2.006

Course Notes

Spring 2009

CHAPTER 9

Viscosity and the Transfer of Momentum in a Fluid

9.1 Introduction

In thermal-fluids engineering, it is usually necessary to move the working fluid of the system from one location to another. During this transport process, the fluid frequently comes into contact with the solid surfaces, or more generally the boundaries, that are used to direct its motion. These may include surfaces that enclose the fluid such as the walls of a conduit through which the fluid is flowing or they may be the surfaces over which the fluid flows such as the wings of an aircraft or the body of an automobile. Whenever the fluid comes into contact with these boundaries, interactions occur that involve the transfer of momentum and energy between the fluid and the boundary as a consequence of the transport properties of the fluid, namely the *viscosity* and the *thermal conductivity*. As a result, gradients of fluid velocity and temperature develop in a direction normal to the surface. Knowing these gradients in velocity and temperature, we can determine the properties of the fluid as a function of position relative to the boundary. The larger the values of the viscosity and the thermal conductivity, the stronger the interaction between the fluid and the boundary. This interaction influences the motion of the fluid in a manner such that strongest influence occurs in the immediate neighborhood of the boundary. This influence diminishes rapidly with distance from the boundary so that far from the boundary, the fluid behaves almost as though it had no viscosity or thermal conductivity and its motion can be described with the aid of the Bernoulli equation that we developed in Chapter 8. However, near the boundary, the effect of the transport properties can be of paramount importance in determining the motion of the fluid and, hence, its performance in the thermal-fluid system.

As we have mentioned previously, an incompressible fluid is an uncoupled system so its thermal and mechanical aspects of behavior can be separated. Therefore, for this fluid model, the effects of viscosity and thermal conductivity can be studied separately. In the present chapter, we shall treat the incompressible fluid as a continuum and focus our attention on the fluid viscosity and the process of momentum transfer between the fluid and its boundaries. We shall develop the "tools" necessary to quantitate this interaction in a wide variety of thermal-fluid systems, both those with "internal flows" such as pipes and those with "external flows" such as airplane wings. Furthermore, we shall quantitate the "strength" of the interaction between the fluid and the boundary, and we shall provide some quantitative measure to the distance over which the effect of the viscosity can be felt in the fluid. In Chapter 11, we shall take up the effect of the fluid thermal conductivity and the resulting energy transfer process between the fluid and its boundaries.

Recall that in Chapter 8 we examined the dynamical behavior of a fluid as it flowed through an open system which we modeled as a control volume. Although the control volume approach is general and can be applied to a control volume of any size or shape, we found in Chapter 8 that it is particularly useful when the control surface that defines the control volume is coincident with walls of a physical device such as a thermal-fluid machine. In such cases, we are able to describe the behavior of the device in terms of the thermodynamic states of the fluid as it crosses the control surface. In using the control volume approach in this manner, we model the state of the fluid crossing the control surface as uniform over the areas of the ports where the fluid enters and leaves the control volume. In reality, the values of the properties that define the state of the fluid vary over these areas for the reasons given above. However, if we know the manner in which the properties vary over the area of interest, we can perform a suitable

averaging process over the area to obtain the appropriate average values of the properties to use in the control volume "conservation" equations. As mentioned above, the "tools" that we shall develop in the present chapter will provide the means of describing the dynamical behavior of the fluid under the influence of its viscosity so that we can determine the manner in which the fluid properties vary over the area of any given port of a thermal-fluid machine. To be sure, the results of this study will be applicable to any situation in which we need to describe the dynamical behavior of a fluid at any point in a flow field, but for the present, this will be one of our primary motivations for the study.

9.2 Viscosity

In order to see the influence of viscosity on fluid behavior, we consider a layer of fluid confined between two infinite parallel flat plates separated by a distance H as shown in Figure 9.1. Because the plates are infinite in extent, the effects of the edges of the plates do not need to be considered. Let the upper plate be in motion with the constant velocity ϑ_0 while the lower plate remains at rest. The fluid can be thought of consisting of many thin layers parallel to the plates such that the fluid in contact with the plates adheres to the plates. This is known as the "no slip" boundary condition. As the upper plate moves relative to the lower plate, the fluid at the upper plate moves with the velocity ϑ_0 while the fluid at the lower plate remains stationary. This induces a steady motion in the fluid in the x-direction as the fluid layers slide over one another. Let the velocity of the fluid in the x-direction at any point between the plates be denoted by ϑ_x. As a consequence of the viscosity of the fluid, there is internal friction between adjacent layers. The layer below the top layer will be dragged in the forward direction by the layer above it, but at a velocity somewhat less than the velocity of the layer above. This layer, in turn, will exert a forward drag on the layer beneath it at reduced velocity and so on through the entire fluid layer. As a result of this motion, there is a velocity gradient $d\vartheta_x/dy$ everywhere in the fluid. In the steady state,

$$\frac{d\vartheta_x}{dy} = \frac{\vartheta_0}{H} \tag{9.1}$$

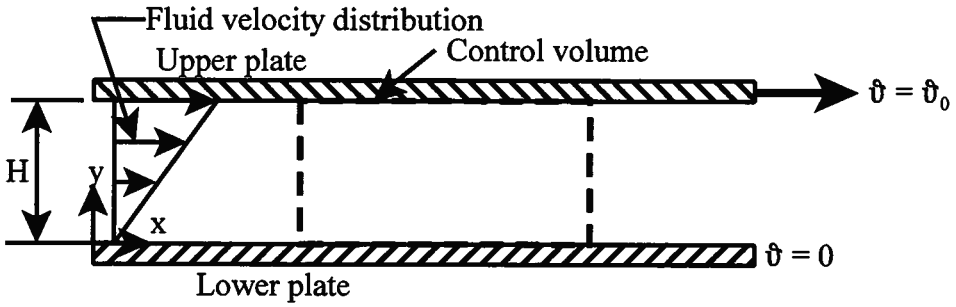

Figure 9.1 Fluid Layer Between Two Flat Plates

This is analogous to the situation in which a deck of playing cards is placed upon a table and a force is exerted on the top card in the plane of this card thereby setting it in motion. The card beneath the top card is dragged along by the friction between the two cards and so on down through the deck until the bottom card is reached which is "stuck" to the table. In the fluid, the frictional forces on the two surfaces of a fluid layer (forward drag on the upper surface and

backward drag on the lower surface) are parallel to the surfaces. Since these forces are in the plane of the surfaces, they tend to shear the layers one over the other. This type of force is known as a shear force, and it gives rise to a type of stress known as a shear stresses which is defined as the shear force divided by the area of the surface over which the force is applied. Since shear stresses, in contrast to the hydrostatic stresses we considered in Chapter 4, are parallel to the surfaces over which they act, we need to specify two directions for a shear stress. By convention, the first of these is the direction normal to the surface over which the force acts and the other is the direction in which it acts. For the case shown in Figure 9.1, the shear stress associated with the relative motion of the two plates is denoted by τ_{yx}.

For the viscous fluids most commonly found in thermal-fluid systems, the shear stress is found to be linearly proportional to the velocity gradient. For this fluid model, known as the Newtonian fluid model, the constant of proportionality is known as the viscosity of the fluid and denoted by the symbol μ. Thus, for the one-dimensional situation shown in Figure 9.1

$$\tau_{yx} = \mu \frac{d\vartheta_x}{dy} \tag{9.2}$$

Physically, this shear stress is the force per unit area that must be applied to the upper plate at all times so that the velocity of the plate can be maintained constant in the presence of the friction in the fluid.

The dissipative nature of the fluid friction manifest in the viscosity of the fluid can be observed by applying the first and second laws of thermodynamics to the control volume fixed in space as shown in Figure 9.1. Let the fluid be modeled as an incompressible fluid. Since the plates are infinite in extent, the fluid has an x-component of velocity only. If the *control volume* (not the plates) has dimensions L in the x-direction, H in the y-direction, and b in the z-direction normal to the plane of the figure, the mass flow rate of the fluid through the control volume in the steady state is given by

$$\dot{m}_{in} = \dot{m}_{out} = \dot{m} = \int_0^H \rho \vartheta_x(y) b dy \tag{9.3}$$

where the fluid velocity $\vartheta_x(y)$ is a function of the distance y measured normal to the plate. By integrating equation (9.1), we can obtain the functional relationship between ϑ_x and y, viz.

$$\vartheta_x = \frac{\vartheta_0}{H} y \tag{9.4}$$

Then equation (9.3) becomes

$$\dot{m} = \int_0^H \rho \frac{\vartheta_0}{H} b y dy = \rho \frac{\vartheta_0 b}{H} \int_0^H y dy = \rho b H \frac{\vartheta_0}{2} = \rho b H \vartheta_{ave} \tag{9.5}$$

Equation (9.5) illustrates the manner in which the average values of the fluid properties can be determined, in this case the average fluid velocity.

Let us examine the fluid control volume of Figure 9.1a in greater detail from the point of view of the forces acting on the fluid control volume in the x-direction. (See Figure 9.1b.)

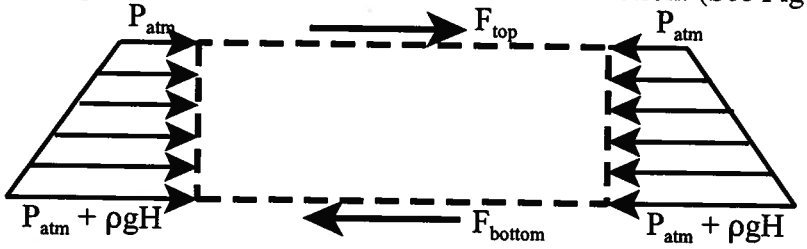

Figure 9.1b Forces on the Control Volume of Figure 9.1a

Since the forces due to normal stresses acting on the ends of the fluid control volume are hydrostatic, the net force acting on the control volume is given by

$$\sum F_x = \left(P_{atm} + \rho g \frac{H}{2}\right) Hb - \left(P_{atm} + \rho g \frac{H}{2}\right) Hb + F_{top} - F_{bottom}$$

$$\sum F_x = \left(P_{atm} + \rho g \frac{H}{2}\right) Hb - \left(P_{atm} + \rho g \frac{H}{2}\right) Hb + \tau_{yx} bL - \tau_{yx} bL = 0$$

where the shear stress acting on the top and bottom surfaces of the fluid control volume are the same since the velocity gradient is constant throughout the fluid layer. (See equation 9.2.) Thus, there is no net force acting on the fluid control volume. This is consistent with the fact that there is no net momentum flow across the control surface for this steady flow situation which can be seen from the equation of linear momentum, viz.

$$\int_{CS} \rho \vec{\vartheta} \left(\vec{\vartheta} \cdot \vec{n}\right) dA = \frac{4}{3} \dot{m} \vartheta_{ave} - \frac{4}{3} \dot{m} \vartheta_{ave} = 0$$

Then for this steady flow situation with no pressure drop in the x-direction, the first law of thermodynamics reduces to

$$\dot{Q} - \dot{W}_{shear} = \dot{m}\left(u_{out} - u_{in}\right) = \dot{m}c\left(T_{out} - T_{in}\right) \tag{9.6}$$

From the definition of the work transfer and the fact that only the boundary mass points on the top of the fluid layer are in motion, the fluid shear power becomes

$$\dot{W}_{shear} = \frac{\delta W_{shear}}{dt} = -\left(F_x\right)_{shear} \frac{dx}{dt} = -F_{top} \frac{dx}{dt} = -\tau_{yx} A \vartheta_0 = -\tau_{yx} bL \vartheta_0 \tag{9.7}$$

Substituting equations (9.1) and (9.2) into equation (9.7), we obtain

$$\dot{W}_{shear} = -\mu \frac{\vartheta_0^{\,2}}{H} bL \tag{9.8}$$

Since the flow is adiabatic, substitution of equation (9.8) into equation (9.6) yields

$$T_{out} = T_{in} + \frac{2\mu \vartheta_0 L}{\rho c H^2} \tag{9.9}$$

Thus as a result of the action of viscosity in the fluid, the temperature of the fluid leaving the control volume is greater than the temperature of the fluid entering the control volume. The rate of entropy generation in the fluid due to viscous dissipation (fluid shear) can be determined by applying the second law of thermodynamics to the control volume. For the adiabatic, steady flow situation shown in Figure 9.1, the second law becomes

$$\dot{S}_{gen} = \dot{m}c\left(s_{out} - s_{in}\right) = \dot{m}c \ln \frac{T_{out}}{T_{in}} \tag{9.10}$$

where we have used the entropy constitutive relation for the incompressible fluid model. Then substituting equation (9.9) into equation (9.10), we obtain

$$\dot{S}_{gen} = \rho \vartheta_0 bc \frac{H}{2} \ln\left(\frac{T_{out}}{T_{in}}\right) = \rho \vartheta_0 bc \frac{H}{2} \ln\left(1 + \frac{2\mu \vartheta_0 L}{\rho c T_{in} H^2}\right) \tag{9.11}$$

From equation (9.11), it is apparent that the more viscous the fluid, i.e., the greater the viscosity of the fluid, the greater the rate of entropy generation. It is also apparent that the smaller the gap between the two plates, the greater the shear and the greater the rate of entropy generation. Note that in the limit of zero viscosity, there is no entropy generation in the control volume due to fluid shear.

For the simple one-dimensional geometry shown in Figure 9.1, we have seen the consequences of fluid shear and the action of viscosity; however, we have not yet seen the relationship between the viscosity and momentum transfer. To do this, we need to examine the fluid on a microscopic scale in which we can identify the individual molecules that make up the fluid. For this purpose, it is most convenient if the fluid is a gas since the kinetic theory of gases molecules is better understood and simpler than that of liquids due primarily to the weak interactions between gas molecules. Suppose the gap between the parallel plates shown in Figure 9.1 is filled with a gas. Consider an imaginary plane located at $y = y_0$ which is being crossed by molecules of gas from above and below. The motion of the molecules in the y- and z-directions is random with zero average velocity, but in the x-direction their average component of velocity is equal to the velocity of bulk motion, $\bar{\vartheta}_x = \vartheta(y)$. Molecules cross the imaginary plane at $y = y_0$ with equal frequency. Each molecule that crosses from above carries with it energy and momentum which are transferred from the layer above to the layer below by the mechanism of molecular collisions. Molecules that cross the plane $y = y_0$ from below transfer energy and momentum from the lower layer to the upper layer. Since there is a velocity gradient in the flowing gas, the molecules, each of mass m, crossing $y = y_0$ from above have a greater average momentum component $m\vartheta_x(y)$ in the x-direction than the molecules below the plane $y = y_0$. Hence, there is a net transfer of momentum from above the plane to below the plane. By Newton's second law of motion, the increase in the x-component of momentum of the lower layer per unit time is equal to the force exerted on it and the decrease in the x-component of momentum of the upper layer is equal to the reaction force. The net effect is the same as if the upper layer exerted a drag force in the x-direction on the lower layer. The net transfer of the x-component of momentum per unit time per unit area of the plane $y = y_0$ is equal to the shear stress τ_{yx} acting on the plane. Thus the viscosity of the gas originates in the net transfer of momentum in the direction of the velocity gradient (but opposite in sense) by molecular collisions.

Using the results of simple kinetic theory of gases, we can develop a quantitative estimate of the viscosity of a gas. Consider again the situation shown schematically in Figure 9.1. Let $m\vartheta_x(y)$ be the x-component of momentum of a gas molecule which varies uniformly in the y-direction due to the velocity gradient in the y-direction associated with the bulk motion of the gas. As we did above, we focus our attention on the imaginary plane $y = y_0$ and determine the net transport of $m\vartheta_x(y)$. The average number of molecules crossing $y = y_0$ per unit area per unit time in either direction is proportional to $n\bar{c}$ where n is the number of molecules per unit volume and $\bar{c}$ is the average velocity of a molecule which is very different from the bulk velocity $\vartheta(y)$. (Typically $\vartheta(y)$ is on the order of 1 m/sec whereas $\bar{c}$ is on the order of 500 m/sec.) When a molecule crosses the $y = y_0$ plane, it carries a value of $m\vartheta_x$ characteristic of that resulting from its last collision. Let $m\vartheta_x(y_0 + \Delta y)$ be the average value of $m\vartheta_x$ transported in the negative y-direction by the molecules crossing $y = y_0$ from above. In the first approximation, Δy represents the average distance a molecule travels since its last collision and is, therefore, equal to the mean free path λ. Then the net amount of $m\vartheta_x$ transported in the negative y-direction is proportional to $n\bar{c}[m\vartheta_x(y_0 + \Delta y) - m\vartheta_x(y_0 - \Delta y)]$. If we perform a Taylor series expansion on the term in square brackets, we get

$$\left[m\vartheta_x(y_0+\Delta y)-m\vartheta_x(y_0-\Delta y)\right] \approx 2\Delta y \frac{d(m\vartheta_x)}{dy} = 2\lambda \frac{d(m\vartheta_x)}{dy} \tag{9.12}$$

By our arguments above, the shear stress in the fluid is proportional to the net transport of the x-

component of momentum, viz.

$$\tau_{yx} = 2an\bar{c}\lambda\frac{d(m\vartheta_x)}{dy} = \varphi(n\bar{c}\lambda)\left(\frac{d(m\vartheta_x)}{dy}\right) = \varphi(mn\bar{c}\lambda)\frac{d\vartheta}{dy} \tag{9.13}$$

where a and φ are constants of proportionality. Then combining equations (9.2) and (9.13), we get

$$\mu = \varphi mn\bar{c}\lambda = \varphi\rho\bar{c}\lambda \tag{9.14}$$

where $\rho = mn$ is the density of the gas. By arguments outside the scope of this treatment, J. C. Maxwell showed in 1860 that $\varphi = 1/3$. Thus since the mean free path λ varies inversely with n, the viscosity μ is independent of density or pressure as confirmed by experiment.

If the molecules are modeled as simple billiard balls with no force of attraction between them, the product $n\lambda$ is independent of temperature. Then since the mean speed of the molecules varies as $T^{1/2}$, the viscosity of gases should vary as $T^{1/2}$. Experiment shows that the temperature dependence of the viscosity of gases is actually stronger than this. In 1893, W. Sutherland showed that by accounting for the weak attractive forces of the gas molecules, the viscosity can be related to the temperature by an expression of the form

$$\mu = A\frac{T^{1/2}}{1+\left(\frac{S^*}{T}\right)} \tag{9.15}$$

where A and S^* are constants now known as the Sutherland constants whose values are determined by experiment. Equation (9.15) gives good agreement with the available data. Representative values of the viscosity of gases commonly used in thermal-fluid systems are listed in Table 9.1 along with their Sutherland constants. Note that in the SI unit system, the units of viscosity are (kg/m sec) or (Pa-sec).

Table 9.1 Viscosity of Common Gases at 300 K and 1 atm[a]

Gas	Viscosity, μ (kg/m sec)	A ($K^{-1/2}$)	S^* (K)
Air	18.53×10^{-6}	1.462×10^{-6}	110
Ammonia, NH_3	10.23×10^{-6}	1.418×10^{-6}	420
Carbon dioxide, CO_2	15.02×10^{-6}	1.596×10^{-6}	252
Helium, He	19.94×10^{-6}	1.535×10^{-6}	100
Hydrogen, H_2	8.949×10^{-6}	6.889×10^{-7}	100
Nitrogen, N_2	17.8×10^{-6}	1.408×10^{-6}	111
Oxygen, O_2	20.65×10^{-6}	1.749×10^{-6}	140
Steam, H_2O (at $P = 3.54 \times 10^3$ N/m^2)	9.195×10^{-6}	2.064×10^{-6}	781

a Except for steam, data derived from *Handbook of Heat Transfer*, ed. by W.M. Rohsenow, J.P. Hartnett, and Y.I. Cho, McGraw-Hill, New York, 3d. ed., 1998, Table 2.10, pp. 2.4-2.11. Data for steam from *NIST/ASME Steam Properties*, NIST Standard Reference Database 10, Version 2.11, by A.H. Harvey, A.P. Peskin, and S.A. Klein.

Although we have examined only gases with respect to the transfer of momentum by molecular collisions, the physics are similar for liquids as well. Of course, the quantitative results will be different for the two types of fluids because the molecules of a liquid are more tightly packed into the volume they occupy and , as a result, they interact with one another more strongly than do the molecules of a gas that occupy an equivalent volume. Because of these strong intermolecular forces, the temperature dependence of the viscosity of liquids is quite different from that of gases. As the temperature of a liquid increases, the liquid expands and the intermolecular forces decrease in magnitude. As a result, the viscosity of a liquid decreases as the temperature increases. The viscosities of some representative liquids are given in Table 9.2.

The important point here is that momentum is transferred in a velocity gradient in the fluid by virtue of collisions between the molecules that make up the fluid as these molecules move from one location to another location of different bulk velocity. This transfer of momentum, in turn, leads to entropy generation in the fluid.

Table 9.2 Viscosity of Some Common Liquids at 300 K and 1 atm[a]

Liquid	Viscosity, μ (kg/m sec)
Ethyl alcohol, C_2H_5OH	10.95×10^{-4}
Octane, C_8H_{18}	5.10×10^{-4}
Engine oil, Mobil 1, 10W-30 (at $T = 40$ C)[b]	506.95×10^{-4}
Castor oil	6500×10^{-4}
Water, H_2O[c]	8.538×10^{-4}

a Handbook of Tables for Applied Engineering Science, ed. by R.E. Bolz and G.L. Tuve, 2nd ed., 1973, CRC press, Cleveland, Ohio, Table 1-46, p. 92. *b* Mobil Oil Co. Product Data Sheet. *c NIST/ASME Steam Properties*, NIST Standard Reference Database 10, Version 2.11, by A.H. Harvey, A.P. Peskin, and S.A. Klein.

9.3 The Total Derivative

We now want to examine the way in which the viscosity of the fluid influences the dynamics of fluid behavior, but in order to do this, we need to study the motion of the fluid by looking at the fluid at the most minute level where it still retains its identity as a continuum. That is, we are going to examine an element of fluid that is so small that we can describe flow phenomena on a point by point basis in space, but is still large enough to contain a sufficiently large number of molecules that the thermal-fluid properties can be described by the continuum constitutive relations introduced previously. In formulating this description, we utilize the "conservation" equations that we developed for the control volume in Chapter 8.

We have already seen in Chapter 8 that there are two alternative descriptions of fluid motion: the Lagrangian approach in which we follow the time history of a fluid particle and the Eulerian approach in which we examine the flow at a particular point in space. The two methods are equivalent and lead to the same end result, but each one has its own set of circumstances for which it is the more appropriate method.

In Chapter 8 we saw that in the Lagrangian approach we were concerned with a control

mass, whereas in the Eulerian approach we were concerned with a control volume. The basic physical laws were originally written for a control mass, and we transformed them by means of an important transformation known as the Reynolds Transport Theorem so that they could be applied to a control volume. We now wish to shrink the size of the control volume down to that of a differential element of volume at some point in space as shown in Figure 9.2. The approach

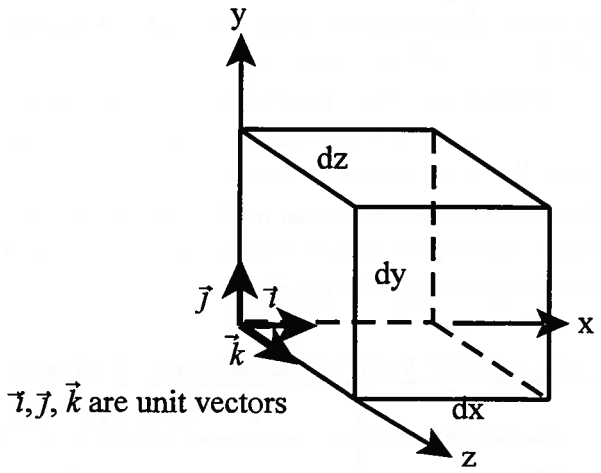

Figure 9.2 Differential Fluid Element

is to follow the time history of a control mass of infinitesimal size, a fluid particle, and to then shrink the time interval of our observation of the history of the particle to zero. In this limit, the fluid particle and the differential volume element become one and the same. The result of this mathematical procedure is the equivalent of the Reynolds Transport Theorem that we used in the case of the finite control volume to transform the time derivative that appears in the Lagrangian approach to the appropriate time derivative for the Eulerian approach. For the differential control volume this transformation is known as the *total derivative* and it provides us with the means to find the proper time rate of change of properties that are specified in terms of both time and the location of the differential control volume in space.

In the Eulerian approach, the properties that describe the flow ρ, T, u, h, s, and $\vec{\vartheta}$ are functions of four independent variables, x, y, z, and t. The values of the properties ρ, T, u, h, s,and $\vec{\vartheta}$ are then specified in terms of the values of the four independent variables, x, y, z, and t. Each property defines a hypersurface in the resulting five-dimensional space. For example,

$$T = T(x, y, z, t) \tag{9.16}$$

defines a hypersurface on which the values of the temperature of the fluid must lie. Similarly, for the velocity vector

$$\vec{\vartheta} = \vartheta_x \vec{i} + \vartheta_y \vec{j} + \vartheta_z \vec{k} \tag{9.17}$$

where

$$\begin{aligned} \vartheta_x &= \vartheta_x(x, y, z, t) \\ \vartheta_y &= \vartheta_y(x, y, z, t) \\ \vartheta_z &= \vartheta_z(x, y, z, t) \end{aligned} \tag{9.18}$$

are the velocity components in the x, y, and z directions.

Consider a fluid particle (which can also be thought of as a control mass denoted by the symbol *CM* as we did in Chapter 8) as it moves a distance Δx, Δy, and Δz in physical space

during the time interval Δt. Let us suppose that we wish to determine the manner in which the fluid temperature changes as the fluid particle moves in space during this time interval. Since the temperature is a function of the four independent variables, x, y, z, and t, it will change by an amount ΔT which will depend upon the amount that each of the independent variables changes. If $\frac{\partial T}{\partial w}$ represents the rate of change of T with respect to the independent variable w, then by the chain rule of differential calculus, the total change in T due to the changes Δw in each of the independent variables is given by

$$\Delta T = \frac{\partial T}{\partial t}\Delta t + \frac{\partial T}{\partial x}\Delta x + \frac{\partial T}{\partial y}\Delta y + \frac{\partial T}{\partial z}\Delta z \tag{9.19}$$

Then if we divide equation (9.19) by Δt, we have

$$\frac{\Delta T}{\Delta t} = \frac{\partial T}{\partial t} + \frac{\partial T}{\partial x}\frac{\Delta x}{\Delta t} + \frac{\partial T}{\partial y}\frac{\Delta y}{\Delta t} + \frac{\partial T}{\partial z}\frac{\Delta z}{\Delta t} \tag{9.20}$$

In the limit as the time interval shrinks to zero ($\Delta t \to 0$), equation (9.20) becomes

$$\left(\frac{dT}{dt}\right)_{CM} = \frac{\partial T}{\partial t} + \left(\frac{dx}{dt}\right)_{CM}\frac{\partial T}{\partial x} + \left(\frac{dy}{dt}\right)_{CM}\frac{\partial T}{\partial y} + \left(\frac{dz}{dt}\right)_{CM}\frac{\partial T}{\partial z} \tag{9.21}$$

where we have used the notation *CM* to identify the derivatives that pertain to the control mass, our fluid particle. Let us now define a new differential operator *D/Dt* such that

$$\frac{D}{Dt} \equiv \left(\frac{d}{dt}\right)_{CM} \tag{9.22}$$

and recognize that the time derivatives of the spatial coordinates traversed by the control mass are simply the instantaneous velocities of the control mass in each of those coordinate directions, viz.

$$\left(\frac{dx}{dt}\right)_{CM} = \vartheta_x, \qquad \left(\frac{dy}{dt}\right)_{CM} = \vartheta_y, \qquad \left(\frac{dz}{dt}\right)_{CM} = \vartheta_z \tag{9.23}$$

Then equation (9.21) becomes

$$\frac{DT}{Dt} = \frac{\partial T}{\partial t} + \vartheta_x\frac{\partial T}{\partial x} + \vartheta_y\frac{\partial T}{\partial y} + \vartheta_z\frac{\partial T}{\partial z} \tag{9.24}$$

where

$$\frac{D}{Dt} = \frac{\partial}{\partial t} + \vartheta_x\frac{\partial}{\partial x} + \vartheta_y\frac{\partial}{\partial y} + \vartheta_z\frac{\partial}{\partial z} \equiv \text{ total derivative} \tag{9.25}$$

Equation (9.24) is also known as the *material derivative* or the *substantial derivative* since it is derived from studying the behavior of a fluid particle. When the total derivative is applied to a property, regardless of whether it is a scalar or a vector, it gives the total time rate of change of that property.

There are two contributions this total time rate of change:

$$\frac{\partial}{\partial t} \tag{9.26}$$

which represents the time rate of change of the property at a given point in space due to the unsteady nature of the flow and is known as the temporal contribution; and

$$\vartheta_x\frac{\partial}{\partial x} + \vartheta_y\frac{\partial}{\partial y} + \vartheta_z\frac{\partial}{\partial z} \tag{9.27}$$

which represents the time rate of change of the property at a given point in space due to the fact

that at a given instant of time, the fluid is at some point in a spatial gradient of that property and is at the same time moving with some velocity in that spatial gradient. This is known as the convective contribution for which the *rate* at which the property changes will depend upon the spatial gradients in the property at the point in question $\left(\frac{\partial}{\partial x}, \frac{\partial}{\partial y}, \text{ and } \frac{\partial}{\partial z}\right)$ *and* the speed at which the fluid is moving at that point (ϑ_x, ϑ_y, and ϑ_z).

To gain some physical sense of the total derivative, consider the following analogy. Imagine yourself riding on a train car or a subway car, and the car is in a tunnel. Suppose that the tunnel is illuminated only by the proverbial light at the end of the tunnel so that the level of illumination in the tunnel will be a function of position in the tunnel as the light entering the tunnel is gradually absorbed by the walls of the tunnel as it travels down the tunnel. That is, there is a spatial gradient in illumination inside the tunnel. The farther into the tunnel the position of observation, the darker it will appear. Now suppose that the car in which you are riding is stopped inside the tunnel and that the intensity of light at the end of the tunnel is modulated in some time-wise fashion such as might occur as a cloud passes over the sun. The time rate of change of light intensity that you would observe by looking out the car window would be that of the rate of change of intensity of the source of illumination. This is equivalent to the first contribution to the total derivative. Now suppose that the light source is fixed in intensity so that there is a fixed spatial gradient in illumination in the tunnel that does not vary with time. Suppose further that the car is now moving in the tunnel. The time rate of change of illumination that you now observe upon looking out the car window will depend upon the spatial gradient in illumination and the speed of the car. This is equivalent to the second contribution to the total derivative.

In a fluid flow field, if the flow is steady, the first contribution to the total derivative vanishes. In a steady, but spatially non-uniform flow field as in a nozzle or diffuser, the fluid velocity can vary in all three directions. As a fluid particle passes through a given point, any one of its properties, such as velocity, changes in response to the spatial variation in the property and the local velocity of the fluid. For example, consider the steady flow of an incompressible fluid in a converging duct as shown in Figure 9.3. As the fluid moves from point A to point B, it speeds up in accordance with the continuity equation. Then even though the flow is steady, the fluid

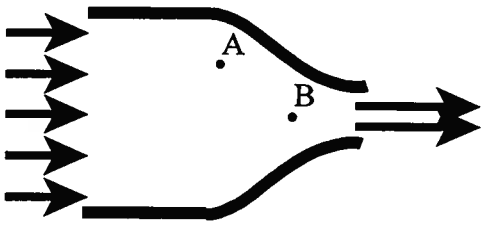

Figure 9.3 Flow in a Converging Duct

accelerates, and this acceleration is described by the convective part of the total derivative.

Thus the total derivative provides information about the rate at which properties of a fluid particle change in the Eulerian approach. In vector notation, it is an operator. Then,

$$\frac{D}{Dt} = \frac{\partial}{\partial t} + \vec{\vartheta} \cdot \nabla \tag{9.28}$$

Note that $\vec{\vartheta} \cdot \nabla$ is not a scalar product but rather an operator such that

$$\vec{\vartheta}\cdot\nabla = \vartheta_x\frac{\partial}{\partial x} + \vartheta_y\frac{\partial}{\partial y} + \vartheta_z\frac{\partial}{\partial z} \tag{9.29}$$

Note also that since

$$\nabla = \frac{\partial}{\partial x}\vec{i} + \frac{\partial}{\partial y}\vec{j} + \frac{\partial}{\partial z}\vec{k}$$
$$\vec{\vartheta} = \vartheta_x\vec{i} + \vartheta_y\vec{j} + \vartheta_z\vec{k} \tag{9.30}$$

$\nabla\cdot\vec{\vartheta}$, known as the divergence, is an operation but $\vec{\vartheta}\cdot\nabla$ is an operator.

$$\nabla\cdot\vec{\vartheta} = \frac{\partial\vartheta_x}{\partial x} + \frac{\partial\vartheta_y}{\partial y} + \frac{\partial\vartheta_z}{\partial z} \tag{9.31}$$

Thus, the total derivative of a scalar property like the density is

$$\frac{D\rho}{Dt} = \frac{\partial\rho}{\partial t} + \vartheta_x\frac{\partial\rho}{\partial x} + \vartheta_y\frac{\partial\rho}{\partial y} + \vartheta_z\frac{\partial\rho}{\partial z} \tag{9.32}$$

whereas the total derivative in a vector property like the velocity becomes

$$\begin{aligned}\frac{D\vec{\vartheta}}{Dt} = &\left(\frac{\partial\vartheta_x}{\partial t} + \vartheta_x\frac{\partial\vartheta_x}{\partial x} + \vartheta_y\frac{\partial\vartheta_x}{\partial y} + \vartheta_z\frac{\partial\vartheta_x}{\partial z}\right)\vec{i}\\ &+\left(\frac{\partial\vartheta_y}{\partial t} + \vartheta_x\frac{\partial\vartheta_y}{\partial x} + \vartheta_y\frac{\partial\vartheta_y}{\partial y} + \vartheta_z\frac{\partial\vartheta_y}{\partial z}\right)\vec{j}\\ &+\left(\frac{\partial\vartheta_z}{\partial t} + \vartheta_x\frac{\partial\vartheta_z}{\partial x} + \vartheta_y\frac{\partial\vartheta_z}{\partial y} + \vartheta_z\frac{\partial\vartheta_z}{\partial z}\right)\vec{k}\end{aligned} \tag{9.33}$$

which is the acceleration of the fluid at some point whose Cartesian coordinates are (x, y, z).

We can now use this total derivative to formulate the various "conservation" equations that apply to the differential control volume of Figure 9.2. In formulating these expressions, for the sake of simplicity, we will consider a two-dimensional differential control volume in each case and then extend the results to the three dimensional case.

9.4 Conservation of Mass

In Chapter 8 we showed that the Reynolds Transport Theorem applied to a control mass reduced to

$$\frac{d}{dt}\int_{CV}\rho dV + \int_{CS}\rho\left(\vec{\vartheta}\cdot\vec{n}\right)dA = 0 \tag{9.34}$$

but for a rigid control volume fixed in space, equation (9.34) reduces to

$$\int_{CV}\frac{\partial\rho}{\partial t}dV + \int_{CS}\rho\left(\vec{\vartheta}\cdot\vec{n}\right)dA = 0 \tag{9.35}$$

Consider the two-dimensional control volume shown in Figure 9.4 with flow through all four of its faces. Because this control volume is of differential size, the first term in equation (9.35) reduces to

$$\int_{CV}\frac{\partial\rho}{\partial t}dV \approx \frac{\partial\rho}{\partial t}dxdy \tag{9.36}$$

and the second term becomes

$$\int_{CS}\rho\left(\vec{\vartheta}\cdot\vec{n}\right)dA = \sum_i\left(\rho_i A_i\vartheta_i\right)_{out} - \sum_i\left(\rho_i A_i\vartheta_i\right)_{in} \tag{9.37}$$

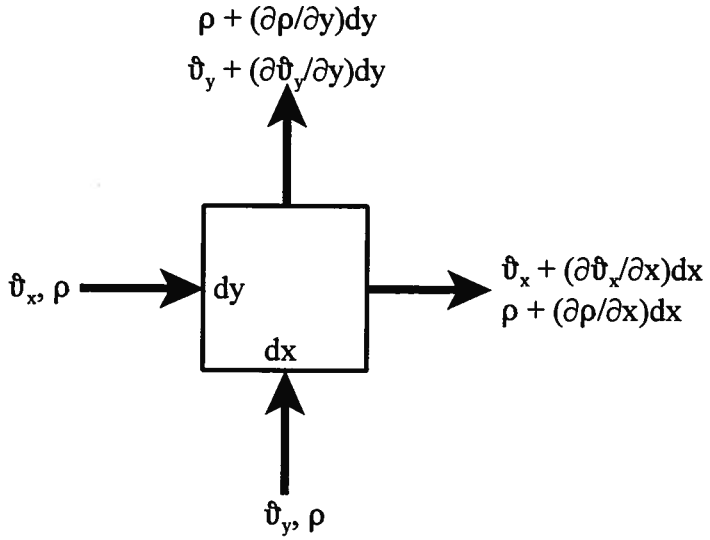

Figure 9.4 Differential Fluid Element Fixed in Space

where

$$\sum_i (\rho_i A_i \vartheta_i)_{out} = \left[\left(\rho + \frac{\partial \rho}{\partial x}dx\right)\left(\vartheta_x + \frac{\partial \vartheta_x}{\partial x}dx\right)\right]dy + \left[\left(\rho + \frac{\partial \rho}{\partial y}dy\right)\left(\vartheta_y + \frac{\partial \vartheta_y}{\partial y}dy\right)\right]dx \quad (9.38)$$

and

$$\sum_i (\rho_i A_i \vartheta_i)_{in} = \rho \vartheta_x dy + \rho \vartheta_y dx \quad (9.39)$$

Carrying out the multiplication in equation (9.38) and neglecting higher order terms, we get

$$\sum_i (\rho_i A_i \vartheta_i)_{out} = \left[\rho \vartheta_x + \rho \frac{\partial \vartheta_x}{\partial x}dx + \vartheta_x \frac{\partial \rho}{\partial x}dx\right]dy + \left[\rho \vartheta_y + \rho \frac{\partial \vartheta_y}{\partial y}dy + \vartheta_y \frac{\partial \rho}{\partial y}dy\right]dx \quad (9.40)$$

Then combining equations (9.37), (9.39), and (9.40), we get

$$\int_{CS} \rho\left(\vec{\vartheta} \cdot \vec{n}\right)dA = \frac{\partial}{\partial x}\left(\rho \vartheta_x\right)dxdy + \frac{\partial}{\partial y}\left(\rho \vartheta_y\right)dxdy \quad (9.41)$$

Substituting equations (9.36) and (9.41) into equation (9.35), we get for the continuity equation

$$\frac{\partial \rho}{\partial t}dxdy + \frac{\partial}{\partial x}\left(\rho \vartheta_x\right)dxdy + \frac{\partial}{\partial y}\left(\rho \vartheta_y\right)dxdy = 0 \quad (9.42)$$

and dividing equation (9.42) through by *dxdy*, we get the two-dimensional continuity equation

$$\frac{\partial \rho}{\partial t} + \frac{\partial}{\partial x}\left(\rho \vartheta_x\right) + \frac{\partial}{\partial y}\left(\rho \vartheta_y\right) = 0 \quad (9.43)$$

but in two dimensions

$$\nabla = \frac{\partial}{\partial x}\vec{i} + \frac{\partial}{\partial y}\vec{j} \quad (9.44)$$

Then the continuity equation in vector notation becomes

$$\frac{\partial \rho}{\partial t} + \nabla \cdot \left(\rho \vec{\vartheta}\right) = 0 \quad (9.45)$$

If we expand equation (9.43), we get

$$\frac{\partial \rho}{\partial t} + \vartheta_x \frac{\partial \rho}{\partial x} + \rho \frac{\partial \vartheta_x}{\partial x} + \vartheta_y \frac{\partial \rho}{\partial y} + \rho \frac{\partial \vartheta_y}{\partial y} = 0$$

$$\left(\frac{\partial \rho}{\partial t}+\vartheta_x\frac{\partial \rho}{\partial x}+\vartheta_y\frac{\partial \rho}{\partial y}\right)+\rho\frac{\partial \vartheta_x}{\partial x}+\rho\frac{\partial \vartheta_y}{\partial y}=0 \tag{9.46}$$

Making use of the definition of the total derivative, we get the vector form of the continuity equation, viz.

$$\frac{D\rho}{Dt}+\rho\nabla\cdot\vec{\vartheta}=0 \tag{9.47}$$

which applies in three dimensions as well.

Note that for an incompressible fluid $D\rho/Dt = 0$ always, so that the continuity equation for this fluid model reduces to $\nabla\cdot\vec{\vartheta}=0$.

9.5 Equation of Linear Momentum for an Inviscid Fluid (Euler Equation)

The differential equation describing the dynamic behavior of a fluid was first derived by Leonhard Euler (1707 - 1783) in 1753 who is the most prolific author of mathematics of all time (886 books and papers). Euler, for whom the Eulerian approach is named, was the first to introduce the concept of the "fluid particle" and, following the example of Daniel Bernoulli with whom he lived from 1730 to 1733, was one of the first mathematicians to use differential and integral calculus to describe fluid behavior. Following Euler's example, we shall first formulate the linear momentum equation for an inviscid fluid model. While this might seem a step backward given the discussion of Section 9.2, the resulting differential equation applies in a fluid flow field remote from the solid surfaces that bound it. In many cases, this is the largest part of the flow. Once we have developed this result, known as the *Euler equation*, we shall use it to determine the effects of the fluid viscosity on the flow.

In formulating the equation of linear momentum, we are concerned with the effects of applied forces acting on the fluid in the flow field. To this end, and keeping with our approach in developing the continuity equation above, we consider the two-dimensional differential control volume shown in Figure 9.5. Two types of forces are of interest here: surface forces and body forces. The only applied surface force that concerns us now is that due to the local pressure acting over each face. The only body force of interest is that due to gravity. If the fluid element is oriented in an arbitrary fashion with respect to gravity, both of these forces contribute to the net force acting along each of the coordinate directions. Then the net force per unit volume F acting

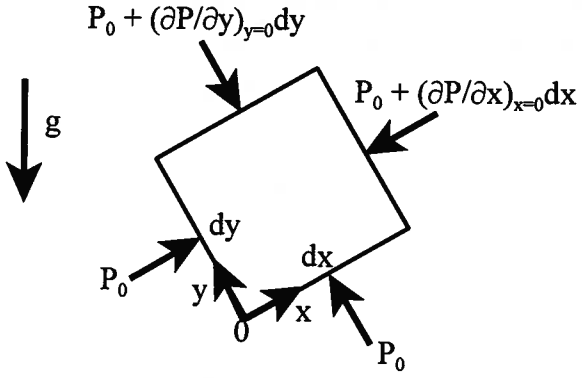

Figure 9.5 Forces Acting on a Differential Fluid Element

on the fluid particle due to surface and body forces is

$$\vec{F}=\vec{F}_{surface}+\vec{F}_{body}=\vec{F}_{\substack{normal\\stresses}}+\vec{F}_{body} \tag{9.48}$$

If we let F_x be the force per unit "volume" $dxdy$ due to normal stresses and body forces acting in the x-direction

$$F_x dxdy = P_0 dy - \left[P_0 + \left(\frac{\partial P}{\partial x} \right)_{x=0} dx \right] dy + \rho_0 g_x dxdy$$

$$F_x dxdy = -\left(\frac{\partial P}{\partial x} \right)_{x=0} dxdy + \rho_0 g_x dxdy \tag{9.49}$$

Similarly for the y-direction, we have

$$F_y dxdy = -\left(\frac{\partial P}{\partial y} \right)_{y=0} dxdy + \rho_0 g_y dxdy \tag{9.50}$$

If we were to extend this analysis to three dimensions in order to include the z-direction as well, we would have

$$F_x dxdydz = -\left(\frac{\partial P}{\partial x} \right)_{x=0} dxdydz + \rho_0 g_x dxdydz$$

$$F_y dxdydz = -\left(\frac{\partial P}{\partial y} \right)_{x=0} dxdydz + \rho_0 g_y dxdydz \tag{9.51}$$

$$F_z dxdydz = -\left(\frac{\partial P}{\partial z} \right)_{z=0} dxdydz + \rho_0 g_z dxdydz$$

Then in vector notation (including all three coordinate directions), the net force per unit volume $dxdydz$ is

$$\vec{F} = \vec{F}_{\substack{normal \\ stresses}} + \vec{F}_{body} = F_x \vec{i} + F_y \vec{j} + F_z \vec{k}$$

$$\vec{F} = \vec{F}_{\substack{normal \\ stresses}} + \vec{F}_{body} = -\left(\frac{\partial P}{\partial x} \vec{i} + \frac{\partial P}{\partial y} \vec{j} + \frac{\partial P}{\partial z} \vec{k} \right) + \rho g_x \vec{i} + \rho g_y \vec{j} + \rho g_z \vec{k} \tag{9.52}$$

where we have dropped the subscript 0 since the result should apply at any point in the flow field. Making use of the gradient operator of equation (9.30), we have

$$\vec{F} = -\nabla P + \rho \vec{g} \tag{9.53}$$

Having determined the net force acting on the fluid element, we can apply Newton's second law of motion: the applied force is equal to the rate of change of momentum of the fluid particle. Using the acceleration vector defined in equation (9.33), we have

$$\vec{F} dxdydz = \rho \frac{D\vec{\vartheta}}{Dt} dxdydz$$

$$\vec{F} = \rho \frac{D\vec{\vartheta}}{Dt} \tag{9.54}$$

Substituting equation (9.53) into (9.54), we obtain the Euler equation

$$\rho \frac{D\vec{\vartheta}}{Dt} = -\nabla P + \rho \vec{g} \tag{9.55}$$

Equation (9.55) represents the equation of linear momentum in the Eulerian approach. Notice that the terms appearing on the right-hand side of equation (9.55) are the forces per unit volume acting on a fluid particle in the flow field. In particular, notice that the "pressure force" per unit volume is due to the gradient in the pressure, not the pressure itself, acting on the fluid particle.

If we divide equation (9.55) through by the density, we obtain an expression in which all of the terms have the units of acceleration, viz.

$$\frac{D\vec{\vartheta}}{Dt} = -\frac{1}{\rho}\nabla P + \vec{g} \tag{9.56}$$

The left-hand side represents the acceleration of a fluid particle in the Eulerian representation while the first term on the right-hand side represents the acceleration of a fluid particle due to the *gradient* in the pressure and the second term on the right-hand side represents the acceleration of a fluid particle due to the effect of gravity. Equation (9.56) is a vector equation since the acceleration is a vector quantity; therefore, equation (9.56) is really three separate equations, one for each coordinate direction.

$$\begin{aligned}
\frac{\partial \vartheta_x}{\partial t} + \vartheta_x\frac{\partial \vartheta_x}{\partial x} + \vartheta_y\frac{\partial \vartheta_x}{\partial y} + \vartheta_z\frac{\partial \vartheta_x}{\partial z} &= -\frac{1}{\rho}\frac{\partial P}{\partial x} + g_x \\
\frac{\partial \vartheta_y}{\partial t} + \vartheta_x\frac{\partial \vartheta_y}{\partial x} + \vartheta_y\frac{\partial \vartheta_y}{\partial y} + \vartheta_z\frac{\partial \vartheta_y}{\partial z} &= -\frac{1}{\rho}\frac{\partial P}{\partial y} + g_y \\
\frac{\partial \vartheta_z}{\partial t} + \vartheta_x\frac{\partial \vartheta_z}{\partial x} + \vartheta_y\frac{\partial \vartheta_z}{\partial y} + \vartheta_z\frac{\partial \vartheta_z}{\partial z} &= -\frac{1}{\rho}\frac{\partial P}{\partial z} + g_z
\end{aligned} \tag{9.57}$$

(Note that if the y-axis is directed vertically upward, $g_x = 0$, $g_y = -g$, and $g_z = 0$.) Since the Euler equation does not include the viscous forces acting on the fluid element, if we apply it to a real fluid that does have viscous effects, it cannot be applied in the region near the solid surfaces that bound the fluid (known as the boundary layer) where there is fluid shear due to the momentum transfer between the wall and the fluid resulting from the action of the viscosity of the fluid. The Euler equation applies only in that region where viscous effects are negligible far from the boundaries. The Euler equation applies to both compressible and incompressible fluid models.

Example 9E.1: In Section 5.3 of Chapter 5 we considered the case for which a piston traveled at constant velocity in a cylinder containing a compressible fluid that we modeled as an ideal gas. We saw that if the motion of the piston was in a direction to compress the gas, there was a compression wave of small amplitude that propagated through the gas with a speed ϑ_s. The compression of the gas that resulted from the passage of the wave was sufficiently rapid that it could be modeled as adiabatic. Furthermore, if the amplitude of the wave was sufficiently small, the compression process could be modeled as reversible as well. Under these conditions, no entropy is generated by the wave (The eventual damping of the wave is another matter entirely!) and the speed is given by

$$\vartheta_s^{\,2} = \left(\frac{\partial P}{\partial \rho}\right)_s$$

where ϑ_s is the speed of sound and the subscript s on the partial derivative indicates that the derivative should be taken in a plane on which the entropy is constant. We showed in Section 5.3 that for the ideal gas model

$$\vartheta_s = \sqrt{\gamma RT}$$

where $\gamma = c_p/c_v$, the ratio of the two specific heats, and R is the gas constant.

We now consider the case for which the motion of the piston is sinusoidal, i.e., the piston moves back and forth (oscillates) in the cylinder such that its position relative to the midpoint of its travel, x_0, is given by

$$x - x_0 = A\sin\omega t$$

where ω is the frequency of the motion in radians and A is the amplitude of the oscillation. As a result of this motion, the gas in the cylinder is alternately compressed and expanded, and the "disturbance" associated with this alternating compression and expansion propagates into the gas inside the cylinder at a velocity of ϑ_s. This "disturbance" constitutes a longitudinal plane wave, a sound wave, propagating from the piston face into the gas. [Note: There are two types of waves in material media that involve a deformation of the medium: (1) those in which the deformation of the medium takes place in the direction of propagation, and (2) those in which the deformation of the medium is perpendicular to the direction of propagation. The first type of wave is known as a *longitudinal* wave, and the second type is known as a *transverse* wave. In a longitudinal wave, the deformation is a compression or expansion of the medium, but in a transverse wave, the deformation is a shearing deformation of the medium. In a solid, both types of waves may exist, but they travel at different velocities with the velocity of the longitudinal wave always the greater of the two. In an inviscid fluid, shear deformations cannot occur so only longitudinal waves are possible.] The sound wave manifests itself as a local perturbation in the density and the pressure of the gas, as well as a perturbation in the local velocity of the gas.

We now show that by applying the continuity equation and the Euler equation to the gas, we can quantitate the behavior of the density of a one-dimensional traveling sound wave propagating from the piston face.

Solution: For the present purpose, we consider the cylinder to be infinitely long so that we do not have to deal with the events that occur when the wave reaches the far end of the cylinder. For the case of a wave propagating in the x-direction only, we can write the continuity equation in the form [*cf.* equation (9.46)]

$$\frac{\partial \rho}{\partial t} + \vartheta_x \frac{\partial \rho}{\partial x} + \rho \frac{\partial \vartheta_x}{\partial x} = 0$$

and the Euler equation [*cf.* equation(9.57)] becomes

$$\rho\left(\frac{\partial \vartheta_x}{\partial t} + \vartheta_x \frac{\partial \vartheta_x}{\partial x}\right) = -\frac{\partial P}{\partial x}$$

Let us now suppose that as a result of the passage of the compression wave (sound wave), the are slight local perturbations in the pressure, density, and velocity of the gas such that

$$P = P_0 + P^*,\ \rho = \rho_0 + \rho^*,\ \text{and}\ \vartheta_x = \vartheta_0 + \vartheta_x^*$$

where the subscript 0 indicates the rest state (so that $\vartheta_0 = 0$) and the starred quantities represent the perturbations associated with the passage of the sound wave.

If we now substitute these quantities into the one-dimensional forms of the continuity equation and the Euler equation and neglect terms that involve the products of the perturbation quantities, we get

$$\frac{\partial \rho}{\partial t} + \vartheta_x \cancel{\frac{\partial \rho_0}{\partial x}} + \cancel{\vartheta_x \frac{\partial \rho^*}{\partial x}} + \rho_0 \frac{\partial \vartheta_x}{\partial x} + \cancel{\rho^* \frac{\partial \vartheta_x}{\partial x}} = 0$$

$$\frac{\partial \rho}{\partial t} + \rho_0 \frac{\partial \vartheta_x}{\partial x} = 0$$

and

$$\rho_0 \frac{\partial \vartheta_x}{\partial t} + \cancel{\rho^* \frac{\partial \vartheta_x}{\partial t}} + \cancel{\vartheta_x \frac{\partial \vartheta_x}{\partial x}} = 0$$

$$\rho_0 \frac{\partial \vartheta_x}{\partial t} = -\frac{\partial P}{\partial x}$$

But

$$\frac{\partial P}{\partial x}=\left(\frac{\partial P}{\partial \rho}\right)_s\left(\frac{\partial \rho}{\partial x}\right)_s=-\vartheta_s^{\,2}\left(\frac{\partial \rho}{\partial x}\right)_s$$

where the subscript s indicates that we are considering reversible, adiabatic (isentropic) compression waves. Then the Euler equation becomes

$$\rho_0\frac{\partial \vartheta_x}{\partial t}=-\vartheta_s^{\,2}\left(\frac{\partial \rho}{\partial x}\right)$$

Now combining this last result with the continuity equation, we get

$$\frac{\partial^2\rho}{\partial t^2}=-\rho_0\frac{\partial}{\partial t}\left(\frac{\partial \vartheta_x}{\partial x}\right)=-\rho_0\frac{\partial}{\partial x}\left(\frac{\partial \vartheta_x}{\partial t}\right)=\rho_0\frac{\partial}{\partial x}\left(\frac{1}{\rho_0}\vartheta_s^{\,2}\frac{\partial \rho}{\partial x}\right)$$

$$\frac{\partial^2\rho}{\partial t^2}=\vartheta_s^{\,2}\frac{\partial^2\rho}{\partial x^2}$$

which is the well-known wave equation. The general solution of this equation is

$$\rho(x,t)=f(x+\vartheta_s t)+g(x-\vartheta_s t)$$

where f and g are arbitrary functions that depend only on the values of $x+\vartheta_s t$ and $x-\vartheta_s t$, respectively. To an observer traveling with velocity $dx/dt = -\vartheta_s$, the value of $x+\vartheta_s t$ would appear constant; thus the first term in the solution represents the motion of a "disturbance" in the negative x-direction. The second term represents another wave moving in the positive x-direction with the velocity $dx/dt = \vartheta_s$. In each case there is no change in the shape and magnitude of the "deformation" as it propagates in its respective direction. Clearly, in the present case we are interested only in the wave propagating in the positive x-direction. Then, guided by the form of the disturbance (the movement of the piston), we can write the solution of the wave equation describing the local density as

$$\rho(x,t)=\rho_0+B\sin\beta(x-\vartheta_s t)$$

where B is the amplitude of the perturbation in the density. At $t = 0$, the profile of this wave is $B\sin\beta x$ which is a sine wave of wavelength $\lambda = 2\pi/\beta$. Then the wave form becomes

$$\rho(x,t)=\rho_0+B\sin\frac{2\pi}{\lambda}(x-\vartheta_s t)$$

At any fixed value of time, say t_0, the density varies sinusoidally in x with a wavelength of λ. At some time Δt later, the whole sinusoidal curve describing the density is displaced in the positive x-direction by an amount $\Delta x = \vartheta_s \Delta t$. This gives rise to the notion of a "traveling" wave. On the other hand, at any fixed position in the cylinder, the density varies sinusoidally with time. Thus, there are *two* sinusoidal variations in this traveling wave.

9.6 Newtonian Fluid Model

We now wish to take into account the effects of viscosity on the dynamic behavior of a fluid as outlined in Section 9.2. In order to do this, we need to develop a fluid model that accounts for the relationship between viscosity and friction in fluid flow fields. Sir Isaac Newton (1643 - 1727) was one of the first to propose such a relationship in 1687 in his treatise of the "new physics," *Philosophiae Naturalis Principia Mathematica*. In *Principia*, Newton concluded that the shear stress developed by fluid friction is given by the product of the coefficient of viscosity and the velocity gradient as shown in equation (9.2). This expression forms the basis of

a model which has become known as the "Newtonian" fluid model in his honor. The Newtonian fluid model states that the viscous stress in a Newtonian fluid is proportional to the rate of strain. The model developed from this simple statement encompasses a vast array of fluids, such as water, air, and oil plus a host of other fluids that are commonly found in thermal-fluid systems. In fact, the Newtonian fluid model is so all-encompassing that the exceptions to it, such as paint, liquid polymers, and a variety of food stuffs, form the basis of a new branch of thermal-fluids engineering known as non-Newtonian fluid mechanics.

Although the Newtonian fluid model applies to both compressible and incompressible fluids, we shall consider here only the incompressible case. While at first glance this may seem overly restrictive, it turns out (as we shall soon show) that the incompressible model applies even to the flow of fluids like gases that we normally think of as being compressible *provided the flow velocities are less than 30 percent of the speed of sound.* The incompressible Newtonian fluid model presents the stress/rate-of-strain relationship in terms of a set of constitutive relations between the shear stresses and the corresponding rates-of-strain in the fluid, viz.

$$\tau_{xx} = 2\mu\frac{\partial \vartheta_x}{\partial x}, \qquad \tau_{yy} = 2\mu\frac{\partial \vartheta_y}{\partial y}, \qquad \tau_{zz} = 2\mu\frac{\partial \vartheta_z}{\partial z}$$

$$\tau_{xy} = \tau_{yx} = \mu\left(\frac{\partial \vartheta_x}{\partial y} + \frac{\partial \vartheta_y}{\partial x}\right)$$

$$\tau_{xz} = \tau_{zx} = \mu\left(\frac{\partial \vartheta_z}{\partial x} + \frac{\partial \vartheta_x}{\partial z}\right) \tag{9.58}$$

$$\tau_{yz} = \tau_{zy} = \mu\left(\frac{\partial \vartheta_y}{\partial z} + \frac{\partial \vartheta_z}{\partial y}\right)$$

where μ is the now familiar coefficient of viscosity. Notice that we have introduced the normal stresses τ_{ii} which are due to extensional rates-of-strain. Since the viscosity is *isotropic* (equal in all directions) in the Newtonian fluid model, these normal stresses are directly proportional to the extensional rates-of-strain with the same constant of proportionality as the shear stresses are proportional to the shear strain rates.

9.7 Navier-Stokes Equation

In order to take into account the effect of viscosity on fluid motion, we need to develop the equation of linear momentum for a viscous fluid. To do this, we need to formulate an expression for the viscous surface forces in terms of the viscous stresses introduced above. Again, in the interests of simplicity, we resort to the two-dimensional differential fluid element shown in Figure 9.6.

If $F_{x,viscous}$ represents the viscous surface force per unit "volume" (the two-dimensional "volume" *dxdy*) acting in the *x*-direction, we have for the *x*-component of the viscous surface force

$$F_{x,viscous}dxdy = -\tau_{xx}dy + \left(\tau_{xx}dy + \frac{\partial \tau_{xx}}{\partial x}dxdy\right) - \tau_{yx}dx + \left(\tau_{yx}dx + \frac{\partial \tau_{yx}}{\partial y}dydx\right)$$

$$F_{x,viscous}dxdy = \frac{\partial \tau_{xx}}{\partial x}dxdy + \frac{\partial \tau_{yx}}{\partial y}dxdy$$

$$F_{x,viscous} = \frac{\partial \tau_{xx}}{\partial x} + \frac{\partial \tau_{yx}}{\partial y} \tag{9.59}$$

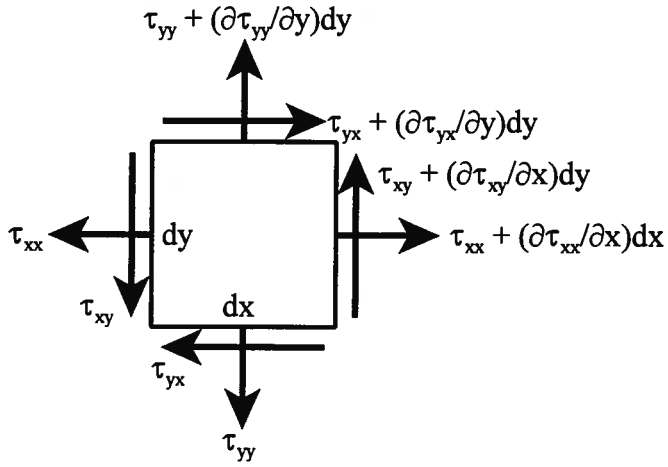

Figure 9.6 Viscous Stresses on a Two-Dimensional Differential Fluid Element

If we extend the result of equation (9.59) to three dimensions, the x-component of the viscous surface force per unit volume ($dxdydz$) becomes

$$F_{x,viscous} = \frac{\partial \tau_{xx}}{\partial x} + \frac{\partial \tau_{yx}}{\partial y} + \frac{\partial \tau_{zx}}{\partial z} \tag{9.60}$$

Similarly for the y- and z-components, we have

$$\begin{aligned} F_{y,viscous} &= \frac{\partial \tau_{xy}}{\partial x} + \frac{\partial \tau_{yy}}{\partial y} + \frac{\partial \tau_{zy}}{\partial z} \\ F_{z,viscous} &= \frac{\partial \tau_{xz}}{\partial x} + \frac{\partial \tau_{yz}}{\partial y} + \frac{\partial \tau_{zz}}{\partial z} \end{aligned} \tag{9.61}$$

If we substitute the stress/rate-of-strain constitutive relations given in equation (9.58) into equations (9.60) and (9.61) and make use of the continuity equation, we obtain for the three components of the viscous surface force per unit volume

$$\begin{aligned} F_{x,viscous} &= \mu\left(\frac{\partial^2 \vartheta_x}{\partial x^2} + \frac{\partial^2 \vartheta_x}{\partial y^2} + \frac{\partial^2 \vartheta_x}{\partial z^2}\right) \\ F_{y,viscous} &= \mu\left(\frac{\partial^2 \vartheta_y}{\partial x^2} + \frac{\partial^2 \vartheta_y}{\partial y^2} + \frac{\partial^2 \vartheta_y}{\partial z^2}\right) \\ F_{z,viscous} &= \mu\left(\frac{\partial^2 \vartheta_z}{\partial x^2} + \frac{\partial^2 \vartheta_z}{\partial y^2} + \frac{\partial^2 \vartheta_z}{\partial z^2}\right) \end{aligned} \tag{9.62}$$

Since the Laplacian operator ∇^2 in Cartesian coordinates is given by $\nabla^2 = \left(\frac{\partial^2}{\partial x^2} + \frac{\partial^2}{\partial y^2} + \frac{\partial^2}{\partial z^2}\right)$, the Laplacian operating on the velocity vector gives

$$\nabla^2 \vec{\vartheta} = \left(\frac{\partial^2 \vartheta_x}{\partial x^2} + \frac{\partial^2 \vartheta_x}{\partial y^2} + \frac{\partial^2 \vartheta_x}{\partial z^2}\right)\vec{i} + \left(\frac{\partial^2 \vartheta_y}{\partial x^2} + \frac{\partial^2 \vartheta_y}{\partial y^2} + \frac{\partial^2 \vartheta_y}{\partial z^2}\right)\vec{j} + \left(\frac{\partial^2 \vartheta_z}{\partial x^2} + \frac{\partial^2 \vartheta_z}{\partial y^2} + \frac{\partial^2 \vartheta_z}{\partial z^2}\right)\vec{k} \tag{9.63}$$

Then we can write the viscous surface force per unit volume in vector form as

$$\vec{F}_{viscous} = \mu \nabla^2 \vec{\vartheta} \tag{9.64}$$

Now we can combine equation (9.53) (the "pressure" force and the body force due to gravity)

and equation (9.64) (the viscous force) to obtain the net force per unit volume acting on a fluid particle, viz.

$$\vec{F}_{net} = \vec{F}_{pressure} + \vec{F}_{body} + \vec{F}_{viscous}$$
$$\vec{F}_{net} = -\nabla P + \rho\vec{g} + \mu\nabla^2\vec{\vartheta} \tag{9.65}$$

If we now substitute equation (9.65) into Newton's second law of motion, equation (9.54), we obtain the well-known Navier-Stokes equation. This is the equation of linear momentum for an

$$\rho\frac{D\vec{\vartheta}}{Dt} = -\nabla P + \rho\vec{g} + \mu\nabla^2\vec{\vartheta} \tag{9.66}$$

incompressible viscous fluid.

It is interesting to note that this equation was first formulated in 1822 by a Frenchman, Claude Louis Marie Henri Navier (1785 - 1836) who was a student of Jean Baptiste Joseph Fourier (1768 - 1830) whom we have already identified for his pioneering contributions to the theory of heat transfer by conduction. Although Navier had the correct form of equation (9.66), he did not fully understand the physics of the situation he was trying to model. He did not understand the concept of shear stress in a fluid, but rather he based his work on an attempt to modify the Euler equation to take into account forces between the molecules in the fluid. In Navier's formulation of equation (9.66), the viscosity appeared as a constant coefficient, but he failed to realize its physical significance. It was not until 1843 that another Frenchman, Jean Claude Barre de Saint-Venant (1797 - 1886) recognized that this coefficient was indeed the viscosity of the fluid. Independently, Sir George Gabriel Stokes (1819 - 1903) published a similar derivation of equation (9.66) in 1845. However, this equation was first viewed with some skepticism. When the Navier-Stokes equation became generally known in the mid-nineteenth century, investigators who tried to apply it to their data for flow in a circular pipe found that sometimes it was valid and sometimes it was not. The reason for this apparent dilemma will become apparent in Section 9.8. Nevertheless, equation (9.66) is an extremely important result in thermal-fluids engineering that now bears the names of Navier and Stokes despite the pivotal role played by Saint-Venant.

For the case of rectangular Cartesian coordinates, we can write the Navier-Stokes equation in component form:

$$\rho\left(\frac{\partial\vartheta_x}{\partial t} + \vartheta_x\frac{\partial\vartheta_x}{\partial x} + \vartheta_y\frac{\partial\vartheta_x}{\partial y} + \vartheta_z\frac{\partial\vartheta_x}{\partial z}\right) = -\frac{\partial P}{\partial x} + \rho g_x + \mu\left(\frac{\partial^2\vartheta_x}{\partial x^2} + \frac{\partial^2\vartheta_x}{\partial y^2} + \frac{\partial^2\vartheta_x}{\partial z^2}\right) \tag{9.67a}$$

$$\rho\left(\frac{\partial\vartheta_y}{\partial t} + \vartheta_x\frac{\partial\vartheta_y}{\partial x} + \vartheta_y\frac{\partial\vartheta_y}{\partial y} + \vartheta_z\frac{\partial\vartheta_y}{\partial z}\right) = -\frac{\partial P}{\partial y} + \rho g_y + \mu\left(\frac{\partial^2\vartheta_y}{\partial x^2} + \frac{\partial^2\vartheta_y}{\partial y^2} + \frac{\partial^2\vartheta_y}{\partial z^2}\right) \tag{9.67b}$$

$$\rho\left(\frac{\partial\vartheta_z}{\partial t} + \vartheta_x\frac{\partial\vartheta_z}{\partial x} + \vartheta_y\frac{\partial\vartheta_z}{\partial y} + \vartheta_z\frac{\partial\vartheta_z}{\partial z}\right) = -\frac{\partial P}{\partial z} + \rho g_z + \mu\left(\frac{\partial^2\vartheta_z}{\partial x^2} + \frac{\partial^2\vartheta_z}{\partial y^2} + \frac{\partial^2\vartheta_z}{\partial z^2}\right) \tag{9.67c}$$

In equation (9.67), there are four unknowns, P, ϑ_x, ϑ_y, and ϑ_z, and we need four equations by which we can solve for these unknowns. For this purpose, the continuity equation must be included along with equation (9.67). For the incompressible fluid model used in the development of equation (9.67), it follows that

$$\frac{D\rho}{Dt} = 0 \tag{9.68}$$

and the continuity equation, equation (9.47), reduces to

$$\nabla\cdot\vec{\vartheta} = 0 \tag{9.69}$$

In Cartesian coordinates, equation (9.69) becomes

$$\frac{\partial \vartheta_x}{\partial x}+\frac{\partial \vartheta_y}{\partial y}+\frac{\partial \vartheta_z}{\partial z}=0 \tag{9.70}$$

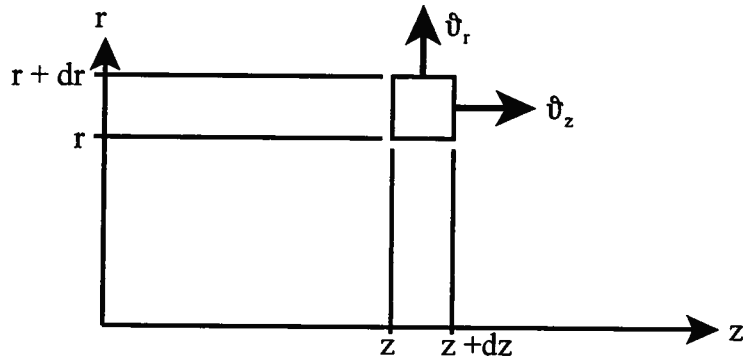

(a) r - z plane

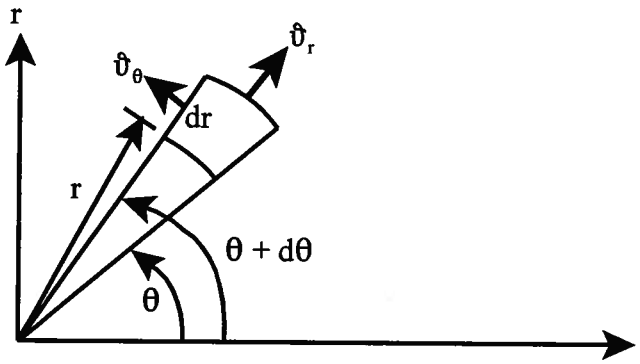

(b) r - θ plane (z-axis normal to plane of figure)

Figure 9.7 Differential Fluid Element in Cylindrical Coordinates

The geometry of many thermal-fluid devices such as pipes, tubes, and cylinders, is cylindrical. The study of the dynamics of fluid flow in these devices is most conveniently accomplished if the Navier-Stokes equation and the continuity equation are posed in cylindrical coordinates r, θ, z, and t. Figure 9.7 shows a differential fluid element in these cylindrical coordinates.

In cylindrical coordinates r, θ, z, and t the continuity equation for the incompressible fluid model is given by

$$\frac{1}{r}\frac{\partial}{\partial r}(r\vartheta_r)+\frac{1}{r}\frac{\partial}{\partial \theta}(\vartheta_\theta)+\frac{\partial}{\partial z}(\vartheta_z)=0 \tag{9.71}$$

The viscous stresses in this coordinate system are given by

$$\tau_{rr}=2\mu\frac{\partial \vartheta_r}{\partial r},\qquad \tau_{\theta\theta}=2\mu\left(\frac{1}{r}\frac{\partial \vartheta_\theta}{\partial \theta}+\frac{\vartheta_r}{r}\right),\qquad \tau_{zz}=2\mu\frac{\partial \vartheta_z}{\partial z}$$

$$\tau_{r\theta}=\tau_{\theta r}=\mu\left[r\frac{\partial}{\partial r}\left(\frac{\vartheta_\theta}{r}\right)+\frac{1}{r}\frac{\partial \vartheta_r}{\partial \theta}\right],\quad \tau_{\theta z}=\tau_{z\theta}=\mu\left(\frac{\partial \vartheta_\theta}{\partial z}+\frac{1}{r}\frac{\partial \vartheta_z}{\partial \theta}\right),\quad \tau_{zr}=\tau_{rz}=\mu\left(\frac{\partial \vartheta_r}{\partial z}+\frac{\partial \vartheta_z}{\partial r}\right) \tag{9.72}$$

The r-, θ-, and z-components of the Navier-Stokes equation in cylindrical coordinates for the incompressible fluid model with constant viscosity are given by, respectively

$$\rho\left(\frac{\partial \vartheta_r}{\partial t}+\vartheta_r\frac{\partial \vartheta_r}{\partial r}+\frac{\vartheta_\theta}{r}\frac{\partial \vartheta_r}{\partial \theta}-\frac{\vartheta_\theta^{\,2}}{r}+\vartheta_z\frac{\partial \vartheta_r}{\partial z}\right)$$
$$=-\frac{\partial P}{\partial r}+\rho g_r+\mu\left[\frac{\partial}{\partial r}\left(\frac{1}{r}\frac{\partial}{\partial r}(r\vartheta_r)\right)+\frac{1}{r^2}\frac{\partial^2 \vartheta_r}{\partial \theta^2}-\frac{2}{r^2}\frac{\partial \vartheta_\theta}{\partial \theta}+\frac{\partial^2 \vartheta_r}{\partial z^2}\right] \tag{9.73a}$$

$$\rho\left(\frac{\partial \vartheta_\theta}{\partial t}+\vartheta_r\frac{\partial \vartheta_\theta}{\partial r}+\frac{\vartheta_\theta}{r}\frac{\partial \vartheta_\theta}{\partial \theta}-\frac{\vartheta_r\vartheta_\theta}{r}+\vartheta_z\frac{\partial \vartheta_\theta}{\partial z}\right)$$
$$=-\frac{1}{r}\frac{\partial P}{\partial \theta}+\rho g_\theta+\mu\left[\frac{\partial}{\partial r}\left(\frac{1}{r}\frac{\partial}{\partial r}(r\vartheta_\theta)\right)+\frac{1}{r^2}\frac{\partial^2 \vartheta_\theta}{\partial \theta^2}-\frac{2}{r^2}\frac{\partial \vartheta_r}{\partial \theta}+\frac{\partial^2 \vartheta_\theta}{\partial z^2}\right] \tag{9.73b}$$

$$\rho\left(\frac{\partial \vartheta_z}{\partial t}+\vartheta_r\frac{\partial \vartheta_z}{\partial r}+\frac{\vartheta_\theta}{r}\frac{\partial \vartheta_z}{\partial \theta}-\frac{\vartheta_\theta^{\,2}}{r}+\vartheta_z\frac{\partial \vartheta_z}{\partial z}\right)$$
$$=-\frac{\partial P}{\partial z}+\rho g_z+\mu\left[\frac{1}{r}\frac{\partial}{\partial r}\left(r\frac{\partial \vartheta_z}{\partial r}\right)+\frac{1}{r^2}\frac{\partial^2 \vartheta_z}{\partial \theta^2}+\frac{\partial^2 \vartheta_z}{\partial z^2}\right] \tag{9.73c}$$

The Navier-Stokes equation is a non-linear, second-order, partial differential equation as is the Euler equation. Because of the non-linear nature of these equations inherent in the convective term on the left-hand side of equation (9.67) [and equation (9.57) as well] there are no general solutions. However, there are solutions of the Navier-Stokes equation in special cases commonly encountered in thermal-fluids engineering for which the non-linear terms vanish. These are known as fully-developed flows in which the viscous forces dominate and occur at low values of the Reynolds number, and we shall discuss several of the more important cases shortly.

Similarly, for flows in which viscous forces are not important, there are solutions of the Euler equation in special cases known as irrotational flows for which the average angular velocity of every fluid particle is zero. With this information, thermal-fluids engineers can determine the pressure distribution over bodies, such as aerodynamic shapes like aircraft wings and fuselages, immersed in the flow. In fact, this work forms a special subset of thermal-fluids engineering known as aerodynamics. Knowing the pressure distribution on these shapes, the aerodynamicist can then calculate the lift force acting on them. While this work is extremely important (particularly in the aircraft industry), it is outside the scope of the present treatment and we shall not consider it here. Rather, we shall focus our attention on the Navier-Stokes equation which will enable us to determine the drag force acting on these shapes. This information will enable us to design the propulsion plants required to power these vehicles.

The development of powerful, high-speed computers has facilitated the solution of both the Navier-Stokes equation and the Euler equation for more complex cases that are beyond our mathematical capabilities to obtain closed form analytical solutions. This has led to a relatively new subset of thermal-fluids engineering known as computational fluid dynamics. These are the techniques used, for example, to solve the Euler equation for an entire commercial aircraft flying at near sonic speed or to solve the Navier-Stokes equation for the flow field characteristics of a viscous fluid such as water flowing through a complex shape such as the impeller of a pump. Unfortunately, these numerical methods are also outside the scope of the present treatment and will not be considered here.

At this point in our development, what we can do is study those special cases for which

we can develop solutions to the Navier-Stokes equation. However, in order to do this, we need a set of boundary conditions. For the Newtonian fluid model, we have two. At the solid surface bounding the fluid (the wall), we have the no-slip boundary condition in which the fluid "sticks" to the wall so that the velocity of the fluid relative to the wall is zero. In addition, there is no flow through the wall. Then for a stationary wall with a fluid flowing in the x-direction, the boundary conditions become

$$\begin{aligned} \vartheta_x &= 0 \quad \text{(no slip boundary condition)} \\ \vartheta_y &= 0 \quad \text{(no flow through the wall boundary condition)} \end{aligned} \tag{9.74}$$

If the fluid is a liquid that forms a free surface as in the case of an open channel flow, for example, there is an additional boundary condition. Suppose for example that the fluid flowing is water and that it forms a free surface with the atmosphere. From Table 9.1, we note that the viscosity of water is

$$\mu_{water} \sim 10^{-3} \text{ kg/m sec}$$

and that of air is

$$\mu_{air} \sim 1.8 \text{ x } 10^{-5} \text{ kg/m sec}$$

Then

$$\frac{\mu_{water}}{\mu_{air}} \sim 50$$

Since the shear stress at the interface between the two fluids is the same, for one-dimensional flow we have

$$(\tau_{air})_{interface} = (\tau_{water})_{interface}$$

or

$$\mu_{air}\left(\frac{d\vartheta_x}{dy}\right)_{air} = \mu_{water}\left(\frac{d\vartheta_x}{dy}\right)_{water}$$

$$\left(\frac{d\vartheta_x}{dy}\right)_{water} = \frac{\mu_{air}}{\mu_{water}}\left(\frac{d\vartheta_x}{dy}\right)_{air} \sim \frac{1}{50}\left(\frac{d\vartheta_x}{dy}\right)_{air}$$

It follows, then, that if we assume the shear stress exerted on the water by the air at the free surface is small, the velocity gradient in the air is also small. Then the velocity gradient in the water is nearly an order of magnitude smaller. Thus we are justified in taking the velocity gradient in the liquid at the free surface to be vanishingly small, i.e., zero. Physically, this is equivalent to saying that the shear stress at the interface is zero. Then despite the fact that the liquid does actually "drag" some of the gas along as it moves, we model the free surface of the liquid as one on which there is no shear stress. The boundary condition at the free surface then becomes

$$\begin{aligned} \tau_{free\ surface} &= 0 \\ \left(\frac{d\vartheta_x}{dy}\right)_{free\ surface} &= 0 \end{aligned} \tag{9.75}$$

9.8 Reynolds Number

As we alluded to in Section 9.8, the solutions that we are about to develop for the Navier-Stokes equation are *mathematically valid* solutions for all values of the parameters involved;

however, experiment shows that these solutions are *physically valid* only for a certain range of these parameters. Outside this range of values, mathematically valid solutions become physically absurd because under certain conditions, the nature of the flow changes dramatically. In the mid-nineteenth century, when the Navier-Stokes equation was applied to flow in a pipe of circular cross-section, this equation predicted a linear relationship between the pressure drop in the flow and the average velocity of the fluid. Experiments showed that sometimes the linear relationship was valid, but at other times the pressure drop depended more nearly upon the square of the velocity as shown schematically (not actual data) in Figure 9.8.

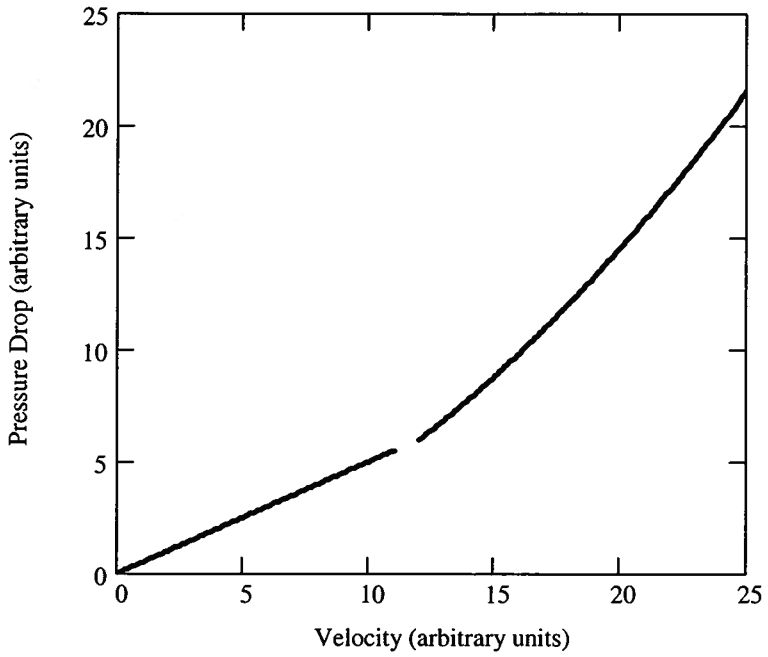

Figure 9.8 Pressure Drop in Pipe Flow (Break in plot indicates change in type of flow.)

It was not until 1883 when Osborne Reynolds (of Reynolds Transport Theorem fame) performed a series of very carefully controlled experiments involving the injection of dye into fluid flowing a circular tube that the underlying physics of this dilemma became apparent. Reynolds found that, indeed, two types of flow do exist: one at relatively low velocities in which the fluid particles slide smoothly past each other in a laminar fashion and produce a linear relationship between pressure drop and average fluid velocity; the other at somewhat higher velocities in which the fluid particles follow a sinuous path that eventually breaks down into a random or turbulent motion and produce a non-linear relationship between pressure drop and average fluid velocity. Reynolds showed that the transition from laminar to turbulent flow depended not just on the velocity, ϑ, of the fluid but on the parameter $\vartheta D\rho/\mu$ where D is the diameter of the circular tube. This dimensionless number is now named the Reynolds number in his honor and is usually designated by the symbol *Re*.

The Reynolds number serves to classify many types of flows, not just flow in a circular pipe, provided that the Reynolds number is properly defined in these other geometries. In general, small values of the Reynolds number imply that laminar flow conditions prevail while large values of the Reynolds number imply that turbulent flow prevails. There is usually a critical value of the Reynolds number at which the transition from laminar to turbulent flow occurs. The numerical value of the critical Reynolds number depends upon the flow geometry. For example, for flow in a circular conduit, the transition from laminar to turbulent occurs at a value of

Reynolds number of approximately 2300. In any given case, the value of the critical Reynolds number will vary somewhat since the transition is also influenced by outside disturbances such as background vibrations in the apparatus or the previous history of the turbulence in the fluid. Thus there is actually a range of values over which one might expect the transition to occur. For the purposes of designing thermal-fluid systems, there is a generally accepted value of the critical Reynolds number for each specific geometry.

Although the Reynolds number is a dimensionless number, it does have a "physical nature" to it. For example, the inertia forces associated with a given flow geometry can be determined from Newton's second law of motion, viz.

$$F_{inertia} = ma \tag{9.76}$$

and the mass m can be written

$$m = \rho V \tag{9.77}$$

where the volume, V, has the dimensions of a characteristic length, L, cubed, L^3. Then

$$m \propto L^3 \tag{9.78}$$

The acceleration can be written

$$a = \frac{d\vartheta}{dt} = \vartheta\frac{d\vartheta}{ds} \tag{9.79}$$

Then

$$a \propto \frac{\vartheta^2}{L} \tag{9.80}$$

Then the inertia force can be written

$$F_{inertia} \propto \left(\rho L^3\right)\left(\frac{\vartheta^2}{L}\right) = \rho\vartheta^2 L^2 \tag{9.81}$$

The viscous force can be written

$$F_{viscous} = \tau A = \mu\left(\frac{d\vartheta}{dy}\right)A \tag{9.82}$$

Then

$$F_{viscous} \propto \mu\left(\frac{\vartheta}{L}\right)L^2 = \mu\vartheta L \tag{9.83}$$

Then the ratio of inertia forces to viscous forces in a given flow geometry with a characteristic length L is given by

$$\frac{F_{inertia}}{F_{viscous}} \propto \frac{\rho\vartheta^2 L^2}{\mu\vartheta L} = \frac{\rho\vartheta L}{\mu} = Re \tag{9.84}$$

Since turbulent conditions prevail at large values of Re, it is apparent that turbulent flow is dominated by inertial forces. Since laminar conditions prevail at small values of Re, laminar flow is dominated by viscous forces.

The Reynolds number has utility not only for establishing the transition from laminar to turbulent flow but also for establishing the similarity between flows. This is known as the Principle of Dynamic Similarity and is the basis of all wind tunnel testing of models of aerodynamic shapes. Consider the case of flow of a uniform fluid stream parallel to the x-axis with velocity ϑ_∞ past a fixed obstacle of given shape, an aerodynamic shape for example, and given orientation whose size is specified by a typical length L. Then we introduce non-

dimensional variables according to the following scheme:

$$\vartheta_x^* = \frac{\vartheta_x}{\vartheta_\infty}, \qquad \vartheta_y^* = \frac{\vartheta_y}{\vartheta_\infty}, \qquad \vartheta_z^* = \frac{\vartheta_z}{\vartheta_\infty}, \qquad P^* = \frac{P}{\rho \vartheta_\infty^{\,2}}$$
$$x^* = \frac{x}{L}, \qquad y^* = \frac{y}{L}, \qquad z^* = \frac{z}{L}, \qquad t^* = \frac{\vartheta_\infty t}{L} \tag{9.85}$$

Then in terms of these new dimensionless variables, the continuity equation for the incompressible fluid model, equation (9.70), becomes

$$\frac{\partial \vartheta_x^*}{\partial x^*} + \frac{\partial \vartheta_y^*}{\partial y^*} + \frac{\partial \vartheta_z^*}{\partial z^*} = 0 \tag{9.86}$$

and the Navier-Stokes equation, equation (9.69), becomes

$$\frac{\partial \vartheta_x^*}{\partial t^*} + \vartheta_x^* \frac{\partial \vartheta_x^*}{\partial x^*} + \vartheta_y^* \frac{\partial \vartheta_x^*}{\partial y^*} + \vartheta_z^* \frac{\partial \vartheta_x^*}{\partial z^*} = -\frac{\partial P^*}{\partial x^*} + \frac{\mu}{\vartheta_\infty L \rho}\left(\frac{\partial^2 \vartheta_x^*}{\partial x^{*2}} + \frac{\partial^2 \vartheta_x^*}{\partial y^{*2}} + \frac{\partial^2 \vartheta_x^*}{\partial z^{*2}}\right) \tag{9.87a}$$

$$\frac{\partial \vartheta_y^*}{\partial t^*} + \vartheta_x^* \frac{\partial \vartheta_y^*}{\partial x^*} + \vartheta_y^* \frac{\partial \vartheta_y^*}{\partial y^*} + \vartheta_z^* \frac{\partial \vartheta_y^*}{\partial z^*} = -\frac{\partial P^*}{\partial y^*} + \frac{\mu}{\vartheta_\infty L \rho}\left(\frac{\partial^2 \vartheta_y^*}{\partial x^{*2}} + \frac{\partial^2 \vartheta_y^*}{\partial y^{*2}} + \frac{\partial^2 \vartheta_y^*}{\partial z^{*2}}\right) \tag{9.87b}$$

$$\frac{\partial \vartheta_z^*}{\partial t^*} + \vartheta_x^* \frac{\partial \vartheta_z^*}{\partial x^*} + \vartheta_y^* \frac{\partial \vartheta_z^*}{\partial y^*} + \vartheta_z^* \frac{\partial \vartheta_z^*}{\partial z^*} = -\frac{\partial P^*}{\partial z^*} + \frac{\mu}{\vartheta_\infty L \rho}\left(\frac{\partial^2 \vartheta_z^*}{\partial x^{*2}} + \frac{\partial^2 \vartheta_z^*}{\partial y^{*2}} + \frac{\partial^2 \vartheta_z^*}{\partial z^{*2}}\right) \tag{9.87c}$$

Notice that the coefficient of the viscous force term, the last term on the right-hand side of equation (9.87), is the inverse of the Reynolds number, $1/Re = \mu/\vartheta_\infty L\rho$. The boundary conditions for the Navier-Stokes equation for this flow configuration are:
At infinity:

$$\vartheta_x = U, \qquad \vartheta_y = 0, \qquad \vartheta_z = 0 \tag{9.88}$$

and at the boundary of the solid obstacle:

$$\vartheta_x = \vartheta_y = \vartheta_z = 0 \tag{9.89}$$

Then for the dimensionless Navier-Stokes equation, equation (9.87), the dimensionless boundary conditions equivalent to equations (9.88) and (9.89) are:

$$\vartheta_x^* = 1, \qquad \vartheta_y^* = 0, \qquad \vartheta_z^* = 0$$
$$\vartheta_x^* = \vartheta_y^* = \vartheta_z^* = 0 \tag{9.90}$$

Thus the solution to equation (9.87) subject to the boundary conditions (9.90) determine ϑ_x^*, ϑ_y^*, ϑ_z^*, and P^*. Then for fluids of different densities and viscosities, for streams of different speeds, and obstacles of different sizes, ϑ_x^*, ϑ_y^*, ϑ_z^*, and P^* will be the same so long as the value of Re is the same. The same is true for any stress component divided by $\rho\vartheta_\infty^{\,2}$. Thus the same value of the Reynolds number insures that the flows will be dynamically similar. Thus a model of an aircraft wing could be tested in a water or wind tunnel at the same Reynolds number that corresponds to actual flight conditions on the full size wing, and the dimensionless values of the lift and drag forces measured on the model would be the same as those on the actual wing. We also infer from this solution to the dimensionless Navier-Stokes equation that in an internal flow, such as we might find in a circular pipe, the pressure gradient in the direction of flow is a function of the value of Re only, or

$$\frac{\partial P^*}{\partial x^*} = f(Re) \tag{9.91}$$

We will make use of this observation later. In fact, in Chapter 10, we will study the process of dimensional analysis in considerable detail since it is a very powerful tool in the analytical and experimental study of thermal-fluid systems. We have included this brief discussion of the Reynolds number at this juncture because it is so intimately connected to the Navier-Stokes equation.

9.9 Laminar Flow

We now examine some classical flow geometries at relatively small values of the Reynolds number (but $Re >> 1$) in which the flow can be classified as laminar. We are motivated by several reasons for doing this: (1) We want to learn how to develop solutions to the Navier-Stokes equation; (2) we want to know what the solutions to the Navier-Stokes equations tell us beyond the obvious velocity distribution in the fluid; (3) we want to try to understand the limitations of the solutions that we do develop, i.e., we want to know what are the other things about the flow that the Navier-Stokes equation cannot tell us; and (4) we want to develop solutions to the Navier-Stokes equation for some common geometries that will be useful to us in the design of thermal-fluid systems.

Example 9E.2: Consider the flow geometry shown in Figure 9E.2 in which a viscous liquid flows steadily down an inclined infinite plane in a uniform film of thickness h. The plane is inclined at an angle θ to the horizontal and the free surface of the liquid is in contact with the atmosphere. The flow is fully developed.

(a) Determine the distribution of pressure, $P(y)$, in the film.

(b) Determine the velocity distribution of the liquid in the film, $\vec{v}_x(y)$.

(c) Determine the shear stress τ_{yx} acting on the surface of the plane.

(d) Determine the volumetric flow rate of liquid in the film, $\dot{V}$.

(e) Determine the average velocity, $\vec{v}_{ave}$, of the liquid in the film.

(f) Determine the steady-state film thickness, h, in terms of the volumetric flow rate, $\dot{V}$, the width of the plate, b, the viscosity of the fluid, μ, and the angle θ.

(g) Determine the rate of entropy generation for a plate of length L.

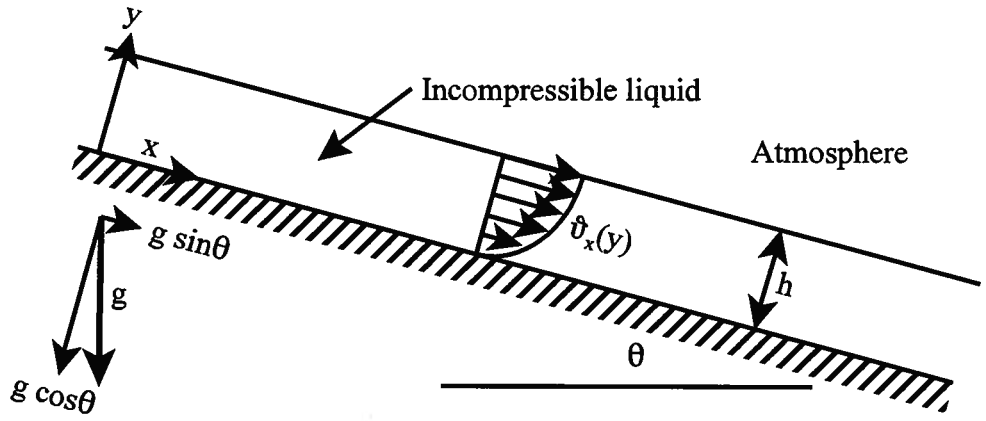

Figure 9E.1 Flow of an Incompressible Fluid Down an Inclined Plane

Solution: (a) The first step in applying the Navier-Stokes equation to a given physical situation is to select the appropriate coordinate system and write down the equation in component form for that geometry. For the case at hand, the rectangular Cartesian coordinate system is the

appropriate coordinate system so we should be working with the Navier-Stokes equation in the form of equation (9.67) and the continuity equation in the form of equation (9.70). For this case the flow is independent of the z-direction, and the flow looks exactly the same at every position along the z-axis. Hence, all derivatives in the z-direction vanish, $\partial/\partial z = 0$. Then since we are working just in x and y coordinate directions, we do not need equation (9.67c) and terms with z-components in them vanish. Since we are looking for the steady flow solution, all the time dependent terms vanish. The fact that the flow is fully developed means that the solution should depend only upon the y-coordinate and not the x-coordinate. That is all properties remain the same regardless the value of x. Then $\partial/\partial x = 0$. In particular,

$$\frac{\partial \vartheta_x}{\partial x} = 0 \quad \text{and} \quad \frac{\partial \vartheta_x}{\partial z} = 0$$

Then

$$\vartheta_x = f(y)$$

and the continuity equation, equation (9.70) reduces to

$$\cancel{\frac{\partial \vartheta_x}{\partial x}} + \frac{\partial \vartheta_y}{\partial y} = 0$$

Then

$$\vartheta_y = f(x, z)$$

but we have already shown that the flow is independent of the x- and z-directions. Then it must be the case that

$$\vartheta_y = \text{constant}$$

From the boundary conditions (9.74), it is apparent that $(\vartheta_y)_{wall} = 0$. Then since ϑ_y = constant, it must be the case that $\vartheta_y = 0$ everywhere. Then equation (9.67b) becomes

$$\rho\left(\cancel{\frac{\partial \vartheta_y}{\partial t}} + \vartheta_x \cancel{\frac{\partial \vartheta_y}{\partial x}} + \cancel{\vartheta_y \frac{\partial \vartheta_y}{\partial y}} + \cancel{\vartheta_z \frac{\partial \vartheta_y}{\partial z}}\right) = -\frac{\partial P}{\partial y} + \rho g_y + \mu\left(\cancel{\frac{\partial^2 \vartheta_y}{\partial x^2}} + \cancel{\frac{\partial^2 \vartheta_y}{\partial y^2}} + \cancel{\frac{\partial^2 \vartheta_y}{\partial z^2}}\right)$$

or

$$\frac{\partial P}{\partial y} = \rho g_y$$

$$\frac{\partial P}{\partial y} = -\rho g \cos\theta$$

Integrating, we get

$$P = -\rho g y \cos\theta + f(x, z)$$

The boundary condition on the pressure is that $P = P_{atm}$ at $y = h$ and is independent of x and z. Then

$$f(x,z) = P_{atm} + \rho g h \cos\theta$$

and the integral becomes

$$P = P_{atm} + (\rho g \cos\theta)(h - y)$$

Physically, this equation says that the pressure distribution across the thickness of the liquid film is the hydrostatic pressure distribution.

(b) Then it follows that

$$\frac{\partial P}{\partial x} = 0$$

Then equation (9.67a) becomes

$$\rho\left(\cancel{\frac{\partial \vartheta_x}{\partial t}} + \vartheta_x \cancel{\frac{\partial \vartheta_x}{\partial x}} + \cancel{\vartheta_y} \frac{\partial \vartheta_x}{\partial y} + \cancel{\vartheta_z} \cancel{\frac{\partial \vartheta_x}{\partial z}}\right) = -\cancel{\frac{\partial P}{\partial x}} + \rho g_x + \mu\left(\cancel{\frac{\partial^2 \vartheta_x}{\partial x^2}} + \frac{\partial^2 \vartheta_x}{\partial y^2} + \cancel{\frac{\partial^2 \vartheta_x}{\partial z^2}}\right)$$

$$0 = \rho g_x + \mu \frac{\partial^2 \vartheta_x}{\partial y^2}$$

Physically, this equation says that the body force per unit volume due to gravity acting on every fluid particle in the liquid film is exactly balanced by the viscous force which acts on the fluid "stuck" to the plane.

As we have already shown, $\vartheta_x = f(y)$. Then above partial derivative becomes an ordinary derivative. Integrating the x-component of the Navier-Stokes equation, we get

$$\frac{d^2 \vartheta_x}{dy^2} = -\frac{\rho g_x}{\mu} = -\rho g \frac{\sin\theta}{\mu}$$

$$\frac{d \vartheta_x}{dy} = -\rho g \frac{\sin\theta}{\mu} y + C_1$$

$$\vartheta_x = -\rho g \frac{\sin\theta}{\mu} \frac{y^2}{2} + C_1 y + C_2$$

with boundary conditions (9.74) and (9.75)

$$(1) \quad \vartheta_x = 0 \qquad \text{at} \quad y = 0$$

$$(2) \quad \frac{d \vartheta_x}{dy} = 0 \qquad \text{at} \quad y = h$$

From the first boundary condition, it follows that $C_2 = 0$. From the second boundary condition, which says that there is no shear stress in the liquid at the liquid-atmosphere interface, we have

$$C_1 = \rho g \frac{\sin\theta}{\mu} h$$

Then the solution of the Navier-Stokes equation for the velocity distribution is

$$\vartheta_x = -\rho g \frac{\sin\theta}{\mu} \frac{y^2}{2} + \rho g \frac{\sin\theta}{\mu} hy$$

$$\vartheta_x = \rho g \frac{\sin\theta}{\mu}\left(hy - \frac{y^2}{2}\right)$$

(c) Then the shear stress acting on any plane in the fluid is given by the first of equations (9.58), viz.

$$\tau_{xy} = \tau_{yx} = \mu\left(\frac{\partial \vartheta_x}{\partial y} + \frac{\partial \vartheta_y}{\partial x}\right)$$

but since we have shown above that $\frac{\partial \vartheta_y}{\partial x} = 0$, the expression for the shear stress becomes

$$\tau_{yx} = \mu \frac{d \vartheta_x}{dy} = (\rho g \sin\theta)(h - y)$$

On the surface of the inclined plate, $y = 0$. Then

$$\left(\tau_{yx}\right)_{\substack{surface \\ of\ plate}} = \rho g h \sin\theta$$

This shear stress is just the x-component of the hydrostatic pressure and acts in the positive x-direction. The force required to hold the plane stationary acts in the negative x-direction and is given by

$$F_{plane} = -\tau_{yx} A = -\rho g h b L \sin\theta$$

where b is the width of the plane normal to the plane of Figure 9E.2 and L is the length of the plane. Notice that the shear force per unit volume of film is exactly equal to the body force acting on that unit volume.

(d) The volumetric flow rate is given by

$$\dot{V} = \int_0^h \vartheta_x b dy = \int_0^h \rho g \frac{\sin\theta}{\mu}\left(hy - \frac{y^2}{2}\right) b dy = \frac{\rho g \sin\theta}{\mu}\frac{bh^3}{3}$$

Clearly, more viscous fluids require thicker films to flow a given volumetric flow rate.

(e) Then the average velocity is given by

$$\vartheta_{ave} = \frac{\dot{V}}{bh} = \frac{\rho g \sin\theta}{\mu}\frac{h^2}{3}$$

(f) The film thickness can be determined from the volumetric flow rate. Thus,

$$h = \left[\frac{3\mu\dot{V}}{\rho g b \sin\theta}\right]^{\frac{1}{3}}$$

Notice that for a film of given thickness, the volumetric flow rate decreases directly as the viscosity of the fluid increases.

(g) The rate of entropy generation is determined from the second law. For an adiabatic, steady-flow film of length L, the second law reduces to

$$\dot{S}_{gen} = \dot{m} c \ln\frac{T_{out}}{T_{in}}$$

where T_{out} is the temperature of the liquid leaving the film and T_{in} is the temperature of the liquid entering the film. These temperatures are determined from the application of the first law to the control volume. Since the pressure over the inlet port is identical to the pressure over the outlet port, the first law for this adiabatic, steady-flow situation reduces to

$$u_{out} - u_{in} = g\left(z_{in} - z_{out}\right) = c\left(T_{out} - T_{in}\right)$$

$$T_{out} = T_{in} + \frac{gL\sin\theta}{c}$$

Since

$$\dot{m} = \rho A \vartheta_{ave} = \rho b h\left(\frac{\rho g \sin\theta}{\mu}\frac{h^2}{3}\right) = \rho\dot{V}$$

the rate of entropy generation for a liquid film of length L, thickness h, and width b is

$$\dot{S}_{gen} = \frac{\rho^2 b h^3 g c \sin\theta}{3\mu}\ln\left(1 + \frac{gL\sin\theta}{cT_{in}}\right) = \rho c\dot{V}\ln\left(1 + \frac{gL\sin\theta}{cT_{in}}\right)$$

Notice that the rate of entropy generation depends only upon the geometry of the film and appears to be independent of the viscosity of the fluid. This is somewhat misleading because in this gravity driven flow, the volumetric flow rate is determined by the viscosity of the fluid and the film thickness.

In developing a solution of the Navier-Stokes equation for this case, the beginning student might be a bit confused about the elimination of certain terms from the component differential equations. In particular, one might reason that we know from our experience in Chapter 8 that a pressure gradient is usually required in the direction of flow of a viscous fluid in order to overcome the effects of viscous dissipation. If that were the case, the x-component of the Navier-Stokes equation would then appear as

$$-\frac{\partial P}{\partial x}+\mu\frac{d^2\vartheta_x}{dy^2}+\rho g_x=0$$

and the y-component would be unchanged from that given above. Then the solution for the velocity distribution would become

$$\vartheta_x=\left(\rho\frac{g\sin\theta}{\mu}-\frac{1}{\mu}\frac{\partial P}{\partial x}\right)\left(hy-\frac{y^2}{2}\right)$$

Since the y-component of the Navier-Stokes equation would be unchanged from that given above, the solution for the pressure distribution given in part (f) above would still be valid. Then the pressure gradient in the direction of flow would be given by

$$\frac{\partial P}{\partial x}=(\rho g\cos\theta)\frac{\partial h}{\partial x}$$

but for the film to be truly fully-developed, the film thickness must be constant in the direction of flow and $\partial h/\partial x = 0$. Then for this case, the pressure gradient in the x-direction must be zero and the x-component of the Navier-Stokes equation is indeed that shown in part (b) above.

Although this solution of the Navier-Stokes equation enables us to characterize this gravity driven, viscosity limited flow completely, there are many things the solution does not tell us. For example, this solution is based upon a simplification of the Navier-Stokes equation that contains only the viscous stresses associated with laminar flow. Therefore, the solution does not tell us when the film will undergo a transition from laminar to turbulent flow which involves the motion of fluid eddies in the flow. As we shall see, the Navier-Stokes equation is capable of describing turbulent flow, but the equation takes on a slightly different form in that case. If the present flow becomes turbulent, the above solution becomes invalid since it assumes that the flow is dominated by viscous forces with no consideration for the inertial forces that are important in turbulent flow. Also, this solution does not tell us the distance the film must travel down the plate before fully-developed flow is established. To determine this length, we would need to solve the Navier-Stokes equation with the non-linear convective terms included. In addition, as anyone who has ever tried to paint a vertical surface has noticed, if too much paint is applied at one time, a film of viscous fluid (albeit a non-Newtonian one), in this case paint, flows down the surface. In a relatively short distance, the advancing front of the paint film breaks up and forms finger-like projections or streaks that painters call "runs". The length of film required for this phenomenon to happen in a Newtonian fluid is not contained in the above solution of the Navier-Stokes equation. It would be necessary for us to do a stability analysis on the advancing film front to determine this distance. The point we are trying to make here is that in any physical situation, the solution of the Navier-Stokes equation can provide us with a lot of information, but that information has its limits in scope and validity. We should not just assume that the solution provides us with a complete picture of the situation.

Example 9E.3: A geometry commonly found in thermal-fluid systems is that of two concentric cylinders, one of which rotates while the other remains stationary: for example, a shaft

rotating in a journal bearing or a fluid viscometer used to measure the viscosity of a fluid. The laminar flow of a liquid in the space between coaxial cylinders is known as *Couette flow* in honor of Maurice Frédéric Alfred Couette, Professor of Physics at the end of the 19th Century at the French provincial university of Angers. Couette published his analysis of this flow geometry and his design of the viscometer in 1890.

There are two possible configurations of this geometry: (1) the inner shaft rotates while the outer cylinder remains stationary; and (2) the outer cylinder rotates while the inner one remains stationary. In either case, the "no-slip" boundary condition causes the fluid "stuck" to the rotating cylinder to be "dragged" along with it while at the same time this boundary condition causes the fluid "stuck" to the stationary cylinder to remain fixed in space. The resulting fluid shear produces a velocity gradient in the fluid and causes the rotating cylinder to exert a torque on the stationary cylinder. In the first configuration, the flow is stable only up to a certain condition whereas in the second configuration, the flow between cylinders has been shown, both theoretically and experimentally, to be inherently stable.

Consider the inherently stable case as shown in Figure 9E.3a. The inner cylinder of radius R_1 is stationary and the outer cylinder of radius R_2 rotates with steady angular velocity ω. The two cylinders are considered long compared to the gap between them which is filled with an incompressible fluid that can be modeled as a Newtonian fluid.

We wish to make the following determinations about the flow field in the gap:

(a) Determine the velocity distribution $\hat{v}_\theta(r)$ in the fluid in the gap.

(b) Determine the torque exerted on the inner cylinder by fluid shear in the gap between the two cylinders.

(c) For a sufficiently small gap, $R_2 - R_1$, this geometry can be modeled as a simple planar shear flow of the type described in Section 9.2 in which the lower plane is stationary and the upper plane moves with velocity $\hat{v}_0 = R_2\omega$. If we take as the limiting criterion the requirement that the shear stress on the stationary plane as predicted by the planar model is within one percent of the shear stress predicted by the concentric cylinder model, what are the conditions for which the planar model is a valid representation of the concentric cylinder geometry?

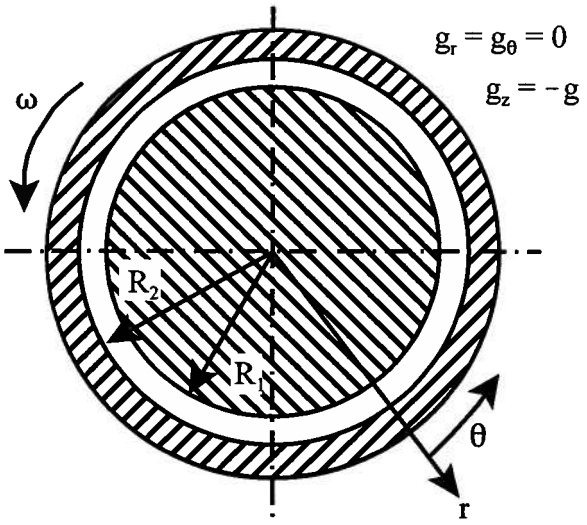

z-axis normal to plane of figure

Figure 9E.3a Rotating Concentric Cylinders

Solution: (a) Since the angular velocity ω is constant, we can model this as a steady flow situation of an incompressible fluid. Then $\partial/\partial t = 0$. For this geometry, there is no flow in the z-direction and there are no variations in any of the flow properties in that direction, i.e., $\partial/\partial z = 0$. The z-component of the Navier-Stokes equation vanishes completely. In addition, the flow is circumferentially symmetric so there is no θ dependence and $\partial/\partial\theta = 0$. Then we are seeking a solution for which ϑ_θ does not depend upon θ. In cylindrical coordinates the continuity equation, equation (9.71), becomes

$$\frac{1}{r}\frac{\partial}{\partial r}(r\vartheta_r)+\frac{1}{r}\frac{\partial}{\partial\theta}(\vartheta_\theta)+\frac{\partial}{\partial z}(\vartheta_z)=0$$

It follows then that

$$r\vartheta_r = \text{constant}$$

Since $\vartheta_r = 0$ at the solid surface of each cylinder, the continuity equation requires that $\vartheta_r = 0$ everywhere. Then the Navier-Stokes equation, equation (9.73a), becomes

$$\rho\left(\frac{\partial\vartheta_r}{\partial t}+\vartheta_r\frac{\partial\vartheta_r}{\partial r}+\frac{\vartheta_\theta}{r}\frac{\partial\vartheta_r}{\partial\theta}-\frac{\vartheta_\theta^{\,2}}{r}+\vartheta_z\frac{\partial\vartheta_r}{\partial z}\right)$$

$$=-\frac{\partial P}{\partial r}+\rho g_r+\mu\left[\frac{\partial}{\partial r}\left(\frac{1}{r}\frac{\partial}{\partial r}(r\vartheta_r)\right)+\frac{1}{r^2}\frac{\partial^2\vartheta_r}{\partial\theta^2}-\frac{2}{r^2}\frac{\partial\vartheta_\theta}{\partial\theta}+\frac{\partial^2\vartheta_r}{\partial z^2}\right]$$

$$-\rho\frac{\vartheta_\theta^{\,2}}{r}=-\frac{\partial P}{\partial r}$$

and the Navier-Stokes equation, equation (9.73b), becomes

$$\rho\left(\frac{\partial\vartheta_\theta}{\partial t}+\vartheta_r\frac{\partial\vartheta_\theta}{\partial r}+\frac{\vartheta_\theta}{r}\frac{\partial\vartheta_\theta}{\partial\theta}-\frac{\vartheta_r\vartheta_\theta}{r}+\vartheta_z\frac{\partial\vartheta_\theta}{\partial z}\right)$$

$$=-\frac{1}{r}\frac{\partial P}{\partial\theta}+\rho g_\theta+\mu\left[\frac{\partial}{\partial r}\left(\frac{1}{r}\frac{\partial}{\partial r}(r\vartheta_\theta)\right)+\frac{1}{r^2}\frac{\partial^2\vartheta_\theta}{\partial\theta^2}-\frac{2}{r^2}\frac{\partial\vartheta_r}{\partial\theta}+\frac{\partial^2\vartheta_\theta}{\partial z^2}\right]$$

or

$$\frac{1}{r}\frac{\partial P}{\partial\theta}=\mu\left[\frac{\partial}{\partial r}\left(\frac{1}{r}\frac{\partial}{\partial r}(r\vartheta_\theta)\right)\right]$$

The question is what to do with the pressure term on the left-hand side of this expression. If we are seeking a solution for which ϑ_θ does not depend upon θ, the right-hand side of this expression is then independent of θ. Then the expression is equivalent to

$$\frac{dP}{d\theta} = \text{constant}$$

If we integrate this, we get

$$P = a\theta + b$$

but symmetry requires that $P(\theta = 0) = P(\theta = 2\pi)$ which is impossible for this functional form. Then it follows that P cannot depend upon θ and

$$\frac{\partial P}{\partial\theta}=0$$

Then the θ-component of the Navier-Stokes equation becomes

$$\frac{d}{dr}\left[\frac{1}{r}\frac{d}{dr}(r\vartheta_\theta)\right]=0$$

Integrate once to get

$$\frac{1}{r}\frac{d}{dr}(r\vartheta_\theta)=C_1$$

$$\frac{d}{dr}(r\vartheta_\theta)=C_1 r$$

Integrate a second time to get

$$r\vartheta_\theta=C_1\frac{r^2}{2}+C_2$$

$$\vartheta_\theta=C_1\frac{r}{2}+C_2\frac{1}{r}$$

with boundary conditions

(1) $\vartheta_\theta=\omega R_2$ at $r=R_2$

(2) $\vartheta_\theta=0$ at $r=R_1$

Substituting the two boundary conditions into the expression for ϑ_θ, we get

$$\omega R_2=C_1\frac{R_2}{2}+C_2\frac{1}{R_2}$$

$$0=C_1\frac{R_1}{2}+C_2\frac{1}{R_1}$$

Solving these two equations simultaneously, we get

$$C_1=\frac{2\omega}{1-\left(\frac{R_1}{R_2}\right)^2} \quad \text{and} \quad C_2=\frac{-\omega R_1^{\,2}}{1-\left(\frac{R_1}{R_2}\right)^2}$$

Substituting the expressions for the constants of integration into the expression for ϑ_θ, we get

$$\vartheta_\theta=\frac{\omega r}{1-\left(\frac{R_1}{R_2}\right)^2}-\frac{\omega\frac{R_1^{\,2}}{r}}{1-\left(\frac{R_1}{R_2}\right)^2}=\frac{\omega R_1}{1-\left(\frac{R_1}{R_2}\right)^2}\left[\frac{r}{R_1}-\frac{R_1}{r}\right]$$

(b) To determine the torque exerted on the inner cylinder, we first calculate the shear stress on that cylinder due to the viscous shear in the fluid. From equation (9.72)

$$\tau_{r\theta}=\mu r\frac{d}{dr}\left(\frac{\vartheta_\theta}{r}\right)=\mu r\frac{d}{dr}\left\{\frac{\omega R_1}{1-\left(\frac{R_1}{R_2}\right)^2}\left[\frac{1}{R_1}-\frac{R_1}{r^2}\right]\right\}=\mu\frac{2\omega}{1-\left(\frac{R_1}{R_2}\right)^2}\frac{R_1^{\,2}}{r^2}$$

At $r=R_1$,

$$\tau_{r=R_1}=\mu\frac{2\omega}{1-\left(\frac{R_1}{R_2}\right)^2}$$

If $\mathcal{T}$ is the torque on the inner cylinder, we have for a cylinder of length L

$$\mathcal{T} = \tau_{r=R_1} A = 2\pi R_1 L \mu \frac{2\omega}{1-\left(\frac{R_1}{R_2}\right)^2}$$

where we have neglected any "end effects" due to flow around the end of the cylinder. Thus, we can use this geometry to determine the viscosity of a fluid simply by measuring the geometry of the apparatus, the angular speed of the outer cylinder, and the torque exerted on the inner cylinder. This torque is typically determined by suspending the inner cylinder from a torsional element like a slender rod (or even a wire for low viscosity fluids) and measuring the twist in the element, usually by means of an optical arrangement employing a laser light source and a mirror attached to the torsional element. One simply measures the displacement of the laser light beam as the mirror is rotated by the torque on the inner cylinder and, hence, the torsional element. Knowing the length between the fixed end of the torsional element and the position of the laser light beam, we can determine the angular displacement of the mirror relative to the fixed end of the torsional element. Simple torsion theory then yields the torque on the element and, hence, the cylinder.

(c) Suppose that we now model the flow in the gap as though it were a planar gap; i.e., we neglect the radius of curvature of the cylinders and treat the flow as shown in Figure 9E.2b. This configuration is known as plane Couette flow and commonly occurs in engineering practice. The question is: "Under what conditions is this a good model of circular Couette flow?"

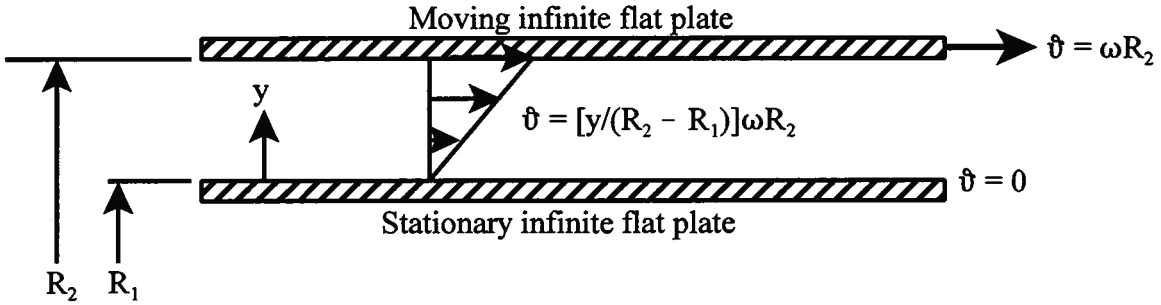

Figure 9E.3b Planar Shear Flow

Consider the shear stress acting on the lower plate.

$$\tau_{planar} = \mu \frac{d\vartheta}{dy} = \mu \frac{\omega R_2}{R_2 - R_1} = \mu \frac{\omega}{1-\frac{R_1}{R_2}}$$

If we had calculated this using the concentric cylinder model, we would have

$$\tau_{r=R_1} = \mu \frac{2\omega}{1-\left(\frac{R_1}{R_2}\right)^2} = \mu \frac{2\omega}{\left(1-\frac{R_1}{R_2}\right)\left(1+\frac{R_1}{R_2}\right)} = \mu \frac{\omega}{\left(1-\frac{R_1}{R_2}\right)} \frac{2}{\left(1+\frac{R_1}{R_2}\right)}$$

Then

$$\frac{\tau_{r=R_1}}{\tau_{planar}} = \frac{2}{\left(1+\frac{R_1}{R_2}\right)}$$

If we require the results of the two models to agree within one percent, we have

$$\frac{\tau_{r=R_1}}{\tau_{planar}} = \frac{2}{\left(1+\frac{R_1}{R_2}\right)} = 1.01$$

$$\frac{R_1}{R_2} = 0.98$$

Then if $R_2 - R_1 < 0.02R_2$, the planar model, which is much simpler to use, will give results with an error of less than one percent.

As we mentioned previously, the configuration that we just considered is inherently stable. However, if we considered the other possible configuration in which the outer cylinder is stationary and the inner cylinder is rotating, it is possible for the flow to become unstable. It is left as an exercise to show that the solution of the Navier-Stokes equation for the velocity distribution for this case is given by

$$v_\theta = \frac{\omega R_1^2}{1-\left(\frac{R_1}{R_2}\right)^2}\left[\frac{1}{r} - \frac{r}{R_2^2}\right]$$

The reason for the instability in this configuration is that the centrifugal force due to the rotation of the inner cylinder tends to drive the fluid toward the outer cylinder. This motion is resisted by a radial viscous force. For certain values of the geometrical and flow parameters, the flow becomes unstable to small disturbances. This instability was studied in great detail in 1923 by Sir Geoffrey I. Taylor (1886 - 1975), famous for his theory of turbulent flow and other fluid flow phenomena. For $R_2 - R_1 << R_1$, Taylor's analysis yielded a well-defined critical value of a dimensionless parameter, now called the "Taylor number" in his honor, at which the base flow becomes unstable to these small disturbances. The Taylor number, Ta, is the ratio of the destabilizing centrifugal force to the stabilizing radial viscous force and is given by

$$Ta = \frac{\rho^2 \omega^2 R_1 (R_2 - R_1)^3}{\mu^2}$$

At the value $Ta_{crit} = 1707.8$, the effect of the destabilizing centrifugal force outweighs the effect of the stabilizing radial viscous force and the instability occurs. The resultant toroidal "Taylor vortices", which are rectangular in cross-section and encircle the inner cylinder, are stacked in the axial direction as shown in Figure 9E.3c. Taylor conducted careful experiments that agreed with his theory within a few percent for a wide range of parameters, thus demonstrating that linear stability analyses can make quantitative predictions of patterns. Taylor's work in 1923 was the first to make a direct comparison between a laboratory experiment and a prediction for the formation of a pattern due to an instability.

It is worth noting at this point that because of the assumptions made at the outset of this analysis, we have a sense that the straightforward solution of the Navier-Stokes equation for this configuration is limited in its validity. However, as Taylor showed, if a small disturbance is introduced into this equation and a new solution obtained, a very different and complex character of the flow is revealed. Thus, the Navier-Stokes equation is very powerful in that it is capable of describing the flow of viscous fluids under wide ranging circumstances, but caution must be exercised in interpreting the applicability of the results. In some cases, one has to know in advance what one is looking for from the Navier-Stokes equation.

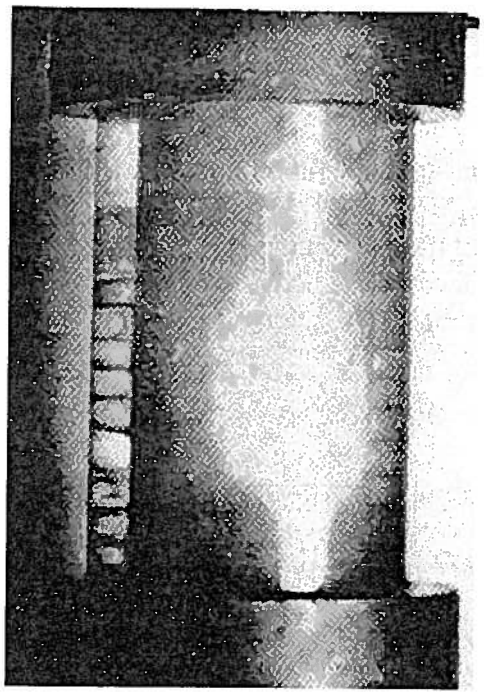

Figure 9E.3c Taylor Vortices Between Rotating Concentric Cylinders
(From *Laminar Boundary Layers*, edited by L. Rosenhead,
Oxford University Press, Oxford, 1963, p. 496f)

Example 9E.4: As shown in Figure 9E.4, a journal bearing for a crankshaft in an automobile engine has a shaft diameter of 75 mm and rides on a film of oil 0.05 mm thick. In a particular application of this bearing, the rotational speed of the crankshaft is 3000 rpm and the bearing is 60 mm long in the plane normal to Figure 9E.4. The viscous dissipation in the oil is accommodated by pumping oil through the gap at a mass flow rate, $\dot{m}_{oil}$, sufficient to produce a temperature increase in the oil of 100 C.

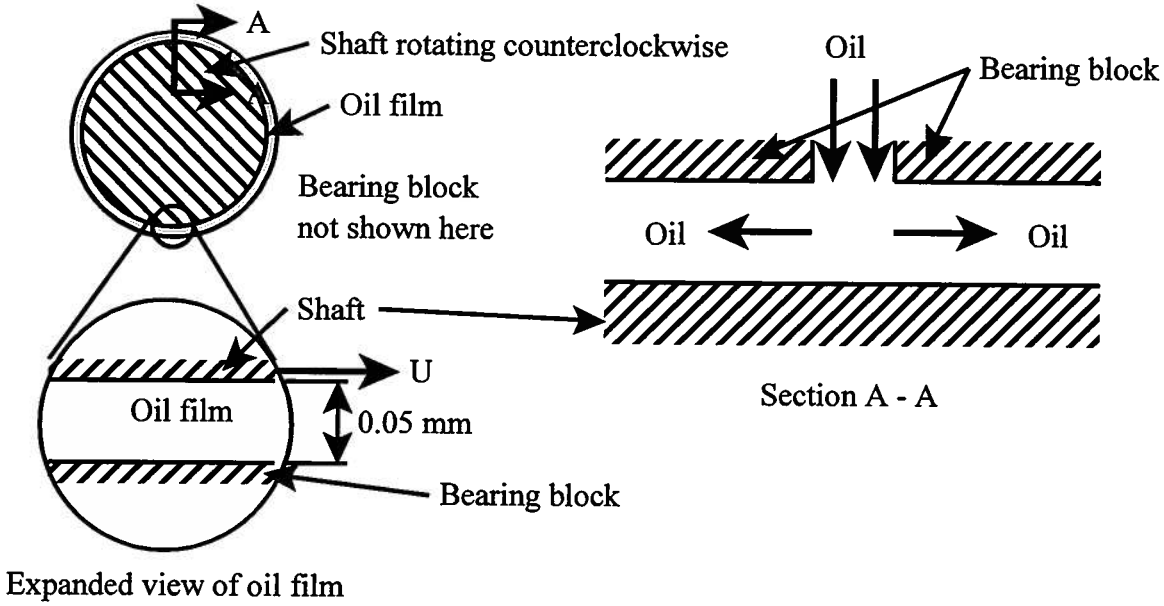

Figure 9E.4 Journal Bearing

The oil properties are as follows: ρ_{oil} = 854 kg/m^3, c_{oil} = 2120 J/kg K, μ_{oil} = 350 x 10^{-4} kg/m sec.

(a) What is the rate of shear work transfer in the bearing?

(b) What is the required mass flow rate of oil through the bearing if the solid surfaces can be modeled as adiabatic?

(c) What is the rate of entropy generation in the oil if the oil enters the bearing at 300 K?

Solution: (a) We saw in Example 9E.3 that if the oil gap is less than 2 percent of the radius of the shaft, we can model the flow in the gap as simple planar shear flow. In the case at hand, 0.02(75 mm) = 1.5 mm. Because the actual oil gap is only 0.05 mm, we can model this bearing as one flat plate moving relative to another. Then

$$\dot{W}_{shear} = -F_{shear}\vartheta_0 = -\tau_{r\theta}A_{surface}\vartheta_0 = -\mu\left(\frac{du}{dy}\right)2\pi RLU = -\mu\left(\frac{R\omega}{a}\right)2\pi RL\vartheta_0$$

$$\vartheta_0 = R\omega = (37.5 \text{ x } 10^{-3} \text{ m})\frac{(3000 \text{ rev/min})(2\pi \text{ radians/rev})}{(60 \text{ sec/min})} = 11.781 \text{ m/sec}$$

$$A_{surface} = 2\pi RL = 2\pi(37.5 \text{ x } 10^{-3} \text{ m})(60 \text{ x } 10^{-3} \text{ m}) = 1.4137 \text{ x } 10^{-2} \text{ m}^2$$

$$\dot{W}_{shear} = -(350 \text{ x } 10^{-4} \text{ kg/m sec})\left(\frac{11.781 \text{ m/sec}}{0.05 \text{ x } 10^{-3} \text{ m}}\right)(1.4137 \text{ x } 10^{-2} \text{ m}^2)(11.781 \text{ m/sec})$$

$$\dot{W}_{shear} = -1.3735 \text{ x } 10^3 \text{ W}$$

(b) For the adiabatic bearing with negligible kinetic and potential energy in the oil, the steady-flow form of the first law for the bearing reduces to

$$-\dot{W}_{shear} = \dot{m}_{oil}c_{oil}(T_{out} - T_{in})$$

$$\therefore \dot{m}_{oil} = \frac{-\dot{W}_{shear}}{c_{oil}(T_{out} - T_{in})} = \frac{1.3735 \text{ x } 10^2 \text{ W}}{(2120 \text{ J/kg K})(100 \text{ C})} = 6.4786 \text{ x } 10^{-3} \text{ kg/sec}$$

(c) Since there is no entropy transfer in an adiabatic bearing, the steady-flow form of the second law for the bearing reduces to

$$\dot{S}_{gen} = \dot{m}_{oil}(s_{out} - s_{in}) = \dot{m}_{oil}c_{oil}\ln\left(\frac{T_{out}}{T_{in}}\right)$$

$$\dot{S}_{gen} = (6.4786 \text{ x } 10^{-3} \text{ kg/sec})(2120 \text{ J/kg K})\ln\left(\frac{400 \text{ K}}{300 \text{ K}}\right) = 3.951 \text{ W/K}$$

This entropy generation is a result of the viscous dissipation in the oil. Ultimately entropy must be transferred at this rate from the oil to the environment in order for the oil situation to be modeled as steady-state. This is the reason that large engines are fitted with oil coolers. Smaller engines rely on simple heat transfer by natural convection from the various external engine surfaces to the environment to cool the oil.

We have just studied two classic examples of flow geometries that illustrate both the power and the limitations of the Navier-Stokes equation in describing the flow of a Newtonian fluid. In both cases we saw that the flow was laminar but could change character as the flow progressed. We also saw that these solutions have practical applications provided we understand the full implications of the solutions. We now wish to extend our study of laminar flows to other special flow geometries that are more commonly found in thermal-fluid systems.

9.9.1 Laminar Internal Flows

The study of laminar flows is naturally divided between "internal flows" and "external flows". Typically, in both of these types of flows, a uniform flow enters a region in which the flow field is bounded in some way by solid boundaries. In the case of internal flows, like the flow of water in a pipe, the solid boundaries completely contain the flow, whereas in external flows, like the flow of air around an aircraft, there are solid objects which are immersed in the flow in some way. In an internal flow, as the uniform flow comes into contact with the solid boundaries, the interaction (momentum transfer) between the fluid and the solid boundaries that define its extent is at first confined to a very small region. But as the flow develops, the effect of the boundaries diffuses into the flow until the influence of the solid boundaries is felt throughout the fluid flow. Thus, in a fully developed internal flow the effect of viscosity extends throughout the flow field. On the other hand, in an external flow, the situation at the outset is similar, but as the flow progresses, the influence of the boundaries is never truly felt throughout the flow field. Rather, the influence of the boundary is confined to a relatively small region known as the *boundary layer*. Inside the boundary layer, viscous effects dominate the behavior of the flow, but outside the boundary layer, the flow is not influenced by the viscosity of the fluid and the fluid can be modeled as though it were inviscid. Because of the simplicity of their solutions of the Navier-Stokes equation, we will first take up the study of laminar internal flows and then follow this with laminar external flows.

9.9.1.1 Laminar Fully-developed Planar Poiseuille Flow The simplest laminar internal flow of a Newtonian fluid is the simple shear flow between infinite parallel flat plates that we discussed in Section 9.2. For that geometry, the flow is actually generated by the viscous drag of the fluid on the moving top plate. The "no-slip" boundary condition of the Newtonian fluid model causes the fluid "stuck" to the top plate to move with the plate. The action of the viscosity of the fluid produces a velocity gradient in the fluid. However, if we now fix the position of both of the plates as shown in Figure 9.9 and we are trying to move a fluid through the space between

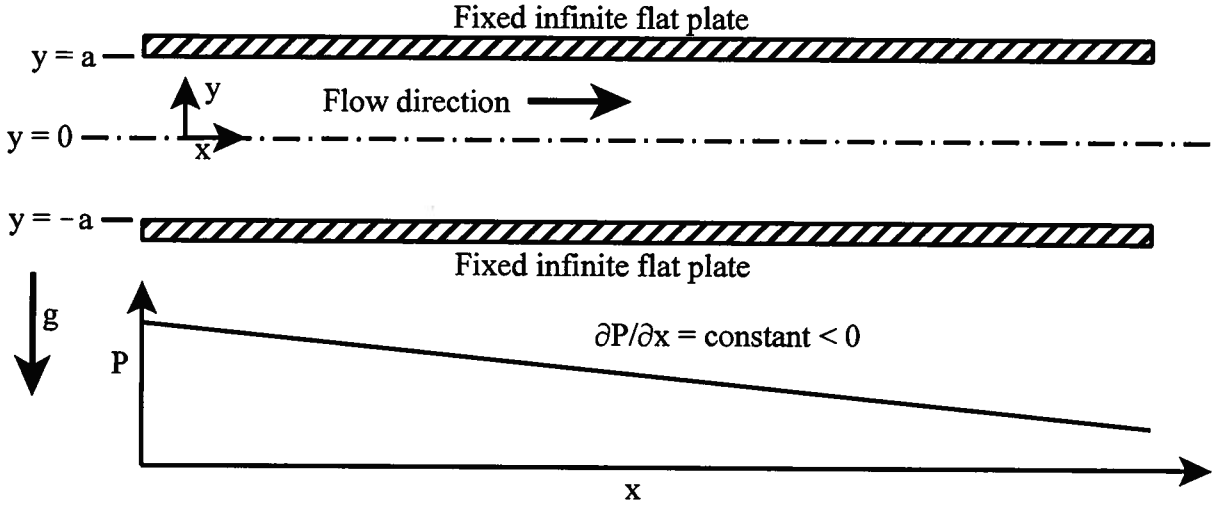

Figure 9.9 Fully-developed Plane Poiseuille Flow Between Fixed Infinite Parallel Flat Plates

them in a steady manner, the action of the viscosity of the fluid requires that we impose (by external means such as a pump) a pressure gradient in the direction of the flow in order to overcome the "viscous drag" of the plates on the fluid. This pressure gradient must be the same

at every position along the x-direction in order to keep the fluid flowing at the same average velocity at each position. This type of flow is known as fully-developed *plane Poiseuille flow* and is just one example of several laminar internal flows driven by a pressure gradient. This class of flows is usually known as "Poiseuille flow" in honor of Jean Marie Louis Poiseuille (1799-1869), a French physician who studied the flow of blood in capillaries. (The unit of viscosity in the cgs system is called the *poise* in his honor.)

Because the flow is fully developed, the flow is steady and the time dependent terms in the Navier-Stokes equation vanish. Also, the flow has the same character at every location along the x-axis, so $\partial/\partial x = 0$. Similarly, the flow is the same in all planes normal to the z-axis, so $\partial/\partial z = 0$. Then from the continuity equation, equation (9.70), we have

$$\cancel{\frac{\partial v_x}{\partial x}} + \frac{\partial v_y}{\partial y} + \cancel{\frac{\partial v_z}{\partial z}} = 0 \tag{9.92}$$

Then v_y = constant. From the boundary condition (9.74), $v_y(\pm a) = 0$. It follows then that $v_y = 0$ everywhere. For the x-component of the Navier-Stokes equation we have

$$\rho\left(\cancel{\frac{\partial v_x}{\partial t}} + v_x\cancel{\frac{\partial v_x}{\partial x}} + \cancel{v_y}\frac{\partial v_x}{\partial y} + \cancel{v_z}\cancel{\frac{\partial v_x}{\partial z}}\right) = -\frac{\partial P}{\partial x} + \cancel{\rho g_x} + \mu\left(\cancel{\frac{\partial^2 v_x}{\partial x^2}} + \frac{\partial^2 v_x}{\partial y^2} + \cancel{\frac{\partial^2 v_x}{\partial z^2}}\right) \tag{9.93}$$

$$-\frac{\partial P}{\partial x} + \mu\frac{\partial^2 v_x}{\partial y^2} = 0$$

For the y-component of the Navier-Stokes equation we have

$$\rho\left(\cancel{\frac{\partial v_y}{\partial t}} + v_x\cancel{\frac{\partial v_y}{\partial x}} + \cancel{v_y}\cancel{\frac{\partial v_y}{\partial y}} + \cancel{v_z}\cancel{\frac{\partial v_y}{\partial z}}\right) = -\frac{\partial P}{\partial y} + \rho g_y + \mu\left(\cancel{\frac{\partial^2 v_y}{\partial x^2}} + \cancel{\frac{\partial^2 v_y}{\partial y^2}} + \cancel{\frac{\partial^2 v_y}{\partial z^2}}\right) \tag{9.94}$$

$$-\frac{\partial P}{\partial y} + \rho g_y = 0$$

For the z-component of the Navier-Stokes equation we have

$$\rho\left(\cancel{\frac{\partial v_z}{\partial t}} + v_x\cancel{\frac{\partial v_z}{\partial x}} + \cancel{v_y}\cancel{\frac{\partial v_z}{\partial y}} + \cancel{v_z}\cancel{\frac{\partial v_z}{\partial z}}\right) = -\frac{\partial P}{\partial z} + \cancel{\rho g_z} + \mu\left(\cancel{\frac{\partial^2 v_z}{\partial x^2}} + \cancel{\frac{\partial^2 v_z}{\partial y^2}} + \cancel{\frac{\partial^2 v_z}{\partial z^2}}\right) \tag{9.95}$$

$$-\frac{\partial P}{\partial z} = 0$$

From the z-component of the Navier-Stokes equation we conclude that the pressure is uniform in the z-direction. From the y-component of the Navier-Stokes equation we conclude that the pressure in the y-direction is hydrostatic. (The dimension in the y-direction is usually small compared to the dimension in the x-direction, so this hydrostatic pressure distribution due to gravity is usually neglected.) From the x-component of the Navier-Stokes equation we have

$$\frac{\partial^2 v_x}{\partial y^2} = \frac{1}{\mu}\frac{\partial P}{\partial x} = \text{constant} \tag{9.96}$$

Thus the viscous force (per unit volume) is just balanced by the "pressure" force (per unit volume). This is typical of fully-developed internal flows. Integrating equation (9.96) twice, we get

$$v_x = \frac{1}{\mu}\left[\frac{\partial P}{\partial x}\frac{y^2}{2} + C_1 y + C_2\right] \tag{9.97}$$

For boundary conditions, we have the "no-slip" condition at the surface of the plates. Then

$$\begin{aligned} &(1) \quad \vartheta_x = 0 \quad \text{at} \quad y = a \\ &(2) \quad \vartheta_x = 0 \quad \text{at} \quad y = -a \end{aligned} \tag{9.98}$$

Applying boundary conditions (9.98), we get

$$0 = \frac{1}{\mu}\left[\frac{\partial P}{\partial x}\frac{a^2}{2} + C_1 a + C_2\right] \tag{9.99}$$

and

$$0 = \frac{1}{\mu}\left[\frac{\partial P}{\partial x}\frac{a^2}{2} - C_1 a + C_2\right] \tag{9.100}$$

Solving these two equations simultaneously, we get

$$\begin{aligned} C_2 &= -\frac{\partial P}{\partial x}\frac{a^2}{2} \\ C_1 &= 0 \end{aligned} \tag{9.101}$$

Then the velocity distribution becomes

$$\vartheta_x = \frac{a^2}{2\mu}\left[\frac{\partial P}{\partial x}\left(\frac{y^2}{a^2} - 1\right)\right] \tag{9.102}$$

Thus the velocity distribution is parabolic with the maximum velocity on the centerline of the channel at $y = 0$. Then

$$\vartheta_{max} = -\frac{\partial P}{\partial x}\frac{a^2}{2\mu} \tag{9.103}$$

and equation (9.102) can be written in non-dimensional form and plotted as shown in Figure 9.10

$$\frac{\vartheta_x}{\vartheta_{max}} = 1 - \left(\frac{y}{a}\right)^2 \tag{9.104}$$

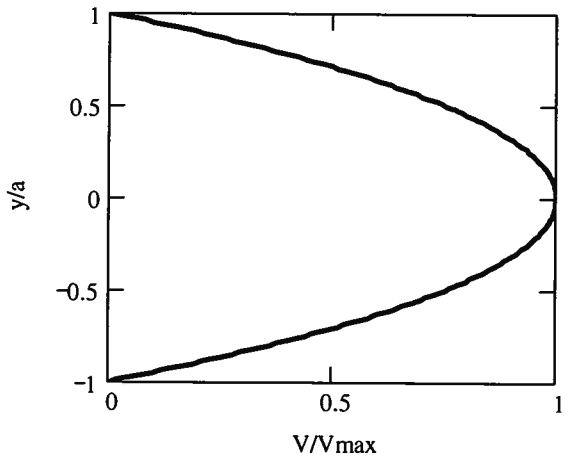

Figure 9.10 Velocity Distribution in Plane Poiseuille Flow Driven by a Pressure gradient

For a channel of width b the volumetric flow rate is given by

$$\dot{V} = \int_0^A \vartheta_x dA = \int_{-a}^{a} \vartheta_x b dy = \frac{\partial P}{\partial x}\frac{a^2 b}{2\mu}\int_{-a}^{a}\left(\frac{y^2}{a^2} - 1\right)dy = -\frac{\partial P}{\partial x}\frac{2a^3 b}{3\mu} \tag{9.105}$$

The average velocity, ϑ_{ave}, is given by

$$\vartheta_{ave} = \frac{\dot{V}}{A} = \left[-\frac{\partial P}{\partial x}\frac{2}{3}\frac{a^3 b}{\mu} \right]\left(\frac{1}{2ab}\right) = -\frac{\partial P}{\partial x}\frac{a^2}{3\mu} = \frac{2}{3}\vartheta_{max} \tag{9.106}$$

For the shear stress in the fluid, we have from equation (9.58)

$$\tau_{yx} = \mu\frac{\partial \vartheta_x}{\partial y} = \frac{\partial P}{\partial x} y \tag{9.107}$$

Thus the shear stress is zero in the center of the gap between the plates and maximum at the surface of the plates.

One of the key issues in the application of the solution that we have just developed is the critical value of the Reynolds number for the transition from laminar to turbulent flow in this configuration. As we have seen in Section 9.8, the definition of the Reynolds number for a particular flow geometry requires the specification of an appropriate characteristic length to describe the geometry. For flow in a circular conduit, the physical diameter of the conduit is the obvious choice for the characteristic length. However, for conduits of non-circular cross-section, the choice may not be so obvious. By convention, the appropriate characteristic length for these geometries is taken to be the *hydraulic diameter* which is defined as

$$D_h = \frac{4A_c}{\wp} \tag{9.108}$$

where A_c is the cross-sectional area of the flow and $\wp$ is the wetted perimeter of the conduit. This definition has been chosen because it yields the physical diameter D of a circular conduit as its hydraulic diameter since $A_c = \pi D^2/4$ and $\wp = \pi D$. For the infinite parallel plate geometry, consider first the case of a duct of rectangular cross-section of height a and width b. Then the hydraulic diameter for that geometry would be

$$D_h = \frac{4(2ab)}{2(2a+b)} = \frac{2(2a)}{\frac{2a}{b}+1} \tag{9.109}$$

Now let $b \to \infty$ since the plates are infinitely wide. Then for the infinite parallel plate geometry

$$D_h = 4a \tag{9.110}$$

and the Reynolds number becomes

$$Re = \frac{4a\rho\vartheta_{ave}}{\mu} \tag{9.111}$$

For this geometry, the lower limit of the critical value of the Reynolds for the transition from laminar to turbulent flow has been determined to be in the range 2200 - 3400 with $Re_{critical} = 2800$ a reasonable value to use for design purposes. For $Re > 2800$, the flow becomes turbulent and equation (9.102) is no longer valid.

9.9.1.2 Laminar flow in the Entry Region for Plane Poiseuille Flow: The flow configuration that we have just studied is known as a fully-developed flow since the effect of the fluid viscosity is felt throughout the flow field and the resulting parabolic velocity distribution has the same appearance (shape) at every value of x. However, this solution to the Navier-Stokes equation for this configuration does not reveal how the flow became fully developed. To see how this happens, we need to examine the *entry region*, the portion of the flow field where this development occurs. The flow field in this entry region can also be described by the Navier-Stokes equation, but now the inertial forces are equally as important as the viscous forces. Since these terms are non-linear, the solution of the Navier-Stokes equation in the entry region is very

complicated mathematically and will not be attempted here; however, there are situations in thermal-fluid systems for which this entry region is important, so it is worth discussing the physics of the situation.

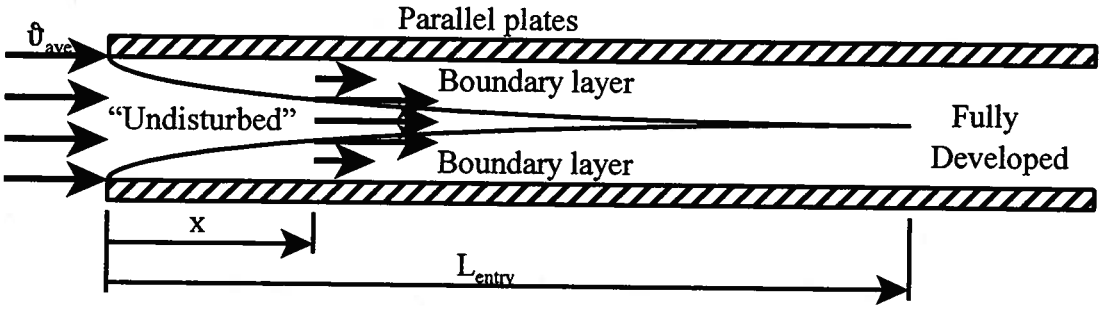

Figure 9.11 Developing Flow in the Entry Region Between Two Parallel Flat Plates

As shown in Figure 9.11, the flow enters the space between plates with a uniform velocity distribution in which the value of $\vartheta_x = \vartheta_{ave}$ is the same at every value of y. As the fluid comes into contact with the upper and lower plates, the fluid at the surface of the plates is slowed to zero velocity as a result of the "no-slip" boundary condition of the Newtonian fluid model. Initially, the influence of the solid boundary is confined to a very small region near the surface of the plates, but as the fluid moves downstream, this region of influence, known as the boundary layer, begins to diffuse further out into the flow in a direction normal to the solid boundary (wall). As the flow progresses in the x-direction, the boundary layer grows in thickness. In the boundary layer, the velocity of the fluid varies in a "smooth" way normal to the wall as the fluid layers slide over one another in a laminar fashion. The fluid velocity at the wall is identically zero while the fluid velocity at the outer limit of the boundary layer is equal to the velocity of the fluid in the "undisturbed" flow that has not yet felt the effect of the wall. Then the average fluid velocity in the boundary layer is less than ϑ_{ave}, and it follows that the average fluid velocity in the "undisturbed" flow must be greater than ϑ_{ave} in order to satisfy the continuity equation. Thus in the "undisturbed" region, the fluid is accelerated as the fluid in the boundary layer is decelerated.

Since the fluid in the "undisturbed" region has not yet felt the influence of the wall (hence the modifier "undisturbed" even though the fluid velocity is rapidly changing in this portion of the flow), viscous effects are negligible here and the fluid can be modeled as an inviscid fluid in this region. It follows, then, that the Bernoulli equation is valid in this region. Thus, as the fluid accelerates in the "undisturbed" region, inertial forces are dominant, and the pressure must decrease in accordance with the Bernoulli equation. At small values of x, the "undisturbed" region is by far the largest portion of the flow field. Then the pressure in this region is impressed upon the flow in the boundary layer. As the value of x increases in the entry region, the pressure falls rapidly in a non-linear manner, in fact as the square of the velocity in the "undisturbed" region.

As we move further and further in the x-direction, the boundary layer grows ever larger at the expense of the "undisturbed" region. As the size of the "undisturbed" region shrinks, the flow continues to accelerate until at some value of $x = L_{entry}$, the boundary layers from the top and bottom plates come together, and the local flow velocity in the disappearing "undisturbed" region has reached its maximum value ϑ_{max}. This is the value of the velocity given in equation (9.103) found on the centerline ($y = 0$) of the fully-developed flow. Thus the flow has become fully-

developed at $x = L_{entry}$. Since the inertial forces are important in the entry region but not in the fully-developed region, we would expect the entry length to depend upon the Reynolds number. Chen[1] has shown that the entry length for plane Poiseuille flow is given by

$$\frac{L_{entry}}{D_h} = 0.011Re + \frac{0.315}{1+0.0175Re} \tag{9.112}$$

As mentioned previously, the flow remains laminar for this configuration for $Re < Re_{critical}$. Then the longest possible entry length would occur at $Re_{critical} = 2800$. Thus from equation (9.112)

$$\left(\frac{L_{entry}}{D_h}\right)_{max} = 30.806 \tag{9.113}$$

an the laminar flow between infinite flat plates spaced a distance $2a$ apart becomes fully developed within $(L_{entry})_{max} = 30.806(D_h) = 30.806(4a) = 123.23a$. Figure 9.12 shows the axial pressure distribution for a sample plane Poiseuille flow of water with $Re = 2800$. The pressure of the water at the inlet to the parallel flat plate geometry is arbitrarily set at $P_{inlet} = 10^6$ N/m^2. The solid line shows the axial pressure distribution assuming fully-developed flow throughout the flow field with no entry region. The dashed line shows the pressure distribution with the effect of the entry region included.

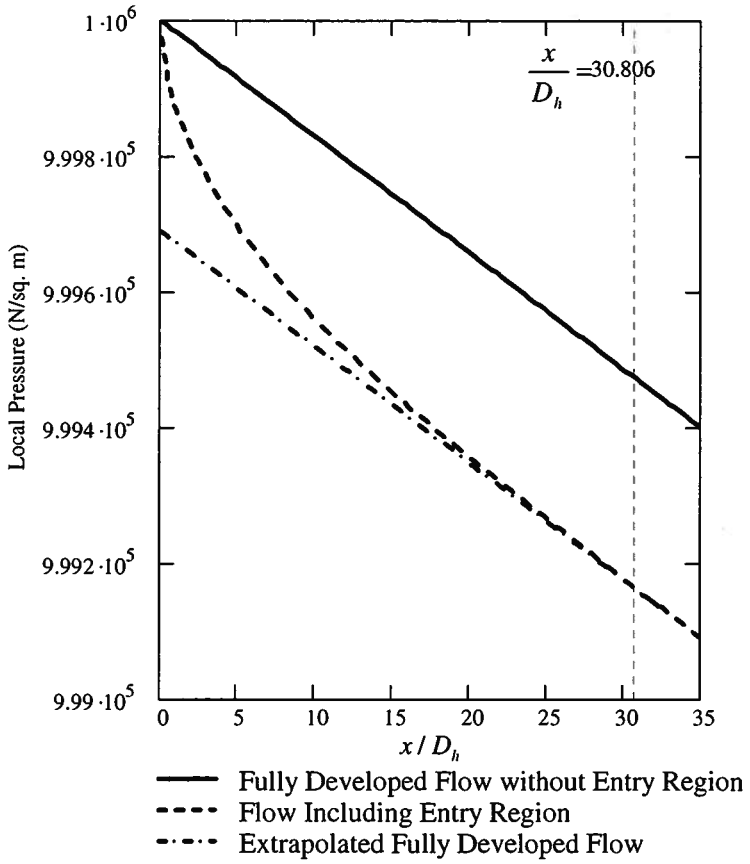

Figure 9.12 Axial Pressure Distribution for Flow of Water Between Infinite Parallel Flat Plates, $Re = 2800$

---

[1] R.Y. Chen, "Flow in the Entrance Region at Low Reynolds Numbers," *J. Fluids Eng.*, (95): 153-158, 1973.

The vertical line indicates the location of the end of the entry region as defined by the full development of the velocity profile (x/D_h = 30.806 for Re = 2800 for this flow configuration). Notice that the pressure with the entry region included is always lower than the pressure without the entry region taken into account. This additional pressure drop is due to the acceleration of the flow in the "undisturbed" region. Notice also that once the flow becomes fully developed, the pressure gradient is the same in both cases. The difference between the extrapolation of the fully-developed flow and the flow in the entry region shows the rapid decrease in pressure due to the acceleration of the "undisturbed" flow in the entry region.

The effect of the entry region on the drop in pressure that accompanies the flow of a viscous fluid in the space between parallel flat plates can be seen more clearly by making use of the pressure drop correlations of Shah and London[2] derived from solutions of the Navier-Stokes equation for the various flow regimes. These correlations are presented in terms of the following dimensionless parameters:

$$\Delta P^* = \frac{P_{inlet} - P}{\frac{\rho \vartheta_{ave}^{\ 2}}{2}} \qquad x^+ = \frac{x}{D_h Re} \tag{9.114}$$

The first of these is the dimensionless pressure drop and the second is the dimensionless length along the axis of the flow channel. According to the work of Shah and London, for laminar flow

$$\left(\Delta P^*\right)_{\substack{fully \\ developed}} = 96x^+$$

$$\left(\Delta P^*\right)_{apparent} = 4x^+ \left[\frac{3.44}{\sqrt{x^+}} + \frac{24 + \frac{0.674}{4x^+} - \frac{3.44}{\sqrt{x^+}}}{1 + 2.9 \text{ x } 10^{-5} \left(x^+\right)^{-2}} \right] \tag{9.115}$$

Equations (9.115) are plotted in Figure 9.13 for a flow with Re = 2800. Notice that the pressure drop with the entry region included is always greater than the pressure drop assuming fully-developed flow. The pressure gradient is very steep in early part of the entry region and becomes a constant value in a relatively short distance. Because of this entry effect, modeling the flow as fully-developed throughout thus introduces an error in calculating the pressure drop. This error becomes negligibly small for very long flow channels. Fortunately, most of the situations encountered in thermal-fluids engineering are of this type. Internal flow channels are frequently, but not always, thousands of diameters in length so the error in calculating the pressure drop with the assumption of fully-developed flow is negligible. In the design of a thermal-fluid system, one must always check to see that this assumption is valid.

---

[2] R. K. Shah and A. L. London, *Laminar Flow Forced Convection in Ducts*, Academic Press, new York, 1978, pp. 40-42 and 168.

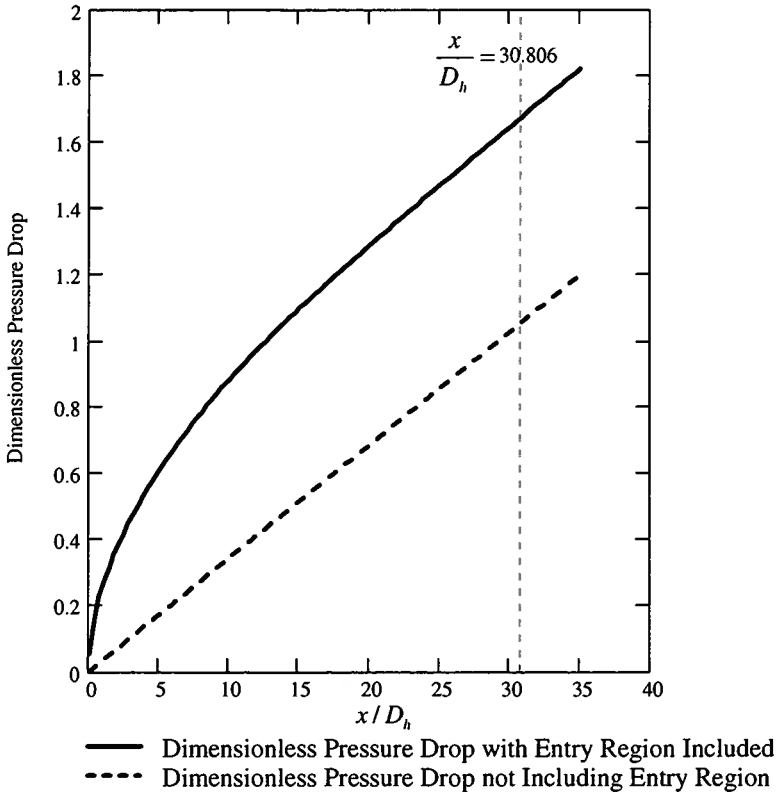

Figure 9.13 Pressure Drop for the Flow of a Viscous Fluid Between Parallel Flat Plates at $Re = 2800$

9.9.1.3 Laminar Couette Flow with a Moving Boundary and a Pressure Gradient: We have already considered the case of a simple shear flow between two parallel flat plates in which one of the plates was moving and the flow was generated by the movement of that plate. We now take up the case in which a pressure gradient is also imposed upon the flow. The flow geometry is shown schematically in Figure 9.14. The upper plate moves with velocity ϑ_0 while

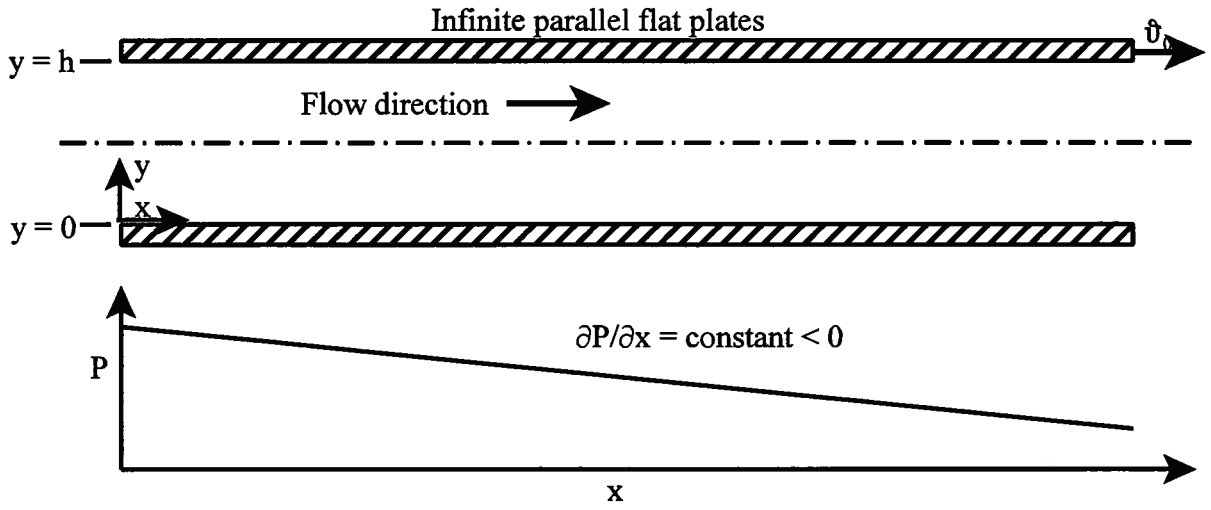

Figure 9.14 Fully-developed Planar Couette Flow with a Moving Boundary

Notice that if the pressure gradient is zero we have the case of the simple shear flow with the linear velocity profile. Thus the general velocity distribution is a simple superposition of a linear

profile typical of the simple shear flow and a parabolic profile typical of flow with a pressure gradient. Superposition of velocity profiles can often be a useful technique for the solution of the Navier-Stokes equation.

Since the velocity profile is a function of y only, the shear stress distribution becomes

$$\tau_{yx} = \mu \frac{\vartheta_0}{h} + h\left(\frac{\partial P}{\partial x}\right)\left[\frac{y}{h} - \frac{1}{2}\right] \tag{9.119}$$

For a channel of width b, the volumetric flow rate becomes

$$\dot{V} = \int_0^h \vartheta_x b dy = \frac{\vartheta_0 hb}{2} - \frac{1}{12\mu}\left(\frac{\partial P}{\partial x}\right)h^3 b \tag{9.120}$$

The average velocity is then given by

$$\vartheta_{ave} = \frac{\dot{V}}{A} = \frac{\vartheta_0}{2} - \frac{1}{12\mu}\left(\frac{\partial P}{\partial x}\right)h^2 \tag{9.121}$$

To determine the maximum velocity in the flow field, we make use of the fact that this occurs where the velocity gradient becomes zero. From equation (9.118) this occurs at

$$y_{\vartheta_{max}} = \frac{h}{2} - \frac{\frac{\vartheta_0}{h}}{\left(\frac{1}{\mu}\right)\left(\frac{\partial P}{\partial x}\right)} \tag{9.122}$$

Thus the location of the point in the flow where the maximum velocity occurs depends upon the magnitude of the pressure gradient as does the value of the maximum velocity itself. Experiment has shown that the laminar flow velocity profile of equation (9.118) is valid up to $Re_{critical} = 1500$ where the Reynolds number is based upon the characteristic length h.

In Figure 9.15 we have plotted in dimensionless form some sample velocity profiles for the three possible cases of the pressure gradient. Notice that if the pressure gradient is negative, meaning that the pressure decreases in the direction of the flow, the flow velocity is always positive. This is known as a favorable pressure gradient and results in flows that are inherently stable. However, if the pressure gradient is positive, meaning that the pressure increases in the direction of flow, it is possible for the velocity profile to have regions where the flow velocity is negative, thereby producing flow reversal. For this reason, this type of pressure gradient is known as an adverse pressure gradient and leads to flows that can become unstable.

As we shall soon see, these cases of flow reversal are extremely important in external flows because they can lead to separation of the flow from the surfaces on which they are occurring. In the case of aerodynamic bodies, this can lead to a significant increase in the drag experienced by the body subjected to the flow. The important point here is that we see that flow reversal can occur when there is an adverse (positive) pressure gradient. Such pressure gradients can occur in external flows when the flow is decelerated as it is on the back side of aerodynamic shapes. This is the reason that aerodynamic shapes such as the bodies of fish are shaped so that the flow on the downstream side of the body is decelerated as slowly as possible. This helps to make the positive pressure gradient as small as possible, thereby minimizing the possibility for flow reversal and eventual separation of the boundary layer from the surface. This separation leads to high aerodynamic drag. In the case of fish, those with poor aerodynamic shapes (high drag) were too slow to escape their faster predators and literally got eaten alive because of poor thermal-fluid design. By the process of natural selection, fish have excellent aerodynamic characteristics.

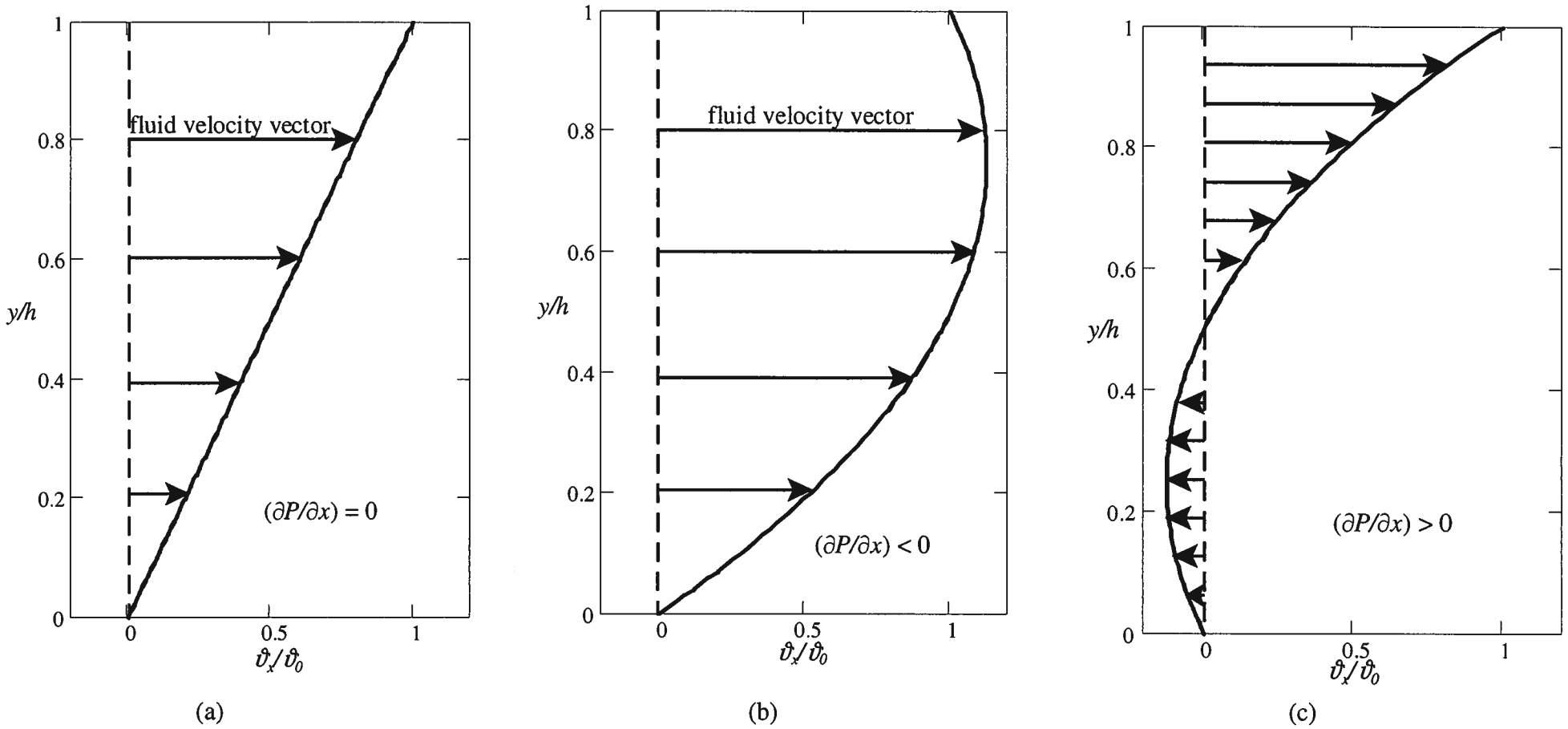

Figure 9.15 The Effect of a Pressure Gradient on Plane Couette Flow

9.9.1.4 Slider Bearings: A common application of the type of flow just considered occurs when the gap h is not a constant but varies slightly along the x-axis. Under these conditions, the pressure gradient is no longer constant. In fact, the pressure varies in the x-direction in such a way that when we integrate this pressure distribution over the upper surface, we find that the flow is capable of supporting a load in the y-direction. The resulting geometry is then a slider bearing capable of supporting enormous loads if properly designed. If we assume that there is no flow in the z-direction and we regard the volumetric flow rate of equation (9.120) as a local value since h is now a function of x, it still must be the case that this flow rate is a constant in the x-direction. Clearly the flow velocity increases as the gap decreases. Then for unit width in the z-direction

$$\frac{d\left(\dot{V}/b\right)}{dx} = \frac{\vartheta_0}{2}\frac{dh}{dx} - \frac{1}{12\mu}\frac{d}{dx}\left(h^3\frac{\partial P}{\partial x}\right) = 0$$
$$\frac{d}{dx}\left(h^3\frac{\partial P}{\partial x}\right) = 6\mu\vartheta_0\frac{dh}{dx} \qquad (9.123)$$

For a channel of variable gap, $h = h(x)$, equation (9.123) determines the approximate pressure distribution provided $dh/dx << 1$. Equation (9.123) is the fundamental equation that describes the performance of simple slider bearings. Notice that due to the presence of the velocity ϑ_0 in equation (9.123), the bearing is hydrodynamic and not hydrostatic. That is, the load carrying capacity (as we shall soon see) is linearly related to the velocity. If $\vartheta_0 = 0$, we have no bearing since that would make the pressure gradient zero. Also note that if ϑ_0 = constant, the pressure distribution depends upon h. We shall now show by way of example that the bearing will respond to an increase in the load by changing the geometry by changing h and/or dh/dx.

Example 9E.4: As shown in Figure 9E.4a, a simple slider bearing has a uniform taper from the inlet, where the gap is H_1, to the exit where the gap is H_2. This gap is filled with oil of viscosity μ and density ρ. The upper surface is stationary and the lower surface moves at a steady velocity ϑ_0. The thickness of the oil film at a location x measured relative to the leading edge of bearing is $h(x)$.

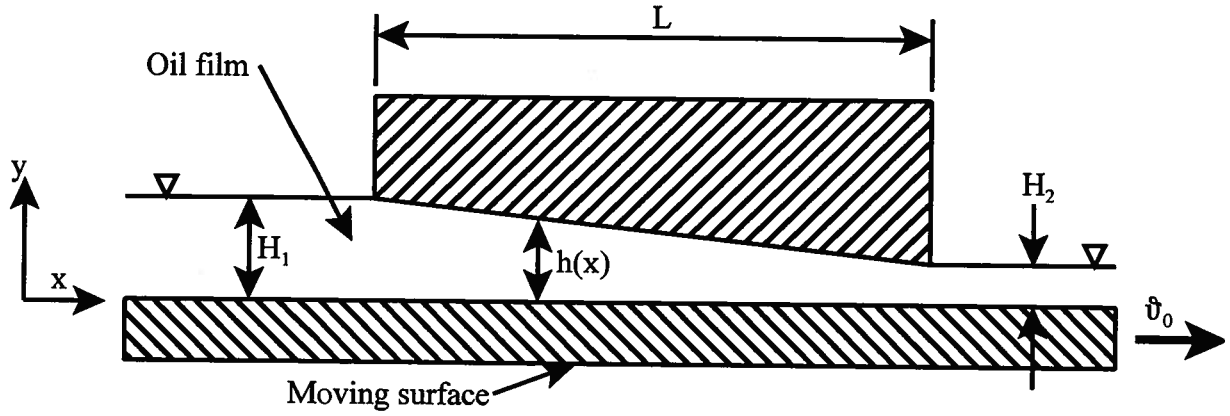

Figure 9E.4a

(a) Show that the pressure gradient along the slider is given by

$$\frac{dP}{dx} = \frac{12\mu\vartheta_0}{h^3}\left(\frac{h}{2} - \frac{H_1H_2}{H_1+H_2}\right)$$

(b) If the pressure at each open end of the bearing is P_{atm}, sketch the pressure profile $P = P(x)$ in the oil film. Find the location the maximum pressure and its value.

(c) If the bearing has dimension b normal to the plane of the sketch, what is the load carrying capacity of the upper block of the bearing?

Solution: (a) The pressure distribution in the bearing is given by equation (9.123). If we integrate this expression with respect to x we obtain

$$\int \frac{d}{dx}\left(h^3 \frac{\partial P}{\partial x}\right) dx = 6\mu v_0 \int \frac{dh}{dx} dx$$

$$h^3 \frac{\partial P}{\partial x} = 6\mu v_0 h + C_1$$

$$\frac{dP}{dx} = \frac{6\mu v_0}{h^2} + \frac{C_1}{h^3}$$

In order to integrate a second time, we note that

$$\frac{dP}{dx} = \frac{dP}{dh}\frac{dh}{dx}$$

but

$$h = H_1 + (H_2 - H_1)\frac{x}{L}$$

Then

$$\frac{dP}{dh} = \left(\frac{L}{H_2 - H_1}\right)\left[\frac{6\mu v_o}{h^2} + \frac{C_1}{h^3}\right]$$

Integrating this expression, we get

$$P = \frac{-6\mu v_0 L}{(H_2 - H_1)}\left(\frac{1}{h}\right) - \left(\frac{C_1 L}{H_2 - H_1}\right)\left(\frac{1}{2h^2}\right) + C_2$$

The boundary conditions are

(1) $P = P_{atm}$ at $h = H_1$

(2) $P = P_{atm}$ at $h = H_2$

Then substituting the boundary conditions and solving for C_1, we get

$$C_1 = -12\mu v_0 \left(\frac{H_1 H_2}{H_1 + H_2}\right)$$

Substituting for C_1 in the expression for dP/dx, we get

$$\frac{dP}{dx} = \frac{12\mu v_0}{h^3}\left[\frac{h}{2} - \frac{H_1 H_2}{H_1 + H_2}\right]$$

(b) The maximum pressure in the oil film can be determined by setting $dP/dx = 0$ and solving for the value of h. Then

$$\frac{h}{2} - \frac{H_1 H_2}{H_1 + H_2} = 0$$

$$h_{P_{max}} = \frac{2H_1 H_2}{H_1 + H_2}$$

Since

$$h = H_1 + (H_1 - H_2)\frac{x}{L}$$

it follows that the maximum pressure in the gap occurs at

$$x = L\frac{H_1}{H_1 + H_2}$$

From the boundary condition (1), we have upon substitution for C_1 and solving for C_2

$$C_2 = P_{atm} + \frac{6\mu v_0 L}{H_2^{\,2} - H_1^{\,2}}$$

and

$$P = P_{atm} + \frac{6\mu v_0 L}{H_2^{\,2} - H_1^{\,2}}\left[1 + \frac{H_1 H_2}{h^2} - \frac{H_2 + H_1}{h}\right]$$

Then the maximum value of the pressure is

$$P_{max} = P_{atm} + \frac{6\mu v_0 L}{(H_1 + H_2)}\frac{(H_1 - H_2)}{4H_1 H_2}$$

We can rewrite the expression for the pressure in dimensionless form.

$$\frac{P - P_{atm}}{6\mu v_0 L \Big/ \left(H_1^{\,2} - H_2^{\,2}\right)} = -\left[1 + \frac{H_1 H_2}{h^2} - \frac{H_2 + H_1}{h}\right]$$

and we can combine it with the expression for $h = h(x)$. This yields an expression for the dimensionless pressure as a function of x. The resulting expression can be plotted as shown in Figure 9E.4b for the cases in which $H_1 = 1$ and $H_2 = 0.99$ and $H_1 = 1$ and $H_2 = 0.97$. Notice that as the slope of the slider increases, the maximum pressure increases and the location of the peak pressure shifts downstream.

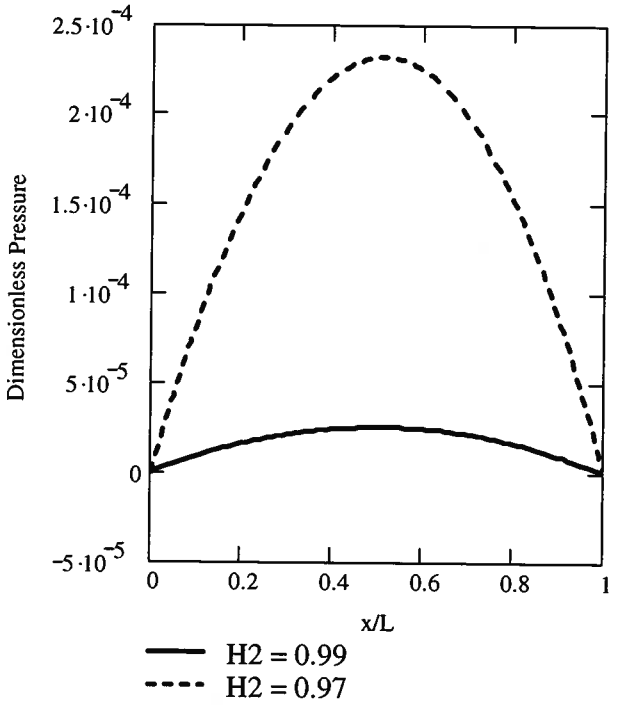

Figure 9E.4b Dimensionless Pressure Distribution Across the Face of a Slider Bearing

(c) The pressure distribution has a parabolic shape that can be integrated to yield the load carrying capability of the bearing.

$$F = \int PdA = \int Pbdx$$

$$\frac{F}{b} = \int_0^L \left(P_{atm} + \frac{6\mu\vartheta_0 L}{H_2^{\,2} - H_1^{\,2}} \left[1 + \frac{H_1 H_2}{\left\{ H_1 - (H_2 - H_1)\frac{x}{L} \right\}^2} - \frac{H_1 + H_2}{\left\{ H_1 - (H_2 - H_1)\frac{x}{L} \right\}} \right] \right) dx$$

Figure 9E.4c shows the force per unit width of a slider bearing with the following operating conditions: ϑ_0 = 10 m/sec; μ = 0.50 kg/m sec; L = 1 m; $H_2 = 0.9H_1$. Note the enormous load

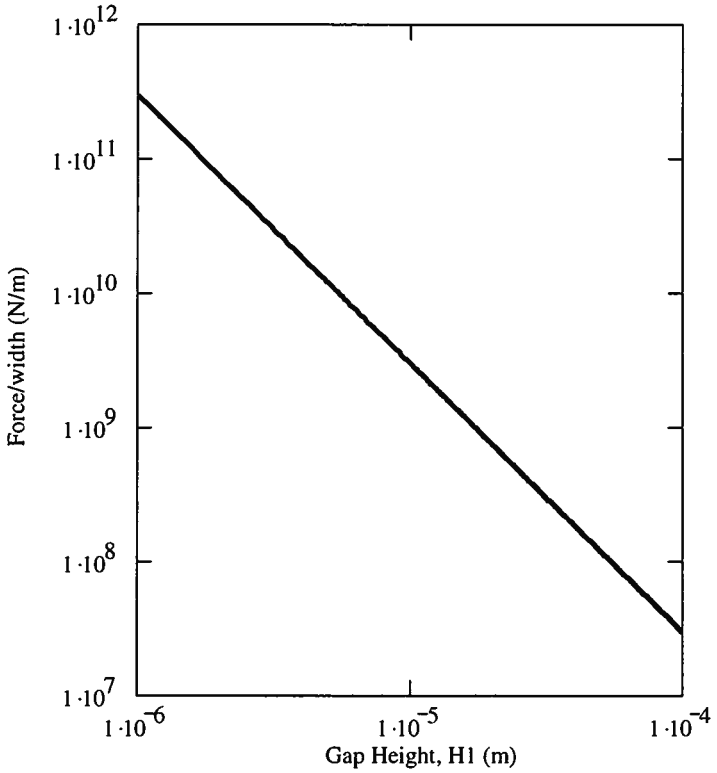

Figure 9E.4c Dependence of Bearing Load Upon Gap Height

carrying capability of the bearing when the oil film is its thinnest. The load carrying capability falls off rapidly as the thickness of the oil film increases. (Note the log-log scale of Figure 9E.4c.) For the thinnest oil films, the machining tolerances of the bearing must be very small in order for the bearing to function as designed. The adjustment of the gap height to a change in load is stable since as load is increased and the gap decreases, the load carrying capability increases. Also note that the larger the angle of inclination of the underside of the bearing, the larger the load. Of course, this increase in the angle has its limits before the assumption of a small angle of inclination is violated and the theory breaks down.

Note also that Boogie boards operate on this principle. In the case of the Boogie board, one has to throw the board to generate a velocity relative to the sheet of water before one jumps on. If there is not sufficient velocity with the proper angle to the water surface, the board sinks when the load is applied. A similar phenomenon applies to the case of a windshield wiper blade sliding over the windshield of an automobile in the rain and to the case of an automobile hydroplaning on a thin film of water on a wet road surface. From Figure 9E.4c, it is not surprising that a 2000 kg automobile can be easily "lifted" (hydroplane) on a thin sheet of water

at turnpike speeds. The faster the speed of the vehicle, the greater the force and the more likely the phenomenon will occur.

9.9.1.5 Fully-developed Laminar Flow in a Circular Conduit: One of the most common geometries for internal flow in thermal-fluid systems is that of a pipe or tube of circular cross-section. For our purposes here, we shall consider the case of steady flow of a fluid in a horizontal pipe with gravity aligned with the vertical, normal to the principal flow direction as shown in Figure 9.16.

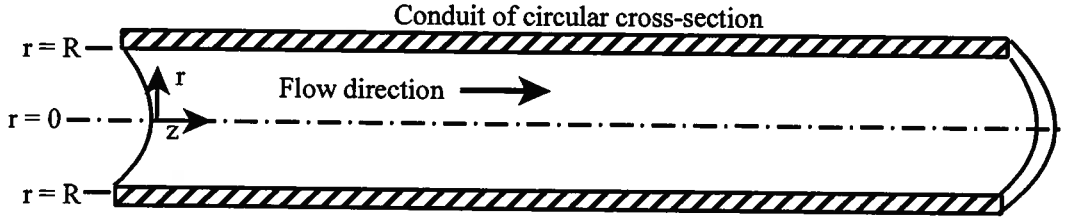

Figure 9.16 Fully-developed Flow in a Circular Conduit

For this geometry, circular coordinates (r, θ, z) are most useful for determining the velocity profile. The z-axis is aligned with the centerline of the pipe and the r-axis is radially outward. We wish to determine the velocity profile for fully-developed steady flow. Under these conditions, there will be no dependence on the z-coordinate so $\partial/\partial z = 0$. In addition, fully-developed flow will be axially symmetric so $\partial/\partial\theta = 0$. Then if there is no swirl, $\vartheta_\theta = 0$, and the continuity equation, equation (9.71), becomes

$$\frac{1}{r}\frac{\partial}{\partial r}(r\vartheta_r)+\frac{1}{r}\frac{\partial}{\partial\theta}(\vartheta_\theta)+\frac{\partial}{\partial z}(\vartheta_z)=0$$
$$\frac{1}{r}\frac{\partial}{\partial r}(r\vartheta_r)=0 \qquad (9.124)$$

Thus, from equation (9.124) it is apparent that $r\vartheta_r$ = constant, but at the wall, $r = R$ and $\vartheta_r = 0$ by the boundary condition, equation (9.74). Then it follows from equation (9.124) that $r\vartheta_r = 0$ and thus $\vartheta_r = 0$ everywhere. Then there is only one velocity component, ϑ_z, and it is a function of r only, $\vartheta_z = \vartheta_z(r)$. Then the r-component of the Navier-Stokes equation, equation (9.73a) becomes

$$\rho\left(\frac{\partial\vartheta_r}{\partial t}+\vartheta_r\frac{\partial\vartheta_r}{\partial r}+\frac{\vartheta_\theta}{r}\frac{\partial\vartheta_r}{\partial\theta}-\frac{\vartheta_\theta^2}{r}+\vartheta_z\frac{\partial\vartheta_r}{\partial z}\right)$$
$$=-\frac{\partial P}{\partial r}+\rho g_r+\mu\left[\frac{\partial}{\partial r}\left(\frac{1}{r}\frac{\partial}{\partial r}(r\vartheta_r)\right)+\frac{1}{r^2}\frac{\partial^2\vartheta_r}{\partial\theta^2}-\frac{2}{r^2}\frac{\partial\vartheta_\theta}{\partial\theta}+\frac{\partial^2\vartheta_r}{\partial z^2}\right] \qquad (9.125a)$$
$$-\frac{\partial P}{\partial r}+\rho g_r=0$$

Thus the pressure is hydrostatic across a plane perpendicular to the z-axis; however, since this dimension is small compared to the axial dimension, the pressure is usually considered uniform over this plane. The θ-component of the Navier-Stokes equation, equation (9.73b) becomes

$$\rho\left(\cancel{\frac{\partial \vartheta_\theta}{\partial t}}+\cancel{\vartheta_r}\cancel{\frac{\partial \vartheta_\theta}{\partial r}}+\cancel{\frac{\vartheta_\theta}{r}}\cancel{\frac{\partial \vartheta_\theta}{\partial \theta}}-\cancel{\frac{\vartheta_r \vartheta_\theta}{r}}+\vartheta_z\cancel{\frac{\partial \vartheta_\theta}{\partial z}}\right)$$

$$=-\frac{1}{r}\frac{\partial P}{\partial \theta}+\cancel{\rho g_\theta}+\mu\left[\frac{\partial}{\partial r}\left(\frac{1}{r}\frac{\partial}{\partial r}\left(r\cancel{\vartheta_\theta}\right)\right)+\frac{1}{r^2}\cancel{\frac{\partial^2 \vartheta_\theta}{\partial \theta^2}}-\frac{2}{r^2}\cancel{\frac{\partial \vartheta_r}{\partial \theta}}+\cancel{\frac{\partial^2 \vartheta_\theta}{\partial z^2}}\right] \tag{9.125b}$$

$$\frac{\partial P}{\partial \theta}=0$$

Thus from equations (9.125a) and (9.125b), it follows that the pressure is a function of z only. The z-component of the Navier-Stokes equation, equation (9.73c) becomes

$$\rho\left(\cancel{\frac{\partial \vartheta_z}{\partial t}}+\cancel{\vartheta_r}\frac{\partial \vartheta_z}{\partial r}+\cancel{\frac{\vartheta_\theta}{r}}\cancel{\frac{\partial \vartheta_z}{\partial \theta}}-\cancel{\frac{\vartheta_\theta^2}{r}}+\vartheta_z\cancel{\frac{\partial \vartheta_z}{\partial z}}\right)$$

$$=-\frac{\partial P}{\partial z}+\cancel{\rho g_z}+\mu\left[\frac{1}{r}\frac{\partial}{\partial r}\left(r\frac{\partial \vartheta_z}{\partial r}\right)+\frac{1}{r^2}\cancel{\frac{\partial^2 \vartheta_z}{\partial \theta^2}}+\cancel{\frac{\partial^2 \vartheta_z}{\partial z^2}}\right] \tag{9.125c}$$

$$\mu\frac{1}{r}\frac{\partial}{\partial r}\left(r\frac{\partial \vartheta_z}{\partial r}\right)=\frac{\partial P}{\partial z}$$

This is the now familiar result for fully-developed internal flow, namely that the viscous force (per unit volume), the left-hand side of equation (9.125c), is balanced by the net pressure force (per unit volume), the right-hand side of equation (9.125c). Equation (9.125c) also presents the interesting result that the left-hand side is a function of r only and the right-hand side is a function of z only. The only way that this can be true is if equation (9.125c) is equal to a constant. It follows, then, that the pressure gradient in the z-direction is a constant, $(\partial P/\partial z)$ = constant. Then equation (9.125c) can be rearranged and integrated. Thus

$$\begin{aligned}
\mu\frac{\partial}{\partial r}\left(r\frac{\partial \vartheta_z}{\partial r}\right)&=r\frac{\partial P}{\partial z}\\
\mu\int\frac{\partial}{\partial r}\left(r\frac{\partial \vartheta_z}{\partial r}\right)dr&=\frac{\partial P}{\partial z}\int r dr\\
\mu r\frac{\partial \vartheta_z}{\partial r}&=\frac{\partial P}{\partial z}\frac{r^2}{2}+C_1\\
\mu\frac{\partial \vartheta_z}{\partial r}&=\frac{\partial P}{\partial z}\frac{r}{2}+\frac{C_1}{r}
\end{aligned} \tag{9.126}$$

Equation (9.126) can be integrated to yield

$$\begin{aligned}
\mu\int\frac{\partial \vartheta_z}{\partial r}dr&=\frac{\partial P}{\partial z}\int\frac{r}{2}dr+C_1\int\frac{dr}{r}\\
\vartheta_z&=\frac{r^2}{4\mu}\left(\frac{\partial P}{\partial z}\right)+\frac{C_1}{\mu}\ln r+C_2
\end{aligned} \tag{9.127}$$

Since the velocity must be finite at the centerline of the conduit, $r = 0$, it must be true that $C_1 = 0$. Alternatively, we could have noticed in equation (9.126) that if the velocity profile is to be axially symmetric about the centerline of the conduit, $r = 0$, it must be true that $\partial \vartheta_z/\partial r = 0$ at the centerline. Then it again follows that $C_1 = 0$. By the "no-slip" boundary condition at the wall of the conduit, $r = R$, the velocity must vanish, $\vartheta_z(R) = 0$. Then

$$C_2 = -\frac{R^2}{4\mu}\left(\frac{\partial P}{\partial z}\right) \tag{9.128}$$

Then substituting the boundary conditions into equation (9.127), we get the velocity profile for fully-developed laminar flow in a circular conduit.

$$\vartheta_z = \frac{r^2}{4\mu}\left(\frac{\partial P}{\partial z}\right) - \frac{R^2}{4\mu}\left(\frac{\partial P}{\partial z}\right) = \frac{1}{4\mu}\left(\frac{\partial P}{\partial z}\right)\left(r^2 - R^2\right) = -\frac{R^2}{4\mu}\left(\frac{\partial P}{\partial z}\right)\left[1 - \left(\frac{r}{R}\right)^2\right] \tag{9.129}$$

This velocity profile is a famous result in thermal-fluids engineering and is named Hagen-Poiseuille flow after the two men who first studied it. In Germany in 1839 G. L. Hagen (1797 - 1884) conducted some very meticulous measurements of the flow of water in small-diameter tubes, using the water temperature instead of the viscosity as one of the parameters. A few years later the French physician Jean Louis Poiseuille (1799 - 1869) repeated the experiments independently, using oil and mercury in addition to water. Although neither Poiseuille nor Hagen really understood the mathematics of the phenomenon, they did appreciate the importance of the pressure drop over the length of the tube (pressure gradient) in determining the magnitude of the flow. It was Hagen who generated and correlated the data in the form of "resistance" plots similar to Figure 9.8 that showed the linear dependence of pressure drop upon the average velocity at low velocities. Hagen even anticipated the work of Osborne Reynolds when he noted in 1854 that the flow was not always laminar, "the efflux jet sometimes being clear and sometimes frothy". Similarly, he found that sawdust suspended in the water sometimes moved in straight lines and sometimes very irregularly. In the latter instances he noted that his linear resistance equation no longer applied. Based on this early work and the subsequent work of Reynolds, we now know that the transition from laminar to turbulent flow in a circular conduit occurs for 2300 $\leq Re_{tr} < 10^4$. As a conservative estimate for design purposes, the critical value of the Reynolds number for this flow configuration is generally considered to be $Re_{critical} = 2100$.

The shear stress distribution for Hagen-Poiseuille flow is given by equation (9.72), viz.

$$\tau_{zr} = \tau_{rz} = \mu\left(\cancel{\frac{\partial \vartheta_r}{\partial z}} + \frac{\partial \vartheta_z}{\partial r}\right)$$

$$\tau_{zr} = \tau_{rz} = \frac{r}{2}\left(\frac{\partial P}{\partial z}\right) \tag{9.130}$$

Thus the shear stress is zero at the centerline and maximum at the wall of the conduit.

The volumetric flow rate is given by

$$\dot{V} = \int_0^R \vartheta_z 2\pi r dr = -\int_0^R \frac{R^2}{4\mu}\left(\frac{\partial P}{\partial z}\right)\left[1 - \left(\frac{r}{R}\right)^2\right] 2\pi r dr = -\frac{\pi R^4}{8\mu}\left(\frac{\partial P}{\partial z}\right) \tag{9.131}$$

Notice that since the pressure gradient is negative (meaning that the pressure decreases in the direction of flow, a condition known as a "favorable" pressure gradient), the volumetric flow rate is positive even though there is a negative sign on the right-hand side of equation (9.131).

The average velocity is given by

$$\vartheta_{ave} = \frac{\dot{V}}{A_c} = \frac{\dot{V}}{\pi R^2} = -\frac{R^2}{8\mu}\left(\frac{\partial P}{\partial z}\right) \tag{9.132}$$

Then the velocity profile of equation (9.129) can be written

$$\vartheta_z = 2\vartheta_{ave}\left[1 - \left(\frac{r}{R}\right)^2\right] \tag{9.133}$$

The maximum velocity can be determined by taking the derivative of equation (9.129) and setting it equal to zero and then solving for the appropriate value of r. Then

$$\frac{d\vartheta_z}{dr} = \frac{r}{2\mu}\left(\frac{\partial P}{\partial z}\right) = 0 \qquad (9.134)$$

$$\therefore r = 0$$

Substituting this value of r into equation (9.129), we get

$$\vartheta_{max} = -\frac{R^2}{4\mu}\left(\frac{\partial P}{\partial z}\right) = 2\vartheta_{ave} \qquad (9.135)$$

Then the velocity profile can be written in the form

$$\vartheta_z = \vartheta_{max}\left[1 - \left(\frac{r}{R}\right)^2\right] \qquad (9.136)$$

This velocity profile is plotted in Figure 9.17 which shows the parabolic nature of the distribution. (The physically meaningless negative values of the parameter r/R are used to show the symmetry of the profile about the centerline, $r = 0$, of the conduit.)

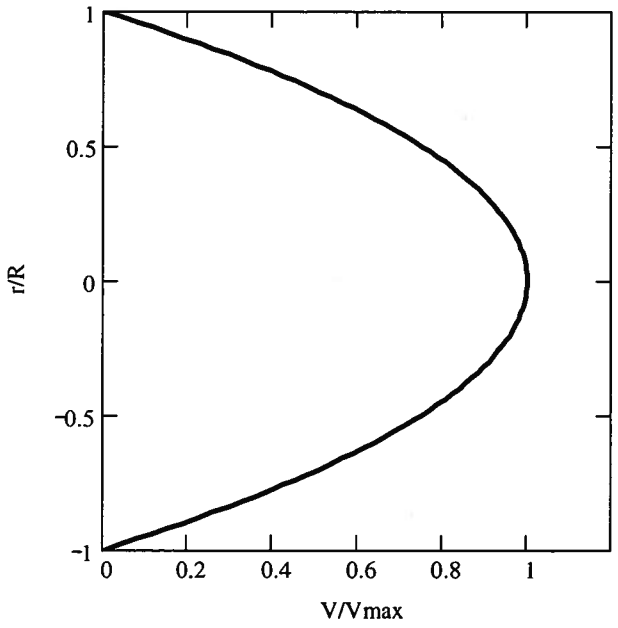

Figure 9.17 Velocity Profile for Fully-developed Laminar Flow in a Circular Conduit

Typically, a thermal-fluid system consists of an assembly of specialized devices of various types, each of which processes the working fluid in some way. These devices are interconnected by circular conduits (pipes) that facilitate the movement of the working fluid from one device to the other. The devices and the pipes are usually, but not always, arranged in a closed circuit so that the working fluid starts out in one location and then passes through all the devices and their interconnecting pipes in succession, and ultimately returns to the starting point. From equation (9.130) it is apparent that in fully developed laminar flow, the amount of incompressible fluid that we can transport, i.e., the volumetric flow rate, through a pipe of fixed dimension is directly proportional to the pressure gradient imposed on the conduit. From the

point of view of a closed circuit of fixed length, this pressure gradient translates into a drop in pressure of the fluid from the beginning of the circuit to its end. Thus, in order for the fluid to flow through the circuit on a continual basis, it is necessary to insert at the start of the circuit a device that increases the pressure of the fluid by the right amount to compensate for the pressure drop around the circuit. The thermal-fluid device that accomplishes this is a pump, but in order to specify the pump required for a given system design, it is necessary to know the magnitude of the pressure drop in the circuit.

To facilitate this design process, thermal-fluids engineers have introduced the concept of a dimensionless parameter known as the friction factor and denoted by the symbol f, that contains the essence of the viscous behavior of a fluid flowing in a conduit. In equation (9.91), we showed that the pressure gradient (expressed in non-dimensional form) in a laminar flow system could be related to the Reynolds number in that system. As we shall now show, for laminar internal flow that relation depends upon the friction factor. Since the pressure gradient appearing in equation (9.131) for the volumetric flow rate for laminar flow in a circular conduit is a constant, it can be integrated for a pipe of length L. Then

$$\begin{aligned} \frac{dP}{dz} &= -\text{constant} = -a \\ \int_{P_1}^{P_2} dP &= -a\int_0^L dz \\ P_2 - P_1 &= -a(L-0) \\ P_1 - P_2 &= aL \\ a &= \frac{P_1 - P_2}{L} \\ \therefore \frac{dP}{dz} &= -\frac{P_1 - P_2}{L} \end{aligned} \tag{9.137}$$

Then we can write equation (9.131) in the form

$$\dot{V} = \frac{\pi R^4}{8\mu}\left(\frac{P_1 - P_2}{L}\right) = \frac{\pi R^4}{8\mu}\frac{\Delta P}{L}$$

$$\frac{\Delta P}{L} = \frac{8\mu}{\pi R^4}\dot{V} = \frac{8\mu}{\pi R^4}\vartheta_{ave}A_c = \frac{8\mu}{\pi R^4}\vartheta_{ave}\pi R^2$$

$$\frac{\Delta P}{L} = \frac{32\mu\vartheta_{ave}}{D^2} = \frac{\mu}{\vartheta_{ave}D\rho}\frac{32\rho\vartheta_{ave}^{\,2}}{D}$$

$$\begin{aligned} \frac{\Delta P}{L} &= \frac{1}{Re}\frac{64}{D}\frac{\rho\vartheta_{ave}^{\,2}}{2} \\ \frac{\Delta P \Big/ \frac{\rho\vartheta_{ave}^{\,2}}{2}}{L/D} &= \frac{64}{Re} \end{aligned} \tag{9.138}$$

The term on the left-hand side of equation (9.138) is the dimensionless pressure gradient of equation (9.91) and the term on the right-hand side of equation (9.138) is the dimensionless parameter defined as the friction factor. Then

$$\frac{\Delta P / \frac{\rho \vartheta_{ave}^{\,2}}{2}}{L/D} \equiv f \tag{9.139}$$

This formulation can be generalized for all internal flows so that the pressure drop can be written

$$\Delta P = f\left(\frac{L}{D_h}\right)\left(\frac{\rho \vartheta_{ave}^{\,2}}{2}\right) \tag{9.140}$$

where for each particular flow configuration specified by the hydraulic diameter, D_h, the friction factor takes on a unique value. For the case of fully-developed laminar flow in a circular conduit

$$f = \frac{64}{Re} \tag{9.141}$$

For the case of fully-developed laminar flow between infinite parallel flat plates, equation (9.115) gives

$$f = \frac{96}{Re} \tag{9.142}$$

Table 9.3 gives the value of the friction factor for fully-developed laminar flow in conduits of different cross-sections, such as triangles, rectangles, and ellipses. In each case, the value of the friction factor has been obtained by solving the Navier-Stokes equation with the appropriate boundary conditions. (Table 9.3 also contains some additional data that we will make use of in Chapter 11.) In the design of thermal-fluid systems, the pressure drop for fully-developed laminar flow in a conduit of particular cross-section and known length is determined by substituting into equation (9.140) the appropriate values for f and D_h obtained from Table 9.3. The value of the critical Reynolds number for the transition from laminar to turbulent flow in these non-circular cross-sections can be conservatively assumed to be the same as that for the circular cross-section with the appropriate value of D_h used in the Reynolds number.

The friction factor used in equation (9.140) is known as the Darcy friction factor in honor of the French engineer Henry Darcy (1803 - 1858) who was an early pioneer in the field fluid dynamics. Henry Darcy is credited with the invention of the modern style Pitot tube, was the first researcher to suspect the existence of the boundary layer in fluid flow, contributed to the development of the Darcy-Weisbach equation for pipe flow resistance (to be introduced later), made major contributions to open channel flow research, and developed Darcy's Law for laminar flow in homogeneous, porous media. Darcy's Law is a foundation stone for several fields of study including ground-water hydrology, soil physics, and petroleum engineering.

In the thermal-fluids engineering literature there is another friction factor, known as the Fanning friction factor, that is sometimes used, especially in the United Kingdom and Europe. In the United States, the literature devoted to heat transfer phenomena also makes frequent use of the Fanning friction factor. The Fanning friction factor is related to the Darcy friction factor in the following way:

$$f_{Darcy} = 4 f_{Fanning} \tag{9.143}$$

In utilizing tabulated data for the friction factor found in the literature, one must always check to see which friction factor is represented. If the data do not specify, one can always check to see how the friction factor for fully-developed laminar flow in a circular conduit is related to the Reynolds number. If the relationship is that of equation (9.141), the data are for the Darcy friction factor. If the constant of proportionality is 16 and not 64, the data are for the Fanning friction factor.

Table 9.3 Friction Factor and Nusselt Number Data for Laminar Flow in Non-circular Conduits

$Re = \frac{\vartheta D_h \rho}{\mu}$ where $D_h = \frac{4A_{cross\text{-}section}}{\wp} = \frac{4A_c}{\wp}$ and $\wp$ is the wetted perimeter

Nu_H is the Nusselt number for constant heat flux and Nu_T is the Nusselt number for constant wall temperature

	Ellipse					Rectangle					Triangle				
b/a	A_c/a^2	$\wp/a$	$f{\cdot}Re$	Nu_H	Nu_T	A_c/a^2	$\wp/a$	$f{\cdot}Re$	Nu_H	Nu_T	A_c/a^2	$\wp/a$	$f{\cdot}Re$	Nu_H	Nu_T
10.00	31.42	4.06	77.26	5.12	3.70	40.00	44.00	84.68	6.78	5.91	10.00	22.10	50.17	2.29	1.34
5.00	15.71	4.20	74.41	4.96	3.77	20.00	24.00	76.28	5.74	4.83	5.00	12.20	51.62	2.51	1.70
2.00	6.28	4.84	67.29	4.56	3.74	8.00	12.00	62.19	4.12	3.39	2.00	6.47	53.28	2.88	2.22
1.00	3.14	6.28	64.00	4.36	3.66	4.00	8.00	56.91	3.61	2.98	1.00	4.83	52.61	3.10	2.46
0.90	2.83	5.97	64.09	4.37	3.66	3.60	7.60	57.04	3.62	2.97	0.90	4.69	52.22	3.12	2.47
0.80	2.51	5.67	64.39	4.39	3.67	3.20	7.20	57.51	3.66	3.01	0.80	4.56	51.84	3.11	2.46
0.70	2.20	5.38	64.98	4.42	3.69	2.80	6.80	58.42	3.75	3.09	0.70	4.44	51.45	3.10	2.45
0.60	1.88	5.11	65.92	4.48	3.72	2.40	6.40	59.92	3.89	3.21	0.60	4.33	51.06	3.06	2.41
0.50	1.57	4.84	67.29	4.56	3.74	2.00	6.00	62.19	4.12	3.39	0.50	4.24	50.49	2.99	2.34
0.40	1.26	4.60	69.18	4.67	3.76	1.60	5.60	65.47	4.47	3.67	0.40	4.15	49.81	2.85	2.18
0.30	0.94	4.39	71.58	4.80	3.78	1.20	5.20	70.05	4.99	4.12	0.30	4.09	49.12	2.71	2.02
0.20	0.63	4.20	74.41	4.96	3.77	0.80	4.80	76.28	5.74	4.83	0.20	4.04	48.63	2.49	1.72
0.10	0.31	4.06	77.26	5.12	3.70	0.40	4.40	84.68	6.78	5.91	0.10	4.01	48.31	2.63	1.37

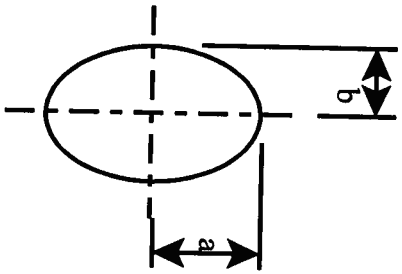

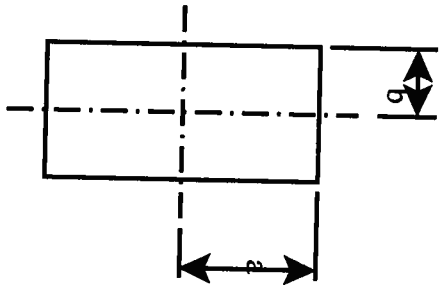

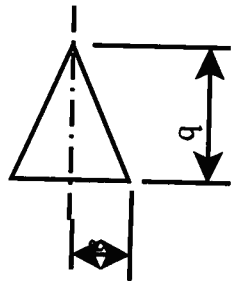

For the fully-developed flow inside the circular conduit, one of the important effects of the fluid friction embodied in the friction factor can be seen from the application of the first law of thermodynamics. For a control volume consisting of a length L of the conduit, there is no heat transfer or shaft work transfer. Furthermore, once the velocity profile becomes fully-developed, the average kinetic energy of the fluid is the same at every location along the axis of the conduit. Then the steady-flow form of the first law becomes

$$h_{out} - h_{in} = 0 \tag{9.144}$$

If we substitute the constitutive relation for the enthalpy for the incompressible fluid model into equation (9.144), we get

$$\begin{aligned} u_{out} - u_{in} &= P_{in} v_{in} - P_{out} v_{out} \\ u_{out} - u_{in} &= v\left(P_{in} - P_{out}\right) = \frac{P_{in} - P_{out}}{\rho} = f\left(\frac{L}{D_h}\right)\left(\frac{\vartheta_{ave}^{\,2}}{2}\right) \end{aligned} \tag{9.145}$$

Thus for this adiabatic, incompressible flow, the effect of the fluid friction manifests itself as the flow work transfer in the conduit which, in turn, results in an increase in the stored thermal energy of the fluid. If we substitute the energy constitutive relation for the incompressible fluid model into equation (9.145), we see that the fluid friction produces a temperature increase in the fluid. Thus,

$$\begin{aligned} c\left(T_{out} - T_{in}\right) &= f\left(\frac{L}{D_h}\right)\left(\frac{\vartheta_{ave}^{\,2}}{2}\right) \\ T_{out} - T_{in} &= \frac{f}{c}\left(\frac{L}{D_h}\right)\left(\frac{\vartheta_{ave}^{\,2}}{2}\right) \end{aligned} \tag{9.146}$$

If we substitute equation (9.141) into equation (9.146), we see that the temperature increase is directly proportional to the fluid viscosity and the average velocity of the fluid.

$$T_{out} - T_{in} = \frac{64}{Re_{D_h}} \frac{1}{c}\left(\frac{L}{D_h}\right)\left(\frac{\vartheta_{ave}^{\,2}}{2}\right) = \frac{32\mu}{\rho D_h} \frac{\vartheta_{ave}}{c}\left(\frac{L}{D_h}\right) \tag{9.147}$$

From the second law of thermodynamics we can calculate the rate of entropy generation for this flow configuration.

$$\dot{S}_{gen} = \dot{m}\left(s_{out} - s_{in}\right) = \dot{m}c \ln\frac{T_{out}}{T_{in}} = \rho c \dot{V} \ln\left(1 + \frac{32\mu L \vartheta_{ave}}{\rho c T_{in} D_h^{\,2}}\right) \tag{9.148}$$

This rate is clearly positive and shows that fluids with higher viscosity generate more entropy for a given flow geometry. Also, the greater the average velocity in a given flow geometry, the greater the rate of entropy generation. Note that this rate of entropy generation is due to the flow work transfer and not the dissipation of kinetic energy in the flow. The kinetic energy of the flow is constant throughout the length of the conduit.

9.9.1.6 Laminar Flow in the Entry Region of a Circular Conduit: The development of fully-developed laminar flow in the circular conduit is analogous to that in the case of infinite parallel flat plates. The only exception is that the entry region in the circular conduit is three-dimensional since the walls wrap around the "undisturbed" region forming a "core" of accelerating flow that can be modeled as inviscid. For uniform velocity at the entrance to the conduit, the boundary layer at the wall starts to grow at the mouth and eventually fills the entire conduit as the flow progresses downstream a distance equal to the entry length, L_{entry}. Within this length, the "undisturbed" flow accelerates until the maximum value of the velocity given by equation

(9.135) is achieved at the centerline. According to Shah and London[3], the entry length data for laminar flow in a circular conduit can be best fit by the relation

$$\left(\frac{L_{entry}}{D_h}\right)_{laminar} = \frac{0.60}{0.035Re+1} + 0.056Re \tag{9.149}$$

Then for flow at the critical value of the Reynolds number, the entry length attains its largest value for laminar flow. Thus, fully-developed flow in a circular conduit occurs within a length of $L \leq 117.61D_h$ depending upon the Reynolds number. The[4] accelerating flow in the "undisturbed" core causes the pressure in the entry region to drop faster than it does in the fully-developed region. Using the dimensionless parameters given in equation (9.114), the dimensionless pressure drop is given by Shah and London[4] as

$$\left(\Delta P^*\right)_{\substack{fully \\ developed}} = 64x^+$$

$$\left(\Delta P^*\right)_{apparent} = 4x^+\left[\frac{3.44}{\sqrt{x^+}} + \frac{16+\frac{1.25}{4x^+}-\frac{3.44}{\sqrt{x^+}}}{1+2.1\text{ x }10^{-4}\left(x^+\right)^{-2}}\right] \tag{9.150}$$

Figure 9.18 shows the axial pressure distribution for a sample flow of water in a pipe with $Re = 2100$ according to equation (9.150).

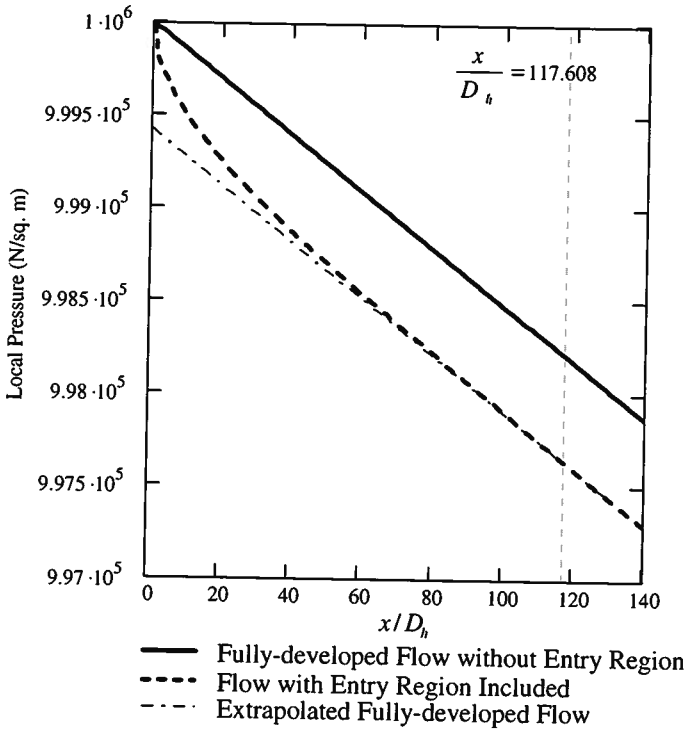

Figure 9.18 Axial Pressure Distribution for Flow of Water in a Pipe, $Re = 2100$

[3] R. K. Shah and A. L. London, *op. cit.*, p. 99.

[4] R. K. Shah and A. L. London, *op. cit.*, p. 98.

The pressure of the water at the inlet to the pipe is $P_{inlet} = 10^6$ N/m^2. The solid line shows the axial pressure distribution assuming fully-developed flow throughout the flow field with no entry region. The dashed line shows the pressure distribution with the effect of the entry region included. This is referred to as the apparent pressure drop. The vertical line indicates the location of the end of the entry region as defined by the full development of the velocity profile (L_{entry} = $117.608D_h$ for Re = 2100 for this flow configuration). Notice that the pressure with the entry region included is always lower than the pressure without the entry region taken into account. This is the case even though the pressure gradient is the same in both cases once the flow becomes fully developed. This is a result of the acceleration of the flow in the "undisturbed" region. Also notice that the pressure gradient becomes constant slightly before the velocity profile becomes fully developed with the entry region included. This is a consequence of the fact that the acceleration of the "undisturbed" region must be complete before the velocity profile can be fully established.

The difference between the extrapolation of the fully-developed flow and the flow in the entry region shows the rapid decrease in pressure due primarily to the acceleration of the "undisturbed" flow in the entry region. Comparing Figures 9.12 and 9.18 we see that the effect of the entry region on the local pressure is greater for the case of the flow in a pipe than for flow between infinite parallel flat plates. This is a manifestation of the three-dimensionality of the flow in the pipe. Equations (9.150) are plotted in Figure 9.19 for a flow with Re = 2100. The behavior of the data is similar to that for the case shown in Figure 9.13. The major difference is the magnitude of the effect of the entry region in the two cases.

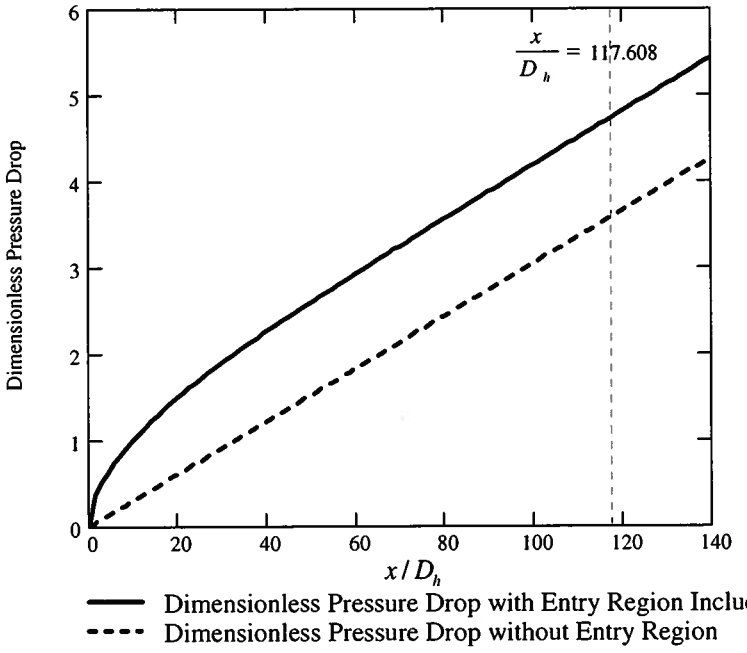

Figure 9.19 Pressure Drop for the Flow of a Viscous Fluid in a Pipe, Re = 2100

Example 9E.5: The fuel injection systems on Diesel engines operate at very high pressures since they inject the fuel directly into the cylinder when the pressure of the air inside the piston-cylinder is at or near its highest level before combustion. Typically the fuel pressure in these injection systems is on the order of 1.4 x 10^7 N/m^2 to 14.0 x 10^7 N/m^2. The fuel lines used

in these engines are relatively small compared to those in a gasoline engine. In a typical application, the fuel line diameter is on the order of $D = 5$ mm.

(a) If the length of the fuel line is on the order of $L = 1$ m, determine the pressure drop in the line if a typical average flow velocity is $\vartheta_{ave} = 1$ m/sec.

(b) Estimate the mass flow rate of diesel fuel resulting from this pressure drop.

The properties of No. 2 Diesel fuel are: $\rho = 920$ kg/m^3, $\mu = 3.96 \times 10^{-3}$ kg/m sec

Solution: (a) Typically in solving these types of problems we calculate the Reynolds number first. Then

$$Re = \frac{\rho \vartheta_{ave} D}{\mu} = \frac{(920 \text{ kg/m}^3)(1 \text{ m/sec})(5 \times 10^{-3} \text{ m})}{3.96 \times 10^{-3} \text{ kg/m sec}} = 1161.6$$

In this case the flow is clearly laminar. The entry length is

$$\frac{L_{entry}}{D} = \frac{0.60}{0.035Re + 1} + 0.056Re = \frac{0.60(1161.6)}{0.035(1161.6) + 1} + 0.056(1161.6) = 81.782$$

$$L_{entry} = 81.782D = 81.782(5 \times 10^{-3} \text{ m}) = 0.40891 \text{ m}$$

Thus, approximately 40 percent of the length of the fuel line is entry length; therefore, it will be necessary to account for entry region effects in computing the pressure drop. We then make use of equation (9.145).

$$(\Delta P^*)_{apparent} = 4x^+ \left[\frac{3.44}{\sqrt{x^+}} + \frac{16 + \frac{1.25}{4x^+} - \frac{3.44}{\sqrt{x^+}}}{1 + 2.1 \times 10^{-4} (x^+)^{-2}} \right]$$

where

$$x^+ = \frac{x}{D_h Re} = \frac{1 \text{ m}}{(0.005 \text{ m})(1161.6)} = 0.17217$$

Then

$$(\Delta P^*)_{apparent} = 4x^+ \left[\frac{3.44}{\sqrt{x^+}} + \frac{16 + \frac{1.25}{4x^+} - \frac{3.44}{\sqrt{x^+}}}{1 + 2.1 \times 10^{-4} (x^+)^{-2}} \right]$$

$$(\Delta P^*)_{apparent} = 4(0.172) \left[\frac{3.44}{\sqrt{0.172}} + \frac{16 + \frac{1.25}{4(0.172)} - \frac{3.44}{\sqrt{0.172}}}{1 + 2.1 \times 10^{-4} (0.172)^{-2}} \right] = 12.223$$

$$\Delta P = 12.223 \left(\frac{\rho \vartheta_{ave}^{\ 2}}{2} \right) = 12.223 \left[\frac{(920 \text{ kg/m}^3)(1 \text{ m/sec})^2}{2} \right] = 5.623 \times 10^3 \text{ N/m}^2$$

If we had assumed fully developed flow, the pressure drop we would have calculated would have been

$$(\Delta P^*)_{\substack{fully \\ developed}} = 64x^+ = 64(0.172) = 11.019$$

$$\Delta P_{\substack{fully \\ developed}} = 11.019 \left(\frac{\rho \vartheta_{ave}^{\ 2}}{2} \right) = 11.019 \left[\frac{(920 \text{ kg/m}^3)(1 \text{ m/sec})^2}{2} \right] = 5.069 \times 10^3 \text{ N/m}^2$$

Then the percent error in assuming fully-developed flow would have been

$$\text{Error} = \frac{5.623 - 5.069}{5.623}(100\%) = 9.86\%$$

In this case the fully-developed flow solution would have underestimated the pressure drop by nearly 10 percent. As we shall see in Section 9.9.2.1, there is a way of eliminating this error without resorting to the tedium inherent in equation (9.145).

(b) To estimate the mass flow rate we must recognize that the pressure drop including the entry effects is not the appropriate one to determine the volumetric flow rate since a portion of the pressure drop is associated with accelerating the "undisturbed" flow in the entry region and does not contribute to the volumetric flow rate in the sense of equation (9.131). Rather, we simply calculate the mass flow rate from the continuity equation. Then

$$\dot{m} = \rho A_c \vartheta_{ave} = \left(920 \text{ kg/m}^3\right)\left(\frac{\pi(0.005 \text{ m})^2}{4}\right)(1 \text{ m/sec}) = 0.0181 \text{ kg/sec}$$

Had we used equation (9.130), we would have obtained

$$\dot{V} = \frac{\pi R^4}{8\mu}\left(\frac{\partial P}{\partial z}\right) = \frac{\pi(0.005)^4}{128\left(3.96 \text{ x } 10^{-3} \text{ kg/m sec}\right)}\left(\frac{5.623 \text{ x } 10^3 \text{ N/m}^2}{1 \text{ m}}\right) = 2.1782 \text{ x } 10^{-5} \text{ m}^3\text{/sec}$$

$$\dot{m} = \rho\dot{V} = \left(920 \text{ kg/m}^3\right)\left(2.1782 \text{ x } 10^{-5} \text{ m}^3/\text{sec}\right) = 0.0200 \text{ kg/sec}$$

which would have overestimated the mass flow rate by approximately 11 percent. The correct result could have been obtained by applying equation (9.131) over that portion of the flow which was fully-developed (approximately the last 0.6 m).

Example 9E.6: In a classroom demonstration of fully-developed flow in a circular conduit, a student immerses a common drinking straw in a bottle of castor oil and fills the straw with castor oil by sucking on the end of it. By quickly placing her finger over the end of the straw, the student is able to hold the castor oil in the straw. The straw is then raised over the mouth of the bottle with its axis aligned vertically, and the finger is removed to allow the castor oil to drain from the straw back into the bottle. By measuring the amount of time required for the straw to empty, the student can actually determine the viscosity of the castor oil if the flow is indeed fully-developed.

(a) If the dimensions of the straw are D = 6 mm and L = 20 cm and the properties of castor oil are ρ = 956.1 kg/m^3 and μ = 0.650 kg/m sec, how long does it take to empty the straw of castor oil if the flow is fully-developed?

(b) Is the assumption of fully-developed flow justified?

Solution: (a) At first glance this would appear to be an unsteady flow situation since we are measuring the amount of time required to empty a control volume, the straw. However, because of the large viscosity of the castor oil, fully-developed steady laminar flow is established almost immediately upon removing the finger. To see that this is the case, first note that with the finger removed, the pressure acting on the oil trapped in the straw is the same at both ends of the straw, namely atmospheric pressure. Then there is no pressure gradient imposed on the flow. Now assume that the flow is indeed steady and solve the appropriate form of the Navier-Stokes equation, viz.

$$\rho\left(\cancel{\frac{\partial \vartheta_z}{\partial t}}+\cancel{\vartheta_r}\frac{\partial \vartheta_z}{\partial r}+\cancel{\frac{\vartheta_\theta}{r}}\cancel{\frac{\partial \vartheta_z}{\partial \theta}}-\cancel{\frac{\vartheta_\theta^2}{r}}+\vartheta_z\cancel{\frac{\partial \vartheta_z}{\partial z}}\right)$$

$$=-\cancel{\frac{\partial P}{\partial z}}+\rho g_z+\mu\left[\frac{1}{r}\frac{\partial}{\partial r}\left(r\frac{\partial \vartheta_z}{\partial r}\right)+\cancel{\frac{1}{r^2}\frac{\partial^2 \vartheta_z}{\partial \theta^2}}+\cancel{\frac{\partial^2 \vartheta_z}{\partial z^2}}\right]$$

$$-\rho g_z=\mu\left[\frac{1}{r}\frac{\partial}{\partial r}\left(r\frac{\partial \vartheta_z}{\partial r}\right)\right]$$

Since $g_z = -g$, the above equation says that in fully developed flow with straw aligned with the z-axis, the body force (per unit volume) due to gravity is just balanced by the viscous force (per unit volume). Notice that this expression is identical to equation (9.125c) except that the "pressure force" is now replaced by the body force. The process of integration is exactly the same, and we end up with an expression nearly identical to equation (9.129) except that the constant pressure gradient is now replaced by the constant body force per unit volume, namely

$$\vartheta_z=\frac{\rho g R^2}{4\mu}\left[1-\left(\frac{r}{R}\right)^2\right]$$

In a manner similar to equation (9.131), we have for the volumetric flow rate

$$\dot{V}=\frac{\pi R^4 \rho g}{8\mu}$$

Since the volumetric flow rate is constant, the amount of time Δt required to empty the straw is

$$\Delta t=\frac{V}{\dot{V}}=\frac{\pi R^2 L}{\pi R^4 \rho g/8\mu}=\frac{8\mu L}{\rho g R^2}=\frac{8(0.650\ \text{kg/m sec})(0.20\ \text{m})}{(956.1\ \text{kg/m}^3)(9.81\ \text{m/sec})(0.003\ \text{m})^2}=12.32\ \text{sec}$$

Thus the time interval is of such a magnitude that it could be measured easily in the classroom. The question remains, however, as to whether the flow is truly fully-developed.

(b) The average velocity for this flow is given by equation (9.132) with the replacement of the pressure gradient by the body force per unit volume.

$$\vartheta_{ave}=\frac{\rho g R^2}{8\mu}=\frac{(956.1\ \text{kg/m}^3)(9.81\ \text{m/sec}^2)(0.003\ \text{m})^2}{8(0.650\ \text{kg/m sec})}=1.6233\ \text{cm/sec}$$

The Reynolds number for this fully-developed laminar flow is then

$$Re=\frac{\rho \vartheta_{ave} D}{\mu}=\frac{(956.1\ \text{kg/m}^3)(0.016233\ \text{m/sec})(0.003\ \text{m})}{0.650\ \text{kg/m sec}}=0.0716$$

The flow is clearly laminar and the viscous forces dominate. The entry length for this flow is given by equation (9.144). Then

$$\frac{L_{entry}}{D_h}=\frac{0.60}{0.035Re+1}+0.056Re=\frac{0.60}{0.035(0.0716)+1}+0.056(0.0716)=0.603$$

$$L_{entry}=(0.603)(0.006\ \text{m})=3.62\ \text{x}\ 10^{-3}\ \text{m}=3.62\ \text{mm}$$

The entry length is only a small fraction (1.81 percent) of the total length of the straw (3.62 mm vs. 200 mm). The time required for the fluid to travel this distance is about 0.223 sec. Thus the flow does indeed become fully-developed relatively quickly, and this method could then be used to determine the viscosity of a highly viscous fluid like castor oil in the classroom.

Example 9E.7: A computer chip fabricated on a silicon substrate is cooled by passing water through many small square channels machined in parallel in the silicon. The channels are 1 mm on each side and are 20 cm long. The pressure drop for the water flowing in a typical channel is $\Delta P = 1.25 \times 10^3$ N/m^2. Determine the mass flow rate of the cooling water for this flow configuration. The thermal-fluid characteristics of water are: ρ=996 kg/m^3, $\mu = 8.67 \times 10^{-4}$ kg/m sec.

Solution: Normally the starting point in the solution is the calculation of the Reynolds number; however, in this case we are unable to do this because neither the velocity nor the mass flow rate are known. If we can determine the velocity, we can get the mass flow rate. Since L/D_h = 200, let us assume that the flow is fully developed and laminar. Then the pressure drop is given by

$$\Delta P = \rho f \left(\frac{L}{D_h}\right)\left(\frac{\vartheta_{ave}^{\,2}}{2}\right)$$

For a square channel D_h is the length of one side, and for fully developed laminar flow in a square channel, Table 9.3 gives

$$fRe_{D_h} = 56.91$$

$$f = \frac{56.91}{Re_{D_h}} = \frac{56.91\mu}{\rho \vartheta_{ave} D_h} = \frac{56.91\left(8.67 \times 10^{-4} \text{ kg/m sec}\right)}{\left(996 \text{ kg/m}^3\right)\left(0.001 \text{ m}\right)\vartheta_{ave}}$$

$$f = \frac{4.9539 \times 10^{-2}}{\vartheta_{ave}}$$

Then

$$\Delta P = \rho\left(\frac{0.049539 \text{ m/sec}}{\vartheta_{ave}}\right)\left(\frac{L}{D_h}\right)\left(\frac{\vartheta_{ave}^{\,2}}{2}\right)$$

$$\therefore \vartheta_{ave} = \frac{2D_h \Delta P}{\rho L(0.049539 \text{ m/sec})} = \frac{2\left(0.001 \text{ m}\right)\left(1.25 \times 10^3 \text{ N/m}^2\right)}{\left(996 \text{ kg/m}^3\right)\left(0.2 \text{ m}\right)\left(0.049539 \text{ m/sec}\right)}$$

$$\vartheta_{ave} = 0.1588 \text{ m/sec}$$

Then the Reynolds number is

$$Re_{D_h} = \frac{\rho \vartheta_{ave} D_h}{\mu} = \frac{\left(996 \text{ kg/m}^3\right)\left(0.1588 \text{ m/sec}\right)\left(0.001 \text{ m}\right)}{8.67 \times 10^{-4} \text{ kg/m sec}} = 181.89$$

The flow is clearly laminar. If we assume that the entry length is on the same order as that for a circular conduit at the same Reynolds number, we have

$$\frac{L_{entry}}{D_h} \approx \frac{0.60}{0.035Re + 1} + 0.056Re = \frac{0.60}{0.035\left(181.89\right) + 1} + 0.056\left(181.89\right) = 10.195$$

Thus the entry length is only 5 percent of the length of the channel, and the assumption of fully developed flow for this case is a reasonable one. Then the mass flow rate of cooling water is

$$\dot{m} = \rho A_c \vartheta_{ave} = \left(996 \text{ kg/m}^3\right)\left(0.001 \text{ m}\right)^2\left(0.1588 \text{ m/sec}\right) = 1.577 \text{ kg/sec}$$

9.9.2 Laminar External Flows

Unlike internal flows, external flows never become fully developed in the sense that the effects of the fluid viscosity are dominant throughout the entire flow geometry as they are in the case of an internal flow, e.g., fully-developed laminar flow in a pipe. In these external flows, the effects of viscosity are confined to small regions near the solid surfaces that bound the flow. These "boundary layers" continue to develop and grow in thickness as the flow proceeds downstream but they never really extend throughout the entire flow field. This means that the nonlinear acceleration terms appearing in the Navier-Stokes equation cannot be neglected as they were for internal flows. Furthermore, within these boundary layers, the fluid velocity changes rapidly in a direction normal to the surface, from zero at the surface to the free-stream value at the outer edge of the boundary layer. This velocity gradient may produce a steep gradient in the shear stress in the fluid. As a result, some of the viscous terms are equally as important as the acceleration terms. Because of the presence of these viscous terms as well as the nonlinear acceleration terms, the solution of the Navier-Stokes equation becomes even more challenging for external flows than it was for internal flows.

The notion that the effects of fluid viscosity can be modeled as being localized to this small region known as the boundary layer was a novel one introduced by Ludwig Prandtl (1875 - 1953) in 1904 and implemented for flow over a flat plate by his student H. Blasius (1883 - 1970) in 1908. For external flows, the introduction of the boundary layer concept represented a major breakthrough that facilitated widespread advances in understanding the effects of fluid viscosity on flow over all sorts of solid bodies.

In the typical external flow situation, a solid body, such as an aircraft or a ship, is moving relative to a fluid which may have a motion of its own. This motion of the fluid in the boundary layers adjacent to the solid surfaces can be described by the Navier-Stokes equation. Outside the boundary layers where the fluid viscosity has no influence on fluid motion, the fluid behaves as though it were inviscid. In this region, the flow can be described by the Euler equation. In the boundary layer, however, the action of fluid viscosity on the solid body results in a velocity gradient in the fluid due to the "no-slip" boundary condition of the Navier-Stokes equation. The net result of this velocity gradient and the action of fluid viscosity leads to a shear stress imposed on the solid surface by the fluid. This shear stress integrated over the surface of the body results in a viscous "drag" force, sometimes called "skin-friction drag," that tends to slow the movement of the body as momentum is transferred from the body to the fluid through this action of viscosity. Initially, the flow in this boundary layer is laminar, but as the boundary layer grows in thickness in the direction of flow, it becomes unstable and the flow undergoes a transition from laminar to turbulent flow. Depending upon the shape of the body, the flow may eventually separate from the body, producing a region of reverse flow or of stagnant fluid. Downstream of this region there is a relatively large "wake" of "disturbed" flow that results in further momentum transfer between the body and the fluid. This produces an additional component of drag known as "profile" drag or "wake" drag. At this point in our development of the subject, we are going to focus on the skin friction drag.

Our approach is to first divide the flow into two regions: (1) the boundary layer flow near the surface of the body where all the viscous effects are confined and (2) the inviscid flow in the free stream outside the boundary layer remote from the surface of the body. We then develop special forms of the components of the Navier-Stokes equation called the boundary layer equations, that apply in the boundary layer. The solution of the boundary layer equations provides us with the velocity profile of the fluid in the boundary layer. From the velocity profile

we can determine the shear stress at the surface of the body, and hence, the skin friction component of the drag on the body. We then determine the shape of the boundary layer so that we can solve the Euler equation for the inviscid flow outside the boundary layer.

In the process of developing the solution for the velocity profile in the boundary layer, we will match the velocity at the outer edge of the boundary layer to the fluid velocity in the mainstream. This is problematic on two counts: (1) we do not really know the location of the outer edge of the boundary layer, and (2) we do not really know the mainstream velocity. In order to resolve this dilemma, we assume that the mainstream velocity is unaffected by the presence of the boundary layer, and we apply this boundary condition by requiring the velocities in the two regions match as the boundary layer thickness becomes infinite. After obtaining the solution for the velocity profile in the boundary layer, we then arbitrarily define the outer limit of the boundary layer as the location at which the fluid velocity in the boundary layer attains 99 percent of the mainstream velocity; however, there is no physical basis for this definition and this choice is arbitrary. We could have just as easily used 95 percent or 90 percent as our definition.

This presents a difficulty when we attempt, after the fact, to determine the effect of the boundary layer on the inviscid flow outside of it by solving the Euler equation in the mainstream. We do not really know the location of the inner boundary of the mainstream. However, closer examination of the physics of the flow in the boundary layer reveals that the retardation of the flow in the boundary layer has the same effect as if we had displaced the streamlines in the mainstream outwardly from the surface of the body by an amount δ^* known as the *displacement thickness* which is related to the boundary layer thickness δ. This displacement, which is a function of x, in turn affects the local velocity and the local pressure in the mainstream since the streamlines are no longer straight but now have some curvature. Thus the inviscid flow in the mainstream "sees" the body *and* the attached boundary layer as a solid streamlined body. Then knowing this displacement thickness, we can determine the flow field around this "streamline body" by solving the Euler equation. We shall demonstrate this approach by considering the example of the flow of a viscous fluid over a flat plate, but first we must develop the boundary layer equations.

9.9.2.1 The Boundary Layer Equations: By its very nature, in its simplest form the boundary layer is a two-dimensional phenomenon. The fluid is flowing in one direction, say the x-direction, and the gradients in velocity and shear stress are occurring in a direction normal to this, say the y-direction. In the laminar boundary layer, the Reynolds number is large but not infinite. Our approach will be to use this fact to simplify the Navier-Stokes equation so that we might develop a solution that describes this two-dimensional situation.

In two-dimensions, the continuity equation and the Navier-Stokes equation in Cartesian coordinates become

$$\frac{\partial \vartheta_x}{\partial x}+\frac{\partial \vartheta_y}{\partial y}=0 \tag{9.151}$$

and

$$\rho\left(\frac{\partial \vartheta_x}{\partial t}+\vartheta_x\frac{\partial \vartheta_x}{\partial x}+\vartheta_y\frac{\partial \vartheta_x}{\partial y}\right)=-\frac{\partial P}{\partial x}+\mu\left(\frac{\partial^2 \vartheta_x}{\partial x^2}+\frac{\partial^2 \vartheta_x}{\partial y^2}\right) \tag{9.152}$$

$$\rho\left(\frac{\partial \vartheta_y}{\partial t}+\vartheta_x\frac{\partial \vartheta_y}{\partial x}+\vartheta_y\frac{\partial \vartheta_y}{\partial y}\right)=-\frac{\partial P}{\partial y}+\mu\left(\frac{\partial^2 \vartheta_y}{\partial x^2}+\frac{\partial^2 \vartheta_y}{\partial y^2}\right) \tag{9.153}$$

respectively, where we have neglected the effect of the gravity body force. (In Chapter 11 we shall see how to deal with this effect.) Let us now non-dimensionalize these three equations in a way that displays the Reynolds number explicitly since the Reynolds number quantitates the relative importance of inertial and viscous effects which are both present in the boundary layer. We can do this by introducing dimensionless parameters in a manner similar to equation (9.85). If L is a characteristic length, ϑ_0 a typical speed, and $Re = \rho L \vartheta_0 / \mu$ the corresponding Reynolds number for the flow as a whole, we can introduce the following set of dimensionless parameters:

$$x^* = \frac{x}{L} \qquad y^* = \frac{y\sqrt{Re}}{L} \qquad t^* = \frac{\vartheta_0 t}{L}$$
$$\vartheta_x^* = \frac{\vartheta_x}{\vartheta_0} \qquad \vartheta_y^* = \frac{\vartheta_y \sqrt{Re}}{\vartheta_0} \qquad P^* = \frac{P}{\rho \vartheta_0^2} \tag{9.154}$$

If we substitute equations (9.154) into equation (9.151), we get the non-dimensional continuity equation, viz.

$$\frac{\partial \vartheta_x^*}{\partial x^*} + \frac{\partial \vartheta_y^*}{\partial y^*} = 0 \tag{9.155}$$

If we substitute equations (9.154) into equations (9.152) and (9.153), we get the component Navier-Stokes equations in non-dimensional form, viz.

$$\frac{\partial \vartheta_x^*}{\partial t^*} + \vartheta_x^* \frac{\partial \vartheta_x^*}{\partial x^*} + \vartheta_y^* \frac{\partial \vartheta_x^*}{\partial y^*} = -\frac{\partial P^*}{\partial x^*} + \frac{1}{Re}\frac{\partial^2 \vartheta_x^*}{\partial x^{*2}} + \frac{\partial^2 \vartheta_x^*}{\partial y^{*2}} \tag{9.156}$$

$$\frac{1}{Re}\left(\frac{\partial \vartheta_y^*}{\partial t^*} + \vartheta_x^* \frac{\partial \vartheta_y^*}{\partial x^*} + \vartheta_y^* \frac{\partial \vartheta_y^*}{\partial y^*}\right) = -\frac{\partial P^*}{\partial y^*} + \frac{1}{Re^2}\frac{\partial^2 \vartheta_y^*}{\partial x^{*2}} + \frac{1}{Re}\frac{\partial^2 \vartheta_y^*}{\partial y^{*2}} \tag{9.157}$$

We now assume that all the derivatives in equations (9.155) through (9.157) are of the same order of magnitude. For the case in which the inertial effects are relatively more important than the viscous effects, the values of Re are large and the limiting forms of equations (9.155) through (9.157) are

$$\frac{\partial \vartheta_x^*}{\partial x^*} + \frac{\partial \vartheta_y^*}{\partial y^*} = 0 \tag{9.153}$$

and

$$\frac{\partial \vartheta_x^*}{\partial t^*} + \vartheta_x^* \frac{\partial \vartheta_x^*}{\partial x^*} + \vartheta_y^* \frac{\partial \vartheta_x^*}{\partial y^*} = -\frac{\partial P^*}{\partial x^*} + \frac{\partial^2 \vartheta_x^*}{\partial y^{*2}} \tag{9.154}$$

$$0 = -\frac{\partial P^*}{\partial y^*}$$

If we now transform these equations back to their dimensional form, we get the boundary layer equations in two dimensions, viz.

$$\frac{\partial \vartheta_x}{\partial x} + \frac{\partial \vartheta_y}{\partial y} = 0 \tag{9.160}$$

$$\rho\left(\frac{\partial \vartheta_x}{\partial t} + \vartheta_x \frac{\partial \vartheta_x}{\partial x} + \vartheta_y \frac{\partial \vartheta_x}{\partial y}\right) = -\frac{\partial P}{\partial x} + \mu \frac{\partial^2 \vartheta_x}{\partial y^2} \tag{9.161}$$

$$0 = -\frac{\partial P}{\partial y} \tag{9.162}$$

Equation (9.162) simply says that the pressure in the boundary layer is uniform at the value in the mainstream flow across each plane x = constant, but not necessarily constant in the direction of flow. It is really equations (9.160) and (9.161) that need to be solved subject to the boundary conditions at the surface $y = 0$

$$\begin{aligned} \vartheta_x &= 0 \quad \text{(no slip boundary condition)} \\ \vartheta_y &= 0 \quad \text{(no flow through the wall boundary condition)} \end{aligned} \tag{9.163}$$

It follows that at the wall, we also have

$$\frac{\partial \vartheta_x}{\partial x} = 0 \qquad \text{and} \qquad \frac{\partial \vartheta_y}{\partial x} = 0 \tag{9.164}$$

At the other extreme, the boundary layer must join the main flow smoothly. The nature of the solutions of the boundary layer equations is such that the mainstream flow is considered to be at infinity. Then

$$\vartheta_x \to \vartheta_0(x) \qquad \text{as} \qquad y \to \infty \tag{9.165}$$

where $\vartheta_0(x)$ is the velocity in the main flow and is in general dependent upon the location x.

The solution of equations (9.160) through (9.162) together with boundary conditions (9.163) through (9.165) provide a description of the flow in a laminar boundary layer. The solutions derived for these equations are not unique in general and may actually provide values of ϑ_y away from the surface that are not physically meaningful. Nevertheless, the solutions of these equations, whose accuracy in many cases varies depending upon the location along the direction of flow, have provided considerable insight into the nature of boundary layer flows. We shall now consider one of these, namely laminar flow over a flat plate, in detail.

9.9.2.2 Laminar Flow Over a Flat Plate: In what has become the classic example of the application of the boundary layer equations, H. Blasius treated the case of steady laminar flow over a flat plate in the absence of a pressure gradient. The fact that the pressure gradient is zero in the boundary layer can be seen by applying the Bernoulli equation in the mainstream flow and invoking equation (9.162). As shown in Figure 9.20, in Blasius's treatment, the flat plate is immersed in a uniform flow of a fluid with constant thermal-fluid properties.

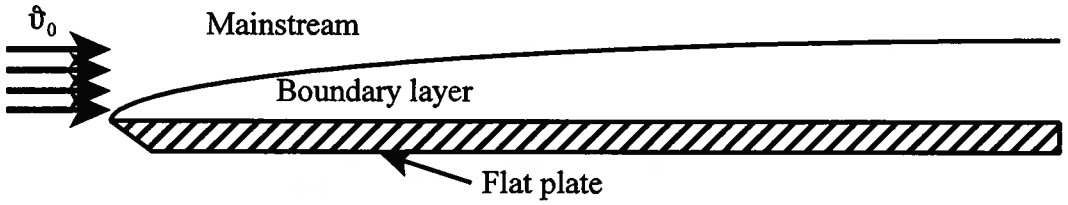

Figure 9.20 Uniform Flow Over a Flat Plate

The uniform velocity is ϑ_0, the density of the fluid is ρ, and the viscosity of the fluid is μ. Under these conditions, the boundary layer equations become

$$\frac{\partial \vartheta_x}{\partial x} + \frac{\partial \vartheta_y}{\partial y} = 0 \tag{9.166}$$

$$\vartheta_x \frac{\partial \vartheta_x}{\partial x} + \vartheta_y \frac{\partial \vartheta_x}{\partial y} = \frac{\mu}{\rho} \frac{\partial^2 \vartheta_x}{\partial y^2} \tag{9.167}$$

In equation (9.167), the term μ/ρ is given a special name, the *kinematic viscosity*. As we shall soon see, this ratio, represented by the symbol ν, plays precisely the same role in momentum transfer that the thermal diffusivity $\alpha = k/\rho c$ plays in heat transfer. Physically, the kinematic viscosity $\nu = \mu/\rho$ is the momentum diffusivity of the fluid and has the units of m^2/sec.

In an attempt to simplify equations (9.166) and (9.167) mathematically, Blasius proposed a coordinate transformation that would reduce these two partial differential equations to a single ordinary differential equation. Prior to Blasius's time, the dynamical behavior of the inviscid model had received extensive study from a mathematical point of view. One of the mathematical techniques used was based upon the premise that there exists a single function, ψ, called the stream function, that satisfies the continuity equation, equation (9.167), exactly if defined properly. If we define the velocity components in the x- and y-directions in the following manner,

$$\vartheta_x \equiv \frac{\partial \psi}{\partial y} \qquad \text{and} \qquad \vartheta_y \equiv -\frac{\partial \psi}{\partial x} \tag{9.168}$$

then it follows that equation (9.167) is satisfied exactly. Blasius adopted this approach and then argued that the velocity profile in the boundary layer should have the same shape at every position x provided it is scaled in some appropriate manner to account for the fact that the boundary layer is growing in thickness as the fluid moves down the plate. That is, the velocity profile is similar at all locations along the plate.

If this is the case, we should be able to express the velocity profile in terms of a dimensionless similarity parameter η that would have the proper scaling built into it. Blasius proposed that the velocity profile in dimensionless form should be a function of this parameter η and that the similarity parameter should be related to the thickness of the boundary layer δ also in dimensionless form. That is,

$$\frac{\vartheta_x}{\vartheta_0} = f'(\eta) \qquad \text{and} \qquad \eta \propto \frac{\delta}{y} \tag{9.169}$$

where f' is the first derivative of a function f. Clearly, from equation (9.169) it follows that the function f is the dimensionless form of the stream function. The reason that the derivative is used instead of the function itself is that the velocity is expressed as a derivative of a stream function in equation (9.168).

Based upon an idea proposed by Stokes in 1851, Blasius argued that the boundary layer thickness should grow like the square root of the position x. Then, in dimensionless form we have

$$\frac{\delta}{x} \propto \frac{1}{\sqrt{Re_x}} \tag{9.170}$$

Then from equation(9.169), the similarity parameter should be of the form

$$\eta = y\sqrt{\frac{\vartheta_0 \rho}{\mu x}} = y\sqrt{\frac{\vartheta_0}{\nu x}} \tag{9.171}$$

Blasius then combined the notion of a stream function as presented in equation (9.168) with his proposed similarity parameter to get the dimensionless stream function, viz.

$$f(\eta) = \frac{\psi}{\sqrt{\nu x \vartheta_0}} \tag{9.172}$$

By formulating the function f in this manner, Blasius was able to get the velocity profile in dimensionless form as he had proposed in equation (9.171), viz.

$$\vartheta_x = \frac{\partial \psi}{\partial y} = \frac{\partial \psi}{\partial \eta}\frac{\partial \eta}{\partial y} = \frac{\partial \psi}{\partial f}\frac{df}{d\eta}\frac{\partial \eta}{\partial y} = \sqrt{\nu x \vartheta_0}\frac{df}{d\eta}\sqrt{\frac{\vartheta_0}{\nu x}} = \vartheta_0 \frac{df}{d\eta}$$
$$\therefore \frac{\vartheta_x}{\vartheta_0} = f'(\eta) \tag{9.173}$$

For the y-component of velocity, we have

$$\vartheta_y = -\frac{\partial \psi}{\partial x} = -\left[\sqrt{\nu x \vartheta_0}\,\frac{\partial f}{\partial x} + \frac{1}{2}\sqrt{\frac{\nu \vartheta_0}{x}}\,f\right] = -\left[\sqrt{\nu x \vartheta_0}\,\frac{df}{d\eta}\left(-\frac{1}{2}\eta\frac{1}{x}\right) + \frac{1}{2}\sqrt{\frac{\nu \vartheta_0}{x}}\,f\right]$$

$$\vartheta_y = \frac{1}{2}\sqrt{\frac{\nu \vartheta_0}{x}}\left[\eta\frac{df}{d\eta} - f\right] \tag{9.174}$$

$$\therefore \frac{\vartheta_y}{\vartheta_0} = \frac{1}{2}\frac{\left[\eta f'(\eta) - f(\eta)\right]}{\sqrt{Re_x}}$$

From equations (9.173) and (9.174), we can form the partial derivatives appearing in equation (9.167). Then

$$\frac{\partial \vartheta_x}{\partial x} = -\frac{\vartheta_0}{2x}\eta\frac{d^2 f}{d\eta^2} = -\frac{\vartheta_0}{2x}\eta f''$$

$$\frac{\partial \vartheta_x}{\partial y} = \vartheta_0\sqrt{\frac{\vartheta_0}{\nu x}}\frac{d^2 f}{d\eta^2} = \vartheta_0\sqrt{\frac{\vartheta_0}{\nu x}}f'' \tag{9.175}$$

$$\frac{\partial^2 \vartheta_x}{\partial y^2} = \frac{\vartheta_0^2}{\nu x}\frac{d^3 f}{d\eta^3} = \frac{\vartheta_0^2}{\nu x}f'''$$

and equation (9.167) becomes

$$2\frac{d^3 f}{d\eta^3} + f\frac{d^2 f}{d\eta^2} = 2f''' + ff'' = 0 \tag{9.176}$$

with boundary conditions

$$\begin{aligned} &(1) \quad f = 0 \quad \text{at} \quad \eta = 0 \\ &(2) \quad \frac{df}{d\eta} = f' = 0 \quad \text{at} \quad \eta = 0 \\ &(3) \quad \frac{df}{d\eta} = f' \to 1 \quad \text{as} \quad \eta \to \infty \end{aligned} \tag{9.177}$$

Given the nonlinear nature of equation (9.176), Blasius expended considerable effort to devise a method to solve it. His method involved formulating infinite series that were evaluated using a recursive scheme. Today, equation (9.176) can be solved numerically rather easily to yield the results shown in Table 9.4. The resulting velocity profile is plotted in Figure 9.21.

There remains the matter of determining the boundary layer thickness from these results. Establishing the outer limit of the boundary layer is a bit ambiguous since the velocity of the fluid in the boundary layer approaches the mainstream value in asymptotic fashion. By convention, we arbitrarily define the boundary layer thickness to be the value of y for which the velocity attains a value equal to 99 percent of the value in the mainstream. Then from Table 9.4, we have

$$\frac{\vartheta_x}{\vartheta_0} = f' = 0.99 \qquad \text{at} \qquad \eta = 4.9 \tag{9.178}$$

Table 9.4 BLASIUS SOLUTION FOR FLOW OVER FLAT PLATE

η	f	f'	f''
0	0	0	0.33216
0.1	1.66077E-3	0.03322	0.33215
0.2	6.64296E-3	0.06643	0.33208
0.3	0.01495	0.09963	0.33191
0.4	0.02657	0.13280	0.33157
0.5	0.04151	0.16593	0.33101
0.6	0.05975	0.19900	0.33018
0.7	0.08130	0.23196	0.32902
0.8	0.10614	0.26479	0.32748
0.9	0.13425	0.29744	0.32553
1.0	0.16562	0.32988	0.32310
1.1	0.20022	0.36204	0.32016
1.2	0.23802	0.39389	0.31668
1.3	0.27898	0.42536	0.31262
1.4	0.32308	0.45639	0.30795
1.5	0.37025	0.48693	0.30266
1.6	0.42044	0.51690	0.29674
1.7	0.47361	0.54626	0.29019
1.8	0.52967	0.57492	0.28300
1.9	0.58857	0.60284	0.27520
2.0	0.65021	0.62994	0.26681
2.1	0.71453	0.65618	0.25787
2.2	0.78142	0.68150	0.24840
2.3	0.85079	0.70585	0.23847
2.4	0.92255	0.72918	0.22813
2.5	0.99659	0.75146	0.21745
2.6	1.07281	0.77266	0.20649
2.7	1.15109	0.79275	0.19532
2.8	1.23132	0.81172	0.18403
2.9	1.31339	0.82956	0.17269
3.0	1.39719	0.84626	0.16137
3.1	1.48261	0.86183	0.15017
3.2	1.56952	0.87630	0.13913
3.3	1.65783	0.88967	0.12835
3.4	1.74742	0.90198	0.11788
3.5	1.83819	0.91326	0.10777
3.6	1.93004	0.92355	0.09808
3.7	2.02287	0.93289	0.08885
3.8	2.11659	0.94133	0.08012
3.9	2.21111	0.94893	0.07190
4.0	2.30635	0.95573	0.06422
4.1	2.40223	0.96179	0.05709
4.2	2.49868	0.96717	0.05051
4.3	2.59564	0.97191	0.04447
4.4	2.69305	0.97608	0.03896
4.5	2.79084	0.97972	0.03397
4.6	2.88897	0.98289	0.02947
4.7	2.98740	0.98563	0.02545
4.8	3.08609	0.98799	0.02186
4.9	3.18499	0.99002	0.01869
5.0	3.28408	0.99174	0.01590

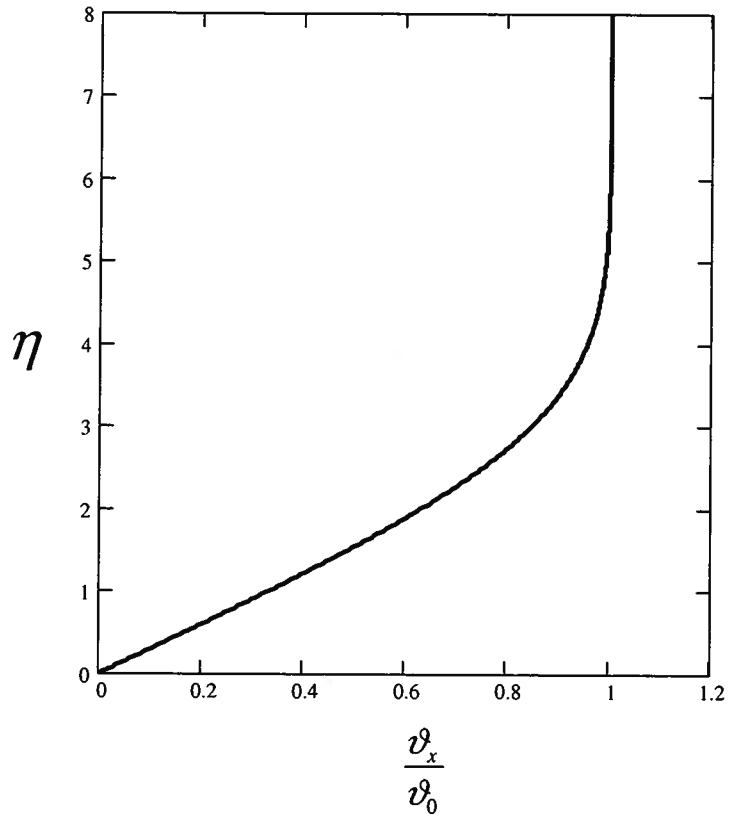

Figure 9.21 Boundary Layer Velocity Profile for a Flat Plate Due to Blasius

Then

$$\eta_{y=\delta} = \delta\sqrt{\frac{\vartheta_0}{\nu x}} = 4.9$$
$$\frac{\delta}{x} = \frac{4.9}{\sqrt{Re_x}} \tag{9.179}$$

where $Re_x = \vartheta_0 x/\nu$ is the local Reynolds number and x is measured from the leading edge of the plate. From equation (9.179) it is apparent that the laminar boundary layer thickness increases as the square root of x.

Our original motivation for studying the laminar boundary layer on a flat plate was to determine the drag force due to skin friction. To this end we compute the shear stress at the wall, τ_w where

$$\tau_w = \mu\left(\frac{\partial \vartheta_x}{\partial y}\right)_{y=0} = \mu\vartheta_0\sqrt{\frac{\vartheta_0}{\nu x}}\left(\frac{d^2 f}{d\eta^2}\right)_{\eta=0} = \mu\vartheta_0\sqrt{\frac{\vartheta_0}{\nu x}}f''_{\eta=0} \tag{9.180}$$

Using the data from Table 9.4, we get

$$\tau_w = 0.332\vartheta_0\sqrt{\frac{\rho\mu^2\vartheta_0}{\mu x}} = \frac{0.332\rho\vartheta_0^2}{\sqrt{Re_x}} \tag{9.181}$$

If we define the friction coefficient, C_f, as

$$C_f \equiv \frac{\tau_w}{\frac{1}{2}\rho\vartheta_0^2} \tag{9.182}$$

the Blasius solution for the flat plate in laminar flow gives

$$C_f = \frac{0.664}{\sqrt{Re_x}} \tag{9.183}$$

For flow on one side of the flat plate, the drag force for a plate of width b and length L is given by

$$F_D = b\int_0^L \tau_w dx = 0.332 b\rho v_0^2 \sqrt{\frac{\mu}{\rho v_0}} \int_0^L \frac{dx}{\sqrt{x}}$$
$$F_D = 0.664 b v_0 \sqrt{\rho \mu v_0 L} \tag{9.184}$$

The drag coefficient, C_D, for one side of the plate is

$$C_D \equiv \frac{F_D}{\frac{1}{2}\rho v_0^2 bL} = \frac{0.664 b v_0 \sqrt{\rho \mu v_0 L}}{\frac{1}{2}\rho v_0^2 bL} = \frac{1.328}{\sqrt{\frac{\rho v_0 L}{\mu}}} = \frac{1.328}{\sqrt{Re_L}} \tag{9.185}$$

All of the results above apply only so long as the flow remains laminar, but unfortunately none of these results tells us when the boundary layer becomes turbulent. For this information, we have to rely upon experimental measurements. These experiments show that there is no specific value of the local Reynolds number, Re_x, at which the transition from laminar to turbulent flow occurs. The data show that the boundary layer on a flat plate in a uniform flow starts out laminar and remains laminar as the flow proceeds down the plate up to a critical value of the local Reynolds number, $Re_{x,critical}$, that depends upon the particular flow situation. In a "very rough" flow $Re_{x,critical}$ can be as small as 8×10^4 whereas in a "very smooth" flow $Re_{x,critical}$ can be as large as 3×10^6. For design purposes, $Re_{x,critical}$ is usually taken to be 5×10^5.

As we shall see, the results above can be applied to many situations in thermal-fluids engineering for which the surfaces can be modeled as flat plates. However, in doing so, we must be mindful of the conditions under which they were formulated. First, in deriving the boundary layer equations, we non-dimensionalized the component Navier-Stokes equations and then neglected certain terms that contained the reciprocal of the Reynolds number. This is valid only insofar as the Reynolds number is large; however, we saw in equations (9.179), (9.181) and (9.183) that the appropriate value of the Reynolds number for these correlations is the *local* Reynolds number for which the appropriate characteristic length is the distance from the leading edge of the plate. Thus, in the neighborhood of the leading edge, this value of the Reynolds number is not large and the Blasius solution is no longer valid in this region because the boundary layer equations on which it is based do not contain the appropriate terms. (This issue has been subsequently addressed in the thermal-fluids engineering literature.) On the other hand, as the flow progresses downstream, the value of x increases, and we can expect the Blasius solution to become more accurate as long as the flow remains laminar.

Second, in postulating a similarity solution, we implicitly assume that the plate extends to infinity in the positive x-direction. If this were not the case and the plate were of finite length L, the trailing edge of the plate would cause a disturbance in the flow that would propagate upstream at the speed of sound by means of pressure waves. The net result would be a change in the velocity profile within the boundary layer that would cause it to be no longer a "similar"one that maintains a fixed shape throughout the length of the plate (assuming that the flow is laminar everywhere). Thus, strictly speaking, the Blasius solution does not apply to a plate of finite length. It is necessary in this case to introduce a set of boundary conditions that apply specifically

to the trailing edge. However, despite this limitation, the Blasius solution in the form of equation (9.184) does provide an estimate of the drag force due to skin friction on one side of the plate. In fact, experimental evidence confirms the validity of equations (9.184) and (9.185) for a plate of length L.

Finally, now that we have obtained a description of the boundary layer, we need to examine our assumption that the uniform flow in the mainstream is not affected by the presence of the boundary layer. This requires a determination of the displacement thickness.

9.9.2.3 The Displacement Thickness: As we have just seen, one of the ways that the boundary layer affects the mainstream flow is the way it affects the continuity of the flow. To see this consider the control volume shown in Figure 9.22. The dimension of the control volume in

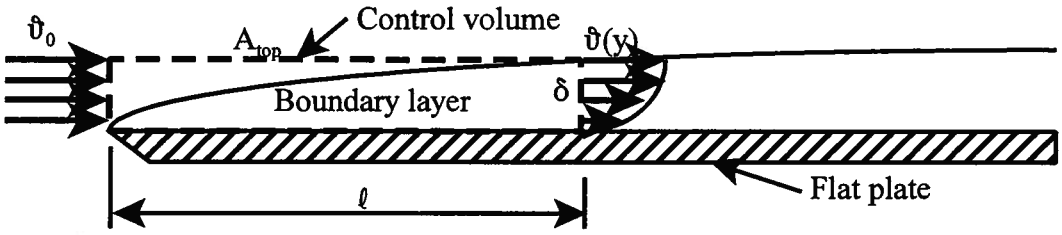

Figure 9.22 Boundary Layer Control Volume

the y-direction is δ and b in the z-direction normal to the plane of Figure 9.22. The fluid velocity entering the control volume is uniform with a value of ϑ_0 and that leaving the control volume is the boundary layer velocity profile shown in Figure 9.21. If we apply continuity in the x-direction we have for the entry and exit planes, respectively

$$\begin{aligned} \dot{m}_{entry} &= \rho b \delta \vartheta_0 \\ \dot{m}_{exit} &= \rho b \int_0^\delta \vartheta_x(y)\, dy \end{aligned} \tag{9.186}$$

Then combining these two expressions we have

$$\dot{m}_{entry} - \dot{m}_{exit} = \rho b \int_0^\delta (\vartheta_0 - \vartheta_x)\, dy > 0 \tag{9.187}$$

since $\vartheta_0 > \vartheta_x$ everywhere in the boundary layer except at the outer edge. Then in order to satisfy continuity, it must be the case that there is some mass flowing through the top area of the control volume, A_{top}. If we had instead selected a streamline as the top boundary of the control volume, there would be no mass flow through this boundary since by definition a streamline is everywhere tangent to the fluid velocity. As shown in Figure 9.23, consider a location L downstream from the leading edge of the plate.

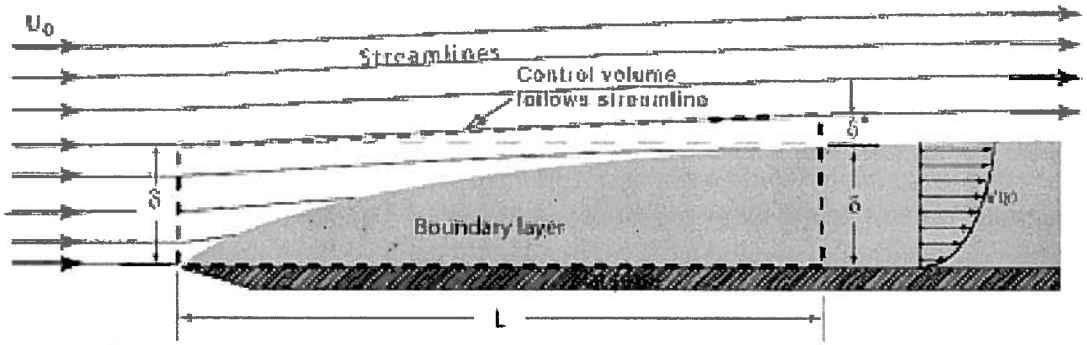

Figure 9.23 Boundary Layer Control Volume

At this location, the boundary layer thickness is δ. At the leading edge, we select a streamline offset from the surface of the plate by a distance δ. At the distance L downstream from the leading edge, this streamline will be displaced from the edge of the boundary layer by an amount δ^*. We now consider the control volume shown in Figure 9.23. Notice that the entry plane extends a considerable distance beyond the boundary layer at the leading edge itself since the Blasius solution is not valid there and hence, we could not define the boundary layer thickness at the leading edge. Then if we apply continuity to this new control volume, we have

$$\begin{aligned} \dot{m}_{in} &= \rho b \delta \vartheta_0 \\ \dot{m}_{out} &= \int_0^{\delta+\delta^*} \vartheta_x(y)\,dy \\ \dot{m}_{in} &= \dot{m}_{out} \end{aligned} \tag{9.188}$$

Evaluating the integrals of equation (9.188), we get

$$\rho b \delta \vartheta_0 = \rho b \int_0^{\delta+\delta^*} \vartheta_x(y)\,dy = \rho b \int_0^{\delta} \vartheta_x(y)\,dy + \rho b \vartheta_0 \int_{\delta}^{\delta+\delta^*} dy$$

$$\rho b \delta \vartheta_0 = \rho b \vartheta_0 \int_0^{\delta} dy = \rho b \int_0^{\delta} \vartheta_x(y)\,dy + \rho b \vartheta_0 \delta^*$$

$$\rho b \vartheta_0 \delta^* = \rho b \vartheta_0 \int_0^{\delta} \left(1 - \frac{\vartheta_x}{\vartheta_0}\right) dy \tag{9.189}$$

$$\delta^* = \int_0^{\delta} \left(1 - \frac{\vartheta_x}{\vartheta_0}\right) dy$$

Physically, the displacement thickness represents the extent of the influence of the viscosity as far as the mass flow rate is concerned. Outside the distance δ^* from the surface of the plate, the flow can be modeled as inviscid as far as mass flow rate is concerned. This distance is a physically meaningful, but not unique, boundary layer thickness. If we substitute the Blasius solution into equation (9.189), we get

$$\delta^* = \int_0^{\infty} \left(1 - \frac{\vartheta_x}{\vartheta_0}\right) dy = \sqrt{\frac{\nu x}{\vartheta_0}} \int_0^{\infty} (1 - f')\,d\eta$$

$$\delta^* = \sqrt{\frac{\nu x}{\vartheta_0}} \lim_{\eta \to \infty} (\eta - f) \tag{9.190}$$

$$\delta^* = 1.719 \sqrt{\frac{\nu x}{\vartheta_0}}$$

where we have extended the upper limit on the integration to infinity since the outer edge of the boundary layer is located there in the Blasius solution. Equation (9.190) can be cast in the same form as equation (9.179) in order to reveal the relative magnitudes of the conventional boundary layer thickness and the displacement thickness.

$$\frac{\delta^*}{x} = \frac{1.719}{\sqrt{Re_x}} \tag{9.191a}$$

Thus the displacement thickness also grows as the square root of x, and for the Blasius solution

$$\delta = 2.85\,\delta^* \tag{9.191b}$$

so that the boundary layer thickness is much greater than the displacement thickness.

Example 9E.8: As shown in Figure 9E.8, air at a temperature of T_{in} = 20 C and a pressure of $P_{in} = 10^5$ N/m^2 enters the space between two infinite parallel plates separated by a distance of $2a$ = 20 cm. The uniform velocity at the entrance to this "parallel plate duct" is ϑ_0 = 0.1 m/sec. A boundary layer grows on each of the two sides of the duct. As the boundary layer grows, the flow in the "undisturbed core" is accelerated. Since the Mach number is so low, the flow can be modeled as incompressible throughout. Then we can use the Blasius solution for flow over a flat plate as a model of the flow in the entry region of the duct by using the displacement thickness δ^* as a measure of the boundary layer thickness in the duct. From this model of the boundary layer thickness, we can determine the behavior of the flow in the undisturbed core and, in turn, make some estimates of the behavior of the flow in the entry region of the parallel plate geometry. Keep in mind that the results that we obtain here are only estimates since the Blasius solution applies only in the case of no pressure gradient in the direction of flow and there is clearly a pressure drop in the entry region of this configuration. We shall also compare these estimates with the accepted models given in Section 9.9.1.1.

For air: $\mu = 1.8 \times 10^{-5}$ kg/m sec, R = 287 J/kg K, c_v = 716 J/kg K

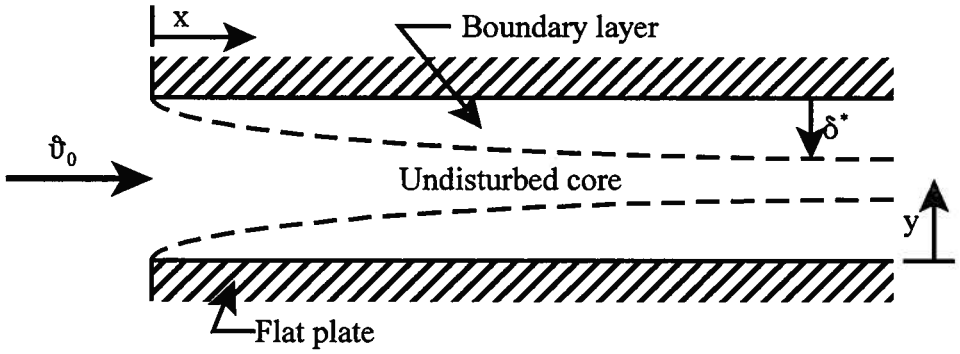

Figure 9E.8

(a) Estimate the average velocity of the flow at a location x = 3 m downstream from the entrance to the duct.

(b) Estimate the average pressure $P_{x=3m}$ in the undisturbed core at this same location.

(c) Use the result of part (b) to compute the apparent friction factor f_{app} for this 3 m length of the duct where

$$\frac{P_{in} - P_{x=3m}}{\frac{1}{2}\rho \vartheta_{ave}^{\ 2}} = f_{app}\frac{4x}{D_h}$$

and D_h is the hydraulic diameter. Recall that for this geometry, $D_h = 4a$ where a is the half distance between the plates. Compare this result with the value calculated from equation (9.115).

(d) Estimate the entry length L_e of this duct, i.e., the length of duct at which the boundary layer just "fills" the duct. Compare this estimate with the value calculated from equation 99.112).

Solution: (a) Since we can model the flow as incompressible and the plates are parallel, the average velocity of this steady flow is constant throughout the length of the duct. Then at a distance of 3 m downstream from the entrance, ϑ_{ave} = 0.1 m/sec. The Reynolds number is

$$Re_{D_h} = \frac{\rho \vartheta_0 D_h}{\mu} = \frac{4(1.189 \text{ kg/m})(0.1 \text{ m/sec})(0.1 \text{ m})}{1.8 \text{ x } 10^{-5} \text{ kg/m sec}} = 2643$$

The flow is laminar since $Re_{Dh} < 2800$.

(b) If we take the displacement thickness δ^* as the boundary layer thickness in the entry region, continuity in the entry region gives

$$\rho \vartheta_0 2a = \rho \vartheta_{core} 2\left(a - \delta^*\right)$$

$$\vartheta_{core} = \vartheta_0 \frac{a}{a - \delta^*}$$

but from equation (9.186)

$$\delta^* = \frac{1.719x}{\sqrt{\frac{\rho \vartheta x}{\mu}}} = 1.719x\sqrt{\frac{\mu}{\rho \vartheta x}}$$

The velocity appearing in this expression according is supposed to be the mainstream velocity which according to the Blasius solution is constant. However, in this case the velocity varies because of the acceleration in the "undisturbed" core. Then the displacement thickness can be written

$$\delta^* = 1.719x\sqrt{\frac{\mu}{\rho \vartheta_{core} x}}$$

Then from continuity we have

$$\vartheta_{core} = \vartheta_0 \frac{a}{a - 1.719x\sqrt{\frac{\mu}{\rho \vartheta_{core} x}}} = \vartheta_0 \frac{1}{1 - \frac{1.719}{a}\sqrt{\frac{\mu x}{\rho \vartheta_{core}}}}$$

Solving this expression for ϑ_0, we get

$$\vartheta_{core} - \frac{1.719\sqrt{\vartheta_{core}}}{a}\sqrt{\frac{\mu x}{\rho}} = \vartheta_0$$

If we let $z = \vartheta_{core}^{1/2}$, we can solve this expression by the quadratic formula. Then at $x = 3$m

$$\vartheta_{core} = 0.144 \text{ m/sec}$$

Since the flow in the "undisturbed" core can be modeled as inviscid, we can apply the Bernoulli equation there. Then the pressure drop from the entrance to the location $x = 3$ m is

$$P_{in} - P_{x=3m} = \frac{\rho\left(\vartheta_{core} - \vartheta_0\right)}{2} = \frac{\left(1.189 \text{ kg/m}^3\right)\left[\left(0.144 \text{ m/sec}\right)^2 - \left(0.100 \text{ m/sec}\right)^2\right]}{2}$$

$$P_{in} - P_{x=3m} = 6.375 \text{ x } 10^{-3} \text{ N/m}^2$$

In order to compare this result with equation (9.115) we first calculate the dimensionless coordinate x^+, viz.

$$x^+ = \frac{x}{D_h Re_{D_h}} = \frac{3 \text{ m}}{4\left(0.1 \text{ m}\right)2643} = 2.838 \text{ x } 10^{-3}$$

Equation (9.115) gives

$$\left(\Delta P^*\right)_{apparent} = 4x^+\left[\frac{3.44}{\sqrt{x^+}} + \frac{24 + \frac{0.674}{4x^+} - \frac{3.44}{\sqrt{x^+}}}{1 + 2.9 \text{ x } 10^{-5}\left(x^+\right)^{-2}}\right]$$

Then

$$\left(\Delta P^*\right)_{apparent} = 4\left(2.838 \text{ x } 10^{-3}\right)\left[\frac{3.44}{\sqrt{\left(2.838 \text{ x } 10^{-3}\right)}} + \frac{24 + \dfrac{0.674}{4\left(2.838 \text{ x } 10^{-3}\right)} - \dfrac{3.44}{\sqrt{\left(2.838 \text{ x } 10^{-3}\right)}}}{1 + 2.9 \text{ x } 10^{-5}\left(2.838 \text{ x } 10^{-3}\right)^{-2}}\right]$$

$$\left(\Delta P^*\right)_{apparent} = 0.779$$

$$\Delta P_{apparent} = \left(\Delta P^*\right)_{apparent}\frac{\rho \vartheta_0^{\,2}}{2} = 0.779\frac{\left(1.189 \text{ kg/m}^3\right)\left(0.1 \text{ m/sec}\right)^2}{2} = 4.634 \text{ x } 10^{-3} \text{ N/m}^2$$

Thus the pressure drop calculated using the flat plate model is about 50 percent greater than that determined from a solution of the Navier-Stokes equation. This is due to the fact that the velocity in the "undisturbed" core is constantly changing throughout the entry length and the Blasius solution cannot accommodate either that or the pressure drop itself.

(c) The apparent friction factor is given by

$$f_{app} = \frac{P_{in} - P_{x=3m}}{\dfrac{\rho \vartheta_0^{\,2}}{2}}\frac{D_h}{4x} = \frac{\left(6.375 \text{ x } 10^{-3} \text{ N/m}^2\right)}{\dfrac{\left(1.189 \text{ kg/m}^3\right)\left(0.1 \text{ m/sec}\right)^2}{2}}\frac{4(0.1 \text{ m})}{4(3 \text{ m})} = 0.036$$

Similarly,

$$f_{app} = \frac{\left(\Delta P^*\right)_{apparent} D_h}{4x} = \frac{(0.779)(0.4 \text{ m})}{4(3 \text{ m})} = 0.026$$

Obviously since the pressure drop is greater by the flat plate model, the friction factor using that model is greater.

(d) From equation (9.106) it is apparent that when the velocity profile becomes fully-developed the maximum velocity, ϑ_{max}, which is on the centerline of the flow, is $1.5\vartheta_0$. Then from continuity (part b above) we again have

$$\vartheta_{core} - \frac{1.719\sqrt{\vartheta_{core}}}{a}\sqrt{\frac{\mu x}{\rho}} = \vartheta_0$$

But now $\vartheta_{core} = 1.5\vartheta_0$. Then

$$1.5\vartheta_0 - \frac{1.719\sqrt{1.5\vartheta_0}}{a}\sqrt{\frac{\mu x}{\rho}} = \vartheta_0$$

$$1.5 - \frac{1.719\sqrt{1.5}}{a}\sqrt{\frac{\mu x}{\rho \vartheta_0}} = 1$$

Since at the entry length $x = L_{entry}$, we have

$$0.5 = \frac{1.719\sqrt{1.5}}{a}\sqrt{\frac{\mu L_{entry}}{\rho \vartheta_0}} = 4\frac{1.719\sqrt{1.5}}{D_h}\sqrt{\frac{\mu L_{entry} D_h}{\rho \vartheta_0 D_h}} = 4(1.719)\sqrt{1.5}\sqrt{\frac{L_{entry}}{D_h}}\frac{1}{\sqrt{Re_{D_h}}}$$

$$\frac{L_{entry}}{D_h} = 3.525 \text{ x } 10^{-3}$$

Equation (9.112) gives for large values of the Reynolds number

$$\frac{L_{entry}}{D_h} \approx 11 \text{ x } 10^{-3}$$

Thus the flat plate model underestimates the entry length because it has the displacement boundary layer growing as the square root of x whereas the acceleration in the core of the planar Couette flow makes the boundary layer grow at a much slower rate. Thus it takes a greater distance for the core velocity to accelerate to the value ϑ_{max} than the flat plate model predicts. However, for a simple estimate of the entry length with no other information available, this would not be an unreasonable result.

The purpose of this example is to show that lacking other information, simple models can often give useful, if approximate, information about flow geometries encountered in thermal-fluids engineering practice.

9.9.2.4 Momentum Thickness: Another effect that the boundary layer has upon the flow is to reduce the momentum flow at any given location along the plate compared with the uniform inviscid flow. This momentum deficit is, of course, the origin of the drag force exerted on the plate by the flow. Theodore von Karman (1881 - 1963), another student of Ludwig Prandtl and the founder of the Jet Propulsion Laboratory during World War II, suggested that there exists a *momentum thickness*, θ, due to this momentum deficit that is analogous to the displacement thickness associated with the deficit in the mass flow due to the presence of the boundary layer.

Von Karman defined θ such that the drag force, F_D, is equal to the flow of the deficit of the momentum in the boundary layer and could be calculated according to

$$F_D = \rho b \vartheta_0^{\,2} \theta \tag{9.192}$$

Consider once again the control volume of Figure 9.22 for a flat plate of width b. If we apply the x-component of the equation of linear momentum to this control volume, we have

$$-F_D = \int_{CV} \rho \vartheta_x \left(\vec{\vartheta} \cdot \vec{n}\right) dA = -\rho b \int_0^{\delta} \vartheta_0^{\,2} dy + \rho b \int_0^{\ell} \vartheta_0 \vartheta_y dx + \rho b \int_0^{\delta} \vartheta_x^{\,2} dy \tag{9.193}$$

where F_D is the drag force exerted on the plate by the fluid stream. The three terms on the right-hand side represent the momentum flows through the left, top, and right faces of the control volume, respectively. To eliminate the term for the momentum flow through the top face, we apply the continuity equation to the control volume. Then

$$-\rho b \delta \vartheta_0 + \rho b \int_0^{\ell} \vartheta_y dx + \rho b \int_0^{\delta} \vartheta_x dy = 0 \tag{9.194}$$

If we multiply equation (9.194) through by ϑ_0 and subtract the result from equation (9.193), we get

$$\begin{aligned} -F_D &= -\rho b \int_0^{\delta} \vartheta_0^{\,2} dy + \rho b \int_0^{\ell} \vartheta_0 \vartheta_y dx + \rho b \int_0^{\delta} \vartheta_x^{\,2} dy + \rho b \delta \vartheta_0^{\,2} - \rho b \vartheta_0 \int_0^{\ell} \vartheta_y dx - \rho b \vartheta_0 \int_0^{\delta} \vartheta_x dy \\ -F_D &= \rho b \int_0^{\delta} \vartheta_x^{\,2} dy - \rho b \vartheta_0 \int_0^{\delta} \vartheta_x dy = \rho b \int_0^{\delta} \left(\vartheta_x^{\,2} - \vartheta_0 \vartheta_x\right) dy \end{aligned} \tag{9.195}$$

Combining equations (9.192) and (9.195), we get

$$F_D = \rho b \vartheta_0^{\,2} \theta = -\rho b \int_0^{\delta} \left(\vartheta_x^{\,2} - \vartheta_0 \vartheta_x\right) dy = \rho b \int_0^{\delta} \vartheta_x \left(\vartheta_0 - \vartheta_x\right) dy \tag{9.196}$$

Then solving for the momentum thickness θ, we get

$$\theta = \int_0^{\delta} \frac{\vartheta_x}{\vartheta_0} \left(1 - \frac{\vartheta_x}{\vartheta_0}\right) dy \tag{9.197}$$

If we substitute the Blasius solution in equation (9.197), we have

$$\theta = \sqrt{\frac{\nu x}{\vartheta_0}} 2 f'' = 0.664 \sqrt{\frac{\nu x}{\vartheta_0}} \tag{9.198}$$

or in the form of equation (9.191)

$$\frac{\theta}{x} = \frac{0.664}{\sqrt{Re_x}} \tag{9.199}$$

Superimposed on the velocity profile, Figure 9.24 shows the relative magnitudes of the various definitions for boundary layer thickness. Each has its own particular physical significance.

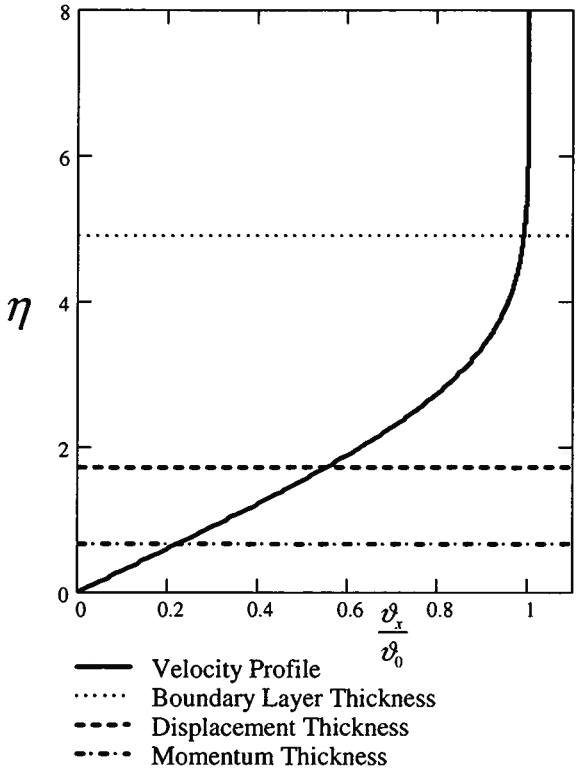

Figure 9.24 Relative Magnitudes of the Boundary Layer, Displacement, and Momentum Thicknesses for Flow Over a Flat Plate

Von Karman also pointed out that the drag force could also be determined from the shear stress on the flat plate. Then

$$F_D = b\int_0^x \tau_w(x)\,dx$$
$$\frac{dF_D}{dx} = b\tau_w \tag{9.200}$$

From equation (9.192) we also have

$$\frac{dF_D}{dx} = \rho b \vartheta_0^2 \frac{d\theta}{dx} \tag{9.201}$$

Combining equations (9.200) and (9.201), we get

$$\tau_w = \rho \vartheta_0^2 \frac{d\theta}{dx} \tag{9.202}$$

Equation (9.202) is known as the momentum integral relation. The local skin friction coefficient, C_f, is defined as

$$C_f \equiv \frac{\tau_w}{\frac{1}{2}\rho \vartheta_0^2} \tag{9.203}$$

For the Blasius solution for laminar flow over a flat plate, we can substitute equations (9.199) and (9.202) into equation (9.203) to get

$$C_f = \frac{0.664}{\sqrt{Re_x}} \tag{9.204}$$

While the displacement thickness, the momentum thickness, and the momentum integral relation seem interesting for the way in which they tie much of the dynamic behavior of the Newtonian fluid model together, they appear at this point to have limited utility since we derived them after we had already developed the Blasius solution for the flat plate. Their value however, lies in the fact that they are integral methods that tend to "average" properties in the boundary layer, and, hence, are less susceptible to the details of the flow. This averaging nature makes them particularly useful for turbulent flows since the solution of the Navier-Stokes equation for turbulent flow is extremely complicated. In the case of turbulent flow, it will be necessary to resort to a semi-empirical determination of the velocity profile in the boundary layer. Then, armed with this velocity profile and the integral methods we have just developed, useful information can be derived for the turbulent flow situation without ever really solving the Navier-Stokes equation. Example 9E.9 illustrates the procedure for a particular laminar velocity profile. As we shall see in Chapter 11, once we can fully describe the momentum transfer process, the description of the energy transfer process follows in a relatively straightforward manner.

Example 9E.9: Because the Blasius solution for the flat plate in laminar flow is numerical and cannot be expressed in closed form, it is a bit unwieldy to employ in practice. For this reason, over the years several different approximations to the Blasius velocity profile have been developed for laminar flow over a flat plate. One such approximation is the parabolic velocity profile originally due to von Karman. For $y \le \delta$, the velocity in the x-direction is given by

$$\frac{\vartheta_x}{\vartheta_0} = 2\left(\frac{y}{\delta}\right) - \left(\frac{y}{\delta}\right)^2$$

and for $y > \delta$

$$\frac{\vartheta_x}{\vartheta_0} = 1$$

The parabolic velocity profile satisfies the boundary conditions

$$(1) \quad \vartheta_x = 0 \quad \text{at} \quad y = 0$$

$$(2) \quad \vartheta_x = \vartheta_0 \quad \text{at} \quad y = \delta$$

As shown in Figure 9E.9, the approximation is quite good through out the thickness of the boundary layer.

(a) For a flat plate of width b, use this parabolic profile to obtain the drag force, F_D, the drag coefficient, C_D, the boundary layer thickness as a function of the position x on the plate, and the skin friction coefficient, C_f.

(b) Estimate the rate of entropy generation in a boundary layer of length ℓ.

(c) Compare the results obtained in part (a) with those obtained from the Blasius solution.

Solution: (a) From equation (9.187), we have

$$F_D = \rho b \vartheta_0^2 \theta$$

Then from equation (9.192) we have

$$\frac{F_D}{\rho b \vartheta_0^2} = \theta = \int_0^\delta \frac{\vartheta_x}{\vartheta_0}\left(1 - \frac{\vartheta_x}{\vartheta_0}\right) dy$$

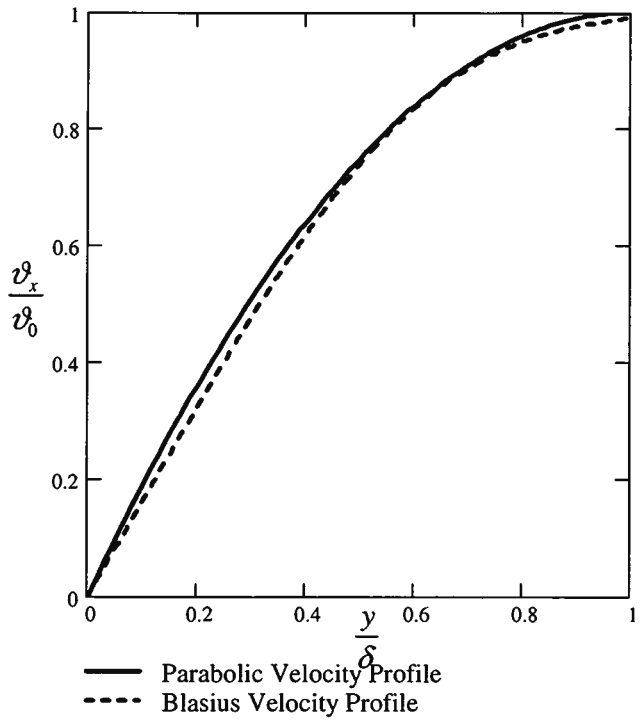

Figure 9E.9 Comparison of the Blasius and Parabolic Velocity Profiles for a Flat Plate

We now substitute the parabolic velocity profile in the integrand. Since the profile is a function of y/δ, let this now become the variable of integration. Then

$$\frac{F_D}{\rho b \vartheta_0^{\,2}\delta} = \frac{\theta}{\delta} = \int_0^1 \frac{\vartheta_x}{\vartheta_0}\left(1-\frac{\vartheta_x}{\vartheta_0}\right) d\left(\frac{y}{\delta}\right)$$

$$\frac{F_D}{\rho b \vartheta_0^{\,2}\delta} = \int_0^1 \left[2\left(\frac{y}{\delta}\right)-\left(\frac{y}{\delta}\right)^2\right]\left[1-2\left(\frac{y}{\delta}\right)+\left(\frac{y}{\delta}\right)^2\right] d\left(\frac{y}{\delta}\right)$$

$$\frac{F_D}{\rho b \vartheta_0^{\,2}\delta} = 2\int_0^1 \left(\frac{y}{\delta}\right) d\left(\frac{y}{\delta}\right) - 5\int_0^1 \left(\frac{y}{\delta}\right)^2 d\left(\frac{y}{\delta}\right) + 4\int_0^1 \left(\frac{y}{\delta}\right)^3 d\left(\frac{y}{\delta}\right) - \int_0^1 \left(\frac{y}{\delta}\right)^4 d\left(\frac{y}{\delta}\right)$$

$$\frac{F_D}{\rho b \vartheta_0^{\,2}\delta} = \frac{2}{15}$$

From the definition of the shear stress in the fluid

$$\tau_w = \mu\left(\frac{\partial \vartheta_x}{\partial y}\right)_{y=0}$$

but if we set $y^* = y/\delta$

$$\frac{\partial \vartheta_x}{\partial y} = \frac{\partial \vartheta_x}{\partial y^*}\frac{\partial y^*}{\partial y} = \left(2\vartheta_0 - 2\vartheta_0 y^*\right)\frac{1}{\delta}$$

Then

$$\tau_w = \left[\frac{2\mu\vartheta_0\left(1-y^*\right)}{\delta}\right]_{y^*=0} = \frac{2\mu\vartheta_0}{\delta}$$

From equation (9.190) we have

$$\tau_w = \frac{1}{b}\frac{dF_D}{dx} = \frac{2\mu\vartheta_0}{\delta}$$

Then

$$F_D\frac{dF_D}{dx} = \frac{2\mu b\vartheta_0}{\delta}\left(\frac{2}{15}\right)\rho b\vartheta_0^{\,2}\delta = \frac{4\mu b^2\vartheta_0^{\,3}}{15}$$

Integrating this expression, we get

$$\int_0^L F_D\frac{dF_D}{dx}dx = \int_0^L \frac{4\mu b^2\vartheta_0^{\,3}}{15}dx$$

$$\frac{F_D^{\,2}}{2} = \frac{4\mu b^2\vartheta_0^{\,3}L}{15}$$

$$F_D = \sqrt{\frac{8\mu b^2\vartheta_0^{\,3}L}{15}}$$

Then the drag coefficient for one side of the plate as defined in equation (9.185) becomes

$$C_D \equiv \frac{F_D}{\frac{1}{2}\rho\vartheta_0^{\,2}bL} = \frac{\sqrt{\frac{8\mu b^2\vartheta_0^{\,3}L}{15}}}{\frac{1}{2}\rho\vartheta_0^{\,2}bL} = \frac{1.461}{\sqrt{\frac{\rho\vartheta_0 L}{\mu}}} = \frac{1.461}{\sqrt{Re_L}}$$

Then

$$F_D = \frac{1.461}{\sqrt{Re_L}}\frac{1}{2}\rho\vartheta_0^{\,2}bL \quad \text{and} \quad F_D = \frac{2}{15}\rho b\vartheta_0^{\,2}\delta$$

Equating these last two expressions, we get

$$\frac{\delta}{L} = \frac{5.477}{\sqrt{Re_L}}$$

and it follows that

$$\frac{\delta}{x} = \frac{5.477}{\sqrt{Re_x}}$$

For the skin friction coefficient C_f, we have from the definition

$$\frac{C_f}{2} = \frac{\tau_w}{\rho\vartheta_0^{\,2}} = \frac{2\mu\vartheta_0}{\delta}\frac{1}{\rho\vartheta_0^{\,2}} = \frac{2\mu}{5.477x}\frac{\sqrt{Re_x}}{\rho\vartheta_0}$$

$$C_f = \frac{0.730}{\sqrt{Re_x}}$$

(b) In order to estimate the rate of entropy generation in this boundary layer based on the incompressible Newtonian fluid model, we must first apply the first law of thermodynamics in order to assess the rate of dissipation of kinetic energy of the fluid in the boundary layer. To do this we employ the control volume shown in Figure 9.22. Since there is no pressure gradient in this steady flow and since the flow is also adiabatic with no shaft work transfer, the first law reduces to

$$0 = (h_{in} - h_{out}) + \left(\frac{\vartheta_{in}^{\,2}}{2} - \frac{\vartheta_{out}^{\,2}}{2}\right)$$

If we now substitute the enthalpy constitutive relation into this expression, we get

$$0 = c\left(T_{in} - T_{out}\right) + v\cancel{\left(P_{in} - P_{out}\right)} + \left(\frac{\vartheta_{in}^{\,2}}{2} - \frac{\vartheta_{out}^{\,2}}{2}\right)$$

$$T_{out} - T_{in} = \frac{1}{2c}\left(\vartheta_{in}^{\,2} - \vartheta_{out}^{\,2}\right)$$

It must be remembered that the kinetic energy terms appearing in this expression are the mass flow rate averaged values over the entry and exit ports. For the entry port the averaging process is trivial since the flow rate is constant over this port, but for the exit port the velocity varies according to the parabolic velocity profile given above. Then

$$\dot{m}\left(\vartheta_{out}^{\,2}\right)_{ave} = \rho b\delta\vartheta_0\left(\vartheta_{out}^{\,2}\right)_{ave} = \rho b\int_0^{\delta}\vartheta_x^{\,3}dy$$

$$\left(\vartheta_{out}^{\,2}\right)_{ave} = \frac{1}{\delta\vartheta_0}\int_0^{\delta}\vartheta_x^{\,3}dy$$

where for the parabolic velocity profile

$$\vartheta_x^{\,3} = \vartheta_0^{\,3}\left[8\left(\frac{y}{\delta}\right)^3 - 12\left(\frac{y}{\delta}\right)^4 + 6\left(\frac{y}{\delta}\right)^5 - \left(\frac{y}{\delta}\right)^6\right]$$

If we change variables by letting $y^* = y/\delta$, we have

$$\int_0^{\delta}\vartheta_x^{\,3}dy = \delta\int_0^{1}\vartheta_x^{\,3}dy^*$$

Substituting for ϑ_x^3 and integrating, we get

$$\int_0^{\delta}\vartheta_x^{\,3}dy = \frac{16}{35}\delta\vartheta_0^{\,3}$$

and

$$\left(\vartheta_{out}^{\,2}\right)_{ave} = \frac{1}{\delta\vartheta_0}\int_0^{\delta}\vartheta_x^{\,3}dy = \frac{1}{\delta\vartheta_0}\frac{16}{35}\delta\vartheta_0^{\,3} = \frac{16}{35}\vartheta_0^{\,2}$$

Then the temperature increase becomes

$$T_{out} - T_{in} = \frac{1}{2c}\left(\vartheta_{in}^{\,2} - \vartheta_{out}^{\,2}\right) = \frac{1}{2c}\left(\vartheta_0^{\,2} - \frac{16}{35}\vartheta_0^{\,2}\right) = \frac{1}{c}\frac{19}{70}\vartheta_0^{\,2}$$

From the second law, we have

$$\dot{S}_{gen} = \dot{m}c\left(s_{out} - s_{in}\right) = \dot{m}c\ln\frac{T_{out}}{T_{in}} = \rho c\dot{V}\ln\left(1 + \frac{T_{out} - T_{in}}{T_{in}}\right)$$

$$\dot{S}_{gen} = \rho cb\delta\vartheta_0\ln\left(1 + \frac{\vartheta_0^{\,2}}{cT_{in}}\frac{19}{70}\right)$$

Thus the rate of entropy generation varies linearly with the boundary layer thickness. Then for a boundary layer of length ℓ, we have

$$\dot{S}_{gen} = \frac{5.477\ell\rho c\vartheta_0}{\sqrt{Re_\ell}}\ln\left(1 + \frac{\vartheta_0^{\,2}}{cT_{in}}\frac{19}{70}\right)$$

Thus, for the flat plate, the rate of entropy generation varies as the square root of the length of the boundary layer.

(c) From these results, it appears that the error associated with the use of the parabolic velocity profile introduces an error of approximately 12 percent. For example,

$$\left|\frac{\delta_{Blasius}-\delta_{parabolic}}{\delta_{Blasius}}\right| = \left|1-\frac{\delta_{parabolic}}{\delta_{Blasius}}\right| = \left|1-\frac{5.477}{4.90}\right| = 0.12$$

Perhaps more importantly, the parabolic velocity profile gives the proper dependence on x for the growth of the boundary layer, namely, the square root of x. There are other analytical forms for the velocity profile that give even greater accuracy, but the method of employing them is precisely the same as that above.

Example 9E.10: As shown in Figure 9E.10a, a flat plate is immersed in a uniform flow of air with a velocity ϑ_0 and zero pressure gradient. The plate is porous with a very large number of uniformly-spaced small holes drilled through it. Air flows through these holes in a direction normal to the plate with a velocity ϑ_{wall} that is the same everywhere, independent of the values of x and y.

(a) Determine the velocity profile of the air for this flow geometry.

(b) Find an expression for the boundary layer thickness of the air flowing over the plate for which the outer limit of the boundary layer is defined as that value of y for which $\vartheta_x = 0.99\,\vartheta_0$.

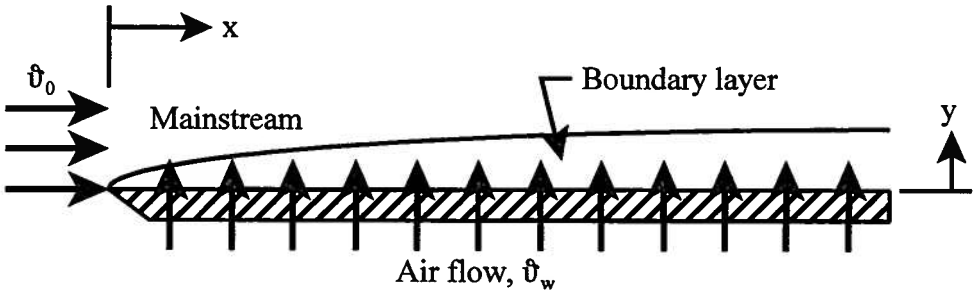

Figure 9E.10a

Solution: (a) We first note that the boundary condition $\vartheta_y = 0$ at $y = 0$ does not hold in this case even though the boundary condition $\vartheta_x = 0$ at $y = 0$ does hold. Thus we cannot use the Blasius solution to describe the flow in this case, and it will be necessary to solve the boundary layer equations specifically for this geometry. We further note that $\vartheta_y = \vartheta_{wall}$ = constant everywhere. Then $\partial\vartheta_y/\partial x = 0$ and from continuity

$$\frac{\partial\vartheta_x}{\partial x}+\frac{\partial\vartheta_y}{\partial y}=0$$

Then it follows that $\vartheta_x = \vartheta_x(y)$. Then the momentum equation, equation (9.156), becomes

$$\rho\left(\frac{\partial\vartheta_x}{\partial t}+\vartheta_x\frac{\partial\vartheta_x}{\partial x}+\vartheta_y\frac{\partial\vartheta_x}{\partial y}\right)=-\frac{\partial P}{\partial x}+\mu\frac{\partial^2\vartheta_x}{\partial y^2}$$

$$\vartheta_y\frac{\partial\vartheta_x}{\partial y}=\frac{\mu}{\rho}\frac{\partial^2\vartheta_x}{\partial y^2}=\nu\frac{\partial^2\vartheta_x}{\partial y^2}$$

$$\therefore \vartheta_{wall}\frac{d\vartheta_x}{dy}=\frac{\mu}{\rho}\frac{d^2\vartheta_x}{dy^2}$$

where we have made use of the fact that the y-component of velocity is ϑ_{wall} everywhere and that the x-component of velocity is a function of y only. We have also introduced the kinematic viscosity, ν. The solution of this second order, ordinary differential equation must satisfy the boundary conditions

$$(1)\quad \vartheta_x = 0 \quad \text{at} \quad y = 0$$

$$(2)\quad \vartheta_x = \vartheta_0 \quad \text{at} \quad y \to \infty$$

The solution of the differential equation is of the form

$$\vartheta_x = Ae^{my} + B$$

Then

$$\frac{d\vartheta_x}{dy} = Ame^{my}$$

$$\frac{d^2\vartheta_x}{dy^2} = Am^2e^{my}$$

Then substituting these expressions into the original differential equation, we get

$$Ame^{my} = \frac{\nu}{\vartheta_{wall}} Am^2e^{my}$$

$$\therefore m = \frac{\vartheta_{wall}}{\nu}$$

Then

$$\vartheta_x = Ae^{\frac{\vartheta_{wall}y}{\nu}} + B$$

From the second boundary condition, it is apparent that only negative values of ϑ_{wall} are allowable if the solution is to remain bounded as we move to the outer edge of the boundary layer where $y \to \infty$. This means that there is suction under the plate. (As we shall see shortly, this is a means of controlling the behavior of the boundary layer.) Applying the second boundary condition, we get the result that $B = \vartheta_0$. Then

$$\vartheta_x = Ae^{\frac{\vartheta_{wall}y}{\nu}} + \vartheta_0$$

Applying the first boundary condition, we get

$$0 = A + \vartheta_0$$

$$\therefore A = -\vartheta_0$$

Then the solution becomes

$$\frac{\vartheta_x}{\vartheta_0} = 1 - e^{\frac{\vartheta_{wall}y}{\nu}} \qquad \vartheta_{wall} < 0$$

(b) The boundary layer thickness is given by

$$\left(\frac{\vartheta_x}{\vartheta_0}\right)_{y=\delta} = 0.99 = 1 - e^{\frac{\vartheta_{wall}\delta}{\nu}}$$

$$\therefore e^{\frac{\vartheta_{wall}\delta}{\nu}} = 0.01$$

$$\frac{\vartheta_{wall}\delta}{\nu} = \ln 0.01$$

$$\frac{\vartheta_{wall}\delta}{\nu} = -4.605$$

Then the boundary layer thickness becomes

$$\delta = -\frac{4.605\nu}{\vartheta_{wall}}$$

Hence, the boundary layer has the same thickness at all locations on the plate, and for a given value of the kinematic viscosity ν, i.e., a given fluid, the thickness of the boundary layer is determined solely by the suction velocity ϑ_{wall}.

Thus, we now have at our disposal a means of controlling the thickness of the boundary layer. The problem is that for a given mainstream velocity, as the boundary layer becomes thinner with an increase in suction velocity, the fluid shear and the skin friction increase. Thus boundary layer suction may not be all that worthwhile as a means of reducing skin friction drag. However, the real reasons that boundary layer suction is of interest are: (1) that it delays separation of the boundary layer from the solid surface thereby reducing profile drag; and (2) that it exerts a stabilizing influence on the laminar flow thereby delaying the onset of the transition to turbulent flow. These are two important flow phenomena that we shall consider in greater detail shortly, but suffice it to say at this point that boundary layer suction is in fact used in some thermal-fluid systems to control the flow configuration. Figures 9E.10b and 9E.10c (from L. Prandtl, *Essentials of Fluid Dynamics*, Hafner Publishing Co., New York, 1952, p.143) show just how dramatic the effect can be.

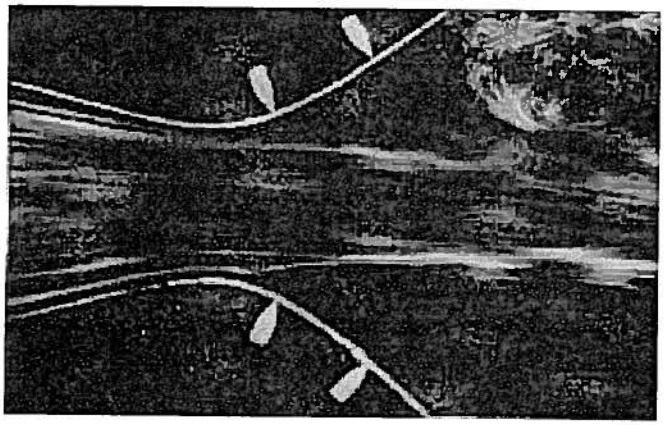

Figure 9E.10b Flow in a Channel with a Sudden Enlargement

Notice in Figure 9E.10b that the flow is separated from the wall in the enlarged section of the channel, but when boundary layer suction is introduced in the portion of the channel where the enlargement occurs, the flow re-attaches to the wall as shown in Figure 9E.10c.

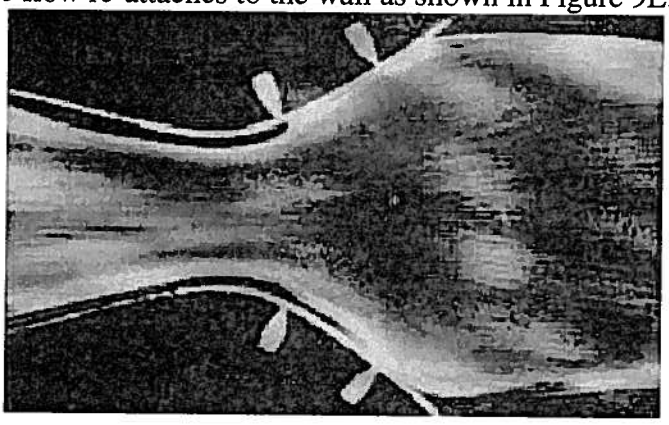

Figure 9E.10c Flow in a Channel with a Sudden Enlargement and Suction at the Wall

9.10 Turbulent Flow

Up to the present time we have been considering flows that are described as laminar in that any perturbation to the flow due to some infinitesimal disturbance is damped out by the action of viscosity. However, we would intuitively expect that if the disturbance became sufficiently large, the flow field could assume another character. As mentioned previously, the experiments of Osborne Reynolds confirmed that this is indeed the case. The Reynolds number provides a good measure of this possibility since it represents the ratio of inertia forces to viscous forces. Thus, at large values of the Reynolds number, we would expect the inertia forces to dominate the flow with the viscous forces exerting little influence on the flow field. At these high Reynolds numbers, perturbations to the flow are no longer subject to the damping action of viscosity. It is now possible, then, for these perturbations to grow in magnitude and thereby destroy the laminar nature of the flow. Such flows are termed *turbulent*, and in fact, most flows commonly encountered in thermal-fluids engineering practice are of this type in which an irregular fluctuation (mixing or eddying motion) is superimposed on the average mainstream flow.

As shown schematically in Figure 9.25, the velocity continually fluctuates about some average value in a manner such that the amplitude of this fluctuation is, in general, of the same order of magnitude as the velocity itself. Not only does the velocity at one point in the flow field fluctuate with time, but also the velocity varies in an irregular fashion from point to point at a particular instant in time. Due to this irregular nature of the velocity, the paths of motion of the fluid particles are highly random which results in an extensive mixing of the fluid and a significant enhancement of the transport of momentum and energy between the fluid and the solid surfaces that bound it. In fact, the effects produced by this mixing motion are such that the viscosity and the thermal conductivity of the fluid appear to have been increased by several orders of magnitude. Unfortunately, the fluctuations in the velocity are so complex that they render the problem inaccessible to mathematical treatment which makes the modeling of turbulent flow one of the major challenges of thermal-fluids engineering.

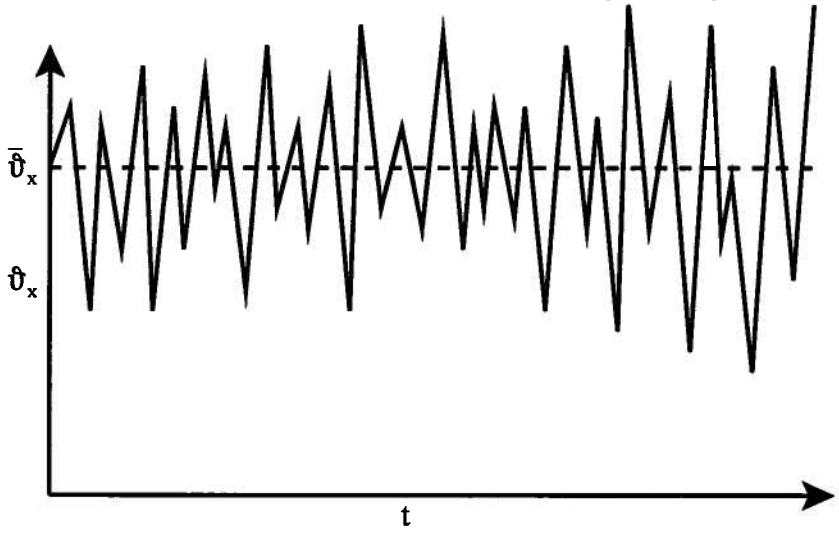

Figure 9.25 Instantaneous Velocity of Fluid in Turbulent Flow at Some Point in Space

The random nature of the motion of the fluid that prevails in turbulent flow fields is similar to that which prevails in the motion of the molecules that make up any physical body. In principle, we could describe the behavior of a macroscopic body by specifying the initial values

of the coordinates and velocities of all the molecules and then integrating the equations of motion for each molecule. This determines the coordinates and velocity of every molecule as a function of time and thereby describes the behavior of the body composed of these molecules. However, since the number of particles making up such a body is incredibly large, the method described is virtually impossible in practice. The resolution of this dilemma lies in the complex and irregular nature of the motion of the molecules themselves. It follows that after a sufficiently long period of time the velocities and coordinates of the molecules assume all possible values so that the effect of the initial conditions is smoothed out and disappears. This condition then permits the use of statistical mechanics to describe the behavior of a macroscopic body in terms of its microscopic components. The situation in turbulent flow is similar to that described above with the fluid particles serving as the analog of the molecules of the body. It follows then that the theory of turbulent flow must be of a statistical nature. Several attempts have been made in this direction; however, to date no complete quantitative theory has been developed. Nevertheless, several important worthwhile results have been deduced using a technique similar to that described below.

At any point in a three-dimensional, fully developed turbulent flow field, the fluid velocity varies with respect to both time and direction. The *instantaneous* velocities and pressure are $\vartheta_{x,i}$, $\vartheta_{y,i}$, $\vartheta_{z,i}$, and P_i while the *time averages* of these quantities are ϑ_x, ϑ_y, ϑ_z, and P where

$$\vartheta_x = \frac{1}{\theta}\int_{t_0}^{t_0+\theta} \vartheta_{x,i}\,dt, \quad \vartheta_y = \frac{1}{\theta}\int_{t_0}^{t_0+\theta} \vartheta_{y,i}\,dt, \quad \vartheta_z = \frac{1}{\theta}\int_{t_0}^{t_0+\theta} \vartheta_{z,i}\,dt, \quad P = \frac{1}{\theta}\int_{t_0}^{t_0+\theta} P_i\,dt \tag{9.205}$$

By virtue of the equations (9.205) it is possible to separate a turbulent flow into a *mean motion* described by (9.205) and into a *fluctuating* or *eddying motion* which represents the amount of fluctuation of the instantaneous quantity from the average quantity. Thus, if ϑ_x', ϑ_y', ϑ_z', and P' denote the fluctuating components, we have

$$\vartheta_{x,i} = \vartheta_x + \vartheta_x', \quad \vartheta_{y,i} = \vartheta_y + \vartheta_y', \quad \vartheta_{z,i} = \vartheta_z + \vartheta_z', \quad P_i = P + P' \tag{9.206}$$

It should be pointed out that the mean values are to be taken over a sufficiently long interval of time, θ, so that they are completely independent of time for a steady flow. Thus, it follows that

$$\overline{\vartheta_x'} = \frac{1}{\theta}\int_{t_0}^{t_0+\theta} \vartheta_x'\,dt = 0, \quad \overline{\vartheta_y'} = \frac{1}{\theta}\int_{t_0}^{t_0+\theta} \vartheta_y'\,dt = 0, \quad \overline{\vartheta_z'} = \frac{1}{\theta}\int_{t_0}^{t_0+\theta} \vartheta_z'\,dt = 0, \quad \overline{P'} = \frac{1}{\theta}\int_{t_0}^{t_0+\theta} P_i\,dt = 0 \tag{9.207}$$

That is, the time average of each of the fluctuating components is zero. By analogy to equations (9.207), the mean square of the velocity fluctuations is defined as

$$\overline{\vartheta_x'^2} = \frac{1}{\theta}\int_{t_0}^{t_0+\theta} \vartheta_x'^2\,dt, \quad \overline{\vartheta_y'^2} = \frac{1}{\theta}\int_{t_0}^{t_0+\theta} \vartheta_y'^2\,dt, \quad \overline{\vartheta_z'^2} = \frac{1}{\theta}\int_{t_0}^{t_0+\theta} \vartheta_z'^2\,dt \tag{9.208}$$

The turbulent shear components (The reason for this name will become apparent shortly.) are

$$\overline{\vartheta_x'\vartheta_y'} = \frac{1}{\theta}\int_{t_0}^{t_0+\theta} \vartheta_x'\vartheta_y'\,dt, \quad \overline{\vartheta_y'\vartheta_z'} = \frac{1}{\theta}\int_{t_0}^{t_0+\theta} \vartheta_y'\vartheta_z'\,dt, \quad \overline{\vartheta_x'\vartheta_z'} = \frac{1}{\theta}\int_{t_0}^{t_0+\theta} \vartheta_x'\vartheta_z'\,dt \tag{9.209}$$

Note that when the mean flow is in one direction, e.g. the x-direction, the mean velocities in the other two directions (y and z) are zero but the fluctuating quantities defined in equations (9.208) and (9.209) are all finite, including those in the y- and z-directions.

Even though the flow is turbulent, the Navier-Stokes equation is still applicable if the instantaneous values of the velocity and pressure are used. For an incompressible Newtonian fluid the relevant component equations are equations (9.67). We shall now show the form that the Navier-Stokes equation takes for the turbulent flow field. For example in the absence of body forces the x-component of the Navier-Stokes equation becomes

$$\rho\left(\frac{\partial \vartheta_{x,i}}{\partial t}+\vartheta_{x,i}\frac{\partial \vartheta_{x,i}}{\partial x}+\vartheta_{y,i}\frac{\partial \vartheta_{x,i}}{\partial y}+\vartheta_{z,i}\frac{\partial \vartheta_{x,i}}{\partial z}\right)=-\frac{\partial P_i}{\partial x}+\mu\left(\frac{\partial^2 \vartheta_{x,i}}{\partial x^2}+\frac{\partial^2 \vartheta_{x,i}}{\partial y^2}+\frac{\partial^2 \vartheta_{x,i}}{\partial z^2}\right) \tag{9.210}$$

and the continuity equation, equation (9.70) becomes

$$\frac{\partial \vartheta_{x,i}}{\partial x}+\frac{\partial \vartheta_{y,i}}{\partial y}+\frac{\partial \vartheta_{z,i}}{\partial z}=0 \tag{9.211}$$

Notice that the convective terms in equation (9.210) can be written

$$\vartheta_{x,i}\frac{\partial \vartheta_{x,i}}{\partial x}+\vartheta_{y,i}\frac{\partial \vartheta_{x,i}}{\partial y}+\vartheta_{z,i}\frac{\partial \vartheta_{x,i}}{\partial z}=\frac{\partial\left(\vartheta_{x,i}\right)^2}{\partial x}+\frac{\partial \vartheta_{x,i}\vartheta_{y,i}}{\partial y}+\frac{\partial \vartheta_{x,i}\vartheta_{z,i}}{\partial z} \tag{9.212}$$

Substituting equation (9.212) into equation (9.210) and collecting like terms, we obtain

$$\rho\frac{\partial \vartheta_{x,i}}{\partial t}=-\frac{\partial P_i}{\partial x}+\frac{\partial}{\partial x}\left(\mu\frac{\partial \vartheta_{x,i}}{\partial x}-\rho{\vartheta_{x,i}}^2\right)+\frac{\partial}{\partial y}\left(\mu\frac{\partial \vartheta_{x,i}}{\partial y}-\rho\vartheta_{x,i}\vartheta_{y,i}\right)+\frac{\partial}{\partial z}\left(\mu\frac{\partial \vartheta_{x,i}}{\partial z}-\rho\vartheta_{x,i}\vartheta_{z,i}\right) \tag{9.213}$$

Now substitute in equation (9.213) the appropriate value for the instantaneous velocity given by equations (9.206). Form the time average in the resulting equation term by term taking into account the following rules in which f and g are two dependent variables whose mean values (denoted by the superscript bar) are to be formed. Let s denote any one of the independent variables x, y, z and t. Then,

$$\overline{\overline{f}}=\overline{f},\quad \overline{f+g}=\overline{f}+\overline{g},\quad \overline{\overline{f}\cdot g}=\overline{f}\cdot\overline{g},\quad \overline{\frac{\partial f}{\partial s}}=\frac{\partial \overline{f}}{\partial s},\quad \overline{\int f ds}=\int \overline{f} ds \tag{9.214}$$

In performing the time averages, we make use of the relations (9.207). For example, making the substitution $\vartheta_{x,i}=\vartheta_x+\vartheta_x'$ in the first term of (9.214), we obtain

$$\frac{\partial \vartheta_{x,i}}{\partial t}=\frac{\partial \vartheta_x}{\partial t}+\frac{\partial \vartheta_x'}{\partial t} \tag{9.215}$$

Taking the time average, we get

$$\overline{\frac{\partial \vartheta_{x,i}}{\partial t}}=\overline{\frac{\partial \vartheta_x}{\partial t}+\frac{\partial \vartheta_x'}{\partial t}}=\overline{\frac{\partial \vartheta_x}{\partial t}}+\overline{\frac{\partial \vartheta_x'}{\partial t}}=\frac{\partial}{\partial t}\overline{\vartheta_x}+\frac{\partial}{\partial t}\overline{\vartheta_x'}=\frac{\partial \vartheta_x}{\partial t} \tag{9.216}$$

Applying this technique to each of the other terms, we obtain

$$\overline{\frac{\partial P_i}{\partial x}}=\frac{\partial P}{\partial x} \tag{9.217}$$

$$\overline{\mu\frac{\partial \vartheta_{x,i}}{\partial x}-\rho{\vartheta_{x,i}}^2}=\mu\frac{\partial \vartheta_x}{\partial x}-\rho{\vartheta_x}^2-\rho\overline{\vartheta_x'^2} \tag{9.218}$$

$$\overline{\mu\frac{\partial \vartheta_{x,i}}{\partial y}-\rho\vartheta_{x,i}\vartheta_{y,i}}=\mu\frac{\partial \vartheta_x}{\partial y}-\rho\vartheta_x\vartheta_y-\rho\overline{\vartheta_x'\vartheta_y'} \tag{9.219}$$

$$\overline{\mu\frac{\partial \vartheta_{x,i}}{\partial z}-\rho\vartheta_{x,i}\vartheta_{z,i}}=\mu\frac{\partial \vartheta_x}{\partial z}-\rho\vartheta_x\vartheta_z-\rho\overline{\vartheta_x'\vartheta_z'} \tag{9.220}$$

Substituting equations (9.217) through (9.220) into equation (9.213), we obtain

$$\begin{aligned}&\rho\left(\frac{\partial \vartheta_x}{\partial t}+\vartheta_x\frac{\partial \vartheta_x}{\partial x}+\vartheta_y\frac{\partial \vartheta_x}{\partial y}+\vartheta_z\frac{\partial \vartheta_x}{\partial z}\right)\\&\quad=-\frac{\partial P}{\partial x}+\mu\left(\frac{\partial^2 \vartheta_x}{\partial x^2}+\frac{\partial^2 \vartheta_x}{\partial y^2}+\frac{\partial^2 \vartheta_x}{\partial z^2}\right)-\frac{\partial \rho\overline{\vartheta_x'^2}}{\partial x}-\frac{\partial \rho\overline{\vartheta_x'\vartheta_y'}}{\partial y}-\frac{\partial \rho\overline{\vartheta_x'\vartheta_z'}}{\partial z}\end{aligned} \tag{9.221}$$

with similar equations for the y- and z-directions.

Comparing equation (9.221) with equations (9.67), we see that for turbulent flow, the Navier-Stokes equation is satisfied provided the mean velocity is used and three additional terms involving the fluctuation components are included in each component equation. These three additional terms have the units of stress and are referred to as the Reynolds stresses in honor of Osborne Reynolds who first derived them. It is customary to group these terms with the viscous terms in the Navier-Stokes equation. In all, there are six independent Reynolds stresses:

three normal stresses $-\rho\overline{\vartheta_x'^2}$, $-\rho\overline{\vartheta_y'^2}$, $-\rho\overline{\vartheta_z'^2}$;

and three shear stresses, $-\rho\overline{\vartheta_x'\vartheta_y'}$, $-\rho\overline{\vartheta_x'\vartheta_z'}$, $-\rho\overline{\vartheta_y'\vartheta_z'}$.

The result of this grouping is that the velocity fluctuations can be regarded as responsible for producing an increase in the shear stress in the fluid.

While the appearance of these Reynolds stresses in the Navier-Stokes equation seems to lend mathematical credence to the notion that they are stresses, we have not yet presented a physical interpretation to confirm this notion. On the one hand, we need to show that physically they are responsible for the transfer of momentum due to turbulence, and on the other hand, we need to show that they affect the flow in much the same manner as the viscous stresses. In this regard, Prandtl in 1925 proposed the following very simple model of turbulence based upon the similarity between the random nature of turbulence and the random nature of molecular motion.

Consider the case of a two-dimensional, parallel turbulent flow in which the average velocity varies only from streamline to streamline. The principal direction of flow is assumed parallel to the x-axis with $\vartheta_y = 0$, $\vartheta_z = 0$, and $\vartheta_x = \vartheta_x(y)$ with $d\vartheta_x/dy > 0$. Then there exists in the flow a velocity profile something like that shown in Figure 9.26.

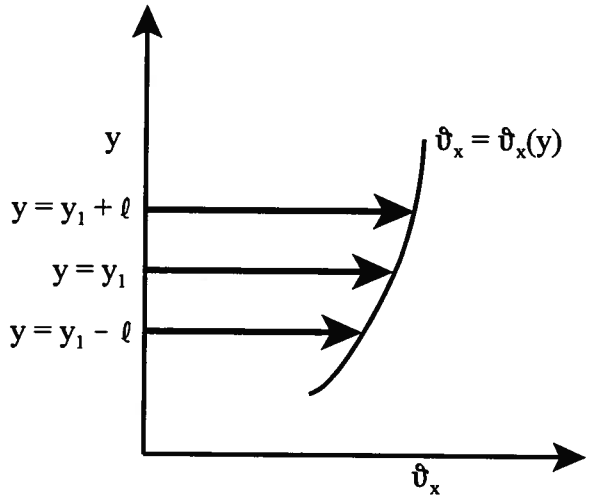

Figure 9.26 Velocity Profile in Turbulent Flow

As the fluid passes along the solid wall that bounds it, a fluid particle traverses some distance in both the x- and y-directions while retaining its momentum parallel to x. Focusing our attention on the plane $y = y_1$, we note that the fluid particle that comes from a layer $(y_1 - \ell)$, and therefore has $\vartheta_y' > 0$, carries with it velocity $\vartheta_x(y_1 - \ell)$ and is displaced transversely a distance ℓ known as the *Prandtl mixing length*. The fluid particle now has an average velocity that is smaller than the average velocity of other fluid particles at its new location. This gives rise to a negative component ϑ_x' in layer y_1 given by

$$\vartheta_x' = \vartheta_x(y_1 - \ell) - \vartheta_x(y_1) = -\ell\left(\frac{d\vartheta_x}{dy}\right)_{y=y_1} \tag{9.222}$$

The transverse component ϑ_y' can be determined from the assumption that two fluid particles that enter the layer at the plane $y = y_1$ from opposite sides approach one another with relative velocity $2\ell d\vartheta_x/dy$ and that this gives rise to transverse fluctuation velocities of the same order of magnitude as the longitudinal fluctuation velocities. Thus

$$\vartheta_y' \sim \ell\left(\frac{d\vartheta_x}{dy}\right)_{y=y_1} \tag{9.223}$$

A similar argument can be applied to a fluid particle that enters the layer from above with $\vartheta_y' < 0$ only now $\vartheta_x' > 0$. Then the product of the two velocities associated with the turbulence is always negative and the relevant Reynolds stress becomes

$$-\rho\overline{\vartheta_x'\vartheta_y'} = \rho\ell^2\left(\frac{d\vartheta_x}{dy}\right)^2 \tag{9.224}$$

Equation (9.224) bears a striking similarity to equation (9.13) with the mixing length playing a role analogous to the mean free path and the fluid particles analogous to the molecules of a gas. Thus momentum transport by eddying particles of fluid is analogous to momentum transport by molecular motion.

One must be careful not to push this analogy too far, however, as there are distinct differences in the underlying physics that limit its validity. In the kinetic theory model, molecules travel a clear path with no interactions occurring between collisions whereas the fluid particles do exchange momentum with surrounding particles during their movement from one location to another. Thus the mixing length is not as well-defined as the mean free path. In addition, with the exception of rarefied gases, the mean free path of the molecules is small compared to typical distances over which the velocity gradient can be viewed as non-linear whereas in the turbulent flow, the size of the typical eddy, as yet undefined, is on the same order as the mixing length ℓ. Nonetheless, this simple model has met with considerable success, particularly for simple shear flows as in the case of turbulent flow in a pipe or turbulent flow over a flat plate.

Equation (9.224) enables us to write the total shear stress in the fluid as the sum of the laminar shear stress and the turbulent or Reynolds shear stress, viz.

$$\tau = \tau_{laminar} + \tau_{turbulent} \tag{9.225}$$

which for two-dimensional flow is

$$\tau = \mu\frac{d\vartheta_x}{dy} - \rho\overline{\vartheta_x'\vartheta_y'} = \mu\frac{d\vartheta_x}{dy} + \mu_T\frac{d\vartheta_x}{dy} \tag{9.226}$$

where μ_T is the *apparent* increase in the viscosity, called the *eddy viscosity*, due to the turbulence in the flow. Since it depends upon the velocity fluctuations which are characteristic of the particular flow field, the eddy viscosity is a property of the flow and must not be regarded as a fluid characteristic like the shear viscosity. It may even vary over the spatial region occupied by the flow. Equation (9.226) can also be written in the form

$$\tau = \rho(\nu + \varepsilon_M)\frac{d\vartheta_x}{dy} \tag{9.227}$$

where ε_M is the *eddy diffusivity* of momentum analogous to the momentum diffusivity characterized by the kinematic viscosity ν. In dimensionless form, the eddy diffusivity is written ε^+ where

$$\tau = \rho\nu\left(1 + \frac{\varepsilon_M}{\nu}\right)\frac{d\vartheta_x}{dy} = \rho\nu\varepsilon^+\frac{d\vartheta_x}{dy} \tag{9.228}$$

9.10.1 Eddies and the Structure of Turbulent Flow

Although eddies are the fundamental reason for enhanced transfer of momentum and energy in turbulent flow, the concept of the "eddy" is not sharply defined. Basically, an eddy of size l represents some sort of coherent motion with a characteristic velocity of $\hat{v}_x(l)$ over this length scale. The characteristic frequency of the eddy is of the order of $\hat{v}_x(l)/l$. Then the irregular motion of turbulent flow can be thought of as a superposition of eddies of different sizes on the mean flow. The process of eddy formation is central to the transport process and can be thought of in the following way. The largest eddies have the largest amplitudes and appear first with a characteristic length l_0 that is of the same order of magnitude as the characteristic length of the flow L. These large eddies have a characteristic velocity $\hat{v}_l$ that is comparable to the mean velocity of the flow $\hat{v}_0$. The characteristic Reynolds number of these large eddies is $Re_l = \hat{v}_l\, l\rho/\mu$ which is of the same order of magnitude as the Reynolds number of the mean flow Re_L. Since this Reynolds number is typically very large in turbulent flow, the effects of viscosity in these large eddies is relatively small and the motion of these eddies can be modeled as inviscid and can be described by the Euler equation. Since an inviscid fluid possesses no dissipation mechanism, it follows that there is no appreciable dissipation of kinetic energy in the large eddies.

However, the large eddies tend to be unstable so they break up into small eddies, thereby transferring kinetic energy from the large eddies into these small eddies in a manner independent of the viscosity of the fluid. These small eddies undergo a further break-up resulting in a transfer of kinetic energy into still smaller eddies. Thus, by means of a practically dissipationless cascade process, momentum and energy pass from the large eddies to the small eddies. In this model, the small eddies, which correspond to high frequencies, participate in the turbulent flow with much smaller amplitudes. They contain only a small part of the total kinetic energy of the fluid, and, therefore, may be regarded as a fine detailed structure superimposed on the large turbulent eddies. It follows that for distances large compared with l, the variation of the fluctuation velocity component is given by the variation in the velocities of the large eddies, namely $\hat{v}_l$. Over distances small compared with l, the fluctuation velocity component is determined by the small eddies and is therefore small compared with $\hat{v}_l$.

Throughout this cascade process, the Reynolds number characteristic of the eddies is decreasing as the characteristic size of the eddies decreases. This process continues until the Reynolds number becomes so small that the viscous effects become the dominant mechanism for dissipating the kinetic energy. The kinetic energy dissipated in this manner ultimately appears as an increase in the stored thermal energy of the fluid. In order to maintain a steady state in the flow field, it is of course necessary to have some external energy source present to continually supply energy to the large eddies. For the case of an incompressible fluid, this energy is supplied by the flow work transfer to the fluid as manifested in the pressure drop in the direction of the average flow.

Although the dissipation is ultimately due to the viscosity, the rate of dissipation is limited by the first step in the cascade. Then its order of magnitude can be determined only by those quantities which characterize the large eddies, namely the fluid density ρ, the dimension l, and the velocity $\hat{v}_l$. The kinetic energy of the large eddies scales according to $\hat{v}_l^2$. Then if ξ represents the rate of energy transfer from the large eddies to the small eddies, it should scale according to the product of the kinetic energy and the frequency of the large eddies, viz.

$$\xi \sim \hat{v}_l^2\left(\frac{\hat{v}_l}{l}\right) \sim \frac{\hat{v}_l^3}{l}$$

which is independent of the viscosity as confirmed by experiment.

In our discussion, we have taken the eddy diffusivity ε_M to be the embodiment of the turbulence. Then if the eddy diffusivity is to characterize the properties of the turbulent flow, its order of magnitude must also be determined by ρ, ϑ_l, and l as per the above discussion. According to equation (9.228), the eddy diffusivity ε_M must have the same dimensions as the kinematic viscosity ν, namely (length)^2/time. The only quantity with these dimensions that can be formed from the combination ρ, ϑ_l, and l is the product $l\vartheta_l$. Then

$$\varepsilon_M \sim l\vartheta_l \tag{9.229}$$

In point of fact, equation (9.229) gives only the manner in which the eddy diffusivity scales with the characteristics of the large eddies. There is a numerical factor of considerable magnitude that would need to be included in equation (9.229) in order to determine the magnitude of the eddy diffusivity. From equation (9.229) the ratio of the eddy diffusivity to the ordinary kinematic viscosity is

$$\frac{\varepsilon_M}{\nu} \sim \frac{l\vartheta_l}{\nu} = Re_l \tag{9.230}$$

so that this ratio scales as the Reynolds number of the large eddies. In light of the large numerical factor in equation (9.229), equation (9.230) is more appropriately written

$$\frac{\varepsilon_M}{\nu} \sim \frac{Re_l}{Re_{critical}} \tag{9.231}$$

where $Re_{critical}$ is that critical value of Reynolds number for which the transition from laminar to turbulent flow occurs. Equation (9.231) shows that for $Re_l << Re_{critical}$, the eddy diffusivity is insignificant and the shear viscosity dominates; consequently, equation (9.227) reduces to the customary laminar flow relation. On the other hand, for $Re_l >> Re_{critical}$, the eddy diffusivity dominates the flow; consequently, under these conditions it is quite often possible to neglect the laminar contribution entirely.

By now it should be obvious that the primary objective of the analysis of turbulent flow is the determination of the eddy diffusivity (or equivalently, the mixing length) that characterizes the flow, preferably in the form ε^+ given by equation (9.228). Once ε^+ is known, the Navier-Stokes equation can be solved to give the average velocity field and the shear stress at the wall. To effect such a solution it is necessary that the boundary conditions be specified. The boundary conditions to be satisfied by the mean velocity components are identical to those of laminar flow, namely all velocity components must vanish at the wall. In addition, all fluctuation velocity components must vanish at the wall which implies that the fluctuation components are very small in the immediate neighborhood of the wall. It follows, then, that immediately adjacent to the wall the only stresses of any consequence are the viscous stresses of laminar flow. Thus in turbulent flow there exists a very thin layer next to the wall that can be modeled as a simple laminar shear flow. In this thin layer known as the *laminar sublayer*, the viscous forces dominate the inertia forces; consequently, there is no turbulence in the laminar sublayer. Any perturbations that occur are quickly damped out by the viscosity. It follows, then, that in this simple shear layer $\varepsilon_M << \nu$ or equivalently $\varepsilon^+ \sim 1$. The velocity profile in this region is a linear one similar to equation (9.4). In spite of the fact that the laminar sublayer is so thin, it plays a significant role in determining the shear at the wall, and hence the viscous drag on the wall, as well as being the major resistance to heat transfer. The shear stress is constant in the laminar sublayer because of the linear velocity profile typical of simple shear flows. Then $\tau = \tau_w$ and equation (9.228) becomes

$$\tau_w = \rho\nu\varepsilon^+ \frac{d\vartheta_x}{dy} = \rho\nu\varepsilon^+ \frac{d\vartheta_x}{dy}$$

$$\frac{\tau_w}{\rho} = \varepsilon^+\nu \frac{d\vartheta_x}{dy} \tag{9.232}$$

The term on the left-hand side of equation (9.232) has the dimensions of a velocity squared. Then we can define a pseudo-velocity, ϑ^*, known as the friction velocity such that

$$\vartheta^* = \sqrt{\frac{\tau_w}{\rho}} \tag{9.233}$$

Then with the aid of equation (9.233), equation (9.232) can be written in dimensionless form, viz.

$$\vartheta^{*2} = \varepsilon^+ \nu \frac{d\vartheta_x}{dy}$$

$$\vartheta^* = \varepsilon^+ \nu \frac{d\left(\vartheta_x / \vartheta^*\right)}{dy} = \varepsilon^+ \nu \frac{d\vartheta^+}{dy} \tag{9.234}$$

$$\varepsilon^+ = \frac{d\left(\vartheta^* y / \nu\right)}{d\vartheta^+} = \frac{dy^+}{d\vartheta^+}$$

where we have introduced the dimensionless distance from the wall, y^+, and the dimensionless velocity, ϑ^+, such that

$$y^+ = \frac{y\vartheta^*}{\nu} \qquad \vartheta^+ = \frac{\vartheta_x}{\vartheta^*} \tag{9.235}$$

From equation (9.235) it can be seen that the quantity y^+ is like a Reynolds number. In the laminar sublayer where $\varepsilon^+ \sim 1$, equation (9.234) becomes

$$\frac{d\vartheta^+}{dy^+} = 1 \tag{9.236}$$

which can be integrated with the boundary condition $\vartheta^+ = 0$ at $y^+ = 0$ to give the linear velocity profile that we expected, viz.

$$\vartheta^+ = y^+ \tag{9.237}$$

which has been shown by experiment to be valid for $y^+ < 5$.

Adjacent to the laminar sublayer is a transitional region known as the *buffer layer.* In the buffer layer the velocity fluctuations are large enough so that the turbulent stresses are comparable to the viscous stresses. The buffer layer provides a smooth transition from the laminar sublayer next to the wall to the *fully turbulent layer* located far from the wall. In this third region, the actual turbulent boundary layer, the Reynolds stresses completely dominate the flow so that $\varepsilon_M >> \nu$ or $\varepsilon^+ >> 1$. In the fully turbulent layer, the shear stress is equal to the Reynolds stress. Then from equation (9.224), we have

$$\tau = \tau_{turbulent} = -\rho\overline{\vartheta_x' \vartheta_y'} = \rho\ell^2\left(\frac{d\vartheta_x}{dy}\right)^2$$

$$\sqrt{\frac{\tau}{\rho}} = \ell\left(\frac{d\vartheta_x}{dy}\right) \tag{9.238}$$

Based upon the experimental evidence, Prandtl suggested that the shear stress could be modeled as being constant across the laminar sublayer, the buffer layer, and the fully turbulent layer as shown schematically in Figure 9.27.

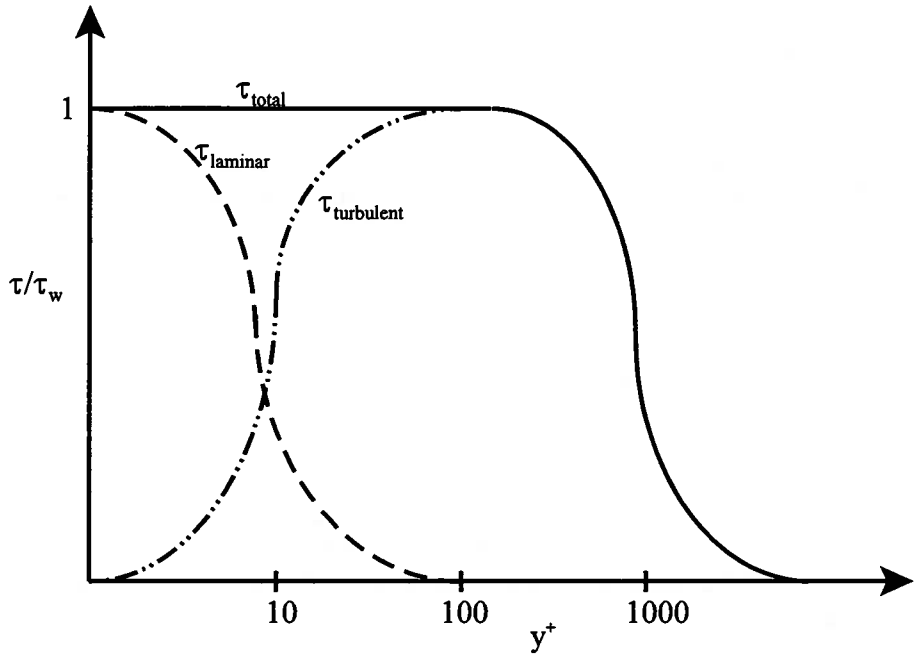

Figure 9.27 Shear Stress Distribution in Turbulent Flow

This is known as the "law of the wall" since the shear stress appearing in equation (9.238) is actually the shear stress at the wall. Then equation (9.238) becomes

$$\sqrt{\frac{\tau_w}{\rho}} = \vartheta^* = \ell\left(\frac{d\vartheta_x}{dy}\right) \tag{9.239}$$

where we have made use of equation (9.233). Prandtl then suggested that the mixing length is proportional to the distance from the wall consistent with our description of the turbulence given above. This suggestion is well supported by the experimental evidence. Then equation (9.239) becomes

$$\vartheta^* = \kappa y \frac{d\vartheta_x}{dy} \tag{9.240}$$

where the constant of proportionality, κ, known as the von Karman constant, is to be determined from the experimental data. Then if we re-arrange equation (9.240), we get

$$d\left(\vartheta_x/\vartheta^*\right) = d\vartheta^+ = \frac{1}{\kappa}\frac{dy}{y} = \frac{1}{\kappa}\frac{dy^+}{y^+} \tag{9.241}$$

Equation (9.241) can be integrated to give

$$\vartheta^+ = \frac{1}{\kappa}\ln y^+ + C \tag{9.242}$$

where the constant of integration, C, is to be determined from the experimental data as shown in Figure 9.28 for both flow in a circular conduit as well as flow over a flat plate.

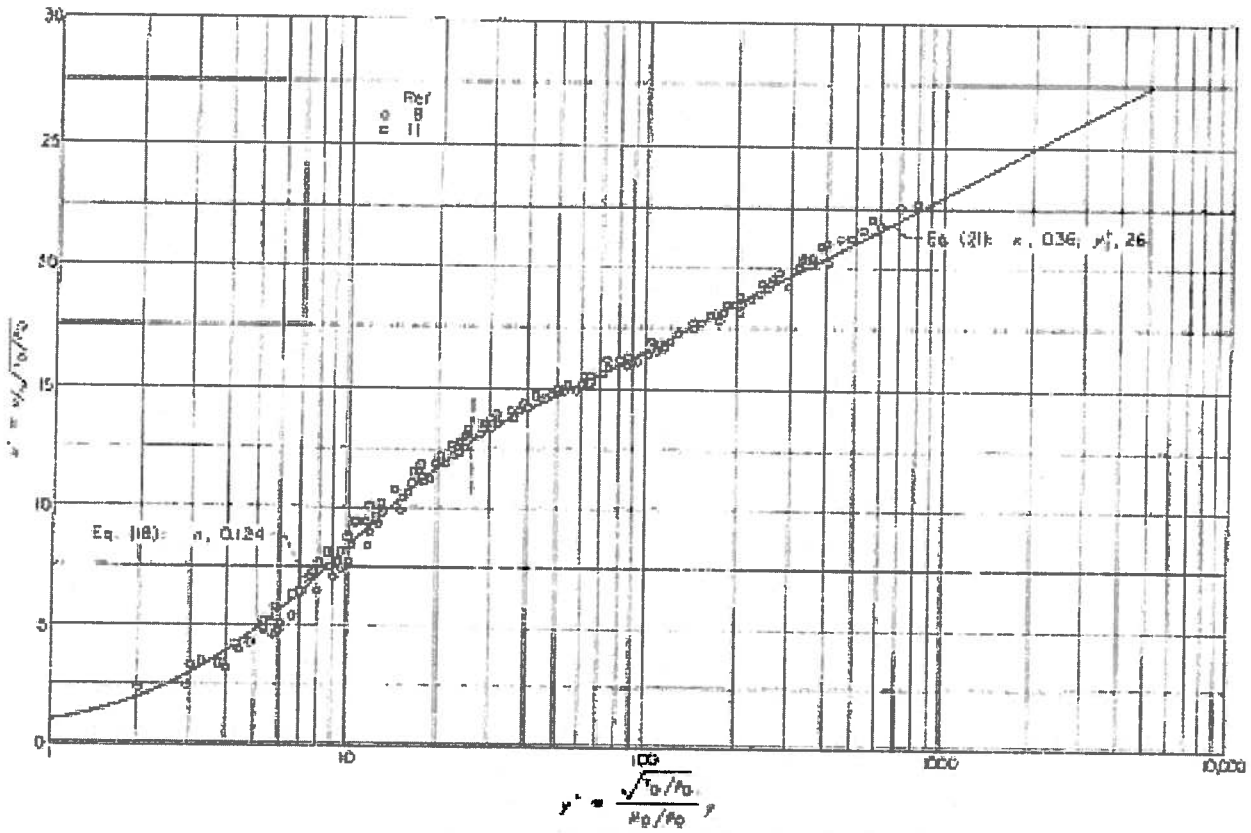

Figure 9.28 Generalized Velocity Distribution for Turbulent Flow
(From Figure 1, NACA Technical Report 1210, *Analysis of Turbulent Heat Transfer, Mass Transfer, and Friction in Smooth Tubes at High Prandtl and Schmidt Numbers*, R. G. Deissler, 1954.)

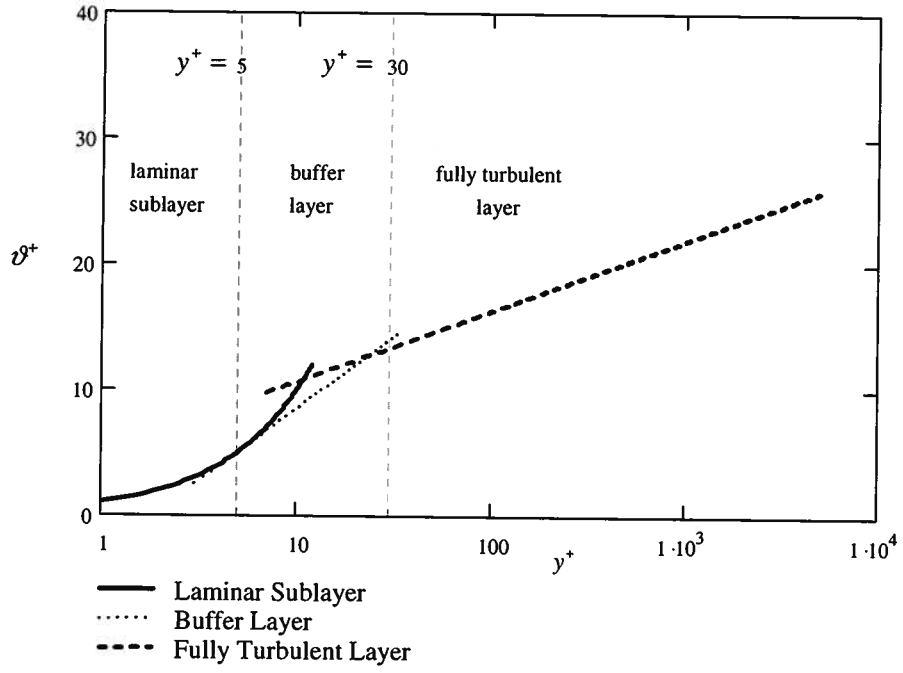

Figure 9.29 Velocity Profiles in Turbulent Boundary Layer

The values that fit the data best are $\kappa = 0.41$ and $C = 5.0$. Then equation (9.242) becomes

$$\vartheta^+ = 2.44 \ln y^+ + 5.0 \tag{9.243}$$

where equation (9.243) is most accurate for $y^+ \geq 30$. In the buffer layer, $5 \leq y^+ < 30$, the velocity profile is best represented by

$$\vartheta^+ = 5 \ln y^+ - 3.05 \tag{9.244}$$

However, as shown in Figure 9.29, this correlation introduces only a small correction to equation (9.243) so it is often neglected. It must be kept in mind that the shear at the wall completely dominates the velocity profile for turbulent flow.

The general structure of turbulent flow discussed above holds for both internal and external flows with some relatively minor differences in each case. Now that we have established the velocity profiles for turbulent flow in the neighborhood of a solid wall, we can use them to determine the characteristics of some turbulent flow geometries, both internal and external, that are important in thermal-fluids engineering.

9.10.2 Turbulent Internal Flows

For obvious reasons, the vast majority of the research in turbulent internal flows has been devoted to studies of flow in a circular conduit. Following this example, we shall consider this case in greater detail than any other. For these internal flows, events at the wall so dominate the flow that even though the flows are driven by a pressure gradient in each case, the velocity profiles are essentially coincident with those developed above for the case of zero pressure gradient. For fully-developed turbulent flow in a circular conduit, the boundary layer extends across the cross-sectional area. The flow consists of a laminar sublayer, a buffer layer, and a fully-turbulent core.

In the laminar sublayer, the velocity profile is the linear one given in equation (9.237) which is valid up to $y^+ < 5$. In order to gain a sense of magnitude of the dimensions of this laminar sublayer in the case of fully-developed turbulent flow in a circular conduit, let us estimate its thickness, δ_L.

$$y^+ = 5$$

$$\frac{\vartheta^* \delta_L}{\nu} = 5$$

$$\frac{\delta_L}{\nu} \sqrt{\frac{\tau_w}{\rho}} = 5 \tag{9.245}$$

where we have made use of the definition of the friction velocity, equation (9.233). The shear stress at the wall is given by equation (9.130). Then

$$\tau_w = \left(\frac{r}{2}\right)_{r=R} \left(\frac{\partial P}{\partial z}\right)_{r=R} = \frac{D}{4} \frac{\Delta P}{L} \tag{9.246}$$

From equation (9.140)

$$\frac{\Delta P}{L} = \frac{\rho f}{D} \left(\frac{\vartheta_{ave}^{\ 2}}{2}\right) \tag{9.247}$$

Substituting equation (9.247) into (9.246), we get

$$\tau_w = \rho \frac{f}{8} \vartheta_{ave}^{\ 2}$$

$$\frac{\tau_w}{\rho} = \frac{f}{8} \vartheta_{ave}^{\ 2} \tag{9.248}$$

Then substituting equation (9.248) into equation (9.245), we get

$$\frac{\vartheta^* \delta_L}{\nu} = \frac{\vartheta_{ave} \delta_L}{\nu}\sqrt{\frac{f}{8}} = 5$$

$$\frac{\delta_L}{D}\frac{\vartheta_{ave} D}{\nu}\sqrt{\frac{f}{8}} = \frac{\delta_L}{D} Re_D \sqrt{\frac{f}{8}} = 5 \tag{9.249}$$

$$\frac{\delta_L}{D} = \frac{5}{Re_D\sqrt{\frac{f}{8}}}$$

We have not yet developed a means of determining the friction factor for turbulent flow. However, for the purposes of an estimate, suppose that the laminar friction factor given in equation (9.141) is still valid for Reynolds numbers close to the laminar-turbulent transition. Then for $Re_D = 4000$, we have

$$f = \frac{64}{Re_D} = \frac{64}{4000} = 0.016 \tag{9.250}$$

and

$$\frac{\delta_L}{D} = \frac{5}{Re_D\sqrt{\frac{f}{8}}} = \frac{5}{4000\sqrt{\frac{0.016}{8}}} = 0.02795 \tag{9.251}$$

A common size for a circular conduit is $D = 25$ mm. Then

$$\delta_L = 0.02795D = 0.02795(0.025\text{ m}) \approx 0.7\text{ mm} \tag{9.252}$$

Clearly the laminar sublayer is quite thin and in fact gets thinner as the Reynolds number increases. It is possible, then, that the asperities on the conduit wall due to casting defects in the case of cast iron pipe or due to scale formation on the wall due to the corrosive nature of a fluid are actually large enough to extend through the laminar sublayer. These asperities can then affect the flow by triggering further turbulence or produce additional friction in the flow. For this reason we then divide our study of turbulent flow in a circular conduit into two domains: (1) flow in a conduit considered hydraulically smooth because the inherent roughness of the conduit wall is much less than the thickness of the laminar sublayer as might be the case for flow in a drawn metal tube or a plastic pipe, and (2) flow in conduits whose walls are inherently so rough that the size of the asperities on the wall are of the same order of magnitude as the thickness of the laminar sublayer.

9.10.2.1 Turbulent Flow in Hydraulically Smooth Conduits: For hydraulically smooth conduits, von Karman proposed what Prandtl called a "middle law" for which the difference between the maximum velocity, ϑ_{max}, found at the centerline of the conduit and the velocity at the distance $y = R - r$ from the wall of the conduit is the product of the friction velocity ϑ^* and a universal function g of the ratio y/r. Then

$$\vartheta_{max} - \vartheta_x(y) = \vartheta^* g\left(\frac{y}{r}\right) \tag{9.253}$$

If we use equation (9.243) for the universal function g, we have

$$\frac{\vartheta_x}{\vartheta^*} = 2.44\ln\frac{y\vartheta^*}{\nu} + 5 = 2.44\ln\frac{(R-r)\vartheta^*}{\nu} + 5 \tag{9.254}$$

If we now evaluate equation (9.254) at the centerline of the conduit, we have

$$\frac{\vartheta_{max}}{\vartheta^*} = 2.44\ln\frac{R\vartheta^*}{\nu} + 5 \tag{9.255}$$

If we now subtract equation (9.254) from equation (9.255), we have

$$\frac{\vartheta_{max}-\vartheta_x}{\vartheta^*}=2.44\ln\frac{R}{R-r} \tag{9.256}$$

which is now known as the *universal defect law* rather than the middle law. Note that by defining the velocity profile in this manner, we have forced the velocity profile to assume the value ϑ_{max} at the centerline with the condition for symmetry, $d\vartheta_x/dr = 0$, satisfied at the centerline as well.

If we now compute the average velocity, ϑ_{ave}, for this flow geometry using equation (9.256) as the velocity profile, we have

$$\vartheta_{ave}=\frac{\dot{V}}{A_c}=\frac{1}{\pi R^2}\left[\int_0^R \vartheta_x 2\pi r dr\right]=\frac{1}{\pi R^2}\left[\int_0^R \vartheta_{max}2\pi r dr-\int_0^R \vartheta^*\left\{2.44\ln R-2.44\ln(R-r)\right\}2\pi r dr\right]$$

$$\vartheta_{ave}=\vartheta_{max}-\frac{3}{2}(2.44)\vartheta^* \tag{9.257}$$

Combining equations (9.257), (9.255), (9.233) and (9.248), we get

$$\begin{aligned}2.44\ln\frac{Re_D}{2}\sqrt{\frac{f}{8}}+5-\frac{3}{2}(2.44)&=\sqrt{\frac{f}{8}}\\ \frac{1}{\sqrt{f}}&=0.8623\ln\left(Re_D\sqrt{f}\right)-1.0200\end{aligned} \tag{9.258}$$

Equation (9.258) is traditionally presented using the base 10 for the logarithm. Then

$$\frac{1}{\sqrt{f}}=1.9856\log_{10}\left(Re_D\sqrt{f}\right)-1.0200 \tag{9.259}$$

The result of equation (9.259) is based upon measurements of the velocity profile in the neighborhood of the wall from which the velocity in the center of the conduit is inferred. Prandtl, together with von Karman, and Nikuradse, decided to improve upon this result by using velocity data actually determined at the center of the conduit. Based on these experimental measurements, the average velocity derived in equation (9.257) becomes

$$\vartheta_{ave}=\vartheta_{max}-4.07\vartheta^* \tag{9.260}$$

Then equation (9.259) becomes

$$\frac{1}{\sqrt{f}}=2.0\log_{10}\left(Re_D\sqrt{f}\right)-0.8 \tag{9.261}$$

which is limited by the experimental data to $3 \times 10^3 < Re_D < 3 \times 10^6$.

Thus, the effects of the fluid viscosity and the turbulence of the flow are manifest in the friction factor used to determine the pressure drop over a given length of conduit according to equation (9.140). Unfortunately, equation (9.261) is a transcendental equation that is rather awkward to use. It is necessary to first guess at a value of f which can be substituted on the right-hand side of equation (9.261) to solve for a new value of f. The process is repeated until the values of f converge.

In an effort to provide the friction factor data in a more tractable form, H. Blasius in 1911 made a critical survey of the then existing experimental results and arranged them in dimensionless form consistent with Reynolds law of similarity. He presented his survey in the form of the coefficient of skin friction, C_f. Thus,

$$\begin{aligned}C_f&=\frac{f}{4}=\frac{0.0791}{Re_D^{\,0.25}}\\ f&=\frac{0.316}{Re_D^{\,0.25}}\end{aligned} \tag{9.262}$$

Subsequent experiments have shown that the validity of this correlation is limited to $3 \times 10^3 < Re_D < 10^5$. More recently, Petukov has suggested that the available data can be better correlated by

$$f = (0.790 \ln Re_D - 1.64)^{-2} \tag{9.263}$$

in the range $10^4 < Re_D < 5 \times 10^6$.

9.10.2.2 Turbulent Flow in Hydraulically Smooth Non-circular Conduits: As an example of the case of turbulent flow in a non-circular conduit, consider the familiar geometry of flow between infinite parallel flat plates as shown in Figure 9.9. If in this case we take $y^* = a - y$, we can write the velocity profile of equation (9.243) in the form

$$\frac{\vartheta_x}{\vartheta^*} = 2.44 \ln \frac{(a-y)\vartheta^*}{\nu} + 5 \tag{9.264}$$

Following the procedure used in the case of a circular conduit, we compute the average velocity ϑ_{ave} according to

$$\vartheta_{ave} = \frac{1}{a}\int_0^a \vartheta_x d(a-y) = -\frac{1}{a}\int_a^0 \vartheta_x dy = -\frac{1}{a}\int_a^0 \vartheta^* \left[2.44 \ln \frac{(a-y)\vartheta^*}{\nu} + 5\right] dy$$

$$\vartheta_{ave} = \vartheta^* \left[2.44 \ln \frac{a\vartheta^*}{\nu} + 2.561\right] \tag{9.265}$$

From equations (9.233) and (9.248) we have

$$\frac{\vartheta_{ave}}{\vartheta^*} = \sqrt{\frac{8}{f}} = 2.44 \ln \frac{a\vartheta^*}{\nu} + 2.561 \tag{9.266}$$

where we have substituted equation (9.265). Since the hydraulic diameter for this geometry is $D_h = 4a$, we can write

$$\frac{a\vartheta^*}{\nu} = \frac{Re_{D_h}}{4}\sqrt{\frac{f}{8}} \tag{9.267}$$

Then we can substitute equation (9.268) into (9.266) to get

$$\frac{1}{\sqrt{f}} = 0.86233 \ln\left(Re_{D_h}\sqrt{f}\right) - 1.1874$$

$$\frac{1}{\sqrt{f}} = 1.9856 \log_{10}\left(Re_{D_h}\sqrt{f}\right) - 1.1874 \tag{9.268}$$

Since equation (9.268) is nearly identical to equation (9.258), we conclude that the dominance of the events in the neighborhood of the wall is so strong, the friction factor data obtained for circular conduits can be applied to non-circular conduits if the diameter D is replaced by the hydraulic diameter $D_h = 4A_c/\wp$ where $\wp$ is the wetted perimeter and A_c is the cross-sectional area. This is in distinct contrast to the case of laminar flow where it was necessary to develop a unique solution of the Navier-Stokes equation for each geometry. The error associated with this replacement is on the order of 10 percent which is adequate accuracy for design purposes.

Before moving on to take up the matter of rough circular conduits, it is worth reflecting for a moment on what we have just accomplished in describing this incredibly complex thermal-fluids phenomenon that we call turbulence. Based upon the randomness of the events in turbulent flow, we proposed a statistical model that we used in the Navier-Stokes equation to identify the effect of the turbulence on the viscous behavior of the fluid. Without solving the Navier-Stokes equation with these new effects included, we then proposed a simple model, based upon the kinetic theory

of gases, to describe these new effects, the Reynolds stresses. We then identified three different regions in the turbulent flow field based upon the degree to which these effects manifest themselves. For each region, we were able to present physical arguments for the nature of the velocity profile in that region. We then made experimental measurements of these velocity profiles, and from the empirical correlations of these data, we were able to determine the effects of both the viscosity and the turbulence embodied in the friction factor. With the aid of the friction factor data we are now able to determine the pressure drop for turbulent flow in a smooth circular conduit. Interestingly enough, we accomplished all this without ever solving the Navier-Stokes equation.

9.10.2.2 Fully-developed Turbulent Flow in Hydraulically Rough Conduits: Despite which relation is used for the friction coefficient, it must be remembered that equations (9.261), (9.262), and (9.263) apply to smooth tubes only. Drawn metallic tubing is considered to be smooth when it is new; however, after it has been in service for sometime, the internal surface of the tube becomes quite rough due to the formation of scale deposits. Furthermore, the inner wall of "standard" pipe is generally quite rough even when new. Since the average roughness of these surfaces is large enough to penetrate through the laminar sublayer, it is worthwhile to develop relationships similar to equations (9.261), (9.262), and (9.263) which will be valid for "rough" tubes. To do this we must formulate a method for determining the degree of roughness of the inner tube wall. The average height of the roughness projections is denoted by k_s, while the radius of the tube is taken to be the average distance from the tube centerline to the inner wall. Therefore, the relative roughness of the tube wall is given by k_s/R. In deriving a general expression for the velocity distribution in rough tubes, Prandtl proposed that the dimensionless distance from the wall y^+ be replaced by the relative roughness y/k_s.

Following this suggestion, in 1933 Johann Nikuradse (1894 - 1979), another student of Prandtl, performed an elaborate set of experiments in which he glued grains of sand, sifted according to size which he denoted by k_s, to the inner walls of otherwise smooth tubes. Nikuradse found from his data that for values of the relative roughness in the range $15 \le R/k_s \le 507$, the velocity profile for large values of the Reynolds number can be written

$$\frac{\vartheta_x}{\vartheta^*} = 2.5 \ln \frac{y}{k_s} + 8.5 \tag{9.269}$$

Computing the average velocity by integrating this profile over the cross-sectional area of the tube, Nikuradse obtained

$$\frac{\vartheta_{ave}}{\vartheta^*} = 2.5 \ln \frac{R}{k_s} + 4.75 \tag{9.270}$$

Von Karman then substituted this result into the combined equations (9.233) and (9.248). Then

$$\frac{1}{\sqrt{f}} = 2.03 \log_{10} \frac{R}{k_s} + 1.68 \tag{9.271}$$

Following this example, Nikuradse found that his friction factor data could be best correlated by

$$f = \left[2.0 \log_{10} \left(\frac{R}{k_s} \right) + 1.74 \right]^{-2} \tag{9.272}$$

This correlation holds only in the "fully rough" regime at large values of the Reynolds number in excess of the value for which

$$Re_{D_h} = \frac{200}{\frac{k_s}{D_h}\sqrt{f}} \tag{9.273}$$

Notice that in the "fully rough" regime, the friction factor is independent of the Reynolds number.

Between the "fully rough" regime bound by equation (9.273) and the laminar flow regime bound by equation (9.141) there is the "transition" regime. For this regime, in 1939 Colebrook combined equation (9.272) and equation (9.261) into a single expression that is the accepted correlation for friction factors for turbulent flow in circular conduits using D and non-circular conduits using D_h. The resulting transcendental equation,

$$\frac{1}{\sqrt{f}} = -2.0\log_{10}\left(\frac{k_s}{3.7D_h} + \frac{2.51}{Re_{D_h}\sqrt{f}}\right) \tag{9.274}$$

proved to be rather inconvenient to use at the time. To help simplify the design process, in 1944 Lewis Ferry Moody (1880 - 1953) plotted the correlations for all three regimes (laminar, fully rough, and transition) on a single graph of friction factor, f, versus Reynolds number, Re_D. This graph has come to be known as the "Moody Diagram" or the "Moody Chart" in honor of its author. Prior to the advent of programmable calculators and personal computers, this was a very important tool for the thermal-fluids engineer in the design of fluid piping systems. Figure 9.30 is the most common form of the Moody Diagram and is presented here more for its historical interest than for its utility since the computational power of computers now facilitates the use of the correlation equation itself.

More recently, Zigrang and Sylvester[5] proposed an explicit correlation of friction factor data that covers all regimes and lends itself more readily to design of turbulent flow systems than the Moody Diagram, viz.

$$f = \left\{-2.0\log_{10}\left[\frac{\left(k_s/D\right)}{3.7} - \frac{4.518}{Re_{D_h}}\log_{10}\left(\left[\frac{\left(k_s/D\right)}{3.7}\right]^{1.11} + \frac{6.9}{Re_{D_h}}\right)\right]\right\}^{-2} \tag{9.275}$$

In order to use the various correlations of friction factor data or the Moody Diagram for thermal-fluids design, it is necessary to have information regarding the equivalent sand grain roughness k_s of conduits fabricated from various materials by various means. Table 9.5 is just such a compilation of data from various sources. The data of Table 9.5, together with the correlations of equations (9.272) and (9.275), can be used most effectively if we make use of Nikuradse's definition of the dimensionless sand grain size k_s^+.

$$k_s^+ = \frac{\vartheta_{ave} k_s}{\nu}\sqrt{\frac{f}{8}} \tag{9.276}$$

The data for the friction factor f can then be classified according to the value of k_s^+:

$$\begin{aligned} &0 < k_s^+ \le 5 && \text{hydraulically smooth} \\ &5 < k_s^+ < 60 && \text{transitionally rough} \\ &60 < k_s^+ && \text{fully rough, } f \text{ independent of } Re_{D_h} \end{aligned} \tag{9.277}$$

The only problem with using this classification is that the friction factor and the average velocity appear as parameters, and they are often the information we seek.

---

[5] Zigrang, D. J. and Sylvester, N. D., "A Review of Explicit Friction Factor Equations," *Trans. ASME, J. of Energy Resources Technology*, 107, 280-283 (1985).

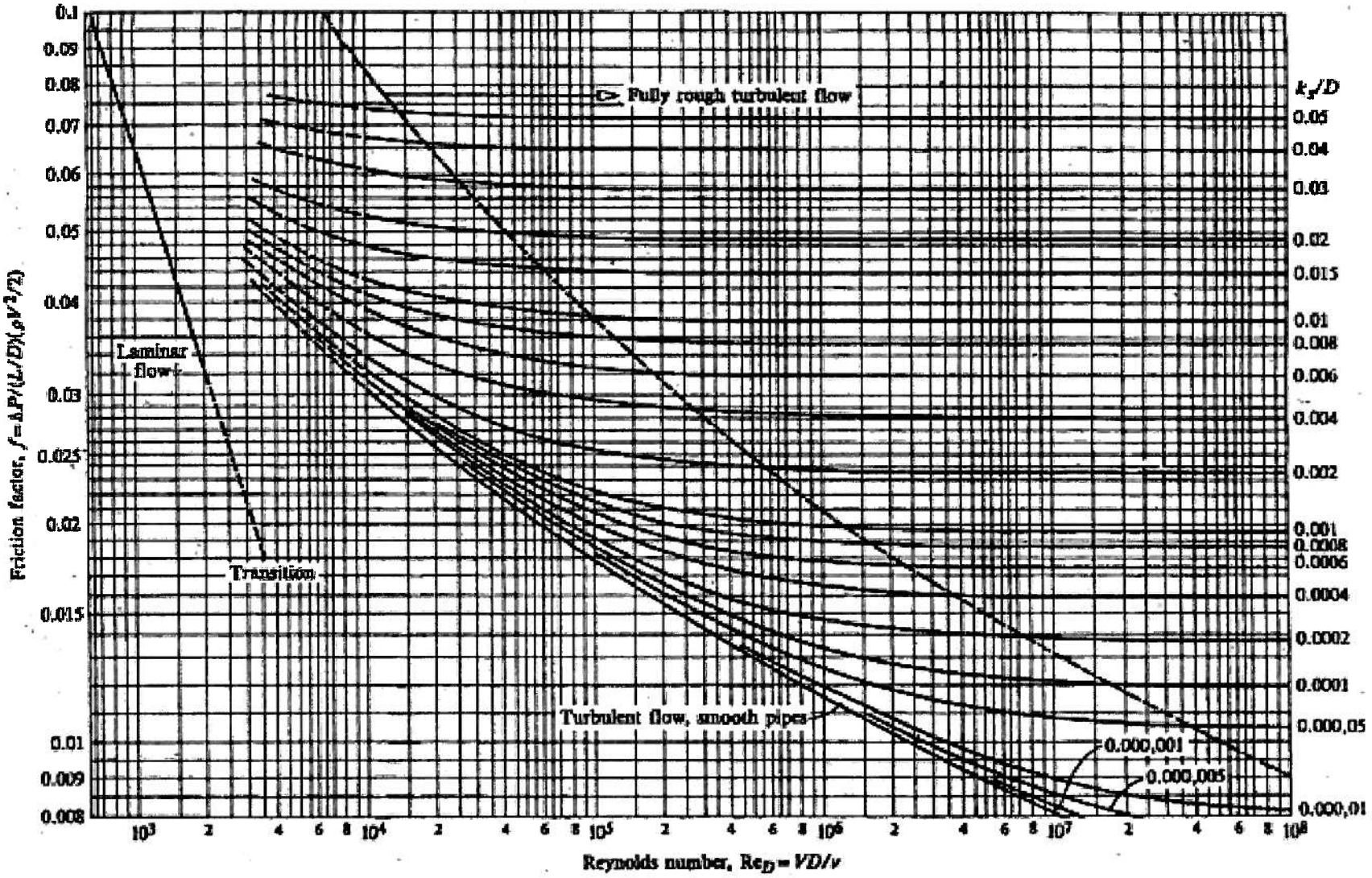

Figure 9.30 Friction Factors for Flow in Circular and Non-circular Conduits
[from Moody, L. F., "Friction Factors for Pipe Flow," *Trans. ASME*, 66, 671-684 (1944)]

Table 9.5 Roughness, k_s, of Various Pipe Configurations

Pipe Configuration	k_s (mm)
Asphalt coated cast iron	0.12
Bituminous lined cast iron	0.0025
Brass	0.0015
Cast iron	0.25
Cement lined cast iron	0.0025
Cement-asbestos	0.3-3
Centrifugally spun cast iron	0.0031
Clay	0.3-3
Commercial steel	0.046
Concrete	0.3-3
Copper	0.0015
Corrugated steel	0.9-9
Drawn tubing	0.0015
Galvanized surface	0.06-0.25
Glass	0.0015
Lead	0.0015
Plastic	0.0015
PVC	Smooth
Riveted steel	0.9-9
Sewer brick	0.3-3
Tin	0.0015
Wood stave	0.18-0.9
Wrought iron	0.046

Source: Johnson, R. W.(editor), *The Handbook of Fluid Dynamics*, CRC Press, Boca Raton, 1998, p. 5-67.

Example 9E.11: As shown in Figure 9E.11, very large cistern is filled with water of density $\rho = 10^3$ kg/m^3 to a depth of $h = 10$ m. Because the water level in the cistern is maintained at a constant level by a well, the water flows from the cistern at a constant rate through a commercial steel pipe of circular cross-section with a diameter of $D = 2.5$ cm and a length of $L =$ 100 m.

(a) Estimate the volumetric flow rate of water from the cistern by modeling the fluid as inviscid.

(b) Estimate the volumetric flow rate of water from the cistern by modeling the fluid as a viscous fluid with a viscosity of $\mu = 8.67 \times 10^{-4}$ kg/m sec.

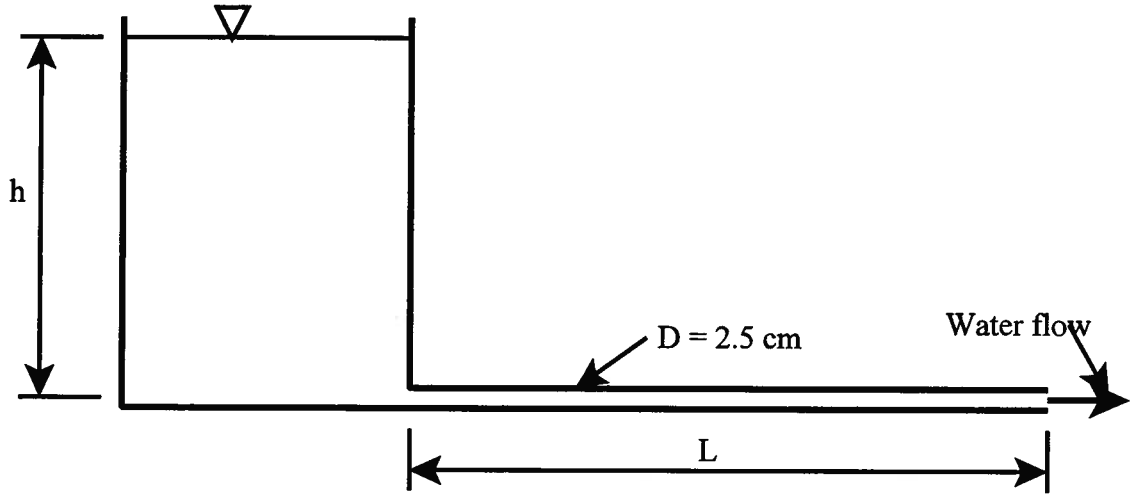

Figure 9E.11

Solution: (a) We begin the solution by assuming that the flow in the discharge pipe is inviscid flow, but we recognize that this is the simplest of all approximations for this flow. This approximation does provide a convenient starting place, however, for more complex models. Consider a streamline that runs from the free surface to the discharge of the pipe. The Bernoulli equation for this streamline is given by

$$\frac{P_1}{\rho}+\frac{\vartheta_1^2}{2}+gz_1=\frac{P_2}{\rho}+\frac{\vartheta_2^2}{2}+gz_2$$

Since $\vartheta_1 = 0$ and $P_1 = P_2 = P_{atm}$, we can write

$$\frac{\vartheta_2^2}{2}=g(z_1-z_2)=gh$$

$$\vartheta_2=\sqrt{2gh}=\sqrt{2\left(9.81\ \text{m/sec}^2\right)(10\ \text{m})}=14.07\ \text{m/sec}$$

Then the volumetric flow rate for this inviscid fluid model becomes

$$\dot{V}=A_c\vartheta_2=\frac{\pi D^2}{4}\vartheta_2=\frac{\pi(0.025\text{m})^2}{4}(14.07\ \text{m/sec})=6.907\ \text{x}\ 10^{-3}\ \text{m}^3/\text{sec}$$

(b) If we now take viscosity into account, we can use the above calculation to estimate the Reynolds number of the flow.

$$Re_D=\frac{\vartheta D\rho}{\mu}=\frac{(14.07\ \text{m/sec})(0.025\ \text{m/sec})\left(10^3\ \text{kg/m}^3\right)}{8.67\ \text{x}\ 10^{-4}\ \text{kg/m sec}}=4.057\ \text{x}\ 10^5$$

Although we know that the effect of viscosity will be to reduce the velocity of flow considerably, the flow does appear from this estimate to be clearly turbulent. Then from equation (9.140), we have

$$\Delta P=\rho f\left(\frac{L}{D}\right)\left(\frac{\vartheta_{ave}^2}{2}\right)$$

$$\vartheta_{ave}=\sqrt{\left(\frac{\Delta P}{\rho}\right)\left(\frac{D}{L}\right)\left(\frac{2}{f}\right)}$$

The pressure of the water at the inlet to the pipe is given by simple hydrostatics. Then

$$\Delta P = (P_{atm} + \rho g h) - P_{atm} = \rho g h$$

$$\vartheta_{ave} = \sqrt{\left(\frac{\rho g h}{\rho}\right)\left(\frac{D}{L}\right)\left(\frac{2}{f}\right)} = \sqrt{(gh)\left(\frac{D}{L}\right)\left(\frac{2}{f}\right)}$$

We know all of these quantities except for the friction factor f. From Table 9.5, we have for commercial steel pipe, $k_s = 0.046$ mm. Then $k_s/D = (0.046 \text{ mm})/(25 \text{ mm}) = 1.84 \times 10^{-3}$. As a first approximation to f, we can assume that the flow is fully rough since this gives a value of f that is independent of the Reynolds number which we do not yet know. From equation (9.272) we have

$$f = \left[2.0 \log_{10}\left(\frac{R}{k_s}\right) + 1.74\right]^{-2}$$

$$f = \left[2.0 \log_{10}\left(\frac{2}{1.84 \times 10^{-3}}\right) + 1.74\right]^{-2} = 0.0164$$

Then

$$\vartheta_{ave} = \sqrt{(9.81 \text{ m/sec}^2)(10 \text{ m})\left(\frac{0.025 \text{ m}}{100 \text{ m}}\right)\left(\frac{2}{0.0164}\right)} = 1.73 \text{ m/sec}$$

and

$$Re_D = \frac{\rho \vartheta_{ave} D}{\mu} = \frac{(10^3 \text{ kg/m}^3)(1.73 \text{ m/sec})(0.025 \text{ m})}{8.67 \times 10^{-4} \text{ kg/m sec}} = 4.987 \times 10^4$$

Based on the new value for the velocity, the flow is still clearly turbulent. The question now is whether it is "fully-rough" as we had assumed. From equation (9.273), the boundary between transition flow and "fully-rough" is

$$Re_D = \frac{200}{\sqrt{f}\left(k_s/D\right)} = \frac{200}{(0.0164)\left(1.84 \times 10^{-3}\right)} = 6.628 \times 10^6$$

Since the Reynolds number is well below this value, we are in the transition region for which equation (9.272) does not hold. Then

$$f = \left\{-2.0 \log_{10}\left[\frac{\left(k_s/D\right)}{3.7} - \frac{4.518}{Re_{D_h}} \log_{10}\left(\left[\frac{\left(k_s/D\right)}{3.7}\right]^{1.11} + \frac{6.9}{Re_{D_h}}\right)\right]\right\}^{-2}$$

$$f = \left\{-2.0 \log_{10}\left[\frac{\left(1.84 \times 10^{-3}\right)}{3.7} - \frac{4.518}{4.987 \times 10^4} \log_{10}\left(\left[\frac{\left(1.84 \times 10^{-3}\right)}{3.7}\right]^{1.11} + \frac{6.9}{4.987 \times 10^4}\right)\right]\right\}^{-2}$$

$$f = 0.02616$$

Since this new value of the friction factor is considerably greater than the value of $f = 0.0164$ that we computed above, we must re-calculate the average velocity. Thus

$$\vartheta_{ave} = \sqrt{(9.81 \text{ m/sec}^2)(10 \text{ m})\left(\frac{0.025 \text{ m}}{100 \text{ m}}\right)\left(\frac{2}{0.02616}\right)} = 1.37 \text{ m/sec}$$

and with this value of the velocity, the Reynolds number becomes

$$Re_D = \frac{\vartheta_{ave} D \rho}{\mu} = \frac{(1.37 \text{ m/sec})(0.025 \text{ m})(10^3 \text{ kg/m}^3)}{8.67 \text{ x } 10^{-4} \text{ kg/m sec}} = 3.949 \text{ x } 10^4$$

Then the new value for the friction factor becomes

$$f = \left\{ -2.0 \log_{10} \left[\frac{(1.84 \text{ x } 10^{-3})}{3.7} - \frac{4.518}{3.949 \text{ x } 10^4} \log_{10} \left(\left[\frac{(1.84 \text{ x } 10^{-3})}{3.7} \right]^{1.11} + \frac{6.9}{3.949 \text{ x } 10^4} \right) \right] \right\}^{-2}$$

$$f = 0.02684$$

Then the new value of the velocity becomes

$$\vartheta_{ave} = \sqrt{(9.81 \text{ m/sec}^2)(10 \text{ m}) \left(\frac{0.025 \text{ m}}{100 \text{ m}} \right) \left(\frac{2}{0.02684} \right)} = 1.35 \text{ m/sec}$$

and the process has converged. Then the volumetric flow rate becomes

$$\dot{V} = A_c \vartheta_{ave} = \frac{\pi D^2}{4} \vartheta_{ave} = \frac{\pi (0.025 \text{ m})^2}{4} (1.35 \text{ m/sec}) = 6.636 \text{ x } 10^{-4} \text{ m}^3/\text{sec}$$

Thus, by neglecting the viscosity, we obtain a volumetric flow rate that is approximately an order of magnitude greater than the estimate that takes the fluid viscosity into account. Notice also that the turbulent viscous flow analysis requires a trial and error solution that does converge after two trials.

9.10.2.3 Velocity Profile Power Law: Let us return for a moment to equation (9.248). If we now substitute into that expression the result from equation (9.262), we get

$$\tau_w = \frac{0.316}{8} \frac{\rho \vartheta_{ave}^2}{Re_D^{1/4}} = 0.0395 \rho \vartheta_{ave}^{7/4} \nu^{1/4} D^{-1/4} \tag{9.278}$$

From equation (9.278), it is apparent that the flow resistance in turbulent flow is proportional to the 1.75 power of the velocity as Hagen's data in 1854 suggested for large values of the flow velocity (large values of the Reynolds number). (See Section 9.9.1.5 and Figure 9.8.) If we substitute equation (9.239) into equation (9.278) and rearrange the terms, we get

$$\left(\frac{\vartheta_{ave}}{\vartheta^*} \right)^{7/4} = \frac{1}{0.0395} \left(\frac{\vartheta^* D}{\nu} \right)^{1/4}$$

$$\frac{\vartheta_{ave}}{\vartheta^*} = 6.3379 \left(\frac{\vartheta^* D}{\nu} \right)^{1/7} \tag{9.279}$$

Equation (9.279) is the first appearance of any kind of a power law for the velocity profile in turbulent flow. Using a power law such as equation (9.279), it can be shown that over a reasonable range of exponents n the mean bulk velocity ϑ_{ave} is approximately 80 percent of the maximum velocity in the tube ϑ_{max}. Then

$$\vartheta_{ave} \approx 0.80 \vartheta_{max} \tag{9.280}$$

Then substituting equation (9.280) into equation (9.279), we get

$$\frac{\vartheta_{max}}{\vartheta^*} = 7.924 \left(\frac{\vartheta^* D}{\nu} \right)^{1/7} = 8.747 \left(\frac{\vartheta^* R}{\nu} \right)^{1/7} \tag{9.281}$$

We now assume that equation (9.281) is valid for any distance y, from the tube wall, not just for the tube centerline where $y = R$. Then equation (9.281) assumes the form

$$\frac{\vartheta_x}{\vartheta^*} = 8.747\left(\frac{\vartheta^* y}{\nu}\right)^{1/7} \tag{9.282}$$

Thus we have succeeded in deriving the *power velocity profile law* from the Blasius friction formula [cf. Equation (9.262)]. Since the Blasius formula is valid only over a limited range of Reynolds numbers, we would expect the 1/7- power velocity distribution law to be similarly restricted.

Encouraged by the result of equation (9.282), Nikuradse conducted an extensive experimental study of the velocity profiles in smooth pipes over a much larger range of Reynolds numbers ($4 \times 10^3 \le Re_D \le 3.2 \times 10^6$) than those that define the limits of the Blasius formula. He found that the results could be correlated by means of the empirical relation

$$\frac{\vartheta_x}{\vartheta_{max}} = \left(\frac{y}{R}\right)^{1/n} = \left(1 - \frac{r}{R}\right)^{1/n} \tag{9.283}$$

where the value of n in the exponent was a function of the Reynolds number. At the lowest value of Reynolds number studied, $n = 6$ and at the highest value of Reynolds number $n = 10$. Although the power velocity profile law is provides a convenient closed form description of the velocity profile for turbulent flow in a pipe, it does have its physical limitations. It predicts infinite velocity gradient at the pipe wall and, hence, cannot be used to evaluate the wall shear stress. Furthermore, it does not produce zero slope at the centerline of the pipe, so it fails to show symmetry about the centerline. Nevertheless, the power velocity profile law does have some utility.

Recalling that the average velocity for flow in a pipe of radius R is defined as

$$\vartheta_{ave} = \frac{\int_0^R \rho \vartheta_x 2\pi r dr}{\rho \pi R^2} \tag{9.284}$$

we can use the empirical velocity profile of equation (9.283) to show that in turbulent flow

$$\frac{\vartheta_{ave}}{\vartheta_{max}} = \frac{2n^2}{(n+1)(2n+1)} \tag{9.285}$$

Table 9.6 shows that as the value of n increases, the ratio of the average velocity to the maximum velocity approaches one. Thus, we conclude that as the Reynolds number of the flow increases, the velocity profile becomes "flatter." Although it applies only to flows at Reynolds numbers of approximately $Re_D = 10^5$, the value $n = 7$ is commonly used as a representative value in equation (9.285).

Table 9.6 Ratio of Average Velocity to Mean Velocity for Turbulent Flow in a Pipe

n	6	7	8	9	10
$\vartheta_{ave}/\vartheta_{max}$	0.791	0.817	0.837	0.852	0.865

9.10.2.4 Turbulent Flow in the Entry Region of a Circular Conduit: Example 9E.11 has not really addressed the issue of the development of the turbulent velocity profile in the entry

region of the conduit. As we saw in the case of laminar flow, there is an entry region for each of these internal flows in which the influence of the viscosity makes itself known across the cross-section of the conduit. Over the distance of the entry length, the boundary layer that forms on the wall at the entrance grows until the boundary layer completely fills the conduit. For the case of turbulent flow, the boundary layer grows more rapidly than in the laminar flow case and the entry length is much shorter.

For the case of turbulent flow in fully-rough circular conduits, Zhiqing[6] combined equations (9.281) and (9.282) to form a power law for the velocity profile in the entry region. He proposed a simple velocity profile in the form

$$\frac{\vartheta_x}{\vartheta_{max}} = \begin{cases} \left(\frac{y}{\delta}\right)^{1/7} & \text{for } 0 \le y \le \delta \\ 1 & \text{for } \delta \le y \le R \end{cases} \tag{9.286}$$

$$\frac{\vartheta_{ave}}{\vartheta_{max}} = 1 - \frac{1}{4}\left(\frac{\delta}{R}\right) + \frac{1}{15}\left(\frac{\delta}{R}\right)^2 \tag{9.287}$$

where δ is the boundary layer thickness which varies with the axial coordinate x according to

$$\frac{x}{D_h Re_{D_h}^{1/4}} = 1.4309\left(\frac{\delta}{R}\right)^{5/4}\left[1 + 0.1577\left(\frac{\delta}{R}\right) - 0.1793\left(\frac{\delta}{R}\right)^2 - 0.0168\left(\frac{\delta}{R}\right)^3 + 0.0064\left(\frac{\delta}{R}\right)^4\right] \tag{9.288}$$

The dimensionless pressure drop defined in equation (9.114) then becomes

$$\left(\Delta P^*\right)_{entry} = \left(\frac{\vartheta_{max}}{\vartheta_{ave}}\right)^2 - 1 \tag{9.289}$$

The hydrodynamic entry length for turbulent flow in a fully-rough circular conduit is then given by

$$\left(\frac{L_{entry}}{D_h}\right)_{turbulent} = 1.359 Re_{D_h}^{1/4} \tag{9.290}$$

By way of comparison, consider two flows in a circular conduit with a Reynolds number of 2300. One of the flows enters a smooth conduit in a laminar fashion while the other enters a fully-rough conduit in a fully-developed turbulent state. In the laminar case, according to equation (9.149), the flow requires approximately 128.8 diameters to become fully-developed Hagen-Poiseuille flow with a parabolic velocity profile while in the turbulent case, according to equation (9.290), the flow requires only 9.4 diameters to become fully-developed turbulent flow with a velocity profile given by equation (9.286). This is clear evidence of the enhanced momentum transport that results from the eddy diffusivity.

9.10.3 Piping Systems

In complex thermal-fluid systems, the working fluid is usually transferred from one system component to another through a piping system consisting of lengths of pipe and various fittings such as elbows, tees, unions, and valves that join these lengths of pipe together. Usually, but not always, the flow in these piping systems is turbulent flow, and these piping systems represent one of the most common applications of the concepts presented in the previous section. In all piping systems, in order to maintain steady flow of the working fluid, it is necessary to provide sufficient flow work transfer in order overcome the viscous dissipation that occurs in the

---

[6] Zhiqing, W., "Study on Correction Coefficients of Laminar and Turbulent Entrance Region Effects in Round Pipe," *Appl. Math. Mech.*, (3/3): 433-446, 1982

various elements of the piping system. This is usually accomplished by means of some sort of pumping apparatus, and in the design of these systems, it is the responsibility of the thermal-fluids engineer to specify the requirements that must be met by this device. In the present section, we shall describe the methods by which the thermal-fluids engineer can determine these requirements.

9.10.3.1 Total Head Loss: Consider the case of a circular conduit of varying cross-section oriented as shown in Figure 9.31. Let us apply the first law of thermodynamics in the form of equation (8.34) to the control volume shown in Figure 9.31.

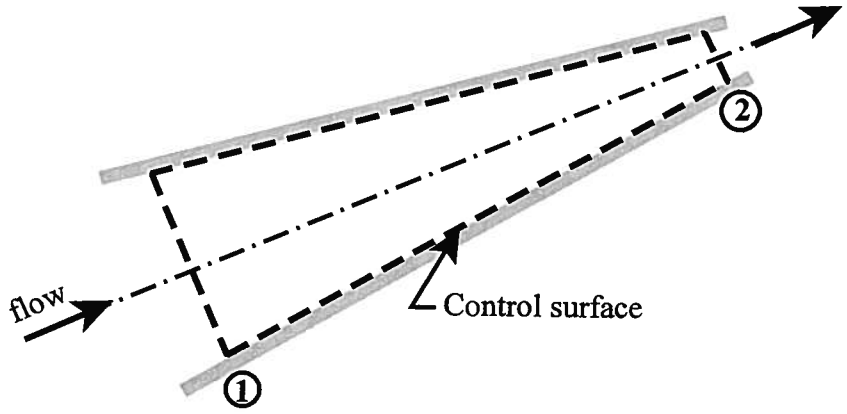

Figure 9.31 Flow in a Circular Conduit of Varying Cross-section

According to equation (8.34), we have

$$\frac{d}{dt}\int_{CV}\rho\left(u+\frac{\vartheta^2}{2}+gz\right)dV=\dot{Q}-\dot{W}_{shear}-\int_{CS}\rho\left(u+\frac{P}{\rho}+\frac{\vartheta^2}{2}+gz\right)\left(\vec{\vartheta}\cdot\vec{n}\right)dA \tag{9.291}$$

In the present case we are interested in steady, adiabatic flow of an incompressible fluid. Through the action of viscosity, there is a shear stress exerted on the lateral surface of the control volume, but since the mass points at this location are not in motion, $\dot{W}_{shear}=0$. Then equation (9.291) becomes

$$\cancel{\frac{d}{dt}\int_{CV}\rho\left(u+\frac{\vartheta^2}{2}+gz\right)dV}=\cancel{\dot{Q}}-\cancel{\dot{W}_{shear}}-\int_{CS}\rho\left(u+\frac{P}{\rho}+\frac{\vartheta^2}{2}+gz\right)\left(\vec{\vartheta}\cdot\vec{n}\right)dA$$

$$\int_{A_2}\rho\vartheta\left(u+\frac{P}{\rho}+\frac{\vartheta^2}{2}+gz\right)dA-\int_{A_1}\rho\vartheta\left(u+\frac{P}{\rho}+\frac{\vartheta^2}{2}+gz\right)dA=0$$

$$\dot{m}\left(u_2-u_1\right)+\dot{m}\left(\frac{P_2}{\rho}-\frac{P_1}{\rho}\right)+\dot{m}g\left(z_2-z_1\right)+\int_{A_2}\rho\vartheta_2\frac{\vartheta_2^{\,2}}{2}dA-\int_{A_1}\rho\vartheta_1\frac{\vartheta_1^{\,2}}{2}dA=0 \tag{9.292}$$

Then

$$\dot{m}\left(\frac{P_1}{\rho}-\frac{P_2}{\rho}\right)+\dot{m}g\left(z_1-z_2\right)+\int_{A_2}\rho\vartheta_1\frac{\vartheta_1^{\,2}}{2}dA-\int_{A_1}\rho\vartheta_2\frac{\vartheta_2^{\,2}}{2}dA=\dot{m}\left(u_2-u_1\right) \tag{9.293}$$

The left-hand side of equation (9.293) is the sum of the rate of flow work transfer (the first term) and the net rate of change of gravitational potential energy and the net rate of change of the kinetic energy of the flow. The right-hand side of equation (9.293) is the rate of increase of stored thermal energy of the flow as a consequence of the viscous dissipation in the control volume. If the flow could be modeled as inviscid and, hence, reversible, the right-hand side of equation (9.293) would vanish. In reality, this is not the case so the right-hand side of equation (9.293) represents the rate at which energy must be supplied to the flow (per unit mass flow rate) by the pumping device in order to maintain steady flow conditions.

For historical reasons that originated with the earliest days of the design of municipal water supply systems, the left-hand side of equation (9.293) is known as the total head loss of the flow denoted by the symbol $h_{l,total}$. It is the quantity that must be determined in order to specify the pumping requirements. In evaluating the head loss, the kinetic energy terms are somewhat more troublesome than the other terms in that the velocity of the fluid at the port varies over the port area. This means that the integral for the kinetic energy term must be evaluated in each case. It would be considerably more convenient if we could use the average velocity instead. This can be accomplished by introducing the *kinetic energy coefficient*, α, defined as

$$\int_A \rho \vartheta_x \frac{\vartheta_x^2}{2} dA = \alpha \dot{m} \frac{\vartheta_{ave}^2}{2}$$

$$\alpha = \frac{\int_A \rho \vartheta_x^3 dA}{\dot{m} \vartheta_{ave}^2} \tag{9.294}$$

For the laminar flow case, we can use equation (9.133) for the velocity profile. Then

$$\alpha = \frac{\int_0^R \rho \left[2\vartheta_{ave} \left(1 - \frac{r^2}{R^2} \right) \right]^3 2\pi r dr}{\left(\rho \vartheta_{ave} \pi R^2 \right) \vartheta_{ave}^2} = \frac{16}{R^2} \int_0^R \left(1 - \frac{r^2}{R^2} \right)^3 r dr = 2 \tag{9.292}$$

where R is the radius of the conduit. For the turbulent flow case, we can use equation (9.283).

$$\alpha = \frac{\int_0^R \rho \left[\vartheta_{max} \left(1 - \frac{r}{R} \right)^{1/n} \right]^3 2\pi r dr}{\left(\rho \vartheta_{ave} \pi R^2 \right) \vartheta_{ave}^2} = \left(\frac{\vartheta_{max}}{\vartheta_{ave}} \right)^3 \frac{2n^2}{(3+n)(3+2n)} \tag{9.293}$$

Table 9.7 shows the values of α for the typical values of n. Recall that n is a function of Reynolds number so α, too, is a function of Reynolds number. However, we observe from Table 9.7 that the dependence of α on n, and by inference on Reynolds number, is rather weak. Moreover, the values of α are only slightly greater than one so that in the case of turbulent flow, α can be taken to be unity with minimal error, particularly in light of the fact that the kinetic energy terms in the expression for total head loss are small compared to the flow work transfer term.

Table 9.7 Dependence of the Kinetic Energy Coefficient on the Value of n

n	6	7	8	9	10
α	1.077	1.058	1.046	1.037	1.031

Then the expression for the total head loss becomes

$$h_{l,total} = \left(\frac{P_1}{\rho} + \alpha_1 \frac{(\vartheta_{ave})_1^2}{2} + gz_1 \right) - \left(\frac{P_2}{\rho} + \alpha_2 \frac{(\vartheta_{ave})_2^2}{2} + gz_2 \right) \tag{9.294}$$

Thus the task of determining the pumping requirements for a piping system becomes one of evaluating equation (9.294). To aid in this process, the total head loss can be rewritten in a slightly different, but equivalent form.

$$h_{l,total} = \left(\frac{P_1}{\rho} - \frac{P_2}{\rho} \right) + \left(\alpha_1 \frac{(\vartheta_{ave})_1^2}{2} - \alpha_2 \frac{(\vartheta_{ave})_2^2}{2} \right) + (gz_1 - gz_2) \tag{9.295}$$

For a unit mass flow rate, the terms on the right-hand side of equation (9.295) represent respectively, the flow work transfer, the change in kinetic energy, and the change in gravitational potential energy of the flow. Of these, the flow work transfer, which embodies the viscous dissipation, typically dominates.

The total head loss is typically divided into two components, one due to the effects of viscous dissipation in the lengths of pipe of constant cross-sectional area in the piping system, the other due to viscous dissipation in the fittings and valves in the system. Since piping systems commonly have extremely long lengths of piping in total (a total length of kilometers is not unusual), this component of the head loss can be quite large so it is referred to as the major head loss, denoted by the symbol $h_{l,major}$. The other component due to the fittings and valves is usually the smaller of the two so it is referred to as the minor head loss, denoted by the symbol $h_{l,minor}$ with a minor head loss contribution from each fitting and valve. Then the total head loss for a piping system with N fittings and valves is given by

$$h_{l,total} = h_{l,major} + \sum_i^N (h_{l,minor})_i = \left(\frac{P_1}{\rho} - \frac{P_2}{\rho} \right) + \left(\alpha_1 \frac{(\vartheta_{ave})_1^2}{2} - \alpha_2 \frac{(\vartheta_{ave})_2^2}{2} \right) + (gz_1 - gz_2) \tag{9.296}$$

We now determine the form for each of the two head loss terms.

9.10.3.2 Major Head Loss: To determine the form for the major head loss term, we consider a special case for which we know the head loss. In particular, consider the case of fully developed turbulent flow of an incompressible fluid in a horizontal conduit of constant cross-sectional area. For this flow configuration, $\alpha_1 = \alpha_2 \approx 1$ and the second term on the right-hand side of equation (9.296) vanishes since the average velocity remains unchanged. Furthermore, for a horizontal conduit, the third term also vanishes. Then for a pipe of diameter D and length L carrying a flow with an average velocity ϑ_{ave}, only the pressure terms remain and the major head loss can be calculated with the aid of equation (9.140), viz.

$$h_{l,major} = \left(\frac{P_1}{\rho} - \frac{P_2}{\rho} \right)_{piping} = f \left(\frac{L}{D} \right) \left(\frac{\vartheta_{ave}^2}{2} \right) \tag{9.297}$$

where the friction factor must be determined from the Reynolds number of the flow. For laminar flow in a conduit of circular with $Re_D \leq 2100$, the friction factor is given by equation (9.141), viz.

$$f = \frac{64}{Re_D} \tag{9.298}$$

For laminar flow in conduits of non-circular cross-section, the hydraulic diameter must be used in evaluating the Reynolds number and the friction factor can then be determined from Table 9.3.

For turbulent flow in smooth pipes of either circular or non-circular cross-section, the friction factor can be determined from equation (9.263), viz.

$$f = \left(0.790 \ln Re_D - 1.64\right)^{-2} \tag{9.299}$$

with the hydraulic diameter used in the evaluation of the Reynolds number.
For rough pipes, the friction factor can be determined from equation (9.275) and the data of Table 9.5, viz.

$$f = \left\{ -2.0 \log_{10} \left[\frac{\left(k_s/D\right)}{3.7} - \frac{4.518}{Re_{D_h}} \log_{10} \left(\left[\frac{\left(k_s/D\right)}{3.7} \right]^{1.11} + \frac{6.9}{Re_{D_h}} \right) \right] \right\}^{-2} \tag{9.300}$$

9.10.3.3 Minor Head Loss: For the minor head loss, the necessary information, with a few exceptions, is usually provided by the manufacturer of the component of interest. There are two methods of reporting the data. In one approach, the minor head loss is taken to depend on the kinetic energy of the flow in a manner similar to the major head loss term, viz.

$$\left(h_{l,minor}\right)_i = K_i \frac{\vartheta_{ave}^{\ 2}}{2} \tag{9.301}$$

where the value of K_i is specific to the component at hand. In the second approach, the minor head loss is evaluated by an expression more closely analogous to the one used in the evaluation of the major head loss with the relevant head loss data expressed in terms of equivalent lengths of straight pipe of the same diameter as the component, viz.

$$\left(h_{l,minor}\right)_i = f \frac{\left(L_e\right)_i}{D} \frac{\vartheta_{ave}^{\ 2}}{2} \tag{9.302}$$

Equations (9.301) and (9.302) each have their advantages and disadvantages and are used with about equal frequency in thermal-fluids engineering practice. In this discussion, we shall use equation (9.301) simply because it provides a sharper contrast between the major and minor head loss terms.

In the following discussion, we present values of the head loss coefficient K_i for a select number of components under turbulent flow conditions. These data are a small sample of the information available in the thermal-fluids engineering literature and are drawn primarily from the comprehensive compilation by R. D. Blevins, *Applied Fluid Dynamics Handbook*, Krieger Publishing Co., Malabar, FL, 1992, Chapter 6. The list of components for which data are presented here includes pipe entrances, enlargements and contractions in pipe cross-sections, and standard fittings.

Pipe Entrances:

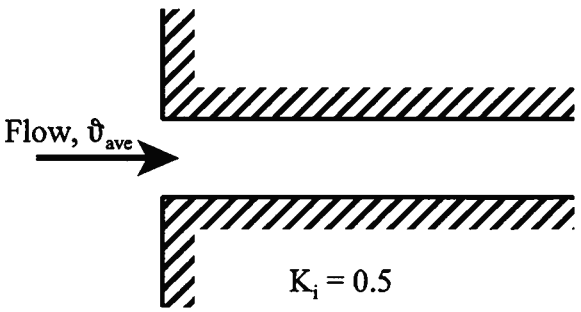

Figure 9.32a Minor Head Loss Coefficient for Square-Edged Entrance

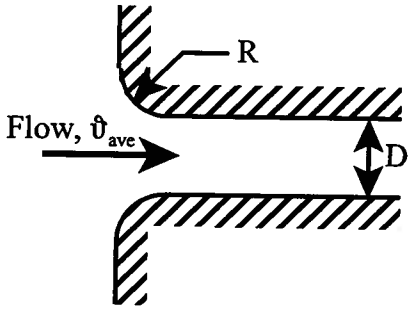

R/D	K_i
0.00	0.50
0.01	0.43
0.02	0.36
0.03	0.31
0.04	0.26
0.05	0.22
0.06	0.20
0.08	0.15
0.12	0.09
0.16	0.06
>0.16	0.03

Figure 9.32b Minor Head Loss Coefficient for Rounded Entrance

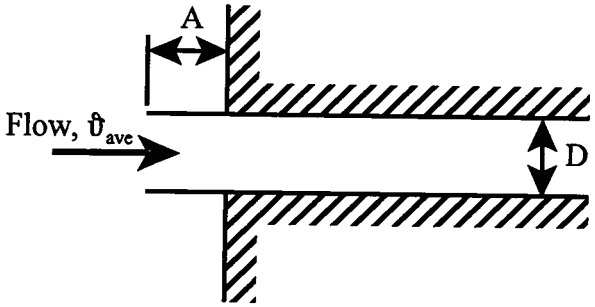

A/D	K_i
0.001	0.63
0.010	0.68
0.100	0.86
0.500	1.00
>0.500	1.00

Figure 9.32c Minor Head Loss Coefficient for Sharp-edged Re-entrant Entrance

Abrupt Enlargements and Contractions:

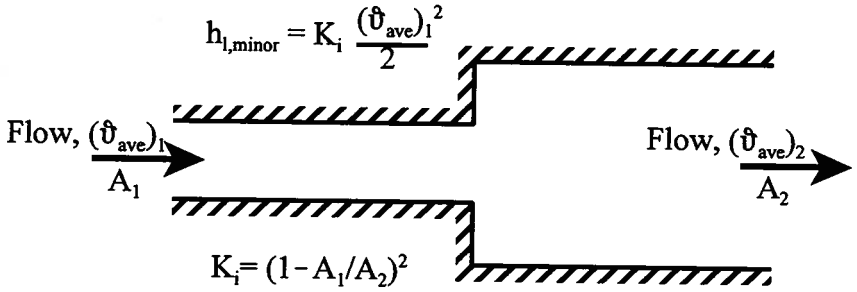

Figure 9.24a Minor Head Loss Coefficient for Abrupt Enlargement

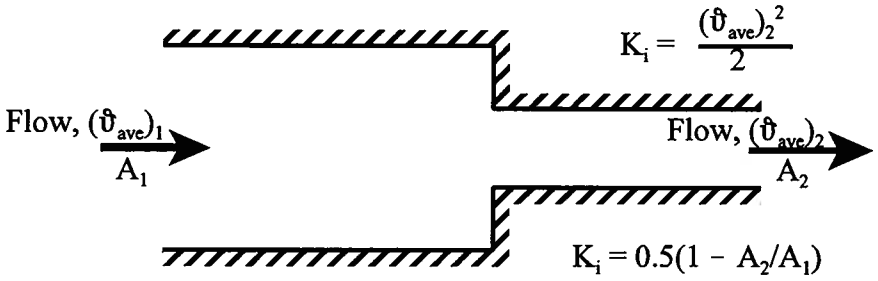

Figure 9.24b Minor Head Loss Coefficient for Abrupt Contraction

Table 9.8 Minor Head Loss Coefficients for Various Fittings and Valves

Valve or Fitting	Nominal Diameter of Fitting, cm					
	2.5	5.0	10	15	20	25
Globe valve, fully open						
Screwed	9	7	5.5			
Flanged	12	9	6	6	5.5	5.5
Gate valve, fully open						
Screwed	0.24	0.18	0.13			
Flanged		0.35	0.16	0.11	0.08	0.06
Foot valve, fully open	0.08 for all sizes					
Swing check valve, fully open						
Screwed	3.0	2.3	2.1			
Flanged	2.0 for all sizes					
Angle valve, fully open						
Screwed	4.5	2.1	1.0			
Flanged		2.4	2.1	2.1	2.1	2.1
Regular elbow, 90°						
Screwed	1.5	1.0	0.65			
Flanged	0.42	0.37	0.31	0.28	0.26	0.25
Long-radius elbow, 90°						
Screwed	0.75	0.4	0.25			
Flanged		0.3	0.22	0.18	0.15	0.14

Source: M. Kutz, *Mechanical Engineers Handbook*, John Wiley, New York, 1998, Table 40.10, p.1321.

Table 9.9 Dimensions for Steel Pipe (American National Standards Institute, ANSI B36.10)

Nominal Size	Pipe OD (in)	Schedule No.	Wall Thkness (in)	ID (in)	Flow Area (in^2)
1/4	0.540	40	0.088	0.364	0.104
		80	0.119	0.302	0.072
3/8	0.675	40	0.091	0.493	0.191
		80	0.126	0.423	0.141
1/2	0.840	40	0.109	0.622	0.304
		80	0.147	0.546	0.234
3/4	1.050	40	0.113	0.824	0.533
		80	0.154	0.742	0.432
1	1.315	40	0.133	1.049	0.864
		80	0.179	0.957	0.719
1-1/4	1.660	40	0.140	1.380	1.50
		80	0.191	1.278	1.28
1-1/2	1.900	40	0.145	1.610	2.04
		80	0.200	1.500	1.77
2	2.375	40	0.154	2.067	3.36
		80	0.218	1.939	2.95
2-1/2	2.875	40	0.203	2.469	4.79
		80	0.276	2.323	4.24
3	3.500	40	0.216	3.068	7.39
		80	0.300	2.900	6.60
4	4.50	40	0.237	4.026	12.73
		80	0.337	3.826	11.50
6	6.625	40	0.280	6.065	28.89
		80	0.432	5.761	26.07
8	8.625	30	0.277	8.071	51.16
		40	0.322	7.981	50.03
		80	0.500	7.625	45.66
10	10.75	30	0.307	10.136	80.69
		40	0.365	10.020	78.85
		XS	0.500	9.750	74.66
		80	0.593	9.564	71.84
12	12.75	30	0.330	12.090	114.8
		ST	0.375	12.000	113.1
		40	0.406	11.938	111.9
		XS	0.500	11.750	108.4
		80	0.687	11.376	71.84

Table 9.9 Notes: Nominal Pipe Sizes (NPS) 1/8 through 12 are known by their nominal diameters in inches. SI standards have not been established as of this writing. The nominal diameter does not indicate a true dimension. All sizes of pipe with NPS 1/8 through NPS 12 have a standardized outside diameter (OD) regardless of Schedule Number or weight. This OD was originally selected so that pipe with a standard wall thickness would have an inside diameter approximately equal to the nominal pipe size. As the Schedule Number or weight changes to accommodate higher working pressures, the wall thickness changes; however, wall thickness affects the inside diameter only. The thicker the wall, the smaller the inside diameter.

In the past, pipe was produced basically in three weights: standard (ST), extra strong (XS), and double extra strong (XXS). In recent years the American National Standards Institute (ANSI) assigned schedule numbers to classify wall thickness for different pressure applications. For NPS1/8 through NPS 10, Schedule 40 is identical with standard weight (ST) pipe. Schedule 80 is identical with extra strong (XS) pipe in nominal NPS 1/8 through NPS 8. Schedules 40 and 80 can vary greatly from standard (ST) and extra strong (XS) pipe in the larger diameters. See ANSI B 36.10.

Useful conversion factors for Table 9.8: To convert from inches to meters, multiply by 2.54×10^{-2}. To convert from $(inches)^2$ to $(meters)^2$ multiply by 6.456×10^{-4}.

In an attempt to establish some correspondence between SI units and the outdated engineering units, "diametre nominel" (DN) has been set as the metric equivalent of Nominal Pipe Sizes (NPS) according to Table 9.10.

Table 9.10 Metric Equivalents (DN) of Nominal Pipe Sizes (NPS)

NPS	⅛	¼	⅜	½	¾	1	1¼	1½	2	2½	3	4	6	8	10	12
DN	6	8	10	15	20	25	32	40	50	65	80	10	15	20	25	30

9.10.3.4 Analysis of Piping Systems: The application of equation (9.296) to a given piping system to determine the pumping requirements embodied in the total head loss is not as straightforward as it might seem on the surface. The difficulty lies in the fact that in a given physical situation, the data for the various head loss terms in equation (9.296) usually depend upon the Reynolds number of the flow, but the Reynolds number depends upon flow velocity which often is not known at the outset. Thus, the analysis of piping systems often requires an iterative procedure in which the thermal-fluids engineer must first guess at a trial solution and then iterate to find the true solution. In the analysis of piping systems there are four different possible situations that present themselves depending upon the information that is known at the outset. We now describe these four different scenarios and offer a plan for approaching each one.

1. *L, D, and $\dot{m}$ (or $\dot{V}$) are known but ΔP is unknown:* In this scenario, the layout of the piping system and the necessary flow rate have been proscribed by the physical configuration of the other systems being connected by the piping. The pump necessary to deliver the working fluid at the specified flow rate must be determined. The dimensions, both length and diameter, of the pipe required together with the fittings and valves necessary to accomplish the connections are known from the piping layout. The performance characteristics of the connecting systems specify the flow rate, either the mass flow rate or the volumetric flow rate. From this information, the flow velocity and the Reynolds number can be determined. Then the friction factor for the pipe and the minor head loss coefficients for the fittings and valves can be determined from the data presented above. Finally, the total head loss and, hence, the pumping requirements can be determined from equation (9.296).

2. *ΔP, $\dot{m}$ (or $\dot{V}$), and D are known but L is unknown:* This scenario is typical of the case in which one of the systems connected by the piping is to be relocated, and it is necessary to determine the length of the new piping configuration to aid in the siting of the component. From the flow rate and the diameter of the pipe, the flow velocity and, hence, the Reynolds number can be determined. From this result and the pressure drop for the configuration, the total head loss can be determined from equation (9.296) and the friction factor can be determined from the correlations. Then equation (9.297) can be solved for the new length of the piping.

3. *ΔP, L, and D are known but $\dot{m}$ (or $\dot{V}$) is unknown:* In this scenario, a pumping device and a piping system exist, and the objective is to determine whether this combination is adequate to meet the flow rate requirement of some other system connected to it. This situation is a bit more complicated than those previously considered since the flow rate and, hence, the flow velocity are unknown. Thus, the Reynolds number is unknown so the friction factor cannot be determined. Without the friction factor, the flow rate cannot be determined. Thus we are faced with making an educated guess at the final result that can then be iterated to obtain the true solution for the flow rate. Two approaches are available to make the "educated guess." In the first approach, the total head loss can be set to zero. Then equation (9.296) can be solved to find the

flow velocity in the absence of friction. This velocity can be used to calculate a Reynolds number that can be used in the appropriate friction factor correlation to obtain a friction factor that can, in turn, be used in equation (9.297) to obtain the new estimate of the major head loss. The new estimate of the minor head loss can be made with the frictionless estimate of the velocity. These estimates of the two head loss contributions can now be used in equation (9.296) to obtain a new estimate of the velocity. This new estimate of velocity that now includes frictional effects can be used to obtain a new estimate of the friction factor, and the whole calculation process can be repeated until the solution for the velocity converges, typically in two iterations. When convergence is obtained, the flow rate can be readily calculated.

In the second approach, the effect of friction can be assumed to be that of the "fully rough" frictional limit for which the friction factor is independent of the Reynolds number [cf. Equation (9.272)]. This estimate of friction factor can be used in equation (9.297) to estimate the velocity provided the minor head loss term is small and that the pressure drop is entirely due to pipe friction. This estimate of velocity can be used to determine a value for Reynolds number that can be used to estimate a new value for the friction factor. The calculation process is then repeated until convergence on the correct value of velocity results.

4. *ΔP, L, and $\dot{m}$ (or $\dot{V}$) are known but D is unknown:* In this scenario, a given pumping device is to be used to pump an incompressible fluid at a predetermined flow rate over a known distance. The diameter of pipe necessary to achieve this is to be determined. This case is similar to case 3 above in that an iterative solution is required because the flow velocity necessary to establish the Reynolds number is unknown. Begin the iterative solution by assuming frictionless flow with zero head loss. Then solve equation (9.296) to determine the flow velocity. Use this flow velocity and the flow rate to determine the "educated guess" at the diameter and the Reynolds number. This estimate of the diameter is the lower bound. Use this Reynolds number to determine the friction factor and then use this friction factor to determine the major head loss from equation (9.297). The minor head loss can be determined from the frictionless velocity and the data for the fittings and valves. Use these results in equation (9.296) to determine a new velocity and subsequently a new Reynolds number. Repeat the analysis as before. Convergence is rapid.

The following examples illustrate the application of the methods of analysis of piping systems.

Example 9E.12: An air impact wrench such as the ones used by NASCAR pit crews to remove the lug nuts from the wheels of race cars, requires a volumetric flow rate of $\dot{V} = 5.4$ CFM at a minimum supply pressure of $P_{supply} = 40$ psi ($\dot{V} = 2.5485 \times 10^{-3}$ m^3/sec at $P_{supply} = 3.77 \times 10^5$ N/m^2) at a temperature of 60 F (288.89 K). The air is supplied through a smooth walled hose with a nominal pipe size of NPS 3/8 and a length of 30 m. It is necessary to determine the pressure drop ΔP through this hose to insure that there is sufficient pressure at the tool for normal operation. The inlet pressure to the hose from the air compressor is P_{inlet}.

For air under these conditions $\mu = 2.0149 \times 10^{-5}$ kg/m sec and $R = 287$ J/kg K.

Solution: This is an example of case 1 above. Let us assume that the flow can be modeled as incompressible even though the working fluid is a gas. We will need to check this later. From Table 9.9 and the conversion factor given in the footnote, the flow area of this "pipe" is

$$A = 0.191 \text{ in}^2 = (0.191 \text{ in}^2)(6.456 \times 10^{-4} \text{ m}^2/\text{in}^2) = 1.2331 \times 10^{-4} \text{ m}^2.$$

Then from continuity, the velocity of flow is

$$\vartheta = \frac{\dot{V}}{A} = \frac{2.5485 \text{ x } 10^{-2} \text{ m}^3/\text{sec}}{1.2331 \text{ x } 10^{-4} \text{ m}^2} = 20.667 \text{ m/sec}$$

This is well below a Mach number of 0.3 since the speed of sound in air under these conditions is on the order of 350 m/sec. Thus we are justified in assuming that the flow can be modeled as incompressible. We need to calculate the density of the air before we can calculate the Reynolds number. Then

$$\rho = \frac{P}{RT} = \frac{3.7711 \text{ x } 10^5 \text{ N/m}^2}{(287 \text{ J/kg K})(288.89 \text{ K})} = 4.5484 \text{ kg/m}^3$$

$$Re = \frac{(20.667 \text{ m/sec})(1.2522 \text{ x } 10^{-2} \text{ m})(4.5484 \text{ kg/m}^3)}{2.0149 \text{ x } 10^{-5} \text{ kg/m sec}} = 58{,}419$$

For this value of Reynolds number for flow in a smooth tube, we can use equation (9.263) to calculate the friction factor, viz.

$$f = (0.790 \ln Re - 1.64)^{-2} = \left[0.790 \ln(58{,}419) - 1.64\right]^{-2} = 0.020231$$

Then from the Darcy-Weisbach Law

$$\Delta P = \rho f \left(\frac{L}{D}\right) \frac{\vartheta_{ave}^{\ 2}}{2} = (4.5484 \text{ kg/m}^3)(0.020)\left(\frac{30 \text{ m}}{1.2522 \text{ x } 10^{-2} \text{ m}}\right) \frac{(20.667 \text{ m/sec})^2}{2}$$

$$\Delta P = 4.7082 \text{ x } 10^4 \text{ N/m}^2$$

Since the discharge pressure from a typical compressor used to provide compressed air to power these tools is on the order of $P_{inlet} = 7.908 \text{ x } 10^5 \text{ N/m}^2$, this pressure drop is only about five percent of the available pressure. Thus a hose of 30 m in length is acceptable for this application.

Example 9E.13: For the tool described in Example 9E.12, determine the maximum length of compressed air hose L_{max} that could be used if the pressure at inlet to the hose is $P_{inlet} = 7.908 \text{ x } 10^5 \text{ N/m}^2$ and $P_{supply} = 3.77 \text{ x } 10^5 \text{ N/m}^2$ is the minimum pressure at the tool that will still permit the tool to operate.

Solution: This is an example of case 2 described above. The volume flow rate specified by the operational requirements of the tool, $\dot{V} = 2.5485 \text{ x } 10^{-3} \text{ m}^3/\text{sec}$, is the same as Example 9E.12. The pressure required at the tool is $P_{supply} = 3.77 \text{ x } 10^5 \text{ N/m}^2$. The inlet pressure to the hose is $P_{inlet} = 7.908 \text{ x } 10^5 \text{ N/m}^2$. Then the maximum allowable pressure drop is

$$\Delta P_{max} = P_{inlet} - P_{supply} = 7.908 \text{ x } 10^5 \text{ N/m}^2 - 3.771 \text{ x } 10^5 \text{ N/m}^2 = 4.137 \text{ x } 10^5 \text{ N/m}^2$$

Since the inside diameter of the hose is the same as Example 9E.12, the velocity and the Reynolds number are the same as those calculated in that example. Thus the friction factor is also the same. Then from the Darcy-Weisbach Law

$$L_{max} = \frac{2D\Delta P_{max}}{\rho f \vartheta_{ave}^{\ 2}} = \frac{2(1.2522 \text{ x } 10^{-2} \text{ m})(4.137 \text{ x } 10^5 \text{ N/m}^2)}{(4.5484 \text{ kg/m}^3)(0.020)(20.667 \text{ m/sec})^2} = 266.65 \text{ m}$$

Example 9E.14: A young child has an aquarium that holds 30 gallons of water. At 8.33 lbm/gal, the weight of the water alone is 250 lbm. Since the child herself weighs only 45 lbm, this tank is hardly something for her to lift when the water needs changing. To draw the dirty water out of the tank she uses a siphon with a geometry as shown in Figure 9E.14. We wish to estimate the maximum flow rate through the smooth-walled siphon tube (I.D. = 8 mm) for the geometry shown taking into account viscous effects. The water can be modeled as an incompressible fluid with a density $\rho = 1000 \text{ kg/m}^3$ and a viscosity of $\mu = 8.67 \text{ x } 10^{-4} \text{ kg/m sec}$. How does this flow rate estimate compare with that for the case in which viscosity is neglected?

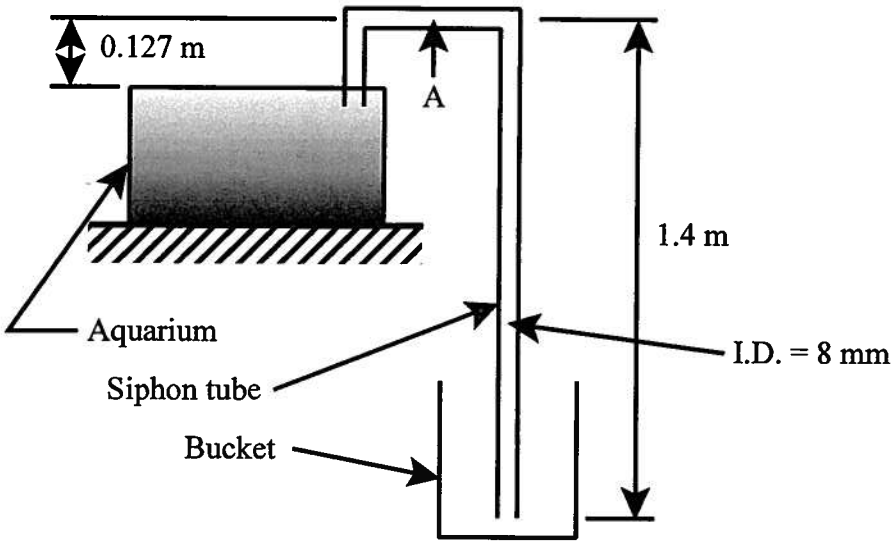

Figure 9E.14 Aquarium Siphon

Solution: The total head loss for this geometry is given by equation (9.296), viz.

$$h_{l,total} = h_{l,major} + \sum_{i}^{N}\left(h_{l,minor}\right)_i = \left(\frac{P_1}{\rho} - \frac{P_2}{\rho}\right) + \left(\alpha_1 \frac{(\vartheta_{ave})_1^{\,2}}{2} - \alpha_2 \frac{(\vartheta_{ave})_2^{\,2}}{2}\right) + (gz_1 - gz_2)$$

The major head loss is given by equation (9.297)

$$h_{l,major} = f\left(\frac{L}{D}\right)\left(\frac{\vartheta_{ave}^{\,2}}{2}\right)$$

and the minor head loss is given by

$$h_{l,minor} = K_1 \frac{\vartheta_{ave}^{\,2}}{2}$$

where K_1 is the head loss coefficient for the re-entrant entrance of the submerged inlet to the siphon tube. If we take location 1 to the free surface of the water in the aquarium, the inlet velocity is effectively zero, and if we also assume turbulent flow (to be checked later), $\alpha_2 = 1$, the total head loss becomes

$$f\left(\frac{L}{D}\right)\frac{\vartheta_{ave}^{\,2}}{2} + K_1 \frac{\vartheta_{ave}^{\,2}}{2} + \frac{\vartheta_{ave}^{\,2}}{2} = \left(\frac{P_1}{\rho} - \frac{P_2}{\rho}\right) + g\left(z_1 - z_2\right)$$

But $P_1 = P_2 = P_{atm}$. Then

$$g\left(z_1 - z_2\right) = \left[f\left(\frac{L}{D}\right) + K_1 + 1\right]\frac{\vartheta_{ave}^{\,2}}{2}$$

If we assume that the siphon tube is submerged to a depth of one tube diameter, Figure 9.32c shows that $K_1 = 1.0$. The difficulty that we now face is that in order to evaluate the friction factor, we need to determine the Reynolds number, but the velocity is as yet unknown. We can make a first guess at the velocity by assuming $f = 0$ in the above expression and solve for ϑ_{ave}. Then

$$\vartheta_{ave} = \sqrt{g\left(z_1 - z_2\right)} = \sqrt{\left(9.81 \text{ m/sec}^2\right)\left(1.4 \text{ m} - 0.127 \text{ m} - 0\right)} = 3.534 \text{ m/sec}$$

Then for this value of velocity, the Reynolds number is

$$Re = \frac{\vartheta_{ave} D \rho}{\mu} = \frac{\left(3.534 \text{ m/sec}\right)\left(0.008 \text{ m}\right)\left(1000 \text{ kg/m}^3\right)}{8.67 \text{ x } 10^{-4} \text{ kg/m sec}} = 32{,}609$$

From equation (9.299), the friction factor is

$$f = (0.790 \ln Re - 1.64)^{-2} = [0.790 \ln(32{,}609) - 1.64]^{-2} = 0.023$$

We can now use this value of f to calculate a new value of ϑ_{ave}. Then

$$\vartheta_{ave} = \left[\frac{2g(z_1 - z_2)}{f\left(\frac{L}{D}\right) + K_1 + 1}\right]^{1/2} = \left[\frac{2(9.81 \text{ m/sec}^2)(1.273 \text{ m})}{0.023\left(\frac{1.527 \text{ m}}{0.008 \text{ m}}\right) + 1 + 1}\right]^{1/2} = 1.977 \text{ m/sec}$$

The new value of Reynolds number is

$$Re = \frac{\vartheta_{ave} D \rho}{\mu} = \frac{(1.977 \text{ m/sec})(0.008 \text{ m})(1000 \text{ kg/m}^3)}{8.67 \text{ x } 10^{-4} \text{ kg/m sec}} = 18{,}242$$

and the new friction factor is

$$f = (0.790 \ln Re - 1.64)^{-2} = [0.790 \ln(18{,}242) - 1.64]^{-2} = 0.0267$$

The third iteration on the velocity gives

$$\vartheta_{ave} = \left[\frac{2g(z_1 - z_2)}{f\left(\frac{L}{D}\right) + K_1 + 1}\right]^{1/2} = \left[\frac{2(9.81 \text{ m/sec}^2)(1.273 \text{ m})}{0.0268\left(\frac{1.527 \text{ m}}{0.008 \text{ m}}\right) + 1 + 1}\right]^{1/2} = 1.874 \text{ m/sec}$$

and the third iteration on the Reynolds number gives

$$Re = \frac{\vartheta_{ave} D \rho}{\mu} = \frac{(1.874 \text{ m/sec})(0.008 \text{ m})(1000 \text{ kg/m}^3)}{8.67 \text{ x } 10^{-4} \text{ kg/m sec}} = 17{,}292$$

and the third iteration on the friction factor gives

$$f = (0.790 \ln Re - 1.64)^{-2} = [0.790 \ln(17{,}292) - 1.64]^{-2} = 0.0272$$

and finally the velocity is

$$\vartheta_{ave} = \left[\frac{2g(z_1 - z_2)}{f\left(\frac{L}{D}\right) + K_1 + 1}\right]^{1/2} = \left[\frac{2(9.81 \text{ m/sec}^2)(1.273 \text{ m})}{0.0272\left(\frac{1.527 \text{ m}}{0.008 \text{ m}}\right) + 1 + 1}\right]^{1/2} = 1.864 \text{ m/sec}$$

Then the flow rate is

$$\dot{V} = A\vartheta_{ave} = \pi \frac{(0.008 \text{ m})^2}{4}(1.864 \text{ m/sec}) = 9.37 \text{ x } 10^{-5} \text{ m}^3/\text{sec}$$

$$\dot{m} = \rho A \vartheta_{ave} = \rho \dot{V} = (1000 \text{ kg/m}^3)(9.37 \text{ x } 10^{-5} \text{ m}^3/\text{sec}) = 0.0937 \text{ kg/sec}$$

For the inviscid case

$$\vartheta_{ave} = \sqrt{2g(z_1 - z_2)} = \sqrt{2(9.81 \text{ m/sec}^2)(1.4 \text{ m} - 0.127 \text{ m} - 0)} = 4.998 \text{ m/sec}$$

$$\dot{V} = A\vartheta_{ave} = \pi \frac{(0.008 \text{ m})^2}{4}(4.997 \text{ m/sec}) = 2.5118 \text{ x } 10^{-4} \text{ m}^3/\text{sec}$$

$$\dot{m} = \rho \dot{V} = (1000 \text{ kg/m}^3)(2.5118 \text{ x } 10^{-4} \text{ m}^3/\text{sec}) = 0.251 \text{ kg/sec}$$

Thus the effect of viscosity reduces the maximum flow rate substantially, by a factor of 2.68.

Example 9E.15: A pumping station for a municipal water system delivers water to a holding reservoir. The pumping station consists of a pump fitted with a globe valve on its discharge followed by a length of pipe of 1250 m followed by a second globe valve at the holding reservoir. The pump characteristics are expressed in terms of the total head loss that it can pump against, in this case $h_{l,total} = 550$ m^2/sec^2, and the volumetric flow rate at that head loss, in this case $\dot{V} = 200$ m^3/hr. The pipe and fittings are made of cast iron, but for a pump of this size, the diameter of the pipe is likely to be large enough that the asperities due to the casting process will be so small relative to the pipe diameter that the pipe can be modeled as smooth. For the water: $\rho = 10^3$ kg/m^3 and $\mu = 10^{-3}$ kg/m sec. Determine the pipe diameter (flanged) appropriate for this pumping station.

Solution: In this case, we have the total head loss so we can write

$$h_{l,total} = \left[f\left(\frac{L}{D}\right) + \sum_{i=1}^{2} K_i \right] \frac{\vartheta_{ave}^{\ 2}}{2}$$

The difficulty is that we need the velocity, as yet unknown, to determine the friction factor used in this equation to solve for the pipe diameter. Thus we are faced with making an educated guess at the velocity (or the pipe diameter) to start an iterative solution. To avoid excessive head losses, these water pumping systems typically use flow velocities such that $\vartheta_{ave} \leq 8$ m/sec. Then as a first try, let us assume $\vartheta_{ave} = 5$ m/sec. Then from continuity

$$D = \sqrt{\frac{4\dot{V}}{\pi \vartheta_{ave}}} = \sqrt{\frac{4(200 \text{ m}^3/\text{hr})}{\pi(3600 \text{ sec/hr})(5 \text{ m/sec})}} = 0.119 \text{ m}$$

From Table 9.10, this is midway between the 4 in and 6 in NPS. Let us choose the larger since this will reduce the velocity and enable us to stay within the typical range for velocity. Then from Table 9.9, $D = 6.0625$ in $= 0.154$ m. and the Reynolds number becomes

$$Re = \frac{\vartheta_{ave} D \rho}{\mu} = \frac{4\dot{V}\rho}{\pi D \mu} = \frac{4(200 \text{ m}^3/\text{hr})(1000 \text{ kg/m}^3)}{\pi(3600 \text{ sec/hr})(0.154 \text{ m})(10^{-3} \text{ kg/m sec})} = 4.5932 \text{ x } 10^5$$

Then the friction factor becomes

$$f = (0.790 \ln Re - 1.64)^{-2} = 0.0133$$

The average velocity is

$$\vartheta_{ave} = \frac{\dot{V}}{A} = \frac{4\dot{V}}{\pi D^2} = \frac{4(200 \text{ m}^3/\text{hr})}{\pi(3600 \text{ sec/hr})(0.154 \text{ m})^2} = 2.983 \text{ m/sec}$$

Then using this result and the data in Table 9.8 for a fully open globe valve for 6 NPS pipe, we get

$$h_{l,total} = \left[f\left(\frac{L}{D}\right) + \sum_{i=1}^{2} K_i \right] \frac{\vartheta_{ave}^{\ 2}}{2} = \left[0.0133\left(\frac{1250 \text{ m}}{0.154 \text{ m}}\right) + 2(6) \right] \frac{(2.983 \text{ m/sec})^2}{2} = 533.7 \text{ m}^2/\text{sec}^2$$

This value of the total head loss is within three percent of the specifications for this pump which is probably within the error limits of the measurements of pump characteristics. Thus the design pipe size for this pumping station would be 6 NPS.

9.10.3.5 Pump Characteristics: Thus far in our discussion of the analysis of piping systems, we have stated that the objective of the analysis is to determine the pumping requirements for the system, but we have not yet explained what those characteristics might be. The object of the pump is to provide the flow work transfer necessary to overcome the total head loss of the piping

system downstream of the pump discharge. Then if we establish a control volume coincident with the walls of the pump and apply the first law to the control volume, we obtain for steady flow operation of the pump

$$\dot{Q}-\dot{W}_{shaft}+\sum_{in}\left[\dot{m}\left(u+\frac{P}{\rho}+\frac{\vartheta^2}{2}+gz\right)\right]_{in}-\sum_{out}\left[\dot{m}\left(u+\frac{P}{\rho}+\frac{\vartheta^2}{2}+gz\right)\right]_{out}=0 \qquad (9.303)$$

Typically, a pump for an incompressible fluid operates in an adiabatic manner. There simply is insufficient residence time of the fluid in the device to establish any significant heat transfer that would enable the fluid to approach thermal equilibrium with the device. Then equation (9.303) becomes

$$\begin{aligned}-\dot{W}_{shaft}&=\dot{m}\left[(u_{out}-u_{in})+\left(\frac{P_{out}}{\rho}-\frac{P_{in}}{\rho}\right)+\left(\frac{\vartheta_{out}^{\ 2}}{2}-\frac{\vartheta_{in}^{\ 2}}{2}\right)+g(z_{out}-z_{in})\right]\\ -\dot{W}_{shaft}&=\dot{m}\left[c(T_{out}-T_{in})+\left(\frac{P_{out}}{\rho}-\frac{P_{in}}{\rho}\right)+\left(\frac{\vartheta_{out}^{\ 2}}{2}-\frac{\vartheta_{in}^{\ 2}}{2}\right)+g(z_{out}-z_{in})\right]\end{aligned} \qquad (9.304)$$

where we have substituted the energy constitutive relation for the incompressible fluid model.

On the right-hand side of equation (9.304), the second term in the square brackets represents the flow work transfer associated with the transfer of the fluid into and out of the pump. This is the reason for the existence of the pump, i.e., to make the outlet pressure of the fluid higher than the inlet pressure of the fluid so that the higher outlet pressure can subsequently be used to drive the flow through the frictional elements (lengths of pipe, fittings, and valves) downstream of the pump. Thus this second term is positive. The third and fourth terms, the kinetic and gravitational potential energy, respectively, are usually small compared with the flow work terms and are often neglected.

On the other hand, the first term in the square brackets on the right-hand side of equation (9.304) represents the increase in stored energy of the fluid due to the irreversible operation of the pump resulting from the viscous behavior of the fluid. This can be seen most easily by applying the second law to the control volume, viz.

$$\begin{aligned}\sum_j\left(\frac{\dot{Q}}{T}\right)_j+\dot{m}(s_{in}-s_{out})+\dot{S}_{gen}&=0\\ \dot{S}_{gen}=-\dot{m}(s_{in}-s_{out})&=\dot{m}c\ln\left(\frac{T_{out}}{T_{in}}\right)\end{aligned} \qquad (9.305)$$

where we have substituted the entropy constitutive relation for the incompressible fluid model. Since the rate of entropy generation will be positive for irreversible operation, the temperature of the fluid, and, hence ,the stored thermal energy, will increase as the fluid passes through the irreversible pump. Thus, like the second term, the first term is also positive for irreversible operation. Clearly, for reversible operation this term is zero.

The net result of these two major energy contributions to the flow is that the shaft power must be negative, i.e., into the pump and, hence, the fluid stream. It follows that the shaft power input to the pump is greater in magnitude for irreversible operation than for reversible operation. Then we can define a pump efficiency η to be

$$\eta=\frac{(\dot{W}_{shaft})_{reversible}}{(\dot{W}_{shaft})_{irreversible}}=\frac{\dot{m}\left[\left(\frac{P_{out}}{\rho}-\frac{P_{in}}{\rho}\right)+\left(\frac{\vartheta_{out}^{\ 2}}{2}-\frac{\vartheta_{in}^{\ 2}}{2}\right)+g(z_{out}-z_{in})\right]}{(\dot{W}_{shaft})_{irreversible}} \qquad (9.306)$$

In the pump industry, the numerator in equation (9.306) is usually referred to as the fluid power and the denominator is referred to as the brake horsepower or shaft power of the drive motor. A typical value for the efficiency of a centrifugal pump is 75 percent.

If we divide the numerator of equation (9.306) by the mass flow rate, we get an expression for the change in stored mechanical energy of the flow through the pump per unit mass which is known as the total dynamic head of the pump, viz.

$$h_{pump} = \left(\frac{P_{out}}{\rho} - \frac{P_{in}}{\rho} \right) + \left(\frac{\vartheta_{out}^{\,2}}{2} - \frac{\vartheta_{in}^{\,2}}{2} \right) + g\left(z_{out} - z_{in} \right) \tag{9.307}$$

Note that equation (9.307) also represents the reversible shaft power added to the flow per unit mass flow rate. If we now subtract equation (9.307) from equation (9.296), we get an expression for the total net head loss for the piping system including the pumping device, viz.

$$h_{l,major} + \sum_{i}^{N} \left(h_{l,minor} \right)_i - h_{pump} = \left(\frac{P_1}{\rho} - \frac{P_2}{\rho} \right) + \left(\alpha_1 \frac{\vartheta_1^{\,2}}{2} - \alpha_2 \frac{\vartheta_2^{\,2}}{2} \right) + g\left(z_1 - z_2 \right) \tag{9.308}$$

where plane 1 refers to the pump inlet and plane 2 refers to the farthest plane of the piping system.

In thermal-fluids engineering practice, the total dynamic head of the pump is usually not the expression given in equation (9.307). In the early days of municipal water systems, the flow was usually driven by gravity alone rather than by mechanical pumps. Based upon this historical practice that dates back to the nineteenth century when the fluid mechanics of water supply systems were first being developed on a rational basis, the term "pump head" usually refers to equation (9.307) divided by the acceleration of gravity g. Then

$$H_{pump} = \frac{h_{pump}}{g} = \left(\frac{P_{out}}{\rho g} - \frac{P_{in}}{\rho g} \right) + \left(\frac{\vartheta_{out}^{\,2}}{2g} - \frac{\vartheta_{in}^{\,2}}{2g} \right) + \left(z_{out} - z_{in} \right) \tag{9.309}$$

which has the units of meters, the height of a column of water that caused the flow. The total head loss then becomes

$$H_{l,total} = \frac{h_{l,total}}{g} = f\left(\frac{L}{D} \right) \frac{\vartheta_{ave}^{\,2}}{2g} + \sum_{i}^{N} K_i \frac{\vartheta_{ave}^{\,2}}{2g} = \left(\frac{P_1}{\rho g} - \frac{P_{in}}{\rho g} \right) + \left(\frac{\vartheta_{out}^{\,2}}{2g} - \frac{\vartheta_{in}^{\,2}}{2g} \right) + \left(z_{out} - z_{in} \right) \tag{9.310}$$

which has the units of meters.

The pump characteristics that are usually most useful in the design of piping systems are the volumetric flow rate, $\dot{V}$ (m^3/hr) and the total dynamic head, H_{pump} (m). There are other pump performance characteristics that are useful, but we shall delay our discussion of these until Chapter 15.

9.10.3.6 Piping Networks: Thus far we have considered only those piping systems for which the components are arranged in series fashion. However, in thermal-fluids engineering practice, it is common to encounter piping networks in which the various components are arranged in both series and parallel configurations simultaneously. The analysis of such configurations can be accomplished by applying the techniques of network analysis except the components in this case are non-linear. In piping networks, all parallel branches have the same pressure drop but different flow rates depending upon the elements that they contain. All elements arranged in series have the same flow rate but different pressure drops depending upon their individual head loss terms.

Example 9E.16: The piping system shown in plan view in Figure 9E.16 consists of two parallel circuits flowing water between two manifolds. The two circuits are in the same horizontal plane. Circuit A is fabricated from 4 NPS cast iron pipe with a flanged globe valve

used to shut off the flow if necessary. Circuit B is fabricated from the same cast iron pipe as circuit A and contains a pump that delivers a volume flow rate of $\dot{V} = 125$ m^3/hr at a head of 33 m. For the water: $\rho = 10^3$ kg/m^3 and $\mu = 10^{-3}$ kg/m sec. Determine the volumetric flow rate of the two circuits together.

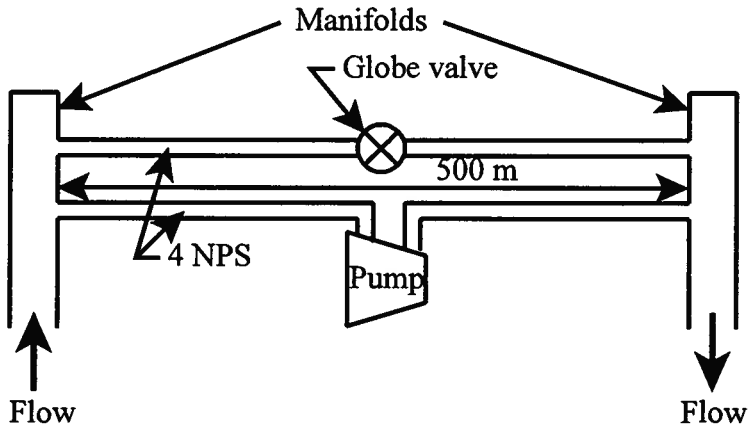

Figure 9E.16 Parallel Piping System (Plan View)

Solution: The pressure drops for the two circuits shown in Figure 9E.16 are the same since they are connected in parallel to the same manifolds. Let the circuit with the pump be circuit A. For this circuit the pressure drop is given by

$$\frac{P_1}{\rho g} - \frac{P_2}{\rho g} = \left[f\left(\frac{L}{D}\right) + K_1 \right] \frac{\vartheta_A^{\,2}}{2g} - H_{pump}$$

where K_1 is the loss coefficient for the entrance to the pipe assumed to be square edged. The flow velocity in circuit A can be determined by the pump through-put (volumetric flow rate). Then for pipe size 4 NPS, $D = 4.026$ in $= 0.1023$ m and $A = 12.73$ in$^2 = 8.2185 \times 10^{-3}$ m^2.

$$\vartheta_A = \frac{\dot{V}}{A} = \frac{\left(125 \text{ m}^3/\text{hr}\right)}{\left(3600 \text{ sec/hr}\right)\left(8.2185\ 10^{-3} \text{ m}^2\right)} = 4.225 \text{ m/sec}$$

Then the Reynolds number for the flow in circuit A is

$$Re_A = \frac{\vartheta_A D \rho}{\mu} = \frac{(4.225 \text{ m/sec})(0.1023 \text{ m})\left(1000 \text{ kg/m}^3\right)}{10^{-3} \text{ kg/m sec}} = 4.3222 \times 10^5$$

For cast iron pipe, Table 9.5 gives $k_s = 0.25$ mm. Then $k_s/D = 2.4438 \times 10^{-6}$ and the friction factor is given by equation

$$f = \left\{ -2.0 \log_{10} \left[\frac{\left(k_s/D\right)}{3.7} - \frac{4.518}{Re_{D_h}} \log_{10} \left(\left[\frac{\left(k_s/D\right)}{3.7} \right]^{1.11} + \frac{6.9}{Re_{D_h}} \right) \right] \right\}^{-2}$$

$$f = \left\{ -2.0 \log_{10} \left[\frac{\left(2.44 \times 10^{-6}\right)}{3.7} - \frac{4.518}{4.32 \times 10^5} \log_{10} \left(\left[\frac{\left(2.44 \times 10^{-6}\right)}{3.7} \right]^{1.11} + \frac{6.9}{4.32 \times 10^5} \right) \right] \right\}^{-2}$$

$$f = 0.0136$$

Then the pressure drop becomes

$$P_1 - P_2 = \left[f\left(\frac{L}{D}\right) + K_1 \right] \frac{\vartheta_A^{\,2} \rho}{2} - H_{pump} \rho g$$

$$P_1 - P_2 = \left[0.0136\left(\frac{500 \text{ m}}{0.1023 \text{ m}}\right) + 0.5 \right] \frac{(4.225 \text{ m/sec})^2 (10^3 \text{ kg/m}^3)}{2} - (33 \text{ m})(10^3 \text{ kg/m}^3)(9.81 \text{ m/sec}^2)$$

$$P_1 - P_2 = 2.7401 \text{ x } 10^5 \text{ N/m}^2$$

Then for circuit B, in order to determine the velocity, we need to have the friction factor which requires the Reynolds number; however, we cannot compute the Reynolds number until we have the velocity. Thus, an iterative solution is required. We then assume as a first estimate that $f_B = f_A$ so that the velocity becomes

$$\vartheta_B = \sqrt{\frac{2(P_1 - P_2)}{\rho\left[f\left(\frac{L}{D}\right) + K_1 + K_2 \right]}} = \sqrt{\frac{2(2.7401 \text{ x } 10^5 \text{ N/m}^2)}{(10^3 \text{ kg/m}^3)\left[0.0136\left(\frac{500 \text{ m}}{0.1023 \text{ m}}\right) + 6 + 0.5 \right]}} = 2.7404 \text{ m/sec}$$

Using this value of velocity we can compute a new value of Reynolds number and a new friction factor. After two iterations we arrive at the result

$$\vartheta_B = 2.637 \text{ m/sec} \quad \text{and} \quad Re = 2.6976 \text{ x } 10^5$$

Then the total flow rate for this parallel circuit becomes

$$\dot{V}_{total} = \dot{V}_A + \dot{V}_B = (\vartheta_A + \vartheta_B) A = (4.225 \text{ m/sec} + 2.637 \text{ m/sec})(8.2185 \text{ x } 10^{-3} \text{ m}^2)$$

$$\dot{V}_{total} = 0.056395 \text{ m}^3/\text{sec} = 203.02 \text{ m}^2/\text{hr}$$

9.10.4 Turbulent External Flows

As we have already discussed in Section 9.9.2.2, in the vicinity of the sharp leading edge of a smooth flat plate, viscous damping ensures that the flow in the boundary layer is laminar even if the flow in the mainstream is turbulent. However, as the laminar boundary layer grows in thickness as the flow proceeds downstream, the flow eventually reaches a location where the characteristic amplitude of the fluctuations inherent in the flow has become so large the viscous forces are no longer able to damp out these disturbances. At this point, the flow in the boundary layer becomes unstable and undergoes a transition to turbulent flow that continues over the remaining length of the plate. In point of fact, the transition from laminar to turbulent flow in the boundary layer is not a sharp one. What happens is that there is a transition region at the end of the laminar region where the laminar boundary layer tries to continue its growth but is constantly being broken up by the instability that derives from the limited damping capabilities of the fluid. Because of this continual destruction and recreation process, transition from laminar to turbulent flow in the boundary layer occurs over a region of the flow rather than at a definite location on the plate. In this transition region, shear stress at the wall increases and the velocity profile undergoes changes in shape as the fully turbulent boundary layer tries to establish itself. Once this occurs, the turbulent boundary layer grows at a much faster rate than that in the laminar region. Of course, as we have already seen in the case of turbulent internal flows, there is a laminar sublayer imbedded in this now fully turbulent boundary layer.

Experimental measurements of this transition phenomenon for a flat plate with zero pressure gradient have reported a range of values of the local Reynolds number at which the transition occurs, typically $6 \times 10^4 < Re_{x,transition} < 5 \times 10^5$. Since these data usually have been obtained in laboratory settings where the conditions are precisely controlled, some investigators believe that these data are artificially high. Kays and Crawford (W. M. Kays and M. E. Crawford, *Convective Heat and Mass Transfer*, 2nd edition, McGraw-Hill, N. Y., 1980, Chapter 10) argue that the results obtained from viscous stability theory might be more appropriate in practice where conditions are not quite so closely controlled, viz. $Re_{x,transition} = 60{,}000$. The location of the transition can also be expressed in terms of the momentum thickness. From equation (9.199),

$$x = \frac{\theta\sqrt{Re_x}}{0.664} \tag{9.311}$$

where θ is the momentum thickness and then

$$Re_{x,transition} = \frac{\vartheta_x x}{\nu} = \frac{\vartheta_x \theta\sqrt{Re_{x,transition}}}{0.664\nu}$$

$$0.664\sqrt{Re_{x,transition}} = \frac{\vartheta_x \theta}{\nu} = Re_{\theta,transition} \tag{9.312}$$

$$Re_{\theta,transition} = 162.65$$

Figure 9.31 shows the fluctuating nature of the outer part of a turbulent boundary layer on a flat plate 3.3 m long suspended in a wind tunnel. Streaklines from a smoke wire near the sharp leading edge are illuminated by a vertical slice of light. (A streamline is the locus of points that are everywhere tangent to the instantaneous velocity vector and cannot be observed directly by

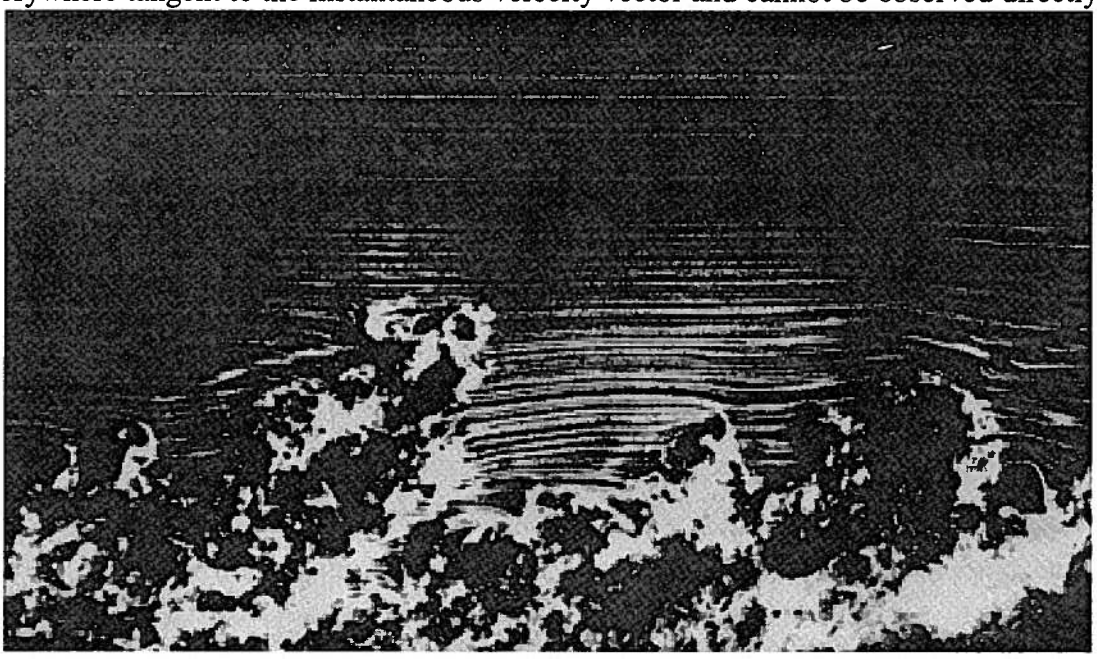

Figure 9.31 Side View of a Turbulent Boundary Layer on a Flat Plate, $Re_\theta = 3500$
(From Figure 157, p. 92 of *An Album of Fluid Motion* by M. Van Dyke, Parabolic Press, Stanford, CA, 1982.)

flow visualization. A pathline is the trajectory of a fluid particle expressed as a function of position and time and is obtained by injecting a dye or some other indicator and observing continuously or photographing with a long exposure time. A streakline is the locus at any instant of all fluid particles that have at some previous time passed through a fixed point in the flow and is obtained by injecting an indicator continuously and observing or photographing instantaneously. In steady flow, all three "lines" are identical, but in unsteady flow, the streamlines, streaklines, and pathlines are all different so that care must be exercised in interpreting the images obtained by various methods of flow visualization. In Figure 9.31, outside the turbulent boundary layer where the flow is steady, the streaklines are identical with the streamlines.) The Reynolds number of the flow in the photograph of Figure 9.31is 3500 as determined by using the momentum thickness as the characteristic length. According to the criterion expressed in equation (9.312), the flow of Figure 9.31 clearly is well into the turbulent regime.

Despite the seemingly chaotic nature of the flow field shown in Figure 9.31, there really is a structure to it. Figure 9.32 shows an image of the laminar sublayer of a turbulent boundary layer on a flat wall. The image was created by introducing a suspension of aluminum particles in a stream of water. The lower portion of the image shows the streaks that result when the sublayer is viewed normal to the wall while the upper portion of the image is a simultaneous side view of the boundary layer formed with the aid of a mirror. The laminar sublayer is clearly evident as is the fully turbulent outer layer.

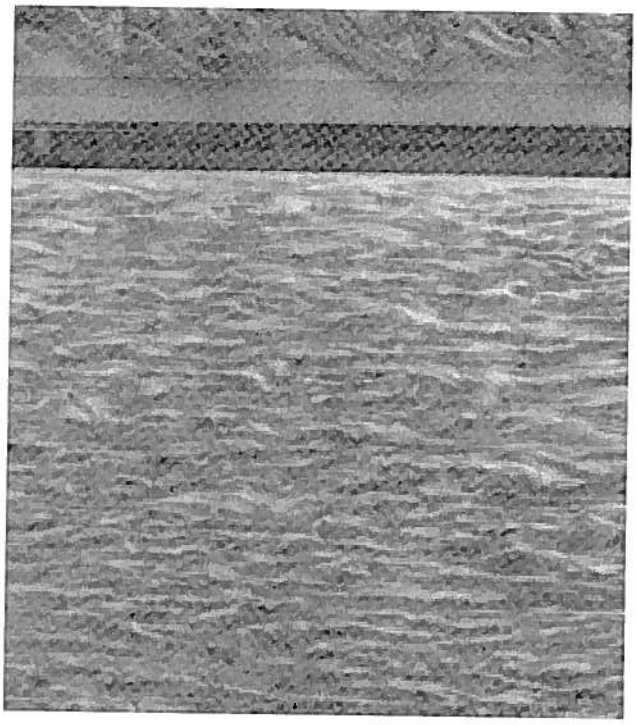

Figure 9.32 Laminar Sublayer of a Turbulent Boundary Layer
(From Figure 159, p. 93 of *An Album of Fluid Motion* by M. Van Dyke, Parabolic Press, Stanford, CA, 1982.)

In internal flows, we focused our interest on the pressure drop required to drive the flow. In contrast, for external flows we are interested in the shear stress that acts on the surface. It is this shear stress that is responsible for the "skin friction drag" experienced by the object. For external flows, the flow is usually driven by the flow external to the boundary layer rather than being driven by a pressure drop in the direction of the flow.

In an attempt to describe the boundary layer on the surface of an object immersed in a flow, we are led to an interesting application of the power velocity profile law developed in Section 9.10.2.2. In that section we showed that the data for the velocity profile in the turbulent boundary layer can be fit approximately with a 1/7th power law. In the analysis of the flow over a flat plate, Von Karman has suggested, in the interests of simplicity, that the similarity solution for the turbulent boundary layer that results for such an external flow can be written in the form

$$\frac{\vartheta_x}{\vartheta_\infty} = \left(\frac{y}{\delta}\right)^{1/7} \tag{9.313}$$

where δ is the bounday layer thickness. Although in the present case we are dealing with the flow over a flat plate, we now borrow some results from turbulent flow in a circular conduit. Recall from equation (9.248) that the shear stress at the wall for turbulent flow in a circular conduit was related to the friction factor by

$$\tau_s = \frac{f}{8}\rho\vartheta_{ave}^{\ 2} \tag{9.314}$$

In 1911 Blasius fit all the data then available for the friction factor for turbulent flow in a circular conduit by the expression

$$f = 0.3164\left(\frac{\vartheta_{ave}D}{\nu}\right)^{-1/4} \tag{9.315}$$

Combining equations (9.314) and (9.315), we get

$$\tau_s = 0.03955\rho\vartheta_{ave}^{\ 1/4}\nu^{1/4}D^{-1/4} \tag{9.316}$$

If we rewrite this result in terms of the radius R of the conduit and recognize that for turbulent flow in this geometry $\vartheta_{ave} = 0.8\vartheta_{max}$, we get

$$\tau_s = 0.0225\rho\vartheta_{max}^{\ 1/4}\left(\frac{\nu}{R}\right)^{1/4} \tag{9.317}$$

Applying equation (9.317) to the case of the flat plate in turbulent flow, we obtain

$$\frac{\tau_s}{\rho\vartheta_\infty^{\ 2}} = 0.0225\left(\frac{\nu}{\vartheta_\infty\delta}\right)^{1/4} \tag{9.318}$$

In our prior discussion of the momentum thickness, we derived the result [equation (9.202)]

$$\tau_s = \rho\vartheta_\infty^{\ 2}\frac{d\theta}{dx} \tag{9.319}$$

where θ is the displacement thickness given by equation (9.197), viz.

$$\theta = \int_0^\delta \frac{\vartheta_x}{\vartheta_\infty}\left(1 - \frac{\vartheta_x}{\vartheta_\infty}\right)dy \tag{9.320}$$

Substituting equation (9.313) into equation (9.320) and carrying out the integration, we get

$$\theta = \frac{7}{72}\delta \tag{9.321}$$

Substituting this result into equation (9.319), we obtain a differential equation for the boundary layer thickness based upon the 1/7th power law similarity solution of equation (9.313), viz.

$$\frac{7}{72}\frac{d\delta}{dx} = 0.0225\left(\frac{\nu}{\vartheta_\infty \delta}\right)^{1/4} \tag{9.322}$$

Integrating equation (9.322) from the leading edge of the plate to the location x, we get

$$\int_0^\delta \delta^{-1/4} d\delta = \frac{0.23143\nu^{1/4}}{\vartheta_\infty^{1/4}} \int_0^x dx$$

$$\delta(x) = 0.37x\left(\frac{\vartheta_\infty x}{\nu}\right)^{-1/5} \tag{9.323}$$

Then from equation (9.321) we get

$$\theta(x) = 0.036x\left(\frac{\vartheta_\infty x}{\nu}\right)^{-1/5} \tag{9.324}$$

We can express the local shear stress on the surface of an object in an external flow in non-dimensional form by defining the local skin friction coefficient C_{fx} as

$$C_{fx} = \frac{\tau_s}{\frac{1}{2}\rho \vartheta_\infty^{\,2}} \tag{9.325}$$

Combining equation (9.325) with equation (9.319), we get

$$C_{fx} = 2\frac{d\theta}{dx} \tag{9.326}$$

Differentiating equation (9.319) and substituting the result into equation (9.326), we get an expression for the local skin friction coefficient on a flat plate, viz.

$$C_{fx} = 0.0576\left(\frac{\vartheta_\infty x}{\nu}\right)^{-1/5} = 0.0576 Re_x^{-1/5} \tag{9.327}$$

Then

$$\frac{C_{fx}}{2} = 0.0288 Re_x^{-1/5}$$

but the experimental data have been found to be better represented by changing the constant slightly so that

$$\frac{C_{fx}}{2} = 0.0296 Re_x^{-1/5} \tag{9.328}$$

which is the commonly accepted correlation in the literature for the local skin friction coefficient for turbulent flow over a smooth flat plate (one side).

The total drag force F_D on one side of a flat plate of length L and width b can be determined by integrating the shear stress on the surface over the area of the plate, viz.

$$F_D = \int_0^L \tau_s b dx \tag{9.329}$$

which is usually expressed in dimensionless form as the drag coefficient C_D such that

$$C_D = \frac{F_D}{\frac{1}{2}\rho \vartheta_\infty^{\,2} bL} = \int_0^1 C_f d\left(\frac{x}{L}\right) \tag{9.330}$$

Substituting equation (9.328) into equation (9.330), we get

$$C_D = 0.0592\int_0^1 Re_x^{-1/5} d\left(\frac{x}{L}\right) = 0.0592\int_0^1 \left(\frac{\vartheta_\infty \rho x}{\mu}\right)^{-1/5} d\left(\frac{x}{L}\right)$$

$$C_D = 0.0592\left(\frac{5}{4}\right)\left(\frac{1}{L}\right)^{1/5}\left(\frac{\vartheta_\infty \rho}{\mu}\right)^{-1/5}\int_0^1 \left(\frac{x}{L}\right)^{-1/5} d\left(\frac{x}{L}\right) \qquad (9.331)$$

$$C_D = 0.074 Re_L^{-1/5}$$

After equations (9.328) and (9.331) had been developed, Prandtl pointed out that they were actually derived on the assumption that the turbulent boundary layer started at the leading edge of the plate. Clearly, this is not the case since there exists a laminar region over a considerable portion of the leading edge even in the case for which the free stream flow is turbulent. The friction force over this leading edge is then considerably less than if the boundary layer had been turbulent from the outset. Prandtl suggested that the turbulent friction force from the leading edge to the to the point of the laminar-turbulent transition be replaced by the laminar friction force over this region. If we use the Blasius solution, equation (9.204), for the laminar region, the integration of the shear stress over the surface of the plate takes on a different form., viz.

$$C_D = \frac{1}{L}\left[\int_0^{x_{transition}} (C_{fx})_{laminar}\, dx + \int_{x_{transition}}^{L} (C_{fx})_{turbulent}\, dx\right]$$

$$C_D = \frac{1}{L}\left[\int_0^{x_{transition}} 0.664 Re_x^{-1/2} dx + \int_{x_{transition}}^{L} 0.0592 Re_x^{-1/5}\right]$$

$$C_D = \frac{\mu}{\vartheta_\infty \rho L}\left[\int_0^{Re_{x,transition}} 0.664 Re_x^{-1/2} d(Re_x) + \int_{Re_{x,transition}}^{Re_L} 0.0592 Re_x^{-1/5} d(Re_x)\right]$$

where we have changed the variable of integration from x to Re_x for simplicity. Carrying out the integration and rearranging the result, we get

$$C_D = 1.328\left(Re_{x,tr}\right)^{-1/2}\left(\frac{Re_{x,tr}}{Re_L}\right) + 0.074 Re_L^{-1/5}\left[1 - \left(\frac{Re_{x,tr}}{Re_L}\right)^{4/5}\right] \qquad (9.332)$$

Of course, the difficulty in applying equation (9.332) in practice is that the transition from laminar to turbulent is not sharply defined because of the continual creation and destruction of the turbulent boundary layer in the transition region. This due in part to the level of turbulence in the free stream. Lacking any other information, it is common practice to assume that the laminar-turbulent transition occurs at a transition Reynolds number of $Re_{x,tr} = 5 \times 10^5$.

When the Reynolds number becomes extremely large, $Re_L > 10^7$, the laminar portion of the boundary layer becomes insignificant. Then using data obtained specifically for this situation and employing the momentum integral approach used above, there results

$$\frac{C_{fx}}{2} = 0.0131 Re_x^{-1/7} \qquad (9.333)$$

and

$$C_D = 0.031 Re_L^{-1/7} \qquad (9.334)$$

The foregoing analysis applies to the case of a smooth flat plate. For the rough flat plate there is no analysis except for the case of the fully rough flat plate for which Mills and Hang [Mills, A. F. and Xu Hang, "On the Skin Friction Coefficient for a Fully Rough Flat Plate," *J. Fluids Engineering*, 105, 364-365, (1983)] suggest

$$C_{fx} = \left(3.476 + 0.707 \ln \frac{x}{k_s} \right)^{-2.46} \quad \text{for} \quad 150 < \frac{x}{k_s} < 1.5 \text{ x } 10^7 \tag{9.335}$$

and

$$C_D = \left(2.635 + 0.618 \ln \frac{L}{k_s} \right)^{-2.57} \quad \text{for} \quad 150 < \frac{L}{k_s} < 1.5 \text{ x } 10^7 \tag{9.336}$$

where as described in section 9.10.2.2 k_s is the average height of the roughness projections with typical values given in Table 9.5.

Example 9E.17: The trailer part of a tractor-trailer highway transport for hauling freight is basically a large box mounted on wheels. The largest size trailer presently allowed on U.S. interstate highways has a length of L = 16 m, a width of W = 2.6 m, and a height of H = 2.9 m. Estimate the engine power required to overcome the just skin friction drag on the trailer alone for a vehicle traveling at a speed of ϑ = 100 km/hr (27.778 m/sec).

For air: ρ = 1.189 kg/m^3 and μ = 1.825 x 10^{-5} kg/m sec

Solution: We can model the surfaces of the box of the trailer as flat plates. Then the Reynolds number based upon the length of the box is

$$Re_L = \frac{\vartheta L \rho}{\mu} = \frac{(27.778 \text{ m/sec})(16 \text{ m})(1.189 \text{ kg/m}^3)}{1.825 \text{ x } 10^{-5} \text{ kg/m sec}} = 2.8956 \text{ x } 10^7$$

For a Reynolds number this large, the laminar portion of the boundary layer can be neglected. Then the drag coefficient can be evaluated from equation (9.334), viz.

$$C_D = 0.031 Re_L^{-1/7} = 0.031 \left(2.8956 \text{ x } 10^7 \right)^{-1/7} = 0.08591$$

For a typical side of width b and length L, the drag force is

$$F_D = C_D \left[\frac{1}{2} \rho \vartheta_\infty^2 bL \right] = (0.08591) \left[\frac{1}{2} (1.189 \text{ kg/m}^3)(27.778 \text{ m/sec})^2 bL \right] = (34.409 \text{ N/m}^2) bL$$

In estimating the drag due to skin friction, we consider only the two vertical sides and the top of the box since the bottom has a number of structural elements and the axle assemblies that affect the character of the flow in this region. Then for the top b = 2.6 m and L = 16 m, and

$$(F_D)_{top} = (39.409 \text{ N/m}^2)(2.6 \text{ m})(16 \text{ m}) = 1639.4 \text{ N}$$

For each of the sides, b = 2.9 m and L = 16 m, and

$$(F_D)_{side} = (39.409 \text{ N/m}^2)(2.9 \text{ m})(16 \text{ m}) = 1828.6 \text{ N}$$

Then the total skin friction drag for the two sides and the top is

$$(F_D)_{total} = (F_D)_{top} + 2(F_D)_{side} = (1639.4 \text{ N}) + 2(1828.6 \text{ N}) = 5296.6 \text{ N}$$

Then the power required to overcome just this component of the drag is given by

$$\wp = (F_D)_{total} \vartheta = (5296.6 \text{ N})(27.778 \text{ N}) = 147.13 \text{ kW} = 197.22 \text{ hp}$$

As we shall see in section 9.11 this is only a fraction of the total drag on the vehicle. A substantial portion of the total drag is associated with the wake of the vehicle.

9.11 Drag

9.11.1 Drag on a Cylinder Immersed in a Flow of an Inviscid Fluid: d'Alembert's Paradox

Perhaps the most dramatic manifestation of the effect of fluid viscosity on the motion of a fluid is evidenced in the production of a drag force acting on bodies immersed in a flowing fluid. (In this discussion of drag we shall make frequent reference to the flow past a cylinder with the axis of the cylinder oriented normal to the direction of the flow since this flow configuration embodies many of the features central to the phenomenon of drag.) If the fluid possessed no viscosity, i.e., were inviscid, there would be no drag. Figure 9.33 shows a physical simulation of a steady, uniform flow of an inviscid incompressible fluid past a cylinder. (The precise manner in which this simulation was achieved is interesting in its own right since it involved the use of a viscous fluid, but since the details are not essential to the present discussion, the reader is referred to the reference from which Figure 9.33 was taken.) The streamlines of the steady flow are visualized by injecting dye into the flow. Note the nearly perfect symmetry of the streamlines.

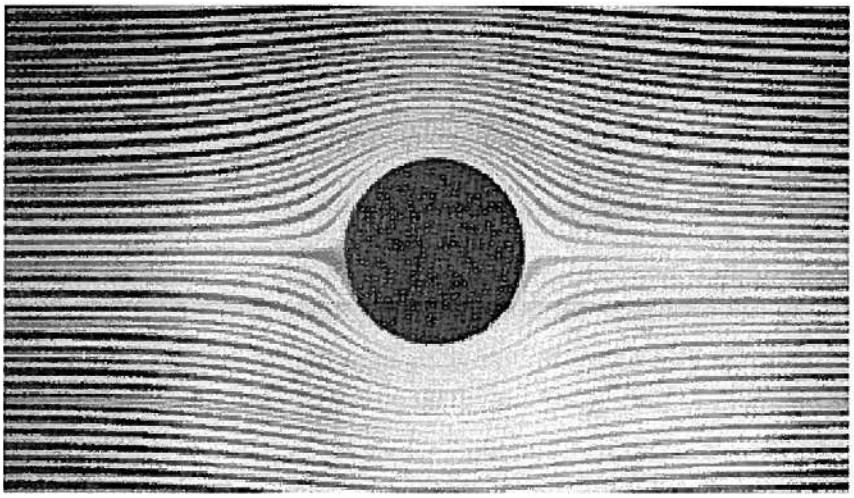

Figure 9.33 Simulation of Flow of an Inviscid Fluid Around a Cylinder
(From Figure 1, p. 8 of *An Album of Fluid Motion* by M. Van Dyke, Parabolic Press, Stanford, CA, 1982.)

As the flow encounters the obstacle represented by the cylinder, the flow in the neighborhood of the cylinder must accelerate in accordance with the continuity equation since a portion of the flow area is taken up by the cylinder. This causes the streamlines to "bunch up" near the surface. The closer together the streamlines, the faster the flow. Clearly, from Figure 9.33 it is apparent that the location of maximum fluid velocity lies at the equator, a position on the surface of the cylinder oriented at an angle 90° to the direction of the free stream. Thus as the fluid travels up the forward facing portion of the cylinder, it accelerates until it reaches its maximum velocity at the equator and then decelerates as it proceeds down the rearward facing portion of the cylinder, eventually reaching the free stream velocity at the rear of the cylinder. (See Figure 9.34.)

From inviscid flow theory, it can be shown that the magnitude of the local velocity $\vec{v}_\theta$ of the fluid on the *surface* of the cylinder is given by

$$\left|\vec{v}_\theta\right| = 2v_\infty \sin\theta \tag{9.337}$$

where ϑ_∞ is the free stream velocity upstream of the cylinder. (The "no-slip" boundary condition does not hold in this case since the fluid is being modeled as inviscid.)

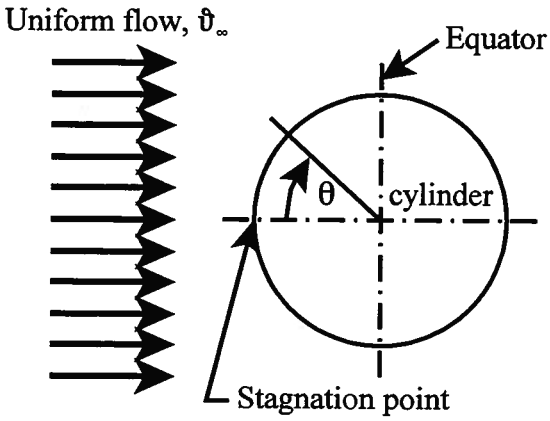

Figure 9.34 Cylinder in Uniform Cross-flow

Since the flow is inviscid and, hence, reversible, the distribution of pressure on the surface of the cylinder is given by the Bernoulli equation

$$\frac{P_\infty}{\rho}+\frac{\vartheta_\infty^{\,2}}{2}=\frac{P_\theta}{\rho}+\frac{\vartheta_\theta^{\,2}}{2} \tag{9.338}$$

If we combine equations (9.337) and (9.338) and solve for P_θ, we get

$$\begin{aligned}\frac{P_\theta}{\rho}+\frac{\left(2\vartheta_\infty\sin\theta\right)^2}{2}&=\frac{P_\infty}{\rho}+\frac{\vartheta_\infty^{\,2}}{2}\\ P_\theta&=P_\infty+\frac{\rho\vartheta_\infty^{\,2}}{2}\left(1-4\sin^2\theta\right)\end{aligned} \tag{9.339}$$

There are two observations that can be made from equation (9.339): (1) the pressure on the surface of the cylinder decreases as the flow moves up the forward facing portion ($0 \le \theta \le \pi/2$) and increases as the flow moves down the rearward facing portion ($\pi/2 \le \theta \le \pi$), and (2) the pressure distribution over the surface of the cylinder is symmetric with respect to the forward facing portion and the rearward facing portion with the minimum pressure at the equator. The pressure distribution can be expressed in dimensionless form as the pressure coefficient C_P, viz.

$$C_P=\frac{P_\theta-P_\infty}{\frac{1}{2}\rho\vartheta_\infty^{\,2}}=1-4\sin^2\theta \tag{9.340}$$

This distribution is shown in Figure 9.35. The symmetry of the pressure distribution means that if we integrate the x-component of it over the entire surface of the cylinder to determine the x-component of the net force exerted on the cylinder by the flow, the result is zero. There is no net force; hence, there is no drag on the cylinder.

$$2\int_0^\pi \frac{P_\theta-P_\infty}{\frac{1}{2}\rho\vartheta_\infty^{\,2}}R\cos\theta d\theta=2\int_0^\pi\left(1-4\sin^2\theta\right)R\cos\theta d\theta=\left[2R\sin\theta\right]_0^\pi-8R\left[\frac{\sin^3\theta}{3}\right]_0^\pi=0 \tag{9.341}$$

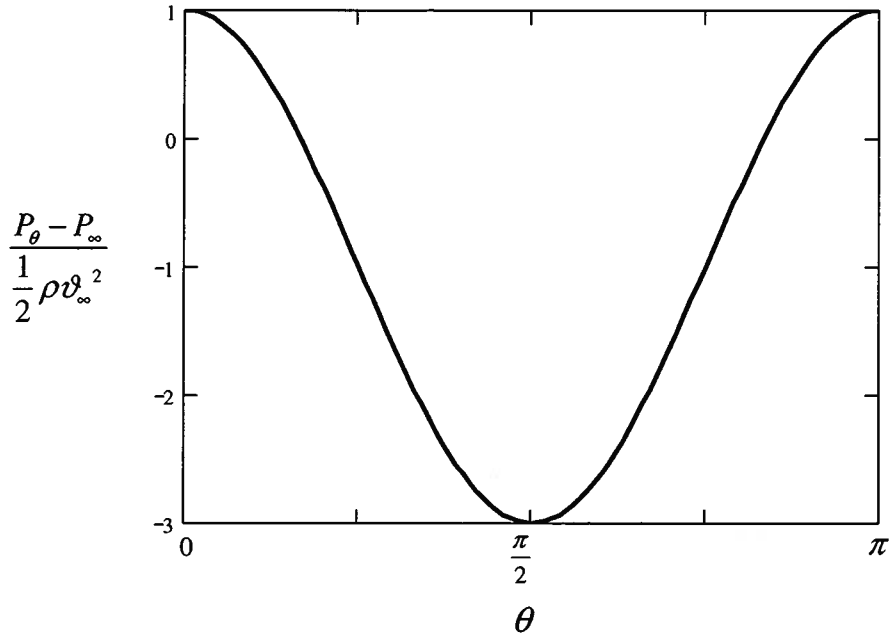

Figure 9.35 Pressure Distribution Over the Surface of a Cylinder Immersed in an Inviscid Flow

In the early days of the study of fluid mechanics, it was thought that this analysis would lead to the correct value of the drag force. When it did not, it was considered a paradox which eventually became known as *d'Alembert's paradox.* In light of our present knowledge of the behavior of fluids and the role that viscosity plays in the development of drag, the result hardly seems paradoxical. In fact, if the result *had* predicted a drag force for the flow of an *inviscid* fluid around a cylinder, that would have been a true paradox! In any case, the name is still used today for historical reasons. It should be noted that this result of zero drag for an inviscid flow applies only to the case of steady flow. If the flow is unsteady, a drag results even for the inviscid model.

9.11.2 The Influence of the Pressure Gradient: Separation of the Flow from the Surface

From our study of the flow of a viscous fluid over a flat plate, we know that in the case of a cylinder with a viscous flow normal to its axis, a boundary layer will develop on the surface of the cylinder beginning from the stagnation point and working its way over the forward facing portion, growing in thickness as the flow progresses toward the equator. As we have discussed before, the flow outside the boundary layer behaves as though it were inviscid and satisfies the Bernoulli equation. All of the influence of viscosity is confined to the boundary layer by definition. For the flat plate the fluid velocity at the outer edge of the boundary layer was the free stream velocity, but in the case of the cylinder, the situation is quite different.

On the cylinder, the boundary layer is quite thin, and the flow velocity at the outer edge of this thin layer is not the free stream velocity but is in fact the velocity that results from the inviscid behavior described above in Section 9.11.1; namely, acceleration of the flow over the forward facing portion and deceleration over the rearward facing portion of the cylinder. Most importantly, as predicted by the Bernoulli equation, the effect of this continual change in the local velocity causes the pressure on the curved surface of the cylinder (actually the pressure on the outer edge of the boundary layer on the curved surface of the cylinder) also to change in the

direction of flow. Since the pressure *across* the boundary layer is constant, this results in a pressure gradient in the boundary layer *in the direction of flow*. This pressure gradient can exert a profound influence on the behavior of the boundary layer and produce a notable difference in the growth of the boundary layer on the curved surface of a cylinder compared with the growth of the boundary layer on a flat plate for which the pressure did not change in the direction of the flow.

This behavior can be illustrated rather simply by writing the Bernoulli equation in differential form for the flow outside the boundary layer, viz.

$$\vartheta_x \frac{d\vartheta_x}{dx} = -\frac{1}{\rho}\frac{dP}{dx} \tag{9.342}$$

where ϑ_x is the local velocity just outside the boundary layer at its outermost edge which changes with x. From equation (9.342), it is apparent that as the flow accelerates in the x-direction, the pressure must decrease, and, conversely, as the flow decelerates, the pressure must increase. Inside the boundary layer, the boundary layer equations must be satisfied on the surface of the object immersed in the flow. At the surface, the boundary conditions of no slip and zero flow through the surface result in

$$\vartheta_x = 0 \quad \text{and} \quad \vartheta_y = 0 \quad \text{at} \quad y = 0 \tag{9.343}$$

Then *at the surface*, equation (9.167) becomes

$$\cancel{\vartheta_x}\frac{\partial \vartheta_x}{\partial x} + \cancel{\vartheta_y}\frac{\partial \vartheta_x}{\partial y} = -\frac{1}{\rho}\frac{dP}{dx} + \frac{\mu}{\rho}\frac{\partial^2 \vartheta_x}{\partial y^2}$$

$$\left(\frac{\partial^2 \vartheta_x}{\partial y^2}\right)_{y=0} = \frac{1}{\mu}\frac{dP}{dx} \tag{9.344}$$

Thus the pressure gradient established by the flow outside the boundary layer determines the curvature of the velocity profile at the surface.

The situation is similar in many respects to the case of planar Couette flow with a pressure gradient as depicted in Figure 9.15. In the general case of an external flow of a viscous fluid over a surface, there are three cases of interest:

1. Zero pressure gradient: $\dfrac{dP}{dx} = 0$ and $\left(\dfrac{\partial^2 \vartheta_x}{\partial y^2}\right)_{y=0} = 0$

In this case, the forward drag of the fluid in the external flow at the outer edge of the boundary layer is sufficient to overcome the retarding drag (shear stress) exerted on the fluid by the surface, and the boundary layer grows as the flow progresses down stream. The flow over a flat plate is an example of this. For the flat plate, note from Figure 9.21 as well as equation (9.176) and the data of Table 9.4 that, indeed, the curvature of the velocity profile derived by Blasius is zero at the surface. This is shown schematically in Figure 9.36a.

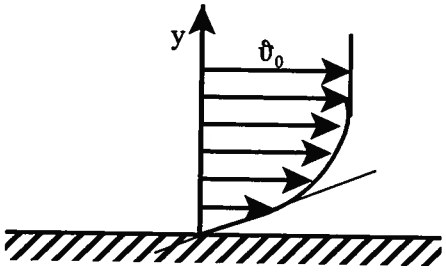

Figure 9.36a Schematic Representation of Velocity Profile with Zero Pressure Gradient

2. Favorable pressure gradient: $\frac{\partial P}{\partial x} < 0$ and $\left(\frac{\partial^2 \vartheta_x}{\partial y^2}\right)_{y=0} < 0$

In this case there are two factors that help to overcome the retarding drag of the surface on the fluid in the boundary layer: the forward drag exerted by the fluid in the external flow at the edge of the boundary layer and the favorable net forward "pressure forces" within the boundary layer. These boundary layers tend to be thinner than the boundary layers that develop without a pressure gradient. For this case, the velocity profile has negative curvature at the wall as shown in Figure 9.36b. Flow over the forward facing portion of a cylinder is an example of a boundary layer with a favorable pressure gradient.

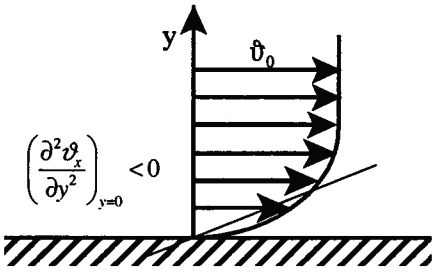

Figure 9.36b Schematic Representation of Velocity Profile with Favorable Pressure Gradient

3. Adverse pressure gradient: $\frac{\partial P}{\partial x} > 0$ and $\left(\frac{\partial^2 \vartheta_x}{\partial y^2}\right)_{y=0} > 0$

In this case there are two factors attempting to *retard* the flow in the boundary layer: the retarding drag of the surface and the adverse net "pressure forces" within the boundary layer which are acting against the direction of the flow. If the forward drag of the fluid in the external flow at the edge of the boundary layer is sufficiently large, it can overcome these retarding influences and the boundary layer will continue to grow in the direction of flow; however, if the drag of the external flow is not sufficiently large, the retarding influences dominate and the flow attempts to reverse direction in response to these retarding influences. It is this latter phenomenon that ultimately causes the boundary layer to separate from the surface. For this case, the velocity profile has negative curvature at the wall as shown in Figure 9.36c. A necessary, but not sufficient, condition for flow reversal is when the velocity gradient at the wall becomes negative. When flow reversal occurs, the velocity profile itself has negative slope at the wall. Flow over the rearward facing portion of a cylinder is an example of flow with an adverse pressure gradient.

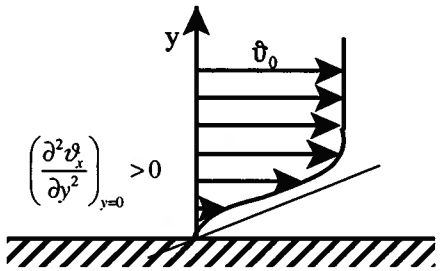

Figure 9.36c Schematic Representation of Velocity Profile with Adverse Pressure Gradient

The latter two conditions above are operative in the case of the cylinder in cross flow. As described in equation (9.340) and shown graphically in Figure 9.35, the flow accelerates over the forward facing portion of the cylinder and the pressure decreases in continuous fashion up to the equator according to the Bernoulli equation. This produces a negative (favorable) pressure gradient in the boundary layer on the forward facing portion. The pressure attains its minimum value at the equator and the pressure gradient reverses sign as the fluid decelerates down the backward facing portion. The question then becomes one of determining where the boundary layer separates from the surface of the cylinder.

Meksyn[7] developed a solution for the boundary layer equation for flow over a cylinder. He assumed that the pressure at the surface of the cylinder could be predicted from the results of the case of an inviscid fluid flowing under the same conditions as the viscous fluid. Following the example of Blasius and other early investigators, he defined a similarity parameter η and a stream function ψ such that

$$\eta = y\sqrt{\frac{2\vartheta_\infty}{\nu\gamma}}\sin(\pi-\theta) \tag{9.345}$$

where θ is defined in Figure 9.34 and

$$\gamma = 2R + \left(R + y + \frac{R^2}{R+y}\right)\cos(\pi-\theta) \tag{9.346}$$

where R is the radius of the surface of the cylinder and y is measured normal to it, and

$$\psi = \sqrt{2\nu\vartheta_\infty\gamma}\,\phi(\eta,\gamma) \tag{9.347}$$

Then the boundary layer equation, equation (9.167), becomes

$$\phi''' + \phi''\phi + \lambda(1-\phi) = 0 \tag{9.348}$$

where the primes denote derivatives with respect to η and

$$\lambda = -\frac{\cos(\pi-\theta)}{\sin^2\left[\dfrac{\pi-\theta}{2}\right]} \tag{9.349}$$

Then the velocity profile at any location defined by θ is

$$\frac{\vartheta_x}{\vartheta_\infty} = \phi'\left[2\sin(\pi-\theta)\right] \tag{9.350}$$

The analysis parallels that for the flat plate and equation (9.348) must be solved numerically in a fashion similar to equation (9.176). Comparison of the results of such a numerical solution with the experimental observations for the velocity profile reveal excellent agreement.

The local coefficient of friction f can be determined from the shear stress on the surface which, in turn, can be determined from the velocity gradient at the surface. Meksyn showed that the coefficient of friction is given by

$$f = 16\sqrt{\frac{\nu}{2R\vartheta_\infty}}\,\phi''(0)\sin^2\frac{\pi-\theta}{2}\cos\frac{\pi-\theta}{2} \tag{9.351}$$

which agrees well with the experimental data. Equation (9.351) is valid up to the point of separation which occurs when the velocity gradient and, hence, the value of f becomes zero. From equation (9.351), separation should occur approximately when $\theta = 95°$. Measured values of the location of the point of separation fall in the range of $85° < \theta < 105°$, depending upon the Reynolds number.

---

[7] Meksyn, D. "The laminar boundary layer equations: I Motion of an elliptic and circular cylinders [sic]," *Proc. Royal Society of London, Series A*, vol. 192, No. 1031,1948, pp. 545-567.

Figure 9.37 shows a circular cylinder in crossflow with a value of Reynolds number of $Re_D = 2000$. The flow visualization is revealed by the introduction of air bubbles in water. The separation of the boundary layer is clearly evident in the photograph as is the turbulent wake.

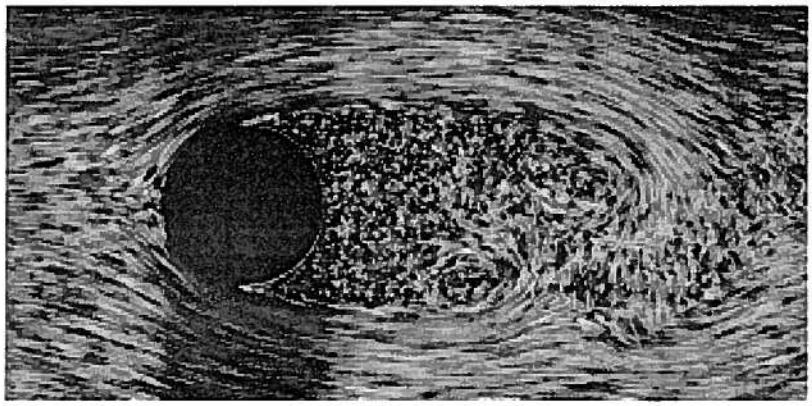

Figure 9.37 Laminar Flow Around Circular Cylinder, $Re_D = 2000$
(From Figure 47, p. 31 of *An Album of Fluid Motion* by M. Van Dyke, Parabolic Press, Stanford, CA, 1982.)

Measurements of the pressure in the wake of a cylinder with $Re_D = 2000$ show that the pressure is essentially uniform across the wake (cf. Figure 9.38 for data at higher values of the Reynolds number) with a pressure coefficient of approximately $C_P \approx -1$ where [cf. Equation (9.340)]

$$C_P = \frac{P_\theta - P_\infty}{\frac{1}{2}\rho v_\infty^{\,2}} \approx -1 \tag{9.352}$$

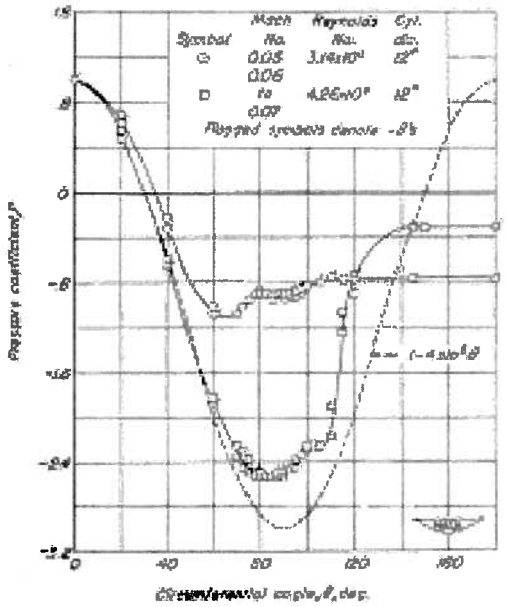

Figure 9.38 Pressure Coefficient for a Cylinder in Crossflow
(From NACA Tech. Note 2960, *Drag of Circular Cylinders for a Wide Range of Reynolds Numbers and Mach Numbers*, F. E. Gowen and E. W. Perkins, 1953, Figure 5.)

Since the pressure varies up to the point of separation according to equation (9.340), it follows that the integration of the pressure distribution over the entire surface of the cylinder yields a net force acting in the direction of flow. This force is a major portion of the drag force that acts on the cylinder. The other contribution to the drag force is, of course, the skin friction resulting from the shear stress at the surface of the cylinder which can be calculated from equation (9.351).

The boundary layer on the surface of the cylinder exhibits a behavior that might not be expected at first glance; namely, as the flow undergoes a transition from laminar to turbulent, the turbulent boundary layer proves to be more stable than the laminar boundary layer and the phenomenon of separation is delayed to a point further along the surface than occurs in laminar flow. Figure 9.39a shows a laminar flow over a convex surface with separation occurring near the apex of the curvature. Figure 9.39b shows a turbulent flow over the same convex surface as Figure 9.39a. In the turbulent case, the boundary layer is thicker than the laminar case, but the boundary layer remains attached far downstream of the point of separation observed in the laminar case.

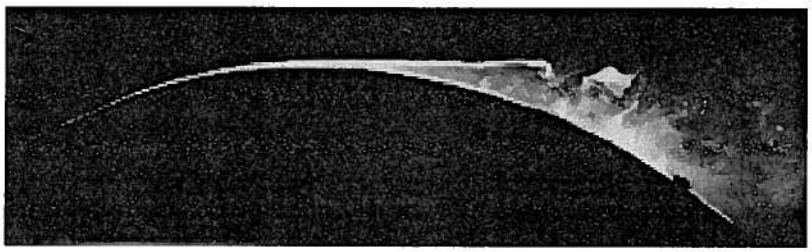

Figure 9.39a Laminar Flow Past a Convex Surface

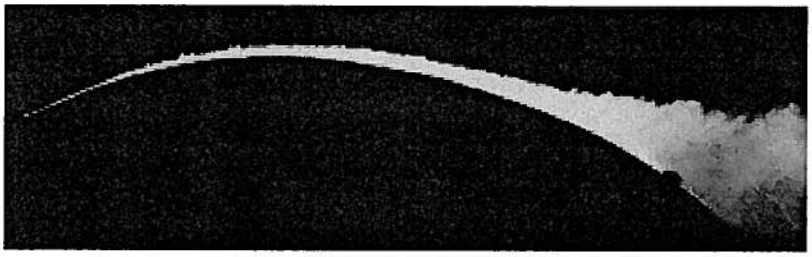

Figure 9.39b Turbulent Flow Past a Convex Surface
(From Figure 156, p. 91 of *An Album of Fluid Motion* by M. Van Dyke, Parabolic Press, Stanford, CA, 1982.)

In the case of flow about a circular cylinder, the observations of Figure 9.39 imply that the wake behind the cylinder will be smaller in turbulent flow than in laminar flow; consequently, wake drag is dramatically reduced in the turbulent case. This phenomenon is shown quite dramatically for the case of flow past a sphere in Figure 9.40. A trip wire has been used to trigger the laminar/turbulent transition in the boundary layer in Figure 9.40b. Note the substantial difference in the size of the wake for the turbulent flow case shown in Figure 9.40b compared with the laminar flow case of Figure9.40a. The small wake in the turbulent case leads to a significant reduction in the drag. We shall return to this point a bit later, but suffice it to say here that this reduction in drag under turbulent flow conditions has implications of considerable practical importance.

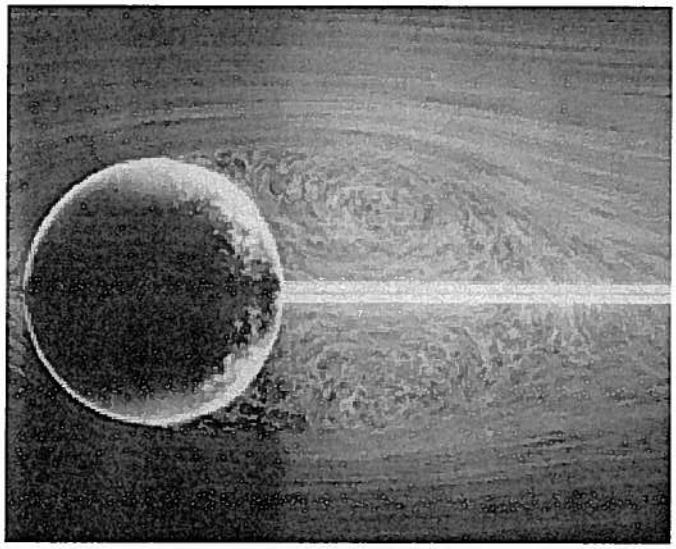

Figure 9.40a Mean Flow Past a Sphere, Re_D = 15,000
(From Figure 56, p. 34 of *An Album of Fluid Motion* by M. Van Dyke, Parabolic Press, Stanford, CA, 1982.)

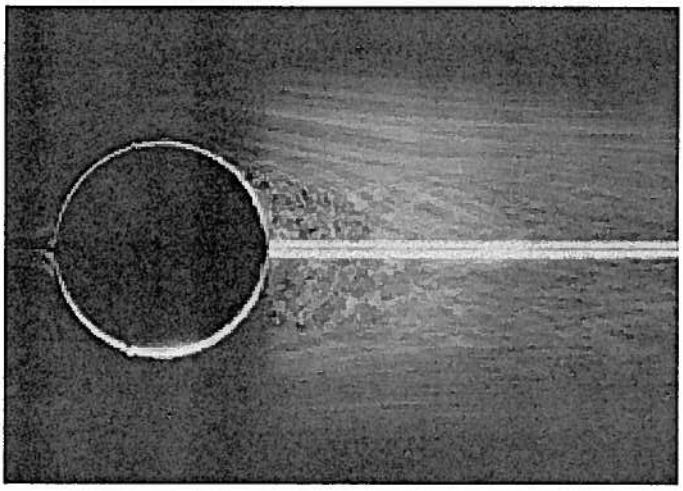

Figure 9.40b Mean Flow Past a Sphere, Re_D = 30,000,
with Boundary Layer Trip Wire Forward of Equator
(From Figure 58, p. 35 of *An Album of Fluid Motion* by M. Van Dyke, Parabolic Press, Stanford, CA, 1982.)

The behavior of the drag for a smooth cylinder of diameter D and length L in crossflow over a wide range of values of the Reynolds number is summarized in Figure 9.41 where the drag coefficient C_D is given by

$$C_D = \frac{F_D}{\frac{1}{2}\rho \vartheta_\infty^{\,2} DL} \tag{9.353}$$

Note the dramatic change in drag coefficient in the range $3.5 \times 10^5 < Re_D < 6 \times 10^5$.

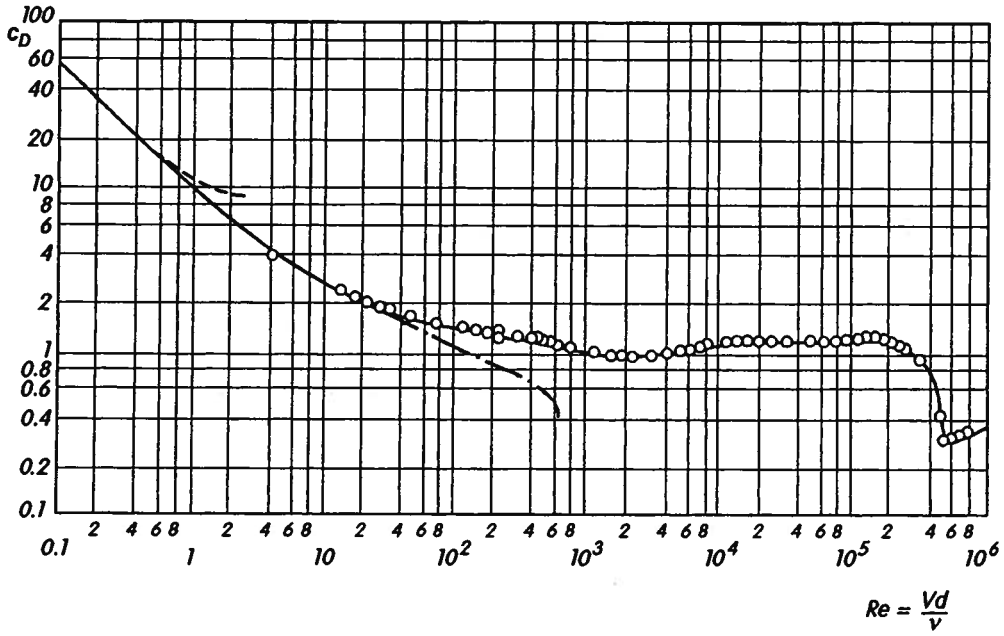

Figure 9.41 Drag Coefficient of a Smooth Cylinder in Crossflow
(From *Boundary Layer Theory*, H. Schlichting and K. Gertsen, Springer, 8th Ed., 2003, Figure 1.12, p. 19. Circles indicate experimental data.)

There are several different flow regimes that can be identified in Figure 9.40, each of which embodies a unique characteristic of the flow that arises not only in the case of flow around a cylinder, but in the flow around other blunt bodies as well. Following the example of Schlichting and Gertsen (H. Schlichting and K. Gertsen, *Boundary Layer Theory*, Springer, 8th Ed., 2003, p. 22; and R. D. Blevins, *Applied Fluid Dynamics Handbook*, Krieger Publishing Co., Malabar, FL, 1992, p. 340.), these are summarized in Table 9.10.

Table 9.10 Flow Regimes for a Circular Cylinder in Crossflow

Reynolds Number Regime	Flow Regime	Illustration	Flow Characteristic	Strouhal Number, Sr	Drag Coefficient, C_D
$0 < Re_D < 5$	creeping flow	Figure 9.42	steady with no wake	NA	$C_D = \frac{8\pi}{Re_D(2.002 - \ln Re_D)}$
$5 < Re_D < 40$	vortex pairs in wake	Figure 9.43	steady symmetric separation	NA	$12.8 > C_D > 1.59$
$40 < Re_D < 90$	onset of Karman vortex street		laminar but unstable wake	NA	$1.59 > C_D > 1.3$
$90 < Re_D < 400$	pure Karman vortex street	Figure 9.44	laminar Karman vortex street	$0.14 < Sr < 0.21$	$1.3 > C_D > 1.17$
$400 < Re_D < 1.3 \times 10^5$	subcritical regime	Figure 9.37	laminar boundary layer with fully turbulent vortex street	$Sr = 0.21$	$C_D \approx 1.17$
$1.3 \times 10^5 < Re_D < 3.5 \times 10^6$	critical regime		transition from laminar to turbulent boundary layer with narrow wake	no organized frequency	$1.17 > C_D > 0.3$
$3.5 \times 10^6 < Re_D$	supercritical regime		re-establishment of turbulent vortex street	$0.25 < Sr < 0.30$	$0.3 < C_D < 0.8$

The Strouhal number appearing in Table 9.10 is the dimensionless frequency of the vortices shed by the cylinder after the boundary layer separates in various flow regimes. In certain regimes, these vortices are stable and are commonly visible. For example, they show quite clearly in satellite views of flows in the atmosphere and in the oceans.
(For example, see http://daac.gsfc.nasa.gov/CAMPAIGN_DOCS/OCDST/vonKarman_vortices.html)
The Strouhal number for a cylinder of diameter D immersed in a flow of velocity ϑ is given by

$$Sr = \frac{fD}{\vartheta} \tag{9.354}$$

where f is now the frequency of oscillation of the vortices in units of Hertz.

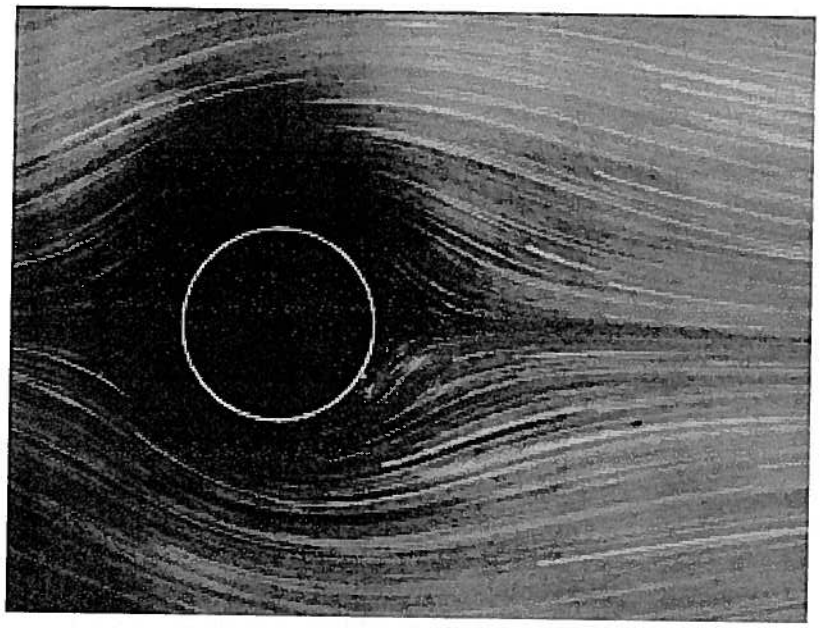

Figure 9.42 Creeping Flow Around a Circular Cylinder, $Re_D = 1.54$
(From Figure 24, p. 20 of *An Album of Fluid Motion* by M. Van Dyke, Parabolic Press, Stanford, CA, 1982.)

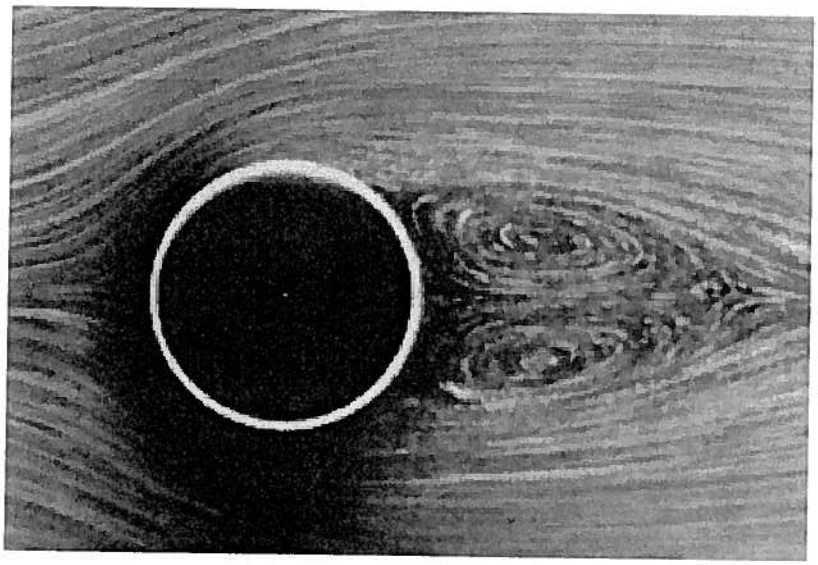

Figure 9.43 Flow Around a Circular Cylinder, $Re_D = 26$.
Note Twin Fixed Föppl Vortices in Wake.
Upper Vortex Rotates Clockwise; Lower Vortex Rotates Counterclockwise.
(From Figure 42, p. 28 of *An Album of Fluid Motion* by M. Van Dyke, Parabolic Press, Stanford, CA, 1982.)

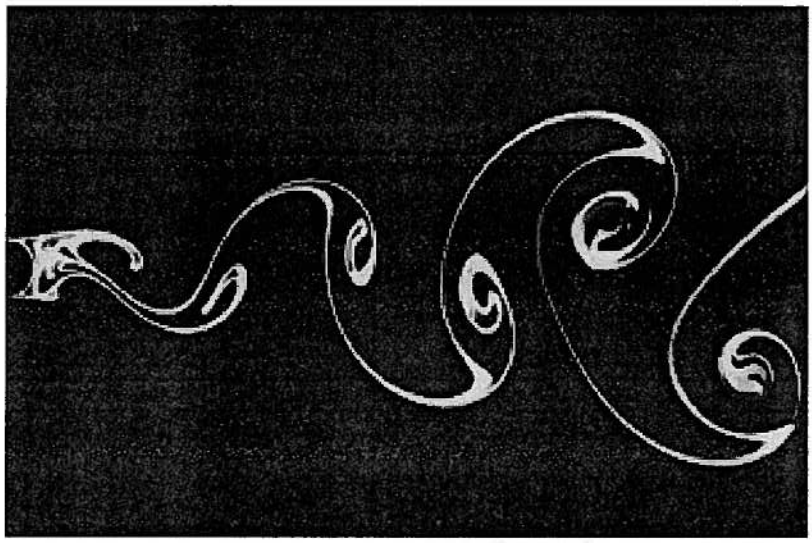

Figure 9.44 Flow Around a Circular Cylinder, Re_D = 140.
Note Well-developed Karman Vortex Street
(From Figure 94, p. 56 of *An Album of Fluid Motion* by M. Van Dyke, Parabolic Press, Stanford, CA, 1982.)

At this point in our discussion, it should be apparent that there are two contributions to the drag on a stationary object immersed in a flowing fluid (or conversely, an object moving through a stationary fluid): (1) skin friction drag due to the shear stress acting on the surface of the object as a consequence of the viscosity of the fluid, and (2) wake drag due to separation of the boundary layer as a consequence of the pressure gradient in the direction of flow imposed on the boundary layer by the "inviscid" flow external to the boundary layer. If we wish to reduce the drag on an object, there is little that we can do to reduce the skin friction component. Even the few changes that can be made may not be worth the effort since this component is the smaller of the two. However, there is a great deal that we can do to reduce wake drag. This is one of the principle objectives of the field of aerodynamics.

In their evolutionary process, fish long ago discovered that one of the principle changes that they could make to reduce the energy expended in swimming while increasing speed markedly, was to alter their body shapes so that the pressure gradient on the downstream portion of their bodies was much smaller in magnitude than the pressure gradient on the upstream portion of their bodies. The result is the characteristic shape of fish that we have all observed in nature. This aerodynamic shape is imitated in the cross-section of aircraft wings. There is one important difference between fish and airfoils. The purpose of the airfoil is to produce a lift force to keep the aircraft in the air while at the same time minimizing the drag force on the wing. This requires the airfoil cross-section to be a asymmetric rather than symmetric as most fish are.

Airfoil design is the result of a good deal of analysis and considerable wind tunnel testing using the principles of dimensional analysis set forth in Chapter 10. The National Advisory Committee for Aeronautics (NACA), the predecessor of the current National Aeronautics and Space Administration (NASA), pioneered the design of aircraft wing sections in the United States in the early part of the 20th century. Many of these early designs are in use to this day. Figure 9.45 shows the streamline flow around one such airfoil shape (NACA 64A015). No separation is evident in this photograph.

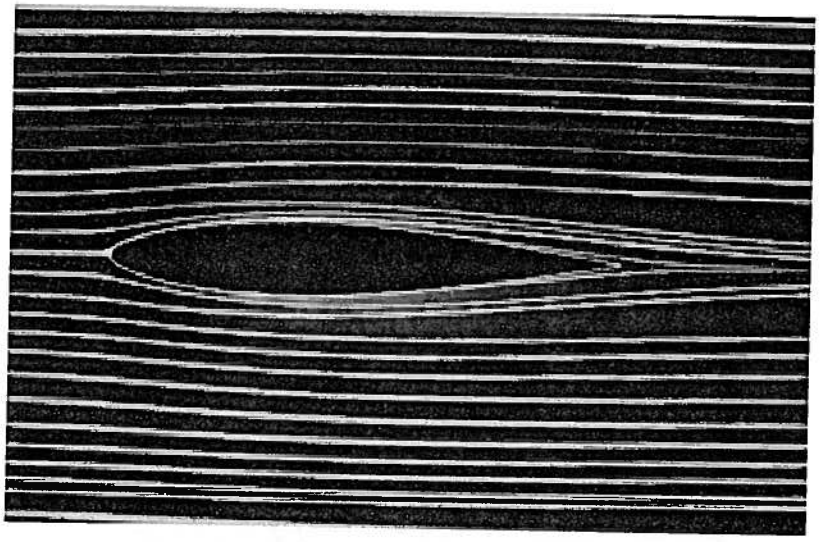

Figure 9.45 Symmetric Plane Flow About NACA Airfoil 64A015 ($Re_L = 7000$)
(From Figure 23, p. 19 of *An Album of Fluid Motion* by M. Van Dyke, Parabolic Press, Stanford, CA, 1982.)

As streamlined and aerodynamic as these airfoil designs may be, the flow about them can be made to separate as evidenced in Figure 9.46. This is usually done by changing the orientation of the airfoil to the principal direction of flow. This maneuver is known as changing the angle of attack. Note the separation of the flow on the upper surface near the trailing edge. The result of this separation is an increase in drag and a loss of lift. The wing on a typical aircraft contains control surfaces known as *flaps* located in the region where the flow is separating in Figure 9.46. The purpose of the flaps is to increase or decrease the drag and lift of the wing during take-off and landing.

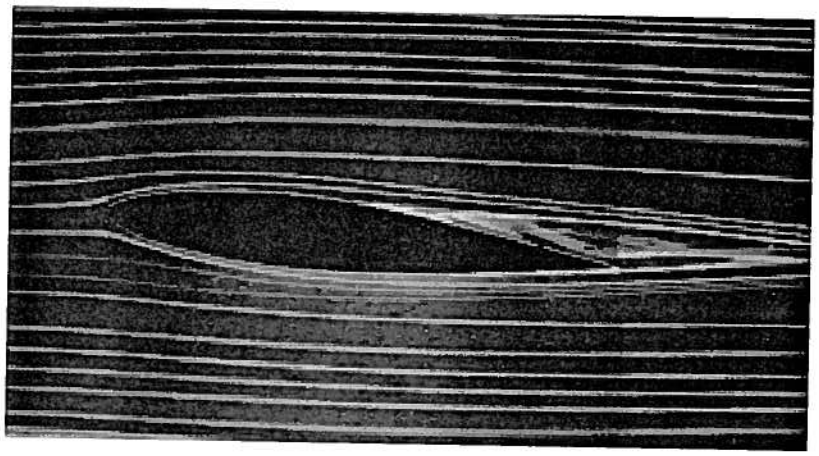

Figure 9.46 Flow About NACA Airfoil 64A015 at an Angle of Attack of 5° ($Re_L = 7000$)
(From Figure 34, p. 25 of *An Album of Fluid Motion* by M. Van Dyke, Parabolic Press, Stanford, CA, 1982.)

As the angle of attack is increased, the point of separation on the upper surface of the wing moves further and further forward until it finally reaches the nose of the wing. (See Figure 9.47.) At this angle of attack, the flow over the upper surface is comprised almost entirely of low-velocity eddy flow. The wing is then said to be "stalled," and the lift of the wing drops

precipitously even though the flow on the underside of the wing is relatively unchanged. In effect, at the stall angle, the wing is about as effective a lifting surface as a flat plate at the same angle of attack. Clearly, stall is an operating condition to be avoided except during landing when it can be used to advantage to return the aircraft to the ground.

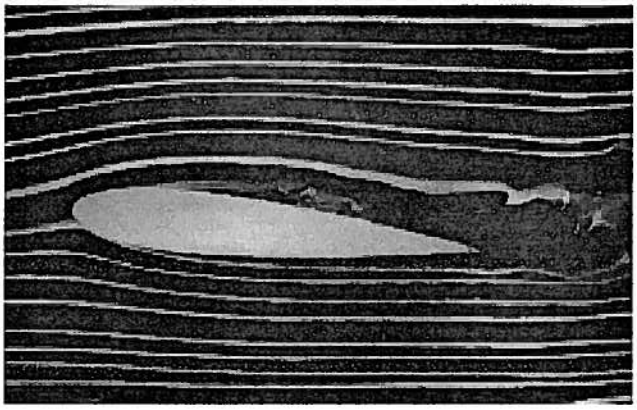

Figure 9.47 Flow About NACA 64A015 Airfoil at Angle of Attack Near Stall
(From Figure 72, p. 41 of *An Album of Fluid Motion* by M. Van Dyke, Parabolic Press, Stanford, CA, 1982.)

Aircraft are not the only vehicles employing aerodynamics to improve performance. Automobiles have shown a trend throughout their history of improving aerodynamics (reducing drag) to improve performance. (See Figure 9.48.) This trend has become more important in recent years as automotive manufacturers have begun employing wind tunnel testing to an ever greater degree in an attempt to improve fuel economy to the highest possible levels for a given body style. Drag coefficients have reached their lowest values ever ($C_D \approx 0.3$) as thermal-fluid engineers in the automotive industry strive for the greatest possible fuel economy. One manufacturer has even resorted to covering the under-carriage with a "belly pan" covered with turbulence promoters in an effort to minimize this contribution to vehicle drag. One danger in this process is that as drag is reduced, lift can improve to the point that it becomes difficult to prevent the vehicle from becoming an aircraft and becoming airborne. Thermal-fluid engineers then work to decrease drag while at the same time maintaining negative lift (down-force) to keep the vehicle on the road, particularly during cornering.

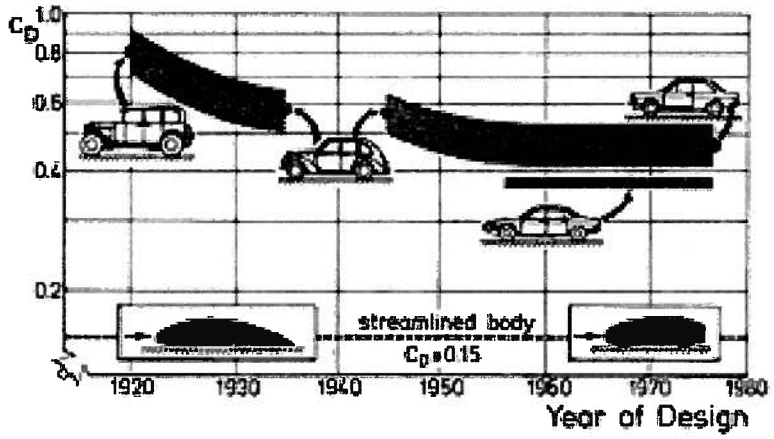

Figure 9.48 Historical Trend of Aerodynamic Drag of the Automobile
(From *Applied Fluid Dynamics Handbook*, R. D. Blevins, Krieger Publishing Co., Malabar, FL, 1992, Fig. 10-32, p. 348.)

PROBLEMS

9.1 The flow of an inviscid fluid around a circular cylinder of radius a centered on the origin is given by, in polar coordinates,

$$\vartheta_r = \vartheta_\infty\left(1-\frac{a^2}{r^2}\right)\cos\theta \quad \text{and} \quad \vartheta_\theta = -\vartheta_\infty\left(1+\frac{a^2}{r^2}\right)\sin\theta$$

where ϑ_∞ is the free stream velocity, a constant.

(a) Check that these forms satisfy the correct boundary condition on the surface of the cylinder and find the velocity at large distances from the cylinder.

(b) Express the pressure on the surface of the cylinder as a pressure coefficient, C_P and sketch the variation of C_P around the cylinder. Note that in this case

$$C_P = \frac{P-P_\infty}{\frac{1}{2}\rho\vartheta_\infty{}^2}$$

where P is the local pressure and P_∞ is the free stream pressure.

(c) Find the maximum speed of the flow over the surface of the cylinder.

9.2 Figure 9P.2 shows a cross-section through the gap between two solid surfaces (which is independent of the direction perpendicular to the page). The fluid flowing in the gap is inviscid and the effect of gravity is negligible.

(a) Sketch the pressure and velocity distribution along the centerline of the gap and along the upper and lower walls.

(b) A short pulse of dye is injected by a rake of probes so that it initially marks a line of fluid particles at AA. Sketch the change in shape of this line of particles as it convects downstream.

Figure 9P.2 Flow in a Gap Between Two Curved Surfaces

9.3 As shown in Figure 9P.3, a viscous, incompressible fluid is flowing in a laminar fashion between two infinite parallel plates.

(a) Starting with the Navier-stokes equation in Cartesian coordinates, show that steady, laminar, incompressible flow of a Newtonian fluid between two parallel plates satisfies the expression

$$\mu\frac{d^2u}{dy^2} = \frac{dP}{dx}$$

Deduce that, if the plates are separated by distance T, the volumetric flow rate per unit width is given by

$$\dot{V} = \frac{T^3}{12\mu}\left|\frac{dP}{dx}\right|$$

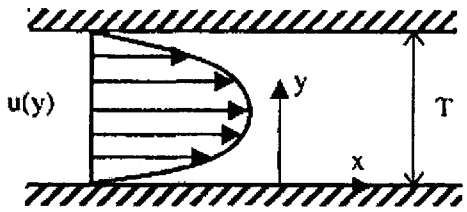

Figure 9P.3 Plane Poiseuille Flow

(b) A horizontal crack forms across a wall of thickness L = 1 m separating two tanks containing water at 20° C. The water surface on one side of the wall is 3m higher than that on the other. The crack is 0.01mm wide and is completely submerged. Find the leakage per unit width of the wall, assuming that the flow is laminar. (μ_{water} = 1x10^3 kg/m sec)

9.4 As shown in Figure 9P.4 below, a Couette flow configuration consists of two infinite parallel plates separated by a gap of height $2h$. The gap is filled with two layers of fluid comprised of two immiscible, incompressible fluids A and B with densities ρ_A and ρ_B ($\rho_B = 0.8\ \rho_A$), respectively, and viscosities μ_A and μ_B ($\mu_B = 0.5\mu_A$), respectively. The two fluid layers are of equal thickness h. The flow of the fluids between the plates is induced by the motion of the bottom plate with constant velocity ϑ_0 relative to the top plate. The pressure gradient in the x-direction is zero.

(a) Derive an expression for the fully-developed velocity profile $\vartheta(y)$ in the gap. Use the coordinate scheme shown in Figure 9P.4. On a carefully proportioned sketch, show this profile. Pay particular attention to the magnitude of the fluid velocity at the midplane of the gap relative to the magnitude of the velocity ϑ_0 of the bottom plate.

For parts (b), (c), and (d), neglect any effects at the edges of the plates.

(b) Derive an expression for the total mass flow rate of fluid for a gap of width b measured normal to the plane of Figure 9P.4.

(c) If the width of the plates is b and the length is L, derive an expression for the power necessary to drive the bottom plate at the constant velocity ϑ_0 relative to the top plate.

(d) If the width of the plates is b and the length is L, derive an expression for the rate of entropy generation in the gap.

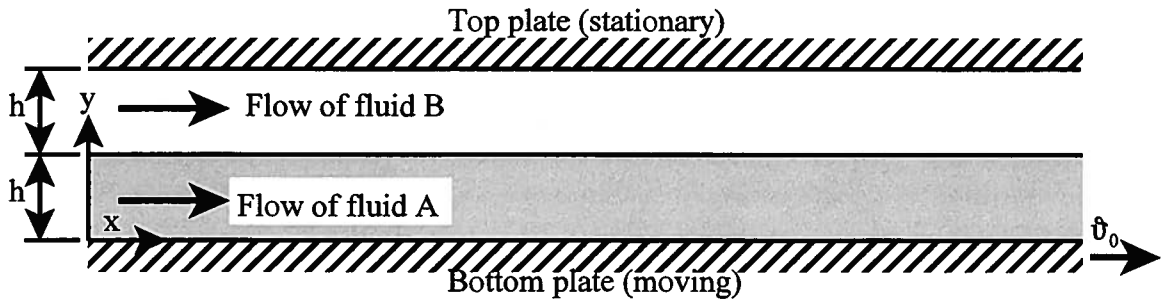

Figure 9P.4 Couette Flow of Two Immiscible, Incompressible Fluids

5. The analysis of Section 9.9.1.4 can be applied to the case of a 'stepped bearing" shown diagrammatically below. The pressures at the left and right hand ends on the bearings may be taken as atmospheric, P_a, (which can be taken as the pressure datum).

(a) Show that, for the flow rates to match in the two parts of the bearing, that the pressure at the step is given by P^* where

$$P^* = \frac{6\mu U(H-h)}{\frac{h^3}{L_1}+\frac{H^3}{L_2}}$$

(Hint: Use a frame of reference moving with the bearing.)

(b) Hence show that the bearing is capable of sustaining a load given by

$$F = \frac{P^*(L_1+L_2)}{2}$$

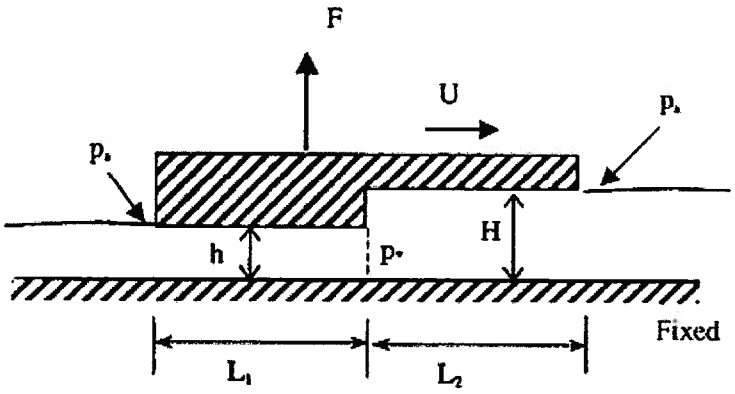

Figure 9P.5 Stepped Bearing

9.6 A viscous liquid flows between two concentric cylinders of radii R_1, R_2 where $R_1 < R_2$. The inner cylinder is at rest and the outer moves parallel to the common axis at speed U. Assuming that the pressure at inlet and outlet to the pipe is atmospheric, show that the velocity profile in the pipe is given by

$$\vartheta(r) = \frac{U}{\ln\left(\frac{R_2}{R_1}\right)}\ln\left(\frac{r}{R_1}\right)$$

9.7 The velocity in the laminar boundary layer on a flat plate in an unbounded stream is often modeled by the form

$$\vartheta = \frac{\vartheta_\infty}{2}\left[3\frac{y}{\delta}-\left(\frac{y}{\delta}\right)^3\right] \quad \text{for} \quad 0 \le y \le \delta \quad \text{and} \quad \vartheta = \vartheta_\infty \quad \text{for} \quad y \ge \delta$$

where ϑ_∞ is the free stream velocity and δ the height of the edge of the boundary layer above the plate. This form is assumed to be valid at each value of x along the length of the plate with δ varying with x.

(a) Explain why the static pressure is approximately uniform throughout the flow and sketch ϑ as a function of y.

(b) Using the result derived in Chapter 9 for mass flow in the boundary layer, find the vertical displacement of the streamline that passes the plate leading edge at a height h in terms of δ.

(c) Again using results from Chapter 9, calculate the total drag force per unit width on the upper side of the plate and the boundary layer thickness at the trailing edge for a plate of length L = 1 m in a stream with a uniform velocity ϑ_∞ of 5 m/sec.

The fluid properties are: $\nu = 1.0 \times 10^{-3}$ m^2/sec and $\rho = 10^3$ kg/m^3

9.8 Water flows through a sudden expansion in a pipe shown in Figure 9P.8. The flow separates from the sharp rim of the smaller pipe, enclosing an almost stagnant region, before mixing in a turbulent manner over a short distance to form a uniform stream at (3).

(a) Explain why the pressure in the stagnant regions marked (a) & (c) on the diagram should be approximately uniform at the same value as that in the region (b).

(b) By applying conservation of mass and conservation of momentum to the control volume shown (because of the short length of (2)-(3), the effect of shear stress on the walls of the larger pipe can be neglected), show that

$$P_{01} - P_{03} = \left(P_1 + \rho\frac{\vartheta_1^2}{2}\right) - \left(P_3 + \rho\frac{\vartheta_3^2}{2}\right) = K\frac{1}{2}\rho\vartheta_1^2$$

where P_{01} and P_{03} are by definition the stagnation pressures at locations (1) and (3), respectively, and $K = \left(1 - \frac{A_1}{A_3}\right)^2$ and where A_1 and A_3 are the cross-sectional areas of inlet and exit.

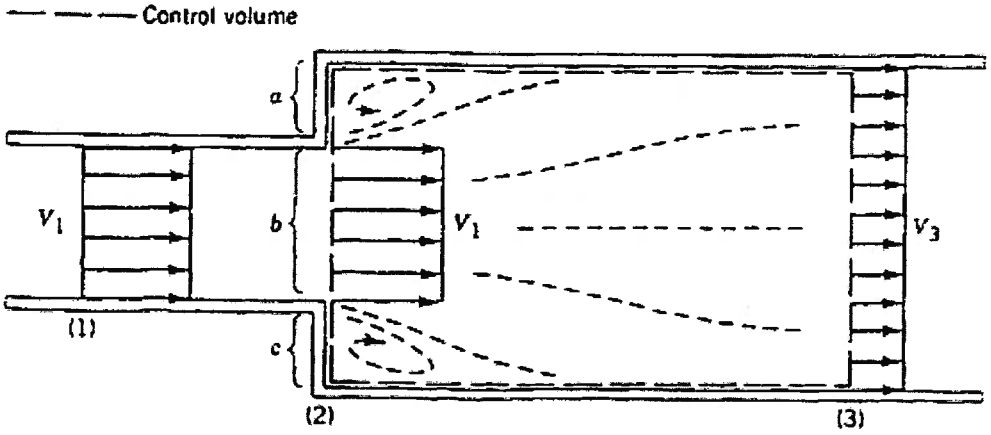

Figure 9P.8 Sudden Expansion

9.9 As shown in Figure 9P.9, two parallel streams of an incompressible fluid each having the same static pressure P_A and a velocity profile that is uniform come together at the location AA′. The two streams mix over a short distance due to the turbulence generated by the unstable shear layer between them.

(a) Assuming that viscous shear stress on the solid surfaces can be neglected, calculate the velocity and static pressure at location BB′, where the mixing is complete.

(b) What is the "loss" of mechanical energy due to the mixing? Where does this energy go?

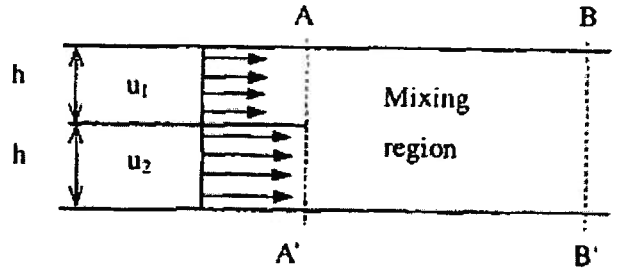

Figure 9P.9 Mixing Streams

9.10 A simple hydrostatic thrust bearing is shown in the Figure 9P.10. Unlike slider bearings, this type of bearing can support a load under static (no motion) conditions. The lubricant is supplied under pressure and fills the recessed region at essentially the supply pressure P_s. The lubricant then slowly flows out between the rotor and the stator as its pressure decreases to atmospheric pressure. Such bearings are useful for supporting very large thrust loads of rotating machinery even under low-speed conditions. The load is determined primarily by the supply pressure that can be maintained in the recess.

For a fixed flow rate of lubricant, the pressure P_s depends upon the film thickness h. Hence, if the lubricant pump flow rate is fixed, the film thickness will decrease as the load F is increased. On the other hand, if a given film thickness must be maintained as the load increases, the lubricant flow rate must then be increased.

In the present analysis, the lubricant is incompressible with density ρ and viscosity μ. The rotor rotates slowly enough that inertial effects can be neglected. Furthermore, we seek a solution for the steady-flow velocity field that is axially symmetric so that $\partial/\partial\theta = 0$ and for which $P = P(r)$. Also the forces due to shear in the radial direction are assumed negligible. That is, the only shear of consequence is due to relative motion of the rotor and stator, and the fluid is in solid body rotation about the z-axis.

(a) Starting with the Navier-Stokes equation and the continuity equation in cylindrical coordinates, show that the r-component equation reduces to

$$\mu\frac{\partial^2 v_r}{\partial z^2} = \frac{\partial P}{\partial r}$$

Similarly, show that the θ-component equation reduces to

$$\frac{\partial^2 v_\theta}{\partial z^2} = 0$$

Also show that the z-component equation vanishes.

(b) Show that

$$v_\theta = r\omega\frac{z}{h}$$

and show that for $b > r > a$,

$$v_r = \frac{1}{2\mu}\frac{dP}{dr}\left(z^2 - hz\right)$$

(c) Show that the volumetric flow rate in the radial direction is given by

$$\dot{V} = -\frac{\pi r h^3}{6\mu}\frac{dP}{dr} = \frac{\pi h^3\left(P_s - P_{atm}\right)}{6\mu\ln\left(\frac{b}{a}\right)}$$

(d) From the expression for the volumetric flow rate, show that since the pressure is a function of r only, the pressure distribution is given by

$$\frac{P_s - P}{P_s - P_{atm}} = \frac{\ln\left(\frac{r}{a}\right)}{\ln\left(\frac{b}{a}\right)}$$

and sketch the pressure distribution in the oil film on the P-r plane.

(e) Show that the load carrying capability of the bearing is F where

$$F = \frac{\pi\left(b^2 - a^2\right)\left(P_s - P_{atm}\right)}{2\ln\left(\frac{b}{a}\right)}$$

(f) Develop an expression for the frictional torque in the bearing due to fluid friction.

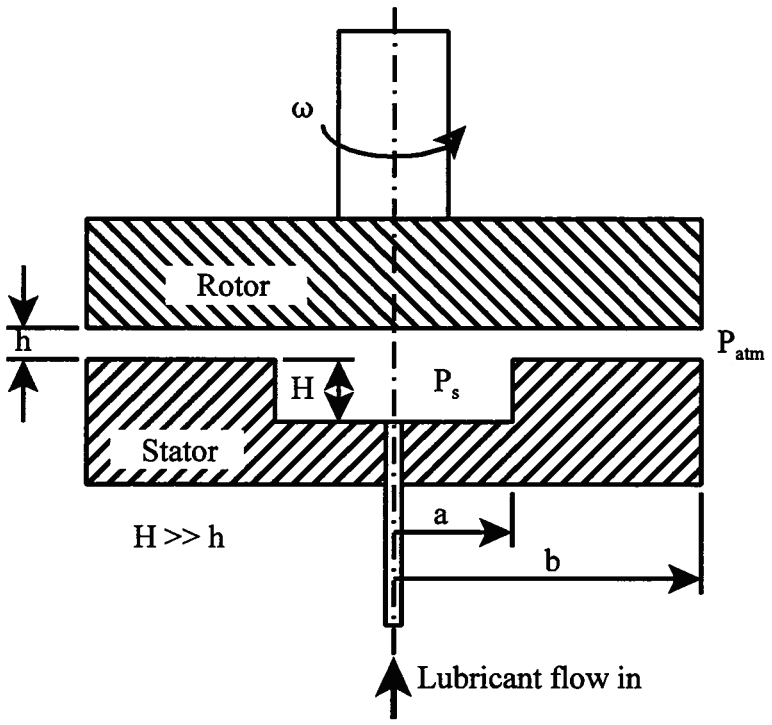

Figure 9P.10 Hydrostatic Thrust Bearing

9.11 A viscosity pump is a simple device for pumping viscous fluids such as lubricating oil. As shown in Figure 9P.11, a typical pump consists of a rotating element of radius R called the rotor mounted in a housing called the stator. These two elements are separated by a narrow gap of dimension h. In operation, oil flows into the gap through the inlet port and is swept around the housing to the outlet port by the viscous drag of the oil acting on the rotor. As a result, the pressure of the oil at the outlet port is higher than the pressure of the oil at the inlet port. In a typical design, $h << R$.

(a) Neglect any leakage due to flow directly from the outlet port to the inlet port and due to flow around the ends of the rotor and determine the following performance parameters as function of the volumetric flow rate through a pump of dimension b normal to the plane of the sketch:

(1) pressure rise in the pump, $P_{out} - P_{in}$
(2) torque on the rotor, T
(3) shaft power required to run the pump, $\dot{W}_{shaft}$
(4) efficiency of the pump, η

(b) For a pump of dimension $R = 2$ cm with an angular velocity of $\omega = 1000$ rpm and pressure rise $P_{out} - P_{in} = 4 \times 10^5$ N/m^2, determine the maximum value of the gap dimension h for which the flow in the gap between the rotor and stator can be modeled as Couette flow between two infinite flat plates with a maximum error of one percent. Determine the Reynolds number for this flow which will remain laminar if the Reynolds number in the gap is less than the critical value of $Re_{crit} = 1500$ where

$$Re = \frac{\vartheta_{ave} h \rho}{\mu}$$

where the density of the oil is $\rho = 883$ kg/m^3 and its viscosity is $\mu = 5030 \times 10^{-4}$ kg/m sec.

(c) The oil for which the properties are given above enters the pump ($b = 3$ cm) at a temperature of $T_{in} = 300$ K. For the conditions determined in part (b) above, estimate the temperature at exit and calculate the rate of entropy generation in the oil if $c = 1900$ J/kg K for the oil.

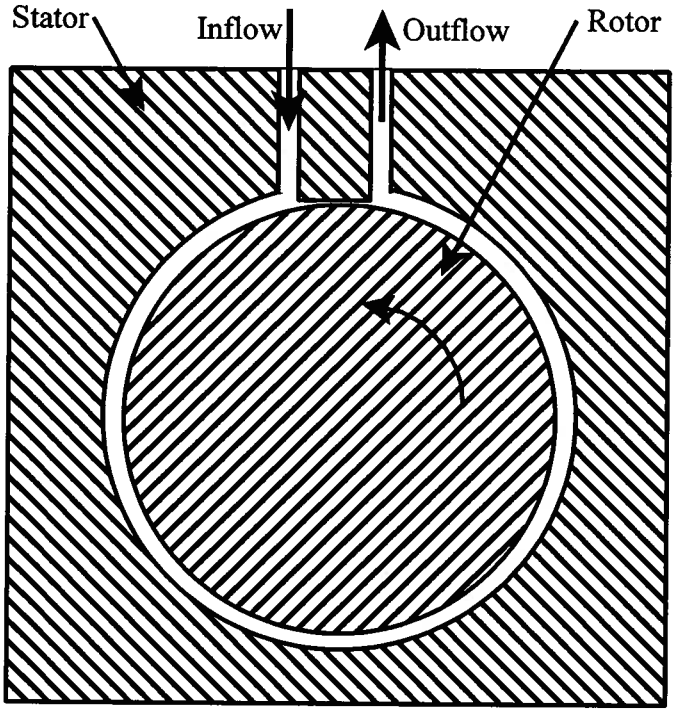

Figure 9P.11 Viscosity Pump

9.12 As shown in Figure 9P.12, a circular disk of radius R is immersed in a fluid of density ρ and viscosity μ. By means of applying a constant force F, the disk is forced down at velocity $\vartheta_0(t)$ onto a flat parallel surface. At any instant of time, the separation of the surfaces is $h(t)$. The motion of the disk is sufficiently slow so that the acceleration and kinetic energy of the fluid can be neglected. The outward viscous flow of the fluid between the surfaces can then be assumed to have the same velocity distribution as a fully developed two-dimensional laminar flow.

(a) Formulate an expression for the pressure distribution in the fluid as a function of the radius r with the boundary condition $P(R) = 0$. Express the result in terms of r, μ, ϑ_0, and h.

(b) Calculate the force F in terms of the same variables.

(c) Find the time t required for the disk to move within a distance h of the lower surface. Assume that for the purposes of this calculation, $h(0) = \infty$.

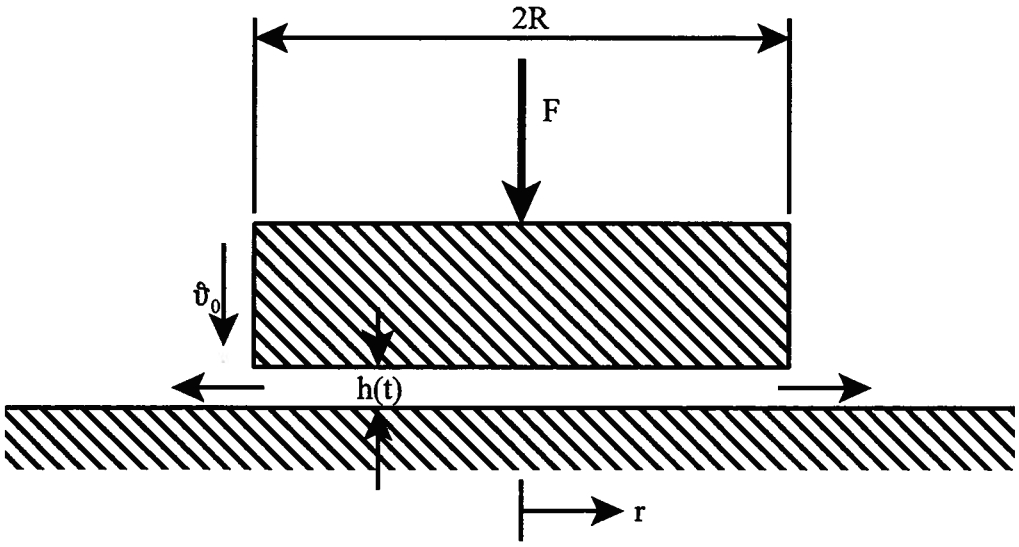

9.13 Figure 9P.13 shows a simple water distribution system. The system is fed by a reservoir connected to a plenum of negligible dimensions by a pipe of diameter $D_1 = 0.5$ m and length $L_1 = 150$ m. Branching out from the plenum is a horizontal pipe of diameter $D_2 = 0.10$ m and length $L_2 = 100$ m and another pipe of diameter $D_3 = 0.15$ m and length $L_3 = 150$ m inclined at an angle of 30° above the horizontal plane. The fourth pipe connected to the plenum is also horizontal and consists of two pipes connected in series. The pipe connected to the plenum is of diameter $D_4 = 0.20$ m and length $L_4 = 100$ m. At its outlet, it is joined to another pipe of diameter $D_5 = 0.10$ m and length $L_5 = 100$ m. The junction of pipes 4 and 5 is a sudden contraction with loss coefficient $K_c = 0.3$ based upon the kinetic energy of the smaller diameter, $(\vartheta_{ave})_5^2/2$. Find the height of the free surface of the water in the supply reservoir so that the velocity of the water at the outlet of pipe 5 is $(\vartheta_{ave})_5 = 20$ m/sec.

For water: density $\rho = 1000$ kg/m^3, viscosity $\mu = 10^{-3}$ kg/m sec.

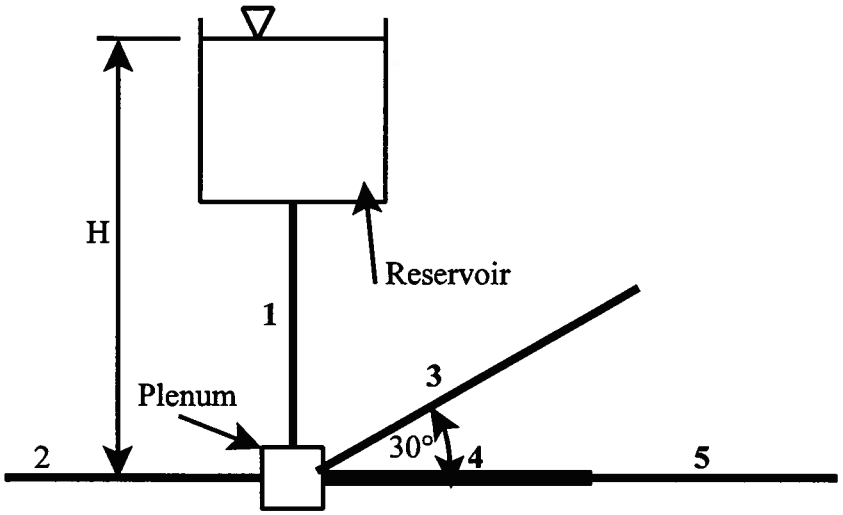

Figure 9P.14 Water Distribution System

9.14 In the cleanup of oil spills from oil tankers on large bodies of water, the oil floats on the surface of the water and is swept into a containment pond by large booms mounted on the bow of another ship. A moving vertical belt, much like that of a belt sander, is used to transport the oil from the water into barges in which it can be processed for safe disposal. In a particular application, it is observed that the belt picks up a layer of oil of thickness h. The belt moves upward with a velocity ϑ and the oil has viscosity μ and density ρ.

(a) Estimate the net volume flow rate V of oil per unit of width of the belt.

(b) Determine the minimum belt velocity necessary to have a net flow of oil upward, and, hence, to keep the fluid on the belt.

(c) For a fixed belt velocity, what thickness h maximizes the volumetric flow rate?

9.15 As shown in Figure 9P.15, a solid cylinder of mass M, length L, and diameter D is falling in a fluid-filled cylinder of diameter $d = D + 2c$ and length ℓ. The fluid can be modeled as a Newtonian fluid with density ρ and viscosity μ. The solid cylinder is made of material with density ρ_s. The ratios c/D and L/ℓ are very small. The solid cylinder has reached terminal velocity ϑ in its descent.

(a) Specify the conditions under which the flow of the fluid in the gap between the two cylinders can be modeled as flow between infinite parallel flat plates.

(b) Using the model of part (a) above, determine the terminal velocity in terms of the geometric parameters and the properties specified.

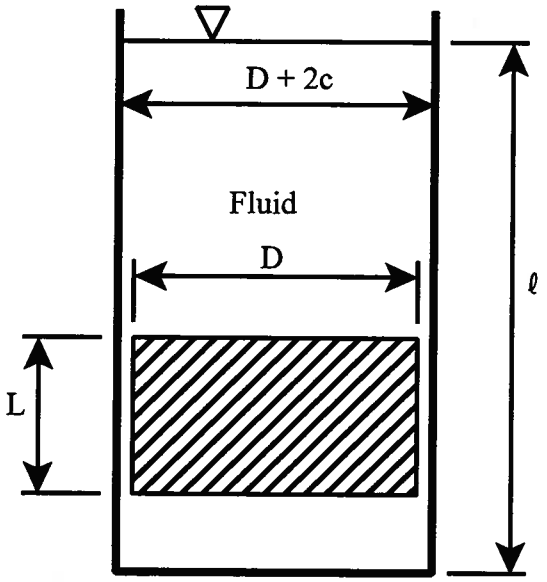

Figure 9P.15 Falling Cylinder

9.16 (a) Sketch the streamlines over the two (two-dimensional) bodies shown in Figure 9P.16 when they are inserted into a uniform ideal, *inviscid* flow from left to right. (The nose of the streamlined body is circular with the same radius as the cylinder). Mark on the sketch the regions of highest and lowest static pressure.

(b) By considering the likely size of any adverse pressure gradients in these ideal flows, explain why the drag on the streamlined body is much less than that on the cylinder for flow at high Reynolds number of a viscous fluid over them from left to right.

(c) Which body will have the least drag for low Reynolds Number flow (i.e. Re << 1)?

cylinder

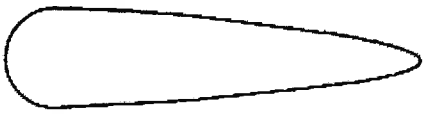

streamlined body

Figure 9P.16 Objects Immersed in a Flowing Fluid

9.17 The measured drag coefficient for a sphere as a function of Reynolds number is as shown in Figure 9P.17a.

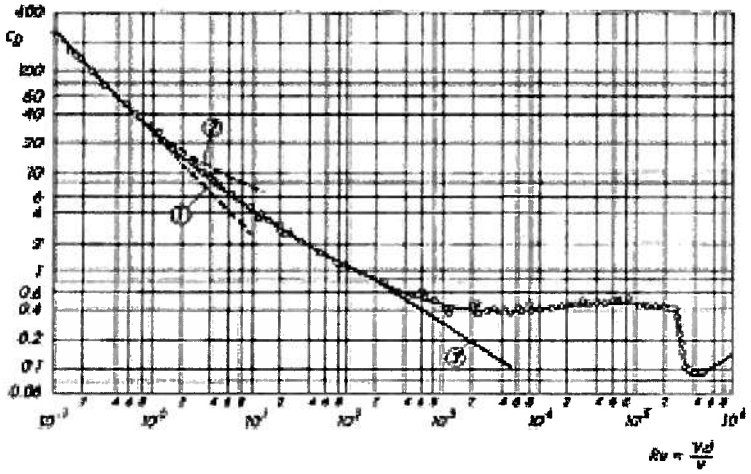

Figure 9P.17a Drag Coefficient for Spheres

(a) Explain why you would expect the drag coefficient to be proportional to Re^{-1} for low values of Re.

(b) Explain why there is a pronounced dip in the value of C_D at high values of Re.

(c) The following table gives typical speeds and sizes of balls used in various sports. Assuming that the kinematic viscosity $\nu = \mu/\rho$ of air is 1.5 x 10^5 m^2/sec, calculate typical Reynolds numbers for the various sports.

	Golf	Cricket	Soccer	Tennis	Baseball
U (m/sec)	70	40	16	50	45
D (m)	0.043	0.068	0.19	0.064	0.075

(d) The effect of surface roughness (defined as the ratio of roughness height to diameter) on C_D is shown in Figure 9P.17b for a particular Reynolds number range. Explain why roughness has this effect.

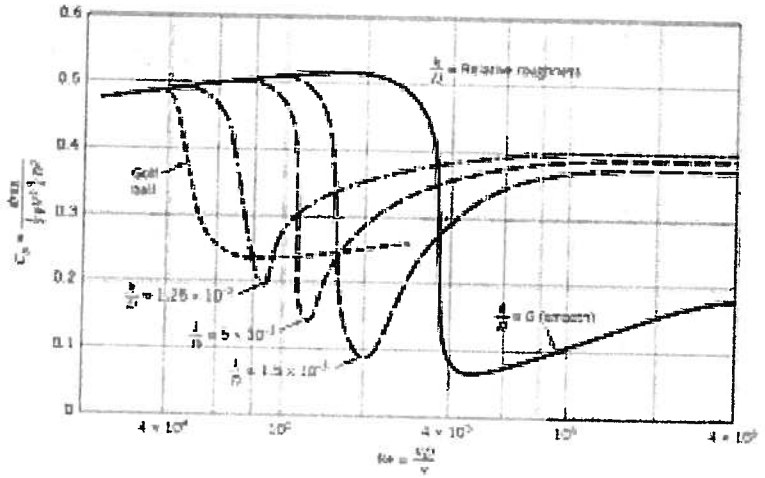

Figure 9P.17b Effect of Surface Roughness on Drag Coefficient for Spheres

9.18 The blood circulatory system in the human body consists of a large diameter vessel (D = 25 mm), the aorta, that carries the oxygenated blood away from the heart to the tissues of the body through a continually branching network of vessels that finally become the capillaries (d = 8 μm). In this particular problem we are concerned with the behavior of the first branch of the aorta under conditions of extreme cardiac output due to maximal exercise. As shown in plan view in Figure 9P.18, the circular, **smooth-walled** aorta branches into two identical circular, **smooth-walled** vessels of equal diameter with equal blood flow rates.

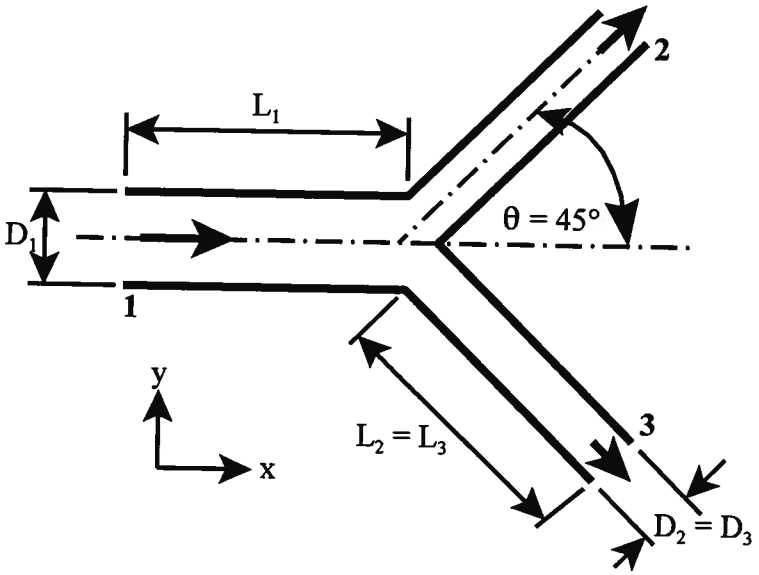

Figure 9P.18 Plan View of Branch in Human Aorta

For this geometry, the aorta and its branches can be modeled as rigid tubes with:

$$D_1 = 0.025 \text{ m}, \quad A_2 = A_3 = \frac{\sqrt{2}}{2} A_1, \quad L_1 = 5D_1, \quad L_2 = L_3 = 5D_2, \quad \dot{V}_1 = 4.167 \text{ x } 10^{-4} \text{ m}^3/\text{sec}$$

The minor head loss due to the branch is given by

$$h_m = \frac{1}{2}\rho v_1^2 K_{12} \quad \text{where} \quad K_{12} = 0.28$$

Although, in general, blood is a non-Newtonian fluid due to the presence of proteins and cellular materials suspended in it, for the purposes here, we can model the blood as a Newtonian fluid with the following properties:

$$\rho = 1050 \text{ kg/m}^3 \quad \text{and} \quad \mu = 3.5 \text{ x } 10^{-3} \text{ kg/m sec}$$

(a) Using the energy equation for fully-developed flow with the major and minor head loss terms included, calculate the pressure drop ΔP between locations 1 and 2 and between locations 1 and 3 for the case in which $P_1 = 1.13 \text{ x } 10^5 \text{ N/m}^2$.

(b) The tissues surrounding this branch must exert a force on the branch itself to keep it from moving within the body. What is the x-component of this force, F_x? Note the sign convention in the sketch above.

(c) What is the y-component of the restraining force, F_y?

9.19 (a) Figure 9P.19 shows a water distribution system from a lower reservoir to two reservoirs at higher level. If the stagnation pressures delivered by the pump to pipes 2 and 3 are equal, show that

$$\mathcal{V}_2^2 = \frac{f_3\left(\frac{L_3}{d_3}\right)\mathcal{V}_3^2 + 2g(y_3 - y_2)}{f_2\left(\frac{L_2}{d_2}\right)}$$

where $\mathcal{V}_2$ and $\mathcal{V}_3$ are the velocities of the flow in pipes 2 and 3.

(b) Find the total flow rate through the pump, V_{pump}, when that through the pipe 3 is $V_3 = 0.115 \text{ m}^3/\text{sec}$.

(c) Find the rise in stagnation pressure across the pump and the power required, assuming that the pump is adiabatic and reversible. (Ignore all losses except those caused by pipe friction.) The density of water is $\rho = 995 \text{ kg/m}^3$.

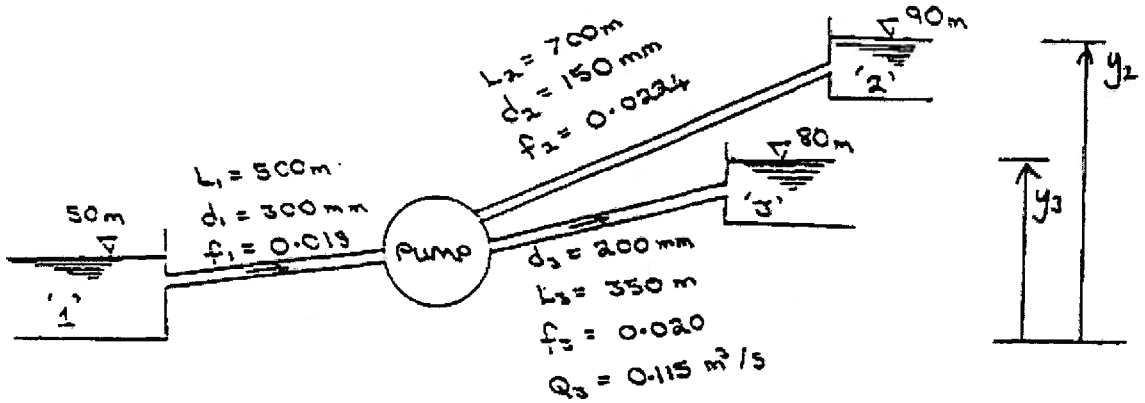

Figure 9.20 Water Distribution Network

9.20 Consider the case of air flowing at a steady rate through a horizontal pipe of constant cross-sectional area. The fully-developed flow configuration is such that the bulk mean temperature of the air is constant at $T_{air} = 27$ C all along the flow direction. At point **A** the pressure is $P_A = 3$ bar and the bulk mean velocity is $\mathcal{V}_A = 160$ m/sec. At point **B** the pressure is $P_B = 2$ bar. The temperature of the pipe wall is $T_{wall} = 43$ C. (1 bar = 10^5 N/m^2)

(a) Calculate the bulk mean velocity $\mathcal{V}_B$ at **B**.

(b) Calculate $\dot{Q}/\dot{m}$, the heat transfer rate per unit mass flow rate of air between points **A** and **B**.

(c) Assuming that the flow is from **A** to **B**, calculate the rate of entropy generation per unit mass flow rate. Suggest a physical cause for the irreversibility, and comment on the validity of the assumption that the flow is from **A** to **B**.

9.21 Air at a pressure of $P_{atm} = 10^5$ N/m^2 and a temperature of $T_{atm} = 20$ C flows along a flat plate whose dimensions are length L and width b. The undisturbed velocity of the air upstream of the leading edge of the plate is $\vartheta_0 = 10$ m/sec. As a result of the action of the viscosity of the air, the air in the neighborhood of the plate is slowed and a boundary layer develops and grows in thickness downstream of the leading edge. At $L = 145$ mm downstream from the leading edge of the plate the boundary layer thickness is $\delta = 2.3$ mm. The velocity profile in the boundary layer at this location is

$$\frac{\vartheta}{\vartheta_0} = \frac{3}{2}\frac{y}{\delta} - \frac{1}{2}\left(\frac{y}{\delta}\right)^2$$

where y is measured normal to the plate. Determine the x-component (horizontal) force per unit of width required to hold the plate stationary if the air can be modeled as incompressible. Note: Only the upper face of the flat plate is exposed to the air flow.

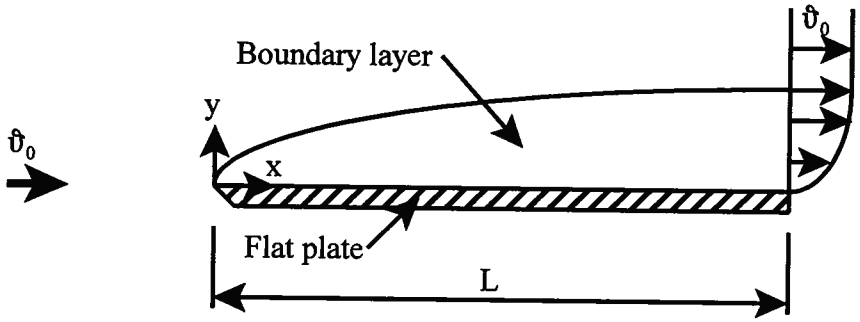

9.22 A "dead-weight" pressure gage tester is a device used to calibrate Bourdon-tube pressure gages. The device shown in Figure 9P.22 consists of a cylinder with a closely fitting piston. The volume between the piston face and the cylinder head is filled with hydraulic oil. Attached to the piston is a pan upon which various masses are placed. By adjusting the mass for a known piston diameter, any desired pressure may be obtained in the oil. In a typical design, the piston uses no piston rings in order to minimize solid friction that would lead to erroneous calibrations. As a consequence, there is some leakage of oil from the cylinder volume to the atmosphere past the piston which causes the piston to descend under the influence of gravity and the viscous drag of the oil in the gap.

In a particular design, the piston diameter is $D = 10$ mm and its length is $L = 70$ mm. The radial clearance is $h = 0.03$ mm, and the oil has a viscosity of $\mu_{oil} = 0.5$ kg/m sec. Atmospheric pressure is $P_{atm} = 10^5$ N/m^2 and $g = 9.81$ m/sec^2.

(a) Assuming no leakage of oil, determine the combined mass of the piston, weights, and pan necessary to produce a pressure of $P_{oil} = 1.5 \times 10^6$ N/m^2 in the oil.

(b) Since the gap thickness is much smaller than the radius of the piston, we can model the leakage of the oil in the gap as a one-dimensional flow as the piston moves. Starting with the Navier-Stokes equations for this one-dimensional flow, show that if we neglect the effect of

gravity in comparison with the viscous effects, the fully-developed laminar velocity profile in the gap is given by

$$\vartheta_x = \frac{\vartheta_0 y}{h} + \frac{1}{2\mu_{oil}}\left(\frac{dP}{dx}\right)\left(y^2 - yh\right)$$

where μ_{oil} is the viscosity of the oil, h is the gap thickness, ϑ_0 is the velocity of the piston (Note that this value is negative.), and dP/dx is the pressure gradient in the flow.

(c) Show that as a result of the pressure gradient, the volumetric flow of oil past the piston per unit depth b measured normal to the plane of the figure (Note that $b = \pi D$.) is

$$\frac{\dot{V}}{b} = \frac{\vartheta_0 h}{2} - \frac{1}{12\mu_{oil}}\left(\frac{dP}{dx}\right)h^3$$

(d) For the mass determined in part (a) above, determine the rate of descent of the piston if drag due to the shear stress acting on the surface of the piston can be neglected.

(e) Calculate the drag force on the piston due to the shear stress acting on the surface of the piston as a result of viscous flow of oil in the gap. How does this compare with the normal force due to the pressure of the oil acting on the face of the piston?

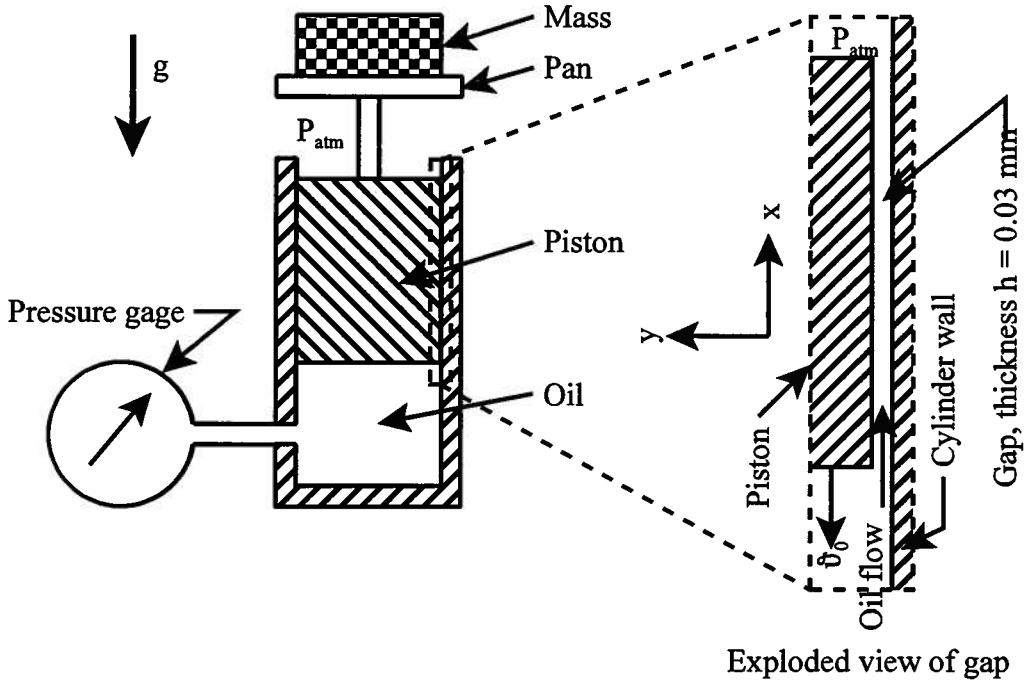

Figure 9P.22

9.23 As shown in Figure 9P.23, a method of coating photographic film with emulsion is to pass the film stock at constant velocity through a bath of liquid emulsion and withdraw the film in the vertical direction. As the film passes through the bath, one side of it becomes coated with liquid emulsion. (The other side is coated with a non-wetting agent that prevents the photographic emulsion from sticking to the film.) Gravity causes the liquid emulsion to drain down, but the continuous motion of the film keeps the liquid emulsion from running off completely. (**Note that the coordinate axes are not in their usual orientation.**)

The film velocity through the bath is ϑ_0; the thickness of the liquid emulsion layer on the film is h; the density of the liquid emulsion is ρ; and the viscosity of the liquid emulsion is μ.

Model the liquid emulsion as a Newtonian fluid. Furthermore, model the flow of the emulsion as a fully developed laminar flow with zero pressure gradient in the x-direction. The viscosity of air is small relative to that of the liquid emulsion.

There are two ways of developing an analysis of this physical situation: one has the coordinate axes attached to the film; the other has the coordinate axes fixed in the room where the film is being coated. Both coordinate schemes are inertial coordinate systems, but they will give different answers for the velocity profile. State which coordinate scheme is to be used in your analysis.

(a) For your coordinate scheme, specify the appropriate boundary conditions at the film/liquid emulsion interface, $y = 0$, and at the liquid emulsion/air interface, $y = h$.

(b) Write the complete expression for the x-component of the Navier-Stokes equation and show that for this physical situation it simplifies to

$$0 = \rho g_x + \mu \frac{\partial^2 \vartheta_x}{\partial y^2}$$

where ϑ_x is the velocity component in the x-direction in your coordinate scheme. In the simplification process, give a reason for the elimination of each term that is dropped from the full form of the Navier-Stokes equation.

(c) Use the simplified Navier-Stokes equation to derive an expression for the velocity profile in the liquid emulsion layer, $\vartheta = \vartheta(x, y)$.

(d) Derive an expression for the shear stress exerted on the film by the liquid emulsion layer, and determine the drag per unit length on the film of width b due to the emulsion layer.

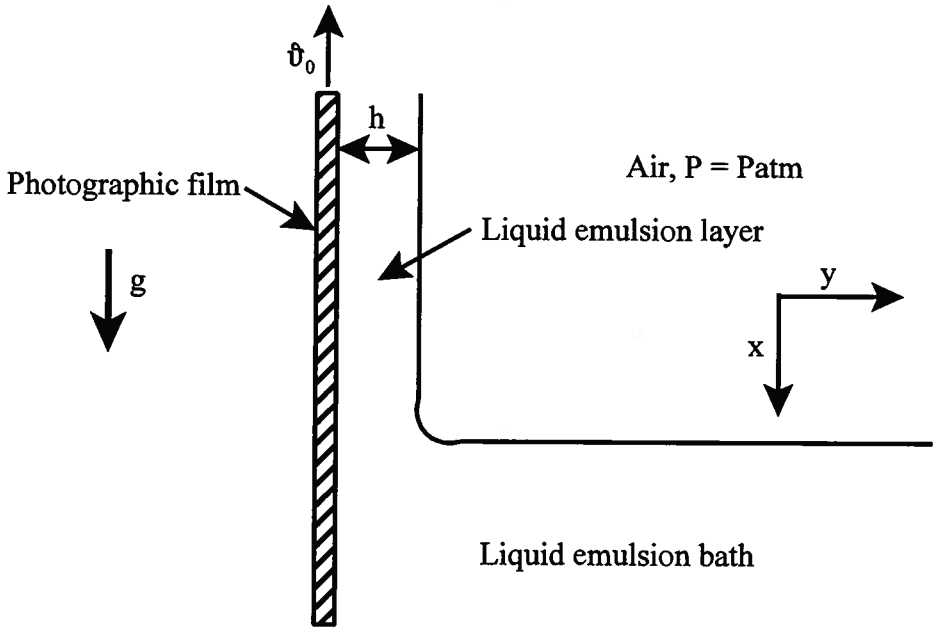

Figure 9P.23

9.24 As shown in Figure 9P.24, a crude oil reservoir in the Bluebell field of northern Utah is being tapped by drilling a well through the natural rock formation in which it is trapped. The reservoir is located 3,000 m below the surface. The pressure in the reservoir at the time the well is drilled is $P_0 = 13.5 \times 10^7$ N/m^2. The viscosity of this light crude oil is $\mu_{oil} = 4 \times 10^{-3}$ kg/m-sec

and its density is ρ_{oil} = 860 kg/m^3. The flow pipe inside the well casing has an inside diameter of 10 cm with a relative roughness of 1 x 10^{-3}.

(a) Estimate the initial volumetric flow rate of oil from this well using the reservoir pressure as the driving pressure to pump the oil to the surface where P_{atm} = 10^5 N/m^2.

(b) If the crude oil is allowed to discharge straight up into the atmosphere in the form of a jet (a "gusher") when it reaches the surface, what is the maximum possible height of the gusher?

(c) This method of using the natural pressure of the oil in the reservoir to pump the oil to the surface is called the "primary recovery". Of course, as the oil is drawn from the reservoir, the pressure in the reservoir will drop and the flow rate will decrease. At what value of the reservoir pressure will the flow rate at the surface decrease to zero?

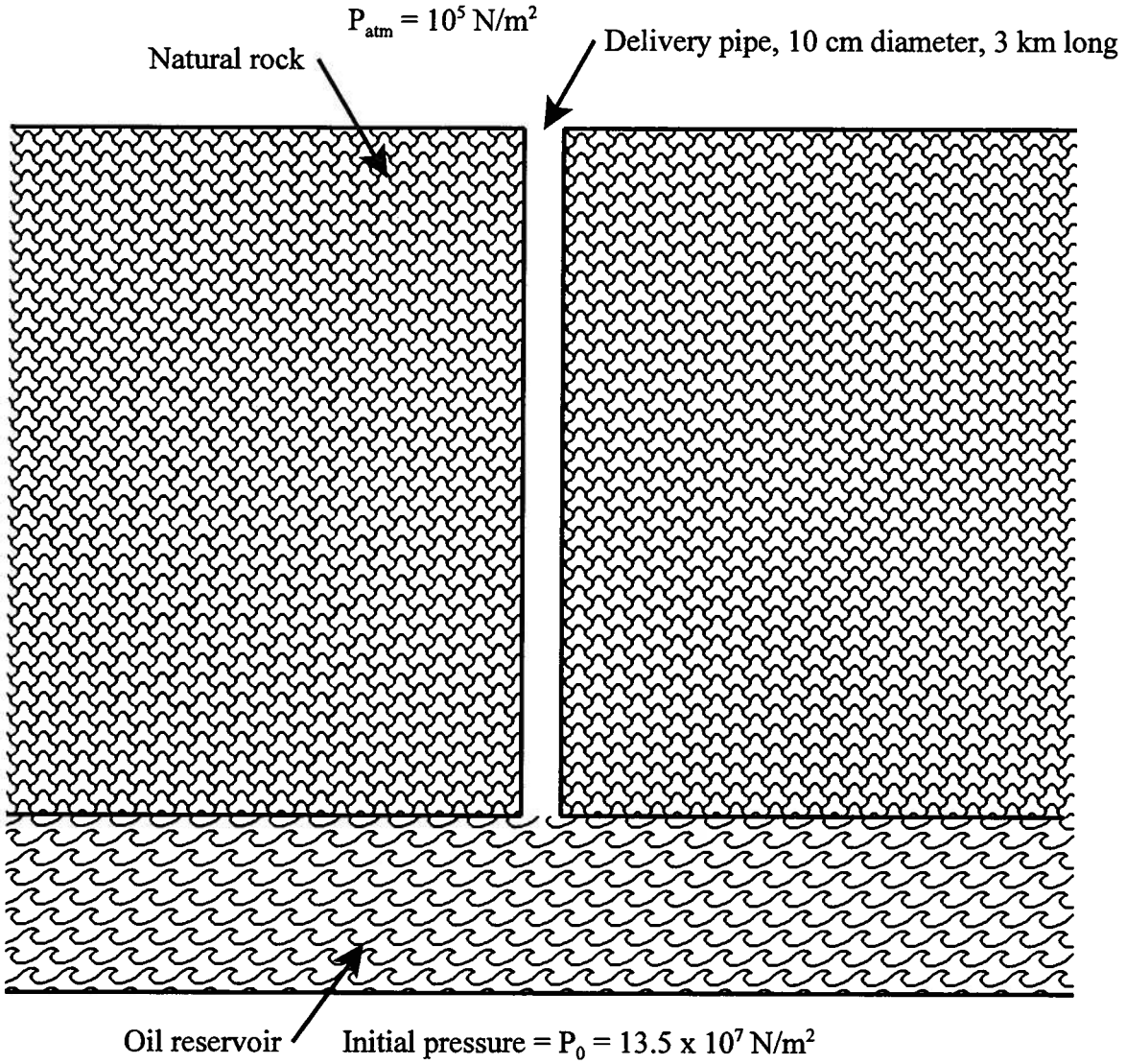

9.25 As shown in Figure 9P.25, a large cistern discharges through a smooth-walled circular pipe with a diameter of D = 10 cm and a length of L = 100 m. The pipe is fitted with a globe valve that is used to regulate the flow rate from the cistern. The water level in the cistern is maintained at a constant value of 30 m above the centerline of the attached pipe.

Determine the maximum volumetric flow rate from the discharge end of the pipe. Include the losses due to the square-edged entrance to the pipe, the globe valve, and the friction of the pipe wall in your analysis. The following data will be useful:

For a square-edged entrance:

$$(h_{lm})_{entrance} = K_1 \frac{\vartheta_{ave}^{\ 2}}{2}$$

where $K_1 = 0.5$ and ϑ_{ave} is the average velocity of flow in the pipe.

For a globe valve in the fully-open position:

$$(h_{lm})_{\substack{globe \\ valve}} = K_2 \frac{\vartheta_{ave}^{\ 2}}{2}$$

where $K_2 = 4.1$ and ϑ_{ave} is the average velocity of flow in the pipe to which the valve is attached.

For water: $\rho = 1000$ kg/m^3, $\mu = 1 \times 10^{-3}$ kg/m sec
For gravity: $g = 9.81$ m/sec^2

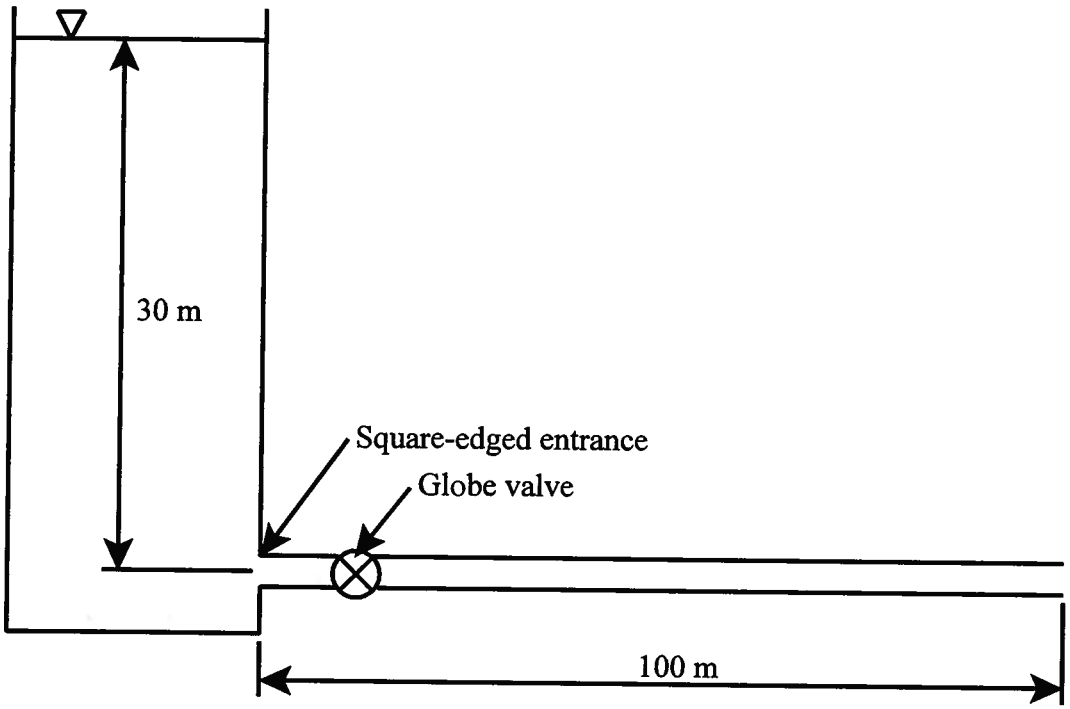

9.26 It has been proposed to construct an inclined tube viscometer as shown in Figure 9P.26. The inclined tube is connected to an infinite supply of the incompressible fluid of density ρ whose viscosity μ is to be measured. In operation, a beaker is to be placed at the discharge end of the tube and the time necessary to collect a fixed volume of the fluid is to be recorded. From these data, the viscosity can be determined.

(a) For the parameters shown in the sketch, show that for certain conditions (which you must specify), the continuity equation in cylindrical coordinates reduces to

$$\frac{1}{r}\frac{\partial}{\partial r}(r\vartheta_r) = 0$$

and use this result to show that there is only one velocity component $\vartheta_z = \vartheta_z(r)$ of consequence.

(b) Using the arguments that you have put forth in part (a) above, show that the relevant form of the Navier-Stokes equation reduces to

$$\frac{1}{r}\frac{\partial}{\partial r}(r\tau) = \frac{d}{dz}(P - \rho g z \sin\theta)$$

where τ is the shear stress and

$$\tau = \mu\left(\frac{\partial \vartheta_z}{\partial r}\right)$$

(c) For the case in which the pressure is atmospheric at both ends of the tube, use the result of part (b) above to derive an expression for the time Δt required to collect a volume V_0 of fluid.

(d) This device cannot be used for just any fluid. What are the conditions that must be satisfied in order for this method to be valid? Express your result in numerical format.

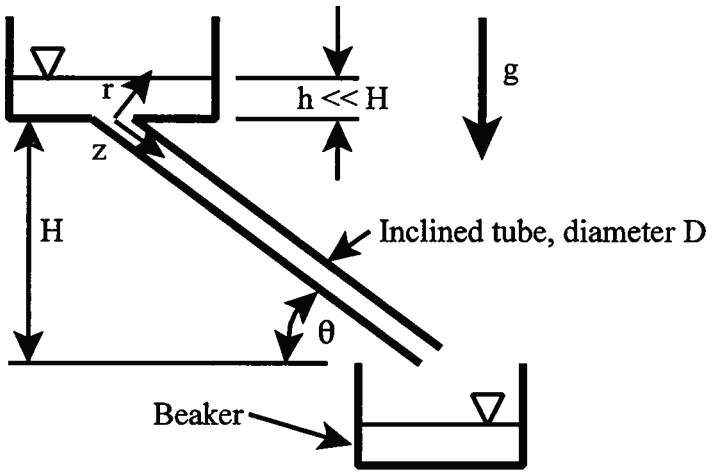

Figure 9P.26

9.27 Consider the case of two concentric tubes for which the radius of the inside wall of the outer tube is R and the radius of the outer wall of the inner tube is κR where $\kappa < 1$. A viscous fluid with viscosity μ flows in a laminar fashion in the annulus between the two tubes.

(a) Show that for fully developed flow in the annulus, the velocity profile is given by

$$\vartheta_z = \frac{(P_1 - P_2)R^2}{4\mu L}\left[1 - \left(\frac{r}{R}\right)^2 - \frac{1-\kappa^2}{\ln\left(1/\kappa\right)}\ln\left(\frac{R}{r}\right)\right]$$

where P_1 is the pressure at some location and P_2 is the pressure at some location a distance L downstream.

(b) Show that the average velocity in the annulus is given by

$$\vartheta_{ave} = \frac{(P_1 - P_2)R^2}{8\mu L}\left[\frac{1-\kappa^4}{1-\kappa^2} - \frac{1-\kappa^2}{\ln\left(1/\kappa\right)}\right]$$

(c) Show that the maximum velocity in the flow is given by

$$\vartheta_{max} = \frac{(P_1 - P_2)R^2}{4\mu L}\left[1 - \lambda^2\left(1 - \ln\lambda^2\right)\right]$$

where

$$\lambda^2 = \frac{1}{2}\frac{1-\kappa^2}{\ln\left(1/\kappa\right)}$$

(d) Sketch the velocity profile in the annulus and label ϑ_{ave} and ϑ_{max}.

(e) Show that the physical situation reduces to flow between parallel plates (plane Poiseuille flow) when

$$\frac{R - \kappa R}{R} \ll 1$$

What is the value of the above ratio for a one percent error associated with the plane Poiseuille flow approximation to the annulus configuration?

9.28 As shown in Figure 9P.28, a viscous fluid is trapped between two parallel infinite flat plates. The plates are separated by a uniform gap of h = 10 mm and are inclined at an angle of 45° to the horizontal. The upper plate moves at a constant velocity of ϑ_0 = 1.5 m/sec relative to the bottom plate, counter to the direction of the fluid flow. The gage pressures at points A and B are P_A = 250 x 10^3 N/m^2 and P_B = 80 x 10^3 N/m^2.

(a) Determine the velocity distribution $\vartheta_x(y)$ of the fluid in the gap.

(b) Determine the shear stress distribution $\tau_{yx}(y)$ in the gap.

(c) Determine the average fluid velocity ϑ_{ave} in the gap.

(d) Determine the maximum fluid velocity ϑ_{max} in the gap and its location.

(e) Determine the power per unit area $\wp$ that must be supplied to the upper plate in order to maintain its velocity constant.

For the fluid: ρ = 1260 kg/m^3 and μ = 0.9 kg/m sec

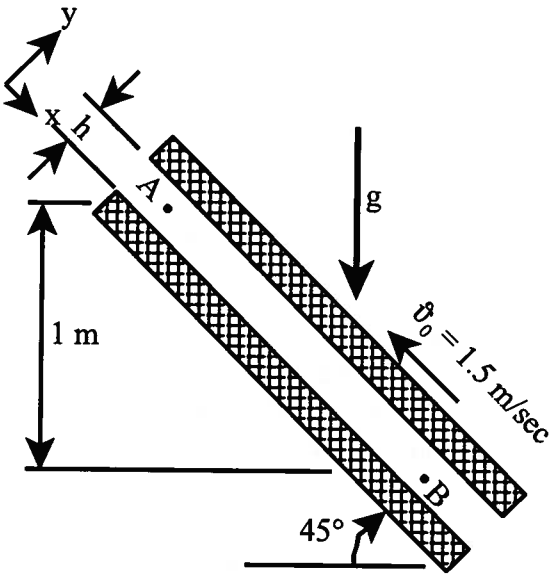

Figure 9P.28

9.29 Consider the boundary layer on a flat plate shown schematically in the sketch below.

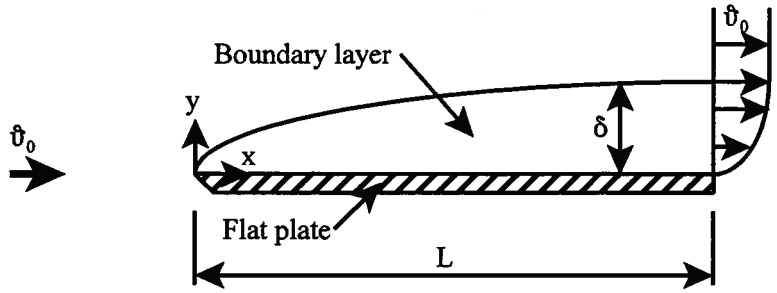

The analysis of this boundary layer can be analyzed in approximate fashion by postulating the form of the velocity distribution in the boundary layer and applying the momentum deficit concept of von Karman. One such velocity profile is given by

$$\vartheta_x = \vartheta_0 \sin\left(\frac{\pi}{2}\frac{y}{\delta}\right)$$

where ϑ_0 is the free stream velocity and $\delta = \delta(x)$ gives the thickness of the boundary layer at any location x measured from the leading edge.

(a) Show that this velocity profile satisfies the no-slip boundary condition at the surface of the plate as well as the requirement that the velocity at the outer edge of the boundary layer must be the free stream velocity, ϑ_0.

(b) Use the momentum integral relation, equation (9.202),

$$\tau_w = \rho \vartheta_0^2 \frac{d\theta}{dx}$$

where θ is the momentum thickness of equation (9.197), viz.

$$\theta = \int_0^\delta \frac{\vartheta_x}{\vartheta_0}\left(1 - \frac{\vartheta_x}{\vartheta_0}\right) dy$$

Together with the definition of the shear stress at the wall

$$\tau_w = \mu\left(\frac{d\vartheta_x}{dy}\right)_{y=0}$$

to show that the friction coefficient C_f for this velocity profile is given by

$$C_f \equiv \frac{\tau_w}{\frac{1}{2}\rho\vartheta_0^2} = \frac{0.655}{\sqrt{Re_x}}$$

(c) Calculate the total drag force for one side of a plate of length L and width b.

(d) Show that the thickness of the boundary layer at any location x for this assumed velocity profile is substantially larger than the corresponding boundary layer thickness for the Blasius profile. How can this be true and yet the difference between the friction coefficients for these two profiles be so small?

9.30 MEMS technology is used to fabricate a heat exchanger from silicon for a micro-turbine system. Air at a temperature of T_{air} = 600 C flows through the passages of the heat exchanger at velocities low enough to be modeled as an incompressible fluid. A design decision has set the

Reynolds number for the flow at $Re_{Dh} = 1000$. The flow channel dimensions are: $H = 2$ mm, $W = 1$ mm, and $L = 1$ m. The thermal-fluid characteristics of the air are:

$\rho_{air} = 0.3988$ kg/m^3 $\quad \mu_{air} = 3.9771 \times 10^{-5}$ kg/m sec $\quad c_P = 1003$ J/kg K $\quad c_v = 716$ J/kg K

(a) Calculate the velocity of the air and show that this velocity results in a Mach number that is less than $M = 0.3$ which is the requirement for the incompressible flow model.

(b) Calculate the pressure drop ΔP for this flow passage. Use the friction factor correlations for laminar flow in a non-circular conduit found in Table 9.3.

9.31 The aorta is the largest blood vessel in the human body with a diameter of $D = 25$ mm. For a person standing erect, the axis of the aorta is vertical, and depending upon the height of the individual, the length of the aorta is approximately $L = 0.5$ m. The volumetric flow rate through the aorta is $V = 4.167 \times 10^{-4}$ m^3/sec. The thermal-fluid characteristics of the blood are:

$$\rho = 1050 \text{ kg/m}^3 \quad \text{and} \quad \mu = 3.5 \times 10^{-3} \text{ kg/m sec}$$

(a) Calculate the Reynolds number in the aorta. Is the flow laminar or turbulent?

(b) Blood proteins and fat globules (drink a milkshake or eat a Krispy Kreme) suspended in the blood may actually be able to damp out disturbances in the flow so that the flow is able to remain laminar at values of the Reynolds number in the transition region $2100 < Re_D < 10^4$. In fact, one can advance a teleological argument that the flow wants to remain laminar for two reasons: (1) to reduce the pressure drop in the flow and thereby impose a lower workload on the pump (heart); and (2) to minimize the mechanical damage that might occur to the fragile red cells and platelets as a result of the turbulence if it were allowed to form. Assuming that the flow is fully developed, calculate the pressure drop in the aorta for the two flow regimes. For the turbulent flow case, evaluate the friction factor from the Petukov correlation of equation (9.263), viz.

$$f = \left(0.7904 \ln Re_D - 1.64\right)^{-2}$$

How do the pressure drops compare? Does the first part of the teleological argument hold?

(c) If the flow is not fully developed, estimate the pressure drop for the two regimes.

CHAPTER 10

Dimensional Analysis

10.1 Introduction

Thus far in our development of thermal-fluids engineering, we have focused on two levels of the physical world. On the one hand, we have studied systems (or objects) and on the other, we have studied their properties (or attributes). We now wish to explore in greater detail the relationship between an object and its attributes, or from a thermal-fluids perspective, a system and its properties. For example, a vehicle may be viewed as an object and some of its many attributes might include its color, its model (sedan, truck, SUV, etc.), its mass, its velocity, and its acceleration to name but a few. Objects have identity and we can use this identity to answer the question, "How many?" As long as the identity is unambiguous, the answer to this question is an unambiguous pure number. For example, consider the set of objects represented by the vehicles in a parking garage. The answer to the question "How many?" can be determined by simply counting the vehicles which results in a pure number, e.g., 27. However, we may also wish to gain information about certain of the attributes of these vehicles. We then ask the question "How much (mass or volume or temperature or pressure, etc.)?" In order to answer this question, we need to make a *measurement*. In the case of the vehicles, for example, if we wanted to know how much mass the vehicles represented in order to design the support structure that would accommodate the vehicles, we would simply measure the mass of each vehicle and then add the results of these measurements together to obtain the total mass.

"Measuring" is a very different operation from "counting." The process of counting results in a *pure* number, but the process of measuring results in an *arbitrary* number whose value will depend upon the *unit system* employed in the measurement process. In the case of the vehicles in the parking garage, we could express the mass in terms of kilograms, pounds-mass, or tons. The number would be different in each case even though it represents the same mass. In order to avoid any ambiguity in communicating the magnitude of an attribute (or a property), we must give the number *and* the units associated with that number in the chosen unit system.

As an example more appropriate to our studies of thermal-fluid systems, suppose that we were interested in the answer to the question "*How much* pressure (the property) does a particular gas (the system) exert on the walls of its container?" We could obtain the desired information by measuring the pressure with an instrument designed for this purpose. In reporting the result of this measurement, there is a wide choice of units available: Pa, MPa, bar, N/m^2, lbf/in^2, atm, and mm Hg to name but a few. The number that specifies the magnitude of the pressure will be different for each of these units, but it will still be the same pressure in each case. For example, in different unit systems, a certain pressure would have the value 10^5 Pa, 0.1 Mpa, 1 bar, 10^5 N/m^2, 14.5 lbf/in^2, 0.987 atm, and 749.88 mm Hg and still be the same identical pressure in every case. Furthermore, if we wish to relate these attributes or properties to other attributes or properties through mathematical relationships such as constitutive relations or fundamental physical laws, we need to ensure that each term in the relationship is in the same system of units. At times, this can be cumbersome and prone to error. On the other hand, if we could somehow remove the units from the parameters appearing in the relationship, we could then remove the arbitrariness from the process and thereby simplify the description of the situation. Our objective in the present chapter is to develop a means of doing just that, i.e., removing the unit system from

our description of physical situations. This process is known as *dimensional analysis*, and it can be a very powerful tool in thermal fluids engineering. As we shall soon see, dimensional analysis has many other benefits, not the least of which is reducing the number of parameters required to describe a physical situation.

10.2 Measurements, Units, and Dimensions

We begin by first examining the measurement process in some detail. As should be obvious from above, the first step in the measurement process is to select the system of units to be used. By international agreement, *Le Système International d'Unitès* (abbreviated SI) has been established as the unit system of choice for science and international commerce. This is the unit system used in this presentation. The choice of unit system determines the base quantities of the system, which for the SI unit system, are: mass (m), length (l), time (t), thermodynamic temperature (T), electric current (I), amount of substance (n), and luminous intensity (I_v). For the thermal-fluid systems of interest at this time, only the first four of the base quantities are relevant, namely mass, length, time, and thermodynamic temperature, and the units of these four base quantities are kg, m, sec, and K, respectively.

All other quantities are deemed derived quantities and are obtained by the mathematical operations of multiplication and division of the base quantities. Examples of derived quantities are density, force, pressure, area, velocity, acceleration, specific volume, energy, entropy, and power. Then any derived thermal-fluid quantity Q in the SI system can be expressed in terms of the thermal-fluid base quantities by an expression of the form

$$Q = m^{\alpha} l^{\beta} t^{\gamma} T^{\delta} \sum_{k=1}^{K} a_k \tag{10.1}$$

where the exponents α, β, γ, and δ are rational numbers that have no units as are the factors a_k. Thus, the SI derived unit of Q becomes $\text{kg}^{\alpha} \cdot \text{m}^{\beta} \cdot \text{sec}^{\gamma} \cdot \text{K}^{\delta}$.

The choice of unit system also determines the *dimensions* of the base quantities. The dimensions are the attributes that need to be measured in order to obtain a numerical value for a certain quantity. For the four base quantities of thermal-fluid systems in the SI unit system (mass, length, time, and thermodynamic temperature), these dimensions are denoted by the symbols M, L, T, and Θ, respectively. Then the *dimension* of a derived quantity Q, denoted by the symbol $[Q]$, is defined to be

$$[Q] = M^{\alpha} L^{\beta} T^{\gamma} \Theta^{\delta} \tag{10.2}$$

where the exponents α, β, γ, and δ are called "dimensional exponents." If the dimensional exponents are all identically zero, the quantity Q is *dimensionless* and can be expressed as a pure number. This is, in fact, the fundamental concept in dimensional analysis. {Note that there is a distinction between the *dimensions* of quantities and the *units* of quantities. The concept of dimension is more fundamental because there are many different unit systems that will be compatible with a given set of dimensions. For example, the now outmoded, but still widely used (in the United States) "Engineering Unit System" with base units lbm, ft, sec, and Rankine is a system that also has the same base dimensions M, L, T, and Θ as the SI unit system. Alternatively, we could choose some other set of dimensions to describe a given physical parameter. For example, the pressure could be described in terms of a set of dimensions consisting of F, L, T, and Θ (force, length, time and thermodynamic temperature, respectively), but of course, this would require a unit system other than SI. None of these alternatives will be considered here because the SI unit system has now been accepted internationally (including in the United States).}

Then for the example at hand, the pressure in the SI system of units is a derived quantity. It is defined as the force divided by the area over which it is applied. {Following the recommendation of the National Institute of Standards and Technology (NIST), this particular choice of wording is preferred to the wording "Pressure is force per unit area." in order to avoid inferring the selection of a particular unit system.} Force itself is also a derived quantity determined by the product of mass and acceleration with acceleration also a derived quantity defined in terms of the second derivative of the position with respect to time.

Then the dimensions of pressure are given by

$$[P]=\left[\frac{F}{A}\right]=\frac{M\left(\frac{L}{T^2}\right)}{L^2}=\frac{M}{LT^2}=ML^{-1}T^{-2} \tag{10.3}$$

Then in this example, the dimensional exponents are $\alpha = 1$, $\beta = -1$, $\gamma = -2$, and $\delta = 0$.The units of pressure in the SI system are then kg · m^{-1} · sec^{-2}. (Note that in the SI system the units of force, kg · m · sec^{-2} occur frequently and are given the special name Newton, denoted by the symbol N. Then the units of pressure become N · m^{-2}, but this, too, appears so frequently it is given the special name Pascal, denoted by the symbol Pa.)

The second step in the measurement process is to determine the number assigned to a particular quantity in the chosen unit system. This is done by noting that each of the base quantities in a particular unit system has a particular definition. For example, the kilogram is defined as the mass of the international prototype of the kilogram. This is a particular mass, m_0, housed at an internationally agreed upon location under specified conditions. Then in principle, the number associated with the mass dimension of a quantity is determined by comparing this mass dimension against the mass of the international prototype of the kilogram or a surrogate. Then this comparison process would yield a result of the form

$$a_1=\left(\frac{m_Q}{m_0}\right)^{\alpha} \tag{10.4}$$

where m_Q is the mass dimension of the quantity, the ratio m_Q/m_0 is a number that represents the number of *units* (hence the origin of the term) of the base quantity m_0 associated with the mass dimension of Q, and α is the appropriate dimensional exponent. Similar operations could, in principle, be carried out for the other dimensions of the quantity Q with results of the form

$$a_2=\left(\frac{l_Q}{l_0}\right)^{\beta}, \quad a_3=\left(\frac{t_Q}{t_0}\right)^{\gamma}, \quad a_4=\left(\frac{\Theta_Q}{\Theta_0}\right)^{\delta} \tag{10.5}$$

Then the magnitude of the number associated with the quantity Q in the chosen unit system is given by

$$|Q| = a_1 a_2 a_3 a_4 \tag{10.6}$$

Clearly, in most physical situations this procedure would not be practical, so measurements are carried out that determine the magnitude of certain convenient derived quantities by using instruments that have been calibrated against agreed standards maintained by designated agencies (NIST in the United States). The final result is of the same form as that given in equation (10.6), however.

To further complicate matters, some derived quantities cannot be measured directly. In such cases, it is necessary for us to determine the magnitude of the derived quantity by utilizing physical laws (that frequently take the form of constitutive relations) that relate the unmeasurable

quantity to those quantities that can be measured. For example, the stored kinetic energy of an object cannot be measured directly so we must use the constitutive relation derived from the first law of thermodynamics that gives the kinetic energy of the object in terms of the measurable quantities mass and velocity. In order for the result of the mathematical operation of multiplying the mass of the object by the square of the velocity and dividing by two to be physically meaningful, the mass and the velocity must be measured in the same system of units. Thus, in a given physical situation, all the measurements must be carried out in the same system of units, and all the terms appearing in the relevant mathematical relations must be in the same system of units for the results of the mathematical operations to be meaningful.

10.3 The Value of Dimensional Analysis in Describing Physical Situations

As mentioned above, dimensional analysis is a process that examines the dimensions of the physical parameters that are used to characterize a given physical situation in order to gain insight into the details of that characterization. As will soon become apparent, this analysis is both powerful and weak at the same time. Dimensional analysis is based upon the fact that a given set of physical parameters can appear in the description of a given physical situation only in a certain dimensionally consistent form, and the process of dimensional analysis provides a method for finding that form. In general, however, dimensional analysis will not provide all the information that we may seek about a particular physical situation, but it can provide insight into the most productive manner in which to treat a given situation.

For example, most thermal fluid systems are far too complicated to be described simply in terms of a solution of the fundamental equations that constitute the model of the situation. Under these circumstances, it is often necessary to resort to experimental measurements made on an "appropriately" scaled model of the system and to then scale up the results of those measurements in the "proper manner" to the full size system. Dimensional analysis offers insights as to the "appropriate" way in which to design the scale model as well as the "proper manner" for scaling the experimental results up from the model to the full scale prototype.

As one of its greatest benefits, dimensional analysis reduces the number of parameters necessary to characterize a system. This can simplify the analysis of the physical situation at hand considerably. Furthermore, if an experiment is to be conducted, dimensional analysis can significantly reduce both the number of parameters to be measured and the number of measurements necessary to fully characterize a system. We will see that this reduction in the number of parameters depends upon the number of dimensions involved.

The results of dimensional analysis also allow the compact (and elegant) presentation of experimental data. Data presented in the proper non-dimensional form usually allow a more general interpretation of the data. We have already seen an example of this in the Moody Diagram in Chapter 9. The axes of the Moody Diagram are the dimensionless friction factor, f, and the Reynolds number, Re, which is also dimensionless. If the pipe friction losses were presented in a dimensional format, a myriad of graphs would be required for different size pipes and different fluids instead of the single graphical presentation developed by Moody.

10.4 An Approach to Dimensional Analysis

We shall use two basic approaches to dimensional analysis. In the first approach, we write all the relevant governing equations and then non-dimensionalize them. In the second approach,

we list those parameters we believe important to the description of a physical situation and then we use the dimensions of those parameters to aid in developing a relationship among them. We have already made use of the first approach in Chapter 6 in our analysis of transient conduction heat transfer and in Chapter 9 for a simple flow. In Chapter 6, the solutions of the time-dependent conduction heat equation and Newton's law of cooling were cast in a non-dimensional form, resulting in two governing dimensionless groups, the Biot number and the Fourier number. In Chapter 9, the Navier-Stokes equations were cast in a non-dimensional form in which a dimensionless number, the Reynolds number, was the critical parameter that insured dimensional similarity. In the second approach, which we have not yet used, a mathematical formalism known as the Buckingham Π-theorem will be used to establish a relationship among the dimensionless parameters that can be formed from the physical parameters of a given situation.

In what follows, we present dimensional analysis by considering several examples. The first will be a fairly intuitive discussion of the simple pendulum. Using only one or two experimental observations and dimensional analysis, we will find the expression for the period of the pendulum. Following this we find the equation of motion for the pendulum. We non-dimensionalize that equation and solve directly for the period of the pendulum, getting the same result as before. We then introduce a more formal procedure for non-dimensionalizing a situation and apply it to the same pendulum. In the second example, we then apply the Buckingham Π-theorem to a simple spring-piston apparatus to infer the functional form of the solution. This is followed with an explicit solution of that situation to show that the solution does indeed fit the form required by dimensional analysis. The third example addresses the analysis of the drag on a baseball followed by analyses of the drag on ships, the heat transfer rate from a cylinder in a fluid flow, and the dynamic behavior of an electrical circuit. The chapter closes with a short discussion of the dimensionless groups commonly found in thermal-fluid systems.

10.5 The Pendulum

A particularly important technological advance for the development of accurate clocks in the sixteenth and seventeenth centuries has been described in an apocryphal story associated with Galileo Galilei. In 1581 he observed the swaying of the long chandeliers in the Pisa cathedral shown in Figure 10.1. As he watched amplitude of the swaying chandeliers decrease, he measured the period of oscillation using his pulse as his timepiece. He observed that the period of the swing of the chandelier was independent of the amplitude of the swing. If the length of the chandelier is 16 m, Galileo would have observed a period of oscillation of 12 heartbeats or 8 seconds (assuming that Galileo had a normal heart rate of 72 beats per minute).

In the analysis of this physical situation, we are interested in developing a relation for the period of oscillation of the pendulum in terms of the physical parameters necessary to characterize it. In one approach, which we will discuss further in a subsequent section, we can write the equations of motion and solve for the period. In this simple physical situation, this can be done quite easily. For more complicated systems, this can be extremely difficult.

Another approach is to list all the physical parameters necessary to describe the situation and try to arrange them in a dimensionally consistent functional form. In this simple example, we will do this on a rather informal basis in order to motivate the more formal procedures that will follow.

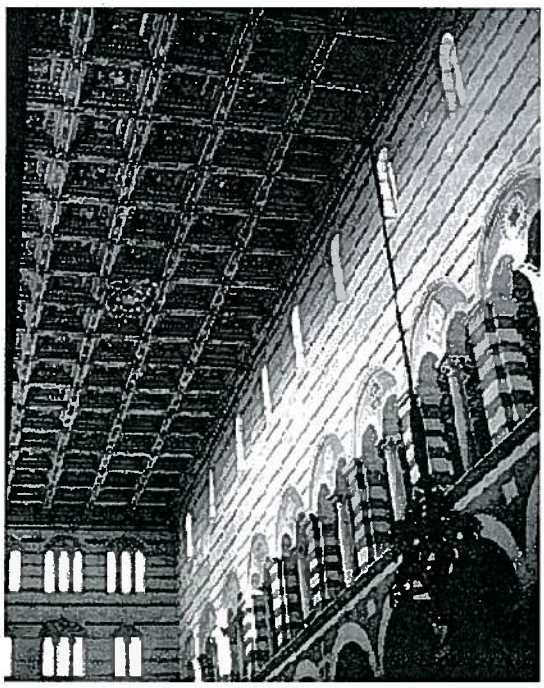

Figure 10.1 An interior view of the Pisa Cathedral showing one of the chandeliers observed by Galileo

10.5.1 Informal Non-Dimensionalization

A simple model of the Pisa Cathedral chandelier, shown in Figure 10.2, consists of the chandelier of mass m on the end of a massless cable of length l. Since the restoring force on the pendulum is due to gravity, the acceleration due to gravity, g, is relevant to determining the period of oscillation, τ. Since the angle the cable makes with the vertical is θ, we shall define the maximum angle the pendulum makes with the vertical as θ_{max}. Following Galileo's lead, we shall presume that the period of oscillation does not depend on the particular angle the pendulum makes at a particular time but only on the maximum amplitude of the oscillation.

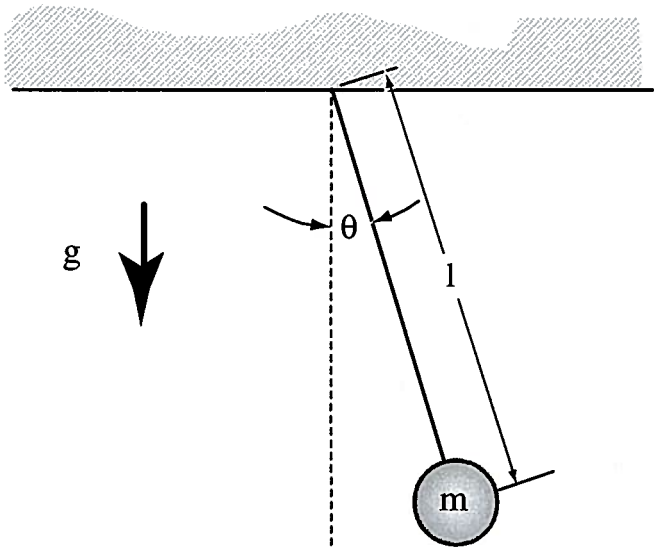

Figure 10.2 A Simple Pendulum

We now have a candidate set of parameters that are relevant to determining the period of oscillation, τ, of the pendulum namely m, l, θ_{max}, and g. More formally,

$$\tau = f\left(m, l, \theta_{max}, g\right) \tag{10.7}$$

where f is the appropriate function relating these parameters. This relation can also be expressed in dimensionless form as

$$\bar{\tau} = \phi\left(\bar{m}, \bar{l}, \theta_{max}, \bar{g}\right) \tag{10.8}$$

where the bar above a parameter indicates the dimensionless form of that parameter and ϕ is the appropriate function relating the dimensionless parameters. Note that θ_{max} (in radians) is already dimensionless since angles are defined as the ratio of the circumferential length subtended by the angle on a circle centered on the vertex of the angle divided by the radius of that circle.

It remains for us to non-dimensionalize each of the parameters. This can be done by looking at all the parameters associated with the situation and combining them to form dimensionless groups. The dimensions of the period of oscillation τ are those of time. The only other parameter that has the dimension of time in it is the gravitational acceleration, g, with dimensions of length divided by time squared. Unfortunately, we need a parameter that has only the dimension of time, not length over time squared. With a moment's reflection, it becomes apparent that if the length and the gravitational acceleration are combined appropriately, namely as the square root of the ratio of l to g, a quantity with units of time can be generated, so that the dimensionless group $\bar{\tau}$ is

$$\bar{\tau} = \frac{\tau}{\sqrt{\frac{l}{g}}} = \tau\sqrt{\frac{g}{l}} \tag{10.9}$$

The dimensionless mass term in equation (10.8) is a problem. All the other parameters in this equation, τ, l, θ_{max}, g do not carry the dimension of mass, and, hence, it is impossible to non-dimensionalize the mass with the chosen set of parameters. We must then reach one of two conclusions: either the mass at the end of the pendulum has no effect on the period of oscillation (and we included it erroneously in the list of relevant parameters) or we have missed other relevant parameters that have the dimension of mass. In this analysis, we will assume that we have included all the important parameters and that the mass was erroneously listed as being important. Thus, there is no $\bar{m}$.

The length l can be non-dimensionalized only by using τ and g. Paralleling the procedure for the non-dimensionalization of τ, the dimensionless length becomes

$$\bar{l} = \frac{l}{g\tau^2} = \left(\frac{1}{\tau}\sqrt{\frac{l}{g}}\right)^2 = \bar{\tau}^{(-2)} \tag{10.10}$$

The dimensionless length is then directly related to the dimensionless period. Similarly, the dimensionless gravitational acceleration is

$$\bar{g} = \frac{g\tau^2}{l} = \left(\tau\sqrt{\frac{g}{l}}\right)^2 = \bar{\tau}^2 \tag{10.11}$$

Then the dimensionless gravity can be explicitly expressed in terms of the dimensionless period. Finally the angular amplitude, θ_{max}, is already dimensionless and hence needs no further attention.

Incorporating our results into equation (10.8), we get

$$\bar{\tau} = \phi\left(\bar{m}, \bar{l}, \theta_{max}, \bar{g}\right) = \phi\left(\bar{l}, \theta_{max}, \bar{g}\right) = \phi\left(\bar{\tau}^{(-2)}, \theta_{max}, \bar{\tau}^2\right) \tag{10.12}$$

Our result shows that the dimensionless period is a function of the angular amplitude of the swing of the pendulum and the dimensionless period. Presumably, some algebra should allow us to bring all the terms containing $\bar{\tau}$ to the left-hand side of the equation allowing us to express the relation as

$$\bar{\tau} = G(\theta_{max}) \tag{10.13}$$

where G is the function that relates $\bar{\tau}$ to θ_{max}. Notice what has happened. Our non-dimensionalization has resulted in an enormous simplification of the problem. Instead of five different parameters (τ, m, l, θ_{max} and g) the description now depends only on two ($\bar{\tau}$ and θ_{max}). If we expand the function G in a Maclaurin series we conclude that the functional relation for the period is

$$\tau\sqrt{\frac{g}{l}} = G(\theta_{max}) = A + B\,\theta_{max} + C\,\theta_{max}{}^2 + \ldots \tag{10.14}$$

where A, B, and C are coefficients in the Maclaurin series. This can be rewritten as

$$\tau = \sqrt{\frac{l}{g}}\left(A + B\,\theta_{max} + C\,\theta_{max}{}^2 + \ldots\right)$$

This is as far as we can go with dimensional analysis. We are now forced to look elsewhere to determine the constants A, B, C etc. Here we have Galileo's experimental observation, namely that the period is independent of the angular amplitude. This leads us to conclude that the coefficients that multiply a power of θ_{max} must all be zero ($B = 0$, $C = 0$, etc.). If we assume that the chandeliers have a length of $l = 16$ m and the period Galileo measured was $\tau = 8$ sec, the constant A is determined to be 6.28. We conclude that the relation for the period of oscillation is

$$\tau = 6.28\sqrt{\frac{l}{g}} \tag{10.15}$$

which is the accepted relation for a small amplitude oscillation of a simple pendulum.

10.5.2 Non-Dimensionalization of the Equations of Motion

A more formal approach to the dimensional analysis of this physical situation is to consider the equations of motion that govern the situation and to non-dimensionalize those equations. The free body diagram for the simple pendulum is shown in Figure 10.3. Gravity acts on the mass in the downward direction with force mg. The angle the cable makes with the vertical is θ. The unit vectors in the radial and angular directions are $\hat{r}$ and $\hat{q}$, respectively. The component of the gravity force in the radial direction is countered by the tension in the cable **T**. The component of the gravity force in the angular direction F_q is not countered by any forces in the wire and has a value of $F_q = -mg\sin\theta$. The acceleration of the mass in the angular direction is

$$a_q = \frac{d^2 s}{dt^2} = \frac{d^2(l\theta)}{dt^2} = l\frac{d^2\theta}{dt^2}$$

Hence, Newton's second law is

$$F_q = ml\frac{d^2\theta}{dt^2} = -mg\sin\theta \tag{10.16}$$

This is a second order ordinary differential equation. To solve this equation fully, we require two initial (or boundary) conditions. In this case, we will assume that at time $t = 0$ the pendulum is released from a position θ_{max} with angular velocity $\dot{\theta}_{max}$. At this point, all we have

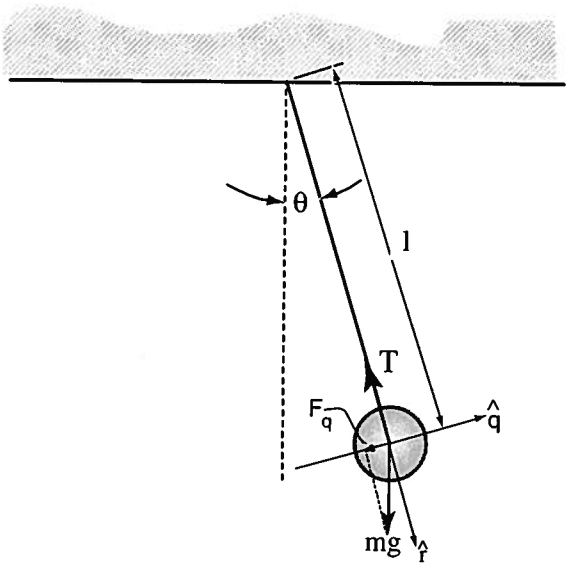

Figure 10.3 A Free Body Diagram for a Simple Pendulum

to do is integrate the equation and apply the boundary conditions for a solution. Dividing equation (10.16) through by m, we get

$$\frac{d^2\theta}{dt^2} = -\frac{g}{l}\sin\theta \tag{10.17}$$

Note that the coefficient of the sine function has the dimension of 1/time^2. The angle θ is dimensionless. [As an aside, the arguments of functions like the sine, the cosine, the tangent and the exponential must be dimensionless. This can be seen most easily by expressing these functions in terms of power series. For example, the exponential function is given by the series

$$e^x = 1 + \frac{x}{1!} + \frac{x^2}{2!} + \frac{x^3}{3!} + \ldots$$

Then if we were to suppose, for instance, that the argument x of the exponential were to have the dimension of length L, the first term would have no dimension since it is a pure number, the second term would have the dimension L, the third dimension L^2 and so on. Since adding objects of different dimension has no meaning, we conclude that x must be dimensionless for the exponential function to have meaning. For example, the argument x could be given by $x = d/D$ where both d and D have the dimension of length.]

Then since g/l has the dimensions of time squared, equation (10.17) can be non-dimensionalized by dividing the equation through by g/l and incorporating it into a dimensionless time t^* where t^* is defined as

$$t^* \equiv t\sqrt{\frac{g}{l}} \tag{10.18}$$

Equation (10.17) then becomes

$$\frac{d^2\theta}{dt^{*2}} = -\sin\theta \tag{10.19}$$

All the parameters in the equation have been non-dimensionalized since both t^* and θ are dimensionless. What remains now is to non-dimensionalize the boundary conditions: θ_{max} is

already dimensionless; and, $\dot{\theta}_{max}$ can be non-dimensionalized by multiplying by $\sqrt{l/g}$ or

$$\dot{\theta}_{max}{}^{*} = \dot{\theta}_{max}\sqrt{\frac{l}{g}} \tag{10.20}$$

The mathematical description of the physical situation has been simplified by non-dimensionalizing the equation of motion and the initial conditions. The original dimensional form of the governing equation, equation (10.17), requires knowledge of four parameters t, g/l, θ_{max}, and $\dot{\theta}_{max}$ to determine θ. The solution has the form

$$\theta = f\left(\frac{g}{l}, t, \theta_{max}, \dot{\theta}_{max}\right) \tag{10.21}$$

where f is the function we would get if we integrated equation (10.17). On the other hand, the dimensionless equations [equation (10.19) and the non-dimensional initial conditions] depend on only three parameters $\left(t^{*}, \theta_{max}, \dot{\theta}_{max}\right)$ rather than the four required by the dimensional one [equation (10.17)]. The solution to equation (10.19) will be of the form

$$\theta = F\left(t^{*}, \theta_{max}, \dot{\theta}_{max}\right) \tag{10.22}$$

where F is the function we would get if we integrated equation (10.19). Once again, the reduction in the number of parameters is *the* major benefit of converting parameters into dimensionless form.

It remains to bring this equation-based analysis back to the result determined through the less formal approach we used earlier. In particular, we are interested in determining the small amplitude period for the pendulum. Making the small amplitude approximation by substituting θ for $\sin\theta$ in equation (10.19) and assuming that the pendulum is released from rest at the maximum angular displacement at time $t = 0$ $\left(\theta = \theta_{max}, \dot{\theta}_{max} = 0\right)$, the solution is

$$\theta = \theta_{max}\cos\left(t^{*}\right) = \theta_{max}\cos\left(t\sqrt{\frac{g}{l}}\right) \tag{10.23}$$

In the absence of friction, the angular displacement must have the value θ_{max} at the end of each period or whenever the argument of the cosine function in equation has the value $2n\pi$ where n is some positive integer indicating the number of periods that the pendulum has traversed. Then for one period when the value of time is τ, we have

$$2\pi = \tau\sqrt{\frac{g}{l}} \tag{10.24}$$

or

$$\tau = 2\pi\sqrt{\frac{l}{g}} \tag{10.25}$$

which is identical to the result that was obtained through a combination of dimensional analysis and experimental observation in section 10.5.1.

Perhaps a few comments are warranted here. In the initial treatment of the pendulum, we depended on our physical intuition and experience to compile a list of the appropriate physical parameters for the situation. By organizing the list into a set of dimensionless groups, we were able to reduce the number of parameters and hence simplify the analysis. Using fairly few

experimental observations, we were able to infer the functional form of the solution. The final result depends very much on the quality of our initial list. In some sense, the choice of our list in the former example is akin to writing the governing equations in the latter.

A proper parameter list is a list of all the physical parameters that appear in the complete set of equations that describe the physical system. It is not always apparent that a particular parameter should or should not be included in the list. For example, if the mass of the supporting cable was included in the above analysis, another dimensionless parameter, the ratio of cable mass to the mass of the pendulum bob, would have appeared in the arguments of the function G in equation (10.13) or

$$\bar{\tau} = G\left(\theta_{max}, \frac{m_{cable}}{m}\right) \tag{10.26}$$

At this juncture, we might well ask why does the non-dimensionalization of the list (or the equation) result in a reduction in the number of parameters? The answer lies in the measurement process. Recall from section 10.2 that a measurement is simply a comparison of the dimension of the parameter with the definition of that dimension. For example, stating that the bob of a pendulum has a mass of two kilograms is really stating that the ratio of the mass of the bob to the mass of the international prototype kilogram is a pure number, e.g., two. The period calculated by equation (10.26) should not depend on such an arbitrary definition as the international prototype mass. The non-dimensionalization of the mass in equation (10.26) removes the arbitrariness from the equation and replaces it with a reference mass that is within the physical system of interest; hence, there is a net reduction in the number of mass ratios from two ($\bar{m}_{cable} = m_{cable}/m_{prototype}$ and $\bar{m} = m/m_{prototype}$) to one (m_{cable}/m).

10.6 Dimensionless Groups and The Buckingham $\prod$-Theorem

With the aid of a simple example, the simple pendulum, we have seen how dimensional analysis can simplify the description of a physical situation. The essence of the process is the formation of dimensionless parameters from dimensional ones. In the example of Section 10.5, we formed these dimensionless parameters, or as they are more commonly known, dimensionless groups (denoted by the symbol Π), in an heuristic way. There is, however, a formal procedure for doing this. Consider first the case in which there are two quantities or physical parameters Q_1 and Q_2 that describe some physical situation. Let us now determine the circumstances under which we can form a dimensionless group Π from the product of Q_1 and some power a of Q_2. Then

$$[\Pi] = \left[Q_1 Q_2^{\,a}\right] = [Q_1]\left[Q_2^{\,a}\right] = 1 \tag{10.27}$$

where we have made use of the fact that Π is dimensionless. Then from equation (10.2), it follows that

$$[Q_1]\left[Q_2^{\,a}\right] = M^{\alpha_1} L^{\beta_1} T^{\gamma_1} \Theta^{\delta_1} \left(M^{\alpha_2} L^{\beta_2} T^{\gamma_2} \Theta^{\delta_2}\right)^a = M^{(\alpha_1 + a\alpha_2)} L^{(\beta_1 + a\beta_2)} T^{(\gamma_1 + a\gamma_2)} \Theta^{(\delta_1 + a\delta_2)} = 1 \tag{10.28}$$

The only way that equation (10.28) can be true is if the exponents of the terms M, L, T, and Θ vanish. Then

$$\begin{aligned} \alpha_1 + a\alpha_2 &= 0 \\ \beta_1 + a\beta_2 &= 0 \\ \gamma_1 + a\gamma_2 &= 0 \\ \delta_1 + a\delta_2 &= 0 \end{aligned} \tag{10.29}$$

and it follows that for this example, Π will be dimensionless if all of the dimensions of Q_2 are directly proportional to the dimensions of Q_1 and a is the constant of proportionality.

Now suppose that we have a more complex situation in which the number of parameters is the same as the number of dimensions which in the thermal-fluids case is four. Then for parameters we have Q_1, Q_2, Q_3, and Q_4 and we wish to know the circumstances under which we can form a dimensionless group Π. Then in the general case, we can write

$$\Pi = Q_1^{\,a} Q_2^{\,b} Q_3^{\,c} Q_4^{\,d} \tag{10.30}$$

where we have raised each of the parameters to some power so that we can apply Euler's theorem for homogeneous functions. Then if Π is dimensionless, we have

$$\begin{aligned} [\Pi] &= \left[Q_1^{\,a} Q_2^{\,b} Q_3^{\,c} Q_4^{\,d}\right] = \left[Q_1^{\,a}\right]\left[Q_2^{\,b}\right]\left[Q_3^{\,c}\right]\left[Q_4^{\,d}\right] = 1 \\ [\Pi] &= M^{(a\alpha_1 + b\alpha_2 + c\alpha_3 + d\alpha_4)} L^{(a\beta_1 + b\beta_2 + c\beta_3 + d\beta_4)} T^{(a\gamma_1 + b\gamma_2 + c\gamma_3 + d\gamma_4)} \Theta^{(a\delta_1 + b\delta_2 + c\delta_3 + d\delta_4)} = 1 \end{aligned} \tag{10.31}$$

Then in order for Π to be dimensionless, the exponents in equation (10.31) must vanish. Then it must be the case that

$$\begin{aligned} a\alpha_1 + b\alpha_2 + c\alpha_3 + d\alpha_4 &= 0 \\ a\beta_1 + b\beta_2 + c\beta_3 + d\beta_4 &= 0 \\ a\gamma_1 + b\gamma_2 + c\gamma_3 + d\gamma_4 &= 0 \\ a\delta_1 + b\delta_2 + c\delta_3 + d\delta_4 &= 0 \end{aligned} \tag{10.32}$$

According to Euler's theorem, in order for there to be a non-trivial solution for a, b, c, and d in the set of equations (10.32), the determinant of the coefficient matrix must be zero. That is, if

$$\begin{vmatrix} \alpha_1 & \alpha_2 & \alpha_3 & \alpha_4 \\ \beta_1 & \beta_2 & \beta_3 & \beta_4 \\ \gamma_1 & \gamma_2 & \gamma_3 & \gamma_4 \\ \delta_1 & \delta_2 & \delta_3 & \delta_4 \end{vmatrix} = 0 \tag{10.33}$$

there is a set of values of a, b, c, and d that will result in Π being dimensionless. However, if the determinant in equation (10.33) is non-zero, it is not possible to form a dimensionless group from Q_1, Q_2, Q_3, and Q_4, and they are said to be dimensionally linearly independent. The coefficients of the unknowns a, b, c, and d appearing in equation (10.32) are the dimensional exponents of the parameters that describe the physical situation at hand and form what is known as the dimensional matrix.

Now to generalize what we have shown above, suppose that we have a physical situation with n parameters of which $n - 1$ are independent. The dependent parameter is related to the independent parameters through a function g such that

dependent

$$Q_1 = g(Q_2, Q_3, \ldots, Q_n) \tag{10.34}$$

where Q_1 is the independent parameter, and $Q_2, \ldots, Q_n$ are the $n - 1$ independent parameters. Equation (10.34) can be expressed in the mathematically equivalent form

$$f(Q_1, Q_2, \ldots, Q_n) = 0 \tag{10.35}$$

where f is an unspecified function different from g. Now for a given unit system, m will be the number of base quantities. As noted previously, for thermal-fluid systems in the SI unit system, $m = 4$. Then the dimensional matrix will be $m \times n$ in size. The rank r of the dimensional matrix is the size of the largest square sub-matrix that has a non-zero determinant. Thus, there are r linearly independent parameters, Q_i. Usually, $r = m$, but there are cases for which $r < m$.

Edgar Buckingham (1867 – 1940), an expert in screw and propeller systems, showed in 1914 that given a relation of the form (10.35), the n parameters can be expressed in $n - r$ independent dimensionless groups, Π_i, that can be expressed in functional form by

$$F(\Pi_1, \Pi_2, \ldots, \Pi_{n-r}) = 0 \tag{10.36}$$

or

$$\Pi_1 = G(\Pi_2, \Pi_3, \ldots, \Pi_{n-r}) \tag{10.37}$$

This result is known as the Buckingham Pi Theorem which we have stated here without proof. Note that this theorem does not predict the functional form of F or G. This must be determined from other information about the physical situation. The $n - r$ dimensionless groups Π_i of equation (10.37) are independent, but an individual dimensionless group Π_i is not independent if it can be formed from a product or quotient of other dimensionless groups.

The Buckingham Pi Theorem forms the basis of dimensional analysis, and there are several different ways to apply it. Each has its own merit, but the following method has proven to be successful for most students:

1. List and count the n parameters required to describe the physical situation. If any important parameters are missing, dimensional analysis will fail.

2. List the dimensions of each variable according to M, L, T, and Θ.

3. Find the value of r. Initially guess r to be equal to the number of different dimensions present and then make sure the there are r parameters that do not form a Π-group. If this is unsuccessful, reduce r by one and look again.

4. Select r parameters which do not form a Π-group among themselves. These parameters are the repeating parameters that will appear in all the Π-groups.

5. Select one of the remaining parameters that is not one of the r repeating parameters and non-dimensionalize that parameter using the r repeating parameters. Repeat the procedure until all the remaining parameters are non-dimensionalized. There should now be $n - r$ Π-groups.

6. Check to see that all proposed Π-groups are dimensionless and write the functional relationship among them in dimensionless form.

As an example of the application of this procedure, let us revisit the pendulum example of Section 10.5 to determine the period in dimensionless form.

Step 1: *List and count the n parameters required to describe the physical situation. If any important parameters are missing, dimensional analysis will fail.*

For the pendulum, the relevant parameters are the period τ, the angular amplitude θ_{max}, the length l, and the gravitational acceleration g. There are four parameters so that $n = 4$. Notice that we have not included the mass in this analysis because our "experience" thus far in this chapter has shown us that this is not an important parameter.

Step 2: *List the dimensions of each variable according to M, L, T, and Θ.*

The dimension of the period, τ, is time or symbolically,

$$[\tau] = T$$

For the angular amplitude, θ_{max}, we have

$$[\theta_{max}] = 1$$

For the length of the pendulum, l, we have

$$[l] = L$$

For the gravity, g, we have

$$[g] = \frac{L}{T^2}$$

Step 3: *Find the value of r. Initially guess r to be equal to the number of different dimensions present and then make sure the there are r parameters that do not form a Π-group. If this is unsuccessful, reduce r by one and look again.*

There are two dimensions (L and T) present in the four parameters listed in Step 2. We now initially guess that $r = 2$. We now look for two parameters that do not in themselves form a Π-group. Let us assume l and g to be those parameters. As stated previously, the general form of a Π-group is a product of powers of parameters that is dimensionless. We now need to show that no products of non-zero powers of l and g can be dimensionless. For this to be true, it must be the case that

$$\left[l^a g^b\right] = L^a \left(\frac{L}{T^2}\right)^b = L^{a+b} T^{-2b} = 1$$

Then since the exponents of the dimensions must vanish, we must have

$$a + b = 0$$
$$-2b = 0$$

and it follows that $a = 0$ and $b = 0$. Thus, we have found two parameters, l and g, that in themselves do not form a dimensionless group; hence $r = 2$.

Step 4: *Select r parameters which do not form a Π-group among themselves. These parameters are the repeating parameters that will appear in all the Π-groups.*

We have already shown in Step 3 that l and g will suffice.

Step 5: *Select one of the remaining parameters that is not one of the r repeating parameters and non-dimensionalize that parameter using the r repeating parameters. Repeat the procedure until all the remaining parameters are non-dimensionalized. There should now be n − r Π-groups.*

Of the original set of n parameters that describe the pendulum, only τ and θ_{max} remain. Then there must be $n - r$ or $4 - 2 = 2$ dimensionless groups. Let us non-dimensionalize τ using the repeating parameters l and g. This will result in the first dimensionless Π-group, Π_1. Symbolically, we must determine the exponents c and d that satisfy the relation

$$[\Pi_1] = \left[\tau l^c g^d\right] = [\tau][l]^c [g]^d = T(L)^c \left(\frac{L}{T^2}\right)^d = L^{c+d} T^{1-2d} = 1$$

Then

$$c + d = 0$$
$$1 - 2d = 0$$

and it follows that $d = ½$ and $c = -½$. Then

$$\Pi_1 = \frac{\tau}{\sqrt{\frac{l}{g}}} = \tau\sqrt{\frac{g}{l}}$$

which is the dimensionless group we determined earlier by heuristic means, equation (10.9). Since the other parameter, θ_{max}, is already dimensionless, it becomes the second dimensionless group.

$$\Pi_2 = \theta_{max}$$

Thus, we have determined the two dimensionless groups relevant to the physical situation of the simple pendulum.

Step 6: *Check to see that all proposed Π-groups are dimensionless and write the functional relationship among them in dimensionless form.*

Π_2 is clearly dimensionless. The dimension of Π_1 is given by

$$[\Pi_1] = \left[\tau\sqrt{\frac{g}{l}}\right] = [\tau]\left[\sqrt{\frac{g}{l}}\right] = T\left(\frac{L}{T^2 L}\right)^{\frac{1}{2}} = \frac{T}{T} = 1$$

Thus Π_1 is also dimensionless.

According to the Buckingham Pi Theorem, there exists a function F such that

$$F(\Pi_1, \Pi_2) = 0$$

or alternatively,

$$\Pi_1 = G(\Pi_2)$$

Then,

$$\tau\sqrt{\frac{g}{l}} = G(\theta_{max})$$

which is precisely the result obtained earlier, equation (10.13).

Note that we have arrived at the same dimensionless equation asserted in our earlier heuristic discussion. This is as far as dimensional analysis can take us. From here, experimental data, models, and theory must be used to gain further insight into the physical situation. For example, in the earlier discussion, we used "Galileo's observations" to determine the functional form for the period of the pendulum, and those observations could be used here as well.

10.7 A Spring-Piston System

We now examine in detail a thermal-fluid system that involves three dimensions, M, L, and T. Let us consider the spring-piston system shown in Figure 10.4 in which an ideal gas, whose ratio of specific heats is γ, is contained in an adiabatic piston-cylinder apparatus. In the initial state, the spring, whose spring constant is k, is in its unstressed state (zero force position) and the piston with mass M_p and area A_p is supported only by the gas at pressure P_i. The gas has an initial volume V_i. If the frictionless piston is displaced from its equilibrium position and

released, the piston will oscillate at a resonant frequency, f_{res}.

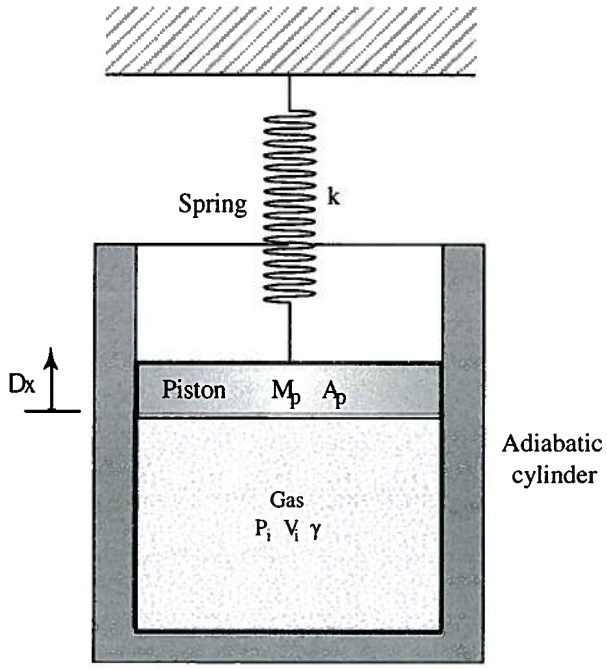

Figure 10.4 A Spring-Piston Apparatus

We are interested in using dimensional analysis to help relate the resonant frequency to the other physical parameters of the system. The six-step procedure described above enables us to achieve this end, and we now apply each step in succession.

Step 1: *List and count the n parameters required to describe the physical situation. If any important parameters are missing, dimensional analysis will fail.*

The important parameters are the ratio of specific heats γ, the piston mass M_p, the piston area A_p, the initial gas pressure P_i, the initial gas volume V_i, and the resonant frequency f_{res}. There are seven parameters so that $n = 7$.

Step 2: *List the dimensions of each variable according to M, L, T, and Θ.*

The dimensions of the seven parameters are

$$[\gamma]=1,\ \left[M_p\right]=M,\ \left[A_p\right]=L^2,\ [P_i]=\left[\frac{F}{A}\right]=\frac{M}{LT^2},\ [V_i]=L^3,\ [k]=\left[\frac{F}{L}\right]=\frac{M}{T^2},\ [f_{res}]=T^{-1}$$

Step 3: *Find the value of r. Initially guess r to be equal to the number of different dimensions present and then make sure that there are r parameters that do not form a Π-group. If this is unsuccessful, reduce r by one and look again.*

In the list above there are three dimensions present, namely M, L, and T, so as a first guess, we assume that $r = 3$. We now must find three parameters that do not in themselves form a Π–group. Clearly, γ is not a candidate since it is already dimensionless and hence forms a Π–group all by itself. Suppose we choose the piston mass M_p, the spring constant k, and the area of the piston A_p. We now must check to see if they form a Π–group. If this were the case,

$$\left[M_p{}^a k^b A_p{}^c\right] = M^a \left(\frac{M}{T^2}\right)^b \left(L^2\right)^c = M^{a+b} L^{2c} T^{-2b} = 1$$

and

$$a+b=0$$
$$2c=0$$
$$-2b=0$$

Then we would have $a = 0$, $b = 0$, and $c = 0$, which would mean that the three chosen parameters are dimensionally independent. Thus we have found the three repeating parameters.

Step 4: *Select r parameters which do not form a Π-group among themselves. These parameters are the repeating parameters that will appear in all the Π-groups.*

The parameters M_p, k, and A_p have been shown to be dimensionally independent, and thus we can use them to non-dimensionalize the remaining four parameters. Note that if it is desired to compare one specific parameter against another in a dimensionless manner, these parameters should not be members of the set of repeating parameters, but rather they should be members of the set of remaining parameters of Step 5. In this manner, the Π-groups that are generated will have each of these parameters of interest appear in only one dimensionless group.

Step 5: *Select one of the remaining parameters that is not one of the r repeating parameters and non-dimensionalize that parameter using the r repeating parameters. Repeat the procedure until all the remaining parameters are non-dimensionalized. There should now be n − r Π-groups.*

In the present case, there are four remaining parameters: f_{res}, γ, P_i, and V_i. We now non-dimensionalize each one of them in turn.

$$\left[\Pi_1\right] = \left[f_{res} M_p{}^d k^e A_p{}^f\right] = \left[f_{res}\right]\left[M_p{}^d\right]\left[k^e\right]\left[A_p{}^f\right] = 1$$

$$\left[\Pi_1\right] = T^{-1} M^d \left(\frac{M}{T^2}\right)^e L^{2f} = M^{d+e} L^{2f} T^{-1-2e} = 1$$

Then

$$d+e=0$$
$$2f=0$$
$$-2e-1=0$$

The solution of this system of equations is $d = -½$, $e = ½$, and f = 0. Then the first dimensionless group is

$$\Pi_1 = f_{res}\sqrt{\frac{M_p}{k}}$$

The second dimensionless group is trivial since γ is already dimensionless.

$$\Pi_2 = \gamma$$

The third dimensionless group is obtained by non-dimensionalizing P_i. Then

$$\left[\Pi_1\right] = \left[P_i M_p{}^g k^h A_p{}^i\right] = \left[P_i\right]\left[M_p{}^g\right]\left[k^h\right]\left[A_p{}^i\right] = 1$$

$$\left[\Pi_1\right] = \left(\frac{M}{LT^2}\right) M^g \left(\frac{M}{T^2}\right)^h L^{2i} = M^{1+g+h} L^{2i} T^{-2-2h} = 1$$

Then

$$1+g+h=0$$
$$-1+2i=0$$
$$-2-2h=0$$

The solution of this system of equations is $g = 0$, $h = -1$, and $i = ½$. Then the third dimensionless group is

$$\Pi_3 = \frac{P_i\sqrt{A_p}}{k}$$

The fourth dimensionless group can be determined by non-dimensionalizing V_i. Then

$$[\Pi_1] = \left[V_i M_p{}^p k^q A_p{}^s\right] = [V_i]\left[M_p{}^p\right]\left[k^q\right]\left[A_p{}^s\right] = 1$$

$$[\Pi_1] = L^3 M^p \left(\frac{M}{T^2}\right)^q L^{2s} = M^{p+q} L^{3+2s} T^{-2q} = 1$$

Then

$$p+q=0$$
$$3+2s=0$$
$$-2q=0$$

The solution of this system of equations is $p = 0$, $q = 0$, and $s = -3/2$. Then the fourth dimensionless group is

$$\Pi_4 = \frac{V_i}{A_p^{\frac{3}{2}}}$$

Thus, we now have four dimensionless groups. We started with seven parameters ($n = 7$) and found that we had three dimensions in that set of parameters so that $r = 3$. We then reduced those seven parameters to four dimensionless groups ($7 - 3 = 4$).

Step 6: *Check to see that all proposed Π-groups are dimensionless and write the functional relationship among them in dimensionless form.*

Each of the Π–groups has been checked and is indeed dimensionless. According to the Buckingham Pi Theorem, there exists a function G such that

$$\Pi_1 = G(\Pi_2, \Pi_3, \Pi_4)$$

or more explicitly

$$f_{res}\sqrt{\frac{M_p}{k}} = G\left(\gamma, \frac{P_i\sqrt{A_p}}{k}, \frac{V_i}{A_p^{\frac{3}{2}}}\right)$$

We now have an expression for the form of the expected relationship amongst the relevant parameters. Realize that the function G is the same regardless of the changes in the physical parameters of the system. For example, doubling the volume of the piston-cylinder apparatus does not change the form of the function G. In addition, if the apparatus is changed in a manner such that the dimensionless groups Π_2, Π_3, and Π_4 remain unchanged, the dimensionless group Π_1 would also remain unchanged since the function G is unaffected by these changes in the physical parameters. Under these conditions, if we denote the physical parameters of the altered apparatus by a prime (′), the resonant frequency of the altered apparatus would be given by

$$\Pi_1' = \Pi_1$$

$$f_{res}' = f_{res}\sqrt{\frac{M_p}{k}}\sqrt{\frac{k'}{M_p'}}$$

Let us explore the physics of this spring-piston apparatus in further detail. We now would like to show that the detailed description of this system does indeed result in a relationship of the type given above. We can most easily demonstrate this by determining the form of the function G shown above. We consider the case of small-amplitude oscillations of the piston. The net force F acting on the piston is the sum of the body force due to gravity, the force due to the pressure of the gas acting over the piston face, and the force exerted by the spring. Then if we take forces acting in the upward direction to be positive as indicated on Figure 10.4, we have

$$F = -M_p g + PA_p - k\Delta x$$

where g is the gravitational constant, P is the pressure of the gas in the cylinder and Δx is the displacement of the piston from the zero force position of the spring as shown on Figure 10.4. Since the velocity of the piston is slow relative to the speed of sound in the gas, we can model the process in the gas as quasi-static with a pressure that is uniform, but changing with time. If the dissipative processes in the gas are negligible because the amplitude of the oscillations is small, we can model the process in the gas as being reversible as well as adiabatic. Then by the second law, the entropy of the gas is constant. If we model the gas as an ideal gas, the isentropic compression process in the gas obeys the relation

$$PV^\gamma = P_i V_i^\gamma$$

where V is the volume of the gas in the cylinder. This volume V is related to the displacement of the piston Δx by

$$V = V_i + A_p \Delta x$$

Combining these expressions results in an expression for the pressure of the gas for any position of the piston.

$$P = \frac{P_i V_i^\gamma}{\left(V_i + A_p \Delta x\right)^\gamma} = P_i \frac{1}{\left(1 + \frac{A_p \Delta x}{V_i}\right)^\gamma}$$

If we use the binomial expansion

$$(1+x)^\gamma = 1 - nx + \frac{n(n+1)}{2!}x^2 - \ldots$$

for the term in the denominator, we get an approximate expression for the pressure in the gas for small displacements Δx.

$$P \approx P_i\left(1 - \gamma\frac{A_p \Delta x}{V_i}\right)$$

Then the net force on the piston becomes

$$F = -M_p g + P_i A_p\left(1 - \gamma\frac{A_p \Delta x}{V_i}\right) - k\Delta x = -M_p g + P_i A_p - \left[\gamma P_i\left(\frac{A_p^2}{V_i}\right) + k\right]\Delta x$$

but the initial position of the piston is one for which the force in the spring is zero. Then in this position, the body force due to gravity is exactly balanced by the force due to the pressure of the gas acting on the face of the piston. Thus

$$M_p g = P_i A_p$$

and the net force on the piston is due to the inertia of the piston by Newton's second law of motion. Then

$$F = M_p \frac{d^2(\Delta x)}{dt^2} = -\left[\gamma P_i \left(\frac{A_p^{\,2}}{V_i}\right) + k\right]\Delta x$$

This is the equation of motion for a simple harmonic oscillator for which the bracketed term serves as an effective spring constant, k_{eff}. Then the resonant frequency of oscillation for the simple harmonic oscillator is

$$f_{res} = \frac{1}{2\pi}\sqrt{\frac{k_{eff}}{M_p}} = \frac{1}{2\pi}\sqrt{\frac{\gamma P_i \left(\frac{A_p^{\,2}}{V_i}\right) + k}{M_p}}$$

This solution can be rewritten in the dimensionless form

$$f_{res}\sqrt{\frac{M_p}{k}} = \frac{1}{2\pi}\sqrt{1 + \frac{\gamma\left(\frac{P_i\sqrt{A_p}}{k}\right)}{\frac{V_i}{A_p^{\frac{3}{2}}}}} = \frac{1}{2\pi}\sqrt{1 + \frac{\Pi_2\Pi_3}{\Pi_4}} = \Pi_1$$

Thus we have now determined the functional form of G. Note that the product of two dimensionless numbers is also dimensionless as is the quotient of two dimensionless numbers. Then we can define a new dimensionless number Π_5 such that

$$\Pi_5 = \frac{\Pi_2\Pi_3}{\Pi_4} = \frac{\gamma P_i A_p^{\,2}}{kV_i}$$

Then

$$\Pi_1 = \frac{1}{2\pi}(1+\Pi_5)^{\frac{1}{2}}$$

If we take the natural logarithm of this expression we get

$$\ln\Pi_1 = \ln\left(\frac{1}{2\pi}\right) + \frac{1}{2}\ln(1+\Pi_5)$$

Thus if were to plot this equation on a set of coordinates with ln Π_1 as the ordinate and ln $(1+\Pi_5)$ as the abscissa, we would have a straight line of slope ½ . This is a common application of dimensional analysis. The function G can often be determined by plotting the dependent dimensionless group, or some function of it such as its logarithm, against some combination of the independent dimensionless groups. The slope of such a plot gives the exponent of the combination and the intercept gives the constant. Of course, knowing which combination of independent dimensionless groups to use is not always obvious and is often a matter of trial and error. For many experimentalists, the manipulation of dimensionless groups in this manner takes on the nature of an art form. Clearly, there are some clues from the physics of the situation as to the way to conduct these manipulations of the data, and we shall say more about this shortly.

10.7 Drag on a Baseball

All baseball fans, to say nothing about batters, are familiar with the speed of a baseball as

it travels from the pitcher to the batter. The speeds of pitches as determined by radar guns are routinely posted during baseball games. Speeds are generally posted to the nearest mile per hour (Clearly, Major League Baseball has not embraced the SI units system.), with typical major league pitchers posting speeds in the range of 80 to 90 miles/hour (mph) while others with "good arms" reach 90 to 100 mph consistently. There are even extreme cases in which speeds as high as 104 mph are attained. These data prompt some questions, such as, "Is the speed over the entire trajectory of the baseball good to 1 mph?" or "How much slower is the baseball traveling when it passes the batter compared to the instant it leaves the pitcher's hand?"

One way we could answer these questions is to measure directly the velocity of the ball using a specialized radar gun, or, alternatively, we could use computational fluid dynamics codes to calculate the drag force on the baseball. Unfortunately, we do not have the resources to do this, but we can gain considerable insight to the situation through dimensional analysis.

We could make measurements in a manner that is more convenient by creating a situation that is dimensionally similar to the actual situation. Then these measurements can be scaled to the circumstances typical of a game. To carry out this approach, we decide to make some drag measurements on a baseball by towing it through water. A friend is willing to take us on her powered skiff so that we can make our measurements. We put weights inside a baseball to try to make it as neutrally buoyant as possible so that the ball tends to "float" underneath the water surface. A small hole is drilled into the baseball and a long line is glued into the hole. The line is connected, in turn, to a spring scale that can be read from the skiff. The tests are conducted by towing the baseball behind the skiff slightly to one side to avoid the propeller wash and to allow the reading of the drag force on the spring scale. The velocity of the skiff can be determined by measuring the time it takes to pass two landmarks that are separated by a known distance. The procedure is shown schematically in Fig. 10.5.

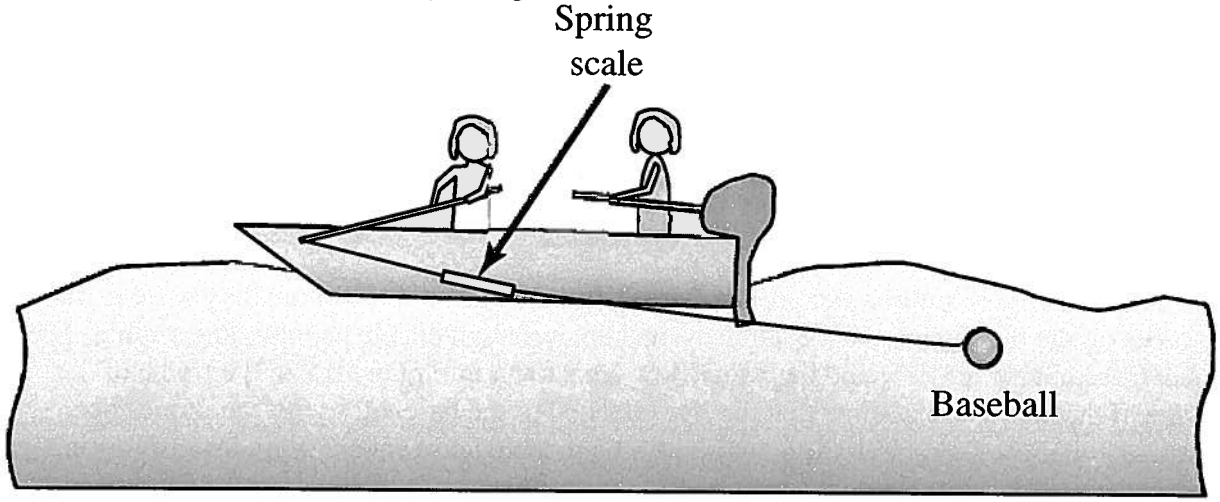

Figure 10.5 A Scheme for Measuring the Drag Force on a Baseball

The data collected for the drag force, F_d, as function of the towing velocity, $\mathcal{V}$, from such an exercise might look like the data listed in Table 10.1. The data are shown graphically in Figure 10.6.

Table 10.1 Drag Force for a Baseball Towed at Different Velocities in Water

Towing Velocity, ϑ (m/sec)	Drag Force, F_d (N)
1	0.8
2	3.4
3	7.7
5	21

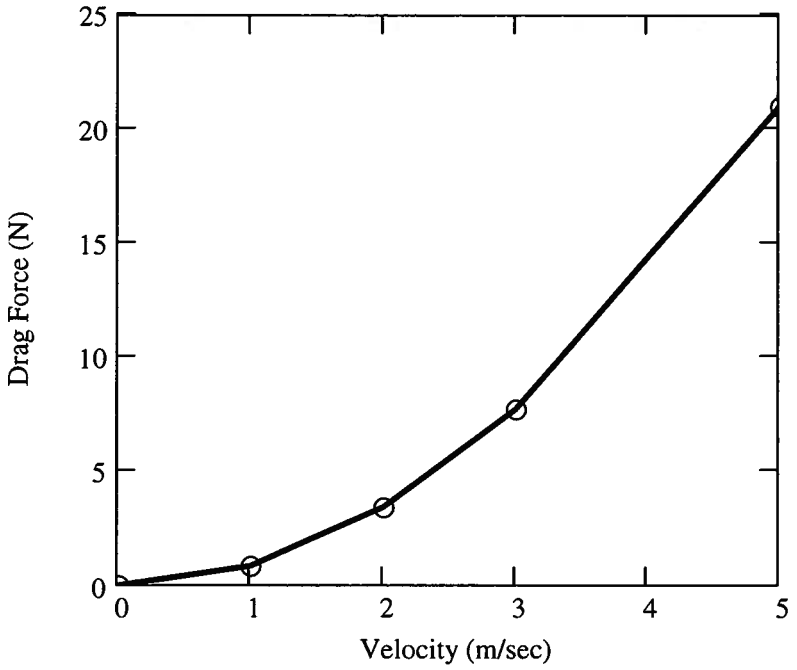

Figure 10.6 Drag on a Baseball Towed in Water

The drag forces in the water are substantial, but we need to know how they scale to the drag forces on the baseball in the air. Dimensional analysis will enable us to do this scaling. The geometry for both the air flow and the water flow are shown in Figure 10.7 in the frame of reference of the ball. If we assume that the line attached to the baseball in the water does not substantially alter the flow field, the situation can be modeled as a sphere of diameter D sitting in a flowing fluid of density ρ and viscosity μ. The uniform upstream velocity of the fluid as it approaches the ball is ϑ. The drag force on the ball is F_d.

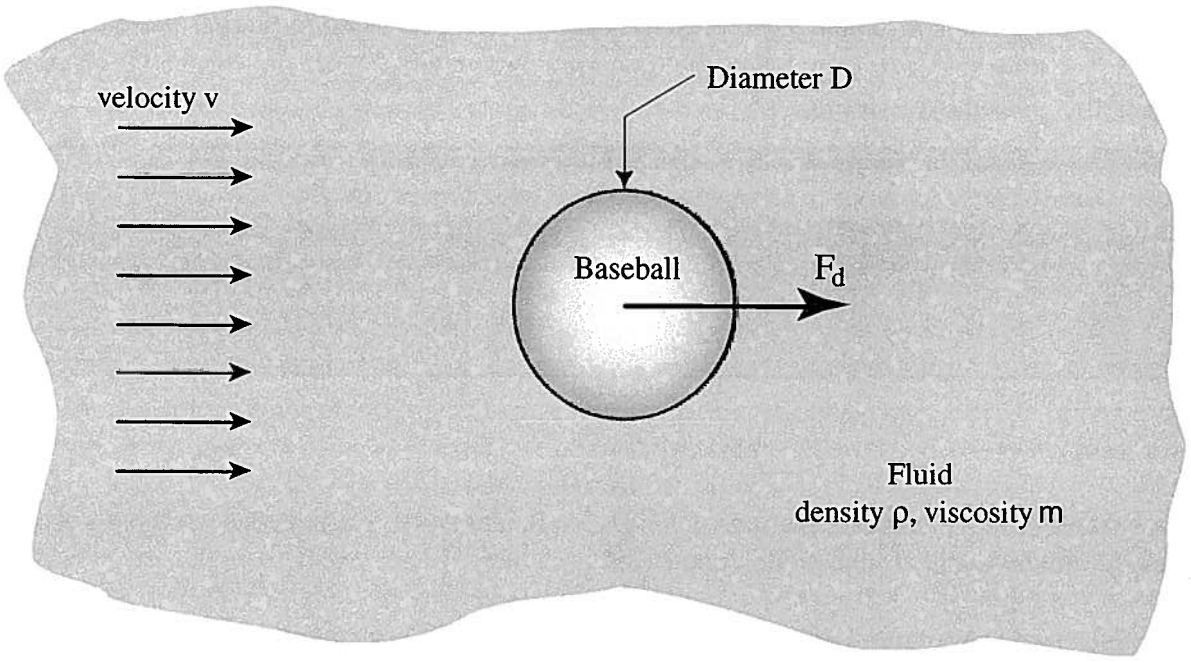

Figure 10.7 The Flow Field from the Perspective of an Observer Located on the Ball

We now perform the dimensional analysis of this situation using the procedure described previously.

Step 1: *List and count the n parameters required to describe the physical situation. If any important parameters are missing, dimensional analysis will fail.*

We have essentially done this step by drawing Figure 10.7. The parameters necessary to describe this physical situation are the drag force, F_d, the velocity of the flow, ϑ, the viscosity of the liquid, μ, the density of the liquid, ρ, and the diameter of the baseball, D. Then $n = 5$.

The mass of the ball and the gravitational constant are not important in this case and should not be included in the dimensional analysis because our intuition tells us that the measured drag force on the baseball in Figure 10.7 would not change if the "baseball" were made of iron or any other material. The fluid is unaware of the mass of the ball. The fluid simply must flow around some fixed rigid sphere.

The buoyancy and gravity forces are normal to the drag force and, hence, are not part of that force. The spring scale does not measure them. Mass and gravity are important only in that the gravity force must match the buoyancy force on the ball so that the ball is dragged under the water and not along the surface of the water. However, if the mass of the ball is too large, the ball will not follow the boat as shown but act as an anchor and hang from the boat almost vertically.

Step 2: *List the dimensions of each variable according to M, L, T, and Θ.*

The dimensions for the parameters are

$$[\rho]=\frac{M}{L^3},\quad [\vartheta]=\frac{L}{T},\quad [D]=L,\quad [\mu]=\frac{M}{LT},\quad [F_d]=\frac{ML}{T^2}$$

Step 3: *Find the value of r. Initially guess r to be equal to the number of different dimensions present and then make sure that there are r parameters that do not form a Π-group. If this is unsuccessful, reduce r by one and look again.*

The dimensions M, L and T are present in the dimensions listed in Step 2. We then guess that $r = 3$. We then select ρ, ϑ, and D as the repeating parameters that do not form a Π–group. Checking this possibility, we find

$$\left[\rho^a \vartheta^b D^c\right] = 1$$

$$\left(\frac{M}{L^3}\right)^a \left(\frac{L}{T}\right)^b (L)^c = 1$$

$$M^a L^{b+c-3a} T^{-b} = 1$$

Then

$$a = 0$$

$$b + c - 3a = 0$$

$$-b = 0$$

The solution of this system of equations is $a = 0$, $b = 0$, and $c = 0$. Then the selected parameters are indeed dimensionally independent, and $r = 3$.

Step 4: *Select r parameters which do not form a Π-group among themselves. These parameters are the repeating parameters that will appear in all the Π-groups.*

The obvious choice for repeating parameters is ρ, ϑ, and D.

Step 5: *Select one of the remaining parameters that is not one of the r repeating parameters and non-dimensionalize that parameter using the r repeating parameters. Repeat the procedure until all the remaining parameters are non-dimensionalized. There should now be n – r Π-groups.*

There are two remaining parameters μ and F_d that we need to non-dimensionalize. Starting with μ, we get

$$\left[\mu \rho^d \vartheta^e D^f\right] = 1$$

$$\frac{M}{LT}\left(\frac{M}{L^3}\right)^d \left(\frac{L}{T}\right)^e (L)^f = 1$$

$$M^{1+d} L^{e+f-1-3d} T^{-1-e} = 1$$

Then

$$1 + d = 0$$

$$e + f - 3d - 1 = 0$$

$$-1 - e = 0$$

The solution of this system of equations is $d = -1$, $e = -1$, and $f = -1$. The resulting dimensionless group is

$$\Pi_1' = \frac{\mu}{\rho \vartheta D}$$

We have included a prime in the notation because this is not the form of the dimensionless group we would like. We would prefer to adopt a more traditional dimensionless group known as the Reynolds number, Re, which is the reciprocal of Π'_1 or

$$\Pi_1 = \frac{\rho v D}{\mu} \equiv Re$$

Note that the dimensionless groups generated using these methods are not unique. As noted previously, any power, product, or quotient of these dimensionless numbers is also an

acceptable dimensionless group. The choice of which dimensionless groups are finally chosen is often dictated by earlier work in the field or by the physics of the situation. There are occasions for which the earlier choices have not been the best way to express the results, and in those cases, the later authors do not follow their predecessors' lead. They usually express their results in terms of a new set of dimensionless parameters more appropriate to the situation.

The next parameter to be non-dimensionalized is the drag force, F_d. Then

$$\left[F_d \rho^g \vartheta^h D^i\right] = 1$$

$$\frac{ML}{T^2}\left(\frac{M}{L^3}\right)^g \left(\frac{L}{T}\right)^h (L)^i = 1$$

$$M^{1+g} L^{1+h+i-3g} T^{-2-h} = 1$$

Then

$$1+g=0$$

$$1+h+i-3g=0$$

$$-2-h=0$$

The solution of this system of equations is $g = -1$, $h = -2$, and $i = -2$, and the resulting dimensionless group is

$$\Pi_2' = \frac{F_d}{\rho \vartheta^2 D^2}$$

Once again we have included a prime in the notation because this is not the final form of the dimensionless group we will choose to use. With a nod to history, we would like to change the denominator of Π_2'. The quantity $\rho\vartheta^2$ appears frequently in fluid mechanics with the quantity ½ attached to it. The quantity $\frac{1}{2}\rho\vartheta^2$ is physically meaningful in that it is the kinetic energy per unit mass carried by a fluid particle. From the energy equation for a control volume, $\frac{1}{2}\rho\vartheta^2$ is the pressure that would result at the point where a fluid particle is brought to rest from the velocity ϑ. This is known as the dynamic pressure in the flow. The dimension of D^2 in the denominator of Π_2' is that of area. A more physically meaningful quantity than D^2 is the projected area of the sphere, $(\pi/4)D^2$. This is the area that an upstream observer would see of the object. The product of a pure number, which is dimensionless, and a dimensionless Π–group is still dimensionless. Then we can legitimately modify Π_2' by multiplying it by any pure number. With this in mind, we propose that the appropriate form for Π_2' is

$$\Pi_2 = \frac{F_d}{\frac{1}{2}\rho\vartheta^2 \frac{\pi}{4} D^2} \equiv C_d$$

where C_d is known as the drag coefficient.

We have non-dimensionalized all non-repeating parameters and in the process have generated two Π–groups. Initially we had $n = 5$ parameters and $r = 3$ dimensions so that we were expecting 5 – 3 = 2 Π-groups.

Step 6: *Check to see that all proposed Π-groups are dimensionless and write the functional relationship among them in dimensionless form.*

Both Π–groups have been checked and are indeed dimensionless. The functional form for the relation of the Π–groups is then

$$\Pi_2 = G(\Pi_1)$$

or

$$C_d = G(Re)$$

This is as far as dimensional analysis can take us. We now need to rely on the data we have taken on our wet baseball. The diameter of a baseball is $D = 7$ cm. For water

$$\rho = 10^3 \text{ kg/m}^3 \qquad \mu = 10^{-3} \text{ kg/m sec}$$

Using these values, we can reformulate the data for the baseball towed in water into dimensionless form and then generate a table of values of C_d versus Re (See Table 10.2.).

Table 10.2 Dimensionless Drag Data for a Baseball Towed in Water

Velocity, ϑ (m/sec)	Drag Force, F_d (N)	C_d	Re
1	0.8	0.415	7×10^4
2	3.4	0.441	14×10^4
3	7.7	0.444	21×10^4
5	21	0.436	35×10^4

A plot of the dimensionless wet baseball data appears in Figure 10.8. Clearly, for Reynolds numbers between 7×10^4 and 3.5×10^5, the drag coefficient remains fairly constant at a value of about 0.43. In symbolic form

$$C_d = G(Re) \approx 0.43 \quad \text{for} \quad 7 \times 10^4 < Re < 35 \times 10^4$$

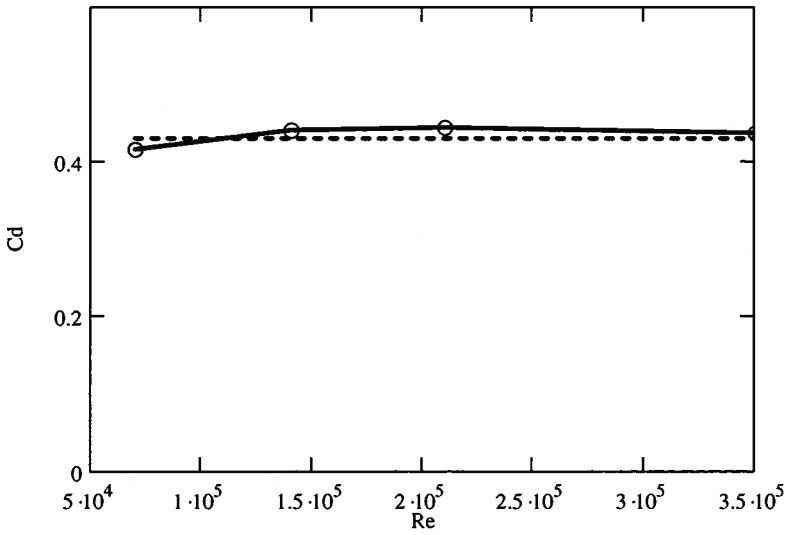

Figure 10.8 Dimensionless Drag Data for a Baseball Towed in Water

In order to use this data to analyze the flight of the ball between the pitcher's mound and the batter, let us assume that a ball is thrown at a velocity of 100 mph or 44.7 m/sec (a very fast ball). The density and viscosity of the air are 1.2 kg/m^3 and 1.8×10^{-5} kg/m sec, respectively. The Reynolds number for the baseball under these conditions is

$$\mathrm{Re} = \frac{\rho \vartheta D}{\mu} = \frac{\left(1.2 \text{ kg/m}^3\right)\left(44.7 \text{ m/sec}\right)\left(7 \text{ x } 10^{-2} \text{ m}\right)}{1.8 \text{ x } 10^{-5} \text{ kg/m sec}} = 2.1 \text{ x } 10^5$$

which is right in the middle of the Reynolds numbers of our wet measurements. Since the Reynolds number for the pitched baseball is between 350,000 and 70,000, C_d must have a value of 0.43. The force on the baseball can be calculated using the definition of the drag coefficient,

$$C_d = 0.43 = \frac{F_d}{\frac{1}{2}\rho \vartheta^2 \frac{\pi}{4} D^2}$$

or

$$F_d = (0.43)\left(\tfrac{1}{2}\rho v^2 \tfrac{\pi}{4} D^2\right) = (0.43)\left[\tfrac{1}{2}\left(1.2 \text{ kg/m}^3\right)\left(44.7 \text{ m/sec}\right)^2 \tfrac{\pi}{4}\left(0.07 \text{ m}\right)^2\right] = 1.984 \text{ N}$$

Assuming that the drag force and the velocity of the ball does not change substantially during the ball's flight from the pitcher's mound to home plate, the change in velocity, $\Delta \vartheta$, can be calculated from

$$\Delta \vartheta \approx \frac{F_d}{m_{ball}} t \approx \frac{F_d}{m_{ball}} \frac{l}{\vartheta_i}$$

where m_{ball} is the mass of the baseball (~0.145 kg), t is the time of flight, l is the distance from the pitcher's mound to home plate (60.5 feet or 18.44 m) and ϑ_i is the velocity of the ball as it leaves the pitcher's hand. The change in the velocity is

$$\Delta \vartheta \approx \frac{\left(1.984 \text{ N}\right)}{\left(0.145 \text{ kg}\right)} \frac{\left(18.44 \text{ m}\right)}{\left(44.7 \text{ m/sec}\right)} = 5.64 \text{ m/sec}$$

Thus, a baseball that is thrown at 44.7 m/sec will slow to 39.1 m/sec by the time it arrives at home plate. In outmoded Engineering Units: a baseball that is thrown at 100 mph will slow to 87 mph by the time it arrives at home plate. For the measurement of pitch speed by a radar gun to have meaning, it is important to measure the speed of the pitch at the same point from pitch-to-pitch.

Although the foregoing discussion provides a reasonable estimate of the effect of drag on a thrown baseball, it simplifies a somewhat complex physical situation. The data employed in the example are data for a smooth sphere similar to a billiard ball. A baseball has a more complex surface due to the presence of the stitched seams. The seams act as turbulence promoters which change the drag characteristics markedly. For a smooth sphere, the data for the drag coefficient as a function of Reynolds number show a pronounced "knee" at a Reynolds number of about 3.8 x 10^5 for which the drag coefficient falls precipitously to a value of about one-tenth its previous value. This knee lies outside the physical capabilities of even the very best major league pitchers. However, the presence of any roughness on the surface of the ball shifts this "knee" in the drag curve to lower values of the Reynolds numbers that are within the capability of good pitchers. The difference between a good fast ball pitcher who can throw in the "high 80s" and a great fast ball pitcher who can "bring it with some serious heat" in the neighborhood of 100 mph is a matter of throwing with enough initial velocity to just clear the "knee" of the curve so that the drag force in the early stage of the flight of the ball is at its lowest possible value. As the ball starts slowing down due to drag, the drag force rises sharply as the Reynolds number decreases into the high drag regime. (See Figure 10.9)

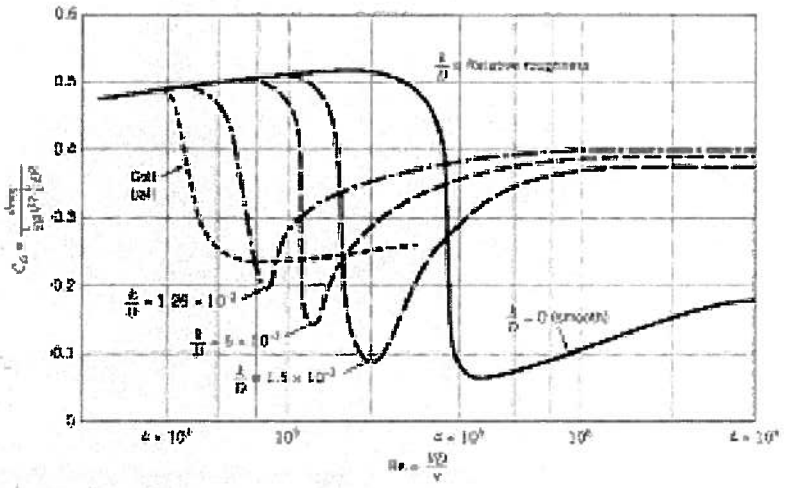

Figure 10.9 Drag Coefficient for Smooth and Rough Spheres
(From *A Physical Introduction to Fluid Mechanics* by Alexander J. Smits, John Wiley & Sons, N. Y. , 2000, p. 317.)

In the early years of baseball, pitchers were not beyond introducing some additional "roughness" of their own through the use of emery cloth concealed in their gloves. Although these early hurlers were completely unaware of the fluid dynamics of the flight of a baseball, they did know that this "emery ball" or "scuffball," as it was called, gave them an advantage. This practice was outlawed in 1919. In modern baseball with its liberal use of new baseballs, astute batters, in an attempt to limit the advantage gained by the pitcher, frequently call for a ball to be removed from play because it has become scuffed by the natural effects of play.

"Junk ball" pitchers who frequently throw a "knuckle ball" or "flutter ball" deliberately throw at low velocity (60 to 70 mph) so that their pitch velocity produces a Reynolds number that lies entirely in the high drag regime. This causes the flight of the ball to drop out of the strike zone as the ball crosses home plate. These pitchers also try to enhance this effect by holding the ball in a manner that minimizes the effect of the seams. If successful, the ball does not rotate, and the flight of the ball is strongly affected by the vortices that are being shed behind the ball in an alternating fashion, one side after the other. This causes the flutter effect of the "knuckler."

10.8 Ship Design

From time immemorial, the hull design of ships had been largely a matter of rule of thumb, complemented by the accumulated experience of the master shipwright. A number of assertions have been made concerning the shape of a high-speed hull ranging from the assertion that the shape of a vessel should have the "shape of a cod" to the assertion that a fast sailboat should take an extreme "plank on edge" shape, i.e., have an extremely small beam to length ratio.

One ship that illustrated the need for a better understanding of the importance of drag on a ship before it was built was the *Great Eastern* shown in Fig. 10.9. She was launched in 1858 with a displacement of 22,500 tons and a length of 693 feet, five times larger than anything else afloat. She remained the longest steamship ever built until 1899 when Oceania surpassed her and became the vessel with the largest displacement until 1906 when Lusitania surpassed her in that category.

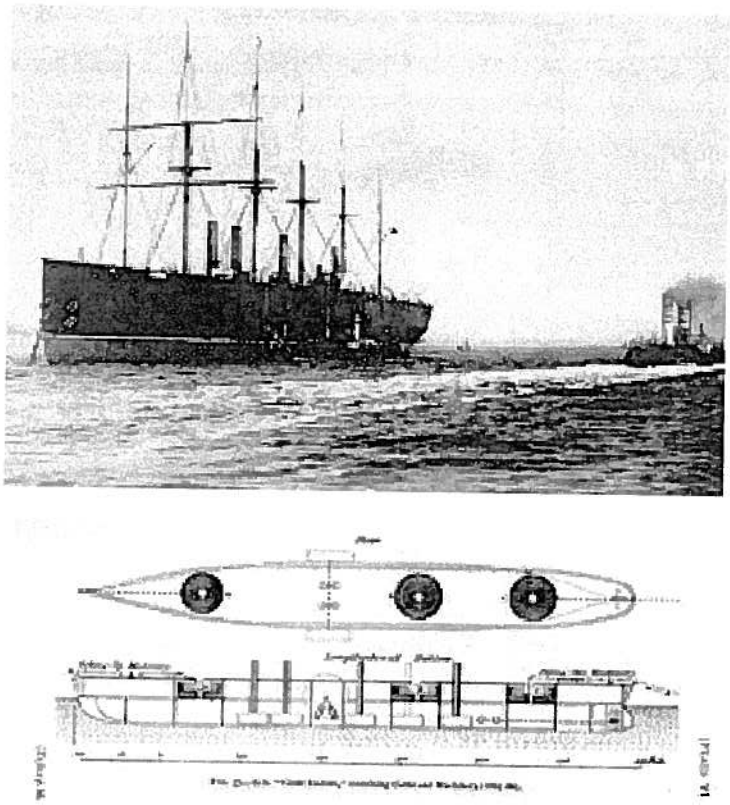

Figure 10.10 The Great Eastern
(The drawing shows her configured for the laying of the Atlantic Cable.)

Great Eastern was built to serve as a steamer on the Britain to Australia route around the Cape of Good Hope. The company that had her built, the Eastern Steam Navigation Company, had decided they wanted a steamer that could carry passengers, substantial cargo, and enough coal to steam from Britain to Australia and back. In 1858, the Suez Canal had not yet been built so that the passage to Australia was around the Cape of Good Hope. The company had determined that the cost of maintaining coaling stations along the route was not economically viable.

Great Eastern was ahead of her time and there was no experience sizing propulsion systems for a ship as large as she was. She had two screw propellers and paddle wheels as well as auxiliary sails for propulsion, but despite all these, she was underpowered. She bankrupted three corporate owners before she was turned to the task of what was ultimately the successful laying the transatlantic cable. Because of her size, she alone could carry enough cable to span the entire distance between Newfoundland and Ireland.

With the dawn of ships that have the size and the cost of construction of Great Eastern, it became imperative to be able to predict the performance of a design before it was implemented in the full scale. Tests on smaller scale prototypes could be made, but the scaling of the test results from the model to the full scale ship remained an uncertainty. This is an ideal role for dimensional analysis. Figure 10.11 shows the basic geometry of a ship on the water.

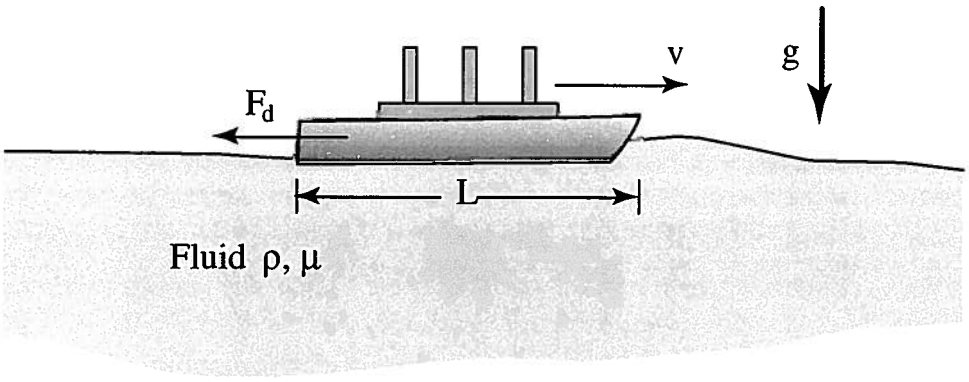

Figure 10.11 Schematic Diagram of a Ship Moving on the Surface of a Large Body of Water

Let us now apply dimensional analysis so that we might determine the appropriate way to scale test model results to the full size ship.

Step 1: *List and count the n parameters required to describe the physical situation. If any important parameters are missing, dimensional analysis will fail.*

In order to determine the required propulsive power for the vessel, we are particularly interested in the drag force on a ship F_d. We believe that the velocity, $\vec{v}$, and the length, L, of the vessel are important in determining the drag. We also believe that the density, ρ, and the viscosity, μ, of the fluid are also important in determining the drag. In addition, because the hull will make waves on the surface of the water we believe that the gravitational acceleration, g, should be included as one of the important parameters to describe the situation because the restoring force for the long wavelength surface waves is gravity.

Presumably the model that we will be testing will be a scale replica of the full size ship. Since we have already shown in equations (10.27) – (10.29) that geometrical similarity results in a common scaling factor for all physical dimensions of a model and a prototype, it is not necessary to include the width and height of the vessel in the list of the important parameters. We will then need only one length on the model to completely specify its size relative to the full-scale ship. We could have chosen the width or the height of the model or a specific diagonal length across the vessel stern, but traditionally the length of the hull is used. If we had included the width, W, and the height, H, as well as the length in the parameter list, we would have found two additional Π–groups that would appear in our analysis, namely W/L and H/L. The values of these Π–groups would be identical in the full-scale prototype and the scale model and their presence in the functional relationship would add no new information.

Additionally, we could have included the surface tension of the water as one of the important parameters. Here our intuition suggests that the drag force would not be influenced a great deal by the surface tension of the fluid. In general, the surface tension affects the surface waves only for short wavelength excitations (millimeter scale). The predominant waves that will be generated by a meter-long scale model, or better still a 200m-long full-scale prototype, are not likely to be on the millimeter scale. Hence we believe that surface tension will not be an important parameter for our analysis.

Step 2: *List the dimensions of each variable according to M, L, T, and Θ.*

The dimensions for the parameters are

$$[\rho]=\frac{M}{L^3},\quad [\vartheta]=\frac{L}{T},\quad [L]=L,\quad [\mu]=\frac{M}{LT},\quad [F_d]=\frac{ML}{T^2},\quad [g]=\frac{L}{T^2}$$

Step 3: *Find the value of r. Initially guess r to be equal to the number of different dimensions present and then make sure that there are r parameters that do not form a Π-group. If this is unsuccessful, reduce r by one and look again.*

The dimensions M, L, and T are present in the dimensions listed in Step 2. We will then guess that $r = 3$. We will select ρ, ϑ, and L as the possible r repeating parameters that do not form a Π–group. Checking to see that these parameters are dimensionally independent, we find

$$\left[\rho^a \vartheta^b L^c\right]=1$$

$$\left(\frac{M}{L^3}\right)^a\left(\frac{L}{T}\right)^b (L)^c=1$$

$$M^a L^{b+c-3a} T^{-b}=1$$

Then

$$a=0$$

$$b+c-3a=0$$

$$-b=0$$

The solution of this system of equations is $a = 0$, $b = 0$, and $c = 0$. Then the parameters ρ, ϑ, and L are dimensionally independent; hence, $r = 3$.

Step 4: *Select r parameters which do not form a Π-group among themselves. These parameters are the repeating parameters that will appear in all the Π-groups.*

We shall select ρ, ϑ, and L as the repeating parameters since they have already been shown to be dimensionally independent.

Step 5: *Select one of the remaining parameters that is not one of the r repeating parameters and non-dimensionalize that parameter using the r repeating parameters. Repeat the procedure until all the remaining parameters are non-dimensionalized. There should now be n − r Π-groups.*

We choose the viscosity as the first non-repeating parameter to non-dimensionalize, and we follow exactly the same procedure as in our previous examples.

$$\left[\mu\rho^d \vartheta^e L^f\right]=1$$

$$\frac{M}{LT}\left(\frac{M}{L^3}\right)^d\left(\frac{L}{T}\right)^e (L)^f=1$$

$$M^{1+d} L^{e+f-1-3d} T^{-1-e}=1$$

Then

$$1+d=0$$

$$-1-e=0$$

$$e+f-1-3d=0$$

The solution of this system of equations is $d = -1$, $e = -1$, and $f = -1$. The resulting dimensionless group is then

$$\Pi_1'=\frac{\mu}{\rho\vartheta L}$$

This Π-group is the reciprocal of the Reynolds number based on the length of the vessel so, bowing to convention, we choose Π_1 to be

$$\Pi_1 = \frac{\rho \vartheta L}{\mu} \equiv Re$$

The next parameter to be non-dimensionalized is the drag force, F_d. Then

$$\left[F_d \rho^h \vartheta^i D^j\right] = 1$$

$$\frac{ML}{T^2}\left(\frac{M}{L^3}\right)^h \left(\frac{L}{T}\right)^i (L)^j = 1$$

$$M^{1+h} L^{1+i+j-3h} T^{-2-i} = 1$$

Then

$$1 + h = 0$$

$$1 + i + j - 3h = 0$$

$$-2 - i = 0$$

The solution of this system of equations is $h = -1$, $i = -2$, and $j = -2$. The resulting dimensionless group is then

$$\Pi_2 = \frac{F_d}{\frac{1}{2}\rho \vartheta^2 L^2} \equiv C_d$$

where C_d is the coefficient of drag. Note that we have inserted the factor of ½ in the denominator for the same reasons discussed in the previous example. For the moment, we use L^2 as a measure of the surface area of the model.

The final Π-group is determined by non-dimensionalizing the gravitational acceleration, g. Then

$$\left[g \rho^k \vartheta^l L^m\right] = 1$$

$$\frac{L}{T^2}\left(\frac{M}{L^3}\right)^k \left(\frac{L}{T}\right)^l (L)^m = 1$$

$$M^k L^{1-3k+l+m} T^{-2-l} = 0$$

Then

$$k = 0$$

$$1 - 3k + l + m = 0$$

$$-2 - l = 0$$

The solution of this system of equations is $k = 0$, $l = -2$, and $m = 1$. The resulting dimensionless group is then

$$\Pi_3' = \frac{gL}{\vartheta^2}$$

This is a perfectly acceptable dimensionless number; however, in the literature, this dimensionless group raised to the −½ power is used or

$$\Pi_3 = \frac{\vartheta}{\sqrt{gL}} \equiv Fr$$

This is the definition of the Froude number, *Fr*, named in honor of William Froude (1810 – 1879), who together with his son Robert Edmund Froude, refined the technique of testing ship

models as an adjunct to the practice of naval architecture.

According to the Buckingham Pi Theorem, there exists a functional relationship of the form

$$\Pi_2 = G(\Pi_1, \Pi_3)$$

or

$$C_d = G(Re, Fr)$$

From this expression, it is clear that in order to derive meaningful results from model tests conducted in a towing tank, both the Reynolds number and the Froude number must be the same in the model and the full-scale prototype. Unfortunately, this is not always possible. For the sake of argument, let us assume that the length model is L_m = 1 m and the length of the prototype is L_p = 100 m. From experience, ships at high cruising speed generate significant surface waves as they move through the water. This can be seen in the full scale in Fig. 10.12 and in towing-tank tests in Fig. 10.13.

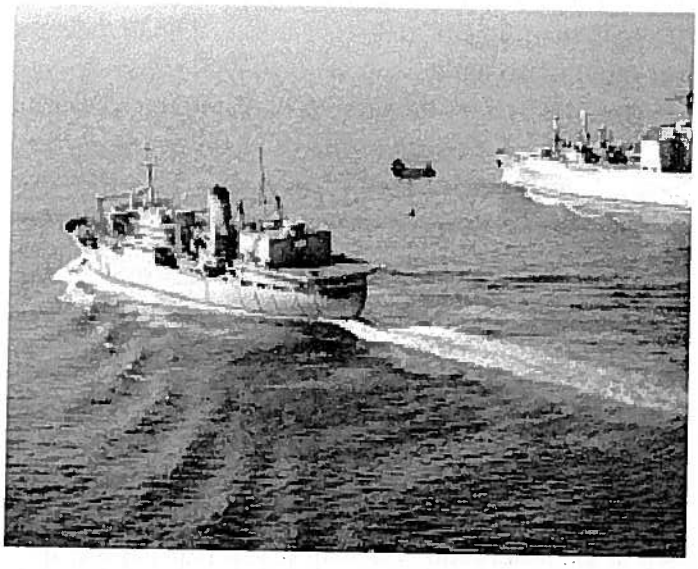

Figure 10.12 Surface Waves Generated by a Ship at Speed (Courtesy U.S. Navy)

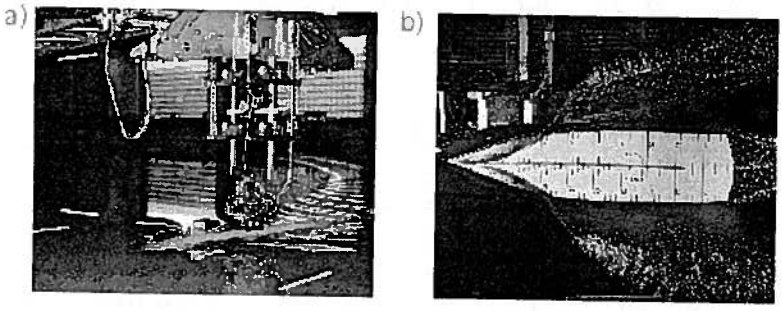

Figure 10.13 a) Test of a Model of a Submarine in a Towing Tank
b) Test of a Model of a Surface Ship Hull in a Towing Tank
(Photographs from Davidson Lab website)

The energy stored and ultimately dissipated in these surface waves comes from the engines of the ship. The Froude number, which is related to the wave speed, should then be a very important parameter in determining the drag on the ship at high cruising speed. Then the Froude numbers in the model tests should match the expected Froude Numbers for the prototype operation. It follows, then, that

$$Fr_{model} = Fr_{prototype}$$

$$\frac{\vartheta_m}{\sqrt{gL_m}} = \frac{\vartheta_p}{\sqrt{gL_p}}$$

$$\frac{\vartheta_m}{\vartheta_p} = \sqrt{\frac{L_m}{L_p}} = \sqrt{\frac{1}{100}} = 0.1$$

As a consequence, a model that is 1/100 the size of the prototype must be towed at 1/10 the speed of the prototype in order to match the wave making patterns of the model and the prototype. Since typical velocities for surface vessels vary from 1 to 20 knots, i.e., 0.51 to 10.2 m/sec, the model velocities then will be in the range of 0.05 to 1 m/sec. The highest model speeds will be a walking pace which seems quite reasonable.

It now remains to match the Reynolds number between the model and the ship.

$$Re_m = Re_p$$

$$\frac{\rho_m \vartheta_m L_m}{\mu_m} = \frac{\rho_p \vartheta_p L_p}{\mu_p}$$

$$\frac{\vartheta_m L_m}{\nu_m} = \frac{\vartheta_p L_p}{\nu_p}$$

where ν is the kinematic viscosity previously defined as μ/ρ. Note that we have already chosen L_m and L_p. The velocity ϑ_p is chosen by virtue of the intended operating speeds of the vessel, and the velocity of the model has already been determined by the Froude number restriction. The kinematic viscosity of the fluid for the prototype (water) has already been chosen. The only parameter left to be chosen is the kinematic viscosity of the fluid in the test tank. The kinematic viscosity of that fluid is

$$\frac{\nu_m}{\nu_p} = \frac{\vartheta_m}{\vartheta_p}\frac{L_m}{L_p} = \sqrt{\frac{L_m}{L_p}}\frac{L_m}{L_p} = \left(\frac{L_m}{L_p}\right)^{\frac{3}{2}} = \left(\frac{1}{100}\right)^{\frac{3}{2}} = 0.001$$

We therefore seek a fluid that has one one-thousandth the kinematic viscosity of water. A list of candidate fluids is shown in Table 10.3.

Table 10.3 Properties of Candidate Test Fluids at 20 C

Liquid	μ (kg/m sec)	ρ (kg/m^3	ν (m^2/sec)	ν_{liquid}/ν_{water}
water	1×10^{-3}	1000	1×10^{-6}	1
gasoline	2.9×10^{-4}	680	4.3×10^{-7}	0.43
ethanol	1.2×10^{-3}	789	1.5×10^{-6}	1.5
refrigerant 12	2.6×10^{-4}	1327	1.95×10^{-7}	0.19
mercury	1.56×10^{-3}	13550	1.15×10^{-7}	0.115

From these data, it is apparent that there are no real fluids that will fulfill our requirements. Mercury is the best with a kinematic viscosity ratio (ν_m/ν_p) of 0.1, but even this toxic fluid is far short of the required ratio of 0.001. The other test fluids also suffer shortcomings such as flammability, toxicity, volatility, etc. We have little choice but to use water as the fluid in the towing tank. However, this presents us with a dilemma; the use of water in the tank means that the Reynolds number cannot be matched between the model and the full scale ship.

In 1872, Froude offered way of resolving this dilemma. He suggested that the viscous effects on the hull of a ship do not significantly affect the hull's wave making action. He also suggested that the viscous effects, embodied in the Reynolds number, and the wave making effects, embodied in the Froude number, were uncoupled as far as the drag on a ship was concerned. (It should be noted that since Reynolds did not present his work concerning the Reynolds number until 1883, we are taking some poetic license here in our interpretation of events.) Froude's assumption can be expressed mathematically in the form,

$$C_d\left(Re, Fr\right) = \Phi(Re) + \Gamma(Fr)$$

where Φ and Γ are functions to be determined. This can be cast in a similar but different form

$$C_d = C_d^{\mu} + C_d^{w}$$

where C_d^{μ} is the coefficient of drag due to viscous effects and C_d^{w} is the coefficient of drag due to wave making. Froude's separation of these two effects in this manner can be argued by realizing that the length scale associated with the wave action is the length of the vessel (observe the wavelengths of the waves in Figure 10.12); whereas, viscous effects are confined to the boundary layer in the immediate neighborhood of the surface of the hull, which according to our previous work in Chapter 9, is of the scale of the boundary layer thickness δ at the location L which in the case of turbulent flow is given by

$$\delta = \left(0.16\, Re^{-\frac{1}{7}}\right) L$$

For a velocity of ϑ = 10 m/s and a length of L = 100 m, the boundary layer thickness is $0.008L$ or 0.8 meters. Thus the length scales between viscous and wave effects differ by a factor larger than 100.

Froude determined C_d^{μ} by towing a flat plate of length L with the same wetted surface area as the ship model. Since the thin plate does not make significant surface waves, $C_d^{\mu} = \Phi(Re)$ can be determined as a function of Reynolds number. Following this, the model can be towed in the towing tank to determine $C_d(Re,Fr)$. With both sets of data, $C_d^{w}(Fr)$ can be determined by taking the difference of C_d and C_d^{μ}. Armed with the functional form of both C_d^{μ} and C_d^{w}, the total drag coefficient can be calculated for the full-scale prototype.

In the foregoing discussion, we have presented the essence of ship model testing, but since this is one of the more intense applications of dimensional analysis, we have included the details of a standard method for scaling towing tank test data as an appendix to this chapter. The boat design illustrated in the appendix is an excellent example of both the methodology of naval architecture and the general technique of dimensional analysis. At this point, however, it is appropriate to continue our discussion of dimensional analysis by examining two additional examples drawn from two very different areas of engineering science.

10.9 Heat Transfer from a Cylinder Immersed in a Flowing Fluid

Dimensional analysis can also be a very powerful tool in analyzing physical situations in which heat transfer is the dominant mode of energy transfer. An example of such a system is the hot-wire anemometer shown in Figure 10.15. In the hot-wire anemometer, a wire is heated by dissipating electrical energy by means of an electrical current passing through the resistance of the wire. The current is adjusted by a feed-back mechanism so that its value is sufficient to maintain the wire at a temperature T_{wire} above the ambient fluid temperature T_{amb}. (The wire is fabricated from a metal such as platinum that has an electrical resistance that is a strong function of the temperature of the wire which serves as the feedback parameter.) The heat transfer rate from the wire to the fluid can be related to the velocity of the fluid, ϑ. Thus once calibrated, the hot wire anemometer can be used to measure the fluid velocity.

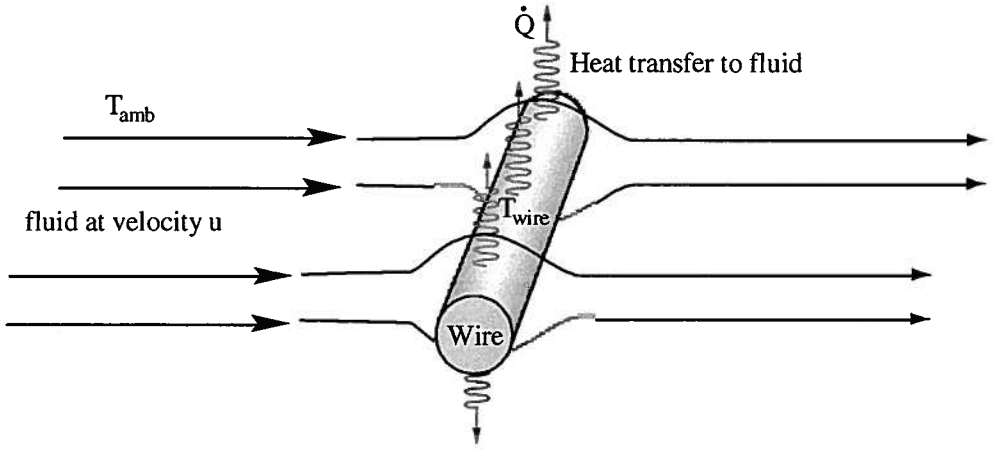

Figure 10.14 Heat Transfer Between a Heated Wire and a Fluid Flowing Past It

In order to design a hot-wire anemometer, we need to find a relation between the convective heat transfer coefficient h and the fluid velocity. Recall that for a situation in which the convective mode of energy transfer dominates

$$h = \frac{\dot{Q}}{A_s\left(T_{wire} - T_{amb}\right)}$$

where A_s is the surface area of the wire in contact with the fluid. One approach is to go into the laboratory and make physical measurements for several different fluids, cylinder diameters, and fluid velocities. Our first set of "measurements" is done with hydrogen gas at T_{amb} = 300 K and a wire with a diameter of D = 100 μm. The second set is done with hydrogen gas at T_{amb} = 300 K and D = 2 cm. The third set is done with carbon dioxide gas at T_{amb} = 300 K and D = 2 cm. Finally, the fourth set is with liquid water at T_{amb} = 350K and a D = 2 cm. For these "measurements," the resulting values of h as a function of fluid velocity are plotted in Figure 10.15 and tabulated in Table 10.4. The measured values of the heat transfer coefficient vary over a range of four orders of magnitude; and, it is not clear from Figure 10.15 how to predict the heat transfer coefficient given a new fluid or a new diameter for the wire.

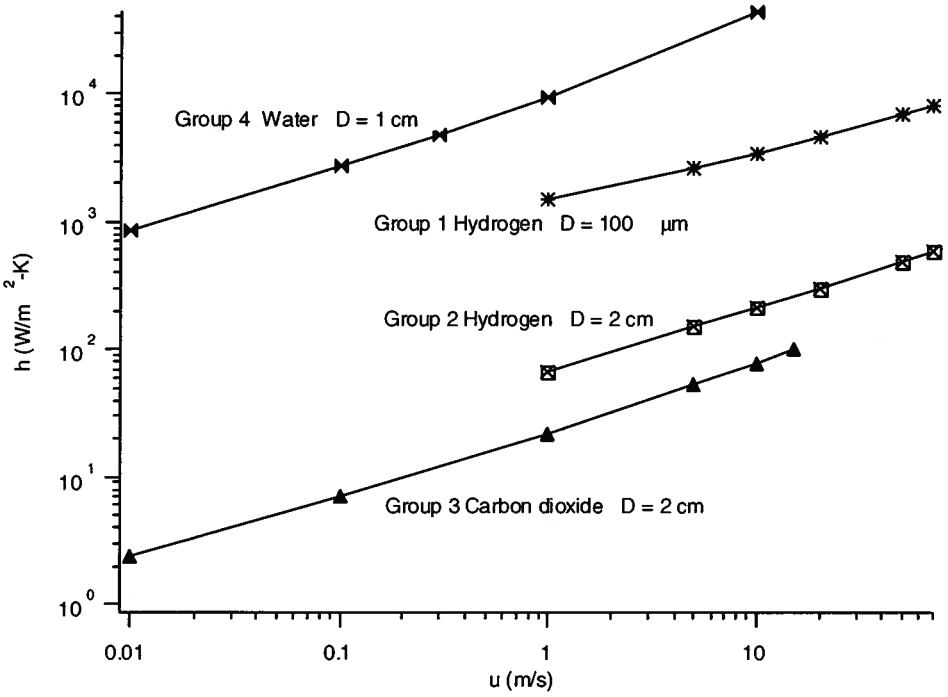

Figure 10.15 Heat Transfer Coefficient for Gases Flowing Past Cylinders

Dimensional analysis can help us make sense of these apparently disparate measurements. Following our well-established procedure, we can develop a dimensionless fuction that relates the dimensionless parameters that describe this situation.

Step 1: *List and count the n parameters required to describe the physical situation. If any important parameters are missing, dimensional analysis will fail.*

The first parameters of interest are the heat transfer coefficient h and the diameter of the "wire" (cylinder) D. The other relevant parameters in this situation are related to the identity of the fluid, namely the density, ρ, viscosity, μ, heat capacity per unit mass (specific heat), c_P, and the thermal conductivity of the fluid, k. With this choice of important parameters, we have combined all the convective heat transfer parameters, namely the heat transfer rate, the surface area of the wire, and the temperatures of the fluid and the wire temperatures into the heat transfer coefficient. We have assumed here that they are not important in themselves but appear only as the group

$$\frac{\dot{Q}}{A_s\left(T_{wire}-T_{amb}\right)}=h$$

in the set of equations that describe this situation. Hence, there are seven parameters that are important in this case, $n = 7$.

Table 10.4 Results of the Heat Transfer measurements on Various Cylinders

Group 1: Hydrogen, T_{amb} = 300 K, D = 100 μm, P = 1atm				
ϑ (m/sec	h (W/m^2 K)	Re	Nu	Pr
1	1490	0.9093	0.7525	0.67
5	2600	4.546	1.313	0.67
10	3424	9.093	1.729	0.67
20	4600	18.19	2.323	0.67
50	6940	45.46	3.505	0.67
70	8100	63.65	4.091	0.67

Group 2: Hydrogen, T_{amb} = 300 K, D = 2 cm, P = 1atm				
ϑ (m/sec	h (W/m^2 K)	Re	Nu	Pr
1	66	182	6.67	0.67
5	150	909	15.2	0.67
10	210	1820	21	0.67
20	300	3640	30	0.67
50	490	9090	49.5	0.67
70	592	12730	59.9	0.67

Group 3: Carbon dioxide, T_{amb} = 300 K, D = 2 cm, P = 1atm				
ϑ (m/sec	h (W/m^2 K)	Re	Nu	Pr
0.01	2.4	23.5	2.65	0.71
0.1	7.07	235	7.81	0.71
1	22	2352	24.31	0.71
5	53	11800	58.56	0.71
10	78	23500	86.2	0.71
15	100	35300	110.5	0.71

Group 4: Water, T_{amb} = 350 K, D = 1 cm, P = 1atm				
ϑ (m/sec	h (W/m^2 K)	Re	Nu	Pr
0.01	843	257	12.60	2.4
0.1	2709	2570	40.49	2.4
0.3	4862	7700	72.68	2.4
1	9610	25700	143.65	2.4
10	43926	257000	656.59	2.4

Step 2: *List the dimensions of each variable according to M, L, T, and Θ.*
For the convective heat transfer case

$$[h]=\frac{M}{\Theta T^3},\quad [D]=L,\quad [\mu]=\frac{M}{LT},\quad [\rho]=\frac{M}{L^3},\quad [\vartheta]=\frac{L}{T},\quad \left[c_p\right]=\frac{L^2}{T^2\Theta},\quad [k]=\frac{ML}{T^3\Theta}$$

Step 3: *Find the value of r. Initially guess r to be equal to the number of different dimensions present and then make sure that there are r parameters that do not form a Π-group. If this is unsuccessful, reduce r by one and look again.*

Unlike our previous examples, in this case there are four dimensions present: M, L, T and Θ. If we assume that $r = 4$, we should be able to reduce the seven variables down to three Π-groups, $n - r = 7 - 4 = 3$. Let us choose D, μ, k and ρ as the 4 potential repeating parameters. We need to ensure that they do not form a Π-group themselves. Checking, we get

$$\left[D^a \mu^b k^c \rho^d\right] = 1$$

$$L^a \left(\frac{M}{LT}\right)^b \left(\frac{ML}{T^3\Theta}\right)^c \left(\frac{M}{L^3}\right)^d = 1$$

$$M^{b+c+d} L^{a-b+c-3d} T^{-b-3c} \Theta^{-c} = 1$$

Then

$$b + c + d = 0$$

$$a - b + c - 3d = 0$$

$$-b - 3c = 0$$

$$-c = 0$$

The solution of this system of equations is $a = 0$, $b = 0$, $c = 0$, and $d = 0$. Then the parameters D, μ, k, and ρ, are dimensionally independent; hence, $r = 4$.

Step 4: *Select r parameters which do not form a Π-group among themselves. These parameters are the repeating parameters that will appear in all the Π-groups.*

We shall select D, μ, k, and ρ, as the repeating parameters since they have already been shown to be dimensionally independent.

Step 5: *Select one of the remaining parameters that is not one of the r repeating parameters and non-dimensionalize that parameter using the r repeating parameters. Repeat the procedure until all the remaining parameters are non-dimensionalized. There should now be n - r Π-groups.*

There are three remaining parameters h, v, and c_p to be non-dimensionalized. Starting with h, we get

$$\left[h D^a \mu^b k^c \rho^d\right] = 1$$

$$\frac{M}{\Theta T^3} L^a \left(\frac{M}{LT}\right)^b \left(\frac{ML}{T^3\Theta}\right)^c \left(\frac{M}{L^3}\right)^d = 1$$

$$M^{1+b+c+d} L^{a-b+c-3d} T^{-3-b-3c} \Theta^{-1-c} = 1$$

Then

$$1 + b + c + d = 0$$

$$a - b + c - 3d = 0$$

$$-3 - b - 3c = 0$$

$$-1 - c = 0$$

The solution of this system of equations is $a = 1$, $b = 0$, $c = -1$, and $d = 0$. The resulting dimensionless group is then

$$\Pi_1 = \frac{hD}{k} \equiv Nu$$

which is known as the Nusselt number, Nu.

The next non-repeating parameter is the velocity, v. Non-dimensionalizing v, we get

$$\left[\vartheta D^d \mu^e k^f \rho^g\right] = 1$$

$$\frac{L}{T}\ L^d \left(\frac{M}{LT}\right)^e \left(\frac{ML}{T^3\Theta}\right)^f \left(\frac{M}{L^3}\right)^g = 1$$

$$M^{e+f+g} L^{1+d-e+f-3g} T^{-1-e-3f} \Theta^{-f} = 1$$

Then

$$e + f + g = 0$$
$$1 + d - e + f - 3g = 0$$
$$-1 - e - 3f = 0$$
$$-f = 0$$

The solution of this system of equations is $d = 1$, $e = -1$, and $f = 0$, and $g = 1$. The resulting dimensionless group is then

$$\Pi_2 = \frac{\rho \vartheta D}{\mu} \equiv Re$$

which we recognize as the Reynolds number.

The final non-repeating parameter is the specific heat capacity, c_P. Non-dimensionalizing this parameter, we get

$$\left[c_P D^i \mu^j k^l \rho^m\right] = 1$$

$$\frac{L^2}{T^2\Theta}\ L^i \left(\frac{M}{LT}\right)^j \left(\frac{ML}{T^3\Theta}\right)^l \left(\frac{M}{L^3}\right)^m = 1$$

$$M^{j+l+m} L^{2+i-j+l-3m} T^{-2-j-3l} \Theta^{-1-l} = 1$$

Then

$$j + l + m = 0$$
$$2 + i - j + l - 3m = 0$$
$$-2 - j - 3l = 0$$
$$-1 - l = 0$$

The solution of this system of equations is $i = 0$, $j = 1$, $l = -1$, and $m = 0$. The resulting dimensionless group is then

$$\Pi_3 = \frac{\mu c_P}{k} \equiv Pr$$

which is known as the Prandtl number, *Pr*. We now have reduced the original seven variables to three Π-groups as expected.

Step 6: *Check to see that all proposed Π-groups are dimensionless and write the functional relationship among them in dimensionless form.*

The three groups we have are indeed dimensionless (we checked again). According to the Buckingham Pi Theorem, the experimental heat transfer results we have presented above can be expressed in the form

$$Nu = G(Re, Pr)$$

Once again, this is as far as dimensional analysis can take us. It is now necessary to use intuition, observation, and analysis to find the functional form of *G*. The Reynolds, Nusselt, and Prandtl

numbers for each of the experimental flows are included in Table 10.4. The fluid physical property values used to determine these dimensionless numbers are shown in Table 10.5. A plot of the Nusselt number data (the non-dimensional heat transfer coefficient) versus the Reynolds number data (the non-dimensional velocity) is shown in Figure 10.16.

Table 10.5 Values of Physical Properties Used to Calculate Data in Table 10.4

Property	Group 1and 2 Hydrogen	Group 3 Carbon Dioxide	Group 4 Water
ρ (kg/m^3)	0.0812	1.788	973
μ (kg/m sec)	8.93×10^{-6}	15.2×10^{-6}	3.79×10^{-4}
c_p (J/kg K)	14780	844	4190
k (W/m K)	0.198	0.0181	0.669

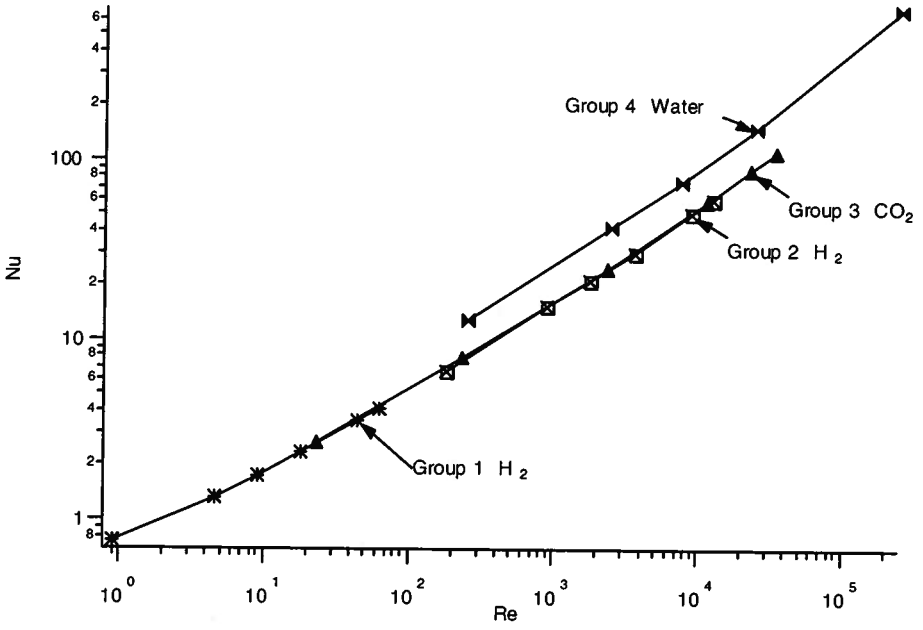

Figure 10.16 Dimensionless Heat Transfer Data for Flow Over a Cylinder (Raw Data Shown in Table 10.4)

It is immediately clear that there has been an overall simplification in presenting the data. Three of the four groups have collapsed onto a single curve. Unfortunately, the Group 4 water data set does not lie on that same curve. This must be the effect of the Prandtl number since the Prandtl number for the water data is 2.4 while that for the gases is substantially different at a value of $Pr \sim 0.7$. Clearly, there must be some way we can factor the Prandtl number into the data, but in order to do this, we need more information. Problems 10.8 and 10.14 explore this possibility so that we can determine the functional form of G in terms of both the Reynolds and Prandtl numbers.

10.10 Electrical Systems

The use of dimensional analysis is not confined to thermal-fluid systems. We have already seen in the case of the simple pendulum that it can be employed for mechanical systems. In this section, we show that it can also be used for electrical systems. By way of example, consider the simple *RLC* filter circuit shown in Figure 10.17. We are interested in the output

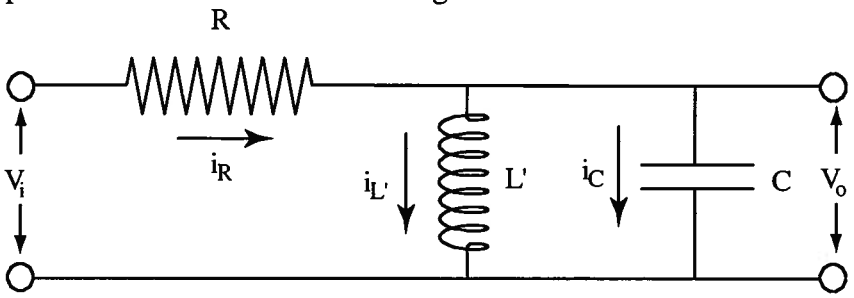

Figure 10.17 A simple *RLC* circuit

voltage amplitude, V_o. The input signal is assumed to be sinusoidal with frequency f and amplitude V_i. We now show the way that dimensional analysis can help us conveniently characterize the relationship between the input and the output of this system.

Step 1: *List and count the n parameters required to describe the physical situation. If any important parameters are missing, dimensional analysis will fail.*

The relevant parameters to describe the behavior of this circuit are the resistance, R, the inductance, $\mathscr{L}$, the capacitance, C, the input voltage amplitude, V_i, the output voltage amplitude, V_o, and the frequency, f. Thus, there are six parameters ($n = 6$).

Step 2: *List the dimensions of each variable according to M, L, T, and Θ.*

In this case, the physics of the situation does not quite match with the thermal-fluid situations we have been examining thus far. If we review the dimensions associated with the SI unit system (See Section 10.1.), we discover that in the case of electrical systems, one of the dimensions is the electrical current, I. Then instead of the appropriate dimensions being M, L, T, and Θ as we had for thermal-fluid systems, we should use M, L, T, and I to describe this situation. Then

$$[V_i]=\frac{M^2L^2}{IT^3},\quad [V_o]=\frac{M^2L^2}{IT^3},\quad [R]=\frac{ML^2}{I^2T^3},\quad [\mathscr{L}]=\frac{ML^2}{I^2T^2},\quad [C]=\frac{I^2T^4}{ML^2},\quad [f]=\frac{1}{T}.$$

Step 3: *Find the value of r. Initially guess r to be equal to the number of different dimensions present and then make sure that there are r parameters that do not form a Π-group. If this is unsuccessful, reduce r by one and look again.*

There are four dimensions present in this set of parameters M, L, T, and I; consequently, we will first guess $r = 4$ and try to reduce the six parameters down to two Π-groups. Let us choose f, C, V_i and R as the potential $r = 4$ parameters. We need to check to see if they form a Π-group by themselves. If they do, then it should be the case that

$$\left[f^a C^b V_i^c R^d\right] = 1$$

$$\frac{1}{T}^a \left(\frac{I^2T^4}{ML^2}\right)^b \left(\frac{M^2L^2}{IT^3}\right)^c \left(\frac{ML^2}{I^2T^3}\right)^d = 1$$

$$M^{-b+2c+d} L^{-2b+2c+2d} T^{-a+4b-3c-3d} I^{2b-c-2d} = 1$$

Then

$$-b+2c+d=0$$
$$-2b+2c+2d=0$$
$$-a+4b-3c-3d=0$$
$$2b-c-2d=0$$

The first two equations of the set establish that $b = d$. The fourth equation shows that $c = 0$. The third equation leads us to the conclusion that there are non-zero solutions to this system of equations. For example, choose $a = b = d = 1$ and the quantity fRC forms a dimensionless Π-group. Thus, we conclude that the parameters f, C, V_i and R are dimensionally dependent. Unfortunately, any choice of four variables from the set of parameters listed in step 1 forms a Π-group. We are then forced to reduce the value of r to a value of 3 and seek three parameters that do not themselves form a Π-group. Let us now choose f, C and V_i. Then

$$\left[f^j C^k V_i^l\right] = 1$$

$$\frac{1}{T}^j \left(\frac{I^2T^4}{ML^2}\right)^k \left(\frac{M^2L^2}{IT^3}\right)^l = 1$$

$$M^{-k+2l} L^{-2k+2l} T^{-j+4k-3l} I^{2k-l} = 0$$

Then

$$-k+2l=0$$
$$-2k+2l=0$$
$$-j+4k-3l=0$$
$$2k-l=0$$

The solution of this system of equations is $j = 0$, $k = 0$, and $l = 0$. Then the parameters f, C, and V_i are dimensionally independent; hence, $r = 3$.

Step 4: *Select r parameters which do not form a Π-group among themselves. These parameters are the repeating parameters that will appear in all the Π-groups.*

We shall select f, C, and V_i, as the repeating parameters since they have already been shown to be dimensionally independent.

Step 5: *Select one of the remaining parameters that is not one of the r repeating parameters and non-dimensionalize that parameter using the r repeating parameters. Repeat the procedure until all the remaining parameters are non-dimensionalized. There should now be n − r Π-groups.*

There are three remaining parameters V_o, R, and $\mathscr{L}$ that need to be non -dimensionalized. Starting with V_o, we get

$$\left[V_o\, f^a C^b V_i^c\right] = 1$$

$$\frac{M^2L^2}{IT^3}\left(\frac{1}{T}\right)^a\left(\frac{I^2T^4}{ML^2}\right)^b\left(\frac{M^2L^2}{IT^3}\right)^c = 1$$

$$M^{2-b+2c}L^{2-2b+2c}T^{-3-a+4b-3c}I^{-1+2b-c} = 1$$

Then

$$2-b+2c=0$$

$$2-2b+2c=0$$

$$-3-a+4b-3c=0$$

$$-1+2b-c=0$$

The solution of this system of equations is $a = 0$, $b = 0$, and $c = -1$. The resulting dimensionless group is then

$$\Pi_1 = \frac{V_o}{V_i}$$

which we probably could have written just by inspection of the parameters without having to go through the details of the dimensional analysis process.

The next non-repeating parameter to be non-dimensionalized is the resistance, R. Hence,

$$\left[R\, f^j C^k V_i^l\right] = 1$$

$$\frac{ML^2}{I^2T^3}\left(\frac{1}{T}\right)^j\left(\frac{I^2T^4}{ML^2}\right)^k\left(\frac{M^2L^2}{IT^3}\right)^l = 1$$

$$M^{1-k+2l}L^{2-2k+2l}T^{-3-j+4k-3l}I^{-2+2k-l} = 1$$

Then

$$1-k-2l=0$$

$$2-2k-2l=0$$

$$-3-j+4k-3l=0$$

$$-2+2k-l=0$$

The solution of this system of equations is $j = 1$, $k = 1$, and $l = 0$. The resulting dimensionless group is then

$$\Pi_2 = f\,RC$$

The final non-repeating parameter is the inductance, $\mathcal{L}$. Non-dimensionalizing this, we get

$$\left[\mathcal{L}\, f^m C^n V_i^p\right] = 1$$

$$\frac{ML^2}{I^2T^2}\left(\frac{1}{T}\right)^m\left(\frac{I^2T^4}{ML^2}\right)^n\left(\frac{M^2L^2}{IT^3}\right)^p = 1$$

$$M^{1-n+2p}L^{2-2n+2p}T^{-2-m+4n-3p}I^{-2+2n-p} = 1$$

Then

$$1-n+2p=0$$

$$2-2n+2p=0$$

$$-2-m+4n-3p=0$$

$$-2+2n-p=0$$

The solution of this system of equations is $m = 2$, $n = 1$, and $p = 0$. The resulting dimensionless group is then

$$\Pi_3 = \mathcal{L} f^2 C$$

We have now reduced the original six parameters to three Π-groups (corresponding to $n - r = 6 - 3 = 3$).

Step 6: *Check to see that all proposed Π-groups are dimensionless and write the functional relationship among them in dimensionless form.*

The three groups we have are indeed dimensionless. (We checked again.) According to the Buckingham Pi Theorem, the response function for this circuit can be expressed in the form

$$\Pi_1 = G(\Pi_2, \Pi_3)$$

$$\frac{V_o}{V_i} = G\left(fRC, f^2 \mathcal{L} C\right)$$

Dimensional analysis has revealed the important groups necessary to describe this physical situation. From the second and third Π-groups, we infer that $1/RC$ and $1/(\mathcal{L}C)^{1/2}$ have the same dimension as frequency. The equation above tells us that the response of the circuit will somehow be scaled by these two frequencies. The function G is known as the transfer function for the circuit and can be determined by examining the circuit in detail.

The current through the resistor, i_R, can be related to the voltage across it by means of Ohm's law, viz.,

$$i_R = \frac{v_i - v_o}{R}$$

Similarly, the current through the inductance, $i_{\mathcal{L}}$, can be related to the voltage across it by means of Ampere's law, viz.,

$$i_{\mathcal{L}} = -\frac{1}{\mathcal{L}} \int v_o \, dt$$

and for the current through the capacitor

$$i_C = C \frac{dv_o}{dt}$$

From Figure 10.17, we realize that Kirchoff's law for current requires that the current through the resistor R must be equal to the sum of the currents through the capacitor and the inductor, or

$$i_R = i_C + i_{\mathcal{L}}$$

$$0 = \frac{v_i - v_o}{R} + \frac{1}{\mathcal{L}} \int v_o \, dt - C \frac{dv_o}{dt}$$

This latter equation is easily solved for the sinusoidal steady state case by assuming the time dependence goes as $e^{j\omega t}$ where $j = \sqrt{-1}$. We substitute $v_o = V_o e^{j\omega t}$ and $v_i = V_i e^{j\omega t}$, where V_o and V_i are the amplitudes of the complex voltages. We do this with the understanding that the meaningful solution is the real part of $V_o e^{j\omega t}$. We then perform the time integration and differentiation, and after some algebra, we arrive at the result

$$\frac{v_o}{v_i} = \frac{1}{\left(1 + \frac{R}{j\omega\mathcal{L}} - j\omega RC\right)}$$

Note that the solution has naturally fallen into a dimensionless form. There are three dimensionless groups in the above expression: (V_o/V_i), ($R/\omega\mathcal{L}$), and (ωRC). We have already found two of these dimensionless groups in our dimensional analysis of the circuit. The third, ($R/\omega\mathcal{L}$), can be written as the quotient of two of the dimensionless groups we found earlier,

$$\Pi_4 = \frac{\Pi_2}{\Pi_3} = \frac{f RC}{f^2 \mathcal{L} C} = \frac{R}{f\mathcal{L}}$$

The ratio of the voltage amplitudes can be made by taking the magnitude of the response equation, resulting in

$$\left|\frac{v_o}{v_i}\right| = \frac{V_o}{V_i} = \frac{1}{\sqrt{1+\left(2\pi(fRC) - \frac{1}{2\pi}\frac{fRC}{f^2\mathcal{L}C}\right)^2}}$$

$$|\Pi_1| = \frac{1}{\sqrt{1+\left(2\pi(\Pi_2) - \frac{1}{2\pi}\frac{\Pi_2}{\Pi_3}\right)^2}}$$

Clearly, the response function can be written in a form consistent with the form we determined by dimensional analysis.

10.11 Physical Significance of Dimensionless Groups

From the examples examined above it would appear that the process of dimensional analysis is purely a mathematical formalism; however, there is actually important physical information conveyed by the dimensionless groups that result from this process. In virtually every case, a dimensionless group represents the ratio of certain physical conditions, and the magnitude of this ratio can be helpful in providing information about the behavior of a particular system in several different ways. One of the most common uses of a dimensionless group is to provide information about the system under limiting physical conditions.

For example, we have already seen in Chapter 6 that the dimensionless group known as the Biot number represents the ratio of the internal resistance to conduction heat transfer to the external resistance to convection heat transfer. Then just knowing the magnitude of the Biot number in a particular situation is equivalent to knowing a substantial amount of information about the physical situation. If the Biot number is "small," we know *a priori* that any irreversibilities that occur as a result of the heat transfer process between a solid and the fluid in which it is immersed will occur within the fluid and not within the solid. The solid will behave as though it is experiencing a reversible heat transfer process. Then if we wish to reduce the magnitude of the entropy generated in the heat transfer process as a whole, we know that we need to focus our attention on the fluid. Conversely, if the Biot number is "large," our attention should be directed to the solid since the dominant irreversibility will be located there. Keep in mind, however, that in order to quantify the concepts of "small" and "large" we need additional information about the physical situation. In the case of the Biot number, previous experience has shown that any value of the Biot number less than 0.1 qualifies as "small," and any value of the Biot number greater than 3 qualifies as "large."

Alternatively, this physical information embodied in a dimensionless group can be a guide to the nature of the physical information that we may need to know about a situation in order to characterize it properly. This can be especially helpful in formulating an analytical

description of a physical situation of interest. For example, we have already seen in Chapter 9 that the Reynolds number represents the ratio of the inertial forces acting in a flow field to the viscous forces acting in that same flow field. Thus, when the value of the Reynolds number is "small," viscous forces tend to dominate, and when the Reynolds number is "large," inertial forces tend to dominate. In Chapter 9 we examined in detail a number cases for which the Reynolds number was "small" and viscous forces were dominant. These examples included, among others, flow of a liquid film down an inclined plane, fully developed laminar flow between infinite parallel flat plates, and fully developed laminar flow inside a conduit of circular cross-section. In each of those cases, we saw that because the Reynolds number was "small," the physical situation could be described by a solution of the Navier-stokes equation in which the non-linear inertial terms could be neglected. It was the magnitude of the Reynolds number that was the clue that such a simplification was possible. Unlike the case of the Biot number, however, the value of the Reynolds number in the cases cited could be on the order of 2000 and still be considered "small." Such additional information becomes known only as a result of experimental investigation or other experience.

Finally, the physical information embodied in the dimensionless groups can useful as an aide to interpreting the results of experimental measurements. We have seen in Figure 10.16, for example, that the heat transfer data for flow of gases over a cylinder resulted in a relatively simple correlation between the Nusselt number and the Reynolds number. However, when we replaced the flowing gas with a flowing liquid like water, the simple correlation broke down. Somehow, it became necessary to incorporate the nature of the fluid into the correlation. The dimensionless group known as the Prandtl number offers a means of accomplishing this. As we will see in greater detail in Chapter 11, the Prandtl number represents the ratio of momentum diffusivity to thermal diffusivity. This ratio is important in convection heat transfer because as the flow field is developing, the velocity profile is developing at one rate while the temperature profile is developing at another rate. The process of convection heat transfer is affected by the relative competition between these two rates. For fluids with "small" values of the Prandtl number, e.g., liquid mercury, the temperature profile becomes established almost immediately while the velocity profile will take much longer to develop. For these fluids, the heat transfer process is dominated by simple thermal conduction down the temperature gradient that has formed in the fluid.

Liquids like water and oil, on the other hand, have relatively large values of the Prandtl number. For such fluids involved in convective heat transfer, the velocity profile develops rapidly, but the temperature profile takes a good bit longer to develop. Since the velocity field can have a strong influence on the transfer of energy by virtue of bulk motion of the fluid in convection heat transfer, fluids with larger values of the Prandtl number tend to have enhanced heat transfer by convection at any given value of the Reynolds number. Thus, the value of the Prandtl number enables us to interpret the experimental data more easily in this case. Again, the interpretation of what constitutes "small" and "large" is unique to this case. For convective heat transfer, a value of unity for the Prandtl number is a rough guide to the demarcation between "small" and "large."

Clearly, dimensional analysis and the dimensionless groups that derive from the process are useful tools in thermal-fluids engineering. The nature of thermal-fluid systems is such that dimensionless groups are frequently used to characterize them. Some of these dimensionless groups occur so frequently and have such special meaning in the history and practice of thermal-fluids engineering they have been given special names, often in honor of the research investigator who first used them.

Some of the more commonly used dimensionless groups in thermal-fluids engineering are listed in Table 10.6. Table 10.7 lists the parameters and their dimensions used in defining the groups.

Table 10.6 Dimensionless Groups Frequently Used to Characterize Thermal-Fluid Systems

GROUP	DEFINITION	INTERPRETATION	USE
Biot number	$Bi = \frac{h_c L}{k_s}$	$\frac{\text{internal resistance to conduction}}{\text{external resistance to convection}}$	Transient forced and natural flows
Eckert number	$Ec = \frac{\frac{1}{2}\vartheta^2}{c_P(\Delta T)}$	$\frac{\text{kinetic energy of flow}}{\text{enthalpy difference in boundary layer}}$	High-speed flows
Euler number	$Eu = \frac{\Delta P}{\rho \vartheta^2}$	$\frac{\text{pressure forces}}{\text{inertia forces}}$	Flow through an orifice
Fourier number	$Fo = \frac{kt}{\rho c L^2} = \frac{\alpha t}{L^2}$	$\frac{\text{rate of conduction heat transfer}}{\text{rate of thermal energy storage}}$	Transient conduction
Froude number	$Fr = \frac{\vartheta}{\sqrt{gL}}$	$\frac{\text{velocity}}{\text{surface wave velocity}}$	Flows with free surface effects
Grashof number	$Gr = \frac{\beta(\Delta T) g L^3}{\nu^2}$	$\frac{\text{(buoyancy forces)(inertia forces)}}{\text{(viscous forces)}^2}$	Natural convection
Mach number	$M = \frac{\vartheta}{a}$	$\frac{\text{inertia forces}}{\text{compressibility forces}}$	High-speed flows
Nusselt number	$Nu = \frac{h_c L}{k}$	$\frac{\text{wall temperature gradient}}{\text{bulk temperature gradient}}$	Forced and natural convection
Peclet number	$Pe = \frac{\rho c_P \vartheta L}{k} = \frac{\vartheta L}{\alpha}$	$\frac{\text{heat transfer by conduction}}{\text{heat transfer by convection}}$	Laminar internal flows; creeping external flows
Prandtl number	$Pr = \frac{\mu c_P}{k} = \frac{\nu}{\alpha}$	$\frac{\text{momentum diffusivity}}{\text{thermal diffusivity}}$	Forced and natural convection
Rayleigh number	$Ra = GrPr$	$\frac{\text{buoyancy forces}}{\text{viscous forces}}$	Natural convection
Reynolds number	$Re = \frac{\vartheta L \rho}{\mu} = \frac{\vartheta L}{\nu}$	$\frac{\text{inertia forces}}{\text{viscous forces}}$	Forced flows
Stanton number	$St = \frac{h_c}{\rho c_P \vartheta}$	$\frac{\text{wall heat transfer rate}}{\text{convection heat transfer rate}}$	Forced flows
Weber number	$We = \frac{\rho \vartheta^2 L}{\sigma}$	$\frac{\text{inertia forces}}{\text{surface tension forces}}$	Two-phase flows
Drag coefficient	$C_D = \frac{F_D}{\frac{1}{2}\rho \vartheta^2 A}$	$\frac{\text{drag force}}{\text{dynamic force}}$	External flows
Friction factor	$f = \frac{\Delta P}{\left(\frac{L}{D}\right)\left(\frac{1}{2}\rho \vartheta^2\right)}$	$\frac{\text{externally applied force}}{\text{dynamic force}}$	Internal flows
Lift coefficient	$C_L = \frac{L}{\frac{1}{2}\rho \vartheta^2 A}$	$\frac{\text{lift force}}{\text{dynamic force}}$	External flows
Pressure coefficient	$C_P = \frac{P - P_\infty}{\frac{1}{2}\rho \vartheta^2}$	$\frac{\text{local pressure difference}}{\text{dynamic pressure}}$	External flows
Skin friction coefficient	$C_f = \frac{\tau_s}{\frac{1}{2}\rho \vartheta^2}$	$\frac{\text{skin friction force}}{\text{dynamic force}}$	External flows

NOTE: In the context of our study of the hydrodynamics of vessels, the Froude number merits special mention. The version of the Froude number expressed in Table 10.6 is technically known as the *first* Froude number. It is used both in the analysis of open channel flows and in the analysis of waves about shapes immersed in deep water. In the case of open channel flows, L is the depth of the channel and ϑ is the average velocity of the flow. The Froude number then represents the ratio of the speed of flow to the speed of a small amplitude surface wave (See Section 5.3.). It should be noted that there are citations in the literature that call the square of this quantity, ϑ^2/gL, the Froude number. This latter dimensionless group is technically known as the *second* Froude number and represents the ratio of the inertial force to the gravitational force.

Table 10.7 Parameters Used to Characterize Thermal-Fluid Systems

Symbol	Description	Dimension $\{MLT\Theta\}$
a	acoustic velocity	L/T
A	surface area or projected area of object	L^2
c	specific heat of an incompressible fluid or solid	$L^2/T^2\Theta$
c_P	specific heat at constant pressure of a compressible fluid	$L^2/T^2\Theta$
D	inside diameter of pipe	L
F_D	drag force on an object	ML/T^2
F_L	lift force on an object	ML/T^2
g	acceleration due to gravity	L/T^2
h	convective heat transfer coefficient	$M/T^3\Theta$
k	thermal conductivity of fluid	$ML/T^3\Theta$
k_s	thermal conductivity of solid	$ML/T^3\Theta$
L	characteristic length	L
P	local pressure	M/LT^2
P_∞	fluid pressure in the free stream	M/LT^2
ΔP	pressure drop in the direction of flow	M/LT^2
t	time	T
T_s	surface temperature	Θ
T_∞	fluid temperature in the free stream	Θ
ΔT	$T_s - T_\infty$	Θ
α	thermal diffusivity	L^2/T
β	fluid coefficient of thermal expansion $\{\beta = -(1/\rho)(\partial\rho/\partial T)_T\}$	Θ^{-1}
μ	fluid viscosity	M/LT
ν	kinematic viscosity ($\nu = \mu/\rho$)	L^2/T
ρ	density	M/L^3
σ	surface tension	M/T^2
τ_s	fluid shear stress acting on a solid surface	M/LT^2
ϑ	local or average fluid velocity	L/T

Appendix 10A

Design of a Sailboat with the Aid of Dimensional Analysis

To demonstrate the utility of dimensional analysis in greater detail, we elaborate here on the methods developed by Froude for the design of the hulls of sailing vessels. In an attempt to substantiate Froude's assertion that the drag on ships due to viscous effects could be treated as uncoupled from the drag due to wave generation effects, the British Admiralty measured the drag on full size ships. In 1871, the 172.5 ft long vessel *Greyhound* was towed off Portsmouth. Data from these tests were compared to tests of a one-sixth scale model of *Greyhound*. The tests were not conclusive in proving Froude's method of scaling the data since the drag on the ship was larger than the drag predicted by the model. This disparity between the measurements was ultimately attributed, in part, to the additional roughness of old copper sheathing on the ship's bottom.

Sometime later in 1950 and 1951, further tests were performed using the 190.5 ft *Lucy Ashton* in Gareloch off the Firth of Clyde. To avoid the influence of a vessel towing her, jet engines were used to propel the *Lucy Ashton*. These tests also showed some disagreement with the results derived using Froude's methods. As a result, several sets of correlations for the skin resistance (resistance due to viscous drag) have been developed. One particularly simple and often used correlation of the viscous drag coefficient on a flat plate, C_f, is the ITTC line, given by

$$C_f = \frac{0.075}{\left[\log_{10}(Re) - 2\right]^2}$$

Here C_f is defined not in terms of the length of the hull squared as suggested in our non-dimensionalization shown in Chapter 10, but rather in terms of the wetted surface area of the hull, S, so that

$$C_f \equiv \frac{F_{D,\,flat\ plate}}{\frac{1}{2}\rho v^2 S}$$

Note again that C_f depends only on the Reynolds number and not on the Froude number. The wave drag coefficient and the total drag coefficient are similarly defined.

$$C_w \equiv \frac{F_{wave\ drag}}{\frac{1}{2}\rho v^2 S}$$

where C_w depends only on the Froude number and not on the Reynolds number and

$$C_{tot} \equiv \frac{F_{total}}{\frac{1}{2}\rho v^2 S}$$

Unfortunately, the viscous drag on a flat plate does not completely capture the viscous drag on a hull. The hull has a shape that will result in a behavior of its boundary layer that is different from that of the flat plate. To compensate for this difference, a form resistance coefficient, κ, has been introduced into the simple additive expression for the total drag coefficient that combines the flat plate viscous drag coefficient and the wave drag coefficient, viz.,

$$C_{tot} = (1+\kappa)C_f + C_w$$

The form resistance coefficient is assumed to be constant and the same for both the model and the full-scale prototype. (Note that in the case of the flat plate, $\kappa = 0$.) The form resistance coefficient can be isolated by dividing the above expression by the flat plate drag coefficient or

$$\frac{C_{tot}}{C_f} = (1+\kappa) + \frac{C_w}{C_f}$$

At very low Froude numbers the vessel does not generate many waves and so the drag coefficient due to wave generation, C_w, will approach zero. It has been found that the ratio C_w/C_f approaches zero as the fourth power of the Froude number or

$$\frac{C_{tot}}{C_f} = (1+\kappa) + \frac{C_w}{C_f} \approx (1+\kappa) + b \cdot Fr^4 \quad \text{for } Fr << 1$$

where b is some coefficient. The value of κ can be determined from the y-intercept, $(1 + \kappa)$, of a plot of the ratio C_{tot}/C_f versus Fr^4.

This approach now enables us to scale test data measured on a model in the towing tank to a full-scale prototype. The results of a towing tank test of a one-twentieth scale model of the sailboat *Boreus* is shown in Table 10A.1. *Boreus* has a waterline length of 18.358 m, a waterline beam (widest width of the boat at the waterline) of 3.263 m, and a draft (vertical distance from the waterline to the keel) of 4.047 m. The total mass of the boat is 26857 kg. The total wetted surface area of the vessel is 71.712 m^2 (These data were provided by Prof. Jerome Milgram of the Department of Naval Architecture and Ocean Engineering , MIT.) We will assume the density of water is 998.178 kg, the kinematic viscosity of the water is 1.10×10^{-6} m^2/sec and the gravitational acceleration 9.806 m/sec^2. The length of the model is 18.358/20 = 0.9179 m. The surface area of the model is $71.712/(20)^2 = 0.17928$ m^2.

Table 10A.1 Drag Force on Model of *Boreus* in the Towing Tank

Model velocity (m/s)	Total drag force on the model (N)
1.1898	0.679
1.9296	1.779
2.4495	3.033
2.8280	4.694
3.2671	9.226
3.4213	11.385
1.4856	1.035
2.2288	2.445
2.5278	3.265
2.8998	5.214
3.5689	13.460
1.6360	1.245
2.2992	2.625
2.5998	3.502
2.9713	5.830
3.7170	15.527
1.7804	1.481
2.3790	2.841
2.0790	2.069
2.6760	3.813
2.7498	4.181
3.1182	7.343

In applying this new approach to the scaling of towing tank test data, the first step is to establish the total coefficient of drag, the Reynolds number and the Froude number for the model tests. In Table 10A.1, the first velocity is 1.1898 m/sec so that the Froude number for this particular test of the model is

$$(Fr)_{model} = \frac{\vartheta}{\sqrt{gL}} = \frac{1.1898 \text{ m/sec}}{\sqrt{(9.806 \text{ m/sec}^2)(0.9179 \text{ m/sec})}} = 0.3966$$

The corresponding drag coefficient for the model is

$$(C_{tot})_{model} = \frac{F_{total}}{\frac{1}{2}\rho\vartheta^2 S} = \frac{0.679 \text{ N}}{\frac{1}{2}(998.178 \text{ kg/m}^3)(1.1898 \text{ m/sec})^2 (0.17928 \text{ m}^2)} = 0.00536$$

The Reynolds number for this velocity is

$$(Re)_{model} = \frac{\rho\vartheta L}{\mu} = \frac{\vartheta L}{\nu} = \frac{(1.1898 \text{ m/sec})(0.9179 \text{ m})}{1.10 \text{ x } 10^{-6} \text{ kg/m sec}} = 9.93 \text{ x } 10^5$$

For a flat plate with the same length and wetted surface area as the model and towed at the same velocity as the model, the viscous drag coefficient is

$$(C_f)_{model} = \frac{0.075}{[\log_{10}(Re) - 2]^2} = \frac{0.075}{[\log_{10}(9.93 \text{ x } 10^5) - 2]^2} = 4.69 \text{ x } 10^{-3}$$

These results and the results of similar calculations for the other data points from the model tests are included in Table 10A.2. The last two columns of this table include the ratio $(C_{tot}/C_f)_{model}$ and Fr^4.

Table 10A.2 Dimensionless Drag Data for the Model of the Sailboat *Boreus*

ϑ_{model} (m/s)	$(F_{total})_{model}$ (N)	$(Fr)_{model}$	$(Re)_{model}$	$(C_{tot})_{model}$	$(C_f)_{model}$	$(C_{tot}/C_f)_{model}$	$(Fr^4)_{model}$
1.1898	0.679	0.3966	$9.93 \text{ x } 10^5$	0.00536	$4.69 \text{ x } 10^{-3}$	1.142	0.0247
1.9296	1.779	0.6432	$1.61 \text{ x } 10^6$	0.00534	$4.24 \text{ x } 10^{-3}$	1.260	0.1711
2.4495	3.033	0.8165	$2.04 \text{ x } 10^6$	0.00536	$4.04 \text{ x } 10^{-3}$	1.400	0.4444
2.8280	4.694	0.9426	$2.36 \text{ x } 10^6$	0.00656	$3.92 \text{ x } 10^{-3}$	1.673	0.7895
3.2671	9.226	1.0890	$2.73 \text{ x } 10^6$	0.00966	$3.81 \text{ x } 10^{-3}$	2.534	1.4063
3.4213	11.385	1.1404	$2.85 \text{ x } 10^6$	0.01087	$3.78 \text{ x } 10^{-3}$	2.877	1.6912
1.4856	1.035	0.4952	$1.24 \text{ x } 10^6$	0.00524	$4.48 \text{ x } 10^{-3}$	1.171	0.0601
2.2288	2.445	0.7429	$1.86 \text{ x } 10^6$	0.00550	$4.11 \text{ x } 10^{-3}$	1.337	0.3046
2.5278	3.265	0.8426	$2.11 \text{ x } 10^6$	0.00571	$4.01 \text{ x } 10^{-3}$	1.424	0.5040
2.8998	5.214	0.9666	$2.42 \text{ x } 10^6$	0.00693	$3.90 \text{ x } 10^{-3}$	1.776	0.8728
3.5689	13.460	1.1896	$2.98 \text{ x } 10^6$	0.01181	$3.75 \text{ x } 10^{-3}$	3.152	2.0025
1.6360	1.245	0.5453	$1.37 \text{ x } 10^6$	0.00520	$4.39 \text{ x } 10^{-3}$	1.186	0.0884
2.2992	2.625	0.7664	$1.92 \text{ x } 10^6$	0.00555	$4.09 \text{ x } 10^{-3}$	1.357	0.3449
2.5998	3.502	0.8666	$2.17 \text{ x } 10^6$	0.00579	$3.99 \text{ x } 10^{-3}$	1.452	0.5639
2.9713	5.830	0.9904	$2.48 \text{ x } 10^6$	0.00738	$3.88 \text{ x } 10^{-3}$	1.900	0.9621
3.7170	15.527	1.2389	$3.10 \text{ x } 10^6$	0.01256	$3.72 \text{ x } 10^{-3}$	3.379	2.3561
1.7804	1.481	0.5934	$1.49 \text{ x } 10^6$	0.00522	$4.31 \text{ x } 10^{-3}$	1.211	0.1240
2.3790	2.841	0.7930	$1.99 \text{ x } 10^6$	0.00561	$4.06 \text{ x } 10^{-3}$	1.382	0.3954
2.0790	2.069	0.6930	$1.73 \text{ x } 10^6$	0.00535	$4.17 \text{ x } 10^{-3}$	1.282	0.2306
2.6760	3.813	0.8920	$2.23 \text{ x } 10^6$	0.00595	$3.97 \text{ x } 10^{-3}$	1.500	0.6330
2.7498	4.181	0.9166	$2.29 \text{ x } 10^6$	0.00618	$3.94 \text{ x } 10^{-3}$	1.567	0.7057
3.1182	7.343	1.0393	$2.60 \text{ x } 10^6$	0.00844	$3.85 \text{ x } 10^{-3}$	2.194	1.1669

These values are plotted in Figure 10A.1 for small values of the Froude number. The best fit to these data is the straight line

$$\left(\frac{C_{tot}}{C_f}\right)_{model} = 1.1262 + 0.6902\left(Fr_{model}\right)^4$$

Then the y-intercept of this line is1.1262; consequently, for this hull, the form resistance coefficient, κ, has a value of 0.1262.

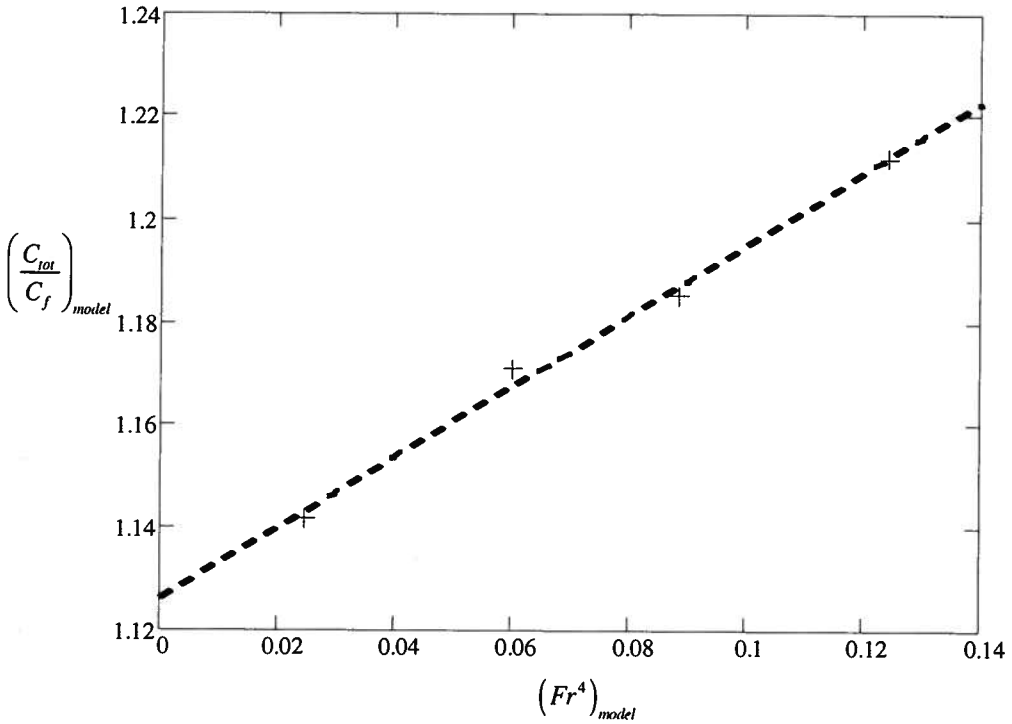

Figure 10A.1 Evaluation of the Form Resistance Coefficient, κ, from Dimensionless Drag Data

We are now in a position to determine C_w as a function of the Froude number. From the expression for the total drag, we have for the results of towing the model with the lowest velocity

$$C_w = C_{tot} - (1+\kappa)C_f = 0.00536 - (1+0.1262)(0.00469) = 7.31 \text{ x } 10^{-5}$$

which corresponds to a Froude number for the model of 0.3966. The full-scale-boat velocity, ϑ_{fs}, associated with this Froude number is

$$\vartheta_{fs} = Fr\sqrt{gL} = 0.3966\sqrt{(9.806 \text{ m/sec}^2)(18.358 \text{ m})} = 5.321 \text{ m/sec}$$

The Reynolds number corresponding to the full scale vessel traveling at this velocity is

$$Re_{fs} = \frac{\vartheta L}{\nu} = \frac{(5.321 \text{ m/sec})(18.358 \text{ m})}{1.10 \text{ x } 10^{-6} \text{ m}^2/\text{sec}} = 8.88 \text{ x } 10^7$$

Then the friction drag coefficient on the full scale vessel becomes

$$\left(C_f\right)_{fs} = \frac{0.075}{\left[\log_{10}\left(Re_{fs}\right) - 2\right]^2} = \frac{0.075}{\left[\log_{10}\left(8.88 \text{ x } 10^7\right) - 2\right]^2} = 2.12 \text{ x } 10^{-3}$$

The total drag coefficient on the full scale vessel traveling at this velocity (5.321 m/sec) becomes

$$(C_{tot})_{fs} = (1+\kappa)(C_f)_{fs} + C_w = 1.1262(2.12 \text{ x } 10^{-3}) + 7.31 \text{ x } 10^{-5} = 2.46 \text{ x } 10^{-3}$$

and the total drag force acting on the full scale vessel can be calculated from the definition of the total drag coefficient,

$$(F_{total})_{fs} = (C_{tot})_{fs}\left(\tfrac{1}{2}\rho \vartheta^2 S\right) = \frac{(2.46 \text{ x } 10^{-3})(998.178 \text{ kg/m}^3)(5.321 \text{ m/sec})^2 (71.712 \text{ m}^2)}{2}$$

$$(F_{total})_{fs} = 2.49 \text{ x } 10^3 \text{ N}$$

These values and the corresponding values for the other velocities are entered in Table 10A.3.

Table 10A.3 Drag Force on the Full-Scale Vessel

Fr	C_w	ϑ_{fs} (m/s)	Re_{fs}	$(C_f)_{fs}$	(C_{tot})	$(F_{total})_{fs}$ (N)
0.3966	$7.31 \text{ x } 10^{-5}$	5.321	$8.88 \text{ x } 10^{7}$	$2.12 \text{ x } 10^{-3}$	$2.46 \text{ x } 10^{-3}$	$2.49 \text{ x } 10^{3}$
0.6432	$5.68 \text{ x } 10^{-4}$	8.630	$1.44 \text{ x } 10^{8}$	$1.98 \text{ x } 10^{-3}$	$2.79 \text{ x } 10^{-3}$	$7.45 \text{ x } 10^{3}$
0.8165	$1.10 \text{ x } 10^{-3}$	10.955	$1.83 \text{ x } 10^{8}$	$1.91 \text{ x } 10^{-3}$	$3.26 \text{ x } 10^{-3}$	$1.40 \text{ x } 10^{4}$
0.9426	$2.14 \text{ x } 10^{-3}$	12.647	$2.11 \text{ x } 10^{8}$	$1.88 \text{ x } 10^{-3}$	$4.25 \text{ x } 10^{-3}$	$2.44 \text{ x } 10^{4}$
1.0890	$5.37 \text{ x } 10^{-3}$	14.611	$2.44 \text{ x } 10^{8}$	$1.84 \text{ x } 10^{-3}$	$7.44 \text{ x } 10^{-3}$	$5.68 \text{ x } 10^{4}$
1.1404	$6.62 \text{ x } 10^{-3}$	15.301	$2.55 \text{ x } 10^{8}$	$1.83 \text{ x } 10^{-3}$	$8.67 \text{ x } 10^{-3}$	$7.27 \text{ x } 10^{4}$
0.4952	$1.99 \text{ x } 10^{-4}$	6.644	$1.11 \text{ x } 10^{8}$	$2.05 \text{ x } 10^{-3}$	$2.51 \text{ x } 10^{-3}$	$3.97 \text{ x } 10^{3}$
0.7429	$8.67 \text{ x } 10^{-4}$	9.968	$1.66 \text{ x } 10^{8}$	$1.94 \text{ x } 10^{-3}$	$3.05 \text{ x } 10^{-3}$	$1.08 \text{ x } 10^{4}$
0.8426	$1.19 \text{ x } 10^{-3}$	11.305	$1.89 \text{ x } 10^{8}$	$1.90 \text{ x } 10^{-3}$	$3.34 \text{ x } 10^{-3}$	$1.53 \text{ x } 10^{4}$
0.9666	$2.54 \text{ x } 10^{-3}$	12.968	$2.16 \text{ x } 10^{8}$	$1.87 \text{ x } 10^{-3}$	$4.64 \text{ x } 10^{-3}$	$2.79 \text{ x } 10^{4}$
1.1896	$7.59 \text{ x } 10^{-3}$	15.961	$2.66 \text{ x } 10^{8}$	$1.82 \text{ x } 10^{-3}$	$9.64 \text{ x } 10^{-3}$	$8.79 \text{ x } 10^{4}$
0.5453	$2.61 \text{ x } 10^{-4}$	7.317	$1.22 \text{ x } 10^{8}$	$2.02 \text{ x } 10^{-3}$	$2.54 \text{ x } 10^{-3}$	$4.87 \text{ x } 10^{3}$
0.7664	$9.46 \text{ x } 10^{-4}$	10.282	$1.72 \text{ x } 10^{8}$	$1.93 \text{ x } 10^{-3}$	$3.12 \text{ x } 10^{-3}$	$1.18 \text{ x } 10^{4}$
0.8666	$1.30 \text{ x } 10^{-3}$	11.627	$1.94 \text{ x } 10^{8}$	$1.90 \text{ x } 10^{-3}$	$3.43 \text{ x } 10^{-3}$	$1.66 \text{ x } 10^{4}$
0.9904	$3.01 \text{ x } 10^{-3}$	13.288	$2.22 \text{ x } 10^{8}$	$1.86 \text{ x } 10^{-3}$	$5.10 \text{ x } 10^{-3}$	$3.23 \text{ x } 10^{4}$
1.2389	$8.37 \text{ x } 10^{-3}$	16.623	$2.77 \text{ x } 10^{8}$	$1.81 \text{ x } 10^{-3}$	$1.04 \text{ x } 10^{-2}$	$1.03 \text{ x } 10^{5}$
0.5934	$3.67 \text{ x } 10^{-4}$	7.962	$1.33 \text{ x } 10^{8}$	$2.00 \text{ x } 10^{-3}$	$2.62 \text{ x } 10^{-3}$	$5.94 \text{ x } 10^{3}$
0.7930	$1.04 \text{ x } 10^{-3}$	10.639	$1.78 \text{ x } 10^{8}$	$1.92 \text{ x } 10^{-3}$	$3.20 \text{ x } 10^{-3}$	$1.30 \text{ x } 10^{4}$
0.6930	$6.50 \text{ x } 10^{-4}$	9.298	$1.55 \text{ x } 10^{8}$	$1.96 \text{ x } 10^{-3}$	$2.85 \text{ x } 10^{-3}$	$8.83 \text{ x } 10^{3}$
0.8920	$1.48 \text{ x } 10^{-3}$	11.968	$2.00 \text{ x } 10^{8}$	$1.89 \text{ x } 10^{-3}$	$3.61 \text{ x } 10^{-3}$	$1.85 \text{ x } 10^{4}$
0.9166	$1.74 \text{ x } 10^{-3}$	12.298	$2.05 \text{ x } 10^{8}$	$1.88 \text{ x } 10^{-3}$	$3.86 \text{ x } 10^{-3}$	$2.09 \text{ x } 10^{4}$
1.0393	$4.11 \text{ x } 10^{-3}$	13.945	$2.33 \text{ x } 10^{8}$	$1.85 \text{ x } 10^{-3}$	$6.19 \text{ x } 10^{-3}$	$4.31 \text{ x } 10^{4}$

Figure 10A.2 shows the relationship between the total drag force, $(F_{tot})_{fs}$, and the velocity, ϑ_{fs}, for the full scale vessel. The data are clearly nonlinear, but they could be used in graphical form to determine the drag force at any velocity. For computational purposes, it is often more convenient to develop an empirical relationship between these data. In the particular case at hand, one convenient way to do this is to non-dimensionalize the drag force with respect to a specific condition. For convenience, let us choose the condition of the vessel for which the velocity is ϑ_{fs} = 5.321 m/sec and the total drag force is $(F_{tot})_{fs}$ = 2490 N. Figure 10A.3 shows the dimensionless values of force that result from dividing all values of force predicted by the modified Froude approach by the selected value. The data are presented in logarithmic form as a way of "compressing" the data and developing a simple curve fit. As shown in Figure 10A.3, the data for the dimensionless drag force can be fit approximately by the equation

$$\left(\frac{F_{tot}}{2490 \text{ N}}\right) = (0.1582)\exp(0.3343\vartheta_{fs})$$

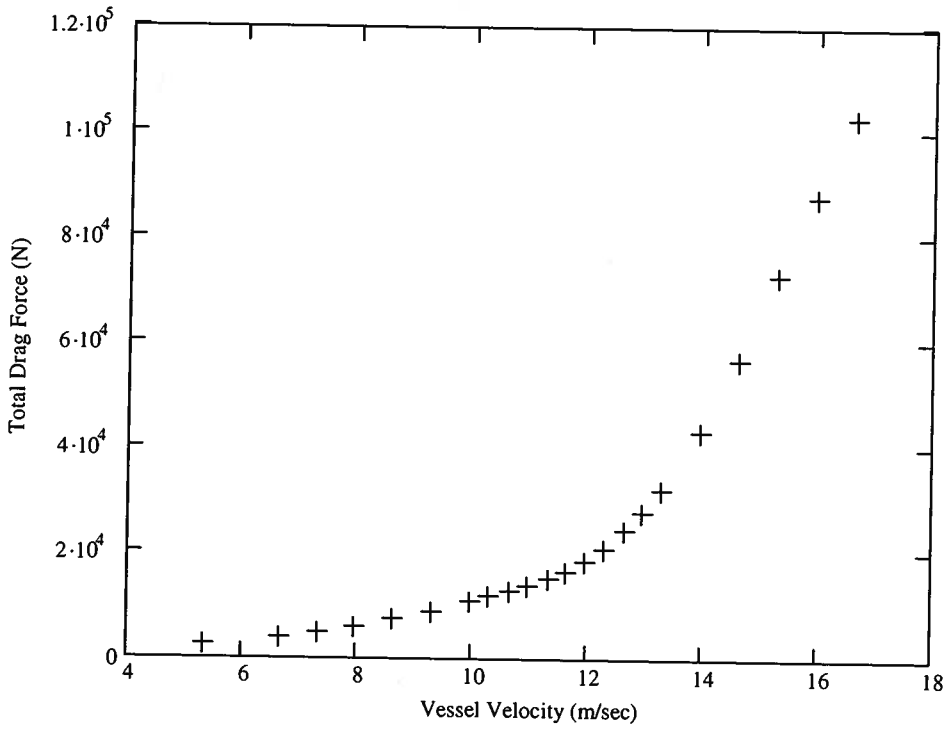

Figure 10A.2 Total Drag Force Acting on the Vessel

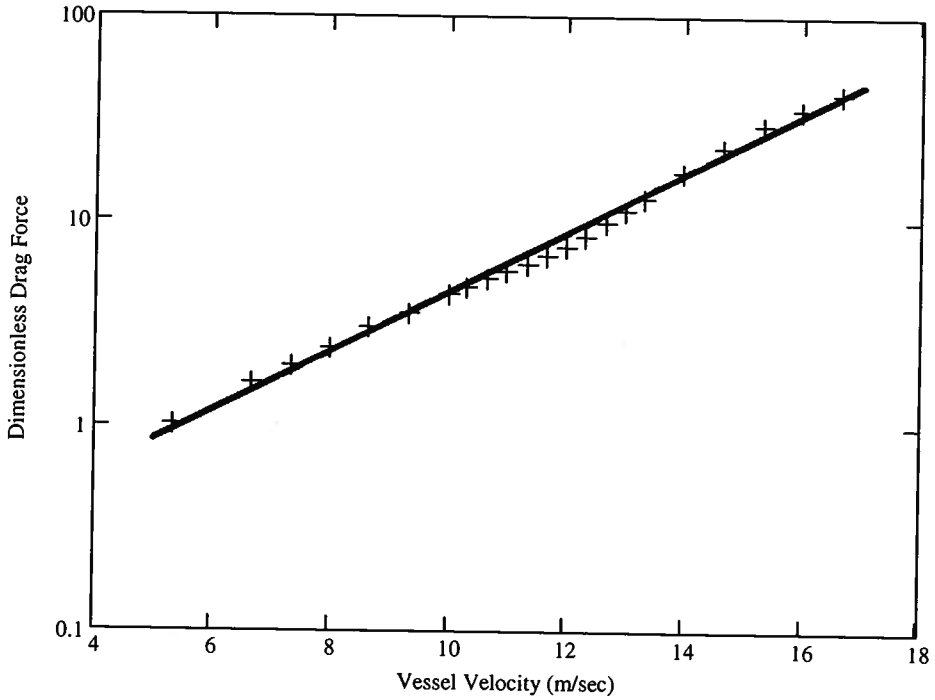

Figure 10A.3 Dimensionless Drag Force

We have chosen to non-dimensionalize the force data in this manner rather than using the drag coefficient because the curve fit given above is simpler than the fit that would be required for the drag coefficient data. The principle is the same in both cases.

As an example of the way in which these results could be used, we can determine the power required to drive the vessel at some particular velocity such as ϑ_{fs} = 9 m/sec. From the

curve fit, we can determine the propulsive force (equal to the drag force at constant vessel velocity) necessary to drive the full scale hull at the selected velocity.

$$(F_{tot})_{fs} = (2940\text{ N})(0.1582)\exp\left[(0.1582)(9\text{ m/sec})\right] = 7983.5\text{ N}$$

The net power required to drive this hull at the selected velocity is simply the product of the force and the velocity or

$$\wp = (F_{tot})_{fs}\left(\vartheta_{fs}\right) = (7983.5\text{ N})(9\text{ m/sec}) = 71.85\text{ kW}$$

Because there are many inefficiencies in the propulsion system (transmission and propeller efficiency, additional drag due to appendages supporting the propeller, etc.), this power is significantly smaller than the power output of the engine required to drive this hull at $\vartheta_{fs} = 9$ m/sec.

Appendix 10B

Strouhal Vortices, the Karman Vortex Street, and the Myth of "Galloping Gertie"

In Chapter 9, we saw that the flow of a fluid like air past bluff bodies such as vehicles and stationary structures generated a wake downstream of the object. We observed that the shape of the wake was a function of the Reynolds number of the flow based upon the incident velocity, $\vec{v}$, of the fluid and some characteristic length of the bluff body. For our purposes here, we wish to consider flow past a cylinder of infinite extent, oriented so that the axis of the cylinder is perpendicular to the plane of the page with the flow of the fluid from left to right. We are interested in flows with Reynolds numbers (based upon the diameter of the cylinder, D) in the range of $50 < Re_D < 10^7$, but especially in the range $600 < Re_D < 6000$. Figure 10B.1 is a photograph of such a flow at a Reynolds number of 120.

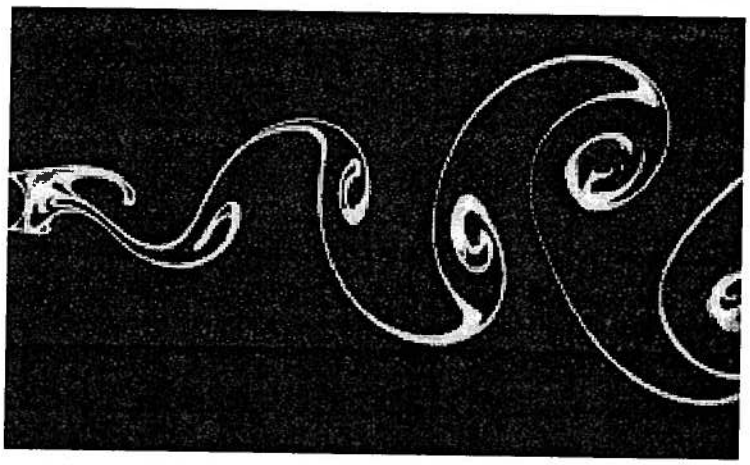

Figure 10B.1 Karman Vortex Street Downstream of a Cylinder, $Re = 120$

Consider a streamline that lies in the horizontal plane containing the axis of the cylinder. The point where this streamline contacts the cylinder is known as the stagnation point. As a fluid particle flows toward the front face of the cylinder, the pressure in the fluid particle rises from the free stream pressure to the stagnation pressure. The high fluid pressure near the stagnation point drives the flow around the cylinder as the boundary layer develops on the forward face. As the flow proceeds away from the stagnation point, the pressure in the free stream decreases as the flow accelerates around the convex shape of the cylinder. When the flow reaches the position where the vertical plane containing the axis of the cylinder intersects the surface of the cylinder (at a point 90° from the stagnation point), the fluid velocity is at a maximum. As the flow tries to proceed down the back face of the cylinder, it decelerates and its pressure increases in an attempt to recover the stagnation pressure at the point diametrically opposite the stagnation point (180° from the stagnation point). However, the skin friction due to viscous shear in the boundary layer decelerates the fluid even faster than the flow geometry would dictate. This combination of retarding forces acting on the flow causes the boundary layer to separate from the surface of the cylinder surface and form two shear layers, one from the top of the cylinder, the other from the bottom.

These shear layers trail behind the cylinder and form the boundaries of the wake. The fluid in the innermost portion of the shear layers that is in contact with the cylinder moves much more slowly than the outermost portion of the shear layers due to the action of viscosity near the surface. This causes the shear layers to roll into the near wake. In this region, they fold up on each other and coalesce into discrete, swirling vortices that alternate positions from the top and the bottom of the cylinder. As shown in Figure 10B.1, a regular pattern of oscillating vortices, called a vortex street, trails the cylinder in the wake. These vortices interact with the cylinder, and because they alternate position from top to bottom, the pressure, and, hence, the forces acting on the top and bottom halves of the cylinder alternate in magnitude causing the net vertical force acting on the cylinder to be alternately positive and negative. This alternating force can cause the cylinder to vibrate transverse to the flow direction depending upon the relative magnitude of the restoring force produced by the elastic behavior of the material of the cylinder. These vibrations can be in the audible portion of the spectrum producing a "hum" or "singing" of the cylinder as in the case of wires stretched between poles in a wind. The vortex street is also the cause of the "chattering" of Venetian blinds in front of an open window on a breezy day. Furthermore, these vortex streets can occur on a global scale as the atmosphere moves over obstacles such as islands as seen in the atmospheric cloud patterns photographed from satellites.

Vortex streets have been the subject of study for centuries. The audible sound induced by a vortex street acting on the wires of an Aeolian harp has been known since ancient times. According to legend, King David hung his harp in an open window and heard it played by the wind. Around the turn of the 16th century, as part of an effort associated with the design of a bridge, Leonardo da Vinci (1452 – 1519) sketched a row of vortices in the wake of a bridge pile in a stream. In 1878, V. Strouhal found that the Aeolian tones generated by a wire in the wind were proportional to the wind speed divided by the wire diameter. He noticed that the sound greatly increased when the natural tones of the wire coincided with the Aeolian tones. In 1879, Lord Rayleigh (1842 – 1919) found that a violin string in a chimney draft vibrated primarily transverse to the flow, rather than in the direction of the flow. When the frequency of this oscillation matched the frequency to which the string was tuned, an Aeolian tone resulted. (The fundamental is never sounded, only the overtone series.) In fact, it was Lord Rayleigh who coined the term "Aeolian tones" after the Greek god of the wind, Aeolus. In 1908, Henri Benard observed that the periodicity of the wake of a cylinder was associated with vortex formation, but it was not until 1912 that Theodore von Karman (1881 – 1963) developed a full quantitative description of the stable street of staggered vortices that forms behind a cylinder in the wake of its flow. The individual vortices are known as *Strouhal vortices* and the phenomenon of the stable vortex street is known as a *Karman vortex street.*

A full analytical description of the Karman vortex street in the wake of a cylinder requires the solution of the time-dependent form of the Navier-Stokes equation, and there are many examples in the literature in which this phenomenon has been addressed by both analytical methods and the methods of computational fluid dynamics. However, it is possible to investigate the importance of the various parameters through dimensional analysis. Let us denote the characteristic frequency of the appearance and disappearance of the vortices by ω, and let us apply the process of dimensional analysis to the description of this situation.

Step 1: *List and count the n parameters required to describe the physical situation. If any important parameters are missing, dimensional analysis will fail.*

In addition to the frequency ω, the first parameters of interest are the velocity of the fluid ϑ and the diameter of the "wire" (cylinder) D. The other relevant parameters in this situation are related to the identity of the fluid, namely the density, ρ, and the viscosity, μ. Temperature is not relevant in this situation although it would be if we were concerned with the heat transfer process associated with the shed of vortices from the cylinder.

Step 2: *List the dimensions of each variable according to M, L, T, and Θ.*

$$[\omega]=\frac{1}{T},\quad [\vartheta]=\frac{L}{T},\quad [D]=L,\quad [\rho]=\frac{M}{L^3},\quad [\mu]=\frac{ML}{T}$$

Step 3: *Find the value of r. Initially guess r to be equal to the number of different dimensions present and then make sure that there are r parameters that do not form a Π-group. If this is unsuccessful, reduce r by one and look again.*

Since there are three dimensions present: M, L, and T, we first guess $r = 3$, and we hope to reduce the five parameters down to two Π-groups, $n - r = 5 - 3 = 2$. Let us choose D, μ, and ϑ as the 3 potential repeating parameters. We need to ensure that they do not form a Π-group themselves. Checking, we get

$$\left[D^a\mu^b\vartheta^c\right]=1$$

$$L^a\left(\frac{M}{LT}\right)^b\left(\frac{L}{T}\right)^c=1$$

$$M^bL^{a-b+c}T^{-b-c}=1$$

Then

$$b=0$$

$$a-b+c=0$$

$$-b-c=0$$

The solution of this system of equations is $a = 0$, $b = 0$, and $c = 0$. Then the parameters D, μ, and ϑ, are dimensionally independent; hence, $r = 3$.

Step 4: *Select r parameters which do not form a Π-group among themselves. These parameters are the repeating parameters that will appear in all the Π-groups.*

We shall select D, μ, and ϑ, as the repeating parameters since they have already been shown to be dimensionally independent.

Step 5: *Select one of the remaining parameters that is not one of the r repeating parameters and non-dimensionalize that parameter using the r repeating parameters. Repeat the procedure until all the remaining parameters are non-dimensionalized. There should now be n - r Π-groups.*

There are two remaining parameters ω and ρ to be non-dimensionalized. Starting with ω, we get

$$\left[\omega\vartheta^dD^e\mu^f\right]=1$$

$$\left(\frac{1}{T}\right)\left(\frac{L}{T}\right)^d\left(L^e\right)\left(\frac{M}{LT}\right)^f=1$$

$$M^fL^{d+e-f}T^{-1-d-f}=1$$

Then

$$f = 0$$
$$d + e - f = 0$$
$$-1 - d - f = 0$$

The solution of this system of equations gives $d = -1$, $e = 1$, and $f = 0$. Then the first dimensionless group is

$$\Pi_1 = \frac{\omega D}{\vartheta}$$

This dimensionless group is known as the Strouhal number, *Sr*, and represents the ratio of the vortex frequency to the characteristic frequency of the flow geometry.

The second dimensionless group can be written by inspection since we have seen it so many times before. It is just the Reynolds number.

$$\left[\rho \vartheta^g D^h \mu^i\right] = 1$$
$$g = 1, \quad h = 1, \quad i = -1$$
$$\Pi_2 = \frac{\vartheta D \rho}{\mu} = Re$$

Step 6: *Check to see that all proposed Π-groups are dimensionless and write the functional relationship among them in dimensionless form.*

The two groups we have are indeed dimensionless (We checked again.). According to the Buckingham Pi Theorem, the experimental results for the characteristic frequency of the vortex street can be expressed in the form

$$Sr = G(Re)$$

Once again, this is as far as dimensional analysis can take us. It is now necessary to employ experimental methods to find the functional form of *G*. Figure 10B.2 shows the values for the modified Strouhal number (frequency in Hz instead of radians/sec) determined by experiment over a wide range of Reynolds numbers. Note that except for the lowest values of the Reynolds number, the value of the Strouhal number is nearly constant at a value of approximately $Sr \approx 0.21$. Then in the case of a wire stretched between two poles in the wind, the frequency of vibration increases as the wind velocity increases.

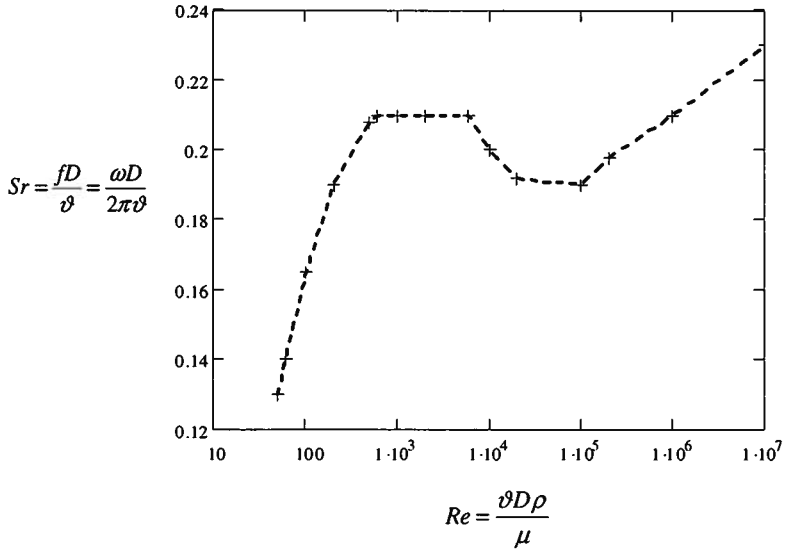

Figure 10B.2 Modified Strouhal Number for Flow Past a Circular Cylinder

Example 10BE.1: Suppose we wish to make an Aeolian harp using a wire of diameter D = 1 mm. If the audible spectrum is considered to be frequencies in the range of 20 Hz $< f <$ 20 kHz, what wind velocity would be required to produce the lowest frequency sound in the audible range? If the highest expected wind velocity is ϑ = 22 m/sec (nearly 50 mph), what is the highest note likely to be produced? Assume that the atmospheric conditions are ρ = 1.177 kg/m^3 and μ = 1.85 x 10^{-5} kg/m sec.

Solution: The lowest value of Reynolds number at which the Karman vortex street can exist is approximately Re = 50 for which Sr = 0.13 (See Figure 10B.2.). Then the air velocity corresponding to this value of the Reynolds number is

$$\vartheta = \frac{\mu(Re)}{D\rho} = \frac{(1.85 \text{ x } 10^{-5} \text{ kg/m sec})(50)}{(0.001 \text{ m})(1.177 \text{ kg/m}^3)} = 0.786 \text{ m/sec}$$

Then the frequency of the lowest note would be

$$f = \frac{\vartheta Sr}{D} = \frac{(0.786 \text{ m/sec})(0.13)}{(0.001 \text{ m})} = 102.18 \text{ Hz}$$

This is well within the audible range and nearly corresponds to the note $G^{\#}{}_2/A^{b}{}_2$. For the highest note, we have for the Reynolds number

$$Re = \frac{\vartheta D\rho}{\mu} = \frac{(22 \text{ m/sec})(0.001 \text{ m})(1.177 \text{ kg/m}^3)}{(1.85 \text{ x } 10^{-5})} = 1399.7$$

From Figure 10B.2, this value of the Reynolds number corresponds to a Strouhal number of Sr = 0.21. Then the frequency is

$$f = \frac{\vartheta Sr}{D} = \frac{(22 \text{ m/sec})(0.21)}{(0.001 \text{ m})} = 4620 \text{ Hz}$$

This frequency is within the audible spectrum and nearly corresponds to the note D_8.

The vibrations induced in structural elements like cylinders, I-beams, and other shapes by the Karman vortex street can be quite dramatic, even apart from the Aeolian tones. In some cases, the vibration of the structure producing the Karman vortex can be catastrophic and lead to ultimate failure if it corresponds to the natural resonant frequency of the structure. An example often given, albeit erroneously, of this phenomenon is the destruction of the Tacoma Narrows Bridge, euphemistically known as "Galloping Gertie," due to gale force cross-winds (18.78 m/sec; 8 on the Beaufort Scale) on November 7, 1940. There are many websites such as:

http://cee.carleton.ca/Exhibits/Tacoma_Narrows/DSmith/photos.html
http://www.nwrain.net/~newtsuit/recoveries/narrows/gg.htm
http://www.enm.bris.ac.uk/research/nonlinear/tacoma/tacnarr.mpg

that show the breakup of the bridge (See Figure 10B.2.), and there have been many references to this spectacular failure both in physics and engineering texts as well as in articles on bridge design.

Unfortunately, many of these treatments are misleading. The facts of the incident are much more complex and quite different from what these reports claim. There has been a natural tendency to oversimplify the situation and to view it as an example of forced resonance in which the vibration of the structure is due to a Karman vortex street down-wind of the bridge deck. Von Karman, himself, was a member of the board of inquiry convened after the failure, and he

showed that the final destructive oscillation at $f_d = 0.2$ Hz was at a frequency quite different from the characteristic frequency of the vortex street. The bridge deck was a simple rectangular box-like structure with dimension $D = 2.438$ m transverse to the flow in the vertical direction and $L = 11.887$ m measured in the direction of flow. For this geometry, the Strouhal number is $Sr = 0.12$ (See Table 10-16, p. 313, *Applied Fluid Dynamics Handbook*, by Robert D. Blevins, Krieger Publishing Co., Malabar, FL, 1992.) Thus for a wind velocity of $\vartheta = 18.78$ m/sec, the characteristic frequency of the vortex street, f_v, is

$$f_v = \frac{\vartheta \cdot Sr}{D} = \frac{(18.78 \text{ m/sec})(0.12)}{2.438 \text{ m}} = 0.924 \text{ Hz} \approx 1 \text{ Hz}$$

Thus, since $f_v \approx 5f_d$, it is reasonable to conclude that the Karman vortex street was not the cause of the failure. To be sure there was a vortex street that induced oscillations in the bridge deck, but these were vertical in nature and began essentially from the day the bridge was opened to traffic on July 1, 1940. In fact, these vertical oscillations were the reason the bridge earned the sobriquet "Galloping Gertie."

There is an excellent review of the aeroelastic behavior of the bridge by Billah and Scanlan (*American Journal of Physics*, Vol. 59, No. 2, February, 1991, pp. 118-124.) They attribute the failure to "an aerodynamically induced condition of *self-excitation* or 'negative damping' in a torsional degree of freedom. This is a phenomenon known as *flutter* that occurs in aircraft structures as well as in stationary structures subject to wind loading. In contrast to the case of aircraft, the air velocities around stationary structures are relatively low and do not influence the vibrational modes that are excited or the frequencies of the ensuing oscillations. As the wind velocities around these structures increase, however, they can cause the normal damping mechanism to reverse sign. This is the *self-excitation* phenomenon characteristic of *flutter* that leads to an unstable oscillation that gradually grows in amplitude. In a sense, flutter is an accident waiting to happen, and it is the job of the thermal-fluids engineer to determine the conditions that will precipitate it. These conditions can be determined by a combination of analysis and experimentation.

The span of the bridge was in three parts with two towers located 335.3 m from each shore. The center span was 853.4 m in length. As Figure 10B.2 clearly shows, it was the center span that failed in a torsional mode. For the purposes of analysis, let us consider a unit length of the center span of the bridge. If α represents the angular displacement of the cross-section of the deck from its equilibrium position, the equation of motion of a unit length of deck in torsion is given by

$$\Im(\alpha, \dot{\alpha}) = I\left\{\ddot{\alpha} + 2\zeta_\alpha \omega_n \dot{\alpha} + \omega_n{}^2 \alpha\right\} \qquad (10B.1)$$

where I is the moment of inertia per unit span about the center of rotation of the cross-section, ζ is the damping coefficient (logarithmic decrement/2π), ω_n is the natural torsional frequency, C_α is the effective spring constant per unit span, and $\Im$ is the torque exciting the torsional oscillation due to aerodynamic loading. Also

$$\dot{\alpha} = \frac{d\alpha}{dt}, \qquad \ddot{\alpha} = \frac{d^2\alpha}{dt^2}, \qquad \omega_n = \sqrt{\frac{C_a}{I}}$$

In equation (10B.1), the moment of inertia per unit span, I, is the analog of the mass per unit span, and the angular displacement, α, is the analog of the linear displacement in Newton's Second Law of Motion. The first term on the right-hand side of equation (10B.1) represents the inertia of the element, the second term represents the damping of the element, and the third term

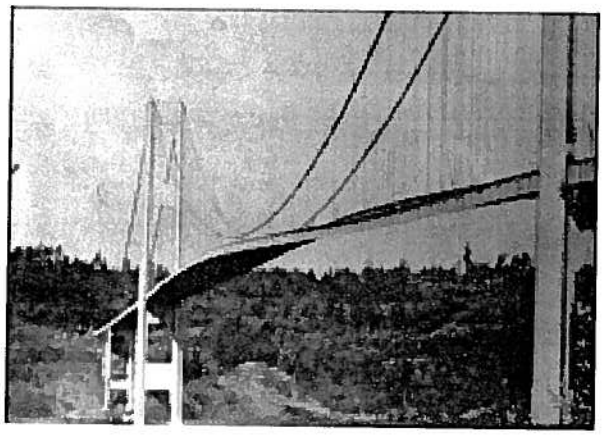

(a)

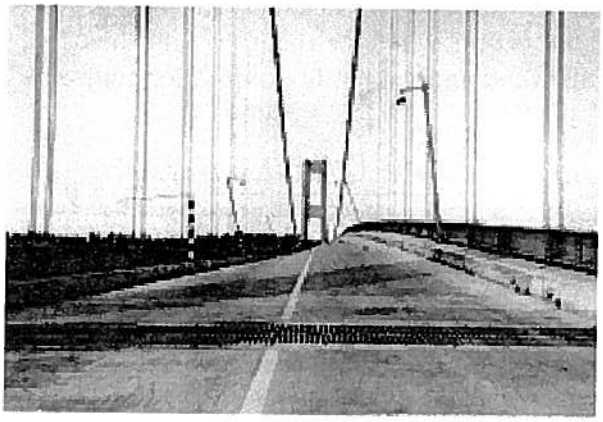

(b)

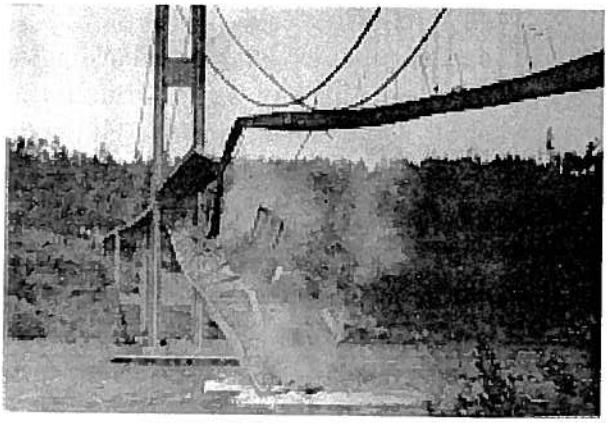

(c)

Figure 10B.2 Failure of "Galloping Gertie," the Tacoma Narrows Bridge, Nov. 7, 1940

represents the elastic restoring force that resists the motion. We assume that the aerodynamic torque can be written

$$\Im(\alpha,\dot{\alpha}) = A_2\dot{\alpha} + A_3\alpha \tag{10B.2}$$

If we combine equations (10B.1) and (10B.2) and non-dimensionalize the result (See Problem 10.8.), we get

$$KA_2^*\left(\frac{\dot{\alpha}L}{\vartheta}\right) + K^2A_3^*\alpha = \frac{I}{\frac{1}{2}\rho\vartheta^2\left(2L^2\right)}\left\{\ddot{\alpha} + 2\zeta_\alpha\omega_n\dot{\alpha} + \omega_n^2\alpha\right\}$$

$$\frac{I}{\frac{1}{2}\rho\vartheta^2\left(2L^2\right)}\left\{\ddot{\alpha} + \left(2\zeta_\alpha\omega_n - \frac{\frac{1}{2}\rho\vartheta^2\left(2L^2\right)KA_2^*}{I}\frac{L}{\vartheta}\right)\dot{\alpha} + \left(\omega_n^2 + K^2A_3^*\right)\alpha\right\} = 0 \tag{10B.3}$$

where ρ is the density of air, L is the length of the deck in the direction of flow, ω is the circular frequency of oscillation, and K is a pseudo-Strouhal number ($K = \omega L/\vartheta$). A_2^* and A_3^* are dimensionless flutter coefficients and are functions of K. Note that $A_1^* \equiv 0$, a coefficient usually related to vertical oscillations which are not relevant here.

The condition for flutter occurs when the damping vanishes, i.e., when the coefficient of $\dot{\alpha}$ is equal to zero. Then for the fundamental mode of vibration with $\omega = \omega_n$, we have from equation (10B.3)

$$2\zeta_\alpha\omega_n - \left(\frac{\frac{1}{2}\rho\vartheta^2\left(2L^2\right)}{I}\right)\left(\frac{\omega_n L}{\vartheta}\right)\frac{L}{\vartheta}A_2^* = 0$$

or

$$A_2^* = \frac{2I\zeta_n}{\rho L^4} \tag{10B.4}$$

For the conditions at Tacoma Narrows, we have

$$\rho = 1.23 \text{ kg/m}^3, \quad L = 11.887 \text{ m}, \quad I = 1.7773 \text{ x } 10^5 \text{ kg m}$$

Then substituting the appropriate values in equation (10B.4), we get

$$A_2^* = 14.474\zeta_n \tag{10B.5}$$

Further development of the flutter analysis requires wind tunnel testing of a model of the bridge section. Following the example of Billah and Scanlan, we construct for incipient flutter the following table of calculated values of A_2^* from equation (10B.5), measured values of (ϑ/fL) from the wind tunnel, and the calculated equivalent values of wind velocity on the bridge for the known fundamental torsional frequency of 0.2 Hz:

Table 10B.1 Conditions for Incipient Flutter

ζ_n	A_2^*	ϑ/fL	$\vartheta_{incipient}$ (m/sec)
0.003	0.043	3.20	7.60
0.005	0.072	3.50	8.31
0.010	0.145	4.30	10.24
0.015	0.217	5.15	12.25
0.020	0.290	5.75	13.68

Billah and Scanlan estimate the value of the damping coefficient for the torsional mode to be $\varsigma_n = 0.005$ which would give a wind velocity of 8.31 m/sec for incipient flutter. In the wind tunnel tests, incipient flutter occurred at an equivalent wind velocity of 7.11 m/sec in the prototype. It is interesting to note that if the data of Table 10B.1 are plotted as in Figure 10B.3 and then extrapolated to a value of $A_2^* = 0$ for which the aeroelastic coefficient reverses sign, we get a wind velocity of 6.54 m/sec. All of the values are consistent with the velocity for incipient flutter. As the wind velocity increases beyond this range as it did on Nov. 7, 1940, the amplitude of the torsional oscillations increases dramatically as seen in Figure 10B.2 which in turn changes the aerodynamic loading of the deck and further exacerbates the situation. Clearly, the conditions leading to the demise of "Galloping Gertie" were not simply a result of the Karman vortex street shed by the bridge deck .

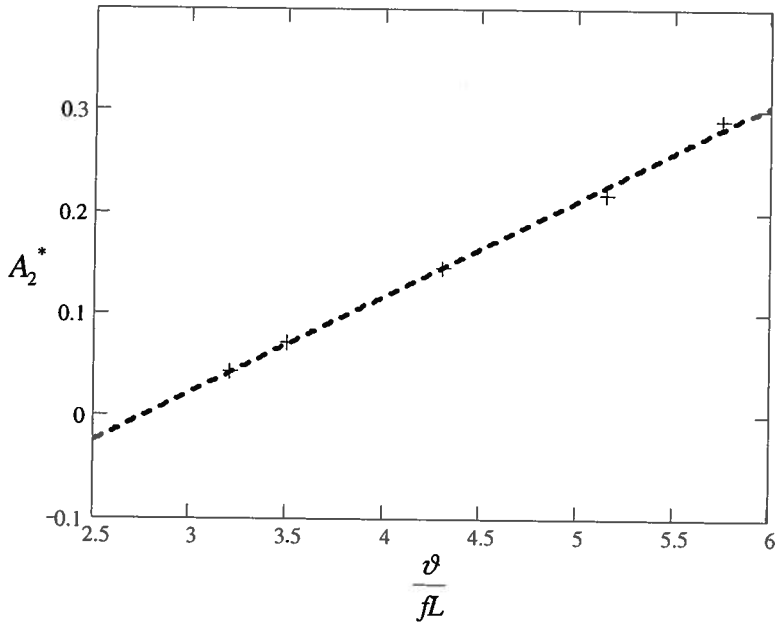

Figure 10B.3 Conditions for Incipient Flutter

PROBLEMS

10.1 Small amplitude surface waves on fluids have been discussed previously in Chapter 5. In these discussions, gravity has been the restoring force in both the deep water and shallow water cases. We are now interested in using dimensional analysis to predict the phase velocity, ϑ, of small-amplitude deep-water surface waves on a fluid of density ρ as a function of wavelength λ as shown in Figure 10P.1.

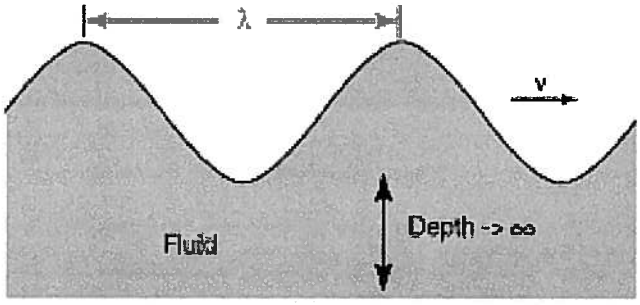

Figure 10P.1

The restoring forces for the fluid are due to gravity, $g = 9.81$ m/sec^2, and surface tension, σ. We believe viscosity and wave amplitude, to first order, are unimportant in determining the velocity of surface waves.

(a) Develop a complete set of Π-groups to describe this physical situation. Choose the physical parameters so that one of these Π-groups can be thought of as the dimensionless gravity and another as the dimensionless surface tension.

(b) Table 10P.1 shows measurements of the wave speed as a function of wavelength for water surface waves. Plot these data on a graph using the Π-groups derived in part (a) above and propose a functional relationship amongst the dimensionless groups.

Table 10P.1

Wavelength (m)	Water Wave velocity (m/sec)
0.001	0.67
0.01	0.245
0.02	0.231
0.06	0.318

(c) If the surface wave speed of a wave of wavelength $\lambda = 7$ mm is $\vartheta = 0.195$ m/sec in pure ethyl alcohol, what is the surface tension of the ethyl alcohol?

For water: $\rho = 1000$ kg/m^3; $\sigma = 0.07118$ J/m^2.
For ethyl alcohol: $\rho = 789.3$ kg/m^3.

10.2 A fluid having density ρ and viscosity μ flows with uniform velocity ϑ between two plates that are separated a distance D. A series of measurements are to be made of the pressure P at a fixed point in the fluid. It is desired to plot the data in the form of a dimensionless pressure Π_P versus a dimensionless quantity Π_ϑ that is linearly proportional to the velocity ϑ.

(a) Find the dimensionless parameters Π_P and Π_ϑ in terms of the remaining physical quantities.

(b) Electric charge is now injected into the fluid and an electric field E is applied that interacts with the charge. The resulting measured pressure in the fluid is now a function of the

applied field E and the dielectric constant in free space ε_0 as well as the remaining appropriate physical parameters. The pressure data can now be plotted as a function of the dimensionless pressure Π_P, the dimensionless parameter Π_ϑ and a new parameter Π_E that is linearly proportional to the electric field E. Determine the additional dimensionless variable Π_E in terms of the remaining physical parameters.

NOTE: The fundamental dimensions of the electric field and the dielectric constant are M, T, L and I. Then the dimensions for E and ε_0 are:

$$[E]=\frac{ML}{IT^3} \quad \text{and} \quad [\varepsilon_0]=\frac{I^2T^4}{ML^3}$$

10.3 Two alternative relationships for the drag force F_D on a sphere of diameter D, moving with velocity ϑ in a fluid, are

$$\frac{F_D}{\rho\vartheta^2D^2}=f_1\left(\frac{\rho\vartheta D}{\mu}\right) \quad \text{and} \quad \frac{F_D}{\mu^2/\rho}=f_2\left(\frac{\rho\vartheta D}{\mu}\right)$$

where f_1 and f_2 are two different functions of the parameter in the parenthesis.

(a) Show that there is no inconsistency between the two expressions.

(b) A sphere of diameter D = 10 cm is to be tested in a water tunnel, in order to simulate the air flow around a spherical ornament 1 m in diameter, which is to be placed at the top of a high building. The maximum possible water speed in the tunnel is 25 m/sec. What is the greatest wind speed for which a dynamically similar test can be arranged?

(c) The force on the sphere in the water tunnel is 500 N when the speed is 25 m/sec. What is the aerodynamic force on the ornament under dynamically similar conditions? Check numerically that the same result is given whichever of the above two dependent dimensionless groups is used for the prediction.

Assume that: ρ_{air} = 1.225 kg/m^3, μ_{air} = 1.79 x 10^{-5} kg/m sec
ρ_{water} = 1000 kg/m^3, μ_{water} = 1.18 x 10^{-3} kg/m sec

10.4 A ship is 70 m long and is designed to travel at a speed of 7 m/sec. A model is made to 1/20 scale and is tested at the Froude number corresponding to that of the full-scale ship.

(a) Calculate the test speed.

(b) In the test, the measured drag is 15 N. Estimate the drag of the ship assuming that half of the measured drag of the model is due to the wave motion and the rest is due to viscous shear stress. Assume that the drag due to viscous shear stress is proportional to $Re_L^{-1/5}$ where Re_L is the Reynolds number based on length.

For water: ρ_{water} = 1000 kg/m^3, μ_{water} = 1.18 x 10^{-3} kg/m sec

10.5 An aircraft is to fly at 275 m/sec at an altitude of 9 km (where the temperature and pressure are T_{atm} = −45 C and P_{atm} = 30 x 10^3 N/m^2). A 1/20 th-scale model is tested in a pressurised wind-tunnel in which the air is at 15 C.

(a) For complete dynamic similarity, what pressure and velocity should be used in the wind-tunnel?

(b) What is then the ratio between the lift on the model and the full-scale lift?

Air can be modeled as an ideal gas with

$$\mu \propto \frac{T^{3/2}}{T+117}$$

10.6 Two smooth horizontal pipes of circular cross-section carry air and water at velocities such that the Reynolds numbers and pressure drops per unit length are the same for each. What is the ratio of the mean velocity of the air in its pipe to that of the water in its pipe?

10.7 When a circular tube of small diameter is dipped into a pool of liquid, surface tension causes a meniscus to form at the free surface of the liquid. This meniscus causes the free surface of the liquid to be depressed or elevated an amount Δh depending upon the contact angle at the liquid-solid-gas interface. Simple experiments show that Δh is a function of the tube diameter, D, the density of the liquid, ρ, gravity, g, and the surface tension (surface force per unit length of free surface), σ.

(a) Find an appropriate set of dimensionless parameters that could be used to correlate the experimental data of Δh vs. σ.

(b) The Bond number is defined as the ratio of gravity forces to surface forces. Can one of the dimensionless parameters in part (a) above be cast in a form similar to the Bond number? Note that it will not be identical to the Bond number since the present physical situation is slightly different from that for which the Bond number was originally derived.

10.8 Consider the physical situation of the Tacoma narrows Bridge undergoing a torsional oscillation. (See Appendix 10B.) In particular, consider a unit length of the midspan subjected to wind loading. There are three parameters necessary to describe the wind: the velocity, $\mathcal{V}$; the air density, ρ; and the viscosity, μ. There are five parameters necessary to describe the unit length of the bridge during the torsional oscillations: the mass moment of inertia (per unit length), I, of the cross-section of the bridge deck about the axis of rotation; the aerodynamic moment, $\mathcal{M}$, acting on the twisting deck; the length of the bridge deck in the direction of flow, L; the torsional spring constant of the unit length of deck, C_α; and the circular frequency of the torsional oscillation, ω.

Develop a set of dimensionless groups to describe this situation and compare your result to the dimensionless groups appearing in equation (10B.3).

10.9 In fully-developed, steady turbulent flow in a pipe of circular cross-section, the heat transfer coefficient h can be argued to depend upon:

(1) a parameter that characterizes the flow, the bulk average fluid velocity $\mathcal{V}$
(2) a parameter that characterizes the geometry of the flow, the diameter of the pipe D
(3) four parameters that characterize the fluid flowing
  (a) the fluid viscosity, μ
  (b) the fluid density, ρ
  (c) the specific heat of the fluid, c_p
  (d) the thermal conductivity of the fluid, k

Use dimensional analysis to show that the appropriate dimensionless groups for this flow are the Nusselt number, the Prandtl number, and the Reynolds number (See Table 10.6). Remember to choose the repeating parameters such that the chosen parameters do not form a dimensionless group. Use the chosen parameters to non-dimensionalize the parameters necessary to characterize this physical situation. For example, consider the fluid velocity $\mathcal{V}$, the thermal conductivity k, and the heat transfer coefficient h to be the necessary parameters in this case.

10.10 According to the Buckingham Pi Theorem, the analysis in Problem 10.9 reveals a relationship amongst the dimensionless groups of the form

$$Nu = f(Re_D, Pr)$$

In 1933, Prof. W. H. McAdams of the Department of Chemical Engineering, MIT, suggested that the functional form of this relationship should be

$$Nu = CRe_D{}^A Pr^B$$

where A, B, and C are constants. Experimental data for h collected for water, air, helium, and oil under various conditions of flow velocities are given in the tables below. Use these data to determine the values of A, B, and C.

For H_2O at $T = 300$ K:
$Pr = 5.9$, $D = 50$ mm, $k = 0.611$ W/m K, $\mu = 8.67 \times 10^{-4}$ kg/m sec, $\rho = 996$ kg/m^3

ϑ (m/sec)	h (W/m^2 K)
0.2	1,049
0.4	1,891
0.7	3,121
1.2	4,108
2.5	9,038
5.6	13,539
8.3	23,118
9.7	21,553
11.8	27,366
12.9	25,173

For air at $T = 350$ K: $Pr = 0.69$, $D = 120$ mm, $k = 0.03$ W/m K, $\mu = 20.54 \times 10^{-6}$ kg/m sec, $\rho =$ 1.012 kg/m^3

ϑ (m/sec)	h (W/m^2 K)
2	7.58
4.3	15.37
7.4	30.32
10.9	31.24
12.7	37.01
15.8	49.80
18.2	51.46
25.4	61.04
33.2	72.79
41	102.84

For helium at $T = 400$ K: $Pr = 0.71$, $D = 200$ mm, $k = 0.178$ W/m K, $\mu = 24.4 \times 10^{-6}$ kg/m sec, $\rho = 0.1218$ kg/m^3

ϑ (m/sec)	h (W/m^2 K)
10	32.63
12.3	37.03
15.8	34.24
19.2	40.38
25.1	53.37
33.3	76.08
41.8	83.11
48.7	99.86
56.9	126.84
71.4	150.19

For oil at $T = 400$ K: $Pr = 154$, $D = 100$ mm, $k = 0.134$ W/m K, $\mu = 88.4 \times 10^{-4}$ kg/m sec, $\rho = 826$ kg/m^3

ϑ (m/sec)	h (W/m^2 K)
1.2	388
2.5	667
5.1	1389
7.3	1519
8.6	2202
9.9	2555
12.4	2424
15.6	2908
18.4	3514
19.5	3006

10.11 As shown in Figure 10P.11a, a vertical flat plate of length L with a temperature T_s is exposed to a fluid whose temperature remote from the plate is T_∞. Since the temperature of the plate is greater than the temperature of the fluid, a fluid particle in contact with the plate will experience a heat transfer interaction with the plate and increase in temperature. As this fluid particle increases in temperature, it expands and its density decreases. Thus it becomes buoyant relative to the cooler, more dense, fluid particles that surround it. The resultant buoyancy force causes the warmer fluid particles to move upward and the cooler fluid particles to move downward. Thus, the fluid is set in motion and convection heat transfer results between the fluid and the plate. This form of convection heat transfer is known as natural convection.

If we are concerned with maintaining the temperature of the plate constant, we need to know the heat transfer coefficient between the plate and the fluid. We expect the heat transfer

process to depend upon the temperature difference between the fluid and the plate, $\Delta T = T_s - T_\infty$; the density of the fluid, ρ; the buoyancy force per unit mass, F_B; the viscosity of the fluid, μ; the specific heat of the fluid, c_P; and the length of the plate, L. We wish to describe the natural convection heat transfer phenomenon in dimensionless form so that we may apply the result to any physical situation regardless of size, temperature, or fluid composition.

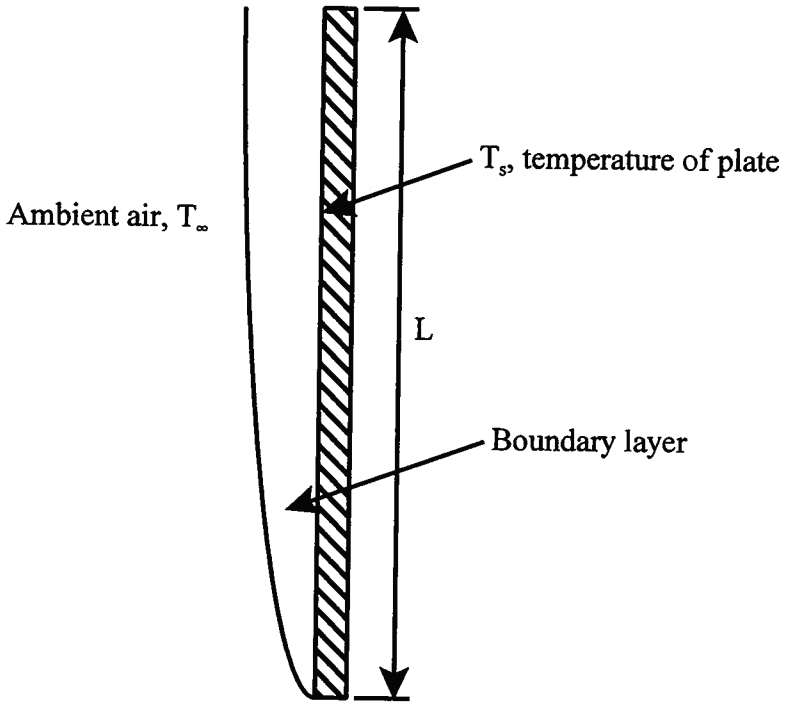

Figure 10P.11a

(a) Form three appropriate dimensionless groups; one each for the heat transfer coefficient h, the buoyancy force per unit mass F_B, and the specific heat c_P. What are the names of these dimensionless parameters?

(b) If we define the coefficient of thermal expansion, β, as the fractional change in density that results as the fluid is heated at constant pressure, viz.

$$\beta = -\frac{1}{\rho}\left(\frac{\partial \rho}{\partial T}\right)_P$$

show that the buoyancy force per unit mass is approximately

$$F_B = -\beta g\left(T_s - T_\infty\right) = -\beta g \Delta T$$

(c) Rewrite the dimensionless buoyancy force to include β, g, and ΔT.

(d) The data shown in Figure 10P.11b were obtained for natural convection heat transfer for air in contact with a hot plate. It has been suggested that the data can be correlated by a power law of the form

$$\Pi_h = C\left(\Pi_{F_B}\right)^n \left(\Pi_{c_P}\right)^m$$

where C, n, and m are constants. From the data given, obtain the value of n.

For air: $\rho = 1.177$ kg/m^3, $\mu = 18.43 \times 10^{-6}$ kg/m sec, $c_P = 1005$ J/kg K, $k = 0.0267$ W/m K

(e) What additional data are required to obtain the value of m?

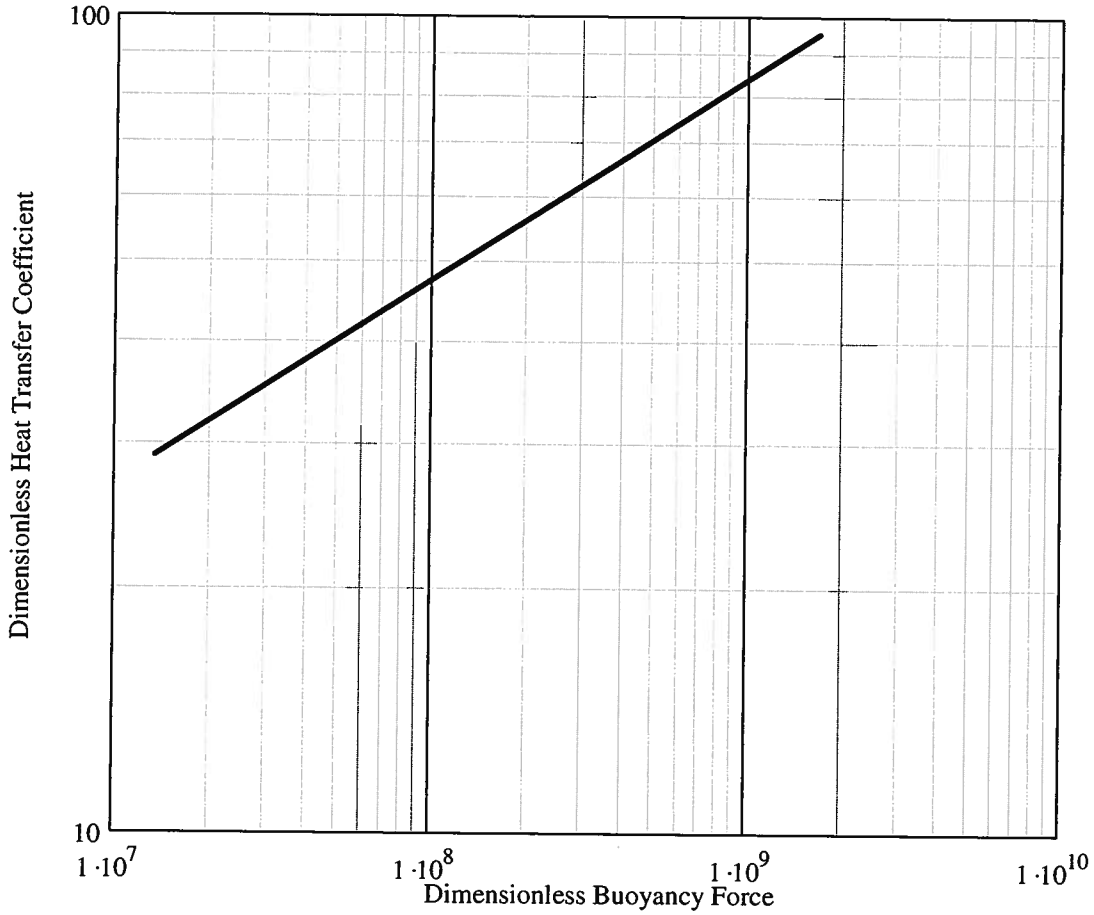

Figure 10P.11b

10.12 One of the techniques often used to measure the viscosity of fluids makes use of an instrument called a rotating cylinder viscometer. As shown in cross-section in Figure 10P.12, the device consists of two coaxial cylinders separated by a small gap filled with the fluid whose viscosity is to be measured. The inner cylinder is suspended from a highly flexible rod (often a wire) while the outer cylinder is set into steady rotational motion ω by means of a motor. By virtue of the action of viscosity of the fluid, a velocity field develops in the fluid such that the fluid in contact with the inner surface of the outer cylinder has tangential velocity $\hat{v}_\theta(R_2) = R_2\omega$ while the velocity of the fluid in contact with the outer surface of the inner cylinder has zero velocity, $\hat{v}_\theta(R_1) = 0$.

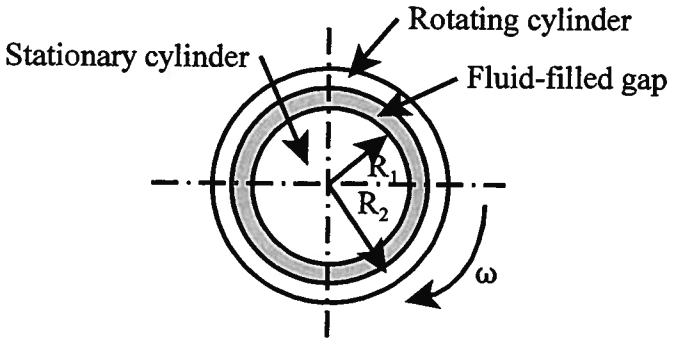

Figure 10P.12

The shear stress acting on the outer surface of the inner cylinder results in a torque acting on the inner cylinder. Because the inner cylinder is suspended from a slender rod fixed at one end, the rod is loaded in torsion and the inner cylinder is displaced some angle Θ such that the moment imposed by the shear stress of the fluid acting on the surface of the cylinder is counteracted by the torsional moment in the rod. Since the shear stress on the inner cylinder is proportional to the viscosity of the fluid, we have an indirect measure of the viscosity of the fluid by measuring the angular displacement Θ of one end of the rod relative to the other.

From the equations of static equilibrium of the rod,

$$\sum M_O = \tau_{r\theta} 2\pi R_1 h - \frac{GI_z\Theta}{L} = 0$$

where $\tau_{r\theta}$ is the shear stress exerted by the fluid on the surface of the cylinder of radius R_1 and height h and G is the shear modulus of the rod of length L with I_z as the polar moment of inertia of the cross-sectional area of the rod about its axis z. Then

$$\tau_{r\theta} = \frac{GI_z\Theta}{2\pi R_1 hL}$$

All of the parameters on the right-hand side of this equation are known from geometry or are measurable. We now need to determine the relationship between the shear stress on the surface of the inner cylinder $\tau_{r\theta}$ and the fluid viscosity μ.

(a) Using the methods of dimensional analysis, find the dimensionless parameters that describe the shear stress in dimensionless form. The parameters that should be included are: r, $\tau_{r\theta}$, ω, R_1, R_2, μ. Take as the repeating parameters ω, μ, R_1.

(b) In cylindrical coordinates, simplify the continuity equation and the Navier-Stokes equation. Assume the following:

1. Steady flow with ω = constant
2. Incompressible fluid model is valid
3. $\vartheta_z = 0$, $\vartheta_r = 0$, $\partial/\partial z = 0$, and $\partial/\partial\theta = 0$

Show that:

$$\vartheta_\theta = \frac{\omega R_1}{1-\left(\frac{R_1}{R_2}\right)^2}\left(\frac{r}{R_1} - \frac{R_1}{r}\right)$$

$$\tau_{r\theta} = \frac{2\mu\omega}{1-\left(\frac{R_1}{R_2}\right)^2}\left(\frac{R_1}{r}\right)^2$$

10.13 There are many examples that show if various objects are geometrically similar, their dynamical properties may obey simple power-law relationships. A good example of this is the mass/velocity relationship of winged objects such as insects, birds, and airplanes.

(a) In Table 10.6 we defined the lift coefficient, C_L, for a typical wing. Wind-tunnel test data show that for a typical wing of projected planar area A at a typical angle of attack (about 6°), the lift coefficient is $C_L = 0.6$. Consider a winged object flying at constant velocity ϑ in air at atmospheric pressure ($P_{atm} = 1.01325 \times 10^5$ N/m^2) and temperature ($T_{atm} = 300$ K) ($\rho_{atm} = 1.1768$ kg/m^3). From a force balance in the vertical direction, show that the mass M of the object and the velocity are related by the expression

$$M = 0.036 A \vartheta^2 \qquad \text{(10P.13a)}$$

(b) If the physical dimensions of all winged objects can be characterized in terms of some multiple of their length l, we can express the projected planar area of the wing, A, as proportional to l^2 and the mass, M, as proportional to the volume, or l^3, show that the mass is proportional to the sixth power of the velocity, viz.,

$$M \propto \vartheta^6$$

(c) Table 10P.1 presents some typical data for winged objects of various kinds. Show that the conclusion of part (b) above is correct *for these data* by forming a Log-Log plot of M versus ϑ^6. Develop a power law relationship between the mass and the velocity in the form

$$M = C\left(\vartheta^6\right)^n$$

and determine the values of C and n.

Table 10P.1 Parameters of Winged Objects

Winged Object	Mass, M (kg)	Lifting Area, A (m^2)	Cruise Velocity, ϑ (m/sec)
Crane fly	30×10^{-6}	7.5×10^{-5}	3
Common starling	0.080	0.02	10.3
Canadian goose	5.7	0.28	23
Cessna Citation	2000	18.2	53.64
Boeing 747	33.34×10^4	511.0	248.11

(d) The *Gossamer Condor* is a human-powered ultra-light aircraft in which the pilot pedals a mechanism that drives the aircraft at a constant velocity of $\vartheta = 5$ m/sec. With the pilot on board, the mass of this airplane is 95.82 kg and it has a wing area of $A = 70$ m^2. Add these data to the plot of part (c) above to show that this aircraft does not satisfy the sixth power scaling law of part (c). Why is this the case?

(e) Following the suggestion of equation (10P.13a) above, form a new Log-Log plot of M versus $A\vartheta^2$ for the data of Table 10P.1.Using the data of Table 10P.1, develop a new power law using these parameters in the form

$$M = \alpha\left(A\vartheta^2\right)^m$$

and determine the values of α and m. Do the data for *Gossamer Condor* fall on the new plot? Why is this the case?

(f) Using the plot of part (e) above, estimate the wing area for a Boeing 767 with $M =$ 179,170 kg and a cruise velocity of $\vartheta = 237$ m/sec. How does this estimate compare with the actual value of $A = 283.85$ m^2?

10.14 A common method of removing unwanted energy and entropy from the surface of an object whose temperature must be controlled, e.g., an electronic device that dissipates electrical energy, is to cover the surface with an appropriate array of fins. (See Chapter 6.) A common fin geometry is that of a flat plate exposed to a flowing stream of some sort of cooling medium such as water or air. Our objective here is to develop a means of predicting the area necessary to

establish heat transfer at some rate predetermined from the electrical characteristics of an electronic device such as the CPU of a personal computer.

One possible model for this situation is that of heat transfer from one side of a flat plate exposed to a flowing stream of fluid. We could analyze this situation by solving the appropriate form of the Navier-Stokes equation to determine the manner in which the boundary layer develops from the leading edge of the plate. In the case of laminar flow, the result would be a self-similar velocity profile of constant shape as we move down the plate from the leading edge. The thickness of the boundary layer is scaled by the distance from the leading edge by means of some sort of dimensionless parameter. This velocity profile is then used in the first law to determine the temperature profile from which we can determine the heat transfer coefficient, h. We shall see how to do this in Chapter 11. For the present, we want to develop a means of utilizing experimental data to make such predictions of the required heat transfer area. Specifically, we want to correlate these data in some useful form.

Consider a flat plate of surface temperature T_s aligned parallel to a steady flow of a fluid with a uniform free-stream velocity. The approaching fluid has a uniform temperature T_∞. The heat transfer coefficient h can be argued to depend upon:

(1) a parameter that characterizes the flow – the bulk average fluid velocity ϑ

(2) a parameter that characterizes the geometry of the flow – the length of the plate L

(3) four parameters that characterize the fluid flowing:

(a) the fluid viscosity, μ

(b) the fluid density, ρ

(c) the specific heat of the fluid, c_P

(d) the thermal conductivity of the fluid, k

(a) Use dimensional analysis to show that the appropriate dimensionless groups for this flow are the Nusselt number, *Nu;* the Prandtl number, *Pr*; and the Reynolds number, *Re* (See Table 10.6). Remember to choose the repeating parameters such that the chosen parameters themselves do not form a dimensionless group. Use the chosen parameters to non-dimensionalize the parameters necessary to characterize this physical situation. For example, consider the fluid velocity ϑ, the thermal conductivity k, and the heat transfer coefficient h to be the necessary parameters in this case.

(b) Table 10P.14a shows actual laboratory measurements of the heat transfer rate from one side of a square flat plate of dimension $L = 30$ cm and surface temperature $T_s = 40$ C immersed in a flow of water with temperature $T_\infty = 20$ C.

Table 10P.14a

ϑ (m/sec)	0.1	0.3	0.5	1.0	2.0	3.0	5.0
Q (W)	760	1400	1700	2600	3400	4300	6000

Use these data to plot on Log-Log coordinates *Nu* versus *Re* for this situation. Use linear regression to develop a correlation of these data in the form

$$Nu = A(Re)^n$$

where A and n are constants. Determine the values of A and n.

(c) In order to determine the influence of fluid properties on the heat transfer coefficient, measurements are made of the heat transfer rate from one side of a square flat plate of dimension $L = 30$ cm and surface temperature $T_s = 40$ C immersed in flows of different fluids with

temperature T_∞ = 20 C. The fluid velocity in each case is the same value $\hat{v}$ = 1 m/sec. The resulting data are shown in Table 10P.14b.

Table 10P.14b

Fluid No.	1	2	3	4	5
μ (kg/m sec)	1.08×10^{-3}	3.00×10^{-3}	1.00×10^{-2}	1.00×10^{-1}	9.00×10^{-4}
ρ (kg/m^3)	1000	980	980	1020	880
k (W/m K)	0.598	1.20	1.20	2.00	1.30
c_P (J/kg K)	4184	2000	2000	1500	900
$\dot{Q}$ (W)	2460	2560	2100	1900	2400

Use these data to plot on Log-Log coordinates (Nu/Re^n) versus Pr for this situation. Use linear regression to develop a correlation of these data in the form

$$\left(\frac{Nu}{Re^n}\right) = C(Pr)^m$$

$$Nu = C(Re)^n (Pr)^m$$

where C and m are constants and n is the value determined in part (b) above. Determine the values of C and m.

(d) For a Pentium©4 CPU running at 3.2 GHz, the maximum power dissipation is 82 W with a maximum value of T_s = 70 C and a maximum value of T_∞ = 45 C. Use the correlation determined in part (c) above to determine the required heat transfer area for an air velocity of $\hat{v}$ = 1 m/sec. Keep in mind that the heat transfer occurs from both sides of the fin, not just the single side used in the correlation, and that this area would be realized by a large array of small fins, not just a single fin.

10.15 No discussion of dimensional analysis would be complete without relating a famous anecdote about the renown British scientist G. I. Taylor. The account presented here is taken from the article by M. P. Brenner and H. A. Stone ("Modern Classical Physics Through the Work of G. I. Taylor", *Physics Today*, May, 2000, p. 20). It seems that "during the early years of World War II, he [Taylor] was told by the British government about the development of the atomic bomb and was asked to think about the mechanical effect produced by such an explosion. He realized that the energy released from the bomb would quickly lose memory of its initial shape and distribution, and would produce a strong shock [wave] in the air."

Taylor assumed that the velocity of the shock wave would be independent of the pressure distribution immediately following the explosion and that the shape of the shock wave in the atmosphere far from the ground would be approximately spherical. Since the shock wave propagates at a velocity greater than the velocity of sound in the atmosphere ahead of it, the air is unaware of the approaching wave. This means that the radius R of the shock wave at any time t would depend only upon the energy that is driving the shock wave through the air, i.e., the energy E instantaneously released by the detonation of the bomb at time t = 0, and the inertia of the

atmosphere, i.e., the density ρ of the undisturbed air that has to be moved in order to make room for the mass of explosion products released by the explosion itself. The pressure of the atmospheric air is not important since the pressure inside the shock wave is several thousand times greater than atmospheric pressure. Only the inertial effect of the atmosphere is important. Thus there are four parameters necessary to describe the physical situation: the energy E released by the blast, the density ρ of atmospheric air, the time t since the blast was detonated, and the radius R of the blast wave, which is a function of t.

(a) Using dimensional analysis, show that there is a single dimensionless group characterizing the blast phenomenon.

$$\Pi_1 = \frac{Et^2}{\rho R^5}$$

Since there is only one dimensionless group, according to the Buckingham Pi Theorem it must be a constant, C. This implies that the radius of the blast wave is given by

$$R = C\left(\frac{E}{\rho}\right)^{1/5} t^{2/5}$$

where C is a constant. By applying the conservation equations for mass, momentum, and energy, Taylor was able to show that the value of $C \sim 1.033$. Therefore, given a picture that shows the radius of the blast, a reference length scale, and the time since the blast, the energy of the blast can be determined. A sequence of such pictures taken at precise time intervals from the instant of the explosion was (publicly!) available and Taylor was able to confirm that the scaling law agreed with the data much to the chagrin of the U.S. military who had given the data the highest level of security classification.

(b) Figure 10P.15 is a sample of the pertinent photographs used by Taylor in his assessment. These are pictures of the blast wave from the first nuclear test labeled Trinity and held on July 16, 1945. The data of Table 10P.15 have been derived from these photos:

Table 10P.15

R (m)	73.85	108.17	176.31
t (sec)	6×10^{-3}	16×10^{-3}	53×10^{-3}

Use these data to form a Log-Log plot of $R^{5/2}$ vs. t and show that Taylor's correlation is correct. Determine the energy yield of the blast and compare this with the reported value of 15 – 16 kilotons of TNT. One kiloton of TNT is equal to 4.184×10^{12} J.

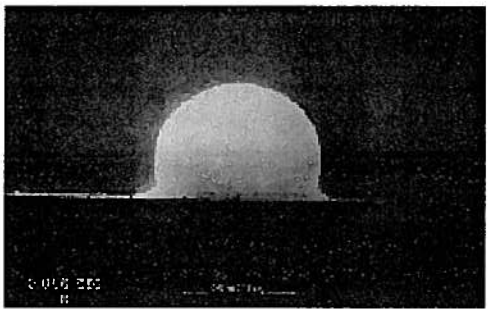

(a) t = 6 milliseconds

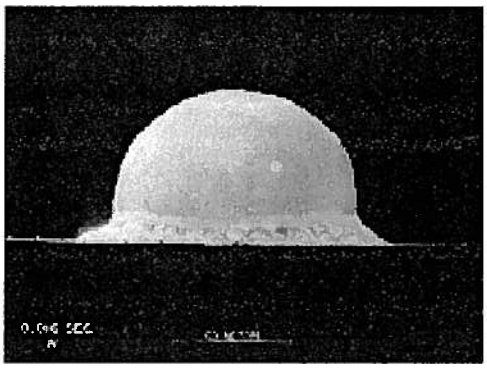

(b) t = 16 milliseconds

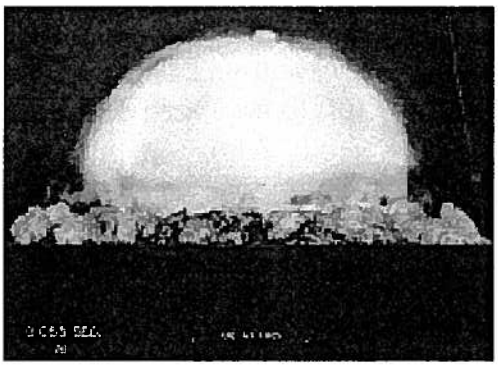

(c) t = 53 milliseconds

Figure 10P.15 Time-lapse Photographs of the First Atomic Bomb Blast July 16, 1945

CHAPTER 11

Thermal Conductivity and Energy Transfer in a Fluid

11.1 Introduction

In Chapter 9 we saw that as a fluid moved over a surface in contact with it, the viscosity of the fluid caused the fluid adjacent to the surface to be slowed by the presence of the surface. We also noted that the fluid closest to the surface was more noticeably affected by the presence of the surface than the fluid that was further from the surface. This observation led to the introduction of the concept of the *momentum boundary layer*, a layer of fluid moving at lower velocity than the fluid in the free stream. In the momentum boundary layer, the fluid velocity relative to the surface increases from zero at the surface to the free stream velocity at the edge of the boundary layer as dictated by the boundary conditions of the situation. In effect, the influence of the surface propagates or diffuses outward from the surface into the fluid in a manner that is determined by the fluid viscosity. In a steady flow situation with a given free stream velocity, at a given location, the larger the viscosity, the thicker the momentum boundary layer. For example, in the case of laminar flow of a fluid of density ρ over a flat plate, we saw that the thickness δ of the momentum boundary layer at a location x was given by the result

$$\delta = 0.664\sqrt{\frac{\mu x}{\rho \vartheta_\infty}} \tag{11.1}$$

where ϑ_∞ was the free stream velocity and μ was the viscosity of the fluid. The combination of terms μ/ρ was given the name kinematic viscosity and represented the momentum diffusivity of the fluid. Thus the boundary layer thickness δ grows in a manner proportional to the square root of the momentum diffusivity.

It can be shown from physical considerations on a molecular scale that a fluid that has viscosity also has thermal conductivity, and that just as the viscosity accounts for the transfer of momentum in the flowing fluid, the thermal conductivity accounts for the transfer of energy in the flowing fluid. The thermal conductivity of the flowing fluid leads to the development of a *thermal boundary layer* in which the thermal influence of the bounding surface is confined. As dictated by the thermal boundary conditions shown schematically in Figure 11.1, the temperature of the fluid varies from the temperature of the surface at the interface between the fluid and the surface to the temperature of the free stream at the edge of the thermal boundary layer. In general, the temperature profile changes in a continuous fashion as we move through the solid surface and into the fluid; however, the slope of the temperature profile, i.e. the temperature gradient normal to the surface, does not. Because of the typically substantial differences in thermal conductivity between fluids and solids, the temperature gradient is usually discontinuous at the interface between the two media. Note, however, that at the interface between the solid and the fluid, the energy conducted down the temperature gradient in the solid to the interface is exactly equal to the energy conducted away from the interface down the temperature gradient in the fluid. In a manner analogous to the growth of the momentum boundary layer, we shall see that the growth of the thermal boundary layer depends upon the thermal diffusivity.

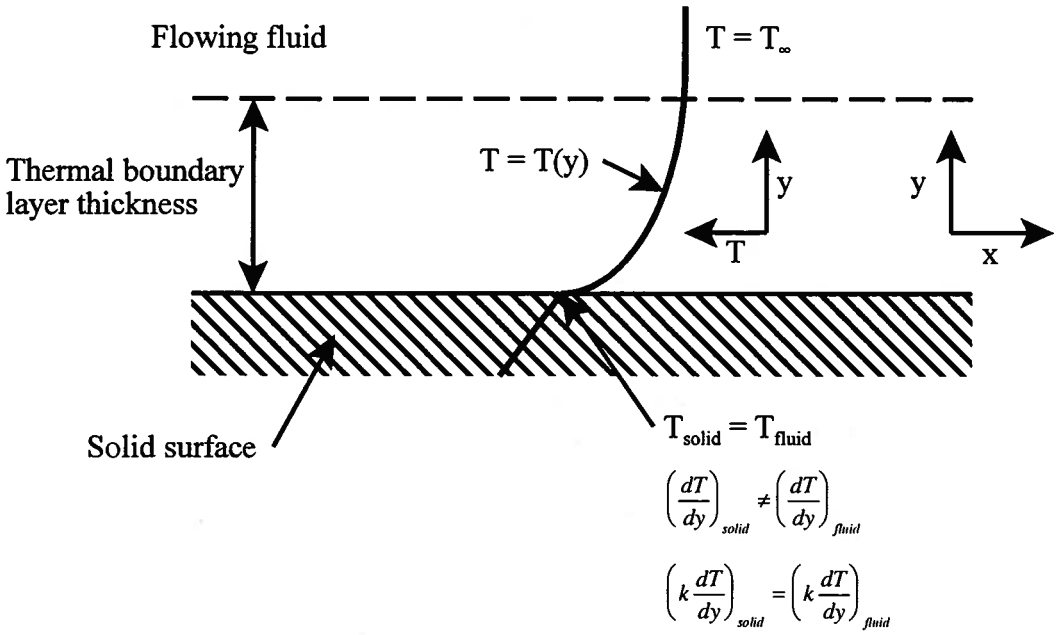

Figure 11.1 Thermal Boundry Layer in Flowing Fluid

Recall from Chapter 10 that the dimensionless number known as the Prandtl number is the ratio of the momentum diffusivity to the thermal diffusivity.

$$Pr \equiv \frac{\mu c_P}{k} = \frac{\mu}{\rho}\frac{\rho c_P}{k} = \frac{\nu}{\alpha} = \frac{\text{momentum diffusivity}}{\text{thermal diffusivity}} \tag{11.2}$$

The range of possible values for the Prandtl number is quite large and depends upon the nature of the fluid. Typically, highly viscous fluids like oils have large values of the Prandtl number and fluids with large thermal conductivities like the liquid metals have small values of the Prandtl number. Gases and water, on the other hand, have values of the Prandtl number on the order of unity. Figure 11.2 shows the spectrum of possible values.

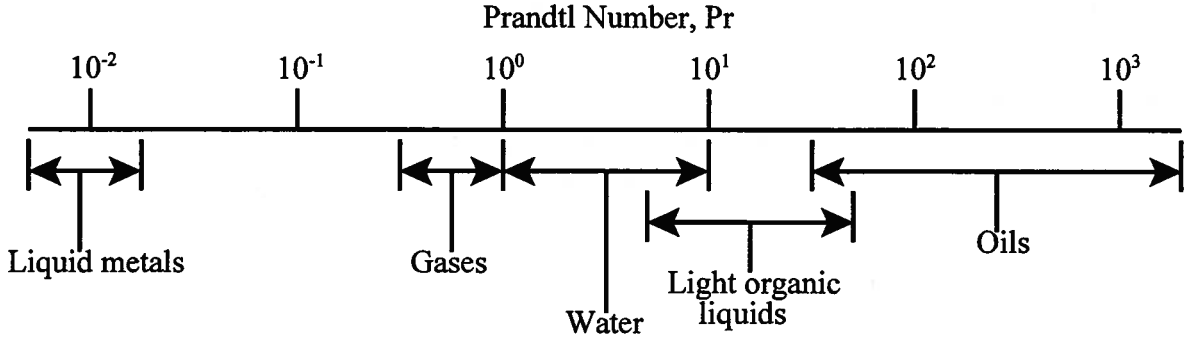

Figure 11.2 Prandtl Number Spectrum of Fluids

It follows, then, that the relative thicknesses of the momentum and thermal boundary layers are determined by the Prandtl number. When the Prandtl number is large, the kinematic viscosity, i.e., the momentum diffusivity, is much larger than the thermal diffusivity and the

retarding influence of the surface on the flow velocity penetrates more deeply into the flowing fluid at any given location than the thermal influence of the heated surface on the temperature of the flowing fluid. Thus, the momentum boundary layer is relative thick compared to the thermal boundary layer. Conversely, when the Prandtl number is small, the thermal diffusivity is much larger than the kinematic viscosity and the thermal influence of the surface penetrates more deeply into the flowing fluid than its retarding influence. Thus, the thermal boundary layer is relatively thick compared to the momentum boundary layer. Clearly, for fluids in which the Prandtl number is of the order of unity, as it is for fluids like air, the two boundary layers are of similar thickness.

In the present chapter, we shall examine in detail the nature of the interplay between the processes of momentum transfer and energy transfer in a flowing fluid. In particular, we shall explore the topic of convection heat transfer (both forced convection and natural convection) between a flowing fluid and the solid surfaces that bound it. We shall consider first the case of internal flows since they are the most common in thermal-fluid systems, and second, the case of external flows. In each case, we shall take up the two flow regimes, laminar and turbulent, separately. Where possible, we shall analyze the basic flow geometries in detail in order to derive the expressions for the convective heat transfer coefficient and report the results in dimensionless form, the Nusselt number, in each case. For more complex flow geometries, we shall simply report the dimensionless correlations of *Nu* vs. *Re* as found in the thermal-fluids literature.

11.2 Forced Convection Heat Transfer to a Fluid in Flowing in a Conduit

As we have seen previously, in thermal-fluid systems the working fluid is usually transported from one system component to another through a conduit such as a circular tube or pipe. As the fluid moves through the conduit in a particular direction in response to a net force imposed in that direction, it may experience interactions with the environment through the walls of the conduit. These interactions may involve the transfer of momentum, energy, and entropy and can have an important influence on the thermodynamic behavior of the thermal-fluid system itself. In Chapter 9 we studied the mechanics of the transport process, i.e. the motion that developed within the fluid in response to the imposed force. We now turn our attention to the thermal interactions that can occur between the flowing fluid and the environment through the solid surfaces of the conduit.

11.2.1 Thermal Entry Length Considerations for Laminar Flow in a Circular Conduit

We saw previously that as a fluid with uniform flow velocity entered the conduit, a finite distance, called the entry length, was required to establish the fully-developed velocity profile over the cross-section of the conduit. For conditions of laminar flow in a circular conduit of inside radius R_i, the fully-developed velocity profile is parabolic and is given by

$$\vartheta(r) = 2\vartheta_{ave}\left[1-\left(\frac{r}{R_i}\right)^2\right] = \vartheta_{max}\left[1-\left(\frac{r}{R_i}\right)^2\right] \tag{11.3}$$

For the case in which the fluid and the tube wall are at the same temperature, the hydrodynamic entry length, L_e, necessary to establish this velocity profile is related to the Reynolds number by the empirical relation of equation (9.149)

$$\left(\frac{L_{entry}}{D_i}\right)_{hy} = \frac{0.60}{0.035Re+1} + 0.056Re \tag{11.4}$$

On the other hand, if the laminar flow is fully-developed hydrodynamically, the velocity profile is already parabolic at the entrance to the conduit. If additionally the temperature of the wall of the conduit is different from that of the fluid, the entry length required for the temperature profile to become fully-developed in the fluid is not only related to both the Reynolds number and the Prandtl number as we might expect, but is also related to the thermal conditions of the wall. If the wall of the conduit has a constant temperature along its length, the thermal entry length is given by

$$\left(\frac{L_{entry}}{D_i}\right)_{\substack{th \\ T=const}} = 0.0334RePr \tag{11.5a}$$

but if the heat flux at the wall is constant, the thermal entry length is given by

$$\left(\frac{L_{entry}}{D_i}\right)_{\substack{th \\ q=const}} = 0.043RePr \tag{11.5b}$$

Equations (11.5) have important implications for the design of heat transfer equipment which frequently uses circular tubes as the major design element. For a given Reynolds number in the flow, the velocity profile will develop very rapidly compared to the development of the temperature profile for a fluid with a large Prandtl number ($Pr >> 1$). The significance of this event is two-fold: (1) the flow will indeed be fully-developed hydrodynamically long before heat transfer processes develop fully as equation (11.5) assumes, and (2) the developing thermal boundary layer must be considered in designing equipment for these fluids since the thermal entry length will typically be longer than the length of the equipment itself. Thus, in heat transfer equipment that use some sort of oil as the working fluid, the thermally fully developed solutions to be developed subsequently will be of little value in the design process; however, as we will show shortly, there are ways of addressing this issue. For fluids with small Prandtl numbers ($Pr << 1$), the situation is reversed. The thermal entry length is much shorter than the hydrodynamic entry length and the flow can be considered fully-developed thermally right from the entrance. Of course, this means that the assumptions leading to equation (11.5) are violated, but as we will soon show, this will have little impact on the design process.

11.2.2 Thermal Entry Length Considerations for Turbulent Flow

In the case of turbulent flow, the question of entry length is somewhat different from that of the laminar flow case. In equation (9.287), we gave the hydrodynamic entry length for a fully rough circular conduit in turbulent flow as

$$\left(\frac{L_{entry}}{D_i}\right)_{hy} = 1.359Re^{1/4} \tag{11.6}$$

Thus the hydrodynamic entry lengths are typically much shorter for turbulent flow than for comparable laminar flows. The behavior of the thermal entry length for a flow that is fully developed hydrodynamically is more complex for turbulent flows than for laminar flows. The influence of Prandtl number is small for large values of Prandtl number but much stronger for small values of the Prandtl number. In nearly every case, the thermal entry length is less than 30 tube diameters.

Example 11E.1: Engines that are used to power vehicles such as snow-mobiles that operate in extreme climates can be difficult to "turn over" after sitting for long periods in the cold outdoors. Because the viscosity of the lubricating oil is so high at low temperatures, the friction

in the engine bearings is excessive. For this reason, engines designed for this purpose often require electric heaters in the tubing used to transport lubricating oil to the engine. Consider the case of a lubricating oil with the following properties at a temperature of T_{env} = 0 C:

ρ = 903.6 kg/m^3, c_P = 1980 J/kg K, k = 0.136 W/m K, μ = 6.86 kg/m sec

In a particular application, the tube diameter is D = 10 mm, and the average velocity of the oil is ϑ = 1 m/sec. The oil heater consists of a length of tube with its circumference wrapped with an electrical resistance heater. Current passed through the electrical resistor (wire) results in Joule heating that transfers energy and entropy to the oil passing through the tube. We wish to determine the minimum length of heater-wrapped tube that will result in the temperature of the oil being affected across the entire cross-section of the flow in the tube.

Solution: The flow in the tube is already fully developed hydrodynamically before it enters the section of tubing wrapped with the heater. Thus we wish to determine the thermal entry length. For any length of tubing greater than this length, the entire cross-section of the flow will be thermally influenced by the action of the heater. Then from equation (11.5b)

$$L_{entry} = 0.043 D Re_D Pr \qquad \texttt{Constant heat flux}$$

The Reynolds number of the flow is

$$Re_D = \frac{\vartheta D \rho}{\mu} = \frac{(1 \text{ m/sec})(0.010 \text{ m})(903.6 \text{ kg/m}^3)}{6.86 \text{ kg/m sec}} = 1.317$$

This is an extremely low value of the Reynolds number, but not uncharacteristic of flows of highly viscous lubricants. The Prandtl number of the fluid is

$$Pr = \frac{\mu c_P}{k} = \frac{(6.86 \text{ kg/m sec})(1980 \text{ J/kg K})}{0.136 \text{ W/m K}} = 9.987 \text{ x } 10^4$$

This is an extremely high value of the Prandtl number, but not uncharacteristic of highly viscous lubricants. Then the entry length becomes

$$L_{entry} = 0.043 D Re_D Pr = 0.043(0.010 \text{ m})(1.317)(9.987 \text{ x } 10^4) = 56.568 \text{ m}$$

This result illustrates the fact that entry lengths in flows of highly viscous fluids such as lubricating oils can be quite long and can often exceed the physical dimensions of the thermal-fluids equipment involved.

11.3 First Law Considerations in Forced Convection Heat Transfer in Internal Flow

Before we attempt to develop the description of the fully-developed temperature profile appropriate for the case of forced convection heat transfer for laminar flow in a circular conduit, it is worthwhile to examine the implications of the first law of thermodynamics in a more general sense. From this analysis, we shall derive expressions for the bulk-mean temperature of the fluid as it flows in the axial direction through the conduit.

The fact that the fluid velocity varies over the cross-section of the conduit in both laminar and turbulent flow means that the thermodynamic state of the fluid will not be uniform over the cross-section. This introduces a slight complication in the application of the first and second laws of thermodynamics for the one-dimensional bulk flow model of the open system or control volume since they are formulated on the basis of a uniform state at any cross-section or port of the system. It becomes necessary, then, to develop some sort of appropriate averaging procedure that will establish the bulk-mean values of the properties of interest. Since the fluid velocity is a

function of the radial location of the fluid element in the conduit, the mass flow rate, $\dot{m}$, is given by

$$\dot{m} = \int_0^{R_i} \rho v_x 2\pi r dr \tag{11.7}$$

where ρ is the local fluid density, v is the axial component of fluid velocity at the radial location r, and R_i is the inside radius of the conduit. In the context of the one-dimensional bulk flow model, the mass flow rate is given by

$$\dot{m} = \rho v_{ave} A_c \tag{11.8}$$

where the cross-sectional area is $A_c = \pi R_i^2$ and v_{ave} is the fluid velocity averaged over the cross-section obtained by equating the equations (11.7) and (11.8).

$$v_{ave} = \frac{\int_0^{R_i} \rho v_x 2\pi r dr}{\rho \pi R_i^2} \tag{11.9}$$

In a similar manner, we can define other bulk-mean properties appropriate to the one-dimensional bulk flow model:

$$h_b = \frac{\int_0^{R_i} \rho v_x h 2\pi r dr}{\dot{m}}$$
$$T_b = \frac{\int_0^{R_i} \rho v_x T 2\pi r dr}{\dot{m}} \tag{11.10}$$

Equations (11.7) through (11.10) provide a means of accounting for the variation of thermodynamic properties over the cross-sectional area of the flow provided that we know the values of the appropriate properties as a function of the distance from the centerline of the conduit. However, the heat transfer interaction that occurs between the fluid flowing in the circular conduit or tube and the walls of the tube produces a variation of thermodynamic properties in the axial direction as well. For example, consider the length of tube L shown in Figure 11.3 with a differential control volume imbedded in it.

If the rate of heat transfer for this differential element is $d\dot{Q}$, then

$$d\dot{Q} = \dot{q}_s 2\pi R_i dx \tag{11.11}$$

where the heat flux at the inner surface of the tube $\dot{q}_s$ is defined as

$$\dot{q}_s = \frac{\dot{Q}}{A_s} \tag{11.12}$$

For steady flow with no shaft work transfer, the first law of thermodynamics for the differential control volume reduces to

$$\cancel{\frac{dE_{cv}}{dt}} = d\dot{Q} - \cancel{\delta \dot{W}_{shaft}} - \dot{m}\left(dh + \cancel{v dv} + \cancel{g dz}\right)$$

$$d\dot{Q} = \dot{m} dh$$

For the appropriate model of the fluid, we now introduce the constitutive relation for the enthalpy. For the case of the ideal gas model,

$$dh = c_p dT$$

and

$$d\dot{Q} = \dot{m} c_p dT \tag{11.13a}$$

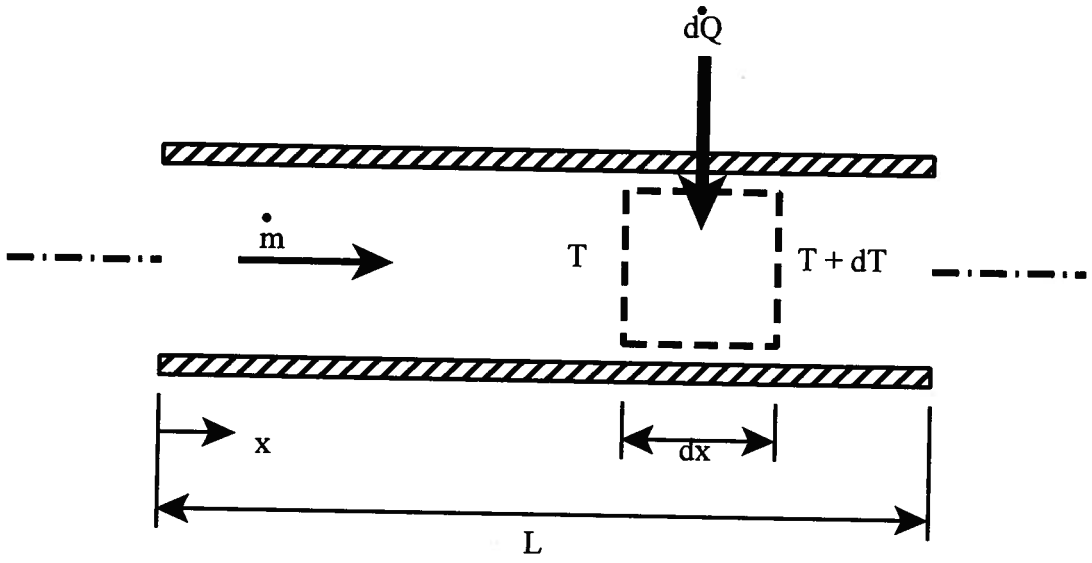

Figure 11.3 Differential Control Volume for a Fluid Flowing in a Circular Conduit

For the incompressible fluid model,

$$dh = d\left(u + \frac{P}{\rho}\right) = cdT + d\left(\frac{P}{\rho}\right)$$

but for heat transfer situations,

$$cdT \gg d\left(\frac{P}{\rho}\right)$$

Then for the incompressible fluid model we usually write (with very small error)

$$d\dot{Q} \approx \dot{m}cdT \tag{11.13b}$$

Because of the similar appearance of equations (11.13a) and (11.13b), we write for the general case

$$d\dot{Q} = \dot{m}c_P dT_b \tag{11.13}$$

where it is understood that the relevant temperature is the one-dimensional bulk flow average temperature for the cross-section and that the incompressible fluid model involves the approximation of equation (11.13b). Then combining equations (11.11) and (11.13), we obtain

$$\frac{dT_b}{dx} = \frac{\dot{q}_s 2\pi R_i}{\dot{m}c_P} \tag{11.14}$$

where the product $\dot{m}c_P$ is known as the *heat capacity rate* or simply the *capacity rate*.

Newton's Law of Cooling defines the coefficient for convective heat transfer between the wall and the fluid, h_c, viz.

$$\dot{q}_s = h_c(T_s - T_b) \tag{11.15}$$

Then combining equations (11.14) and (11.15), we obtain

$$\boxed{\frac{dT_b}{dx} = \frac{2\pi R_i h_c}{\dot{m}c_P}(T_s - T_b)} \tag{11.16}$$

Equation (11.16) can be integrated to determine the variation in the bulk-mean temperature along

the axis of the tube. In carrying out the integration, we note that for flow in a tube, the quantity $2\pi R_i/\dot{m}c_P$ is a constant and does not vary with x. The value of the heat transfer coefficient, h_c, does vary with x in the entry region but then becomes constant when the flow becomes fully developed. The solution of equation (11.16) for $T_b(x)$ will then depend upon the manner in which the temperature of the surface of the tube, T_s, varies with x.

In engineering practice, there are two special boundary conditions with regard to heat transfer interactions at the inner surface of the conduit that are important either because they describe the physical situation exactly or because they represent reasonable models of the real situation. These are the cases of *constant surface heat flux* and *constant surface temperature*. Because of their importance, we will consider them separately.

11.3.1 Constant Surface Heat Flux

There are many situations in engineering practice for which the heat flux at the surface of the tube is constant. This might occur, for example, if the tube wall were wrapped with an electrical resistance heater and a constant electrical current were passed through it. Then for a tube of length L, the total rate of heat transfer over the length of the tube is

$$\dot{Q} = 2\pi R_i L \dot{q}_s \tag{11.17}$$

and the expression for the axial variation of the one-dimensional bulk flow average temperature becomes

$$\frac{dT_b}{dx} = \frac{2\pi R_i \dot{q}_s}{\dot{m}c_P} \tag{11.18}$$

Since the right-hand side of this expression is constant, the variation of T_b with x is linear and the integration of this expression is straightforward.

$$\int_{T_{b,in}}^{T_b(x)} dT_b = \frac{2\pi R_i \dot{q}_s}{\dot{m}c_P} \int_0^x dx \tag{11.19}$$

or

$$T_b(x) = T_{b,in} + \frac{2\pi R_i \dot{q}_s}{\dot{m}c_P} x \tag{11.20}$$

From Newton's Law of Cooling, it is apparent that when h_c becomes constant as it does in the region of fully developed flow, the temperature difference $(T_s - T_b)$ also becomes constant. Then the axial temperature distribution appears as shown in Figure 11.4 for $T_{b,in}$ = 100 C and $\dot{Q}/\dot{m}c_P$ = 50 C. Notice that $T_b(x)$ is indeed linear and that the temperature difference $(T_s - T_b)$ is constant except in the entry region where the heat transfer coefficient is a strong function of the axial coordinate x. Notice also in Figure 11.4 that in the entry region where the flow is not fully developed, it is the bulk-flow average temperature of the fluid and not the conduit wall temperature that varies in a linear fashion as required by equation (11.18). The developing thermal conditions in the flow in this region manifest themselves in the changing radial temperature distribution, not in the bulk average temperature. This means that the fluid temperature at the wall changes as does the heat transfer coefficient. The first law of thermodynamics and the constant surface heat flux require that the rate of change of the bulk-mean temperature be constant as the fluid moves down the conduit. Thus, the variation in heat transfer coefficient in the entry region causes the surface temperature of the tube to vary in a non-linear manner in the axial direction until the flow becomes fully developed. From that point on, the difference between the temperature of the surface and the bulk-mean temperature of the fluid

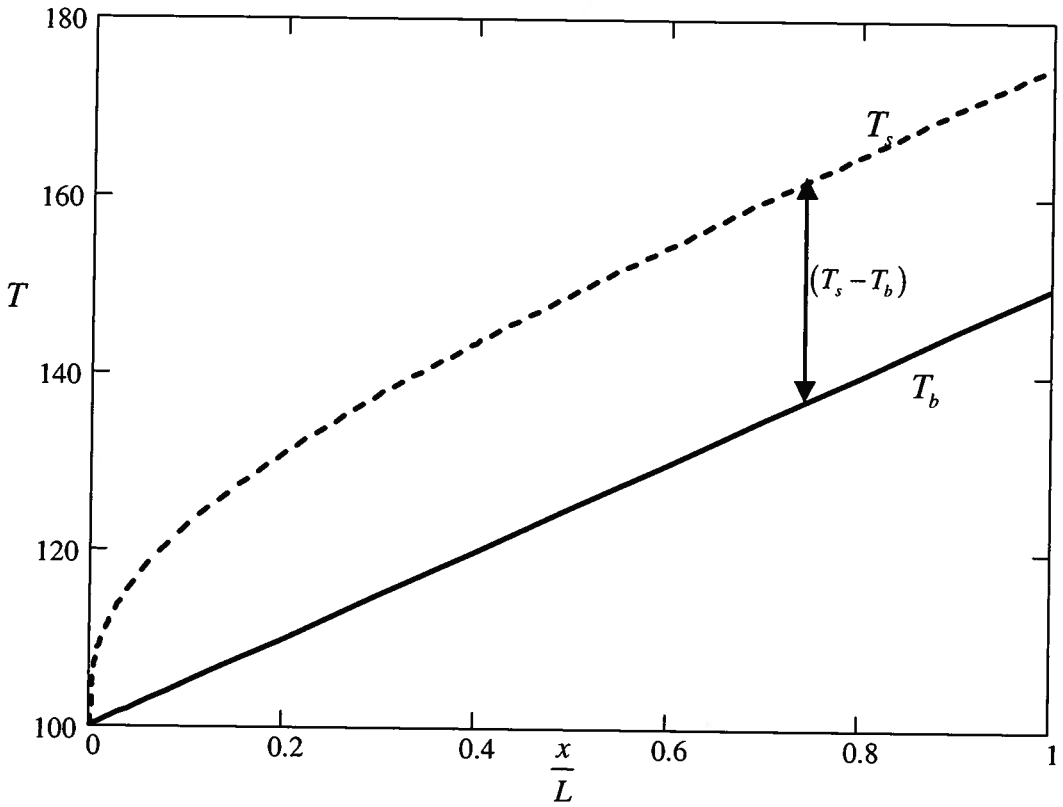

Figure 11.4 Axial Temperature Distribution for Convection in a Circular Conduit with Constant Surface Heat Flux

becomes constant since the heat transfer coefficient is now constant. Of course, the boundary conditions on the flow require that the fluid temperature at the conduit surface be identical with the surface temperature of the conduit, so this temperature tracks the conduit surface temperature in the direction of flow. Notice that since we did not have to specify the character of the flow, that is whether it is laminar or turbulent, the first law analysis of this situation applies to both laminar and turbulent flow situations.

Example 11E.2: Water at a pressure of $P_{in} = 4 \times 10^5$ N/m^2 flows in a heated section of tubing of length $L = 10$ m and diameter $D = 20$ mm. In this section, the flow is fully developed both hydrodynamically and thermally. The water flows at an average velocity of $\hat{v}_{ave} = 1$ m/sec and enters this section with a bulk-mean temperature of $T_{b,in} = 20$ C. The constant heat flux at the wall of the tube is $\hat{q} = 250$ kW/m^2, and the constant heat transfer coefficient for forced convection in this section is $h_c = 6750$ W/m^2 K. The tubing is made of polyvinyl chloride (PVC) plastic with a melting point of $T_{mp} = 150$ C. We wish to determine the maximum temperature of the tube wall in order to ensure that the PVC tubing can safely operate at the temperatures achieved in this system. In this situation, the thermal-fluid characteristics of the water are:

$\rho = 977.76$ kg/m^3, $c_P = 4190.1$ J/kg K, $k = 0.66313$ W/m K, $\mu = 4.0389 \times 10^{-4}$ kg/m sec

Solution: To calculate the maximum tube wall temperature, we first calculate the bulk-mean temperature of the water at the end of the heated section. Since we have a constant heat flux at the wall, we can use equation (11.20) to find the axial temperature distribution in the tube flow, viz.

$$T_{b,out} = T_{b,in} + \frac{\pi D L \dot{q}}{\dot{m} c_P}$$

We need to first calculate the mass flow rate through the tube. Thus,

$$\dot{m} = \rho A_c \vartheta_{ave} = \rho \pi \frac{D^2}{4} \vartheta_{ave} = \left(977.76 \text{ kg/m}^3\right) \pi \frac{(0.020 \text{ m})^2}{4} (1 \text{ m/sec}) = 0.3072 \text{ kg/sec}$$

Then

$$T_{b,out} = T_{b,in} + \frac{\pi D L \dot{q}}{\dot{m} c_P} = 20 \text{ C} + \frac{\pi (0.020 \text{ m})(10 \text{ m})\left(2.5 \text{ x } 10^5 \text{ W}\right)}{(0.3072 \text{ kg/sec})(4190.1 \text{ J/kg K})} = 142.04 \text{ C}$$

The tube wall temperature can be determined from Newton's Law of Cooling, viz.

$$\boxed{\dot{q} = h_c \left(T_{s,out} - T_{b,out}\right)}$$

$$T_{s,out} = T_{b,out} + \frac{\dot{q}}{h_c} = 142.04 + \frac{2.5 \text{ x } 10^5 \text{ W}}{6750} = 179.08 \text{ C}$$

Clearly this temperature exceeds the melting point of PVC and tube failure will result. Thus, if the bulk-mean temperature at the outlet is a functional requirement, it will be necessary to seek an alternative material for the construction of the tube. On the other hand, if the issue is one of simply providing cooling to the heater, one could increase the mass flow rate through the tube which will have the dual effect of reducing the bulk-mean temperature of the water at the outlet and, as we shall see shortly, increasing the forced convection heat transfer coefficient, h_c. Both effects will reduce $T_{s,out}$.

Note that the bulk-mean temperature of the water at outlet from the heater section is higher than the normal boiling point of water at atmospheric pressure. This is possible because the pressure of the water is significantly higher than atmospheric pressure. The boiling point for water at $P_{in} = 4 \text{ x } 10^5$ N/m^2 is $T = 143.61$ C. The reasons for this behavior will be taken up in Chapter 13.

11.3.2 Constant Surface Temperature

In many thermal-fluid systems, the surface temperature of the tube is constant (or nearly so), usually by virtue of heat transfer to a second fluid medium flowing over the outer surface. A typical situation is the change of phase of a fluid on the outside surface of the tube as in a condenser. Under these conditions, the expression for the axial temperature gradient in the fluid becomes

$$\frac{dT_b}{dx} = \frac{2\pi R_i}{\dot{m} c_P} h_c (T_s - T_b) \tag{11.21}$$

In contrast to the constant heat flux case, the temperature gradient in the constant wall temperature case is not constant because neither h_c nor $(T_s - T_b)$ is constant. Since T_s is constant, $dT_b = -d(T_s - T_b)$. Then if we write $\Delta T = (T_s - T_b)$, equation (11.21) becomes a differential equation for the new parameter ΔT, viz.

$$\frac{dT_b}{dx} = -\frac{d(\Delta T)}{dx} = \frac{2\pi R_i}{\dot{m} c_P} h_c \Delta T \tag{11.22}$$

Then, separating variables and integrating from the inlet of the tube to the outlet of the tube, we get an expression relating the temperature difference at the outlet of the conduit to the

temperature difference at the inlet of the conduit, viz.

$$\int_{\Delta T_{in}}^{\Delta T_{out}} \frac{d(\Delta T)}{\Delta T} = -\frac{2\pi R_i}{\dot{m}c_P}\int_0^L h_c dx \tag{11.23}$$

or

$$\ln\frac{\Delta T_{out}}{\Delta T_{in}} = -\frac{2\pi R_i L}{\dot{m}c_P}\bar{h}_c \tag{11.24}$$

where we have made use of the definition of the average heat transfer coefficient, viz.

$$\bar{h}_c = \frac{1}{L}\int_0^L h_c dx \tag{11.25}$$

Thus the axial temperature profile in the fluid can be written

$$\frac{T_s - T_{b,out}}{T_s - T_{b,in}} = \exp\left(-\frac{2\pi R_i L}{\dot{m}c_P}\bar{h}_c\right) = \frac{\Delta T_{out}}{\Delta T_{in}} \tag{11.26}$$

For the axial temperature distribution we can rewrite equation (11.26) in the form

$$\frac{T_s - T_b(x/L)}{T_s - T_{b,in}} = \exp\left[-\left(\frac{\pi DL}{\dot{m}c_P}\right)\left(\frac{x}{L}\right)\right]$$

which is plotted in Figure 11.5 for the case in which

$$\frac{\pi DL}{\dot{m}c_P} = 2.5 \quad \text{and} \quad T_s = 100\ \text{C} \quad \text{and} \quad T_s - T_{b.in} = 10\ \text{C}$$

Clearly, the difference between the temperature of the surface of the conduit and the bulk-mean temperature of the fluid varies along the conduit axis.

From the first law,

$$\dot{Q} = \dot{m}c_P(T_{b,out} - T_{b,in}) = -\dot{m}c_P\left[(T_s - T_{b,out}) - (T_s - T_{b,in})\right] \tag{11.27}$$

or

$$\dot{Q} = -\dot{m}c_P(\Delta T_{out} - \Delta T_{in}) \tag{11.28}$$

If we now rewrite equation (11.26) for the axial temperature profile to yield an expression for the *capacity rate*, we obtain

$$\dot{m}c_P = -\frac{2\pi R_i L\bar{h}_c}{\ln\dfrac{\Delta T_{out}}{\Delta T_{in}}} \tag{11.29}$$

If we now substitute equation (11.29) into equation (11.27), we obtain an expression for Newton's Law of Cooling for the whole tube, viz.

$$\dot{Q} = \bar{h}_c 2\pi R_i L\frac{\Delta T_{out} - \Delta T_{in}}{\ln\dfrac{\Delta T_{out}}{\Delta T_{in}}} = \bar{h}_c A_s \Delta T_{LM} \tag{11.30}$$

where, for this situation in which the temperature difference between the conduit wall and the fluid varies along the length of the flow conduit, we have introduced the concept of the *log mean temperature difference*, ΔT_{LM}, as the appropriate temperature difference driving the heat transfer interaction described by Newton's Law of Cooling, viz.

$$\Delta T_{LM} = \frac{\Delta T_{out} - \Delta T_{in}}{\ln\dfrac{\Delta T_{out}}{\Delta T_{in}}} \tag{11.31}$$

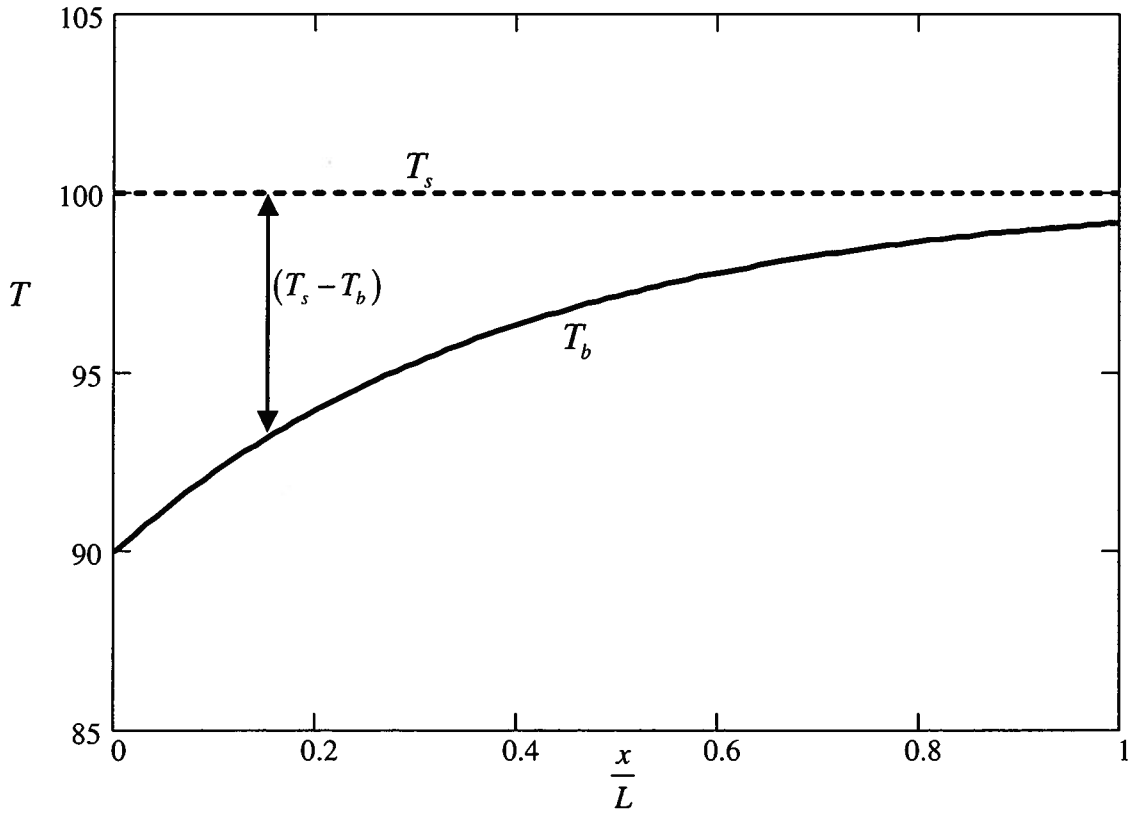

Figure 11.Axial Temperature Distribution for Forced Convection in a Circular Conduit with Constant Surface Temperature

Note that equations (11.26) and (11.30) also can be applied to a slightly different heat transfer situation from the one just described. As shown schematically in cross-section in Figure 11.6, instead of a constant tube surface temperature we have a fluid with constant temperature

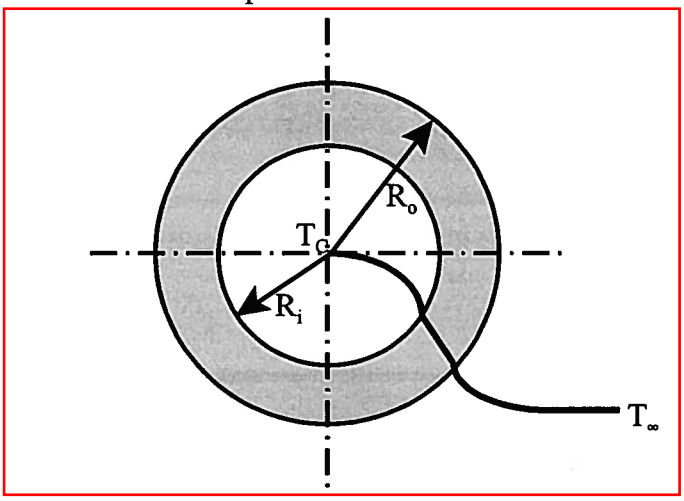

Figure 11.6 Heat Transfer from a Fluid Flowing in a Pipe to an External Fluid of Temperature T_∞

flowing over the outside of the tube with a corresponding average heat transfer coefficient $\overline{h_{c,o}}$, and radial temperature gradient as shown. If the temperature of this external fluid remote from the external surface of the tube has the fixed value T_∞, Newton's Law of Cooling becomes

$$\dot{Q} = \overline{U} A_s \Delta T_{LM} \tag{11.32}$$

where

$$\frac{\Delta T_{out}}{\Delta T_{in}} = \frac{T_\infty - T_{b,out}}{T_\infty - T_{b,in}} = \exp\left(-\frac{2\pi R_i L}{\dot{m} c_P} \overline{U} \right) \tag{11.33}$$

and the log mean temperature difference is calculated according to equation (11.32). The overall heat transfer coefficient $\overline{U}$ is calculated by recognizing that the energy associated with the heat transfer from the external fluid to the internal fluid must past through three thermal resistances in series:

(1) the convection thermal resistance between the internal fluid and the inside of the tube wall given by equation (6.14)

$$R_{\substack{convection \\ inside}} = \frac{1}{2\pi R_i L \overline{h_{c,i}}} \tag{11.34}$$

(2) the conduction thermal resistance of the tube wall itself given by equation (6.34)

$$R_{\substack{conduction \\ wall}} = \frac{\ln \frac{R_o}{R_i}}{2\pi k_{wall} L} \tag{11.35}$$

(3) the convection thermal resistance between the external fluid and the outside of the tube wall also given by equation (6.14)

$$R_{\substack{convection \\ outside}} = \frac{1}{2\pi R_o L \overline{h_{c,o}}} \tag{11.36}$$

Then upon combining equations (11.32) through (11.34), we get

$$\overline{U}_i A_{s,i} = \overline{U}_o A_{s,o} = \left[\frac{1}{2\pi R_i L \overline{h_{c,i}}} + \frac{\ln \frac{R_o}{R_i}}{2\pi k_{wall} L} + \frac{1}{2\pi R_o L \overline{h_{c,o}}} \right]^{-1} \tag{11.37}$$

where $\overline{U_i}$ is the overall heat transfer coefficient based upon the internal surface area of the tube $A_{s,i}$ and $\overline{U_o}$ is the overall heat transfer coefficient based upon the external surface area of the tube $A_{s,o}$.

Example 11E.3: A "moonshiner" (a producer of illegal alcoholic liquor known as "white lightening" in a home still in a rural area of the U.S.) produces liquor with the highest possible concentration in a simple still – 96 percent ethanol by volume (192 proof). [This is known as an *azeotrope* which is the concentration for which the liquid and vapor have the same concentration of the more volatile component.] The liquor comes from the still in vapor form at a pressure of P_s = 2 x 10^5 N/m^2 and is condensed at constant pressure to the liquid form at a temperature of 95.6 C. For bottling purposes, the moonshiner wishes to cool the liquor in a simple heat exchanger

consisting of a length L of thin-walled copper tubing with a diameter of D = 10 mm formed into a series of coils. By the time the liquor reaches the cooler, its temperature has reached $T_{b,in}$ = 90 C. The desired outlet temperature is $T_{b,out}$ = 30 C. The liquor flows through the tubing at an average velocity of ϑ = 1 m/sec. The coils of copper tubing are immersed in a large water bath contained in a surplus oil drum now filled with water at a constant temperature of T_w = 20 C. The coils are cooled by the water by a process known as natural convection with a resulting average heat transfer coefficient of $\overline{h_o}$ = 800 W/m^2 K. The forced convection heat transfer coefficient for the liquor inside the tubing is $\overline{h_i}$ = 1880 W/m^2 K. The moonshiner wishes to determine the length L of copper tubing required for this simple heat exchanger.

For the liquor:

ρ = 738.55 kg/m^3, c = 2890 J/kg K, k = 0.167 W/m K, μ = 0.588 x 10^{-3} kg/m sec

Solution: The heat transfer experienced by the liquor as it flows through the tubing can be determined by the first law, viz.

$$\dot{Q} = \dot{m}c\left(T_{b,in} - T_{b,out}\right)$$

where

$$\dot{m} = \rho A_c \vartheta_{ave} = \rho\pi\frac{D^2}{4}\vartheta_{ave} = \left(738.55\ \text{kg/m}^3\right)\pi\frac{(0.010\ \text{m})^2}{4}(1\ \text{m/sec}) = 0.0580\ \text{kg/sec}$$

Then

$$\dot{Q} = (0.0580\ \text{kg/sec})(2890\ \text{J/kg K})(30\ \text{C} - 90\ \text{C}) = -1.0058\ \text{x}\ 10^4\ \text{W}$$

The negative sign indicates that the heat transfer is from the liquor to the cooling water. From Newton's Law of Cooling, this same heat transfer rate is given by

$$\dot{Q} = UA\Delta T_{LM}$$

where UA is the overall heat transfer coefficient given by equation (11.37) and ΔT_{LM} is the log-mean temperature difference given by equation (11.31). Then

Log Mean logic

$$\Delta T_{in} = T_{b,in} - T_w = 90\ \text{C} - 20\ \text{C} = 70\ \text{C}$$

$$\Delta T_{out} = T_{b,out} - T_w = 30\ \text{C} - 20\ \text{C} = 10\ \text{C}$$

$$\Delta T_{LM} = \frac{\Delta T_{out} - \Delta T_{in}}{\ln\dfrac{\Delta T_{out}}{\Delta T_{in}}} = \frac{70\ \text{C} - 10\ \text{C}}{\ln\dfrac{70\ \text{C}}{10\ \text{C}}} = 30.834\ \text{C}$$

The overall heat transfer coefficient contains the unknown length L. Then we write

$$UA = \left[\frac{1}{\pi DL\overline{h_{c,i}}} + \frac{1}{\pi DL\overline{h_{c,o}}}\right]^{-1} = \left(\frac{1}{L}\right)^{-1}\left[\frac{1}{\pi D\overline{h_{c,i}}} + \frac{1}{\pi D\overline{h_{c,o}}}\right]^{-1} = L\left[\frac{1}{\pi D\overline{h_{c,i}}} + \frac{1}{\pi D\overline{h_{c,o}}}\right]^{-1}$$

$$ua = \frac{UA}{L} = \left[\frac{1}{\pi D\overline{h_{c,i}}} + \frac{1}{\pi D\overline{h_{c,o}}}\right]^{-1} = \left[\frac{1}{\pi(0.010\ \text{m})\left(1880\ \text{W/m}^2\ \text{K}\right)} + \frac{1}{\pi(0.010\ \text{m})\left(800\ \text{W/m}^2\ \text{K}\right)}\right]^{-1}$$

$$ua = 17.63\ \text{W/m K}$$

Notice that we have neglected the thermal resistance of the tubing since it is thin-walled and it is fabricated from copper which has a very high thermal conductivity (k_{Cu} = 384 W/m K). Then Newton's Law of Cooling can be written

$$\dot{Q} = uaL\Delta T_{LM}$$

$$L = \frac{\dot{Q}}{ua\Delta T_{LM}} = \frac{1.0058 \text{ x } 10^4 \text{ W}}{(17.63 \text{ W/m K})(30.834 \text{ C})} = 18.5 \text{ m}$$

This is the length of copper tubing required to provide sufficient surface area for the cooling of the liquor.

As we have mentioned previously, the velocity of the fluid flowing inside the conduit is not uniform over the cross-sectional area of the conduit. In fact it varies from one radial position to another. It now remains for us to determine the manner in which this velocity distribution establishes the temperature profile for the laminar flow conditions in the conduit. Since the flow velocity governs the amount of time available for any fluid element to experience a heat transfer interaction with the wall or other fluid elements, we must use this velocity profile to determine the temperature profile and the rate of heat transfer that results. Using Newton's Law of Cooling, we can then determine the heat transfer coefficient, h_c.

11.4 Forced Convection Heat Transfer in Laminar Flow in a Circular Conduit

The basic approach is to determine the temperature profile in the fluid in the radial direction in order to establish the temperature gradient in the fluid at the wall of the conduit. From this temperature gradient and the Fourier Conduction Law, we can determine the heat flux at the wall in the fluid. We can then use this heat flux together with Newton's Law of Cooling to determine the convective heat transfer coefficient, h_c. Of course, the radial temperature profile in the fluid is determined by the residence time of the fluid at any location. This, in turn, is a function of the velocity profile in the fluid. Thus, it is necessary to first solve the momentum equation to determine the velocity profile. For the laminar flow case, we have already done this and obtained the result shown in equation (11.3).

11.4.1 Constant Surface Heat Flux in Forced Convection Heat Transfer

As before, we first consider the case in which the heat flux at the wall of the conduit is constant. We now assume that the flow is laminar and is fully developed both hydrodynamically and thermally. That is, we assume that we are examining the flow far enough from the entry region that the temperature profile will be a function of radial position only, independent of the axial coordinate. Thus, in all that follows, $L >> L_{th}$, where L_{th} is given by equation (11.5).

Equation (11.20) gives the axial temperature profile for flow in a conduit with a constant surface heat flux. While this result relates the heat flux at the surface to the axial gradient in the one-dimensional bulk-flow average temperature, we can generalize it to any radial location in the fluid. For example, consider the annular differential control volume shown in Figure 11.7. The first law gives

$$\left[\dot{q}2\pi rdx\right]_{r+dr} - \left[\dot{q}2\pi rdx\right]_r = \rho v h(x)2\pi rdr - \rho v h(x+dx)2\pi rdr \qquad (11.38)$$

where $\dot{q}$ is the local heat flux and $h(x + dx)$ and $h(x)$ are the specific enthalpies of the fluid at the locations $x + dx$ and x, respectively. Using the constitutive relation for the specific enthalpy (mindful of the approximation involved in the case of the incompressible fluid), we have

$$\begin{aligned} h(x) &= c_p T(x) \\ h(x+dx) &= c_p T(x+dx) \end{aligned} \qquad (11.39)$$

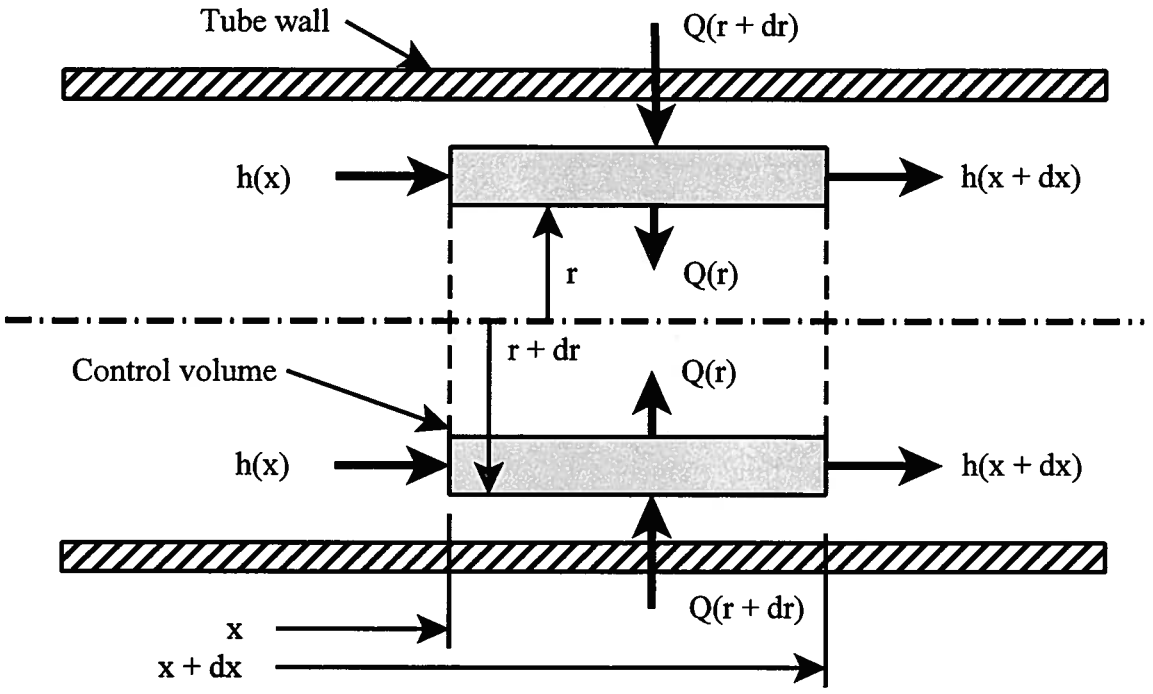

Figure 11.7 Differential Control Volume for Laminar Flow Heat Transfer in a Circular Conduit

If we expand the various terms in Taylor series, we get

$$\begin{aligned}\left[\dot{q}2\pi r dx\right]_{r+dr} &= \left[\dot{q}2\pi r dx\right]_r + \frac{\partial}{\partial r}\left[\dot{q}2\pi r dx\right]_r dr \\ \rho\vartheta c_P T(x+dx)2\pi r dr &= \left[\rho\vartheta c_P T(x) + \rho\vartheta c_P \frac{\partial}{\partial x}T(x)dx\right]2\pi r dr\end{aligned} \tag{11.40}$$

Substituting equations (11.40) into equation (11.38) and then collecting terms and dividing through by $2\pi\rho c_P dr dx$, we get

$$\vartheta\frac{\partial T}{\partial x} = -\frac{1}{\rho c_P}\frac{1}{r}\frac{\partial}{\partial r}(r\dot{q}) \tag{11.41}$$

but from Fourier's Law of Conduction

$$\dot{q} = -k\left(\frac{\partial T}{\partial r}\right) \tag{11.42}$$

Then

$$\vartheta\frac{\partial T}{\partial x} = \frac{k}{\rho c_P}\frac{1}{r}\frac{\partial}{\partial r}\left(r\frac{\partial T}{\partial r}\right) = \frac{\alpha}{r}\frac{\partial}{\partial r}\left(r\frac{\partial T}{\partial r}\right) \tag{11.43}$$

For the case of constant heat flux at the surface, we have already seen that even though T_s and T_b vary along the axis of the tube, the relative shape of the temperature profile (like the velocity profile) does not change along the axis of the tube. That is, $T_s(x)$ - $T_b(x)$ and $T_s(x)$ - $T(r,x)$ are independent of x as we have already seen. Then, it follows that the dimensionless temperature

difference should also be independent of x, viz.

$$\frac{\partial}{\partial x}\left[\frac{T_s(x)-T(r,x)}{T_s(x)-T_b(x)}\right]=0 \tag{11.44}$$

If we carry out the differentiation and solve for $\frac{\partial T}{\partial x}$, we obtain

$$\frac{\partial T}{\partial x}=\frac{dT_s}{dx}-\frac{(T_s-T)}{(T_s-T_b)}\frac{dT_s}{dx}+\frac{(T_s-T)}{(T_s-T_b)}\frac{dT_b}{dx} \tag{11.45}$$

but from Figure 11.5 it is apparent that beyond the entry length

$$\frac{dT_s}{dx}=\frac{dT_b}{dx} \tag{11.46}$$

Then it follows that

$$\frac{\partial T}{\partial x}=\frac{dT_b}{dx} \tag{11.47}$$

Then equation (11.43) becomes

$$\vartheta\frac{dT_b}{dx}=\frac{\alpha}{r}\frac{\partial}{\partial r}\left(r\frac{\partial T}{\partial r}\right) \tag{11.48}$$

Since the temperature difference T - T_b is independent of x, we can write

$$T-T_b=\Re(r) \tag{11.49}$$

Substituting equations (11.3) and (11.49) into equation (11.48), we get for laminar flow

$$2\vartheta_{ave}\left[1-\left(\frac{r}{R}\right)^2\right]\frac{dT_b}{dx}=\frac{\alpha}{r}\frac{d}{dr}\left(r\frac{d\Re}{dr}\right) \tag{11.50}$$

Our task of determining the temperature profile in the case of laminar flow in a circular conduit with a constant heat flux at the surface is reduced to evaluating the function $\Re(r)$ in equation (11.50). To do this, we note that we have already shown in equation (11.18) that

$$\frac{dT_b}{dx}=\frac{2\pi R_i\dot{q}_s}{\dot{m}c_P}=\frac{2\dot{q}_s}{\rho\vartheta_{ave}c_PR_i}=\text{ constant} \tag{11.51}$$

Combining equations (11.50) and (11.51), we get

$$\left[1-\left(\frac{r}{R}\right)^2\right]\frac{4\dot{q}_s}{kR_i}=\frac{1}{r}\frac{d}{dr}\left(r\frac{d\Re}{dr}\right) \tag{11.52}$$

with the following boundary conditions

$$\left(\frac{dT}{dr}\right)_{(r=0)}=\left(\frac{d\Re}{dr}\right)_{(r=0)}=0 \tag{11.53}$$

and

$$T(R_i)=T_s(R_i) \qquad \text{or} \qquad \Re(R_i)=T_s-T_b \tag{11.54}$$

Integrating equation (11.52) once, we get

$$\frac{d\Re}{dr}=\frac{4\dot{q}}{kR_i}\left[\frac{r}{2}-\frac{r^3}{4R_i^2}\right]+\frac{C_1}{r} \tag{11.55}$$

By equation (11.53), $C_1 = 0$. Substituting this result into equation (11.55) and integrating, we get

$$\Re = \frac{4\dot{q}_s}{kR_i}\left[\frac{r^2}{4} - \frac{r^4}{16R_i^2}\right] + C_2 \tag{11.56}$$

By equation (11.54), it follows that

$$T = T_s - \frac{4\dot{q}_s}{kR_i}\left[\frac{3R_i^2}{16} - \frac{r^2}{4} - \frac{r^4}{16R_i^2}\right] \tag{11.57}$$

We can now substitute this result into equation (11.10) and integrate over the cross-section of the tube to obtain the one-dimensional bulk-flow average temperature. There results

$$T_b = T_s - \frac{11}{24}\frac{\dot{q}_s R_i}{k} \tag{11.58}$$

We can now combine equation (11.58) with Newton's Law of Cooling to obtain an expression for the heat transfer coefficient, viz.

$$h_c = \frac{\dot{q}_s}{(T_s - T_b)} = \frac{24}{11}\frac{k}{R_i} = \frac{48}{11}\frac{k}{D_i} \tag{11.59}$$

Equation (11.59) can be rearranged into a dimensionless form, viz.

$$Nu_D = \frac{h_c D_i}{k} = \frac{48}{11} = 4.364 \tag{11.60}$$

Always for constant heat flux

where we have introduced the dimensionless Nusselt number, Nu_D, which can be interpreted physically in the following manner. The heat flux at the wall of the tube can be calculated in two different ways: either by Newton's Law of Cooling or by evaluating the Fourier Conduction Law from the temperature profile in the fluid at the wall. Since they must give us the same result, we can equate them. Thus,

$$\dot{q}_s = h_c(T_s - T_b) = -k\left(\frac{\partial T}{\partial r}\right)_{(r=R_i)} \tag{11.61}$$

If we multiply both sides of equation (11.61) by D_i and solve for the Nusselt number, we get

$$Nu_D = \frac{h_c D_i}{k} = -\frac{2R_i}{(T_s - T_b)}\left(\frac{\partial T}{\partial r}\right)_{(r=R_i)} \tag{11.62}$$

Since $(T_s - T_b)/R_i$ is a measure of the average temperature gradient in the fluid across the conduit, the Nusselt number is the ratio of the temperature gradient at the surface to the average temperature gradient in the fluid. The larger the value of the Nusselt number, the steeper the temperature gradient at the surface in proportion to the average temperature gradient in the fluid.

11.4.2 Constant Surface Temperature in Forced Convection Heat Transfer

We have just shown that the ratio implied in the expression for the Nusselt number, equation (11.62), is a constant for the case of a constant heat flux at the surface. This result is a consequence of the fact that in the fully developed flow, the shapes of both the velocity profile and the temperature profile do not change in the direction of flow along the axis of the conduit. Since this is also true in the case of laminar flow in a circular conduit with an isothermal wall, we would expect a similar result.

For the case of the constant surface temperature, equation (11.48) becomes

$$\vartheta\left(\frac{T_s - T}{T_s - T_b}\right)\frac{dT_b}{dx} = \frac{\alpha}{r}\frac{\partial}{\partial r}\left(\frac{\partial T}{\partial r}\right) \tag{11.63}$$

with boundary conditions

$$T(R_i) = T_s \tag{11.64}$$

and

$$\left(\frac{\partial T}{\partial r}\right)_{(r=0)} = 0 \tag{11.65}$$

As before, substituting the velocity profile from equation (11.3), we get the new form of equation (11.63).

$$2\vartheta_{ave}\left[1-\left(\frac{r}{R}\right)^2\right]\left(\frac{T_s - T}{T_s - T_b}\right)\frac{dT_b}{dx} = \frac{\alpha}{r}\frac{\partial}{\partial r}\left(\frac{\partial T}{\partial r}\right) \tag{11.66}$$

Equation (11.66) is usually solved by the method of successive approximations. Equation (11.57) is substituted for T in equation (11.66) and the resulting polynomial expression is integrated to obtain a new temperature profile. This new profile is now substituted back into the original expression and the process is repeated. For each new temperature profile, the Nusselt number is calculated and the process of integration of equation (11.66) is repeated until the value of the Nusselt number converges. The limiting value for this case of constant surface temperature is

$$Nu_D = 3.66 \tag{11.67}$$

11.4.4 Developing Laminar Flows or Entrance Effects in Forced Convection Heat Transfer

The results of the analyses embodied in equations (11.60) and (11.67) enable us to determine the heat transfer coefficients for laminar flow of incompressible fluids in two important heat transfer configurations commonly encountered in engineering practice. Equations (11.60) and (11.67) are applicable as long as two important criteria are met:

(1) the **flow must be laminar**, i.e. $Re \leq 2300$, and

(2) the **flow must be fully developed**

While these two criteria are satisfied in many practical situations, there are also many situations for which they are not met, and the practicing thermal-fluids engineer must be prepared to address them. Let us consider these two criteria separately beginning with the second.

In section 11.2.1 we touched briefly on the thermal entrance effects for which the flow was fully developed hydrodynamically but not thermally. Because the heat transfer coefficient is so large in the immediate vicinity of the thermal entrance to the conduit ($h_c \to \infty$) relative to the fully developed value downstream, the effect of the thermally developing flow on the *average* heat transfer coefficient for a long conduit is felt even for relatively large values of L/D. This is particularly troublesome in the case of the constant wall temperature because the heat transfer rate and the axial temperature profile for a single conduit both depend upon the average heat transfer coefficient $\overline{h}_c$ [*cf.* equations (11.26) and (11.30).]. For this reason, the case of the constant surface temperature studied in Section 11.3 has been analyzed in detail to determine the effects of the thermal entry region. For example, see W. M. Kays, M. E. Crawford, and B. Weigand, *Convective Heat and Mass Transfer*, 4th Edition, McGraw-Hill, N. Y., 2005, Chapter 8. However, these results, shown in graphical form in Figure 11.8, are unwieldy to work with in closed form. Consequently, the results of the analysis have been fit with a dimensionless correlation, equation (11.68), that lends itself more readily to calculation by the practicing thermal-fluids engineer. This correlation is also plotted in Figure 11.8.

For a circular conduit with a constant surface temperature in hydrodynamically fully

developed flow, the average Nusselt number is given by

$$\overline{Nu_D} = 3.66 + \frac{0.065(D/L)Re_D Pr}{1 + 0.045\left[(D/L)Re_D Pr\right]^{2/3}} \tag{11.68}$$

For the case in which the surface heat flux is constant, the situation is somewhat different from the case of constant surface temperature. For a single conduit, the heat transfer for the whole conduit can be evaluated directly from the heat flux so there is no need for the average heat transfer coefficient. However, as we shall see in Chapter 12, in a two-fluid heat exchanger, the average Nusselt number is required to determine the overall heat transfer coefficient as in equation (11.37). Furthermore, there are physical situations where the flow is already fully developed hydrodynamically but not thermally. Such might be the case, for example, for a conduit with a heater mounted on the wall far downstream of the physical entrance to the conduit. In the heated region, the Nusselt number and, hence, the heat transfer coefficient will no longer be a constant, but rather, will be a function of position in the direction of flow.

Again, the aforementioned reference, W. M. Kays, M. E. Crawford, and B. Weigand, *Convective Heat and Mass Transfer*, 4th Edition, McGraw-Hill, N. Y., 2005, Chapter 8, presents an analysis of this situation in detail and the results are shown in Figure 11.8 along with a curve fit to the analytical results. In this case, two curve fits are required:

$$\begin{aligned} \overline{Nu_D} &= 1.953\left[\left(D/L\right)Re_D Pr\right]^{1/3} \quad \text{for} \quad \left(D/L\right)Re_D Pr \le 0.03 \\ \overline{Nu_D} &= 4.364 + 0.0722\left(D/L\right)Re_D Pr \quad \text{for} \quad \left(D/L\right)Re_D Pr > 0.03 \end{aligned} \tag{11.69}$$

For the two limiting cases involving laminar flow that we have just considered, the conduit length for which the thermal development is important is given by equations (11.5a) and (11.5b), and these cases have been studied in detail. Figure 11.8 shows in graphical form the results of these analytical studies. However, there are other situations in which we must also consider the possibility that the flow is not fully developed either thermally or hydrodynamically. That is, both the velocity and the temperature profiles are developing simultaneously. As we discussed in section 11.2.1, this is quite likely the case in the entrance region of flow in a tube for fluids with large values of the Prandtl number. Again the Nusselt number and the heat transfer coefficient are functions of position in the direction of flow.

While both thermal entrance effects and combined thermal and hydrodynamic effects can be treated using the model techniques described above, the methods of analysis are beyond the scope of this treatment. Instead we present the results in graphical form in Figure 11.8 drawn from the work of Kays and Crawford (W. M. Kays and M. E. Crawford, *Convective Heat and Mass Transfer*, 2nd edition, McGraw-Hill, N. Y., 1980, Chapter 8). Note that the local Nusselt number becomes infinite at $x = 0$ and the results are plotted as a function of the inverse of the Graetz number, Gz, where

$$Gz^{-1} = \frac{x/D}{Re_D Pr} \tag{11.68}$$

Note that the thermal entry length is independent of the Prandtl number, but the combined entry length depends upon Prandtl number. Note also that the plots approach equations (11.60) and (11.66) in the limit of large values of x/D, i.e. small values of the Graetz number.

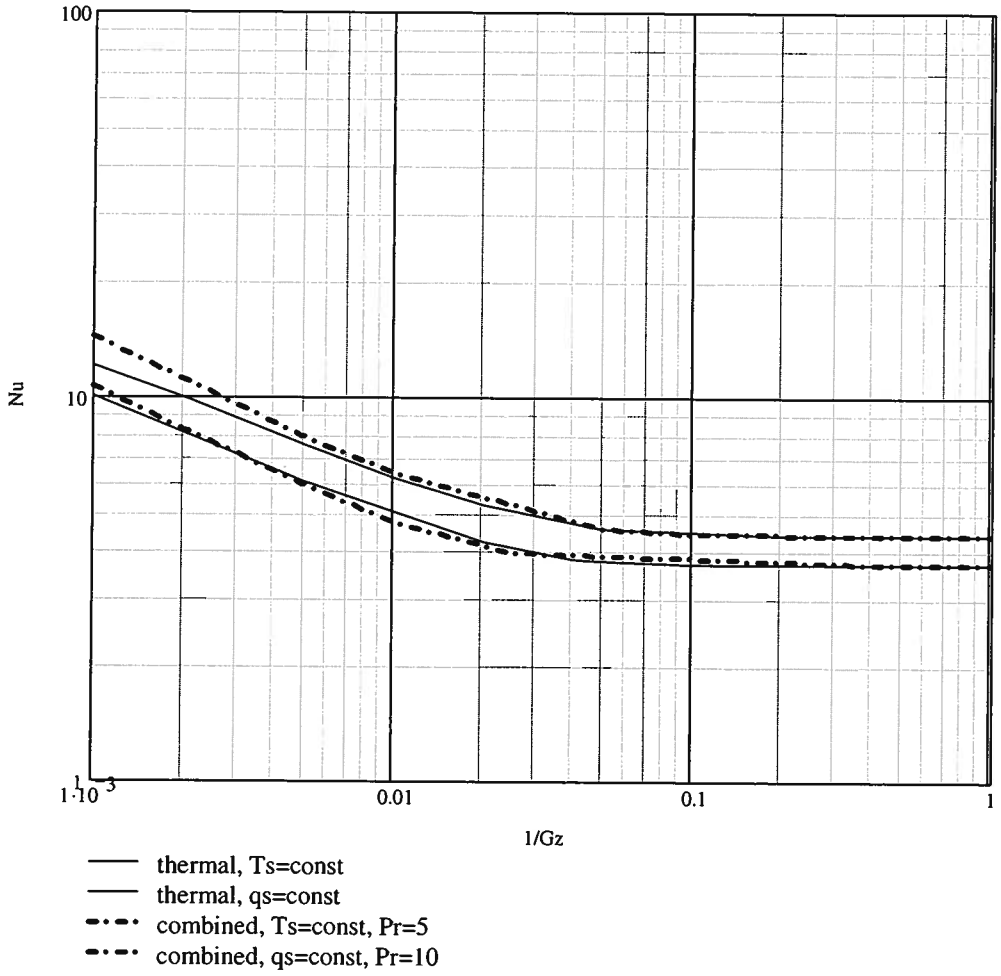

Figure 11.8 Local Nusselt Number for Developing Flows

Example 11E.4: The rules for international hockey require that the rink must be 61 m long by 26 m wide. Testing has shown that the ideal ice surface temperature for skating should be $T_{ice} = -5$ C. The temperature of the air immediately above the ice surface is to be maintained at a constant temperature of $T_{air} = 3.5$ C.

As shown in Figure 11E.4, the ice is 2 cm thick and is formed on a concrete slab 12 cm thick. The midplane of this concrete slab is also the midplane of an array of pipes carrying a heat transfer fluid known as Dowtherm SR-1, consisting of 50% ethylene glycol (antifreeze) and 50% water plus some anti-corrosion additive. This configuration enables us to model the midplane of the pipes as an isothermal surface 6 cm below the bottom of the ice slab. Heat transfer analysis of the ice surface shows that the temperature of the midplane of the concrete, which is also the surface temperature of the pipes, is $T_s = -18$ C.

The ethylene glycol piping consists of thin-walled mild steel tubing with an inside diameter of $D = 10$ mm. The piping is configured so that the supply and return headers are placed across the middle of the rink with a typical tube running from the supply header to the end of the rink and returning to the return header. The mass flow rate for each tube is $m_e = 0.0656$ kg/sec. The bulk-mean temperature of the ethylene glycol solution at the inlet to each tube is $T_{b,in} = -20$

C. We wish to determine the exit temperature of the coolant and the heat transfer rate for each tube.

For Dowtherm SR-1: $\rho = 1088.15$ kg/m^3, $c = 3129$ J/kg K, $k = 0.3442$ W/m K,
$\mu = 2.2082 \times 10^{-2}$ kg/m sec, $Pr = 200.7$

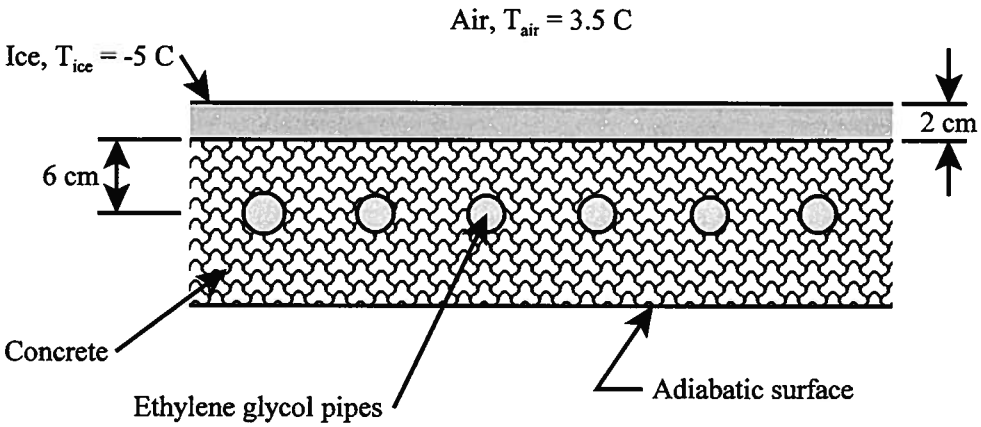

Figure 11E.4

Solution: We first determine the Reynolds number.

$$Re_D = \frac{4\dot{m}}{\pi\mu D} = \frac{4(0.0656 \text{ kg/sec})}{\pi\left(2.2082 \times 10^{-2} \text{ kg/m sec}\right)} = 378$$

Clearly, the flow is laminar. If we knew the value of the average heat transfer coefficient for the tube, we could use equation (11.26) to determine the outlet temperature of the coolant. From equation (11.69)

$$Nu = 3.66 + \frac{0.065\left(\frac{D}{L}\right)Re_D Pr}{1 + 0.045\left[\left(\frac{D}{L}\right)Re_D Pr\right]^{2/3}} = 3.66 + \frac{0.065\left(\frac{0.010 \text{ m}}{61 \text{ m}}\right)(378)(200.7)}{1 + 0.045\left[\left(\frac{0.010 \text{ m}}{61 \text{ m}}\right)(378)(200.7)\right]^{2/3}} = 4.311$$

Then

$$\overline{h_c} = Nu\frac{k}{D} = 4.311\frac{0.3442 \text{ W/m K}}{0.010 \text{ m}} = 148.39 \text{ W/m}^2 \text{ K}$$

From equation (11.26)

$$\frac{T_s - T_{b,out}}{T_s - T_{b,in}} = \exp\left(-\frac{\pi D L \overline{h_c}}{\dot{m}c}\right)$$

$$T_{b,out} = T_s - \left(T_s - T_{b,in}\right)\exp\left(-\frac{\pi D L \overline{h_c}}{\dot{m}c}\right)$$

$$T_{b,out} = -18 \text{ C} - \left[(-18 \text{ C}) - (-20 \text{ C})\right]\exp\left[-\frac{\pi(0.010 \text{ m})(61 \text{ m})(148.39 \text{ W/m}^2 \text{ K})}{(0.0656 \text{ kg/sec})(3129 \text{ J/kg K})}\right]$$

$$T_{b,out} = -18.5 \text{ C}$$

Then the heat transfer rate for each tube can be computed from the first law, viz.

$$\dot{Q} = \dot{m}c\left(T_{b,out} - T_{b,in}\right) = (0.0656 \text{ kg/sec})(3129 \text{ J/kg K})\left[(-18.5 \text{ C}) - (-20 \text{ C})\right] = 307.69 \text{ W}$$

We can also evaluate the heat transfer rate from Newton's Law of Cooling, viz.

$$\dot{Q} = \overline{h}_c A_s \Delta T_{LM} = \overline{h}_c \pi D L \Delta T_{LM}$$

where the log-mean temperature difference is given by

$$\Delta T_{LM} = \frac{\left(T_s - T_{b,out}\right) - \left(T_s - T_{b,in}\right)}{\ln\left(\dfrac{T_s - T_{b,out}}{T_s - T_{b,in}}\right)} = \frac{\left[(-18 \text{ C}) - (-18.5 \text{ C})\right] - \left[(-18 \text{ C}) - (-20 \text{ C})\right]}{\ln\left\{\dfrac{\left[(-18 \text{ C}) - (-18.5 \text{ C})\right]}{\left[(-18 \text{ C}) - (-20 \text{ C})\right]}\right\}} = 1.082 \text{ C}$$

Then

$$\dot{Q} = \left(148.39 \text{ W/m}^2 \text{ K}\right)\pi(0.010 \text{ m})(61 \text{ m})(1.082 \text{ C}) = 307.69 \text{ W}$$

which is precisely the same result obtained from the first law.

11.5 Forced Convection Heat Transfer in Laminar Flow in a Non-Circular Conduit

There are many cases in the practice of thermal fluids engineering in which the working fluid is transported through a conduit for which the cross-sectional area perpendicular to the direction of flow is not circular, but the flow is laminar nonetheless. Such cases are common in nanotechnology, for example, for which the fabrication processes of necessity often result in flow channels of square, rectangular, or even triangular cross-section. Since the characteristic dimension of these channels is extremely small, the relevant Reynolds numbers that characterize the flow are small, thereby resulting in laminar flow. Provided that the requirements for continuum conditions are fulfilled, the heat transfer process in these cases can be analyzed utilizing the approach discussed above. However, the non-circular geometry of the channel complicates the form of the Navier-Stokes equation somewhat so that the solution is less straightforward than shown above for the circular case. Fortunately, these geometries have been studied in great detail (see R. K. Shah and A. L. London, *Laminar Flow Forced Convection in Ducts*, in *Advances in Heat Transfer*, Supplement 1, ed. By T. F. Irvine and J. P. Hartnett, Academic Press, 1978.), and the results of these analyses have been cast in a dimensionless form that readily lends itself to the application of a wide variety of thermal-fluid engineering situations. Table 11.1 summarizes these results for both the friction factor, f, and the Nusselt number for both constant heat flux at the wall, Nu_H, and constant wall temperature, Nu_T. Note that in the case of the elliptic channel, the cross-section becomes circular for the case in which $b/a = 1.00$. Thus, Table 11.1 contains results for conduits of both circular and non-circular cross-section.

Table 11.1 Friction Factor and Nusselt Number Data for Laminar Flow in Non-circular Conduits

$Re = \frac{\vartheta D_h \rho}{\mu}$ where $D_h = \frac{4A_{cross\cdot section}}{\wp} = \frac{4A_c}{\wp}$ and $\wp$ is the wetted perimeter

Nu_H means constant heat flux and Nu_T means constant wall temperature

	Ellipse					Rectangle					Triangle				
b/a	A_c/a^2	$\wp/a$	$f\cdot Re$	Nu_H	Nu_T	A_c/a^2	$\wp/a$	$f\cdot Re$	Nu_H	Nu_T	A_c/a^2	$\wp/a$	$f\cdot Re$	Nu_H	Nu_T
10.00	31.42	4.06	77.26	5.12	3.70	40.00	44.00	84.68	6.78	5.91	10.00	22.10	50.17	2.29	1.34
5.00	15.71	4.20	74.41	4.96	3.77	20.00	24.00	76.28	5.74	4.83	5.00	12.20	51.62	2.51	1.70
2.00	6.28	4.84	67.29	4.56	3.74	8.00	12.00	62.19	4.12	3.39	2.00	6.47	53.28	2.88	2.22
1.00	3.14	6.28	64.00	4.36	3.66	4.00	8.00	56.91	3.61	2.98	1.00	4.83	52.61	3.10	2.46
0.90	2.83	5.97	64.09	4.37	3.66	3.60	7.60	57.04	3.62	2.97	0.90	4.69	52.22	3.12	2.47
0.80	2.51	5.67	64.39	4.39	3.67	3.20	7.20	57.51	3.66	3.01	0.80	4.56	51.84	3.11	2.46
0.70	2.20	5.38	64.98	4.42	3.69	2.80	6.80	58.42	3.75	3.09	0.70	4.44	51.45	3.10	2.45
0.60	1.88	5.11	65.92	4.48	3.72	2.40	6.40	59.92	3.89	3.21	0.60	4.33	51.06	3.06	2.41
0.50	1.57	4.84	67.29	4.56	3.74	2.00	6.00	62.19	4.12	3.39	0.50	4.24	50.49	2.99	2.34
0.40	1.26	4.60	69.18	4.67	3.76	1.60	5.60	65.47	4.47	3.67	0.40	4.15	49.81	2.85	2.18
0.30	0.94	4.39	71.58	4.80	3.78	1.20	5.20	70.05	4.99	4.12	0.30	4.09	49.12	2.71	2.02
0.20	0.63	4.20	74.41	4.96	3.77	0.80	4.80	76.28	5.74	4.83	0.20	4.04	48.63	2.49	1.72
0.10	0.31	4.06	77.26	5.12	3.70	0.40	4.40	84.68	6.78	5.91	0.10	4.01	48.31	2.63	1.37

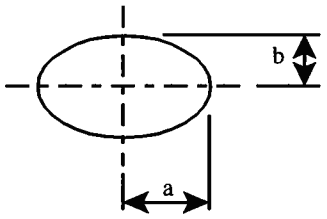

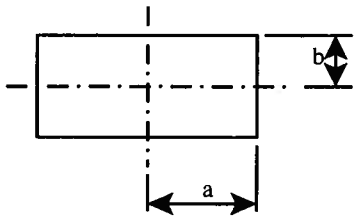

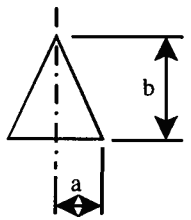

11.5 Forced Convection Heat Transfer to a Fluid in Turbulent Flow in a Conduit

For hydrodynamically fully developed turbulent flow in a circular conduit with $Re_D > 10^4$, the thermal entry length for fluids with Prandtl numbers on the order of unity is typically short with $(L_{th}/D) < 15$. For fluids with small values of the Prandtl number, the thermal entry length is somewhat longer $(L_{th}/D) < 40$. In the present section we shall develop the appropriate relationships that describe the energy transfer that results for fully developed turbulent flow in a circular conduit.

Note that the results of section 11.3 hold for the turbulent case as well as the laminar case since at no time during the derivations of the relevant equations of those sections did we specify the character of the flow. Thus the axial temperature profiles are of the same form for both laminar and turbulent flow for each separate case of flow with constant heat flux at the wall and flow with az constant wall temperature. The laminar and turbulent cases differ in detail, however, since the values of the relevant convection heat transfer coefficients depend markedly upon the nature of the flow. We now proceed to develop the appropriate expressions for the Nusselt number in turbulent flow in a circular conduit.

The complicated nature of turbulent flow defies an analytical treatment of energy transfer analogous to the treatment of the laminar flow case. The source of the complexity is the fact that even though the first law in the form of equation (11.43) is applicable to both laminar and turbulent flow, in turbulent flow the energy transfer process involves both convection, i.e., mass motion due to eddy transport, and simple conduction down the temperature gradient. Thus, a detailed description of energy transfer in turbulent flow requires a knowledge of the velocity fluctuations introduced previously in our study of momentum transfer in turbulent flow. To address this matter, we follow the example of Reynolds. The velocity fluctuations of turbulent flow produce a vigorous exchange of momentum between fluid layers and the boundaries of the fluid. This momentum exchange which is manifested in an increase in both the wall shear stress and the velocity gradient at the wall is characterized by an apparent increase in the viscosity of the fluid. However, in addition to enhancing the transfer of momentum, turbulent mixing due to the motion of eddies in the flow field enhances the transfer of energy as well. This increase in the rate of heat transfer which is manifested in an increase in the temperature gradient at the wall can be characterized (by analogy with momentum transfer) by an apparent increase in the thermal conductivity of the fluid.

We could follow a procedure similar to that used to solve the first law, equation (11.43), for the laminar flow case. For turbulent flow, equation (11.43) is first modified to account for the enhanced energy transfer due to eddy transport, viz.

$$\rho \vartheta c_P \frac{\partial T}{\partial x} = \frac{1}{r}\frac{\partial}{\partial r}\left[r(k + k_t)\frac{\partial T}{\partial r} \right] \tag{11.69}$$

where k_t is the eddy contribution to the apparent thermal conductivity which is a function of r and hence kept inside the brackets. Equation (11.69) can be rearranged to give

$$\vartheta \frac{\partial T}{\partial x} = \frac{1}{r}\frac{\partial}{\partial r}\left[r(\alpha + \varepsilon_H)\frac{\partial T}{\partial r} \right] = \frac{1}{r}\frac{\partial}{\partial r}\left[r\left(\frac{\upsilon}{Pr} + \frac{\varepsilon_M}{Pr_t} \right)\frac{\partial T}{\partial r} \right] \tag{11.70}$$

where ε_H is the eddy diffusivity of heat. Since the Prandtl number of a fluid is defined as the ratio of the momentum diffusivity to the thermal diffusivity, we can, by analogy, define a turbulent Prandtl number, Pr_t, as

$$Pr_t = \frac{\varepsilon_M}{\varepsilon_H} \tag{11.71}$$

Unlike the laminar case, the convection term appearing on the left-hand side of equation (11.70) is negligible compared to the radial conduction which is now enhanced by the turbulent eddies. If we define a coordinate system measured from the wall $y = R_i - r$, we are then left to solve

$$\left(\frac{\upsilon}{Pr}+\frac{\varepsilon_M}{Pr_t}\right)\frac{\partial T}{\partial y} = constant = \dot{q}_s \tag{11.72}$$

to obtain the temperature distribution in the radial direction. Typically, we assume that the mechanism for energy transport is identical to the mechanism for momentum transport in fully turbulent flow, i.e., $Pr_t = 1$. To achieve a solution to equation (11.72), the flow field is broken into three separate regions representing the laminar sublayer, the buffer layer, and the fully turbulent core with a different temperature distribution for each. These temperature distributions are combined with Newton's Law of Cooling to give the convective heat transfer coefficient. The resulting expression is somewhat ponderous and is useful only in illustrating the magnitudes of the various regions of the flow. It is not widely used in thermal-fluids engineering practice. The preferred approach is that due to an idea originally proposed by Reynolds.

Recall from our previous discussion of momentum transfer in turbulent flow that we expressed the total shear stress in a turbulent flow field as the sum of a laminar contribution and a turbulent contribution, viz.

$$\tau = \rho(\upsilon+\varepsilon_M)\frac{d\vartheta}{dy} \tag{11.73}$$

where ε_M is the eddy diffusivity of momentum. Then by analogy, we treat the energy transfer in a similar fashion, viz.

$$\dot{q} = -\rho c_P\left(\frac{k}{\rho c_P}+\varepsilon_H\right)\frac{dT}{dy} = -\rho c_P(\alpha+\varepsilon_H)\frac{dT}{dy} \tag{11.74}$$

where ε_H is again the eddy diffusivity of heat. Using the turbulent Prandtl number, Pr_t, defined in equation (11.71), we can write equation (11.74) in the form

$$\dot{q} = -\rho c_P\left(\frac{\upsilon}{Pr}+\frac{\varepsilon_M}{Pr_t}\right)\frac{dT}{dy} \tag{11.75}$$

Reynolds originally considered the case in which $Pr = 1$ and $Pr_t = 1$ throughout the flow field and postulated that for this case the velocity and the temperature profiles for turbulent flow are identical. This implies that the same mechanisms control both momentum and energy transfer. The velocity and temperature profiles in the forms $\vartheta/\vartheta_{ave}$ and $(T-T_s)/(T_b-T_s)$ must, therefore, have identical forms. Then

$$\frac{d}{dy}\left(\frac{\vartheta}{\vartheta_{ave}}\right) = \frac{d}{dy}\left(\frac{T-T_s}{T_b-T_s}\right) \tag{11.76}$$

Combining equations (11.73), (11.75), and (11.76), we get

$$\dot{q} = \frac{k}{\mu}\left(\frac{T_s-T_b}{\vartheta_{ave}}\right)\tau_s \tag{11.77}$$

but Newton's Law of Cooling gives

$$\dot{q} = h_c(T_s-T_b) \tag{11.78}$$

and the definition of the Darcy friction factor gives

$$\tau_s = \frac{f\rho\vartheta_{ave}^{\,2}}{8} \tag{11.79}$$

Then, combining equations (11.77), (11.78), and (11.79) and casting the result in dimensionless form, we get

$$Nu_D = \frac{f}{8} Re_D \tag{11.80}$$

Equation (11.80) is one form of the model known as the *Reynolds analogy*.

This well-known result for turbulent flow is limited in that it applies only to fluids for which $Pr = 1$ (typically air and water at high temperatures). In an attempt to remove this limitation, Prandtl modified Reynolds original approach. Prandtl divided the total flow field into two regions: a laminar sublayer and a turbulent layer. At sufficiently large distances from the wall in the fully turbulent layer, the eddy diffusivity of momentum, and by analogy the eddy diffusivity of heat, assume values which are so large in comparison with the molecular viscosity, μ, and the molecular thermal conductivity, k, that the latter can often be neglected with respect to the former. On the other hand, in the laminar sublayer where turbulent fluctuations are nonexistent, the reverse is true and the eddy coefficients may be neglected. Experimental measurements have shown that even though the Prandtl number may be different from unity in the laminar sublayer, the turbulent Prandtl number may still be unity in the turbulent layer ($Pr_t = 1$ but $Pr \neq 1$). Under these circumstances, the Reynolds analogy of equation (11.80) is no longer valid. In the Prandtl approach, for the laminar sublayer the eddy coefficients vanish, and equations (11.73) and (11.75) can be written

$$\frac{\dot{q}}{\tau} = -\frac{k}{\mu}\frac{dT}{d\vartheta} \tag{11.81}$$

In the turbulent layer where μ and k can be neglected and $Pr_t = 1$, these equations become

$$\frac{\dot{q}}{\tau} = -c_P \frac{dT}{d\vartheta} \tag{11.82}$$

Prandtl now integrated these expressions assuming that the temperature at the wall was a constant, T_s, and that the velocity and temperature at the outer edge of the laminar sublayer were ϑ_L and T_L, respectively. Prandtl argued that the ratio $\dot{q}/\tau$ remains constant throughout the boundary layer and obtained for the laminar sublayer

$$\frac{\dot{q}}{\tau} = -\frac{k}{\mu}\frac{T_L - T_s}{\vartheta_L} = -\frac{k}{\mu\vartheta_{ave}}\frac{T_L - T_s}{\frac{\vartheta_L}{\vartheta_{ave}}} \tag{11.83}$$

and for the turbulent layer

$$\frac{\dot{q}}{\tau} = -c_P \frac{T_L - T_b}{\vartheta_L - \vartheta_{ave}} \tag{11.84}$$

Since $\dot{q}/\tau$ is constant, we can equate equations (11.83) and (11.84) to obtain

$$Pr(T_s - T_b) = -\frac{\vartheta_{ave}}{\vartheta_L}\left[1 + \frac{\vartheta_L}{\vartheta_{ave}}(Pr - 1)\right](T_L - T_s) \tag{11.85}$$

but Newton's Law of Cooling gives

$$h_c = \frac{\dot{q}}{T_s - T_b} \tag{11.86}$$

Then combining equations (11.85) and (11.86), we get

$$h_c = -\frac{Pr}{1 + \frac{\vartheta_L}{\vartheta_{ave}}(Pr - 1)}\frac{\dot{q}\frac{\vartheta_L}{\vartheta_{ave}}}{(T_L - T_s)} \tag{11.87}$$

Combining equations (11.83) and (11.87), we get

$$h_c = \frac{1}{1+\frac{\vartheta_L}{\vartheta_{ave}}(Pr-1)}\frac{c_p\tau}{\vartheta_{ave}} \tag{11.88}$$

Introducing the definition of the friction coefficient, equation (11.79), into equation (11.88) and casting the result in dimensionless form, we get

$$Nu_D = \frac{\frac{f}{8}Re_D Pr}{1+\frac{\vartheta_L}{\vartheta_{ave}}(Pr-1)} \tag{11.89}$$

which is known as the Prandtl analogy.

Note that before equation (11.89) can be applied to a particular physical situation, we must first specify the ratio $\vartheta_L/\vartheta_{ave}$. On the basis of experimental observations and "the law of the wall," Prandtl proposed the following velocity profiles for the two regions of flow in a circular conduit:

$$\begin{aligned} 0 \le y^+ \le 11.5 \qquad & \vartheta^+ = y^+ \\ y^+ > 11.5 \qquad & \vartheta^+ = 2.5\ln y^+ + 5.5 \end{aligned} \tag{11.90}$$

Then at the outer edge of the laminar sublayer

$$y^+ = \frac{\delta\vartheta^*\rho}{\mu} = 11.5 \tag{11.91}$$

From the definition of the friction velocity, ϑ^*,

$$\tau_s = \rho\vartheta^{*2} = \frac{f}{8}\rho\vartheta_{ave}{}^2 \tag{11.92}$$

and the fact that at the edge of the laminar sublayer

$$y^+ = \vartheta^+ = \frac{\vartheta_L}{\vartheta^*} = 11.5 \tag{11.93}$$

we have

$$\frac{\vartheta_L}{\vartheta_{ave}} = 11.5\sqrt{\frac{f}{8}} \tag{11.94}$$

Then the Prandtl analogy for turbulent flow in a circular conduit becomes

$$Nu_D = \frac{\frac{f}{8}Re_D Pr}{1+11.5\sqrt{\frac{f}{8}}(Pr-1)} \tag{11.95}$$

On the basis of more recent experimental evidence, the Prandtl analogy has been modified by Gnielinski to produce a correlation that is applicable to turbulent flow in smooth circular conduits over a larger range of Reynolds numbers ($2300 \le Re_D \le 5 \times 10^6$) and Prandtl numbers ($0.5 \le Pr \le 2000$):

$$Nu_D = \frac{\frac{f}{8}(Re_D - 1000)Pr}{1+12.7\sqrt{\frac{f}{8}}(Pr^{2/3}-1)} \tag{11.96}$$

For smooth circular conduits, the friction factor is given by the Moody diagram or the correlation

$$f = (0.790 \ln Re_D - 1.64)^{-2} \tag{11.97}$$

Equation (11.96) for turbulent flow applies to both wall conditions considered previously for conditions of laminar flow: constant heat flux at the wall and constant wall temperature. The requisite thermal property data should be evaluated at the mean temperature between the wall temperature and the bulk mean temperature of the fluid. Note that equation (11.96) can be applied to turbulent flow in conduits of non-circular cross-section by using the hydraulic diameter, D_h, in place of the diameter where

$$D_h = \frac{4A_c}{\wp} \tag{11.98}$$

and A_c is the cross-sectional area of the flow and $\wp$ is the wetted perimeter.

11.6 Forced Convection Heat Transfer in External Flows – Flow Over a Flat Plate

External flows differ from the internal flows we have just discussed in two important respects. On the one hand, the boundary layer that develops as a result of the interaction between the viscous fluid and the bounding surface is free to grow in an unbounded fashion. That is, as we have already seen in the case of the hydrodynamic boundary layer developing on a flat plate for example, the boundary layer can continue to grow as the flow proceeds down the surface of the plate. The same is true for the thermal boundary layer. In the course of its growth, the thermal boundary layer continues to interact with the bounding surface on one side and the free stream of flowing fluid on the other. The external thermal boundary layer never grows to such an extent that it completely dominates the entire flow field as was the case for an internal flow.

On the other hand, the external boundary layer never becomes fully developed in the sense of an internal flow where the velocity profile remains unchanged once the flow has proceeded beyond the entry length. The temperature profile in an internal flow retains its shape once fully developed, but the magnitude of the temperature of the fluid does as a result of heat transfer interactions between the fluid and the wall in the direction of flow. In the case of the external flow, although the velocity profile has the same shape due to the self-similar nature of the flow as the fluid proceeds down the surface, the dimension of the profile normal to the bounding surface does change as the flow progresses. In fact, as the flow progresses over the surface, it reaches a point where the boundary layer has grown so large, the influence of viscosity is no longer able to damp out the small perturbations to the flow (the eddies) that are always trying to develop as a result of the inherent roughness of the bounding surface. The character of the flow then undergoes a transition from laminar to turbulent. As we have already seen from our discussion in Chapter 9 for the case of the hydrodynamic boundary layer, the mechanism of momentum transfer is very different for these types of flow. Similarly, the mechanism of energy transfer between the wall and the fluid is very different between these two types of flow. The important point is that, in the case of external flow over a surface of typical dimensions, we must consider both a laminar region and a turbulent region in the same flow field whereas for an internal flow, we could confine our attention and our analysis to a single type of flow.

In our development of the topic of forced convection heat transfer in external flows, we shall focus on the case of flow over a flat plate since that geometry is by far the most common in thermal-fluids engineering. We shall consider the case of laminar flow and then the case of turbulent flow.

11.6.1 Laminar Flow Over a Flat Plate in Forced Convection Heat Transfer

Consider the case of a flat plate maintained at a uniform surface temperature T_s by some external means. The plate is immersed in a flow which has a uniform free-stream velocity $\vec{v}_\infty$ and a uniform free-stream temperature T_∞ upstream from the plate. As shown in Figure 11.9, as the flow encounters the plate, the action of viscosity causes the fluid adjacent to the plate to be slowed by the presence of the plate. As a consequence, a velocity profile develops in the fluid such that the fluid immediately adjacent to the plate assumes the velocity of the plate, the "no-slip" boundary condition of Chapter 9 while the fluid a short distance from the surface of the plate has a finite velocity that is somewhat less than the free-stream velocity. Although the influence of the plate truly can be felt no matter how far we might get away from the plate, the effect does become negligible in a relatively short distance measured normal to the surface. This narrow region of influence is modeled as the boundary layer as suggested by Prandtl.

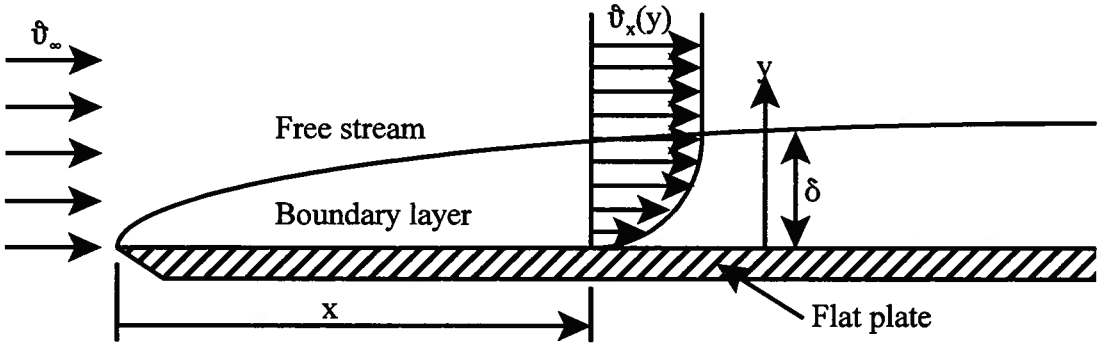

Figure 11.9 Velocity Boundary Layer on a Flat Plate

Since the fluid particles in the boundary layer spend more time in the neighborhood of the surface than the fluid particles remote from the surface, they have more time to try to reach thermal equilibrium with the plate. As a result, the temperatures of these fluid particles take on values between the surface temperature of the plate T_s and the free-stream temperature of the fluid T_∞. The actual values depend upon the distance from the surface of the plate as well the character of the flow and the thermal-fluid properties of the fluid. The variation in the values of the temperature occurs in a continuous fashion with distance normal to the plate. At distances remote from the surface, the residence time of the fluid particles is too low to have any effect on the temperature of the fluid. This establishes the outer limit of a thermal boundary layer in the fluid which may be thicker or thinner than the velocity boundary layer depending on the value of the Prandtl number of the fluid. As we shall soon see, in the special (but common) case for which $Pr = 1$, the thermal boundary layer has the same thickness as the velocity boundary layer. (We expected this based upon our discussion in section 11.1.)

The analysis of the thermal boundary layer for this flow geometry follows the same pattern as that used for the analysis of the internal flows shown above. We first solve the Navier-Stokes equation for the geometry of interest in order to establish the velocity profile in the flow. This we have already done for the case of the flat plate. The result is the well-known Blasius solution derived in Chapter 9. We then use this result in the appropriate form of the first law for the geometry at hand. For flow over a flat plate, we have not yet developed the appropriate form of the first law. To accomplish this we consider a differential control volume in the boundary

layer of Figure 11.9. A differential control volume of unit width normal to the plane of the page would appear as shown in Figure 11.10.

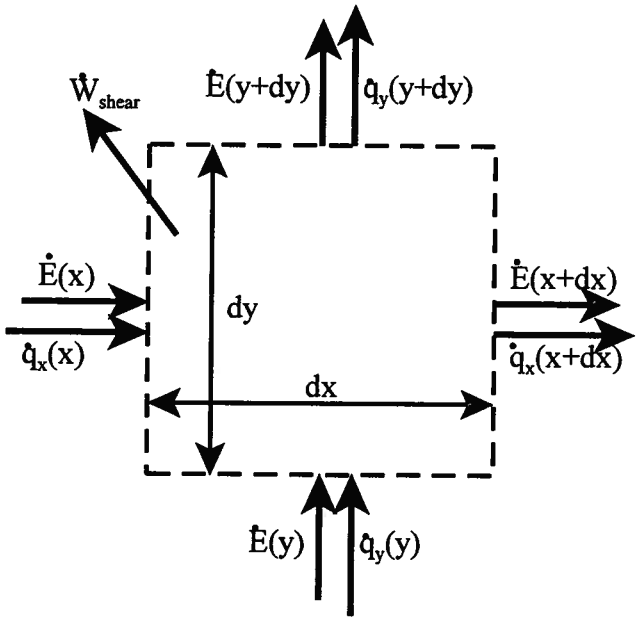

Figure 11.10 Differential Control Volume

The terms like $\dot{E}(x)$ represent the rate of flow of energy stored within the mass that enters the control volume at the location x. This term includes kinetic and gravitational potential energy as well as the flow work transfer and, in the case of the incompressible fluid model, the stored thermal energy. (See Chapter 8.) The terms like $\dot{q}_x(x)$ represent the rate of energy transfer by conduction (the heat flux) in the x-direction at the location x. (See Chapter 6.) The term $\dot{W}_{shear}$ represents the rate at which the shear stresses in the fluid result in a work transfer for the control volume.

When the appropriate forms of the various terms are substituted into the first law, we obtain after a considerable amount of algebraic manipulation (See Appendix 11A.) The following form of the first law:

$$\rho c\left(\vartheta_x\frac{\partial T}{\partial x}+\vartheta_y\frac{\partial T}{\partial y}\right)=k\left(\frac{\partial^2 T}{\partial x^2}+\frac{\partial^2 T}{\partial y^2}\right)-P\left(\frac{\partial \vartheta_x}{\partial x}+\frac{\partial \vartheta_y}{\partial y}\right)+\mu\left(\frac{\partial \vartheta_x}{\partial y}\right)^2 \qquad (11.99)$$

To first order, the kinetic and gravitational potential energy of the incompressible fluid are unchanged as it flows at a steady rate through the control volume. Thus the only stored energy change of consequence is the change in stored thermal energy. The terms on the left-hand side of equation (11.99) represent the net rate at which the stored thermal energy of the fluid is changed as it flows through the control volume. As we have seen in Chapter 9, the flow work transfer for the incompressible fluid just compensates for the work transfer associated with the viscous forces acting on the control volume. Thus those terms cancel out and do not appear in equation (11.99). On the right-hand side of equation (11.99), we are then left the energy transfer to the fluid via conduction (the first term), the work transfer associated with the compressibility of the fluid (the second term), and the viscous dissipation in the fluid (the third term).

For the incompressible fluid model the two-dimensional form of the continuity equation,

equation (9.70), reduces to

$$\frac{\partial \vartheta_x}{\partial x}+\frac{\partial \vartheta_y}{\partial y}=0 \tag{11.100}$$

Thus the second term on the right-hand side of equation (11.99) vanishes as we would expect from the fact that the fluid is incompressible. Furthermore, the third term on the right-hand side also can be neglected in all cases except those involving very high speed flow or those involving the flow of highly viscous fluids such as oils. Then equation (11.99) reduces to

$$\rho c\left(\vartheta_x\frac{\partial T}{\partial x}+\vartheta_y\frac{\partial T}{\partial y}\right)=k\left(\frac{\partial^2 T}{\partial x^2}+\frac{\partial^2 T}{\partial y^2}\right) \tag{11.101}$$

We now note that from our experience with the momentum equation in the boundary layer, the gradients in the direction of flow are small compared to the gradients transverse to the flow. Thus the first term in the parenthesis on the right-hand side of equation (11.101) can be neglected in comparison with the second term in the parenthesis. We can not simplify the left-hand side of equation (11.101) because the first term in the parenthesis is the product of a large velocity and a small gradient while the second term is the product of a small velocity and a large gradient. Thus the to terms are of the same order. Then the boundary layer form of the first law becomes

$$\vartheta_x\frac{\partial T}{\partial x}+\vartheta_y\frac{\partial T}{\partial y}=\alpha\frac{\partial^2 T}{\partial y^2} \tag{11.102}$$

where we have made use of the definition of the thermal diffusivity, $\alpha = k/\rho c$.

11.6.1.1 The Reynolds Analogy. We now note, as Osborne Reynolds did in 1874, that equation (11.102) is precisely the same form as the momentum equation for the boundary layer, equation (9.167), with the velocity component ϑ_x in the derivatives replaced by the temperature and the momentum diffusivity ν replaced by the thermal diffusivity α. Furthermore, the boundary conditions are the same for the two cases:

$$\vartheta_x = 0 \text{ and } T - T_s = 0 \text{ at } y = 0$$
$$\vartheta_x \to \vartheta_\infty \text{ and } T \to T_\infty \text{ as } y \to \infty$$

In fact, if $\alpha = \nu$, that is if $Pr = 1$, the same function will satisfy both equations. If the equation is cast in dimensionless form, the coefficient on the right-hand side of equation (11.102) becomes the reciprocal of the Prandtl number. Then for $Pr = 1$, the shapes of the dimensionless temperature profile and the dimensionless velocity profile are identical and they grow at the same rate so that $\delta_\vartheta = \delta_T$.

Suppose we now define a dimensionless temperature profile $\theta(\eta)$ such that

$$\theta(\eta)=\frac{T(\eta)-T_s}{T_\infty-T_s}=\frac{\vartheta_x(\eta)}{\vartheta_\infty} \tag{11.103}$$

Then

$$\frac{\partial}{\partial y}\left(\frac{T-T_s}{T_\infty-T_s}\right)=\frac{\partial}{\partial y}\left(\frac{\vartheta_x}{\vartheta_\infty}\right) \tag{11.104}$$

The heat flux at the surface of the plate is given by the Fourier Conduction Law, viz.

$$\dot{q}=-k\left(\frac{\partial T}{\partial y}\right)_{y=0}=-k\left[\frac{\partial}{\partial y}\left(\frac{T-T_s}{T_\infty-T_s}\right)\right]_{y=0} \tag{11.105}$$

but the shear stress at the surface is

$$\tau_s = \mu\left(\frac{\partial \vartheta_x}{\partial y}\right)_{y=0} = \mu\left[\frac{\partial}{\partial y}\left(\frac{\vartheta_x}{\vartheta_\infty}\right)\right]_{y=0} \tag{11.106}$$

For the case in which $Pr = 1$, we can combine equations (11.104), (11.105), and (11.106) to get

$$\dot{q} = \frac{k}{\mu}\frac{T_s - T_\infty}{\vartheta_\infty}\tau_s \tag{11.107}$$

If we now introduce Newton's Law of Cooling, we get

$$h(T_s - T_\infty) = \frac{k}{\mu}\frac{(T_s - T_\infty)}{\vartheta_\infty}\tau_s \tag{11.108}$$

Equation (11.108) can be rewritten in the dimensionless form

$$\frac{h_x x}{k} = \frac{1}{2}\frac{\vartheta_\infty x \rho}{\mu}\frac{\tau_s}{\frac{1}{2}\rho\vartheta_\infty^{\,2}} \tag{11.109}$$

or from Table 10.7

$$Nu_x = Re_x \frac{C_f}{2} \tag{11.110}$$

where we have made use of the definition of the local skin friction coefficient C_f given in equation (9.203). Equation (11.110) is known as the *Reynolds analogy*.

Note that the two definitions presented in equations (9.203) and (11.79) can be combined to give the relationship between the Darcy friction factor f and the skin friction coefficient C_f which is also known as the Fanning friction factor [see equation (9.143)], viz.

$$C_f = \frac{f}{4} \tag{11.111}$$

Thus equations (11.80) and (11.110) are identical except that in one case the conduit diameter D is the characteristic length, and in the other case the distance from the leading edge of the plate is the characteristic length.

From equation (9.204) we have

$$C_f = \frac{0.664}{\sqrt{Re_x}} \tag{9.204}$$

Then for the case of a fluid with $Pr = 1$ flowing in a laminar fashion over a flat plate, equation (11.110) becomes

$$Nu_x = 0.332 Re^{1/2} \quad \text{with} \quad Pr = 1 \tag{11.112}$$

Thus for a special (but common) case of $Pr = 1$, we have actually achieved a solution of the first law for laminar flow over a flat plate, without explicitly solving the partial differential equation. The problem is, we do not know the influence of the Prandtl number for fluids with $Pr \neq 1$. We now proceed to do this with the aid of the Blasius solution for the boundary layer form of the Navier-Stokes equation. Before we do this, however, it is appropriate to make two observations concerning the Reynolds analogy of equation (11.110).

Although the foregoing development of the Reynolds analogy utilized the situation of laminar flow over a flat plate, the concept is general and can be applied to other geometrical shapes and to turbulent flow as we have already seen in equation (11.79). In fact, the Reynolds analogy finds its greatest importance in the case of turbulent flows because of the extraordinary

complexity of these flow fields. In those cases for which a more precise correlation between the Nusselt number and the Reynolds and Prandtl numbers is unavailable, the Reynolds analogy is often the only means available to model the physical situation.

Finally, it should be noted that in 1874 Reynolds did not present the analogy concept in quite the manner presented here. Rather, he argued that the heat transfer actually experienced by a surface relative to the maximum heat transfer that could be realized in allowing the surface to run down to equilibrium with the fluid should be equal to the amount of momentum transfer between the fluid and the surface relative to the maximum amount of momentum that could be transferred by bringing the fluid to rest relative to the surface. Equation (11.107) is the modern mathematical equivalent of Reynolds's argument on a rate basis.

11.6.1.2 Extension of the Reynolds Analogy to the case with $Pr \neq 1$. Note that equation (11.103) is related to the Blasius function, viz.

$$\theta(\eta)=\frac{T(\eta)-T_s}{T_\infty-T_s}=\frac{\vartheta_x(\eta)}{\vartheta_\infty}=\frac{df}{d\eta} \tag{11.113}$$

where as before

$$\eta = y\sqrt{\frac{\vartheta_\infty}{xv}} \tag{11.114}$$

Then the stream function becomes once again

$$\psi = \sqrt{vx\vartheta_\infty}\, f(\eta) \tag{11.115}$$

Then from the continuity equation, equation (11.100), we have

$$\vartheta_x = \vartheta_\infty f'(\eta) \tag{11.116}$$

and

$$\vartheta_y = \sqrt{\frac{v\vartheta_\infty}{x}}\frac{(\eta f'-f)}{2} \tag{11.117}$$

Substituting equations (11.114) through (11.117) into the first law, equation (11.102), we get

$$-\vartheta_\infty f'\left(-\frac{\eta}{2x}\right)\frac{d\theta}{d\eta}-\frac{1}{2}\sqrt{\frac{v\vartheta_\infty}{x}}(\eta f'-f)\sqrt{\frac{\vartheta_\infty}{vx}}\frac{d\theta}{d\eta}=\alpha\frac{\vartheta_\infty}{vx}\frac{d^2\theta}{d\eta^2} \tag{11.118}$$

which reduces to

$$-\frac{1}{2}f\frac{d\theta}{d\eta}=\frac{\alpha}{v}\frac{d^2\theta}{d\eta^2} \tag{11.119}$$

or

$$\frac{d^2\theta}{d\eta^2}+\frac{1}{2}(f)Pr\frac{d\theta}{d\eta}=0 \tag{11.120}$$

Thus the partial differential equation has been converted into an ordinary differential equation. The original boundary conditions were

$$\begin{aligned} T &= T_s \quad \text{at} \quad y=0 \\ T &= T_\infty \quad \text{at} \quad y=\infty \end{aligned} \tag{11.121}$$

which with the change of variables now become

$$\begin{aligned} \theta &= 0 \quad \text{at} \quad \eta=0 \\ \theta &= 1 \quad \text{at} \quad \eta=\infty \end{aligned} \tag{11.122}$$

If we make another change of variables such that

$$p = \frac{d\theta}{d\eta} \tag{11.123}$$

equation (11.120) becomes

$$\frac{dp}{d\eta} + \frac{1}{2} f \cdot Pr \cdot p = 0 \tag{11.124}$$

which can be integrated to obtain

$$\begin{aligned} \ln p &= -\frac{1}{2} Pr \int_0^\eta f d\eta + C_1 \\ p &= \frac{d\theta}{d\eta} = C_2 \exp\left[-\frac{1}{2} Pr \int_0^\eta f d\eta \right] \end{aligned} \tag{11.125}$$

Equation (11.125) can be integrated to yield

$$\theta(\eta) = C_2 \int_0^\eta \exp\left[-\frac{1}{2} Pr \int_0^\eta f d\eta \right] d\eta \tag{11.126}$$

Applying the second boundary condition to equation (11.126), we get

$$\theta = \frac{\int_0^\eta \exp\left[-\frac{1}{2} Pr \int_0^\eta f d\eta \right] d\eta}{\int_0^\infty \exp\left[-\frac{1}{2} Pr \int_0^\eta f d\eta \right] d\eta} \tag{11.127}$$

If we recall the original Blasius equation, equation (9.176), we can recast equation (11.127) in the form

$$\theta(\eta) = \frac{\int_0^\eta (f'')^{Pr} d\eta}{\int_0^\infty (f'')^{Pr} d\eta} \tag{11.128}$$

which can be evaluated numerically using the values given in Table 9.4. However, what we are really after here is a dimensionless solution that will give us the Nusselt number in terms of the Reynolds number and the Prandtl number. If we recognize that the rate at which energy is convected away by the fluid is precisely the energy conducted down the temperature gradient in the fluid, we can combine Newton's law of Cooling with the Fourier Conduction Law in the fluid. Then we have

$$h_x (T_s - T_\infty) = -k \left(\frac{\partial T}{\partial y} \right)_{y=0} \tag{11.129}$$

where h_x is the local value of the convection heat transfer coefficient. In terms of the variables we have employed in the solution thus far we have

$$\left(\frac{\partial T}{\partial y} \right)_{y=0} = -(T_s - T_\infty) \sqrt{\frac{\vartheta_\infty}{\nu x}} \left(\frac{d\theta}{d\eta} \right)_{\eta=0} = -(T_s - T_\infty) \sqrt{\frac{\vartheta_\infty}{\nu x}} \frac{1}{\int_0^\infty (f'')^{Pr} d\eta} \tag{11.130}$$

If we now solve equation (11.129) for the heat transfer coefficient h_x and make use of equation (11.130), we get

$$h_x = \sqrt{\frac{\vartheta_\infty}{\nu x}} \frac{k}{\int_0^\infty (f'')^{Pr} d\eta} \tag{11.131}$$

If we now define a local value of the Nusselt number, Nu_x, we get

$$Nu_x = \frac{h_x x}{k} = \sqrt{\frac{\vartheta_\infty x}{\nu}} \frac{1}{\int_0^\infty (f'')^{Pr}\, d\eta} = \frac{\sqrt{Re_x}}{\int_0^\infty (f'')^{Pr}\, d\eta} \tag{11.132}$$

If we now rearrange equation (11.132) in the following form, we can generate from Table 9.4 a table of values for the ratio $Nu_x/Re_x^{1/2}$ as in Table 11.2.

$$\frac{Nu_x}{\sqrt{Re_x}} = \frac{1}{\int_0^\infty (f'')^{Pr}\, d\eta} \tag{11.133}$$

Table 11.2

Pr	0.5	0.7	1.0	7.0	10.0	15.0
$Nu_x(Re_x)^{-1/2}$	0.259	0.292	0.332	0.645	0.730	0.835

If we now plot the data of Table 11.2, we can develop a correlation of the form $Nu_x = \phi(Re_x, Pr)$.

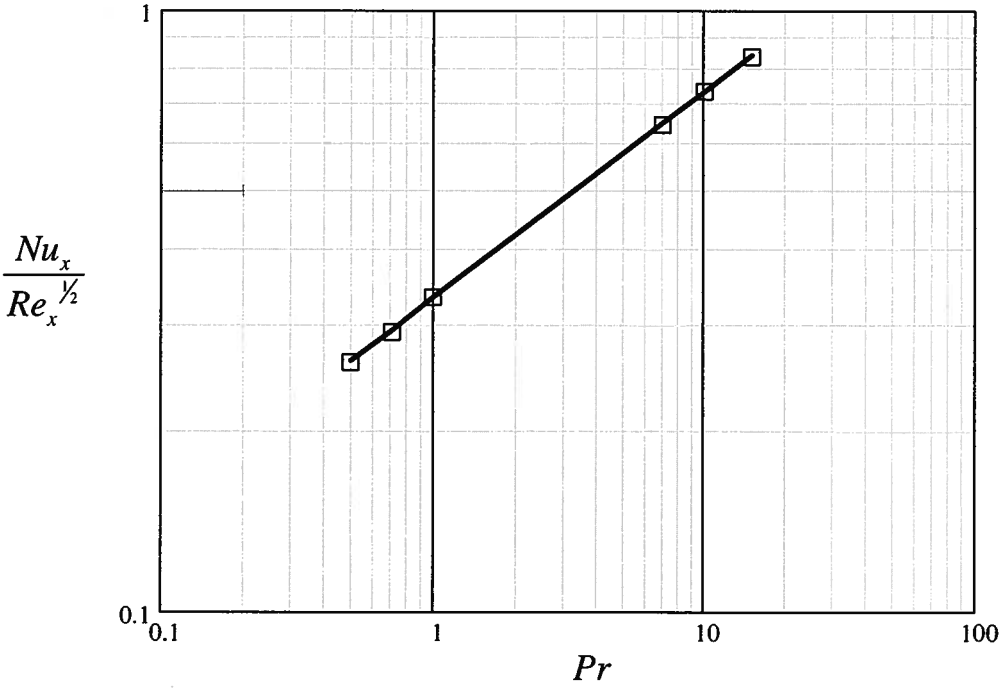

Figure 11.11 Heat Transfer Correlation for Flow Over a Flat Plate

If we use a linear regression analysis and force the fitted line to go through the point for $Pr = 1$, we can correlate the local Nusselt number with the Reynolds number and the Prandtl number for a flat plate in laminar flow as

$$Nu_x = 0.332 Re_x^{1/2} Pr^{0.3437} \tag{11.134}$$

which for simplicity has historically been written in the form

$$Nu_x = 0.332 Re_x^{1/2} Pr^{1/3} \tag{11.135}$$

From equation (11.131), it is apparent that for a given free-stream velocity of a given fluid, the form of the local heat transfer coefficient h_x is

$$h_x = \frac{C}{\sqrt{x}} \tag{11.136}$$

where C is a constant. Then the average heat transfer coefficient for a flat plate of length L is given by $\overline{h_L}$ where

$$\overline{h_L} = \frac{1}{L}\int_0^L h_x dx = \frac{C}{L}\int_0^L \frac{dx}{\sqrt{x}} = \frac{2C}{\sqrt{L}} = 2h_{x=L} \tag{11.137}$$

Then the Nusselt number for a flat plate of length L in laminar flow becomes Nu_L where

$$Nu_L = 0.664 Re_L^{1/2} Pr^{1/3} \tag{11.138}$$

and the Reynolds number is evaluated at the length L.

Consider a typical application of equation (11.135) involving the flow of air at a velocity of $\vartheta = 0.9$ m/sec over a flat plate of length $L = 1$ m. The kinematic viscosity of the air at a temperature of $T = 300$ K is $\nu = 15.66 \times 10^{-6}$ m^2/sec and the thermal conductivity is $k = 0.0267$ W/m K. The local convection heat transfer coefficient h_x exhibits the behavior shown in Figure 11.12 which is typical of all cases involving flow over an isothermal flat plate.

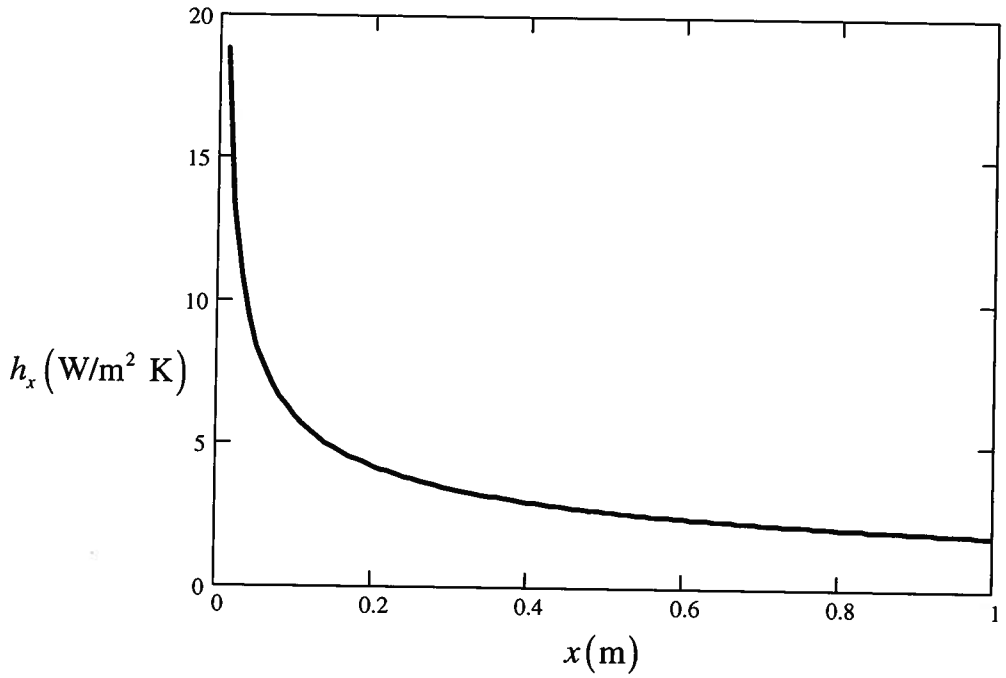

Figure 11.12 Local Convection Heat Transfer Coefficient for Laminar Flow Over a Flat Plate

According to equation (11.135), the local heat transfer coefficient varies as the inverse of the square root of the distance from the leading edge of the plate. Thus at the leading edge, the heat transfer coefficient is infinite and decays rapidly with distance from the leading edge. The portion of the flat plate downstream from the leading edge is much less effective as a heat transfer surface than the portion right near the leading edge. This observation is a guiding principle in the design of flat-plate like surfaces, such as this rectangular pin fins, for the control of surface temperatures. If the fins are short in the direction of flow (chord length) and are staggered so that they are not shielded from the oncoming fluid stream by their neighbors, the

heat transfer will be dominated by this effect of the leading edge and the heat transfer coefficient for convection over the fin will have the largest possible value for a given fluid velocity. There results, then, a reduction in the total fin surface area which reduces the cost of the finned surface.

11.6.2 Turbulent Flow Over a Flat Plate in Forced Convection Heat Transfer

The flow field in the neighborhood of the surface of an external flow has many perturbations to it due to small fluctuations in both flow velocity and local pressure of the flow as well as perturbations due to the roughness of the surface itself. In laminar flow, these small perturbations are damped out through the action of fluid viscosity, but as the flow progresses downstream from the leading edge, it becomes increasingly difficult for the fluid to damp out these small perturbations. Eventually, the perturbations become large and the flow becomes unstable. The flow then undergoes a transition from laminar flow to turbulent flow. Experimental measurements of this transition phenomenon have reported a range of values of the local Reynolds number at which the transition occurs, typically $3 \times 10^5 < Re_{x,transition} < 5 \times 10^5$. Since these data have been typically obtained in laboratory settings where the conditions are precisely controlled, some investigators believe that these data are artificially high. Kays and Crawford (W. M. Kays and M. E. Crawford, *Convective Heat and Mass Transfer*, 2nd edition, McGraw-Hill, N. Y., 1980, Chapter 10) argue that the results obtained from viscous stability theory might be more appropriate in practice where conditions are not quite so closely controlled, viz. $Re_{x,transition} = 60{,}000$.

The analysis of the case of heat transfer in turbulent flow over a flat plate is usually treated by means of the Reynolds analogy or the Prandtl analogy. Here we make use of the latter in the form of equation (11.95) because it includes the effects of Prandtl number. We now rewrite this expression for the flat plate case in the customary manner using the local skin friction coefficient C_{fx} instead of the Darcy friction factor.

$$Nu_D = \frac{\frac{C_{fx}}{2} Re_D Pr}{1 + 11.5\sqrt{\frac{C_{fx}}{2}}(Pr - 1)} \tag{11.139}$$

It now remains for us to determine the skin friction coefficient for the case at hand.

It has been found that the data for the velocity profile in the turbulent boundary layer can be fit approximately with a 1/7th power law. Von Karman has suggested, in the interests of simplicity, that the similarity solution for the turbulent boundary layer be written in the form

$$\frac{\vartheta_x}{\vartheta_\infty} = \left(\frac{y}{\delta}\right)^{1/7} \tag{11.140}$$

where δ is the bounday layer thickness. We now borrow some results from turbulent flow in a circular conduit. Recall from equation (9.248) that the shear stress at the wall for turbulent flow in a circular conduit was related to the friction factor by

$$\tau_s = \frac{f}{8} \rho \vartheta_{ave}^{\ 2} \tag{11.141}$$

In 1911 Blasius fit all the data then available for the friction factor for turbulent flow in a circular conduit by the expression

$$f = 0.3164 \left(\frac{\vartheta_{ave} D}{\nu}\right)^{-1/4} \tag{11.142}$$

Combining equations (11.141) and (11.142), we get

$$\tau_s = 0.03955 \rho \vartheta_{ave}^{\ 1/4} \nu^{1/4} D^{-1/4} \tag{11.143}$$

If we rewrite this result in terms of the radius R of the conduit and recognize that for turbulent flow in this geometry $\vartheta_{ave} = 0.8\,\vartheta_{max}$, we get

$$\tau_s = 0.0225\rho\vartheta_{max}^{1/4}\left(\frac{\nu}{R}\right)^{1/4} \tag{11.144}$$

For the flat plate in turbulent flow, equation (11.144) becomes

$$\frac{\tau_s}{\rho\vartheta_\infty^{\,2}} = 0.0225\left(\frac{\nu}{\vartheta_\infty\delta}\right)^{1/4} \tag{11.145}$$

In our prior discussion of the momentum thickness, we derived the result [equation (9.202)]

$$\tau_s = \rho\vartheta_\infty^{\,2}\frac{d\theta}{dx} \tag{11.146}$$

where θ is the displacement thickness given by equation (9.197), viz.

$$\theta = \int_0^\delta \frac{\vartheta_x}{\vartheta_\infty}\left(1-\frac{\vartheta_x}{\vartheta_\infty}\right)dy \tag{11.147}$$

Substituting equation (11.140) into equation (11.147) and carrying out the integration, we get

$$\theta = \frac{7}{72}\delta \tag{11.148}$$

Substituting this result into equation (11.146), we obtain a differential equation for the boundary layer thickness based upon the 1/7th power law similarity solution of equation (11.140), viz.

$$\frac{7}{72}\frac{d\delta}{dx} = 0.0225\left(\frac{\nu}{\vartheta_\infty\delta}\right)^{1/4} \tag{11.149}$$

Integrating equation (11.149) from the leading edge of the plate to the location x, we get

$$\begin{aligned}\int_0^\delta \delta^{-1/4}d\delta &= \frac{0.23143\nu^{1/4}}{\vartheta_\infty^{\,1/4}}\int_0^x dx \\ \delta(x) &= 0.37x\left(\frac{\vartheta_\infty x}{\nu}\right)^{-1/5}\end{aligned} \tag{11.150}$$

Then from equation (11.148) we get

$$\theta(x) = 0.036x\left(\frac{\vartheta_\infty x}{\nu}\right)^{-1/5} \tag{11.151}$$

but the definition of the local skin friction coefficient C_{fx} is

$$C_{fx} = \frac{\tau_s}{\frac{1}{2}\rho\vartheta_\infty^{\,2}} \tag{11.152}$$

Combining equation (11.152) with equation (11.146), we get

$$C_{fx} = 2\frac{d\theta}{dx} \tag{11.153}$$

Differentiating equation (11.146) and substituting the result into equation (11.153), we get

$$C_{fx} = 0.0576\left(\frac{\vartheta_\infty x}{\nu}\right)^{-1/5} = 0.0576Re_x^{-1/5} \tag{11.154}$$

Then

$$\frac{C_{fx}}{2} = 0.0288 Re_x^{-1/5}$$

but the experimental data have been found to be better represented by changing the constant slightly so that

$$\frac{C_{fx}}{2} = 0.0296 Re_x^{-1/5} \tag{11.155}$$

which is the commonly accepted correlation in the literature.

To determine the Nusselt number, equation (11.155) can be substituted into the Prandtl analogy, equation (11.95). Because of the scatter in the experimental data, it has been customary in practice to simplify the correlation by dividing both sides of equation (11.95) by the numerator on the right-hand side and to evaluate numerically the quantity

$$\frac{Nu_x}{\left(C_{fx}/2\right) Re_x Pr}$$

in the neighborhood of $Pr = 1$ over the range of Reynolds numbers $5 \times 10^5 \le Re_x \le 10^7$. The results for each value of Prandtl number are averaged over the range of values of Reynolds numbers. These results are then plotted vs. Pr on Log-Log coordinates as in Figure 11.13.

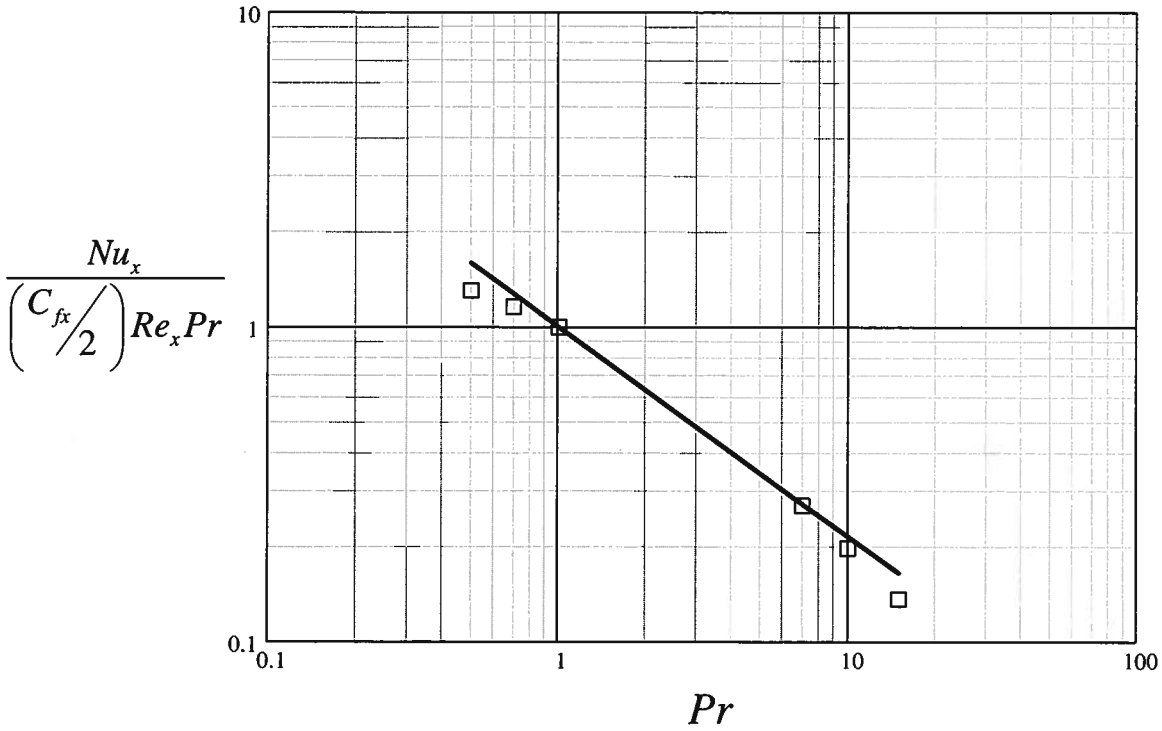

Figure 11.13 Heat Transfer Correlation for Turbulent Flow Over a Flat Plate, $5 \times 10^5 \le Re_x \le 10^7$

The data are then fit using linear regression analysis. The result is

$$\frac{Nu_x}{\left(C_{fx}/2\right) Re_x Pr} = Pr^{-2/3} \tag{11.156}$$

Equation (11.156) can then be rewritten in the form

$$Nu_x = 0.0296 Re_x^{4/5} Pr^{1/3} \tag{11.157}$$

which is the equation of the line plotted in Figure 11.13. Comparison of this expression with the recent experimental data suggests that the fit could be improved by modifying the constant and the exponent on Pr slightly, viz.

$$Nu_x = 0.029 Re_x^{0.8} Pr^{0.43} \tag{11.158}$$

Finally, we note that the flow is not turbulent over the entire flat plate. As mentioned above, the flow is initially laminar and then undergoes a transition to turbulent flow at some distance downstream from the leading edge. Exactly where this transition occurs is still the subject of study, but the generally accepted values are in the range of $6 \times 10^4 < Re_{x,tr} < 5 \times 10^5$. Then the heat transfer coefficient averaged over the length of the plate L becomes

$$h_L = \frac{1}{L}\left[\int_0^{x_{tr}} h_{x,laminar}\,dx + \int_{x_{tr}}^{L} h_{x,turbulent}\,dx\right] \tag{11.159}$$

If we substitute equations (11.135) and (11.158) into equation (11.159), we get an expression for the Nusselt number averaged over the length of the plate L.

$$Nu_L = 0.0664 Re_{tr}^{1/2} Pr^{1/3} + 0.036 Re_L Pr^{0.43}\left[1 - \left(\frac{Re_{tr}}{Re_L}\right)^{0.8}\right] \tag{11.160}$$

Clearly, the application of equation (11.160) depends upon the value of Re_{tr} used.

11.7 Free Convection Heat Transfer

Convection heat transfer, unlike conduction and radiation heat transfer, involves the motion of a fluid past a solid surface. Thus far in our development of the topic, we have focused our attention on situations in which the motion of the fluid was induced by external means – either by an imposed pressure gradient produced by a compressor or pump or by imposed motion resulting from the motion of a boundary such as a fan or turbine blade. However, there is another important class of convective motions in which the fluid motion is induced *naturally* by buoyancy forces generated within the fluid itself.

As we have discussed in detail in Chapter 4, buoyancy forces arise from non-uniform pressure distributions that can ultimately be traced to density differences. For example, consider the Ping-Pong ball held completely submerged in a body of water as shown in Figure 11.14. A

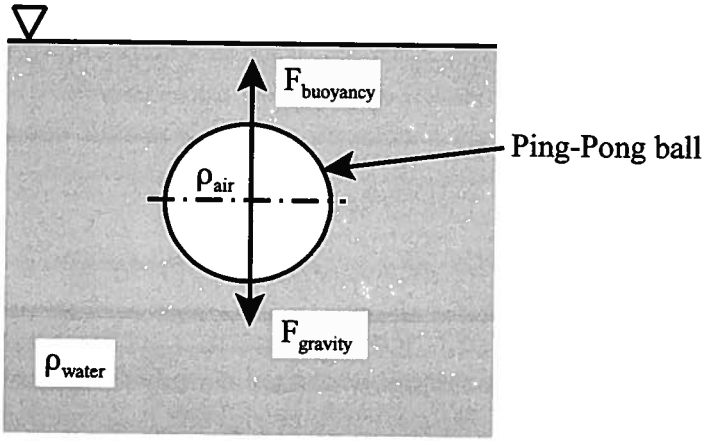

Figure 11.14 Buoyancy of Submerged Ping-Pong Ball

buoyancy force acting on the ball arises from the fact that the pressure on the top surface of the Ping-Pong ball is less than the pressure on the bottom surface of the ball. When this pressure distribution is integrated over the entire surface of the ball, a buoyancy force in the upward direction results. This buoyancy force is greater than the body force due to gravity acting in the downward direction. As a result, there is a *net* upward force acting on the ball that can be expressed in terms of the difference in the densities of the air inside the ball and of the surrounding water that is displaced by submerging the ball. (Clearly we are neglecting the mass of the thin shell that comprises the wall of the ball.) This expression is the fundamental equation of hydrostatics for submerged objects of uniform density.

$$F_{net} = F_{buoyancy} - F_{gravity} = (\rho_{water} - \rho_{air})\, g V_{ball}$$

$$F_{net} = (\rho_{fluid} - \rho_{object})\, g V_{object}$$

This net upward force causes a motion of the object in the upward direction. In the case of the Ping-Pong ball, the ball rushes to the surface upon being released.

In a similar manner, if a solid object in contact with a fluid medium has a surface temperature different from that of the surrounding fluid, the temperature difference causes a heat transfer interaction between the fluid and the solid that can create a localized density *gradient* within the bulk of the fluid. This density gradient can create a buoyancy force on some parts of the fluid that ultimately leads to local motion within the fluid itself that we call *free convection* or *natural convection*. The classic configuration is one in which a fluid layer is heated from below or cooled from above. The fluid density gradient that results is unstable since in both cases the denser fluid lies above the less dense fluid. A small perturbation to this unstable fluid layer causes the fluid to break up into vertical cells of fluid of polygonal section, usually known as *convection cells* or *Bénard cells* in honor of Henri Bénard who first studied them experimentally in 1901. Within these cells, the magnitude of the body force due to gravity acting on a typical fluid element produces a *net* force on the element that causes the more dense fluid elements to fall and the less dense fluid elements to rise. The ensuing fluid motion occurs on a local level within each one of the many cells of circulating fluid that are now distributed throughout the fluid. It was Lord Rayleigh who first described this motion in mathematical terms in 1916.

It is clear, then, that the appearance of the free convection phenomenon in a fluid is dependent upon the development of a density gradient by thermal means. For the incompressible fluid model that we have used thus far to describe most of the dynamical behavior of fluids, the density is taken to be a constant, independent of temperature. Clearly, in order to describe the free convection phenomenon in this model, it is necessary for us to relax this constraint and now allow the fluid density to depend upon the local temperature. Since the density gradients that drive the motion are small, we can expand the density in a Taylor series expansion of the temperature, viz.

$$\rho = \rho_0 + \left(\frac{\partial \rho}{\partial T}\right)_0 dT + \ldots \approx \rho_0 \left[1 + \beta_0 (T - T_0)\right] \tag{11.161}$$

where we have retained just the linear term of the expansion. ρ_0 is the density at some Kelvin reference temperature T_0, and the coefficient β_0 evaluated at the same reference temperature is known as the coefficient of thermal expansion (volumetric) and is defined as the fractional change in the specific volume per unit change in temperature at constant pressure, viz.

$$\beta \equiv \frac{1}{v}\left(\frac{\partial v}{\partial T}\right)_p = -\frac{1}{\rho}\left(\frac{\partial \rho}{\partial T}\right)_p \tag{11.162}$$

For the ideal gas model, $P = \rho RT$ and equation (11.162) gives a particularly simple result, viz.

$$\beta = -\frac{1}{\rho}\left(\frac{\partial(P/RT)}{\partial T}\right)_P = -\frac{1}{(P/RT)}\left(-\frac{P}{RT^2}\right) = \frac{1}{T} \qquad (11.163)$$

For more complex fluids like liquids, the value of β must be determined experimentally or from complex property constitutive relations derived from experimental data. Some values for representative liquids at a temperature of $T_0 = 300$ K are given in Table 11.3 along with the corresponding value for the ideal gas model at this temperature.

Table 11.3 Coefficient of Thermal Expansion (Volumetric) of Selected Liquids at $T_0 = 300$ K

Fluid	β (K)$^{-1}$
Mercury	1.8×10^{-4}
Water	2.75×10^{-4}
Glycerine	5.4×10^{-4}
Gasoline (octane)	7.2×10^{-4}
Turpentine	9.9×10^{-4}
Ethyl Alcohol	1.1×10^{-3}
Methyl Alcohol	1.4×10^{-3}
Ideal Gas (all)	3.33×10^{-3}

Note that β is positive and typically has a small value so that to first order, liquids can be modeled as incompressible. In that sense, free convection can be viewed as a second order phenomenon. Clearly, the ideal gas has the largest value of the coefficient of thermal expansion and is therefore the most susceptible to free convection phenomena. It is not surprising, then, that free convection phenomena occur readily in the atmosphere and are responsible for much of the weather on the planet Earth.

Although we have not yet discussed the behavior of fluids that can change phase, it is worth noting in passing that water is anomalous with respect to its thermal expansion behavior. Water is unusual in that under conditions for which the liquid and vapor can co-exist in equilibrium, the liquid phase has a local maximum density at $T = 3.9982$ C (277.15 K) so that β becomes zero at that temperature and subsequently changes sign and becomes negative for saturation temperatures down to the triple point ($T_{T.P.} = 0.01$ C), the state in which the vapor, liquid, and solid phases can co-exist in equilibrium. This behavior happens to be extremely important for life on earth. In a stationary pool of water, such as a lake, that is cooling through radiative and/or convective heat transfer to the surroundings, the packets of water that reach a temperature of 4 C are locally more dense than both warmer and colder packets of water and thus sink to the bottom of the pool. The colder water then rises to the surface where it freezes, thus forming a layer of ice above the liquid water at the bottom of the pool. Although this layer of ice has a higher value of thermal conductivity than the liquid water, it does present a large thermal resistance to the atmosphere compared with the thermal resistance associated with the convective

and radiative cooling processes at the air/liquid water interface. This solid ice layer prevents the liquid water beneath it from cooling further and thus protects fish and other life forms from death by freezing during winter (or extinction during ice ages!).

The change in local density with temperature also results in changes in other properties such as the refractive index of the fluid. These changes in refractive index distort light passing through the fluid, and it is these local variations that we see when we see observe natural convection in the surroundings. For example, when driving down a paved road in summer, the road visible in the distance appears to "shimmer" as the light rays from it are deflected by the convection cells near the road surface. Similarly, the steam rising off the bare head of a hot, helmetless football player sitting on the side lines of Lambeau field in winter develops a swirling motion due to local density variations.

11.7.1 Modes of Free Convection

As we described above, free convection phenomena result from local spatial density gradients within a fluid, but the coefficient of thermal expansion is defined in equation (11.162) in terms of the change in density with temperature. This coefficient of thermal expansion can be related to the spatial gradients in density by using the product rule, viz.

$$\left(\frac{\partial \rho}{\partial x}\right)_P = \left(\frac{\partial \rho}{\partial T}\right)_P \left(\frac{\partial T}{\partial x}\right)_P = -\beta\rho\left(\frac{\partial T}{\partial x}\right)_P \qquad (11.164)$$

Thus the analysis of free convection flows is reduced to one of determining the temperature gradients that lead to the density gradients that drive the free convection phenomena. The free convection motions that arise from these temperature gradients may be subdivided simply into two classes depending upon whether the fluid motion occurs *adjacent to* or *away from* the rigid boundary responsible for the temperature gradients.

Images of two free convection flows are shown in Figure 11.15. These images have been formed using interferometry to produce fringes from local refractive index changes in the fluid resulting from local density gradients due to local temperature gradients. The lines thus correspond to isodensity lines, which at the nearly constant pressure present in the flow field, are also isotherms. If the free convection occurs near a rigid wall as in Figure 11.15a, then it is only logical that we try to describe the flow in terms of a free convection *boundary layer* similar to that of the forced convection flow. However, as we shall see shortly, the shape and rate of growth in this boundary layer is very different from that of the forced convection case since the fluid motion is induced by the local change in density rather than by being imposed externally. A familiar example of such a boundary layer is the one that occurs spontaneously on the inside of a window on a cold winter day. If one places the back of the hand close to, but not touching, a single pane glass window, one can just detect the slowly moving free convection air flow as the warm air in the room experiences a heat transfer interaction with the cold glass surface.

In the absence of a bounding rigid surface, the convective fluid motion can be thought of as a *plume* or *buoyant jet* as shown in Figure 11.15b. The difference between this case and the previous one is clearly seen in the shapes of the fringes, which are constant density contours, at the middle of the plume. Such configurations occur commonly in chimneys and in environmental or geophysical flows within the atmosphere and ocean. This is the classic case of a fluid heated from below or cooled from above as studied by Rayleigh and many others since.

Finally, it is worth noting that although these images show an *upward motion* due to local heating of the fluid with the resulting expansion of fluid elements, identical but opposite motions can occur from local cooling of fluid elements. The same correlations may be used in both cases;

the change in the sign of the temperature difference simply leads to a change in the sign of the heat transfer interaction (positive or negative when viewed from the perspective of the fluid) and a change in the direction of the heat flux (away from or towards the wall).

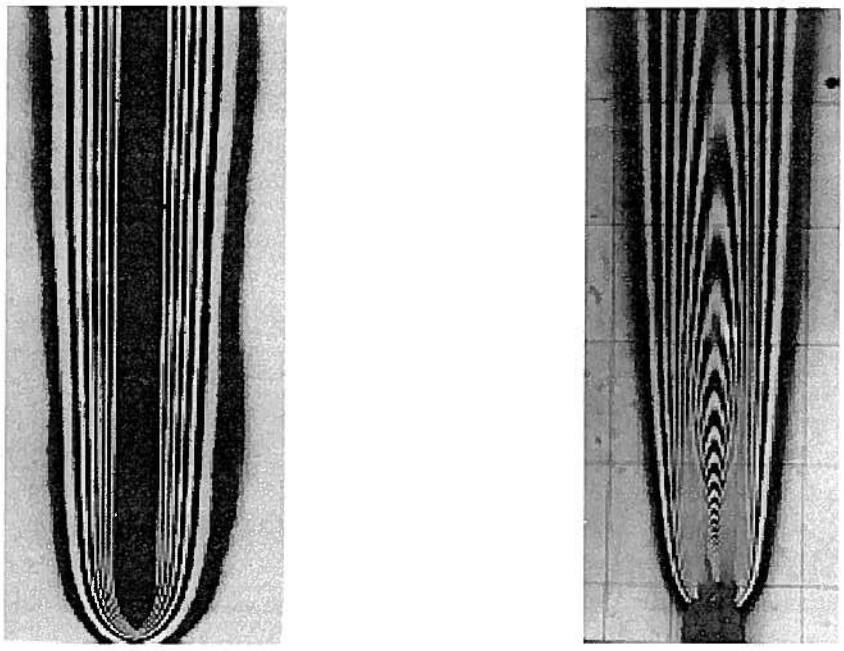

(a) (b)

Figure 11.15 Images of Free Convection
(a) Natural convection boundary layer on a heated vertical flat plate
(b) A thermal plume above a heated horizontal plate located at the bottom of the picture
(from Van Dyke, *An Album of Fluid Motion*, Parabolic Press, 1981)

11.7.2 Free Convection on a Vertical Flat Plate

Consider the configuration shown in Fig 11.15a, namely the free convection thermal boundary layer that forms along the surface of a vertical flat plate that is at a temperature T_s different from the temperature T_∞ of the surrounding fluid far outside the boundary layer. This is a geometry that occurs frequently in thermal-fluid systems, so it is only natural that we attempt to develop a means of evaluating the heat transfer that occurs between the plate and the fluid as a result of the ensuing free convection flow. The analysis of this configuration is somewhat more complicated than the case of forced convection flow that we considered earlier because the flow occurs as a result of the heat transfer process itself rather than being imposed by external means. As a consequence, the Navier-Stokes equation (the equation of motion) becomes coupled with the first law of thermodynamics for the configuration. This means that we can no longer solve the appropriate form of the Navier-Stokes equation first to obtain the velocity profile in the fluid, and then use this result to solve the first law for the temperature distribution and the subsequent heat transfer coefficient. In the case of free convection flows, the momentum boundary layer and the thermal boundary layer are essentially one and the same and develop together. This complicates the analysis considerably. Therefore, rather than attempt to solve the problem exactly, as we did for the case of forced convection over a flat plate, we employ the methods of dimensional

analysis first to establish the dimensionless parameters that can be used to describe the situation, and then we consider the *balance of forces* acting on a fluid element in the boundary layer and the manner in which they *scale* with the fundamental thermal-fluid and geometric parameters of the situation to obtain an approximate form for the relationship between these dimensionless parameters.

11.7.2.1 Dimensional analysis. Let us determine the dimensionless groups that characterize the dynamics of the coupling between the fluid motion and the heat transfer in the freely-convecting boundary layer shown schematically in Figure 11.16. We can accomplish this by applying the methodology that we developed for this purpose in Chapter 10.

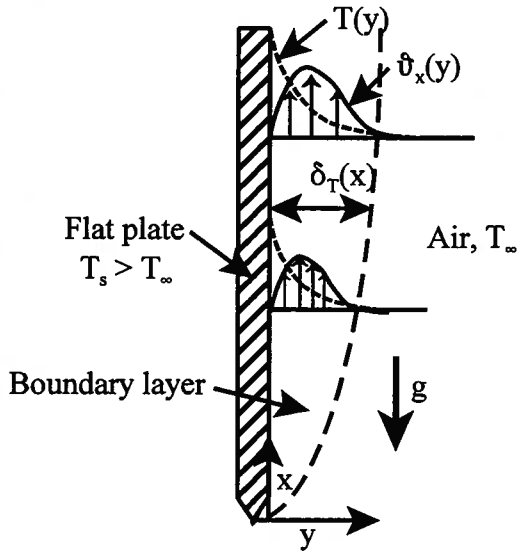

Figure 11.16 Free Convection Boundary Layer on a Vertical Flat Plate

Step 1: *List and count the n parameters required to describe the physical situation. If any important parameters are missing, dimensional analysis will fail.*

Based on the foregoing discussion, we expect the heat transfer process embodied in the heat transfer coefficient, h, to depend upon the temperature difference between the fluid and the plate, $\Delta T = T_s - T_\infty$; the density of the fluid, ρ; the buoyancy force per unit mass, F_B; the viscosity of the fluid, μ; the specific heat of the fluid, c_P; the thermal conductivity of the fluid, k; the acceleration of gravity, g; and the length of the plate, L. There are nine parameters so $n = 9$.

Step 2: *List the dimensions of each variable according to M, L, T, and Θ.*

$$[h]=\frac{M}{\Theta T^3},\ [\Delta T]=\Theta,\ [\rho]=\frac{M}{L^3},\ [F_B]=\frac{L}{T^2},\ [\mu]=\frac{M}{LT},$$

$$[c_P]=\frac{L^2}{\Theta T^2},\ [k]=\frac{ML}{\Theta T^2},\ [g]=\frac{L}{T^2},\ [L]=L$$

Step 3: *Find the value of r. Initially guess r to be equal to the number of different dimensions present and then make sure the there are r parameters that do not form a Π-product. If this is*

unsuccessful, reduce r by one and look again.

We initially guess $r = 4$ since there are four dimensions. Then we should be able to reduce the nine parameters down to five Π-groups, $n - r = 9 - 4 = 5$. Let us choose ρ, c_P, k, and L as the 4 potential repeating parameters. We need to ensure that they themselves do not form a Π-group. Checking, we get

$$\left[\rho^a c_P{}^b k^c L^d\right] = 1$$

$$\left(\frac{M}{L^3}\right)^a \left(\frac{L^2}{\Theta T^2}\right)^b \left(\frac{M}{\Theta T}\right)^c (L)^d = 1$$

$$M^{a+c} L^{-3a+2b+d} T^{-2b+c} \Theta^{-b-c} = 1$$

$$a + c = 0$$

$$-3a + 2b + d = 0$$

$$-2b + c = 0$$

$$-b - c = 0$$

The solution of this system of equations is $a = 0$, $b = 0$, $c = 0$, and $d = 0$. Then the parameters ρ, c_P, k, and L are dimensionally independent; hence, $r = 4$.

Step 4: *Select r parameters which do not form a Π-product among themselves. These parameters are the repeating parameters that will appear in all the Π-groups.*

We shall select ρ, c_P, k, and L as the repeating parameters since they have already been shown to be dimensionally independent.

Step 5: *Select one of the remaining parameters that is not one of the r repeating parameters and non-dimensionalize that parameter using the r repeating parameters. Repeat the procedure until all the remaining parameters are non-dimensionalized. There should now be n - r Π-groups.*

We have already gained some experience in working with a similar collection of parameters in situations involving heat transfer. When non-dimensionalize the heat transfer coefficient h, we will get the Nusselt number, Nu. This will be our first Π-group.

$$\Pi_1 = \frac{hL}{k} = Nu$$

When non-dimensionalize the viscosity μ, we will get the Prandtl number, Pr. This will be our second Π-group.

$$\Pi_2 = \frac{\mu c_P}{k} = Pr$$

The third dimensionless group results from non-dimensionalizing ΔT, viz.

$$\left[\Delta T \rho^a c_P{}^b k^c L^d\right] = 1$$

$$\Theta\left(\frac{M}{L^3}\right)^a \left(\frac{L^2}{\Theta T^2}\right)^b \left(\frac{ML}{\Theta T^3}\right)^c L^d = 1$$

$$M^{a+c} L^{-3a+2b+c+d} T^{-2b-3c} \Theta^{1-b-c} = 1$$

$$a + c = 0$$

$$-3a + 2b + c + d = 0$$

$$-2b - 3c = 0$$

$$1 - b - c = 0$$

The solution of this system of equations is $a = 2$, $b = 3$, $c = -2$, and $d = 2$. Then

$$\Pi_3 = \frac{\Delta T \rho^2 c_P{}^3 L^2}{k^2} = \left(\frac{c_P \Delta T}{\vartheta^2}\right)\left(\frac{\rho \vartheta L}{\mu}\right)^2\left(\frac{\mu c_P}{k}\right)^2 = \left(\frac{1}{2Ec}\right) Re^2 Pr^2$$

where Ec is the Eckert number (See Table 10.6.) and is important only in high-speed flows where the velocity ϑ is appreciable (typically a value approaching the speed of sound). Since the velocities in free convection are extremely slow, we do not expect Π_3 to be of any significance in the present situation. It is still a valid dimensionless group, however. The fourth dimensionless group results from non-dimensionalizing F_B, viz.

$$\left[F_B \rho^a c_P{}^b k^c L^d\right] = 1$$

$$\left(\frac{L}{T^2}\right)\left(\frac{M}{L^3}\right)^a\left(\frac{L^2}{\Theta T^2}\right)^b\left(\frac{ML}{\Theta T^3}\right)^c L^d = 1$$

$$M^{a+c} L^{1-3a+2b+c+d} T^{-2-2b-3c} \Theta^{-b-c} = 1$$

$$a + c = 0$$

$$1 - 3a + 2b + c + d = 0$$

$$-2 - 2b - 3c = 0$$

$$-b - c = 0$$

The solution of this system of equations is $a = 2$, $b = 2$, $c = -2$, and $d = 3$. Then

$$\Pi_4 = \frac{F_B \rho^2 c_P{}^2 L^3}{k^2} = \left(\frac{F_B \rho^2 L^3}{\mu^2}\right)\left(\frac{\mu c_P}{k}\right)^2 = \left(\frac{F_B L^3}{\nu^2}\right) Pr^2$$

where ν is the kinematic viscosity, $\nu = \mu/\rho$. We can express the buoyancy force in terms of the other parameters and thereby clarify the first term in parentheses on the right-hand side of the above expression. The buoyancy force per unit volume is

$$\hat{F}_B = (\rho_\infty - \rho) g$$

and the buoyancy force per unit mass becomes

$$F_B = \frac{(\rho_\infty - \rho)}{\rho} g$$

but the thermal expansion coefficient can be written

$$\beta \equiv -\frac{1}{\rho}\left(\frac{\partial \rho}{\partial T}\right)_P \approx -\frac{1}{\rho}\frac{(\rho - \rho_\infty)}{(T - T_\infty)} \tag{11.165}$$

Then the buoyancy force per unit mass becomes

$$F_B = \beta g (T - T_\infty) \approx \beta g (T_s - T_\infty)$$

Then the first term on the right-hand side of Π_4 becomes

$$\frac{F_B L^3}{\nu^2} = \frac{\beta g (T_s - T_\infty) L^3}{\nu^2} = Gr$$

This dimensionless parameter is known as the *Grashof number* and is denoted by the symbol Gr. Physically the Grashof number represents the ratio of the product of the buoyancy force and the inertia force to the square of the viscous force, i.e.,

$$Gr \sim \frac{(\text{buoyancy force})(\text{inertia force})}{(\text{viscous force})^2}$$

Since Gr depends directly upon L^3 and inversely upon ν^2, it can be a very large number (as large as 10^{10}) for typical convection flows in fluids with small kinematic viscosities such as gases.

The fifth dimensionless group will turn out to have precisely the same form as the fourth dimensionless group because g has the same dimensions as F_B, namely L/T^2. Thus

$$\Pi_5 = \left(\frac{gL^3}{\nu^2}\right) Pr^2$$

The term in parentheses can easily be converted into the Grashof number by multiplying by the dimensionless group $\beta(T_s - T_\infty)$. As a result, we cannot expect to learn anything from the dimensionless group Π_5 that we cannot already learn from the Grashof number.

Step 6: *Check to see that all proposed P-groups are dimensionless and write the functional relationship among them in dimensionless form.*

The five Π-groups are indeed dimensionless (We checked.). Then according to the Buckingham Pi Theorem, the free convection heat transfer analysis can be presented in a relationship of the form

$$Nu = G(Gr, Pr)$$

Once again, this is as far as dimensional analysis can take us. To determine the form of the function G, we need to examine the governing equations in detail and perhaps perform some experimental measurements.

11.7.2.2 Scaling of the free convection boundary layer. We now proceed to analyze the way in which the boundary layer thickness develops along the plate. The expected variations of the velocity profile and temperature in the boundary layer are shown in Figure 11.16. Note that since the two motions are coupled, there is only *one* boundary layer with a thickness we simply denote by $\delta(x)$. The velocity is zero both on the surface of the plate (the familiar "no slip" boundary condition) as well as far from the plate where the fluid is quiescent. In the boundary layer, the fluid velocity increases with distance along the plate as the fluid elements are heated, expand, and begin to rise due to the buoyancy effect. The temperature difference between the plate and the fluid far from the plate is *always* $\Delta T = T_s - T_\infty$ but the gradient $\partial T/\partial y$ in the boundary layer actually *decreases* as we move along the plate due to the outward diffusion of thermal energy from the surface of the plate into the fluid. Since the momentum transfer and the heat transfer are coupled in this case, once we have determined the velocity profile, we can see how the slope of the temperature difference changes. We can then compute the local heat flux at each point, and from this determine the local Nusselt number. Integrating the local Nusselt number along the plate will finally lead to an expression for the average Nusselt number as a function of the Grashof number and Prandtl number.

Consider a control volume in the natural convection boundary layer shown in Fig. 11.16. The lateral extent of the control volume is $\delta(x)$ and the components of the velocity vector in the x-direction and the y-direction are v_x and v_y, respectively. The motion in the boundary layer is steady from the point of view of an observer stationary in space (Eulerian view). However, from the point of view of an observer moving with the fluid (Lagrangian view), the motion is unsteady. Thermal energy diffuses in the y-direction away from the wall and the fluid particles near the wall expand and thus experience a buoyancy force which causes them to accelerate vertically upwards until this buoyancy force is just balanced by the viscous drag force. This motion convects thermal energy with the fluid. These physical statements are embodied in the

conservation equations for mass and linear momentum (Navier-Stokes equation) and the first law. The thermal-fluid properties of the fluid can be considered constant except for the variation of density with temperature in the gravitational body force term of the Navier-Stokes equation since it is this term which drives the flow. (Without this term there would be no free convection.) The effect of the temperature dependence of the other properties is to modify the numerical constants in the solution in a simple, but weak fashion. This simplification is known as the *Boussinesq approximation.*

Employing the Boussinesq approximation, we can now write the governing equations in two-dimensional form. The continuity equation becomes

$$\frac{\partial \vartheta_x}{\partial x}+\frac{\partial \vartheta_y}{\partial y}=0 \tag{11.166}$$

and the x-component of the Navier-Stokes equation becomes

$$\rho\left(\vartheta_x\frac{\partial \vartheta_x}{\partial x}+\vartheta_y\frac{\partial \vartheta_y}{\partial y}\right)=-\frac{\partial P}{\partial x}+\mu\left(\frac{\partial^2 \vartheta_x}{\partial x^2}+\frac{\partial \vartheta_y}{\partial y^2}\right)-\rho g \tag{11.167}$$

where we have made use of the fact that the gravity vector lies in the negative x-direction in this case. We note that at the outer edge of the boundary layer, the pressure gradient in the direction of flow is simply the hydrostatic variation in pressure, viz.

$$\left(\frac{\partial P}{\partial x}\right)_{y\to\infty}=-\rho_\infty g \tag{11.168}$$

To first order, the pressure gradient in the y-direction is zero. Then equation (11.168) gives the pressure gradient in the x-direction within the boundary layer. Substituting equation (11.168) into equation (11.167), we obtain

$$\rho\left(\vartheta_x\frac{\partial \vartheta_x}{\partial x}+\vartheta_y\frac{\partial \vartheta_y}{\partial y}\right)=\mu\left(\frac{\partial^2 \vartheta_x}{\partial x^2}+\frac{\partial \vartheta_y}{\partial y^2}\right)-(\rho-\rho_\infty)g \tag{11.169}$$

Substituting equation (11.165) into equation (11.169), we get

$$\rho\left(\vartheta_x\frac{\partial \vartheta_x}{\partial x}+\vartheta_y\frac{\partial \vartheta_y}{\partial y}\right)=\rho\beta g\,(T-T_\infty)+\mu\left(\frac{\partial^2 \vartheta_x}{\partial x^2}+\frac{\partial \vartheta_y}{\partial y^2}\right) \tag{11.170}$$

The first law for this case becomes

$$\rho c_P\left(\vartheta_x\frac{\partial T}{\partial x}+\vartheta_y\frac{\partial T}{\partial y}\right)=k\left(\frac{\partial^2 T}{\partial x^2}+\frac{\partial^2 T}{\partial y^2}\right) \tag{11.171}$$

The description of the boundary layer for free convection on an isothermal vertical flat plate can be determined by solving equations (11.166), (11.170), and (11.171) subject to the boundary conditions of "no slip" at the wall and "no temperature jump" at the wall, viz.

$$\vartheta_x=0 \text{ and } \vartheta_y=0 \quad \text{at} \quad y=0$$

$$\vartheta_x=0 \quad \text{at} \quad y\to\infty$$

$$T=T_s \quad \text{at} \quad y=0$$

$$T=T_\infty \quad \text{at} \quad y\to\infty$$

Unfortunately, we cannot use the same approach that we used in the case of forced convection over a flat plate, namely, solve the Navier-Stokes equation for the velocity profile and then use this velocity profile in the first law to determine the temperature profile. In the present case, equations (11.170) and (11.171) are coupled through the coefficient of expansion, β. We could

introduce a coupled similarity variable and then use this to derive a set of coupled ordinary differential equations from equations (11.170) and (11.171) that could be solved numerically. At this time, however, we do not know what that similarity variable might be.

To gain some insight to this situation, let us determine the magnitude of each variable that appears in the governing equations. In contrast to the case of forced convection, the present case has no externally imposed fluid velocity by which all the other terms can be scaled. For the free convection case the velocity in the x-direction is an unknown and changes with x as the fluid accelerates up the plate. Then we write

$$x = x, \quad \vartheta_x \simeq U(x), \quad (T - T_\infty) \simeq (T_s - T_\infty) = \Delta T_s, \quad y \simeq \delta(x), \quad \vartheta_y \simeq V(x) \tag{11.172}$$

Then from equations (11.172) we have

$$\frac{\partial \vartheta_x}{\partial x} \simeq \frac{U(x)}{x} \quad \text{and} \quad \frac{\partial \vartheta_y}{\partial y} \simeq \frac{V(x)}{\delta(x)}$$

Then the continuity equation (11.166) becomes

$$\frac{U(x)}{x} + \frac{V(x)}{\delta(x)} = 0$$

or

$$V(x) \simeq U(x)\frac{\delta(x)}{x} \tag{11.173}$$

Since by definition the boundary layer is thin, $\delta(x) << x$ and it follows from equation (11.173) that $V(x) << U(x)$ and the flow is almost parallel to the plate. Then following the example of the continuity equation, the Navier-Stokes equation, with the aid of equation (11.173), becomes

$$\rho\left[U(x)\frac{U(x)}{x} + \left(\frac{\delta(x)U(x)}{x}\right)\frac{U(x)}{\delta(x)}\right] \simeq \rho\beta g\Delta T_s + \mu\left(\underline{\frac{U(x)}{x^2}} + \frac{U(x)}{\left[\delta(x)\right]^2}\right) \tag{11.174}$$

In equation (11.174), the two terms in the brackets on the left-hand side are of the same order and can be combined; however, on the right-hand side, the underlined term in the viscous drag term is much smaller than the second term because $\delta(x) << x$. Then we can be neglect it by comparison. Then combining the remaining terms equation (11.174) and dividing by ρ, we get

$$\frac{\left[U(x)\right]^2}{x} \simeq \beta g\Delta T_s + \frac{\nu U(x)}{\left[\delta(x)\right]^2} \tag{11.175}$$

where we have made use of the definition of the kinematic viscosity, $\nu = \mu/\rho$.

Using the same approach on the first law, equation (11.171) becomes

$$\rho c_P\left(U(x)\frac{\Delta T_s}{x}\right) \simeq k\frac{\Delta T_s}{\left[\delta(x)\right]^2} \tag{11.176}$$

Solving equation (11.176) for $U(x)$, we get the behavior of the convection velocity with respect to the position on the plate, viz.

$$U(x) \simeq \left(\frac{k}{\rho c_P}\right)\frac{x}{\left[\delta(x)\right]^2} = \frac{\alpha x}{\left[\delta(x)\right]^2} \tag{11.177}$$

where we have made use of the thermal diffusivity, $\alpha = k/\rho c_P$. Since $U(x) \sim x/t$, it follows from equation (11.177) that

$$\delta(x) \propto \sqrt{t} \tag{11.178}$$

and the boundary layer thickness does indeed grow in a diffusive fashion. The difference between this result and a similar result for the case of forced convection is that in the free convection case the velocity $U(x)$ itself varies along the plate. Thus, we need to eliminate it from the coupled equations (11.175) and (11.176). Combining these two equations, we get

$$\frac{1}{x}\frac{\alpha^2 x^2}{\left[\delta(x)\right]^4} \simeq \beta\Delta T_s + \nu\alpha\frac{x}{\left[\delta(x)\right]^4} \tag{11.179}$$

Dividing equation (11.179) by ν^2, we get

$$Pr^{-2}\frac{x}{\left[\delta(x)\right]^4} \simeq \frac{\beta g\Delta T_s}{\nu^2} + Pr^{-1}\frac{x}{\left[\delta(x)\right]^4} \tag{11.180}$$

Equation (11.180) can be written in more general terms as

$$f(Pr)\frac{x}{\left[\delta(x)\right]^4} \simeq \frac{\beta g\Delta T_s}{\nu^2} \tag{11.181}$$

where $f(Pr)$ is a function of Pr^{-1} and Pr^{-2}. Solving equation (11.181) for the boundary layer thickness, we get

$$\delta(x) \simeq \left(\frac{\beta g\Delta T_s}{\nu^2}\right)^{-1/4} f(Pr)\, x^{1/4} \tag{11.182}$$

Equation (11.182) shows that the free convection boundary layer grows along the plate as $x^{1/4}$ which is markedly different from the forced convection boundary layer which grows as $x^{1/2}$. Non-dimensionalizing the boundary layer thickness in equation (11.182), we get

$$\frac{\delta(x)}{x} \simeq \left(\frac{\beta g(T_s - T_\infty)x^3}{\nu^2}\right)^{-1/4} f(Pr)^{1/4} = Gr_x^{-1/4}\left[f(Pr)\right]^{1/4} \tag{11.183}$$

where we have introduced the local Grashof number, Gr_x.

Having obtained an expression for the development of the free convection boundary layer along the plate, we can now explore the details of the development of the dimensionless heat transfer coefficient, i.e. the Nusselt number, along the plate. The heat flux at the surface can be expressed either in terms of the temperature gradient in the fluid at the surface of the plate, or equivalently, in terms of Newton's law of cooling, viz.

$$-k\left(\frac{\partial T}{\partial y}\right)_{y=0} = \dot{q}_s = h(T_s - T_\infty) \tag{11.184}$$

Since the temperature gradient at the wall decreases along the plate as the boundary layer grows with x, it is clear that on the right-hand side of equation (11.184) we should expect the heat transfer coefficient $h(x)$ to also vary with x. We may estimate the wall temperature gradient as

$$\frac{\partial T}{\partial y} \simeq \frac{T_s - T_\infty}{\delta(x)} \tag{11.185}$$

Then combining equations (11.182), (11.184), and (11.185), we get

$$-\frac{k(T_s - T_\infty)}{xGr_x^{-1/4} f(Pr)} \simeq h(x)(T_s - T_\infty) \tag{11.186}$$

Introducing the definition of the local Nusselt number into equation (11.186), we get

$$Nu_x = \frac{h(x)x}{k} \simeq Gr_x^{1/4}\left[f(Pr)\right]^{-1/4} \tag{11.187}$$

Thus we have now determined the functional form of the relationship derived from the dimensional analysis. In order to evaluate the precise form of equation (11.187), we need to develop the similarity solution.

For design purposes it is often more convenient to express heat transfer correlations in terms of an *average* heat transfer coefficient. From equation (11.187) we can readily determine the average Nusselt number over a vertical plate of length L as

$$Nu_L = \frac{1}{L}\int_0^L Nu_x dx = \frac{\left[f(Pr)\right]^{-1/4}}{L}\int_0^L \left(\frac{\beta g(T_s - T_\infty)}{\nu^2}\right) x^{3/4} dx = \frac{4}{3} Nu_{x=L} \tag{11.188}$$

Thus the average value of the Nusselt number over the length of the plate is 1/3 larger than the local value at $x = L$. This result is a consequence of the fact that the temperature gradient, and, hence, the heat flux, actually *decreases* along the plate as the boundary layer diffuses outward and becomes thicker.

11.7.2.3 Similarity solution for free convection on a vertical flat plate. Now that we have determined the manner in which the boundary layer thickness scales with distance along the plate, we can develop the appropriate similarity parameter that will lead to a solution of the coupled governing equations. To this end, we introduce the stream function ψ such that the continuity function is automatically satisfied, viz.

$$\vartheta_x = \frac{\partial \psi}{\partial y} \quad \text{and} \quad \vartheta_y = -\frac{\partial \psi}{\partial x} \tag{11.189}$$

where the similarity variable is given by

$$\eta = \left(\frac{Gr_x}{4}\right)^{1/4} \frac{y}{x} \quad \text{and} \quad \psi = 4\nu \left(\frac{Gr_x}{4}\right)^{1/4} f(\eta) \tag{11.190}$$

Then the velocity components become

$$\vartheta_x = 2\sqrt{\beta g x (T_s - T_\infty)}\, f' \quad \text{and} \quad \vartheta_y = \left[\frac{\beta g \nu^2 (T_s - T_\infty)}{4x}\right]^{1/4} (\eta f' - 3f) \tag{11.191}$$

and the dimensionless temperature is given by

$$\theta = \frac{T - T_\infty}{T_s - T_\infty} \tag{11.192}$$

Substituting equations (11.191) and (11.192) into equations (11.170) and (11.171), we are able to reduce the coupled partial differential equations into a pair of coupled ordinary differential equations, viz.

$$\begin{aligned} f''' + 3ff'' - 2f'^2 + \theta &= 0 \\ \theta'' + 3(Pr) f\theta' &= 0 \end{aligned} \tag{11.193}$$

with boundary conditions

$$\begin{aligned} f = 0 \quad \text{and} \quad f' = 0 \quad \text{at} \quad \eta &= 0 \\ f' = 0 \quad \text{at} \quad \eta &\to \infty \\ \theta = 1 \quad \text{at} \quad \eta &= 0 \\ \theta = 0 \quad \text{at} \quad \eta &\to \infty \end{aligned} \tag{11.194}$$

There is no known analytic solution for equations (11.193) so we must rely on numerical solutions with the Prandtl number as a parameter. The difficulty with numerical solutions is that the velocity gradient f'' and the temperature gradient θ' must be known at the wall in order for

the velocity to vanish and the temperature to decay to T_∞ as $\eta \to \infty$. For some representative values of the Prandtl number, White (Frank M. White, *Viscous Fluid Flow*, McGraw-Hill, Boston, 1991, p. 326.) suggests the values for these gradients as shown in Table 11.4.

Table 11.4 Dimensionless Velocity Gradients and Temperature Gradients at the Surface for Free Convection Flow Over a Vertical Flat Plate

Pr	$f''(0)$	$\theta'(0)$
0.10	0.8591	-0.2301
1	0.6422	-0.5671
10	0.4192	-1.1237
100	0.2517	-2.1913

Using the data of Table 11.4, we can obtain a numerical solution of equations (11.193). The results are shown graphically in Figures 11.17 and 11.18.

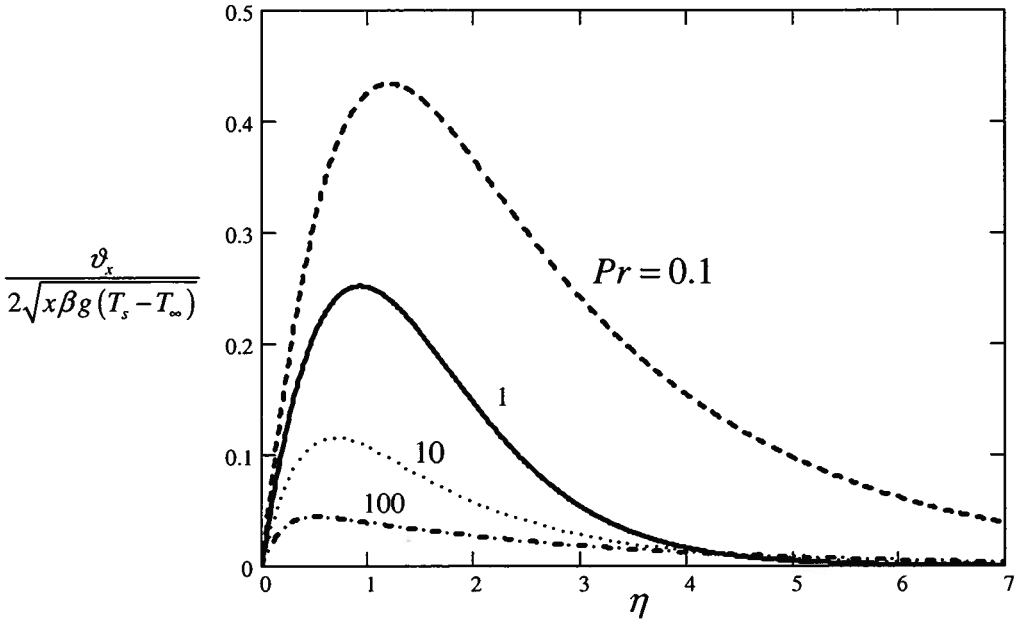

Figure 11.17 Velocity Profile in Free Convection Boundary Layer on Vertical Flat Plate

In order to fit the Nusselt number data resulting from the foregoing numerical solutions for various values of the Prandtl number, Churchill and Usagi (S. W. Churchill and R. Usagi, "A General Expression for the Correlation of Rates of Transfer and Other Phenomena," *AIChE Journal*, 18, pp. 1121-1128, 1972) curve fit the data and proposed a Prandtl number function Ψ such that

$$\Psi = \left[1 + \left(\frac{0.492}{Pr}\right)^{9/16}\right]^{-16/9} \tag{11.195}$$

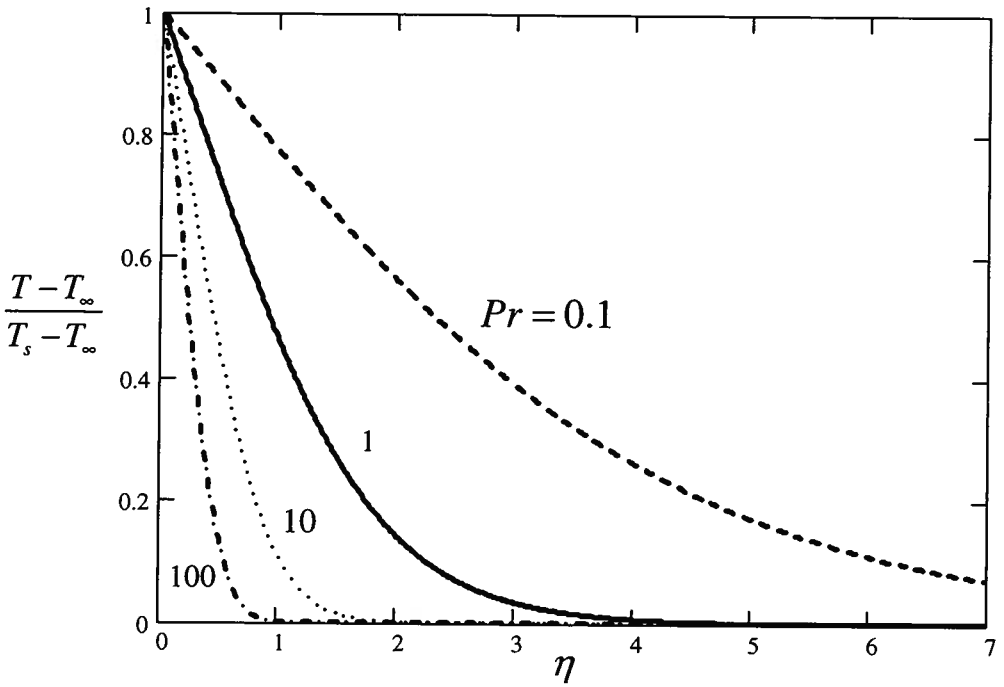

Figure 11.18 Temperature Profile in Free Convection Boundary Layer on Vertical Flat Plate

In the laminar regime ($Ra_L \leq 10^9$), this function is to be used with the following curve fit for the average Nusselt number for free convection over a vertical flat plate as determined by Churchill and Chu (S. W. Churchill and H. H .S. Chu, "Correlating Equations for Laminar and Turbulent Free Convection from a Vertical Plate," *International Journal of Heat and Mass Transfer*, **18**, pp. 1323-1329, 1975), viz.

$$Nu_L = 0.68 + 0.670\left(Ra\Psi\right)^{1/4} \tag{11.196}$$

where we have introduced the *Rayleigh number*, $Ra = GrPr$.

Thus for the case of free convection over a vertical flat plate, we have shown through a combination of dimensional analysis and approximate or 'scaling' analysis of the governing equations, that laminar free convection gives rise to a slowly-growing boundary layer described by equation (11.182) and an average Nusselt number given by equation (11.196). As we have shown, the coupled nature of the heat transfer and fluid flow means that both of these results depend on the dimensionless *Grashof number* raised to the 1/4 power. This result is quite robust and we should expect it to be repeated for other geometries that are more difficult to analyze exactly.

11.7.2.4 Turbulent free convection. Based on our experience with forced convection, we fully expect the laminar free convection boundary layer to become unstable at some point and to undergo a transition to a turbulent boundary layer. Figure 11.19 shows a typical free convection flow experiencing just such a transition.

In the case of free convection on the vertical flat plate, as the fluid rises up the plate, the velocity increases as indicated by equation (11.177). In fact, the velocity increases as $x^{1/2}$.

$$U(x) \simeq \frac{x}{\left[\delta(x)\right]^2} \simeq \frac{x}{\left(x^{1/4}\right)^2} \simeq \frac{x}{x^{1/2}} \simeq x^{1/2}$$

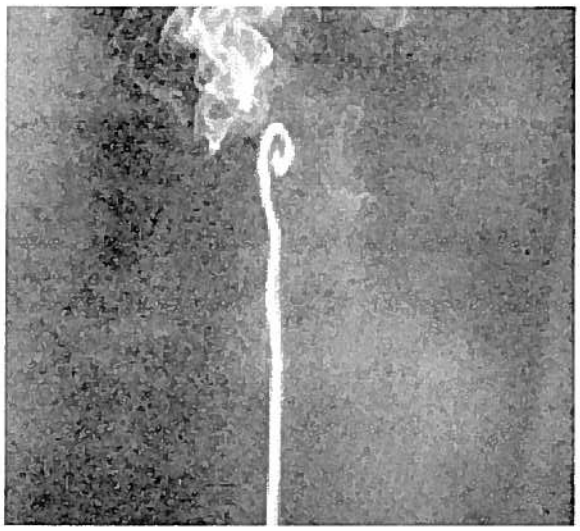

Figure 11.19 A Free Convection Smoke Plume Develops Waves and Becomes Turbulent

The local Grashof number, Gr_x, also increases just as the local Reynolds number, Re_x, increased during laminar forced convection over a flat plate. Then, at some value of the Grashof number, even under carefully controlled conditions, small perturbations to the flow will eventually grow and the flow will become turbulent. This turbulence leads to disruption of the laminar boundary layer and rapid mixing of the rising warmer fluid with the surrounding colder air. The mixing then enhances energy transport between the plate and the fluid. Experiments and calculations show that for the free convection boundary layer adjacent to a flat plate, the critical conditions for the laminar/turbulent transition occur at a critical Rayleigh number of $Ra_{x,critical} = 10^9$. For a given temperature difference between the plate and the fluid, this value of the Rayleigh number can be used to determine the location where the laminar/turbulent transition occurs. Beyond this point, the fluid motion is turbulent and the correlation of equation (11.196) no longer applies. For $10^9 \leq Ra_L \leq 10^{12}$, Churchill and Chu (*op. cit.*) suggest that the average value of the Nusselt number can be determined from

$$Nu_L = 0.68 + 0.670\left(Ra_L \Psi\right)^{1/4}\left(1 + 1.6 \text{ x } 10^{-8} Ra_L \Psi\right)^{1/12} \qquad (11.197)$$

where the Prandtl number function Ψ is given by equation (11.195).

11.8 Combined Free and Forced Convection

Another very common situation encountered in automotive engineering and in micro-electronic applications consists of combined natural and forced convection. For example, in the latter case, a small fan may be mounted close to a hot surface such as a circuit board populated with integrated circuits that dissipate power and which are normally cooled by natural convection. If the surface temperature T_s as monitored by a surface mounted thermocouple exceeds a critical value, the fan may be actuated and air will be blown across the surface to enhance the overall heat transfer coefficient and assist in the removal of excess thermal energy. We may wish to know which process dominates the overall heat transfer, free or forced convection. From the definition of the Grashof number, it is clear that it provides a dimensionless measure of the inertial and buoyancy forces in the fluid. This measure may be compared with the

appropriate measure of the inertial forces in the corresponding forced convection configuration which characterizes the growth of the thermal boundary layer and the average Nusselt number. The dimensionless ratio Gr_L/Re_L^2 thus provides information about the relative magnitude of free and forced convection.

Three limiting cases can be identified, viz.

$$\frac{Gr_L}{Re_L^{\,2}} \begin{cases} \ll 1 \text{ Free convection negligible} \\ \simeq 1 \text{ Both effects important} \\ \gg 1 \text{ Forced convection negligible} \end{cases} \tag{11.198}$$

As the velocity ϑ_0 of the forced fluid stream is increased, it is clear from equation (11.198) that free convection becomes progressively less important. In general, analysis of a situation for which $0.1 \leq Gr_L/Re_L^2 \leq 10$ requires the development of specialized correlations for the actual geometry and conditions.

11.9 Convection Heat Transfer Correlations for Other Geometries

The foregoing discussion of this chapter has attempted to present the underlying physics of convection heat transfer for both forced convection and free convection phenomena. The discussion has also attempted to present the typical methods employed in the analysis of the quantitative aspects of these phenomena in the context of some common situations that occur in the practice of thermal-fluids engineering. Clearly, given the scope of the subject, this treatment has of necessity been illustrative rather than exhaustive. The methodology presented, however, is common to all situations that might arise in the practice of the profession. Specific convection correlations that should prove useful to the practicing thermal-fluids engineer are summarized in Table 11.5.

Table 11.5 Heat Transfer Correlation Equations of $Nu = \phi(Re,Pr)$ for Various Configurations

	Configuration	Correlations	Comments
1	Turbulent flow in smooth ducts with fully developed hydrodynamics and heat transfer	$f = \left(0.790 \cdot \ln \mathrm{Re}_{D_h} - 1.64\right)^{-2}; \quad 10^4 < \mathrm{Re}_{D_h} < 5\times10^6$ $\mathrm{Nu}_{D_h} = \dfrac{(f/8)\left(\mathrm{Re}_{D_h} - 1000\right)\mathrm{Pr}}{1+12.7(f/8)^{1/2}\left(\mathrm{Pr}^{2/3}-1\right)}; \quad 3000 < \mathrm{Re}_{D_h} < 10^6$ $0.5 < \mathrm{Pr}$	Hydraulic Diameter: $D_h = \dfrac{4A_c}{\wp}$, where $\wp$ is the wetted perimeter Exponents for property and temp ratio corrections for duct flows (*s:* refers to wall; *b:* to bulk): Flow / Fluid / Wall / m / n Laminar / Liquids / Heating / 0.58 / -0.11 (μ_s/μ_b) / Cooling / 0.50 / -0.11 Gases / Heating / 1 / 0 (T_s/T_b) / Cooling / 1 / 0 Turbulent / Liquids / Heating / 0.25 / -0.25 (μ_s/μ_b) / Cooling / 0.25 / -0.11 Gases / Heating / -0.2 / -0.55 (T_s/T_b) / Cooling / -0.1 / 0.0 for use with the following ratios: $\dfrac{f}{f_b} = \left(\dfrac{\mathrm{Pr}_s}{\mathrm{Pr}_b}\right)^m$ or $\left(\dfrac{\mu_s}{\mu_b}\right)^m$ or $\left(\dfrac{T_s}{T_b}\right)^m$ $\dfrac{\mathrm{Nu}}{\mathrm{Nu}_b} = \left(\dfrac{\mathrm{Pr}_s}{\mathrm{Pr}_b}\right)^n$ or $\left(\dfrac{\mu_s}{\mu_b}\right)^n$ or $\left(\dfrac{T_s}{T_b}\right)^n$
2	Laminar flow in a pipe with fully developed hydrodynamics: T_{wall} uniform $\dfrac{\dot{Q}}{A}$ uniform	$f = \dfrac{64}{\mathrm{Re}_D}; \quad \mathrm{Re}_D < 2300$ $\overline{\mathrm{Nu}}_D = 3.66 + \dfrac{0.065(D/L)\mathrm{Re}_D\,\mathrm{Pr}}{1+0.04\left[(D/L)\mathrm{Re}_D\,\mathrm{Pr}\right]^{2/3}}; \quad \mathrm{Re}_D < 2300$ $\overline{\mathrm{Nu}}_D = 4.364 + 0.0722(D/L)\mathrm{Re}_D\mathrm{Pr} \quad \mathrm{Re}_D < 2300$	
3	Laminar flow between parallel plates with fully developed hydrodynamics	$f = \dfrac{96}{\mathrm{Re}_{D_h}}; \quad \mathrm{Re}_{D_h} < 2800$ $D_h = \dfrac{4A_c}{\wp} = 2\times\text{plate spacing}$ $\overline{\mathrm{Nu}}_{D_h} = 7.54 + \dfrac{0.03(D_h/L)\mathrm{Re}_{D_h}\,\mathrm{Pr}}{1+0.016\left[(D_h/L)\mathrm{Re}_{D_h}\,\mathrm{Pr}\right]^{2/3}}; \quad \mathrm{Re}_{D_h} < 2800$ $\overline{\mathrm{Nu}}_{D_h} = 8.235 + 0.0364(D_h/L)\mathrm{Re}_{D_h}\,\mathrm{Pr} \quad \mathrm{Re}_{D_h} < 2800$	
4	Laminar boundary layer on a flat plate	$\overline{C}_f = 1.328\,\mathrm{Re}_L^{-1/2}; \quad 10^3 < \mathrm{Re}_L \le 5\times10^5$ $\overline{\mathrm{Nu}} = 0.664\,\mathrm{Re}_L^{1/2}\,\mathrm{Pr}^{1/3}; \quad 10^3 < \mathrm{Re}_L \le 5\times10^5, \quad 0.5 < \mathrm{Pr}$	
5	Turbulent boundary layer on a smooth flat plate	$\overline{C}_f = 1.328\,\mathrm{Re}_{tr}^{-1/2}\left(\dfrac{\mathrm{Re}_{tr}}{\mathrm{Re}_L}\right) + \dfrac{0.523}{\ln^2 0.06\,\mathrm{Re}_L} - \left(\dfrac{\mathrm{Re}_{tr}}{\mathrm{Re}_L}\right)\dfrac{0.523}{\ln^2 0.06\,\mathrm{Re}_{tr}}$ $\mathrm{Re}_{tr} < \mathrm{Re}_L < 10^9$ $\overline{\mathrm{Nu}} = 0.664\,\mathrm{Re}_{tr}^{1/2}\,\mathrm{Pr}^{1/3} + 0.036\,\mathrm{Re}_L^{0.8}\,\mathrm{Pr}^{0.43}\left[1-\left(\mathrm{Re}_{tr}/\mathrm{Re}_L\right)^{0.8}\right]$ $\mathrm{Re}_{tr} < \mathrm{Re}_L < 3\times10^7, \quad 0.7 < \mathrm{Pr} < 400$	$\mathrm{Re}_{tr} = 50{,}000 - 500{,}000$ Lower values are characteristic of practical situations where disturbing factors such as roughness and vibration are present

6	Flow across a cylinder	$C_D = 1 + \dfrac{10}{\mathrm{Re}_D^{2/3}}; \quad 1 < \mathrm{Re}_D < 10^4$ $\mathrm{Nu}_D = 1.15 \cdot \mathrm{Re}_D^{1/2}\,\mathrm{Pr}^{1/3}; \quad 0.5 < \mathrm{Pr}$ $\overline{\mathrm{Nu}}_D = 0.3 + \dfrac{0.62\,\mathrm{Re}_D^{1/2}\,\mathrm{Pr}^{1/3}}{\left[1+(0.4/\mathrm{Pr})^{2/3}\right]^{1/4}}; \quad \mathrm{Re}_D < 10^4,\ 0.5 < \mathrm{Pr}$ $= 0.3 + \dfrac{0.62\,\mathrm{Re}_D^{1/2}\,\mathrm{Pr}^{1/3}}{\left[1+(0.4/\mathrm{Pr})^{2/3}\right]^{1/4}}\left[1+\left(\dfrac{\mathrm{Re}_D}{282{,}000}\right)^{1/2}\right];$ $2\times10^4 < \mathrm{Re}_D < 4\times10^5$ $= 0.3 + \dfrac{0.62\,\mathrm{Re}_D^{1/2}\,\mathrm{Pr}^{1/3}}{\left[1+(0.4/\mathrm{Pr})^{2/3}\right]^{1/4}}\left[1+\left(\dfrac{\mathrm{Re}_D}{282{,}000}\right)^{5/8}\right]^{4/5};$ $4\times10^5 < \mathrm{Re}_D < 5\times10^6$ $\overline{\mathrm{Nu}}_D = \dfrac{1}{0.8237 - \ln(\mathrm{Re}_D\,\mathrm{Pr})^{1/2}}; \quad \mathrm{Re}_D\,\mathrm{Pr} < 0.2$	C_D = Drag force / $\left(\frac{1}{2}\rho v^2 A_f\right)$ Nu_D: stagnation line local Nusselt number
7	Flow across a sphere	$C_D = \dfrac{24}{\mathrm{Re}_D}; \quad \mathrm{Re}_D < 0.5$ $C_D \cong \dfrac{24}{\mathrm{Re}_D}\left(1+\dfrac{\mathrm{Re}_D^{2/3}}{6}\right); \quad 2 < \mathrm{Re}_D < 500$ $C_D \cong 0.44; \quad 500 < \mathrm{Re}_D < 2\times10^5$ $\mathrm{Nu}_D = 1.32\,\mathrm{Re}_D^{1/2}\,\mathrm{Pr}^{1/3}; \quad 0.5 < \mathrm{Pr}$ $\overline{\mathrm{Nu}}_D = 2 + \left(0.4\,\mathrm{Re}_D^{1/2} + 0.06\,\mathrm{Re}_D^{2/3}\right)\mathrm{Pr}^{0.4};$ $3.5 < \mathrm{Re}_D < 8\times10^4,\ 0.7 < \mathrm{Pr} < 380$	Use mean film temperature; or better results can be obtained using a viscosity ratio correction with n = -1/4 applied to the convection contribution Nu_D: stagnation line local Nusselt number
8	Laminar natural-convection boundary layer on a vertical wall	$\overline{\mathrm{Nu}}_L = 0.68 + 0.670(\mathrm{Ra}_L\Psi)^{1/4}; \quad \mathrm{Ra}_L < 10^9$ $\Psi = \left[1+\left(\dfrac{0.492}{\mathrm{Pr}}\right)^{9/16}\right]^{-16/9}$	
9	Turbulent natural-convection boundary layer on a vertical wall	$\overline{\mathrm{Nu}}_L = 0.68 + 0.670(\mathrm{Ra}_L\Psi)^{1/4}\left(1+1.6\times10^{-8}\mathrm{Ra}_L\Psi\right)^{1/12};$ $\Psi = \left[1+\left(\dfrac{0.492}{\mathrm{Pr}}\right)^{9/16}\right]^{-16/9} \quad 10^9 < \mathrm{Ra}_L < 10^{12}$	

10	Natural convection on a horizontal cylinder	$\overline{\mathrm{Nu}}_D = 0.36 + \dfrac{0.518 \cdot \mathrm{Ra}_D^{1/4}}{\left[1+(0.559/\mathrm{Pr})^{9/16}\right]^{4/9}}; \qquad 10^{-4} < \mathrm{Ra}_D \le 10^9$ $\overline{\mathrm{Nu}}_D = \left\{0.60 + 0.387\left[\dfrac{\mathrm{Ra}_D}{\left[1+(0.559/\mathrm{Pr})^{9/16}\right]^{16/9}}\right]^{1/6}\right\}^2; \quad 10^9 \le \mathrm{Ra}_D$	
11	Natural convection on a sphere	$\overline{\mathrm{Nu}}_D = 2 + \dfrac{0.589 \cdot \mathrm{Ra}_D^{1/4}}{\left[1+(0.469/\mathrm{Pr})^{9/16}\right]^{4/9}}; \quad \mathrm{Ra}_D \le 10^{11}; \; 0.5 < \mathrm{Pr}$	
12	Natural convection on a heated horizontal plate facing down or a cooled plate facing up	$\overline{\mathrm{Nu}}_L = 6.5\left[1 + 0.38\dfrac{L}{W}\right]\left[(1+X)^{0.39} - X^{0.39}\right]\mathrm{Ra}_L^{0.13}$ $X = 13.5\mathrm{Ra}_L^{-0.16} + 2.2\left(\dfrac{L_a}{L}\right)^{0.7}$ $10^6 < \mathrm{Ra}_L < 10^{10}; \; 0.7 < \mathrm{Pr} < 4800; \; 0 < \dfrac{L_a}{L} < 0.2$	W is the length of the longer side, L is the length of the shorter side, L_a is the length of the adiabatic extensions 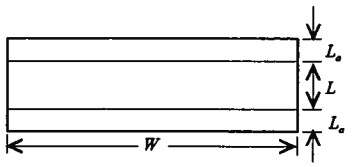
13	Natural convection on a heated horizontal plate facing up or a cooled plate facing down	$\overline{\mathrm{Nu}}_L = 0.54\mathrm{Ra}_L^{1/4}; \qquad 10^5 < \mathrm{Ra}_L < 2\times10^7$ $\overline{\mathrm{Nu}}_L = 0.14\mathrm{Ra}_L^{1/3}; \quad 2\times10^7 < \mathrm{Ra}_L < 3\times10^{10}$	L is the length of the shorter side
14	Natural convection across vertical cavities with insulated horizontal surfaces, $1<H/L<10$	$1 < H/L < 2$: $\overline{\mathrm{Nu}}_L = 0.18\left(\dfrac{\mathrm{Pr}}{0.2+\mathrm{Pr}}\mathrm{Ra}_L\right)^{0.29}; \quad 10^3 < \dfrac{\mathrm{Pr}}{0.2+\mathrm{Pr}}\mathrm{Ra}_L$ $2 < H/L < 10$: $\overline{\mathrm{Nu}}_L = 0.22\left(\dfrac{\mathrm{Pr}}{0.2+\mathrm{Pr}}\mathrm{Ra}_L\right)^{0.28}\left(\dfrac{H}{L}\right)^{-1/4}; \quad \mathrm{Ra}_L < 10^{10}$	H is the height of the cavity, L is the length of the cavity
15	Natural convection between concentric cylinders	$\dfrac{k_{eff}}{k} = 0.386\left(\dfrac{\mathrm{Pr}}{0.861+\mathrm{Pr}}\right)^{1/4}\mathrm{Ra}_{\mathrm{cyl}}^{1/4}; \quad 10^2 < \mathrm{Ra}_{\mathrm{cyl}} < 10^7$ $\mathrm{Ra}_{\mathrm{cyl}} = \dfrac{\left[\ln(D_o/D_i)\right]^4}{\left[\frac{1}{2}(D_o - D_i)\right]^3\left(D_o^{-3/5} + D_i^{-3/5}\right)^5}\mathrm{Ra}_L$	Valid only for $k_{eff}/k > 1$ k_{eff} is the effective thermal conductivity, for use in $\dot{Q} = \dfrac{2\pi k_{eff} L(T_1 - T_2)}{\ln(r_2/r_1)}$

16	Natural convection between concentric spheres	$\frac{k_{eff}}{k} = 0.74\left(\frac{\mathrm{Pr}}{0.861+\mathrm{Pr}}\right)^{1/4} \mathrm{Ra}_{sph}^{1/4}; \quad 10^2 < \mathrm{Ra}_{sph} < 10^4$ $\mathrm{Ra}_{sph} = \frac{\frac{1}{2}(D_o - D_i)}{(D_o D_i)^4} \frac{\mathrm{Ra}_L}{\left(D_o^{-7/5} + D_i^{-7/5}\right)^5}$	Valid only for $k_{eff}/k > 1$ k_{eff} is the effective thermal conductivity, for use in $\dot{Q} = \frac{4\pi k_{eff}(T_1 - T_2)}{1/r_1 - 1/r_2}$
17	Natural convection across thin enclosures ($H/L > 10$)	$0 \le \theta < 60°$: $\overline{\mathrm{Nu}}_L = 1 + 1.44\left[1 - \frac{1708}{\mathrm{Ra}_L \cos\theta}\right]\left\{1 - \frac{1708(\sin 1.8\theta)^{1.6}}{\mathrm{Ra}_L \cos\theta}\right\} + \left[\left(\frac{\mathrm{Ra}_L \cos\theta}{5830}\right)^{1/3} - 1\right]; \quad 0 < \mathrm{Ra}_L < 10^5$ $\theta = 60°$: $\overline{\mathrm{Nu}}_{L,60°} = \max\{\mathrm{Nu}_1, \mathrm{Nu}_2\}; \quad 0 < \mathrm{Ra}_L < 10^7$ $\mathrm{Nu}_1 = \left\{1 + \left[\frac{0.0936\mathrm{Ra}_L^{0.314}}{1 + \frac{0.5}{\left[1+(\mathrm{Ra}_L/3160)^{20.6}\right]^{0.1}}}\right]^7\right\}^{1/7}$ $\mathrm{Nu}_2 = \left(0.104 + \frac{0.175}{H/L}\right)\mathrm{Ra}_L^{0.283}$ $60° < \theta < 90°$ $\overline{\mathrm{Nu}}_L = \left(\frac{90-\theta}{30}\right)\overline{\mathrm{Nu}}_{L,60°} + \left(\frac{\theta - 60}{30}\right)\overline{\mathrm{Nu}}_{L,90°}$ $\theta = 90°$: $\overline{\mathrm{Nu}}_{L,90°} \cong 1; \quad \mathrm{Ra}_L \le 10^3$ $\overline{\mathrm{Nu}}_{L,90°} = \max\{\mathrm{Nu}_1, \mathrm{Nu}_2, \mathrm{Nu}_3\}; \quad 10^3 < \mathrm{Ra}_L < 10^7$ $\mathrm{Nu}_1 = 0.0605\mathrm{Ra}_L^{1/3}$ $\mathrm{Nu}_2 = \left\{1 + \left[\frac{0.104\mathrm{Ra}_L^{0.293}}{1+(6310/\mathrm{Ra}_L)^{1.36}}\right]^3\right\}^{1/3}$ $\mathrm{Nu}_3 = 0.242\left(\frac{\mathrm{Ra}_L}{H/L}\right)^{0.272}$	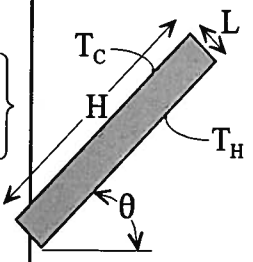 *Schematic of an inclined enclosure* All properties to be evaluated at $T_r = \frac{1}{2}(T_H + T_C)$ If a term in square brackets is negative, set it equal to zero. Strictly speaking, these correlations are for gases only; however, the equation for $0 \le \theta < 60°$ can also be used for liquids of moderate Prandtl number

18	Flow through tube banks, with N rows of tubes transverse to the flow 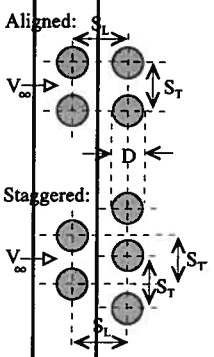	$N<10$: $\overline{\mathrm{Nu}}_D = \dfrac{1+(N-1)\Phi}{N}\overline{\mathrm{Nu}}^{1}_D$ $10 \le N$: $\overline{\mathrm{Nu}}^{10+}_D = \Phi\overline{\mathrm{Nu}}^{1}_D$ $\Phi_{\text{aligned}} = 1+\dfrac{0.7}{\Psi^{1.5}}\cdot\dfrac{(S_L/S_T-0.3)}{(S_L/S_T+0.7)^2}$ $\Phi_{\text{staggered}} = 1+\dfrac{2}{3P_L}$ where, for $P_L<1$: $\Psi = 1-\dfrac{\pi}{4P_TP_L}$ $1\le P_L$: $\Psi = 1-\dfrac{\pi}{4P_T}$	$\overline{\mathrm{Nu}}^{1}_D = \overline{\mathrm{Nu}}_D$ from item 6 with Re_D based on the average velocity in the space between two adjacent tubes, $\overline{\vartheta} = \vartheta_o\dfrac{S_T}{S_T-(\pi/4)D}$, where ϑ_o is the velocity of the fluid in the empty cross section of the shell or duct Φ is an arrangement factor, S_L is the transverse pitch, S_T is the longitudinal pitch, $P_T = S_T/D$ is the dimensionless transverse pitch, $P_L = S_L/D$ is the dimensionless longitudinal pitch
19	Flow through packed beds	$\dfrac{dP}{dx} = \dfrac{150\mu V}{L^2}+\dfrac{1.75\rho V^2}{L}$; $1<\mathrm{Re}<10^4$ $V = \dfrac{\dot m}{\rho\varepsilon_v A_c}$, $L = d_p\left(\dfrac{\varepsilon_v}{1-\varepsilon_v}\right)$, $d_p = 6\dfrac{V_p}{A_p}$ $\varepsilon_v = \dfrac{\text{Bed Volume - Packing Volume}}{\text{Bed Volume}}$ $\mathrm{Nu} = (0.5\mathrm{Re}^{1/2}+0.2\mathrm{Re}^{2/3})\mathrm{Pr}^{1/3}$; $0.5<\mathrm{Pr}<20$, $20<\mathrm{Re}<10^4$	Viscosity ratio with n = -0.14 V is the characteristic velocity, L is the characteristic length, d_P is the effective particle diameter, V_P is the total particle volume, A_P is the total particle surface area, $a = \dfrac{A_P}{V_P}(1-\varepsilon_v)$ is the specific surface area of a packed bed
20	Flow through perforated plates	$\mathrm{Eu} = 8.17\,\mathrm{Re}^{-0.55}(1.707-\varepsilon_p)^2$; $20<\mathrm{Re}<150$ $\mathrm{Eu} = 0.5(1.707-\varepsilon_p)^2$; $150<\mathrm{Re}<3000$ $\mathrm{St} = C\,\mathrm{Re}^n\,\mathrm{Pr}^{-2/3}$; $0.5<\mathrm{Pr}$, $300<\mathrm{Re}<3000$ $C = 3.6\times10^{-4}\left[(1-\varepsilon_p)\varepsilon_p-0.2\right]^{-2.07}$ $n = -4.36\times10^{-2}\varepsilon_p^{-2.34}$; $0.3<\varepsilon_p<0.6$	$\mathrm{Re} = \dfrac{Gd}{\mu}$; G is the mass velocity through the holes of diameter d $\mathrm{Eu} = \dfrac{\Delta P\rho}{G^2}$; ΔP for a single plate ε_p = plate open-area ratio Equation for Strouhal number is valid for gases and for liquids of moderate Prandtl number

21	Rotating disk in a quiescent fluid	$\mathrm{Nu}_r = \dfrac{0.585\,\mathrm{Re}_r^{1/2}}{0.6/\mathrm{Pr} + 0.95/\mathrm{Pr}^{1/3}}; \quad \mathrm{Re}_r < 2.4\times10^5$ $\mathrm{Nu}_r = 0.021\,\mathrm{Re}_r^{0.8}\,\mathrm{Pr}^{1/3}; \quad 0.5 < \mathrm{Pr}, \quad 2.4\times10^5 < \mathrm{Re}_r$	
22	Rotating sphere in a quiescent fluid	$\overline{\mathrm{Nu}}_D = 0.43\,\mathrm{Re}_D^{0.5}\,\mathrm{Pr}^{0.4};$ $10^2 < \mathrm{Re}_D < 5\times10^5, \quad 0.7 < \mathrm{Pr}$ $\overline{\mathrm{Nu}}_D = 0.066\,\mathrm{Re}_D^{0.67}\,\mathrm{Pr}^{0.4};$ $5\times10^5 < \mathrm{Re}_D < 7\times10^6, \; 0.7 < \mathrm{Pr}$	
23	Horizontal rotating cylinder in a quiescent fluid	$\overline{\mathrm{Nu}}_D = 0.133\,\mathrm{Re}_D^{2/3}\,\mathrm{Pr}^{1/3}; \quad 0.7 < \mathrm{Pr} < 670,$ $4.7\left(\dfrac{\mathrm{Gr}_D^{\,3}}{\mathrm{Pr}}\right)^{0.137} < \mathrm{Re}_D < 4.3\times10^5$	Lower limit on Re_D is due to natural convection effects
24	Turbulent flow in a rough pipe	$f = \left\{-2.0\log\left[\dfrac{(k_s/R)}{7.4} - \dfrac{5.02}{\mathrm{Re}_D}\log\left(\dfrac{(k_s/R)}{7.4} + \dfrac{13}{\mathrm{Re}_D}\right)\right]\right\}^{-2}$ $\mathrm{St} = \dfrac{f/8}{0.9 + (f/8)^{1/2}\left[g(h^+,\mathrm{Pr}) - 7.65\right]}; \quad 60 < k_s^+$	Options for $g(h^+,\mathrm{Pr})$: 1. Sand grain indentation, $g = 4.8(h^+)^{0.2}\,\mathrm{Pr}^{0.44}; \; 1 < \mathrm{Pr} < 6$ 2. Rectangular transverse ribs with $10 < p/h < 40$, $g = 4.3(h^+)^{0.28}\,\mathrm{Pr}^{0.57}; \; 0.7 < \mathrm{Pr} < 40$ 3. General, $g = 0.55(h^+)^{1/2}(\mathrm{Pr}^{2/3} - 1) + 9.5; \; 0.5 < \mathrm{Pr}$
25	Turbulent boundary layer on a fully rough flat plate	$C_{fx} = \left(3.476 + 0.707\ln\dfrac{x}{k_s}\right)^{-2.46}; \quad 150 < \dfrac{x}{k_s} < 1.5\times10^7, \quad 60 < k_s^+$ $\overline{C}_f = \left(2.635 + 0.618\ln\dfrac{L}{k_s}\right)^{-2.57}; \quad 150 < \dfrac{L}{k_s} < 1.5\times10^7, \quad 60 < k_s^+$ $\mathrm{St}_x = \dfrac{\frac{1}{2}C_{fx}}{0.9 + \left(\frac{1}{2}C_{fx}\right)^{1/2}\left[g(h^+,\mathrm{Pr}) - 7.65\right]}; \quad 60 < k_s^+$	

Problems

11.1 Water flows at an average velocity of ϑ_{ave} = 1 m/sec through a smooth, circular conduit whose diameter is D = 25 mm. The water can be modeled as an incompressible fluid with constant average properties ρ = 990.63 kg/m^3, μ = 6.0678 x 10^{-4} kg/m sec, and c = 4180 J/kg K. There is a uniform, constant heat flux at the wall of $\dot{q}''_w$. In a section where the flow is fully developed, the water enters at a bulk mean temperature of $T_{b,in}$ = 20 C. At a distance L = 10 m down the conduit the bulk mean temperature of the fluid is $T_{b,out}$ = 70 C.

(a) What is the value of the heat flux $\dot{q}''_w$?

(b) Show that the temperature profile in both the fluid and the conduit wall are linear with x, the distance measured along the conduit axis from the entry point to the exit point in this region of fully developed flow.

(c) Calculate the rate of entropy transfer to the fluid at the interface between the conduit and the fluid in the section of interest.

(d) Calculate the rate of entropy generation $\dot{S}_{gen}$ for the control volume bounded by the inside of the conduit wall and the planes perpendicular to the conduit axis at x = 0 and $x = L$.

(e) Explain why the entropy generation has the value that it does.

11.2 In the transport of oil via pipeline, whether for cross country transport such as the Alaskan pipeline or for supply of fuel oil to a power plant, the oil is heated to some elevated temperature in order to reduce its viscosity and, hence, the power required to pump it. Although the pipe is insulated, there are heat losses along its length that cause the temperature of the oil to drop to levels that result in unacceptably high pumping power requirements. Thus, it is necessary to install heaters and pumping stations at periodic intervals along the length of the pipeline.

In the design of a section of the Alaskan pipeline, an insulated steel pipe of length L = 100 km and diameter d = 1.2 m is buried a depth z = 3 m below the surface of the ground. The thickness of the insulation around the pipe is 0.15 m so that the outside diameter of the buried pipe with its insulation becomes D = 1.5 m. The oil enters this section of the pipeline at a mean temperature of $T_{b,i}$ = 120 C and a flow rate of $\dot{m}$ = 500 kg/sec. The surface temperature of the soil is T_s = −40 C.

(a) For a case in which the surface temperature of the pipe is constant, the thermal resistance of the soil geometry above the pipeline, R_s, is given by

$$R_s = \frac{\ln\left(\frac{4z}{D}\right)}{2\pi k_s L}$$

where the thermal conductivity of the soil is k_s = 0.5 W/m K. Calculate the bulk mean temperature of the oil leaving this section of the pipeline, $T_{b,o}$, at L = 100 km assuming that the surface temperature of the pipe is constant.

(b) Calculate the total heat loss from this section of the pipeline in order to determine the power requirement for the heater for the next section.

(c) Is the assumption of constant surface temperature of the pipe a reasonable one?

For the oil: ρ_o = 900 kg/m^3, $c_{P,o}$ = 2000 J/kg K, ν_o = 8.5 x 10^{-4} m^2/sec, k_o = 0.140 W/m K
The thermal conductivity of the insulation is k_i = 0.05 W/m K.

11.3 The Ocean Thermal Energy Conversion (OTEC) system is an attempt by thermal-fluids engineers to exploit the variation in temperature that exists in the ocean. Cold water can be found at the lower depths and warm water, in the form of the Gulf Stream, can be found near the surface. Since the volumes of water are huge, large amounts of power can be "produced" by using these "bodies" of water as heat reservoirs even though the temperature difference between them is relatively small. Obviously the efficiency is going to be low, but as they say, "The price is right."

As shown in Figure 11P.3, one design calls for cold water from the lower depths to be pumped up to the surface where it can pass through a heat exchanger and serve as the low temperature heat reservoir. The pipe for this purpose is bare aluminum with D_i = 1 m and D_o 1.15 m. The volumetric flow rate inside the pipe is $\dot{V}$ = 1.3 m^3/sec at 5 C. There is an external crossflow current of $\hat{v}$ = 60 cm/sec with a temperature of 15 C.

(a) Estimate the drag on the pipe (per meter of length) due to the external current.

(b) For a one meter length of pipe, estimate the heat transfer in the radial direction between the internal flow and the external flow.

(c) Estimate the increase in temperature of the internal flow per meter of length of pipe.

For water at 5 C: ρ_5 = 999.92 kg/m^3, c_5 = 4205.5 J/kg K, μ_5 = 1.5183 x 10^{-3} kg/m sec,
k_5 = 0.57052 W/m K

For water at 15 C: ρ_{15} = 999.06 kg/m^3, c_{15} =4188.8 J/kg K, μ_{15} = 1.1376 x 10^{-3} kg/m sec,
k_{15} = 0.58933 W/m K

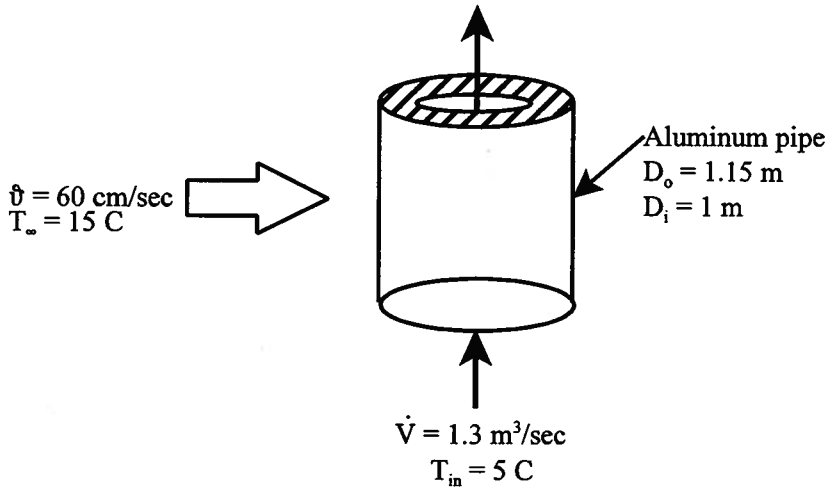

Figure 11P.3

11.4 "Cold plates" are devices that are commonly used to maintain safe operating temperatures of electrically dissipative electronic components that are mounted on them. The design of the cold plate consists of a slab of material of high thermal conductivity with passages cast or machined in it. Coolant of some sort, often in the form of cooling water, flows through these passages to remove the energy dissipated and the entropy generated by the electronic component. By virtue of its high thermal conductivity, the slab can be modeled as isothermal. In operation, the slab achieves a uniform temperature different from the temperature of the coolant passing through it. The operating temperature of the electronic component will depend upon the thermal contact resistance between the electronic components and the cold plate.

The cold plate shown in cross-section in Figure 11P.4, consists of a thick slab of aluminum 15 cm wide by 22 cm long with 8 circular cooling passages 6 mm in diameter cast in it. Water enters each channel with a mass flow rate of 0.24 kg/sec and a temperature of 25 C. The electronic components mounted on the slab dissipate a total power of 1.2 kW.

(a) If the thermal contact resistance between the electronic components and the cold plate is $R_{th} = 5 \times 10^{-3}$ C/W, estimate the operating temperature of the electronic components.

(b) Estimate the rate of entropy generation of the electronic components.

(c) Estimate the pressure drop for the water if the passages are smooth.

For cast aluminum: $k_{Al} = 168$ W/m K

For water: $\rho_w = 1000$ kg/m^3, $c_w = 4178$ J/kg K, $\mu_w = 8.67 \times 10^{-4}$ kg/m sec, $k_w = 0.611$ W/m K

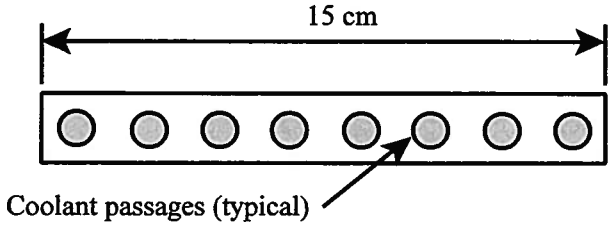

Figure 11P.4

11.5 As part of the air-conditioning system of a large commercial building, a long, $L = 15$ m, thin-walled uninsulated duct, $D = 0.3$ m, is used to route chilled air at a mass flow rate of 0.05 kg/sec through the attic space of the building. The temperature of the attic air is 37 C, and natural convection between this air and the duct results in a heat transfer coefficient of $h_{c,o} = 2$ W/m^2 K on the outer surface of the duct. Chilled air enters the duct at a temperature of $T_{b,in} = 7$ C.

(a) What is the exit temperature of the air, $T_{b,out}$?

(b) If the duct is now insulated by wrapping it with a 1 cm thick layer of fiberglass, $k = 0.038$ W/m K, what is the exit temperature? Assume the value of $h_{c,o}$ is unchanged.

(c) For the configuration of part (a) above, what is the rate of entropy generation for a control volume that is drawn around the duct and the boundary layer on the outside of it?

The thermal properties of air are: $\rho = 1.177$ kg/m^3, $c_P = 1005$ J/kg K, $\mu = 18.43 \times 10^{-6}$ kg/m sec, $k = 0.0267$ W/m K

11.6 A typical microprocessor (CPU) for a personal computer consists of number of transistors mounted on a slab of silicon bonded to a metal or metal oxide substrate. The switching of the capacitive elements at high frequency results in the dissipation of electrical energy causing the microprocessor to increase in temperature. In earlier CPU designs, the amount of energy dissipated was of such a magnitude that it usually could be removed by natural convection heat transfer from the surface of the device. Device design consisted of a thin layer of silicon bonded to an aluminum substrate 2 mm thick.

As shown in cross-section in Figure 11P.6a, the aluminum substrate is a square 5 cm on each side. The semi-conductor layer is located on the back of the substrate which is mounted directly on the circuit board which is fabricated from a plastic composite material of very low thermal conductivity. For this reason, this back surface can be modeled as adiabatic. Because of

the particular shape of the fixture that holds the chip, the edges of the aluminum can also be modeled as adiabatic.

In slightly newer designs, the Intel Pentium© processor employed a more sophisticated chip design that incorporated a greater number of transistors fabricated in a thinner layer of silicon bonded to the aluminum substrate. For a Pentium© MMX processor running at 233 MHz, the rate of power dissipation was measured to be 17 W. This chip was cooled by forced convection.

(a) Consider first the older design cooled by natural convection. If the maximum allowable temperature of the semi-conductor is 65 C and the natural convection heat transfer coefficient for the flat surface of the CPU (without fins) is h_c, describe a heat transfer model (thermal resistance circuit), not including thermal radiation, that will enable you to determine the maximum allowable rate of dissipation of electrical energy in the semi-conductor.
For aluminum: k_{al} = 174 W/m K; ρ_{al} = 2770 kg/m^3; c_{al} = 875 J/kg K.
For air: k_{air} = 0.0281 W/m K, ρ_{air} = 1.106 kg/m^3, $c_{P,air}$ 1005 J/kg K, μ_{air} = 19.29 x 10^{-6} kg/m sec

(b) Using the model described in part (a) above, calculate the maximum allowable rate of energy dissipation for natural convection cooling with an air temperature of 35 C.

(c) By incorporating a small fan on the chip package as shown in Figure 11P.6b, the cooling mechanism was transformed from natural convection to forced convection with a larger convection heat transfer coefficient h_c. Show that for an air velocity of 1 m/sec in the forced convection mode, the cooling of the Pentium© MMX design is still inadequate unless the surface area of the chip is increased by adding fins. What number of fins will provide adequate cooling with a typical pin fin size of 3 mm diameter and 12 mm length?

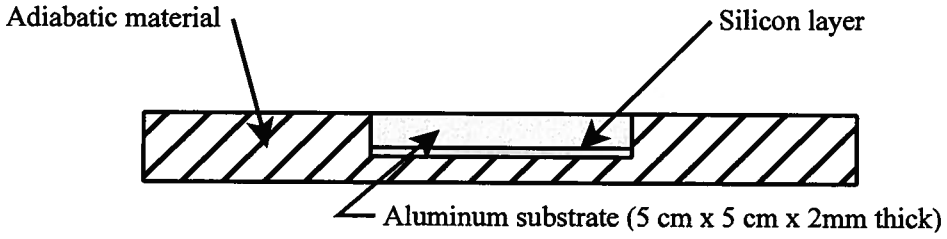

Figure 11P.6a

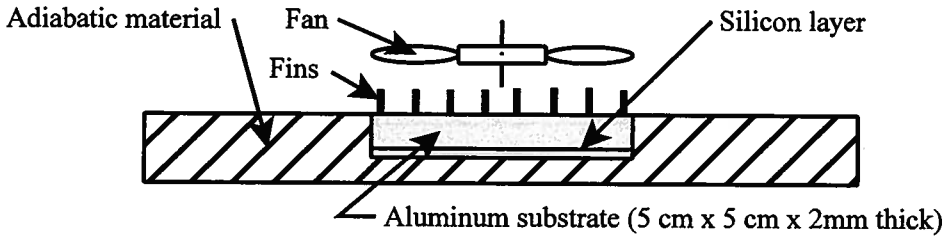

CROSS-SECTION OF PENTIUM PROCESSOR

Figure 11P.6b

11.7 A heat exchanger used to condense water vapor in a desalination plant consists of many tubes through which sea water passes while the vapor condenses on the outer surface of the tubes. In a particular design, a typical tube is fabricated from monel metal (a copper-nickel alloy

that is corrosion resistant with k = 23 W/m K) with an inside diameter of D_i = 19.1 mm and a wall thickness of t = 1.07 mm. The length of the tube is L = 15 m. The sea water flowing on the inside of the tube enters at $T_{b,in}$ = 15 C and exits at $T_{b,out}$ = 25 C. The flow velocity of the sea water is ϑ = 5 m/sec. The temperature of the condensing water vapor is constant at T_{vapor} = 30 C, and the heat transfer coefficient for condensation on the outside of the tubes is h_o = 1500 W/m^2 K.

(a) Calculate the Reynolds number of the sea water flowing in the heat exchanger.

(b) Estimate the heat transfer rate possible with a typical tube.

For sea water:

ρ = 1024 kg/m^3, μ = 1.072 x 10^{-3} kg/m sec, c = 3994 J/kg K, k = 0.600 W/m K

11.8 As shown in Figure 11P.8, a smooth, thin-walled steel pipe of diameter D = 0.1 m and length L = 25.0 m passes through a vat containing a slurry which is held at a constant temperature of 70 C. The heat transfer coefficient between the slurry in the vat and the pipe wall is known to be $h_{c,o}$ = 100 W/m^2 K. Water is pumped through the pipe for an extended period of time.

(a) The outlet temperature of the water flowing in the pipe is measured to be $T_{b,out}$ = 31.0 C. The mass flow rate of the water through the pipe is $\dot{m}_{water}$ = 2 kg/sec, and the length of the pipe is L = 25 m. Under these conditions, what is the inlet temperature $T_{b,in}$ of the water?

(b) What is the pressure drop of the water as it flows through the pipe?

Thermal properties of water: ρ_{water} = 1000 kg/m^3, k_{water} = 0.611 W/m K, c_{water} = 4178 J/m K, μ_{water} = 8.67 x 10^{-4} kg/m sec

Thermal properties of the slurry: ρ_{slurry} = 1100 kg/m^3, μ_{slurry} = 20 x 10^{-4} kg/m sec

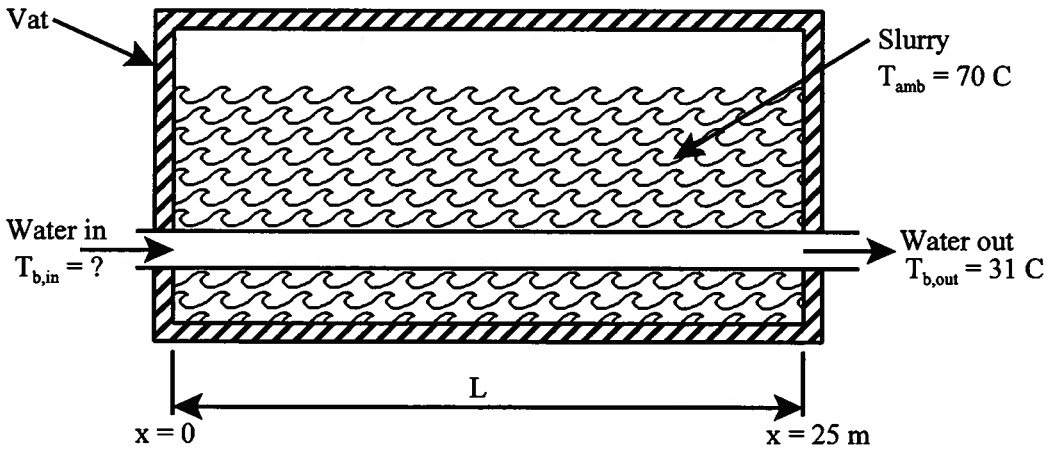

Figure 11P.8

11.9 A section of copper tubing 10 mm in diameter and 10 m long carries water at high pressure in fully developed flow. The water enters the section at a temperature of $T_{b,in}$ = 22 C and the tube wall is maintained at a temperature of T_s = 125 C. Because the water is under high pressure, the water does not boil. Two flow regimes are being considered:

(1) Re = 2 x 10^3 and (2) Re = 2 x 10^4

For each flow regime, compute the following:

(a) The pressure drop in the flow.

(b) The heat transfer coefficient, h_c, of the flow.

(c) The outlet temperature of the water, $T_{b,out}$.

(d) The net rate of entropy convected out of the tube by the water, $\dot{m}(s_{out} - s_{in})$.

(e) The rate of entropy transfer at the interface between the water and the inside of the tube wall.

(f) The rate of entropy generation due to viscous dissipation in the flow, $\left(\dot{S}_{GEN}\right)_{viscous}$

(g) The rate of entropy generation due to the heat transfer process, $\left(\dot{S}_{GEN}\right)_{h.t.}$

For this example:

Compare the results of these calculations for the two flow regimes. What conclusions can you draw regarding laminar vs. turbulent flow? What conclusions can you draw regarding the irreversibility of viscous dissipation vs. the irreversibility of heat transfer?

11.10 Exhaust gases from an oven are discharged through a tall vertical stack. In order to meet certain EPA regulations, it is necessary to know the mean outlet temperature of the exhaust gas from the stack, $T_{b,out}$, and the temperature of the surface of the stack at outlet, $T_{s,o}$. The section of stack of interest is a non-insulated, thin-walled smooth cylinder with a diameter $D = 0.5$ m and a length $L = 6.0$ m. The exhaust gas flow rate is $\dot{m}_{gas} = 0.5$ kg/sec, and the mean temperature of the gas entering the section of interest is $T_{b,in} = 575$ C. The ambient air temperature is $T_\infty = 10$ C and the wind velocity transverse to the axis of the stack is $\mathcal{V} = 5$ m/sec.

Assuming that the flow entering the stack is fully developed and that thermal radiation can be neglected, estimate the temperatures $T_{b,out}$ and $T_{s,o}$.

For the exhaust gas: $\rho_{gas} = 0.435$ kg/m^3, $(c_P)_{gas} = 1099$ J/kg K, $\mu_{gas} = 36.98 \times 10^{-6}$ kg/m sec,
$k_{gas} = 57.3 \times 10^{-3}$ W/m K, $Pr_{gas} = 0.709$

For the air: $\rho_{air} = 1.2306$ kg/m^3, $(c_P)_{air} = 1006.1$ J/kg K, $\mu_{air} = 1.7757 \times 10^{-5}$ kg/m sec,
$k_{air} = 0.02504$ W/m K, $Pr_{air} = 0.7135$

11.11 A hot-wire anemometer is a device used to measure the velocity of a gas stream flowing over it. The device is in the form of a small diameter, electrically conducting wire stretched between rigid, thermally non-conducting supports. The gas flow is normal to the axis of the wire. An electrical current is passed through the wire such that the "steady-state" temperature of the wire is established when the rate of electrical energy dissipation in the wire is exactly balanced by the rate of heat transfer between the wire and the flowing gas stream. If thermal conduction through the supports and thermal radiation from the surface of the wire are assumed negligible, the dominant mode of heat transfer is convection from the surface of the wire. The measured steady temperature of the wire can then be directly related to the velocity of the gas stream. The temperature of the wire is determined by means of a previous calibration of temperature vs. electrical resistance in a non-flow configuration.

In a particular application of an anemometer, the wire is made of tungsten with a diameter of $D = 20$ μm and a length between supports of $L = 2$ mm. The steady temperature of the wire is 40 C when exposed to flowing air with a temperature of 27 C. The current flowing through the wire is 150 mA and the electrical resistivity of the tungsten at 40 C is $\rho_{elect} = 5.51$ micro-ohms cm. Note that the electrical resistance of a wire is given by

$$R_{elect} = \frac{\rho_{elect} L}{A}$$

where A is the cross-sectional area of the wire.

(a) Determine the velocity of the air flowing over the wire.
(b) What is the Biot number for this configuration?
(c) What is the time constant of this device?
(d) Could this device be used to measure local fluctuations of velocity in a turbulent flow of air? If so, what is the highest frequency of fluctuations that could be measured?

For tungsten: $\rho_W = 19{,}300$ kg/m^3, $c_W = 132$ J/kg K, $k_W = 174$ W/m K
For air: $\rho = 1.1614$ kg/m^3, $c_P = 1007$ J/kg K, $\mu = 184.6 \times 10^{-7}$ kg/m sec, $k = 0.0263$ W/m K

11.12 Small spheres of lead, known as "shot", are used in the manufacture of shotgun shells and other items that require small diameter lead spheres. The lead shot are manufactured by cooling molten lead droplets in air. The requisite heat transfer process is provided by allowing the droplets to fall through ambient air in a tower designed specifically for this purpose. The lead is cooled by forced convection over the surface of the sphere and the small spheres are collected at the bottom of the tower.

(a) In a particular design, 3 mm diameter lead spheres with an initial temperature of 601 K are cooled by forced convection during free fall in ambient air with a temperature of 300 K. Assume that the spheres are released with an initial velocity of zero and are allowed to fall freely through the air in the tower with g = 9.81 m/sec^2. Assume that the spheres immediately reach terminal velocity. The drag coefficient of a sphere is given by

$$C_D = \frac{F_D}{\frac{1}{2}\rho v^2 A}$$

where F_D is the drag force on the sphere, ρ is the density of the air flowing over the sphere, v is the velocity of the air relative to the sphere, and A is the cross-sectional area of the sphere projected normal to the direction of flow of the air over the sphere. The value of C_D can be determined from Figure 11P.12 for which the following curve fit has been proposed:

$$C_D = \frac{24}{Re_D} \qquad Re_D \le 1$$

$$C_D = \frac{24}{Re_D^{0.646}} \qquad 1 < Re_D \le 400$$

$$C_D = 0.5 \qquad 400 < Re_D \le 3 \times 10^5$$

$$C_D = \left(3.66 \times 10^{-4}\right) Re_D^{0.4275} \qquad 3 \times 10^5 < Re_D \le 2 \times 10^6$$

$$C_D = 0.18 \qquad Re_D > 2 \times 10^6$$

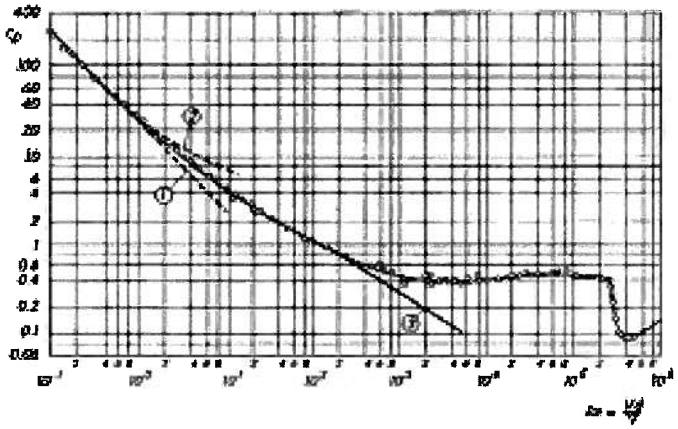

Figure 11P.12

What is the Biot number for this situation? Formulate an appropriate model to describe the temperature at the center of the sphere as the sphere cools. Use this model to determine the height of the tower H necessary to reduce the temperature of the center of the lead sphere to 180 C. Is the assumption of terminal velocity for most of the distance traveled by the sphere a reasonable one?

(b) Calculate the entropy transfer for the lead for this cooling process.

(c) Calculate the entropy change of the air for this process.

(d) Calculate the entropy transfer for the air for this process.

(e) Calculate the entropy generated in this cooling process, and comment on the reversibility of this process and identify the source of the irreversibility if there is one.

For lead: $\rho = 11340$ kg/m^3, $c = 129$ J/kg K, and $k = 34$ W/m K.
For air: $\rho_{air} = 1.311$ kg/m^3, $c_{P,air} = 1009$ J/kg K, and $k_{air} = 0.0249$ W/m K

11.13 Water at high pressure is flowing through the horizontal aluminum square duct shown in cross-section in Figure 11P.13. An electric current flows in the walls of the duct in the direction of flow which is normal to the plane of the figure. The inside surfaces of the duct are smooth, and the outside surfaces are insulated so that all the energy dissipated in the walls flows into the water. At any plane perpendicular to the direction of flow of the water, the temperature of the inside surface of the duct is uniform in the circumferential direction. However, since the heat flux at the wall due to the Joule heating is $\dot{q}'' = 300$ W/m^2, the surface temperature of the duct wall varies in the axial direction. Consider the last 10 m of the duct in which the flow is fully developed hydrodynamically and thermally. The bulk mean temperature of the water entering this region is $T_{b,in} = 450$ K. Two flow rates are being considered for the cooling water:

For the case in which the water flow rate is $\dot{m}_{water} = 0.027$ kg/sec:

(a) Estimate the pressure drop over the length $L = 10$ m.

(b) Estimate the inside wall temperature at the end of the duct.

For the case in which the water flow rate is $\dot{m}_{water} = 2.7$ kg/sec:

(c) Estimate the pressure drop over the length $L = 10$ m for this new flow rate.

(d) Using the Reynolds analogy, estimate the inside wall temperature at the end of the duct for this new flow rate.

(e) If the Gnielinski correlation for $Nu_D = \phi(f, Re_D, Pr)$ can be considered to predict the heat transfer coefficient h_c with an accuracy of 100 percent, what is the error from using the Reynolds analogy in part (d) above?

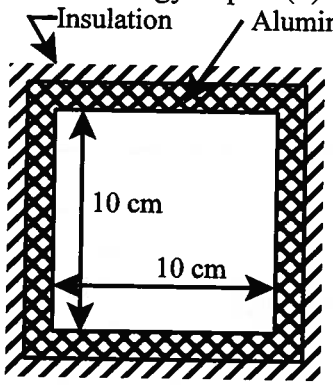

Figure 11P.13

For water at $T = 450$ K: $\rho = 890.47$ kg/m^3, $c = 4400$ J/kg K, $\mu = 152 \times 10^{-6}$ kg/m sec,
$k = 0.678$ W/m K, $Pr = 0.99$

11.14 As shown in Figure 11P.14, a kiln for the "firing" of ceramic materials such as toilet bowls and bathtubs is fired by natural gas which produces high-temperature products of combustion used to increase the temperature of the ceramics to the appropriate firing temperature. After the products of combustion pass over the ceramics, they are discharged to the atmosphere via a tall, thin-walled cicrcular stack whose diameter is $D = 0.5$ m. In order to predict the dispersion of the exhaust gases once they are discharged to the atmosphere, it is essential to know the temperature of the exhaust gases as they leave the stack. In addition, the exhaust gases contain water vapor from the oxidation of the hydrogen in the natural gas. If the stack surface temperature reaches the temperature of 150 C, the water vapor will condense on the walls and lead to corrosion ("rusting out") of the stack. Also, any sulfur dioxide formed during the combustion process will react with the condensed water vapor to form sulfuric acid which is a dangerous pollutant. The exhaust gases enter the stack at a temperature of $T_{b,in} = 600$ C and a mass flow rate of $\dot{m}_{gas} = 0.5$ kg/sec.

(a) As the thermal-fluids engineer on the job, you are asked to determine the maximum stack height that will avoid the condensation problem for weather conditions that include a wind flowing normal to the stack with a velocity of $\vartheta_{wind} = 10$ m/sec and a temperature of $T_{atm} = -10$ C.

(b) What is the discharge temperature, $T_{b,out}$, of the exhaust gases leaving the stack for the conditions specified in part (a) above?

(c) For the stack height determined in part (a) above, is the buoyancy force sufficient to "drive" the flow of exhaust gases or will some sort of blower be required?

For the gases entering the stack: $\rho_{gas} = 0.427$ kg/m^3, $(c_P)_{gas} = 1123$ J/kg K,
$\mu_{gas} = 34.2 \times 10^{-6}$ kg/m sec, $k_{gas} = 0.055$ W/m K
For the atmosphere: $\rho_{atm} = 1.360$ kg/m^3, $(c_P)_{atm} = 1009$ J/kg K, $\mu_{atm} = 16.63 \times 10^{-6}$ kg/m sec,
$k_{atm} = 0.0242$ W/m K

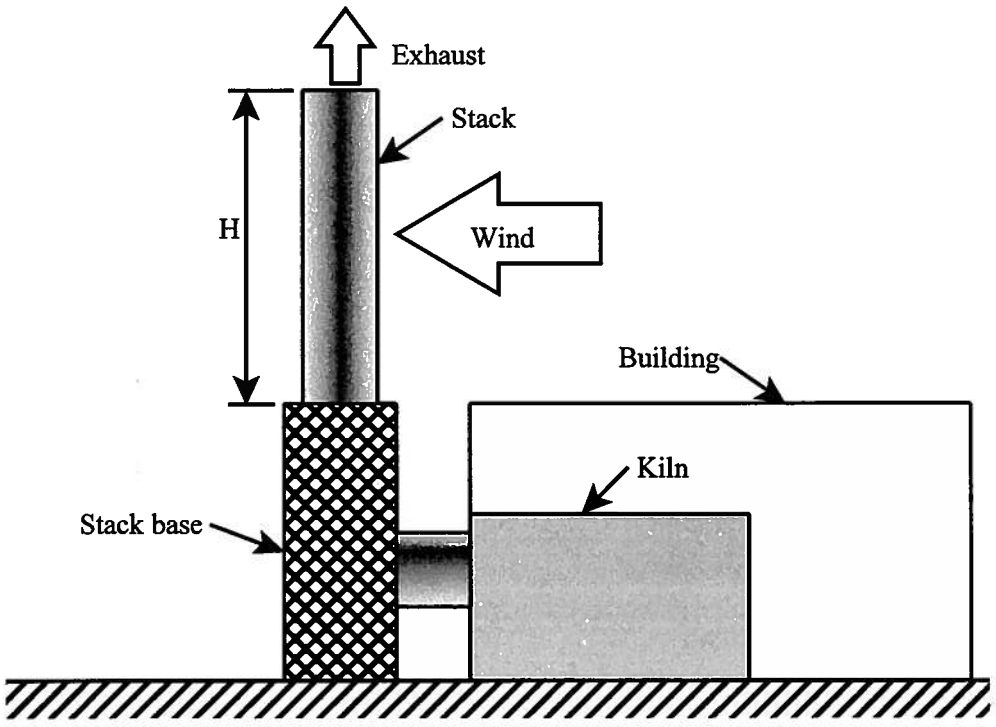

Figure 11P.14

11.15 A plate-type heat exchanger consists of an array of thin flat aluminum (k_{Al} = 175 W/m K) plates parallel to one another and separated by a distance of 5 mm. The length of each plate is L = 750 mm and the width is W = 150 mm. The fluid flows in a counterflow configuration with alternate streams of hot and cold water as shown in cross-section in Figure 11P.15. Consider a single plate and half of the flow on each side as constituting a heat exchanger configuration.

(a) Estimate the overall heat transfer coefficient of this configuration.

(b) Estimate the rate of heat transfer through a single plate.

(c) Determine the fluid outlet temperatures for each stream.

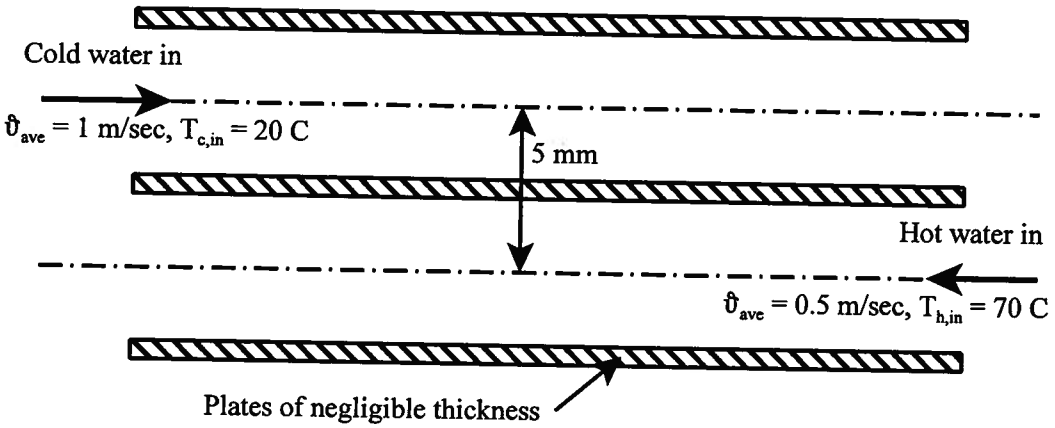

For water at 20 C: $\rho_{20} = 998.21$ kg/m^3, $(c_P)_{20} = 4184.1$ J/kg K, $k_{20} = 0.59846$ W/m K,
$\mu_{20} = 1.0016 \times 10^{-3}$, $Pr_{20} = 7.0026$

For water at 70 C: $\rho_{70} = 977.76$ kg/m^3, $(c_P)_{70} = 4190.1$ J/kg K, $k_{70} = 0.66313$ W/m K,
$\mu_{70} = 4.0389 \times 10^{-4}$, $Pr_{70} = 2.5521$

11.16 As we have seen in Chapter 9, detailed solution of the time-dependent three-dimensional flow that develops in a pipe at high Reynolds number – turbulent flow – is extremely difficult; however, following the example of Prandtl, we can use dimensional analysis to gain insight into the parameters that are important. Prandtl (in 1930) postulated that the velocity ϑ_x very near the wall must depend only on the distance y away from the wall and on the fluid properties that are important near the wall such as the shear stress τ_w, the viscosity μ, and the density ρ. That is,

$$\vartheta_x = f(\tau_w, \mu, \rho, y) \tag{1}$$

(a) How many dimensionless groups should we expect from this postulate? Choose the wall shear stress and the fluid density as two of the repeated variables (plus as many others as might be needed) and give the dimensionless form of the above equation.

(b) Why would it be incorrect to also include the velocity gradient $\frac{\partial u}{\partial y}$ the equation (1)?

(c) By noting that the Π group containing velocity is dimensionless and can thus be written as a ratio of velocities $\frac{\vartheta_x}{\vartheta^*}$ give a definition of ϑ^*. This parameter is known as the friction velocity. Re-express the other Π groups and the dimensionless equation in terms of this characteristic velocity. The result is known as the *Law of the Wall* and forms the basis for all existing theories of turbulent pipe flows.

(d) Very close to the wall, this law should take a special limiting form since we know that the no-slip boundary condition must still be satisfied right at the wall, i.e., $\vartheta_x = 0$ at $y = 0$. Thus

we can use a Taylor series expansion for very small distances ($y << 1$) away from the wall itself. Starting from the expansion,

$$\vartheta_x(y) \cong \vartheta_x(0) + \left(\frac{\partial \vartheta_x}{\partial y}\right)_{y=0} dy + \ldots$$

eliminate $\frac{\partial \vartheta_x}{\partial y}$ in favor of other parameters in equation (1) and then rearrange the result to give an equation for the "law of the wall" in dimensionless form using the variables identified in (c) above.

11.17 Consider a 1 cm thick plate glass window in a large office building that is 2m high and 10 m long. On a night when the outside air temperature is $T_{out} = -10$ C, the inside air temperature is $T_{in} = 20$ C. Assume that the air outside and inside the cafeteria is still. Compute the heat transfer through this window due to natural convection on the inside and outside surfaces.

For air at -10 C: $\rho_{-10} = 1.3245$ kg/m^3, $(c_P)_{-10} = 1005.8$ J/kg K, $k_{-10} = 0.02361$ W/m K,
$\mu_{-10} = 1.6753 \times 10^{-5}$, $Pr_{20} = 0.7137$
For air at 20 C: $\rho_{20} = 1.1885$ kg/m^3, $(c_P)_{20} = 1006.4$ J/kg K, $k_{20} = 0.02574$ W/m K,
$\mu_{20} = 1.8249 \times 10^{-5}$, $Pr_{20} = 0.7134$

11.18 In one design of indoor ice rinks, an array of pipes carrying refrigerant is placed a small distance above a plane surface, often concrete or packed sand as shown in Figure 11P.18. The area is flooded with water and the refrigerant is circulated at low temperature, thereby freezing the water. In Figure 11P.18, the water layer thickness, H, is 60 mm with the refrigerant tubes centrally placed, the refrigerant tube diameter, D, is 12 mm, the centerline separation of the tubes, S, is 50 mm, and the length of each tube, L, is 5 m. All the tubes are fed from a common manifold such that the bulk mean temperature of the fluid entering each tube is $T_{b,in} = -33$ C and the mass flow rate for each tube is $\dot{m} = 0.02$ kg/sec. The refrigerant is liquid throughout the flow with the following properties: $c_P = 900$ J/kg K, $k = 0.07$ W/m K, $\mu = 3.5 \times 10^{-4}$ kg/m sec.
For the water: $\rho = 10^3$ kg/m^3 and the latent heat of fusion is $h_{sf} = 3.34 \times 10^5$ J/kg

(a) For the case in which the water is well-stirred (no spatial temperature gradients), we are interested in the phase change from saturated liquid water to saturated solid ice. Assume that the tube wall temperature is uniform at the saturation temperature of the ice (not a bad assumption since $k_{ice} > 3k_{water}$). Estimate the bulk mean temperature of the refrigerant as it leaves the tube, $T_{b,out}$.

(b) What is the rate of heat transfer for a single tube?

(c) Estimate the length of time required to freeze the entire water layer.

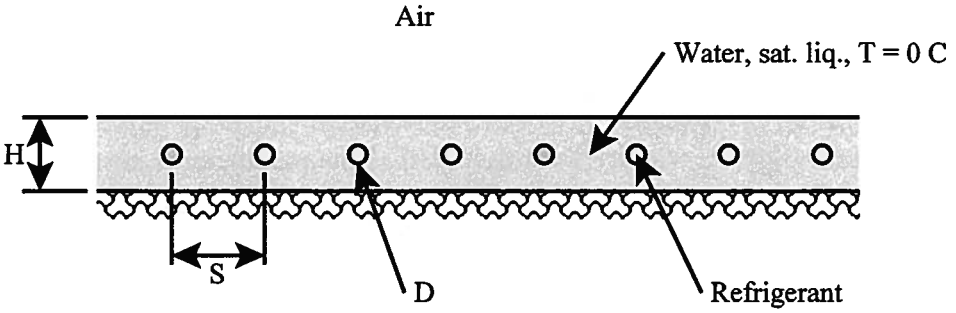

Figure 11P.18

CHAPTER 12

Heat Exchangers

12.1 Introduction

For proper operation, many thermal-fluid systems require heat transfer between a solid boundary and a flowing fluid or between two fluid streams separated by a solid wall. The required heat transfer and concomitant entropy transfer is usually accomplished in a dedicated system component known as a *heat exchanger*. The primary objective of the heat exchanger may be to change the thermodynamic state of the fluid stream(s) or, alternatively, to remove or add energy (and entropy) to the solid boundary.

Examples of heat exchangers used to accomplish the first objective include the *boiler* and *superheater* which are used in a steam power plant to increase the temperature, enthalpy, and entropy of the steam before it flows into the positive shaft work machines (turbines or expansion engines) of the cycle. Similarly, the *condensers* of the steam power plant are heat exchangers used to reduce the energy, enthalpy, and entropy of the steam before it flows into the negative shaft work machines (pumps) of the plant. Heat exchangers of this type are also found in refrigeration plants where they are used to increase the energy, enthalpy, and entropy of the refrigerant while it is in thermal communication with the substance being refrigerated. These heat exchangers are known as *evaporators* while the heat exchangers used to communicate with the "heat sink" of the refrigeration plant are known as *condensers* because they decrease the energy, enthalpy, and entropy of the refrigerant, often at constant temperature.

Examples of heat exchangers used to accomplish the second objective are those which attempt to maintain a desired operating temperature of a surface as in the cooling jacket of an internal combustion engine or the cooling fins of a passive thermal control device for an electronic component. In large rotating electrical machines like electrical generators, the electrical windings are carefully designed to be heat exchangers for heat transfer to the ambient air which is circulated by fans on the rotor. In fact, the power rating of the machine is determined by the effectiveness of the heat transfer from the windings and the maximum operating temperature for the insulation.

A nuclear power reactor is an example of a device in which both objectives are equally important. The temperature of the nuclear fuel elements must be kept at a safe level while the thermodynamic state of the coolant, which also serves as the working fluid for the power cycle, must be changed significantly by the heat transfer interaction. Clearly the range of applications of heat exchangers is very wide.

In those heat exchangers in which the change of state of the fluid is of prime importance, it is usually desirable to effect the heat transfer while generating as little entropy as possible. This requires that the fluid must achieve thermal equilibrium with the heating or cooling element. In general, since the rate of heat transfer decreases with a decrease in temperature difference between the two media, the time required to achieve thermal equilibrium becomes inconveniently large. Therefore, thermal equilibrium can only be approached as a limit of the operating conditions. The closeness of the approach to thermal equilibrium, and conversely, the rate of entropy generation is a suitable compromise between the fluid velocity, the temperature difference for heat transfer, and the surface area for heat transfer. This compromise varies with the application depending upon the relative importance of weight, size, irreversibility, cost, and

other factors; however, regardless of the level of compromise, the fluid velocity is usually so low that the pressure drop necessary to move the fluid through the heat exchanger is negligible to first order. Thus, the heat exchanger operates at essentially constant pressure. Furthermore, these low values of fluid velocity usually mean that the kinetic energies of the fluid streams are negligible. Also, the gravitational potential energy of the fluid is negligible compared to the heat transfer across the fluid boundaries. Then for the control volume of a typical fluid stream in a heat exchanger as shown in Figure 12.1, the first law becomes

$$\dot{Q} = \dot{m}\left(h_{out} - h_{in}\right) \tag{12.1}$$

Equation (12.1) is consistent with the notion that the fluid velocity should be as low as possible if the enthalpy change of the fluid is to be as large as possible for a given heat transfer rate. The smaller the mass flow rate, the larger the change in enthalpy for a given heat transfer rate. These low mass flow rates insure that the pressure drop due to fluid friction is negligible.

On the other hand, when the temperature of the apparatus is of prime importance, the situation is somewhat different since the main objective is to establish heat transfer at the maximum rate through a given surface area. Under these circumstances, a large mass flow rate is used with a resulting small change in the enthalpy of the fluid. In such cases, the pressure drop due to fluid friction is usually significantly larger than in the previous case.

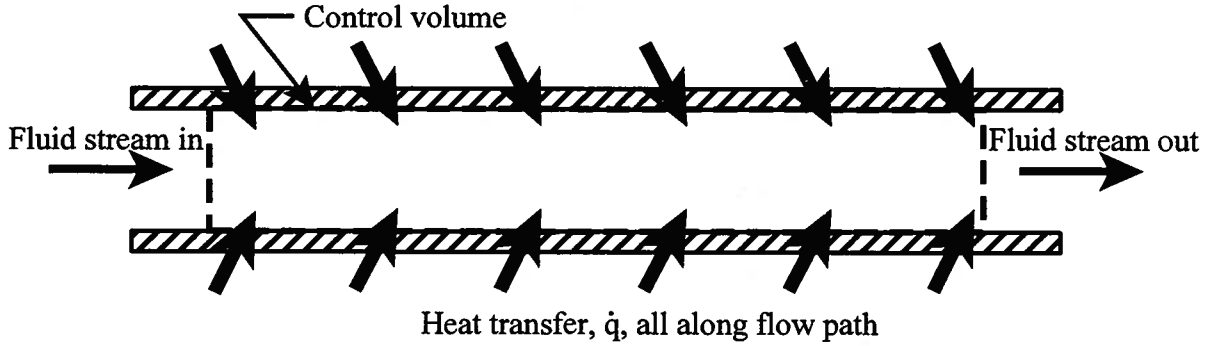

Figure 12.1 Heat Transfer to Fluid Stream in Heat Exchanger

The relationship between the fluid temperature and the enthalpy appearing in equation (12.1) will depend upon the fluid model used. For the ideal gas model, the enthalpy constitutive relation is $dh = c_P dT$ and equation (12.1) becomes

$$\dot{Q} = \dot{m}c_P\left(T_{out} - T_{in}\right) \tag{12.2}$$

For the incompressible fluid model, the enthalpy constitutive relation is $dh = cdT + vdP$ and equation (12.1) becomes

$$\dot{Q} = \dot{m}c\left(T_{out} - T_{in}\right) + \dot{m}v\left(P_{out} - P_{in}\right) \tag{12.3}$$

but given the fact that we can model the flow as constant pressure, the second term on the right-hand side of equation (12.3) becomes negligible in this limit. Even in those cases for which the pressure drop is non-zero, the magnitude of the second term on the right-hand side of equation (12.3) is negligible compared with the first term for a heat transfer of any appreciable magnitude. It is common practice in thermal-fluids engineering to write the first law for a heat exchanger for both the ideal gas model and the incompressible fluid model as equation (12.2) with the subscript in the case of the incompressible fluid model serving as a reminder that the flow is modeled as constant pressure. The product $\dot{m}c_P$ is known as the *heat capacity rate* or simply the *capacity rate* of the fluid stream.

12.2 Heat Exchangers with Two Fluid Streams

The most common configuration for heat exchangers used in thermal-fluid systems is one in which the heat transfer occurs between two fluid streams *a* and *b* as shown in Figure 12.2. For this case, the first law for the control volume becomes

$$\dot{m}_a(h_a)_{in} + \dot{m}_b(h_b)_{in} = \dot{m}_a(h_a)_{out} + \dot{m}_b(h_b)_{out}$$

$$\dot{m}_a\left[(h_a)_{in} - (h_a)_{out}\right] = \dot{m}_b\left[(h_b)_{out} - (h_b)_{in}\right] \qquad (12.4)$$

$$\dot{Q}_a = \dot{m}_a c_{Pa}\left[(T_a)_{in} - (T_a)_{out}\right] = \dot{m}_b c_{Pb}\left[(T_b)_{out} - (T_b)_{in}\right] = -\dot{Q}_b$$

where we have made use of equation (12.2) for the individual streams. Note the fact that the heat exchanger is adiabatic with respect to the environment so that from the point of view of the individual streams

$$\dot{Q}_a = -\dot{Q}_b \qquad (12.5)$$

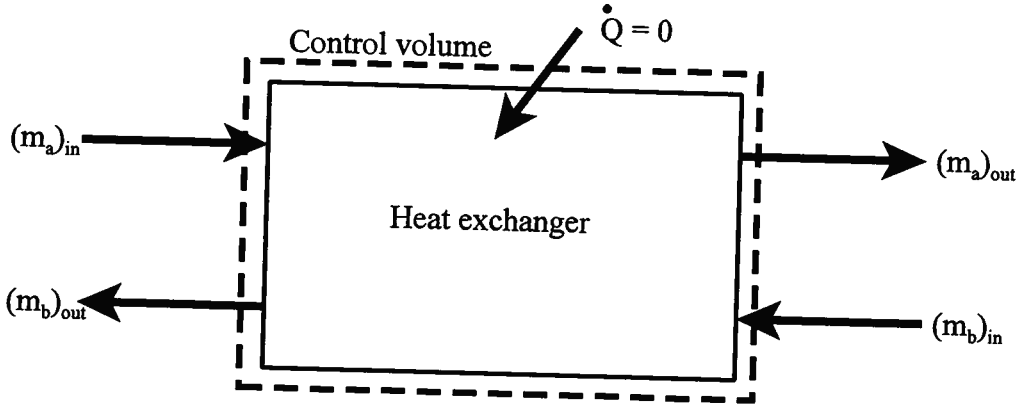

Figure 12.2 Externally Adiabatic Heat Exchanger with Two Fluid Streams

In a heat exchanger with two fluid streams, the extent of the approach to thermal equilibrium between the two streams depends upon the resistance to heat transfer between the two streams. The simplest model for the kinetics of the heat transfer process is that the heat transfer rate is proportional to the temperature difference between the two streams and the surface area available for heat transfer between them. For stream *b*, for example, the heat transfer rate is given by

$$\dot{Q}_b = UA(T_a - T_b) \qquad (12.6)$$

where A is the surface area available for heat transfer between the two streams and $(T_a - T_b)$ is some appropriate temperature difference between the two streams *a* and *b* that serves as the driving force for the heat transfer interaction. The constant of proportionality U appearing in equation (12.6) is known as the *overall heat transfer coefficient* and is a complicated function of the internal geometry of the heat exchanger, the individual fluid velocities, the thermophysical properties of the fluids, and the material of construction of the heat exchanger. The temperature difference $(T_a - T_b)$ is also a function of the flow geometry. We now proceed to develop each of these terms in detail.

12.2.1 The Log Mean Temperature Difference

Figure 12.3 shows a simple heat exchanger with two fluid streams flowing in the same direction. This configuration is known as a parallel flow heat exchanger. The axial temperature

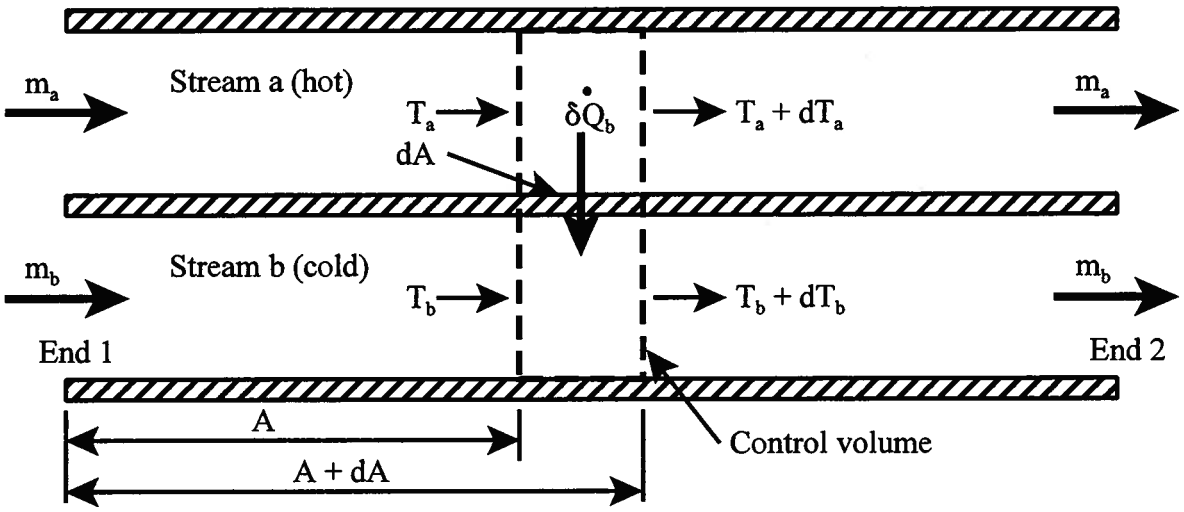

Figure 12.3 Parallel Flow Configuration for a Two-stream Heat Exchanger

distribution for this configuration is determined by considering the differential control volume of Figure 12.3. The first law gives

$$\delta\dot{Q}_a = \dot{m}_a c_{Pa} dT_a \tag{12.7}$$

and

$$\delta\dot{Q}_b = \dot{m}_b c_{Pb} dT_b \tag{12.8}$$

with

$$\delta\dot{Q}_a = -\delta\dot{Q}_b \tag{12.9}$$

Since stream a is the hot stream, $\delta\dot{Q}_b$ is positive, dT_a is negative, and dT_b is positive. The local rate of heat transfer between the two streams can also be obtained by applying Newton's Law of Cooling, viz.

$$\delta\dot{Q}_b = U\left(T_a - T_b\right) dA \tag{12.10}$$

We now define the temperature difference between streams to be ΔT where

$$\Delta T = T_a - T_b \tag{12.11}$$

where T_a and T_b are measured at the same axial position in the heat exchanger. Then

$$d\left(\Delta T\right) = dT_a - dT_b \tag{12.12}$$

Combining equations (12.7) through (12.9) with equation (12.12), we get

$$d\left(\Delta T\right) = \frac{\delta\dot{Q}_a}{\dot{m}_a c_{Pa}} - \frac{\delta\dot{Q}_b}{\dot{m}_b c_{Pb}} = -\delta\dot{Q}_b\left(\frac{1}{\dot{m}_a c_{Pa}} + \frac{1}{\dot{m}_b c_{Pb}}\right) \tag{12.13}$$

Substituting equation (12.10) into equation (12.13), we get

$$\frac{d\left(\Delta T\right)}{\Delta T} = -\left(\frac{1}{\dot{m}_a c_{Pa}} + \frac{1}{\dot{m}_b c_{Pb}}\right) U dA \tag{12.14}$$

Equation (12.14) can be integrated from one end of the heat exchanger to the other to give

$$\int_{\Delta T_1}^{\Delta T_2} \frac{d(\Delta T)}{\Delta T} = -\left(\frac{1}{\dot{m}_a c_{Pa}} + \frac{1}{\dot{m}_b c_{Pb}}\right) U \int_0^{A_T} dA$$

$$\ln\left(\frac{\Delta T_2}{\Delta T_1}\right) = -\left(\frac{1}{\dot{m}_a c_{Pa}} + \frac{1}{\dot{m}_b c_{Pb}}\right) UA_T \qquad (12.15)$$

Substituting equation (12.4) into equation (12.15), we get

$$\ln\frac{\Delta T_2}{\Delta T_1} = \left[(T_{b2} - T_{b1}) - (T_{a2} - T_{a1})\right]\frac{UA_T}{\dot{Q}_b} = \left[(T_{b2} - T_{a2}) - (T_{b1} - T_{a1})\right]\frac{UA_T}{\dot{Q}_b} = \left[\Delta T_2 - \Delta T_1\right]\frac{UA_T}{\dot{Q}_b} \qquad (12.16)$$

Equation (12.16) can be rearranged to give

$$\dot{Q}_b = \left[\frac{\Delta T_2 - \Delta T_1}{\ln\frac{\Delta T_2}{\Delta T_1}}\right] UA_T = UA_T \Delta T_{LM} \qquad (12.17)$$

where we have made use of the concept of the *log mean temperature difference*, ΔT_{LM}.

2=out
1=in

$$\Delta T_{LM} = \frac{\Delta T_2 - \Delta T_1}{\ln\frac{\Delta T_2}{\Delta T_1}} \quad \text{hot - cold} \qquad (12.18)$$

Thus we have now established the proper temperature difference to use in Newton's Law of Cooling applied to one stream of the heat exchanger.

12.2.2 The Axial Temperature Profile in a Two-fluid Stream Heat Exchanger

If we combine equations (12.11), (12.15), and (12.4), we can obtain (after considerable algebraic manipulation) the temperature distribution in each of the fluid streams. For the parallel flow configuration we have

$$T_b - T_{b1} = \frac{(T_{a1} - T_{b1})}{\left(1 + \frac{\dot{m}_b c_{Pb}}{\dot{m}_a c_{Pa}}\right)}\left[1 - \exp\left\{-\left(\frac{1}{\dot{m}_a c_{Pa}} + \frac{1}{\dot{m}_b c_{Pb}}\right)UA\right\}\right]$$

$$T_{a1} - T_a = \frac{\dot{m}_b c_{Pb}}{\dot{m}_a c_{Pa}}\frac{(T_{a1} - T_{b1})}{\left(1 + \frac{\dot{m}_b c_{Pb}}{\dot{m}_a c_{Pa}}\right)}\left[1 - \exp\left\{-\left(\frac{1}{\dot{m}_a c_{Pa}} + \frac{1}{\dot{m}_b c_{Pb}}\right)UA\right\}\right] \qquad (12.19)$$

where the area A is allowed to increase in the direction of flow. Figure 12.4 shows these temperature distributions for a representative case of parallel flow in which the axial coordinate along the direction of flow is A/A_T. The specific values of the relevant parameters used in plotting Figure 12.4 are:

$$\frac{\dot{m}_b c_{Pb}}{\dot{m}_a c_{Pa}} = 2 \quad \text{and} \quad \frac{UA_T}{\dot{m}_a c_{Pa}} = 2$$

From Figure 12.4 we note that the temperature change from inlet to outlet is largest for the stream with the smaller capacity rate, $\dot{m}c_P$.

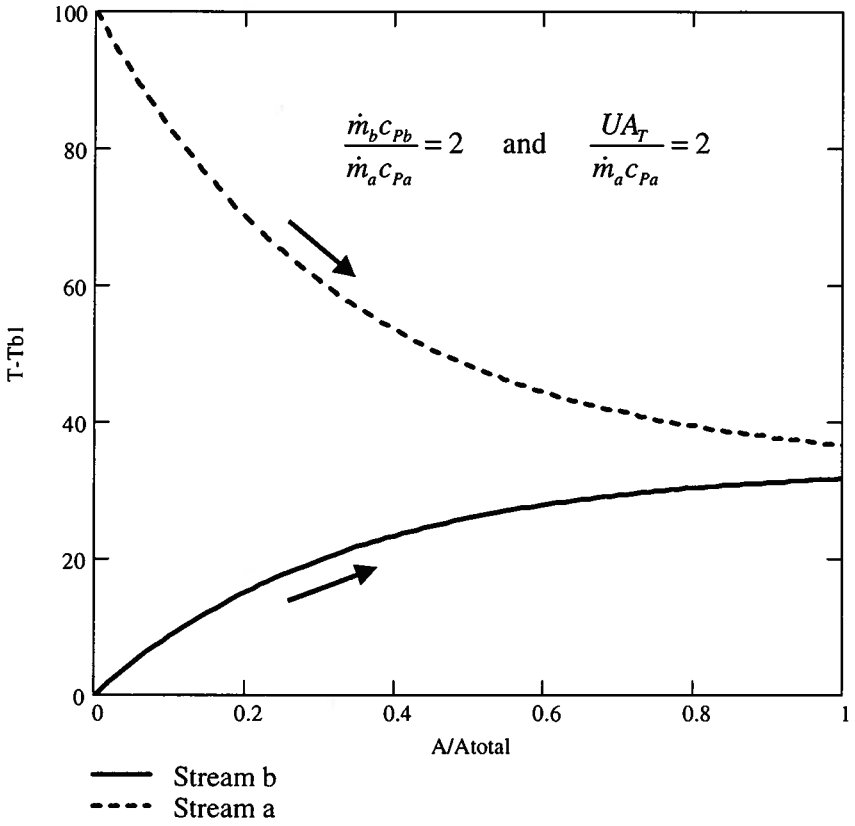

Figure 12.4 Temperature Distributions for a Two-stream, Parallel Flow Heat Exchanger

Figure 12.5 shows the counterflow configuration for a heat exchanger with two fluid streams in which one stream is flowing in the opposite direction from the other. The axial temperature distribution can be determined in the same manner as for the parallel flow heat

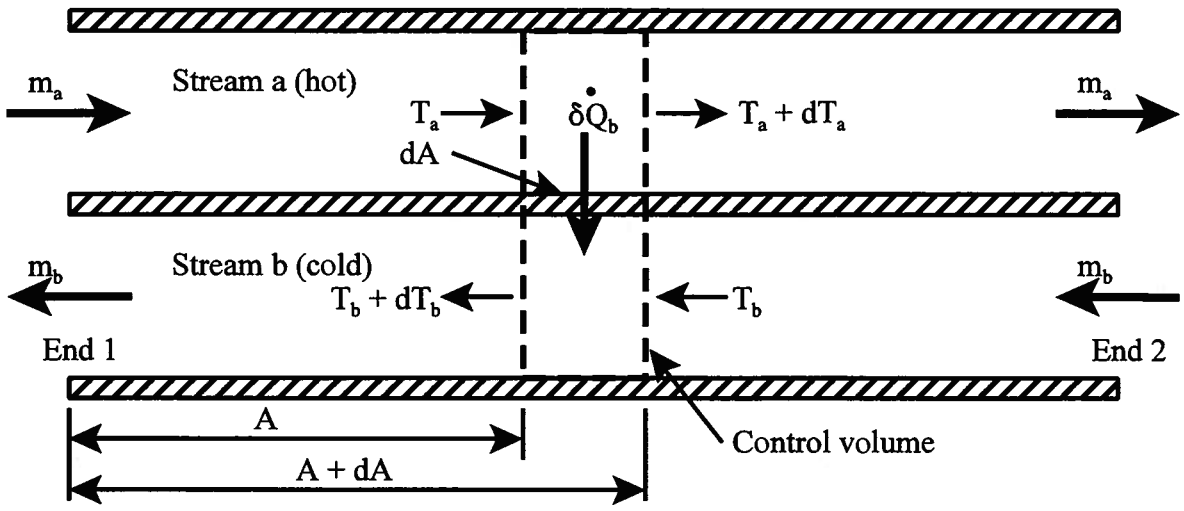

Figure 12.5 Counterflow Configuration for a Two-stream Heat Exchanger

exchanger except that now a negative sign appears in front of each $\dot{m}_b$ since it is now going in the opposite direction. The principal equations that change are (12.8) and (12.15) which becomes

$$\ln\left(\frac{\Delta T_2}{\Delta T_1}\right) = -\left(\frac{1}{\dot{m}_a c_{Pa}} - \frac{1}{\dot{m}_b c_{Pb}}\right) UA_T \tag{12.20}$$

Note that equations (12.17) and (12.18) remain unchanged. Equation (12.20) shows that a two-stream counterflow heat exchanger with identical capacity rates in the two streams has the same ΔT at each end of the heat exchanger. In fact, for this arrangement the ΔT is constant along the length of the heat exchanger as long as the two capacity rates are identical.

For the counterflow configuration, the temperature distributions are given by

$$T_{b1} - T_b = \frac{(T_{a1} - T_{b1})}{\left(\frac{\dot{m}_b c_{Pb}}{\dot{m}_a c_{Pa}} - 1\right)}\left[1 - \exp\left\{-\left(\frac{1}{\dot{m}_a c_{Pa}} - \frac{1}{\dot{m}_b c_{Pb}}\right) UA\right\}\right]$$

$$T_{a1} - T_a = \frac{\dot{m}_b c_{Pb}}{\dot{m}_a c_{Pa}} \frac{(T_{a1} - T_{b1})}{\left(\frac{\dot{m}_b c_{Pb}}{\dot{m}_a c_{Pa}} - 1\right)}\left[1 - \exp\left\{-\left(\frac{1}{\dot{m}_a c_{Pa}} - \frac{1}{\dot{m}_b c_{Pb}}\right) UA\right\}\right] \tag{12.21}$$

Figure 12.6 shows these temperature distributions for a representative case of counterflow in which the axial coordinate along the direction of flow is A/A_T. The specific values of the relevant parameters used in plotting Figure 12.6 are identical to those of Figure 12.4.

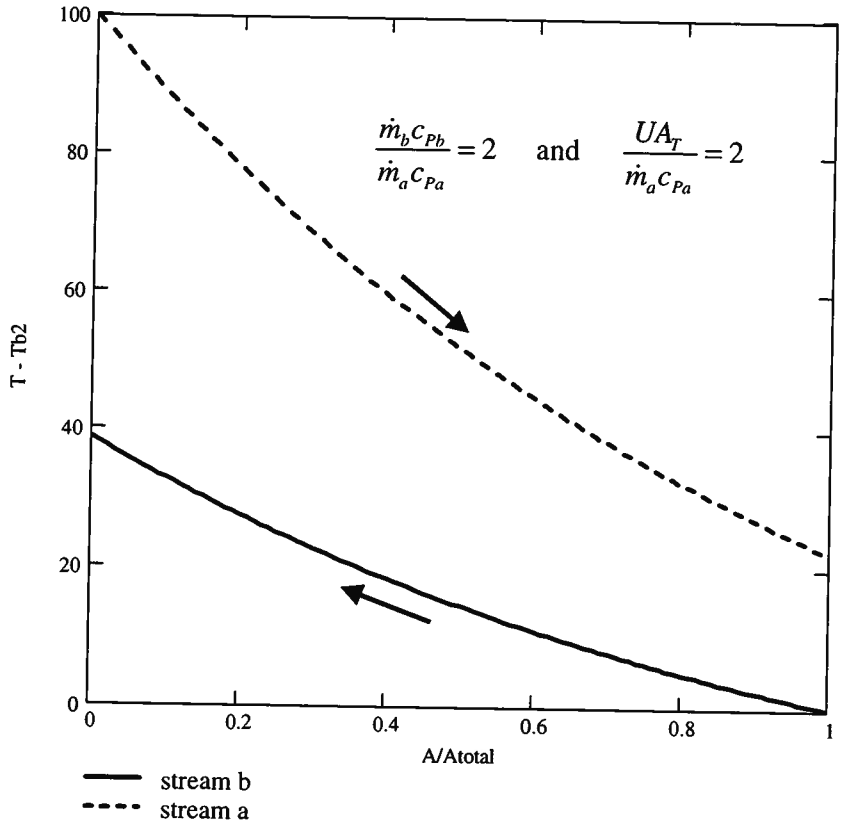

Figure 12.6 Temperature Distributions for a Two-stream, Counterflow Heat Exchanger

From Figure 12.6 it is apparent that the temperature difference between the two streams decreases in the direction of flow of the stream with the smaller capacity rate, $\dot{m}c_P$. We also note, as before, that the temperature change from inlet to outlet is largest for the stream with the smaller capacity rate, $\dot{m}c_P$. Indeed, these two observations are true for heat exchangers in general.

12.3 Second Law Considerations of Heat Exchanger Performance

For the control volume shown in Figure 12.2, the second law of thermodynamics takes the form

$$\frac{d}{dt}(S_{CV}) = \sum_j \left(\frac{\dot{Q}}{T}\right)_j + \sum_{in}(\dot{m}s)_{in} - \sum_{out}(\dot{m}s)_{out} + \dot{S}_{gen} \tag{12.22}$$

Since the heat exchanger operates in the steady flow condition and since the control surface shown is modeled as adiabatic, equation (12.22) reduces to

$$\begin{aligned} \dot{S}_{gen} &= \sum_{out}(\dot{m}s)_{out} - \sum_{in}(\dot{m}s)_{in} \\ \dot{S}_{gen} &= \dot{m}_a\left[(s_a)_{out} - (s_a)_{in}\right] + \dot{m}_b\left[(s_b)_{out} - (s_b)_{in}\right] \end{aligned} \tag{12.23}$$

If the fluid can be modeled as incompressible, we can substitute the entropy constitutive relation given in section 4.3.2 so that equation (12.23) becomes

$$\dot{S}_{gen} = \dot{m}_a c_a \ln\frac{(T_a)_{out}}{(T_a)_{in}} + \dot{m}_b c_b \ln\frac{(T_b)_{out}}{(T_b)_{in}} \tag{12.24}$$

If the fluid can be modeled as an ideal gas, we can substitute the entropy constitutive relation given in section 4.3.3 so that equation (12.23) becomes

$$\dot{S}_{gen} = \dot{m}_a c_{Pa} \ln\frac{(T_a)_{out}}{(T_a)_{in}} - \dot{m}_a R \ln\frac{(P_a)_{out}}{(P_a)_{in}} + \dot{m}_b c_{Pb} \ln\frac{(T_b)_{out}}{(T_b)_{in}} - \dot{m}_b R \ln\frac{(P_b)_{out}}{(P_b)_{in}} \tag{12.25}$$

but since heat exchangers are modeled as constant pressure devices to first order, equation (12.25) reduces to

$$\boxed{\dot{S}_{gen} = \dot{m}_a c_{Pa} \ln\frac{(T_a)_{out}}{(T_a)_{in}} + \dot{m}_b c_{Pb} \ln\frac{(T_b)_{out}}{(T_b)_{in}}} \tag{12.26}$$

which is identical to equation (12.24) with the additional reminder in the subscript of the specific heat that the heat transfer process is being modeled as a constant pressure process.

The second law requires that the rate of entropy generation must always be positive or, in the reversible limit, zero. Then equation (12.26) sets the limits on the inlet and outlet temperatures that will satisfy the second law. It is interesting to note that there are many combinations of inlet and outlet temperatures that will satisfy the first law that will not also satisfy the second law. It is imperative, then, that one must always check to see that any heat exchanger configuration of interest satisfies both the first law and the second law simultaneously. It is particularly worth noting that it is possible mathematically to create a heat exchanger design that will satisfy both the first law and the second law simultaneously but not achieve the specified inlet and outlet conditions physically because the mathematically specified inlet and outlet temperatures require that the axial temperature profiles of the two streams cross. This means that at some point in the direction of flow, the stream that was the hotter of the two

suddenly became the colder of the two and vice versa. Then at some later point in the flow, the stream that was originally the hotter of the two but is now the colder one once again becomes the hotter stream. This, of course, is physically impossible. What happens is that at the point where the temperature profiles would cross, the temperature profiles touch and the rest of the heat exchanger becomes inoperative because the two fluid streams have reached a state of mutual thermal equilibrium. In order to make sure that this situation does not occur with a given heat exchanger design, one must check to see that the second law is satisfied at every plane perpendicular to the direction of flow. This is especially important for a case in which the specific heats of the fluids are functions of temperature and/or pressure.

Example 12E.1: As a thermal systems design engineer working for a company that manufactures paint and solvents, you are asked to design a simple heat exchanger to cool toluene (lacquer thinner) from the temperature at which it leaves the fractionation column to a temperature appropriate for packaging, say 25 C. To carry out the design, you decide to set the mass flow rate of the toluene to be $\dot{m} = 1$ kg/sec. In the final heat exchanger design, you know you can simply scale accordingly to accommodate the actual flow rate of the toluene. As an initial approach, you decide to examine both parallel flow and counterflow configurations. The heat exchanger is to be of the simple concentric tube design with the toluene flowing in the inner tube and the coolant, water, flowing in the annulus between the two tubes as shown in Figure 12E.1.

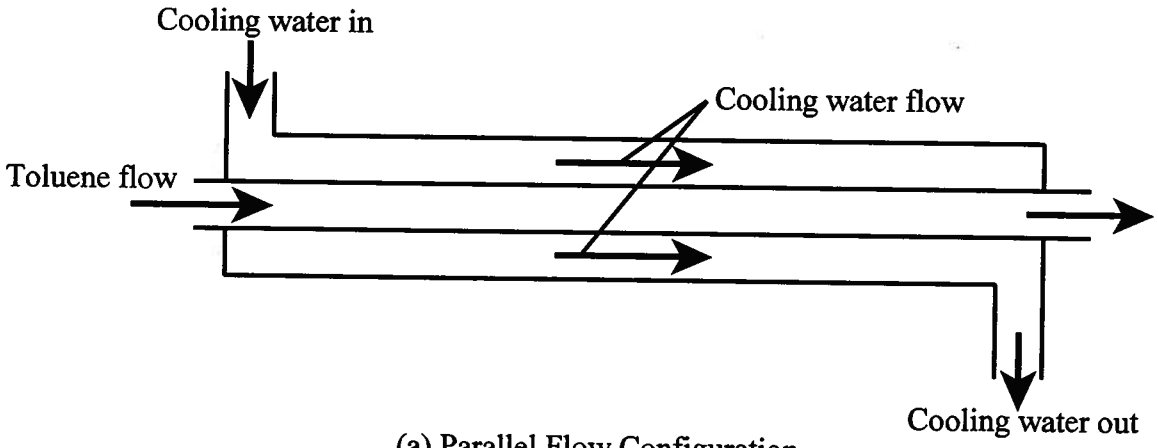

(a) Parallel Flow Configuration

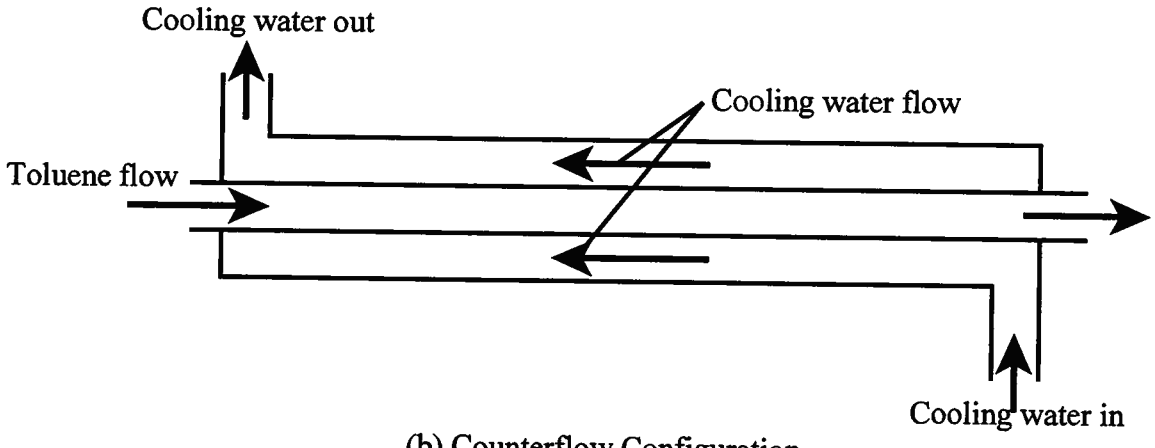

(b) Counterflow Configuration

Figure 12E.1 Simple Concentric Tube Heat Exchanger Design

The toluene enters the heat exchanger at a temperature T_{in} = 100 C and leaves at the temperature T_{out} = 25 C. The water enters the annulus at a temperature of $T_{w,in}$ = 20 C. One of the objectives is to use as little water as possible to do the job. As an initial assumption, assume turbulent flow throughout.

The thermal properties of toluene are:

$$\rho = 867 \text{ k/m}^3,\ c = 1690 \text{ J/kg K},\ \mu = 587 \text{ x } 10^{-6} \text{ kg/m sec},\ k = 0.160 \text{ W/m K}$$

The thermal properties of water are:

$$\rho_w = 989 \text{ k/m}^3,\ c_w = 4174 \text{ J/kg K},\ \mu_w = 5.84 \text{ x } 10^{-4} \text{ kg/m sec},\ k_w = 0.641 \text{ W/m K}$$

Solution: To begin the design, let us assume that for the toluene, Re = 86,000. (This is not a purely arbitrary choice as we will discover later.) There are other parameters that we need to establish in order to carry out the design. Specifically, the Prandtl number Pr

$$Pr = \frac{\mu c_P}{k} = \frac{(587 \text{ x } 10^{-6} \text{ kg/m sec})(1690 \text{ J/kg K})}{0.160 \text{ W/m K}} = 6.2$$

and the inner pipe diameter D_i necessary to handle this mass flow rate.

$$D_i = \frac{4\dot{m}}{\pi \mu Re} = \frac{4(1 \text{ kg/sec})}{\pi(587 \text{ x } 10^{-6} \text{ kg/m sec})(86{,}000)} = 0.025 \text{ m}$$

The flow velocity is then

$$\vartheta = \frac{4\dot{m}}{\rho \pi D_i^2} = \frac{4(1 \text{ kg/sec})}{\pi(867 \text{ k/m}^3)(0.025 \text{ m})^2} = 2.309 \text{ m/sec}$$

Alternatively, we could have chosen the diameter of the inner tube to be some standard diameter of tubing. Fortunately, the above value is such a diameter. As a design choice, we assume the tubing to be drawn stainless steel tubing which for the purposes here can be considered to be hydrodynamically smooth. Then the friction factor is given by the friction factor correlation of Petukhov given in equation (11.97), viz.

$$f = (0.790 \ln Re - 1.64)^{-2} = [0.790 \ln(86{,}000) - 1.64]^{-2} = 0.019$$

Alternatively, we could have obtained this value from the Moody diagram, Figure 9.30.

In order to determine the required length of the inner pipe, we need to determine the heat transfer coefficient $h_{c,i}$. This requires that we first calculate the Nusselt number. In the present case, the appropriate correlation for the Nusselt number for this turbulent flow is given by equation (11.96). Then

$$Nu_{D_i} = \frac{\frac{f}{8}(Re - 1000)Pr}{1 + 12.7\sqrt{\frac{f}{8}}(Pr^{2/3} - 1)} = \frac{\frac{0.019}{8}(86{,}000 - 1000)6.2}{1 + 12.7\sqrt{\frac{0.019}{8}}(6.2^{2/3} - 1)} = 498.883$$

Then the heat transfer coefficient becomes

$$h_{c,i} = Nu_{D_i}\frac{k}{D_i} = (498.883)\left(\frac{0.160 \text{ W/m K}}{0.025 \text{ m}}\right) = 3165 \text{ W/m}^2 \text{ K}$$

The requisite heat transfer between the two fluid streams can be determined by applying the first law to the flow in the inner pipe. Then

$$\dot{Q}_i = -\dot{m}c(T_{in} - T_{out}) = -(1 \text{ kg/sec})(1950 \text{ J/kg K})(100 \text{ C} - 25 \text{ C}) = -1.268 \text{ x } 10^5 \text{ W}$$

For the parallel flow configuration, the water enters the annulus at a temperature of 20 C and at

best can achieve a maximum temperature of 25 C. Then the water flow rate is determined by the first law applied to the water, viz.

$$\dot{Q}_i = \dot{m}_w c_w \left(T_{w,out} - T_{w,in}\right) = -\dot{Q}_o$$

$$\dot{m}_w = \frac{-\dot{Q}_o}{c_w \left(T_{w,out} - T_{w,in}\right)} = \frac{1.268 \text{ x } 10^5 \text{ W}}{(4174 \text{ J/kg K})(24 \text{ C} - 20 \text{ C})} = 7.592 \text{ kg/sec}$$

In order to determine the appropriate size for the annulus, we assume an appropriate value for the Reynolds number in the annulus. The larger the value of Re_w, the smaller the value of the diameter of the outside tube. The choice is somewhat arbitrary. Let $Re_w = 5 \text{ x } 10^5$. Then for the mass flow rate just calculated for the water, the hydraulic diameter of the annulus is D_{hw} where

$$D_{hw} = \frac{4\dot{m}_w}{\pi \mu_w Re_w} = \frac{4(7.592 \text{ kg/sec})}{\pi\left(5.84 \text{ x } 10^{-4} \text{ kg/m sec}\right)\left(5 \text{ x } 10^5\right)} = 0.033 \text{ m}$$

By definition, the hydraulic diameter of the annulus is four times the cross-sectional area divided by the wetted perimeter. Then since we are assuming that the wall thickness is zero for the purposes of this illustration, the diameter of the outside pipe is given by

$$D_{hw} = \frac{4A_c}{\wp} = \frac{4\left(\frac{\pi D_o^{\,2}}{4} - \frac{\pi D_o^{\,2}}{4}\right)}{\pi D_o - \pi D_i}$$

$$D_o^{\,2} - D_{hw} D_o - \left(D_i^{\,2} + D_{hw} D_i\right) = 0$$

$$D_o^{\,2} - (0.033 \text{ m}) D_o - \left((0.025 \text{ m})^2 + (0.033 \text{ m})(0.025 \text{ m})\right) = 0$$

$$D_o = 0.058 \text{ m}$$

The friction factor for the annulus is given by

$$f = (0.790 \ln Re - 1.64)^{-2} = \left[0.790 \ln\left(5 \text{ x } 10^5\right) - 1.64\right]^{-2} = 0.013$$

and the Prandtl number for the water is

$$Pr_w = \frac{\mu_w c_w}{k_w} = \frac{\left(5.84 \text{ x } 10^{-4} \text{ kg/m sec}\right)(4174 \text{ J/kg K})}{(0.641 \text{ W/m K})} = 3.803$$

The literature reports that for the geometry selected for this parallel flow heat exchanger, namely an annulus with the outer tube insulated on the outside and the heat transfer occurring across the outer surface of the inner tube, the appropriate correlation for heat transfer to the annulus is

$$Nu_A = \frac{\frac{f}{8}(Re - 1000) Pr}{1 + 12.7\sqrt{\frac{f}{8}}\left(Pr^{2/3} - 1\right)}\left[0.86\left(\frac{D_i}{D_o}\right)^{-0.16}\right]$$

Then

$$Nu_A = \frac{\frac{0.013}{8}\left(5 \text{ x } 10^5 - 1000\right) 3.803}{1 + 12.7\sqrt{\frac{0.013}{8}}\left(3.803^{2/3} - 1\right)}\left[0.86\left(\frac{0.025 \text{ m}}{0.058 \text{ m}}\right)^{-0.16}\right] = 1760$$

Then the heat transfer coefficient in the annulus becomes

$$h_{c,o} = Nu_A \frac{k_w}{D_{hw}} = 1760 \frac{0.641 \text{ W/m K}}{0.033 \text{ m}} = 8590 \text{ W/m}^2 \text{ K}$$

Then the overall heat transfer coefficient per unit length of the inner tube is

$$ua = \frac{UA}{L} = \left[\frac{1}{\pi D_i h_{c,i}} + \frac{1}{\pi D_i h_{c,o}} \right]^{-1}$$

$$ua = \left[\frac{1}{\pi(0.025 \text{ m})(3165 \text{ W/m}^2 \text{ K})} + \frac{1}{\pi(0.025 \text{ m})(8590 \text{ W/m}^2 \text{ K})} \right]^{-1} = 183.253 \text{ W/m K}$$

For this parallel flow configuration, the log mean temperature difference can be computed from the temperatures at the two ends of the heat exchanger. Then

$$\Delta T_1 = (T_{in} - T_{w,in}) = (100 \text{ C} - 20 \text{ C}) = 80 \text{ C} \quad \text{and} \quad \Delta T_2 = (T_{out} - T_{w,out}) = (25 \text{ C} - 24 \text{ C}) = 1 \text{ C}$$

$$\Delta T_{LM} = \frac{\Delta T_1 - \Delta T_2}{\ln \frac{\Delta T_1}{\Delta T_2}} = \frac{80 \text{ C} - 1 \text{ C}}{\ln \frac{80 \text{ C}}{1 \text{ C}}} = 18.028 \text{ C}$$

From Newton's law of cooling, we can obtain the overall heat transfer coefficient *UA*.

$$UA = \frac{\dot{Q}_o}{\Delta T_{LM}} = \frac{1.268 \text{ x } 10^5 \text{ W}}{18.028 \text{ K}} = 7031 \text{ W/K}$$

Then the length of the inner tube becomes

$$L = \frac{UA}{ua} = \frac{7031 \text{W/K}}{183.253 \text{ W/m K}} = 38.366 \text{ m}$$

Thus the design results in a double tube, parallel flow heat exchanger 38.37 m long with an inner tube diameter D_i = 25 mm and an outer tube diameter D_o = 58 mm. At this point we should check to see that the pressure drop is something reasonable. On the toluene side

$$\Delta P_t = f \frac{L}{D_i} \rho \frac{\vartheta^2}{2} = 0.019 \left(\frac{38.37 \text{ m}}{0.025 \text{ m}} \right) (867 \text{ k/m3}) \frac{(2.309 \text{ m/sec})^2}{2} = 6.53 \text{ x } 10^4 \text{ N/m}^2$$

This is a bit high for a heat exchanger, but it can be easily met with a pump of small size. On the water side, we have

$$\Delta P_w = f_w \frac{L}{D_i} \rho_w \frac{\vartheta_w^2}{2} = 0.013 \left(\frac{38.37 \text{ m}}{0.033 \text{ m}} \right) (989 \text{ k/m}^3) \frac{(0.538 \text{ m/sec})^2}{2} = 2.203 \text{ x } 10^3 \text{ N/m}^2$$

This is a much more modest pressure drop typical of heat exchangers of this type.

For the counterflow design, the correlation equations are the same; however, the value of ΔT_{LM} is different and the value of *UA* also will be different. The water enters at $T_{w,in}$ = 20 C and now leaves at a much higher temperature but less than the entering temperature of the toluene. As a first try let the temperature at exit be 65 C. Then from the first law

$$\dot{m}_w = \frac{\dot{Q}_o}{c_w (T_{w,out} - T_{w,in})} = \frac{1.268 \text{ x } 10^5 \text{ W}}{(4174 \text{ J/kg K})(65 \text{ C} - 20 \text{ C})} = 0.675 \text{ kg/sec}$$

Since the temperature change for the water is now significantly larger than in the case of parallel flow, we can try a smaller value of the Reynolds number on the water side. Let $Re_w = 5 \text{ x } 10^4$. Then the hydraulic diameter for the water becomes

$$D_{hw} = \frac{4\dot{m}_w}{\pi \mu_w Re_w} = \frac{4(0.675 \text{ kg/sec})}{\pi(5.84 \text{ x } 10^{-4} \text{ kg/m sec})(5 \text{ x } 10^4)} = 0.029 \text{ m}$$

As before,

$$D_{hw} = \frac{4A_c}{\wp} = \frac{4\left(\frac{\pi D_o^2}{4} - \frac{\pi D_o^2}{4}\right)}{\pi D_o - \pi D_i}$$

$$D_o^2 - D_{hw} D_o - \left(D_i^2 + D_{hw} D_i\right) = 0$$

$$D_o^2 - (0.029 \text{ m}) D_o - \left((0.025 \text{ m})^2 + (0.029 \text{ m})(0.025 \text{ m})\right) = 0$$

$$D_o = 0.054 \text{ m}$$

The friction factor for the annulus is given by

$$f = (0.790 \ln Re - 1.64)^{-2} = \left[0.790 \ln\left(5 \text{ x } 10^4\right) - 1.64\right]^{-2} = 0.021$$

and the Prandtl number for the water is the same as that calculated above, namely, $Pr = 3.803$. Since we are still using the annulus geometry, the correlation for the Nusselt number is the same as above, namely

$$Nu_A = \frac{\frac{f}{8}(Re - 1000) Pr}{1 + 12.7\sqrt{\frac{f}{8}}\left(Pr^{2/3} - 1\right)}\left[0.86\left(\frac{D_i}{D_o}\right)^{-0.16}\right]$$

Then

$$Nu_A = \frac{\frac{0.021}{8}\left(5 \text{ x } 10^4 - 1000\right)3.803}{1 + 12.7\sqrt{\frac{0.013}{8}}\left(3.803^{2/3} - 1\right)}\left[0.86\left(\frac{0.025 \text{ m}}{0.054 \text{ m}}\right)^{-0.16}\right] = 245.23$$

Then the heat transfer coefficient in the annulus becomes

$$h_{c,o} = Nu_A \frac{k_w}{D_{hw}} = 245.23 \frac{0.641 \text{ W/m K}}{0.033 \text{ m}} = 1363 \text{ W/m}^2 \text{ K}$$

Then the overall heat transfer coefficient per unit length of the inner tube is

$$ua = \frac{UA}{L} = \left[\frac{1}{\pi D_i h_{c,i}} + \frac{1}{\pi D_i h_{c,o}}\right]^{-1}$$

$$ua = \left[\frac{1}{\pi(0.025 \text{ m})(3165 \text{ W/m}^2 \text{ K})} + \frac{1}{\pi(0.025 \text{ m})(1363 \text{ W/m}^2 \text{ K})}\right]^{-1} = 75.504 \text{ W/m K}$$

For this counterflow configuration, the log mean temperature difference can be computed from the temperatures at the two ends of the heat exchanger. Then

$$\Delta T_1 = \left(T_{in} - T_{w,in}\right) = (100 \text{ C} - 65 \text{ C}) = 35 \text{ C} \quad \text{and} \quad \Delta T_2 = \left(T_{out} - T_{w,out}\right) = (25 \text{ C} - 20 \text{ C}) = 5 \text{ C}$$

$$\Delta T_{LM} = \frac{\Delta T_1 - \Delta T_2}{\ln \frac{\Delta T_1}{\Delta T_2}} = \frac{35 \text{ C} - 5 \text{ C}}{\ln \frac{35 \text{ C}}{5 \text{ C}}} = 15.417 \text{ C}$$

From Newton's law of cooling, we can obtain the overall heat transfer coefficient *UA*.

$$UA = \frac{\dot{Q}_o}{\Delta T_{LM}} = \frac{1.268 \text{ x } 10^5 \text{ W}}{15.417 \text{ K}} = 8221 \text{ W/K}$$

Then the length of the inner tube becomes

$$L = \frac{UA}{ua} = \frac{8221 \text{W/K}}{75.504 \text{ W/m K}} = 108.888 \text{ m}$$

Thus the design results in a double tube, counterflow heat exchanger 108.89 m long with an inner tube diameter D_i = 25 mm and an outer tube diameter D_o = 54 mm. At this point we should check to see that the pressure drop is something reasonable. On the toluene side

$$\Delta P_t = f \frac{L}{D_i} \rho \frac{\vartheta^2}{2} = 0.019 \left(\frac{108.888 \text{ m}}{0.025 \text{ m}} \right) (867 \text{ k/m3}) \frac{(2.309 \text{ m/sec})^2}{2} = 1.853 \text{ x } 10^5 \text{ N/m}^2$$

This is high for a heat exchanger, but it can be easily met with a pump of small size if necessary. Other factors may dictate choosing the parallel flow design instead. On the water side, we have

$$\Delta P_w = f_w \frac{L}{D_{hw}} \rho_w \frac{\vartheta_w^{\,2}}{2} = 0.021 \left(\frac{108.888 \text{ m}}{0.029 \text{ m}} \right) (989 \text{ k/m}^3) \frac{(0.644 \text{ m/sec})^2}{2} = 1.627 \text{ x } 10^4 \text{ N/m}^2$$

This is a reasonable pressure drop.

In comparing the two designs, we see that the length of the parallel flow configuration is significantly shorter than the length of the counterflow design; thus, the capital cost of the parallel flow design would be substantially less than the cost of the counterflow design. However, the required mass flow rate of the coolant in the parallel flow design is more than ten times the mass flow rate of the coolant in the counterflow design; thus, the operating cost of the parallel flow design is substantially more than the operating cost of the counterflow design. The thermal-fluid engineer is then faced with with making a trade-off between operating cost and capital cost. The choice would be dictated by other factors. For example, if the design is to be in service for an extended period of time, it might be possible to amortize the capital cost with the savings on the operating costs.

There is another issue to be considered in this design. The irreversibility inherent in both designs generates entropy that must be dealt with in some other portion of the system. The costs in terms of system performance due to this entropy generation may completely overshadow the other costs mentioned above. To determine the relative merits of these two designs from the point of view of the entropy, we need to evaluate the rate of entropy generation in each design by applying the second law in each case. The second law applied to the steady-flow, externally adiabatic heat exchanger reduces to

$$\dot{S}_{gen} = \dot{m}_w \left[(s_w)_{out} - (s_w)_{in} \right] + \dot{m} \left[(s)_{out} - (s)_{in} \right]$$

$$\dot{S}_{gen} = \dot{m}_w c_w \ln \frac{(T_w)_{out}}{(T_w)_{in}} + \dot{m} c \ln \frac{(T)_{out}}{(T)_{in}}$$

For the parallel flow design, the rate of entropy generation becomes

$$\dot{S}_{gen} = (7.592 \text{ kg/sec})(4174 \text{ J/kg K}) \ln \left(\frac{297 \text{ K}}{293 \text{ K}} \right) + (1 \text{ kg/sec})(1690 \text{ J/kg K}) \ln \left(\frac{298 \text{ K}}{393 \text{ K}} \right)$$

$$\dot{S}_{gen} = 50.309 \text{ W/K}$$

For the counterflow design, the rate of entropy generation becomes

$$\dot{S}_{gen} = (7.592 \text{ kg/sec})(4174 \text{ J/kg K}) \ln \left(\frac{338 \text{ K}}{293 \text{ K}} \right) + (1 \text{ kg/sec})(1690 \text{ J/kg K}) \ln \left(\frac{298 \text{ K}}{393 \text{ K}} \right)$$

$$\dot{S}_{gen} = 23.159 \text{ W/K}$$

Thus, the rate of entropy generation for the counterflow design is less than half that of the parallel flow design. This parameter alone may be the determining factor in picking one design over the other.

The present example tends to over-simplify the task of designing a simple heat exchanger for this application. We made a number of arbitrary decisions concerning water outlet temperature and Reynolds number of the water flow. These need to be examined in detail by performing a parameter study. For example, consider the counterflow heat exchanger design. Let us assume that the toluene side of the heat exchanger is fixed at a diameter of 25 mm , a mass flow rate of 1 kg/sec, an inlet temperature of 100 C, and an outlet temperature of 25 C. For the cooling water side, let us consider several different designs in which we allow the outlet temperature to vary from 25 C to 95 C and the Reynolds number to vary from 5 x 10^4 to 5 x 10^5. Using the methods described above, we find that for various values of the Reynolds number the length of the heat exchanger takes the form shown in Figure 12E.2.

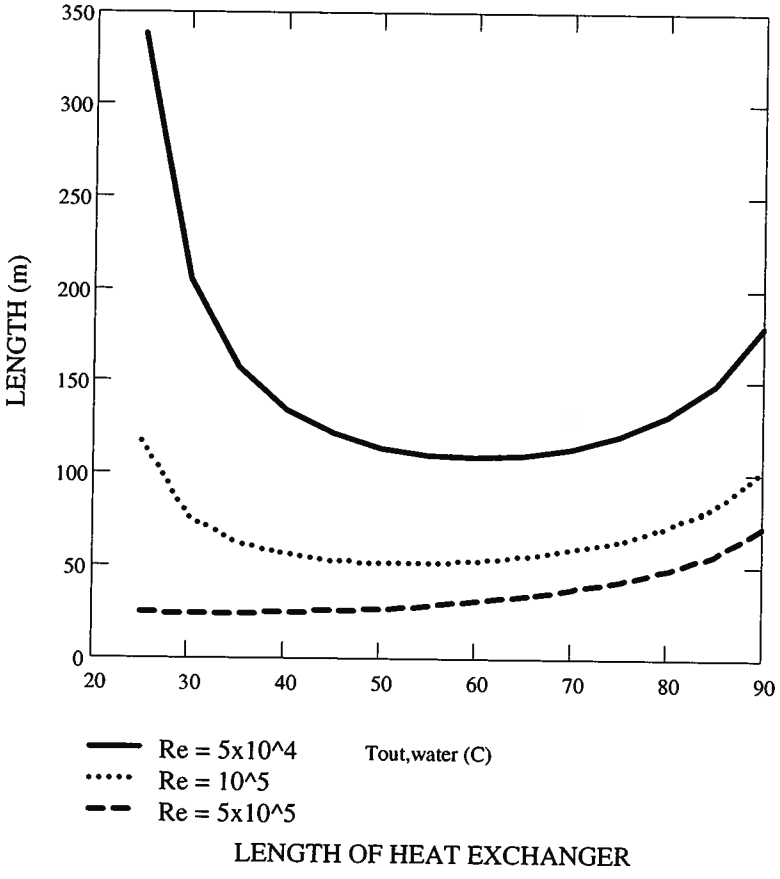

Figure 12E.2 Heat Exchanger Length for Various Flow Rates

Note that the length actually experiences a minimum. There are two competing effects at work here. One is the fact that ΔT_{LM} decreases as the water outlet temperature increases. See Figure 12E.3.

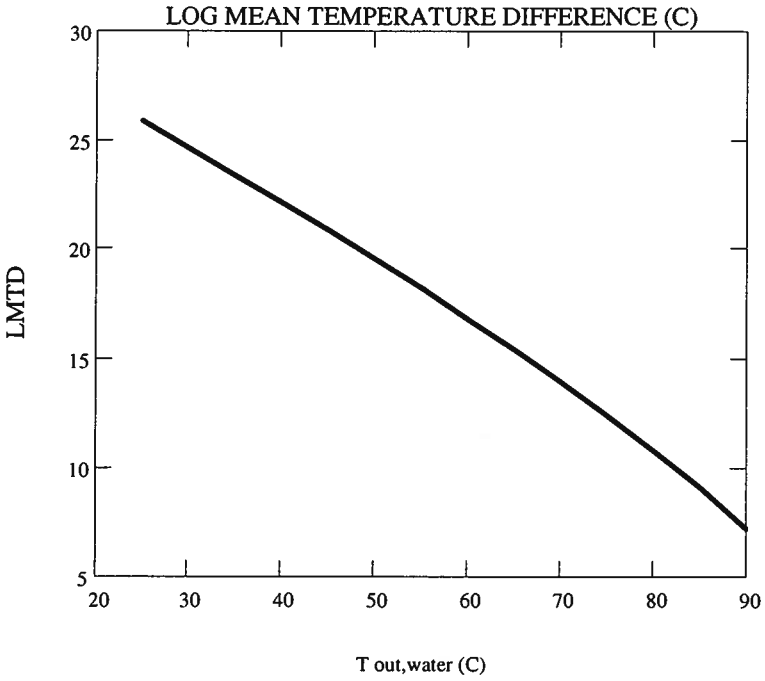

Figure 12E.3 Log Mean Temperature Difference for Various Cooling Water Outlet Temperatures

Thus there is a smaller temperature difference available to maintain the fixed heat transfer rate. As a consequence, the area of the heat exchanger must increase as the outlet temperature increases. However, at lower outlet temperatures, another phenomenon occurs . As the outlet temperature decreases, the outside diameter of the annulus must increase significantly in order to accommodate the increased water flow rate mandated by the first law. See Figure 12E.4.

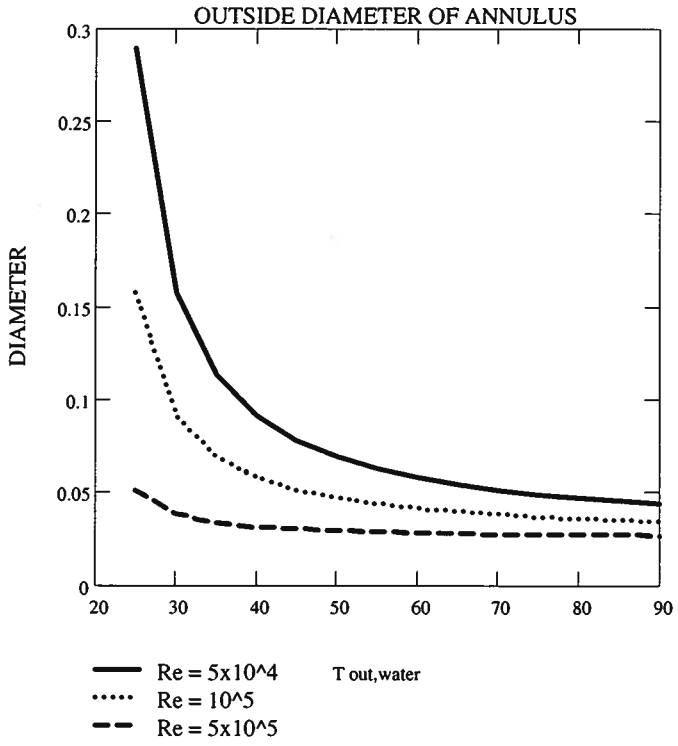

Figure 12E.4 Annulus Diameter for Various Cooling Water Outlet Temperatures

At fixed Reynolds number, this has the effect of reducing the temperature gradient at the wall for a given bulk mean temperature. The net result is that the heat transfer coefficient decreases as shown in Figure 12E.5. Thus the conductance at the wall decreases necessitating a larger surface area.

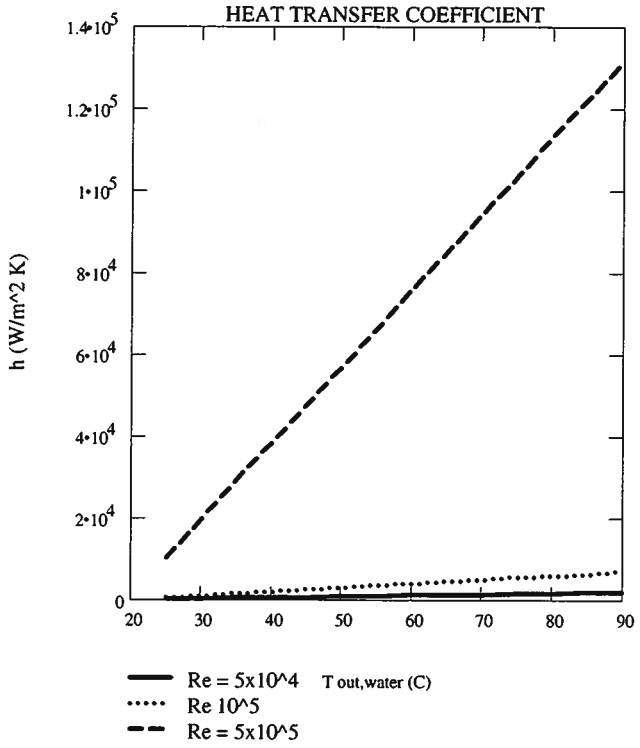

Figure 12E.5 Heat Transfer Coefficient of the Cooling Water

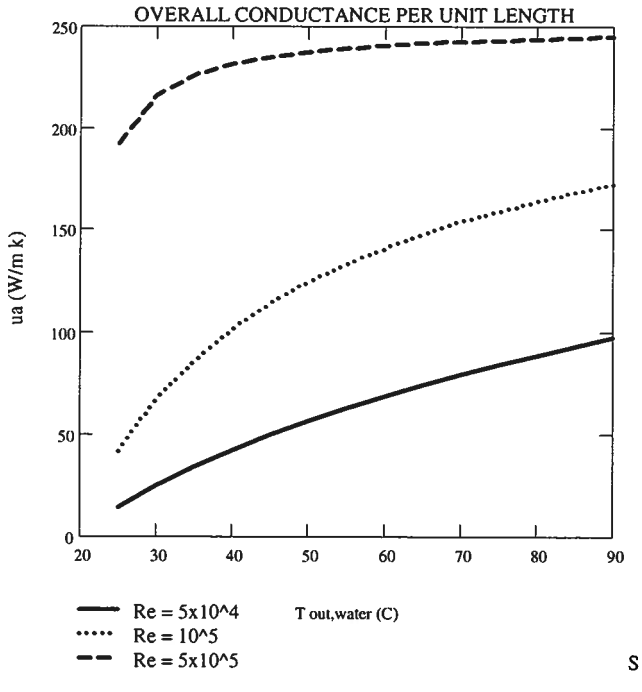

Figure 12E.6 Overall Heat Transfer Coefficient Per Unit Length

The rate of entropy generation is as shown in Figure 12E.7. Clearly it decreases as the outlet temperature increases because the temperature difference across which the heat transfer occurs decreases.

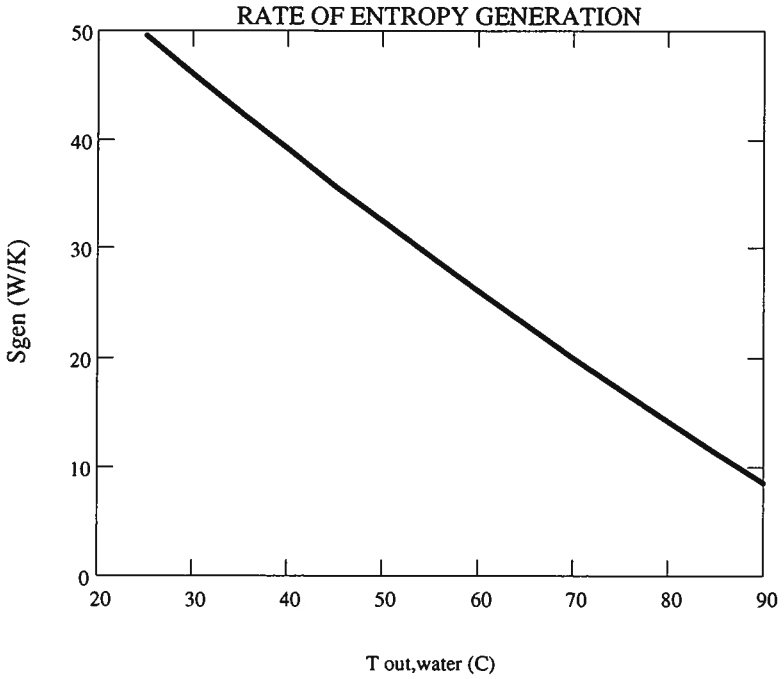

Figure 12E.7 Rate of Entropy Generation for the Counterflow Configuration

In this particular case the rate of entropy generation is not quite so important as it would be in an energy conversion system where it would decrease the output directly, but it does reflect itself in the amount of cooling water that the design consumes.

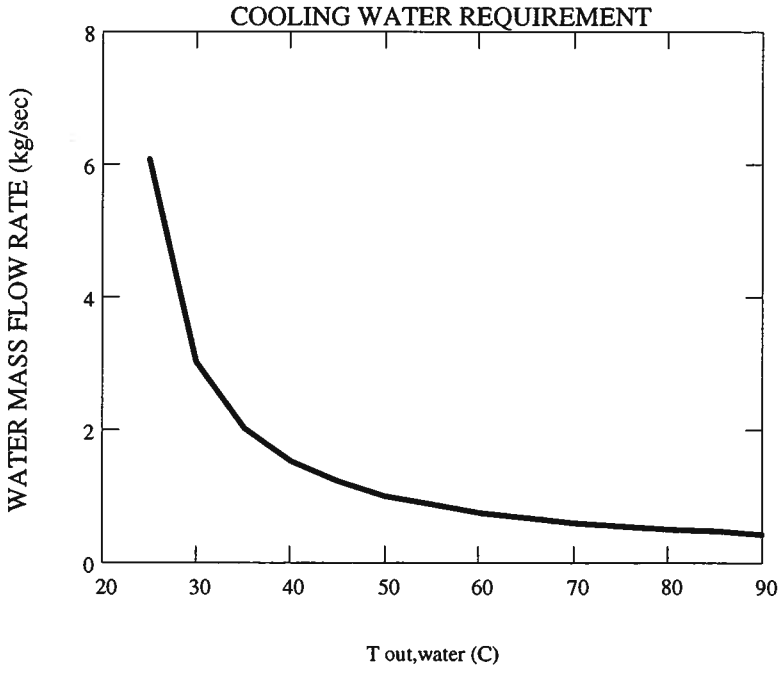

Figure 12E.8 Cooling Water Requirements

12.2.3 Flow Configurations Other Than Parallel Flow and Counterflow

While the two flow geometries considered above are adequate to provide the necessary heat transfer between two fluid streams in many cases, there are situations in which some other flow configuration is more desirable or even required. For example, in order to provide the most intimate contact possible between the two fluid streams, thermal-fluids engineers have developed complex flow geometries such as crossflow in which either one or both of the fluids is mixed in the thermal sense. These flow configurations often use the available hardware in a more efficient manner than is possible with the simple parallel flow or counterflow geometries. Many other configurations are also possible and the choices are limited only by the imagination of the designer.

For each of these geometries, the first law of equation (12.4) still applies; however, for each different geometry, the rate equation of equation (12.6) requires a new expression for the appropriate temperature difference that serves as the driving force for the heat transfer interaction between the two fluid streams. The expression for the log mean temperature difference developed in section 12.2.2 is limited strictly to the two specific flow configurations considered there. Unfortunately, the more complex the flow geometry, the more complicated the analysis. In some cases the treatment is virtually intractable, and rather than attempt these difficult formulations in each case, thermal-fluids engineers have developed a semi-empirical approach based upon that of the preceding sections. Unfortunately, this method is convenient to use only for a limited number of geometries and is not widely used in modern thermal-fluids engineering practice. We present it here simply for historical completeness since it was the earliest method for dealing with complex geometries and is sometimes still found in the heat exchanger literature.

In this method, known as the mean temperature difference (MTD) method, the heat transfer rate between the two fluid streams is given by the rate equation

$$\dot{Q} = UAF\Delta T_{LM,CF} \tag{12.22}$$

where all terms are as before except that $\Delta T_{LM,CF}$ represents the log mean temperature difference for the counterflow configuration and the factor F represents the degree of departure of the actual mean temperature difference from the counterflow log mean temperature difference, viz.

$$F = \frac{\Delta T_{actual}}{\Delta T_{LM,CF}} \tag{12.23}$$

The factor F, which should not be interpreted as some sort of heat exchanger effectiveness, is a function of two dimensionless groups P_1 and R_1 where

$$P_1 = \frac{(T_a)_{out} - (T_a)_{in}}{(T_b)_{in} - (T_a)_{in}} \quad \text{and} \quad R_1 = \frac{(T_b)_{in} - (T_b)_{out}}{(T_a)_{out} - (T_a)_{in}} \tag{12.24}$$

For all flows other than parallel flow, the log mean temperature difference for counterflow is given by equation (12.18) with

$$\Delta T_1 = (T_{hot})_{in} - (T_{cold})_{out} \quad \text{and} \quad \Delta T_2 = (T_{hot})_{out} - (T_{cold})_{in} \tag{12.25}$$

where we have now explicitly identified which stream is the hotter and which stream is the colder. For parallel flow, the log mean temperature difference is again given by equation (12.18) with

$$\Delta T_1 = (T_{hot})_{in} - (T_{cold})_{in} \quad \text{and} \quad \Delta T_2 = (T_{hot})_{out} - (T_{cold})_{out}$$

for which the factor F becomes unity.

For the case of the shell and tube heat exchanger shown schematically in Figure 12.7, the values for the factor F are shown in Figure 12.8.

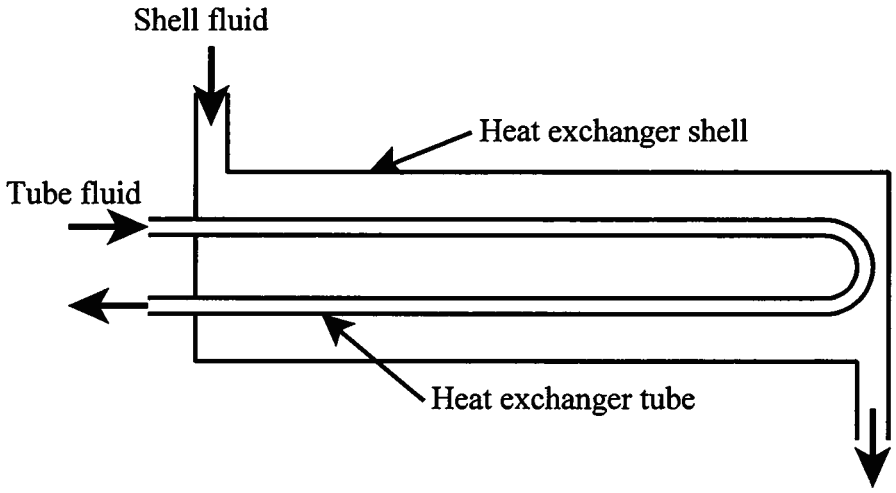

Figure 12.7 Shell-and-tube Heat Exchanger Schematic

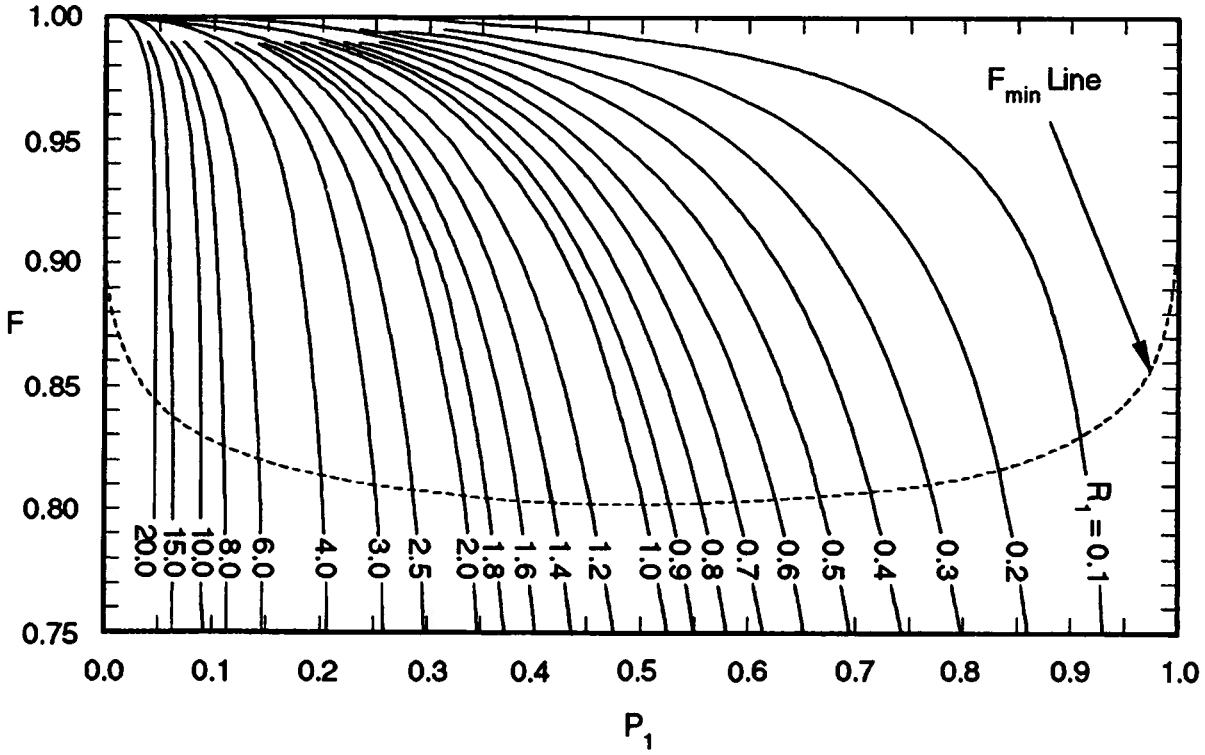

Figure 12.8 The LMTD Correction Factor for a Shell-and-tube Heat Exchanger
(From *Handbook of Heat Transfer*, ed. byW.M. Rohsenow, J.P. Hartnett, and Y.I. Cho, McGraw-Hill, N.Y., 1998, Chapter 17, *Heat Exchangers* by R.K. Shah and D.P. Sekulic, p. 17.33)

12.3 The ε - *NTU* Method of Heat Exchanger Analysis

In determining the states of the working fluid in a given heat exchanger application, the method employed depends upon the information available. If the four temperatures, two inlet temperatures and two outlet temperatures, are known, equation (12.18) gives the log mean temperature difference, ΔT_{LM}, equation (12.4) gives the heat transfer rate, and equation (12.17) gives the required heat exchanger specification, UA_T. This method is known as the *Mean Temperature Difference* method and is denoted as *MTD*. It should be noted that the *MTD* method of analyzing heat exchanger performance is useful only in limited circumstances.

In particular, if the capacity rates for the two fluid streams are known and two of the inlet temperatures and one of the outlet temperatures are known, the first law, equation (12.4), can be used to determine the other outlet temperature. The log mean temperature difference for the counterflow configuration, $\Delta T_{LM,CF}$, can then be determined from equation (12.18). Then a chart similar to Figure 12.8 can be used to determine the appropriate value of the factor F for the configuration being analyzed. Then from the first law and Newton's Law of Cooling in the form of equation (12.22), we can determine the value of the product UA_T for the heat exchanger. Using this value of UA_T, we can select the heat exchanger appropriate for the application at hand from data supplied by heat exchanger manufacturers. Alternatively, we could design a heat exchanger using the appropriate heat transfer correlations for the configuration selected.

On the other hand, if the two inlet temperatures, the capacity rates, and the UA_T product are known, equation (12.4) must be solved simultaneously with equation (12.15) or (12.20) for the two unknown temperatures. Equation (12.6) or, in the case of a flow configuration other than parallel or counterflow, equation (12.22) then gives the required heat transfer rate. This procedure usually requires an iterative solution and can be quite tedious.

Fortunately, there is an alternate method of heat exchanger analysis available known as the $\varepsilon - NTU$ method that does not require iteration. The essence of the method lies in the definition of the heat exchanger efficiency, ε, or as it is more commonly known, the heat exchanger effectiveness. By definition, the heat exchanger effectiveness is the ratio of the actual heat transfer rate from one stream to the other divided by the maximum possible heat transfer rate for the given set of inlet temperatures.

As we have shown in section 12.2, the fluid stream with the smaller value of the capacity rate $C_{min} = (\dot{m}c_P)_{min}$ will experience the larger change in temperature in the direction of flow. In addition, the highest temperature in the heat exchanger is the inlet temperature of the hot stream, $T_{h,in}$, and the lowest temperature is the inlet temperature of the cold stream, $T_{c,in}$. Thus the largest possible temperature change in either stream would occur for the case in which one of the temperatures is equal to $T_{h,in}$ and the other temperature is equal to $T_{c,in}$. At best, this combination of temperatures is possible only for the stream with the lower capacity rate, $C_{min} = (\dot{m}c_P)_{min}$. Then the maximum heat transfer rate that is physically possible in the heat exchanger would be $\dot{Q}_{max}$ where

$$\dot{Q}_{max} = (\dot{m}c_P)_{min}(T_{h,in} - T_{c,in}) = C_{min}(T_{h,in} - T_{c,in}) \tag{12.27}$$

At first glance, it would appear that equation (12.27) cannot be correct since $C_{max}(T_{h,in} - T_{c,in})$ would give a larger numerical value. However, while this is true mathematically, this latter combination would violate the first law and is, therefore, not an acceptable statement of the maximum possible heat transfer in the heat exchanger. For example if the stream with the maximum capacity rate C_{max} were to experience the maximum change in temperature ΔT_{max}, the

first law would require

$$C_{max}\Delta T_{max} = C_{min}\Delta T_{min}$$

which clearly leads to an absurdity.

$$\frac{C_{max}}{C_{min}} = \frac{\Delta T_{min}}{\Delta T_{max}} \Rightarrow \text{absurdity}$$

It follows, then, that the heat exchanger effectiveness can be expressed in two ways guaranteed to be equivalent by the first law.

$$\varepsilon = \frac{\dot{Q}}{\dot{Q}_{max}} = \frac{C_c\left(T_{c,out} - T_{c,in}\right)}{C_{min}\left(T_{h,in} - T_{c,in}\right)} = \frac{C_h\left(T_{h,in} - T_{h,out}\right)}{C_{min}\left(T_{h,in} - T_{c,in}\right)} \tag{12.28}$$

The overall thermal conductance for the heat exchanger can be expressed in dimensionless form as

$$NTU = \frac{UA}{C_{min}} \tag{12.29}$$

where the symbol *NTU* stands for the *number of transfer units*. The $\varepsilon - NTU$ methods postulates the existence of a function ϕ such that

$$\varepsilon = \phi\left(NTU, C^*\right) \tag{12.30}$$

where the capacity ratio C^* is given by

$$C^* = \frac{C_{min}}{C_{max}} \tag{12.31}$$

As an example of the development of the functional relationship between ε and *NTU*, consider the case of a two-stream heat exchanger with parallel flow such that the capacity rate of the hotter stream, C_h, is the smaller of the two capacity rates, $C_h = C_{min}$. Then

$$\varepsilon = \frac{C_h\left(T_{h,in} - T_{h,out}\right)}{C_{min}\left(T_{h,in} - T_{c,in}\right)} = \frac{\left(T_{h,in} - T_{h,out}\right)}{\left(T_{h,in} - T_{c,in}\right)} \tag{12.32}$$

and

$$C^* = \frac{C_{min}}{C_{max}} = \frac{\dot{m}_h c_{P,h}}{\dot{m}_c c_{P,c}} = \frac{\dot{Q}}{\left(T_{h,in} - T_{h,out}\right)} \frac{\left(T_{c,out} - T_{c,in}\right)}{\dot{Q}} = \frac{\left(T_{c,out} - T_{c,in}\right)}{\left(T_{h,in} - T_{h,out}\right)} \tag{12.33}$$

From equation (12.15) we have

$$\ln\left(\frac{\Delta T_2}{\Delta T_1}\right) = -\left(\frac{1}{\dot{m}_h c_{P,h}} + \frac{1}{\dot{m}_c c_{P,c}}\right) UA_T$$

$$\ln\left[\frac{T_{h,out} - T_{c,out}}{T_{h,in} - T_{c,in}}\right] = -\left(\frac{1}{C_h} + \frac{1}{C_c}\right) UA_T \tag{12.34}$$

$$\ln\left[\frac{T_{h,out} - T_{c,out}}{T_{h,in} - T_{c,in}}\right] = -\frac{UA_T}{C_{min}}\left(1 + \frac{C_{min}}{C_{max}}\right) = -NTU\left(1 + C^*\right)$$

Then

$$\frac{T_{h,out} - T_{c,out}}{T_{h,in} - T_{c,in}} = \exp\left[-NTU\left(1 + C^*\right)\right] \tag{12.35}$$

But adding and subtracting $T_{h,in}$ in the numerator of the left-hand side of equation (12.35) and making use of the first law, we get

$$\frac{T_{h,out}-T_{c,out}}{T_{h,in}-T_{c,in}}=\frac{T_{h,out}-T_{h,in}+T_{h,in}-T_{c,out}}{T_{h,in}-T_{c,in}}=\frac{\left(T_{h,out}-T_{h,in}\right)+\left(T_{h,in}-T_{c,in}\right)-\frac{C_{min}}{C_{max}}\left(T_{h,out}-T_{h,in}\right)}{T_{h,in}-T_{c,in}}$$

or

$$\frac{T_{h,out}-T_{c,out}}{T_{h,in}-T_{c,in}}=-\varepsilon+1-C^*\varepsilon=1-\varepsilon\left(1+C^*\right) \tag{12.36}$$

Combining equations (12.35) and (12.36), we get

$$\varepsilon=\frac{1-\exp\left[-NTU\left(1+C^*\right)\right]}{1+C^*} \tag{12.37}$$

Similar analyses can be carried out for other heat exchanger configurations. The results are summarized in Table 12.1.

In practice, the steps to be carried out in applying the $\varepsilon-NTU$ method for the analysis of a heat exchanger can be best summarized as follows:

Case I: Given U, C_c, C_h, and the temperatures $T_{h,in}$, $T_{h,out}$, $T_{c,in}$, and $T_{c,out}$, find A_T.

1. Select a heat exchanger configuration.
2. Calculate ε from equation (12.28).
3. Calculate $C^* = C_{min}/C_{max}$.
4. Use the correlation equation from Table 12.1 to find the value of NTU appropriate for the heat exchanger configuration selected.
5. Calculate A_T from the definition of NTU, equation (12.29).

Case II: Given A_T, U, C_c, C_h, $T_{h,in}$, and $T_{c,in}$, find T_{out}.

1. Select a heat exchanger configuration.
2. Calculate NTU from the definition, equation (12.29).
3. Calculate $C^* = C_{min}/C_{max}$.
4. Calculate $\dot{Q}=\varepsilon C_{min}\left(T_{h,in}-T_{c,in}\right)$.
5. Calculate

$$T_{c,out}=T_{c,in}+\frac{\dot{Q}}{C_c} \quad \text{and} \quad T_{h,out}=T_{h,in}-\frac{\dot{Q}}{C_h}$$

In both cases listed above, the overall heat transfer coefficient, U, is assumed to be known. Frequently, this information is available from the manufacturer who has determined the value of U from data derived from tests on the actual heat exchanger configuration of interest. However, there are other cases, such as the design of a heat exchanger custom configured to meet the unique requirements of a particular application, in which the value of U is not available by this means. Under these circumstances, it may be necessary to determine the value of U from the application of heat transfer correlations similar to those presented in Chapter 11. Example 12E.3 illustrates this procedure.

Table 12.1 Heat Exchanger Correlation Equations for ε and *NTU*

$$C = \dot{m}c_p \quad ; \quad C^* = \frac{C_{min}}{C_{max}} \quad ; \quad \varepsilon = \frac{\dot{Q}}{\dot{Q}_{max}} = \frac{C_h\left(T_{h,in} - T_{h,out}\right)}{C_{min}\left(T_{h,in} - T_{c,in}\right)} = \frac{C_c\left(T_{c,out} - T_{c,in}\right)}{C_{min}\left(T_{h,in} - T_{c,in}\right)} \quad ; \quad NTU = \frac{UA_T}{C_{min}}$$

	Configuration	Correlation for $\varepsilon = f(\mathrm{NTU}, C^*)$	Correlation for $\mathrm{NTU} = f(\varepsilon, C^*)$
1	Single stream; heat exchangers with $C^* = 0$	$\varepsilon = 1 - \exp(-\mathrm{NTU})$	$\mathrm{NTU} = -\ln(1-\varepsilon)$
2	Concentric tube: parallel flow	$\varepsilon = \dfrac{1-\exp\left[-\mathrm{NTU}(1+C^*)\right]}{1+C^*}$	$\mathrm{NTU} = -\dfrac{1}{C^*+1}\cdot\ln\left[1-\varepsilon(1+C^*)\right]$
3	Concentric tube: counter flow	$\varepsilon = \dfrac{1-\exp\left[-\mathrm{NTU}(1-C^*)\right]}{1-C^*\cdot\exp\left[-\mathrm{NTU}(1-C^*)\right]}$	$\mathrm{NTU} = \dfrac{1}{C^*-1}\cdot\ln\left(\dfrac{\varepsilon-1}{\varepsilon C^*-1}\right) \quad (C^*<1)$ $\mathrm{NTU} = \varepsilon/(1-\varepsilon) \quad (C^*=1)$
4	Shell and tube: one shell pass; 2, 4, ... tube passes	$\varepsilon = \varepsilon_1 = 2\left\{1+C^*+\left[1+(C^*)^2\right]^{1/2}\cdot\dfrac{1+\exp\left(-\mathrm{NTU}\left[1+(C^*)^2\right]^{1/2}\right)}{1-\exp\left(-\mathrm{NTU}\left[1+(C^*)^2\right]^{1/2}\right)}\right\}^{-1}$	$\mathrm{NTU} = -\left[1+(C^*)^2\right]^{-1/2}\cdot\ln\left(\dfrac{E-1}{E+1}\right)$ where $E_{\text{one shell pass}} = \dfrac{\frac{2}{\varepsilon}-(1+C^*)}{\left[1+(C^*)^2\right]^{1/2}}$,
5	Shell and tube: n shell passes; 2n, 4n , ... tube passes	$\varepsilon = \left[\left(\dfrac{1-\varepsilon_1\cdot C^*}{1-\varepsilon_1}\right)^n - 1\right]\cdot\left[\left(\dfrac{1-\varepsilon_1\cdot C^*}{1-\varepsilon_1}\right)^n - C^*\right]^{-1}$ where ε_1 is defined in (4), and calculated using *NTU* per shell pass (e.g. *NTU* / *n*) where *NTU* appears	$E_{n\text{ shell passes}} = \dfrac{2\cdot\left(\frac{F-C^*}{F-1}\right)-(1+C^*)}{\left[1+(C^*)^2\right]^{1/2}}$, and $F = \left(\dfrac{\varepsilon\cdot C^*-1}{\varepsilon-1}\right)^{1/n}$
6	Single-pass cross-flow: both fluids unmixed	$\varepsilon = 1-\exp\left\{-\dfrac{\mathrm{NTU}^{0.22}}{C^*}\cdot\left[1-\exp\left(-C^*\cdot\mathrm{NTU}^{0.78}\right)\right]\right\}$	Iterate the $\varepsilon = f(\mathrm{NTU}, C^*)$ correlation for unmixed single-pass cross-flow
7	Single-pass cross-flow: both fluids mixed	$\varepsilon = \left[\dfrac{1}{1-\exp(-NTU)} + \dfrac{C^*}{1-\exp(-C^*\cdot NTU)} - \dfrac{1}{NTU}\right]^{-1}$	Iterate the $\varepsilon = f(\mathrm{NTU}, C^*)$ correlation for mixed single-pass cross-flow
8	Single-pass cross-flow: C_{min} unmixed and C_{max} mixed	$\varepsilon = \dfrac{1}{C^*}\cdot\left\{1-\exp\left(-C^*\left[1-\exp(-\mathrm{NTU})\right]\right)\right\}$	$\mathrm{NTU} = -\ln\left[1+\dfrac{1}{C^*}\cdot\ln\left(1-\varepsilon\cdot C^*\right)\right]$
9	Single-pass cross-flow: C_{min} mixed and C_{max} unmixed	$\varepsilon = 1-\exp\left\{-\dfrac{1}{C^*}\left[1-\exp\left(-C^*\cdot\mathrm{NTU}\right)\right]\right\}$	$\mathrm{NTU} = -\dfrac{1}{C^*}\cdot\ln\left[1+C^*\ln(1-\varepsilon)\right]$

Adapted from: Tables 8.3a and 8.3b *Basic Heat and Mass Transfer*, by A.F. Mills, and
Tables 11.3 and 11.4 in *Introduction to Heat and Mass Transfer* by Frank P. Incropera and David P. DeWitt

Note from Table 12.1 that the counterflow configuration has the largest value of the heat exchanger effectiveness, ε, for given values of NTU and C^* compared to all other configurations. In this sense, the counterflow configuration provides maximum performance in terms of utilization of heat exchanger surface area.

In applying the $\varepsilon - NTU$ method, there are two special cases worthy of note. The first of these is the special case in which the heat exchanger effectiveness approaches unity. This can occur only for a counterflow heat exchanger for which the two capacity rates are equal. That is, $C_{min} = C_{max}$. From the first law in the form of equation (12.4), it is apparent that when the capacity rates are equal, the temperature changes in the direction of flow for the two streams are equal to each other. In addition, from the definition of the effectiveness, equation (12.32), it is apparent that a value of unity for the effectiveness requires that the outlet temperature of the hot stream must be equal to the inlet temperature of the cold stream and the outlet temperature of the cold stream must be equal to the inlet temperature of the hot stream. Thus, in the limit of an effectiveness of unity, the ΔT is zero throughout the heat exchanger and it follows that the log mean temperature difference for the heat exchanger is zero. From the second law for the heat exchanger, equation (12.26), it is apparent that the rate of entropy generation vanishes and the heat exchanger becomes reversible in this limit. In addition, the rate equation requires that the overall conductance, UA_T, must be infinite if the heat transfer rate is finite. (As a practical consideration, it should be pointed out that the effectiveness can approach unity for some complex heat exchanger designs that are not simple counterflow. For these configurations the overall conductance approaches infinity, and thermal conduction in the solid parts that make up the heat exchanger becomes important. This effect has been neglected in the present discussion. The effect is that the heat exchanger tries to become isothermal by virtue of conduction in the solid parts that make up the heat exchanger. This can have an adverse effect on heat exchanger performance.) On the basis of the foregoing discussion, the heat exchanger effectiveness can be thought of as the ratio of the actual heat transfer rate to the heat transfer rate in a reversible heat exchanger with the same two inlet states, the same minimum capacity rate, but a different maximum capacity rate.

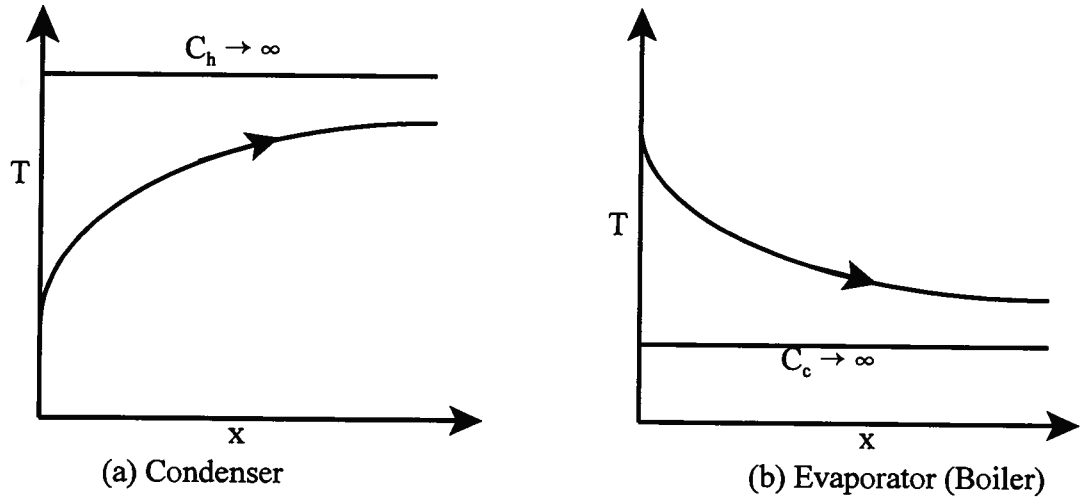

Figure 12.9 Heat Exchangers with One Fluid Changing Phase

The second special case occurs when one of the fluid streams undergoes a change of phase as a result of the heat transfer with the other stream. This is the case in a boiler or an evaporator and in a condenser. Since the heat transfer process in the heat exchanger is modeled

as constant pressure, it follows that the fluid stream undergoing the phase change does not change temperature. This has the effect of making that fluid stream appear as though it had an infinite capacity rate. The situation is shown schematically in Figure 12.9.

In both of the cases depicted in Figure 12.9, $C^* = 0$ and the $\varepsilon - NTU$ correlations reduce to

$$\varepsilon = 1 - \exp(-NTU) \quad \text{and} \quad NTU = -\ln(1-\varepsilon) \tag{12.38}$$

as shown in case 1 of Table 12.1.

Example 12E.2: In open heart surgery, the oxygen requirements of the patient can be reduced substantially by reducing the core body temperature of the patient. This is known as induced *hypothermia*. To achieve this state of the patient, the patient is placed on a heart-lung machine in which the patient's own heart is by-passed so that it can be "freed" for the surgical procedure. The heart-lung machine contains a heat exchanger which is used to cool the patient's blood before the surgery and to re-warm it afterward. It is proposed that a concentric tube counterflow heat exchanger shown schematically in Figure 12E.2, of length 4 m be used for heating the blood post-operatively, with the thin-walled inner tube carrying the blood having a diameter of 60 mm and the insulated outer tube carrying the heating water having a diameter of 80 mm.

(a) Calculate the overall heat transfer coefficient U for the following operating conditions: $T_{h,in} = 90$ C, $\dot{m}_h = 0.10$ kg/sec, $T_{c,in} = 18$ C, $\dot{m}_c = 0.05$ kg/sec

(b) What is the temperature of the blood leaving the heat exchanger?

For water: $k_{water} = 0.652$ W/m K, $\rho_{water} = 985$ kg/m^3, $c_{water} = 4178$ J/kg K,
$\mu_{water} = 4.92 \times 10^{-4}$ kg/m sec, $Pr_{water} = 3.153$
For blood: $k_{blood} = 0.602$ W/m K, $\rho_{blood} = 998$ kg/m^3, $c_{blood} = 3500$ J/kg K,
$\mu_{blood} = 9.68 \times 10^{-4}$ kg/m sec, $Pr_{blood} = 5.628$

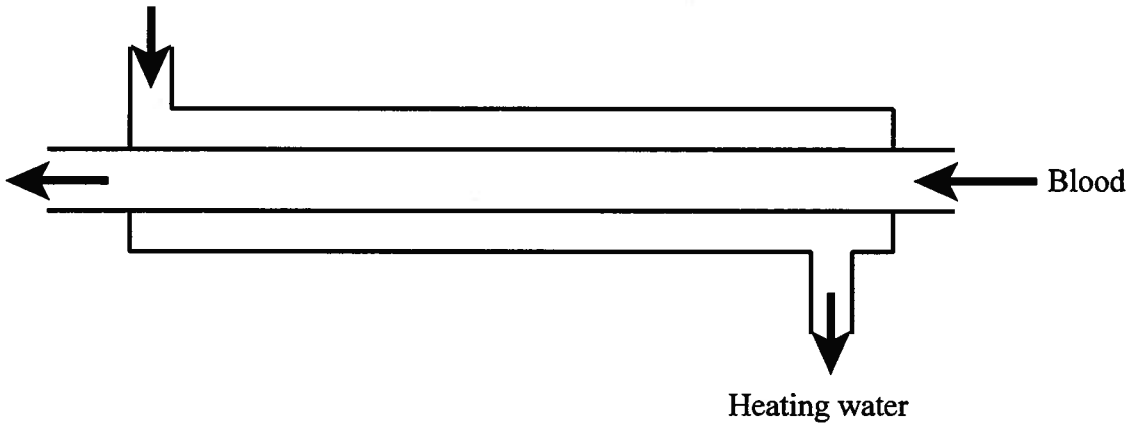

Figure 12E.2 Counterflow Heat Exchanger for Warming Blood

Solution: (a) In order to determine the overall heat transfer coefficient, U, we need to first calculate the thermal resistances on the inside wall and the outside wall of the inner tube. We first calculate the Reynolds number of the flow in the inner tube. (In the calculations that follow, we denote the properties of the blood by the subscript c since the blood is on the cold side of the heat exchanger and the properties of the water by the subscript h since the water is on the hot side of the heat exchanger.)

$$Re_c = \frac{4\dot{m}_c}{\pi D_i \mu_c} = \frac{4(0.05 \text{ kg/sec})}{\pi(0.060 \text{ m})(9.68 \times 10^{-4} \text{ kg/m sec})} = 1096$$

Thus the flow of the blood in the inner tube is laminar. This is to be expected since the laminar flow condition minimizes the mechanical damage to the formed elements of the blood, e.g., red blood cells, white blood cells, platelets, etc. The Nusselt number for this flow is given by

$$Nu_c = 3.66 + \frac{0.065\left(\frac{D_i}{L}\right)Re_c Pr_c}{1+0.04\left[\left(\frac{D_i}{L}\right)Re_c Pr_c\right]^{2/3}} = 3.66 + \frac{0.065\left(\frac{0.060\text{ m}}{4\text{ m}}\right)(1096)(5.628)}{1+0.04\left[\left(\frac{0.060\text{ m}}{4\text{ m}}\right)(1096)(5.628)\right]^{2/3}} = 6.968$$

Then the heat transfer coefficient and the corresponding thermal resistance for the cold side is

$$h_c = Nu_c\frac{k_c}{D_i} = 6.968\frac{0.602\text{ W/m K}}{0.060\text{ m}} = 69.91\text{ W/m}^2\text{ K}$$

$$R_c = \frac{1}{h_c \pi D_i L} = \frac{1}{(69.91\text{W/m}^2\text{ K})\pi(0.060\text{ m})(4\text{ m})} = 0.0190\text{ K/W}$$

For the hot side of the heat exchanger, the Reynolds number depends upon the hydraulic diameter, D_h, which for an annulus becomes $D_h = D_o - D_i = 0.020$ m. Then

$$Re_h = \frac{4\dot{m}_h}{\pi D_h \mu_h} = \frac{4(0.10\text{ kg/sec})}{\pi(0.020\text{ m})(4.92\text{ x }10^{-4}\text{ kg/m sec})} = 1.294\text{ x }10^4$$

Since this is turbulent flow in an annulus, the friction factor and the corresponding Nusselt number are given by

$$f = (0.79\ln Re_h - 1.64)^{-2} = \left[0.79\ln\left(1.294\text{ x }10^4\right) - 1.64\right]^{-2} = 0.029$$

$$Nu_h = \frac{\frac{f}{8}(Re_h - 1000)Pr_h}{1+12.7\sqrt{\frac{f}{8}}\left(Pr_h^{2/3}-1\right)}\left[0.86\left(\frac{D_i}{D_o}\right)^{-0.16}\right]$$

$$Nu_h = \frac{\frac{0.029}{8}\left[\left(1.294\text{ x }10^4\right)-1000\right](3.153)}{1+12.7\sqrt{\frac{0.029}{8}}\left[(3.153)^{2/3}-1\right]}\left[0.86\left(\frac{0.060}{0.080}\right)^{-0.16}\right]$$

$$Nu_h = 65.937$$

Then the heat transfer coefficient and corresponding thermal resistance on the hot side of the heat exchanger are

$$h_h = Nu_h\frac{k_h}{D_h} = 65.937\frac{0.652\text{ W/m K}}{0.020\text{ m}} = 2149.6\text{ W/m}^2\text{ K}$$

$$R_h = \frac{1}{h_h \pi D_i L} = \frac{1}{(2149.6\text{ W/m}^2\text{ K})\pi(0.060\text{ m})(4\text{ m})} = 6.170\text{ x }10^{-4}\text{ K/W}$$

Then the overall thermal conductance and the overall heat transfer coefficient are given by

$$UA = (R_c + R_h)^{-1} = \left(0.0190\text{ K/W} + 6.170\text{ x }10^{-4}\text{ K/W}\right)^{-1} = 51.051\text{ W/K}$$

$$U_i = \frac{UA}{\pi D_i L} = \frac{51.051\text{ W/K}}{\pi(0.060\text{ m})(4\text{ m})} = 67.708\text{ W/m}^2\text{ K}$$

(b) The temperature of the blood leaving the heat exchanger can be determined from the heat exchanger effectiveness. Then

$$NTU = \frac{UA}{C_{min}} = \frac{UA}{C_c} = \frac{51.051 \text{ W/K}}{(0.050 \text{ kg/sec})(3500 \text{ J/kg K})} = 0.292$$

$$\varepsilon = \frac{1-\exp\left[-NTU\left(1-C^*\right)\right]}{1-C^*\exp\left[-NTU\left(1-C^*\right)\right]} = \frac{1-\exp\left[-(0.292)(1-0.419)\right]}{1-0.419\exp\left[-(0.292)(1-0.419)\right]} = 0.241$$

$$T_{c,out} = T_{c,in} + \varepsilon\left(T_{h,in} - T_{c,in}\right) = 18 \text{ C} + (0.241)(90 \text{ C} - 18 \text{ C}) = 35.368 \text{ C}$$

This temperature is a reasonable value since blood components are damaged by temperatures in excess of 42 C. Also blood at this temperature will restore the patient to normal body temperature, 37 C, in a short time.

Example 12E.3: The exhaust stream from a large industrial furnace contains a significant amount of energy that we wish to recover by placing a "waste heat" recovery heat exchanger in the stack as shown in Figure 12E.3. The heat exchanger consists of a tube bank arranged in a square array of 95 thin-walled tubes in a staggered configuration with 5 rows of ten tubes each alternating with 5 rows of 9 tubes each. Each tube has a diameter of D = 25 mm and a length of L = 4 m. The transverse pitch of the array is S_T = 50 mm and the longitudinal pitch is S_L = 50 mm. Pressurized water at a flow rate of $\dot{m}_w$ = 0.025 kg/sec makes a single pass through each of the tubes, and the exhaust gas has a uniform upstream velocity of ϑ_g = 5 m/sec. The stack has a diameter of 4 m. Assume that the water flow is fully developed. The inlet temperature of the water for each tube is $T_{water,in}$ = 300 K and the exhaust gas enters the tube array at a uniform temperature of $T_{gas,in}$ = 800 K.

(a) Calculate the overall heat transfer coefficient, U, for this cross-flow configuration.

(b) Calculate the outlet temperatures of the two fluid streams, $T_{water,out}$ and $T_{gas,out}$.

For the water: $\rho_{water} = 10^3$ kg/m^3, c_{water} = 4180 J/kg K, $\mu_{water} = 855 \times 10^{-6}$ kg/m sec,
k_{water} = 0.612 W/m K, Pr_{water} = 5.84

For the exhaust gas: ρ_{gas} = 0.435 kg/m^3, $(c_P)_{gas}$ = 1099 J/kg K, $\mu_{gas} = 36.98 \times 10^{-6}$ kg/m sec,
$k_{gas} = 57.3 \times 10^{-3}$ W/m K, Pr_{gas} = 0.709

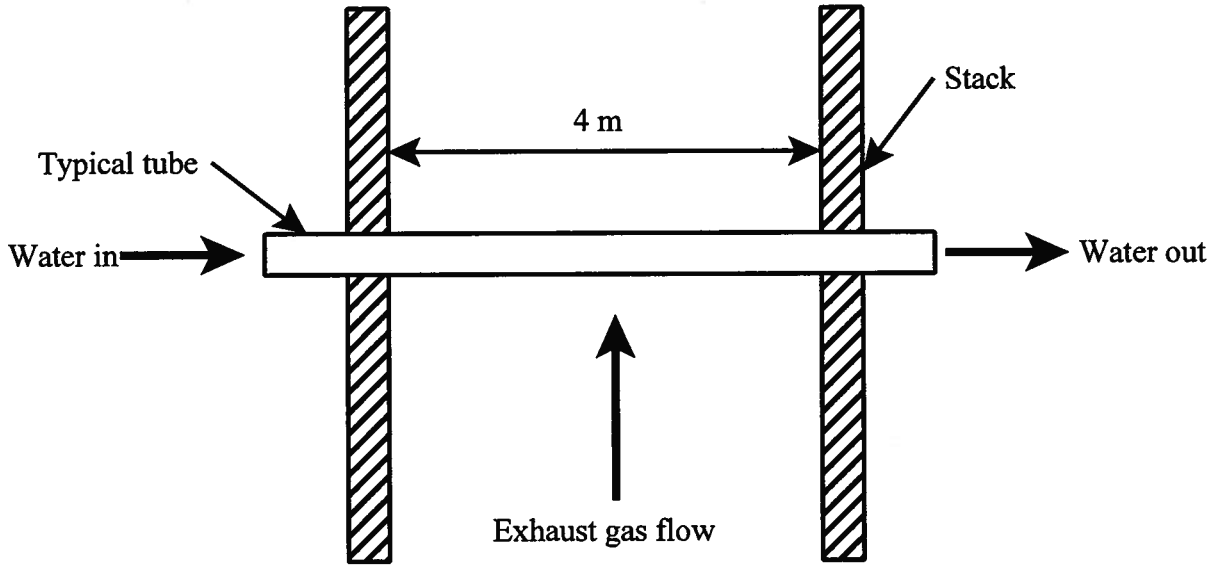

Figure 12E.3 Waste Heat Recovery System

Solution: (a) We first calculate the Reynolds number of the water flow.

$$Re_w = \frac{4\dot{m}_w}{\pi D \mu_w} = \frac{4(0.025 \text{ kg/sec})}{\pi(0.025 \text{ m})(8.55 \text{ x } 10^{-4} \text{ kg/m sec})} = 1489$$

Clearly, the water flow is laminar. Then from correlation number 2 of Table 11.5

$$Nu_w = 3.66 + \frac{0.065\left(\frac{D}{L}\right)Re_w Pr_w}{1+0.04\left[\left(\frac{D}{L}\right)Re_w Pr_w\right]^{2/3}} = 3.66 + \frac{0.065\left(\frac{0.025 \text{ m}}{4 \text{ m}}\right)(1489)(5.84)}{1+0.04\left[\left(\frac{0.025 \text{ m}}{4 \text{ m}}\right)(1489)(5.84)\right]^{2/3}} = 5.905$$

Then the convective heat transfer coefficient for the water flow is

$$h_{c,w} = Nu_w \frac{k_w}{D} = 5.905 \frac{0.612 \text{ W/m K}}{0.025 \text{ m}} = 144.547 \text{ W/m}^2 \text{ K}$$

For the flow over the tube array, we need to calculate the average velocity in the array. Then from correlation number 18 of Table 11.5

$$\bar{\vartheta} = \vartheta_g \frac{S_T}{S_T - \left(\frac{\pi}{4}\right)D} = (5 \text{ m/sec}) \frac{0.050 \text{ m}}{0.050 \text{ m} - \left(\frac{\pi}{4}\right)(0.025 \text{ m})} = 8.233 \text{ m/sec}$$

Then the Reynolds number for the exhaust gas flow is

$$Re_g = \frac{\bar{\vartheta} D \rho_g}{\mu_g} = \frac{(8.233 \text{ m/sec})(0.025 \text{ m})(0.435 \text{ kg/m}^3)}{36.98 \text{ x } 10^{-6} \text{ kg/m sec}} = 2421$$

Then from correlation number 6 of Table 11.5

$$\overline{Nu}_D^{1} = 0.3 + \frac{0.62 Re_g^{1/2} Pr_g^{1/3}}{\left[1+\left(\frac{0.4}{Pr_g}\right)^{2/3}\right]^{1/4}} = 0.3 + \frac{0.62(2421)^{1/2}(0.709)^{1/3}}{\left[1+\left(\frac{0.4}{0.709}\right)^{2/3}\right]^{1/4}} = 24.184$$

For the array, correlation 18 gives

$$P_L = \frac{S_L}{D} = \frac{0.050 \text{ m}}{0.025 \text{ m}} = 2$$

$$\Phi_{staggered} = 1 + \frac{2}{3P_L} = 1 + \frac{2}{3 \cdot 2} = 1.333$$

$$\overline{Nu}_D^{10+} = \Phi_{staggered} \overline{Nu}_D^{1} = (1.133)(24.184) = 32.246$$

Then the heat transfer coefficient for convection on the outside of a single tube in the array is

$$h_{c,g} = \overline{Nu}_D^{10+} \frac{k_g}{D} = 32.246 \frac{0.0573 \text{ W/m K}}{0.025 \text{ m}} = 73.908$$

Then the thermal resistances on the inside and the outside of a tube are, respectively

$$R_i = \frac{1}{h_{c,w} \pi D L} = \frac{1}{(144.547 \text{ W/m}^2 \text{ K})\pi(0.025 \text{ m})(4 \text{ m})} = 0.022 \text{ K/W}$$

$$R_o = \frac{1}{h_{c,g} \pi D L} = \frac{1}{(73.908 \text{ W/m}^2 \text{ K})\pi(0.025 \text{ m})(4 \text{ m})} = 0.043 \text{ K/W}$$

Then the thermal conductance of an individual tube in the array is

$$UA = \left(R_i + R_a\right)^{-1} = \left(0.022\ \text{K/W} + 0.043\ \text{K/W}\right)^{-1} = 15.363\ \text{W/K}$$

The temperature of the water at the outlet from a tube is

$$T_{w,out} = T_{g,in} - \left(T_{g,in} - T_{w,in}\right)\exp\left(-\frac{UA}{\dot{m}_w c_w}\right)$$

Where does this come from?

$$T_{w,out} = 800\ \text{K} - (800\ \text{K} - 300\ \text{K})\exp\left(-\frac{15.363\ \text{W/K}}{(0.025\ \text{kg/sec})(4180\ \text{J/kg K})}\right)$$

$$T_{w,out} = 368.361\ \text{K}$$

Then the capacity rates for the water and the exhaust gases are

$$\dot{m}_g = \rho_g \pi \frac{L^2}{4} \vartheta_g = \left(0.435\ \text{kg/m}^3\right)\pi \frac{(4\ \text{m})^2}{4}(5\ \text{m/sec}) = 27.332\ \text{kg/sec}$$

$$C_g = \dot{m}_g c_{Pg} = (27.332\ \text{kg/sec})(1099\ \text{J/kg K}) = 3.004\ \text{x}\ 10^4\ \text{W/K} = C_{max}$$

$$C_w = \dot{m}_w c_w N_{tubes} = (0.025\ \text{kg/sec})(4180\ \text{J/kg K})(95\ \text{tubes}) = 9928\ \text{W/K} = C_{min}$$

$$C^* = \frac{C_{min}}{C_{max}} = \frac{9928\ \text{W/K}}{3.004\ \text{x}\ 10^4\ \text{W/K}} = 0.331$$

Then the heat exchanger effectiveness is

$$\varepsilon = \frac{C_w\left(T_{b,out} - T_{b,in}\right)}{C_{min}\left(T_{g,in} - T_{b,in}\right)} = \frac{(9928\ \text{W/K})(368.361\ \text{K} - 300\ \text{K})}{(9928\ \text{W/K})(800\ \text{K} - 300\ \text{K})} = 0.137$$

Then the correlation number 9 of Table 12.1 gives for crossflow with the fluid with C_{max} mixed

$$NTU = -\ln\left[1 + \frac{1}{C^*}\ln\left(1 - \varepsilon C^*\right)\right] = -\ln\left[1 + \frac{1}{0.331}\ln\left(1 - (0.137)(0.331)\right)\right] = 0.151$$

$$UA_{array} = NTU \cdot C_{min} = (0.151)(9928\ \text{W/K}) = 1496\ \text{W/K}$$

$$A_{array} = \pi D L N_{tubes} = \pi(0.025\ \text{m})(4\ \text{m})(95\ \text{tubes}) = 29.845\ \text{m}^2$$

$$U = \frac{UA_{array}}{A_{array}} = \frac{1496\ \text{W/K}}{29.845\ \text{m}^2} = 50.133\ \text{W/m}^2\ \text{K}$$

(b) The result for the outlet temperature of the water is given above

$$T_{w,out} = 368.361\ \text{K}$$

For the outlet temperature of the exhaust gas, we make use of the heat exchanger effectiveness, viz.

$$\dot{Q}_{max} = C_{min}\left(T_{g,in} - T_{w,in}\right) = (9928\ \text{W/K})(800\ \text{K} - 300\ \text{K}) = 4.964\ \text{x}\ 10^6\ \text{W}$$

$$T_{g,out} = T_{g,in} - \frac{\varepsilon \dot{Q}_{max}}{C_g} = 800\ \text{K} - \frac{0.137\left(4.964\ \text{x}\ 10^6\ \text{W}\right)}{3.004\ \text{x}\ 10^4\ \text{W/K}} = 777.407\ \text{K}$$

Then the "waste heat recovered" can be determined from either the water side or the exhaust gas side, viz.

$$\dot{Q}_g = \dot{m}_g c_{Pg}\left(T_{g,out} - T_{g,in}\right) = (27.332\ \text{kg/sec})(1099\ \text{J/kg K})(777.407\ \text{K} - 800\ \text{K})$$

$$\dot{Q}_g = -6.787\ \text{x}\ 10^5\ \text{W}$$

$$\dot{Q}_w = \dot{m}_w c_w N_{tubes}\left(T_{w,out} - T_{w,in}\right) = (0.025 \text{ kg/sec})(4180 \text{ J/kg K})(95 \text{ tubes})(368.361 \text{ K} - 300 \text{ K})$$

$$\dot{Q}_w = 6.787 \text{ x } 10^5 \text{ W}$$

Example 12E.4: Saturated steam from a manufacturing process is to be condensed at a pressure of $P_{sat} = 10^5$ N/m^2 in a shell-and-tube heat exchanger with one shell pass and two tube passes. Saturated H_2O vapor enters the shell with an enthalpy of $h_g = 2674.9$ kJ/kg and saturated liquid H_2O leaves with an enthalpy of $h_f = 417.50$ kJ/kg. The saturation temperature of the steam is $T_{sat} = 99.61$ C.

Cooling water enters the tubes at $T_{w,in} = 14$ C with an average velocity of $\vartheta_{ave} = 3.5$ m/sec. The tubes are thin-walled and made of copper with a diameter of $D = 14$ mm and a length of $L = 0.5$ m per pass. The convective heat transfer coefficient for condensation on the outer surface of the tubes is $h_o = 21{,}800$ W/m^2 K.

(a) Determine the bulk mean outlet temperature of the water.

(b) Find the number of tubes/pass required to condense steam at the rate of 2.3 kg/sec.

Solution: (a) We first need to establish the relevant fluid properties. Clearly the temperature of the water inside the tubes is going to increase as a result of the heat transfer process. Then the average temperature of the water is higher than the inlet temperature. Let us assume that the average bulk mean temperature of the water is 20 C. Then

$$\rho_{20} = 998.21 \text{ kg/m}^3 \quad c_{20} = 4184.1 \text{ J/kg K} \quad k_{20} = 0.59846 \text{ W/m K} \quad Pr_{20} = 7.0026$$

$$\mu_{20} = 1.0016 \text{ x } 10^{-3} \text{ kg/m sec}$$

We begin by calculating the Reynolds number and the associated friction factor for the flow of the water inside the tubes.

$$Re_w = \frac{\vartheta_w D \rho_{20}}{\mu_{20}} = \frac{(3.5 \text{ m/sec})(0.014 \text{ m})\left(998.21 \text{ kg/m}^3\right)}{1.0016 \text{ x } 10^{-3} \text{ kg/m sec}} = 4.883 \text{ x } 10^4$$

$$f = \left(0.79 \ln \text{Re}_w - 1.64\right)^{-2} = \left[0.79 \ln\left(4.883 \text{ x } 10^4\right) - 1.64\right]^{-2} = 0.021$$

Then the Nusselt number and the resulting heat transfer coefficient for the flow inside the tubes becomes

$$Nu_w = \frac{\frac{f}{8}(Re_w - 1000)Pr_{20}}{1 + 12.7\sqrt{\frac{f}{8}}\left(Pr_{20}^{2/3} - 1\right)} = \frac{\frac{0.021}{8}\left[\left(4.883 \text{ x } 10^4\right) - 1000\right](7.0026)}{1 + 12.7\sqrt{\frac{0.021}{8}}\left[(7.0026)^{2/3} - 1\right]} = 322.713$$

$$h_{c,i} = Nu_w \frac{k_{20}}{D} = 322.713 \frac{0.59846 \text{ W/m K}}{0.014 \text{ m}} = 1.3795 \text{ x } 10^4 \text{ W/m}^2 \text{ K}$$

Then the thermal resistances for heat transfer across the tube wall are

$$R_i = \frac{1}{h_{c,i}\pi D(2 \cdot L)} = \frac{1}{\left(1.3795 \text{ x } 10^4 \text{ W/m}^2 \text{ K}\right)\pi(0.014 \text{ m})(1 \text{ m})} = 1.648 \text{ x} 10^{-3} \text{ K/W}$$

$$R_o = \frac{1}{h_o \pi D(2 \cdot L)} = \frac{1}{\left(2.1800 \text{ x } 10^4 \text{ W/m}^2 \text{ K}\right)\pi(0.014 \text{ m})(1 \text{ m})} = 1.0430 \text{ x } 10^{-3} \text{ K/W}$$

Then the thermal conductance of a single tube is

$$UA = \left(R_i + R_o\right)^{-1} = \left(1.6482 \text{ x } 10^{-3} \text{ K/W} + 1.0430 \text{ x } 10^{-3} \text{ K/W}\right)^{-1} = 371.594 \text{ W/K}$$

We now calculate the number of transfer units for a single tube.

$$\dot{m}_w = \rho_{20}\pi\frac{D^2}{4}\vartheta_w = \left(998.21\ \text{kg/m}^3\right)\pi\frac{(0.014\ \text{m})^2}{4}(3.5\ \text{m/sec}) = 0.5378\ \text{kg/sec}$$

$$C_w = \dot{m}_w c_{20} = (0.5378\ \text{kg/sec})(4184.1\ \text{J/kg K}) = 2250.3\ \text{W/K}$$

$$NTU = \frac{UA}{C_w} = \frac{371.594\ \text{W/K}}{2250.3\ \text{W/K}} = 0.1651$$

Then the heat exchanger effectiveness can be determined from correlation number 1 of Table 12.1, viz.

$$\varepsilon = 1 - \exp(-NTU) = 1 - \exp(-0.1651) = 0.1522$$

The outlet temperature of the water inside the tubes can be calculated from the effectiveness.

$$T_{w,out} = T_{w,in} + \varepsilon\left(T_{h.in} - T_{w,in}\right) = 14\ \text{C} + (0.1522)(99.61\ \text{C} - 14\ \text{C}) = 27.88\ \text{C}$$

(b) The number of tubes required can be determined from the load on the condenser and the heat transfer rate per tube.

$$\dot{Q}_{steam} = \dot{m}_{steam}\left(h_g - h_f\right) = (2.3\ \text{kg/sec})\left[\left(2674.1\ \text{x}\ 10^3\ \text{J/kg}\right) - (417.50\ \text{J/kg})\right]$$

$$\dot{Q}_{steam} = 5.1920\ \text{x}\ 10^6\ \text{W}$$

$$\dot{Q}_{tube} = \dot{m}_w c_w\left(T_{w,out} - T_{w,in}\right) = (0.5378\ \text{kg/sec})(4184.1\ \text{J/kg K})(27.88\ \text{C} - 14\ \text{C})$$

$$\dot{Q}_{tube} = 2.8982\ \text{x}\ 10^4\ \text{W/tube}$$

$$N_{tubes} = \frac{\dot{Q}_{steam}}{\dot{Q}_{tube}} = \frac{5.1920\ \text{x}\ 10^6\ \text{W}}{2.8982\ \text{x}\ 10^4\ \text{W/tube}} = 179.15\ \text{tubes} \approx 180\ \text{tubes}$$

Problems

12.1 As shown in the sketch below, the feedwater heater for the boiler of a large power plant supplies water at the mass flow rate of $\dot{m}_{fw} = 10^4$ kg/hr at a pressure of $P_{t2} = 10^6$ N/m^2 and a temperature of $T_{t2} = 65$ C. The inlet temperature of the feedwater to the heater is $T_{t1} = 20$ C. The heater heat exchanger design is of the shell and tube type with a single shell pass and two tube passes in which saturated vapor H_2O at a pressure of $P_{s1} = 1.4 \times 10^5$ N/m^2 enters the shell side and exits as saturated liquid at the same pressure. The overall heat transfer coefficient is $U =$ 2000 W/m^2 K.

(a) What is the temperature of the fluid exiting the shell? Sketch the axial temperature distribution in the heat exchanger.

(b) Using the NTU method, determine the required heat transfer area.

(c) What is the rate of condensation $\dot{m}_{condensation}$ for the H_2O on the shell side?

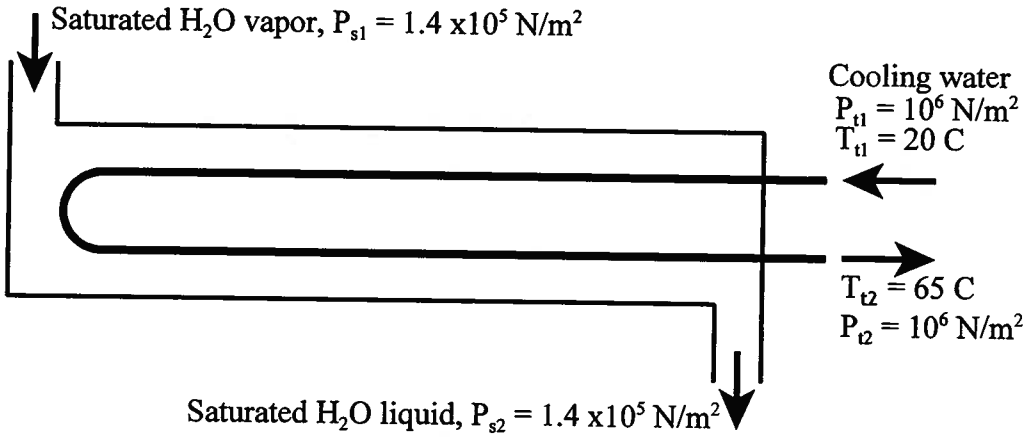

12.2 Our objective here is to design a counterflow heat exchanger to function as the primary heat exchanger in a small combined-cycle power plant. The high temperature stream is air which enters the heat exchanger at a temperature of $T_{h,i} = 600$ C at a mass flow rate of 84 kg/sec. The low temperature stream is H_2O at a pressure of 35 x 10^6 N/m^2 which enters the heat exchanger at a temperature of $T_{c,i} = 20$ C with a mass flow rate of 15 kg/sec and flows through the heat exchanger at nearly constant pressure. At this pressure, H_2O will not experience a phase change at any temperature.

As shown schematically in the sketch below, the heat exchanger is a shell and tube design in which the counterflow configuration is achieved by bending the tubes in a U-shape inside the shell. A longitudinal baffle in the horizontal plane forces the flow on the shell side to follow a counterflow path. However, vertical baffles on each side of the horizontal baffle force the flow on the shell side to pass back and forth over the tubes in a cross-flow pattern as the fluid moves along the axis of the heat exchanger. The net result is a well-mixed fluid on the shell side traveling in a counterflow direction. The convective heat transfer coefficient for the air on the shell side is $h_o = 10{,}000$ W/m^2 K. The tube side of the heat exchanger consists of 20 brass tubes ($k_{brass} = 111$ W/m K) each with a total length of 140 meters with I.D. = 19.3 mm and O.D. = 25.4 mm.

(a) Determine the Reynolds number for the H_2O flowing in the tubes.

(b) Using the appropriate correlation equation, determine the heat transfer coefficient h_i for the H_2O inside the tubes.

(c) Calculate the overall heat transfer coefficient U for a single tube based on the outside area of the tube for the shell and tube geometry.

(d) For this counterflow configuration, use the ε-*NTU* method to determine to determine $T_{air,out}$ and $T_{water,out}$.

(e) Calculate the pressure drop for the H_2O flowing inside the tubes.

For air: ρ_{air} = 0.56 kg/m^3, c_P = 1003 J/kg K, k_{air} = 0.04598 W/m K, μ_{air} = 30.497 x 10^{-6} kg/m sec
For H_2O: ρ_{water} = 565.15 kg/m^3, c_{water} = 5814.3 J/kg K, k_{water} = 0.3673 W/m K, μ_{water} = 5.2168 x 10^{-4} kg/m sec

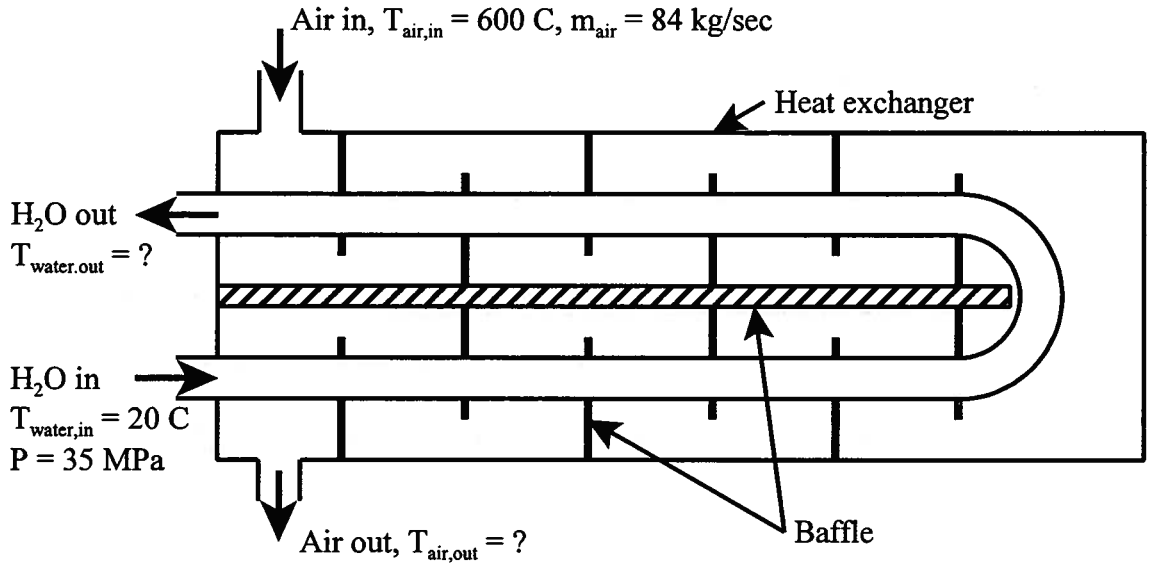

12.3 The lubricating oil for a large industrial gas turbine is to be cooled in a simple counterflow double-pipe heat exchanger. The mass flow rate of cooling water through the inner tube is $\dot{m}_c$ = 0.2 kg/sec, while the mass flow rate of oil through the outer annulus is $\dot{m}_h$ = 0.4 kg/sec. The oil and water enter at temperatures of 60 C and 30 C, respectively. The inside diameter of the tube is 25 mm and the inside diameter of the outer annulus is 45 mm. The outlet temperature of the oil is 40 C. Neglect the thermal resistance of the tube wall.

(a) Using the *NTU* method, calculate the length *L* of the heat exchanger.

(b) Calculate the pressure drops for both oil and water.

For the water: ρ_{water} = 10^3 kg/m^3, c_{water} = 4180 J/kg K, μ_{water} = 855 x 10^{-6} kg/m sec,
k_{water} = 0.612 W/m K, Pr_{water} = 5.84
For the oil: ρ_{oil} = 871 kg/m^3, c_{oil} = 1990 J/kg K, μ_{oil} = 1370 x 10^{-4} kg/m sec,
k_{oil} = 0.1425 W/m K, Pr_{oil} = 1910

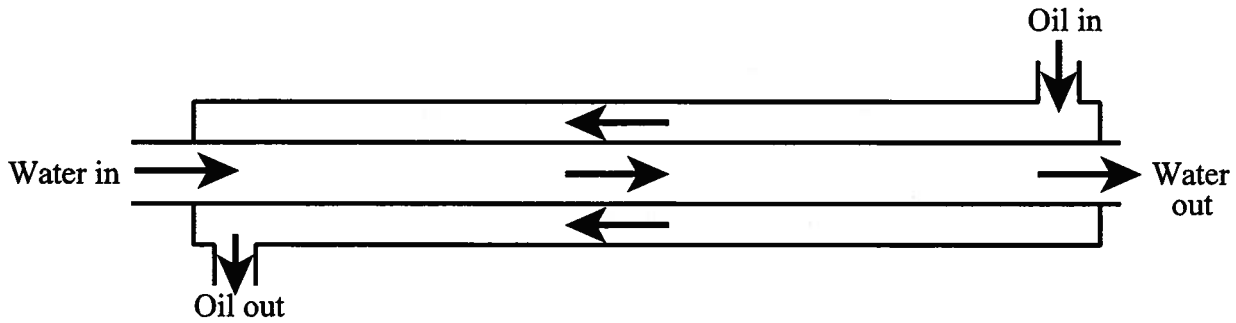

12.4 As shown in Figure 12P.4, a counterflow heat exchanger for a hydrogen cryogenic refrigeration system is to be fabricated by welding two stainless steel tubes together. The system has a balanced flow with the capacity rates identical in the two tubes. The mass flow rate in each tube is $\dot{m} = 6.0 \times 10^{-6}$ kg/sec. The cold stream enters at a temperature of $T_{c,in} = 11$ K and must be heated to a temperature of $T_{c,out} = 300$ K. The hot stream enters at a temperature of $T_{h,in} = 310$ K. The average pressure on the cold side is $P_c = 667$ N/m^2, and the allowable pressure drop on the cold side is $\Delta P_c = 80$ N/m^2. The wall thickness of the tubes is $t = 1$ mm and the tube walls can be modeled as fins of the appropriate length. That is, think of the joined tube walls as forming fins with the base of the fin at the weld and the insulated tip at the midpoint of the circumference opposite the weld in each tube. Thus, the two tubes together form two pairs of fins, each pair consisting of one hot fin and one cold fin joined at the base. Since the temperature difference between the two tubes is nearly constant along the length, the configuration can be modeled as one of constant wall heat flux. At these low flow rates, the flow can be modeled as laminar. (You will need to confirm this.) Determine the tube diameter and the tube length.

For hydrogen at 150 K: $\rho = 0.16156$ kg/m^3, $c_P = 12.60 \times 10^3$ J/kg K, $\mu = 56.0 \times 10^{-7}$ kg/m sec, $k = 0.101$ W/m K, $Pr = 0.699$

HINT: This situation requires a bit of modeling. You may have to iterate to find the final solution.

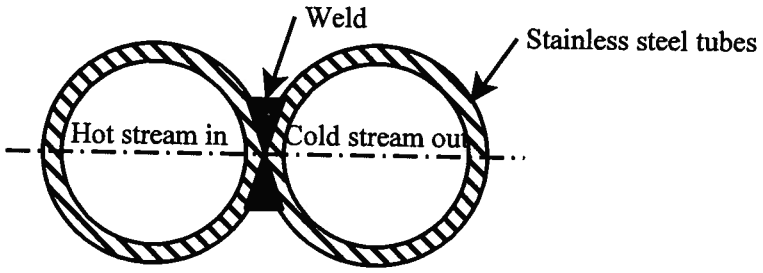

Figure 12P.4

12.5 A combustion apparatus discharges a gas stream at a temperature of 950 K and a mass flow rate of 5.4 kg/sec. As shown in Figure 12P.5, the gas stream is to be passed through a heat exchanger that will provide the high temperature heat transfer to a reversible cycle that operates with the atmosphere as the low temperature heat reservoir. Two heat exchanger designs are being considered, and both produce the same exit temperature for the combustion gases.

In the first design, the heat exchanger consists of 100 identical thin-walled, smooth tubes with an I.D. of $D = 50$ mm and a length of $L = 9.5$ m with a constant wall temperature maintained at $T_s = 400$ K by means of an evaporating fluid that serves as the working fluid for the reversible cycle.

In the second design, by some clever means, the working fluid for the cycle (now a liquid different from the first case) enters the heat exchanger at 400 K and leaves at a temperature such that the temperature difference is the same at both ends of the heat exchanger.

The properties of the combustion gases are: $c_P = 1057$ J/kg K, $\rho = 0.683$ kg/m^3, $k = 0.0383$ W/m K, $\mu = 25.1 \times 10^{-6}$ kg/m sec

For the first heat exchanger design, calculate the following:

(a) the heat transfer coefficient, h_c, for the combustion gases

(b) the exit temperature and pressure drop for the combustion gases

For the two heat exchanger designs, sketch the axial temperature profiles and calculate the following:

(c) the rate of heat transfer from the combustion gases to the cycle

(d) the power output from the cycle

Answer the following questions:

(e) Are the two answers for part (c) the same? Why?

(f) Are the two answers for part (d) the same? Why?

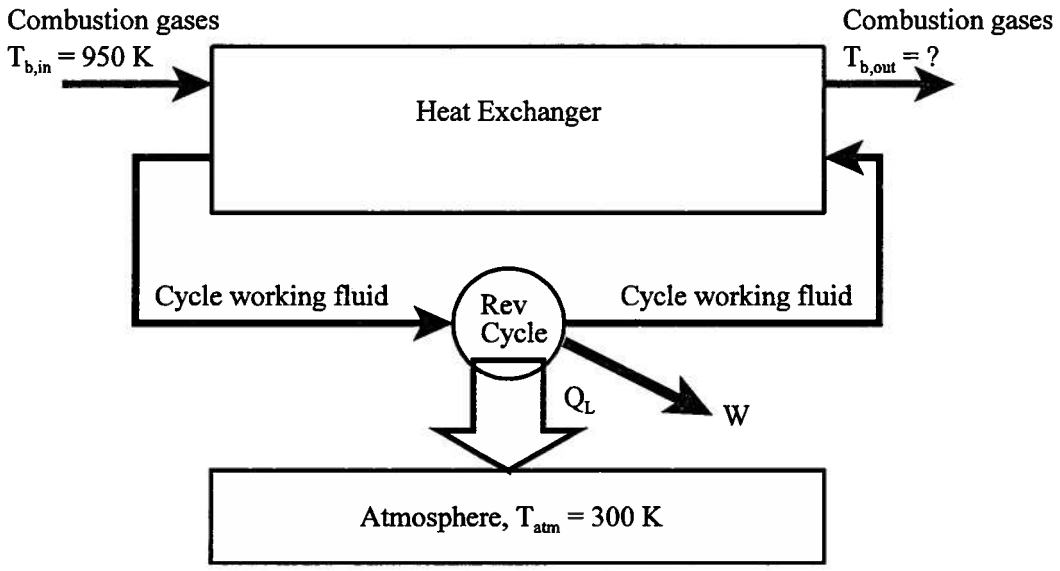

Figure 12P.5

12.6 A particular manufacturing process requires air at a temperature of 340 K. The available air supply is at a temperature of 280 K. Your job as a thermal systems design engineer is to design a heater to raise the temperature of the air to the required value. The basic design is to wrap an electric heating tape around a section of tubing in the air supply piping. Existing piping limits your design to a thin-walled, smooth stainless steel tube with an I.D. of D = 25.4 mm and a length of L = 0.5 m. Process requirements set the average air velocity at 30 m/sec with air of the following properties (assumed constant): c_P = 1005 J/kg K, ρ = 1.141 kg/m^3, k = 0.0274 W/m K, μ = 18.87 x 10^{-6} kg/m sec. For fully developed hydrodynamics and heat transfer the appropriate correlations for turbulent flow would be:

$$f = (0.790 \ln Re_D - 1.64)^{-2} \text{ and}$$

$$(Nu_D)_{L=\infty} = \frac{\left(\frac{f}{8}\right)(Re_D - 1000)\,\mathrm{Pr}}{1 + 12.7\sqrt{\frac{f}{8}}\left(\mathrm{Pr}^{\frac{2}{3}} - 1\right)}$$

with

$$f = 0.021 \quad \text{and} \quad (Nu_D)_{L=\infty} = 97.154$$

As an astute young engineer, you are concerned that 0.5 m may be too short a distance to achieve

fully developed hydrodynamics and heat transfer. A search of the literature turns up the following reference: *Convective Heat and Mass Transfer*, 2nd Edition, by William M. Kays and Michael E. Crawford, McGraw-Hill, 1980. Chapter 13 of this text offers the following data for the configuration at hand (although not quite in this form):

x^+	0	$1x10^{-4}$	$2x10^{-4}$	$3x10^{-4}$	$4x10^{-4}$	$5x10^{-4}$	$6x10^{-4}$	$8x10^{-4}$	$9x10^{-4}$	10^{-3}
Nu_x	164.721	126.282	115.422	110.099	106.848	104.637	103.041	100.922	100.2	99.628
x^+	$1.5x10^{-3}$	$2x10^{-3}$	$2.5x10^{-3}$	$3x10^{-3}$	$3.5x10^{-3}$	$4x10^{-3}$	$4.5x10^{-3}$	$5x10^{-3}$	$6x10^{-3}$	10^{-2}
Nu_x	98.059	97.493	97.281	97.202	97.172	97.161	97.156	97.155	97.154	97.154

$$x^+ = \frac{2(x/D)}{RePr} \quad \text{and} \quad Nu_x = Nu(x^+)$$

(a) Calculate the Reynolds number and confirm that the flow is indeed turbulent.

(b) Calculate the heater power requirements for steady flow operation.

(c) Plot the tube wall temperature and the bulk mean temperature of the fluid as a function of x, the distance from the start of the heated section in the direction of flow.

(d) Calculate the log mean temperature difference and U for this configuration.

(e) What is the thermal entry length (definition is arbitrary; you specify) for this flow?

(f) How does this information help you in the design process? Could $L = 0.25$ m?

12.7 A tractor-trailer (an 18 wheeler) has a gross vehicle mass of 4×10^4 kg. It presents a frontal area of 4 m in height and 2.6 m in width and is traveling up a 10 percent grade (10 m rise/100 m horizontal distance) at a steady speed of 100 km/hr. It has a standard fairing with a drag coefficient of $C_D = 0.96$. The rolling resistance of this vehicle at this speed is known to be 125 HP. At this level of performance, the engine dissipates an additional amount of power in the coolant in the cooling system equal to 60 percent of the shaft power output. The heat exchanger in the cooling system (a.k.a. "the radiator") is a crossflow design with both fluids unmixed. The coolant flows in the tubes with atmospheric air flowing over the outside of the tubes. The coolant enters the heat exchanger at a temperature of $T_{h,in} = 100$ C and exits at a temperature of $T_{h,out} = 75$ C. The air enters at a temperature of $T_{c,in} = 37$ C and exits at some unknown temperature. The heat exchanger effectiveness is $\varepsilon = 0.8$.

(a) Determine the necessary value of UA for this heat exchanger.

(b) Determine the bulk mean temperature of the air leaving "the radiator."

Note: An approximate expression used by many authors for the heat exchanger effectiveness of the crossflow heat exchanger with both fluids unmixed as in this application is given by

$$\varepsilon = 1 - \exp\left\{\frac{NTU^{0.22}}{C_{min}/C_{max}}\left[\exp\left(-\frac{C_{min}}{C_{max}}NTU^{0.78}\right) - 1\right]\right\}$$

For the coolant: $\rho_{coolant} = 1048.1$ kg/m^3, $c_{coolant} = 3650$ J/kg K
For the air: $\rho_{air} = 1.141$ kg/m^3, $(c_P)_{air} = 1005$ J/kg K

12.8 A local company, Lytron, the Total Thermal Solutions Company™, makes many different types of heat exchangers. One of their product lines is cold plates. A particular model, CP-15, is shown in Figure 12P.8 taken from their website http://www.lytron.com/about/index.htm . The intended application is to mount dissipative electronic packages on the smooth top surface so that the cold plate can maintain the proper operating temperature of the electronics.

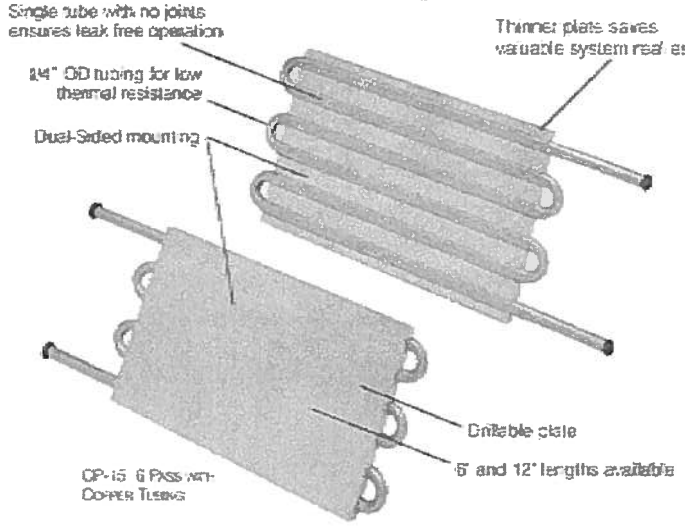

Figure 12P.8 Lytron Cold Plate, Model CP-15

The device consists of an aluminum casting (k_{Al} = 169.2 W/m K) with a length of copper tubing shaped as shown and pressed into groves cast into the underside of the aluminum casting. The casting is 6 inches long (15.24 cm) and 3.75 inches (9.35 cm) wide. The thickness of the casting is 0.3125 inches (7.938 mm). The copper tubing has an outside diameter of 0.25 inches (D_o = 6.350 mm) and an inside diameter of D_i = 4.826 mm. The length of copper tubing in contact with the aluminum casting is L = 0.9144 m. The copper tubing is pressed into the bottom of the aluminum casting so that there is a thin layer, t = 1.5875 mm, of aluminum between the smooth top surface of the aluminum casting and the outer wall of the copper tubing.

Lytron reports the thermal performance of the device based on actual heat transfer test results. Performance is expressed in terms of a thermal resistance $\Re$ defined such that

$$\Re = \frac{\left(T_s - T_{b,in}\right)}{\dot{Q}}$$

where T_s is the temperature of the top surface of the aluminum casting and $T_{b,in}$ is the bulk-mean temperature of the cooling water at entrance to the smooth copper tubing. For the model CP-15, T_s = 65 C and $T_{b,in}$ = 20 C so that $\Re$ = 0.0182 C/W with a water flow rate of $\dot{V}$ = 0.75 gallons/min ($\dot{V}$ = 4.731 x 10^{-5} m^3/sec).

One deficiency of the design arises from the fact that by pressing the copper tubing into the casting without using a low thermal resistance bonding material between the two mating surfaces, there is a thermal contact resistance between the copper tubing and the casting. This results in a reduction in thermal performance of the device. Our objective here is to determine the thermal contact resistance to see if it might be worth altering the assembly process to reduce this contact resistance and thereby increase the thermal performance of the device.

For water at 20 C: ρ = 998.21 kg/m^3, c = 4184.1 J/kg K, k = 0.59846 W/m K,

μ = 1.0016 x 10^{-3} kg/m K, Pr = 7.0026

(a) For the performance data given, determine the heat transfer rate $\dot{Q}_P$ for the present configuration of the CP-15 cold plate.

(b) Calculate the Reynolds number for the flow inside the copper tube.

(c) Calculate the convective heat transfer coefficient, h_i, for the inside of the smooth copper tube.

(d) For a thermal resistance model that has the conduction thermal resistance of the thin layer of aluminum t in series with the convection thermal resistance of the inside of the copper tube, calculate the temperature of the cooling water at exit from the copper tube.

(e) From the first law, calculate the rate of heat transfer $\dot{Q}_F$ to the cooling water. Note that this result ignores the contact resistance and, hence, represents the maximum possible rate of heat transfer.

(f) From the value of $\dot{Q}_P$ and the first law, calculate the temperature of the cooling water at the outlet of the copper tube during the heat transfer test. Use this bulk-mean outlet temperature to determine the value of ΔT_{LM} during the test.

(g) Consider a thermal resistance circuit consisting of the thin aluminum layer of thickness t, the contact resistance between the outside of the copper tube and the aluminum casting, and the convection resistance inside the copper tube. Formulate an expression for the overall thermal conductance UA of this circuit. Use this expression together with the values of ΔT_{LM} and $\dot{Q}_P$ to estimate the value of the contact resistance. Compare the magnitude of this thermal resistance with that associated with the convection process inside the copper tube.

(h) Plot the thermal performance of the device that could be realized by reducing the contact resistance by 20, 40, 60, and 80 percent. Show $\dot{Q}_F$ on the plot.

12.9 Direct immersion cooling is a technology used in the thermal control of electronic components. In this technology, the electronic chips in a system, such as a supercomputer, are immersed directly in a dielectric heat exchange fluid such as Fluorinert manufactured by 3M Co. The Fluorinert absorbs energy and entropy directly from the electronics package usually, by boiling heat transfer or spray cooling, and is then circulated to a heat exchanger where it gives up this energy and entropy to cooling water.

The following is excerpted from an article by Robert E. Simons, an expert in direct immersion cooling:
(*cf.* http://www.electronics-cooling.com/Resources/EC_Articles/MAY96/may96_04.htm)

"An example of a large scale forced convection fluorocarbon cooling system is provided by the CRAY-2 supercomputer [5]. As shown schematically in Figure 5 [Figure 12P.9a], stacks of electronic module assemblies were cooled by a forced flow of FC-77 in parallel across each module assembly. Each module assembly consisted of 8 printed circuit boards on which were mounted arrays of single chip carriers. A total flow rate of 70 gpm [$\mathcal{V} = 4.416 \times 10^{-3}$ m^3/sec] was used to cool 14 stacks containing 24 module assemblies each. The power dissipated by a module assembly was reported to be 600 to 700 watts. Coolant was supplied to the electronics frame by two separate frames containing the required pumps and water-cooled heat exchangers to reject the total system heat load to customer supplied chilled water."

Reference 5 of Simons article:
5. Danielson, R.D., Krajewski, N., and Brost, J., *Cooling a Superfast Computer*, Electronic Packaging and Production, pp. 44-45, July 1986.

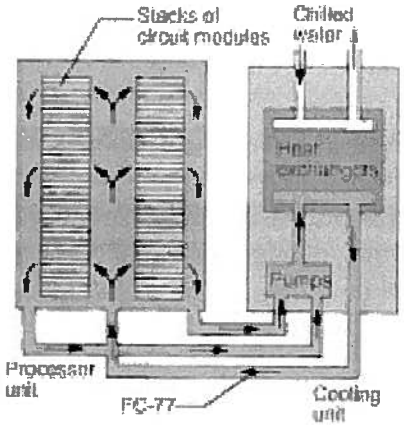

Figure 12P.9a: CRAY-2 liquid immersion cooling system

For FC-77: $\rho = 1780$ kg/m^3, $c = 1100$ J/kg K, $k = 0.063$ W/m K, $\mu = 1.3 \times 10^{-3}$ kg/m sec
For water: $\rho = 999.25$ kg/m^3, $c = 4189.6$ J/kg K, $k = 0.58753$ W/m K, $\mu = 1.1683 \times 10^{-3}$ kg/m sec

(a) Calculate C_h. If the inlet temperature of the FC-77 to the stacks is $T_{h,out} = 20$ C, calculate the required outlet temperature from the stacks, $T_{h,in}$.(Note: Temperatures are labeled referenced to the heat exchanger, not the stacks.)

(b) The heat exchanger of choice is a shell and tube exchanger in which each tube makes two shell passes (down the length of the shell and back) and the cooling water makes one shell pass as shown in Figure 12P.9b. There are 88 thin-walled tubes each with diameter $D = 8$ mm. Chilled cooling water enters the heat exchanger at $T_{c,in} = 10$ C and exits at $T_{c,out} = 18$ C. The heat transfer coefficient on the water side is $h_c = 1.094 \times 10^4$ W/m^2 K. Calculate C_c and C_{min}.

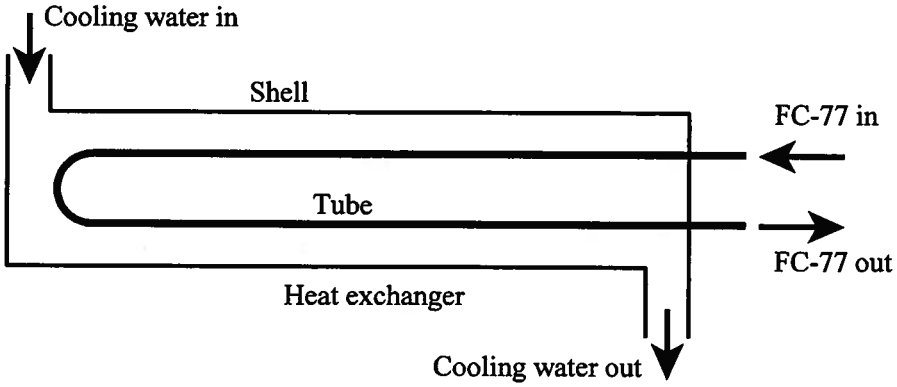

Figure 12P.9b Shell and Tube Heat Exchanger Schematic

(d) Calculate ε and NTU.
(e) Calculate UA and UA/tube.
(f) Calculate UA/L for a single tube. Calculate the length of each tube.

Chapter 13

Thermodynamic Properties of the Pure Substance Model

13.1 Introduction

In developing the first and second laws of thermodynamics in the preceding chapters, we have used simple models to represent the thermodynamic behavior of a system. The constitutive relations for the equilibrium properties of these models embody the essential elements of thermodynamic behavior and serve to illustrate the use of the laws of thermodynamics. Unfortunately, because of their simplicity, these special models are incapable of representing certain significant aspects of thermodynamic behavior. Accordingly, in this chapter, we consider the constitutive relations for the more complex *simple system* model. By definition, a *simple system* is a thermodynamic system without significant effects from the following phenomena:

(1) Surface forces from capillarity and surface tension.
(2) Forces due to gravitational, electric, and magnetic fields.
(3) Shear stresses resulting from the distortion of solids.
(4) Bulk motion.

In keeping with our simplified approach, the simple system model is still an idealization of thermodynamic behavior. In the model, the state of stress is hydrostatic everywhere and all body forces due to external force fields are taken to be insignificant. The state of stress is hydrostatic if the force per unit area acting on a test plane is independent of the orientation of the plane at each point within the system. A solid under uniform three-dimensional compression or tension will not have shear stresses. This classification may seem highly restrictive since these phenomena are present in so many physical situations; however, experience shows that the simple system represents the significant coupled thermodynamic behavior of many systems. The most significant characteristic of the simple system model is that the pressure is uniform and hydrostatic at equilibrium and all reversible work transfer is given by $W = \int P\, dV$. Here P is the uniform pressure of the system and V is the volume of the system. When no chemical reactions are involved, the simple system model becomes the pure substance model. The definition of a *pure substance* is:

> A pure substance is a simple system which is uniform and invariable in chemical composition.

Further, the internal energy, U, of the pure substance can be changed *reversibly* only by heat transfer or by work transfer associated with the uniform pressure of the system and the displacement of the system boundary, that is, the reversible work transfer is given by the integral $\int P\, dV$. This restriction on the *reversible* work transfer requires that bulk motion, gravity, surface tension, solid shear stresses, electric fields, and magnetic fields all have an insignificant influence on the thermodynamic equilibrium properties of the pure substance. With all of these influences eliminated, the requirement for mechanical equilibrium is that the pressure is uniform throughout the system and that the force on the boundary of the system is directly related to this uniform pressure. In addition, the requirement for thermal equilibrium is that the temperature is uniform throughout the system. In some cases the influence of bulk velocity and gravity are included;

however, the energies associated with these effects are considered to be uncoupled from the internal energy, U, in the manner described in Chapter 4. Each of these effects, which are ignored for the pure substance, represent reversible methods of work transfer in addition to $\int P\,dV$, and thus would add to the complexity of the interactions between the system and the environment. The incompressible fluid model and the ideal gas model that we introduced previously are both special cases of the pure substance. In particular, the incompressible fluid model is, in effect, the degenerate case of the pure substance in which the volume is constant and no reversible work transfer is possible. In the more general case, the pure substance describes the properties of a chemically pure material in the gaseous, liquid, and solid forms, or any combination of the three. In addition, the pure substance describes the properties of a mixture of gases if no liquefaction or solidification takes place. For example, air may be modeled as a pure substance in the gaseous state; however, if some of the air condenses into liquid, the liquid will be richer in oxygen than the remaining gas. This condition then violates the requirement that a pure substance be uniform in composition. The pure substance model also describes the properties of a solution if no solidification or vaporization takes place. A solution of salt in water may be modeled as a pure substance, but if freezing takes place, the solid will be of lower salt concentration than the remaining liquid, again violating the uniform composition requirement. On the other hand, pure H_2O may be modeled as a pure substance in the solid, liquid, or gaseous form or any combination of the three.

13.2 Independent Properties of the Pure Substance Model

In establishing the independent properties of the pure substance model, we make use of a fundamental principle, the *state principle.* This principle, although deduced by empirical means, is based upon the observation of so many thermodynamic systems that it can be regarded as a fundamental law of thermodynamics. The *state principle*, stated rather simply, is:

> Any two independent properties are sufficient to establish a stable equilibrium thermodynamic state of a simple system. For each identifiable departure from the requirements for a simple system, one additional independent property is necessary.

Note that the state principle is restricted to *stable* equilibrium thermodynamic states rather than to equilibrium states in general. Stable equilibrium states are those equilibrium states for which a finite change of state can occur only if there is some corresponding change of state in the environment. Since most equilibrium thermodynamic states are of this type, this restriction poses no serious limitations from a thermodynamic point of view. The significance of the state principle itself is contained in the fact that it establishes in a formal way the minimum number of properties necessary to describe the state of a thermodynamic system.

A convenient, but not necessarily unique, interpretation of this principle is that there is one independent property associated with each reversible mode of energy interaction. The only reversible mode of work transfer for the simple system is given (in differential form) by $P\,dV$. In this case, the volume V can be regarded as the independent property describing the work transfer. Similarly, we have seen in Section 7.7 that the reversible heat transfer for any system is given (in differential form) by $T\,dS$. For the heat transfer interaction, the entropy assumes the role of the independent property. Thus for the pure substance, the simple system of interest there, the first law of thermodynamics in differential form becomes

$$dU = TdS - PdV \tag{13.1}$$

The first law of thermodynamics guarantees that the internal energy is a property; consequently, equation (13.1) has an integrated form

$$U = U(S,V) \tag{13.2}$$

Equation (13.2) expresses the internal energy of a pure substance in terms of the two independent properties entropy and volume. According to the state principle, only two independent properties are necessary to describe the equilibrium state of a pure substance; equations (13.1) and (13.2) are just such a description. Therefore, equations (13.1) and (13.2) relate equilibrium states and are valid regardless of whether the interactions experienced by the pure substance during the change of state are reversible or irreversible. Another way of interpreting this result is to note that any one equilibrium state of a pure substance can be reached (in principle) from any other equilibrium state by a series of reversible processes. In this manner, we can establish for every equilibrium state the value of any property (relative to some datum state). Equation (13.1) is an interrelation among the system properties that must be satisfied for every infinitesimal change of state. From the change of state itself, we cannot establish whether reversible or irreversible interactions were involved; however, equation (13.1) is true regardless of the nature of the interactions. The important point is that the product $T\,dS$ represents the heat transfer and the product $P\,dV$ represents the work transfer only for reversible interactions. In the case of irreversible interactions, the product $T\,dS$ exceeds the actual heat transfer by the same amount that $P\,dV$ exceeds the actual work transfer.

Although we have just established the entropy and volume as a set of independent properties for a pure substance, we are by no means restricted to this set. That is, any other two properties of the pure substance could be selected as the independent set provided, of course, that the two properties really are independent. For example, in the case of the ideal gas, the temperature and the pressure form a set of independent properties, but the temperature and the internal energy do not. This is because the internal energy is a function of only temperature for the ideal gas. As we shall see later, the temperature and the pressure are not a set of independent properties for the states of a pure substance in which the vapor and liquid forms coexist in equilibrium.

Although equation (13.1) has been discussed in the context of a pure substance, the equation is equally applicable to any simple system. In fact, equation (13.1) occupies a rather special position in thermodynamics, and for this reason, some authors refer to it as the *canonical relation.* The significance of equation (13.1) lies in the fact that there is a great deal of information that can be obtained from it. For example, if we mechanically restrain a simple system so that its volume is fixed, it cannot experience any reversible work transfer. If we further isolate it so that it cannot experience any heat transfer or irreversible work transfer, either internal or external, its entropy is fixed. Under these circumstances, equation (13.1) can be shown to indicate that the internal energy is an extremum. In more advanced treatments, stability considerations reveal that this extremum is a minimum. The very foundation of thermodynamics is that, under these imposed restrictions, the system will achieve a unique state as determined by the entropy and volume, and that the internal energy of this state is smaller than all other states of the system with the same entropy and volume. By definition, this state is the stable equilibrium state and all other states with the same entropy and volume are non-equilibrium states. Thus, equation (13.1) is not necessarily satisfied for non-equilibrium states. Equation (13.1) serves to distinguish between *extensive* properties and *intensive* properties. The extensive properties energy, entropy, and volume are directly proportional to the mass present in the system. For example, if a pure substance system at equilibrium is subdivided into two subsystems the value

of each extensive property of the subsystem will be less than the value for the total system. The value of an extensive property for a composite system is the sum of the values for that property for the subsystems.

The intensive properties, temperature and pressure, in equation (13.1) are the properties with values that are not changed by subdivision of the system. The intensive properties can be defined at a point within a system and have values which are uniform for the equilibrium states of a pure substance. For non-equilibrium states the intensive properties may be non uniform or may be undefined. Another noteworthy feature of the canonical relation is that the thermodynamic properties appear as pairs which are said to be canonically conjugate. For example, the temperature and the entropy are canonically conjugate properties that completely describe a reversible heat transfer interaction while the pressure and the volume are canonically conjugate properties that completely describe a reversible work transfer interaction. Note that in each case the pair of properties consists of one intensive property such as the temperature or pressure, and one extensive property such as the entropy or volume. We can generalize these observations to the case of closed systems which cannot be classed as simple. For each independent, reversible interaction capable of altering the internal energy of the system, there is a pair of properties, one intensive and one extensive, that completely describes the interaction. The set of independent extensive properties associated with these interactions represents the minimum number of properties necessary to specify the stable equilibrium state of a given system. Since all of the properties affect the internal energy, they are coupled. The simplest form for the constitutive relations are then equations that express each of the intensive properties in terms of all of the independent extensive properties. For each aspect of system behavior that is uncoupled, there is not only an independent property that is used to describe the interaction but also a separate stored energy form. Note that the conditions of equilibrium require that the intensive property associated with each possible reversible interaction be uniform. When two systems (or subsystems) are not in a state of mutual equilibrium, the difference in their intensive properties serves as the driving potential for the interaction which will bring the systems to a state of mutual equilibrium characterized by equal intensive properties.

Equation (13.1) can also be expressed in terms of specific properties, which are the extensive properties per unit mass of the system. If we divide equation (13.1) by the mass of the system we have

$$d\left(\frac{U}{m}\right) = Td\left(\frac{S}{m}\right) - Pd\left(\frac{V}{m}\right) \tag{13.3}$$

or

$$du = Tds - Pdv \tag{13.4}$$

Here u is the specific internal energy, U/m, s is the specific entropy, S/m, and v is the specific volume V/m. As we will discuss in detail later, the specific properties may be multivalued in a pure substance in an equilibrium state, when more than one of the liquid, gaseous or solid forms are present.

13.3 Equilibrium Liquid-Vapor States

One of the primary reasons for formulating the pure substance model is to be able to model the thermodynamic behavior of a substance that can experience changes between the solid, liquid, and gaseous forms. None of the other system models that we have considered previously is capable of experiencing such a transformation.

The transformation between gaseous and liquid forms has a high degree of thermodynamic coupling and is thus quite important in thermo-mechanical energy conversion. It is natural to begin the discussion of the pure substance with the consideration of liquid-vapor equilibrium states.

As a consequence of the state principle, any two independent properties are sufficient to fix the state of a pure substance. Thus, an expression relating any other property to the two independent properties selected for the characterization of the state constitutes a valid constitutive relation, or equation of state. It is often convenient to graphically represent the equilibrium states of a pure substance in terms of this constitutive relation. Accordingly, we most commonly use a two-dimensional representation in which one independent property appears as the abscissa, the dependent property appears as the ordinate, and the other independent property appears as a parameter indexing the family of curves. The constitutive relations for pure substances are usually determined by actual measurements of the properties. The pressure-volume-temperature relation is very common since these properties are most easily measured. There is no one universal constitutive relation which will model all of the pure substances. However, with a few notable exceptions, the equilibrium thermodynamic behavior of most pure substances is qualitatively the same. Thus, to illustrate the general thermodynamic behavior of a pure substance (in a qualitative fashion, of course) it is sufficient to perform a hypothetical experiment on a hypothetical pure substance. To this end, consider the following situation in which a unit of mass of a pure substance, for example a gas, is enclosed in a piston-cylinder apparatus and the whole configuration is in thermal equilibrium with a heat reservoir at the temperature T (*cf.* Figure 13.1).

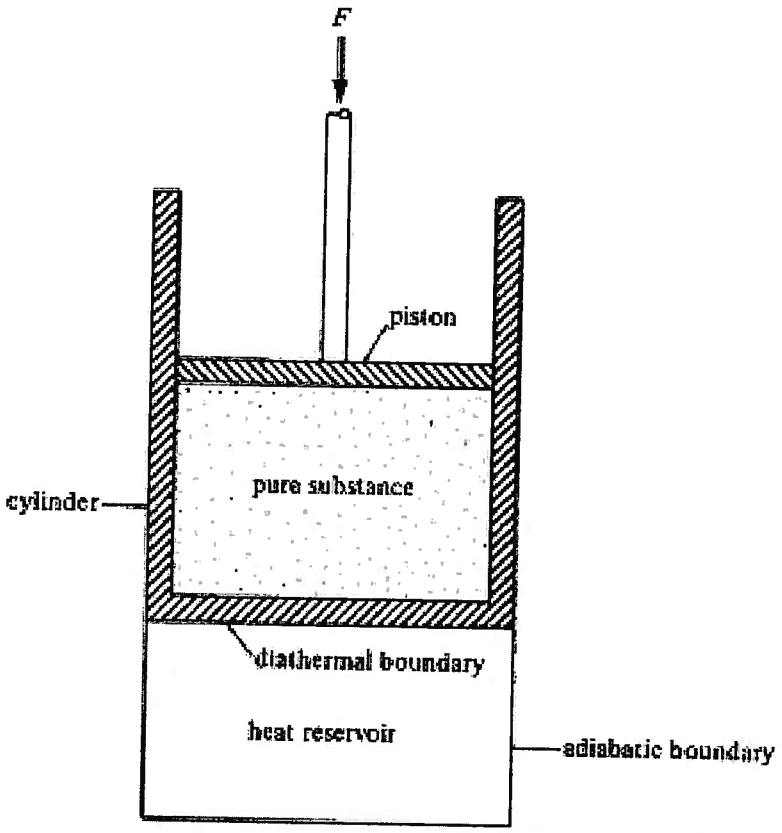

Figure 13.1 Piston-cylinder Apparatus for Isothermal Processes in the Pure Substance Model

We now proceed to compress the pure substance by decreasing the volume. If we perform this compression at a sufficiently slow rate, the temperature of the substance will remain fixed at T_1 since the system is in thermal communication with the heat reservoir. As we might expect, the pressure of the substance will increase during this compression process. To be more specific, if we decrease the volume from v_a to v_b (Figure 13.2) while the temperature remains constant at T_1, the pressure increases accordingly from P_a to P_b. In fact, if we were to monitor the pressure constantly during this process *a-b,* we would find that it would trace out the path *a-b* shown on Figure 13.2. Clearly, because of the manner in which we are performing the experiment, the states which lie on the line *a-b* are equilibrium states.

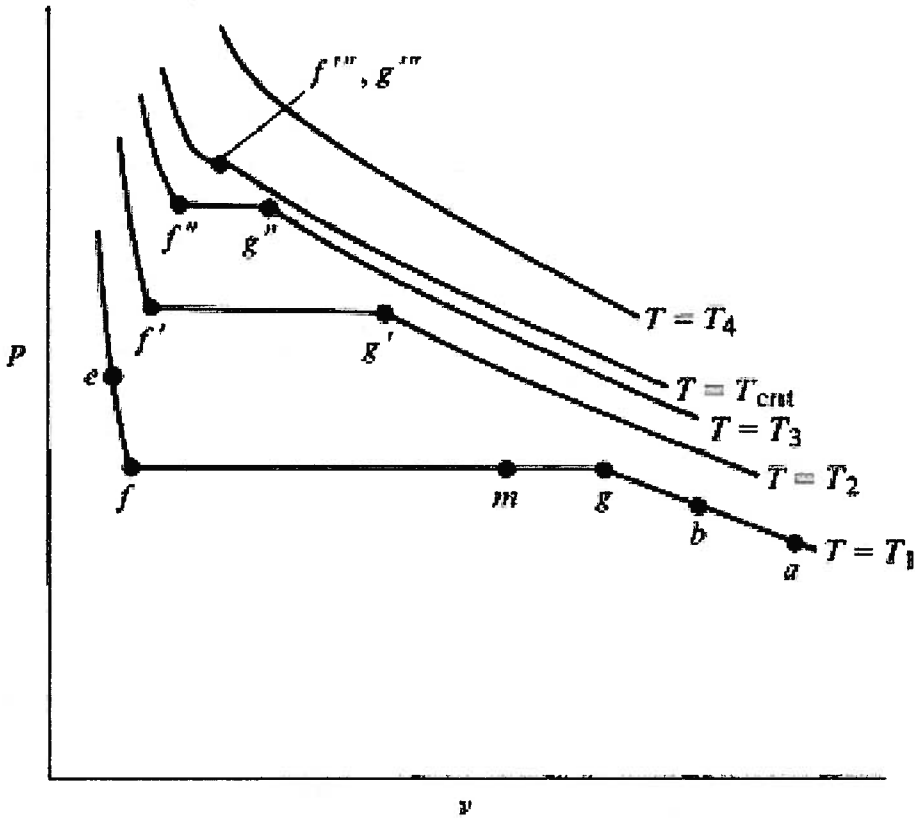

Figure 13.2 Isotherms for the Pure Substance Model

If we were to continue to decrease the volume in the manner described above, we would continue to see a corresponding increase in pressure until the state g is reached. Suddenly, when this state is reached, the pressure ceases to increase with a further decrease in volume. In fact, if we were to continue to decrease the volume to v_m for example, the pressure in state *m* would still be identical to that in state *g*. Obviously, something drastic happened when the system reached state *g*. Closer inspection of the apparatus reveals that when the system reached state *g*, the substance was present only in the gaseous form. For all volumes less than v_g, the liquid form of the pure substance was present. Further, as the system progressed from state *g* to state *m*, the amount of the liquid form increased while the amount of gas, or vapor as it is often called, decreased.

If we examine the liquid form more closely, we find that the state of the liquid is homogeneous, that is, uniform throughout its extent. Similar inspection of the vapor form reveals that it, too, is homogeneous in state. The conditions of thermal and mechanical equilibrium

require that the temperatures and the pressures for these two forms be identical. However, in spite of the homogeneity that exists within the two forms, the only properties that are the same for these two forms of the pure substance are the temperature and pressure. All of the specific properties, such as entropy, energy, and volume, have different values for the two forms, but each of these properties is uniform throughout the extent of the particular form. Thus, the liquid and the vapor forms have the same intensive state, that is, temperature and pressure, but different thermodynamic states. In order to better describe this situation, J. Willard Gibbs introduced the concept *of phase* which he defined in the following manner:

> *A phase* is the collection of all macroscopic parts of the system with the same homogeneous thermodynamic state. That is, all parts of a system which have identical and uniform values for each of the specific properties as well as identical and uniform temperature and pressure are said to constitute one phase.

Thus, in state *m* described above, the liquid form and the vapor form constitute separate, distinct phases, namely, the liquid phase and the vapor phase. State *m* is said to be a *two-phase state* or *mixed state* in which the two phases are in equilibrium.

As we continue to decrease the volume of the pure substance from state *m* in the manner described previously, we find that both the pressure and temperature remain constant. All during this process, the amount of liquid present continues to increase while the amount of vapor present continues to decrease. Suddenly, when we reach state *f,* we find that the vapor has vanished. Only the liquid phase is present. If we now continue to decrease the volume of the pure substance to *ve,* for example, we find that the pressure again increases. Then, it is apparent that unlike single phase states the pressure and temperature are *not* independent properties when two phases of a pure substance exist together in equilibrium. Thus, a two-phase state can be specified only by temperature *or* pressure *and* some other property such as volume.

In proceeding from state g to state *f,* the pure substance is said to have experienced a *change in phase* or *phase transition* since only the vapor phase is present in state g while only the liquid phase is present in state f. A definite change in the specific properties is associated with this phase change which took place both at constant temperature and at constant pressure. The locus of equilibrium states traced out by the system while in thermal communication with the heat reservoir at the temperature T_1 is represented on the pressure-volume plane as a continuous line known as an *isotherm.* Notice from Figure 13.2 that at the two states *g* and *f*, the isotherm, $T = T_1$, undergoes a discontinuous change in slope. That is, between states *g* and *f*, $(\partial P/\partial v)_T = 0$ while everywhere else $(\partial P/\partial v)_T < 0$. A discontinuous change of slope of this type is characteristic of phase changes which occur at constant temperature and pressure.

If we were to perform the same experiment while the system was in thermal communication with a heat reservoir at a temperature T_2, where $T_2 > T_1$, we would observe the same general behavior. That is, the pressure would continue to increase with a decrease in volume until some state *g ′* is reached. For this state, the slope of the isotherm $T = T_2$ changes discontinuously to zero as the liquid phase appears. The pressure and temperature remain constant as the volume is decreased until the state *f ′* is reached. For this state the slope of the isotherm again changes discontinuously, this time from zero to something less than zero, as the vapor phase vanishes. From this state on, the pressure increases as the volume is decreased. Once again, the states between *g ′* and *f ′* are two phase states with liquid and vapor phases. As the volume is decreased from *v* at *g′* to *v* at *f ′* the relative amount of the liquid phase present increases from zero at *g ′* to all liquid at *f ′*. Associated with this phase change at constant pressure

and temperature is a definite change in the specific properties such as the specific volume. Of course the pressure and temperature are not independent properties during the phase change $g'-f'$. The locus of equilibrium states for the system while in communication with the heat reservoir at T_2 is shown on Figure 13.2 as the isotherm $T = T_2$.

If we were to perform this same experiment on this apparatus while it was in thermal communication with a heat reservoir at a temperature T_3, where $T_3 > T_2 > T_1$, the system would trace out the isotherm $T = T_3$ as shown in Figure 13.2. Notice that this isotherm possesses the same general characteristics as the previous two isotherms, $T = T_1$ and $T = T_2$. However, in comparing the three isotherms $T = T_1$, $T = T_2$, and $T = T_3$, we note the occurrence of a rather curious phenomenon. The change in specific volume associated with the phase change at constant pressure and temperature decreases as the temperature at which the experiment is executed increases. Changes in all other specific properties behave in a similar manner. Apparently, the liquid and vapor phases are becoming more and more similar in nature as the temperature is increased. The question then arises as to whether there exists some critical temperature $T = T_c$ for which there is no difference in specific properties between the liquid and vapor phases. For such a temperature there must exist a state for which there is no distinction between the liquid and vapor phases. Such a critical temperature does indeed exist, and the *critical state,* is the state at the critical temperature for which the liquid and vapor phases are identical. In this state the isotherm $T = T_c$ undergoes an inflection with $(\partial P/\partial v)_T = 0$ and $(\partial^2 P/\partial v^2)_T = 0$ (*cf.* Figure 13.2). No other state possesses this feature. Thus, the critical state is a unique state and every pure substance is observed to possess only one.

For experiments carried out at higher temperatures, we find that the isotherms, for example $T = T_4$, $T_4 > T_c$, possess no discontinuity of slope. Everywhere $(\partial P/\partial v)_T < 0$ if $T > T_c$. Along such isotherms, sometimes called *supercritical isotherms*, the pressure increases continuously as the volume is decreased. As is shown on Figure 13.2, no liquid-vapor phase change occurs. If we again look at the collection of isotherms that we have generated in our hypothetical experiment, we note that we can form the locus of states for which the slope $(\partial P/\partial v)_T < 0$ changes discontinuously. These states, because of this change in slope, are very special states that we call *saturation states.* The saturation states are those states of the pure substance for which $(\partial P/\partial v)_T = 0$ and only one phase is present. The locus of saturated states for a typical pure substance is shown in Figure 13.3. Any saturated state for which $v < v_C$ is known as a *saturated liquid state.* On the other hand, any saturated state for which $v > v_c$ is known as a *saturated vapor state.* A change in phase from a saturated liquid state to a saturated vapor state is commonly known as *boiling, evaporation* or *vaporization.* Conversely, a change in phase from a saturated vapor state to a saturated liquid state is commonly known as *condensation* or *liquefaction.* The locus of saturated liquid states and the locus of saturated vapor states meet at the critical state since in this state the two phases, liquid and vapor, are identical. By way of convention we denote the specific properties of the saturated vapor state with the subscript g (gas) and the specific properties of the saturated liquid state by the subscript f (liquid). Thus, the specific volume of the saturated vapor state would be v_g while that of the saturated liquid state would be v_f. For a given temperature, there is at most one and only one set of liquid-vapor saturation states. Further, there is a unique pressure, known as the *saturation pressure* or *vapor pressure* that corresponds to a given temperature for which a saturated liquid state and a saturated vapor state can coexist. Conversely, to any one pressure at which the two types of saturated states can coexist there corresponds a single temperature known as the *saturation temperature, dew point temperature*, or *boiling point temperature.* There is a definite relationship between the saturation temperature and saturation pressure.

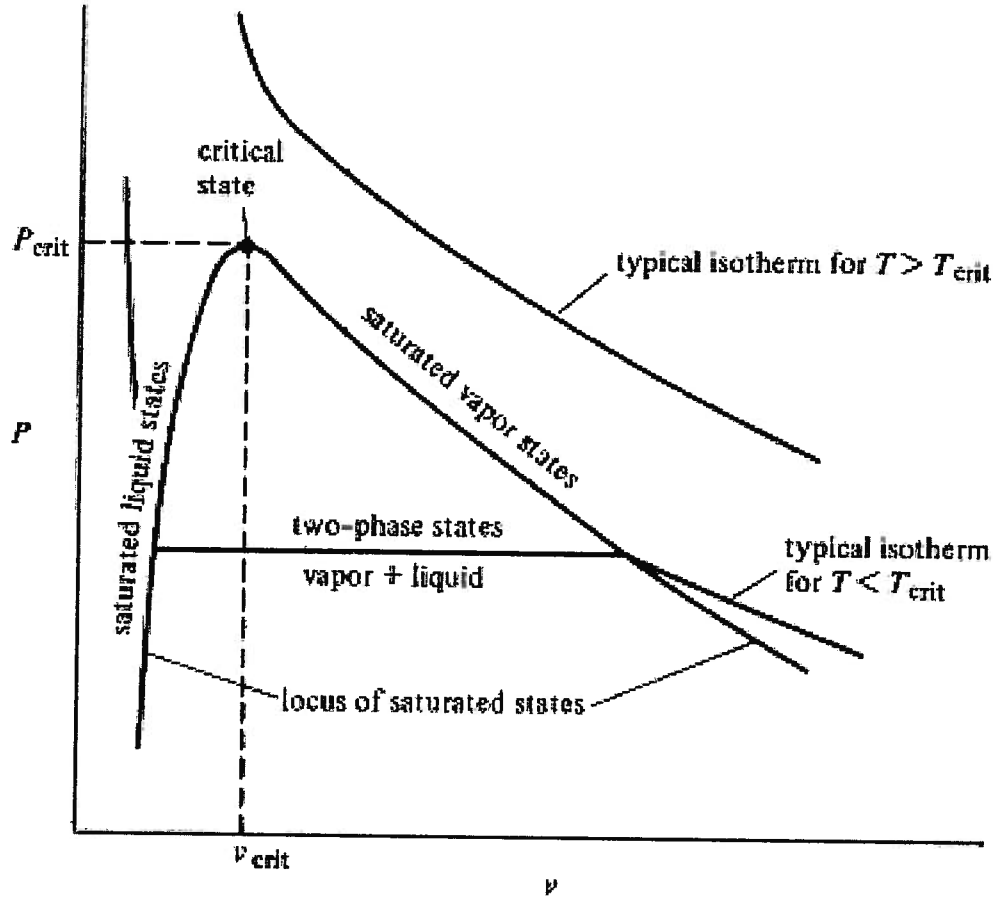

Figure 13.3 Pressure-volume Diagram of Vapor-liquid Two-phase States for Pure Substance Model

In Figure 13.3 there are other regions of interest in addition to the region of two-phase states. For example, at a given temperature, those states for which $v > v_g$ are known as *superheated vapor* states. Note that for these states the temperature is greater than the saturation temperature at the pressure of the state, hence the name superheated vapor. The difference in these two temperatures is often called the *degree of superheat.* All superheated vapor states are single phase states since they involve the vapor phase only.

Another region of interest in Figure 13.3 involves those states at a given temperature for which $v < v_f$. Note that for these single phase (liquid) states, the pressure is greater than the saturation pressure that corresponds to the temperature of the state. For this reason, states of this group are often called *compressed liquid states.* For these same states we note that the temperature of the state is lower than the saturation temperature which corresponds to the pressure of the state. Accordingly, these states are sometimes referred to as *subcooled liquid states.*

There is one other region of interest in Figure 13.3. This region involves states which are most appropriately termed supercritical states, but because of their special nature, we shall delay their discussion until later.

13.4 Critical State

We have already introduced the existence of a special state, known as the critical state,

for which the saturated liquid and vapor phases become identical. We have also pointed out that the isotherm for this state, i.e. the critical isotherm, possesses an inflection point for which both the slope and the curvature of the isotherm vanish. That is, $(\partial P/\partial v)_{T=T\text{crit}} = 0$, and $(\partial^2 P/\partial v^2)_{T=T\text{crit}} = 0$. The critical state is specified by means of its pressure, the critical pressure, and its temperature, the critical temperature. Since the common substances with critical temperatures near room temperature have rather high critical pressures (on the order of 60 MPa), the critical state is not within our everyday experience. However, because the critical state exhibits such unusual behavior, it is worthwhile to study the nature of this state and its neighbors even though such states are not encountered at moderate temperatures and pressures.

The physical behavior of a pure substance in states near the critical state can be illustrated by considering several simple thermodynamic processes. If a substance at state *a,* with specific volume v_a ($v_a > v_{crit}$) as shown in Figure 13.4, is compressed at constant temperature T ($T > T_{crit}$)

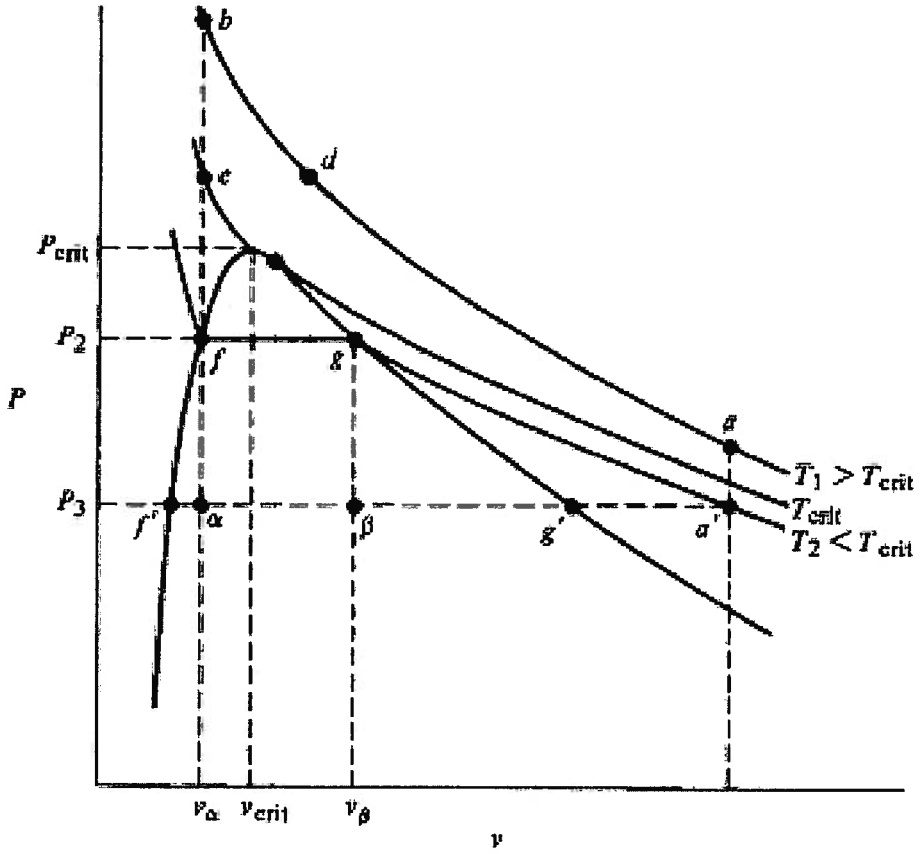

Figure 13.4 Thermodynamic Processes for the Pure Substance Model

to a specific volume v_b ($v_b < v_{crit}$), the state of the system will remain homogeneous throughout the process. One could then say that the substance had been compressed to state *b* without any condensation. On the other hand, suppose the substance in state *a* had been first cooled to state *a'*, where $v_a = v_{a'}$ and $T_{a'} = T_2 < T_{crit}$. If the substance in this state is now compressed at constant temperature, the substance will begin to condense when state *g* (saturated vapor) is reached, and will continue to condense at constant pressure until state *f* (saturated liquid) is reached. The system at state *f* may now be heated at constant volume to state *b* without passing through any two phase states. Thus, in the first process (*a* to *b*) the substance at *a* was still vapor when it reached state *b*. In the second series of processes, the substance at state *a'* condensed to liquid

before reaching the same state b. Is the substance at state b liquid or vapor? The only completely satisfactory way out of this paradox is to abandon the simple idea that every state of a given material can be uniquely classified as a solid, liquid, or vapor. In fact, at the critical point the system is entirely liquid and vapor at the same time since the distinction between liquid and vapor has vanished. It follows that any liquid can be changed to a vapor without a change of phase (i.e. passing through two-phase states) by a series of processes which take place at temperatures and pressures in excess of their critical values. In a strict sense the terms liquid and vapor can be applied only to the phases of the two-phase states. The location of a boundary between liquid and vapor in the supercritical region would be completely arbitrary.

Historically the term vapor was applied to that form of a substance which could be compressed to two-phase states while at room temperature, that is, to substances with critical temperatures above room temperature. The term permanent gases was originally applied to hydrogen, oxygen, and carbon monoxide because the behavior of these gases is such that their two-phase states cannot be reached by compression at room temperature. The critical temperature of these substances is below room temperature. Now it is common, but not universal, to use the term vapor for states with $v > v_{crit}$ and $T < T_{crit}$, the term liquid for states with $v < v_f$ and $P < P_{crit}$, and the term supercritical for states with either $P > P_{crit}$ or $T > T_{crit}$.

An additional feature of the supercritical states is illustrated by the constant pressure process d to e shown in Figure 13.4. Since the pressure is greater than the critical pressure, the constant pressure cooling from state d to e cannot reach the two-phase region and no condensation can occur. Conversely, the system at state e cannot be made to evaporate by a constant pressure heating.

Subcritical states also exhibit unusual behavior. Consider first a substance in the state α shown in Figure 13.4. The pressure in this state, P_3, is less than the saturation pressure corresponding to the saturated liquid state with the same specific volume as this state, $v < v_{crit}$. Clearly this state is a mixture of liquid and vapor phases. The properties of the liquid present are the properties characteristic of the saturated liquid at the pressure P_3 (state f'), and the properties of the vapor present are the properties characteristic of the saturated vapor at the pressure P_3 (state g'). If this system is enclosed in a rigid container and heated, the pressure and the temperature will increase while the total volume remains constant. The temperature in each state is the saturation temperature corresponding to the pressure of the two phases. Because of the increase in temperature, the liquid phase will expand and increase in specific volume along the saturated liquid line from $v_{f'}$ to v_f. In the vapor phase, the effect of the increase in pressure overshadows the effect of the increase in temperature, and the specific volume decreases from $v_{g'}$ to v_g along the saturated vapor line. Since the amount of liquid present is large relative to the amount of vapor present, the expansion of the liquid is larger than is necessary to compress vapor; consequently, the vapor condenses. By the time the pressure has reached P_2, all of the vapor has condensed and only liquid remains. Thus, we have condensed the vapor in the system by heating.

If the system at state β has an initial specific volume v such that $v > v_{crit}$, the expansion of the liquid when heated is not sufficient to compress the vapor, and thus some of the liquid must evaporate in order to increase the density of the vapor. This evaporation process continues until finally only vapor is present at state g. If the initial specific volume is such that $v = v_{crit}$, the two effects balance and the system remains in a two-phase state up to the critical point. When the experiment is carried out in a container with glass viewing ports, the approach to the critical state is easily followed by shaking the container and observing the wave action at the interface between the liquid and vapor phases. This wave motion is driven by the difference in the density

of the two phases of the pure substance; thus, as the density of the vapor approaches the density of the liquid, the wave motion becomes very slow until finally, at the critical point, the interface separating the liquid and vapor just fades away. At the critical point, the fluid usually appears to change color as it preferentially scatters light fron the liquid droplets or vapor bubbles remaining in the vapor or liquid phases. The scattering phenomenon may become so strong that the fluid appears reasonably opaque.

The critical constants of a great many pure substances have been compiled in the International Critical Tables. Every pure substance has a critical state; however, some substances decompose chemically before the critical state can be reached. On the other hand, there are some materials with critical states at temperatures and pressures which are above the available experimental range. Consequently, these critical states have never been observed experimentally.

13.5 Equilibrium Liquid-Solid and Vapor-Solid States

In Sections 13.3 and 13.4 we have described the nature of various equilibrium states of the pure substance model. The states described there were by no means inclusive since a solid phase is possible for the pure substance model. Thus, two other types of two-phase states are possible-liquid-solid two-phase states and vapor-solid two-phase states. Since these two-phase states occur at extremes in temperatures and pressures, it is difficult to represent them on the P-v plane with liquid-vapor two-phase states. Accordingly, we expand that portion of the P-v plane in the vicinity of these two-phase states. Figure 13.5 is an example of such an expansion.

In general, these states exhibit a behavior similar to the liquid-vapor two-phase states. That is, if we were to extend the isotherms as in Figure 13.5 to include the solid phase, we would find much the same behavior that we observed in the liquid-vapor region. The slope of an isotherm is less than zero everywhere except in the two-phase regions where $(\partial P/\partial v)_T = 0$. There exist saturated solid, liquid, and vapor states for which there is only one phase and $(\partial P/\partial v)_T = 0$. For all two-phase states, pressure and temperature are related so that an additional property is required to specify the state. Definite changes in the values of the specific properties are associated with a change in phase at constant temperature and pressure. From Figure 13.5 it is apparent that if the isothermal compression process producing the change in phase is carried out at sufficiently low temperature, the vapor phase will condense directly to the solid phase without ever becoming liquid. In distinct contrast to liquid-vapor two-phase states, there is no critical state within our physical experience for which the liquid and solid become indistinguishable or for which the vapor and solid become indistinguishable.

A phase change from saturated liquid to saturated solid is commonly referred to as *freezing* while the reverse change of phase is known as *melting.* (Note that the saturated liquid phase in equilibrium with the saturated solid phase is completely different from the saturated liquid phase in equilibrium with the saturated vapor phase.) A phase change from saturated vapor to saturated solid is commonly known *as frosting* while the reverse change of phase is referred to as *sublimation.* The properties that establish these states are also given special names. At a given pressure, the temperature for which the solid and liquid phases can coexist in equilibrium is known as the *melting point* or *freezing point.* The pressure at which these two phases coexist for a given temperature is called simply the *saturation pressure.* Solid and vapor phases at a given pressure can coexist in equilibrium at a temperature known as the *sublimation point* or *frost point.* For a given temperature, the pressure at which the solid and vapor phases are in equilibrium is also known as the *saturation pressure.*

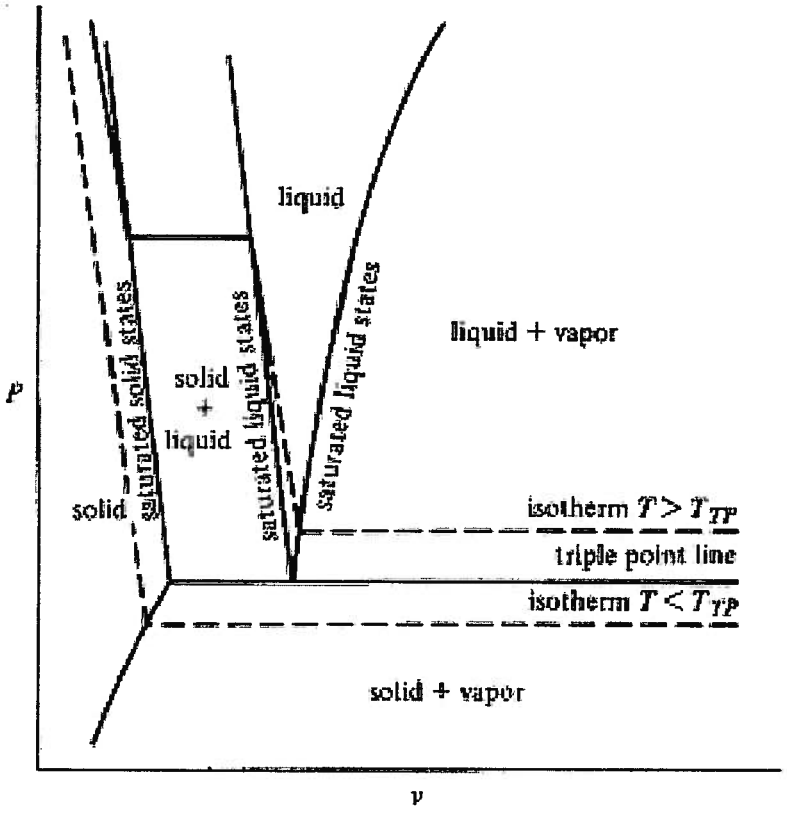

Figure 13.5 Equilibrium States in the Solid-liquid Region of the *P-v* Plane of a Pure Substance that Contracts upon Freezing

In dealing with the solid phase, we note that there are two phenomena peculiar to this phase only. The first of these is a consequence of the variety of possible molecular orientations in the solid phase. As a result, some pure substances are capable of forming more than one solid phase, usually of different crystal structure. Thermodynamically, the two-phase state formed by two solid phases in equilibrium is much the same as the two-phase states that we have already discussed. Two-phase states of this type, as well as liquid-solid two-phase states, are of major importance in metallurgical thermodynamics. The second peculiarity of the solid phase is a consequence of the nature of intermolecular forces at close molecular spacings typical of the solid phase. These forces can be of two distinctly different types which can cause the substance to expand or contract upon freezing. That is, for a freezing process that takes place at constant pressure and temperature, the change in specific volume associated with the liquid-to-solid phase change may be either positive or negative according to whether the substance expands or contracts. All other specific properties, however, decrease during the freezing process. Thus, in the neighborhood of the liquid-solid equilibrium states, the *P-v* plane would have the appearance of Figure 13.5 for a substance that contracts upon freezing or the appearance of Figure 13.6 for a substance that expands upon freezing. Figure 13.6 is difficult to visualize because it is a two-dimensional projection of a folded surface. For example, it is impossible to reach the saturated solid state from the saturated liquid state by isothermal compression along the isotherm shown in Figure 13.6. Although such behavior would at first sight seem anomalous, one of the most common substances known, water, behaves in this manner. In fact, it is because of this behavior that ice floats in liquid water.

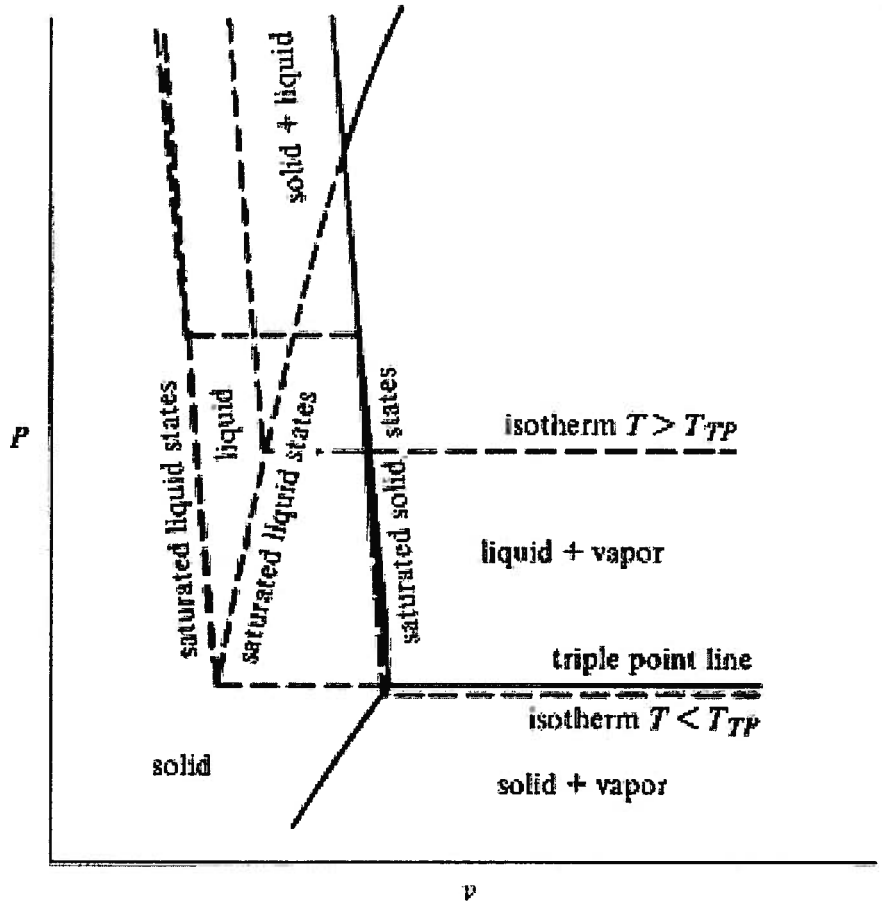

Figure 13.6 Equilibrium States in the Liquid-solid Region of the *P-v* Plane of a Pure Substance that Expands Upon Freezing

13.6 Equilibrium Solid-Liquid-Vapor States

The final combination of phases in the pure substance model is a state of mutual equilibrium among the solid phase, the liquid phase, and the vapor phase. These three-phase equilibrium states are unique in that they occur only at one temperature and one pressure for a given pure substance. This intensive state is known as the *triple point.* Thus, for the pure substance model a three-phase equilibrium state is even more restrictive than a two-phase equilibrium state because the temperature and pressure are not only related but they are fixed. Neither temperature nor pressure can be arbitrarily established if the three phases are to remain in equilibrium. For an isothermal compression process carried out at the triple point temperature, the vapor phase can condense to either the solid or the liquid.

Although three-phase states are unique with regard to their intensive state, they still possess considerable freedom with regard to their extensive states. At the triple point, each of the specific properties (e.g. the specific volume) has a unique value; however, the relative amounts of the three phases present can be varied over a relatively large range so that there is essentially an infinite number of three-phase states. For this reason, the locus of three-phase states is a line in the *P-v* plane (cf. Figures 13.5 and 13.6). This line joins the saturated solid, saturated liquid, and saturated vapor states. Note that at the triple point there is a single saturated liquid state. With the exception of helium, all real substances possess a triple point. Helium, however, cannot exist as a solid under its own vapor pressure and can only be solidified, even at temperatures

near 0 K, at pressures in excess of 25 atmospheres. At any lower pressure, helium remains liquid to the lowest temperatures attainable.

13.7 Gibbs Phase Rule

In comparing the mutual equilibrium that prevails in three-phase states, two-phase states, and single-phase states for a given pure substance, we make an interesting observation. Three-phase states can occur only at a single intensive state. That is, only at a unique combination of temperature and pressure will we find the solid, liquid, and vapor phases in equilibrium for a given substance. On the other hand, two-phase states can occur at a variety of temperatures and pressures, and we are free to arbitrarily specify either the temperature *or* the pressure. Of course, once we have specified one of these properties, the other is automatically determined since there is a unique relationship between pressure and temperature for two-phase states. Finally, we note that singit-phase states can occur at any combination of pressure and temperature. There is no restriction placed on the intensive properties of a single-phase state. Temperature and pressure are independent properties for these states.

An alternate way of making this observation is to note from Figure 13.7 that three-phase states are confined to a single point in the P-T plane, two-phase states can occur only along certain lines in the P-T plane, but single-phase states can occur anywhere in the P-T plane. Note from Figure 13.7 the two possible configurations of the intensive states of a pure substance. One for the substance that contracts upon freezing, Figure 13.7(a), and the other for the substance that expands upon freezing, Figure 13.7(b). The two differ in the sign of the slope of the line that represents the locus of solid-liquid two-phase states. The significance of the term triple point becomes immediately apparent from Figure 13.7.

J. Willard Gibbs generalized these observations of the number of independent intensive properties in the form of an empirical expression which is now known as the *Gibbs phase rule.*

$$f = 2 + c - \zeta \tag{13.5}$$

Here f is the number of thermodynamic degrees of freedom, that is, the number of intensive properties which can be arbitrarily specified, c is the number of chemically independent components, and ζ is the number of phases present. For a pure substance, c must be 1 since only one component is present. Then Gibbs phase rule reduces to

$$f = 3 - \zeta \tag{13.6}$$

Thus, if only one phase is present, $\zeta = 1$ and $f = 2$. Then the pressure and temperature can be fixed arbitrarily, and the system is said to be *divariant.* If there are two phases present, $\zeta = 2$ and $f = 1$. Then only the temperature *or* the pressure, but not both, can be fixed arbitrarily. Once one of these properties is specified, the other is automatically determined in order to preserve the equilibrium between the two phases. The system is then said to be *monovariant.* Finally, if three phases are present, $\zeta = 3$ and $f = 0$. Thus, no intensive property can be arbitrarily fixed. The intensive state is automatically specified by virtue of the equilibrium among the three phases. The system is then said to be *invariant.* Note that the three phases involved need not be solid, liquid, and vapor. There can be two or even three solid phases involved, and the Gibbs phase rule will still be valid.

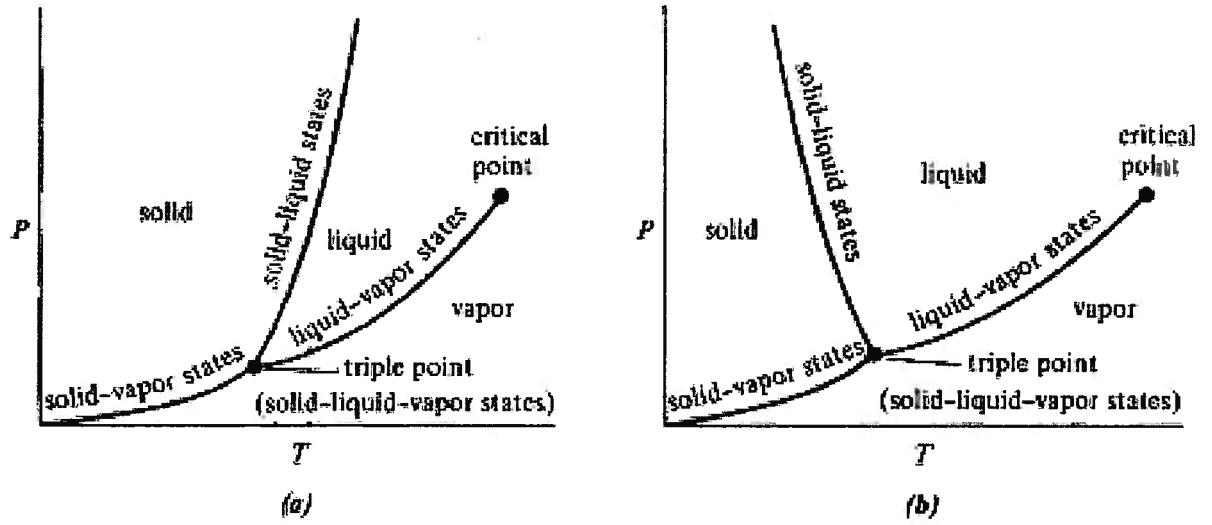

Figure 13.7 (a) Intensive States of the Pure Substance Model that Contracts upon Freezing
(b) Intensive States of the Pure Substance Model that Expands upon Freezing

13.8 Energy Interactions During Changes of Phase

Change of phase processes at constant pressure are important practical processes for the pure substance. Since the two phases are in equilibrium with each other during such a change of phase, it follows from our previous discussions in this chapter that if the pressure remains constant, then the temperature must also remain constant. Under these circumstances, the evaluation of the energy interactions becomes particularly simple. For example, consider the case of a phase change from saturated liquid to saturated vapor due to a heat transfer process in which the temperature and pressure of the pure substance are always constant. If the process is reversible, the only work transfer (for a unit mass of the substance) is $\int Pdv$, but since the pressure is constant,

$$(W_{f-g})_{rev} = mP(v_g - v_f) \tag{13.7}$$

Here the subscript f refers to the saturated liquid and the subscript g refers to the saturated vapor. The first law of thermodynamics requires

$$Q_{f-g} - W_{f-g} = m(u_g - u_f) \tag{13.8}$$

When we substitute equation (13.7) for the work transfer, the required heat transfer for the system is

$$(Q_{f-g})_{rev} = m[(u+Pv)_g - (u+Pv)_f] = m[h_g - h_f] \tag{13.9}$$

In equation (13.9) we have used the property *enthalpy* defined as

$$H = U + PV = mh = m(u+Pv) \tag{13.10}$$

(Although the enthalpy has a special significance in the present case, we shall see later that it has an even greater significance in the case of the open system.) If the system were initially all saturated liquid and finally all saturated vapor, then

$$(Q_{f-g})_{rev} = m(h_g - h_f) = mh_{fg} \tag{13.11}$$

The quantity h_{fg} is called the *latent heat* of vaporization and involves the same historic misnomer as the specific heat. The term latent heat originated in caloric theory which attempted to describe all thermal processes in terms of the simple concepts of stored heat. We now know these simple

concepts to be adequate only for pure thermal systems. The term latent heat was used in contrast to the term *sensible heat* in an attempt to justify the absence of the temperature increase expected in the common case. In spite of its name, the latent heat h_{fg} is generally useful for liquid-vapor phase changes at constant pressure. For example, if a saturated liquid confined in a cylinder at constant pressure is evaporated by an adiabatic, irreversible process such as stirring the fluid with a paddle wheel, the work transfer *to* the fluid is given by the latent heat h_{fg}.

The heat transfer required for a reversible evaporation at constant temperature and pressure may also be determined directly from the second law of thermodynamics.

$$\left(Q_{f-g}\right)_{rev} = m\int_f^g Tds \tag{13.12}$$

Since the temperature is constant in the present case, the integration of equation (13.12) is straightforward. Thus,

$$\left(Q_{f-g}\right)_{rev} = mT\left(s_g - s_f\right) = mTs_{fg} \tag{13.13}$$

When we equate this result to the heat transfer computed with the first law, equation (13.11), we obtain the important relation

$$Ts_{fg} = h_{fg} \tag{13.14}$$

which must be satisfied by the specific properties of two phases in equilibrium.

Although we have calculated the heat transfer and work transfer for the case of a liquid-vapor phase change, the analysis is also valid for solid-liquid and solid-vapor phase changes. In each case, it is simply a matter of using the properties for the appropriate saturated states.

13.9 Phase Equilibrium

The results of equation (13.14) can be used to establish an additional requirement for equilibrium between two phases in the pure substance model. Equation (13.14) can be rewritten in the form

$$h_g - Ts_g = h_f - Ts_f \tag{13.15}$$

Making use of the definition of the Gibbs free energy equation (7.88), we can write equation (13.15) in the form

$$g_g = g_f \tag{13.16}$$

Equation (13.16) is a general result and holds for any two phases of a pure substance in equilibrium. Thus for such a system, the specific Gibbs free energy is the same for both phases. This result is consistent with the second law limit on the work transfer (equation (7.89)) for the evaporation of a saturated liquid at constant temperature and pressure since the reversible work transfer other than $\int Pdv$ is zero.

We have now developed an additional requirement for thermodynamic equilibrium of a pure substance in a multiphase state. This requirement is that the specific Gibbs free energy be uniform throughout the system if the system is to be at equilibrium with respect to mass passing from one phase to another. Thus, the specific Gibbs free energy, h - Ts, plays the same role with respect to mass transfer between phases as the temperature plays with respect to heat transfer and the pressure plays with respect to work transfer by means of mechanical motion. Accordingly, equation (13.1) can be modified to allow for interactions involving mass transfer. For a pure substance,

$$dU = Tds - Pdv + gdm \tag{13.17}$$

Here m is the mass of the system and g is the specific Gibbs free energy. For a closed system, the mass is constant, and equation (13.17) reduces to equation (13.1). The open system is another matter altogether since mass can be transferred across the open system boundary.

In more complex cases in which the system is made up of a number of different substances and chemical reactions are possible, a property called the chemical potential must be uniform throughout the system for equilibrium with respect to mass transfer between phases. Thus, in the simple case of the pure substance the chemical potential reduces to the Gibbs free energy.

13.10 Thermodynamic Surfaces

In the preceding section we have assumed that all the equilibrium properties of the pure substance are known. Because of the complex thermodynamic behavior of the pure substance we cannot evaluate these properties from simple algebraic constitutive relations of the type we have used previously. Instead, we must rely upon the values of properties determined from experimental measurements. We have already seen that it is possible to represent the thermodynamic properties of the pure substance model in terms of curves plotted on an appropriate set of coordinates. Although such a representation is often very convenient, it suffers from two disadvantages. First, for clarity, the data must be presented as a family of curves spaced at reasonable intervals while the actual physical data vary continuously. Interpolation must be used to obtain data for engineering calculations from the two-dimensional graphical representation. The accuracy of this method is at best limited. Second, the two-dimensional graphical representation is sometimes difficult to interpret. This situation is particularly true in the case of the pure substance that expands on freezing (*cf.* Figure 13.6). Thus, it is worthwhile to consider a representation that does not involve these disadvantages. We recognize that according to the state principle, we can specify the state of a pure substance by establishing the values of two independent properties. Any other property can then be related to these two through the appropriate set of constitutive relations. These constitutive relations can be reduced to a single expression for the desired property as a function of the two independent properties. For a unit mass of the pure substance this single expression can be represented as a surface in a three-dimensional coordinate space defined by the two independent properties and the property of interest. Such a surface is called a *thermodynamic surface*, and for a unit mass of a given pure substance, every equilibrium state of the substance must lie somewhere on the surface.

The most common, and perhaps most useful, thermodynamic surface is the three-dimensional representation of the P-v-T data for the pure substance. These three properties are the easiest properties to measure. Figure 13.8 shows schematically typical P-v-T surfaces for two classes of pure substances – those that contract upon freezing and those that expand upon freezing. In this representation the interrelation between temperature and pressure for two-phase states becomes immediately apparent. Because of this interrelationship the loci of all two-phase states are surfaces whose generators are normal to the pressure-temperature plane and parallel to the volume axis. A single curved surface of this type is often called a *ruled surface*. There are three such regions of two phases. All three of these ruled surfaces intersect at a particular value of the pressure and temperature, the triple point. The locus of the intersection is actually a line called the triple line and every three-phase state for a unit mass of the pure substance must lie somewhere on this line. Although the three ruled surfaces have the same temperature and pressure at their line of intersection, they each have a different slope. These slopes, however, do not vary with the average specific volume of the three-phase state.

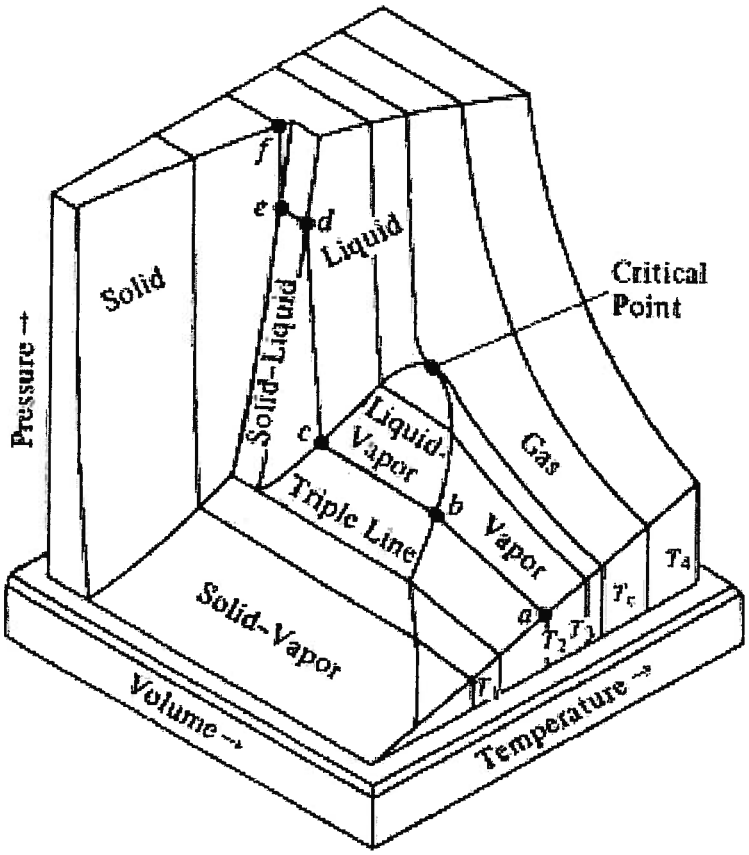

Figure 13.8(a) P-v-T Surface for a Pure Substance that Contracts upon Freezing

On the *P-v-T* surface the saturated states lie on the lines of intersection between the ruled surfaces representing the two-phase states and the double curved surfaces representing the single-phase states. In Figure 13.8 the relative magnitudes of the volume changes associated with constant pressure phase changes are greatly exaggerated. The volume change for the constant pressure liquid-solid phase change is extremely small (too small to show unless exaggerated) relative to the volume change for either the vapor-liquid or vapor-solid phase change which are both of the same order of magnitude.

Note that there are two distinct differences between the *P-v-T* surfaces shown in Figures 13.8 (a) and 13.8 (b). The first difference is the location of the liquid-solid two-phase surface with respect to the location of the liquid-vapor two-phase surface. In Figure 13.8 (a) we see that at the triple point, the volume change for the vapor-liquid phase change is smaller than the volume change for the vapor-solid phase change. Thus, at this pressure the specific volume of the solid is smaller than the specific volume of the liquid, and the substance contracts upon freezing. On the other hand, in Figure 13.8 (b) we note that at the triple point the volume change for the vapor-liquid phase change is greater than the volume change for the vapor-solid phase change. Hence, at this pressure the specific volume of the solid is greater than the specific volume of the liquid, and the substance expands upon freezing. This difference between Figures 13.8 (a) and 13.8 (b) becomes even more obvious when we project the *P-v-T* surface onto the already familiar *P-v* plane as in Figures 13.5 and 13.6.

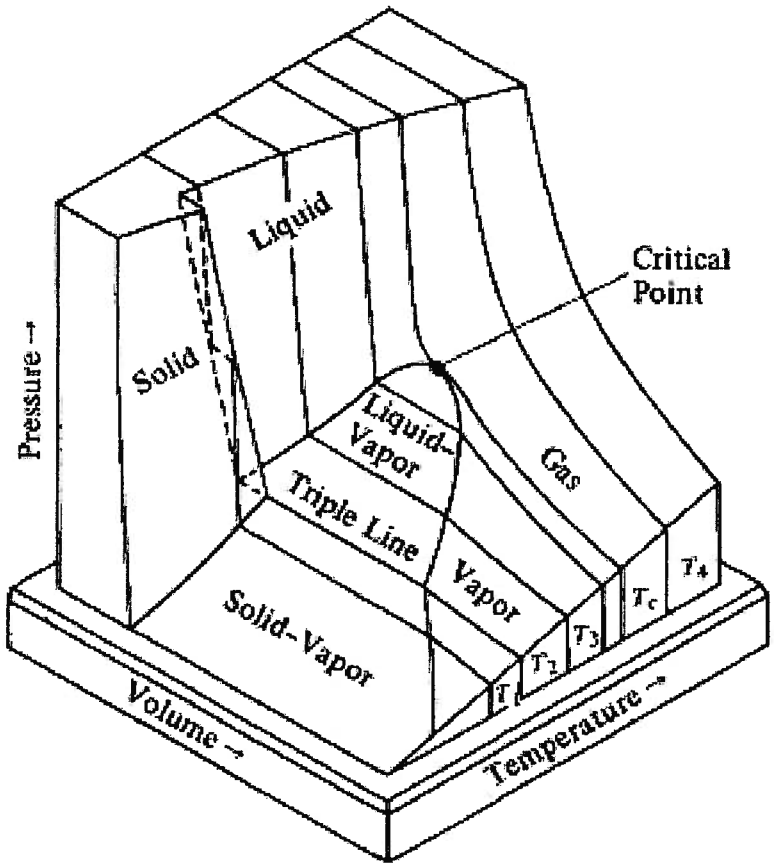

Figure 13.8(b) *P-v-T* surface for a substance that expands upon freezing

The second difference between Figures 13.8 (a) and 13.8 (b) is in the sign of the slope of the ruled surface representing the liquid-solid two-phase states. In Figure 13.8 (a) it is clear that an increase in pressure results in an increase in the freezing point. This situation is also typical of the liquid-vapor and solid-vapor two-phase states for which an increase in pressure causes an increase in the saturation temperature. For a substance that expands upon freezing, the liquid-solid two-phase states exhibit the anomalous behavior that an increase in pressure results in a decrease in the freezing point, a distinct contrast to other two-phase states. The projection of the *P-v-T* surface onto the *P-T* plane as in Figure 13.7 reveals this difference in even more striking fashion.

By now it is obvious that the *P-v-T* surface for a pure substance provides a great deal of information about the equilibrium thermodynamic behavior of the substance. However, we must remember that the actual *P-v-T* surface of a given pure substance may look radically different from the two schematic surfaces that we have just considered. For example, one of the most common of all pure substances, water, exhibits unusual behavior of its *P-v-T* surface at high pressures. When water freezes at pressures that are within our normal range of experience (e.g. several atmospheres), it expands. Thus the solid form, ice, will float on the surface of the liquid. At extremely high pressures (thousands of atmospheres), the solid form becomes more dense than the liquid and hence will not float. This type of behavior together with the seven different solid phases of ice is shown in Figure 13.9. The important point to remember is that regardless of the anomalies that might occur, *every* equilibrium state of a unit mass of a pure substance must lie somewhere on the *P-v-T* surface.

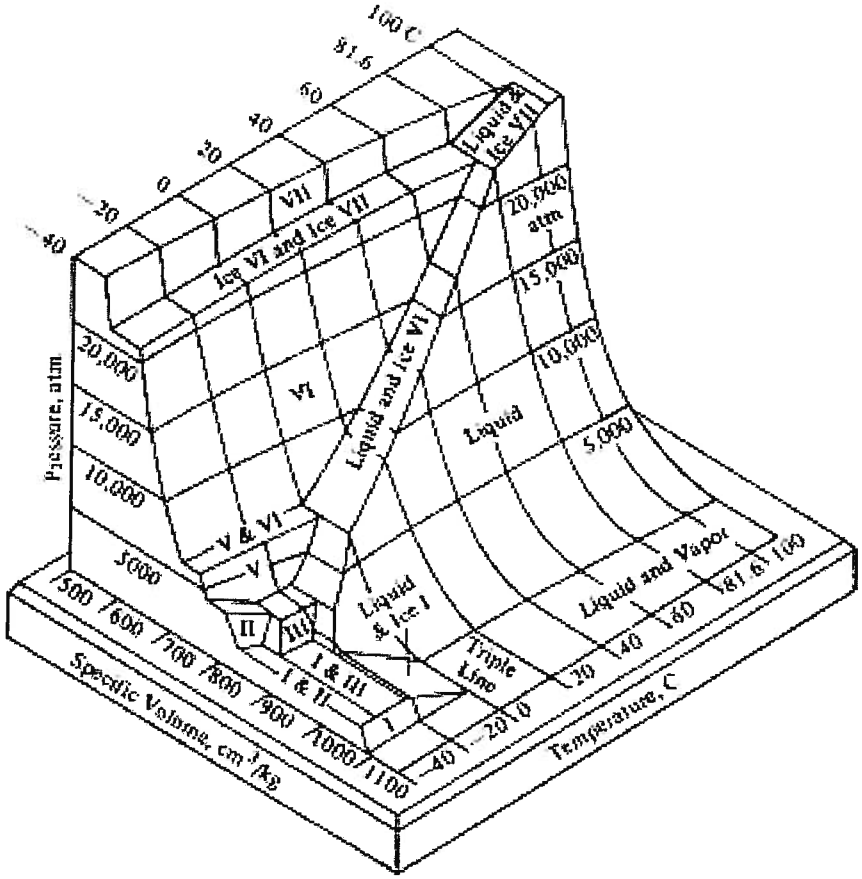

Figure 8.9 *P-v-T* Surface of Water at High Pressure

Figure reprinted from Lee and Sears, *Thermodynamics: An Introductory Text for Engineering Students*, © 1963, Addison-Wesley Publishing Company, Inc., page 42, figure 2-11.

The *P-v-T* surface is just one example of the many possible thermodynamic surfaces that we can construct. Each one serves some special purpose; however, these surfaces are awkward to use. For this reason, we usually rely on projections of these surfaces onto one of the coordinate planes for a graphical representation of the states of the pure substance model. In spite of their limitations, these projections are quite often useful because the liquid-vapor two-phase states are of most interest.

13.11 Tabulation of the Thermodynamic Properties of the Pure Substance Model

In the previous section we saw that all possible thermodynamic states of a pure substance can be represented by a surface in a three-dimensional coordinate space. In principle, a collection of such surfaces could be used to record all of the thermodynamic properties; however, this is certainly not a very practical method. A more convenient record of the properties is the projections of these surfaces onto appropriate two-dimensional planes such as the *P-v* plane (*cf.* Figure 13.3) or the *T-s* plane (*cf.* Figure 13.10). These two projections are useful since the interactions for quasi-static processes are easily depicted on these planes. On the *P-v* plane, the quasi-static work transfers are $\int Pdv$ while on the *T-s* plane reversible heat transfers are $\int Tds$. The data plotted on these planes are determined by experimental measurement of the properties of interest. Using elaborate curve-fitting and smoothing routines, we can establish the values of the properties for any particular state. These are the values that are then plotted on the two-dimensional planes such as Figure 13.10.

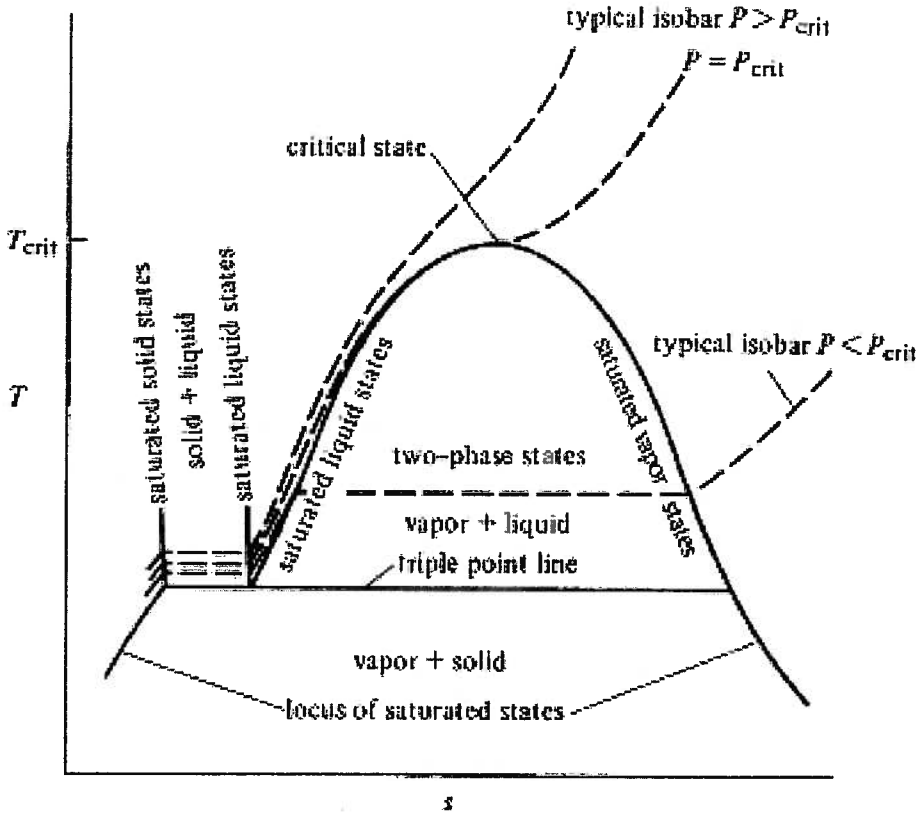

Figure 13.10 Temperature-entropy Diagram of the Pure Substance Model

Since any property diagram of any reasonable size is limited in accuracy to a few percent, tables of the values of the thermodynamic properties are more useful for accurate engineering calculations. These tables of values are established by employing the empirical curve-fits described above. For pure substance models that find wide-spread use in the design and analysis of thermal-fluid systems, great care is taken to insure that the curve-fits are mathematically and thermodynamically robust, not only in the fits themselves but also in their first and second derivatives. The mathematical formalisms based upon the laws of thermodynamics and presented in detail in Chapter 14 are used extensively for this purpose.

In particular, the pure substance model for H_2O has been the subject of considerable attention in this regard since it is so widely used in energy conversion systems throughout the world . An international commission with representatives from many nations has reviewed the considerable amounts of data that have been generated by investigators in these many nations. By international agreement, particular forms for the curve fits have been established. These closed form expressions are then used to generate the data presented in tabular form. For other pure substance models, a somewhat lesser effort has been devoted to the experimental and mathematical formulation of the relevant data. These efforts are often overseen by professional societies such as the American Society of Mechanical Engineers (ASME) and the American Society of Refrigeration and Air-conditioning Engineers (ASHRAE), or by national commissions such as the National Institute of Standards and Technology (NIST) in the United States. Similar efforts are pursued in other nations as well. In recent years, the results of these diverse studies have often been made available in the form of software that can be used on personal computers or is available on the World Wide Web. (For example, see the Chemistry WebBook maintained

by NIST at the website http://webbook.nist.gov/chemistry/.) In the present work, we shall make use of the tabular form of the data generated by these software packages, but the approach described herein can be applied to data generated by any of the aforementioned methods.

Typically, these tables are a listing of the values of the specific volume, specific entropy, specific enthalpy, and specific internal energy at convenient intervals of temperature and pressure. The listing is usually in the form of a matrix with the rows and columns corresponding to either a fixed temperature or a fixed pressure. Table 13.1 is an example extracted from the tabulated properties of H_2O given in Appendix A. To determine the values of the specific properties for a known state, we simply select the appropriate column corresponding to the pressure of the system and search down this column until we reach the appropriate row corresponding to the temperature of the system. The values of u, v, s, and h can be read directly from the entry in the tables. To calculate the total value of these properties we simply multiply the specific value by the mass of the system. The intervals of temperature and pressure used in full and complete tables are selected to permit linear interpolation with reasonable accuracy. Abstracted tables for several pure substances are given in Appendix A.

This scheme of tabulation is sufficient for those states in which only one phase of the pure substance is present. However, for two-phase states the situation is a bit more complicated since the pressure and temperature are no longer independent of one another. Fortunately, each of the two phases involved is in a single-phase saturated state so that for a given temperature or pressure it is possible to tabulate the specific properties for each of the two coexistent phases. A table of thermodynamic properties of these saturated states is called a *saturation table.* Either the temperature or the pressure is selected as the independent property and is indexed at convenient intervals to permit linear interpolation. The value of the other intensive property (pressure or temperature) is usually included in the list of tabulated properties. Table 13.2 is an example, excerpted from Appendix A, of a saturation table for equilibrium liquid-vapor two-phase states of H_2O with the temperature as the independent property. Abstracted tables for the saturated states for several pure substances are given in Appendix A.

Table 13.1 also lists the two-phase states for the pressure values listed at the top of the table. The saturation temperature corresponding to the pressure is listed in parentheses after the pressure. The values of the specific properties of saturated liquid (subscript f states) at each pressure are in row one of the table (indicated by "Sat liq" in the left column). The values for saturated vapor (subscript g states) are given in row three (indicated by "Sat vap"). The difference between saturated vapor properties and saturated liquid properties (subscript fg) are given in row two (indicated by "Evap"). At each pressure the states above the horizontal line are compressed liquid states and the states below are superheated vapor states.

Table 13.1

PROPERTIES OF H_2O

$P(T_{sat})$	1 x 10⁴ N/m² (45.81 C)			
Temp [C]	v [m³/kg]	u [kJ/kg]	h [kJ/kg]	s [kJ/kg K]
Sat. Liq.	1.0103E-03	191.80	191.81	0.6492
Evap.	14.669	2245.4	2392.1	7.5010
Sat. Vap.	14.670	2437.2	2583.9	8.1488
0.00	1.0002E-03	-0.0420	-0.0320	-0.0002
10	1.0003E-03	42.020	42.030	0.1511
20	1.0018E-03	83.911	83.921	0.2965
30	1.0044E-03	125.74	125.75	0.4368
40	1.0079E-03	167.53	167.54	0.5724
50	14.869	2443.3	2592.6	8.1741
60	15.336	2457.8	2611.2	8.2328
70	15.801	2472.3	2630.3	8.2886
80	16.267	2486.7	2649.3	8.3430
90	16.732	2501.1	2668.4	8.3971
100	17.196	2515.5	2687.5	8.4488
120	18.124	2544.4	2725.6	8.5464
140	19.050	2573.4	2763.9	8.6434
160	19.976	2602.6	2802.3	8.7341
180	20.901	2631.8	2840.8	8.8212
200	21.825	2661.3	2879.6	8.9048
220	22.750	2691.1	2918.6	8.9852
240	23.674	2721.0	2957.8	9.0635
260	24.598	2751.2	2997.2	9.1390
280	25.522	2781.6	3036.8	9.2118
300	26.445	2812.3	3076.7	9.2827
320	27.369	2843.2	3116.9	9.3505
340	28.293	2874.3	3157.3	9.4166
360	29.216	2905.7	3197.8	9.4837
380	30.140	2937.4	3238.8	9.5473
400	31.063	2969.3	3279.9	9.6094
420	31.986	3001.5	3321.4	9.6700
440	32.910	3034.0	3363.0	9.7283
460	33.833	3066.7	3405.0	9.7873
480	34.756	3099.8	3447.3	9.8441
500	35.680	3132.3	3489.7	[illegible]
520	36.603	3166.4	3532.4	9.9544
540	37.526	3200.3	3575.5	10.006
560	38.449	3234.3	3618.8	10.061
580	39.372	3268.7	3662.4	10.113
600	40.296	3303.3	3706.3	10.163
620	41.219	3338.2	3750.4	10.213
640	42.142	3373.6	3794.9	10.262
660	43.065	3408.9	3839.6	10.311
680	43.988	3444.7	3884.6	10.358
700	44.911	3480.9	3930.0	10.406
720	45.834	3517.4	3975.5	10.452
740	46.758	3553.8	4021.3	10.498
760	47.681	3590.7	4067.1	10.543
780	48.604	3627.9	4113.9	10.587
800	49.527	3665.3	4160.6	10.631
850	51.835	3760.2	4278.6	10.738
900	54.143	3856.8	4398.3	10.841
950	56.450	3955.2	4519.7	10.941
1000	58.758	4055.2	4643.0	11.043
1100	63.373	4260.0	4893.7	11.233
1200	67.988	4470.2	5150.7	11.413
1300	72.604	4687.4	5413.4	11.584

$P(T_{sat})$	2 x 10⁴ N/m² (60.06 C)				3 x 10⁴ N/m² (69.10 C)			
Temp [C]	v [m³/kg]	u [kJ/kg]	h [kJ/kg]	s [kJ/kg K]	v [m³/kg]	u [kJ/kg]	h [kJ/kg]	s [kJ/kg K]
Sat. Liq.	1.0172E-03	251.40	251.42	0.8320	1.0223E-03	289.24	289.27	0.9441
Evap.	7.6470	2204.6	2357.5	7.0752	5.2274	2174.8	2335.3	6.8234
Sat. Vap.	7.6480	2456.0	2608.9	7.9072	5.2284	2467.7	2624.5	7.7675
0.00	1.0002E-03	-0.0418	-0.0218	-0.0002	1.0002E-03	-0.0417	-0.0117	-0.0002
10	1.0003E-03	42.020	42.040	0.1511	1.0003E-03	42.019	42.049	0.1511
20	1.0018E-03	83.911	83.931	0.2965	1.0018E-03	83.910	83.940	0.2965
30	1.0044E-03	125.73	125.75	0.4368	1.0044E-03	125.73	125.76	0.4368
40	1.0079E-03	167.52	167.54	0.5724	1.0079E-03	167.52	167.55	0.5724
50	1.0121E-03	209.33	209.34	0.7038	1.0121E-03	209.33	209.36	0.7038
60	1.0171E-03	251.16	251.18	0.8313	1.0171E-03	251.15	251.18	0.8313
70	7.8826	2470.7	2628.3	7.9848	5.2428	2469.1	2626.3	7.7727
80	8.1170	2485.3	2647.7	8.0392	5.4018	2484.6	2646.6	7.8282
90	8.3516	2499.8	2666.9	8.0947	5.5590	2499.0	2665.8	7.8837
100	8.5850	2514.5	2686.2	8.1263	5.7151	2513.5	2685.0	7.9365
120	9.0516	2543.6	2724.6	8.2288	6.0274	2542.9	2723.7	8.0373
140	9.5164	2572.8	2763.1	8.3229	6.3384	2572.0	2762.3	8.1334
160	9.9805	2602.9	2801.6	8.4131	6.6487	2601.5	2801.0	8.2248
180	10.444	2631.4	2840.3	8.5004	6.9584	2631.0	2839.8	8.3123
200	10.907	2661.0	2879.2	8.5843	7.2677	2660.7	2878.7	8.3964
220	11.370	2690.8	2918.2	8.6651	7.5768	2690.6	2917.8	8.4773
240	11.833	2720.8	2957.4	8.7431	7.8855	2720.5	2957.1	8.5554
260	12.295	2751.0	2996.9	8.8185	8.1941	2750.8	2996.6	8.6309
280	12.757	2781.4	3036.6	8.8916	8.5026	2781.3	3036.3	8.7041
300	13.219	2812.1	3076.5	8.9625	8.8110	2811.9	3076.2	8.7750
320	13.682	2843.0	3116.7	9.0314	9.1192	2842.9	3116.4	8.8439
340	14.144	2874.2	3157.1	9.0983	9.4274	2874.0	3156.8	8.9110
360	14.606	2905.6	3197.7	9.1635	9.7356	2905.5	3197.5	8.9763
380	15.068	2937.3	3238.6	9.2272	10.044	2937.2	3238.5	9.0399
400	15.530	2969.2	3279.8	9.2893	10.352	2969.1	3279.6	9.1026
420	15.991	3001.4	3321.2	9.3499	10.660	3001.5	3321.1	9.1627
440	16.453	3033.9	3362.9	9.4090	10.968	3033.7	3362.8	9.2220
460	16.915	3066.6	3404.9	9.4673	11.276	3066.5	3404.7	9.2800
480	17.377	3099.6	3447.1	9.5241	11.584	3099.5	3447.0	9.3368
500	17.838	3132.8	3489.6	9.5794	11.891	3132.7	3489.5	9.3925
520	18.300	3166.3	3532.4	9.6344	12.199	3166.3	3532.3	9.4471
540	18.762	3200.3	3575.6	[illegible]	12.507	3200.1	3575.3	9.5007
560	19.224	3234.3	3618.7	9.7406	12.815	3234.2	3618.6	9.5534
580	19.685	3268.8	3662.5	9.7923	13.123	3268.6	3662.2	9.6051
600	20.147	3303.3	3706.2	9.8431	13.431	3303.0	3706.0	9.6559
620	20.609	3338.2	3750.4	9.8930	13.738	3338.1	3750.3	9.7060
640	21.070	3373.4	3794.9	9.9424	14.046	3373.3	3794.7	9.7553
660	21.532	3408.8	3839.5	9.9906	14.354	3408.8	3839.5	9.8036
680	21.993	3444.7	3884.5	10.039	14.662	3444.6	3884.5	9.8514
700	22.455	3480.7	3929.8	10.086	14.970	3480.7	3929.8	9.8984
720	22.917	3517.1	3975.4	10.132	15.277	3517.0	3975.4	9.9446
740	23.378	3553.7	4021.3	10.178	15.585	3553.7	4021.2	9.9902
760	23.840	3590.6	4067.4	10.223	15.893	3590.6	4067.4	10.035
780	24.301	3627.8	4113.9	10.267	16.201	3627.8	4113.8	10.080
800	24.763	3665.3	4160.6	10.311	16.508	3665.3	4160.8	10.124
850	25.917	3760.2	4278.6	10.419	17.278	3760.2	4278.5	10.232
900	27.071	3856.9	4398.3	10.523	18.047	3856.8	4398.3	10.336
950	28.225	3955.3	4519.7	10.624	18.816	3955.2	4519.7	10.437
1000	29.379	4055.2	4642.8	10.723	19.585	4055.2	4643.0	10.536
1100	31.686	4260.0	4893.7	10.913	21.124	4260.0	4893.7	10.726
1200	33.994	4470.8	5150.7	11.093	22.663	4470.8	5150.7	10.906
1300	36.302	4687.3	5413.4	11.268	24.201	4687.3	5413.4	11.078

$P(T_{sat})$	5 x 10⁴ N/m² (81.33 C)				7 x 10⁴ N/m² (89.95 C)				$P(T_{sat})$
Temp [C]	v [m³/kg]	u [kJ/kg]	h [kJ/kg]	s [kJ/kg K]	v [m³/kg]	u [kJ/kg]	h [kJ/kg]	s [kJ/kg K]	Temp [C]
Sat. Liq.	1.0299E-03	340.49	340.54	1.0912	1.0360E-03	376.68	376.75	1.1921	Sat. Liq.
Evap.	3.2390	2142.7	2304.7	6.5018	2.3649	2117.2	2283.7	6.2883	Evap.
Sat. Vap.	3.2400	2483.2	2646.2	7.5930	2.3659	2493.9	2660.4	7.4790	Sat. Vap.
0.00	1.0002E-03	-0.0413	0.0087	-0.0002	1.0002E-03	-0.0408	0.0291	-0.0001	0.00
10	1.0003E-03	42.018	42.068	0.1511	1.0003E-03	42.016	42.086	0.1511	10
20	1.0018E-03	83.909	83.959	0.2965	1.0018E-03	83.908	83.978	0.2965	20
30	1.0044E-03	125.73	125.78	0.4367	1.0044E-03	125.73	125.79	0.4367	30
40	1.0079E-03	167.52	167.57	0.5724	1.0079E-03	167.52	167.59	0.5724	40
50	1.0121E-03	209.32	209.37	0.7038	1.0121E-03	209.32	209.39	0.7038	50
60	1.0171E-03	251.15	251.21	0.8313	1.0171E-03	251.14	251.23	0.8313	60
70	1.0228E-03	293.03	293.08	0.9551	1.0227E-03	293.03	293.10	0.9551	70
80	1.0292E-03	334.95	335.01	1.0756	1.0290E-03	334.96	335.03	1.0755	80
90	3.3235	2496.3	2662.6	7.6415	2.3655	2494.0	2659.6	7.4790	90
100	3.4180	2511.5	2682.4	7.6953	2.4340	2509.4	2679.8	7.5344	100
120	3.6080	2541.3	2721.7	7.7998	2.5710	2539.7	2719.7	7.6383	120
140	3.7980	2570.9	2760.7	[illegible]	2.7064	2569.7	2759.1	7.7384	140
160	3.9833	2600.6	2799.7	7.9868	2.8420	2599.5	2798.4	7.8323	160
180	4.1690	2630.2	2838.7	8.0746	2.9768	2629.4	2837.8	7.9177	180
200	4.3562	2660.0	2877.8	8.1597	3.1109	2659.3	2877.0	8.0024	200
220	4.5421	2689.9	2917.0	8.2404	3.2449	2689.3	2916.2	8.0840	220
240	4.7278	2720.0	2956.4	8.3187	3.3789	2719.5	2955.7	8.1624	240
260	4.9134	2750.3	2996.0	8.3943	3.5079	2749.8	2995.4	8.2382	260
280	5.0988	2780.8	3035.8	8.4676	3.6460	2780.4	3035.2	8.3119	280
300	5.2843	2811.6	3075.8	8.5388	3.7725	2811.2	3075.3	8.3827	300
320	5.4693	2842.5	3116.0	8.6076	3.9056	2842.2	3115.6	8.4518	320
340	5.6544	2873.7	3156.5	8.6747	4.0373	2873.4	3156.1	8.5190	340
360	5.8395	2905.2	3197.2	8.7431	4.1660	2904.9	3196.8	8.5844	360
380	6.0244	2936.9	3238.1	8.8038	4.3018	2936.7	3237.6	8.6481	380
400	6.2094	2968.9	3279.3	8.8658	4.4341	2968.6	3279.0	8.7163	400
420	6.3943	3001.1	3320.8	8.9266	4.5665	3000.8	3320.5	8.7710	420
440	6.5792	3033.6	3362.5	8.9858	4.6985	3033.4	3362.3	8.8364	440
460	6.7641	3066.3	3404.5	9.0440	4.8306	3066.1	3404.3	8.8925	460
480	6.9489	3099.3	3446.7	9.1008	4.9627	3099.1	3446.5	8.9453	480
500	7.1338	3132.6	3489.3	9.1564	5.0948	3132.4	3489.1	9.0011	500
520	7.3180	3166.1	3532.1	9.2113	5.2258	3165.9	3531.8	9.0642	520
540	7.5034	3199.9	3575.2	9.2648	5.3589	3199.8	3574.9	9.1156	540
560	7.6881	3234.1	3618.5	9.3175	5.4909	3233.9	3618.3	9.1680	560
580	7.8729	3268.4	3662.1	[illegible]	5.6230	3268.3	3661.9	9.2038	580
600	8.0576	3303.1	3706.0	9.4201	5.7548	3300.0	3705.8	9.2706	600
620	8.2424	3338.0	3750.1	9.4701	[illegible]	3337.9	3750.0	9.3207	620
640	8.4271	3373.2	3794.6	9.5193	6.0189	3373.1	3794.5	9.3699	640
660	8.6118	3408.7	3839.3	9.5670	6.1508	3408.6	3839.2	9.4124	660
680	8.7965	3444.5	3884.4	9.6155	6.2828	3444.4	3884.3	9.4661	680
700	8.9812	3480.6	3929.7	9.6625	6.4148	3480.5	3929.5	9.5072	700
720	9.1659	3517.0	3975.3	9.7089	6.5467	3516.9	3975.2	9.5535	720
740	9.3506	3553.6	4021.1	9.7546	6.6787	3553.6	4021.0	9.6063	740
760	9.5353	3590.5	4067.3	9.7994	6.8106	3590.4	4067.2	9.6444	760
780	9.7200	3627.7	4113.7	9.8443	6.9425	3627.8	4113.6	9.6888	780
800	9.9047	3665.2	4160.4	9.8882	7.0745	3665.1	4160.3	9.7339	800
850	10.366	3760.1	4278.4	9.9957	7.4043	3760.1	4278.4	9.8404	850
900	10.828	3856.8	4398.2	10.100	7.7341	3856.7	[illegible]	9.9447	900
950	11.290	3955.1	4519.6	10.201	8.0639	3955.1	4519.6	10.046	950
1000	11.751	4055.1	4642.7	10.300	8.3937	4055.1	4642.6	10.145	1000
1100	12.674	4259.8	4893.7	10.490	9.0533	4259.8	4893.6	10.334	1100
1200	13.598	4470.7	5150.7	10.670	9.7129	4470.7	5150.6	10.515	1200
1300	14.521	4687.3	5413.3	10.843	10.370	4687.2	5413.1	10.688	1300

Table 13.2

ROPERTIES OF SATURATED H_2O

T [C]	T [K]	P_{sat} [N/m²]	v_f [m³/kg]	v_{fg} [m³/kg]	v_g [m³/kg]	u_f [kJ/kg]	u_{fg} [kJ/kg]	u_g [kJ/kg]	h_f [kJ/kg]	h_{fg} [kJ/kg]	h_g [kJ/kg]	s_f [kJ/kg K]	s_{fg} [kJ/kg K]	s_g [kJ/kg K]
0.01	273.16	6.1166E+02	1.0002E-03	205.99	205.99	0.00	2374.90	2374.90	6.1233E-04	2500.90	2500.90	0.00	9.1555	9.1555
5	278.15	8.7258E+02	1.0001E-03	147.01	147.01	21.02	2360.76	2381.78	21.02	2489.04	2510.06	0.0763	8.9485	9.0248
10	283.15	1.2282E+03	1.0003E-03	106.30	106.30	42.02	2346.65	2388.65	42.02	2477.19	2519.21	0.1511	8.7487	8.8998
15	288.15	1.7058E+03	1.0008E-03	77.874	77.875	62.98	2332.51	2395.49	62.98	2465.35	2528.33	0.2245	8.5558	8.7803
20	293.15	2.3393E+03	1.0018E-03	57.756	57.757	83.91	2318.41	2402.32	83.91	2453.52	2537.43	0.2965	8.3695	8.6660
25	298.15	3.1698E+03	1.0030E-03	43.336	43.337	104.83	2304.30	2409.13	104.83	2441.68	2546.51	0.3672	8.1894	8.5566
30	303.15	4.2470E+03	1.0044E-03	32.877	32.878	125.73	2290.18	2415.91	125.73	2429.82	2555.55	0.4368	8.0152	8.4520
35	308.15	5.6290E+03	1.0060E-03	25.205	25.206	146.63	2276.04	2422.67	146.63	2417.92	2564.55	0.5051	7.8469	8.3517
40	313.15	7.3849E+03	1.0079E-03	19.514	19.515	167.53	2261.86	2429.39	167.53	2406.00	2573.51	0.5724	7.6831	8.2555
45	318.15	9.5950E+03	1.0099E-03	15.251	15.252	188.43	2247.65	2436.08	188.43	2394.00	2582.43	0.6386	7.5247	8.1633
50	323.15	1.2352E+04	1.0121E-03	12.026	12.027	209.33	2233.40	2442.73	209.34	2381.95	2591.29	0.7038	7.3710	8.0748
55	328.15	1.5762E+04	1.0146E-03	9.563	9.564	230.24	2219.10	2449.34	230.26	2369.83	2600.09	0.7680	7.2218	7.9898
60	333.15	1.9946E+04	1.0171E-03	7.666	7.667	251.16	2204.74	2455.90	251.18	2357.65	2608.83	0.8313	7.0768	7.9081
65	338.15	2.5042E+04	1.0199E-03	6.193	6.194	272.09	2190.32	2462.41	272.12	2345.38	2617.50	0.8937	6.9358	7.8295
70	343.15	3.1201E+04	1.0228E-03	5.039	5.040	293.03	2175.85	2468.88	293.07	2333.03	2626.10	0.9551	6.7989	7.7540
75	348.15	3.8595E+04	1.0258E-03	4.129	4.129	313.99	2161.26	2475.24	314.03	2320.57	2634.60	1.0156	6.6654	7.6812
80	353.15	4.7414E+04	1.0291E-03	3.404	3.405	334.96	2146.60	2481.56	335.01	2308.01	2643.02	1.0756	6.5355	7.6111
85	358.15	5.7867E+04	1.0324E-03	2.826	2.826	355.95	2131.85	2487.81	356.01	2295.32	2651.33	1.1348	6.4088	7.5434
90	363.15	7.0182E+04	1.0360E-03	2.359	2.359	376.97	2117.00	2493.97	377.04	2282.49	2659.53	1.1932	6.2852	7.4781
95	368.15	8.4608E+04	1.0396E-03	1.9795	1.9805	398.00	2102.04	2500.04	398.09	2269.52	2667.61	1.2504	6.1647	7.4151
100	373.15	1.0142E+05	1.0435E-03	1.6707	1.6711	419.06	2086.98	2506.02	419.17	2256.40	2675.57	1.3072	6.0468	7.3541
105	378.15	1.2080E+05	1.0474E-03	1.4173	1.4184	440.15	2071.75	2511.90	440.27	2243.12	2683.39	1.3633	5.9318	7.2952
110	383.15	1.4338E+05	1.0516E-03	1.2092	1.2097	461.26	2056.41	2517.67	461.42	2229.64	2691.06	1.4188	5.8193	7.2381
115	388.15	1.6918E+05	1.0559E-03	1.0346	1.0355	482.41	2040.92	2523.33	482.59	2215.99	2698.58	1.4737	5.7091	7.1829
120	393.15	1.9867E+05	1.0603E-03	0.8902	0.8913	503.60	2025.26	2528.86	503.81	2202.12	2705.93	1.5279	5.6012	7.1291
125	398.15	2.3224E+05	1.0649E-03	0.7700	0.7709	524.83	2009.44	2534.27	525.07	2188.03	2713.10	1.5816	5.4954	7.0770
130	403.15	2.7028E+05	1.0697E-03	0.6693	0.6980	546.09	1993.44	2539.53	546.38	2173.70	2720.08	1.6348	5.3918	7.0264
135	408.15	3.1320E+05	1.0746E-03	0.5807	0.5817	567.41	1977.24	2544.65	567.74	2159.13	2726.87	1.6872	5.2900	6.9772
140	413.15	3.6154E+05	1.0798E-03	0.5074	0.5085	588.77	1960.85	2549.62	589.16	2144.28	2733.44	1.7392	5.1901	6.9293
145	418.15	4.1568E+05	1.0850E-03	0.4449	0.4460	610.19	1944.23	2554.42	610.64	2129.16	2739.80	1.7907	5.0919	6.8826
150	423.15	4.7616E+05	1.0906E-03	0.3914	0.3925	631.66	1927.38	2559.05	632.18	2113.75	2745.93	1.8418	4.9953	6.8371
155	428.15	5.4380E+05	1.0992E-03	0.3454	0.3465	653.19	1910.32	2563.51	653.79	2098.02	2751.81	1.8924	4.9002	6.7926
160	433.15	6.1923E+05	1.1020E-03	0.3057	0.3068	674.79	1892.99	2567.78	675.47	2081.97	2757.44	1.9426	4.8065	6.7491
165	438.15	7.0303E+05	1.1080E-03	0.2713	0.2724	696.48	1875.39	2571.86	697.24	2065.57	2762.81	1.9923	4.7143	6.7066
170	443.15	7.9218E+05	1.1143E-03	0.2415	0.2426	718.20	1857.53	2575.73	719.08	2048.82	2767.90	2.0417	4.6233	6.6650
175	448.15	8.9260E+05	1.1207E-03	0.2155	0.2166	740.02	1839.37	2579.39	741.02	2031.69	2772.71	2.0906	4.5335	6.6241
180	453.15	1.0028E+06	1.1274E-03	0.1927	0.1939	761.92	1820.91	2582.83	763.06	2014.16	2777.21	2.1392	4.4448	6.5840
185	458.15	1.1235E+06	1.1343E-03	0.1728	0.1739	783.91	1802.13	2586.04	785.19	1996.22	2781.41	2.1875	4.3572	6.5447
190	463.15	1.2562E+06	1.1416E-03	0.1552	0.1566	806.00	1783.01	2589.01	807.43	1977.85	2785.28	2.2356	4.2704	6.5059
195	468.15	1.3988E+06	1.1492E-03	0.1397	0.1409	828.18	1763.56	2591.74	829.79	1959.03	2788.82	2.2832	4.1846	6.4678
200	473.15	1.5549E+06	1.1565E-03	0.1261	0.1277	850.47	1743.78	2594.20	852.27	1939.74	2792.01	2.3306	4.0997	6.4302
205	478.15	1.7243E+06	1.1646E-03	0.1139	0.1151	872.87	1723.63	2596.40	874.88	1919.95	2794.83	2.3777	4.0153	6.3930
210	483.15	1.9077E+06	1.1727E-03	0.1031	0.1043	895.39	1703.02	2598.31	897.63	1899.64	2797.27	2.4246	3.9316	6.3563

We can now use these tabulated specific properties of the two saturated phases to evaluate the extensive properties of a two-phase state simply by computing the values of these extensive properties for the separate phases and then summing the values for all the phases present. Since the state of each phase is saturated, the value of an extensive property for a given phase is obtained by multiplying the tabulated value of the specific property for the saturated state of the phase by the mass of the phase. The volume for a two-phase state is the sum of the volume of the liquid phase, $V_f = m_f v_f$, and the volume of the vapor phase, $V_g = m_g v_g$, as in equations (13.18) and (13.19).

$$V = V_f + V_g \tag{13.18}$$

or

$$V = m_f v_f + m_g v_g \tag{13.19}$$

In equation (13.19) the subscript f denotes the saturated liquid phase and the subscript g the saturated vapor phase. The relations for the other extensive properties are of the same form.

$$U = m_f u_f + m_g u_g \tag{13.20}$$

$$S = m_f s_f + m_g s_g \tag{13.21}$$

$$H = m_f h_f + m_g h_g \tag{13.22}$$

Equations (13.19) through (13.22) show that the extensive properties of a system in a two-phase state depend upon the relative amounts of the two phases. Thus, a system in a two-phase state can have as one of its independent properties a property that expresses the relative mass in the two phases. For historical reasons, this property is called the *quality,* denoted by the symbol x, and is defined for liquid-vapor two-phase states as *the fraction of the mass in the vapor phase.* Thus,

$$x = \frac{m_g}{m_f + m_g} = \frac{m_g}{m} \tag{13.23}$$

The quality is often expressed in percent. As an alternate description of a liquid-vapor two-phase state, we often employ the property called the *moisture content,* denoted by the symbol y, which is defined as *the fraction of the mass in the liquid phase.* Then

$$y = \frac{m_f}{m_f + m_g} = \frac{m_f}{m} \tag{13.24}$$

For two-phase states that are nearly all saturated liquid, the moisture content is more convenient than the quality in characterizing the state. Conversely, for two-phase states that are nearly all saturated vapor, the quality is more convenient than the moisture content. From equations (13.23) and (13.24) it follows that

$$x + y = 1 \tag{13.25}$$

Thus, when a system enters the two-phase region of the P-v-T surface, we lose either the temperature or the pressure as an independent property, but we gain the quality or the moisture content as an independent property. Then, in accordance with the state principle, the two independent properties necessary to specify the state of the pure substance in the two-phase region, could be (T, x) or (P, x) or (T, y) or (P, y).

The average value for a specific property of a two-phase state is defined as the corresponding total extensive property divided by the total mass of the system. For example, the average specific volume of a two-phase state is

$$v = \frac{V}{m} \tag{13.26}$$

It must be remembered that this is not a true specific property since a random sample from the two-phase state might contain only a single phase, and therefore will not have this volume per unit mass. The value presented in equation (13.26) is the value averaged over all the mass in the system. Substituting equation (13.19) into equation (13.26), we obtain

$$v = \frac{m_f v_f + m_g v_g}{m_f + m_g} \tag{13.27}$$

and

$$v = \frac{m_f}{m_f + m_g} v_f + \frac{m_g}{m_f + m_g} v_g \tag{13.28}$$

Substituting equations (13.23) and (13.24) into equation (13.28), we obtain

$$v = y v_f + x v_g \tag{13.29}$$

or

$$v = (1 - x) v_f + x v_g \tag{13.30}$$

Equation (13.30) can be rearranged to give

$$v = v_f + x(v_g - v_f) \tag{13.31}$$

or

$$v = v_f + x v_{fg} \tag{13.32}$$

Here v_{fg} is a symbol representing the difference in the specific volume for the saturated liquid and vapor phases, $v_{fg} = v_g - v_g$. This specific volume difference is a property fixed by the saturation temperature or pressure and is often tabulated for convenience in calculation. In a similar fashion, the average values of the other specific properties can be calculated.

$$u = u_f + x u_{fg} \tag{13.33}$$

$$h = h_f + x h_{fg} \tag{13.34}$$

$$s = s_f + x s_{fg} \tag{13.35}$$

In many practical situations it is necessary to compute the properties of a two-phase state from a knowledge of the temperature or pressure and the value of an extensive property and the mass of the system. We begin the calculation by first dividing the extensive property by the mass, thereby converting the extensive property into an average specific property. We next establish that the system is indeed in a two-phase state. This information is obtained by recalling that the specification of the temperature or the pressure immediately fixes all saturated specific properties of the two phases. Then, if the average specific property that we have just calculated has a value between the two tabulated saturation values for that property at the given temperature or pressure, the system is in a two-phase state. However, if the value of the specific property had been less than the value of that specific property for the saturated liquid state at the system temperature or pressure, the system would have been in a compressed liquid state. Conversely, if the value of the specific property had been greater than the value of that specific property for the saturated vapor state, the system would have been in a superheated vapor state.

Once we have established the fact that the system is in a two-phase state, we next compute the quality of the two-phase state by substitution of the known specific property into the appropriate equation of equations (13.32) through (13.35). The value for the quality together with the tabulated values for the saturated properties then permits us to evaluate all other average specific properties for the two-phase state. These specific properties can then be converted into extensive properties simply by multiplying by the mass.

Example 13E.1: A system with a total volume of $V = 3\ m^3$ contains a mass of $m = 2$ kg of H_2O at a pressure of $P = 7 \times 10^4\ N/m^2$. What is the entropy of this fluid?

Solution: Following the procedure described above, we first calculate the average specific volume.

$$v = \frac{V}{m} = \frac{3\ m^3}{2\ kg} = 1.5\ m^3/kg$$

Entering the table of properties of H_2O at a pressure of $P = 7 \times 10^4\ N/m^2$, we find at the top of the column for this pressure the specific volume of saturated liquid and of saturated vapor.

$$v_f = 1.0360E-3\ m^3/kg \quad \text{and} \quad v_g = 2.365\ m^3/kg$$

Since $1.0360E-3 < 1.5 < 2.365$, the system is in a two-phase state. We now compute the quality. From equation (13.32)

$$x = \frac{v - v_f}{v_{fg}} = \frac{v - v_f}{v_g - v_f} = \frac{1.5\ m^3/kg - 1.0360 \times 10^{-3}\ m^3/kg}{2.365\ m^3/kg - 1.0360 \times 10^{-3}\ m^3/kg} = 0.634$$

Then according to equation (13.35) the specific entropy becomes

$$s = s_f + s_{fg} = 1.1919\ kJ/kg\ K + (0.634)(6.2878\ kJ/kg\ K)$$

$$s = 1.1919\ kJ/kg\ K + 3.9865\ kJ/kg\ K = 5.1784\ kJ/kg\ K$$

The total entropy of the H_2O is then

$$S = ms = (2\ kg)(5.1784\ kJ/kg\ K) = 10.3568\ kJ/kg$$

13.12 The Clapeyron Relation

In Sections 13.3 and 13.5, we showed that the temperature and pressure of a two-phase equilibrium state are interrelated in a way established by equation (13.16). This equation requires that the value of the specific Gibbs free energy for the two phases be identical. Thus, g_{fg} is identically zero and the average specific Gibbs free energy for the two phases taken together is equal to the value given in equation (13.15). This value is independent of the relative amounts of the two phases present and does not depend upon the quality, x (or the moisture content, y), of the two-phase system.

If the temperature T of this two-phase system is now changed by an infinitesimal amount dT to a new value $T + dT$, the pressure P will also change an infinitesimal amount dP to $P + dP$ in order to preserve the equilibrium between the two phases. Since the two phases remain in equilibrium, this change of state follows the locus of saturated states, also known as the *vapor pressure curve* or the *saturation curve*. These infinitesimal changes in the intensive properties are related by the expression

$$dP = \left(\frac{dP}{dT}\right)_{sat} dP \tag{13.36}$$

Here $(dP/dT)_{sat}$ is the slope of the vapor pressure curve.

This infinitesimal change in the intensive state of the two-phase system causes the specific Gibbs free energy to change from g to $g + dg$. Since the specific Gibbs free energy is given by

$$g = u + Pv - Ts \tag{13.37}$$

the infinitesimal change in the Gibbs free energy becomes

$$dg = du + Pdv + vdp - Tds - sdT \tag{13.38}$$

Substituting equation (13.4) into equation (13.38), we obtain

$$dg = Tds - Pdv + Pdv + vdP - Tds - sdT = vdP - sdT \tag{13.39}$$

Equation (13.39) can be rewritten with the aid of equation (13.36), viz.

$$dg = \left[-s + v\left(\frac{dP}{dT}\right)_{sat} \right] dT \tag{13.40}$$

Since the states involved are two-phase states, we can make use of equations (13.32) and (13.35) and write equation (13.40) in the form

$$dg = \left[-s_f - xs_{fg} + \left(v_f + xv_{fg}\right)\left(\frac{dP}{dT}\right)_{sat} \right] dT \tag{13.41}$$

or

$$dg = \left\{ -s_f + v_f\left(\frac{dP}{dT}\right)_{sat} + x\left[-s_{fg} + v_{fg}\left(\frac{dP}{dT}\right)_{sat} \right] \right\} dT \tag{13.42}$$

Since the Gibbs free energy for a two-phase equilibrium state must be independent of the quality, x, the coefficient of the quality in equation (13.42) must vanish. Then

$$-s_{fg} + v_{fg}\left(\frac{dP}{dT}\right)_{sat} = 0 \tag{13.43}$$

Solving equation (13.43) for the slope of the vapor pressure curve, we obtain

$$\left(\frac{dP}{dT}\right)_{sat} = \frac{s_{fg}}{v_{fg}} \tag{13.44}$$

We can substitute equation (13.14) into equation (13.44) and obtain an alternate expression for the slope of the vapor pressure curve, viz.

$$\left(\frac{dP}{dT}\right)_{sat} = \frac{h_{fg}}{Tv_{fg}} \tag{13.45}$$

Both equations (13.44) and (13.45) are known as the *Clapeyron relation* in honor of Emile Clapeyron (1799 – 1864), a French mining engineer who was one of the early designers of steam locomotives. Clapeyron was the first thermodynamicist to develop Sadi Carnot's ideas in mathematical form. Clapeyron's work laid the foundation for the formalization of the first and second laws of thermodynamics.

It is to be noted that although we have derived this expression for liquid-vapor two-phase equilibrium states, this result is a general one and holds for any two phases in equilibrium. One useful application of the Clapeyron relation is to determine the slope of the line representing the locus of two-phase equilibrium states in the pressure-temperature plane (*cf.* Figure 13.7). Notice that this slope is expressed in terms of the difference in the saturation properties for the two phases of the particular intensive state. Actually, a particular combination of temperature and pressure represents an infinite number of equilibrium two-phase states which differ in the relative amounts of the two phases present. As a consequence, each of these two-phase states will be represented by the same point with the same slope on the pressure-temperature plane. Thus, any thermodynamic surface that uses the pressure, temperature, and some specific extensive property as coordinates (for example, the *P-v-T* surface) will be a surface of single curvature in the two-phase region as described in Section 13.10.

Equation (13.44) or (13.45) also illustrates the difference between Figures 13.7 (a) and 13.7 (b). For a pure substance that contracts upon freezing, the numerator and the denominator

on the right side of equation (13.45) have the same sign. This indicates that the slope of the locus of solid-liquid states is positive as shown in Figure 13.7 (a). Comparatively, for a pure substance that expands upon freezing, the numerator and denominator on the right side are of opposite sign so that the slope of the locus of solid-liquid states is negative as in Figure 13.7 (b). In this sense the Clapeyron relation is a good example of the manner in which the equilibrium between phases restricts the behavior of the intensive state in order to preserve this equilibrium.

The equation of the vapor pressure curve can be obtained by integrating either equation (13.44) or (13.45). For example, the difference in saturation pressure between any two-phase equilibrium states 1 and 2 at different temperatures T_1 and T_2 is given by

$$P_2 - P_1 = \int_{T_1}^{T_2} \frac{h_{fg}}{v_{fg}} \frac{dT}{T} \tag{13.46}$$

Because the specific enthalpy and specific volume of saturated states depend upon the temperature, the integral in equation (13.46) is complicated and usually must be evaluated numerically from curve fits to the experimental data.

Rudolf Clausius (1822 – 1888), a German theoretical physicist who debunked the caloric theory of heat used by his predecessors and thereby became the first investigator to formalize the first and second laws of thermodynamics without resorting to that artifice, proposed a simplification of the Clapeyron relation that has become known as the *Clausius-Clapeyron relation*. Clausius argued that in the case of liquid-vapor equilibrium states and also solid-vapor equilibrium states, the denser phase has a specific volume that is typically several orders of magnitude smaller than the specific volume of the less dense phase (the vapor). Therefore, the specific volume of this phase can be neglected in comparison with that of the vapor phase , i.e., $v_f << v_g$ and $v_s << v_g$. Then the Clapeyron relation becomes

$$\left(\frac{dP}{dT}\right)_{sat} \approx \frac{h_{fg}}{Tv_g} \tag{13.47}$$

Clausius then argued that (1) the latent heat can be modeled as constant (This is very nearly true for the solid-vapor latent heat, but only approximately true for the liquid-vapor latent heat.) and (2) the vapor phase can be modeled as an ideal gas (Again, this is very nearly true for the vapor in equilibrium with the solid because of the very low pressures involved, but only approximately true for the vapor in equilibrium with the liquid because of the significantly higher pressures.). Then equation (13.47) can be written

$$\left(\frac{dP}{dT}\right)_{sat} \approx \frac{h_{fg}P}{RT^2} \tag{13.48}$$

Then in the context of these applications, we can now separate variables and integrate equation (13.48) in closed form, viz.

$$\frac{dP}{P} = \frac{h_{fg}}{R}\frac{dT}{T^2} \tag{13.49}$$

or

$$\begin{aligned} \int_{P_1}^{P_2} \frac{dP}{P} &= \frac{h_{fg}}{R}\int_{T_1}^{T_2} \frac{dT}{T^2} \\ \ln\left(\frac{P_2}{P_1}\right) &= -\frac{h_{fg}}{R}\left(\frac{1}{T_2} - \frac{1}{T_1}\right) \end{aligned} \tag{13.50}$$

For the purpose of curve-fitting experimental data for the vapor pressure curve, equation (13.50) is often written in the form

$$\ln P = A - \frac{B}{T} \tag{13.51}$$

where A and B are constants determined by the "best fit" to the experimental data. Both equations (13.50) and (13.51) are referred to as the Clausius-Clapeyron relation. Clearly, this relation is only approximately true with the error dependent upon the details of the application.

There is one other useful application of the Clapeyron relation. Since pressure, temperature, and specific volume are readily measured, equation (13.46) can be used to obtain the latent heat from such measurements. In those cases for which the latent heat is also measured, the Clapeyron relation provides a useful check on the consistency of the data.

13.12 Metastable States

All of the equilibrium properties of the pure substance model that we have been discussing thus far are in fact the properties of *stable equilibrium* states. A system can change from one stable equilibrium state to another only if there is a corresponding, finite, permanent change of state of the environment of the system. *Metastable* equilibrium states are states of a system that can be changed at a finite rate to some other stable equilibrium state by means of a finite, but temporary, change of state of the environment in excess of a certain minimum value. In other words, when a system is in a metastable equilibrium state, a fluctuation of sufficient magnitude in the state of the environment can cause the system to experience a change of state at a finite rate. On the other hand, had the initial state of the system been a stable equilibrium state, no finite change of state could have occurred.

For example, when very clean deaerated water is heated at constant pressure in a new glass container without blemishes, the water can be heated significantly above the boiling point corresponding to the pressure without the appearance of any bubbles of the vapor phase. This liquid is termed a superheated liquid and is in a metastable state because the introduction of a small quantity of the vapor phase will cause the rapid (explosive) change to a stable two-phase state consisting of a liquid phase and a vapor phase in mutual equilibrium. The superheated liquid is maintained in the metastable state by the action of surface tension which is ignored in considerations of the pure substance. The extra energy needed to form the liquid surface of the first vapor bubble prevents bubble formation. As a result of metastability of the liquid-vapor phase change, a boiling liquid will normally be at a temperature somewhat higher than the saturation temperature corresponding to the pressure.

Metastable states are also associated with the freezing of a liquid. A clean liquid may be supercooled considerably below the freezing point without the formation of any solid phase. Here again the system is maintained in the metastable state by the surface energy required to form the first small crystal of solid. The introduction of a small amount of solid will produce a rapid solidification in a supercooled liquid. A metastable state associated with a phase change is a single-phase state where at stable equilibrium two phases are present. The energy associated with the formation of the first particle of the second phase is not available so the substance remains in the single phase. Quite often the necessary energy is provided by an external perturbation such as a vibration, and the substance violently reverts to the stable two-phase state.

In some situations metastable states can be used to advantage. In fact many heat treating and other metallurgical processes involve freezing the material in a metastable state by cooling

the substance at a rate sufficient to prevent the formation of the stable equilibrium state. Another example of the useful exploitation of metastable states is the bubble chamber used to detect the presence of high energy nuclear and subnuclear particles. The particles pass through a liquid, usually liquid hydrogen, which has been intentionally placed in a metastable superheated liquid state. The interaction between the particles and the liquid releases sufficient energy to produce a series of bubbles along the path of the particles.

On the other hand, metastable states can sometimes be troublesome. For example, the steam (vapor) flowing at high speed through the nozzles and blades of a steam turbine may be supercooled well below the saturation temperature corresponding to the local pressure. Suddenly, the stream of vapor is perturbed sufficiently to produce a liquid nucleus, and a rapid condensation process ensues, perhaps resulting in mechanical damage to the turbine blades.

13.13 Applications of the Pure Substance Model

In the present chapter we have described the thermodynamic properties of the pure substance model from a phenomenological point of view. This model is very general for a simple system without chemical reactions. Because of this general nature, the pure substance model is useful in a very broad range of physical situations and thus occupies a prominent position in thermal-fluids engineering and the science of thermodynamics, in general. The general nature of the model requires more care in the application of the first and second laws of thermodynamics than was necessary for the ideal gas model. The possibility of a phase change in the pure substance model necessitates the evaluation of properties from tables or charts or software. As we saw in Section 13.9, the proper use of these calculational aids requires that we first establish the number and nature of the phases present in a given state. Having done this, we can then apply the first and second laws of thermodynamics by using the appropriate set of data to evaluate the relevant properties.

The method of analysis for a change of state in the pure substance model are best illustrated by the following numerical examples.

Example 13E.2: A closed, rigid container with an internal volume of $V = 1$ m^3 contains a mass $m = 2$kg of H_2O at a pressure of $P_1 = 7 \times 10^4$ N/m^2. The H_2O experiences a positive, reversible heat transfer changing its state until the final pressure is $P_2 = 3 \times 10^5$ N/m^2.

(a) What are the initial and final temperatures, T_1 and T_2, of the H_2O?

(b) What are the values of the quality, x_1 and x_2, of the H_2O in the initial and final states?

(c) What is the work transfer, $W_{1\text{-}2}$, experienced by the H_2O during the change of state?

(d) What is the heat transfer, $Q_{1\text{-}2}$, experienced by the H_2O during the change of state?

Solution: (a) From the table of the properties of H_2O at pressure of $P_1 = 7 \times 10^4$ N/m^2, we have

$$v_f = 1.0359 \times 10^{-3} \text{ m}^3/\text{kg} \quad \text{and} \quad v_g = 2.3648 \text{ m}^3/\text{kg}$$

The specific volume of the H_2O in the container is

$$v_1 = \frac{V}{m} = \frac{1 \text{ m}^3}{2 \text{ kg}} = 0.5 \text{ m}^3/\text{kg}$$

Since at this pressure $v_f < v_1 < v_g$, the H_2O in the initial state is a two-phase mixture of vapor and liquid. Therefore, the temperature of the H_2O in this state is the saturation temperature at the pressure $P_1 = 7 \times 10^4$ N/m^2. From the top of the pressure column in the table, this temperature is $T_1 = 89.93$ C (the number in parentheses after the pressure). For the final state with an absolute

pressure of $P_2 = 3 \times 10^5$ N/m^2, the table gives $v_f = 1.0732 \times 10^{-3}$ m^3/kg and $v_g = 0.6058$ m^3/kg. Since the tank is closed, the total mass of H_2O (liquid and vapor) does not change. Also, since the tank is rigid, its volume does not change. Thus, $v_2 = 0.5$ m^3/kg. Again, since $v_f < v_2 < v_g$ at this new pressure, the final state is a two-phase state with a temperature equal to the saturation temperature at $P_2 = 3 \times 10^5$ N/m^2. From the table, $T_2 = 133.52$ C. The path of the process would appear as shown in the P-v and T-s diagrams in Figure 13E.2.

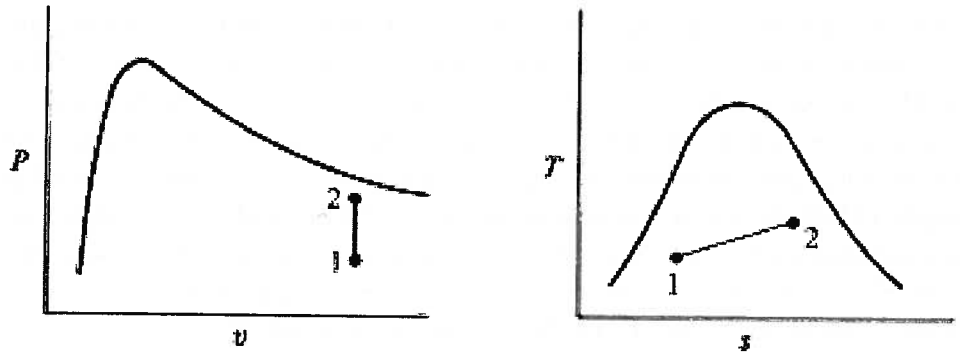

Figure 13E.2 P-v and T-s Diagrams of a Reversible Constant Volume Process in the Two-phase Region of the Pure Substance Model

(b) The quality in both the initial and the final state is determined from the average specific volume which is 0.5 m^3/kg for both states. Then from equation (13.31)

$$x = \frac{v - v_f}{v_g - v_f}$$

The value for the initial state is

$$x_1 = \frac{0.5 \text{ m}^3/\text{kg} - 0.001036 \text{ m}^3/\text{kg}}{2.365 \text{ m}^3/\text{kg} - 0.001036 \text{ m}^3/\text{kg}} = 0.2111$$

For the final state

$$x_2 = \frac{0.5 \text{ m}^3/\text{kg} - 0.0010732 \text{ m}^3/\text{kg}}{0.6058 \text{ m}^3/\text{kg} - 0.0010732 \text{ m}^3/\text{kg}} = 0.8250$$

(c) Since we are modeling the H_2O as a pure substance, the only possible work transfer in this reversible case is associated with the displacement of the boundary of the system. Since the container is rigid and since the two phases fill the container, there is no work transfer for this reversible process. That is,

$$W_{1-2} = \int P dv$$

(d) From the first law of thermodynamics,

$$Q_{1-2} = U_2 - U_1 + W_{1-2}$$

which in this case reduces to

$$Q_{1-2} = U_2 - U_1$$

since $W_{1-2} = 0$. From equation (13.33),

$$u = u_f + u_{fg}$$

Then for the initial state, the table gives $u_f = 376.68$ kJ/kg and $u_{fg} = 2117.2$ kJ/kg and

$$u_1 = 376.68 \text{ kJ/kg} + (0.2111)(2117.2 \text{ kJ/kg}) = 823.62 \text{ kJ/kg}$$

For the final state, the table gives $u_f = 561.10$ kJ/kg and $u_{fg} = 1982.1$ kJ/kg. Then

$$u_2 = 561.10 \text{ kJ/kg} + (0.825)(1982.1 \text{ kJ/kg}) = 2196.3 \text{ kJ/kg}$$

Then the heat transfer for this reversible constant volume change of state is

$$Q_{1-2} = (2.0 \text{ kg})(2196.3 \text{ kJ/kg} - 823.62) = 2745.4 \text{ kJ}$$

Although not an issue in this particular example, students are cautioned about the units used in tabulations of thermodynamic properties. In the interest of conserving space in the tables, the units for both energy and enthalpy are kJ/kg, but the units that result from forming the product Pv are J/kg if the units for P are N/m^2 and the units for v are m^3/kg. Thus, the units of the integral of Pdv for the work transfer will be three orders of magnitude different from the order of magnitude of the units for tabulated values of energy. This can be the source of considerable error when working from tabulated properties unless care is exercised in carrying out the calculations.

Example 13E.3: A closed system contains $m = 0.10$ kg of H_2O at a temperature of $T_1 =$ 180 C and at a pressure of $P_1 = 10^5$ N/m^2. The H_2O is expanded to a final pressure of $P_2 = 2 \times 10^4$ N/m^2 by means of a process that can be modeled as adiabatic and reversible.

(a) What is the temperature, T_2, of the H_2O in the final state?

(b) What is the heat transfer, $Q_{1\text{-}2}$, for the H_2O during the expansion process?

(c) What is the work transfer, $W_{1\text{-}2}$, for the H_2O during the expansion process?

Solution: (a) Since the process connecting the end states is both reversible and adiabatic, the second law of thermodynamics, equation (7.35), shows that the entropy of the steam is constant during this process. From the table of the properties of H_2O, the initial state is clearly a superheated state with $s_2 = s_1 = 7.7503$ kJ/kg K. For the final state at $P_2 = 2 \times 10^4$ N/m^2, the table also shows that $s_f = 0.8320$ kJ/kg K, $s_g = 7.9072$ kJ/kg K, and $s_{fg} = 7.0752$ kJ/kg K. Thus, since $s_f < s_2 < s_g$ at the pressure $P_2 = 2 \times 10^4$ N/m^2, the final state must be a two-phase state. From equation (13.35)

$$x_2 = \frac{s_2 - s_f}{s_{fg}} = \frac{7.7503 \text{ kJ/kg K} - 0.8320 \text{ kJ/kg K}}{7.0752 \text{ kJ/kg K}} = 0.9778$$

Clearly the temperature in this final state is the saturation temperature at $P_2 = 2 \times 10^4$ N/m^2. From the table, $T_2 = 60.06$ C. The path of the process would appear as shown in the P-v and T-s diagrams in Figure 13E.3.

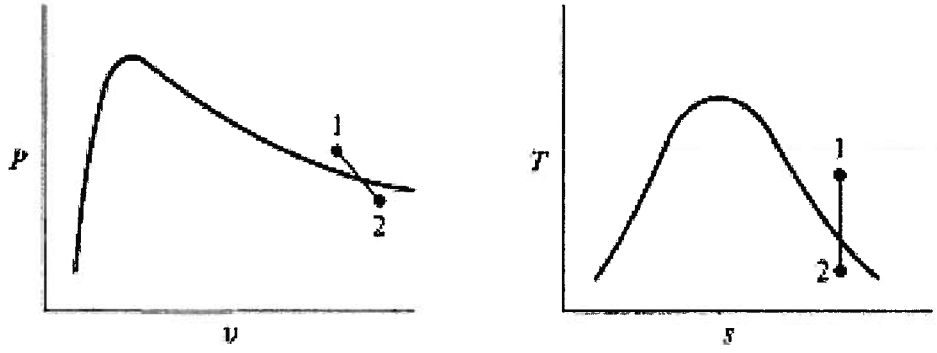

Figure 13E.3 P-v and T-s Diagrams for a Reversible Adiabatic Process in the Pure Substance Model

(b) Since process the process is being modeled as adiabatic and reversible, there is no heat transfer during the expansion.

$$Q_{1-2} = 0$$

(c) To determine the work transfer, we use the first law of thermodynamics.

$$W_{1-2} = Q_{1-2} - (U_2 - U_1)$$

or since the process is adiabatic,

$$W_{1-2} = -(U_2 - U_1) = -m(u_2 - u_1)$$

From equation (13.33) and the data of the table, the specific internal energy of the final state is

$$u_2 = 251.40 \text{ kJ/kg} + (0.9778)(2204.6 \text{ kJ/kg}) = 2407.1 \text{ kJ/kg}$$

For the specific internal energy of the initial state, the table gives

$$u_1 = 2628.1 \text{ kJ/kg}$$

Thus,

$$W_{1-2} = (0.10 \text{ kg})(2628.1 \text{ kJ/kg} - 2407.1 \text{ kJ/kg}) = 22.10 \text{ kJ}$$

Example 13E.4: A piston-cylinder apparatus is fitted with a frictionless piston capable of maintaining a constant absolute pressure of $P = 10^5$ N/m^2 on a mass $m = 0.1$ kg of H_2O. The H_2O, which is all saturated liquid in the initial state, is heated reversibly until all of the liquid is converted to saturated vapor.

(a) What are the temperatures, T_1 and T_2, of the H_2O in the initial and final states?

(b) What is the reversible heat transfer, Q_{1-2}, necessary to achieve this change of state?

(c) What is the reversible work transfer, W_{1-2}, associated with this change of state?

Solution: (a) Since the process involves a change of state from saturated liquid to saturated vapor at constant pressure and since the pressure and temperature are directly related for two-phase equilibrium states of a pure substance, the temperature must also remain constant throughout the process. The temperature is the saturation temperature corresponding to the pressure of the system, $P = 10^5$ N/m^2. From the table of the properties of H_2O, the saturation temperature corresponding to this pressure is $T_{sat} = T_2 = 99.61$ C. Thus the path of this process would appear as shown in the P-v and T-s diagrams in Figure 13E.4.

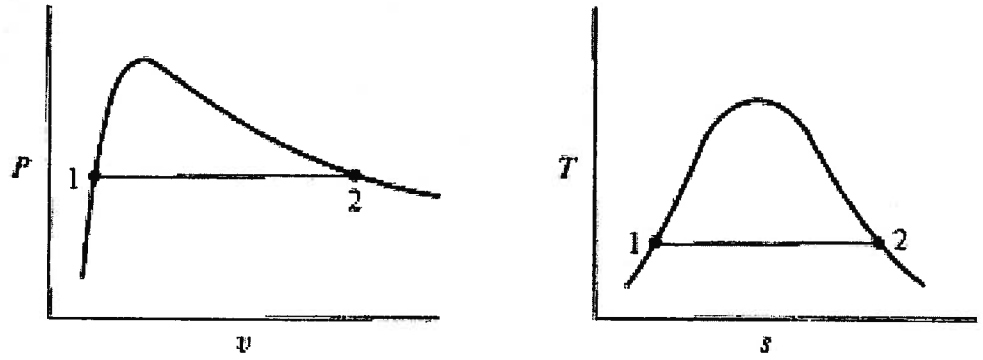

Figure 13E.4 P-v and T-s Diagrams for a Reversible Constant Pressure Phase Change in the Pure Substance Model

(b) Since the process from state 1 to state 2 is quasi-static and isothermal, we can according to the second law of thermodynamics calculate the heat transfer for this process from the relation

$$Q_{1-2} = mT(s_2 - s_1)$$

Since state 1 is a saturated liquid state and state 2 is a saturated vapor state, the expression for the heat transfer reduces to

$$Q_{1-2} = mT\left(s_g - s_f\right) = mTs_{fg}$$

From the tabulated properties for the pure substance model of H_2O at $P = 10^5$ N/m^2, $s_{fg} = 6.0560$ kJ/kg K. Then since $T = 99.61$ C + 273.15 K = 372.76 K

$$Q_{1-2} = (0.1 \text{ kg})(372.76 \text{ K})(6.0560 \text{ kJ/kg K}) = 225.74 \text{ kJ}$$

Alternatively, we could have calculated the heat transfer from the first law of thermodynamics. For this reversible constant pressure process the first law can be written

$$Q_{1-2} - mP\left(v_2 - v_1\right) = m\left(u_2 - u_1\right)$$

or

$$Q_{1-2} = m\left(u_2 - u_1\right) + mP\left(v_2 - v_1\right) = m\left(h_2 - h_1\right)$$

Again since the end states are saturated states, this expression reduces to

$$Q_{1-2} = mh_{fg} = (0.10 \text{ kg})(2257.4 \text{ kJ/kg}) = 225.74 \text{ kJ}$$

(c) The work transfer for this reversible constant pressure process is

$$W_{1-2} = mP\left(v_2 - v_1\right)$$

Since the end states are saturated states,

$$W_{1-2} = mP\left(v_g - v_f\right) = mPv_{fg}$$

From the table, $v_g = 1.6939$ m^3/kg, $v_f = 1.0432 \times 10^{-3}$ m^3/kg, and $v_{fg} = 1.6929$ m^3/kg. Then

$$W_{1-2} = (0.10 \text{ kg})\left(10^5 \text{ N/m}^2\right)\left(1.6929 \text{ m}^3/\text{kg}\right) = 1.6929 \times 10^4 \text{ J} = 16.93 \text{ kJ}$$

Note the units. Note also that the above results are in distinct contrast to what we would have expected from an ideal gas. For the pure substance model, since two phases are present, the temperature also remains constant even though we are only maintaining the pressure constant by physical means. For the ideal gas model the constant temperature requires that the internal energy be constant. Then according to the first law of thermodynamics, the work transfer and heat transfer are equal. Clearly this is not the case in the present example for which the heat transfer is a whole order of magnitude greater than the work transfer. Obviously the internal energy in the present case is not constant. In fact the change in internal energy is equal to mu_{gf}

$$m\left(u_2 - u_1\right) = mu_{fg} = (0.10 \text{ kg})(2088.2 \text{ kJ/kg}) = 208.82 \text{ kJ}$$

Example 13E.5: Consider two separate systems A and B. System A consists of a rigid vessel that contains $m_A = 1$ kg of saturated liquid H_2O at a pressure of $P_{A1} = 10^5$ N/m^2. System B consists of a similar rigid vessel that contains $m_B = 1$ kg of saturated vapor H_2O at the same pressure of $P_{B1} = 10^5$ N/m^2. The contents of each vessel experience reversible heat transfer until the pressure reaches $P_{A2} = P_{B2} = 4 \times 10^5$ N/m^2 in each case.

(a) What is the volume of each vessel?

(b) On a single set of axes representing P, the pressure of the H_2O, on the vertical axis and v, the specific volume of the H_2O, on the horizontal axis, sketch the locus of states that each system passes through during the quasi-static heat transfer process. Be sure to include the locus of saturated states.

(c) What are the temperatures, T_{A2} and T_{B2}, of the H_2O in each vessel, respectively, at the conclusion of the heat transfer process? Why is T_{A2} different from T_{B2}?

(d) Calculate the heat transfers, $(Q_{1-2})_A$ and $(Q_{1-2})_B$, experienced by the two systems, respectively. Why is $(Q_{1-2})_A$ different from $(Q_{1-2})_B$?

Solution:(a) Since system A is a saturated liquid, its volume is

$$V_A = m_A v_A = (1 \text{ kg})(1.0432 \times 10^{-3} \text{ m}^3/\text{kg}) = 1.0432 \times 10^{-3} \text{ m}^3$$

Since system B is a saturated vapor, its volume is

$$V_B = m_B v_B = (1\text{ kg})(1.6939\text{ m}^3/\text{kg}) = 1.6939\text{ m}^3$$

(b)

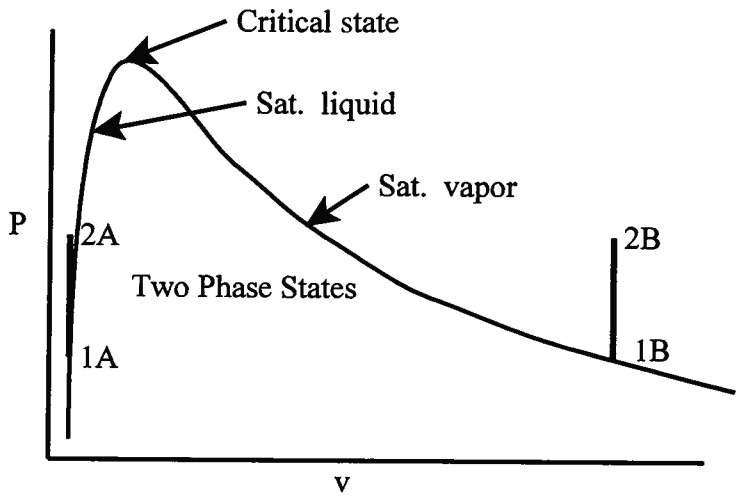

(c) To determine the temperature in the final state in each case, we make use of the fact that the volume does not change in either case. Then, we have in each case two independent properties, P and V, in the final state. Then the final temperature can be determined from the tabulated properties, viz.

$$P_{A2} = 4 \text{ x } 10^5\text{ N/m}^2,\ v_{A2} = v_{A1} = 1.0432 \text{ x } 10^{-3}\text{ m}^3/\text{kg} : T_{A2} = 100\text{ C}$$
$$P_{B2} = 4 \text{ x } 10^5\text{ N/m}^2,\ v_{B2} = v_{B1} = 1.6939\text{ m}^3/\text{kg} : T_{B2} = 1195.2\text{ C}$$

The two temperatures are different because system A is a liquid which is very weakly coupled so its temperature changes only a modest amount for a given change in pressure, but system B is a vapor which is very strongly coupled which results in a large temperature change for a given pressure change.

(d) To determine the heat transfer, it is necessary to apply the first law in each case. Since the vessels are rigid, there is no work transfer. Then the first law for these closed systems reduces to

$$(Q_{1-2})_A = U_{A2} - U_{A1} = m_A(u_{A2} - u_{A1}) = (1\text{ kg})(418.97\text{ kJ/kg} - 417.40\text{ kJ/kg}) = 1.57\text{ kJ}$$

$$(Q_{1-2})_B = U_{B2} - U_{B1} = m_B(u_{B2} - u_{B1}) = (1\text{ kg})(4456.8\text{ kJ/kg} - 2505.6\text{ kJ/kg}) = 1951.2\text{ kJ}$$

Once again the coupling comes into play producing a huge difference between these two results.

Example 13E.6: Cryogens, low-temperature liquefied gases, are stored in vessels known as Dewars. A Dewar storage vessel consists of a double-walled container with the space between the walls evacuated and filled with some low-density solid material designed to reduce the thermal radiation from the high temperature outer wall to the low temperature inner wall. In a particular design, a Dewar for storing liquid N_2 has a volume of V = 160 liters with a residual heat leak of $\dot{Q}$ = 1.67 W. Because of the residual heat leak, N_2 vapor must be continually vented to the atmosphere through a vent valve in order to maintain the internal pressure at $1\text{x}10^5\text{ N/m}^2$. As an added safety feature, the Dewar is also fitted with a relief valve that "blows" when the internal pressure reaches a dangerously high level.

In a particular incident, a Dewar initially contains V_{f1} = 140 liters of liquid N_2 in equilibrium with V_{g1} = 20 liters of vapor at a pressure of $P_1 = 1 \text{ x } 10^5\text{ N/m}^2$. The vent valve becomes blocked causing the internal pressure of the Dewar to rise to a value of $P_2 = 5 \text{ x } 10^5\text{ N/m}^2$. At this pressure, the relief valve "blows" and releases N_2 very rapidly until the internal pressure falls to $P_3 = 1\text{x}10^5\text{ N/m}^2$.

(a) How long did it take before the relief valve "blew" in this incident?

(b) We are interested in determining the amount of N_2 that remained in the Dewar after the relief valve finished venting N_2 to the atmosphere. Formulate an appropriate model for the process experienced by this N_2 during the "blow down" process, and use this model to estimate the amount of N_2 that remained in the Dewar by the time the pressure fell to $P_3 = 1 \times 10^5$ N/m^2. Specify the state of the N_2.

Solution: (a) The process of heat transfer to the liquid nitrogen container occurs while the nitrogen is held at constant volume. Then from the first law for the nitrogen as a system, we have

$$Q_{1-2} = m_{N_2}(u_2 - u_1) = \dot{Q}\Delta t$$

where the $\dot{Q}$ is the heat leak into the Dewar. It is necessary for us to first determine the mass of nitrogen in the Dewar in order to evaluate the necessary properties.

$$V_{f_1} = 0.140 \text{ m}^3 = m_{f_1} v_{f_1}$$

$$m_{f_1} = \frac{0.140 \text{ m}^3}{1.236 \text{ x } 10^{-3} \text{ m}^3/\text{kg}} = 113.269 \text{ kg}$$

$$V_{g_1} = 0.020 \text{ m}^3 = m_{g_1} v_{g_1}$$

$$m_{g_1} = \frac{0.020 \text{ m}^3}{0.2195 \text{ m}^3/\text{kg}} = 0.091 \text{ kg}$$

$$m_{N_2} = 113.269 \text{ kg} + 0.091 \text{ kg} = 113.36 \text{ kg}$$

$$x_1 = \frac{m_{g_1}}{m_{N_2}} = \frac{0.091 \text{ kg}}{113.36 \text{ kg}} = 8.038 \text{ x } 10^{-4}$$

$$v_1 = v_{f1} + x_1 v_{fg_1} = v_{f1} + x_1(v_{g_1} - v_{f_1})$$

$$v_1 = 1.236 \text{ x } 10^{-3} \text{ m}^3/\text{kg} + (8.038 \text{ x } 10^{-4})(0.2195 \text{ m}^3/\text{kg} - 1.236 \text{ x } 10^{-3} \text{ m}^3/\text{kg})$$

$$v_1 = 1.411 \text{ x } 10^{-3} \text{ m}^3/\text{kg}$$

$$u_1 = u_{f_1} + x_1(u_{g_1} - u_{f_1})$$

$$u_1 = -121.7 \text{ kJ/kg} + (8.038 \text{ x } 10^{-4})(177.1 \text{ kJ/kg}) = -121.558 \text{ kJ/kg}$$

For the state at the end of the constant volume heat transfer process, we have

$$v_2 = v_1 = v_{f_2} + x_2 v_{fg_2}$$

$$x_2 = \frac{v_2 - v_{f_2}}{v_{fg_2}} = \frac{1.411 \text{ x } 10^{-3} \text{ m}^3/\text{kg} - 1.381 \text{ x } 10^{-3} \text{ m}^3/\text{kg}}{0.04712 \text{ m}^3/\text{kg}} = 6.459 \text{ x } 10^{-4}$$

$$u_2 = u_{f_2} + x_2 u_{fg_2} = -86.76 \text{ kJ/kg} + (6.459 \text{ x } 10^{-4})(-149.9 \text{ kJ/kg}) = -86.857 \text{ kJ/kg}$$

$$Q = (113.36 \text{ kg})[-86.857 \text{ kJ/kg} - (-121.558 \text{ kJ/kg})] = 3.934 \text{ x } 10^6 \text{ J}$$

$$\Delta t = \frac{Q}{\dot{Q}} = \frac{3.934 \text{ x } 10^6 \text{ J}}{1.67 \text{ J/sec}} = 2.355 \text{ x } 10^6 \text{ sec} = 654.304 \text{ hr}$$

(b) To estimate the amount of nitrogen that remains in the Dewar after the explosion, we consider the control volume shown in Figure 13E.6. We model the control volume as adiabatic in light of the rapid nature of the process and the considerable insulation on the outside of the Dewar. If we further model the state of the fluid inside the Dewar as one of uniform state, this is equivalent to modeling the process experienced by the nitrogen inside the Dewar as a reversible

one since the fluid passes through a series of equilibrium states. Since the two-phase nitrogen that remains in the Dewar experiences a reversible, adiabatic process, its entropy will be unchanged throughout the process.

The rationale for this model is that the nitrogen escaping from the Dewar provides an inertial resistance to the expanding nitrogen as it tries to accelerate the escaping vapor through the relief valve. The flow resistance encountered by the escaping vapor as it passes through the valve is due to its viscosity. These resistances combine to make the process in the expanding nitrogen look like a quasi-static process. That is, if we were to imagine an interface between the escaping vapor and the expanding two-phase nitrogen, the motion of this interface would be slow relative to the rate at which mechanical equilibrium is being established in the expanding two-phase nitrogen. Note that this observation applies only to the nitrogen that remains in the Dewar and that the overall process of discharging the nitrogen from the Dewar is not reversible due to the irreversibility of the nitrogen flowing through the flow resistance presented by the relief valve.

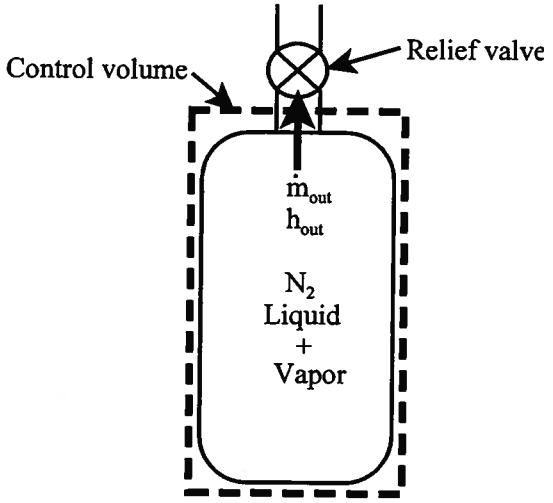

Figure 13E.6 Dewar Control Volume

From the first law for the control volume, we have

$$\left(\frac{dE}{dt}\right)_{CV} = \cancel{\dot{Q}} - \cancel{\dot{W}_{shaft}} + \dot{m}_{in}\left(h + \cancel{\frac{v^2}{2}} + gz\right)_{in} - \dot{m}_{out}\left(h + \cancel{\frac{v^2}{2}} + \cancel{gz}\right)_{out}$$

According to the uniform state model, the left-hand side becomes

$$\frac{d}{dt}(mu)_{CV} = -\dot{m}_{out}h_{out}$$

Substituting the continuity equation, we obtain for the first law

$$\frac{d}{dt}(mu)_{CV} = h_{out}\frac{dm_{CV}}{dt}$$

If we now integrate this expression over the time duration of the blow down process, we obtain

$$\int_0^{t_0}\frac{d}{dt}(mu)_{CV}\,dt = \int_0^{t_0} h_{out}\frac{dm_{CV}}{dt}dt$$

$$\left[(mu)_{CV}\right]_{t=t_0} - \left[(mu)_{CV}\right]_{t=0} = \int_0^{t_0} h_{out}\frac{dm_{CV}}{dt}dt$$

$$m_3u_3 - m_2u_2 = \int_0^{t_0} h_{out}\frac{dm_{CV}}{dt}dt$$

In order to integrate the right-hand side of this expression, we must be cognizant of the fact that the pressure of the nitrogen in the Dewar is continually decreasing as the blow down process progresses. This means that the value of the enthalpy of the fluid leaving the Dewar changes with time. Then if there is always liquid and vapor nitrogen in equilibrium with one another inside the Dewar throughout the blow down process, the pressure of the two phases inside the Dewar will always be the saturation pressure which, of course, is changing with time. Then first law can be written

$$m_3u_3 - m_2u_2 = \int_{(P_{sat})_2}^{(P_{sat})_3} h_{out}(P_{sat})\frac{dm_{CV}(P_{sat})}{dt}\frac{dt}{dP_{sat}}dP_{sat}$$

where the notation $h_{out}(P_{sat})$ and $m_{CV}(P_{sat})$ is intended to indicate that the values of h_{out} and m_{CV} depend upon the instantaneous value of the saturation pressure. Given the complex dependence of the properties on the saturation pressure, it is necessary to evaluate this expression numerically recognizing that there is a constraint on the volume of the nitrogen. For each state i that the expanding nitrogen passes through, we have the requirement that it must fill the Dewar at all times. Then

$$V_{Dewar} = m_i v_i = m_i\left(v_{fi} + x_i v_{fgi}\right)$$

Carrying out the integration numerically, we obtain the result $m_3 = 93.909$ kg.

It is worth noting that an approximate result can be obtained by assuming that the value of h_{out} is constant. This is reasonable in the present case since $h_{out} = h_g$ varies by about 15 percent over the range of pressures involved. Then the first law becomes

$$m_3u_3 - m_2u_2 = h_{out}\left(m_3 - m_2\right)$$

$$m_3\left(u_{f3} + x_3u_{fg3}\right) - m_2u_2 = h_{out}m_3 - h_{out} - m_2$$

At first glance it would appear that there are two unknowns in this equation, m_3 and x_3, but the constraint on the volume eliminates one of these, viz.

$$V_{Dewar} = m_3v_3 = m_3\left(v_{f3} + x_3v_{fg3}\right)$$

$$x_3 = \left(\frac{V_{Dewar}}{m_3} - v_{f3}\right)\frac{1}{v_{fg3}}$$

Substituting this result into the integrated form of the first law and solving for m_3, we get

$$m_3 = \frac{m_2u_2 - h_{out}m_2 - \dfrac{u_{fg3}V_{Dewar}}{v_{fg3}}}{u_{f3} - \dfrac{u_{fg3}v_{f3}}{v_{fg3}} - h_{out}}$$

From part (a) above, $u_2 = -86.857$ kJ/kg and $m_2 = 113.36$ kg. At $P_{sat} = 5 \times 10^5$ N/m^2, $h_g = 86.523$ kJ/kg and at $P_{sat} = 1 \times 10^5$ N/m^2, $h_g = 77.073$ kJ/kg. The numerical average of these two values for the enthalpy is $h_{out} = 81.798$ kJ/kg. At $P_3 = 1 \times 10^5$ N/m^2, $u_{f3} = -122.37$ kJ/kg, $u_{fg3} = 177.496$ kJ/kg, $v_{f3} = 1.22398 \times 10^{-3}$ m^3/kg, and $v_{fg3} = 0.21823$ m^3/kg. The volume of the Dewar is $V_{Dewar} = 0.160$ m^3. Substituting these values and solving for m_3, we get $m_3 = 93.822$ kg. Compared with the numerical integration, this results in an error that is on the order of 0.1 percent. Note that not all approximations are this good. In this case, the range of pressures involved is relatively small so the approximation works quite well. In general, the error would be larger.

Example 13E.7: A rigid, insulated vessel is fitted with a single port for filling and emptying. Initially, the valve on the port is closed after the vessel has been evacuated. The vessel

is to be filled with H_2O from a supply line with constant supply conditions of P_s = 1 x 10^6 N/m^2 and T_s = 300 C. The valve is opened and H_2O is allowed to flow until the pressure in the vessel reaches P_2 = 1 x 10^6 N/m^2. At this time the valve is closed.

(a) What is the temperature, T_2, of the H_2O in the vessel the instant the valve is closed?

(b) Why is the temperature of the H_2O in the vessel different from the temperature of the H_2O in the charging line at the instant mechanical equilibrium is established between the contents and the H_2O in the supply line?

(c) The H_2O is now allowed to come to thermal equilibrium with the environment at T_{env} = 40 C. What is the pressure, P_3, of the H_2O in the vessel at this time?

(d) What is the heat transfer, $Q_{2\text{-}3}$, for the H_2O during the thermal equilibration process?

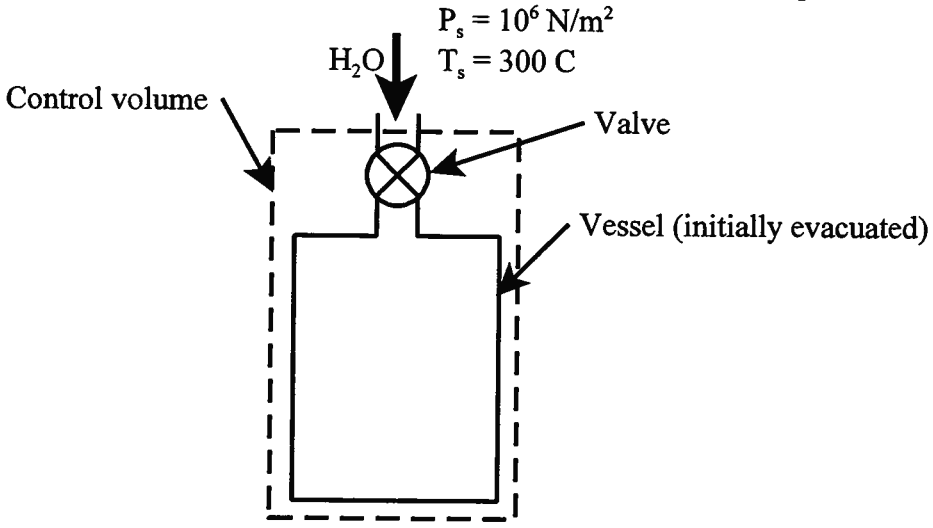

Figure 13E.7

Solution: (a) The vessel being filled can be modeled as an open system since mass flows across its boundary. Schematically, the system would appear as shown in Figure 13E.7. Since the filling process occurs so rapidly, there is no time for heat transfer. There is obviously no shaft work transfer and kinetic and potential energies are negligible. The first law for this control volume with unsteady flow and a uniform state is given by

$$\frac{\partial}{\partial t}(E_{CV}) = \frac{\partial}{\partial t}(m_{CV}u_{CV}) = \dot{m}_{in}h_{in}$$

but the continuity equation gives

$$\frac{\partial}{\partial t}m_{CV} = \dot{m}_{in} - \dot{m}_{out} = \dot{m}_{in} - 0$$

Then the first law becomes

$$\frac{\partial}{\partial t}(m_{CV}u_{CV}) = h_{in}\frac{\partial}{\partial t}m_{CV}$$

Since h_{in} is constant, we can integrate this expression. Then

$$m_2u_2 - m_1u_1 = h_{in}(m_2 - m_1)$$

$$m_2u_2 = m_2h_{in}$$

$$u_2 = h_{in}$$

Then from the tabulated properties of H_2O, it follows that $u_2 = h_{in}$ = 3051.2 kJ/kg. Then interpolating linearly, we get T_2 = 456.53 C.

(b) The temperature of the steam inside the vessel immediately upon establishing

mechanical equilibrium is higher than the temperature of the steam in the supply line because of the flow work done on the steam in order to push it inside the vessel. Remember that the first mass element that enters the evacuated vessel will fill the vessel immediately upon entry. Then the next mass element that enters has to compress the fluid (vapor) already in the vessel. This adiabatic compression of mass elements that entered the vessel previously continues until mechanical equilibrium (but not thermal equilibrium) is established between the vessel contents and the steam in the supply line. Thus the temperature of the steam in the vessel is higher than the temperature of the steam in the supply line due to the fact that the rate processes responsible for establishing mechanical equilibrium are significantly faster than the rate processes responsible for establishing thermal equilibrium.

(c) After the valve is closed, the vessel acts like a closed system. Then for the thermal equilibration process which occurs at constant volume, the specific volume of the steam remains constant. Thus

$$v_3 = v_2 = 0.33355 \text{ m}^3/\text{kg}$$

This value of the specific volume lies between the values of the specific volume s for the saturated liquid and the saturated vapor at 40 C. Thus the pressure of the steam at 40 C is the saturation pressure, $P_3 = 7.384 \text{ x } 10^3 \text{ N/m}^2$.

(d) The equilibration process occurs at constant volume. Thus, there is no work transfer during this process. Then the first law gives

$$Q_{2-3} = m(u_3 - u_2)$$

but

$$v_3 = v_{f_3} + x_3 v_{fg_3} = 1.0078 \text{ x } 10^{-3} \text{ m}^3/\text{kg} + x_3 19.522 \text{ m}^3/\text{kg}$$

$$x_3 = \frac{0.33355 \text{ m}^3/\text{kg} - 1.0078 \text{ x } 10^{-3} \text{ m}^3}{19.522 \text{ m}^3/\text{kg}} = 0.017034$$

$$u_3 = u_{f_3} + x_3 u_{fg_3} = 167.56 \text{ kJ/kg} + (0.01703)(2262.6 \text{ kJ/kg}) = 206.10 \text{ kJ/kg}$$

Then the heat transfer per unit mass of H_2O in the vessel is

$$q = u_3 - u_2$$

$$q = 206.10 \text{ kJ/kg} - 3051.2 \text{ kJ/kg} = -2845.1 \text{ kJ/kg}$$

Example 13E.8: As shown schematically in Figure 13E.8, a manufacturing plant has a stream of saturated H_2O vapor available at a mass flow rate of $\dot{m}_1 = 1$ kg/sec and a temperature of $T_s = 300$ C, but it needs two streams of H_2O vapor, one stream at a pressure of $P_2 = 2 \text{ x } 10^6 \text{ N/m}^2$ and a temperature of $T_2 = 400$ C, the other at a pressure of $P_3 = 10^5 \text{ N/m}^2$ and a temperature of $T_3 = 200$ C. It is proposed to split the supply stream into the two required streams in a steady flow system whose only interaction is a heat transfer with the environment at a temperature of $T_{atm} = 300$K.

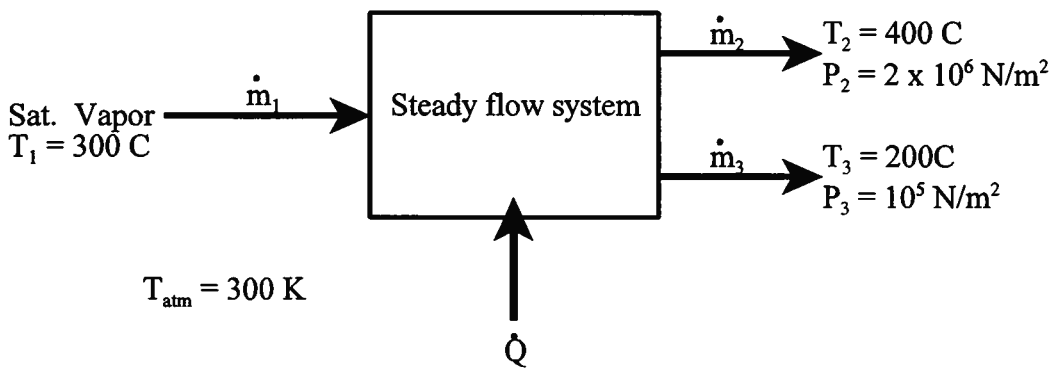

Figure 13E.8

(a) Calculate the mass flow rates of streams 2 and 3.

(b) If the system operates in a reversible manner, what is the magnitude and direction of the heat transfer rate? What is the effect of irreversibility on this heat transfer rate and the flow rates?

Solution: (a) For this open system in steady flow, we have for the continuity equation

$$\dot{m}_1 = 1 \text{ kg/sec} = \dot{m}_2 + \dot{m}_3$$

$$\dot{m}_3 = 1 - \dot{m}_2$$

The first law reduces to

$$\dot{Q} = \dot{m}_2 h_2 + \dot{m}_3 h_3 - \dot{m}_1 h_1 = \dot{m}_2 h_2 + (1 - \dot{m}_2) h_3 - h_1$$

$$\dot{Q} = \dot{m}_2 (3248.3 \text{ kJ/kg}) + (1 - \dot{m}_2)(2875.5 \text{ kJ/kg}) - (1 \text{ kg/sec})(2749.6 \text{ kJ/kg})$$

$$\dot{Q} = 125.90 \text{ kW} + \dot{m}_2 (372.80 \text{ kJ/kg})$$

If the system is reversible, the second law gives

$$\dot{Q} = T_{atm} \left[\dot{m}_2 s_2 + (1 - \dot{m}_2) s_3 - s_1 \right]$$

$$\dot{Q} = (300 \text{ K}) \left[\dot{m}_2 (7.1292 \text{ kJ/kg K}) + (1 - \dot{m}_2)(7.8356 \text{ kJ/kg K}) - (1 \text{ kg/sec})(5.7059 \text{ kJ/kg K}) \right]$$

$$\dot{Q} = 638.91 \text{ kW} - \dot{m}_2 (211.92 \text{ kJ/kg})$$

Solving the expressions simultaneously, we get

$$\dot{m}_2 = 0.877 \text{ kg/sec}$$

$$\dot{m}_3 = 0.123 \text{ kg/sec}$$

(b) The heat transfer for reversible operation is then given by either the first law or the second law, viz.

$$\dot{Q} = 638.91 \text{ kW} - (0.877 \text{ kg/sec})(211.92 \text{ kJ/kg}) = 452.98 \text{ kW}$$

Note that the heat transfer is positive, i.e., into the system. If the operation is irreversible, the effect is to reduce this heat transfer rate since entropy is now being generated within the control volume thereby reducing the need for positive entropy transfer from the environment, and hence, heat transfer, across the control surface. However, since the energy associated with this heat transfer interaction is the source of the flow work driving the high energy (actually, high enthalpy) flow, stream 2, the reduced heat transfer will result in a reduction in the flow rate in stream 2 and an increase in the flow rate of stream 1, the less energetic (lower enthalpy) stream.

13.14 Heat Transfer Interactions in the Pure Substance Model

The fact that the pure substance can experience a change in phase as a result of a heat transfer interaction gives rise to two new mechanisms of heat transfer that we have not considered heretofore. As described in Section 13.5, the transformation of a saturated liquid into a saturated vapor at constant pressure, and, hence, constant temperature, is known as *evaporation* or *boiling* and constitutes one of these new mechanisms. The other mechanism is associated with the reverse phase transformation from saturated vapor to saturated liquid and is known as *liquefaction* or *condensation*. From a physical point of view, both boiling heat transfer and condensation heat transfer are exceedingly complex and necessitate expanding the pure substance model in order to account for the surface forces that are essential to both mechanisms. This has presented a considerable challenge to the thermal-fluid engineer – a challenge more than worth

the effort since the heat fluxes that result from these two mechanisms are quite high and can reach magnitudes of one megawatt/square meter or higher. This means that these processes can be valuable design tools to the thermal-fluid engineer since high heat fluxes can result in a considerable reduction in the size of heat transfer equipment with a concomitant reduction in the cost of the apparatus.

Because of the complexities of the physics of these processes, analytical models that can be used to predict their behavior are also complex and in many cases only approximations of the true situation. Nonetheless, because of their importance in the design of thermal-fluid equipment, these mechanisms have been the subject of intense investigation by thermal-fluid engineers for more than half a century and these investigations continue to this day. The result of all this effort has been a basic understanding of the underlying physics of the mechanisms and the formulation of heat transfer correlations that are useful to the thermal-fluid engineer in the design of devices that exploit these mechanisms. In the present section, we shall examine these mechanisms in some detail and present useful correlations of their behavior.

13.14.1 Boiling Heat Transfer

The fundamental process of boiling heat transfer involves a solid surface in contact with a liquid which may be either a saturated liquid or a subcooled liquid. Typically, the temperature of the solid surface at the interface with the liquid is higher than the saturation temperature of the liquid corresponding to its pressure by an amount $\Delta T = T_s - T_{sat}$. The boiling mechanism that ensues is a function of the magnitude of ΔT and the conditions of the surface such as its surface condition, the material of construction, and its orientation with respect to the gravity vector.

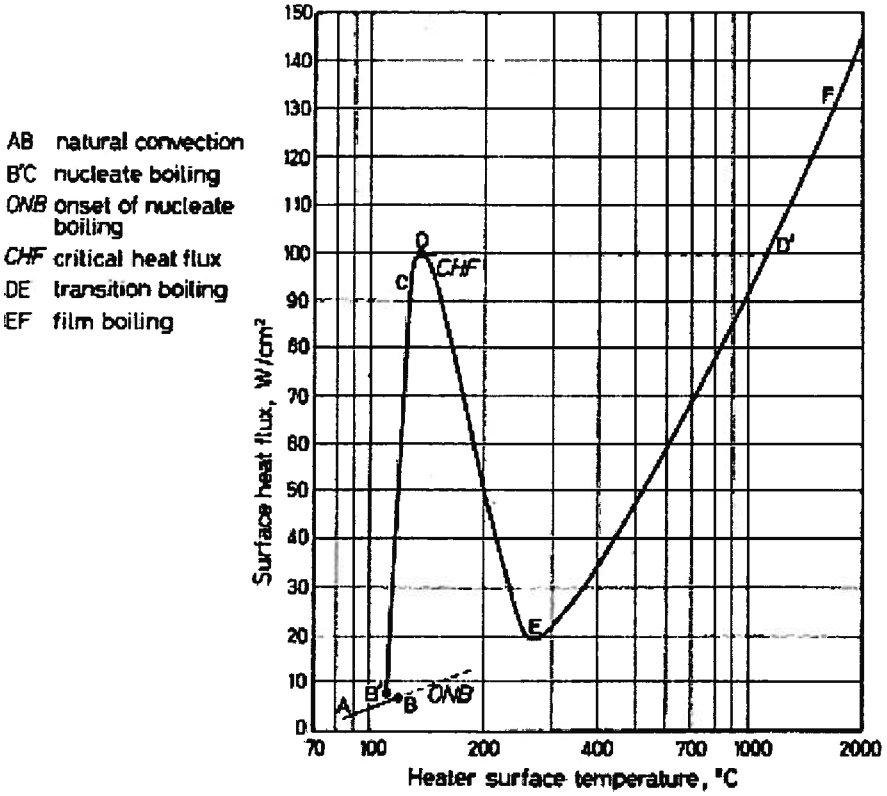

Figure 13.11 Pool Boiling Heat Transfer Data for H_2O at Atmospheric Pressure (From J. G. Collier and J. R. Thome, *Convective Boiling and Condensation*, 3rd Edition, Oxford University Press, 1999, p. 149, Fig. 4.10.)

Consider a typical boiling heat transfer condition known as *pool boiling* since the liquid experiencing the phase transformation exists as a pool of liquid sitting on a heater surface. (Later we shall consider the case in which the liquid is moving with some velocity past the heater surface. This latter case is known as forced convection boiling.) Figure 13.11 shows the surface heat flux for a pool of saturated liquid H_2O on a horizontal heater surface at atmospheric pressure.

The details of the boiling heat transfer mechanism change as the value of ΔT increases. Several different regimes can be identified on Figure 13.11,and these are shown schematically in Figure 13.12:

(1) natural convection, path A to B
(2) nucleate boiling, path B′ to D
(3) transition boiling, path D to D′
(4) film boiling, D′ to F

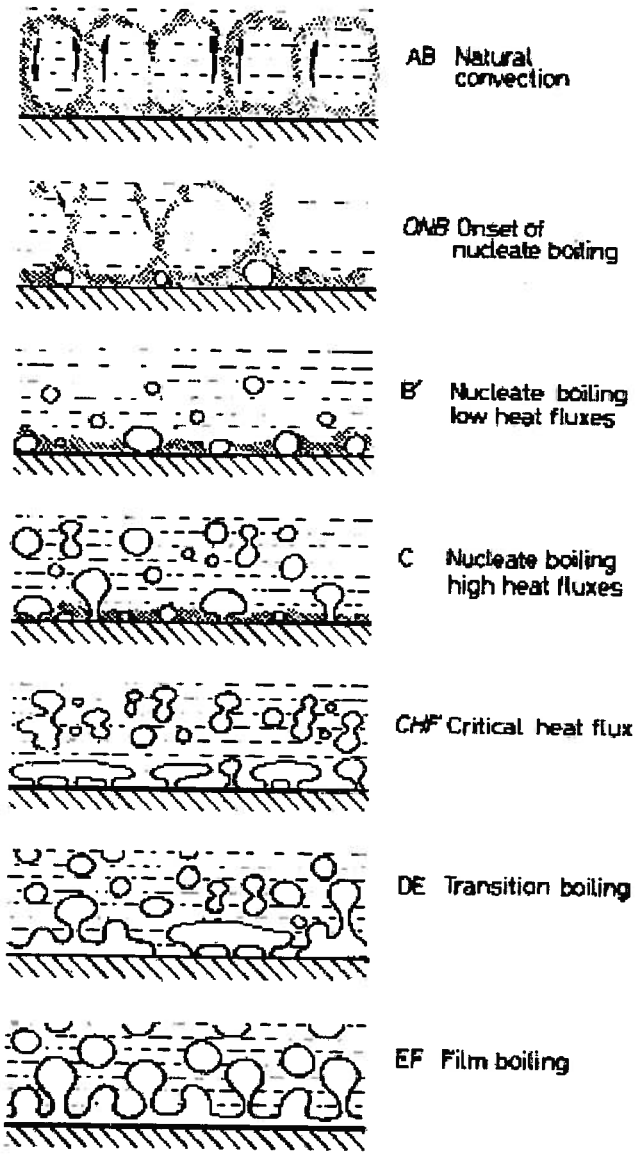

Figure 13.12 Regimes of Pool Boiling
(From J. G. Collier and J. R. Thome, *Convective Boiling and Condensation*, 3rd Edition, Oxford University Press, 1999, p. 150, Fig. 4.11.)

13.14.1.1 Natural Convection: As heater power is increased and the surface temperature of the heater increases from 70 C to 100 C and beyond, the data follow the curve from A to B′ to C to D in the natural convection and nucleate boiling regimes. In the range A to B, the heat transfer mechanism is by free convection from a heated horizontal surface facing up as we discussed in Section 11.7. The resulting free convection cells are shown schematically in Figure 13.12 and the heat transfer data can be correlated by the expression

$$Nu = 0.14[GrPr]^{1/3}$$

$$\frac{hD}{k_f} = 0.14\left[\left(\frac{\beta g \Delta T D^3 \rho_f^2}{\mu_f^2}\right)\left(\frac{\mu c_P}{k}\right)_f\right]^{1/3} \tag{13.52}$$

Notice that the free convection regime continues into the range where the surface temperature exceeds the saturation temperature, T_{sat} = 100C. This is due to the fact that the vapor in the bubbles that are trying to form on the heater surface must have some superheat to compensate for the surface energy associated with the vapor-liquid interface of the bubbles. In order to provide the necessary superheat, there must be a temperature gradient in the liquid pool in the neighborhood of the heater surface. This gradient provides a means for the energy and entropy to flow from the heater surface into the liquid pool. Clearly this is not a true equilibrium situation in the sense of the pure substance model discussed thus far. The liquid layer with the temperature gradient is a superheated liquid since its temperature exceeds the saturation temperature, and it is, therefore, in a metastable state as described in Section 13.12. However, we can use the equilibrium pure substance model to gain some understanding of the basic physics of the boiling heat transfer mechanism.

13.14.1.2 Bubble Dynamics: Despite the presence of the aforementioned temperature gradient at the heater surface, the bulk of the liquid is at the saturation temperature dictated by the externally imposed pressure, atmospheric pressure in the case under consideration. The localized temperature gradient plays a key role in the formation of the vapor-liquid interface associated with the boiling heat transfer mechanism. Consider a spherical bubble in local thermodynamic equilibrium with the layer of superheated liquid in which it is immersed as shown in Figure 13.13.

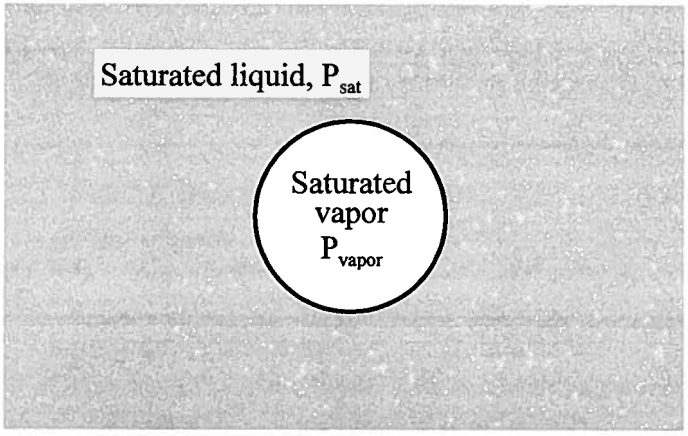

Figure 13.13 Vapor Bubble in Equilibrium with Liquid

Consistent with the pure substance model, gravity effects on the local pressure in the liquid are

assumed negligible. Then for a liquid at nearly uniform temperature except for the metastable layer, the pressure exerted by the liquid on the vapor bubble is the saturation pressure. Since the vapor bubble sits in the temperature gradient at the heater surface, the vapor phase is in thermal equilibrium with the liquid at its local temperature. Thus, the vapor pressure inside the bubble is greater than the saturation pressure of the liquid pool that surrounds it. For this value of the pressure exerted by the vapor, there is only one size vapor bubble that can exist in mechanical equilibrium with the saturated liquid. The radius of this bubble is known as the critical radius and is denoted by the symbol R_c. We can determine the critical radius by considering a free-body consisting of half the bubble as shown in Figure 13.14.

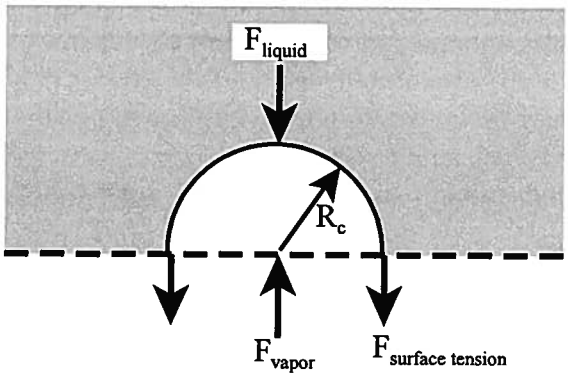

Figure 13.14 Free-body Diagram of Bubble

The condition of mechanical equilibrium between the bubble and the liquid requires

$$\sum F = 0$$

$$F_{\substack{surface\\tension}} + F_{liquid} - F_{vapor} = 0 \tag{13.53}$$

$$2\pi R_c \sigma + \pi R_c^{\,2} P_{sat} - \pi R_c^{\,2} P_{vapor} = 0$$

where σ denotes the surface tension of the liquid-vapor interface. Then the critical radius is

$$R_c = \frac{2\sigma}{P_{vapor} - P_{sat}} \tag{13.54}$$

In equation (13.54), the value of P_{vapor} is determined by the thermal equilibrium between vapor and liquid phases at the local temperature in the gradient where the bubble is located. The value of P_{sat} is the value of the externally imposed pressure on the liquid pool. From equation (13.54), we have

$$P_{vapor}\left(T_{vapor}\right) - P_{liquid}\left(T_{sat}\right) = \frac{2\sigma}{R_c} \tag{13.55}$$

Thus, equation (13.55) shows that in order to produce a vapor bubble in a liquid with a surface tension σ, the temperature of the vapor in the bubble must be greater than the saturation temperature of the bulk liquid far removed from the heater surface. This is the point B′ in Figure 13.11 which represents a departure from the pure substance model since we are now accounting for surface effects. The degree of superheat can be determined explicitly by substituting equation (13.55) into the Clausius-Clapeyron equation in the form of equation (13.50) and solving for the superheat, viz.

$$T_{vapor} - T_{sat} = \Delta T = \frac{RT_{sat}^2}{h_{fg}} \frac{2\sigma}{P_{sat} R_c} \tag{13.56}$$

The experimental data of Figure 13.11 show that the onset of nucleate boiling occurs

when the surface temperature of the heater exceeds the saturation temperature by approximately 10 C. Thus at atmospheric pressure, T_{sat} = 100 C, P_{sat} = 1.01325 x 10^5 N/m^2, σ = 0.05891 N/m, and P_{sat} (110 C) = 1.4338 x 10^5 N/m^2. From equation (13.54) we have for the critical radius

$$R_c = \frac{2(0.05891\ \text{N/m})}{1.4338 \times 10^5\ \text{N/m}^2 - 1.01325 \times 10^5\ \text{N/m}^2} = 2.802 \times 10^{-6}\ \text{m} \qquad (13.57)$$

This is the size of equilibrium vapor bubbles consistent with the superheat associated with the onset of nucleate boiling; however, these bubbles are not stable with respect to small perturbations in their size. Bubbles with a radius smaller than R_c will collapse spontaneously, and bubbles with a larger radius will grow.

The bubble nucleation process does not occur homogeneously in the superheated liquid. It requires a surface on which the bubbles can nucleate and grow before being released into the liquid pool. Microscopic examination of the heater surface reveals that the surface is not a true plane, but is, in fact, rough and covered with a large number of small pits or cavities of a myriad of shapes and sizes. Vapor bubbles tend to form in these cavities at specific locations called *nucleation sites* as shown schematically in Figure 13.15. A vapor nucleus forms in the cavity and

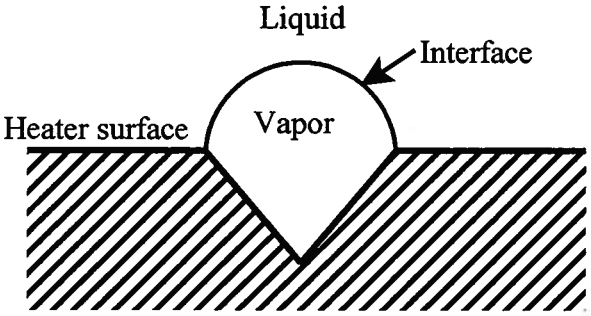

Figure 13.15 Vapor Bubble Forming in Cavity

grows through conduction heat transfer from the solid into the vapor. The mass of the vapor nucleus increases by evaporation at the liquid-vapor interface and in the process pushes the interface out of the cavity. Depending upon the *contact angle* between the liquid and the solid, a cap of some shape forms on the vapor and this vapor cap expands along the surface involving a number of nucleation sites as the heat transfer process continues. In the case of water on most metallic surfaces, the contact angle is approximately 90° resulting in a vapor cap that is nearly hemispherical. Eventually these hemispherical vapor bubbles break away from the cavity and become spherical when a balance is achieved between the surface forces associated with the liquid-vapor interface (surface tension) and the net body force due to gravity acting on the vapor mass and the buoyancy force due to the displaced liquid. Then

$$\sum F = 0$$

$$F_{\substack{surface\\tension}} + F_{gravity} - F_{buoyancy} = 0 \qquad (13.58)$$

$$2\pi R_b \sigma + \frac{2}{3}\pi R_b^3 \rho_g g - \frac{2}{3}\pi R_b^3 \rho_f g = 0$$

and the radius of the bubble at break-away becomes R_b where

$$R_b = \left[\frac{3\sigma}{(\rho_f - \rho_g)g}\right]^{1/2} \qquad (13.59)$$

For pool boiling of H_2O at atmospheric pressure, ρ_f = 958.35 kg/m^3 and ρ_g = 0.59817 kg/m^3 with

$\sigma = 0.05891$ N/m. Then

$$R_b = \sqrt{\frac{3(0.05891 \text{ N/m})}{(958.35 \text{ kg/m}^3 - 0.59817 \text{ kg/m}^3)(9.81 \text{ m/sec}^2)}} = 4.337 \text{ x } 10^{-3} \text{ m} \qquad (13.60)$$

In reality, the bubble growth process is somewhat more complicated than described above and results in slightly smaller bubbles than calculated in equation (13.60). The inertia of the surrounding liquid and the rate at which the latent heat can be conducted to the interface play important roles and produce bubble break-away diameters for H_2O in the range of 1 to 2.5 mm.

Since the boiling heat transfer process occurs at essentially the saturation pressure of the pool, each vapor bubble formed carries with it the latent heat of the vapor mass (*cf.* Section 13.8) plus whatever superheat developed in the vapor before it leaves the surface. The latent heat carried by each bubble is the same for bubbles of equal size, but the number per unit area increases as ΔT increases. The frequency with which bubbles leave the surface also contributes to the heat flux. Typically for H_2O, this frequency is on the order of 20 to 40 bubbles per second. Initially, the nucleation sites are few in number, but their number increases dramatically as the value of ΔT increases by a small amount. This is part of the reason for the steep slope of the portion of the boiling curve labeled B′ – D in Figure 13.11. Also, the size of the bubbles tends to increase as ΔT increases and there is some coalescence of bubbles with increasing ΔT as shown in Figure 13.12.

The net result of this complex process of bubble growth and release is that the typically large values of the latent heat of pure substances gives rise to very large values of the heat fluxes in nucleate boiling. The maximum value of the nucleate boiling heat flux for H_2O, $\mathring{q}_{crit} = 126$ W/cm^2 = 1.26 MW/m^2, is attained at point D in Figure 13.11. The particular value of $\mathring{q}_{crit}$ is somewhat variable from one experiment to another depending upon the presence of gases and other impurities dissolved in the liquid as well as the specific condition of the heater surface. Regardless of these experimental variations, point D is characterized by the fact that the all possible nucleation sites have become actively involved in the nucleate boiling heat transfer process.

If the heater power is increased at point D, the surface temperature suddenly increases while the surface heat flux holds constant at the critical value of $\mathring{q}_{crit}$ until point D′ is reached. At point D′, the surface temperature for pool boiling of H_2O is approximately 1200 C and the regime of boiling shifts from *nucleate boiling* to *film boiling* as the multitude of vapor bubbles on the heater surface coalesce and the surface becomes blanketed with H_2O vapor (*cf.* Figure 13.12). Because of the large sudden increase in surface temperature as the boiling regime changes character, point D is often referred to as the *burn-out heat flux.* Initially, the principal heat transfer mechanism in this vapor blanket is conduction and the vapor blanket acts as a thermal resistance between the heater surface and the pool of liquid. The thickness of this vapor blanket grows as heater power is increased and more vapor is generated. Thus, the value of ΔT must increase as heater power is increased. As heater power is increased still further, the surface temperature increases in the film boiling regime as long as the heater material does not melt since surface temperatures have now become quite high. As the value of ΔT increases, radiation heat transfer begins to play a role, and the heat transfer process in film boiling becomes one of combined conduction and thermal radiation.

It is important to note that the boiling heat transfer curve exhibits a marked *hysteresis.* If heater power is decreased from point F, the heater surface temperature follows the path F to D′ and then to E, not D, where it suddenly shifts at constant heat flux to the nucleate boiling portion

of the curve B′ – C. Further decrease in heater power reduces the heater surface temperature along B′– C. Thus, the *transition boiling* regime D – E is never actually realized in this simple heated surface experiment. (The data for the portion of the curve D – E are determined in experiments that use a surface in which boiling heat transfer occurs on one side and condensation heat transfer [*cf.* Section 13.14.2] occurs on the other.)

13.14.1.3 Nucleate Boiling: Given the complexity of the boiling phenomena, it is not surprising that the correlation of boiling heat transfer data has proven to be one of the more challenging issues that thermal-fluid engineers have faced. To this date, most of the attempts at formulating useful correlations have relied heavily on the pioneering work of Warren M. Rohsenow of the Massachusetts Institute of Technology. In 1952, Rohsenow argued that since the increased heat transfer rate in pool boiling probably results from the increased agitation of the liquid due to the motion of the bubbles being released from the surface with a concomitant transfer of energy primarily from the surface directly to the liquid, there should exist a Reynolds number Re_b based on bubble dynamics that accounts for these effects. Following the example of single-phase forced convection correlations, Rohsenow postulated the existence of a dimensionless correlation of the form

$$Nu_b = \phi\left(Re_b, Pr_f\right) \tag{13.61}$$

where Nu_b is an appropriately defined bubble Nusselt number and Pr_f is the Prandtl number of the saturated liquid. The success of this approach, of course, depends upon selecting the proper definitions for the dimensionless parameters. For the characteristic length, L_c, Rohsenow chose a simplified form of the critical bubble radius shown in equation (13.59), viz.

$$L_c = \left[\frac{\sigma}{g\left(\rho_f - \rho_g\right)}\right]^{1/2} \tag{13.62}$$

Then the bubble Nusselt number becomes

$$Nu_b = \frac{\dot{q}L_c}{\left(T_{surface} - T_{sat}\right)k_f} \tag{13.63}$$

where $\dot{q}$ is the measured heat flux for a given surface temperature $T_{surface}$ as reported in Figure 13.11 for example. The velocity that should be used in the bubble Reynolds number is the mass average velocity of the vapor receding from the surface, viz.

$$\vartheta_b = \frac{\dot{q}}{\rho_g h_{fg}} \tag{13.64}$$

Then

$$Re_b = \frac{\vartheta_b \rho_g L_c}{\mu_f} = \frac{\dot{q}L_c}{\mu_f h_{fg}} = \frac{\dot{q}}{\mu_f h_{fg}}\left[\frac{\sigma}{\left(\rho_f - \rho_g\right)g}\right]^{1/2} \tag{13.65}$$

In its final form, the correlation proposed in equation (13.61) should include the effects of the surface, e.g., roughness, wetability, etc. This Rohsenow accomplished by the inclusion of a factor C_{sf} that accounts for the nature of the heating surface-fluid combination. In dimensionless form, the nucleate boiling heat transfer data can then be correlated as follows:

$$\frac{c_{Pf}\left(T_{surface} - T_{sat}\right)}{h_{fg}} = C_{sf}\left\{\frac{\dot{q}}{\mu_f h_{fg}}\left[\frac{\sigma}{\left(\rho_f - \rho_g\right)g}\right]^{1/2}\right\}^{1/3} Pr^n \tag{13.66}$$

Note that the dimensionless group appearing on the left-hand side of equation (13.66) occurs

frequently in heat transfer correlations involving a change of phase and is called the Jakob number in honor of Max Jakob (1879 – 1955), a German physicist who was one of the early pioneers in thermal-fluids engineering. Physically the Jakob number, *Ja*, usually represents the ratio of the sensible heat of the liquid phase to the latent heat of a pure substance. In the present case, the definition of the Jakob number is modified slightly to represent the ratio of the superheat of the liquid phase to the latent heat, viz.

$$Ja = \frac{c_{P,f}\left(T_{surface} - T_{sat}\right)}{h_{fg}} \tag{13.67}$$

The dimensionless correlation of equation (13.66) can be recast in dimensional form, viz.

$$\dot{q} = \mu_f h_{fg}\left[\frac{g(\rho_f - \rho_g)}{\sigma}\right]^{1/2}\left(\frac{c_{P,f}(T_{surface} - T_{sat})}{C_{sf} h_{fg} Pr_f^{\,n}}\right)^3 \tag{13.68}$$

where the values of C_{sf} and n are given in Table 13.3 and all other fluid properties are evaluated at T_{sat}. Notice that the nucleate boiling heat flux is proportional to $(T_{surface} - T_{sat})^3$ which accounts for the sharp rise in heat flux as the liquid superheat increases. As mentioned above this increase is due to the rapid increase in active nucleation sites associated as the heating surface temperature increases.

Table 13.3 Nucleate Boiling Parameters

FLUID-SURFACE COMBINATION	C_{sf}	n
Water-copper		
Scored	0.0068	1.0
Polished	0.0128	1.0
Lapped	0.0147	1.0
Water-stainless steel		
Chemically etched	0.0133	1.0
Mechanically polished	0.0132	1.0
Ground and polished	0.0080	1.0
Teflon-pitted	0.0058	1.0
Water-brass	0.0060	1.0
Water-nickel	0.0060	1.0
Water-platinum	0.0130	1.0
n-Pentane-copper		
Polished	0.0154	1.7
Lapped	0.0049	1.7
Emery rubbed	0.0074	1.7
n-Pentane-polished nickel	0.0127	1.7
Benzene-chromium	0.101	1.7
Carbon tetrachloride-polished copper	0.0070	1.7
Ethyl alcohol-chromium	0.0027	1.7

Lacking other information, try $C_{sf} = 0.013$ as a first approximation.

(Adapted from J. G. Collier and J. R. Thome, *Convective Boiling and Condensation*, 3rd Edition, Oxford University Press, 1999, p. 154, Table 4.2.)

Despite the considerable effort expended by many investigators over the years to develop accurate correlations of nucleate boiling heat transfer data, the correlation of equation (13.68) has proven to be only an approximation to the actual data. In some cases, the accuracy is quite good, but in others, it is little more than an order of magnitude estimate. There are simply too many physical variations related to dissolved gases, surface contaminants, surface finishes and the like that can affect the prediction of the nucleate boiling heat flux with any consistent accuracy. Fortunately, it is the critical heat flux, $\dot{q}''_{crit}$, that designers have to worry about, and this point on the boiling curve has been correlated with a more acceptable level of accuracy.

13.14.1.4 Critical Heat Flux: The critical heat flux is limited by the rate at which vapor can leave the surface since all possible nucleation sites have been activated and the frequency of bubble break-away is essentially fixed. If we let ϑ_{max} be the maximum possible velocity with which vapor can leave the heater surface, the critical heat flux is given by

$$\dot{q}_{crit} = C_{max}\rho_g \vartheta_{max} h_{fg} \tag{13.69}$$

where C_{max} is a constant that essentially accounts for the geometry of the heater surface. The maximum vapor velocity can be estimated by considering a unit mass of vapor as an isolated system hydrodynamically and applying the first law. Then the kinetic energy acquired by the vapor bubble leaving the surface comes at the expense of the change in gravitational potential energy of the bubble volume as it moves between the liquid and vapor phases over the characteristic length of nucleate boiling. Then

$$\frac{1}{2}\rho_g \vartheta_{max}^2 = \left(\rho_f - \rho_g\right) g L_c \tag{13.70}$$

Solving equation (13.70) for the maximum velocity, we get

$$\vartheta_{max} = \sqrt{2}\left[\frac{\sigma g\left(\rho_f - \rho_g\right)}{\rho_g^2}\right]^{1/4} \tag{13.71}$$

Combining equations (13.69) and (13.71), we get

$$\dot{q}_{crit} = K h_{fg}\left[\sigma g \rho_g^2\left(\rho_f - \rho_g\right)\right]^{1/4} \tag{13.72}$$

where the constant K is given by the data in Table 13.4. To use the data of Table 13.4, it is first necessary to determine the size of the heater surface relative to the characteristic length L_c given by equation (13.62). For example, for a horizontal cylinder of radius R

$$R^* = \frac{R}{L_c} \tag{13.73}$$

The correlation of equation (13.72) has an accuracy of approximately 20 percent provided the heater dimensions are not too small. If $L \leq 0.38$ mm, surface tension forces dominate and the correlation breaks down. As L decreases further, the boiling curve becomes monotonic. For very fine wires, the heat transfer process passes directly from free convection to film boiling.

Equation (13.72) is used in practice to establish the maximum possible heat flux that a surface can sustain without risk of melting or incurring temperatures so high that mechanical failure is likely. The heater surface is then designed to operate at some fraction of $\dot{q}''_{crit}$ that provides a reasonable margin of safety. For the pool boiling curve of Figure 13.11, we can establish the value of $\dot{q}''_{crit}$ with the aid of equation (13.72). For pool boiling of H_2O at atmospheric pressure, $\rho_f = 958.35$ kg/m^3 and $\rho_g = 0.59817$ kg/m^3 with $\sigma = 0.05891$ N/m. Then

$$\dot{q}_{crit} = Kh_{fg}\left[\sigma g \rho_g^2 \left(\rho_f - \rho_g\right)\right]^{1/4}$$

$$\dot{q}_{crit} = 0.149\left(2256.40 \text{ x } 10^3 \text{ J/kg}\right)\left[\begin{array}{r}\left(0.05891 \text{ N/m}\right)\left(9.81 \text{ m/sec}^2\right)\left(0.59817 \text{ kg/m}^3\right)^2 \cdot \\ \cdot\left(958.35 \text{ kg/m}^3 - 0.59817 \text{ kg/m}^3\right)\end{array}\right]^{1/4}$$

$$\dot{q}_{crit} = 1.261 \text{ x } 10^6 \text{ W/m}^2 \qquad (13.74)$$

This result compares favorably with the data shown in Figure 13.11. Example 13E.9 illustrates the way in which the critical heat flux correlation is used to set the operating conditions of boiling heat transfer apparatus.

Table 13.4 Critical Heat Flux Parameters

Geometry	K	Dimension	Range
Infinite flat plate	0.149	width or diameter	$L^* \geq 2.7$
Small flat heater	$0.149(12\pi L_c^2)$/Area	width or diameter	$0.07 \leq L^* \leq 0.2$
Horizontal cylinder	$0.1165 + 0.297\exp(-3.44\sqrt{R^*})$	radius R	$R^* \geq 0.15$
Large horizontal cylinder	0.118	radius R	$R^* \geq 1.2$
Small horizontal cylinder	$0.123/(R^*)^{0.25}$	radius R	$0.15 \leq R^* \leq 1.2$
Large sphere	0.110	radius R	$R^* \geq 4.26$
Small sphere	$0.227/(R^*)^{0.5}$	radius R	$R^* \leq 4.26$
Small horizontal ribbon oriented vertically #	$0.154/(H^*)^{0.25}$	height of side H	$0.15 \leq H^* \leq 2.96$
Small horizontal ribbon oriented vertically %	$0.183/(H^*)^{0.25}$	height of side H	$0.15 \leq H^* \leq 5.86$
Any large finite body	~0.118	length L	$\sim L^* \geq 4$
Small slender cylinder of any cross section	$0.183/(P^*)^{0.25}$	transverse perimeter P	$0.15 \leq P^* \leq 5.86$

Heated on both sides
% One side insulated

(Adapted from J. G. Collier and J. R. Thome, *Convective Boiling and Condensation*, 3rd Edition, Oxford University Press, 1999, p. 165, Table 4.4.)

Example 13E.9: A common type of electric boiler used in many industrial applications makes use of an immersion heater that uses some sort of electrically resistive element connected to the electrical grid. A simple example of this design is shown in Figure 13E.9 and consists of a tube (D = 10 mm) bent in a U-shape with an electrical resistance heater inside. The electrical leads for the heater are then brought out from the ends of the resistor so that one lead emerges from each end of the U-tube. The wires are then connected to an electrical circuit which provides the necessary power to operate the heater. The heaters are usually inserted into a pool of liquid so that the axis of the tube is horizontal.

In a particular heater design, the heater is being used to boil water. The outside surface of the tube exposed to the water is mechanically polished stainless steel. The electrical resistor is sized so that the heater operates with a heat flux that is 30 % of the critical heat flux.

(a) What is the surface temperature of the stainless steel tube when operating as designed in a pool of saturated liquid H_2O at a temperature of T_{sat} = 100 C?

(b) If the total length of the heater is 1 m, determine the electrical power that must be supplied to operate the heater.

(c) What is the mass flow rate of the saturated vapor H_2O exiting from the boiler?

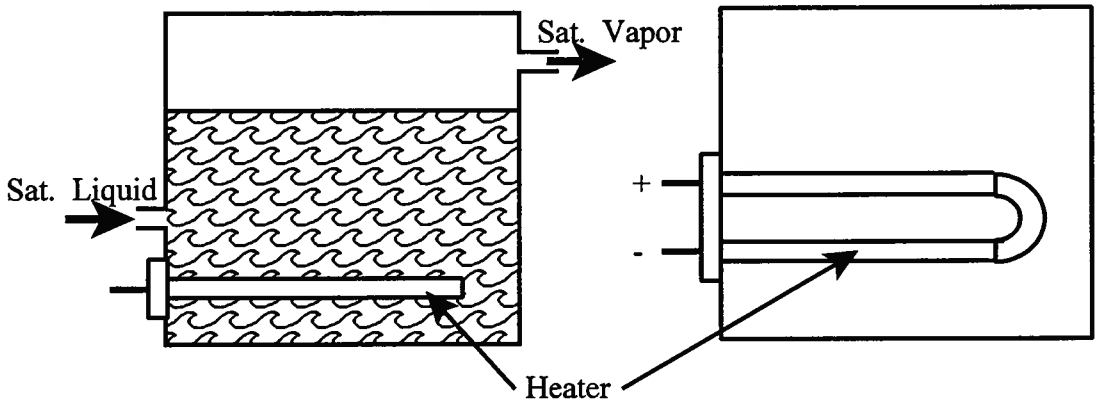

Figure 13E.9

Solution: (a) We first need to determine the critical heat flux, $\dot{q}''_{max}$, for this geometry. From equation (13.72)

$$\dot{q}''_{max} = Kh_{fg}\left[\sigma g \rho_g^{\,2}\left(\rho_f - \rho_g\right)\right]^{1/4}$$

The value of K can be determined from Table 13.4. We first need to determine the characteristic length from equation (13.62) so that we can determine the appropriate value of the dimensionless radius. For pool boiling of H_2O at T_{sat} = 100 C, ρ_f = 958.35 kg/m^3 and ρ_g = 0.59817 kg/m^3 with σ = 0.05891 N/m

$$L_c = \left[\frac{\sigma}{g\left(\rho_f - \rho_g\right)}\right]^{1/2}$$

$$L_c = \left[\frac{0.05891\ \text{N/m}}{\left(9.81\ \text{m/sec}^2\right)\left(958.35\ \text{kg/m}^3 - 0.59817\ \text{kg/m}^3\right)}\right]^{1/2} = 2.504 \times 10^{-3}\ \text{m}$$

Then the dimensionless radius of the heater tube is

$$R^* = \frac{R}{L_c} = \frac{5 \text{ x } 10^{-3} \text{ m}}{2.50 \text{ x } 10^{-3} \text{ m}} = 2$$

According to Table 13.4, this tube qualifies as a large horizontal cylinder with $K = 0.118$. Then the critical heat flux for this geometry is

$$\dot{q}_{max} = 0.118(2256.40 \text{ kJ/kg})\left[\left(0.58917 \text{ N/m}^2\right)^2\left(9.81 \text{ m/sec}^2\right)\left(958.35 \text{ kg/m}^2 - 0.59817 \text{ kg/m}^2\right)\right]^{\frac{1}{4}}$$

$$\dot{q}_{max} = 9.988 \text{ x } 10^5 \text{ W/m}^2$$

Then the heat flux for the heater is

$$\dot{q} = 0.3\dot{q}_{max} = 0.3(9.988 \text{ x } 10^6 \text{ W/m}^2) = 2.996 \text{ x } 10^5 \text{ W/m}^2$$

Since the heat flux is less than the critical heat flux, we can use the nucleate boiling correlation of equation (13.68) to estimate the surface temperature. Then, solving equation (13.68) for the tube surface temperature, we get

$$T_{surface} = T_{sat} + \frac{C_{s,f} h_{fg} Pr_f}{c_{P,f}}\left\{\frac{q}{\mu_f h_{fg}\left[\frac{\sigma}{g\left(\rho_f - \rho_g\right)}\right]^{\frac{1}{2}}}\right\}^{\frac{1}{3}}$$

$$T_{surface} = (100 \text{ C}) + \frac{0.0132(2256.4 \text{ kJ/kg})(1.749)}{4215.7 \text{ J/kg K}} \cdot$$

$$\cdot\left\{\frac{2.996 \text{ x } 10^5 \text{ W/m}^2}{\left(2.817 \text{ x } 10^{-4} \text{ kg/m sec}\right)(2256.4 \text{ kJ/kg})\left[\frac{0.5891 \text{ N/m}}{(9.81 \text{ m/sec}^2)(958.35 \text{ kg/m}^3 - 0.59817 \text{ kg/m}^3)}\right]^{\frac{1}{2}}}\right\}^{\frac{1}{3}}$$

$$T_{surface} = 113.1 \text{ C}$$

This result is really only an estimate since equation (13.68) is only an approximate correlation because of all the unknowns and, in this case, there is quite likely some further error introduced by the fact that equation (13.68) was formulated for a horizontal flat plate and not a horizontal cylinder. The one redeeming feature of this calculation is that we are solving for the surface temperature which involves a cube root operation that tends to reduce the error.

(b) The electrical power required to operate the heater is simply the total heat transfer rate from the heater. Thus,

$$\wp = \dot{Q} = \dot{q}A_{surface} = \dot{q}\pi DL$$

$$\wp = \left(2.996 \text{ x } 10^5 \text{ W/m}^2\right)\pi(0.010 \text{ m})(1 \text{ m}) = 9.41 \text{ kW}$$

(c) To determine the mass flow rate of saturated vapor out of the boiler, we apply the first law to the boiler. Then

$$\dot{Q} = \dot{m}\left(h_g - h_f\right) = \dot{m}h_{fg}$$

but from Newton's Law of Cooling

$$\dot{Q} = \dot{q}A_{surface} = \dot{q}\pi DL$$

Then

$$\dot{m} = \frac{\dot{q}\pi DL}{h_{fg}} = \frac{(2.996 \text{ x } 10^5 \text{ W/m}^2)\pi(0.010 \text{ m})(1 \text{ m})}{2256.4 \text{ kJ/kg}} = 4.172 \text{ x } 10^{-3} \text{ kg/sec}$$

It is interesting to note in this example that the electrical power requirement is sufficient to operate three to five large homes and yet it is capable of generating only four grams of steam per second. This gives some perspective to the magnitude of the latent heat of vaporization of water.

13.14.1.5 Film Boiling: From the data of Figure 13.11, it is apparent that in film boiling, the portion of the boiling curve labeled E – F, results in heater surface temperatures that are relatively high due to the large thermal resistance presented by the vapor film. Therefore, film boiling is not widely used as a cooling mechanism in thermal-fluids equipment since this puts the equipment at risk for material failures. One notable exception is cryogenic equipment that operate with fluids at very low temperatures. For this type of equipment, the resulting high surface temperatures are still within the range of normal temperatures for most materials.

The phenomenon of film boiling is an interesting mix of hydrodynamics and heat transfer. The physical situation is an inherently unstable one with a more dense fluid, the liquid, sitting on top of a less dense fluid, the vapor. Basically, the momentum of the vapor leaving the heater surface is so high, the liquid no longer wets the heater surface. However, the interface between the two phases is subject to perturbations due to the motion of the vapor that escapes the vapor blanket through the interface as bubbles. This bubble movement is regular in both time and space with a wavelength characteristic of a Taylor instability of wavelength

$$\lambda_c = 2\pi\left[\frac{\sigma}{g\left(\rho_f - \rho_g\right)}\right]^{1/2} \tag{13.74}$$

When the vapor generation rate becomes too low to sustain this Taylor instability, the vapor blanket breaks down and the liquid wets the surface. This corresponds to point E on the boiling curve of Figure 13.11. This point is known as the *Leidenfrost point* [first reported by the German physician Johann Gottlobb Leidenfrost (1715 – 1794) in 1756 in a paper: *A Tract About Some Qualities of Common Water*] and represents the minimum heat flux, $\dot{q}_{min}$, necessary to sustain film boiling. For a horizontal, flat heater surface

$$\dot{q}_{min} = 0.09\rho_g h_{fg}\left[\frac{g\sigma\left(\rho_f - \rho_g\right)}{\left(\rho_f + \rho_g\right)^2}\right]^{1/4} \tag{13.75}$$

In stable film boiling, since the liquid is no longer in contact with the heater surface, bubble transport is no longer the fundamental mechanism for energy transfer between the surface and the liquid pool. Heat transfer now occurs by conduction through the moving vapor film (convection) and thermal radiation across it because of the relatively high surface temperatures. The relative contributions of the two mechanisms depend heavily upon the details of the physical situation, and the two contributions are usually treated independently.

Since the complex dynamics of bubble formation and growth are no longer an issue, the analysis of the film boiling regime is somewhat more straightforward than the nucleate boiling regime. The presence of a vapor film on the heater surface with a phase change taking place naturally leads us to view the convection heat transfer contribution as analogous to film-wise condensation. In fact, for many geometries, the film condensation correlations are used directly for this contribution. Rather than take up the details of modeling film-wise heat transfer at this juncture, we shall delay the detailed analysis of this heat transfer mechanism until Section 13.4.2 where we shall take up the treatment of film-wise condensation. Instead, we simply present here the results of the correlations appropriate for film boiling heat transfer.

In dimensionless form, the convection contribution can be determined from correlations

similar in form to equation (13.61), viz.

$$\overline{Nu}_{L_C} = \frac{\bar{h}_{conv} L_C}{k_g} = C_{fb}\left[\frac{g(\rho_f - \rho_g)h'_{fg} L_C^{\,3}}{\nu_g k_g (T_{surface} - T_{sat})}\right]^{1/4} \tag{13.76}$$

where the superscribed bar indicates values averaged over the length of the surface. C_{fb} is a film boiling constant that accounts for the geometry of the surface on which the vapor film has formed; k_g is the thermal conductivity of the vapor; $\nu_g = \mu_g / \rho_g$ is the kinematic viscosity of the vapor; and L_C is a characteristic length that describes the geometry. Values for the film boiling parameters are given in Table 13.5 for various geometries. Note that the latent heat of vaporization has been modified to account for the superheat in the film [G. F. Hewitt, *Boiling*, Chapter 15, in *Handbook of Heat Transfer*, 3rd Edition, ed. by W. M. Rohsenow, J. P. Hartnett, and Y. I. Cho, McGraw-Hill, N. Y., 1998, p. 15.72.] viz.

$$h'_{fg} = h_{fg} + 0.34 c_{P,f}(T_{surface} - T_{sat}) \tag{13.77}$$

Table 13.5 Film Boiling Geometrical Parameters

SHAPE	C_{fb}	L_c
Horizontal cylinder	0.62	diameter, D
Sphere	0.67#	diameter, D
Plane vertical surface	0.943	vertical length, L
Horizontal surface	0.425	$L_C = \sqrt{\sigma / (\rho_f - \rho_g) g}$

(Adapted from L. S. Tong and Y. S. Tang, *Boiling Heat Transfer and Two-Phase Flow*, 2nd Edition, Taylor and Francis Publishers, Washington, D. C., 1997, pp. 103 – 107.)
From A. F. Mills, *Heat Transfer*, Richard D. Irwin, Inc., Boston, 1992, p. 640.

As mentioned above, the thermal radiation contribution to film boiling is usually treated independently of the convection contribution. The two effects are then simply added together with some sort of weighting function to obtain the net film boiling heat transfer coefficient, h_{fb}, viz.

$$h_{fb} = h_{conv} + J h_{rad} \tag{13.78}$$

where h_{conv} is the contribution to the heat transfer coefficient due to convection as determined from equation (13.76), h_{rad} is the contribution due to thermal radiation, and J is the weighting function. Over the years, many different approaches have been suggested for the evaluation of J with the simplest being $J = 0.75$. Thus,

$$h_{fb} = h_{conv} + 0.75 h_{rad} \tag{13.79}$$

The radiation contribution to the heat transfer contribution is given by

$$h_{rad} = \frac{\sigma_{SB} \mathscr{F} \left(T_{surface}^4 - T_{sat}^4\right)}{T_{surface} - T_{sat}} \tag{13.80}$$

where σ_{SB} is the Stefan-Boltzmann radiation constant ($\sigma_{SB} = 5.67 \times 10^{-8}$ W/m^2 K^4) and $\mathscr{F}$ is the

shape factor that accounts for the geometry and non-ideal behavior of the radiating surfaces. The simplest model for the radiation contribution is to treat the vapor-liquid interface and the heating surface as infinite parallel plates with the emissivity of the heater surface denoted by ε and the absorptivity of the liquid-vapor interface denoted by α. Then if we model the liquid-vapor interface as an ideal radiator, a black body, $\alpha = 1$ and

$$\mathcal{F} = \frac{1}{\varepsilon} + \frac{1}{\alpha} - 1 = \frac{1}{\varepsilon} \tag{13.81}$$

Then equation (13.80) becomes

$$h_{rad} = \frac{\sigma_{SB}\varepsilon\left(T_{surface}^4 - T_{sat}^4\right)}{T_{surface} - T_{sat}} \tag{13.82}$$

Example 13E.10: During installation of the electric heater for the simple pool boiler of Example 13E.9, a construction worker inadvertently wires the heater in a 480 V circuit instead of a 240 V circuit. Thus the power dissipated in the resistor is now 4 times what it was designed for. If the melting point of the stainless steel is 1400 C, is there a danger of a melt-down of the heater due to this improper installation?

Solution: We note that if the electrical resistance of the heater is a constant, the power level with the incorrect wiring will now be four times the design power level. Then the new heat flux will be

$$\dot{q}_{new} = 4\dot{q} = 4(2.996 \text{ x } 10^5 \text{ W/m}^2) = 1.198 \text{ x } 10^6 \text{ W/m}^2$$

This new heat flux exceeds the critical heat flux for this geometry, $\dot{q}_{crit}^{\circ} = 9.988 \text{ x } 10^5 \text{ W/m}^2$. We now determine the heat flux that the heater could sustain if it operated at the melting point of the stainless steel. Then the heater will operate in the film boiling range. If the melting point of the stainless steel is 1400 C, the convection contribution to the film boiling heat transfer coefficient at this wall temperature is from equations (13.76) and (13.75) with data from Table 13.5

$$h_{conv} = 0.62\frac{k_g}{D}\left[\frac{g\left(\rho_f - \rho_g\right)\left\{h_{fg} + 0.34c_{P,f}\left(T_{wall} - T_{sat}\right)\right\}D^3\rho_g}{\mu_g k_g\left(T_{wall} - T_{sat}\right)}\right]^{\frac{1}{4}} = 61.994 \text{ W/m}^2 \text{ K}$$

where we have evaluated all the fluid properties at the saturation temperature. Now if we take the emissivity of the stainless steel to be $\varepsilon = 0.16$, we have from equation (13.82)

$$h_{rad} = \frac{\left(5.67 \text{ x } 10^{-8} \text{ W/m}^2 \text{ K}^4\right)(0.16)\left[(1673.15 \text{ K})^4 - (373.15 \text{ K})^4\right]}{1673.15 \text{ K} - 373.15 \text{ K}} = 67.695 \text{ W/m}^2 \text{ K}$$

Then the heat transfer coefficient for film boiling becomes

$$h_{fb} = h_{conv} + 0.75h_{rad} = 61.994 \text{ W/m}^2 \text{ K} + 0.75\left(67.695 \text{ W/m}^2 \text{ K}\right) = 112.766 \text{ W/m}^2 \text{ K}$$

Then the heat flux for a surface temperature of 1400 C is

$$\dot{q}_{1400} = h_{fb}\left(T_{wall} - T_{sat}\right) = (112.766 \text{ W/m}^2 \text{ K})(1400 \text{ C} - 100 \text{ C}) = 1.466 \text{ x } 10^5 \text{ W/m}^2$$

$$\dot{q}_{1400} \ll \dot{q}_{new}$$

This is essentially an order of magnitude less than the heat flux due to the electrical power dissipation in the heater. Thus, there will most surely be a meltdown of the heater.

13.14.1.6 Internal Forced Convection Boiling: In the sections immediately preceding this, we gained considerable insight to the heat transfer mechanisms associated with boiling in the pure substance model by studying pool boiling phenomena. While there are many physical situations that can be modeled as pool boiling, by far the greatest number of applications of boiling heat transfer found in thermal-fluids engineering practice involve heat transfer to a flowing fluid. Typical examples include the steam generator of a thermodynamic energy

conversion plant, the evaporator in a refrigeration plant, and a boiling water nuclear reactor (BWR).

In these systems, there is heat transfer by the simultaneous mechanisms of forced convection due to the fluid flow and boiling heat transfer due to the behavior of the pure substance in a saturated state. As we have already seen, the analysis of each of these mechanisms is challenging in its own right, but when both mechanisms are present simultaneously, the complexity of the situation is further compounded by the coupling that exists between the fluid mechanics of the situation and the heat transfer processes. The heat transfer processes result in the coexistence of the two phases, liquid and vapor, and the individual phases each have their own peculiar hydrodynamic behavior manifested in the flow patterns themselves as well as the pressure drop required to drive the flow. The hydrodynamics, in turn, limits the possible heat transfer by virtue of the nature of the phase in contact with the wall at any instant of time.

Since we are dealing with two phases that have markedly different densities, the orientation of the flow conduit with respect to the gravity field can have a profound effect on the both the hydrodynamics and the heat transfer processes in the flow. Figure 13.16 shows the

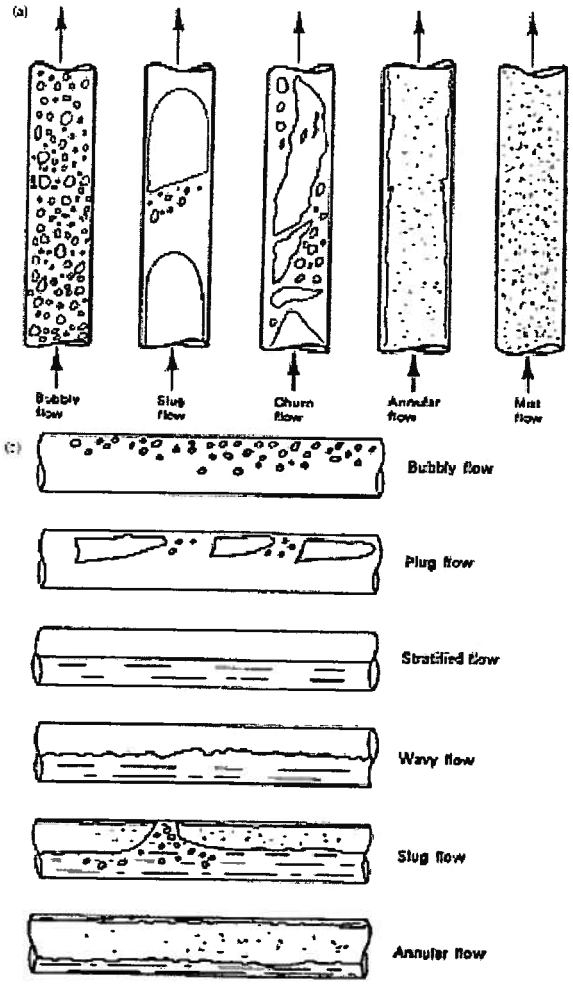

Figure 13.16 Typical Two-phase Flow Patterns
(a) Vertical Flow
(b) Horizontal Flow

(From L. S. Tong and Y. S. Tang, *Boiling Heat Transfer and Two-Phase Flow*, 2nd Edition, Taylor and Francis Publishers, Washington, D. C., 1997, Fig. 3.1, p. 121.)

remarkable influence of gravity on the flow patterns that occur when both the liquid and the vapor phases are present in the flow. In horizontal flow geometries, the effect of the body force due to gravity tends to cause the less dense phase, the vapor, to sequester in the upper protion of the conduit. This usually results in a stratification of the flow that might not otherwise be stratified in vertical flow geometries. Some industrial applications favor one orientation, while others favor another. For example, steam generators in large, central energy conversion plants tend to favor vertical flow configurations due in large part to their size and their desire to have as small a "footprint" as possible, while the refrigeration industry tends to favor the horizontal configuration since it is more compatible with the other components found in refrigeration plants.

Each flow pattern results in its own particular response to the influences of fluid viscosity and thermal conductivity on the processes of momentum and energy transport. While it is impossible to characterize all of these situations in detail, it is possible to develop some correlations that can be applied to typical applications, at least in an approximate manner. There have been developed flow maps that attempt to establish the conditions under which the various flow patterns occur. Figures 13.17 and 13.18 are examples of these maps for adiabatic flows. For each region, correlations have been developed to describe the flow in quantitative terms.

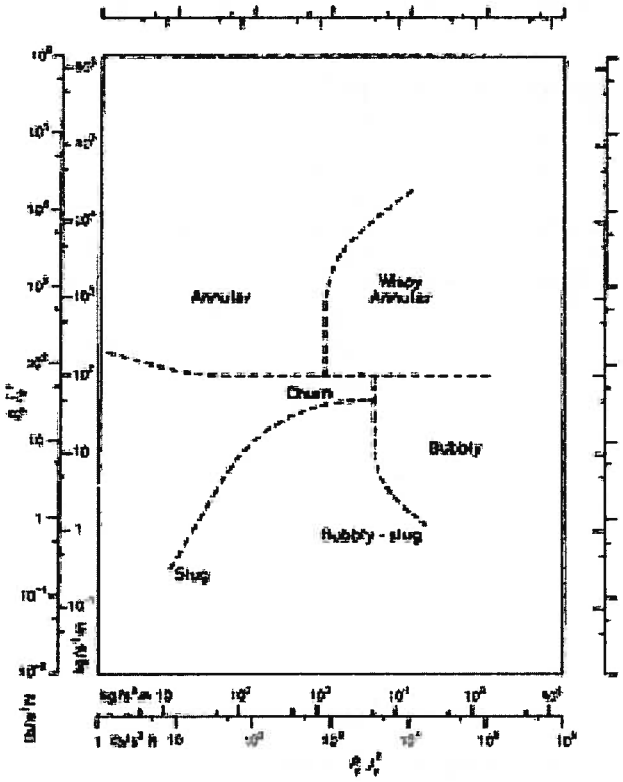

Figure 13.17 Flow Patterns for vertical Two-phase Flow Upward
(From J. G. Collier and J. R. Thome, *Convective Boiling and Condensation*, 3rd Edition, Oxford University Press, 1999, p. 19, Fig. 1.5.)

In Figure 13.17, the flow patterns are characterized by a single set of parameters defined in the following manner:

$$\rho_f j_f^2 = \frac{\left[\frac{\dot{m}}{A_c}(1-x)\right]^2}{\rho_f} \quad \text{and} \quad \rho_g j_g^2 = \frac{\left[\frac{\dot{m}}{A_c}x\right]}{\rho_g} \tag{13.83}$$

where A_c is the cross-sectional area of the conduit with mass flow $\dot{m}$ of quality x. The parameter j with a subscript f or g depending upon the phase of interest, represents the superficial velocity of the phase. This is a defined velocity (rather than a true physical velocity) in which the particular phase of interest is assumed to occupy the entire cross-section of the conduit. Then the product ρj^2 as defined in equation (13.83) represents the superficial momentum flux of the phase of interest. Then in Figure 13.17, for example, vertical annular flows are characterized by high momentum fluxes of the vapor phase and low momentum fluxes of the liquid phase. Notice that in these two-phase flows, the two phases do not necessarily have the same velocity. In fact, that would be the exception rather than the rule. In the analysis of these flows, it is then necessary to consider the drag that one phase imposes on the other. This is just one of the many complexities that prevail in these two-phase flows.

In Figure 13.18, it is acknowledged that the flow patterns involve very different kinds of flow and that no single set of parameters could describe them all. Hence, the notion of using a single set is abandoned, and, instead, several different sets of parameters are required to characterize each of the flow patterns. These parameters are based, in part, on the homogeneous model of two-phase flow that ignores the details of the flow patterns and simply separates the pressure gradient in a two-phase flow into three separate contributions: one due to fluid friction, $(dP/dz)_F$; one due to momentum changes in the flow, $(dP/dz)_M$; and one due to the effects of gravity, $(dP/dz)_G$. This empirical model then assumes that these effects can be linearly superposed so that the net pressure gradient in the flow is given by

$$\frac{dP}{dz} = \left(\frac{dP}{dz}\right)_F + \left(\frac{dP}{dz}\right)_M + \left(\frac{dP}{dz}\right)_G \tag{13.84}$$

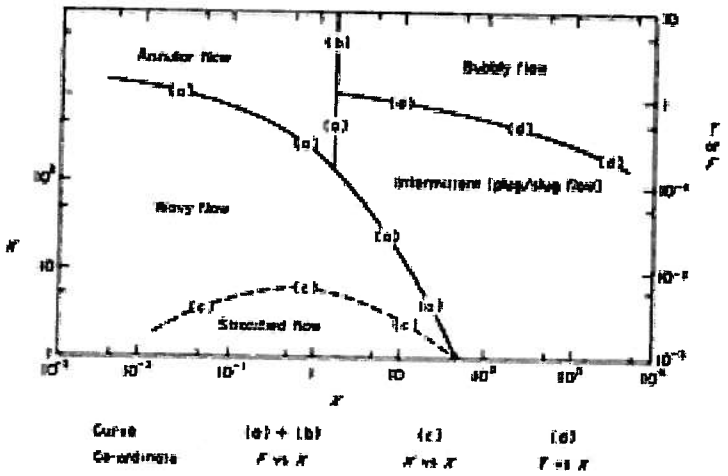

Figure 13.18 Flow Patterns for Horizontal Two-phase Flow
(From J. G. Collier and J. R. Thome, *Convective Boiling and Condensation*, 3rd Edition, Oxford University Press, 1999, p. 22, Fig. 1.7.)

The details of these contributions are given below, but this model is required first to establish the parameters of the flow. The first of these is the Lockhart-Martinelli parameter, X, that is one of the fundamental parameters of two-phase flow and is defined as

$$X = \left[\frac{\left(\frac{dP}{dz}\right)_{Ff}}{\left(\frac{dP}{dz}\right)_{Fg}}\right]^{1/2} \tag{13.85}$$

where the subscript *Ff* denotes the frictional contribution to the pressure gradient due to the liquid phase as if it existed alone, and the subscript *Fg* is similarly defined for the vapor phase.

The parameter F appearing in Figure 13.18 is a modified Froude number defined as

$$F = \left(\frac{\rho_g}{\rho_f - \rho_g}\right)^{1/2} \left(\frac{j_g}{\sqrt{Dg\cos\theta}}\right) \tag{13.86}$$

where D is the diameter of the conduit and θ is the angle of inclination of the conduit with respect to the horizontal. This modified Froude number is relevant to two-phase flows with a liquid-vapor interface and accounts for the wave behavior that appears in the flow.

The parameter K describes the rate of dissipation of kinetic energy in the flow and is defined as

$$K = \left[\frac{\rho_f \rho_g j_g^2 j_f}{(\rho_f - \rho_g)\mu_f g\cos\theta}\right]^{1/2} \tag{13.86}$$

Finally the parameter T (which is not to be confused with the temperature, but is just a poor choice of symbols) is defined as

$$T = \left[\frac{\left(\frac{dP}{dz}\right)_{Ff}}{(\rho_f - \rho_g) g\cos\theta}\right]^{1/2} \tag{13.87}$$

In determining the pressure gradient in the two-phase flow from equation (13.84), the velocities of the two phases are assumed to be the same. The average density of the two phases is taken to be

$$\frac{1}{\rho} = \frac{1}{\rho_f} + x\left(\frac{1}{\rho_f} - \frac{1}{\rho_g}\right) = \frac{x\rho_f + (1-x)\rho_g}{\rho_f \rho_g} \tag{13.88}$$

Then from the definition of the friction factor, equation (9.139), we have for the friction component of the pressure gradient

$$\left(\frac{dP}{dz}\right)_F = -\frac{f}{2\rho D}\left(\frac{\dot{m}}{A_c}\right)^2 \tag{13.89}$$

where the friction factor can be determined from Figure 9.30 or equation (9.275). The Reynolds number to be used in this evaluation is given by

$$Re = \frac{4\dot{m}}{\pi D \mu^*} \tag{13.90}$$

where we have introduced a pseudo-viscosity, μ^*, to account for the fact that the influence of the vapor phase on the pressure gradient increases as the quality increases. This pseudo-viscosity is given by

$$\frac{1}{\mu^*} = \frac{x}{\mu_v} + \frac{1-x}{\mu_l} \tag{13.91}$$

which clearly tends to the proper values at the limiting values of the quality, viz. $x = 0$ and $x = 1$.

The momentum contribution to the pressure drop accounts for the momentum changes that occur in the flow as the density of the flow changes in response to the attendant changes in

phase. Since the mass flow rate is constant in the direction of flow regardless of possible changes in phase, we can write

$$\left(\frac{dP}{dz}\right)_M = \left(\frac{\dot{m}}{\rho A_c}\right)^2 \frac{d\rho}{dz} \tag{13.92}$$

which shows that as the density of the flow decreases in the direction of the flow path, that is ($d\rho/dz < 0$), the pressure gradient must be negative since the flow must accelerate.

The gravity contribution to the pressure gradient is given by

$$\left(\frac{dP}{dz}\right)_G = -\rho g \sin\theta \tag{13.93}$$

where θ is measured from the horizontal. Then equations (13.89), (13.92), and (13.93) must be combined in equation (13.84) to determine the total pressure gradient for the flow.

Keep in mind that the approach presented above is but the simplest of treatments of this complicated subject. There are several specialized treatments that give far more detail than is possible in an introductory treatment such as the present study, and the reader is referred to these for additional information. For example, see:

1. *Convective Boiling and Condensation*, 3rd Edition, J. G. Collier and J. R. Thome, Oxford University Press, Oxford, 1999.

2. *Boiling Heat Transfer and Two-Phase Flow*, 2nd Edition, L. S. Tong and Y. S. Tang, Taylor and Francis Publishers, Washington, D. C., 1997.

3. *Liquid-Vapor Phase-Change Phenomena: An Introduction to the Thermophysics of Vaporization and Condensation Processes in Heat Transfer Equipment*, V. P. Carey, Taylor and Francis Publishers, Washington, D. C., 1992.

Figure 13.19 shows the various regions of heat transfer that occur during convective boiling in a tube. The fluid begins as a single phase liquid with heat transfer occurring as single phase forced convection heat transfer (Region A). At some point, (Region B) some nucleation sites become active and vapor begins to form while the fluid is still a subcooled liquid. This heat transfer mechanism is known as subcooled nucleate boiling and is driven by a surface temperature that is slightly above the saturation temperature of the liquid. In regions A and B, the bulk mean temperature of the fluid is increasing to the saturation temperature which is attained in region C. The heat transfer mechanism now becomes saturated nucleate boiling and is marked by the fact that the tiny vapor bubbles that have formed at the nucleation sites on the surface begin to coalesce and form fairly large bubbles that give rise to slug flow. The boundary of this region is identified by the fact that the quality of the fluid begins to change and the enthalpy of the fluid now becomes a function of the distance along the flow coordinate z, viz.

$$h(z - z_{SC}) = h_f + x(z - z_{SC})h_{fg} \tag{13.94}$$

where z_{SC} denotes the point in the flow where saturation conditions are attained. Since changes in kinetic energy due to acceleration of the flow are small compared to the changes in enthalpy, the first law reduces to

$$\dot{Q} = \dot{q}A_{surface} = \left(\frac{\dot{m}}{A_c}\right) A_c \left(h - h_f\right) \tag{13.95}$$

Substituting equation (13.96) into equation (13.95), we obtain the quality as a function from the location where saturation is attained, viz.

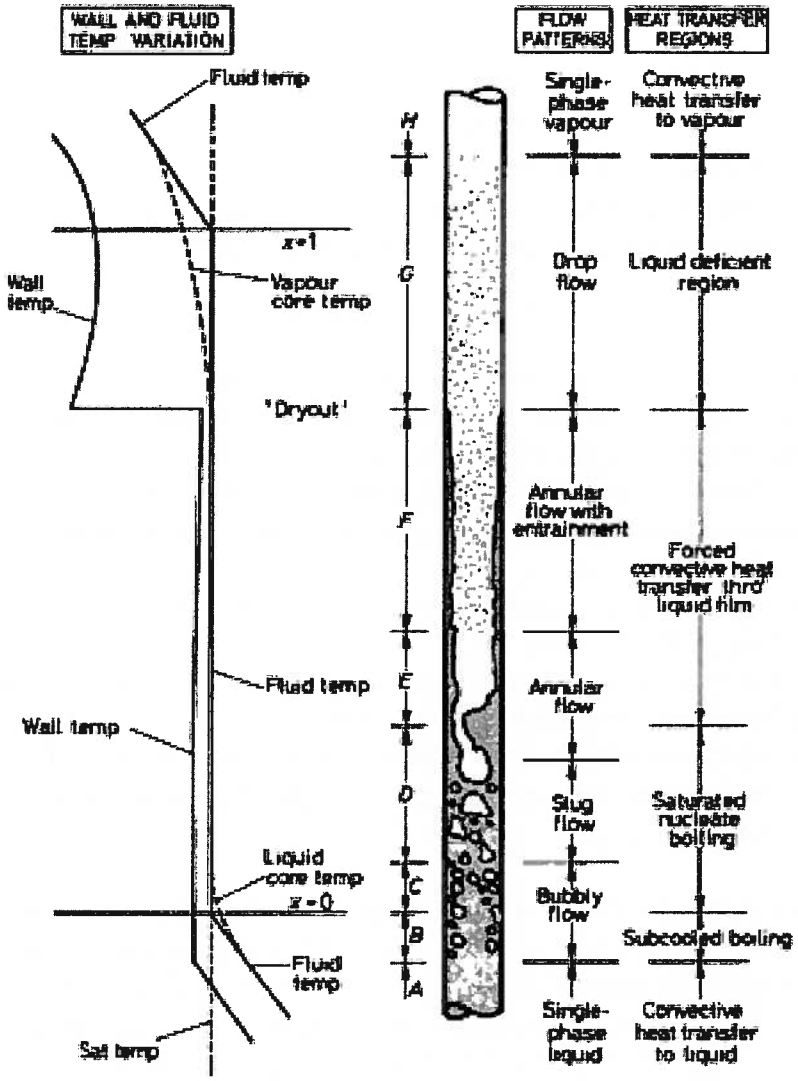

Figure 13.19 Regions of Heat Transfer in Convective Boiling
(From J. G. Collier and J. R. Thome, *Convective Boiling and Condensation*, 3rd Edition, Oxford University Press, 1999, p. 170, Fig. 4.21.)

$$\dot{q}A_{surface} = \left(\frac{\dot{m}}{A_c}\right) A_c x h_{fg}$$

$$x = \frac{\dot{q}A_{surface}}{\left(\frac{\dot{m}}{A_c}\right) A_c h_{fg}} = \frac{\dot{q}\pi D\left(z - z_{SC}\right)}{\left(\frac{\dot{m}}{A_c}\right)\pi\frac{D^2}{4}h_{fg}} = \frac{4\dot{q}}{Dh_{fg}\left(\frac{\dot{m}}{A_c}\right)}\left(z - z_{SC}\right) \tag{13.96}$$

At some point during the saturated nucleate boiling stage, the growing vapor bubbles coalesce in the central core of the flow and produce an annular flow with the liquid sequestered at the tube wall and the vapor in the core. The heat transfer mechanism now transitions to one of forced convection in the liquid film with evaporation at the liquid-vapor interface. This covers regions E and F. Eventually, all of the liquid evaporates at the location denoted "dryout" and the

heat transfer mechanism undergoes yet another transition to one in which the surface temperature experiences a sharp increase. Downstream of this point, the flow consists of dispersed bubbles (Region G) that gradually evaporate and produce a true dry vapor flow with no liquid phase present (Region H). Because of the steep rise in surface temperature at the dryout point, it is an important feature of convective boiling heat transfer. The increase in temperature can result in severe damage to thermal-fluid equipment such as evaporators, boilers, and nuclear reactors.

Each of the regions delineated in figure 13.19 has its own complex physical phenomena that have been studied in detail. The result of these studies is a set of complex analytical tools that describe the heat transfer processes of each region and are given in the three references listed above. The early work in the field relied on correlations of pool boiling heat transfer data of the type given above and forced convection correlations of the type given in Chapter 11. These two correlations were then combined in some empirical manner to yield the heat transfer coefficient for flow boiling. The early work has been valuable because it led to a fuller understanding of the phenomena attendant to flow boiling heat transfer. In recent years, however, the advent of high speed personal computers and the introduction of new flow boiling data have lead to empirical approaches which tend to lump all the flow boiling phenomena into a single expression for the direct correlation of data which have both greater accuracy and ease of evaluation than the earlier treatments. In this introductory presentation, it is not possible to include all the details developed in the earlier work so we present, instead, one of the more recent simplified correlations reported by Klimenko. (V. V. Klimenko, "A generalized correlation for two-phase forced flow heat transfer – second assessment", *International Journal of Heat and Mass Transfer*, Vol. 33, No. 10, pp. 2073 – 2088, 1990.)

Klimenko's model essentially takes the many different regions shown in Figure 13.19 and lumps them into two separate regions: one that involves forced convection nucleate boiling and a second one involving forced convection vaporization typical of the annular flow regime. The demarcation between these two regions is established by the value of the convective boiling number, N_{CB}, where

$$N_{CB} = \left(\frac{\dot{m}}{A_c}\right)\left(\frac{h_{fg}}{q}\right)\left[1 + x\left(\frac{\rho_f}{\rho_g} - 1\right)\right]\left(\frac{\rho_g}{\rho_f}\right)^{1/3} \tag{13.97}$$

The cross-over from forced convection nucleate boiling to forced convection vaporization occurs for the value of $N_{CB} = 1.6 \times 10^4$. That is, for $N_{CB} < 1.6 \times 10^4$, forced convection nucleate boiling prevails, and for $N_{CB} > 1.6 \times 10^4$, forced convection vaporization prevails.

The forced convection nucleate boiling contribution is given by

$$Nu_b = CPe_m^{0.6} Pr_f^{-0.33} \left(\frac{P_{sat} L_c}{\sigma}\right)^{0.54} \left(\frac{k_{surface}}{k_f}\right)^{0.12} \tag{13.98}$$

where the Nusselt number for forced convection nucleate boiling, Nu_b, is

$$Nu_b = \frac{h_b L_c}{k_f} \tag{13.99}$$

where L_c is the characteristic length for boiling (also known as the Laplace constant) given by equation (13.62). In equation (13.98) Pe_m is the modified Peclet number

$$Pe_m = \frac{qL_c \rho_f c_{Pf}}{h_{fg} \rho_g k_f} \tag{13.100}$$

and Pr_f is the Prandtl number for the liquid phase. The constant C appearing in equation (13.98) depends upon the nature of the fluid and is given in Table 13.6.

Table 13.6 Constants in the Forced Convection Nucleate Boiling Correlation

Fluid	C	Pr
Freons (R-22, R-134a, R-113, etc.)	7.6×10^{-3}	3.8 ± 2.5
Organic fluids	6.8×10^{-3}	3.5 ± 1.3
Cryogenic fluids	6.1×10^{-3}	1.6 ± 1.0
H_2O	4.9×10^{-3}	1.2 ± 0.4

The forced convection vaporization contribution is given by

$$Nu_c = 0.087 Re_m^{0.6} Pr_f^{1/6} \left(\frac{\rho_g}{\rho_f}\right)^{0.2} \left(\frac{k_{surface}}{k_f}\right)^{0.09} \tag{13.101}$$

where forced convection vaporization Nusselt number, Nu_c, is given by

$$Nu_c = \frac{h_c L_c}{k_f} \tag{13.102}$$

and Re_m is the Reynolds number of the two-phase mixture, viz.

$$Re_m = \left(\frac{\dot{m}}{A_c}\right)\left[1 + x\left(\frac{\rho_f}{\rho_g} - 1\right)\right]\frac{L_c}{\mu_f} \tag{13.103}$$

Then for two-phase flow in vertical and horizontal conduits when the perimeter is fully wetted by liquid and $1.2 \times 10^4 < N_{CB} < 2.0 \times 10^4$, the appropriate correlation is

$$Nu_{TP} = \max\left[Nu_b ; Nu_c\right] \tag{13.104}$$

where Nu_b and Nu_c are given by equations (13.98) and (13.101), respectively. If $N_{CB} < 1.2 \times 10^4$, equation (13.98) is the appropriate correlation, and if $N_{CB} > 2.0 \times 10^4$, equation (13.101) is the appropriate correlation.

Example 13E.11: The steam generator of an energy conversion plant that uses H_2O as the working fluid is constructed with a "water tube wall" consisting of a collection of stainless steel tubes (D = 16 mm, k_s = 15.2 W/m K) welded together, side-by-side, with their axes parallel and vertical. The heat flux is $\dot{q}$ = 10^6 W/m^2 and the mass flux is $\dot{m}/A_c$ = 500 kg/m^2 sec. The H_2O flows vertically upward, and at some point in the flow the saturation temperature is T_{sat} = 200 C with a quality of x = 0.02. At this location in the flow, we wish to determine the temperature of the tube wall, and the local pressure gradient in the flow.

Solution: From the property tables for the pure substance model for H_2O, we have the following properties at T_{sat} = 200 C:

$$P_{sat} = 1.5549 \times 10^6 \text{ N/m}^2 \quad \sigma = 0.03768 \text{ N/m sec} \quad Pr_f = 0.9104 \quad k_f = 0.66331 \text{ W/m K}$$

$$\rho_f = 864.66 \text{ kg/m}^3 \quad \rho_g = 7.8610 \text{ kg/m}^3 \quad h_f = 0.85227 \times 10^6 \text{ J/kg} \quad h_{fg} = 1.93974 \times 10^6 \text{ J/kg}$$

We first calculate the convective boiling number from equation (13.97), viz.

$$N_{CB} = \left(\frac{\dot{m}}{A_c}\right)\left(\frac{h_{fg}}{q}\right)\left[1 + x\left(\frac{\rho_f}{\rho_g} - 1\right)\right]\left(\frac{\rho_g}{\rho_f}\right)^{1/3}$$

$$N_{CB} = \left(500 \text{ kg/m}^2 \text{ sec}\right)\left(\frac{1.9397 \times 10^6 \text{ J/kg}}{10^6 \text{ W/m}^2}\right)\left[1 + 0.02\left(\frac{864.66 \text{ kg/m}^3}{7.8610 \text{ kg/m}^3} - 1\right)\right]\left(\frac{7.8610 \text{ kg/m}^3}{864.66 \text{ kg/m}^3}\right)^{1/3}$$

$$N_{CB} = 643.68$$

Thus, at this point in the flow, the heat transfer process is dominated by forced convection nucleate boiling as we would have expected given the small value of the quality. Then the heat transfer coefficient should be calculated from equation (13.98) with $C = 4.9 \times 10^{-3}$. Then we must first calculate the modified Peclet number Pe_m. For this we need the specific heat at constant pressure for the liquid, $c_{Pf} = 4495.9$ J/kg K and the Laplace constant, L_c, viz.

$$L_c = \sqrt{\frac{\sigma}{g(\rho_f - \rho_g)}} = \sqrt{\frac{0.03768 \text{ N/m}}{(9.81 \text{ m/sec}^2)(864.66 \text{ kg/m}^3 - 7.861 \text{ kg/m}^3)}} = 2.117 \times 10^{-3} \text{ m}$$

Then

$$Pe_m = \frac{\dot{q} L_c \rho_f c_{Pf}}{h_{fg} \rho_g k_f} = \frac{(10^6 \text{ W/m}^2)(2.117 \times 10^{-3} \text{ m})(864.66 \text{ kg/m}^3)(4495.8 \text{ J/kg K})}{(1.93974 \times 10^6 \text{ J/kg})(7.861 \text{ kg/m}^3)(0.66331 \text{ W/m K})} = 813.759$$

Then

$$Nu_b = C Pe_m^{0.6} Pr_f^{-0.33} \left(\frac{P_{sat} L_c}{\sigma}\right)^{0.54} \left(\frac{k_{surface}}{k_f}\right)^{0.12}$$

$$Nu_b = 4.9 \times 10^{-3} (813.759)^{0.6} (0.9104)^{-0.33} \left[\frac{(1.5549 \times 10^6 \text{N/m}^2)(2.117 \times 10^{-3} \text{ m})}{0.03768 \text{ N/m}}\right]^{0.54} \cdot \left(\frac{15.2 \text{ W/m K}}{0.66331 \text{ W/m K}}\right)^{0.12}$$

$$Nu_b = 163.985$$

Then the heat transfer coefficient for forced convection nucleate boiling becomes

$$h_b = Nu_b \frac{k_f}{L_c} = 163.985 \left(\frac{0.66331 \text{ W/m K}}{2.117 \times 10^{-3} \text{ m}}\right) = 5.137 \times 10^4 \text{ W/m}^2 \text{ K}$$

Then the tube wall temperature is given by Newton's Law of Cooling, viz.

$$T_{wall} = T_{sat} + \frac{\dot{q}}{h_b} = 200 \text{ C} + \frac{10^6 \text{ W/m}^2}{5.137 \times 10^4 \text{ W/m}^2 \text{ K}} = 219.47 \text{ C}$$

The average density of the two phases is

$$\rho = \frac{\rho_f \rho_g}{x\rho_f + (1-x)\rho_g} = \frac{(864.66 \text{ kg/m}^3)(7.861 \text{ kg/m}^3)}{0.02(864.66 \text{ kg/m}^3) + (1-0.02)(7.861 \text{ kg/m}^3)} = 271.92 \text{ kg/m}^3$$

The mass flow rate is

$$\dot{m} = \left(\frac{\dot{m}}{A_c}\right) A_c = (500 \text{ kg/m}^2 \text{ sec}) \frac{\pi (0.016 \text{ m})^2}{4} = 0.1005 \text{ kg/sec}$$

The pseudo-viscosity of the two-phase mixture is

$$\frac{1}{\mu^*} = \frac{x}{\mu_g} + \frac{1-x}{\mu_f} = \frac{0.02}{1.5715 \times 10^{-5} \text{ kg/m sec}} + \frac{1-0.02}{1.3432 \times 10^{-4} \text{ kg/m sec}}$$

$$\mu^* = 1.1670 \times 10^{-4} \text{ kg/m sec}$$

Then the Reynolds number for the flow is

$$Re = \frac{4\dot{m}}{\pi D \mu^*} = \frac{4(0.1005 \text{ kg/sec})}{\pi (0.016 \text{ m})(1.1670 \times 10^{-4} \text{ kg/m sec})} = 6.8549 \times 10^4$$

Then the friction factor is

$$f = (0.7904 \ln Re - 1.64)^{-2} = \left[0.7904 \ln (68549) - 1.64\right]^{-2} = 0.0195$$

Then the pressure gradient due to friction is

$$\left(\frac{dP}{dz}\right)_F = -\frac{f}{2\rho D}\left(\frac{\dot{m}}{A_c}\right)^2 = -\frac{0.0195\left(500 \text{ kg/m}^2 \text{ sec}\right)^2}{2\left(271.92 \text{ kg/m}^3\right)\left(0.016 \text{ m}\right)} = -560.93 \text{ N/m}^3$$

The pressure gradient due to changes in momentum can be calculated from equation (13.92), viz.

$$\left(\frac{dP}{dz}\right)_M = \left(\frac{\dot{m}}{\rho A_c}\right)^2 \frac{d\rho}{dz}$$

But we can expand the spatial gradient of density with the aid of the chain rule, viz.

$$\frac{d\rho}{dz} = \frac{d\rho}{dx}\frac{dx}{dz}$$

The first derivative on the right-hand side can be evaluated with the aid of equation (13.88), viz.

$$\frac{d\rho}{dx} = \frac{-\rho_f \rho_g \left(\rho_f - \rho_g\right)}{\left[x\rho_f + (1-x)\rho_g\right]^2}$$

$$\frac{d\rho}{dx} = \frac{-\left(864.66 \text{ kg/m}^3\right)\left(7.861 \text{ kg/m}^3\right)\left(864.66 \text{ kg/m}^3 - 7.861 \text{ kg/m}^3\right)}{\left[0.02\left(864.66 \text{ kg/m}^3\right) + (1-0.02)\left(7.861 \text{ kg/m}^3\right)\right]^2} = -9320.2 \text{ kg/m}^2$$

The second derivative on the right-hand side can be evaluated from equation (13.92), viz.

$$\frac{dx}{dz} = \frac{4\dot{q}}{Dh_{fg}}\left(\frac{\dot{m}}{A_c}\right)^{-1} = \frac{4\left(10^6 \text{ W/m}^2\right)}{\left(0.016 \text{ m}\right)\left(1.93974 \text{ x } 10^6 \text{ J/kg}\right)\left(500 \text{ kg/m}^2 \text{ sec}\right)} = 0.2578 \text{ m}^{-1}$$

Then the pressure gradient due to momentum changes is

$$\left(\frac{dP}{dz}\right)_M = \left(\frac{\dot{m}}{\rho A_c}\right)^2 \frac{d\rho}{dz} = \frac{\left(\dot{m}/A_c\right)^2}{\rho^2}\frac{d\rho}{dx}\frac{dx}{dz}$$

$$\left(\frac{dP}{dz}\right)_M = \frac{\left(500 \text{ kg/m}^2 \text{ sec}\right)^2}{\left(271.92 \text{ kg/m}^3\right)^2}\left(-9320.2 \text{ kg/m}^3\right)\left(0.2578 \text{ m}^{-1}\right) = -8123.1 \text{ N/m}^3$$

The pressure gradient due to the gravity body force is

$$\left(\frac{dP}{dz}\right)_G = -\rho g = \left(271.92 \text{ kg/m}^3\right)\left(9.81 \text{ m/sec}^2\right) = -2667.5 \text{ N/m}^3$$

Finally, the total pressure gradient is

$$\frac{dP}{dz} = \left(\frac{dP}{dz}\right)_F + \left(\frac{dP}{dz}\right)_M + \left(\frac{dP}{dz}\right)_G$$

$$\frac{dP}{dz} = \left(-560.93 \text{ N/m}^3\right) + \left(-8123.1 \text{ N/m}^3\right) + \left(-2667.5 \text{ N/m}^3\right) = -1.1352 \text{ x } 10^4 \text{ N/m}^3$$

Example 13.12: Consider the steam generator of Example 13.11. Let us examine the situation further along a typical tube near the "dryout" point where the quality is $x = 0.98$.

(a) At this location, calculate the tube wall temperature and estimate the length of tube over which the phase change occurs.

(b) Calculate the local pressure gradient.

Solution: (a) The thermal-fluid properties of interest are identical to those listed in Example 13.11. Then the convective boiling number now becomes

$$N_{CB} = \left(\frac{\dot{m}}{A_c}\right)\left(\frac{h_{fg}}{q}\right)\left[1+x\left(\frac{\rho_f}{\rho_g}-1\right)\right]\left(\frac{\rho_g}{\rho_f}\right)^{1/3}$$

$$N_{CB} = \left(500 \text{ kg/m}^2 \text{ sec}\right)\left(\frac{1.9397 \text{ x } 10^6 \text{ J/kg}}{10^6 \text{ W/m}^2}\right)\left[1+0.98\left(\frac{864.66 \text{ kg/m}^3}{7.8610 \text{ kg/m}^3}-1\right)\right]\left(\frac{7.8610 \text{ kg/m}^3}{864.66 \text{ kg/m}^3}\right)^{1/3}$$

$$N_{CB} = 2.1824 \text{ x } 10^4$$

This is clearly a situation in which forced convection vaporization dominates and the Nusselt number is given by equation (13.101), viz.

$$Nu_c = 0.087 Re_m^{0.6} Pr_f^{1/6}\left(\frac{\rho_g}{\rho_f}\right)^{0.2}\left(\frac{k_{surface}}{k_f}\right)^{0.09}$$

where the relevant value of the Reynolds number is

$$Re_m = \left(\frac{\dot{m}}{A_c}\right)\left[1+x\left(\frac{\rho_f}{\rho_g}-1\right)\right]\frac{L_c}{\mu_f}$$

$$Re_m = \left(500 \text{ kg/m}^2 \text{ sec}\right)\left[1+0.98\left(\frac{864.66 \text{ kg/m}^3}{7.861 \text{ kg/m}^3}\right)\right]\frac{2.1173 \text{ x } 10^{-3} \text{ m}}{1.3432 \text{ x } 10^{-4} \text{ kg/m sec}}$$

$$Re_m = 8.4974 \text{ x } 10^5$$

Then

$$Nu_c = 0.087\left(8.4974 \text{ x } 10^5\right)^{0.6}(0.9104)^{1/6}\left(\frac{7.861 \text{ kg/m}^3}{864.66 \text{ kg/m}^3}\right)^{0.2}\left(\frac{15.2 \text{ W/m K}}{0.66331 \text{ W/m K}}\right)^{0.09}$$

$$Nu_c = 160.116$$

Then the heat transfer coefficient becomes

$$h_c = Nu_c\frac{k_f}{L_c} = 106.116\left(\frac{0.66331 \text{ W/m K}}{2.1173 \text{ x } 10^{-3} \text{ m}}\right) = 5.0161 \text{ x } 10^4 \text{ W/m}^2 \text{ K}$$

Then the wall temperature at this location becomes

$$T_{wall} = T_{sat} + \frac{\dot{q}}{h_c} = 200 \text{ C} + \frac{10^6 \text{ W/m}^2}{5.0161 \text{ x } 10^4 \text{ W/m}^2 \text{ K}} = 219.94 \text{ C}$$

Thus the tube wall temperature is essentially constant over the region where the phase change is taking place. The length of this region is given by the first law

$$\dot{q}\pi DL = \left(\frac{\dot{m}}{A_c}\right)A_c h_{fg}$$

$$L = \left(\frac{\dot{m}}{A_c}\right)\frac{A_c h_{fg}}{\dot{q}\pi D} = \left(\frac{\dot{m}}{A_c}\right)\frac{h_{fg}D}{4\dot{q}} = \left(500 \text{ kg/m}^2 \text{ sec}\right)\frac{\left(1.93974 \text{ x } 10^6 \text{ J/kg}\right)\left(0.016 \text{ m}\right)}{4\left(10^6 \text{ W/m}^2\right)} = 3.88 \text{ m}$$

(b) To determine the pressure gradient due to fluid friction, we first calculate the pseudo-viscosity, viz.

$$\frac{1}{\mu^*} = \frac{x}{\mu_g}+\frac{1-x}{\mu_f} = \frac{0.98}{1.5715 \text{ x } 10^{-5} \text{ kg/m sec}}+\frac{1-0.98}{1.4332 \text{ x } 10^{-4} \text{ kg/m sec}} = 1.60 \text{ x } 10^{-5} \text{ kg/m sec}$$

Then the Reynolds number becomes

$$Re = \frac{4\dot{m}}{\pi D \mu^*} = \frac{4(0.1005 \text{ kg/sec})}{\pi(0.016 \text{ m})(1.60 \text{ x } 10^{-5} \text{ kg/m sec})} = 5.0008 \text{ x } 10^5$$

Then the friction factor becomes

$$f = (0.7904 \ln Re - 1.64)^{-2} = \left[0.7904 \ln(5.0008 \text{ x } 10^5) - 1.64\right]^{-2} = 0.0131$$

Then the pressure gradient due to friction becomes

$$\left(\frac{dP}{dz}\right)_F = -\frac{f}{2\rho D}\left(\frac{\dot{m}}{A_c}\right)^2 = -\frac{0.0131(500 \text{ kg/m}^2 \text{ sec})^2}{2(271.92 \text{ kg/m}^3)(0.016 \text{ m})} = -377.26 \text{ N/m}^3$$

As in Example 13.11, the pressure gradient due to momentum changes is given by

$$\left(\frac{dP}{dz}\right)_M = \left(\frac{\dot{m}}{\rho A_c}\right)^2 \frac{d\rho}{dz}$$

and

$$\frac{d\rho}{dz} = \frac{d\rho}{dx}\frac{dx}{dz}$$

where

$$\frac{d\rho}{dx} = \frac{-\rho_f \rho_g (\rho_f - \rho_g)}{\left[x\rho_f + (1-x)\rho_g\right]^2}$$

and

$$\frac{d\rho}{dx} = \frac{-(864.66 \text{ kg/m}^3)(7.861 \text{ kg/m}^3)(864.66 \text{ kg/m}^3 - 7.861 \text{ kg/m}^3)}{\left[0.98(864.66 \text{ kg/m}^3) + (1-0.98)(7.861 \text{ kg/m}^3)\right]^2} = -8.1077 \text{ kg/m}^2$$

and from Example 13.11, $dx/dz = 0.2578 \text{ m}^{-1}$. Then

$$\frac{d\rho}{dz} = (-8.1077 \text{ kg/m}^3)(0.2578 \text{ m}^{-1}) = -2.0899 \text{ kg/m}^3$$

and the pressure gradient due to momentum changes becomes

$$\left(\frac{dP}{dz}\right)_M = \left(\frac{\dot{m}}{\rho A_c}\right)^2 \frac{d\rho}{dz} = \frac{(\dot{m}/A_c)^2}{\rho^2}\frac{d\rho}{dx}\frac{dx}{dz}$$

$$\left(\frac{dP}{dz}\right)_M = \frac{(500 \text{ kg/m}^2 \text{ sec})^2}{(271.92 \text{ kg/m}^3)^2}(-2.0899 \text{ kg/m}^3)(0.2578 \text{ m}^{-1}) = -7.066 \text{ N/m}^3$$

which is quite small since most of the mass has already been converted from liquid to vapor. The pressure gradient due to the gravity body force is identical to Example 13.11. Then

$$\left(\frac{dP}{dz}\right)_G = -\rho g = (271.92 \text{ kg/m}^3)(9.81 \text{ m/sec}^2) = -2667.5 \text{ N/m}^3$$

and the total pressure gradient is given by

$$\frac{dP}{dz} = \left(\frac{dP}{dz}\right)_F + \left(\frac{dP}{dz}\right)_M + \left(\frac{dP}{dz}\right)_G$$

$$\frac{dP}{dz} = (-377.26 \text{ N/m}^3) + (-7.0663 \text{ N/m}^3) + (-2667.5 \text{ N/m}^3) = -3.0518 \text{ x } 10^3 \text{ N/m}^3$$

Comparing this result with that of Example 13.11, we see that the pressure gradient decreases as the mass is converted from the liquid phase to the vapor phase. Eventually, in vertical upward flow, the largest contribution to the pressure gradient is due to the gravity body force.

13.14.2 Condensation Heat Transfer

Consider the physical situation in which a solid surface with a temperature $T_{surface}$ is exposed to a saturated vapor at a pressure P_{sat} with a corresponding saturation temperature T_{sat}. If $T_{surface} < T_{sat}$ some of the vapor will condense and form the liquid phase. Since the condensation process involves the transfer of the latent heat, it usually gives rise to relatively high heat fluxes with correspondingly high heat transfer coefficients. For this reason, the condensation process plays an important role in thermal-fluids engineering practice and is the dominant mechanism of heat transfer in a large class of thermal-fluids engineering equipment, known as *condensers*, that are commonly found in energy conversion plants and refrigeration plants. The condensation process is also important in the processing of many materials such as the refinement of petroleum and the desalination of water to name only two of many examples.

The condensation process is a complex one that can proceed by both homogeneous nucleation and heterogeneous nucleation mechanisms. Of these, the heterogeneous mechanism involving some sort of foreign body or surface imperfection is by far the most common. When the vapor condenses on the solid surface, it forms nuclei which grow and can form liquid droplets leading to a phenomenon known as *dropwise condensation*. In dropwise condensation, the liquid droplets are dispersed over the surface with the condensation occurring at very localized sites. These liquid droplets eventually coalesce to form much larger droplets which then move over the surface under the influence of gravity body forces or drag forces. This gives rise to very high heat transfer coefficients since the area involved in the heat transfer process is so small.

On the other hand, these nuclei may involve the formation of a liquid film leading to a phenomenon known as *filmwise condensation*. In filmwise condensation, the liquid is dispersed over the condensing surface in a more or less uniform manner and moves under the influence of gravity. As a result, the heat transfer coefficients characteristic of filmwise condensation are typically smaller than those characteristic of dropwise condensation, usually by an order of magnitude or more. This offers the possibility that condensers involving dropwise condensation can be made much smaller and at lower cost. Unfortunately, despite the fact that dropwise condensation is the phenomenon commonly observed on the outside surface of a cold beverage container, for reasons explained below, dropwise condensation is not easily achieved nor maintained in industrial equipment.

Whether the condensation process proceeds in a dropwise or filmwise manner depends upon whether the liquid formed "wets" the surface. The wetting of the surface is a result of the contact angle between the liquid-vapor interface and the condensing surface. If the vapor involved in the condensation process is H_2O and the resulting liquid phase wets the surface, the surface is said to be *hydrophilic* whereas if the surface is not wet by the liquid, the surface is said to be *hydrophobic*. A hydrophobic surface results in dropwise condensation and a hydrophilic surface results in filmwise condensation. Surfaces can be made hydrophobic or hydrophilic by treatment with appropriate chemical agents, so in principle at least, the thermal-fluids engineer has some flexibility in the design of condensing surfaces.

Since condensing surfaces ultimately must transfer the energy and entropy to some other fluid medium, the surface must have good conduction heat transfer characteristics. For this reason, metals are the materials of choice for condensing surfaces. Clean metal surfaces tend to be hydrophobic and contaminated metal surfaces tend to be hydrophilic. However, clean metal

surfaces usually become quickly contaminated due to impurities in the prevailing environment and revert to hydrophilic character. Many polymer surfaces are naturally hydrophobic but have poor conduction heat transfer characteristics and therefore are not used as condensing surfaces. The net result of all these considerations is that filmwise condensation is the more common mechanism in condensing equipment and, for this reason, will be considered here in detail.

The study of the condensation heat transfer process naturally divides into two classifications: external condensation and internal condensation. External condensation commonly occurs on the walls of vessels that are exposed to saturated vapors, as is the case of the cold beverage container in a humid environment, or it may occur when saturated vapors are exposed to tubes in which a cooling medium is flowing as is the case on the shell side in a shell-and-tube condenser. Internal condensation commonly occurs inside tubes in which a saturated vapor is flowing, as is the case of the condenser in a household refrigerator. In either case, the temperature of the condensing surface is less than the saturation temperature of the vapor to which it is exposed. We begin our analysis with the case of external condensation.

13.14.2.1 Filmwise Condensation on a Vertical Flat Plate

The most widely used formulation of filmwise condensation is that due to Nusselt who presented the following treatment in 1916. Consider the case of a vertical flat plate that bounds a volume containing a saturated vapor at a pressure P_{sat} and a temperature T_{sat}. The temperature of the plate surface is maintained at the value $T_{surface}$. Since $T_{surface} < T_{sat}$, a liquid film of thickness δ forms on the surface of the plate.

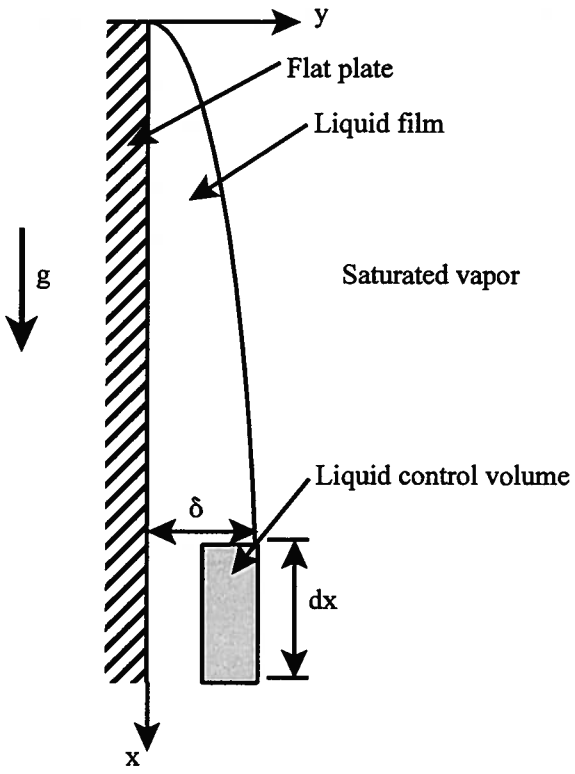

Figure 13.20 Liquid Film Condensing on a Vertical Flat Plate

As shown in Figure 13.20, the condensing liquid film forms at the leading edge of the plate, $x = 0$, and descends down the plate under the influence of a body force that is the net result of the gravity body force and the buoyancy force provided by the displacement of the vapor. In the Nusselt analysis of this situation, it is assumed that the flow in the film is laminar. Then the motion of this liquid film is retarded by a shear force due to the shear stress in the film. In the

steady state when inertial effects are no longer operative, the body force is just balanced by the shear force and the velocity profile in the film becomes fully developed. Then for the differential liquid control volume of length dx identified in Figure 13.20, the equation of motion reduces to

$$(\delta - y)dx(\rho_f - \rho_g)g = \mu_f\left(\frac{d\vartheta_x}{dy}\right)dx \tag{13.105}$$

Then separating variables and integrating equation (13.105) from the surface of the plate where the liquid velocity is zero to some arbitrary location y in the film where the velocity is ϑ_x, we get

$$\frac{(\rho_f - \rho_g)g}{\mu_f}\int_0^{\delta}(\delta - y)dy = \int_0^{\vartheta_x} d\vartheta_x$$

$$\vartheta_x = \frac{(\rho_f - \rho_g)g}{\mu_f}\left[\delta y - \frac{y^2}{2}\right] \tag{13.106}$$

If we define the mass flow rate per unit film width Γ as

$$\Gamma = \rho_f \int_0^{\delta} \vartheta_x dy \tag{13.107}$$

we can substitute equation (13.106) and integrate to get

$$\Gamma = \frac{\rho_f(\rho_f - \rho_g)g}{\mu_f}\int_0^{\delta}\left(\delta y - \frac{y^2}{2}\right)dy = \frac{\rho_f(\rho_f - \rho_g)g}{\mu_f}\frac{\delta^3}{3} \tag{13.108}$$

but this is a local result since the film thickness varies in the x-direction due to the condensation. To account for this, we differentiate equation (13.108) with respect to δ. Then

$$\frac{d\Gamma}{d\delta} = \frac{\rho_f(\rho_f - \rho_g)g\delta^2}{\mu_f} \tag{13.109}$$

There exists in the film a temperature gradient given by

$$\frac{dT}{dy} = \left(\frac{T_{sat} - T_{surface}}{\delta}\right) \tag{13.110}$$

Then for a differential control volume of the film of length dx and thickness δ, the rate of heat transfer across the film by conduction from the liquid-vapor interface to the surface of the plate is given by

$$d\dot{Q} = \dot{q}dx = \frac{k_f(T_{sat} - T_{surface})dx}{\delta} \tag{13.111}$$

At the liquid-vapor interface of the differential element, there is a heat transfer due to the condensation process at the interface (Here.), viz.

$$d\dot{Q} = \dot{q}dx = h_{fg}\frac{d\Gamma}{dx}dx = h_{fg}\frac{d\Gamma}{d\delta}\frac{d\delta}{dx}dx \tag{13.112}$$

where we have neglected subcooling in the liquid in comparison with the latent heat. Combining equations (13.109), (13.111), and (13.112), we get a differential equation for $\delta = \delta(x)$

$$\frac{d\delta}{dx} = \frac{k_f\mu_f(T_{sat} - T_{surface})}{\rho_f(\rho_f - \rho_g)gh_{fg}\delta^3} \tag{13.113}$$

Integrating equation (13.113) with respect to x, we get

$$\int_0^\delta \delta^3 d\delta = \frac{k_f \mu_f \left(T_{sat} - T_{surface}\right)}{\rho_f \left(\rho_f - \rho_g\right) g h_{fg}} \int_0^x dx$$

$$\delta = \left[\frac{4 k_f \mu_f x \left(T_{sat} - T_{surface}\right)}{\rho_f \left(\rho_f - \rho_g\right) g h_{fg}}\right]^{1/4} \tag{13.114}$$

The heat flux can be determined in two ways – either by Newton's Law of Cooling applied between the condensing surface and the vapor, or by the Fourier Conduction Law applied across the film. Both approaches yield the same result and can, therefore, be equated. Thus, the condensation heat transfer coefficient becomes

$$h_{cond} = \frac{k_f \left(\partial T / \partial y\right)_{wall}}{T_{sat} - T_{wall}} = \frac{k_f}{\delta} \tag{13.115}$$

In Nusselt's original formulation, he non-dimensionalized the heat transfer coefficient in terms of the local coordinate x. This non-dimensional parameter is now known as the Nusselt number and takes the form

$$Nu_x = \frac{h_{cond} x}{k_f} = \frac{x}{\delta} = \left[\frac{\rho_f \left(\rho_f - \rho_g\right) g h_{fg} x^3}{4 k_f \mu_f x \left(T_{sat} - T_{surface}\right)}\right]^{1/4} \tag{13.116}$$

where we have made use of equation (13.115).

If the condensing film remains laminar over its entire length, we can determine the average heat transfer coefficient to be

$$\overline{h_{cond}} = \frac{1}{L}\int_0^L h_{cond}\left(x\right) dx = \frac{1}{L}\int_0^L \frac{k_f}{\delta} dx = \frac{1}{L}\left[\frac{\rho_f k_f{}^3 \left(\rho_f - \rho_g\right) g h_{fg}}{\mu_f x \left(T_{sat} - T_{surface}\right)}\right]^{1/4} \int_0^L \frac{dx}{\left(4x\right)^{1/4}}$$

$$\overline{h_{cond}} = \left[\frac{\rho_f k_f{}^3 \left(\rho_f - \rho_g\right) g h_{fg}}{\mu_f L \left(T_{sat} - T_{surface}\right)}\right]^{1/4} \frac{4}{3(4)^{1/4}} = 0.943 \left[\frac{\rho_f k_f{}^3 \left(\rho_f - \rho_g\right) g h_{fg}}{\mu_f L \left(T_{sat} - T_{surface}\right)}\right]^{1/4} \tag{13.117}$$

Then the average value of the Nusselt number over the length of the plate becomes

$$\overline{Nu_L} = \frac{\overline{h_{cond}} L}{k_f} = 0.943 \left[\frac{\rho_f \left(\rho_f - \rho_g\right) g h_{fg} L^3}{\mu_f k_f \left(T_{sat} - T_{surface}\right)}\right]^{1/4} \tag{13.118}$$

It must be remembered that this result is valid only so long as the film remains laminar.

One of the shortcomings of the Nusselt model for laminar film condensation of a vapor on a vertical flat plate is that it fails to account for the convection of energy as the liquid moves through the control volume. As is evident from equation (13.112), the heat flux into the differential control volume is assumed to be simply due to the latent heat of the condensing vapor. In reality, there is a temperature gradient in the liquid and the liquid becomes subcooled as it moves through the control volume. In order to account for this effect, it is necessary to rewrite the first law for the differential control volume in the form so that the new form of equation (13.112) becomes

$$d\dot{Q} = \dot{q} dx = \frac{k_f \left(T_{sat} - T_{surface}\right) dx}{\delta} = h_{fg} \frac{d\Gamma}{dx} dx + \left[\frac{d}{dx}\int_0^\delta \rho_f c_{Pf} \vartheta_x \left(T_{sat} - T\right) dy\right] dx \tag{13.119}$$

Equation (13.119) simply is a statement of the fact that the energy that enters the surface of the

plate by conduction in the liquid at the surface of the plate, is the net result of the condensation heat flow and the difference between the enthalpy of the liquid entering and leaving the differential control volume in the x-direction. If we now substitute the velocity profile of equation (13.106) and the linear temperature profile in the liquid

$$\frac{T_{sat}-T}{T_{sat}-T_{surface}}=1-\frac{y}{\delta} \tag{13.120}$$

into equation (13.119), we get

$$d\dot{Q}=h_{fg}\frac{d\Gamma}{dx}dx+\left[\frac{d}{dx}\int_0^{\delta}\rho_f c_{Pf}\frac{(\rho_f-\rho_g)g}{\mu_f}\left[\delta y-\frac{y^2}{2}\right]\left(T_{sat}-T_{surface}\right)\left(1-\frac{y}{\delta}\right)dy\right]dx \tag{13.121}$$

$$d\dot{Q}=h_{fg}\frac{d\Gamma}{dx}dx+\frac{\rho_f(\rho_f-\rho_g)g}{\mu_f}c_{Pf}\left(T_{sat}-T_{surface}\right)\left[\frac{d}{dx}\int_0^{\delta}\left(\delta y-y^2-\frac{y^2}{2}+\frac{y^3}{2\delta}\right)dy\right]dx$$

which after carrying out the integration and rearranging terms becomes

$$d\dot{Q}=h_{fg}\frac{d\Gamma}{dx}dx+\frac{\rho_f(\rho_f-\rho_g)g}{\mu_f}c_{Pf}\left(T_{sat}-T_{surface}\right)\frac{d}{dx}\left(\frac{\delta^3}{8}\right)dx$$

$$d\dot{Q}=h_{fg}\frac{d\Gamma}{dx}dx+\frac{d(3\Gamma)}{dx}\frac{c_{Pf}\left(T_{sat}-T_{surface}\right)}{8}dx$$

$$\frac{k_f\left(T_{sat}-T_{surface}\right)dx}{\delta}=h_{fg}\left[1+\frac{3}{8}\frac{c_{Pf}\left(T_{sat}-T_{surface}\right)}{h_{fg}}\right]dx$$

$$\frac{k_f\left(T_{sat}-T_{surface}\right)dx}{\delta}=h_{fg}^{*}\frac{d\Gamma}{dx}dx \tag{13.122}$$

where

$$h_{fg}^{*}=h_{fg}\left\{1+\frac{3}{8}\left[\frac{c_{Pf}\left(T_{sat}-T_{surface}\right)}{h_{fg}}\right]\right\} \tag{13.123}$$

Since equation (13.122) is identical in form to the combination of equations (13.112) and (13.113), we can account for the effect of subcooling in the liquid by simply replacing the latent heat h_{fg} in equations (13.116) and (13.118) by a pseudo-latent heat h_{fg}^{*} given by equation (13.123). A more detailed analysis by Rohsenow (Rohsenow, W. M., "Heat Transfer and Temperature Distribution in Laminar Film Condensation," *Transactions of the ASME*, vol. 78, pp. 1645 – 1648, 1956.) shows that the temperature distribution is not linear, but slightly curved, and that the film thickness is slightly greater than that predicted by equation (13.114). The net result is that the heat transfer rate is slightly greater than that predicted by the Nusselt analysis. Rohsenow showed that these additional effects can be introduced into the Nusselt analysis by modifying the constant in equation (13.123) so that the pseudo-latent heat becomes

$$h_{fg}'=h_{fg}\left\{1+0.68\left[\frac{c_{Pf}\left(T_{sat}-T_{surface}\right)}{h_{fg}}\right]\right\} \tag{13.124}$$

In our analysis of the condensing film, we could have followed the example of Mills (Mills, A. F., *Heat Transfer*, Richard D. Irwin Publishers, Boston, MA, Chapter 7, 1992) and adopted an approach slightly different from that of Nusselt. The film Reynolds number is defined

in terms of the mean velocity and the hydraulic diameter of the film. Thus,

$$Re_\Gamma = \frac{4\Gamma}{\mu_f} \tag{13.125}$$

where Γ is the mass flow rate per unit width of film whose local thickness $\delta(x)$ is given by equation (13.114). Then

$$Re_\Gamma = \frac{4g\delta^3(\rho_f - \rho_g)\rho_f}{3\mu_f^2} \tag{13.126}$$

However, typically $\rho_g << \rho_f$ and ρ_g can be neglected in comparison to ρ_f. Then

$$Re_\Gamma = \frac{4g\delta^3\rho_f^2}{3\mu_f^2} = \frac{4}{3}\left(\frac{g}{\nu_f^2}\right)\delta^3 \tag{13.127}$$

If we now define a characteristic length for condensation L_{cond} such that

$$L_{cond} = \left(\frac{\nu_f^2}{g}\right)^{1/3} \tag{13.128}$$

the film Reynolds number becomes

$$Re_\Gamma = \frac{4}{3}\left(\frac{\delta}{L_{cond}}\right)^3 \tag{13.129}$$

We now define the Nusselt number for condensation in terms of this characteristic length L_{cond} as

$$Nu_{cond} = \frac{h_{cond}L_{cond}}{k_f} = \frac{h_{cond}\left(\nu_f^2/g\right)^{1/3}}{k_f} \tag{13.130}$$

While the film thickness δ might seem to be the appropriate length scale to use in the definition of the Nusselt number, L_{cond} is a better choice since δ is unknown and must be determined separately. If we substitute equations (13.115) and (13.129) into equation (13.130), we have the dimensionless relation

$$Nu_{cond} = \left(\frac{3}{4}Re_\Gamma\right)^{-1/3} \tag{13.131}$$

which depends only on the local value of δ and is valid only so long as the film remains laminar.

The falling film is inherently unstable with the possibility of small amplitude waves forming on the surface at any value of the film Reynolds number. However, it has been shown by experiment that by the time the film Reynolds number reaches a value of $Re_\Gamma = 33$, the probability of wave formation is high enough that equation (13.131) is no longer valid. Beyond this value, the film takes on a character known as "wavy laminar" with small amplitude waves appearing on the interface between the vapor and the liquid. In this regime, which persists up to a film Reynolds number of approximately $Re_\Gamma = 1600$, the experimental data of Chun and Seban (Chun, K. R. And Seban, R. A., "Heat Transfer to Evaporating Liquid Films," *Journal of Heat Transfer*, vol. 93, pp. 391 – 396, 1971.) for the condensation Nusselt number can be correlated by

$$Nu_{cond} = 0.822Re_\Gamma^{-0.22} \tag{13.132}$$

In the range of Reynolds numbers $1400 < Re_\Gamma < 2000$, the laminar film undergoes a transition to a fully turbulent film. In this turbulent regime, according to the work of Chun and

Seban (*op. cit.*), the condensation Nusselt number can be correlated by the expression

$$Nu_{cond} = 3.8 \times 10^{-3}\ Re_{\Gamma}^{0.4} Pr_f^{0.65} \tag{13.133}$$

For the average value of the Nusselt number over the length of the vertical flat plate, L, we must integrate the above results. If we take x to be the local position measured from the top of the wall and if we assume the liquid film to be saturated liquid at the vapor/liquid interface with a temperature gradient within the film, it follows that the enthalpy carried into the film by the condensing vapor must be conducted away through the wall (assuming subcooling of the film is negligible relative to the latent heat). Then for a unit width of the plate

$$k_f \left(\frac{\partial T}{\partial y}\right)_{y=0} = \frac{k_f \left(T_{sat} - T_{surface}\right)}{\delta} = h_{fg} \frac{d\Gamma}{dx} \tag{13.134}$$

Substituting the expressions for the local values of Re and Nu, we get

$$\frac{dx}{\left(\nu_f^{\,2}/g\right)^{\frac{1}{3}}} = \frac{\mu_f h_{fg}}{4k_f \left(T_{sat} - T_{surface}\right) Nu} dRe_{\Gamma} \tag{13.135}$$

But since the Prandtl number for the liquid in the film is given by

$$Pr_f = \frac{\mu_f c_{Pf}}{k_f} \tag{13.136}$$

and the Jakob number is given by

$$Ja_f = \frac{c_{Pf}\left(T_{sat} - T_{surface}\right)}{h_{fg}} \tag{13.137}$$

we can write

$$\frac{dx}{\left(\nu_f^{\,2}/g\right)^{1/3}} = \frac{Pr_f}{4Ja_f} \frac{dRe_{\Gamma}}{Nu} \tag{13.138}$$

If the condensation begins at $x = 0$ with $\Gamma = 0$ and $Re = 0$, we can integrate equation (13.138) over a length L down the wall to get

$$\frac{L}{\left(\nu_f^{\,2}/g\right)^{1/3}} = \frac{Pr_f}{4Ja_f} \int_0^{Re_L} \frac{dRe_{\Gamma}}{Nu} \tag{13.139}$$

We can define the average Nusselt number for this length of film to be

$$\overline{Nu_{cond}} = \frac{\overline{h_{cond}} \left(\nu_f^{\,2}/g\right)^{1/3}}{k_f} \tag{13.140}$$

The average heat transfer coefficient can be determined by applying the first law to a unit width of the plate over the length L and combining it with Newton's Law of Cooling. Then

$$\dot{Q} = \Gamma_L h_{fg} = \overline{h_{cond}} L \left(T_{sat} - T_{surface}\right) = \frac{\mu_f h_{fg}}{4} Re_L \tag{13.141}$$

where the subscript L on the mass flow rate indicates that equation (13.108) should be evaluated at a value of δ at $x = L$. Combining equations (13.140) and (13.141), we get

$$\overline{Nu_{cond}} = \frac{Pr_f}{4Ja_f} \frac{\left(\nu_f^{\,2}/g\right)^{1/3}}{L} Re_L \tag{13.142}$$

We can carry out the integration of equation (13.139) over the length L and solve for the average Reynolds number.

For example, substituting equation (13.131) into equation (13.139), we get

$$\frac{L}{\left(\nu_f^2/g\right)^{1/3}} = \frac{Pr_f}{4Ja_f}\int_0^{Re_L}\frac{dRe_\Gamma}{Nu} = \frac{Pr_f}{4Ja_f}\int_0^{Re_L}\frac{dRe_\Gamma}{\left(\frac{3}{4}Re\right)^{-1/3}} = \frac{Pr_f}{4Ja_f}\left(\frac{3}{4}\right)^{4/3}Re_L^{4/3} \qquad (13.143)$$

Equation (13.143) can be solved for Re_L to give

$$Re_L = \frac{4}{3}\left[\frac{4Ja_f}{Pr_f}\frac{L}{\left(\nu_f^2/g\right)^{1/3}}\right]^{3/4} < 30 \quad \text{(laminar)} \qquad (13.144)$$

Substituting equation (13.144) into equation (13.142), we get

$$\overline{Nu}_{cond} = \frac{4}{3}\left[\frac{Pr_f}{4Ja_f}\frac{\left(\nu_f^2/g\right)^{1/3}}{L}\right]^{1/4} \qquad (13.145)$$

Similarly, for the wavy-laminar regime, substituting equations (13.132) into (13.139) and integrating, we get

$$33 < Re_L = \left[\frac{4Ja_f}{Pr_f}\frac{L}{\left(\nu_f^2/g\right)^{1/3}}\right]^{0.82} < Re_{tr} \quad \text{(wavy laminar)} \qquad (13.146)$$

and the Nusselt number becomes

$$\overline{Nu}_{cond} = \left[\frac{Pr_f}{4Ja_f}\frac{\left(\nu_f^2/g\right)^{1/3}}{L}\right]^{0.18} \qquad (13.147)$$

where the transition Reynolds number for a turbulent film is in the range $1400 < Re_{tr} < 2000$ with $Re_{tr} = 1600$ a typical value.

In the turbulent regime, the location of the transition from wavy-laminar to turbulent is obtained by substituting equations (13.131) and (13.132) into equation (13.139), integrating and solving for the location of the transition, viz.

$$\frac{x_{tr}}{\left(\nu_f^2/g\right)^{1/3}} = 1.00\frac{Pr_f}{4Ja_f}Re_{tr}^{1.22} \qquad (13.148)$$

Now substitute equation (13.133) into equation (13.139) and integrate to get

$$\frac{L}{\left(\nu_f^2/g\right)^{1/3}} = \frac{x_{tr}}{\left(\nu_f^2/g\right)^{1/3}} + \frac{Pr_f^{0.35}}{4(3.8\times10^{-3})(0.6)Ja_f}\left[Re_L^{0.6} - Re_{tr}^{0.6}\right] \qquad (13.149)$$

Upon solving equation (13.149) for Re_L and substituting into equation (13.142), we get

$$\overline{Nu}_{cond} = \frac{Pr_f}{4Ja_f}\frac{\left(\nu_f^2/g\right)^{1/3}}{L}\left[\frac{9.12\times10^{-3}Ja_f(L-x_{tr})}{\left(\nu_f^2/g\right)^{1/3}Pr_f^{0.35}} + Re_{tr}^{0.6}\right]^{10/6} \qquad (13.150)$$

13.14.2.2 Filmwise Condensation on a Horizontal Cylinder

As mentioned previously, another common example of external condensation is the heat transfer process that occurs in a shell-and-tube condenser when a saturated vapor flows in the shell and is exposed to the outside wall of the tubes in which a low temperature fluid is flowing. Filmwise condensation results, and since the diameter of a typical tube is small, the resulting film Reynolds number is small. Thus, the flow in the film is laminar in character. Under these circumstances, the Nusselt model is applicable with minor modifications. In addition, as we mentioned in Section 13.14.1.5, the results of this analysis are applicable to film boiling as well.

The geometry of interest is essentially a horizontal cylinder with an isothermal outer surface as shown in Figure 13.21.

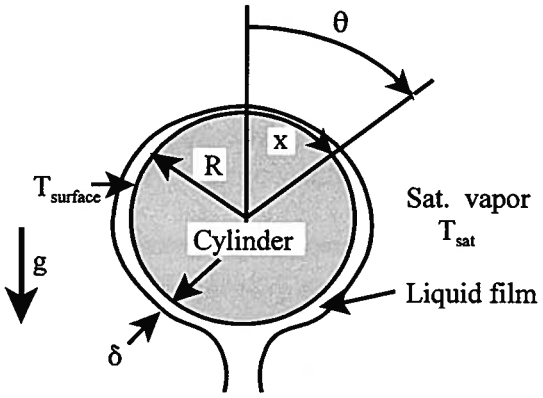

Figure 13.21 Horizontal Cylinder with Condensing Film

The condensing film begins at the position $\theta = 0$ and increases in thickness δ as the film flows down over the surface of the cylinder under the influence of gravity. For a unit width of the film measured along the horizontal axis of the cylinder, the first law is the same as equation (13.134), viz.

$$d\dot{Q} = h_{fg}\frac{d\Gamma}{dx}dx = \frac{k_f\left(T_{sat} - T_{surface}\right)}{\delta}dx \tag{13.134}$$

where we have once again neglected the subcooling in the film. Since the body force per unit volume is now $g\sin\theta$, the laminar velocity profile in the film becomes [*cf.* Equation (13.106)]

$$\vartheta_x = \frac{\left(\rho_f - \rho_g\right)g\sin\theta}{\mu_f}\left(y\delta - \frac{y^2}{2}\right) \tag{13.152}$$

and the mass flow rate per unit width of film measured along the axis of the cylinder is [*cf.* equation (13.109)]

$$\Gamma = \frac{\rho_f\left(\rho_f - \rho_g\right)g\sin\theta}{\mu_f}\int_0^\delta\left(\delta y - \frac{y^2}{2}\right)dy = \frac{\rho_f\left(\rho_f - \rho_g\right)g\sin\theta}{\mu_f}\frac{\delta^3}{3} \tag{13.153}$$

Then

$$\delta = \Gamma^{1/3}\left[\frac{3\mu_f}{\rho_f\left(\rho_f - \rho_g\right)g\sin\theta}\right]^{1/3} \tag{13.154}$$

Since $x = R\theta$, we have

$$\frac{d\Gamma}{dx} = \frac{d\Gamma}{d\theta}\frac{d\theta}{dx} = \frac{1}{R}\frac{d\Gamma}{d\theta} \tag{13.155}$$

Substituting equations (13.154) and (13.155) into equation (13.134), we get

$$\Gamma^{1/3} d\Gamma = \frac{Rk_f \left(T_{sat} - T_{surface}\right)}{h_{fg}} \left[\frac{\rho_f \left(\rho_f - \rho_g\right) g}{3\mu_f}\right]^{1/3} \sin^{1/3}\theta d\theta \tag{13.156}$$

which can be integrated

$$\int_0^{\Gamma_h} \Gamma^{1/3} d\Gamma = \frac{Rk_f \left(T_{sat} - T_{surface}\right)}{h_{fg}} \left[\frac{\rho_f \left(\rho_f - \rho_g\right) g}{3\mu_f}\right]^{1/3} \int_0^{\pi} \sin^{1/3}\theta d\theta$$

$$\frac{3}{4}\Gamma_h^{4/3} = \frac{2.5871}{3^{1/3}} \frac{Rk_f \left(T_{sat} - T_{surface}\right)}{h_{fg}} \left[\frac{\rho_f \left(\rho_f - \rho_g\right) g}{\mu_f}\right]^{1/3}$$

$$\Gamma_h = 1.9232 \left[\frac{R^3 k_f{}^3 \left(T_{sat} - T_{surface}\right)^3 \rho_f \left(\rho_f - \rho_g\right) g}{h_{fg}{}^3 \mu_f}\right]^{1/4} \tag{13.157}$$

where Γ_h is the mass flow rate per unit axial width over one-half the cylinder. Then for a control volume surrounding the entire cylinder, the heat transfer rate per unit axial width, in the absence of subcooling of the liquid, becomes

$$\dot{Q} = 2\Gamma_h h_{fg} = \pi D \overline{h_{cond}} \left(T_{sat} - T_{surface}\right) \tag{13.158}$$

Solving equation(13.158) for the condensing heat transfer coefficient and substituting equation (13.157), we get

$$\overline{h_{cond}} = 0.728 \left[\frac{\rho_f (\rho_f - \rho_g) g h_{fg} k_f{}^3}{\mu_f D (T_{sat} - T_{surface})}\right]^{1/4} \tag{13.159}$$

and the average Nusselt number becomes

$$\overline{Nu_D} = \frac{\overline{h_{cond}} D}{k_f} = 0.728 \left(\frac{Ra^*}{Ja}\right)^{1/4} \tag{13.160}$$

where Ra^* is a modified form of the Rayleigh number

$$Ra^* = \frac{\rho_f \left(\rho_f - \rho_g\right) g D^3 Pr_f}{\mu_f{}^2} \tag{13.161}$$

and Ja is the Jakob number.

In most condenser designs, the tubes used as conduits of the cooling medium are arranged in some sort of array, either an in-line array or a staggered array depending upon the particular design of the heat exchanger. In either case, there is usually one tube above another which results in the liquid flowing off the upper tube onto the lower tube. There results, then, a cascading liquid sheet with the surface tension of the liquid preserving the integrity of the sheet as it moves downward in the tube array. In actual fact, the surface tension causes the sheet to break up into columns of the liquid (*cf.* Figure 13.22.).

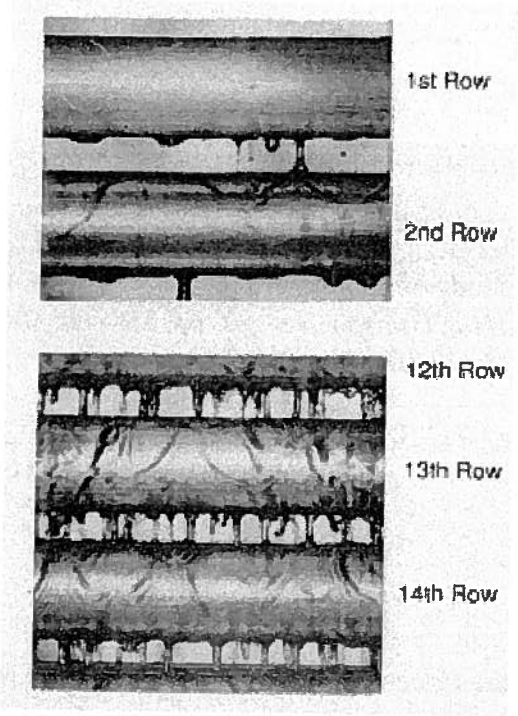

Figure 13.22 Photograph of Cascading Condensing Liquid on a Tube Bundle
(From J. G. Collier and J. R. Thome, *Convective Boiling and Condensation*, 3rd Edition, Oxford University Press, 1999, p. 451, Fig. 10.7.)

Nusselt was able to extend the analysis of equation (13.156) by recognizing that the liquid flowing over the surface of one tube was comprised of two components: the vapor condensing on that tube and the liquid draining down from the tube above. Thus, the limits of integration on equation (13.157) are changed so that for the *i*th tube in the column of tubes

$$\Gamma_{i,bottom}^{4/3} - \Gamma_{i,top}^{4/3} = 2.3917\left[\frac{R^3 k_f{}^3 \left(T_{sat} - T_{surface}\right)^3 \rho_f \left(\rho_f - \rho_g\right) g}{h_{fg}{}^3 \mu_f}\right]^{1/3} \tag{13.162}$$

Continuity requires

$$\Gamma_{i,bottom}^{4/3} - \Gamma_{i-1,bottom}^{4/3} = 2.3917\left[\frac{R^3 k_f{}^3 \left(T_{sat} - T_{surface}\right)^3 \rho_f \left(\rho_f - \rho_g\right) g}{h_{fg}{}^3 \mu_f}\right]^{1/3} \tag{13.163}$$

Then it follows that

$$\Gamma_{i,bottom}^{4/3} = i\, 2.3917\left[\frac{R^3 k_f{}^3 \left(T_{sat} - T_{surface}\right)^3 \rho_f \left(\rho_f - \rho_g\right) g}{h_{fg}{}^3 \mu_f}\right]^{1/3} \tag{13.164}$$

Then for the *i*th tube, the equivalent of equation (13.158) becomes

$$2h_{fg}\Gamma_{i,bottom} = \pi D\overline{h_{cond}}\left(T_{sat} - T_{surface}\right) \tag{13.165}$$

Then for N tubes placed one above the other, the average condensing heat transfer coefficient for

each tube in the array becomes

$$\overline{h_{cond}} = 0.728\left[\frac{\rho_f(\rho_f-\rho_g)gh_{fg}k_f^{\,3}}{ND\mu_f(T_{sat}-T_{surface})}\right]^{1/4} \tag{13.166}$$

Since we have shown in equation (13.123) that the liquid film between tubes is subcooled by an amount $(3/8)(T_{sat} - T_{surface})$, it is possible that additional condensation occurs on this portion of the liquid film. If we assume that all of this subcooling is consumed by condensation, Chen (Chen, M. M., "An Analytical Study of Laminar Film Condensation, Part 2: Single and Multiple Horizontal Tubes," *Journal of Heat Transfer*, vol. 83, pp. 55 – 60, 1961.) has shown that the numerical coefficient in equation (13.166) becomes

$$\overline{h_{cond}} = 0.728\left[1+0.2(N-1)\frac{c_{Pf}\left(T_{sat}-T_{surface}\right)}{h_{fg}}\right]\left[\frac{\rho_f(\rho_f-\rho_g)gh_{fg}k_f^{\,3}}{ND\mu_f(T_{sat}-T_{surface})}\right]^{1/4} \tag{13.167}$$

provided that

$$\left[(N-1)\frac{c_{Pf}\left(T_{sat}-T_{surface}\right)}{h_{fg}}\right] < 2 \tag{13.168}$$

It should be noted that the foregoing analyses do not account for superheat of the vapor, shear at the vapor-liquid interface, and non-condensable gases. For consideration of these and other effects, the reader should consult more advanced treatments of the subject such as those cited previously.

13.14.2.3 Condensation Inside a Horizontal Tube

In many applications of condenser designs, the condensation process occurs within a tube instead of on the outside of a tube. Such is the case, for example, in the condenser of a household refrigerator. These condensers are usually modeled as three separate heat exchangers in series. The first heat exchanger is the *desuperheater* which operates entirely in the single phase superheated vapor region with the fluid entering as a superheated vapor and exiting as a saturated vapor. Analysis of this section employs the heat transfer correlations of Chapter 11. The fluid then passes to the *condenser* proper where the conversion from saturated vapor to saturated liquid occurs. The analysis of this component makes use of the correlations described below. Finally, there is the *subcooled liquid* heat exchanger where the saturated liquid is subcooled below the saturation temperature. This component is also analyzed using the correlations of Chapter 11.

In the condenser proper, the analysis is complicated by the fact that the character of the flow changes as the heat transfer process takes place. As the flow progresses from the inlet where the fluid is essentially saturated vapor, $x \approx 1$, to the outlet where the fluid is essentially saturated liquid, $x \approx 0$, the flow can assume various forms as shown in Figure 13.23. Under these circumstances, it is first necessary to establish the flow regime before proceeding with the analysis. Berber, et al. (G. Berber, J. W. Palen, and J. Taborek, "Prediction of Tubeside Condensation of Pure Components Using Flow Regime Criteria," *International Journal of Heat Transfer*, vol. 83, pp. 471 – 476, 1980.) propose classifications for the flow regimes based upon the dimensionless mass velocity of the vapor phase, viz.

$$j_g^* = \frac{x(\dot{m}/A_c)}{\left[g\rho_g\left(\rho_f-\rho_g\right)D\right]^{1/2}} \tag{13.169}$$

and the Lockhart-Martinelli parameter, X_{tt}

$$X_{tt} = \left(\frac{1-x}{x}\right)^{0.9}\left(\frac{\rho_g}{\rho_f}\right)^{0.5}\left(\frac{\mu_f}{\mu_g}\right)^{0.1} \tag{13.170}$$

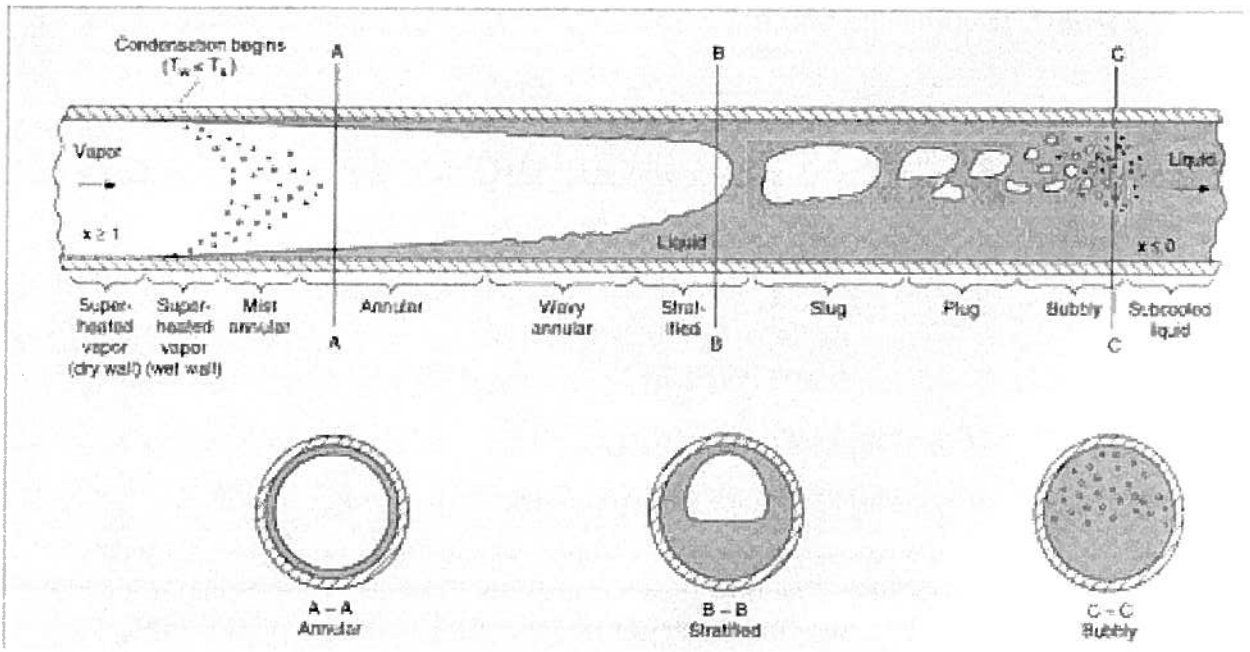

Figure 13.23 Flow Regimes in a Horizontal Condenser Tube
(From P. J. Marto, "Condensation," in *Handbook of Heat Transfer*, 3rd Ed., edited by W. M. Rohsenow, J. P. Hartnett, and Y. I. Cho, McGraw-Hill, N. Y., 1998, Chapter 14, 14.32, Fig. 14.21.)

The flow regimes are:

$$\begin{aligned} j_g^* > 1.5 \quad & X_{tt} < 1.0 \quad \text{mist and annular flows} \\ j_g^* < 0.5 \quad & X_{tt} < 1.0 \quad \text{wavy and stratified flows} \\ j_g^* < 0.5 \quad & X_{tt} > 1.5 \quad \text{slug flow} \\ j_g^* > 1.5 \quad & X_{tt} > 1.5 \quad \text{bubble flow} \end{aligned} \tag{13.171}$$

The analysis proceeds by breaking the condenser up into discrete elements of length ΔL along the flow axis and establishing the flow condition for that element. Then the first law combined with Newton's Law of Cooling for the element in question becomes

$$\Delta\dot{Q} = h_{cond}\pi D\Delta L\left(T_{sat} - T_{surface}\right) = \dot{m}h_{fg}\Delta x \tag{13.172}$$

where the fractional decrease in the quality Δx is taken as the independent variable. Then the length of the element ΔL is given by

$$\Delta L = \frac{\dot{m}h_{fg}\Delta x}{h_{cond}\pi D\left(T_{sat} - T_{surface}\right)} \tag{13.173}$$

where h_{cond} is the local value of the condensing heat transfer coefficient determined from one of the following correlations. The total length of the tube is then the sum of all the ΔL.

Since the vapor velocity is typically high ($j_g^* > 1.5$) in condensers, the flow is often *annular* in character along most of its length. Gravitational effects are negligible and the flow is turbulent with the condensate forming as a thin annular film along the tube wall with no stratification. For this regime, Traviss et al. (D. P. Traviss, W. M. Rohsenow, and A. B. Baron, "Forced Convection Condensation inside Tubes: A Heat Transfer Equation for Condenser Design," *ASHRAE Transactions*, vol. 79,pp. 157 – 165, 1972.) suggest the following correlation:

$$Nu_{cond} = \frac{Pr_f Re_f^{0.9}}{F_2} F_1 \qquad 0.15 < F_1 < 15$$

$$Re_f = \frac{(\dot{m}/A_c)(1-x)D}{\mu_f}$$

$$F_1 = 0.15\left[\frac{1}{X_{tt}} + \frac{2.85}{X_{tt}^{0.476}}\right] \tag{13.174}$$

$$F_2 = 0.707 Pr_f Re_f^{0.5} \qquad Re_f < 50$$

$$F_2 = 5Pr_f + 5\ln\left[1 + Pr_f\left(0.0964 Re_f^{0.585} - 1\right)\right] \qquad 50 < Re_f < 1125$$

$$F_2 = 5Pr_f + 5\ln\left(1 + 5Pr_f\right) + 2.5\ln\left(0.0031 Re_f^{0.812}\right) \qquad Re_f > 1125$$

As the condensation process proceeds, the vapor velocity decreases ($j_g^* < 0.5$) and the flow cannot sustain annular flow. The flow then becomes dominated by the gravitational body force acting on the liquid. Then the condensate forms a thin film on the top portion of the tube wall that flows downward along the wall under the influence of gravity. The liquid then collects in the lower portion of the tube and the flow becomes stratified. This situation is similar to the case of filmwise condensation on the outside of a cylinder as described in Section 13.14.2.2. The condensation heat transfer coefficient can then be correlated by a modified Nusselt form, viz.

$$h_{cond} = 0.728K\left[\frac{\rho_f(\rho_f - \rho_g)g h_{fg} k_f^{\,3}}{ND\mu_f(T_{sat} - T_{surface})}\right]^{1/4}$$

$$K = \left[1 - \left(\frac{1-x}{x}\right)\left(\frac{\rho_g}{\rho_f}\right)^{2/3}\right]^{-3/4} \tag{13.175}$$

where the factor K accounts for the fraction of the tube surface that is stratified. Typically, the quality is low, $x < 0.2$ and the Reynolds number of the flow becomes laminar due to the large difference in viscosity between the liquid and vapor.

The pressure drop in the tube can be calculated by again breaking the length of the tube into discrete elements as was done for the heat transfer analysis and determining the pressure gradient at the midpoint of each element by means of equation (13.84). Then the pressure drop for that element is given by

$$\Delta P = \left(\frac{dP}{dz}\right)\Delta L \tag{13.176}$$

The total pressure drop is then the sum of the individual pressure drops.

13.15 Thermosyphons and Heat Pipes

One of the most interesting applications of the pure substance model is that of the heat pipe, the forerunner of which was the thermosyphon. These devices typically operate in the steady-state with the purpose of maintaining some object at constant the temperature by transferring large amounts of energy and entropy through a small temperature difference, thereby generating little entropy in the process. The device accomplishes this feat by utilizing a pure substance as the working fluid and exploiting the latent heat of the substance as the means of transporting the large amount of energy in a relatively compact system. The high heat transfer rates then become a consequence of the large heat fluxes associated with the processes of boiling and condensation in the pure substance. As it turns out, the sequence of processes experienced by the working fluid in a heat pipe or thermosyphon is quite similar, in part, to the sequence of processes experienced by the working fluid in a Rankine heat engine cycle (to be discussed in detail in Chapter 16). While modern heat pipes were originally developed for the space program, the most common application of the heat pipe at the present time is the cooling of electronic devices such as the central processing unit (CPU) of a laptop computer.

13.15.1 Thermosyphons

The thermosyphon is not a new concept. The original manifestation of the thermosyphon was presented in a series of patents by the Perkins family filed in the United Kingdom over the time period ranging from the mid-nineteenth century to the early twentieth century. The U. K. patent filed by Jacob Perkins in 1836 showed a configuration, now known as the Perkins tube, that closely resembles the present-day heat pipe. More recently in 1929, Gay obtained a U. S. patent for a device that was basically a collection of Perkins tubes used to transfer energy and entropy between a hot fluid stream and a cold fluid stream. In 1944, Gaugler obtained a patent for a thermosyphon used to transfer a refrigeration load (by evaporating a liquid) at an elevated location to a lower elevation by using capillary forces to return the condensed liquid from the lower location to the higher location; however, it was not until 1966 that the term "heat pipe" was coined in a U. S. patent granted to G. Grover of the Los Alamos National Laboratory.

As shown in Figure 13.24, the thermosyphon, in its simplest form, consists of a boiler and a condenser connected by two conduits that facilitate the transport of mass between them. In a typical application, the boiler is placed in contact with an object, such as an electronic device, that is generating entropy by irreversibly "dissipating" energy. In order to maintain the surface temperature of the object constant, it is necessary to transport the generated entropy and "dissipated" energy to an energy and entropy sink, such as the atmosphere, usually in a location remote from the object being cooled. The dissipated energy, in the form of a heat flux, flows from the object, through a thermal resistance, into the boiler that contains a pure substance in a two-phase state of liquid and vapor. This heat flux converts some liquid into vapor which is then transported upward through a conduit to the condenser. The condenser is in contact with the energy and entropy sink through another thermal resistance. The temperature of the inner surface of the condenser is less than the saturation temperature of the vapor, thereby resulting in condensation of the vapor on this surface. The liquid thus formed then flows by gravity back to the boiler where the process begins once again. If all the conduit hardware can be modeled as adiabatic, it follows that $\dot{Q}_{in} = \dot{Q}_{out}$.

In the steady state, the temperature of the pure substance in the boiler is determined by the thermal resistance between the surface of the object being cooled and the pure substance, the surface temperature of the object, and the heat flux from the object. Typically, the surface

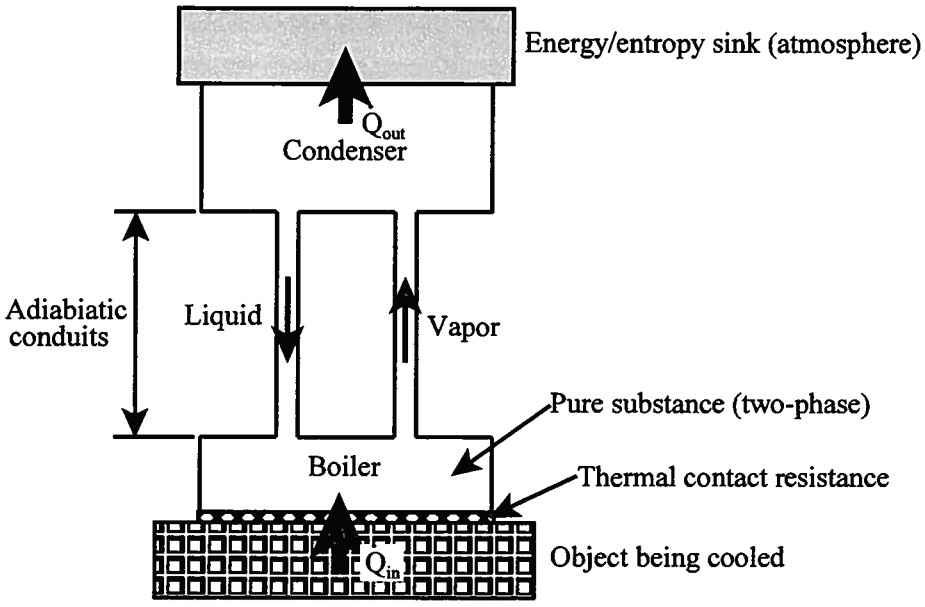

Figure 13.24 Simple Thermosyphon Configuration

temperature of the object is a design parameter usually fixed by the desired operating conditions of the object. The temperature of the pure substance fixes the pressure in the boiler since the pure substance is in a two-phase state. This pressure is the inlet pressure for the vapor conduit. The temperature of the pure substance in the condenser is determined by the heat flux, the thermal resistance between the energy/entropy sink and the pure substance, and the temperature of the energy/entropy sink. This temperature fixes the pressure in the condenser since there are two phases present. This now establishes the pressure drop across the vapor conduit. The mass flow rate through the vapor conduit is determined by the heat transfer rate and the latent heat of vaporization of the pure substance. The first law for the vapor conduit determines the change in velocity of the vapor as it flows through the conduit. For the established pressure drop, the size of the vapor conduit (*L*/*D* ratio) can then be determined by applying the Darcy-Weisbach Law and the friction factor data for the conduit.

For the liquid conduit, the design is complicated by the fact that in the steady state, the flow of the liquid is counter to the pressure drop between the boiler and the condenser and, therefore, depends upon a balance between the body force due to gravity that drives the flow and the combined effect of the normal surface forces (due to pressure) and shear forces, both of which oppose the flow. (As we shall see shortly, the heat pipe introduces additional forces that aid in the transport of liquid against the adverse pressure gradient.) This means that the length of this conduit is an important design consideration since the pressure drop is fixed by the operating conditions in the boiler and the condenser, and, as the Navier-Stokes equation shows, it is the pressure gradient that determines the normal force per unit volume acting on the fluid contained within the conduit at any instant of time.

The thermal-fluid behavior of a thermosyphon can be best illustrated by considering a specific example as shown in Example 13.13.

Example 13.13: The objective in the present example is to design a thermosyphon to cool the CPU, a Pentium® 4 processor manufactured by the Intel Corporation, for a personal computer. The specifications set by Intel are that the maximum allowable case temperature of the

CPU is T_{case} = 70.8 C. Due primarily to the high-speed switching of the capacitive elements of the CPU, the Pentium® 4 dissipates 115 W of electrical power in the steady state. The thermosyphon must be capable of providing adequate cooling to maintain the case temperature at the maximum value when the environmental temperature, the energy sink temperature, reaches a maximum value of T_{env} = 38 C. The thermosyphon is attached to the CPU case with a thermal interface material (TIM) that has a thermal resistance of R_{TIM} = 0.04 C/W. The contact area between the case of the CPU and the boiler is a square 31 mm on a side. The condenser surface is a square of aluminum 10 cm on a side. We wish to specify the design of a thermosyphon, using H_2O as the working fluid, adequate to provide the necessary cooling of the CPU.

Solution: If we assume that the material of construction of the boiler is of high thermal conductivity such as copper or aluminum, the only thermal resistances of consequence between the case of the CPU and the bulk liquid of the pure substance working fluid of the thermosyphon are those of the TIM and the boiling interface of the pure substance/boiler surface. In order to evaluate the thermal resistance, or alternatively, the heat transfer coefficient of the boiling heat transfer process in the boiler, we must establish approximately the operating temperature of the boiler. The temperature difference between the isothermal boiler surface and the isothermal case of the CPU is given by

$$T_{case} - T_{\substack{boiler \\ surface}} = \dot{Q} R_{TIM}$$

$$T_{case} - T_{\substack{boiler \\ surface}} = (115 \text{ W})(0.04 \text{ C/W}) = 4.6 \text{ C}$$

Then

$$T_{\substack{boiler \\ surface}} = T_{case} - 4.6 \text{ C} = 70.8 \text{ C} - 4.6 \text{ C} = 66.2 \text{ C}$$

The heat flux into the boiler is

$$\dot{q} = \frac{\dot{Q}}{A_s} = \frac{115 \text{ W}}{(3.1 \text{ cm})^2} = 11.967 \text{ W/cm}^2$$

Although Figure 13.11 is for boiling at atmospheric pressure, we can use this plot to establish the boiling regime. Figure 13.11 shows that this heat flux is clearly in the nucleate boiling regime for water. Then the temperature difference between the boiler surface and the pool of water is given by equation (13.68), viz.

$$T_{\substack{boiler \\ surface}} - T_{sat} = \frac{C_{sf} h_{fg} Pr_f^n}{c_{P,f}} \left\{ \frac{\dot{q}}{\mu_f h_{fg}} \left[\frac{\sigma}{g(\rho_f - \rho_g)} \right]^{1/2} \right\}$$

From Figure 13.11 (which is for T_{sat} = 100 C), it would appear that the ΔT between the boiler surface and the pool of saturated liquid in the present case is on the order of 15 C. Then if we use the properties of H_2O at a temperature of 50 C, we should be able to determine a good estimate of the saturation temperature of the liquid. Then from the tabulated properties of H_2O at T_{sat} = 50 C, we have

$$h_{fg} = 2381.95 \text{ kJ/kg} \quad \rho_f = 988.00 \text{ kg/m}^3 \quad \rho_g = 0.083147 \text{ kg/m}^3 \quad Pr_f = 3.5531$$

$$\sigma = 0.06794 \text{ N/m} \quad c_{P,f} = 4181.5 \text{ J/kg K} \quad \mu_f = 5.4683 \text{ x } 10^{-4} \text{ kg/m sec}$$

From Table 13.3 for water on a copper surface, C_{sf} = 0.0128 and n = 1.00 so that

$$T_{\substack{boiler\\surface}} - T_{sat} = \frac{0.0128\left(2381.95 \text{ x } 10^3 \text{ J/kg}\right)(3.5531)}{4181.5 \text{ J/kg K}} \bullet$$

$$\bullet \left\{ \frac{11.967 \text{ x } 10^4 \text{ W/m}^2}{\left(5.47 \text{ x } 10^{-4} \text{ kg/m sec}\right)\left(2.382 \text{ x } 10^6 \text{ J/kg}\right)} \left[\frac{0.0674 \text{ N/m}}{\left(9.81 \text{ m}^2/\text{sec}\right)\left(988 \text{ kg/m}^3 - 0.0831 \text{ kg/m}^3\right)} \right]^{1/2} \right\}^{1/3}$$

$$T_{\substack{boiler\\surface}} - T_{sat} = 16.2 \text{ C}$$

Then

$$T_{sat} = T_{\substack{boiler\\surface}} - 16.2 \text{ C} = 66.2 \text{ C} - 16.2 \text{ C} = 50 \text{ C}$$

Thus the properties that we used in the calculation were the correct ones. The value of T_{sat} = 50 C sets the pressure in the boiler at P_{sat} = 1.2352 x 10^4 N/m^2. In general, this procedure is an iterative one in which one assumes a value of the saturation temperature and then calculates the ΔT between the surface and the bulk liquid. If this value of the ΔT does not give the value of the saturation temperature assumed, it is then necessary to guess a new value and repeat the calculation. In the present case, we got lucky, but in general, convergence is rapid.

The conditions in the condenser are determined by the heat transfer between the wall of the condenser and the environment. In the present case, we will assume that the saturation temperature of the fluid in the condenser is T_{sat} = 49 C, P_{sat} = 1.1752 x 10^4 N/m^2. This is an arbitrary choice for the conditions of this design. As we shall see shortly, the design is actually dominated by the fluid mechanics in the adiabatic tubes connecting the boiler and condenser. In practice, we want to make the saturation temperature in the condenser as close as possible to the saturation temperature of the boiler so that we obtain as small a temperature difference through which the heat transfer would occur. This, after all, is the point of the thermosyphon. The values chosen here are strictly for the purposes of illustrating the method of design, rather than optimizing the design.

In the design process, it is essential that the thermal-fluids engineer have access to software that provides the necessary thermal-fluid properties of the pure substance model. Tables of properties alone are not sufficiently precise for this kind of work over small temperature differences. The National Institute of Standards and Technology (NIST) has developed the requisite software for a wide variety of pure substance models which can be purchased over the Internet from the website: http://www.nist.gov. The present case employs the software package entitled: *Steam, NIST Standard Reference Database 10.*

If we apply the first law to the adiabatic vapor conduit as a control volume, we have for steady flow conditions

$$\cancel{\frac{dE_{cv}}{dt}} = \cancel{\dot{Q}} - \cancel{\dot{W}_{shaft}} + \dot{m}_{in}\left(h_{in} + \frac{\vartheta_{in}^2}{2} + gz_{in}\right) - \dot{m}_{out}\left(h_{out} + \frac{\vartheta_{out}^2}{2} + gz_{out}\right)$$

$$\dot{m}_{in}\left(h_{in} + \frac{\vartheta_{in}^2}{2} + gz_{in}\right) = \dot{m}_{out}\left(h_{out} + \frac{\vartheta_{out}^2}{2} + gz_{out}\right)$$

The mass flow rates into and out of the conduit are identical, so we only need concern ourselves with the terms in parentheses. Given the typical size of a thermosyphon, the gravitational potential energy terms are negligible. Similarly, the kinetic energy terms are negligible compared

with the enthalpy terms. (We shall confirm this subsequently.) Then it follows that

$$h_{in} = h_{out}$$

Since the outlet enthalpy is identical to the inlet enthalpy, but the outlet pressure is lower than the inlet pressure, it follows from the pure substance model that the H_2O is slightly superheated at outlet from the vapor conduit. We then have two independent properties to establish the state of the H_2O at the outlet of the conduit: the enthalpy, $h_{out} = h_{in} = 2591.29$ kJ/kg; and the outlet pressure, $P_{out} = 1.1752 \times 10^4$ N/m^2. From the aforementioned software,

$$\rho_{out} = 0.079115 \text{ kg/m}^3 \quad \text{and} \quad \mu_{out} = 1.06143 \times 10^{-5} \text{ kg/m sec}$$

We now need to establish the cross-sectional area of the vapor conduit. The mass flow rate of vapor $\dot{m}_g$ is given by the first law applied to the boiling process at the surface of the boiler, viz.

$$\dot{Q} = \dot{m}_g h_{fg}$$

$$\dot{m}_g = \frac{\dot{Q}}{h_{fg}} = \frac{115 \text{ W}}{2381.95 \times 10^3 \text{ J/kg}} = 4.828 \times 10^{-5} \text{ kg/sec}$$

We now need to establish the vapor velocity in the conduit. The speed of sound (from the aforementioned software using methods to be developed in Chapter 14) at the inlet is $a_{in} = 443.2$ m/sec. If we wish to maintain incompressible flow in the conduit, the velocity must be such that the Mach number is less than $M_{in} = 0.3$. A velocity of $\vartheta_{in} = 50$ m/sec should be sufficient. Then from continuity,

$$A_c = \frac{\dot{m}_g}{\rho_{in}\vartheta_{in}} = \frac{4.828 \times 10^{-5} \text{ kg/sec}}{(0.083147 \text{ kg/m}^3)(50 \text{ m/sec})} = 1.1613 \times 10^{-5} \text{ m}^2$$

Then the diameter becomes

$$D = \sqrt{\frac{4A_c}{\pi}} = \sqrt{\frac{4(1.1613 \times 10^{-5} \text{ m}^2)}{\pi}} = 3.845 \times 10^{-3} \text{ m}$$

The pressure difference between the boiler and condenser can be sustained by a conduit of diameter $D = 3.845$ mm only if the length is right for the mass flow rate $\dot{m}_g = 0.0483$ g/sec. The proper length can be determined by applying the Darcy-Weisbach Law. The Reynolds number of the flow at the inlet is

$$Re_{in} = \frac{\vartheta_{in} D \rho_{in}}{\mu_{in}} = \frac{(50 \text{ m/sec})(3.845 \times 10^{-3} \text{ m})(0.083147 \text{ kg/m}^3)}{1.0616 \times 10^{-5} \text{ kg/m sec}} = 1505.9$$

The flow is clearly laminar for a circular conduit. The velocity of the superheated vapor at outlet can be determined by applying continuity, viz.

$$\vartheta_{out} = \frac{\dot{m}_g}{\rho_{out} A_c} = \frac{4.828 \times 10^{-5} \text{ kg/sec}}{(0.079115 \text{ kg/m}^3)(1.1613 \times 10^{-5} \text{ m}^2)} = 52.548 \text{ m/sec}$$

Thus, there is a slight change in velocity of the vapor, not as a consequence of compressibility which we have neglected here because of the low Mach number, but, rather, as a consequence of the behavior of the pure substance model. [At this juncture we can justify neglecting the kinetic energy terms in the first law in comparison with the enthalpy terms. To wit,

$$h_{in} = 2591.29 \times 10^3 \text{ J/kg} = 2.591 \times 10^6 \text{ N-m/kg} = 2.591 \times 10^6 \text{ m}^2/\text{sec}^2$$

$$\frac{\vartheta_{in}^2}{2} = \frac{(50 \text{ m/sec})^2}{2} = \frac{2500}{2} \text{ m}^2/\text{sec}^2 = 1.250 \times 10^3 \text{ m}^2/\text{sec}^2$$

Thus

$$\frac{\vartheta_{in}^2/2}{h_{in}} \approx 0.05\%$$

and the approximation is justified.]

We can now determine the arithmetic average of the thermal-fluid properties for the inlet and outlet conditions of the conduit. Then

$\vartheta_{ave} = 51.27$ m/sec and $\rho_{ave} = 0.0811$ kg/m^3 and $\mu_{ave} = 1.0616 \text{ x } 10^{-5}$ kg/m sec

Then the average value of the Reynolds number becomes

$$Re_{ave} = \frac{\vartheta_{ave} D \rho_{ave}}{\mu_{ave}} = \frac{(51.27 \text{ m/sec})(3.85 \text{ x } 10^{-3} \text{ m})(0.0811 \text{ kg/m}^3)}{1.0615 \text{ x } 10^{-5} \text{ kg/m sec}} = 1506.9$$

Then the friction factor becomes

$$f_{ave} = \frac{64}{Re_{ave}} = \frac{64}{1506.9} = 0.0425$$

The length of conduit required to sustain the requisite pressure drop with this vapor flow rate is then given by the Darcy-Weisbach Law, viz.

$$L = \frac{2D\Delta P}{\rho_{ave} f_{ave} \vartheta_{ave}^2} = \frac{2(3.845 \text{ x } 10^{-3} \text{ m})(600.9 \text{ N/m}^2)}{(0.0811 \text{ kg/m}^3)(0.0425)(51.27 \text{ m/sec})^2} = 0.510 \text{ m}$$

In order to establish the conditions in the condenser, we need to know the temperature of the condensing surface. The temperature of this surface is required in equation (13.118). This can be determined only by assuming a value and then performing the analysis to determine the heat transfer coefficient for condensation, h_{cond}. From this value of h_{cond}, the thermal resistance per unit area of the condensing surface can be determined. Since in this case the heat transfer and the surface area of the condensing surface are known, the calculated value of h_{cond} can be used in Newton's Law of Cooling to determine the surface temperature. If this value of $T_{surface}$ does not agree with the value originally assumed, we need to estimate a new value and repeat the calculation until convergence is obtained. In this particular example, we have already done this iteration and have found $T_{surface} = 48.41234$ C. (The approximations involved in the Nusselt analysis of film condensation do not merit this level of precision, but the calculation is sensitive to the value of this parameter; hence, we have used an unusual number of significant figures in this example.) This temperature and the temperature of the energy and entropy sink, in this case the environment, determines the convection heat transfer between the surface and the sink. This temperature difference should be sufficient to do the job; however, it will require a finned outer surface and most likely a fan to increase the convection heat transfer coefficient over the fins. This part of the analysis employs the methods and correlations of Chapter 11, as well as the analysis of Section 6.6 of Chapter 6, and is left as an exercise for the reader. For our present purposes, we shall focus on the condensation heat transfer in the thermosyphon.

For saturated H_2O at $T_{sat} = 49$ C, we have

$h_{fg} = 2384.36$ kJ/kg $\rho_f = 988.45$ kg/m^3 $\rho_g = 0.079343$ kg/m^3

$c_{P,f} = 4181.3$ J/kg K $\mu_f = 5.5613 \text{ x } 10^{-4}$ kg/m sec $k_f = 0.64236$ W/m K

To calculate h_{cond}, we first need h_{fg}' as given by equation (13.124). Then

$$h_{fg}{}' = h_{fg}\left\{1+0.68\left[\frac{c_{Pf}\left(T_{sat}-T_{surface}\right)}{h_{fg}}\right]\right\}$$

$$h_{fg}{}' = \left(2384.36 \text{ x } 10^3 \text{ J/kg}\right)\left\{1+0.68\left[\frac{(4181.3 \text{ J/kg K})(49 \text{ C}-48.41234 \text{ C})}{\left(2384.36 \text{ x } 10^3 \text{ J/kg}\right)}\right]\right\}$$

$$h_{fg}{}' = 2.3860 \text{ x } 10^6 \text{ J/kg}$$

Then from equation (13.118), we have

$$\overline{Nu_L} = \frac{\overline{h_{cond}}L}{k_f} = 0.943\left[\frac{\rho_f\left(\rho_f-\rho_g\right)gh_{fg}L^3}{\mu_f k_f\left(T_{sat}-T_{surface}\right)}\right]^{1/4}$$

$$\overline{Nu_L} = 0.943\left[\frac{\left(988.45 \text{ kg/m}^3\right)^2\left(1-\frac{0.0793 \text{ kg/m}^3}{988.45 \text{ kg/m}^3}\right)\left(9.81 \text{ m/sec}^2\right)\left(2.3860 \text{ x } 10^6\right)(0.100 \text{ m})^3}{\left(5.5613 \text{ x } 10^{-4} \text{ kg/m sec}\right)(0.64236 \text{ W/m K})(49 \text{ C}-48.41234 \text{ C})}\right]^{1/4}$$

$$\overline{Nu_L} = 3046.5$$

and

$$h_{cond} = \overline{Nu_L}\frac{k_f}{L} = 3046.5\frac{0.64236 \text{ W/m K}}{0.100 \text{ m}} = 1.9569 \text{ x } 10^4 \text{ W/m}^2 \text{ K}$$

Then the heat transfer rate is

$$\dot{Q} = h_{cond}L^2\left(T_{sat}-T_{surface}\right) = \left(1.9569 \text{ x } 10^4 \text{ W/m}^2 \text{ K}\right)(0.100 \text{ m})^2(49 \text{ C}-48.84307 \text{ C}) = 115 \text{ W}$$

This heat transfer rate does indeed match the heat transfer rate in the boiler. Thus, we chose the correct value for the condensing surface temperature.

We now examine the liquid conduit to determine the geometry necessary to sustain the pressure difference between the boiler and condenser. In this case, the flow is driven by gravity counter to the pressure drop. Since the pressure drop is small and the mass flow rate in this case is also small, we would expect the Reynolds number to be small and the flow to be laminar. Then the Navier-Stokes equation can be solved for the velocity profile. Thus, if we take the z-direction to be positive downward and the flow to be solely in this direction, the z-component of the Navier-Stokes equation in cylindrical coordinates becomes

$$\rho\left(\frac{\partial \vartheta_z}{\partial t}+\vartheta_z\frac{\partial \vartheta_z}{\partial z}\right) = -\frac{\partial P}{\partial z}+\rho g_z+\mu\left[\frac{1}{r}\frac{\partial}{\partial r}\left(r\frac{\partial \vartheta_z}{\partial r}\right)\right]$$

For fully developed flow the left-hand side of this expression vanishes. Then

$$\rho g-\frac{\Delta P}{L} = -\mu\left[\frac{1}{r}\frac{d}{dr}\left(r\frac{d\vartheta_z}{dr}\right)\right]$$

Integrating this expression twice and applying the boundary conditions for the liquid conduit

$$\vartheta_z = 0 \quad \text{at} \quad r = R_f \quad \text{and} \quad \frac{d\vartheta_z}{dr} = 0 \quad \text{at} \quad r = 0$$

we get

$$\vartheta_z = \frac{R_f{}^2}{4\mu}\left(\rho g-\frac{\Delta P}{L_f}\right)\left(1-\frac{r^2}{R_f{}^2}\right)$$

and

$$\vartheta_{ave} = \frac{D_f^{\,2}}{32\mu}\left(\rho g - \frac{\Delta P}{L_f}\right) \quad \text{and} \quad \dot{m} = \rho \vartheta_{ave} A_c$$

Then from the Darcy-Weisbach Law

$$L_f = \frac{\Delta P}{\rho_f g - \dfrac{128\mu_f \dot{m}}{\pi \rho_f D_f^{\,4}}}$$

where L_f represents the length of the liquid conduit. Given the high density of the liquid, the liquid conduit should be much smaller than the vapor conduit. Assume that this conduit is a capillary of diameter $D_f = 1$ mm. Then the length of the conduit becomes

$$L_f = \frac{\Delta P}{\rho_f g - \dfrac{128\mu_f \dot{m}}{\pi \rho_f D_f^{\,4}}}$$

$$L_f = \frac{600.9 \text{ N/m}^2}{\left(988.45 \text{ kg/m}^3\right)\left(9.81 \text{ m/sec}^2\right) - \dfrac{128\left(5.5613 \text{ x } 10^{-5} \text{ kg/m sec}\right)\left(4.828 \text{ x } 10^{-5} \text{ kg/sec}\right)}{\pi\left(988.45 \text{ kg/m}^3\right)\left(1 \text{ x } 10^{-3} \text{ m}\right)^4}}$$

$$L_f = 0.070 \text{ m}$$

The average velocity of the liquid in the conduit is given by

$$\left(\vartheta_f\right)_{ave} = \frac{D_f^2}{32\mu_f}\left(\rho_f g - \frac{\Delta P}{L_f}\right)$$

$$\left(\vartheta_f\right)_{ave} = \frac{\left(1 \text{ x } 10^{-3} \text{ m}\right)^2}{32\left(5.5613 \text{ x } 10^{-5} \text{ kg/m sec}\right)}\left[\left(988.45 \text{ kg/m}^3\right)\left(9.81 \text{ m/sec}^2\right) - \frac{600.9 \text{ N/m}^2}{0.070 \text{ m}}\right]$$

$$\left(\vartheta_f\right)_{ave} = 0.0622 \text{ m/sec}$$

The Reynolds number for this flow rate is then

$$Re_f = \frac{\left(\vartheta_f\right)_{ave} D_f \rho_f}{\mu_f} = \frac{\left(0.0622 \text{ m/sec}\right)\left(0.001 \text{ m}\right)\left(988.45 \text{ kg/m}^3\right)}{5.5613 \text{ x } 10^{-5} \text{ kg/m sec}} = 110.53$$

which is clearly laminar flow.

13.5.2 Heat Pipes

In Example 13.13 we note that the vapor conduit is significantly longer than the liquid conduit. If the physical separation of the boiler and condenser is dictated by the shorter of the two, it would be necessary for the longer conduit transporting the vapor to be formed into a helix (similar to a coil spring) with a coil diameter appropriate for the given installed boiler/condenser separation. Upon further consideration of the design of the thermosyphon, it would appear desirable to have a single conduit with the liquid flowing downward along the wall under the influence of gravity and the vapor traveling upward in the core of the conduit under the influence of the pressure difference between the boiler and the condenser. However, it is clear from the analysis of Example 13.13 that for a conduit of length appropriate to sustain the pressure difference in the vapor, there must be some additional force applied to the liquid since the shear

stress in the liquid at the wall would be too large for gravity alone to drive the liquid flow. One possibility would be to line the conduit with a wick-like material that would provide an additional force due to capillarity in the wick. This, in fact, is precisely what makes a heat pipe different from a thermosyphon. In the heat pipe configuration, the single conduit can be made sufficiently large so that the boiler and condenser can be built into opposite ends with the vapor traveling in the core and the liquid moving in the opposite direction in the wick material lining the wall. If the wick material is properly chosen, the capillary force can dominate the liquid flow and the heat pipe can be used in an orientation, e.g., horizontal, in which the liquid flow is not dependent on gravity alone. Figure 13.25 shows such a configuration schematically.

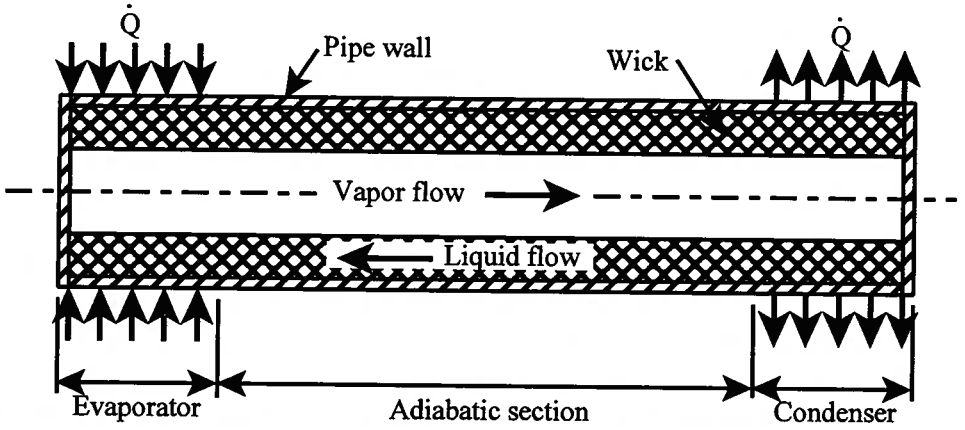

Figure 13.25 Simple Heat Pipe Schematic

For the heat pipe depicted in Figure 13.25 with a constant value of heat flux that is identical in both the evaporator and condenser sections, the mass flow rate, $\dot{m}_g$, of the vapor through the device varies along the length as shown schematically in Figure 13.26. The force necessary to

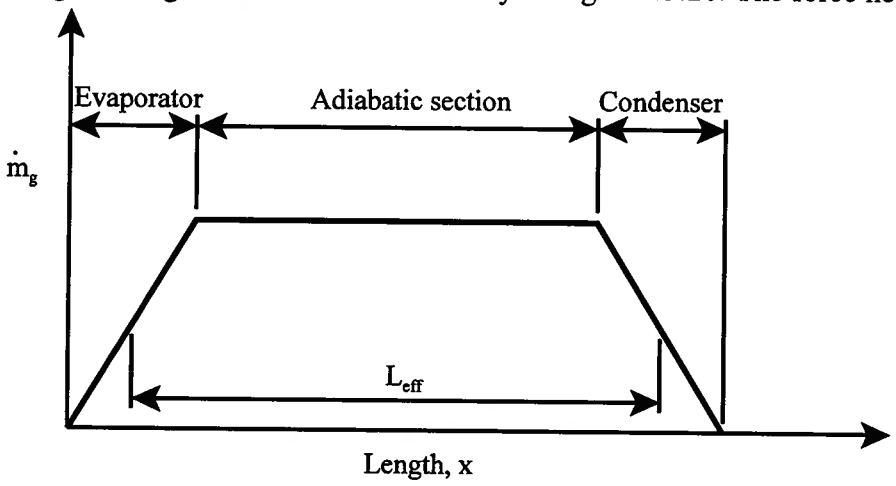

Figure 13.26 Distribution of Vapor Mass Flow Rate in a Heat Pipe

drive the vapor flow through the central core of the heat pipe is provided by the difference in saturation pressure between the two ends of the device due to the temperature difference between the evaporator section and the condenser section. For steady operation, there must be a similar distribution of mass flow in the wick, but in the opposite sense. Clearly, if the saturation pressure alone were imposed on the liquid/vapor interface in the two ends of the heat pipe, liquid flow

would be in the wrong direction because of the adverse pressure gradient. Fortunately, the capillary forces in the wick are sufficient to provide the pumping power necessary to move the liquid through the wick against the vapor pressure gradient. These forces are a consequence of the structure of the wick and the surface tension force acting at the interface between the liquid and the vapor phases in the pores of the wick.

To understand the nature of these forces, we first consider the case of a liquid drop on a solid surface immersed in a pure vapor as shown in Figure 13.27.

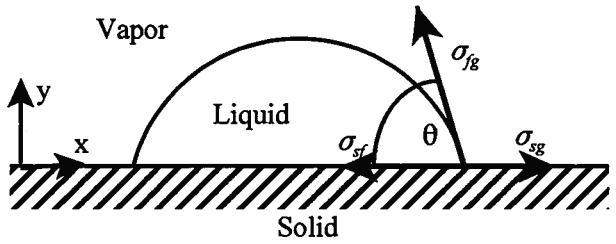

Figure 13.27 Single Drop of Liquid on a Solid Surface Immersed in a Pure Vapor

The base of the drop forms a circle where it comes in contact with the surface. Along the circumference of this circle, the interface between the vapor and the liquid forms the angle θ, known as the *contact angle*, which is measured in the liquid phase. This region where all three phases – solid, liquid, and vapor – are in contact with one another is often referred to as the *triple interface*. If thermodynamic equilibrium exists among all three phases (Note that the solid phase is of a substance different from the liquid and vapor phases.), i.e., there is no evaporation or condensation occurring at liquid/vapor interface, the volume of the drop is constant and the drop is in static equilibrium. As shown in Figure 13.27, at the triple interface there are three surface tension forces acting: one between the liquid and vapor, σ_{fg}; one between the vapor and solid, σ_{sg}; and one between the solid and liquid, σ_{sf}. Mechanical equilibrium requires that there can be no net force acting on the drop. For the x-direction, it must be the case that

$$\sum F_x = 0$$

$$\sigma_{sg} - \sigma_{sf} - \sigma_{fg}\cos\theta = 0$$

$$\sigma_{sg} = \sigma_{sf} + \sigma_{fg}\cos\theta \qquad (13.177)$$

which is known as the Neuman equation. For the y-direction, the elastic modulus of the solid is so high that it is capable of always producing a force that exactly offsets the y-component of the surface tension between the liquid and vapor phases with no deformation of the surface.

In the case of a heat pipe, the contact angle θ shown in Figure 13.27 is a characteristic of the liquid-solid combination and plays an important role in the operation of the heat pipe. In equation (13.177), six possibilities present themselves:

$$\sigma_{sg} \geq \sigma_{sf} + \sigma_{fg} \quad \Rightarrow \quad \theta = 0 \quad \Rightarrow \quad \text{liquid completely "wets" this surface as a film}$$

$$\sigma_{sg} < \sigma_{sf} + \sigma_{fg} \text{ and } \sigma_{sg} > \sigma_{sf} \quad \Rightarrow \quad 0 < \theta < \frac{\pi}{2} \quad \Rightarrow \quad \text{liquid "wets" this surface} \qquad (13.178)$$

$$\sigma_{sg} = \sigma_{sf} \quad \Rightarrow \quad \theta = \frac{\pi}{2} \quad \Rightarrow \quad \text{liquid "wets" this surface}$$

$$\sigma_{sg} < \sigma_{sf} + \sigma_{fg} \text{ and } \sigma_{sg} < \sigma_{sf} \quad \Rightarrow \quad \frac{\pi}{2} < \theta < \pi \quad \text{liquid does not "wet" surface;} \qquad (13.178)$$

$$\sigma_{sg} = \sigma_{sf} + \sigma_{fg} \quad \Rightarrow \quad \theta = \pi \quad \Rightarrow \quad \text{liquid is "completely non-wetting" on this surface}$$

In order for a wick material to be effective in a heat pipe, it must be "wet" by the working fluid with a contact angle between 0 and $\pi/2$, the smaller, the better.

In the simplest heat pipe design, the wick material is a porous medium usually made up of a matrix of very small diameter wires or particles of powder in which the working fluid is "drawn up" into the pores by capillary action. In Figure 13.28, a typical pore is represented by a tube of small inside diameter (a capillary tube) open at both ends with one end immersed into a large pool of liquid that is in thermodynamic equilibrium with its vapor. The liquid rises in the tube due to the *resultant* of the surface tension forces acting along the line of contact between liquid and solid surface of the tube wall. At a distance H relative to the free surface of the pool, the interface in the tube attains mechanical equilibrium. If we consider the free body consisting of the mass of liquid contained in the tube between the interface and the plane of the free surface of the pool of liquid remote from the outside surface of the tube, we see that this state of equilibrium is governed by a balance between the forces due to pressure acting on the ends of the column of liquid, the body force due to gravity acting on the mass of liquid M, and the force due to surface tension at the interface.

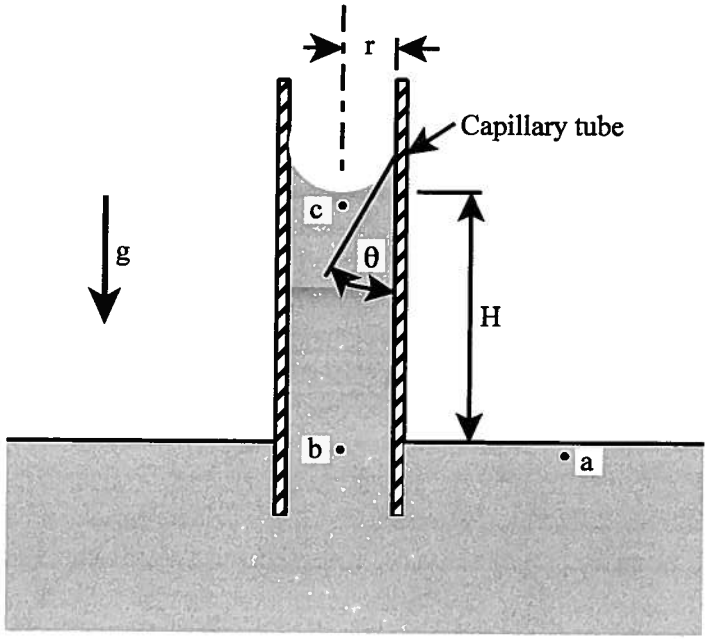

Figure 13.28 Capillary Tube with End Immersed in a Liquid

As shown in Chapter 4, the pressure is uniform on horizontal planes in a continuous liquid. Then $P_a = P_b$ and relative to point c,

$$P_a = P_c + \rho_g g H = P_b \tag{13.179}$$

Mechanical equilibrium requires

$$\sum F_z = 0$$

$$\pi r^2 P_c - \pi r^2 P_b - 2\pi r\sigma\cos\theta + Mg = 0$$

$$\pi r^2 \rho_f g H = \pi r^2 \left(P_b - P_c\right) + 2\pi r\sigma\cos\theta \tag{13.180}$$

Substituting equation (13.179) into equation (13.180), we get

$$\pi r^2 \left(\rho_f g H\right) = \pi r^2 \left(\rho_g g H\right) + 2\pi r\sigma\cos\theta$$

$$H\left(\rho_f g - \rho_g g\right) = \frac{2\sigma\cos\theta}{r}$$

$$H = \frac{2\sigma\cos\theta}{r}\left(\frac{1}{\rho_f g - \rho_g g}\right) \tag{13.181}$$

Thus the height of the liquid column H in a capillary tube depends directly upon the *resultant* surface tension force.

Note that equation (13.181) can be rearranged to give

$$H = 2\cos\theta\left(\frac{L_C^2}{r}\right) = \left(2L_C\cos\theta\right)\left(\frac{L_C}{r}\right) \tag{13.182}$$

where the quantity L_C is the capillary length (also known as the Laplace constant) and is given by

$$L_C = \sqrt{\frac{\sigma}{\left(\rho_f - \rho_g\right)g}} \tag{13.183}$$

which we have already introduced in equation (13.62) as the characteristic length scale for phenomena that involve surface tension in a significant way. Notice that when $r << L_C$, surface tension dominates and the value of H becomes large, but when $r >> L_C$, surface tension is relatively unimportant and the value of H becomes quite small. Figure 13.30 shows the values of the capillary length for water over a range of temperatures from room temperature to nearly the critical temperature. At the critical temperature, T_{crit} = 373.95 C, the concept of phase vanishes and all surfaces become bathed in the critical fluid.

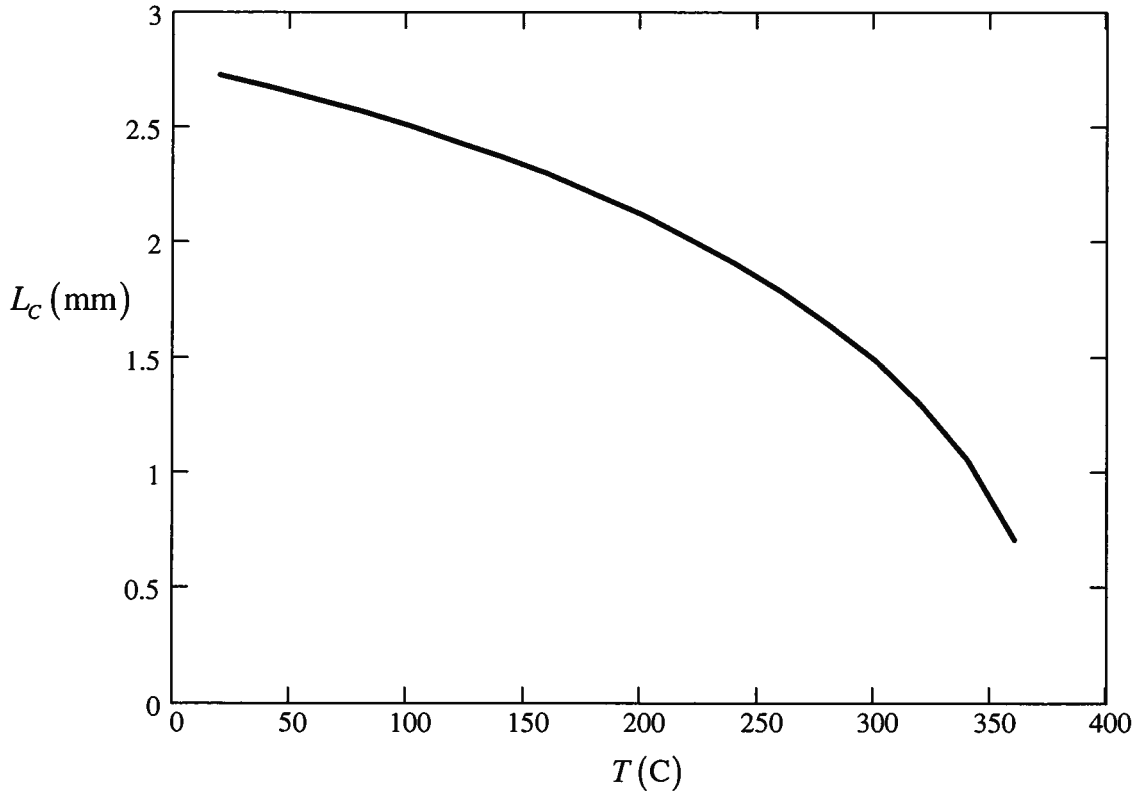

Figure 13.30 Capillary Length for H_2O

Suppose for a moment that the upper end of the capillary tube is closed. Now consider the situation as the capillary tube is gradually withdrawn from the liquid pool so that the volume of

the vapor space increases. Since the approach to mechanical equilibrium is much faster than the approach to thermal equilibrium, the vapor in the tube expands initially to fill the increased volume thereby reducing its pressure and temperature. In order to maintain the column of liquid in the tube in mechanical equilibrium, the contact angle at the wall decreases in an attempt to increase the surface tension contribution to the condition of mechanical equilibrium. Meanwhile, the reduced pressure of the vapor causes some liquid to evaporate in an attempt to restore thermal equilibrium. The sequence of events is a dynamic one that causes the contact angle under conditions of evaporation to be less than the contact angle in the static equilibrium state. In a similar manner, if the tube with the closed end is depressed into the liquid pool, the pressure of the vapor increases as the vapor is compressed into a smaller volume. The contact angle decreases as the vapor begins to condense to restore thermodynamic equilibrium. Thus, under conditions of condensation, the contact angle is greater than the contact angle in the equilibrium case. Then for a given saturation temperature, $\theta_{evap} < \theta_{cond}$. As we shall see, this behavior of the contact angle during evaporation and condensation is crucial to the operation of the heat pipe.

In Figure 13.28, if thermodynamic equilibrium prevails, the pressure in the vapor phase at points *a* and *c* is the equilibrium vapor pressure of the pure substance model, P_{sat}, the pressure of the liquid just below the curved interface at point *c* is less than P_{sat} by the amount ΔP where

$$\Delta P = P_a - P_c = \rho_f g H - \rho_g g H = H\left(\rho_f g - \rho_g g\right) \tag{13.184}$$

This is the pressure difference across a stable curved interface between two phases. In Figure 13.28, the liquid/vapor interface in the capillary tube and the liquid/vapor interface of the pool were in thermal and mechanical communication with one another through the vapor phase whose saturation pressure was determined by the uniform equilibrium temperature of the physical situation. In the case of the heat pipe, the situation is somewhat different. In both the evaporator and condenser sections, the liquid/vapor interfaces of the various pores communicate with each other through a vapor that has gradients in both temperature and pressure. Nonetheless, the two situations are similar. The pressure of the liquid just below the liquid vapor interface is less than the local vapor pressure. In a heat pipe with a simple wick, the reduced pressure in the liquid phase at the vapor/liquid interface in the pores of the wick provides the pumping power necessary to pull the liquid through the pores.

Substituting equation (13.183) into equation (13.184), we obtain

$$(\Delta P)_{interface} = \frac{2\sigma\cos\theta}{r} \tag{13.185}$$

Since the temperature in the evaporator section is different from that of the condenser section, the values of $(\Delta P)_{interface}$ are different for the evaporator and condenser sections of the heat pipe.

$$\Delta P_{evap} = \left(\frac{2\sigma\cos\theta}{r}\right)_{evap} \tag{13.186}$$

and

$$\Delta P_{cond} = \left(\frac{2\sigma\cos\theta}{r}\right)_{cond} \tag{13.187}$$

In equations (13.186) and (13.187), there are two competing effects. In the evaporator section where the temperature is the highest, the surface tension is the lowest which tends to reduce this pressure difference and, hence, increase the pressure in the liquid phase. On the other hand, in the evaporator section, the contact angle is smaller than in the condenser section which tends to increase the pressure difference across the interface and thereby reduce the pressure in the liquid. This situation is shown schematically in Figure 13.31 for the liquid/vapor interfaces in the evaporator and condenser sections.

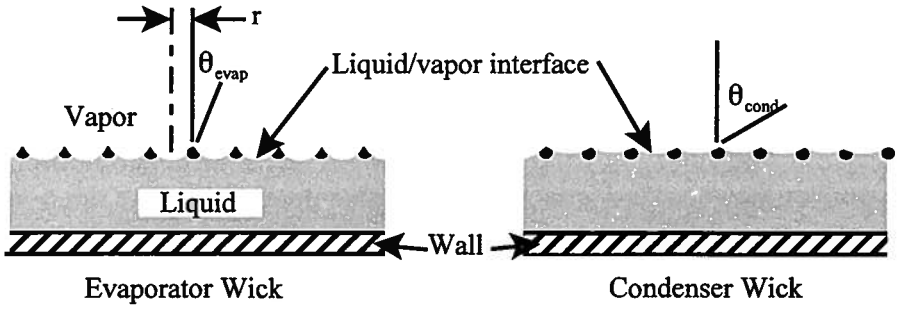

Figure 13.31 Contact Angles in Evaporator and Condenser Sections

In the limiting case, $\theta_{evap} = 0$ and $\theta_{cond} = \pi/2$. Then in the liquid phase, the limiting pressures at the liquid/vapor interface are given by

$$\left(P_{evap}\right)_{min} = \left(P_{sat}\right)_{evap} - \frac{2\sigma_{evap}}{r} \quad \text{and} \quad \left(P_{cond}\right)_{max} = \left(P_{sat}\right)_{cond} \tag{13.188}$$

Since in general $(P_{sat})_{evap} > (P_{sat})_{cond}$ and $(P_{sat})_{cond}$ decreases with temperature, there is a maximum temperature difference between the evaporator and condenser sections at which the pressure differential in the liquid phase between the condenser and evaporator vanishes. This means that in order to have sufficient pumping power in the wick, the heat pipe should be designed so that the temperature difference between the evaporator and condenser sections is as small as possible. Figure 13.32 illustrates the minimum operating pressure in the condenser for a heat pipe using water as the working fluid with a temperature of 70 C in the evaporator section as in Example 13.13. These data were obtained by plotting equations (13.188) for this design.

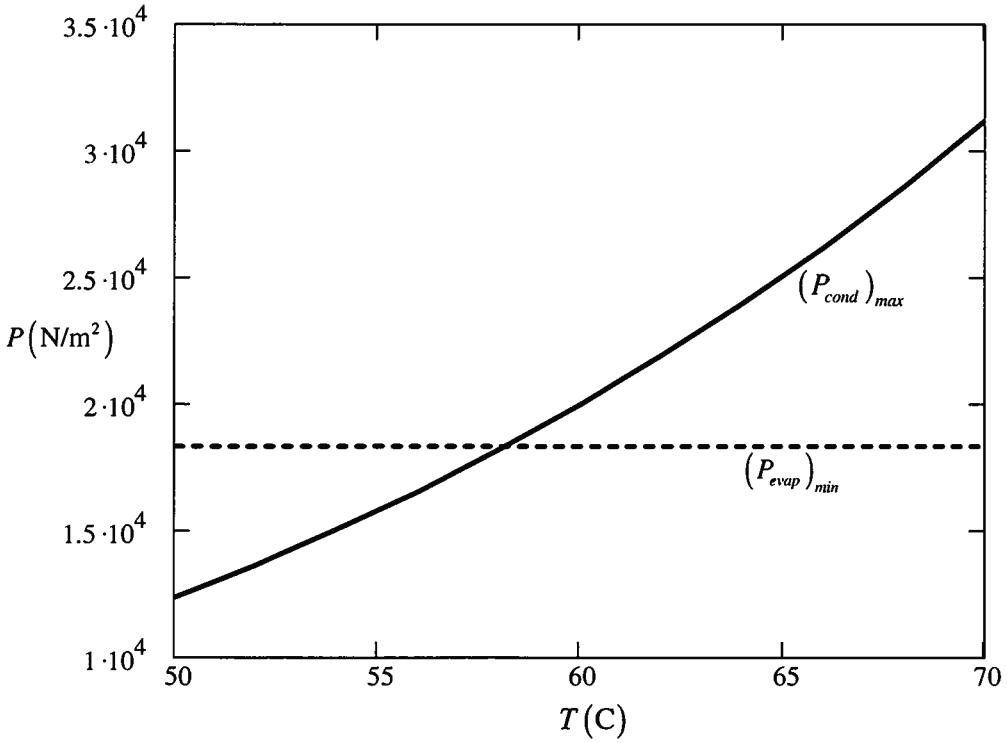

Figure 13.32 Limiting Pressures in the Liquid Phase in the Evaporator and Condenser Sections

From Figure 13.32, it is apparent that the minimum condenser temperature is 58 C. For condenser temperatures less than 58 C, the pressure in the condenser is less than the minimum possible liquid pressure at the interface in the evaporator section, $(P_{evap})_{min}$. Thus, there would be insufficient pressure in the liquid in the condenser section to overcome the pressure drop in the liquid phase in the wick between the condenser and evaporator sections. In practice, the temperature in the condenser section would have to be substantially higher than this minimum value. This condition dictates that, in general, heat pipe designs should have small temperature differences between evaporator and condenser sections. Then the other operating features of the heat pipe have to be designed around the chosen temperature difference for the heat transfer rate desired.

As we have seen in the case of the thermosyphon, the mass flow rate in the device depends directly upon the heat transfer rate and inversely upon the latent heat of vaporization of the working fluid. This sets the mass flow rate not only of the vapor in the core of the heat pipe but also of the liquid in the wick. The resulting pressure distributions in the vapor and liquid phases are shown schematically in Figure 13.33.

In the condenser section for the vapor phase, there are two contributions to the pressure drop. Firstly, there is an inertial effect due to the fact that mass is being added along the flow path by virtue of the evaporation process itself. This causes the flow to accelerate along the flow

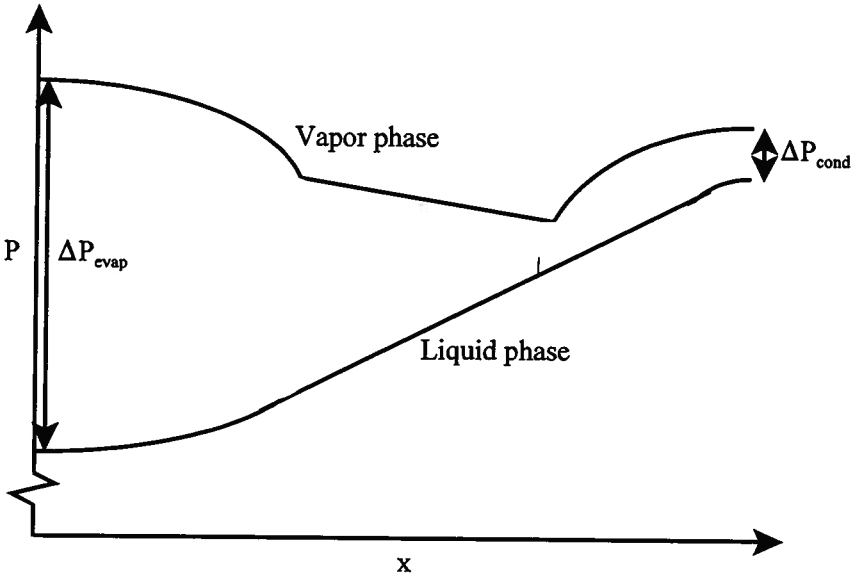

Figure 13.33 Pressure Distribution in the Vapor and Liquid Phase in a Wick-type Heat Pipe

path which makes the pressure drop nonlinear with respect to the flow coordinate. Secondly, there is a viscous effect due to the viscous shear at the liquid/vapor interface. This viscous effect is moderated by the fact that mass is being added to the flow (analogous to "blowing" in single phase flow) along the flow path. This has the effect of increasing the thickness of the boundary layer at the interface which reduces the shear stress and, hence, the viscous contribution to the pressure drop. The net result is a pressure distribution that is non-linear in the evaporator section. The pressure gradient increases in the direction of flow due to the acceleration of the flow associated with the mass addition.

In the adiabatic section, the situation is a bit more straightforward since the mass flow rate is essentially constant. There is some acceleration of the flow as the density of the vapor

increases in the flow direction. To a first approximation, the pressure gradient is constant and the pressure drop is determined by the friction between the vapor and the liquid/vapor interface.

In the condenser section, the flow is again more complicated. Since mass is now being removed from the flow, there is some pressure recovery as the flow decelerates. The viscous contribution increases since the loss of mass reduces the thickness of the boundary layer at the liquid/vapor interface (analogous to "suction" in a single phase flow). This increases the viscous shear. The net result is a pressure distribution that is non-linear with the pressure gradient steepest near the adiabatic section.

In most heat pipe designs, the Mach number in the vapor flow is less than 0.3 which means that the flow can be treated as incompressible. Although the flow is usually laminar in the vapor phase, which makes the solution of the Navier-Stokes equation somewhat more tractable, the analysis of the flow field is complicated not only by the inertial effects and the mass flow in the radial direction, but also by the fact that the flow is not fully developed. The flow of the vapor is essentially all "entry length" throughout the length of the heat pipe. While these various factors often counteract one another and can be ignored in an approximate description of the flow field, a more complete treatment usually requires the use of numerical methods.

For the liquid flowing through the wick of a horizontal heat pipe, the flow quickly becomes fully developed since the Reynolds number is small, and, hence, can be modeled as flow through a porous medium with the flow described by a phenomenological relation known as Darcy's Law, viz.

$$\Delta P_{liquid} = \frac{\mu_f L_{effective} \vartheta_D}{K} = \frac{\mu_f L_{effective} \dot{m}}{K \rho_f A_{wick}} \tag{13.189}$$

where μ_f is the average viscosity of the liquid, $L_{effective}$ is the effective length of the heat pipe, ϑ_D is the one-dimensional mass-averaged flow velocity, and K is the permeability of the wick. All of our ignorance of the details of the flow in the wick are buried in the permeability which is determined from measurements of the pressure drop and the application of Darcy's Law. The value for the permeability is highly dependent upon the structure of the wick with values ranging from 9×10^{-13} m^2 to 30×10^{-10} m^2. (Note that the magnitude of the permeability in SI units is so small, data are often reported in the units of Darcys where 1 Darcy = 9.87×10^{-13} m^2.)

For a horizontal heat pipe, the maximum heat transfer rate is given by

$$\dot{Q}_{max} = \dot{m}_{max} h_{fg} \tag{13.190}$$

From equation (13.189), the maximum mass flow rate is given by

$$\dot{m}_{max} = (\Delta P)_{max} \frac{K \rho_f A_{wick}}{\mu_f L_{eff}} \tag{13.191}$$

where the maximum pressure drop in the wick, $(\Delta P)_{max}$, is given by equation (13.188), viz.

$$(\Delta P)_{max} = (P_{cond})_{max} - (P_{evap})_{min} = (P_{sat})_{cond} - (P_{sat})_{evap} + \frac{2\sigma}{r} \tag{13.192}$$

If the temperature difference between evaporator and condenser is small, $(P_{sat})_{cond} \approx (P_{sat})_{evap}$ and

$$(\Delta P)_{max} \approx \frac{2\sigma}{r} \tag{13.193}$$

Then combining equations (13.190), (13.191), and (13.193), we obtain for a horizontal heat pipe

$$\dot{Q}_{max} \approx \left(\frac{\sigma \rho_f h_{fg}}{\mu_f} \right) \left(\frac{2KA_{wick}}{L_{effective}} \right) \tag{13.194}$$

The first term in parentheses contains only thermodynamic and transport properties of the working liquid phase and thus provides a means of evaluating the prospective working fluids for a heat pipe employing a simple wick design. This quantity is often referred to as the figure of merit for the working fluid and is designated by the symbol N_f. Thus,

$$N_f = \frac{\sigma \rho_f h_{fg}}{\mu_f} \tag{13.195}$$

Using the pure substance model, we can evaluate equation (13.195) for various working fluids. Figure 13.34 shows the results of these calculations which are quite useful in selecting a working fluid to use in a simple wick-type heat pipe for a given application.

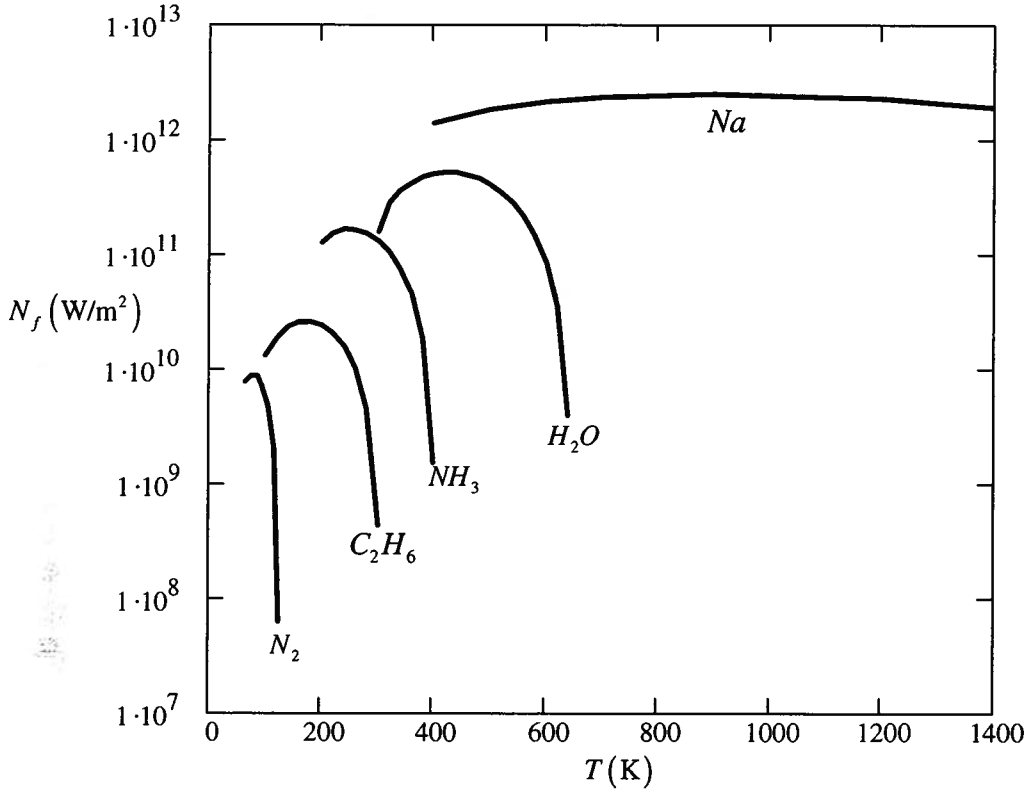

Figure 13.34 Figure of Merit N_f for Various Working Fluids in a Wick-type Heat Pipe

The foregoing discussion describes the behavior of a wick-type heat pipe whose performance is limited by the ability of the wick to transport the liquid phase through capillary forces. This type of limitation, known as the *capillary limit*, is not the only phenomenon that limits heat pipe performance. At low operating temperatures, saturation pressures in the pure substance model are also low and, in fact, may not be sufficient to overcome the viscous pressure drop in the vapor phase. Under these conditions, the vapor may not flow at all, and the heat pipe shuts down. This limitation, known as the *viscous limit*, occurs in heat pipes designed for cryogenic temperatures and in those cases when a heat pipe operates at temperatures below its normal range of operating temperatures, such as at startup. In the latter case, the viscous limit can be overcome by increasing the heat transfer rate into the evaporator, thereby increasing the rate of mass addition along the flow path in the evaporator section. As we have seen in Figure 13.33, increasing the mass flow rate along the flow path causes the flow to accelerate which, in turn, causes the pressure to drop in the direction of flow. However, there is a limit to the acceleration

of the flow. At some point in time, the flow velocity at the exit from the evaporator section will reach the velocity of sound, and the flow will become "choked" as a consequence of the incomplete pressure recovery in the condenser. Had the pressure recovery process in the condenser been reversible, pressure recovery would be complete and the flow could accelerate to supersonic velocities, but the irreversible nature of the pressure recovery process, primarily due to viscous dissipation, causes the flow to become choked so that reductions in the temperature in the condenser section have no effect on the heat transfer rate. This limitation, known as the *sonic limit*, occurs most frequently in heat pipes employing liquid metals as the working fluid.

The motion of the vapor in the central core of the heat pipe is countercurrent to the flow of the liquid in the wick. The relative motion of the two phases results in a shear stress being imposed on the liquid/vapor interface that opposes the motion of the liquid. If great enough in magnitude, this shear stress can cause the pores in the wick in the condenser section to become flooded as liquid is driven back into the condenser section. In addition, this shear stress could, in principle, cause waves to form on the interface that could eventually lead to droplets of liquid breaking away from the interface and becoming entrained in the vapor flow. Eventually, the evaporator section would become "starved' and dry out (at least partially) leading to a significant degradation in heat pipe performance. This phenomenon is known as the *entrainment limit.* While there have been many studies of this phenomenon, both analytical and experimental, there is no hard evidence that the entrainment limit has ever occurred in a functioning heat pipe. It is believed that the pores of the wick prevent the formation of waves of sufficient wavelength to result in entrainment of the liquid in the vapor.

Finally, there are two limiting conditions that have to do with the heat transfer between the shell of the heat pipe and the energy sink and energy source. If the thermal resistance between the shell of the condenser section and the energy sink is of sufficient magnitude, the temperature of the shell of the condenser becomes too great for efficient condensation to take place on the liquid/vapor interface in the condenser section. The heat transfer rate due to condensation then becomes the rate limiting step in the operation of the heat pipe. This condition is known as the *condensation limit.* Similarly, in the evaporator section, if the heat flux on the shell is too large, nucleate boiling occurs and the wick becomes blocked by the formation of vapor which inhibits the flow of liquid into the wick of the evaporator section. This is known as the *boiling limit.*

The various limits are summarized in Figure 13.35 which is a schematic representation of

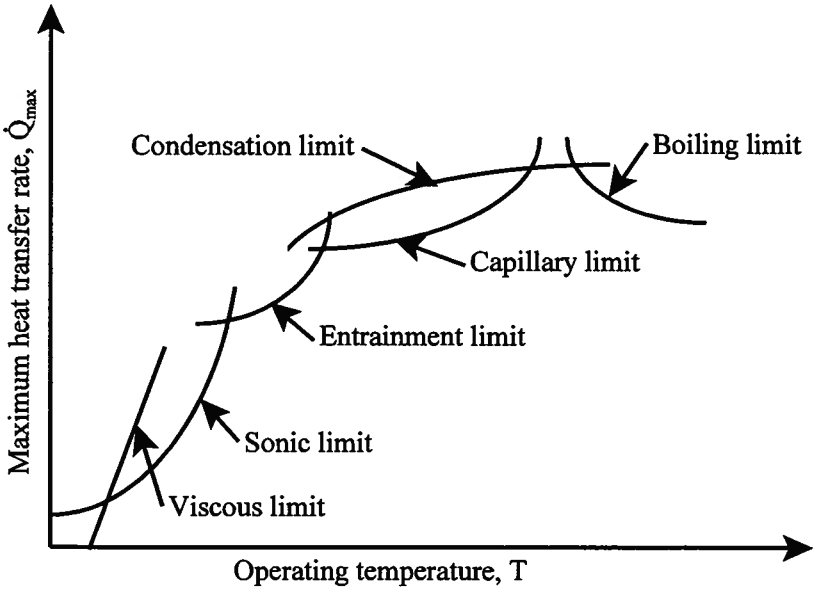

Figure 13.35 Schematic Performance Map of a Typical Heat Pipe Design

the performance map of a typical heat pipe design. Although a number of different limitations on the performance of a heat pipe have been identified, the capillary limit tends to be the dominant one.

In conclusion, the heat pipe is an important means of heat transfer whose operation relies heavily upon the detailed behavior of a working fluid that can be modeled as a pure substance. As we have attempted to show in the foregoing discussion, the heat pipe is a means of transferring large amounts of energy and entropy in a relatively compact device of simple construction. Furthermore, the heat pipe presents an opportunity to transfer this energy with minimal entropy generation. For these reasons, the use of heat pipes in various commercial products and industrial designs is becoming increasingly widespread. Most significantly, the successful operation of high performance electronic devices, such as laptop computers, depends heavily upon heat pipe technology. For a more detailed discussion of heat pipe design and the role of the pure substance model in those designs, the reader is referred to the literature on the subject. Two excellent summaries of the subject are: *Heat Pipe Science and Technology*, A. Faghiri, Taylor and Francis Publishers, N. Y., 1995; and *An Introduction to Heat Pipes: Modeling, Testing, and Applications*, G. P. Peterson, John Wiley and Sons, N. Y., 1994.

Problems

13.1 A boiling water nuclear reactor contains m kg of saturated liquid water at 260 C. In case the reactor pressure vessel fails, a secondary containment vessel must be provided to avoid the spread of radioactive water.

(a) How large must the secondary containment vessel be if the maximum design pressure is $P_{max} = 2 \times 10^5$ N/m^2 and the space between the reactor and the containment vessel is initially at zero pressure?

(b) In the case of a sudden release of the H_2O, it would be reasonable to assume that pressure equilibrium would be established in a time too short for significant heat transfer to the H_2O. Determine the final temperature of the H_2O.

13.2 A rigid, sealed container of liquid and vapor H_2O is heated at constant volume.

(a) Find the proportions *by volume* of liquid and vapor H_2O sealed in the container at atmospheric pressure that will pass through the critical state when heated quasi-statically.

(b) What is the necessary heat transfer to the contents of the container between atmospheric pressure and the critical state if the enclosed volume is $V = 8 \times 10^{-6}$ m^3 ?

13.3 A rigid, closed vessel is charged with carbon dioxide at 20 C. If the initial charge contains the correct proportions of saturated liquid and saturated vapor, the carbon dioxide will pass through the critical state when heated quasi-statically with the fill line closed off. In the initial state, what are the proper proportions by volume of liquid and vapor CO_2 that will produce the desired change of state?

13.4 One kg of refrigerant R-134a at an initial pressure of 7×10^5 N/m^2 and 30 C undergoes an adiabatic free expansion (unrestrained expansion into a vacuum) in which the final volume is 15 times the original volume ($V_2 = 15V_1$). Find the changes in the temperature and in the entropy for this process for each of the following models for the refrigerant:

(a) The ideal gas model for R-134a with $R = 81.490$ J/kg K

(b) The pure substance model for R-134a

13.5 One kg of nitrogen at a temperature of $T_1 = 300$ K and a pressure of $P_1 = 10^5$ N/m^2 is compressed reversibly and isothermally to a pressure of $P_2 = 2 \times 10^7$ N/m^2.

(a) Using the ideal gas model for nitrogen, compute the work transfer $W_{1\text{-}2}$ and heat transfer $Q_{1\text{-}2}$ for the compression process.

(b) Using the tabulated properties of nitrogen based on the pure substance model, compute the work transfer $W_{1\text{-}2}$ and heat transfer $Q_{1\text{-}2}$ for the process.

(c) What error is involved in using the ideal gas model at these temperatures and pressures?

(d) Repeat parts (a) through (c) above for a reversible isothermal compression process between the same two limiting pressures but at a temperature of $T_1 = 90$ K.

(e) From these results, what conclusions can you draw regarding the limitations of the ideal gas model?

13.6 A new method of stress-relieving metal castings has been developed. The method, known as "cryo-quenching", consists of plunging the casting into liquid nitrogen at a pressure of 10^5 N/m^2 and allowing the casting to attain thermal equilibrium with the liquid before it is removed. In a

particular application of this technique, a steel casting of m_{steel} = 10 kg is to be cooled at a constant pressure of $P = 10^5$ N/m^2 from a temperature of 300 K to the saturation temperature of nitrogen. Only 5 kg of nitrogen are available, not all of which are liquid. The casting can be modeled as a pure thermal system with a specific heat of c_{steel} = 0.419 kJ/kgK.

(a) What is the minimum fraction of the mass of nitrogen that must be liquid in order to attain an equilibrium temperature equal to the saturation temperature of nitrogen at a pressure of $P = 10^5$ N/m^2 ?

(b) From an explicit calculation of the entropy change of some suitably defined system, determine whether the cryo-quenching process is reversible or irreversible.

13.7 A Dewar storage vessel has a volume of 25 liters (1 liter = 10^{-3} m^3) and contains liquid and vapor nitrogen at $P = 10^5$ N/m^2. At some particular instant of time when the Dewar contains 22 liters of liquid and 3 liters of vapor, the vapor vent tube is accidentally sealed off. Heat transfer calculations show that the heat transfer from the environment to the liquid nitrogen across the vacuum space is 1.67 J/s. Stress analysis shows that the containment vessel will rupture when the internal pressure reaches $P_{rupture} = 5 \times 10^5$ N/m^2.

(a) How long will it take to rupture the vessel?

(b) Estimate how much mass will be lost if the vapor vent tube is opened when the pressure reaches $P_{rupture} = 5 \times 10^5$ N/m^2.

13.8 As shown in Figure 13P.8, a mass of of water m = 5 kg are contained in a vertical cylinder at T_1 = 40 C by a frictionless piston with a mass such that the pressure on the water is $P_1 = 1.4 \times 10^6$ N/m^2. The water experiences a quasi-static heat transfer, causing the piston to rise until it reaches the stops at which point the volume inside the cylinder is V_2 = 0.5 m^3. The heat transfer process continues until the water exists as a saturated vapor in state 3.

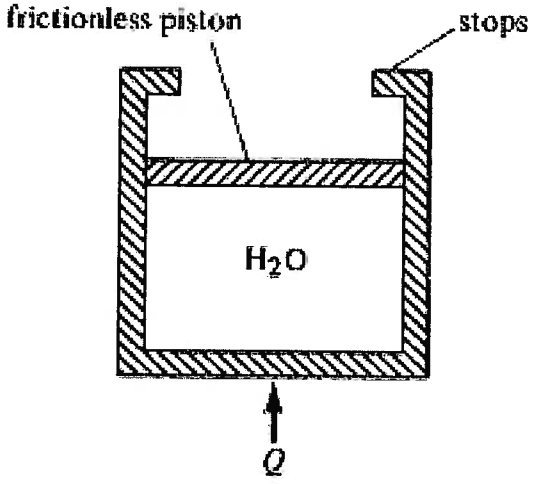

Figure 13P.8

(a) Show the heat transfer process on a T-s diagram.
(b) What is the pressure P_3 of the vapor in the cylinder in state 3?
(c) Determine the heat transfer to the H_2O for this process 1 → 3.
(d) Evaluate the work transfer from the H_2O to the piston.

13.9 The piston-cylinder apparatus shown in Figure 13P.9 is fitted with a leakproof, frictionless piston loaded with enough weights to maintain a pressure of $P_{piston} = 1 \times 10^6$ N/m^2. Initially the

piston rests upon stops so that the volume trapped in the cylinder is $V_1 = 0.01$ m^3. This volume is initially filled with 1 kg of refrigerant 134a at a pressure of $P_1 = 4 \times 10^4$ N/m^2. The refrigerant now experiences a quasi-static heat transfer until its temperature reaches $T_3 = 180$ C.

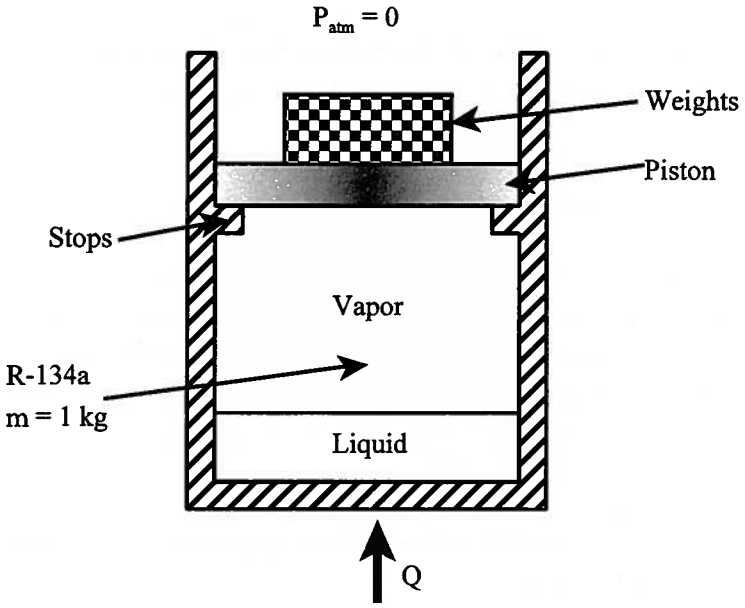

Figure 13P.9

(a) Show the path of the process on P-v and T-s diagrams.
(b) What is the temperature in the initial state, state 1?
(c) What fraction of the total mass is liquid in state 1?
(d) What fraction of the initial volume V_1 is occupied by the liquid?
(e) What is the temperature of the refrigerant as the piston just begins to lift off of the stops in state 2?
(f) What is the heat transfer necessary to just lift the piston off the stops in state 2?
(g) What is the work transfer experienced by the Freon during the process by which it is heated from its initial temperature T_1 to $T_3 = 170$ C?

13.10 As shown in Figure 13P.10, an adiabatic cylinder is fitted with a frictionless, adiabatic piston and a weight such that a pressure of 8×10^5 is required to support it. The volume between the piston face and the end of the cylinder is partitioned off into two volumes A and B (not equal) by a thin, rigid, adiabatic membrane. The volume between the piston face and the membrane, volume A, contains 10 kg of R-134a with an initial quality of $x_{A1} = 0.5$. The other volume, volume B, initially contains 3 kg of R-134a at a pressure of 4×10^5 N/m^2 and a temperature of 30 C. At some instant of time, the membrane is destroyed and the system consisting of the 13 kg of R-134a comes to a new equilibrium state.
(a) Calculate the quality of the R-134a in the final equilibrium state.
(b) What is the final volume of the R-134a?
(c) Calculate the work transfer experienced by the R-134a.
(d) Calculate the entropy generated in the run down to equilibrium.

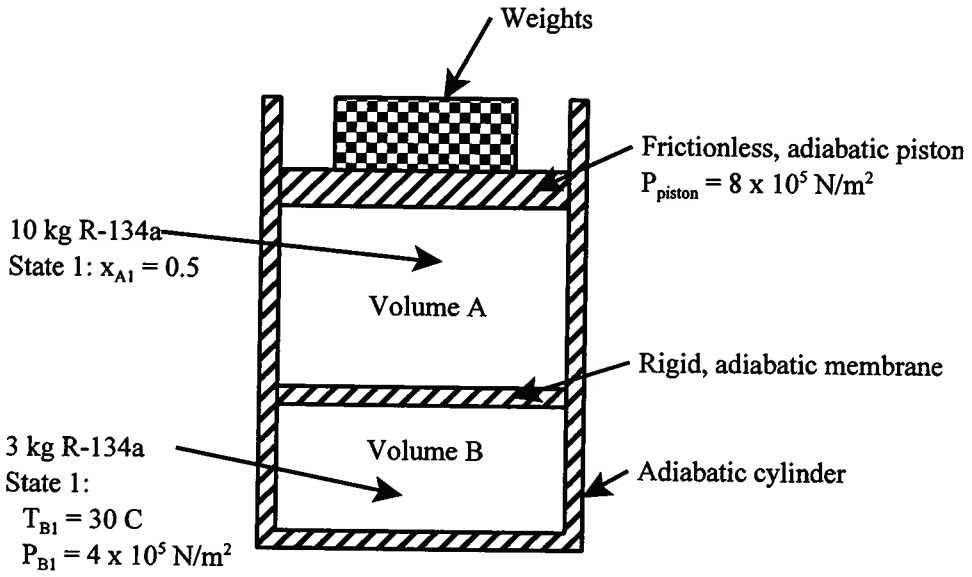

Figure 13P.10

13.11 Consider a system of H_2O consisting of 1 kg of vapor, 1 kg of liquid, and 1 kg of solid all in thermodynamic equilibrium (state 1). The mixture is stirred by a paddle wheel while the volume remains constant until all the solid has melted (state 2). In a second process the stirring is continued at constant volume until only vapor remains (state 3). In an alternative process the system at state 2 is stirred at constant pressure until only vapor remains (state 4).
Note: Data for the triple point of H_2O are given below.

(a) What are the mass proportions of liquid and vapor at state 2?

(b) Determine the temperature, pressure and volume for states 3 and 4.

(c) What are the paddle wheel work transfers for process 1-2, process 2-3, and process 2-4 if these processes are adiabatic?

(d) What is the entropy change for each of the three processes?

Triple Point Data for H_2O
$P_{TP} = 611.3$ N/m², $T_{TP} = 0.01$ C

Phase	Enthalpy (kJ/kg)	Specific Volume (m³/kg)	Entropy (kJ/kgK)
Solid	-333.40	1.0908×10^{-3}	-1.221
Liquid	0.01	1.0002×10^{-2}	0.0000
Vapor	2501.4	206.1	9.156

13.12 A heat engine design consists of a cylinder containing 1 kg of H_2O closed by a slowly moving piston traveling back and forth between two extreme positions so that the H_2O executes a cycle. At one of these extreme positions, the specific volume available to the H_2O is 0.300 m³/kg while at the other extreme position the specific volume available is 1.344 m³/kg. Two heat reservoirs are available, one at $T_H = 260$ C and another at $T_L = 140$ C. During the progress of the piston from one extreme position to the other, the steam experiences reversible heat transfer at

such a rate as to keep the temperature of the H_2O constant and equal to the temperature of one of the heat reservoirs. With the piston at either end, the steam experiences reversible heat transfer so that the temperature changes from the temperature of one heat reservoir to the temperature of the other heat reservoir.

(a) Show the cycle on *P-v* and *T-s* diagrams. Label all the states and be sure to include the locus of saturated states on these diagrams.

(b) Find the net work transfer per cycle $\oint \delta W$ for the engine.

(c) Find the energy conversion efficiency η of the engine.

13.13 Consider the system shown in Figure 13P.13. Tank *A* initially contains $m_{A1} = 5$ kg of H_2O at $P_{A1} = 6 \times 10^5$ N/m^2, $T_{A1} = 200$ C, and is connected through a valve to cylinder *B* fitted with a frictionless piston. An internal pressure of 1.2×10^5 N/m^2 is required to support the mass of the piston. Also, the piston rests on stops so that the initial volume of *B* is $V_{B1} = 0.5$ m^3. This volume is initially evacuated, $P_{B1} = 0$. The connecting valve is opened until the pressure in *A* is reduced to 1.2×10^5 N/m^2. The entire process by which the contents of tank *A* and cylinder *B* come to mechanical, but not thermal, equilibrium can be modeled as adiabatic. In addition, the H_2O that remains in *A* can be modeled as having undergone a reversible adiabatic process. Determine the work transfer to the piston and the final temperature of the steam in cylinder *B*. Note that the final temperatures in tank *A* and cylinder *B* are not equal.

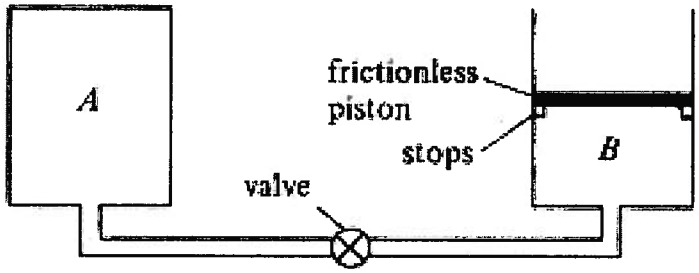

Figure 13P.13

13.14 As shown in Figure 13P.14, a piston-cylinder apparatus is fitted with a weighted, frictionless piston with an area of $A_p = 1$ m^2. The cylinder is initially filled with H_2O at $T_1 = 250$ C. The initial volume $V_1 = 1$ m^3 is half filled with saturated liquid and half filled with saturated vapor. The H_2O experiences a reversible heat transfer that causes the piston to rise in the cylinder. In state 2, the cylinder contains saturated vapor only and, the piston just makes contact with the pure translational spring ($k = 2.0703 \times 10^6$ N/m) above it. The reversible heat transfer process continues causing the spring to be compressed until the pressure of the H_2O in the cylinder reaches $P_3 = 8 \times 10^6$ N/m^2.

(a) In the initial state, what are m_f and m_g and x_1?

(b) What is the volume occupied by the H_2O in state 2?

(c) Show the path of the process 1→2→3 on a *P-v* diagram that also includes the locus of saturated states. Make sure that state 3 is properly located relative to the critical state. By shading the appropriate area on this diagram, show the work transfer from the H_2O to the piston for the process 1→2→3 and the work transfer from the H_2O to the spring for the process 2→3.

(d) What is the temperature T_3 of the H_2O in state 3?

(e) What is the energy change of the spring for the process 2→3?
(f) What is the energy change of the weighted piston for the process 1→2→3?
(g) What is the heat transfer $Q_{1\text{-}3}$?

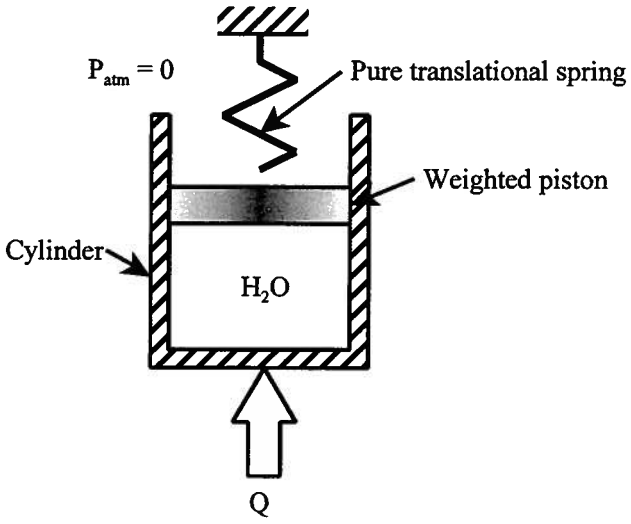

Figure 13P.14

13.15 A rigid, adiabatic container is divided into two compartments *A* and *B* which are separated by a rigid, adiabatic membrane as shown in Figure 13P. 15. Compartment *A* contains $m_A = 2$ kg of saturated vapor CO_2 at $T_{A1} = -50$ C and compartment *B* contains $m_B = 8$ kg of saturated liquid CO_2 at $T_{B1} = 22.5$ C. The rigid, adiabatic membrane is then destroyed, and all of the CO_2 comes into a new equilibrium state.

(a) Determine the temperature and pressure of the CO_2 in the final equilibrium state.
(b) What is the quality of the CO_2 in the final equilibrium state?

HINT: Establish two independent equations for the final quality. Iterate with the saturation table to find the temperature which gives the same quality in both equations.

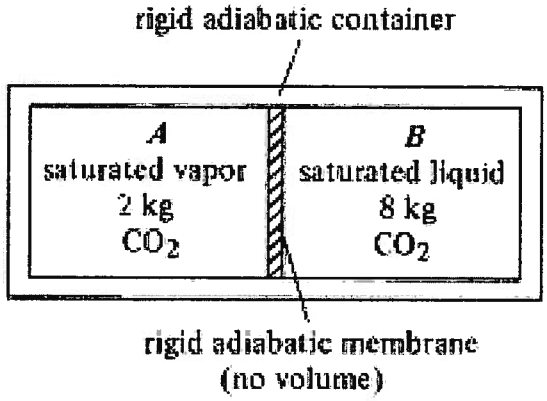

Figure 13P.15

13.16 As shown in Figure 13.16, a rigid, adiabatic vessel of volume $V = 1$ m^3 initially contains $m_1 = 2$ kg of H_2O at a pressure of $P_1 = 2 \times 10^5$ N/m^2. Additional H_2O is added from a charging line

whose conditions are shown in the sketch. When the contents of the vessel reach mechanical equilibrium with the H_2O in the charging line, the valve connecting the charging line to the vessel is closed.

(a) What is the initial temperature, T_1, of the H_2O in the vessel?

(b) What is the pressure, P_2, of the H_2O in the vessel when the valve is closed?

(c) Show the states 1 and 2 on a P-v diagram that includes the locus of saturated states.

(d) Estimate the mass, m_2, of H_2O in the vessel when the valve is closed.

(e) Specify the state of the state of the H_2O in the vessel when the valve is closed.

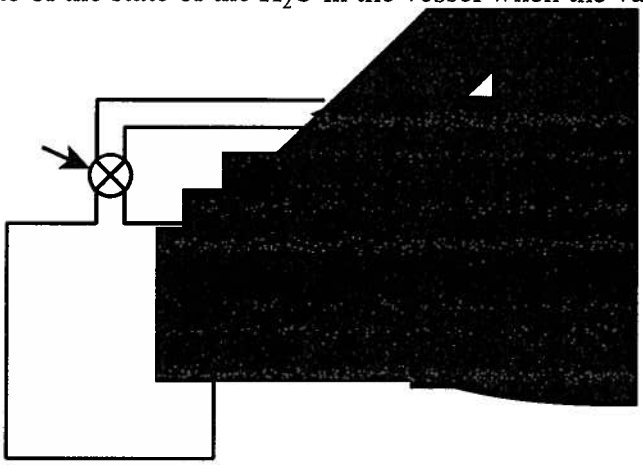

Figure 13P.16

13.17 An inexpensive way of making a Dewar for the storage of cryogens is to manufacture the walls of the Dewar from polystyrene foam (k_{foam} = 0.023 W/m K) that can be foamed in a mold of the appropriate geometry. Consider such a spherical Dewar, shown in Figure 13P.17, with a wall thickness of t = 2 cm and a radius of R = 1 m. In the initial state, the Dewar contains, *by volume*, 50 percent saturated liquid nitrogen and 50 percent saturated vapor nitrogen in equilibrium. The Dewar sits in a room with fixed environmental conditions of T_{atm} = 300 K and $P_{atm} = 10^5$ N/m^2. As the liquid boils due to the parasitic heat leak, the nitrogen vapor created vents through a hole in the top of the sphere such that no pressure drop is required for the saturated vapor to escape.

(a) What is the temperature of the nitrogen in the initial state?

(b) What is the mass of the nitrogen in the Dewar in the initial state?

(c) What is the quality of the nitrogen in the initial state?

(d) Estimate the rate of heat transfer from the room into the nitrogen if the heat transfer coefficient for convection and radiation from the outside surface is h_o = 8 W/m^2 K and the average heat transfer coefficient between the nitrogen and the inside wall of the Dewar is $h_i = 10^3$ W/m^2 K.

(e) Estimate the time required for enough liquid to boil away so that the Dewar contains only saturated nitrogen vapor.

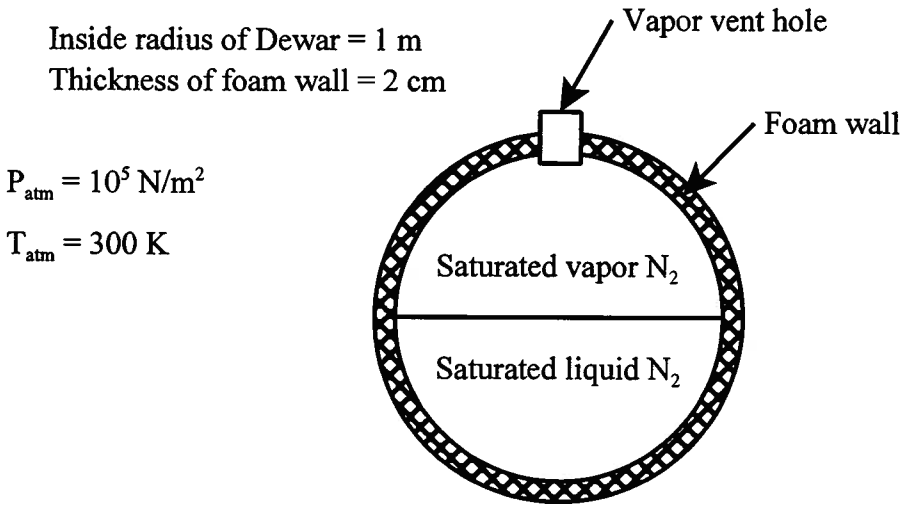

Figure 13P.17

13.18 As shown in Figure 13P.18, a container is divided into two volumes A and B. In the initial state, volume A contains H_2O in the critical state ($V_{A1} = 0.5$ m^3) and volume B is evacuated. A crack forms in the adiabatic wall separating volumes A and B, and H_2O **slowly** leaks from volume A into volume B. As a result of the resistance to flow in the crack, the weights and the piston that bounds volume A slowly descend, compressing the H_2O such that the H_2O that **remains** in volume A passes through a sequence of equilibrium states until the piston comes to rest on the stops, thereby leaving a volume of 0.25 m^3 in volume A ($V_{A2} = 0.25$ m^3). When the flow through the crack stops and the pressure of the H_2O is uniform throughout volumes A and B, $P_{A2} = P_{B2} = 10^7$ N/m^2.

The boundary of the H_2O, i.e. the interface between the H_2O and the walls of both volumes A and B, is adiabatic at all times.

(a) What is the temperature and pressure of the H_2O in the initial state?

(b) Show by means of proper thermodynamic arguments that the mass remaining in volume A in state 2 is $m_{A2} = 26.825$ kg.

(c) What is the quality x_{A2} in volume A in state 2?

(d) What is the volume of volume B?

(e) For a system consisting of all the H_2O, what is the entropy generation for the process by which the H_2O runs down to the final equilibrium state from the initial state?

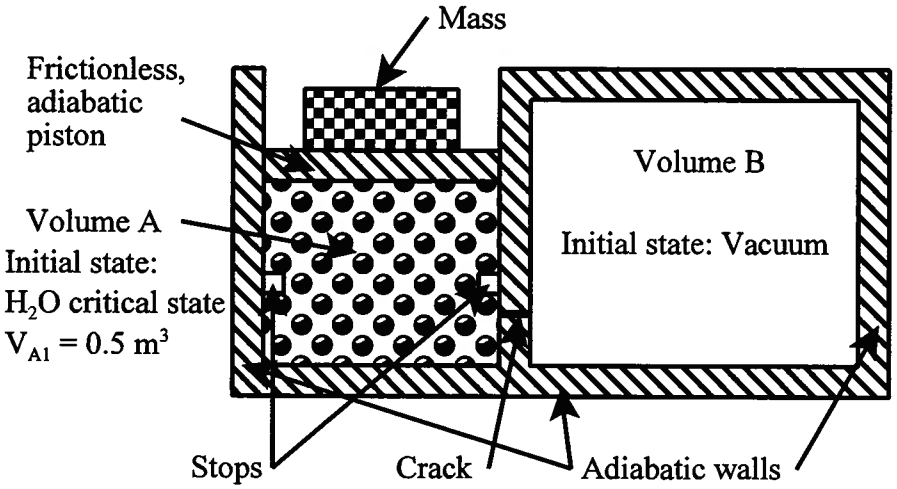

Figure 13P.18

13.19 A steam catapult in the form of a horizontal piston-cylinder apparatus is to be used to launch aircraft from the deck of an aircraft carrier. The steam that is available for this purpose is at a pressure of $P_1 = 8 \times 10^6$ N/m^2 and a temperature of $T_1 = 540$ C. For the purpose of designing this catapult, assume that the steam can be expanded reversibly and adiabatically to a pressure of $P_2 = 1 \times 10^5$ N/m^2. The aircraft, $m_{plane} = 1.5 \times 10^5$ kg, is to be launched with a velocity of $\vartheta_{plane} = 60$ m/sec after starting from rest. Half of the energy required for the launch comes from the aircraft power plant and the rest is to be provided by the catapult. As a first approximation, assume that work done against the atmosphere is negligible. The steam required for the launch is to be stored in a rigid pressure vessel called an accumulator.

(a) What is the volume, V_1, of the accumulator required to store steam for one launch?

(b) If the length of the catapult is $L = 200$ m, what is the diameter?

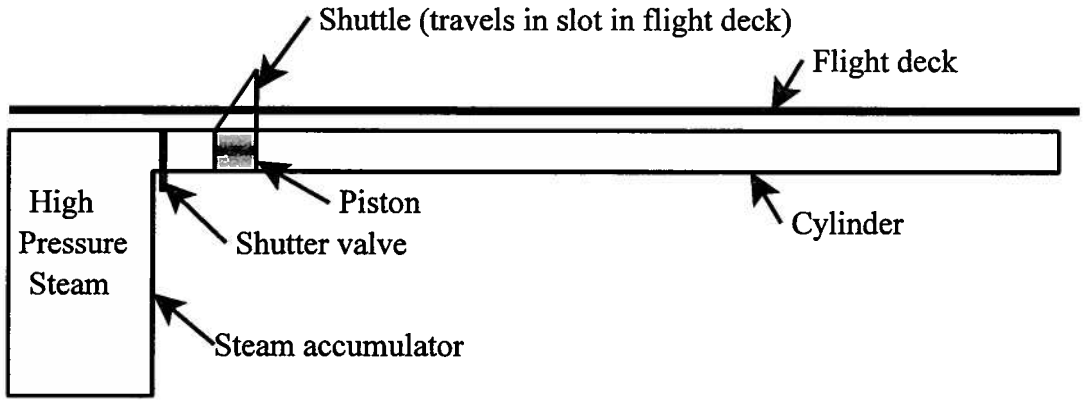

Steam Catapult for Launching Aircraft

Figure 13P.19

13.20 As shown in Figure 13P.20, a reversible cyclic device operates between two streams of H_2O flowing in pipes. Stream A has a mass flow rate of $\dot{m}_A = 2$ kg/sec and enters its pipe at a temperature of $T_{1A} = 20$ C and a pressure of $P_{1A} = 2 \times 10^5$ N/m^2. Stream B enters its pipe at a temperature of $T_{1B} = 500$ C and a pressure of $P_{1B} = 2 \times 10^5$ N/m^2. The H_2O flows in the pipes with negligible pressure drop. Stream A exits from its pipe at a quality of $x_{2A} = 0.8$. Stream B exits from its pipe as a two-phase, liquid-vapor equilibrium state. The reversible, cyclic device experiences a work transfer with the environment at a rate of $\dot{W} = 717.8$ kW.

(a) What is the temperature T_{2A} at the exit of stream A?

(b) What is the temperature T_{2B} at the exit of stream B?

(c) What is the state of the H_2O at the exit of stream B?

(d) What is the mass flow rate $\dot{m}_B$?

(e) Show the paths of the processes in streams A and B on a single set of *T-s* coordinates that also includes the locus of saturated liquid and vapor states.

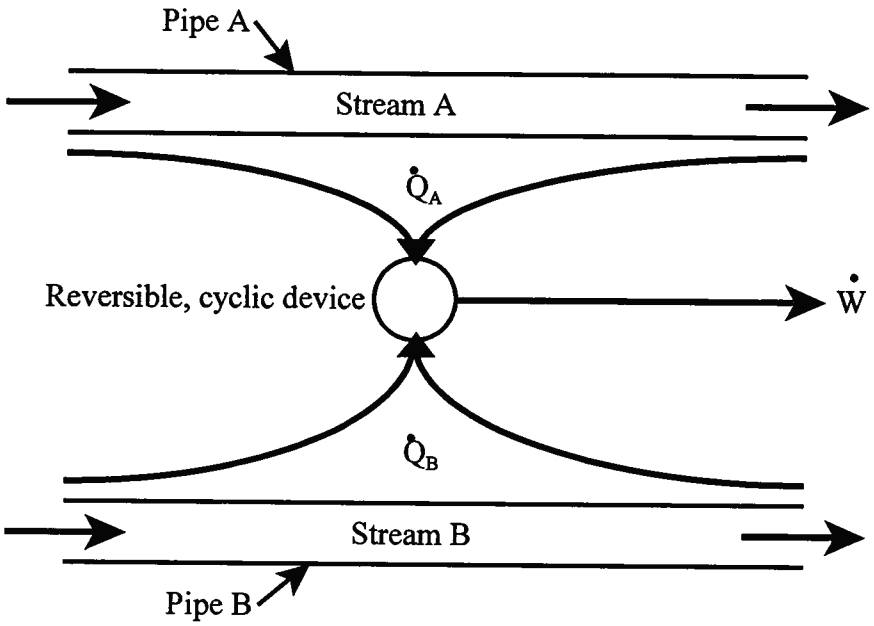

Figure 13P.20

13.21 As shown in Figure 13P.21, a rigid vessel contains m_A = 1 kg of saturated liquid H_2O at a temperature of T_{A1} = 320 C in the initial state. This vessel is adiabatic everywhere except where it is connected to a thermal conductor. This thermal conductor is connected through a thermal switch to a cylinder containing m_B = 1 kg of H_2O initially in a two-phase state. The cylinder is fitted with a weighted piston such that the contents of the cylinder must exert a pressure of P_B = 10^5 N/m^2 in order to support the piston. This cylinder and piston are also adiabatic everywhere except where the thermal conductor makes contact with the cylinder.

The thermal switch is closed and the contents of the rigid vessel run down to thermal equilibrium with the contents of the piston-cylinder apparatus. The thermal resistance of the thermal circuit is such that the processes in the H_2O can be modeled as quasi-static. In its **final state**, the H_2O in the piston-cylinder apparatus is a saturated vapor.

(a) On a single *P-v* diagram, show the locus of saturated states and show the paths of the processes of the H_2O in the rigid vessel *A* and in the piston-cylinder apparatus *B*.

(b) What is the final equilibrium temperature T_{A2} of the H_2O in the rigid vessel?

(c) What is the final equilibrium pressure P_{A2} of the H_2O in the rigid vessel?

(d) For the contents of the rigid vessel, determine the volume V_{A2f} occupied by the liquid phase in the final state.

(e) For the contents of the piston-cylinder apparatus, determine the specific volume v_{B1} of the two-phase H_2O in the initial state.

(f) For a system consisting of all the H_2O, what is the entropy generation for the process by which the H_2O runs down to the final equilibrium state from the initial state?

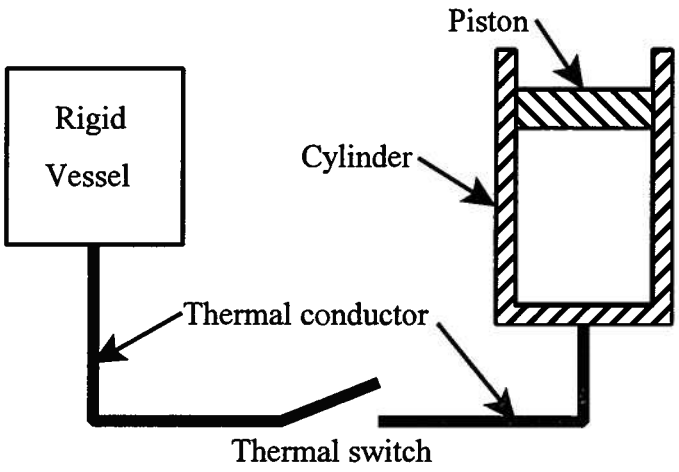

Figure 13P.21

13.22 A supply line contains H_2O at its critical point. The line is capable of supplying any amount of this H_2O without changing the state of the H_2O in the line. A rigid tank, initially evacuated, is connected to the supply line through a valve. The valve is opened and H_2O is allowed to flow into the tank until the pressure inside the tank reaches $P_2 = 10^5$ N/m^2. The tank volume is $V_T = 0.1$ m^3.

(a) What is the state of the H_2O in the tank when the pressure reaches $P_2 = 10^5$ N/m^2?

(b) What is the mass of the H_2O in the tank when $P_2 = 10^5$ N/m^2?

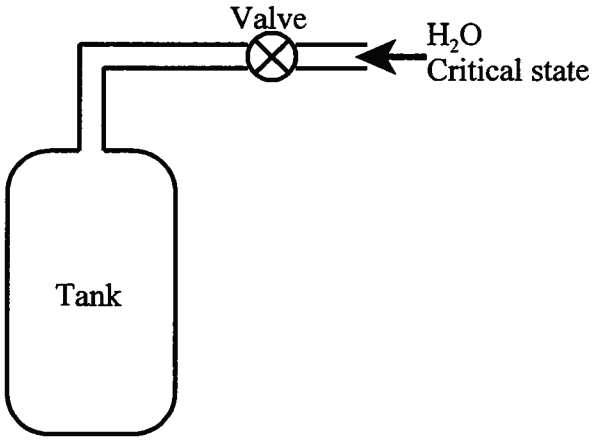

Figure 13P.22

13.23 In a classroom demonstration of the triple point of N_2 shown schematically in Figure 13P.23, a Dewar contains an initial mass of $m_1 = 1$ kg of saturated liquid N_2 at the pressure 10^5 N/m^2 and a negligible amount of vapor in equilibrium with the liquid. A vacuum pump is connected to the vapor space of the Dewar and nitrogen is removed from the Dewar by reducing the pressure of the vapor phase in equilibrium with the liquid phase. This causes some of the liquid to evaporate in an attempt to replace the vapor removed by the pump. As the liquid evaporates, the latent heat necessary to convert liquid into vapor is provided by the liquid that remains behind. This, in turn, causes the temperature of the remaining liquid to drop in accordance with the reduced vapor pressure. The reduction in pressure can be continued until the triple point pressure is reached. If the pumping process is continued further, it is possible to

convert the remaining nitrogen into solid nitrogen in equilibrium with nitrogen vapor at the triple point pressure.

(a) Estimate the mass of N_2 that must be removed by the vacuum pump in order to convert all the remaining liquid into saturated liquid N_2 at the triple point.

(b) When all the liquid N_2 has been transformed into solid and vapor N_2 (no liquid) at the triple point, how much N_2 remains?

(c) How much of the remaining mass of N_2 is in the vapor phase?

The following data for nitrogen at the triple point may be useful:

$$T_{TP} = 63 \text{ K}, \; P_{TP} = 0.1249 \times 10^5 \text{ N/m}^2$$

$$h_s = -25.75 \text{ kJ/kg}, \; h_f = 0 \text{ kJ/kg}, \; h_g = 216.0 \text{ kJ/kg}$$

$$v_s = 1.129 \times 10^{-3} \text{ m}^3\text{/kg}, \; v_f = 1.152 \times 10^{-3} \text{ m}^3\text{/kg}, \; v_g = 1.487 \text{ m}^3\text{/kg}$$

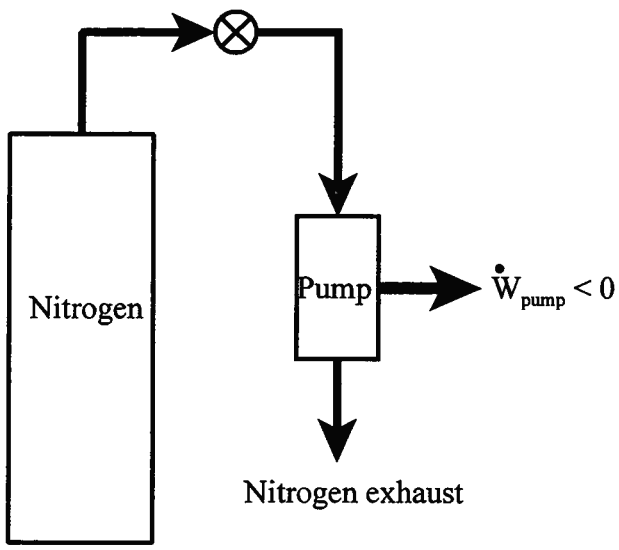

Figure 13P.23

13.24 As shown in Figure 13P.24, an adiabatic piston-cylinder apparatus is divided into two separate compartments of equal volume, $V = 1 \text{ m}^3$, by means of a thin rigid membrane. One compartment contains saturated liquid refrigerant R-22 in the initial state $T_1 = 20$ C, while the other compartment is evacuated. The adiabatic piston is loaded with a mass such that a pressure of $P_{piston} = 10^5 \text{ N/m}^2$ is required to support it in mechanical equilibrium. In the initial state, a pin holds the piston in a fixed position.

(a) The membrane ruptures and the R-22 expands to fill the entire volume of the cylinder. The R-22 is allowed to come to equilibrium in state 2. Calculate P_2 and T_2.

(b) The pin is now removed and the piston is free to move. After some time the R-22 and the piston reach a new equilibrium state 3. Calculate V_3 and T_3.

(c) Calculate the interactions for the various changes of state.

(d) For the R-22 as a system, calculate the entropy transfer for the two process, 1 → 2 and 2 → 3. Calculate the change of entropy of the R-22 for these two processes. From these data, what conclusions can be drawn regarding their reversibility?

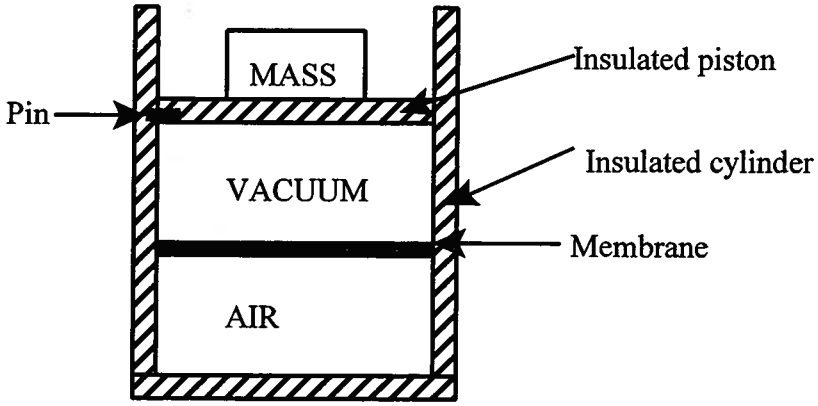

Figure 13P.24

13.25 As shown in Figure 13P.25, a rigid tank of volume $V = 10^3$ m^3 is thermally connected to a reversible cyclic device. In the initial state, the tank is filled with saturated H_2O vapor at a temperature of $T_1 = 40$ C. The H_2O is then cooled to a temperature of $T_2 = 30$ C by means of the cyclic system that operates in an integral number of reversible cycles. The cyclic system uses the atmosphere at a temperature of $T_{atm} = 35$ C as a heat reservoir.

(a) Calculate the heat transfer from the H_2O to the cyclic system.

(b) Calculate the work transfer experienced by the cyclic system in order to provide the heat transfer of part (a) above.

(c) Calculate the mass of saturated liquid H_2O that forms inside the tank during the cooling process.

(d) Calculate the change in entropy of the atmosphere at a result of the interaction between the H_2O and the cyclic device.

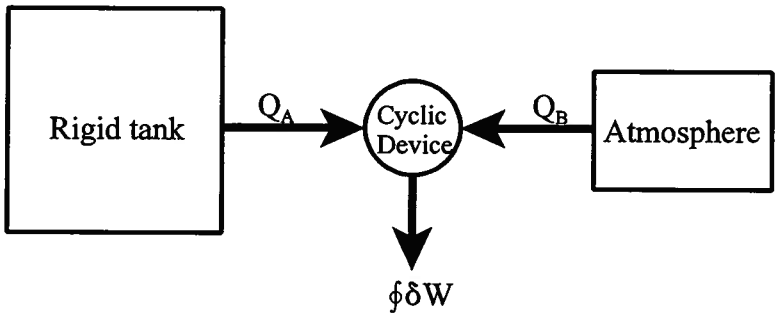

Figure 13P.25

13.26 A pressure cooker is a device used to process foodstuffs by cooking them at elevated temperatures in order to reduce the cooking time. The elevated temperatures are achieved by cooking the foodstuffs in an H_2O environment at pressures higher than atmospheric. Consider the following example. A pressure cooker consisting of a rigid vessel with an effective internal volume of $V = 1$ m^3 is filled with saturated H_2O at a pressure of $P_1 = 1 \times 10^5$ N/m^2 in the proportions 10% of the volume saturated liquid and 90% of the volume saturated vapor (state 1). The vessel is sealed, and the vessel and its contents experience a positive quasi-static heat transfer until the internal pressure reaches $P_2 = 2 \times 10^5$ N/m^2 (state 2). At this time, a relief valve opens and allows saturated vapor to escape as the heat transfer process continues at constant

pressure until only saturated vapor remains in the pressure cooker (state 3). At this time, the relief valve closes and the heat transfer process becomes negative as the contents are cooled until the internal pressure reaches $1x10^5$ N/m^2 (state 4). The pressure cooker is now opened and the foodstuffs are removed.

(a) Show the states and the processes on *P-v* and *T-s* diagrams.
(b) Calculate the mass of liquid, m_f, and the mass of vapor, m_g, in states 1 and 2.
(c) Calculate the heat transfer, $Q_{1\text{-}2}$, and work transfer, $W_{1\text{-}2}$, for the process 1 → 2.
(d) Calculate the mass, m_3, of H_2O in the pressure cooker in state 3.
(e) Calculate the heat transfer, $Q_{2\text{-}3}$, to the pressure cooker for the process 2 → 3.
(f) Calculate the heat transfer, $Q_{3\text{-}4}$, and work transfer, $W_{3\text{-}4}$, for the process 3 → 4.
(g) Calculate the proportions by volume of liquid and vapor in state 4.

13.27 The manufacture of paper consumes enormous amounts of energy. A new paper mill is presently being designed for Bucksport, Maine. The mill is to produce 10^9 kg of paper (dry) per year. As shown in Figure 13P.27, wood pulp enters the mill as a slurry of wood fibers suspended in water. The wood pulp is 95% water and 5% wood fibers by mass. The water can be assumed to enter as saturated liquid at 25 C and leave as saturated vapor at 25 C. The wood fibers enter the mill at 25 C, and the paper leaves the mill dry at 25 C. In the preliminary design of the mill, we would like to estimate the minimum energy requirements, both heat transfer and work transfer, of the mill as it interacts with the environment at 25 C. Wood fibers and paper can be modeled as incompressible materials with density ρ_s = 900 kg/m^3 and c = 1.38 kJ/kg K.

(a) Estimate $\dot{Q}_{min}$ and $\dot{W}_{min}$.
(b) Prove that these values are indeed the minimum values for the interactions.

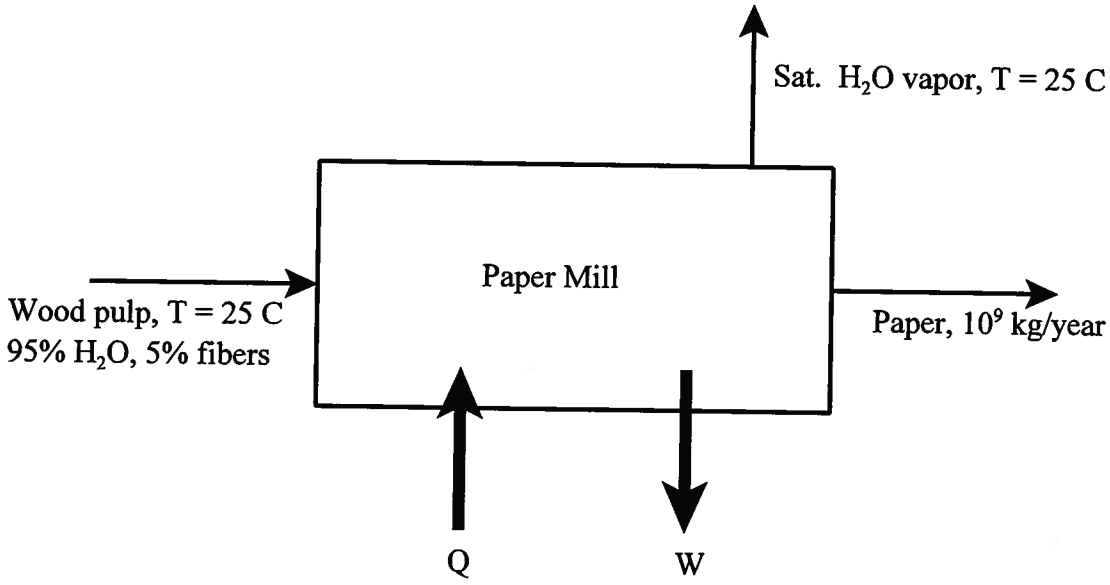

Figure 13P.27

13.28 The objective is to design a steam-powered catapult for launching jet aircraft from the deck of an aircraft carrier. As shown in Figure 13P.28a, the shuttle, or trolley, of the steam catapult is connected to the aircraft by its launch bar and is propelled along a track in the deck by two

pistons which are directly connected to it. The pistons travel in two steam cylinders that are placed side by side under the deck and extend the whole length of the track. Steam pressure acts directly on these pistons and propels them along the cylinders. The comparatively light pistons and the shuttle are the only moving parts of the catapult.

The sketch illustrates an aircraft secured by its launch bar to the shuttle and held back against the thrust of its own engines. The nose gear launch equipment is designed to assist in launching aircraft by attaching the nose wheel strut to the towing mechanism of the catapult by way of the launch bar. A holdback device is connected between the aircraft holdback fitting and the holdback attachment point on the deck. The holdback restrains the aircraft against forward movement prior to actual catapult firing. The capacity selector valve (CSV) system allows for the catapult officer to set the desired energy level of the launch. The catapult officer uses the type of aircraft, aircraft weight, aircraft configuration, wind conditions, and the desired excess aircraft airspeed to find the correct CSV setting from aircraft launching bulletins that are prepared for each type of ship. When the aircraft is ready to be launched with its engines at full power, the launching valves are opened and steam is admitted from the receivers to the after side of the main pistons in the power cylinders. The force on the pistons generated by this steam breaks a calibrated weak link in the holdback and accelerates the pistons, shuttle, and aircraft to the required speed along the deck. At the end of the catapult power stroke, the aircraft automatically disengages from the catapult and continues the launch under its own power. The catapult retraction system can then be actuated to return the catapult shuttle to battery position.

Figure 13.28b shows a cross-section through the catapult and illustrates how the two power cylinders are installed side by side in the trough formed in the flight deck. This trough is closed by two portable tracks or portions of deck which carry the channel-shaped rails in which the shuttle runs upon its rollers.

The body of the shuttle is in the shape of an inverted ``T'' of which the upper part projects through a slot between the two channel rails above the deck and forms the hook to which the towing bridle is attached. The flange of the ``T'' on the underside is furnished at each edge with "dogs" which engage in corresponding "dogs" in the driving key attached to the piston. The two pistons and the shuttle are constrained to move axially, but have freedom relative to each other so that slight movement of the track or cylinders is possible. The dogs are provided with ample bearing surfaces. The length of the accelerating stroke, and therefore of the assembled cylinder, is only limited by the length of the ship, but it is necessary to stop the piston assemblies and shuttle when they have reached the end of their available stroke.

At the end of the power stroke, the spear sections of the piston assemblies engage the water brakes. The brake unit consists of two fixed cylinders, or chambers, which are kept full of water using centrifugal action of a vortex induced in each chamber by jets of water. The tapered spear enters the orifice at the chamber's mouth, displacing water aft through the gradually reducing area between the orifice and the entering spear. This action develops high pressure in the brake chambers, which acts on the spears to stop the pistons and the shuttle.

The rotary retraction engine uses hydraulic pressure from the catapult hydraulic system to operate a hydraulic motor and wind mechanism, which feeds the cables on and off the drum to operate the launching shuttle "grab." After each shot, the "grab" is propelled the full length of the launching stroke, where it latches onto the shuttle. The motion is reversed to return the pistons and shuttle to the starting position in preparation for the next launch.

The current design of the steam catapult is capable of launching a Grumman F-14A Tomcat aircraft of mass m = 35,805 kg at a speed of ϑ = 71.4 m/sec with a catapult piston stroke of L = 76.2 m. Each of the two engines of the Tomcat develop a static thrust of F_t = 9.2963 x 10^4 N. The two Westinghouse A2W pressurized water nuclear reactors (PWR) of the aircraft carrier

are capable of providing wet steam at a pressure of $P_{supply} = 6.72 \times 10^6$ N/m^2, $T_{sat} = 283.1$ C, and a quality of $x_1 = 0.9975$. The saturation properties of this steam are:

$v_f = 1.3427 \times 10^{-3}$ m^3/kg, $v_g = 2.8652 \times 10^{-2}$ m^3/kg, $u_f = 1244.1$ kJ/kg, $u_g = 2583.6$ kJ/kg

$h_f = 1253.1$ kJ/kg, $h_g = 2776.2$ kJ/kg, $s_f = 3.0969$ kJ/kg K, $s_g = 5.8352$ kJ/kg K

Estimate the diameter of each of the two pistons and the volume of the steam receivers used to store the steam for each launch.

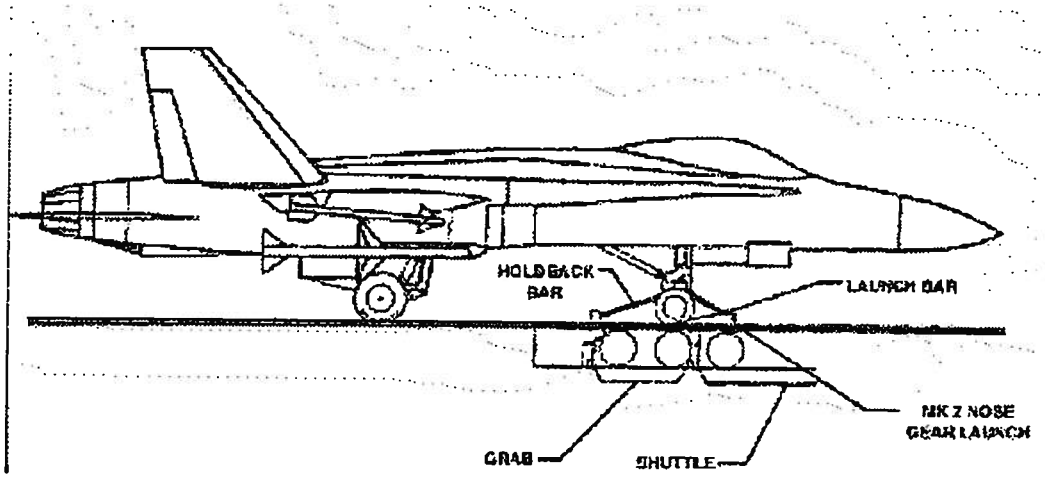

Figure 13.28a Aircraft in Launch Position

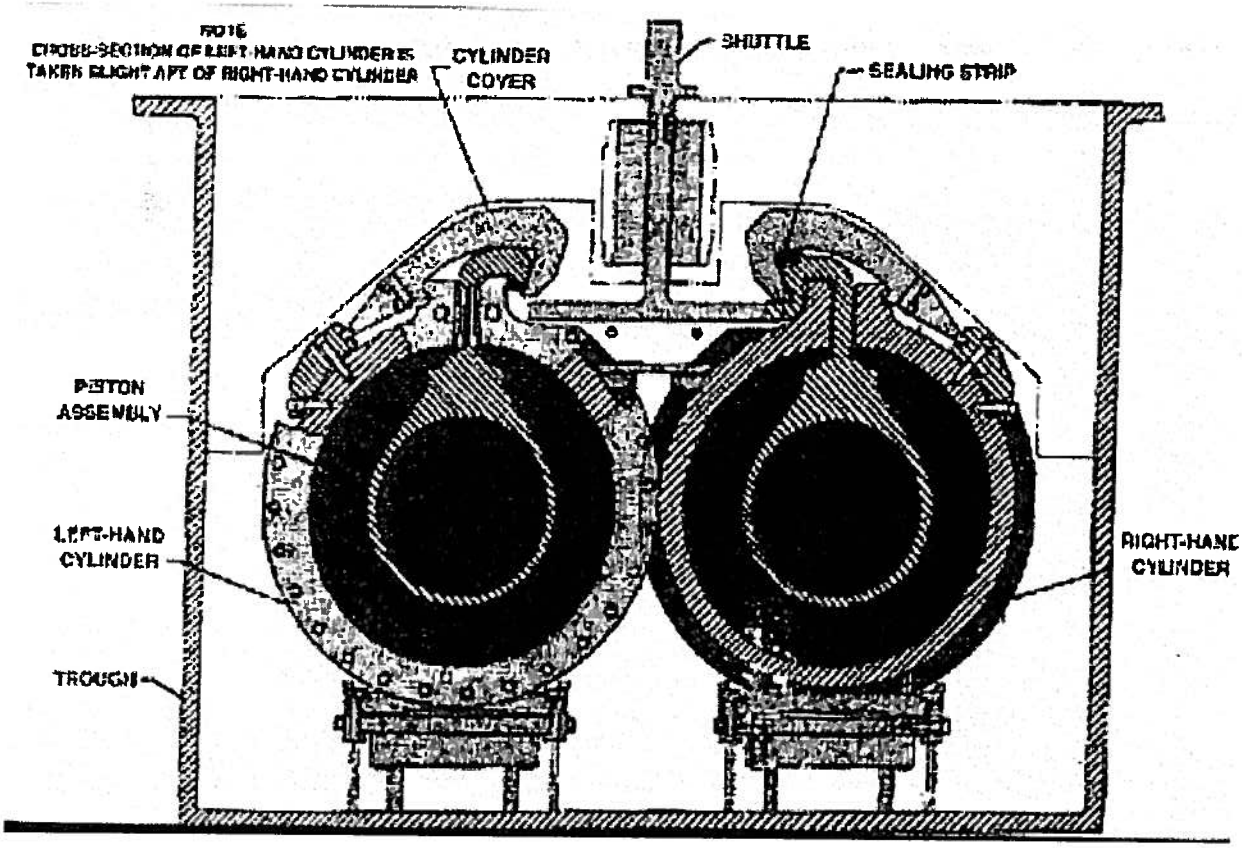

Figure 13.28b Cross-sectional View of Piston Assembly

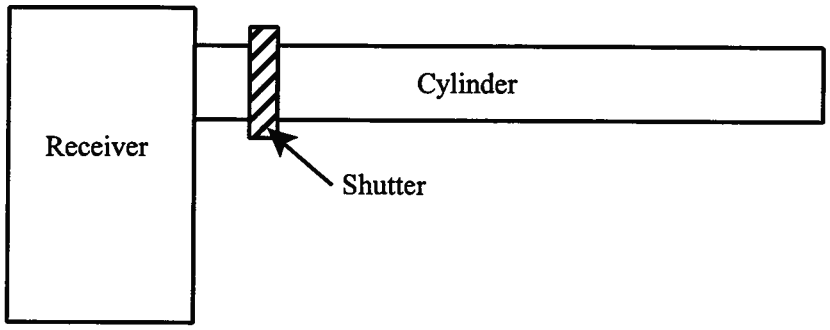

Figure 13.28c Receiver-Cylinder Schematic

13.29 One of the design limitations in the large scale integration of electronic devices is the cooling requirements of the individual chips that make up the device. One method of cooling that has been developed to address this problem uses a dielectric fluid, such as refrigerant R-134a, that has a low boiling point. The particular design under consideration uses a modular approach in which an array of chips is housed in a compartment fitted with a condenser coil in the top of the compartment. As shown in Figure 13.29, a pool of boiling R-134a is used to cool the array of chips located on the floor of the module, and the vapor thus produced is condensed on the cooling coil and allowed to drip down into the pool. Thus there is a circuit of R-134a in which the refrigerant alternates between the two phases, liquid and vapor.

The module is sealed so that the temperature of the two-phase R-134a inside is $T_{sat} = 40$ C when the unit is working. Integrated circuits (ICs) are embedded in an adiabatic ceramic substrate with one surface exposed. The ICs are submerged in the liquid phase and cooled by nucleate boiling on the exposed surface. The maximum allowable surface temperature of the ICs is $T_w = 50$ C. The vapor produced by the boiling heat transfer rises to the top of the cooling module where it comes into contact with a coiled copper tube cooled by water circulating through it. The vapor condenses, and the condensate drips down into the pool of liquid below. The copper tube is 2 m long with an I.D. of 8 mm and an O.D. of 10 mm. The water enters the tube at a temperature of 10 C with a mass flow rate of 0.05 kg/sec.

For the chip/R-134a interface: $C_{s,f} = 0.004$ and $n = 1.7$

For copper: $k_{Cu} = 401$ W/m K

(a) Determine the heat transfer rate for the coolant.

(b) What is the temperature of the coolant at exit from the module?

(c) If each IC has an exposed surface area 24 mm^2, calculate the maximum allowable power dissipation in each IC.

(d) How many circuits can be accommodated by this design?

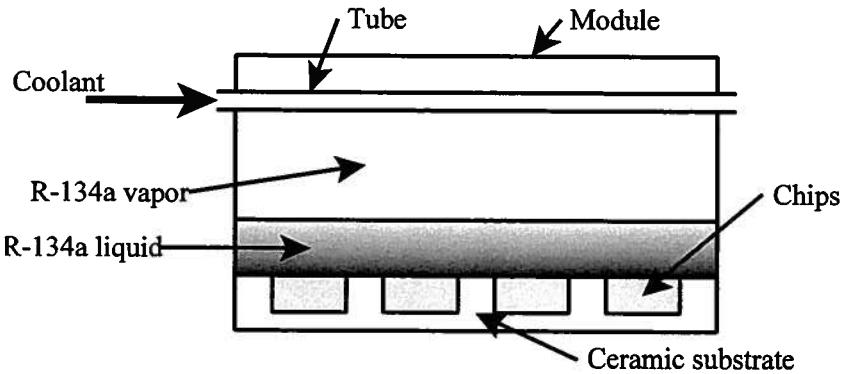

Figure 13P.29

13.30 As shown in Figure 13P.30, a vessel is divided into two chambers separated by a wall that is adiabatic everywhere except for a square 2m on each side. This square is made of copper 5 mm thick (k_{Cu} = 401 W/m K). On one side of the wall is saturated R-134a at a temperature of 35 C. On the other side of the wall is saturated H_2O, T_{sat} = 45 C, that is condensing in a filmwise manner on the copper surface. As a result of the condensing heat transfer in the H_2O, the R-134a experiences nucleate boiling. The resulting vapor is removed and the mass is replaced by an equal mass of saturated liquid so that saturation conditions are maintained in the R-134a. Similarly, the condensate that forms is removed and replaced by an equal mass of saturated H_2O vapor.

For the copper/R-134a interface: $C_{s,f}$ = 0.0154 and n = 1.7

(a) Estimate the temperature of the copper plate assuming the thermal resistance of the plate is negligible. Is this a reasonable assumption?

(b) Estimate the mass rates (kg/sec) of evaporation and condensation for the two fluids.

HINT: The solution of this problem requires a trial and error approach in which one first guesses the temperature of the copper plate and then determines the heat flux due to boiling in the R-134a. This now establishes the heat flux on the H_2O side. One then needs to check to see that the assumed value for the temperature of the plate will sustain that heat flux in the H_2O. If not, pick a new value for the temperature of the plate and try again.

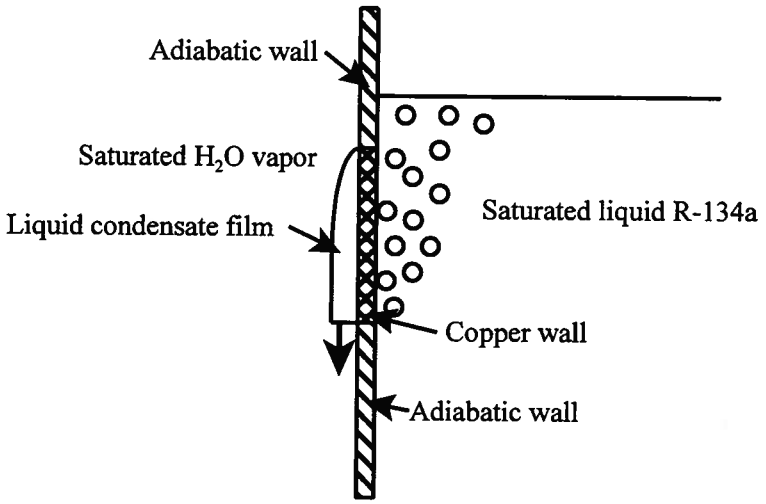

Figure 13P.30

13.31 A thermosyphon (sometimes called a Perkins tube) is a device for transporting energy and entropy from one region to another by means of boiling and condensation of a working fluid. Typically a thermosyphon consists of a tube closed at both ends and filled with a fluid in the right proportions of liquid and vapor so that the liquid-filled portion of the tube is in contact with the energy source (high temperature heat reservoir) while the other end is in contact with the energy sink (low temperature heat reservoir). The liquid filled portion of the tube is called the boiling section and the vapor filled section is called the condensation section. Depending upon the application, these two sections may be separated by an insulated section.

In a particular application of the device, two streams of water, one stream at 85 C, the other at 50 C, are separated by an adiabatic membrane. A thermosyphon made from a stainless steel tube, k_s = 14.9 W/m K, with I.D. = 19 mm and O.D. = 25 mm is filled with pure water. As shown in Figure 13P.31, the hot stream flows at 0.3 m/sec while the cold stream is stagnant (zero velocity with heat transfer by natural convection). The total length of the tube is 1.3 m with a

boiling section 0.3 m long and a condensation section 1 m long. Vapor condenses on the inside of the condenser section and falls as a film to maintain the level in the boiler section. Calculate the heat transfer rate from the hot stream to the cold stream.
Note that the state of the water inside the tube needs to be determined. HINT: The state of the water inside the tube is approximately saturated H_2O at a temperature in the neighborhood of 65 C.

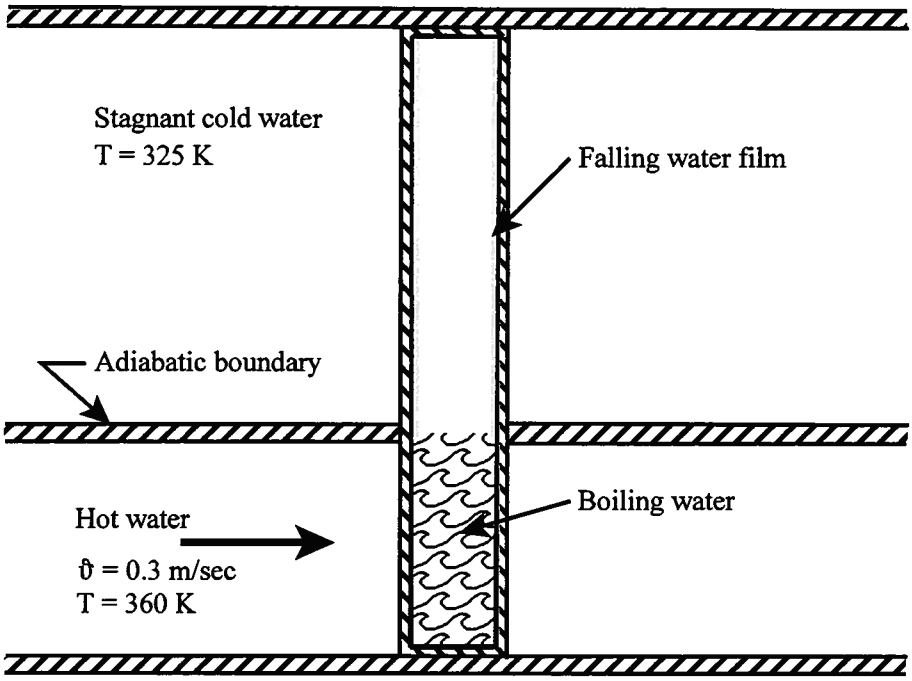

Figure 13P.31

13.32 For forced convection boiling in smooth tubes, one approach to estimating the heat flux combines the heat transfer coefficients in a linear fashion for the separate effects of boiling and forced convection. In this method, the Rohsenow correlation for nucleate boiling of equation (13.68) is used together with Newton's law of Cooling to determine a heat transfer coefficient h_b, and the Dittus-Boelter correlation is used to predict the forced convection contributions with the constant 0.023 in the Dittus-Boelter correlation replaced by the value 0.019, viz.

$$Nu_D = 0.019 Re_D^{0.8} Pr^{0.4}$$

The convection heat transfer coefficient h_c is then simply added to h_b to get h_{total}. In this analysis, we wish to compare this simple approximation with the results of the more complex approach suggested in the boiling heat transfer correlation of equation (13.98). As a test case, consider water with a bulk mean velocity of 1.5 m/sec and a bulk mean temperature of 95 C flowing through a horizontal brass tube (k_{brass} = 127.8 W/m K) with an I.D. = 15 mm and a tube wall temperature of 110 C.

(a) Estimate the rate of heat transfer per unit length of the tube for the two correlations.

(b) Which correlation would you choose? Why?

(c) For the approximate method estimate the length of tube necessary to convert saturated liquid into saturated vapor at 95 C. What is the pressure drop for this tube?

The thermal properties of water at 95 C are:
ρ_l = 961.82 kg/m^3, ρ_v = 5.0457 x 10^{-4} kg/m^3, h_{fg} = 2270.2 x 10^3 J/kg, $c_{P,l}$ = 4212 J/kg K, $c_{P,v}$ = 2014 J/kg K, μ_l = 295.8 x 10^{-6} kg/m sec, μ_v = 11.81 x 10^{-6} kg/m sec, k_l = 0.678 W/m K, k_v = 24.34 x 10^{-3} W/m K, σ = 59.9 x 10^{-3} N/m

13.33 Saturated steam from a manufacturing process is to be condensed at a pressure of 1 atm (T_{sat} = 100 C) in a shell-and-tube heat exchanger with one shell pass and two tube passes. Cooling water enters the tubes at $T_{w,in}$ = 15 C with an average velocity of $\mathcal{V}_{ave}$ = 3.5 m/sec. The tubes are thin-walled and made of copper with a diameter of D = 14 mm and a length of L = 0.5 m.

(a) Find the number of tubes/pass required to condense steam at the rate of 2.3 kg/sec.

(b) Determine the bulk mean outlet temperature of the water.

(c) What is the maximum possible condensation rate that could be achieved with this heat exchanger with the same mass flow rate for the water and inlet temperature of the water?

13.34 The fuel rods, known as "pins", in a boiling water nuclear reactor are designed with hollow cylindrical cores that act as a channels for coolant flow. In a particular design shown in Figure 13P.34, the diameter of this circular channel is 5 mm with a length of 1.2 m. Water at a pressure of 5 x 10^6 N/m^2 and a temperature of 210 C enters the channel with an average velocity of 6 m/sec. The heat flux due to the fission of the uranium fuel is uniform along the length of the pin and has a value of

$$\frac{\dot{Q}}{A} = 2.2 \text{ MW / m}^2$$

Assume that the flow is fully developed thermally and hydrodynamically. Assume that the wall of the pin is thin enough that it is at uniform temperature across any plane normal to its axis. That is, assume that the temperature of the pin is a function of x only where x is the direction of flow of the coolant. Assume that nucleate boiling dominates along the channel.

(a) Plot the wall temperature of the pin as a function of x. What is the temperature of the wall at the coolant exit?

(b) What is the state of the coolant at exit?

(c) Estimate the pressure drop for the coolant over the length of the channel.

For uranium: k = 32 W/m K

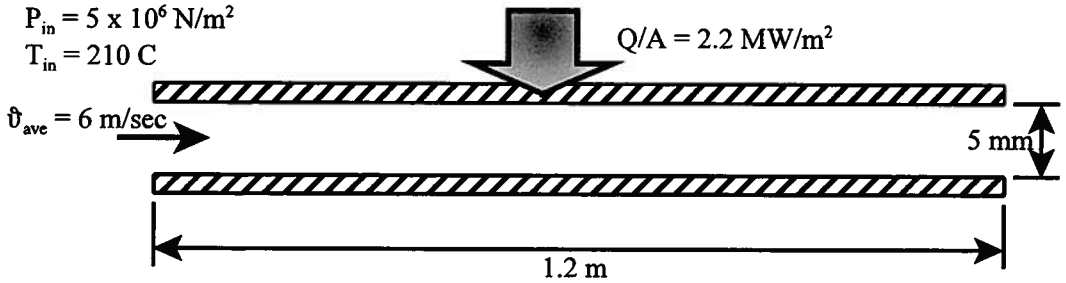

Figure 13P.34

13.35 As shown in Figure 13P.35, an aluminum rod 10 cm in diameter emerges from the final set of rollers in a rolling mill at a velocity of 1 m/sec and a uniform temperature of 450 C. As the rod leaves the rollers, a low-velocity stream of water at a temperature of 100 C flows across the rod. As an expert in thermal-fluids engineering, you are being asked to evaluate the cooling process. Specifically, the manufacturing engineers wish to know the length of the water stream such that film boiling will persist over the entire length of rod cooled by the water.

The transition from film boiling to nucleate boiling occurs at (T_{wall} - T_{sat}) = 30 C. Assume that the rod is at uniform temperature at any cross-section throughout the film boiling process.

(a) Estimate the length L.

(b) Prove that the rod can be modeled as being at uniform temperature over any cross-section.

For the aluminum: $\rho_s = 2770$ kg/m^3, $c_s = 875$ J/kg K, $k_s = 186$ W/m K, $\varepsilon_s = 0.3$
The Stefan-Boltzmann radiation constant is $\sigma_{SB} = 5.67 \times 10^{-8}$ W/m^2 K^4

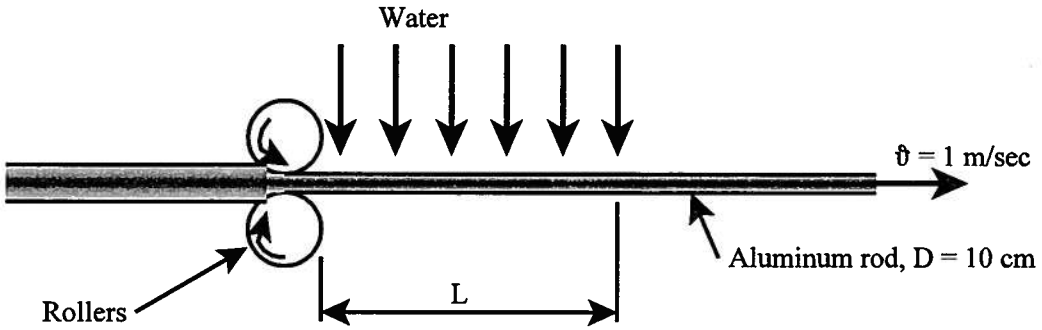

Figure 13P.37

Chapter 14

Mathematical Foundations of the Pure Substance Model

14.1 Introduction

In the previous chapter we treated the pure substance model from a phenomenological point of view. That is, we subjected a pure substance to a series of hypothetical experiments that enabled us to determine qualitatively the general behavior of the pure substance. We then showed how the various phases interact to maintain equilibrium, and we illustrated the use of the properties to determine the thermodynamic behavior of the system.

In this chapter, we shall show that as a consequence of the first and second laws of thermodynamics, the properties of the pure substance model are related to one another by a set of mathematical relations that we call thermodynamic functions. Further, we shall show the influence of this interrelationship on the equilibrium among phases and the manner in which we can develop simple models to describe the behavior of the pure substance model in certain localized domains. We further demonstrate the use of the thermodynamic functions to determine all of the properties of the pure substance model from a minimum number of experimental measurements. Finally, we conclude by establishing the criteria for the stability of thermodynamic systems and the implications of these criteria for the relative magnitudes of certain properties.

14.2 Thermodynamic Functions

Recall that for a closed system we have defined the canonical relation of thermodynamics, equation (13.1), to be

$$du = Tds - Pdv \tag{14.1}$$

where we have written equation (14.1) for a unit mass. The first law of thermodynamics guarantees that u is a property so that equation (14.1) can always be integrated to give the functional relation between the internal energy, the entropy, and the volume. Thus,

$$u = u(s, v) \tag{14.2}$$

where the specific entropy, s, and the specific volume, v, are the independent variables of the function. The *state principle* guarantees that equation (14.1) is complete so that the variables s and v are sufficient to specify completely every equilibrium state of the pure substance for which s and v are actually independent.

14.2.1 Equilibrium States on the Energy Surface

Before we explore the mathematical properties of the energy surface, equation (14.2), and their implications for the thermodynamic properties of a system, it is worth noting that this relation represents all the information concerning the equilibrium states of a system. For example, consider an isolated system comprised of several subsystems separated from one another by various constraints which become internal to the larger composite system. The composite system is initially in an equilibrium state consistent with the constraints. When these internal constraints are removed, the system seeks a new equilibrium state consistent with the requirements for an isolated system, namely that the energy and the volume be constant ($du = 0$ and $dv = 0$). During the run down to equilibrium, the system maximizes the entropy by internal heat transfer and work transfer processes that generate entropy. The final equilibrium state is the state with the largest value of entropy consistent with the fixed value of energy and volume of the original state of the composite system.

Alternatively, the situation can be viewed from an energy perspective. If the entropy and volume are fixed ($ds = 0$ and $dv = 0$), the run down to equilibrium is characterized by the energy seeking a minimum value consistent with the fixed valued of entropy and volume. Since the composite system is no longer constrained with respect to heat transfer, we have from the second law

$$ds = \frac{\delta Q}{T} + \delta s_{gen} = 0 \tag{14.3}$$

Then

$$\delta Q = -T\delta s_{gen} \tag{14.4}$$

Then the first law gives

$$du = \delta Q - \delta W = \delta Q - \cancel{P dv} \tag{14.5}$$

$$du = -T\delta s_{gen} \tag{14.6}$$

Thus, the system decreases in energy as entropy is generated during the run down to equilibrium. In the equilibrium state, the process is complete and the energy decreases no further. Then $du = 0$ and the energy is a minimum for the fixed value of s and v.

The surface represented by equation (14.2) in the three-dimensional space spanned by u, s, and v contains all the equilibrium states of the system and provides all thermodynamic information about the system. That is, all of the equilibrium properties of a system can be derived from this surface, $u = u(s,v)$, and the first and second laws of thermodynamics. The function that represents the surface is holomorphic meaning that it is infinitely often differentiable and can be described by its Taylor series. As we shall see, this type of behavior is extremely important in the determination of the thermodynamic properties from the surface and in the practical determination of the surface from experimental data.

Example 14E.1: As shown in Figure 14E.1(a), a system consists of a rigid volume, $V = 1$ m^3, divided into two compartments, A and B, by a frictionless, adiabatic piston. Initially, the compartments are of equal volume and contain air that can be modeled as an ideal gas with $R = 287$ J/kg K and $c_v = 716$ J/kg K. In the initial state, $T_{A1} = 300$ K and $T_{B1} = 600$ K with $P_{A1} = P_{B1} = 10^5$ N/m^2. Consider the two following situations.

(a) In the first case, the rigid volume is adiabatic so that the composite system consisting of the two compartments constitutes an isolated system with fixed energy ($du = 0$) and fixed volume ($dv = 0$). At some point in time, the adiabatic nature of the piston breaks down and the piston develops a finite value of thermal conductivity greater than zero. Thus, the contents of the two compartments are allowed to experience heat transfer with one another. Determine the equilibrium state and show that during the run down to equilibrium, the entropy of this composite system is maximized and attains its maximum value in the equilibrium state.

(b) In the second case, the rigid volume is no longer adiabatic but the value of entropy is fixed ($ds = 0$) as is the value of the volume ($dv = 0$). Again, the adiabatic nature of the piston breaks down and the piston develops a finite value of thermal conductivity greater than zero. The contents of the two compartments are now allowed to experience heat transfer with one another. Determine the equilibrium state and show that during the run down to equilibrium, the energy of this composite system is minimized and attains its minimum value in the equilibrium state.

(c) Compare the results of parts (a) and (b) above and discuss their differences.

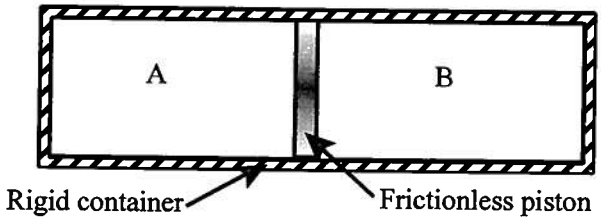

Figure 14E.1(a)

Solution: (a) The mass of the gas on each side of the piston is given by the ideal gas property constitutive relation, viz.

$$m_A = \frac{P_{A1}V_{A1}}{RT_{A1}} = \frac{(10^5 \text{ N/m}^2)(0.50 \text{ m}^3)}{(287 \text{ J/kg K})(300 \text{ K})} = 0.581 \text{ kg}$$

$$m_B = \frac{P_{B1}V_{B1}}{RT_{B1}} = \frac{(10^5 \text{ N/m}^2)(0.50 \text{ m}^3)}{(287 \text{ J/kg K})(600 \text{ K})} = 0.290 \text{ kg}$$

Since the total energy of the composite system is fixed in this case and since the total volume is also fixed, the first law establishes the final equilibrium temperature, viz.

$$\cancel{Q_{1-2}} - \cancel{W_{1-2}} = (U_2 - U_1)_{A+B} = (U_2 - U_1)_A + (U_2 - U_1)_B = 0$$

$$(U_2 - U_1)_A + (U_2 - U_1)_B = m_A c_v (T_2 - T_{A1}) + m_A c_v (T_2 - T_{A1}) = 0$$

$$(0.581 \text{ kg})(716 \text{ J/kg K})(T_2 - 300 \text{ K}) + (0.290 \text{ kg})(716 \text{ J/kg K})(T_2 - 600 \text{ K}) = 0$$

$$T_2 = 400 \text{ K}$$

The equilibrium volume is given by the property constitutive relation and the mechanical equilibrium of the piston, viz.

$$P_{A2} = \frac{m_A RT_{A2}}{V_{A2}} = P_{B2} = \frac{m_B RT_{B2}}{V_{B2}}$$

From the conservation of volume,

$$V_{A2} = 1 - V_{B2}$$

Combining these last two equations and solving for the equilibrium volumes, we get

$$V_{B2} = \frac{m_B RT_2}{m_B RT_2 + m_A RT_2}$$

$$V_{B2} = \frac{(0.290 \text{ kg})(287 \text{ J/kg K})(400 \text{ K})}{(0.290 \text{ kg})(287 \text{ J/kg K})(400 \text{ K}) + (0.581 \text{ kg})(287 \text{ J/kg K})(400 \text{ K})} = 0.333 \text{ m}^3$$

$$V_{A2} = 1 \text{ m}^3 - 0.333 \text{ m}^3 = 0.667 \text{ m}^3$$

These properties define the unique equilibrium state that satisfies the first law and the condition that the temperatures on both sides of the piston be equal. However, if we allow the temperatures on the two sides of the piston to be unequal, there are many combinations of T_{A2} and T_{B2} that will satisfy the first law. A sample of these is shown in Figure 14E.1(b).

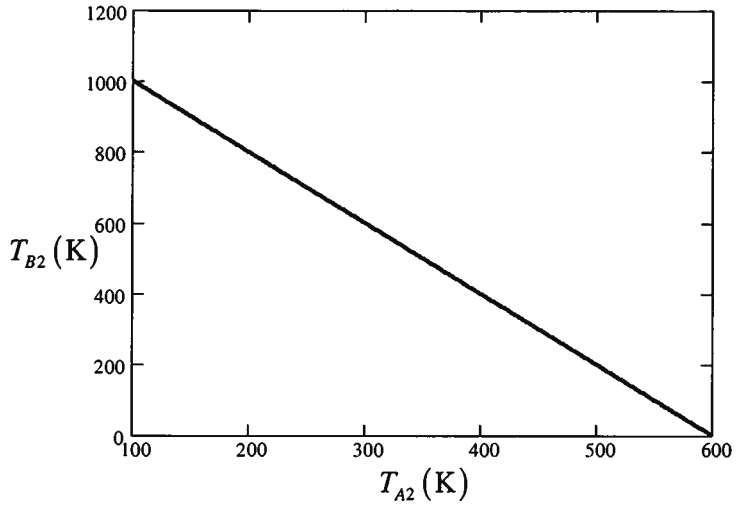

Figure 14E.1(b) Gas Temperatures that Satisfy the First Law

The change in entropy for the composite system that results from the lack of thermal equilibrium between the gases in the two chambers can be determined from the second law applied to the composite system, viz.

$$(S_2 - S_1)_{A+B} = (S_2 - S_1)_A + (S_2 - S_1)_B$$

$$(S_2 - S_1)_{A+B} = m_A c_v \ln\frac{T_{A2}}{T_{A1}} + m_A R \ln\frac{V_{A2}}{V_{A1}} + m_B c_v \ln\frac{T_{B2}}{T_{B1}} + m_B R \ln\frac{V_{B2}}{V_{B1}}$$

If we substitute the temperatures shown in Figure 14E.1(b) into this expression, we obtain the results shown in Figure 14E.1(c).

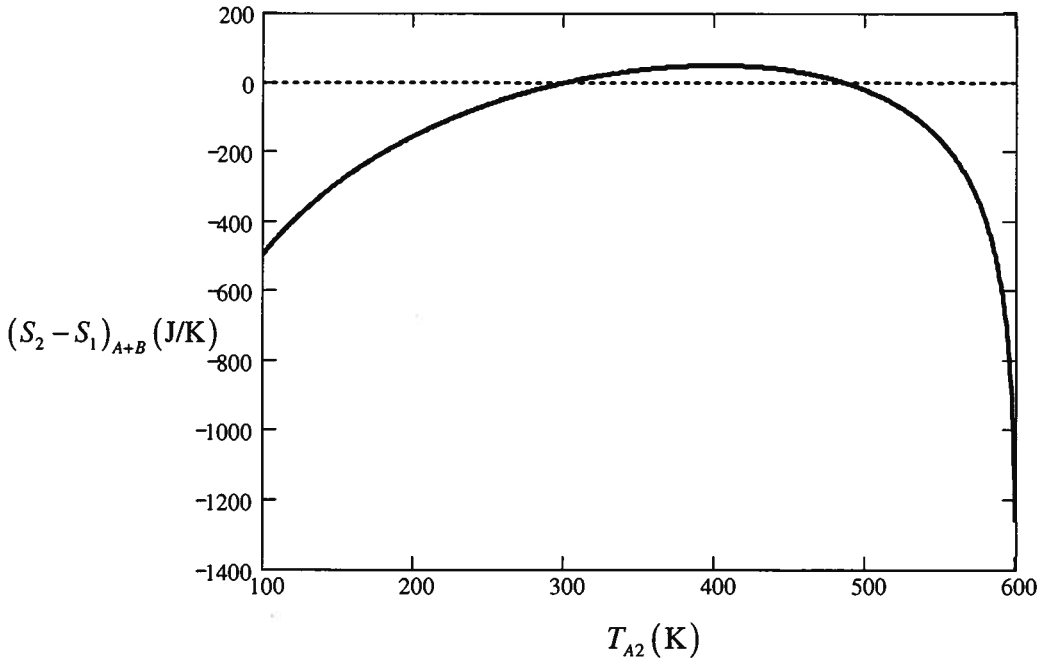

Figure 14E.1(c) Entropy Change in the Composite System

Notice that of the results shown in Figure 14E.1(c), only those for which $(S_2 - S_1)_{A+B} \geq 0$ are physically meaningful. Most importantly, notice that the maximum value for the change in

entropy occurs in the equilibrium state and that in this state, $ds = 0$.

(b) If we now adopt the energy point of view, we have $ds = 0$ and $dv = 0$. The equilibrium state can then be determined by finding the temperature for which the entropy change is zero.

$$(S_2 - S_1)_{A+B} = (S_2 - S_1)_A + (S_2 - S_1)_B = 0$$

$$(S_2 - S_1)_{A+B} = m_A c_v \ln\frac{T_{A2}}{T_{A1}} + m_A R \ln\frac{V_{A2}}{V_{A1}} + m_B c_v \ln\frac{T_{B2}}{T_{B1}} + m_B R \ln\frac{V_{B2}}{V_{B1}} = 0$$

Figure 14E.1(d) shows the values of T_{A2} and T_{B2} that satisfy this constraint. The first law for this situation is

$$Q_{1-2} - \cancel{W_{1-2}} = (U_2 - U_1)_{A+B} = (U_2 - U_1)_A + (U_2 - U_1)_B$$

$$Q_{1-2} = (U_2 - U_1)_A + (U_2 - U_1)_B = m_A c_v (T_2 - T_{A1}) + m_A c_v (T_2 - T_{A1})$$

$$Q_{1-2} = (0.581\text{ kg})(716\text{ J/kg K})(T_2 - 300\text{ K}) + (0.290\text{ kg})(716\text{ J/kg K})(T_2 - 600\text{ K})$$

If we plot the change in energy for the temperatures shown in Figure 14E.1(d), we obtain Figure 14E.1(e). We note that the energy change attains its minimum value in the equilibrium state for which $T_{A2} = 369.49$ K.

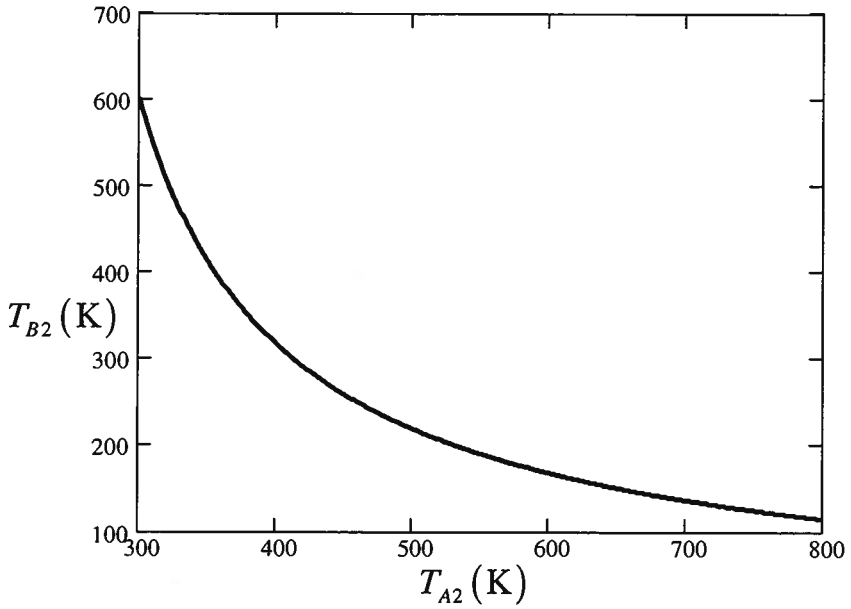

Figure 14E.1(d) Gas Temperatures that Satisfy the Constraint $ds = 0$

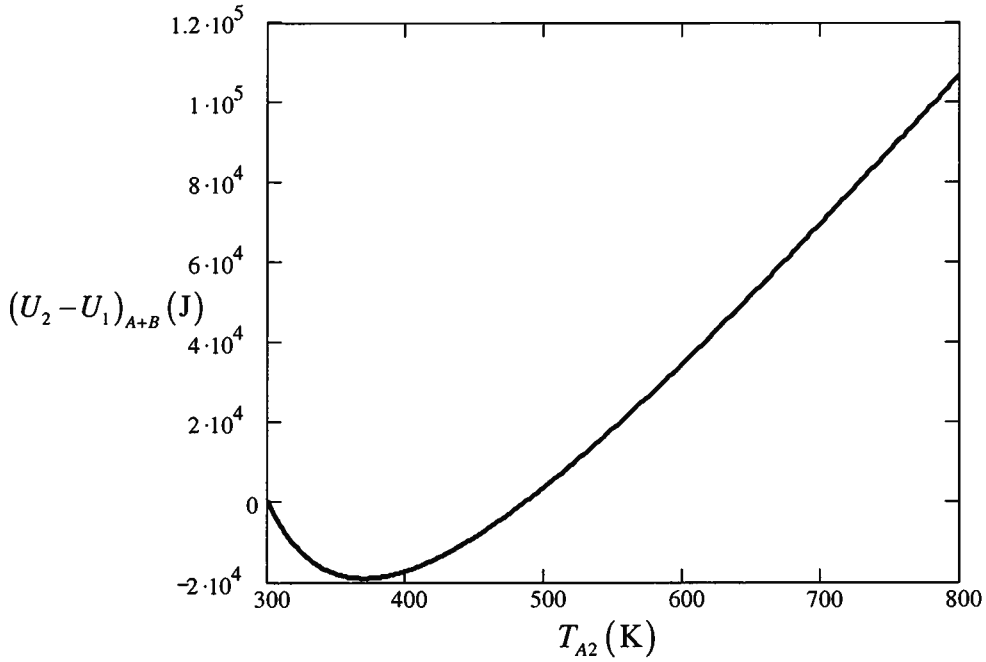

Figure 14E.1(e) Change in Energy of the Composite System

(c) In comparing the results of parts (a) and (b), we note that the equilibrium states for the two cases are different which is to be expected since the constraints on the system are different for the two cases. In part (a) the system is isolated and no heat transfer is allowed; however, in part (b), the system is no longer isolated with respect to heat transfer and the system ends up in a lower energy state. In each case, we are looking at a particular plane that intersects the surface described by the characteristic function. In the first case the surface is $s = s(u,v)$ and we are looking at the states on a plane u = constant [Figure 14E.1(c)]. We note that the equilibrium state is the one for which the entropy is maximum on this plane. In the second case, the surface is $u = u(s,v)$ and we are looking at states on a plane s = constant [Figure 14E.1(e)]. The equilibrium state is the one for which the energy is minimum on this plane.

14.2.2 Mathematical Properties of the Energy Surface

Equation (14.2) implies mathematically that the internal energy is a state function and that we could write the total differential of the internal energy in the form

$$du = \left(\frac{\partial u}{\partial s}\right)_v ds + \left(\frac{\partial u}{\partial v}\right)_s dv \tag{14.7}$$

Upon comparing equations (14.1) and (14.7), we conclude that the following identities must exist, viz.

$$T \equiv \left(\frac{\partial u}{\partial s}\right)_v \quad \text{and} \quad -P \equiv \left(\frac{\partial u}{\partial v}\right)_s \tag{14.8}$$

In an abstract mathematical sense, these identities can be taken as the *definitions* of temperature and pressure. These definitions are abstract in that they presuppose the existence of the function $u(s,v)$. In a practical sense, the reverse is true. That is, we must first have working definitions of temperature and pressure in order to establish the actual function $u(s,v)$ from experimental data.

In the canonical relation, equation (14.1), we observe that the thermal variables (properties) T and s are associated in a single term (the reversible heat transfer interaction).

Although so associated, the variables (properties) T and s are different in nature in that the temperature is *intensive* and *dependent* while the entropy is *extensive* and *independent*. For these reasons, the variables (properties) T and s are termed *conjugate*. For analogous reasons, the mechanical variables (properties) P and v are also termed conjugate. Note that in each conjugate pair of variables the intensive property, T or P, acts as the "force"(or the potential) for the associated interaction, heat transfer or work transfer, and the extensive property is the "displacement" i.e., the quantity that is transferred across the system boundary during the interaction.

If we examine equations (14.2), (14.7) and (14.1), we see that equation (14.2) contains all of the information necessary to completely specify all reversible interactions for a given path for the pure substance in terms of the independent properties s and v. The temperature and the pressure are obtained from equations (14.8) in terms of s and v. Thus, the reversible heat transfer, and the reversible work transfer for a given path are completely specified in terms of s and v, viz.

$$(Q_{1-2})_{rev} = \int_1^2 Tds = \int_1^2 \left(\frac{\partial u}{\partial s}\right)_v ds \tag{14.9}$$

$$(W_{1-2})_{rev} = \int_1^2 Pdv = \int_1^2 \left(\frac{\partial u}{\partial v}\right)_s dv \tag{14.10}$$

Note that although equations (14.9) and (14.10) are path dependent, the first law guarantees that their difference is not path dependent. As a consequence, the canonical relation is an exact differential. That is, if we consider two different equilibrium states 1 and 2 on the surface $u = u(s,v)$ and we proceed from state 1 to state 2 along two different paths A and B, the values of the integrals in equations (14.9) and (14.10) will be different so that

$$\left[(Q_{1-2})_{rev}\right]_{pathA} \neq \left[(Q_{1-2})_{rev}\right]_{pathB} \quad \text{and} \quad \left[(W_{1-2})_{rev}\right]_{pathA} \neq \left[(W_{1-2})_{rev}\right]_{pathB} \tag{14.11}$$

However, the first law of thermodynamics guarantees that

$$\left[(Q_{1-2})_{rev} - (W_{1-2})_{rev}\right]_{pathA} = \left[(Q_{1-2})_{rev} - (W_{1-2})_{rev}\right]_{pathB} \tag{14.12}$$

14.2.3 The Characteristic Thermodynamic Functions and the Legendre Transformation

Since $u(s,v)$ interrelates both pairs of the conjugate variables (properties) for the two reversible energy transfer interactions, the function $u(s,v)$ may be thought of as a complete constitutive relation for the pure substance. In contrast, given T and P, in order to have the same information as is implied by $u(s,v)$, we must have both T as a function of s and v, *i.e.*, $T(s,v)$, and P as a function of s and v, *i.e.*, $P(s,v)$. The function $T(s,v)$ is necessary to integrate Tds (the reversible heat transfer) and the function $P(s,v)$ is necessary to integrate Pdv (the reversible work transfer).

A single thermodynamic function of one thermal variable (T or s) and one mechanical variable (P or v) that yields the two conjugate variables (s or T) and (v or P) by partial differentiation is called a *characteristic thermodynamic function.* Thus, $u(s,v)$ is one such function. A characteristic thermodynamic function contains complete information about the thermodynamic properties of a pure substance and is therefore a complete constitutive relation for the substance. Given the set of four variables (properties) s, v, T, and P, we can construct four such characteristic thermodynamic functions by taking different pairs of properties as independent. The choices of pairs that will lead to the four possible characteristic functions are:

$$s,v \quad s,P \quad T,v \quad T,P$$

Each characteristic function is the integral of an exact differential expression similar to the

canonical relation, equation (14.1). The corresponding characteristic thermodynamic functions for the pairs of properties given above are, in the order given, the internal energy, u, the enthalpy, h, the Helmholtz free energy, f, and the Gibbs free energy, g.

We can think of the independent variables (properties) as a set of coordinates, so that the various characteristic thermodynamic functions should be obtainable from one another by means of a suitable transformation of coordinates. This transformation can be readily executed by employing the Legendre transformation (*cf.* Callen, H. B., *Thermodynamics and an Introduction to Thermostatistics*, 2nd edition, John Wiley, New York, 1985, pp. 137 – 145.). The Legendre transformation leads us to the following rule for transforming the canonical relation:

> To replace one of the independent variables (properties) in an exact differential such as the canonical relation with its conjugate variable (property), subtract from the differential of the dependent variable the differential of the product of the two conjugate variables (properties).

Thus, starting with the differential of the internal energy and applying the rule to each variable (property) in turn, we obtain the three other characteristic functions. In particular, we obtain the second characteristic function by replacing v with P, viz.

$$du - d\left[(-P)v\right] = d\left(u + Pv\right) = Tds - Pdv + Pdv + vdP \tag{14.13}$$

This simplifies to

$$dh = Tds + vdp \tag{14.14}$$

where we have made use of the definition of the specific enthalpy, viz.

$$h \equiv u + Pv \tag{14.15}$$

Equation (14.14) can then be integrated to give the characteristic thermodynamic function

$$h = h\left(s, P\right) \tag{14.16}$$

By comparing the total differential of equation (14.16) with equation (14.14), we obtain the identities

$$T = \left(\frac{\partial h}{\partial s}\right)_P \quad \text{and} \quad v = \left(\frac{\partial h}{\partial P}\right)_s \tag{14.17}$$

Observe that in applying the rule for the transformation of independent variables (properties) we have carefully associated the proper sign with the variable as required by the canonical form, equation (14.1). For example we used $(-P)$ instead of P. The third characteristic function is obtained by replacing s with T, viz.

$$du - d\left(Ts\right) = d\left(u - Ts\right) = Tds - Pdv - Tds - sdT \tag{14.18}$$

which simplifies to

$$df = -sdT - Pdv \tag{14.19}$$

where we have made use of the definition of the specific *Helmholtz free energy*, f, viz.

$$f \equiv u - Ts \tag{14.20}$$

Integration of equation (14.19) then gives the characteristic function

$$f = f\left(T, v\right) \tag{14.21}$$

and the identities

$$-s=\left(\frac{\partial f}{\partial T}\right)_s \quad \text{and} \quad -P=\left(\frac{\partial f}{\partial v}\right)_s \tag{14.22}$$

The fourth characteristic function and the associated relations are obtained by replacing v with $-P$ and s with T, viz.

$$du-d\left[(-P)v\right]-d\left(Ts\right)=Tds-Pdv+Pdv+vdP-Tds-sdT \tag{14.23}$$

$$d\left(u+Pv-Ts\right)=d\left(h-Ts\right)=dg=-sdT+vdP \tag{14.24}$$

where we have made use of the definition of the specific *Gibbs free energy*, g. viz.

$$g\equiv h-Ts \tag{14.25}$$

Integration of equation (14.25) yields the characteristic thermodynamic function

$$g=g\left(T,P\right) \tag{14.26}$$

with the definitions

$$-s=\left(\frac{\partial g}{\partial T}\right)_P \quad \text{and} \quad v=\left(\frac{\partial g}{\partial P}\right)_T \tag{14.27}$$

14.3 Maxwell Relations

The first and second laws of thermodynamics guarantee that the quantities *u, h, f,* and g are themselves properties and that variations in these properties can be expressed as exact differentials. When these properties are expressed in terms of the proper set of conjugate variables (properties), they become characteristic functions, and the conjugate variables (properties) can be obtained from the coefficients of the differentials of the independent variables (properties). Since the total differential of a property is an exact differential, the second-order partial derivatives of the dependent variables (properties) are symmetric. This implies that the order of partial differentiation is immaterial so that the mixed second-order partial derivatives are equal. That is, given an analytic function $z = z(x,y)$ with an exact differential dz,

$$\left\{\frac{\partial}{\partial x}\left[\left(\frac{\partial z}{\partial y}\right)\right]_x\right\}_y=\left\{\frac{\partial}{\partial y}\left[\left(\frac{\partial z}{\partial x}\right)\right]_y\right\}_z \tag{14.28}$$

If we apply this requirement to the canonical relation, equation (14.1), we obtain

$$\left\{\frac{\partial}{\partial v}\left[\left(\frac{\partial u}{\partial s}\right)\right]_v\right\}_s=\left\{\frac{\partial}{\partial s}\left[\left(\frac{\partial u}{\partial v}\right)\right]_s\right\}_v \tag{14.29}$$

Substituting equations (14.8) into equation (14.29), we have

$$\left(\frac{\partial T}{\partial v}\right)_s=-\left(\frac{\partial P}{\partial s}\right)_v \tag{14.30}$$

Similarly, for the enthalpy, equation (14.16), we have

$$\left\{\frac{\partial}{\partial P}\left[\left(\frac{\partial h}{\partial s}\right)\right]_P\right\}_s=\left\{\frac{\partial}{\partial s}\left[\left(\frac{\partial h}{\partial P}\right)\right]_s\right\}_P \tag{14.31}$$

Substituting equations (14.17) into equation (14.31), we obtain

$$\left(\frac{\partial T}{\partial P}\right)_s=\left(\frac{\partial v}{\partial s}\right)_P \tag{14.32}$$

For the Helmholtz free energy, equation (14.20), we have

$$\left\{\frac{\partial}{\partial T}\left[\left(\frac{\partial f}{\partial v}\right)\right]_T\right\}_v = \left\{\frac{\partial}{\partial v}\left[\left(\frac{\partial f}{\partial T}\right)\right]_v\right\}_T \tag{14.33}$$

Substitution of equations (14.22) into equation (14.33) yields

$$-\left(\frac{\partial P}{\partial T}\right)_v = -\left(\frac{\partial s}{\partial v}\right)_T \tag{14.34}$$

Finally, for the Gibbs free energy, equation (14.25), we have

$$\left\{\frac{\partial}{\partial P}\left[\left(\frac{\partial g}{\partial T}\right)\right]_P\right\}_T = \left\{\frac{\partial}{\partial T}\left[\left(\frac{\partial g}{\partial P}\right)\right]_T\right\}_P \tag{14.35}$$

Substituting equations (14.27) into equation (14.35), we obtain

$$-\left(\frac{\partial s}{\partial P}\right)_T = \left(\frac{\partial v}{\partial T}\right)_P \tag{14.36}$$

The four equations (14.30), (14.32), (14.34) and (14.36) are known as the Maxwell relations in honor of James Clerk Maxwell (1831 – 1879) who presented them formally in a lecture on thermodynamic surfaces in 1876. These expressions show that the properties *s, v, T,* and *P* are interrelated while equations (14.8), (14.17), (14.22), and (14.27) relate these four properties to the characteristic thermodynamic functions (complete constitutive relations).

Notice that these partial differential relations, the Maxwell relations, have a certain symmetry to them. On one side of the equal sign, the numerator contains a thermal property (either *s* or *T*) while the denominator contains a mechanical property (either *P* or *v*) with the conjugate thermal property held constant. On the other side of the equal sign, the numerator contains a mechanical property (either *P* or *v*) while the denominator contains a thermal property (either *s* or *T*) with the conjugate mechanical property held constant. As we shall soon see, the Maxwell relations contain a wealth of information regarding the physical behavior of substances. For this reason, it is useful to summarize them in a systematic manner as shown in Table 14.1. It is worth noting that the mathematical relations summarized in Table 14.1 provide more than just a formal mathematical relationship amongst the various properties that we use to describe the thermodynamic behavior of substances. In particular, the Maxwell relations provide a metric of the thermodynamic coupling that exists in the substance to which they are applied. For example, as we shall soon show for the case of the incompressible fluid model, which is uncoupled, all four Maxwell relations reduce to zero, a sure indication of uncoupled behavior. For the pure substance, in general, each of the Maxwell relations provides specific information about some aspect of thermodynamic coupling. Equation (14.45) provides the classic measure of coupling, the magnitude of the temperature change that results from an isentropic expansion. Equation (14.46) gives the magnitude of the volume change that results from a heat transfer to the substance at constant pressure. Equation (14.47) gives the pressure increase that results from a temperature increase at constant volume. Equation (14.48) reveals the expansion of the substance as the temperature increases at constant pressure.

Most importantly, these eight equations taken together enable us to evaluate a complete and consistent set of thermodynamic properties from experimental measurements of a minimal number of properties. They also make it possible for us to determine the values of certain thermodynamic properties that cannot be measured directly. We now proceed to illustrate the utility of the relations contained in Table 14.1.

Table 14.1
Thermodynamic Relations

I. The characteristic thermodynamic functions

Property	*Characteristic Function*	*Exact Differential*	
$u = u$	$u = u(s,v)$	$du = Tds - Pdv$	(14.37)
$h = u + Pv$	$h = h(s,P)$	$dh = Tds + vdP$	(14.38)
$f = u - Ts$	$f = f(T,v)$	$df = -sdT - Pdv$	(14.39)
$g = h - Ts$	$g = g(T,P)$	$dg = -sdT + vdP$	(14.40)

II. The first partial derivatives of the characteristic functions

$$T = \left(\frac{\partial u}{\partial s}\right)_v = \left(\frac{\partial h}{\partial s}\right)_P \tag{14.41}$$

$$-P = \left(\frac{\partial u}{\partial v}\right)_s = \left(\frac{\partial f}{\partial v}\right)_T \tag{14.42}$$

$$-s = \left(\frac{\partial f}{\partial T}\right)_v = \left(\frac{\partial g}{\partial T}\right)_P \tag{14.43}$$

$$v = \left(\frac{\partial h}{\partial P}\right)_s = \left(\frac{\partial g}{\partial P}\right)_T \tag{14.44}$$

III. The symmetric, mixed second partial derivatives of the characteristic functions, the Maxwell relations

$$\frac{\partial^2 u}{\partial s \partial v} = \left(\frac{\partial T}{\partial v}\right)_s = -\left(\frac{\partial P}{\partial s}\right)_v \tag{14.45}$$

$$\frac{\partial^2 h}{\partial s \partial P} = \left(\frac{\partial T}{\partial P}\right)_s = \left(\frac{\partial v}{\partial s}\right)_P \tag{14.46}$$

$$\frac{\partial^2 f}{\partial T \partial v} = -\left(\frac{\partial s}{\partial v}\right)_T = -\left(\frac{\partial P}{\partial T}\right)_v \tag{14.47}$$

$$\frac{\partial^2 g}{\partial T \partial P} = -\left(\frac{\partial s}{\partial P}\right)_T = \left(\frac{\partial v}{\partial T}\right)_P \tag{14.48}$$

Example 14E.2: The Clapeyron relation, equation (13.45), gives the slope of the locus of two-phase states on the *P-T* plane, viz.

$$\left(\frac{dP}{dT}\right)_{sat} = \frac{h_{fg}}{Tv_{fg}}$$

In section 13.12, we derived this relation from the fact that the Gibbs free energy per unit mass for a two-phase state was the same value for the two phases, $g_f = g_g$. Show that the Clapeyron relation also can be derived directly from one of Maxwell's equations.

Solution: An alternate method of deriving the Clapeyron relation involves the use of one of Maxwell's relations, equation (14.47), viz.

$$\left(\frac{\partial s}{\partial v}\right)_T = \left(\frac{\partial P}{\partial T}\right)_v$$

The left side of equation (14.47) represents the change in entropy per unit change in volume for an isothermal change of state. Thus for isothermal change of phase, the left side of equation (14.47) becomes

$$\left(\frac{\partial s}{\partial v}\right)_T = \frac{s_g - s_f}{v_g - v_f}$$

If we substitute this expression into equation (14.47), we obtain

$$\left(\frac{\partial P}{\partial T}\right)_v = \frac{s_g - s_f}{v_g - v_f}$$

For the case in which there are two phases in equilibrium, the left side of this expression becomes an ordinary derivative since the pressure is a function of the temperature only. Furthermore, the intersection of a plane of constant volume and the P-v-T surface in the two phase region is a a single line representing the locus of two-phase states. Then

$$\left(\frac{dP}{dT}\right)_{sat} = \frac{s_{fg}}{v_{fg}}$$

Again, substitution of equation (13.14) into this equation yields equation (13.45).

14.4 Calculation of Thermodynamic Properties from P-v-T Data and Partial Derivatives

From a phenomenological point of view, we have already discussed in considerable detail the thermodynamic behavior of the pure substance model. We have shown how this behavior can be demonstrated by experiment. We also have shown how we can use the properties of the pure substance model, in tabular or graphical form, to evaluate the response of the pure substance model to various processes. However, this approach presupposes that by some means we have already established the properties of the pure substance. The most obvious method to establish these properties is by direct measurement; however, there are certain properties that cannot be readily measured, and we must rely on some other indirect method for their evaluation. This indirect method takes advantage of the interrelationships that exist between properties that can be measured and those that cannot. In fact, the formation of this indirect method is one of the motives for developing the relations of Sections 14.2 and 14.3.

The properties most readily and accurately measured are the pressure, specific volume, and temperature. These three properties together form the P-v-T data and the P-v-T surface that we have already discussed in detail. In addition to measurements of P-v-T data, the various partial derivatives of the P-v-T surface are often measured directly. The most readily measured partial derivatives are the coefficient of thermal expansion, $(1/v)(\partial v/\partial T)_P$, the isothermal compressibility, $-(1/v)(\partial v/\partial P)_T$, and the constant-volume pressure coefficient, $(1/P)(\partial P/\partial T)_v$.

Although P-v-T data are usually the most accurate and readily available thermodynamic properties, these data by themselves are not sufficient to formulate a complete constitutive relation (characteristic thermodynamic function) for the substance. A minimum amount of

thermal data must be combined with the P-v-T data to complete the constitutive relations and specify the internal energy, the enthalpy, and the entropy. Normally the specific heats at zero pressure are the most reliable data for this purpose. Other thermal data which may be useful are the specific heat at constant pressure, the specific heat at constant volume, the Joule-Thomson coefficient, and the constant-temperature coefficient.

14.4.1 Definitions of Partial Differential Coefficients

A number of useful properties are defined in terms of various partial derivatives of the thermodynamic functions for the pure substance.

The *specific heat at constant volume* is a property defined by the partial derivative

$$c_v \equiv \left(\frac{\partial u}{\partial T}\right)_v \tag{14.49}$$

For a quasi-static constant volume process in a pure substance, the first law of thermodynamics shows that the property c_v relates the differential heat transfer interaction to the differential change in the temperature. Thus,

$$(\delta Q)_{\substack{quasi-static \\ constant\ volume}} - mPdv = mdu \tag{14.50}$$

If we write $u = u(T,v)$, the change in the internal energy for an infinitesimal change of state at constant volume can be written

$$du = \left(\frac{\partial u}{\partial T}\right)_v dT + \cancel{\left(\frac{\partial u}{\partial v}\right)_T dv} = c_v dT$$

since dv is zero. Then equation (14.50) becomes

$$(\delta Q)_{\substack{quasi-static \\ dv=0}} = mc_v dT \tag{14.51}$$

Thus, physically, the specific heat at constant volume represents the quasi-static heat transfer per unit temperature change per unit mass for a system whose volume is held constant, viz.

$$c_v = \frac{1}{m}\frac{(\delta Q)_{\substack{quasi-static \\ dv=0}}}{dT} \tag{14.52}$$

The *specific heat at constant pressure* is a property defined by the partial derivative

$$c_P = \left(\frac{\partial h}{\partial T}\right)_P \tag{14.53}$$

For a quasi-static process in a pure substance at constant pressure, the first law of thermodynamics shows that the property c_P relates the differential heat transfer interaction to the differential temperature change.

$$(\delta Q)_{\substack{quasi-static \\ constant\ pressure}} - mPdv = mdu \tag{14.54}$$

Since the pressure is constant, equation (14.54) can be written

$$(\delta Q)_{\substack{quasi-static \\ dP=o}} = m\left[du + d(Pv)\right] = mdh \tag{14.55}$$

If we write $h = h(T,P)$, the total differential of the enthalpy in this case becomes

$$dh = \left(\frac{\partial h}{\partial T}\right)_P dT + \cancel{\left(\frac{\partial h}{\partial P}\right)_T dP} = c_P dT \tag{14.56}$$

since dP is zero. Then equation (14.55) can be written in the form

$$(\delta Q)_{\substack{quasi-static \\ dP=o}} = mc_P dT \tag{14.57}$$

which may be rearranged to give

$$c_P = \frac{1}{m}\frac{(\delta Q)_{\substack{quasi-static \\ dP=0}}}{dT} \tag{14.58}$$

Thus, physically the specific heat at constant pressure represents the quasi-static heat transfer per unit temperature change per unit mass for a system whose pressure is held constant.

The *Joule-Thomson coefficient,* μ_{JT}, is the property that gives the increase in the temperature per unit increase in the pressure for a process in which the enthalpy remains constant. Thus,

$$\mu_{JT} = \left(\frac{\partial T}{\partial P}\right)_h \tag{14.59}$$

The *constant-temperature coefficient,* c_T, is the property that gives the increase in the enthalpy per unit increase in the pressure for an isothermal process. Thus,

$$c_T = \left(\frac{\partial h}{\partial P}\right)_T \tag{14.60}$$

The *coefficient of thermal expansion,* β, is the property that gives the fractional increase in the specific volume per unit increase in the temperature while the substance remains at a constant pressure. Hence,

$$\beta = \frac{1}{v}\left(\frac{\partial v}{\partial T}\right)_P \tag{14.61}$$

This property, β, is a measure of the coupling between the thermal property temperature and the mechanical property volume.

The *isothermal compressibility, K,* is the property which gives the fractional decrease in the specific volume per unit increase in the pressure while the substance remains at a constant temperature. Thus,

$$K = -\frac{1}{v}\left(\frac{\partial v}{\partial P}\right)_T \tag{14.62}$$

This property, K, is a measure of the compressibility of the substance in the absence of any thermal effects due to temperature changes. In a sense, this property is the "isothermal spring constant".

14.4.2 Mathematical Relations Between Partial Derivatives

In order to be able to use successfully the differential relations amongst thermodynamic properties summarized in Table 14.1, we need to recall several relations particularly useful for the manipulation of variables as previously developed in the differential calculus of a function of two variables. The most useful are:

the reciprocal relation:

$$\left(\frac{\partial x}{\partial y}\right)_z = \frac{1}{\left(\partial y / \partial x\right)_z} \tag{14.63}$$

the chain rule:

$$\left(\frac{\partial x}{\partial y}\right)_z = \left(\frac{\partial x}{\partial w}\right)_z \Big/ \left(\frac{\partial y}{\partial w}\right)_z \tag{14.64}$$

the cyclical relation:

$$\left(\frac{\partial x}{\partial y}\right)_z \left(\frac{\partial y}{\partial z}\right)_x \left(\frac{\partial z}{\partial x}\right)_y = -1 \tag{14.65}$$

In addition, the substitution rule is often useful. For example, suppose there exists a function $z = z(x,y)$ with total differential

$$dz = \left(\frac{\partial z}{\partial x}\right)_y dx + \left(\frac{\partial z}{\partial y}\right)_y dy \tag{14.66}$$

If we wish to reformulate the function $z(x,y)$ in terms of properties w and y as independent variables, we first write the implicit relation for z in terms of the new variables, viz.

$$z = z(w, y) \tag{14.67}$$

and the total differential expressed in terms of the new set of independent variables, viz.

$$dz = \left(\frac{\partial z}{\partial w}\right)_y dw + \left(\frac{\partial z}{\partial y}\right)_w dy \tag{14.68}$$

In order to eliminate the old independent variable x in equation (14.66), we write x in terms of the new independent variables w and y, viz.

$$x = x(w, y) \tag{14.69}$$

with the total differential

$$dx = \left(\frac{\partial x}{\partial w}\right)_y dw + \left(\frac{\partial x}{\partial y}\right)_w dy \tag{14.70}$$

Substituting equation (14.70) into equation (14.66), we obtain

$$dz = \left(\frac{\partial z}{\partial w}\right)_y \left[\left(\frac{\partial x}{\partial w}\right)_y dw + \left(\frac{\partial x}{\partial y}\right)_w dy\right] + \left(\frac{\partial z}{\partial y}\right)_w dy \tag{14.71}$$

or

$$dz = \left[\left(\frac{\partial z}{\partial x}\right)_y \left(\frac{\partial x}{\partial w}\right)_y\right] dw + \left[\left(\frac{\partial z}{\partial x}\right)_y \left(\frac{\partial x}{\partial y}\right)_w + \left(\frac{\partial z}{\partial y}\right)_x\right] dy \tag{14.72}$$

But equation (14.72) must give the same value for dz as equation (14.68) for all values of dw and dy. Hence, the coefficients of dw and dy must be equal. Equating the coefficients, we obtain

the substitution rule:

$$\left(\frac{\partial z}{\partial w}\right)_y = \left(\frac{\partial z}{\partial x}\right)_y \left(\frac{\partial x}{\partial w}\right)_y \tag{14.73}$$

and

$$\left(\frac{\partial z}{\partial y}\right)_w = \left(\frac{\partial z}{\partial y}\right)_x + \left(\frac{\partial z}{\partial x}\right)_y \left(\frac{\partial x}{\partial y}\right)_w \tag{14.74}$$

14.4.3 Guidelines for the Manipulation of Thermodynamic Properties

The results of the preceding sections provide the mathematical basis for the relations amongst equilibrium thermodynamic properties and their derivatives. We now provide a set of guidelines for the manipulation of these properties from one form to another. Typically, as we shall show in the next section, the properties available for such manipulations are in the form of

P-v-T relationships. It is convenient, then, to express the derivatives of the properties in these terms. Following the example of Callen (Callen, H. B., *Thermodynamics and an Introduction to Thermostatistics*, 2nd edition, John Wiley, New York, 1985, pp. 186 – 189.), we offer the following set of guidelines that have been shown to be useful for this purpose:

1. If any of the derivatives contain any of the properties *f*, *g*, *h*, and *u*, bring them one by one to the numerator and eliminate them by means of equations (14.41) through (14.44) or the substitution rule and equations (14.37) through (14.40).

2. If any of the derivatives contain the entropy, bring it to the numerator by means of one of the mathematical relations for partial derivatives. If one of the four Maxwell relations, equations (14.45) through (14.48), does not eliminate the entropy, use the chain rule for partial derivatives to obtain a partial derivative of the form $\partial s/\partial T$. This derivative is then one of the specific heats, equations (14.49) and (14.53).

3. Now eliminate the dependent variable (property) of the *P-v-T* formulation by bringing it to the numerator by means of the cyclic relation and the chain rule. If the *P-v-T* formulation is in the form $v(P,T)$, eliminate the volume in this manner. Conversely, if the *P-v-T* formulation is in the form $P(v,T)$, eliminate the pressure in this manner. The remaining derivatives are now expressed in terms of the derivatives of the *P-v-T* formulation.

4. The original derivatives have now been expressed in terms of c_v, c_P and the derivatives of the *P-v-T* formulation. If desired, one of the specific heats can be eliminated by the equation

$$c_P - c_v = \frac{Tv\beta^2}{\kappa} \tag{14.75}$$

or

$$c_P - c_v = \frac{T\left[\left(\frac{\partial P}{\partial T}\right)_v\right]^2}{-\left(\frac{\partial P}{\partial v}\right)_T} \tag{14.76}$$

Example 14E.3: (a) Show that the Joule-Thomson coefficient can be expressed in the following form:

$$\mu_{JT} \equiv \left(\frac{\partial T}{\partial P}\right)_h = \frac{v}{c_P}(\beta T - 1)$$

(b) Show that for the ideal gas model, the Joule-Thomson coefficient is identically zero.

Solution: Following guideline number 1, we bring the enthalpy to the numerator with the aid of the cyclical relation, equation (14.65), viz.

$$\mu_{JT} = \left(\frac{\partial T}{\partial P}\right)_h = -\frac{\left(\frac{\partial h}{\partial P}\right)_T}{\left(\frac{\partial h}{\partial T}\right)_P} = -\frac{\left(\frac{\partial h}{\partial P}\right)_T}{c_P}$$

For the numerator in the above expression, we make use of the substitution rule, equation (14.74)

in the following manner. We write $h = h(T,P)$.
Then

$$h = h(T,P)$$

$$dh = \left(\frac{\partial h}{\partial T}\right)_P dT + \left(\frac{\partial h}{\partial P}\right)_T dP$$

From equation (14.38) we have

$$dh = Tds + vdP$$

If we now write $s = s(T,P)$, we have

$$s = s(T,P)$$

$$ds = \left(\frac{\partial s}{\partial T}\right)_P dT + \left(\frac{\partial s}{\partial P}\right)_T dP$$

We now substitute this result into the exact differential for the enthalpy to get

$$dh = T\left[\left(\frac{\partial s}{\partial T}\right)_P dT + \left(\frac{\partial s}{\partial P}\right)_T dP\right] + vdP = \left(\frac{\partial h}{\partial T}\right)_P dT + \left(\frac{\partial h}{\partial P}\right)_T dP$$

$$dh = T\left(\frac{\partial s}{\partial T}\right)_P dT + \left[T\left(\frac{\partial s}{\partial P}\right)_T + v\right] dP = \left(\frac{\partial h}{\partial T}\right)_P dT + \left(\frac{\partial h}{\partial P}\right)_T dP$$

Equating coefficients, We get

$$T\left(\frac{\partial s}{\partial T}\right)_P = \left(\frac{\partial h}{\partial T}\right)_P = c_P$$

where we have made use of equation (14.53) and

$$\left(\frac{\partial h}{\partial P}\right)_T = T\left(\frac{\partial s}{\partial P}\right)_T + v = -T\left(\frac{\partial v}{\partial T}\right)_P + v$$

where we have made use of one of the Maxwell relations, equation (14.48). Then using equation (14.53) for the denominator of the Joule-Thomson coefficient, we have

$$\mu_{JT} = \left(\frac{\partial T}{\partial P}\right)_h = \frac{1}{c_P}\left[T\left(\frac{\partial v}{\partial T}\right)_P - v\right]$$

From the definition of the coefficient of thermal expansion, equation (14.61), the first term in square brackets becomes

$$\left(\frac{\partial v}{\partial T}\right)_P = \beta v$$

Then the Joule-Thomson coefficient becomes

$$\mu_{JT} = \left(\frac{\partial T}{\partial P}\right)_h = \frac{1}{c_P}\left[T\left(\frac{\partial v}{\partial T}\right)_P - v\right] = \frac{v}{c_P}(\beta T - 1)$$

(b) For the ideal gas model, $Pv = RT$ and the coefficient of thermal expansion becomes

$$(\beta)_{\substack{ideal \\ gas}} = \frac{1}{v}\left(\frac{\partial v}{\partial T}\right)_P = \frac{1}{v}\frac{\partial}{\partial T}\left(\frac{RT}{P}\right)_P = \frac{1}{v}\left(\frac{R}{P}\right) = \frac{1}{T}$$

Then the Joule-Thomson coefficient for the ideal gas model becomes

$$(\mu_{JT})_{\substack{ideal \\ gas}} = \left(\frac{\partial T}{\partial P}\right)_h = \frac{v}{c_P}(\beta T - 1) = \frac{v}{c_P}\left(\frac{1}{T}T - 1\right) = \frac{v}{c_P}(1-1) = 0$$

Example 14E.4: As shown in Figure 14E.4, a rigid, adiabatic container is divided into two chambers of equal volume by means of a frictionless adiabatic piston. One chamber contains a unit mass of gas at a pressure of P_1 and a temperature of T_1 while the other chamber is evacuated. The piston is held in the initial position by means of a pin. The pin is removed and the gas expands to a new volume V_2.

(a) Show that the temperature change experienced by the gas is given by

$$T_2 - T_1 = \int_{v_1}^{v_2} \left[\frac{P}{c_v} - \frac{T\beta}{c_v \kappa} \right] dv$$

(b) Show that the temperature change for the ideal gas model is identically zero.

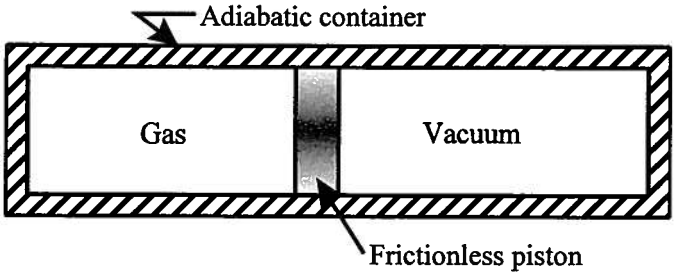

Figure 14E.1 Free Expansion of a Gas

Solution: (a) Consider the system consisting of the gas. Given the nature of the boundary of this system, there is no heat transfer experienced by the gas during the motion of the piston. Also, since there is no force exerted by the vacuum on the piston, there is no work transfer experienced by the gas even though there is motion of the boundary. Then from the first law, the energy of the gas is constant. Then the temperature change of the gas is given by

$$dT = \left(\frac{\partial T}{\partial v} \right)_u dv$$

Following guideline number 1, we have

$$\left(\frac{\partial T}{\partial v} \right)_u = -\frac{\left(\frac{\partial u}{\partial v} \right)_T}{\left(\frac{\partial u}{\partial T} \right)_v} = -\frac{1}{c_v} \left(\frac{\partial u}{\partial v} \right)_T$$

where we have made use of equation (14.49). We now write the internal energy as a function the volume and the temperature, viz.

$$u = u(v,T)$$

$$du = \left(\frac{\partial u}{\partial v} \right)_T dv + \left(\frac{\partial u}{\partial T} \right)_v dT$$

However, the canonical relation also gives an expression for the differential of the internal energy, viz.

$$du = Tds - Pdv$$

If we now write the entropy as a function of the volume and the temperature, we have

$$s = s(v,T)$$

$$ds = \left(\frac{\partial s}{\partial v}\right)_T dv + \left(\frac{\partial s}{\partial T}\right)_v dT$$

We now substitute this last expression into the canonical relation to get

$$du = T\left[\left(\frac{\partial s}{\partial v}\right)_T dv + \left(\frac{\partial s}{\partial T}\right)_v dT\right] - Pdv = \left[T\left(\frac{\partial s}{\partial v}\right)_T - P\right]dv + T\left(\frac{\partial s}{\partial T}\right)_v dT$$

Equating coefficients in the two expressions for the differential in the internal energy, we get

$$T\left(\frac{\partial s}{\partial T}\right)_v = \left(\frac{\partial u}{\partial T}\right)_v = c_v$$

and

$$\left(\frac{\partial u}{\partial v}\right)_T = T\left(\frac{\partial s}{\partial v}\right)_T - P = T\left(\frac{\partial P}{\partial T}\right)_v - P$$

where we have made use of Maxwell relation (14.47). From the cyclical relation, equation (14.65), we have

$$\left(\frac{\partial P}{\partial T}\right)_v = -\frac{\left(\frac{\partial v}{\partial T}\right)_P}{\left(\frac{\partial v}{\partial P}\right)_T} = \frac{\beta v}{\kappa v} = \frac{\beta}{\kappa}$$

where we have made use of equations (14.61) and (14.62). Then the temperature change during the free expansion of the gas becomes

$$dT = -\frac{1}{c_v}\left(T\frac{\beta}{\kappa} - P\right)dv$$

$$T_2 - T_1 = \int_{v_1}^{v_2}\left(\frac{P}{c_v} - \frac{\beta T}{c_v \kappa}\right)dv$$

(b) For the ideal gas model

$$\beta = \frac{1}{v}\frac{\partial}{\partial T}\left(\frac{RT}{P}\right)_P = \frac{1}{v}\left(\frac{R}{P}\right) = \frac{1}{T}$$

$$\kappa = -\frac{1}{v}\frac{\partial}{\partial P}\left(\frac{RT}{P}\right)_T = \frac{1}{v}\left(\frac{RT}{P^2}\right) = \frac{1}{P}$$

Then

$$(T_2 - T_1)_{\substack{ideal \\ gas}} = \int_{v_1}^{v_2}\left(\frac{P}{c_v} - \frac{\beta T}{c_v \kappa}\right)dv = \int_{v_1}^{v_2}\left(\frac{P}{c_v} - \frac{PT}{c_v T}\right)dv = \int_{v_1}^{v_2}\left(\frac{P}{c_v} - \frac{P}{c_v}\right)dv = 0$$

14.5 Determination of the Characteristic Functions from *P-v-T* Formulations

The problem of determining the complete and consistent constitutive relation for a pure substance will illustrate the use of the thermodynamic and mathematical relations that we have just enumerated. Normally, the starting point is the *P-v-T* data for the substance. These data are obtained by measuring the equilibrium pressure and the corresponding equilibrium temperature

for a measured mass of the substance contained in a vessel of known volume. The P-v-T data can be measured with the best accuracy since the volume is the easiest extensive property to measure, and the intensive properties P and T are uniform at equilibrium. Next, curve fitting techniques are used (in three dimensions) to smooth the experimental P-v-T data. This must be done with accuracy in the derivatives of the P-v-T surface since these derivatives are necessary to determine the other properties.

In principle the P-v-T data are fitted with an explicit analytical function with sufficient accuracy for the determination of the entropy and the internal energy or the enthalpy. This explicit analytical function is the P-v-T constitutive relation and is usually called the equation of state for the substance. The ideal situation would be to have a single P-v-T function (equation of state) that can be valid for the solid, liquid, and vapor phases; however, the P-v-T behavior of the various phases is so significantly different that the development of a single P-v-T function (equation of state) valid for all three phases is virtually impossible to achieve. The common approach is to develop P-v-T functions that are valid only for certain regions of the P-v-T surface. It is then necessary for us to insure that these different P-v-T functions match at the boundaries of the various regions – a difficult task that involves matching not only the properties themselves but their derivatives as well. More recently, improved computational capabilities have allowed the formulation of a characteristic function directly from experimental data (*cf.* Keenan, J. H., Keyes, F. G., Hill, P. G., and Moore, J. G., *Steam Tables*, John Wiley, New York, 1969, p. 134.). With this technique it has been possible to describe both liquid and vapor phases with a single equation which yields all of the other thermodynamic properties by appropriate differentiation.

The problem of evaluation of properties can be simplified considerably if we use simple models that embody the essential features of certain limited regions of the P-v-T surface of the pure substance. These simple models are expressed as simplified equations of state (P-v-T functions) which actually form subclasses of the more general pure substance model. In the following sections, we develop in a more formal manner than heretofore, two such models that represent two important regions of the P-v-T surface, namely the incompressible fluid model and the ideal gas model.

14.5.1 Incompressible Fluid Model

For example, in the liquid phase region of the P-v-T surface we note that the specific volume is relatively insensitive to changes in pressure and temperature. That is, it is necessary to change the pressure or temperature by very large amounts in order to effect a significant change in volume. Since in many engineering situations the temperature and pressure changes are relatively small, we can safely model the behavior of liquids in these cases by a fluid of constant specific volume known as the *incompressible fluid.*

The equation of state which defines the incompressible fluid is simply

$$v = \text{constant} \tag{14.77}$$

The P-v-T surface is thus a plane perpendicular to the specific volume axis, and all equilibrium states of the fluid lie on this plane. Thus, the two derivatives $(\partial v/\partial T)_P$ and $(\partial v/\partial P)_T$ are both zero which means the coefficient of thermal expansion, β, and the isothermal compressibility, κ, are identically zero. When we employ this model in actual engineering situations, we allow the intersection of this plane with the specific volume axis to shift from one location to another, depending upon the circumstances. In this sense, the specific volume at the point of intersection represents the average specific volume of the fluid suitable for the prevailing conditions of pressure and temperature.

In spite of the extreme simplicity of the model, it is very useful in many engineering situations; therefore, it is important to establish its properties. Specifically these are the enthalpy,

the internal energy, and the entropy. Since we have an equation of state of the form $v(T,P)$, we seek expressions for the properties of the form $h(T,P)$, $u(T,P)$, and $s(T,P)$. To determine $h(P,T)$ we integrate

$$dh = \left(\frac{\partial h}{\partial P}\right)_T dP + \left(\frac{\partial h}{\partial T}\right)_P dT \tag{14.78}$$

The coefficient $(\partial h/\partial T)_P$ is by definition c_P, equation (14.53). The coefficient $(\partial h/\partial P)_T$ is expressed in terms of the P-v-T formulation by using the substitution technique, equations (14.70) through (14.74), on the characteristic function equation (14.38), viz.

$$dh = Tds + vdP \tag{14.79}$$

Equation (14.79) implies $h(s,P)$ which we must reformulate as $h(T,P)$. To change the independent property from s to T, we consider $s(T,P)$ which implies the total differential of s is

$$ds = \left(\frac{\partial s}{\partial T}\right)_P dT + \left(\frac{\partial s}{\partial P}\right)_T dP \tag{14.80}$$

Substituting for ds in equation (14.79), we have

$$dh = \left[T\left(\frac{\partial s}{\partial P}\right)_T + v\right]dP + T\left(\frac{\partial s}{\partial T}\right)_P dT \tag{14.81}$$

Thus, comparing equations (14.78) and (14.81) we have

$$\left(\frac{\partial h}{\partial T}\right)_P = c_P = T\left(\frac{\partial s}{\partial T}\right)_P \tag{14.82}$$

and

$$\left(\frac{\partial h}{\partial P}\right)_T = T\left(\frac{\partial s}{\partial P}\right)_T + v \tag{14.83}$$

When we use the Maxwell relation, equation (14.48), we have

$$\left(\frac{\partial h}{\partial P}\right)_T = v - T\left(\frac{\partial v}{\partial T}\right)_P \tag{14.84}$$

Equation (14.78) then becomes

$$dh = \left[v - T\left(\frac{\partial v}{\partial T}\right)_P\right]dP + c_P dT \tag{14.85}$$

Since the coefficient of thermal expansion for the incompressible fluid is identically zero, equation (14.85) reduces further to

$$dh = vdP + c_P dT \tag{14.86}$$

Since v is constant and the second mixed partial derivatives are equal,

$$\frac{\partial}{\partial P}\left[\left(\frac{\partial h}{\partial T}\right)_P\right]_T = \frac{\partial}{\partial T}\left[\left(\frac{\partial h}{\partial P}\right)_T\right]_P \tag{14.87}$$

$$\left[\frac{\partial}{\partial P}c_P\right]_T = T\left(\frac{\partial^2 v}{\partial T^2}\right)_P = 0 \tag{14.88}$$

which implies that c_P is a function of temperature only. Equation (14.86) can then be integrated simply to give

$$h_2 - h_1 = v(P_2 - P_1) + \int_{T_1}^{T_2} c_P(T)\,dT \tag{14.89}$$

From the definition of h we get $u = h - Pv$. Thus,

$$u_2 - u_1 = \int_{T_1}^{T_2} c_P(T)\,dT \tag{14.90}$$

Equation (14.91) now can be used to evaluate c_v, viz.

$$c_v = \left(\frac{\partial u}{\partial T}\right)_v = c_P \tag{14.91}$$

Hence, for the incompressible fluid the specific heat c_v and the specific heat c_P are the same. Therefore, the incompressible fluid has a specific heat, c, that must be a function of the temperature only. Equation (14.90) then becomes

$$u_2 - u_1 = \int_{T_1}^{T_2} c(T)\,dT \tag{14.92}$$

Often the temperature dependence of the specific heat is weak and the specific heat can be taken to be constant so that equation (14.92) can be integrated simply to obtain the energy constitutive relation of the incompressible fluid as presented earlier in Section 4.4, viz.

$$u_2 - u_1 = c(T_2 - T_1) \tag{14.93}$$

The entropy of the incompressible fluid can be determined by integrating equation (14.80). When equation (14.82) and the Maxwell relation, equation (14.48), are substituted, equation (14.80) then becomes

$$ds = -\left(\frac{\partial v}{\partial T}\right)_P dP + \frac{c_P}{T} dT \tag{14.94}$$

Again since the coefficient of thermal expansion of the incompressible fluid is identically zero, equation (14.94) reduces to

$$ds = \frac{c(T)}{T} dT \tag{14.95}$$

Integrating equation (14.95), we have

$$s_2 - s_1 = \int_{T_1}^{T_2} \frac{c(T)}{T} dT \tag{14.96}$$

Again, if the temperature dependence of the specific heat is weak, it can be treated as a constant and equation (14.96) can be integrated to obtain the entropy constitutive relation of the incompressible fluid as presented earlier in Section 4.4, viz.

$$s_2 - s_1 = c \ln \frac{T_2}{T_1} \tag{14.97}$$

Equations (14.93) and (14.97) show that the equilibrium properties of the incompressible fluid are identical to those of a pure thermal system, equations (3.9) and (7.44). Since the specific volume is constant, the reversible work transfer associated with the normal displacement of the boundary of an incompressible pure substance is zero. That is,

$$W_{1-2} = m \int_{v_1}^{v_2} P dv = 0 \tag{14.98}$$

Then the first law of thermodynamics for reversible processes in the incompressible fluid is identical to that of the pure thermal system, viz.

$$Q_{1-2} = U_2 - U_1 = m \int_{T_1}^{T_2} c dT \tag{14.99}$$

since the normal displacement of the boundary is the only relevant work transfer. In spite of its simplicity, the incompressible fluid model finds widespread use in predicting the thermodynamic

behavior of liquid systems. It is particularly useful in the science of fluid mechanics since compressibility effects are often negligible, and the uncoupled mechanical aspects associated with the bulk motion of the fluid are dominant.

Example 14E.5: Consider the situation in which a viscous incompressible fluid is flowing at a steady rate through a well-insulated horizontal tube.

(a) Show that the temperature of the fluid must increase in the direction of flow.

(b) Estimate the magnitude of the effect for water modeled as an incompressible fluid.

Solution: (a) Consider a control volume consisting of the fluid inside the tube that lies between planes normal to the tube axis located at x and $x+dx$. The first law for this control volume is given by

$$\cancel{\delta Q} - \cancel{\delta W_{shaft}} + dh + \vartheta d\vartheta + g dz = 0$$

Since the kinetic energy of the flow and the gravitational potential energy of the flow are constant, the first law reduces to

$$dh = 0$$

This implies that h = constant. Since the fluid is viscous, we can expect a pressure drop in the direction of flow; thus, $dP < 0$. Then the temperature change in the direction of flow is given by

$$dT = \left(\frac{\partial T}{\partial P}\right)_h dP$$

But

$$\left(\frac{\partial T}{\partial P}\right)_h = -\frac{\left(\frac{\partial h}{\partial P}\right)_T}{\left(\frac{\partial h}{\partial T}\right)_P} = -\frac{1}{c_P}\left(\frac{\partial h}{\partial P}\right)_T = -\frac{1}{c_P}\left[v - T\left(\frac{\partial v}{\partial T}\right)_P\right] = -\frac{v}{c_P}$$

where we have made use of equation (14.84). Since the coefficient of thermal expansion of the incompressible fluid is identically zero, we have

$$dT = -\frac{v}{c_P} dP$$

Since $dP < 0$ in the direction of flow, it follows from the above result that $dT > 0$ in the direction of flow. Notice that this result could have also been obtained directly from the first law and the characteristic function form of the enthalpy, viz.

$$dh = 0 = Tds + vdP$$

For the incompressible fluid model, the entropy has a unique form for its constitutive relation, viz.

$$ds = \frac{c_P}{T} dT$$

$$c_P dT = -v dP$$

$$dT = -\frac{v}{c_P} dP$$

(b) For water, $v = 10^{-3}$ m^3/kg and $c_P = 4187$ J/kg K. Then

$$dT = -\frac{v}{c_P} dP = -\frac{10^{-3}\ \text{m}^3/\text{kg}}{4187\ \text{J/kg K}} dP = -\left(2.388 \times 10^{-7}\ \text{K m}^2/\text{N}\right) dP$$

Clearly, the pressure drop would have to be very, very large for the temperature change to be

anything significant.

14.5.2 Ideal Gas Model

The ideal gas model is the simple model for the P-v-T behavior of the vapor phase of the pure substance. The ideal gas model is an approximation of the behavior of the vapor phase that steadily improves as the pressure approaches zero. In fact, it describes exactly the behavior of a vapor in the limit of zero pressure. As previously cited in Chapter 4, the P-v-T constitutive relation (equation of state) for a unit mass of an ideal gas is

$$Pv = RT \tag{14.100}$$

This P-v-T surface is a hyperbolic paraboloid.

This unusually simple form of the P-v-T constitutive relation for the ideal gas model, equation (14.100), is responsible for its simple thermodynamic behavior. One of the significant aspects of this behavior is the fact that both the internal energy and the enthalpy depend on the temperature only. We can illustrate this fact by the following arguments. Let us assume that the pressure and the internal energy are functions of the temperature and the volume. Then,

$$P = P(T,v) \quad \text{and} \quad u = u(T,v) \tag{14.101}$$

The total differential du is then

$$du = \left(\frac{\partial u}{\partial T}\right)_v dT + \left(\frac{\partial u}{\partial v}\right)_T dv \tag{14.102}$$

The coefficient $(\partial u/\partial T)_v$ is by definition c_v, equation (14.49). The coefficient $(\partial u/\partial v)_T$ is expressed in the P-v-T formulation by using the substitution rule on equation (14.37), viz.

$$du = Tds - Pdv \tag{14.103}$$

Assuming that there exists a function $s(T,v)$, we obtain

$$ds = \left(\frac{\partial s}{\partial T}\right)_v dT + \left(\frac{\partial s}{\partial v}\right)_T dv \tag{14.104}$$

Substituting equation (14.104) into equation (14.103), we obtain

$$du = T\left(\frac{\partial s}{\partial T}\right)_v + \left[T\left(\frac{\partial s}{\partial v}\right)_T - P\right]dv \tag{14.105}$$

Comparing equations (14.102) and (14.105), we obtain

$$\left(\frac{\partial u}{\partial T}\right)_v = c_v = T\left(\frac{\partial s}{\partial T}\right)_v \tag{14.106}$$

and

$$\left(\frac{\partial u}{\partial v}\right)_T = T\left(\frac{\partial s}{\partial v}\right)_T - P \tag{14.107}$$

Substituting one of the Maxwell relations, equation (14.47), into equation (14.107), we obtain

$$\left(\frac{\partial u}{\partial v}\right)_T = T\left(\frac{\partial P}{\partial T}\right)_v - P \tag{14.108}$$

From the ideal gas equation of state, equation (14.100), we get

$$\left(\frac{\partial P}{\partial T}\right)_v = \frac{R}{v} \tag{14.109}$$

Substituting equations (14.109) and (14.100) into equation (14.108), we obtain

$$\left(\frac{\partial u}{\partial v}\right)_T = \frac{RT}{v} - P = P - P = 0 \tag{14.110}$$

Thus, the internal energy is independent of the volume, and equation (14.102) reduces to

$$du = c_v dT \tag{14.111}$$

which permits us to write

$$c_v = \frac{du}{dT} \tag{14.112}$$

Hence, for the ideal gas model, the partial derivative of equation (14.106) reduces to an ordinary derivative. Equation (14.111) can be integrated simply to give

$$u_2 - u_1 = \int_{T_1}^{T_2} c_v dT \tag{14.113}$$

From the definition of enthalpy, $h = u + Pv$, we have from equation (14.113)

$$h_2 - h_1 = R(T_2 - T_1) + \int_{T_1}^{T_2} c_v dT \tag{14.114}$$

Differentiation of equation (14.114) with respect to T gives

$$\frac{dh}{dT} = R + c_v \tag{14.115}$$

which we have already stated without proof in equation (5.66). In an alternate method of deriving the energy and enthalpy of an ideal gas, we assume that the volume and the enthalpy are functions of temperature and pressure, viz.

$$v = v(T,P) \quad \text{and} \quad h = h(T,P) \tag{14.116}$$

The total differential dh is then

$$dh = \left(\frac{\partial h}{\partial T}\right)_P dT + \left(\frac{\partial h}{\partial P}\right)_T dP \tag{14.117}$$

This is the same formulation that we employed for the incompressible fluid. By using the substitution rule on the characteristic function, we obtained equations (14.82) through (14.85) which are generally applicable for this formulation in terms of T and P. We need only form the appropriate partial derivatives of the ideal gas equation of state, $v(T,P)$ and substitute them into the equations. The ideal gas equation of state yields

$$\left(\frac{\partial v}{\partial T}\right)_P = \frac{R}{P} \tag{14.118}$$

Thus, equation (14.84) becomes

$$\left(\frac{\partial h}{\partial P}\right)_T = v - \frac{RT}{P} = v - v = 0 \tag{14.119}$$

and the enthalpy of the ideal gas model is independent of pressure. Therefore, equation (14.85) reduces to

$$dh = c_P dT \tag{14.120}$$

which permits us to write

$$c_P = \frac{dh}{dT} \tag{14.121}$$

Thus, for the ideal gas model the partial derivative of equation (14.82) becomes an ordinary derivative, and equation (14.120) can be integrated to give

$$h_2 - h_1 = \int_{T_1}^{T_2} c_P dT \tag{14.122}$$

In general, the specific heats c_P and c_v are functions of temperature. As a typical example, the specific heat c_v for a gas composed of diatomic molecules is shown in Figure 14.1 as a function of temperature.

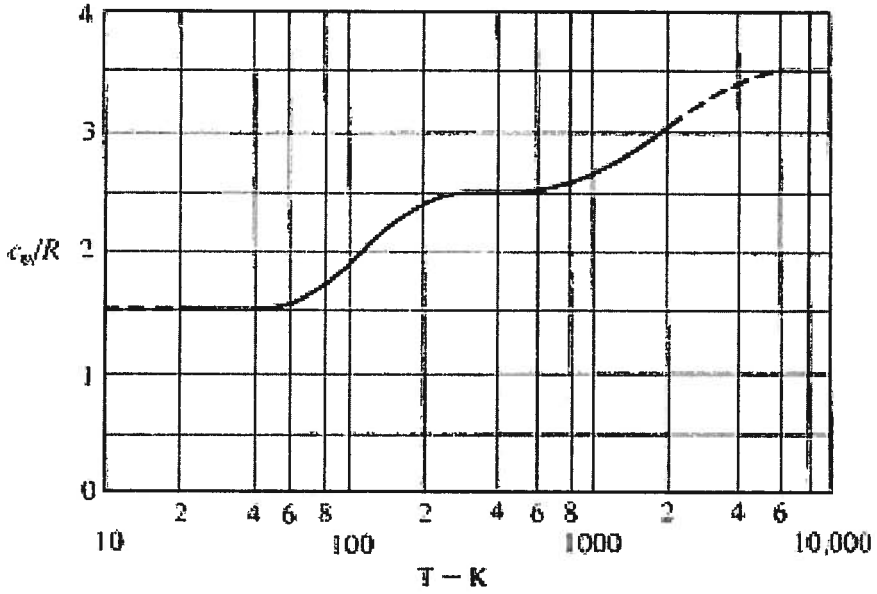

Figure 14.1 Specific Heat at Constant Volume for the Diatomic Ideal Gas Model
(from *Introduction to Modern Physics,* Richmyer and Kennard, 1947, by permission McGraw-Hill Book Co.)

The simple classical statistical mechanical model for the ideal gas shows that the specific heat c_v is related to the number of mechanical coordinates, n, required to specify the mechanical state of a single molecule by the relation

$$c_v = \frac{n}{2} R \tag{14.123}$$

In Figure 14.1 the three plateaus for which the specific heat is constant over a temperature range correspond to temperature regions within which the bahavior of the gas is well represented by the classical statistical mechanics model. For the lowest temperature plateau, the required mechanical coordinates are simply the three translational coordinates. In the middle plateau, two rotational coordinates are necessary in addition to three translational coordinates. In the highest plateau, additional coordinates are necessary because of a vibration between the two atoms in the diatomic molecule. A quantum statistical mechanical model is necessary to represent adequately the behavior of the specific heat in the regions between the classical specific heat plateaus. Quantum statistics predicts the occupation of the energy levels associated with rotation and vibration of the molecule as the temperature of the gas is increased. In more complex molecules the regions of classical behavior are eliminated by overlapping regions of quantum mechanical behavior.

In spite of its limitations for more complex molecules, the classical microscopic model of the ideal gas gives useful results for ideal gases composed of simple molecules. For example the specific heat

$$c_v = \frac{3}{2}R \tag{14.124}$$

is quite accurate for monatomic ideal gases over a wide range of temperatures, while the specific heat

$$c_v = \frac{5}{2}R \tag{14.125}$$

is quite accurate for diatomic ideal gases over a wide range of temperatures. In addition, this model shows that the specific heat ratio, $\gamma = c_P/c_v$, should vary from a maximum of 5/3 for a monatomic gas to a limit of unity for a gas composed of complex molecules, such as a hydrocarbon.

$$1.67 \geq \gamma > 1 \tag{14.126}$$

For most of the common gases the quantum mechanical model has been worked out in detail from spectroscopic measurements. The evaluation of the ideal gas specific heat or internal energy for the substance from this microscopic model is a numerical procedure, and the results are presented in tabular form. These results for a number of common gases have been collected in hard copy form (Keenan, J. H. and Kaye, J., *Gas Tables*, John Wiley, New York, 1948) and electronic form (*cf.* http://webbook.nist.gov/chemistry/ published by the National Institute for Standards and Technology). The ideal gas specific heats have also been empirically curve fitted with simple functions of temperature over a limited range of temperature. These specific functions are usually given in thermodynamic data books (*cf.* Hilsenrath, Joseph, et al., *Tables of Thermodynamic and Transport Properties*, Pergamon Press, New York, 1960 and *Data Book,* Thermophysical Properties Research Center Purdue University, Lafayette, Indiana, 1964, Vol. 2, Chapter 5.).

There are in common use two formulations of the entropy of the ideal gas that depend on the particular set of properties considered independent. In one case, we have $s(v,T)$ while in the other we have $s(P,T)$. Let us now consider the first possibility, $s(v,T)$. Then

$$ds = \left(\frac{\partial s}{\partial v}\right)_T dv + \left(\frac{\partial s}{\partial T}\right)_v dT \tag{14.127}$$

From equation (14.106) it follows that

$$\left(\frac{\partial s}{\partial T}\right)_v = \frac{c_v}{T} \tag{14.128}$$

From the Maxwell relation of equation (14.47) we have

$$\left(\frac{\partial s}{\partial v}\right)_T = \left(\frac{\partial P}{\partial T}\right)_v \tag{14.129}$$

Then combining equations (14.127), (14.128), and (14.129), we obtain

$$ds = \left(\frac{\partial P}{\partial T}\right)_v dv + \frac{c_v}{T}dT \tag{14.130}$$

For the ideal gas we can substitute equation (14.109) into equation (14.130), viz.

$$ds = \frac{R}{v}dv + \frac{c_v}{T}dT \tag{14.131}$$

Integrating equation (14.131), we obtain

$$s_2 - s_1 = R \ln \frac{v_2}{v_1} + \int_{T_1}^{T_2} \frac{c_v}{T} dT \tag{14.132}$$

Now consider the second possibility $s(T,P)$. Then,

$$ds = \left(\frac{\partial s}{\partial T}\right)_P dT + \left(\frac{\partial s}{\partial P}\right)_T \tag{14.133}$$

From equation (14.82), it follows that

$$\left(\frac{\partial s}{\partial T}\right)_P = \frac{c_P}{T} \tag{14.134}$$

From the Maxwell relation of equation (14.48), we have

$$\left(\frac{\partial s}{\partial P}\right)_T = -\left(\frac{\partial v}{\partial T}\right)_P \tag{14.135}$$

Then combining equations (14.133), (14.134), and (14.135), we obtain

$$ds = -\left(\frac{\partial v}{\partial T}\right)_P dP + \frac{c_P}{T} dT \tag{14.136}$$

For the ideal gas we can substitute equation (14.119) into equation (14.136) to obtain

$$ds = -\frac{R}{P} dP + \frac{c_P}{T} dT \tag{14.137}$$

Integrating equation (14.137), we obtain the entropy constitutive relation for the ideal gas model, viz.

$$s_2 - s_1 = -R \ln \frac{P_2}{P_1} + \int_{T_1}^{T_2} \frac{c_P}{T} dT \tag{14.138}$$

In the more general case, the specific heat is a function of temperature only and the integral in equation (14.132) or equation (14.138) depends only upon T_1 and T_2. If we define a function $\phi(T)$ by the relation

$$\phi(T) = \int_{T=T_0}^{T} \frac{c_P}{T} dT \tag{14.139}$$

then equation (14.138) becomes

$$s_2 - s_1 = -R \ln \frac{P_2}{P_1} + \phi(T_2) - \phi(T_1) \tag{14.140}$$

The function $\phi(T)$ has been evaluated for a number of common gases and is given in the tabulation by Keenan and Kaye (Keenan, J. H. and Kaye, J., *Gas Tables*, John Wiley, New York, 1948). The use of the function $\phi(T)$ and equation (14.138) makes the calculation of entropy changes for the ideal gas with variable specific heats as simple as those with constant specific heats. The *Gas Tables* also tabulate functions for rapid calculation of the pressure and volume ratios for isentropic (constant entropy) processes of an ideal gas with variable specific heats. A complete explanation and further reference in the use of these functions can be found in the *Gas Tables*. The use of these tabulations has become somewhat obsolete in recent years in light of the software available for personal computers, particularly the databases available from NIST.

If the states of interest lie in a region where the temperature dependence of the specific heat is weak, we can treat the specific heat as a constant and integrate equations (14.111), (14.114), (14.132), and (14.138), respectively

$$u_2 - u_1 = c_v (T_2 - T_1) \tag{14.141}$$

$$h_2 - h_1 = c_P (T_2 - T_1) \tag{14.142}$$

$$s_2 - s_1 = R \ln \frac{v_2}{v_1} + c_v \ln \frac{T_2}{T_1} \tag{14.143}$$

and

$$s_2 - s_1 = c_P \ln \frac{T_2}{T_1} - R \ln \frac{P_2}{P_1} \tag{14.144}$$

which we have stated previously in the context of the constitutive relations for the ideal gas model.

Example 14E.6: The speed of sound, a, in a pure substance is defined as

$$a^2 \equiv \left(\frac{\partial P}{\partial \rho} \right)_s$$

(a) Show that for the ideal gas model the speed of sound becomes

$$a^2 = \gamma RT$$

where $\gamma = c_P/c_v$.

(b) Calculate the speed of sound in Nitrogen at a temperature of $T = 300$ K and a pressure of $P = 1 \times 10^5$ N/m^2. For nitrogen $R = 296.81$ J/kg K and $\gamma = 1.4$.

Solution: (a) Note that the Maxwell relations and the characteristic functions are given in terms of v not ρ. Then it is worthwhile to express the definition of the speed of sound in terms of v instead of ρ, viz.

$$\left(\frac{\partial P}{\partial \rho} \right)_s = \left(\frac{\partial P}{\partial v} \right)_s \left(\frac{dv}{d\rho} \right)_s$$

Since $\rho = 1/v$,

$$\left(\frac{d\rho}{dv} \right)_s = -\frac{1}{v^2}$$

and

$$a^2 = -v^2 \left(\frac{\partial P}{\partial v} \right)_s$$

Then following guideline number 2, we get

$$a^2 = \left(\frac{\partial P}{\partial v} \right)_s \left(\frac{dv}{d\rho} \right)_s = -v^2 \frac{-\left(\frac{\partial s}{\partial v} \right)_P}{\left(\frac{\partial s}{\partial P} \right)_v} = v^2 \frac{\left(\frac{\partial s}{\partial T} \right)_P \left(\frac{\partial T}{\partial v} \right)_P}{\left(\frac{\partial s}{\partial T} \right)_v \left(\frac{\partial T}{\partial P} \right)_v} = v^2 \frac{c_P}{c_v} \frac{\left(\frac{\partial T}{\partial v} \right)_P}{\left(\frac{\partial T}{\partial P} \right)_v}$$

For the ideal gas model, the partial derivatives appearing above are given by

$$\left(\frac{\partial T}{\partial v} \right)_P = \frac{\partial}{\partial v} \left(\frac{Pv}{R} \right)_P = \frac{P}{R}$$

$$\left(\frac{\partial T}{\partial P} \right)_v = \frac{\partial}{\partial P} \left(\frac{Pv}{R} \right)_v = \frac{v}{R}$$

Then

$$a^2 = \gamma v^2 \frac{P}{R} \frac{R}{v} = \gamma Pv = \gamma RT$$

(b) Substituting the appropriate values, we get

$$a = \sqrt{(1.4)(296.81 \text{ J/kg K})(300 \text{ K})} = 353.07 \text{ m/sec}$$

This value is quite close to the value given in NIST Database 23, viz. a = 353.16 m/sec. Note that the value of the speed of sound for the ideal gas model depends only upon temperature and is independent of pressure. The pure substance model shows that this not the case. For example, at a temperature of T = 300 K and a pressure of $P = 10^7$ N/m^2, the value given in NIST Database 23 is a = 379.52 m/sec. Thus, we have further proof that the ideal gas model is limited in its applicability to states at low pressure.

Example 14E.7: In the combustion chamber of an internal combustion engine, nitrogen gas, a natural component of the air used in the combustion process, experiences a change of state 1 → 2 such that T_1 = 300 K, $P_1 = 10^5$ N/m^2 and T_2 = 1500 K, $P_2 = 6 \times 10^5$ N/m^2. Model the nitrogen as an ideal gas and calculate the change in entropy of the gas taking into account the temperature dependence of the specific heat. From the NIST Chem Web Book, the Shomate correlation for the specific heat is given by

$$c_{P0}(T) = \frac{1000 \text{ K}}{M}\left(A + Bt + Ct^2 + Dt^3 + \frac{E}{t^2}\right)$$

where t = T(K)/1000 K, M is the molecular weight of nitrogen (28.013 kg/kg-mole) and

$$A = 26.09200 \text{ J/kg-mole (K/1000)}$$

$$B = 8.218801 \text{ J/kg-mole (K/1000)}$$

$$C = -1.976141 \text{ J/kg-mole (K/1000)}$$

$$D = 0.159274 \text{ J/kg-mole (K/1000)}$$

$$E = 0.044434 \text{ J/kg-mole (K/1000)}$$

Solution: The function c_{P0} is shown in Figure 14E.7. From equation (14.139), we have

$$\phi(T_2) - \phi(T_1) = \int_{T_1}^{T_2} \frac{c_{P0}(T)}{T} dT = \frac{100 \text{ K}}{M} \int_{t_1}^{t_2} \frac{c_{P0}(t)}{t} dt$$

$$\phi(1500 \text{ K}) - \phi(300 \text{ K}) = \frac{100 \text{ K}}{28.013 \text{ kg/kg-mole}} \int_{0.3}^{1.5} \left(\frac{A}{t} + B + Ct + Dt^2 + \frac{E}{t^3}\right) dt$$

$$\phi(1500 \text{ K}) - \phi(300 \text{ K}) = 1.790 \times 10^3 \text{ J/kg K}$$

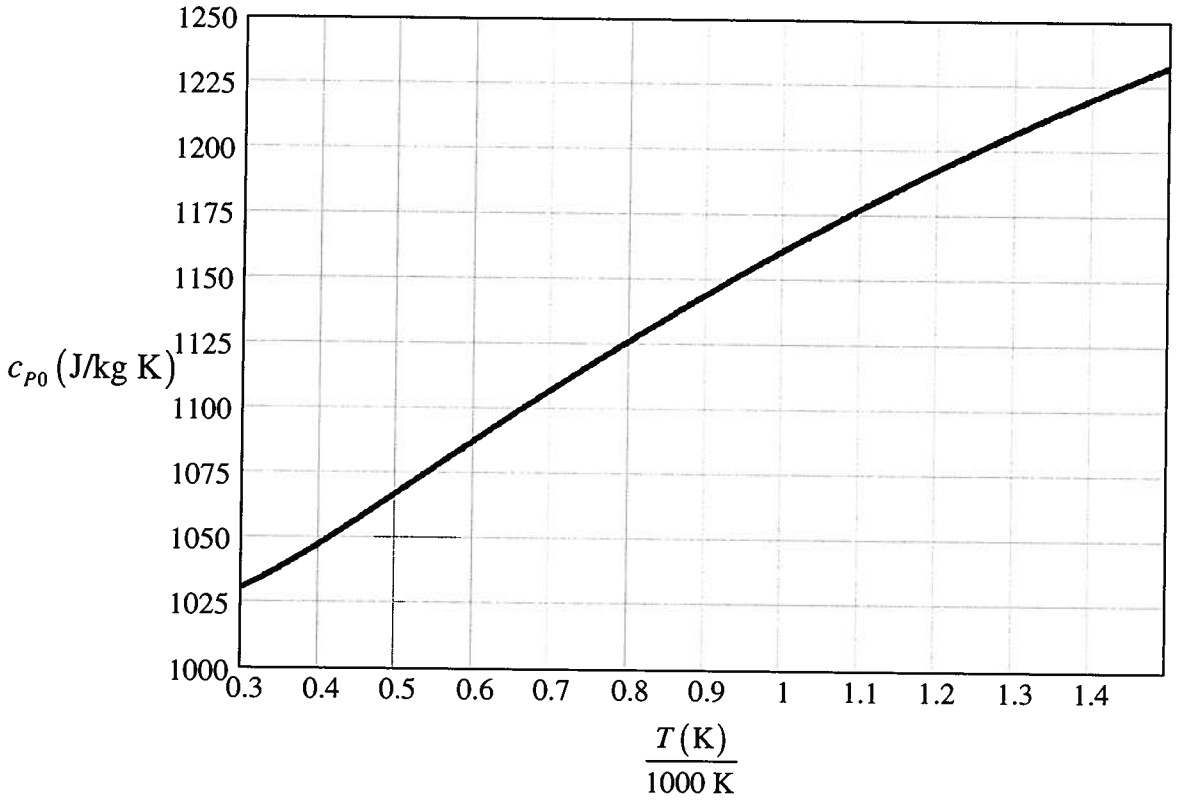

Figure 14E.7 Temperature Dependence of the Specific Heat at Constant Pressure for Nitrogen

From equation (14.140), we have

$$s_2 - s_1 = -R\ln\frac{P_2}{P_1} + \phi(T_2) - \phi(T_1) = -(296.808\ \text{J/kg K})\ln\frac{6\ \text{x}\ 10^5\ \text{N/m}^2}{10^5\ \text{N/m}^2} + 1.790\ \text{x}\ 10^3\ \text{J/kg K}$$

$$s_2 - s_1 = 1258\ \text{J/kg K}$$

If we had assumed that the specific heat were constant at the temperature of 300 K, we would have obtained

$$s_2 - s_1 = -R\ln\frac{P_2}{P_1} + c_{P0}\ln\frac{T_2}{T_1} = -(296.808\ \text{J/kg K})\ln\frac{6\ \text{x}\ 10^5\ \text{N/m}^2}{10^5\ \text{N/m}^2} + (1031\ \text{J/kg K})\ln\frac{1500\ \text{K}}{300\ \text{K}}$$

$$s_2 - s_1 = 1127\ \text{J/kg K}$$

The assumption of constant specific heat results in an error of about 10 percent.

14.6 Thermodynamic Properties from *P-v-T* Surfaces

In the previous section we developed techniques for calculating the thermodynamic properties of simple models of the *P-v-T* surface of the pure substance. In this section, we will show how these techniques can be applied to the more general case. The major difference between the simple and general case is the manner in which we integrate the differential expressions of the properties. For example, in Sections 14.5.1 and 14.5.2 we saw that certain partial differential coefficients, notably the specific heats, played an important role in the evaluation of other properties such as the internal energy, the enthalpy, and the entropy. For simple models like the incompressible fluid and the ideal gas, these partial differential

coefficients assumed very simple forms (usually constants) which made the integration of relevant expressions trivial. In general, however, the formulations of the partial differential coefficients in terms of the properties pressure, volume, and temperature are exceedingly complex and render the integration of relevant expressions difficult. Fortunately, we can partially reduce these complexities by selection of a path of integration that passes through states for which the ideal gas model is valid. This will allow us to express the partial differential coefficients in very simple form. By employing such paths for integration, we can evaluate all of the thermodynamic properties from minimum experimental data. A complete set of P-v-T data and the specific heats for the ideal gas (low density) states are all that are required. The P-v-T data must provide accurate values for the partial derivatives of the P-v-T function.

The specific heats, $c_{v\infty}$ and c_{P0}, of the ideal gas states are themselves measured by indirect methods. As outlined earlier, there exist quantum mechanical models for the behavior of the ideal gas. When we use these models together, with the emission and absorption spectra for the substance at very low pressures, we obtain the specific heats $c_{v\infty}$ and c_{P0}.

There are two methods of proceeding with the calculations of the thermodynamic properties depending on the way that the P-v-T data have been formulated (curve fitted). One method is used for $P = P(v,T)$ and a second method is used for $v = v(P,T)$. When the formulation is $P = P(v,T)$, the convenient independent properties are v and T. The other thermodynamic properties are in the form $u = u(v,T)$, $h = h(v,T)$, and $s = s(v,T)$. To determine the internal energy, $u(v,T)$, we must integrate equation (14.102).

$$du = \left(\frac{\partial u}{\partial T}\right)_v dT + \left(\frac{\partial u}{\partial v}\right)_T dv \tag{14.145}$$

When we perform the operations described in Section 14.5.2, equation (14.145) becomes

$$du = c_v dT + \left[T\left(\frac{\partial P}{\partial T}\right)_v - P\right] dv \tag{14.146}$$

Here we have combined equations (14.106), (14.108), and (14.145).

If we select the path of integration for changes in u so that the temperature changes only when the substance is in ideal gas states ($P \to 0$, $v \to \infty$), the specific heat c_v becomes the ideal gas specific heat $c_{v\infty}$ and the volume contribution to the internal energy change vanishes. Then, the change in u is composed of an ideal gas term that depends on temperature only plus non-ideal gas correction terms. To perform the integration in this manner, we need explicit functions for $c_{v\infty}(T)$ and $P(v,T)$. Note, however, that the accuracy of the resulting internal energy will depend upon the accuracy of the derivative of $P(v,T)$.

For computing the difference in internal energy between two states 1 and 2 by this method, the most convenient path for integration of equation (14.144) is at constant temperature ($T = T_1$) from v to $v \to \infty$ ($\rho = 0$). Next integrate at constant volume $v \to \infty$ ($\rho = 0$) from T to T_2. For this part of the integration the substance is in ideal gas states. Finally, integrate at constant temperature ($T = T_2$) from $v \to \infty$ to v_2. This path is shown on the v-T plane in Figure 9.2 (a) and on the ρ-T plane in Figure 9.2 (b). The mathematical formulation for this path of integration is

$$u_2 - u_1 = \left[\int \left[T\left(\frac{\partial P}{\partial T}\right)_v - P\right] dv\right]_{T=T_1} + \left[\int_{T_1}^{T_2} c_{v\infty} dT\right]_{v\to\infty} + \left[\int \left[T\left(\frac{\partial P}{\partial T}\right)_v - P\right] dv\right]_{T=T_2} \tag{14.147}$$

In most practical cases the expressions for $P(T,v)$ and c_v are too complex to be integrated in closed form; therefore, the integrals of equation (14.147) are normally evaluated numerically with the aid of a computer.

The entropy, $s(v,T)$, can be evaluated in a manner similar to the internal energy, $u(v,T)$. In this case we must integrate equation (14.127) to get

$$ds = \left(\frac{\partial s}{\partial v}\right)_T dv + \left(\frac{\partial s}{\partial T}\right)_v dT \tag{14.148}$$

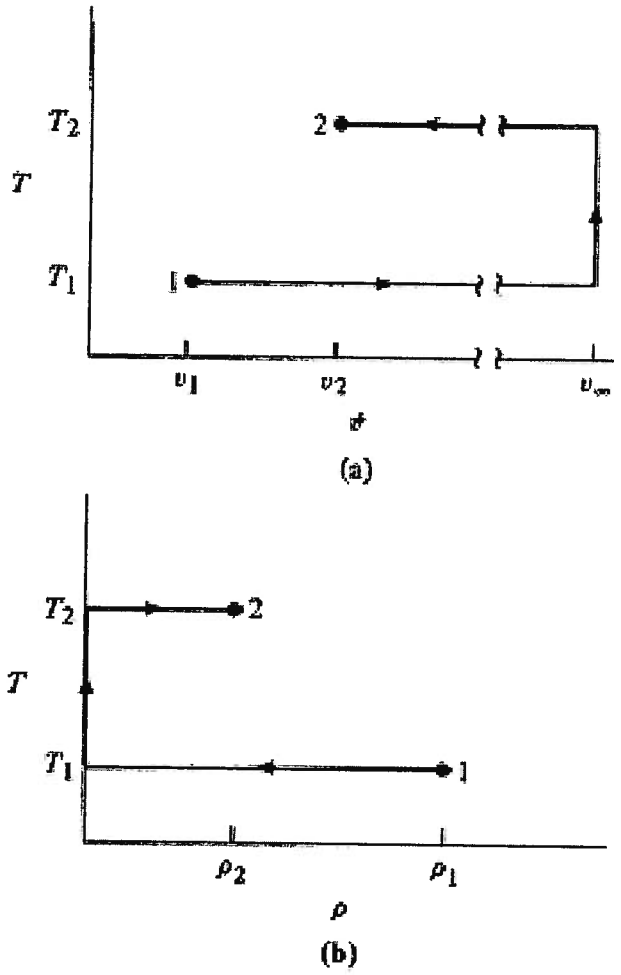

Figure 14.2 (a) and (b) Paths of Integration for Property Calculations

Following the steps shown in Section 14.5.2, we obtain equation (14.130).

$$ds = \left(\frac{\partial P}{\partial T}\right)_v dv + \frac{c_v}{T} dT \tag{14.149}$$

If we wish to employ the ideal gas specific heats for the integration, equation (14.149) must be modified to avoid the unbounded entropy at infinite volume, but the modification must permit equation (14.149) to be separated into the ideal gas entropy plus a correction term. From equation (14.131), it is apparent that adding and subtracting the term $(R/v)dv$ in equation (14.149) will achieve the desired result. Then

$$ds = \left[\left(\frac{\partial P}{\partial T}\right)_v - \frac{R}{v}\right] dv + \frac{R}{v} dv + \frac{c_v}{T} dT \tag{14.150}$$

Here the last two terms are the ideal gas terms of equation (14.131), and the first term approaches zero as the volume becomes infinite.

For the difference in entropy between two states 1 and 2, the most convenient path for

integration of equation (14.150) is the path shown in Figures 14.2 (a) and (b). That is, first integrate at constant temperature ($T = T_1$) from v to $v \to \infty$ ($\rho = 0$), then integrate at constant volume $v \to \infty$ ($\rho = 0$) from T to T_2. Finally, integrate at constant temperature ($T = T_2$) from $v \to \infty$ to v_2. Equation (14.150) then becomes

$$s_2 - s_1 = R\ln\frac{v_2}{v_1} + \left[\int_{T_1}^{T_2}\frac{c_{v\infty}}{T}dT\right]_{v\to\infty} + \left[\int_{v_1}^{v\to\infty}\left[\left(\frac{\partial P}{\partial T}\right)_v - \frac{R}{v}\right]dv\right]_{T=T_1} + \left[\int_{v\to\infty}^{v_2}\left[\left(\frac{\partial P}{\partial T}\right)_v - \frac{R}{v}\right]dv\right]_{T=T_2} \quad (14.151)$$

Here again, the actual integrals are normally evaluated numerically.

The enthalpy can now be determined from the internal energy by means of the definition of h.

$$h(v,T) = u(v,T) + v\left[P(v,T)\right] \quad (14.152)$$

The free energies, f and g, can also be evaluated from the definitions

$$f(v,T) = u(v,T) - T\left[s(v,T)\right] \quad (14.153)$$

and

$$g(v,T) = h(v,T) - T\left[s(v,T)\right] \quad (14.154)$$

When the P-v-T data have been formulated as $v = v(P,T)$, a method very similar to the one previously described is normally employed to obtain the calculated thermodynamic properties. In this case the independent variables are P and T so the appropriate starting point is the evaluation of the enthalpy $h(P,T)$. Thus, we must integrate equation (14.79).

$$dh = \left(\frac{\partial h}{\partial P}\right)_T dP + \left(\frac{\partial h}{\partial T}\right)_P dT \quad (14.155)$$

When we follow the steps shown in Section 14.6.1, equation (14.153) becomes

$$dh = \left[v - T\left(\frac{\partial v}{\partial T}\right)_P\right]dP + c_P dT \quad (14.156)$$

Normally the path of integration used in integrating equation (14.156) is chosen so that the ideal gas specific heat c_{P0} is employed. Then, for the difference in enthalpy between two states 1 and 2, the path of integration is the one shown in Figure 14.2 (c). That is, $T = T_1$ from P_1 to $P = 0$, at $P = 0$ from T_1 to T_2, and at $T = T_2$ from $P = 0$ to P_2.

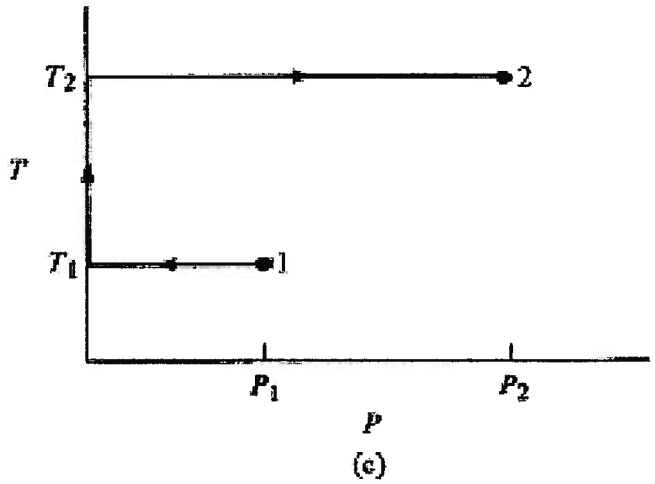

Figure 14.2(c) Path of Integration for the Enthalpy and Entropy Constitutive Relations of a Pure Substance

For this path, the integrated form of equation (14.156) is

$$h_2 - h_1 = \left[\int_{P_1}^{P=0}\left[v - T\left(\frac{\partial v}{\partial T}\right)_P\right]dP\right]_{T=T_1} + \left[\int_{T_1}^{T_2} c_{P0}\,dT\right]_{P=0} + \left[\int_{P=0}^{P_2}\left[v - T\left(\frac{\partial v}{\partial T}\right)_P\right]dP\right]_{T=T_2} \tag{14.157}$$

To determine the entropy $s(P,T)$, we must integrate equation (14.131).

$$ds = \left(\frac{\partial s}{\partial T}\right)_P dT + \left(\frac{\partial s}{\partial P}\right)_T dP \tag{14.158}$$

When we follow the steps shown in Section 14.5.2, equation (14.158) becomes

$$ds = -\left(\frac{\partial v}{\partial T}\right)_P dP + \frac{c_P}{T}dT \tag{14.159}$$

When we integrate equation (14.159) along the path shown in Figure 14.2 (c), we obtain the difference in entropy between any two states 1 and 2.

$$s_2 - s_1 = -R\ln\frac{P_2}{P_1} + \left[\int_{T_1}^{T_2}\frac{c_{P0}}{T}dT\right]_{P=0} + \left[\int_{P_1}^{P=0}\left[\frac{R}{P} - \left(\frac{\partial v}{\partial T}\right)_P\right]dP\right]_{T=T_1} + \left[\int_{P=0}^{P_2}\left[\frac{R}{P} - \left(\frac{\partial v}{\partial T}\right)_P\right]dP\right]_{T=T_2} \tag{14.160}$$

The other properties can now be determined from the following definitions:

$$u(P,T) = h(P,T) - P\left[v(P,T)\right] \tag{14.161}$$

$$f(P,T) = u(P,T) - T\left[s(P,T)\right] \tag{14.162}$$

$$g(P,T) = h(P,T) - T\left[s(P,T)\right] \tag{14.163}$$

We have now developed methods for determining a characteristic thermodynamic function from the *P-v-T* formulation (and its partial derivatives) and a specific heat as a function of temperature at one particular pressure. Since this information provides us with a complete constitutive relation, it will always be possible to express any combination of thermodynamic properties and their derivatives in terms of the measurable thermodynamic properties. An adequate set of measurable properties is the *P-v-T* formulation (and its partial derivatives) plus a specific heat.

14.7 Special Formulations of the *P-v-T* Data for the Pure Substance Model

From the discussions of the preceding section, it is clear that the functional form used to represent the *P-v-T* data plays an important role in the calculation of thermodynamic properties. It should come as no surprise, then, that many (in excess of 85) formulations, or equations of state, have been reported in the literature. In general these formulations are restricted to the vapor phase, but some can be extrapolated to the liquid phase. They vary considerably in complexity, and with one exception, the van der Waals equation, are not based upon rational physical arguments. All have two or more adjustable constants; hence, they are quite useful for curve fitting and interpolating existing *P-v-T* data. In this section we present several of the more widely used *P-v-T* constitutive relations, usually referred to as equations of state, in the order of their increasing complexity.

14.7.1 Van Der Waals Equation of State

The equation suggested by J. D. van der Waals in 1873 represents in a qualitative manner

the *P-v-T* characteristics of both the liquid and vapor phases. In addition, the equation has a critical state and approaches ideal gas behavior as the pressure approaches zero. Although the van der Waals equation does not represent the properties of any given substance with accuracy, it is still very useful since it is the simplest model of a substance which explains the departures from ideal gas behavior. Whereas in the ideal gas model the molecules exert no mutual influence on one another except possibly during short time collisions (The ideals gas model is sometimes referred to as a *collisionless gas.*), van der Waals suggested a molecular model in which the molecules each have a finite volume and exert long range attractive forces on one another. The net result of this model is that not all of the physical volume of the container is available to the molecules of the gas and that the force that the molecules exert on the container wall is reduced by the attractive force exerted on a molecule by its neighbors. The van der Waals equation of state then assumes the form

$$P = \frac{RT}{v-b} - \frac{a}{v^2} \tag{14.164}$$

Here the constant b is the volume excluded by the dimensions of the molecules themselves and the constant a accounts for the attractive forces between molecules. The numerical values of these two constants can be related to the critical state by recognizing that the critical isotherm must have a horizontal inflection point at the critical state. That is, in the critical state

$$\left(\frac{\partial P}{\partial v}\right)_T = \left(\frac{\partial^2 P}{\partial v^2}\right)_T = 0 \tag{14.165}$$

Applying this condition to the van der Waals equation of state and solving the resulting equations for the properties in the critical state, v_c, P_c, and T_c, we obtain

$$v_c = 3b \qquad P_c = \frac{a}{27b^2} \qquad RT_c = \frac{8a}{27b} \tag{14.166}$$

Solving for the constants a and b, we obtain the results

$$a = \frac{27}{64}\frac{R^2T_c^2}{P_c} \qquad b = \frac{1}{8}\frac{RT_c}{P_c} \tag{14.167}$$

At temperatures below the critical temperature, the van der Waals equation of state provides a qualitative description of liquid-vapor two-phase states. If we rewrite equation (14.164) in the form

$$Pv^3 - (bP + RT)v^2 + av - ab = 0 \tag{14.168}$$

we have a polynomial that is third order in volume. At temperatures below T_c, a given isotherm (line of constant temperature) has three volumes for each pressure over a range of pressure, as is shown schematically in Figure 14.3. The multiple values of volume at a given T and P allow the van der Waals equation to represent two-phase states which have a range of volume for a given combination of T and P. In fact, the van der Waals equation provides a simple model of the phase change. For the isotherm $T = T_1$ shown in Figure 14.3 the slope $(\partial P/\partial v)_T$ is positive in the region from m to n. As we shall show later in this chapter, this positive slope indicates that the gas is mechanically unstable in this region. If we have some gas at state o and a part of the gas happens to decrease in volume slightly, its pressure will decrease. The remainder of the gas expands and increases in pressure. This process accelerates, and finally a part of the gas has condensed to liquid at f and the remainder of the gas expands to vapor at g. The line f to g then represents the two-phase states composed of saturated liquid, state f, and saturated vapor, state g.

For mechanical and thermal equilibrium, the pressure and temperature must be the same for states *f* and *g*. In addition we showed in Section 13.9, equation (13.16), that the Gibbs free energy must be the same for states *f* and *g* to remain in equilibrium. This requirement for equilibrium with respect to mass transfer between phases determines the saturation pressure for each isotherm, that is, determines the vertical position of line *f* to *g* in Figure 14.3.

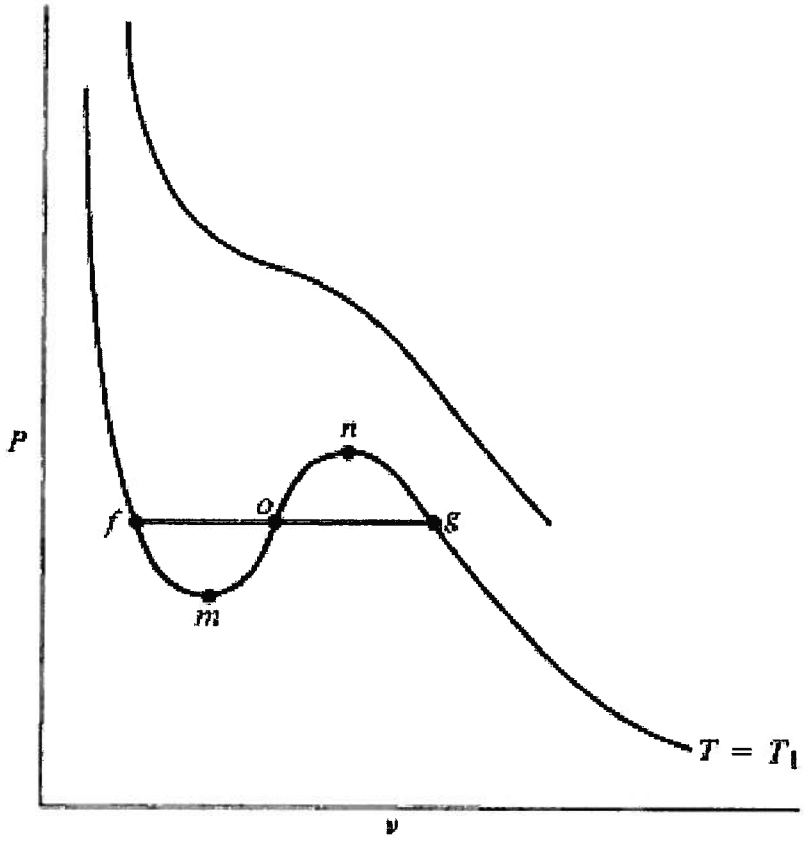

Figure 14.3 Isotherms of a van der Waals Gas

The equilibrium condition between the vapor and liquid phases is expressed by the equality of the Gibbs free energies for these two states *g* and *f* as shown in Figure 14.3, viz.

$$g_g = g_f \tag{14.169}$$

Since $dg = -sdT + vdP$ and T = constant, we have along the path *f-m-o-n-g*

$$\int_{g_f}^{g_g} dg = g_g - g_f = 0 = \int_{P_f}^{P_m} vdP + \int_{P_m}^{P_o} vdP + \int_{P_o}^{P_n} vdP + \int_{P_n}^{P_g} vdP \tag{14.170}$$

which we can rewrite in the form

$$\int_{P_m}^{P_o} vdP - \int_{P_m}^{P_f} vdP = \int_{P_g}^{P_n} vdP - \int_{P_o}^{P_n} vdP \tag{14.171}$$

The first integral on the left hand side of equation (14.171) represents the area under that portion of the curve *m-o* while the second integral on the left hand side of equation (14.171) represents the area under that portion of the curve *f-m*. Thus the entire left hand side of equation (14.171) represents the area enclosed by the curve *m-o-f-m*. Similarly, the right hand side of equation (14.171) represents the area enclosed by the curve *g-n-o-g*. Clearly, by equation (14.171) the two areas in question are equal. This is equivalent to writing

$$\int_{v_f}^{v_g} P dv = P_{sat}\left(v_g - v_f\right) \tag{14.172}$$

which determines the vertical position of the line *f* to *g* which is known as the saturation pressure corresponding to the temperature represented by the isotherm on Figure 14.3.

The saturation pressure for the isotherm may also be determined by considering a cycle proceeding along the path *f-m-o-n-g* and returning along *g-o-f*. If by some hypothetical means we could keep the unstable equilibrium states from collapsing, this would be a reversible cycle in communication with a single heat reservoir (all states in the cycle at the same *T*). The second law then requires no net heat transfer for the cycle which means that, by the first law, the net work transfer for the cycle is also zero; hence, the isobar *g-o-f* is located so that the area between the curve *f-m-o* and the isobar is equal to the area between the curve *o-n-g* and the isobar.

The states represented by curve *g-n* are metastable vapor states which are stable except to the formation of a finite drop of the liquid phase. The states represented by curve *f-m* are metastable liquid states which are stable except to the formation of a finite bubble of the vapor phase.

The behavior of the van der Waals model perhaps can be made more revealing if the properties are expressed in dimensionless form such that

$$P_r = \frac{P}{P_c} \qquad T_r = \frac{T}{T_c} \qquad v_r = \frac{v}{v_c} \tag{14.173}$$

where the subscript *r* is used to denote *reduced properties*. Making use of equations (14.166), (14.167), and (14.173), we can rewrite equation (14.164) in the dimensionless form

$$P_r = \frac{8T_r}{3v_r - 1} - \frac{3}{v_r^{\,2}} \tag{14.174}$$

Figure 14.4 shows a typical isotherm, $T_r = 0.87$, for the van der Waals model for nitrogen. From the pure substance model for nitrogen (NIST Database 23, v. 7.0): $P_c = 3.3958 \times 10^6$ N/m^2, $T_c =$ 126.19 K, and $v_c = 3.19198 \times 10^{-3}$ m^3/kg.

In dimensionless form, equation (14.172) becomes

$$\int_{(v_f)_r}^{(v_g)_r} P_r dv_r = (P_{sat})_r\left[(v_g)_r - (v_f)_r\right] \tag{14.175}$$

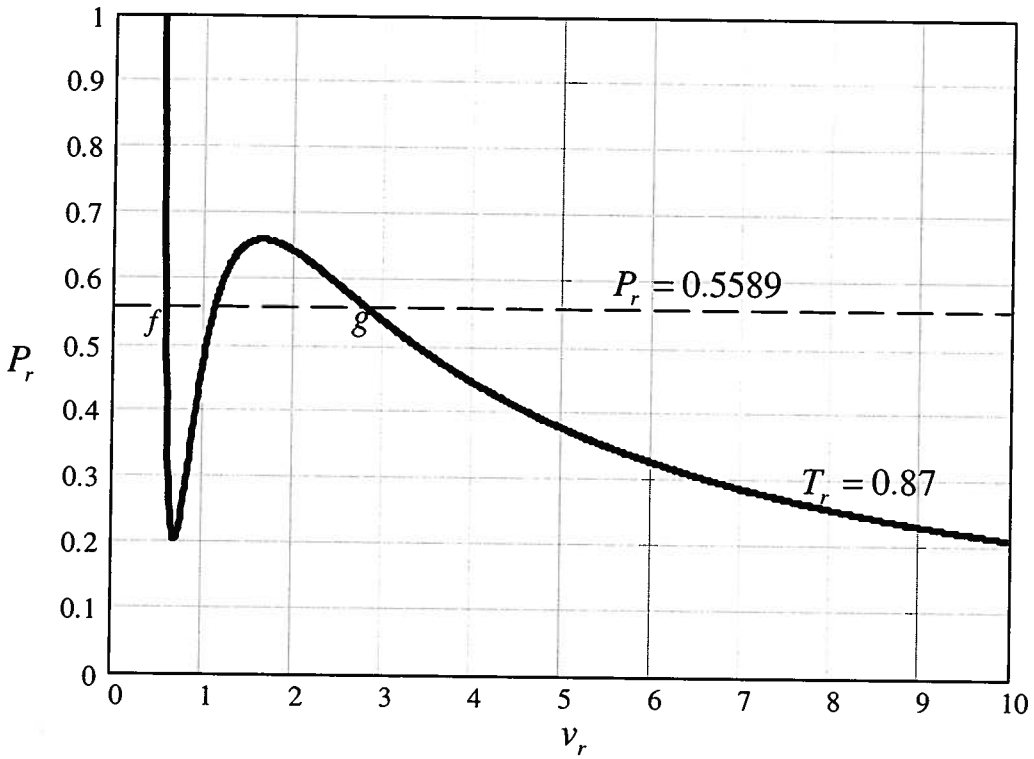

Figure 14.4 The Dimensionless Form of the van der Waals Model for Nitrogen

In Figure 14.4, the dimensionless isobar for the saturation pressure corresponding to the dimensionless isotherm $T_r = 0.87$ can be determined by substituting equation (14.174) into equation (14.175) and carrying out the integration. There results an equation for $(v_g)_r$ and $(v_f)_r$ as a function of T_r, viz.

$$\ln\left[3(v_g)_r - 1\right] + \frac{9}{4T_r}\frac{1}{(v_g)_r} - \frac{1}{3(v_g)_r - 1} = \ln\left[3(v_f)_r - 1\right] + \frac{9}{4T_r}\frac{1}{(v_f)_r} - \frac{1}{3(v_f)_r - 1} \quad (14.176)$$

Equation (14.176) yields a unique combination of $(v_g)_r$ and $(v_f)_r$ for each value of $T_r \leq 1$. These values of $(v_g)_r$ and $(v_f)_r$ can be substituted into equation (14.164) to obtain the value of the dimensionless saturation pressure corresponding to T_r. If these calculations are carried out for all values of $T_r \leq 1.0$, we can generate the locus of saturated states as shown in Figure 14.5.

Then for the isotherm $T_r = 0.87$ of Figure 14.4, $(P_{sat})_r = 0.5589$ with $(v_g)_r = 2.7909$ and $(v_f)_r = 0.5712$. For nitrogen, we can compare these results with those obtained from the aforementioned pure substance model as shown in Table 14.2.

Table 14.2
Comparison of the van der Waals Model and the Pure Substance Model of Nitrogen for $T = 109.79$ K

Model	P_{sat} (N/m^2)	v_g (m^3/kg)	v_f (m^3/kg)
van der Waals	1.8979×10^6	8.9089×10^{-3}	1.8233×10^{-3}
pure substance	1.4480×10^6	1.6202×10^{-2}	1.6049×10^{-3}

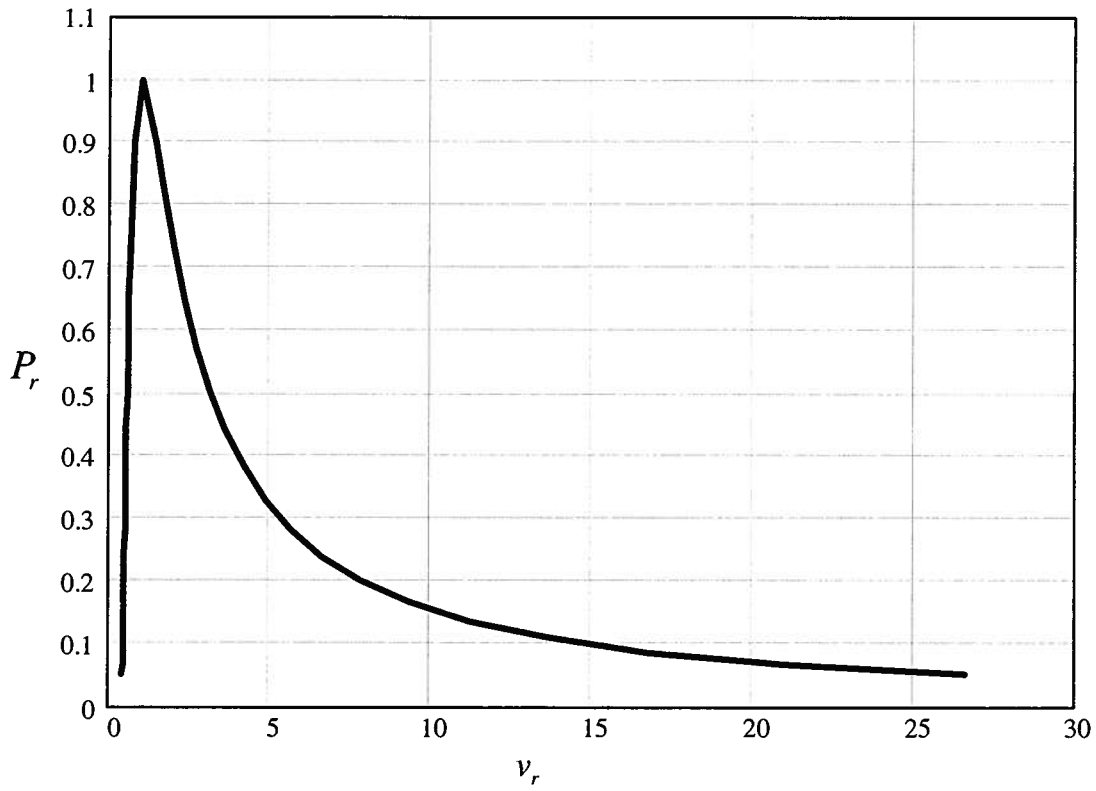

Figure 14.4 Locus of Saturated States for the van der Waals Model

From Table 14.2 it is evident that while the van der Waals model does a reasonable job of representing the overall physical behavior of thermal fluids, it does not yield the properties with any degree of accuracy that would make it a useful predictive model.

One interesting feature of the van der Waals model is shown in Figure 14.5. For certain values of the temperature, the values of the pressure predicted by the van der Waals model are negative. While at first glance this may seem to be physically unrealistic, it has been shown by careful experimentation that liquids are capable of sustaining quite large values of tension (negative pressure) under the right circumstances.

14.7.2 Dieterici Equation of State

This equation is an empirical improvement upon the van der Waals equation of state. It has the form

$$P = \frac{RT}{v-b}\exp\left(-\frac{a}{vRT}\right) \tag{14.177}$$

Here the two constants may be expressed in terms of the critical temperature and pressure, or they may be adjusted to fit the P-v-T data for two particular states. In this latter case the equation of state is used as an interpolation formula for the P-v-T data between the two fixed states.

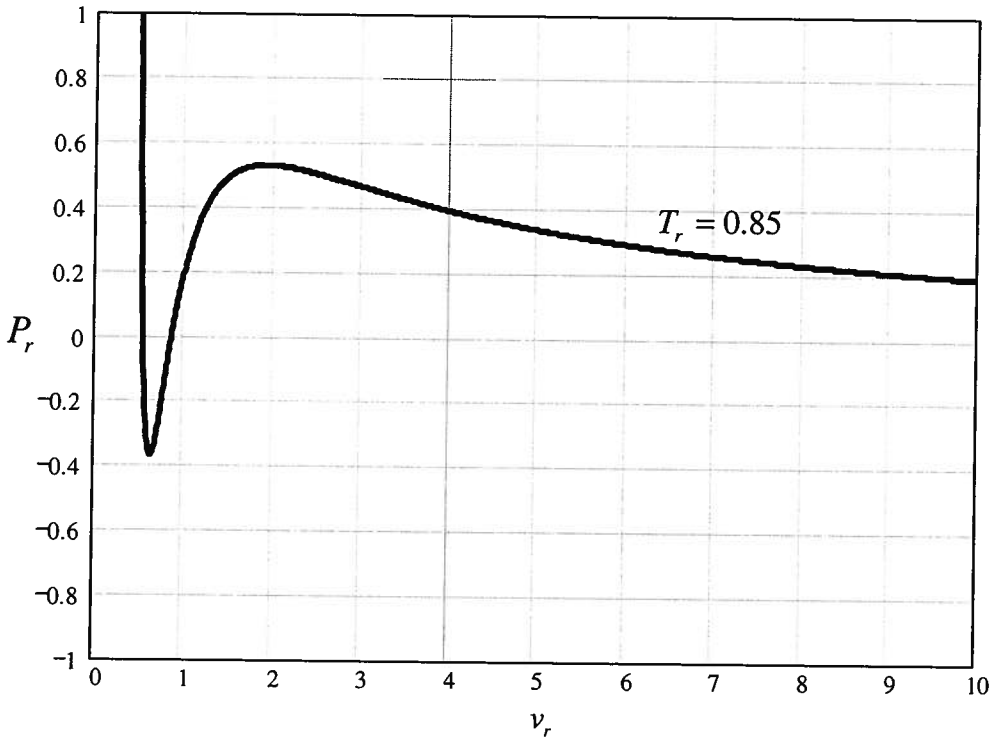

Figure 14.5 van der Waals Isotherm with Negative Pressures

14.7.3 Beattie-Bridgeman Equation of State

In order to obtain a fit to the P-v-T data of gases over a broader range of states, Beattie and Bridgeman proposed the following equation of state which contains five constants in addition to the gas constant R, viz.

$$P = \frac{RT}{v^2}(1-\varepsilon)(v+B) - \frac{A_0}{v^2}\left(1-\frac{a}{v}\right) \tag{14.178}$$

where

$$\varepsilon = \frac{C}{vT^3} \quad \text{and} \quad B = B_0\left(1-\frac{b}{v}\right) \tag{14.179}$$

The values of the constants for some common gases are given in Table 14.3.

Table 14.3
Constants for the Beattie-Bridgeman Equation of State

Gas	Formula	R J/kgK	A_0 Nm^4/kg^2	a m^3/kg	B_0 m^3/kg	b m^3/kg	C m^3K^3/kg
Ammonia	NH_3	488.15	836.16	1.00012 E−2	2.0052 E−3	1.1223 E−2	2.8003 E+5
Air		286.95	157.12	6.6674 E−4	1.5919 E−3	−3.801 E−5	1.498 E+3
Argon	A	208.14	81.99	5.8290 E−4	9.8451 E−4	0.0	1.499 E+3
n-Butane	C_4H_{10}	143.15	534.57	2.09388 E−3	4.2391 E−3	1.6225 E−3	6.0267 E+4
Carbon dioxide	CO_2	188.93	262.07	1.62129 E−3	2.3811 E−3	1.6444 E−3	1.4997 E+4
Carbon monoxide	CO	296.90	173.78	9.3457 E−4	1.8023 E−3	2.4660 E−4	1.498 E+3
Ethane	C_2H_6	276.62	659.89	1.95030 E−3	3.1283 E−3	6.3740 E−4	2.995 E+4
Ethylene	C_2H_4	296.58	793.50	1.77812 E−3	4.3370 E−3	1.2835 E−3	8.092 E+3
Ethyl ether	$C_4H_{10}O$	112.22	577.59	1.67748 E−3	6.1350 E−3	1.6137 E−3	4.499 E+3
Helium	He	2078.18	136.79	1.49581 E−2	3.5004 E−3	0.0	9.955
n-Heptane	C_7H_{16}	83.01	551.18	2.00398 E−3	7.0733 E−3	1.9159 E−3	3.992 E+4
Hydrogen	H_2	4115.47	4904.92	−2.50530 E−3	1.0376 E−2	−2.1582 E−2	2.4942 E+2
Methane	CH_4	518.60	897.96	1.15744 E−3	3.4854 E−3	−9.9013 E−4	8.003 E+3
Neon	Ne	411.98	52.89	1.08815 E−3	1.0207 E−3	0.0	50.10
Nitrogen	N_2	296.69	173.54	9.3394 E−4	1.8011 E−3	−2.4660 E−4	1.498 E+3
Nitrous oxide	N_2O	188.83	261.83	1.62005 E−3	2.3799 E−3	1.6431 E−3	1.498 E+4
Oxygen	O_2	259.79	147.56	8.0097 E−4	1.4452 E−3	1.3148 E−4	1.498 E+3
Propane	C_3H_8	188.67	622.24	1.66125 E−3	4.1082 E−3	9.7452 E−4	2.719 E+4

14.7.4 Benedict-Webb-Rubin Equation of State

Benedict, Webb, and Rubin have generalized the Beattie-Bridgeman equation of state, equation (14.178), to cover a broader range of states. The resulting equation of state has been tailored to represent the P-v-T data of hydrocarbons in particular and contains eight constants in addition to the gas constant .

$$P=\frac{RT}{v}+\left(B_0RT-A_0-\frac{C_0}{T^2}\right)\frac{1}{v^2}+\left(bRT-a\right)\frac{1}{v^3}+\frac{\alpha a}{v^6}+\frac{c\left(1+\gamma/v^2\right)}{T^2}\frac{1}{v^3}\exp\left(-\frac{\gamma}{v^2}\right) \qquad (14.180)$$

The values of the constants for a number of different gases are given in Table 14.4.

Table 14.4
Empirical Constants for the Benedict-Webb-Rubin Equation of State

Gas	*Formula*	A_0 Nm^4/kg^2	B_0 m^3/kg	C_0 Nm^4K^2/kg^2
Methane	CH_4	7.31195 E+2	2.65735 E−3	8.89635 E+6
Ethylene	C_2H_4	4.30550 E+2	1.98649 E−3	1.69071 E+7
Ethane	C_2H_6	4.66269 E+2	2.08914 E−3	2.01509 E+7
Propylene	C_3H_6	3.50217 E+2	2.02308 E−3	2.51642 E+7
Propane	C_3H_8	3.58575 E+2	2.20855 E−3	2.65194 E+7
i-Butane	C_4H_{10}	3.07308 E+2	2.36826 E−3	2.55256 E+7
i-Butylene	C_4H_8	2.88571 E+2	2.06958 E−3	2.98871 E+7
n-Butane	C_4H_{10}	3.02865 E+2	2.14127 E−3	2.98168 E+7
i-Pentane	C_5H_{12}	2.49391 E+2	2.22006 E−3	3.40357 E+7
n-Pentane	C_5H_{12}	2.37376 E+2	2.17426 E−3	4.13424 E+7
n-Hexane	C_6H_{14}	1.97242 E+2	2.06498 E−3	4.53487 E+7
n-Heptane	C_7H_{16}	1.77041 E+2	1.98756 E−3	4.79543 E+7

Gas	a Nm^7/kg^2	b m^6/kg^2	c Nm^4K^2/kg^2	α m^6/kg^2	γ m^6/kg^2
Methane	12.1466	1.31523 E−5	6.2577 E+4	3.01853 E−8	2.33469 E−5
Ethylene	1.19119	1.09451 E−5	9.7139 E+4	8.08173 E−9	1.17469 E−5
Ethane	1.28892	1.23191 E−5	1.22361 E+5	8.97220 E−9	1.30701 E−5
Propylene	1.05482	1.05806 E−5	1.39829 E+5	6.13014 E−9	1.03453 E−5
Propane	1.12224	1.15892 E−5	1.52759 E+5	7.09776 E−9	1.13317 E−5
i-Butane	1.00195	1.25806 E−5	1.47891 E+5	5.48279 E−9	1.00799 E−5
i-Butylene	0.97316	1.10774 E−5	1.58056 E+5	5.16963 E−9	9.41616 E−6
n-Butane	0.97334	1.18582 E−5	1.63610 E+5	5.62184 E−9	1.00799 E−5
i-Pentane	1.01546	1.28545 E−5	1.87887 E+5	4.53682 E−9	8.90805 E−6
n-Pentane	1.10159	1.28545 E−5	2.22807 E+5	4.83038 E−9	9.13893 E−6
n-Hexane	1.12913	1.47181 E−5	2.40013 E+5	4.40244 E−9	8.99353 E−6
n-Heptane	1.04602	1.51575 E−5	2.49275 E+5	4.33982 E−9	8.97754 E−6

14.7.5 Virial Equation of State

Closer inspection of equations (14.164), (14.177), (14.179), and (14.180) reveals that all of these equations of state are of the form

$$\frac{Pv}{RT} = 1 + \frac{B(T)}{v} + \frac{C(T)}{v^2} + \frac{D(T)}{v^3} + \ldots \tag{14.181}$$

where $B(T)$, $C(T)$, $D(T)$, . . . are all functions of temperature only and are known as the second, third, fourth, . . . virial coefficients respectively. Equation (14.181) itself is known as the virial

equation of state and was originally proposed by Clausius as an improvement over the ideal gas model. By arguments involving a microscopic model, it can be shown that the virial coefficients account for the interaction forces among molecules and that their magnitude depends upon the nature of the microscopic model used to describe the forces of interaction. Of course, equation (14.181) can also be used in an empirical fashion in which case the virial coefficients simply become parameters whose magnitudes can be adjusted to fit the P-v-T data of the particular gas. For this reason, some form of virial equation of state is frequently used to fit P-v-T because it offers the advantage that the number of virial coefficients can be increased to whatever number is necessary to achieve the desired level of accuracy for the numerical representation of the data.

14.8 The Principle of Corresponding States and the Generalized Equation of State

The principle of corresponding states is used in engineering practice when the thermodynamic behavior of the substance is not known and the ideal gas model is not adequate. J. D. van der Waals, who was the first individual to formulate this empirical principle, noted that all substances possess a critical state – the state on the critical isotherm for which the inflection point and the point of zero slope are coincident. van der Waals' idea was to express the P-v-T data of a pure substance in terms of the pressure, temperature, and the volume of the critical state. He postulated a universal function among these critical properties to establish the P-v-T data in any other state. The properties, which are normalized with respect to the critical properties, are called the *reduced properties* P_r, T_r, and v_r. They were defined previously in equation (14.173) as

$$P_r = \frac{P}{P_c}, T_r = \frac{T}{T_c}, \text{ and } v_r = \frac{v}{v_c} \tag{14.182}$$

where the critical properties are denoted by the subscript c. (Values of the critical properties for some common pure substances are listed in Table 14.5.) The empirical principle of corresponding states may then be expressed as follows:

All substances obey the same equation of state expressed in terms of the reduced properties.

According to the state principle, a stable, single-phase equilibrium state may be established by specifying any two independent properties chosen from of the three properties P, v, and T. Then, the principle of corresponding states implies that any dimensionless group of properties is a universal function of any two of the three reduced properties. In particular the compressibility factor, z, where

$$z = \frac{Pv}{RT} \tag{14.183}$$

can be written as a universal function of the reduced volume and temperature, viz.

$$z = \frac{Pv}{RT} = f(T_r, v_r) \tag{14.184}$$

Table 14.5
Critical Constants

Gas	Formula	Molecular Weight	Critical Temperature, T_c K	R	Critical Pressure, P_c atm	N/m^2	Critical Volume, v_c $m^3/kg\text{-}mole$	ω
Acetic acid	$C_2H_4O_2$	60.03	594.8	1070.6	57.2	5.79 E + 6	0.1711	0.454
Acetylene	C_2H_2	26.02	309	556	62	6.28 E + 6	0.1130	0.184
Ammonia	NH_3	17.03	405.5	729.8	111.3	1.127 E + 7	0.0724	0.250
Argon	A	39.944	151	272	48.0	4.86 E + 6	0.0749	−0.004
Benzene	C_6H_6	78.11	562	1012	48.6	4.92 E + 6	0.2604	0.212
Bromine	Br_2	159.832	584	1052	102	1.033 E + 7	0.1355	0.132
n-Butane	C_4H_{10}	58.120	425.2	765.2	37.5	3.80 E + 6	0.2547	0.193
Carbon dioxide	CO_2	44.01	304.2	547.2	72.9	7.38 E + 6	0.0943	0.225
Carbon monoxide	CO	28.01	133	240	34.5	3.49 E + 6	0.0930	0.049
Carbon tetrachloride	CCl_4	153.84	556.4	1001.5	45.0	4.56 E + 6	0.2760	0.194
Chlorine	Cl_2	70.914	417	751	76.1	7.71 E + 6	0.1243	0.073
Chloroform	$CHCl_3$	119.39	536.6	965.8	54.0	5.47 E + 6	0.2404	0.216
Decane	$C_{10}H_{22}$	142.17	619.4	1115	21.24	2.152 E + 6	0.6113	0.490
Deuterium (normal)	D_2	4.00	38.4	69.1	16.4	1.66 E + 6	—	−0.130
Dichlorodifluoro-methane Freon-12	CCl_2F_2	120.92	384.7	692.4	39.6	4.01 E + 6	0.2179	0.176
Dichlorofluoro-methane Freon-21	$CHCl_2F$	102.93	451.7	813.0	51.0	5.17 E + 6	0.1973	—
Ethane	C_2H_6	30.068	305.5	549.8	48.2	4.88 E + 6	0.1480	0.098
Ethyl alcohol	C_2H_5OH	46.07	516.0	929.0	63.0	6.38 E + 6	0.1673	0.635
Ethyl chloride	C_2H_5Cl	64.50	460.4	828.7	52	5.27 E + 6	0.1961	0.190
Ethyl ether	$C_4H_{10}O$	74.08	466.0	838.8	35.5	3.60 E + 6	0.2822	0.281
Ethylene	C_2H_4	28.052	282.4	508.3	50.5	5.12 E + 6	0.1243	0.085
Helium	He^4	4.003	5.3	9.5	2.26	2.29 E + 5	0.0578	−0.387
Helium[a]	He^3	3.00	3.34	6.01	1.15	1.16 E + 5	—	—
Heptane	C_7H_{16}	100.12	540.17	972.31	27.00	2.735 E + 6	0.4108	0.351

Although equation (14.184) is the form in which the principle of corresponding states was originally proposed, the critical volume has proven to be difficult to measure with any degree of accuracy. Therefore, it is more convenient to express the compressibility factor in terms of the reduced pressure and temperature. Thus,

$$z = \frac{Pv}{RT} = z(T_r, P_r) \tag{14.185}$$

In place of the actual reduced volume we use a pseudo-reduced volume, v_r', where

$$v_r' = \frac{v}{RT_c/P_c} = z\frac{T_r}{P_r} \tag{14.186}$$

Rather than attempting to formulate the analytical expression of equation (14.185), we find it

Table 14.5 (continued)
Critical Constants

Gas	Formula	Molecular Weight	Critical Temperature, T_c K	R	Critical Pressure, P_c atm	N/m²	Critical Volume, v_c m³/kg-mole	ω
n-Hexane	C_6H_{14}	86.172	507.9	914.2	29.9	3.03 E + 6	0.3678	0.296
Hydrogen (normal)	H_2	2.016	33.3	59.9	12.8	1.30 E + 6	0.0649	−0.220
Hydrogen cyanide	HCN	27.02	456.7	822.1	50	5.07 E + 6	0.1349	0.407
Krypton	Kr	83.7	209.4	376.9	54.3	5.50 E + 6	0.0924	−0.002
Methane	CH_4	16.042	191.1	343.9	45.8	4.64 E + 6	0.0993	0.008
Methyl alcohol	CH_3OH	32.04	513.2	923.7	78.5	7.95 E + 6	0.1180	0.559
Methyl chloride	CH_3Cl	50.49	416.3	749.3	65.9	6.68 E + 6	0.1430	0.156
Neon	Ne	20.183	44.5	80.1	26.9	2.72 E + 6	0.0417	0.0
Nitric oxide	NO	30.01	179	323	65	6.58 E + 6	0.0578	0.607
Nitrogen	N_2	28.016	126.2	227.1	33.5	3.39 E + 6	0.0899	0.040
Nitrous oxide	N_2O	44.02	309.7	557.4	71.7	7.26 E + 6	0.0962	0.160
Nonane	C_9H_{20}	128.16	596	1072	22.86	2.316 E + 6	0.5532	0.444
Octane	C_8H_{18}	114.14	569.4	1024.9	24.66	2.498 E + 6	0.4901	0.394
Oxygen	O_2	32.00	158.4	278.6	50.1	5.08 E + 6	0.0780	0.021
Pentane	C_5H_{12}	72.09	470.3	846.6	33.04	3.347 E + 6	0.3103	0.231
Propane	C_3H_8	44.094	370.0	665.9	42.0	4.25 E + 6	0.1998	0.152
Propene	C_3H_6	42.078	365.0	656.9	45.6	4.62 E + 6	0.1811	0.148
Propyne	C_3H_4	40.062	401	722	52.8	5.35 E + 6	—	0.218
Sulfur dioxide	SO_2	64.06	430.7	775.2	77.8	7.88 E + 6	0.1218	0.251
Sulfur trioxide	SO_3	80.06	491.5	884.7	83.6	8.47 E + 6	0.1268	0.410
Toluene	C_7H_8	92.06	593.8	1068.8	41.6	4.21 E + 6	0.3153	0.257
Trichlorofluoro-methane Freon-11	CCl_3F	137.38	471.2	848.1	43.2	4.38 E + 6	0.2479	0.188
Water	H_2O	18.016	647.4	1165.3	218.3	2.211 E + 7	0.0562	0.344
Xenon	Xe	131.3	289.75	521.55	58.0	5.88 E + 6	0.1186	0.002

more practical to establish the compressibility factor from experimental measurements and to present the data in the form of a graph of z as a function of P_r with T_r and v_r' as parameters. The original compressibility charts were prepared by averaging data for the following seven gases: H_2, N_2 , CO_2, NH_3 , CH_4, C_3H_8, C_5H_{12}. The latest versions of the compressibility charts, for example Figure 14.6 (Reprinted by permission of E. F. Obert, University of Wisconsin.), have increased this number to thirty. Because the gases used in the averaging process include many types of molecules, the resulting chart cannot be expected to reproduce absolutely the properties of any one of the gases listed. However, more accurate charts can be prepared by averaging data of molecules which are more nearly the same type. In spite of these limitations, the use of Figure 14.6 to obtain a value of z at a given T_r and P_r should lead to errors less than 4 to 6 percent except near the critical state where z is a strong function of T_r and P_r. In employing the compressibility chart for engineering calculations, any two of the three properties T_r, P_r, or v_r' are used to find the compressibility factor, z. This quantity is then used in the relation

$$Pv = zRT \tag{14.187}$$

to find the third property of state. Equation (14.187) is known as the *generalized equation of state*. As such, it is a two-parameter equation of state.

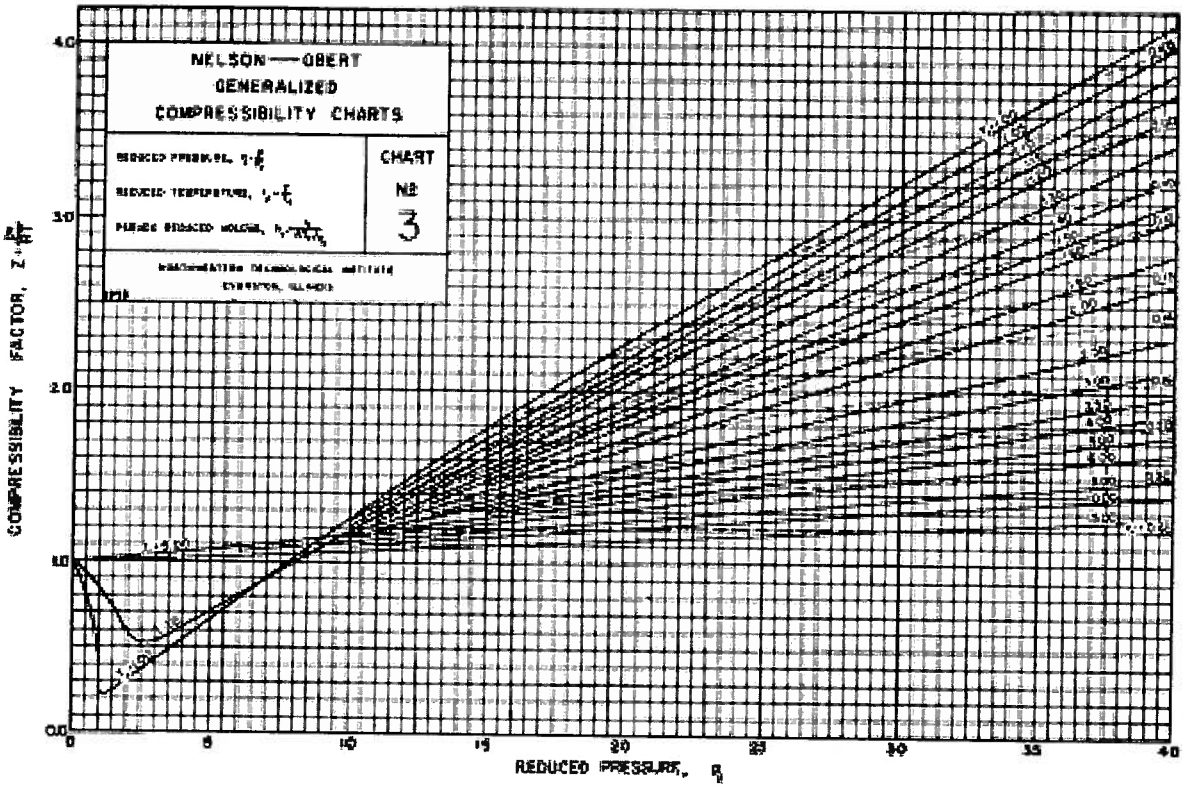

Figure 14.6(a) Generalized Compressibility Chart

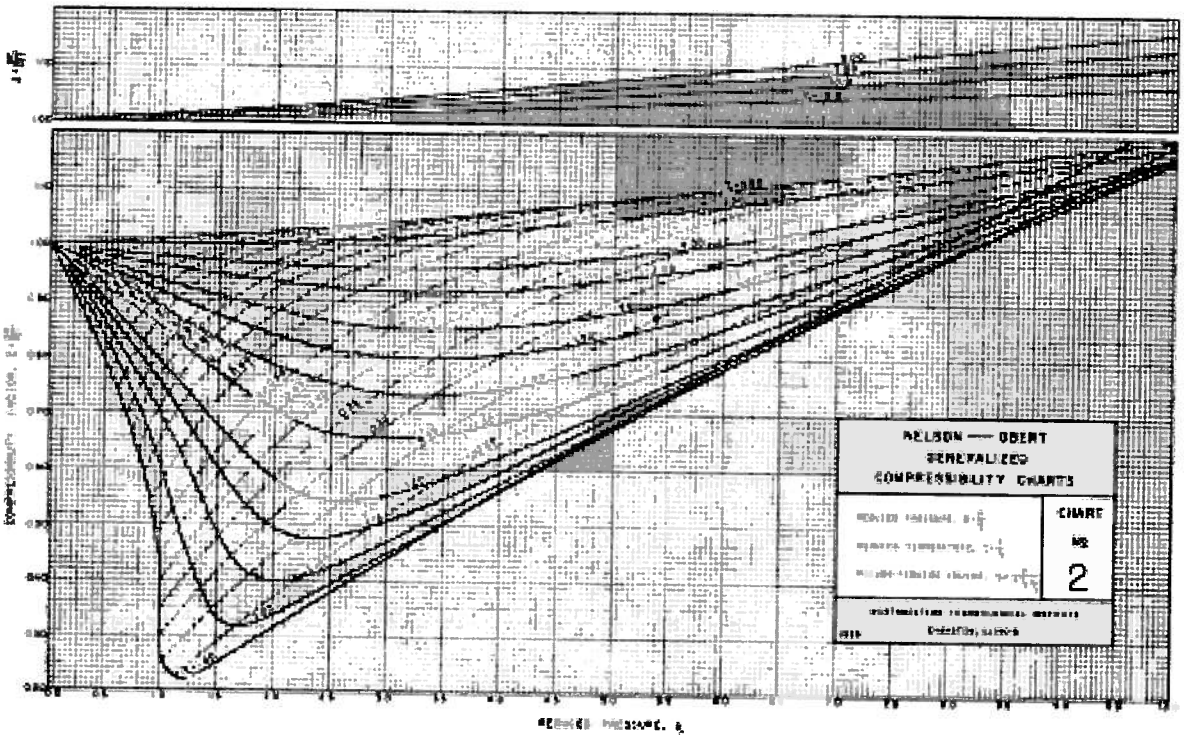

Figure 14.6(b) Generalized Compressibility Chart

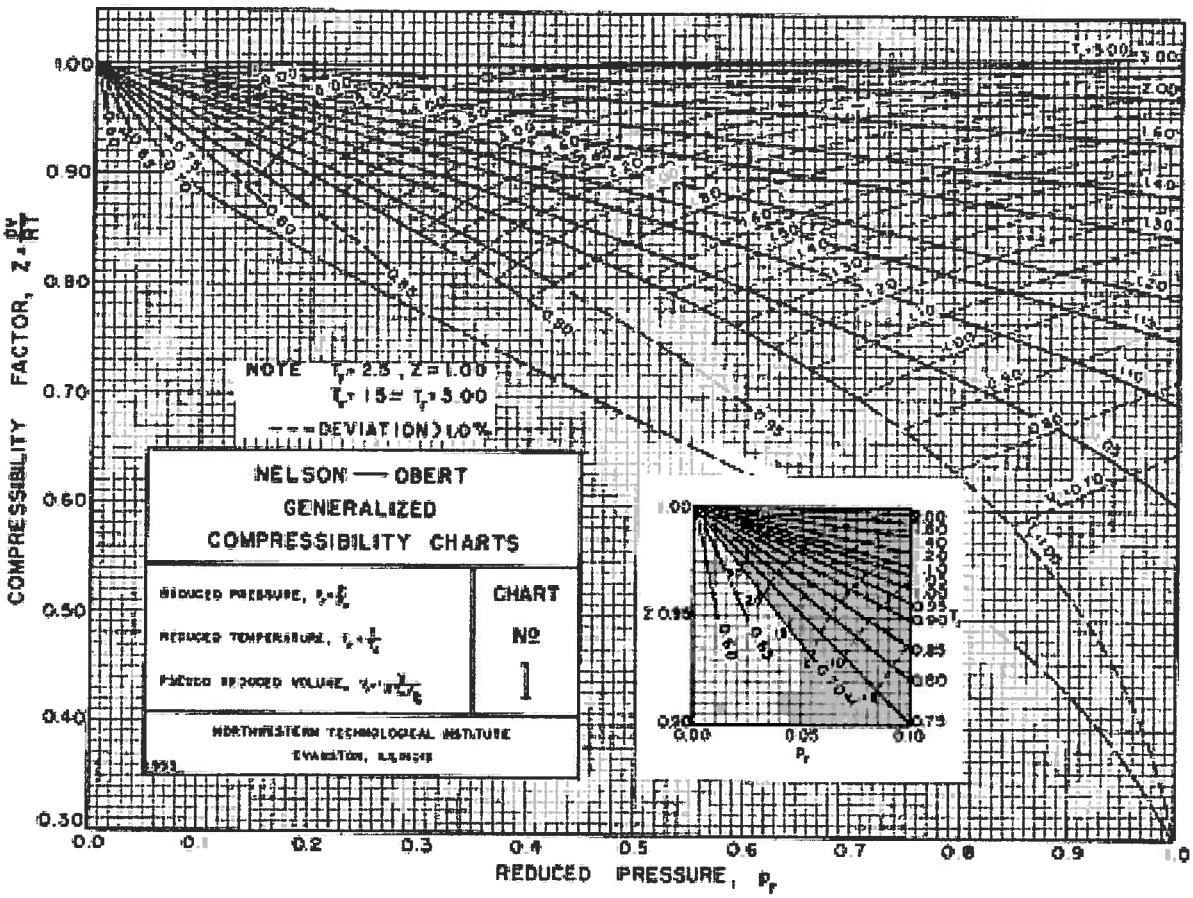

Figure 14.6(c) Generalized Compressibility Chart

In an attempt to improve the accuracy of the two-parameter generalized equation of state, it has been suggested that an additional third parameter be introduced into the expression for z given by equation (14.185). Lee and Kesler (Lee, B. I. and Kesler, M. G., "A Generalized Thermodynamic Correlation Based on Three-Parameter Corresponding States," AIChE Journal, Vol. 21, No. 3, pp. 510-527, May, 1975.) have suggested that the Pitzer acentric factor, ω, defined by the expression

$$\omega = -\log\left(P_{vap}\right)_{T_r=0.7} - 1.000 \tag{14.188}$$

be used for this purpose. In equation (14.188), $(P_{vap})_{Tr=0.7}$ is the vapor pressure of the fluid evaluated at $T_r = 0.7$. This factor, which is a measure of the non-spherical nature of the molecular force field ($\omega = 0$ for a noble gas with spherical symmetry, such as helium), is then used in a linear expansion of the compressibility factor.

$$z = z^{(0)}\left(T_r, P_r\right) + \omega z^{(1)}\left(T_r, P_r\right) \tag{14.189}$$

where $z^{(0)}$ applies to spherical molecules and $z^{(1)}$ is a deviation function. Values of $z^{(0)}$ and $z^{(1)}$ are tabulated in Tables 14.6 and 14.7 (from Lee and Kesler, *op. cit.*) for various values of T_r and P_r. The value of ω to be used in equation (14.189) is given for various fluids in Table 14.5.

Once we have generated the P-v-T data of a substance by means of the generalized compressibility factor, z, we can use these data and the methods of Section 14.7 to establish the other properties such as the enthalpy and entropy. The values of these two properties are most conveniently presented in terms of the deviation from the ideal gas model. Since these properties

Table 14.6
Values of $z^{(0)}$ in Equation (14.189)

	P_r						
T_r	0.010	0.050	0.100	0.200	0.400	0.600	0.800
0.30	0.0029	0.0145	0.0290	0.0579	0.1158	0.1737	0.2315
0.35	0.0026	0.0130	0.0261	0.0522	0.1043	0.1564	0.2084
0.40	0.0024	0.0119	0.0239	0.0477	0.0953	0.1429	0.1904
0.45	0.0022	0.0110	0.0221	0.0442	0.0882	0.1322	0.1762
0.50	0.0021	0.0103	0.0207	0.0413	0.0825	0.1236	0.1647
0.55	0.9804	0.0098	0.0195	0.0390	0.0778	0.1166	0.1553
0.60	0.9849	0.0093	0.0186	0.0371	0.0741	0.1109	0.1476
0.65	0.9881	0.9377	0.0178	0.0356	0.0710	0.1063	0.1415
0.70	0.9904	0.9504	0.8958	0.0344	0.0687	0.1027	0.1366
0.75	0.9922	0.9598	0.9165	0.0336	0.0670	0.1001	0.1330
0.80	0.9935	0.9669	0.9319	0.8539	0.0661	0.0985	0.1307
0.85	0.9946	0.9725	0.9436	0.8810	0.0661	0.0983	0.1301
0.90	0.9954	0.9768	0.9528	0.9015	0.7800	0.1006	0.1321
0.93	0.9959	0.9790	0.9573	0.9115	0.8059	0.6635	0.1359
0.95	0.9961	0.9803	0.9600	0.9174	0.8206	0.6967	0.1410
0.97	0.9963	0.9815	0.9625	0.9227	0.8338	0.7240	0.5580
0.98	0.9965	0.9821	0.9637	0.9253	0.8398	0.7360	0.5887
0.99	0.9966	0.9826	0.9648	0.9277	0.8455	0.7471	0.6138
1.00	0.9967	0.9832	0.9659	0.9300	0.8509	0.7574	0.6353
1.01	0.9968	0.9837	0.9669	0.9322	0.8561	0.7671	0.6542
1.02	0.9969	0.9842	0.9679	0.9343	0.8610	0.7761	0.6710
1.05	0.9971	0.9855	0.9707	0.9401	0.8743	0.8002	0.7130
1.10	0.9975	0.9874	0.9747	0.9485	0.8930	0.8323	0.7649
1.15	0.9978	0.9891	0.9780	0.9554	0.9081	0.8576	0.8032
1.20	0.9981	0.9904	0.9808	0.9611	0.9205	0.8779	0.8330
1.30	0.9985	0.9926	0.9852	0.9702	0.9396	0.9083	0.8764
1.40	0.9988	0.9942	0.9884	0.9768	0.9534	0.9298	0.9062
1.50	0.9991	0.9954	0.9909	0.9818	0.9636	0.9456	0.9278
1.60	0.9993	0.9964	0.9928	0.9856	0.9714	0.9575	0.9439
1.70	0.9994	0.9971	0.9943	0.9886	0.9775	0.9667	0.9563
1.80	0.9995	0.9977	0.9955	0.9910	0.9823	0.9739	0.9659
1.90	0.9996	0.9982	0.9964	0.9929	0.9861	0.9796	0.9735
2.00	0.9997	0.9986	0.9972	0.9944	0.9892	0.9842	0.9796
2.20	0.9998	0.9992	0.9983	0.9967	0.9937	0.9910	0.9886
2.40	0.9999	0.9996	0.9991	0.9983	0.9969	0.9957	0.9948
2.60	1.0000	0.9998	0.9997	0.9994	0.9991	0.9990	0.9990
2.80	1.0000	1.0000	1.0001	1.0002	1.0007	1.0013	1.0021
3.00	1.0000	1.0002	1.0004	1.0008	1.0018	1.0030	1.0043
3.50	1.0001	1.0004	1.0008	1.0017	1.0035	1.0055	1.0075
4.00	1.0001	1.0005	1.0010	1.0021	1.0043	1.0066	1.0090

Table 14.6(continued)
Values of $z^{(0)}$ for Equation (14.189)

P_r							
1.000	1.200	1.500	2.000	3.000	5.000	7.000	10.000
0.2892	0.3470	0.4335	0.5775	0.8648	1.4366	2.0048	2.8507
0.2604	0.3123	0.3901	0.5195	0.7775	1.2902	1.7987	2.5539
0.2379	0.2853	0.3563	0.4744	0.7095	1.1758	1.6373	2.3211
0.2200	0.2638	0.3294	0.4384	0.6551	1.0841	1.5077	2.1338
0.2056	0.2465	0.3077	0.4092	0.6110	1.0094	1.4017	1.9801
0.1939	0.2323	0.2899	0.3853	0.5747	0.9475	1.3137	1.8520
0.1842	0.2207	0.2753	0.3657	0.5446	0.8959	1.2398	1.7440
0.1765	0.2113	0.2634	0.3495	0.5197	0.8526	1.1773	1.6519
0.1703	0.2038	0.2538	0.3364	0.4991	0.8161	1.1241	1.5729
0.1656	0.1981	0.2464	0.3260	0.4823	0.7854	1.0787	1.5047
0.1626	0.1942	0.2411	0.3182	0.4690	0.7598	1.0400	1.4456
0.1614	0.1924	0.2382	0.3132	0.4591	0.7388	1.0071	1.3943
0.1630	0.1935	0.2383	0.3114	0.4527	0.7220	0.9793	1.3496
0.1664	0.1963	0.2405	0.3122	0.4507	0.7138	0.9648	1.3257
0.1705	0.1998	0.2432	0.3138	0.4501	0.7092	0.9561	1.3108
0.1779	0.2055	0.2474	0.3164	0.4504	0.7052	0.9480	1.2968
0.1844	0.2097	0.2503	0.3182	0.4508	0.7035	0.9442	1.2901
0.1959	0.2154	0.2538	0.3204	0.4514	0.7018	0.9406	1.2835
0.2901	0.2237	0.2583	0.3229	0.4522	0.7004	0.9372	1.2772
0.4648	0.2370	0.2640	0.3260	0.4533	0.6991	0.9339	1.2710
0.5146	0.2629	0.2715	0.3297	0.4547	0.6980	0.9307	1.2650
0.6026	0.4437	0.3131	0.3452	0.4604	0.6956	0.9222	1.2481
0.6880	0.5984	0.4580	0.3953	0.4770	0.6950	0.9110	1.2232
0.7443	0.6803	0.5798	0.4760	0.5042	0.6987	0.9033	1.2021
0.7858	0.7363	0.6605	0.5605	0.5425	0.7069	0.8990	1.1844
0.8438	0.8111	0.7624	0.6908	0.6344	0.7358	0.8998	1.1580
0.8827	0.8595	0.8256	0.7753	0.7202	0.7761	0.9112	1.1419
0.9103	0.8933	0.8689	0.8328	0.7887	0.8200	0.9297	1.1339
0.9308	0.9180	0.9000	0.8738	0.8410	0.8617	0.9518	1.1320
0.9463	0.9367	0.9234	0.9043	0.8809	0.8984	0.9745	1.1343
0.9583	0.9511	0.9413	0.9275	0.9118	0.9297	0.9961	1.1391
0.9678	0.9624	0.9552	0.9456	0.9359	0.9557	1.0157	1.1452
0.9754	0.9715	0.9664	0.9599	0.9550	0.9772	1.0328	1.1516
0.9865	0.9847	0.9826	0.9806	0.9827	1.0094	1.0600	1.1635
0.9941	0.9936	0.9935	0.9945	1.0011	1.0313	1.0793	1.1728
0.9993	0.9998	1.0010	1.0040	1.0137	1.0463	1.0926	1.1792
1.0031	1.0042	1.0063	1.0106	1.0223	1.0565	1.1016	1.1830
1.0057	1.0074	1.0101	1.0153	1.0284	1.0635	1.1075	1.1848
1.0097	1.0120	0.0156	1.0221	1.0368	1.0723	1.1138	1.1834
1.0115	1.0140	1.0179	1.0249	1.0401	1.0747	1.1136	1.1773

Table 14.7
Values of $z^{(1)}$ for Equation (14.189)

	P_r						
T_r	0.010	0.050	0.100	0.200	0.400	0.600	0.800
0.30	−0.0008	−0.0040	−0.0081	−0.0161	−0.0323	−0.0484	−0.0645
0.35	−0.0009	−0.0046	−0.0093	−0.0185	−0.0370	−0.0554	−0.0738
0.40	−0.0010	−0.0048	−0.0095	−0.0190	−0.0380	−0.0570	−0.0758
0.45	−0.0009	−0.0047	−0.0094	−0.0187	−0.0374	−0.0560	−0.0745
0.50	−0.0009	−0.0045	−0.0090	−0.0181	−0.0360	−0.0539	−0.0716
0.55	−0.0314	−0.0043	−0.0086	−0.0172	−0.0343	−0.0513	−0.0682
0.60	−0.0205	−0.0041	−0.0082	−0.0164	−0.0326	−0.0487	−0.0646
0.65	−0.0137	−0.0772	−0.0078	−0.0156	−0.0309	−0.0461	−0.0611
0.70	−0.0093	−0.0507	−0.1161	−0.0148	−0.0294	−0.0438	−0.0579
0.75	−0.0064	−0.0339	−0.0744	−0.0143	−0.0282	−0.0417	−0.0550
0.80	−0.0044	−0.0228	−0.0487	−0.1160	−0.0272	−0.0401	−0.0526
0.85	−0.0029	−0.0152	−0.0319	−0.0715	−0.0268	−0.0391	−0.0509
0.90	−0.0019	−0.0099	−0.0205	−0.0442	−0.1118	−0.0396	−0.0503
0.93	−0.0015	−0.0075	−0.0154	−0.0326	−0.0763	−0.1662	−0.0514
0.95	−0.0012	−0.0062	−0.0126	−0.0262	−0.0589	−0.1110	−0.0540
0.97	−0.0010	−0.0050	−0.0101	−0.0208	−0.0450	−0.0770	−0.1647
0.98	−0.0009	−0.0044	−0.0090	−0.0184	−0.0390	−0.0641	−0.1100
0.99	−0.0008	−0.0039	−0.0079	−0.0161	−0.0335	−0.0531	−0.0796
1.00	−0.0007	−0.0034	−0.0069	−0.0140	−0.0285	−0.0435	−0.0588
1.01	−0.0006	−0.0030	−0.0060	−0.0120	−0.0240	−0.0351	−0.0429
1.02	−0.0005	−0.0026	−0.0051	−0.0102	−0.0198	−0.0277	−0.0303
1.05	−0.0003	−0.0015	−0.0029	−0.0054	−0.0092	−0.0097	−0.0032
1.10	−0.0000	0.0000	0.0001	0.0007	0.0038	0.0106	0.0236
1.15	0.0002	0.0011	0.0023	0.0052	0.0127	0.0237	0.0396
1.20	0.0004	0.0019	0.0039	0.0084	0.0190	0.0326	0.0499
1.30	0.0006	0.0030	0.0061	0.0125	0.0267	0.0429	0.0612
1.40	0.0007	0.0036	0.0072	0.0147	0.0306	0.0477	0.0661
1.50	0.0008	0.0039	0.0078	0.0158	0.0323	0.0497	0.0677
1.60	0.0008	0.0040	0.0080	0.0162	0.0330	0.0501	0.0677
1.70	0.0008	0.0040	0.0081	0.0163	0.0329	0.0497	0.0667
1.80	0.0008	0.0040	0.0081	0.0162	0.0325	0.0488	0.0652
1.90	0.0008	0.0040	0.0079	0.0159	0.0318	0.0477	0.0635
2.00	0.0008	0.0039	0.0078	0.0155	0.0310	0.0464	0.0617
2.20	0.0007	0.0037	0.0074	0.0147	0.0293	0.0437	0.0579
2.40	0.0007	0.0035	0.0070	0.0139	0.0276	0.0411	0.0544
2.60	0.0007	0.0033	0.0066	0.0131	0.0260	0.0387	0.0512
2.80	0.0006	0.0031	0.0062	0.0124	0.0245	0.0365	0.0483
3.00	0.0006	0.0029	0.0059	0.0117	0.0232	0.0345	0.0456
3.50	0.0005	0.0026	0.0052	0.0103	0.0204	0.0303	0.0401
4.00	0.0005	0.0023	0.0046	0.0091	0.0182	0.0270	0.0357

Table 14.7(continued)
Values of $z^{(1)}$ for Equation (14.189)

P_r							
1.000	1.200	1.500	2.000	3.000	5.000	7.000	10.000
−0.0806	−0.0966	−0.1207	−0.1608	−0.2407	−0.3996	−0.5572	−0.7915
−0.0921	−0.1105	−0.1379	−0.1834	−0.2738	−0.4523	−0.6279	−0.8863
−0.0946	−0.1134	−0.1414	−0.1879	−0.2799	−0.4603	−0.6365	−0.8936
−0.0929	−0.1113	−0.1387	−0.1840	−0.2734	−0.4475	−0.6162	−0.8606
−0.0893	−0.1069	−0.1330	−0.1762	−0.2611	−0.4253	−0.5831	−0.8099
−0.0849	−0.1015	−0.1263	−0.1669	−0.2465	−0.3991	−0.5446	−0.7521
−0.0803	−0.0960	−0.1192	−0.1572	−0.2312	−0.3718	−0.5047	−0.6928
−0.0759	−0.0906	−0.1122	−0.1476	−0.2160	−0.3447	−0.4653	−0.6346
−0.0718	−0.0855	−0.1057	−0.1385	−0.2013	−0.3184	−0.4270	−0.5785
−0.0681	−0.0808	−0.0996	−0.1298	−0.1872	−0.2929	−0.3901	−0.5250
−0.0648	−0.0767	−0.0940	−0.1217	−0.1736	−0.2682	−0.3545	−0.4740
−0.0622	−0.0731	−0.0888	−0.1138	−0.1602	−0.2439	−0.3201	−0.4254
−0.0604	−0.0701	−0.0840	−0.1059	−0.1463	−0.2195	−0.2862	−0.3788
−0.0602	−0.0687	−0.0810	−0.1007	−0.1374	−0.2045	−0.2661	−0.3516
−0.0607	−0.0678	−0.0788	−0.0967	−0.1310	−0.1943	−0.2526	−0.3339
−0.0623	−0.0669	−0.0759	−0.0921	−0.1240	−0.1837	−0.2391	−0.3163
−0.0641	−0.0661	−0.0740	−0.0893	−0.1202	−0.1783	−0.2322	−0.3075
−0.0680	−0.0646	−0.0715	−0.0861	−0.1162	−0.1728	−0.2254	−0.2989
−0.0879	−0.0609	−0.0678	−0.0824	−0.1118	−0.1672	−0.2185	−0.2902
−0.0223	−0.0473	−0.0621	−0.0778	−0.1072	−0.1615	−0.2116	−0.2816
−0.0062	0.0227	−0.0524	−0.0722	−0.1021	−0.1556	−0.2047	−0.2731
0.0220	0.1059	0.0451	−0.0432	−0.0838	−0.1370	−0.1835	−0.2476
0.0476	0.0897	0.1630	0.0698	−0.0373	−0.1021	−0.1469	−0.2056
0.0625	0.0943	0.1548	0.1667	0.0332	−0.0611	−0.1084	−0.1642
0.0719	0.0991	0.1477	0.1990	0.1095	−0.0141	−0.0678	−0.1231
0.0819	0.1048	0.1420	0.1991	0.2079	0.0875	0.0176	−0.0423
0.0857	0.1063	0.1383	0.1894	0.2397	0.1737	0.1008	0.0350
0.0864	0.1055	0.1345	0.1806	0.2433	0.2309	0.1717	0.1058
0.0855	0.1035	0.1303	0.1729	0.2381	0.2631	0.2255	0.1673
0.0838	0.1008	0.1259	0.1658	0.2305	0.2788	0.2628	0.2179
0.0816	0.0978	0.1216	0.1593	0.2224	0.2846	0.2871	0.2576
0.0792	0.0947	0.1173	0.1532	0.2144	0.2848	0.3017	0.2876
0.0767	0.0916	0.1133	0.1476	0.2069	0.2819	0.3097	0.3096
0.0719	0.0857	0.1057	0.1374	0.1932	0.2720	0.3135	0.3355
0.0675	0.0803	0.0989	0.1285	0.1812	0.2602	0.3089	0.3459
0.0634	0.0754	0.0929	0.1207	0.1706	0.2484	0.3009	0.3475
0.0598	0.0711	0.0876	0.1138	0.1613	0.2372	0.2915	0.3443
0.0565	0.0672	0.0828	0.1076	0.1529	0.2268	0.2817	0.3385
0.0497	0.0591	0.0728	0.0949	0.1356	0.2042	0.2584	0.3194
0.0443	0.0527	0.0651	0.0849	0.1219	0.1857	0.2378	0.2994

can be readily evaluated for the ideal gas model, the enthalpy and entropy of the generalized real substance can be evaluated by simply adding to the ideal gas result the contribution due to "real" effects as determined from the generalized compressibility factor. To evaluate the enthalpy we employ equation (14.156) since the independent variables in equation (14.189) are temperature and pressure. The "real" effect due to the deviation from the ideal gas model is defined as the enthalpy departure function. Specifically, the enthalpy departure function for a state defined by T_1 and P_1 is given by

$$\left(h_{ideal} - h_{actual}\right)_{T_1} = h_{T_1,P=0} - h_{T_1,P_1} \tag{14.190}$$

Equation (14.156) then allows us to evaluate the enthalpy departure in terms of $v(T,P)$, viz.

$$\left(h_{ideal} - h_{actual}\right)_{T_1} = \int_{P}^{P=0} \left[v - T\left(\frac{\partial v}{\partial T}\right)_P \right]_{T=T_1} dP \tag{14.191}$$

We must now express equation (14.191) in dimensionless form in terms of P_r, T_r and the compressibility z. From the definitions of P_r, T_r and z we have

$$P = P_c P_r \Rightarrow dP = P_c dP_r \tag{14.192}$$

$$T = T_c T_r \Rightarrow dT = T_c dT_r \tag{14.193}$$

and

$$v = \frac{zRT_c}{P_c}\frac{T_r}{P_r} \tag{14.194}$$

With these relations, the derivative $(\partial v/\partial T)_P$ becomes

$$\left(\frac{\partial v}{\partial T}\right)_P = \frac{zR}{P_c}\frac{1}{P_r} + \frac{R}{P_c}\frac{T_r}{P_r}\left(\frac{\partial z}{\partial T_r}\right)_{P_r} \tag{14.195}$$

The integrand of equation (14.191) then becomes

$$v - T\left(\frac{\partial v}{\partial T}\right)_P = \frac{zRT_c}{P_c}\frac{T_r}{P_r} - \frac{zRT_c}{P_c}\frac{T_r}{P_r} - \frac{RT_c}{P_c}\frac{T_r^2}{P_r}\left(\frac{\partial z}{\partial T_r}\right)_{P_r} \tag{14.196}$$

Equation (14.194) can then be written in terms of the reduced properties as

$$\left(h_{ideal} - h_{actual}\right)_{T_1} = RT_c \left[\int_{P_r=0}^{P_r} T_r^2 \left(\frac{\partial z}{\partial T_r}\right)_{P_r} d\left(\ln P_r\right) \right]_{T=T_1} \tag{14.197}$$

where the limits of integration have been reversed. By using an analytical expression for the compressibility factor given in equation (14.181), Lee and Kesler (*op. cit.*) have been able to express the enthalpy departure function in the form

$$\left(h_{ideal} - h_{actual}\right) = \frac{RT_c}{M}\left[\left(\frac{h_{ideal} - h_{actual}}{RT_c}\right)^{(0)} + \omega\left(\frac{h_{ideal} - h_{actual}}{RT_c}\right)^{(1)} \right] \tag{14.198}$$

where the terms $[(h_{ideal} - h_{actual})/RT_c]^{(0)}$ and $[(h_{ideal} - h_{actual})/RT_c]^{(1)}$ are given in Tables 14.7 and 14.8 and have the same meaning as $z^{(0)}$ and $z^{(1)}$ in equation (14.182). A pseudo-analytical technique suitable for programming this approach on a computer is described in detail by Lee and Kesler. (Lee, B. I. and Kesler, M. G., "A Generalized Thermodynamic Correlation Based on Three-Parameter Corresponding States," AIChE Journal, Vol. 21, No. 3, pp. 510-527, May, 1975.)

Table 14.8

Values of $\left(\frac{h_{ideal} - h_{actual}}{RT_c}\right)^{(0)}$ for Equation (14.198)

	P_r						
T_r	0.010	0.050	0.100	0.200	0.400	0.600	0.800
0.30	6.045	6.043	6.040	6.034	6.022	6.011	5.999
0.35	5.906	5.904	5.901	5.895	5.882	5.870	5.858
0.40	5.763	5.761	5.757	5.751	5.738	5.726	5.713
0.45	5.615	5.612	5.609	5.603	5.590	5.577	5.564
0.50	5.465	5.463	4.459	5.453	5.440	5.427	5.414
0.55	0.032	5.312	5.309	5.303	5.290	5.278	5.265
0.60	0.027	5.162	5.159	5.153	5.141	5.129	5.116
0.65	0.023	0.118	5.008	5.002	4.991	4.980	4.968
0.70	0.020	0.101	0.243	4.848	4.838	4.828	4.818
0.75	0.017	0.088	0.183	4.687	4.679	4.672	4.664
0.80	0.015	0.078	0.160	0.345	4.507	4.504	4.499
0.85	0.014	0.069	0.141	0.300	4.309	4.313	4.316
0.90	0.012	0.062	0.126	0.264	0.596	4.074	4.094
0.93	0.011	0.058	0.118	0.246	0.545	0.960	3.920
0.95	0.011	0.056	0.113	0.235	0.516	0.885	3.763
0.97	0.011	0.054	0.109	0.225	0.490	0.824	1.356
0.98	0.010	0.053	0.107	0.221	0.478	0.797	1.273
0.99	0.010	0.052	0.105	0.216	0.466	0.773	1.206
1.00	0.010	0.051	0.103	0.212	0.455	0.750	1.151
1.01	0.010	0.050	0.101	0.208	0.445	0.728	0.102
1.02	0.010	0.049	0.099	0.203	0.434	0.708	1.060
1.05	0.009	0.046	0.094	0.192	0.407	0.654	0.955
1.10	0.008	0.042	0.086	0.175	0.367	0.581	0.827
1.15	0.008	0.039	0.079	0.160	0.334	0.523	0.732
1.20	0.007	0.036	0.073	0.148	0.305	0.474	0.657
1.30	0.006	0.031	0.063	0.127	0.259	0.399	0.545
1.40	0.005	0.027	0.055	0.110	0.224	0.341	0.463
1.50	0.005	0.024	0.048	0.097	0.196	0.297	0.400
1.60	0.004	0.021	0.043	0.086	0.173	0.261	0.350
1.70	0.004	0.019	0.038	0.076	0.153	0.231	0.309
1.80	0.003	0.017	0.034	0.068	0.137	0.206	0.275
1.90	0.003	0.015	0.031	0.062	0.123	0.185	0.246
2.00	0.003	0.014	0.028	0.056	0.111	0.167	0.222
2.20	0.002	0.012	0.023	0.046	0.092	0.137	0.182
2.40	0.002	0.010	0.019	0.038	0.076	0.114	0.150
2.60	0.002	0.008	0.016	0.032	0.064	0.095	0.125
2.80	0.001	0.007	0.014	0.027	0.054	0.080	0.105
3.00	0.001	0.006	0.011	0.023	0.045	0.067	0.088
3.50	0.001	0.004	0.007	0.015	0.029	0.043	0.056
4.00	0.000	0.002	0.005	0.009	0.017	0.026	0.033

Table 14.8(continued)

Values of $\left(\frac{h_{ideal} - h_{actual}}{RT_c}\right)^{(0)}$ for Equation (14.198)

P_r							
1.000	*1.200*	*1.500*	*2.000*	*3.000*	*5.000*	*7.000*	*10.000*
5.987	5.975	5.957	5.927	5.868	5.748	5.628	5.446
5.845	5.833	5.814	5.783	5.721	5.595	5.469	5.278
5.700	5.687	5.668	5.636	5.572	5.442	5.311	5.113
5.551	5.538	5.519	5.486	5.421	5.288	5.154	4.950
5.401	5.388	5.369	5.336	5.270	5.135	4.999	4.791
5.252	5.239	5.220	5.187	5.121	4.986	4.849	4.638
5.104	5.091	5.073	5.041	4.976	4.842	4.704	4.492
4.956	4.945	4.927	4.896	4.833	4.702	4.565	4.353
4.808	4.797	4.781	4.752	4.693	4.566	4.432	4.221
4.655	4.646	4.632	4.607	4.554	4.434	4.303	4.095
4.494	4.488	4.478	4.459	4.413	4.303	4.178	3.974
4.316	4.316	4.312	4.302	4.269	4.173	4.056	3.857
4.108	4.118	4.127	4.132	4.119	4.043	3.935	3.744
3.953	3.976	4.000	4.020	4.024	3.963	3.863	3.678
3.825	3.865	3.904	3.940	3.958	3.910	3.815	3.634
3.658	3.732	3.796	3.853	3.890	3.856	3.767	3.591
3.544	3.652	3.736	3.806	3.854	3.829	3.743	3.569
3.376	3.558	3.670	3.758	3.818	3.801	3.719	3.548
2.584	3.441	3.598	3.706	3.782	3.774	3.695	3.526
1.796	3.283	3.516	3.652	3.744	3.746	3.671	3.505
1.627	3.039	3.442	3.595	3.705	3.718	3.647	3.484
1.359	2.034	3.030	3.398	3.583	3.632	3.575	3.420
1.120	1.487	2.203	2.965	3.353	3.484	3.453	3.315
0.968	1.239	1.719	2.479	3.091	3.329	3.329	3.211
0.857	1.076	1.443	2.079	2.807	3.166	3.202	3.107
0.698	0.860	1.116	1.560	2.274	2.825	2.942	2.899
0.588	0.716	0.915	1.253	1.857	2.486	2.679	2.692
0.505	0.611	0.774	1.046	1.549	2.175	2.421	2.486
0.440	0.531	0.667	0.894	1.318	1.904	2.177	2.285
0.387	0.466	0.583	0.777	1.139	1.672	1.953	2.091
0.344	0.413	0.515	0.683	0.996	1.476	1.751	1.908
0.307	0.368	0.458	0.606	0.880	1.309	1.571	1.736
0.276	0.330	0.411	0.541	0.782	1.167	1.411	1.577
0.226	0.269	0.334	0.437	0.629	0.937	1.143	1.295
0.187	0.222	0.275	0.359	0.513	0.761	0.929	1.058
0.155	0.185	0.228	0.297	0.422	0.621	0.756	0.858
0.130	0.154	0.190	0.246	0.348	0.508	0.614	0.689
0.109	0.129	0.159	0.205	0.288	0.415	0.495	0.545
0.069	0.081	0.099	0.127	0.174	0.239	0.270	0.264
0.041	0.048	0.058	0.072	0.095	0.116	0.110	0.061

Table 14.9

Values of $\left(\frac{h_{ideal} - h_{actual}}{RT_c}\right)^{(1)}$ for Equation (14.198)

	P_r						
T_r	0.010	0.050	0.100	0.200	0.400	0.600	0.800
0.30	11.098	11.096	11.095	11.091	11.083	11.076	11.069
0.35	10.656	10.655	10.654	10.653	10.650	10.646	10.643
0.40	10.121	10.121	10.121	10.120	10.121	10.121	10.121
0.45	9.515	9.515	9.516	9.517	9.519	9.521	9.523
0.50	8.868	8.869	8.870	8.872	8.876	8.880	8.884
0.55	0.080	8.211	8.212	8.215	8.221	8.226	8.232
0.60	0.059	7.568	7.570	7.573	7.579	7.585	7.591
0.65	0.045	0.247	6.949	6.952	6.959	6.966	6.973
0.70	0.034	0.185	0.415	6.360	6.367	6.373	6.381
0.75	0.027	0.142	0.306	5.796	5.802	5.809	5.816
0.80	0.021	0.110	0.234	0.542	5.266	5.271	5.278
0.85	0.017	0.087	0.182	0.401	4.753	4.754	4.758
0.90	0.014	0.070	0.144	0.308	0.751	4.254	4.248
0.93	0.012	0.061	0.126	0.265	0.612	1.236	3.942
0.95	0.011	0.056	0.115	0.241	0.542	0.994	3.737
0.97	0.010	0.052	0.105	0.219	0.483	0.837	1.616
0.98	0.010	0.050	0.101	0.209	0.457	0.776	1.324
0.99	0.009	0.048	0.097	0.200	0.433	0.722	1.154
1.00	0.009	0.046	0.093	0.191	0.410	0.675	1.034
1.01	0.009	0.044	0.089	0.183	0.389	0.632	0.940
1.02	0.008	0.042	0.085	0.175	0.370	0.594	0.863
1.05	0.007	0.037	0.075	0.153	0.318	0.498	0.691
1.10	0.006	0.030	0.061	0.123	0.251	0.381	0.507
1.15	0.005	0.025	0.050	0.099	0.199	0.296	0.385
1.20	0.004	0.020	0.040	0.080	0.158	0.232	0.297
1.30	0.003	0.013	0.026	0.052	0.100	0.142	0.177
1.40	0.002	0.008	0.016	0.032	0.060	0.083	0.100
1.50	0.001	0.005	0.009	0.018	0.032	0.042	0.048
1.60	0.000	0.002	0.004	0.007	0.012	0.013	0.011
1.70	0.000	0.000	0.000	−0.000	−0.003	−0.009	−0.017
1.80	−0.000	−0.001	−0.003	−0.006	−0.015	−0.025	−0.037
1.90	−0.001	−0.003	−0.005	−0.011	−0.023	−0.037	−0.053
2.00	−0.001	−0.003	−0.007	−0.015	−0.030	−0.047	−0.065
2.20	−0.001	−0.005	−0.010	−0.020	−0.040	−0.062	−0.083
2.40	−0.001	−0.006	−0.012	−0.023	−0.047	−0.071	−0.095
2.60	−0.001	−0.006	−0.013	−0.026	−0.052	−0.078	−0.104
2.80	−0.001	−0.007	−0.014	−0.028	−0.055	−0.082	−0.110
3.00	−0.001	−0.007	−0.014	−0.029	−0.058	−0.086	−0.114
3.50	−0.002	−0.008	−0.016	−0.031	−0.062	−0.092	−0.122
4.00	−0.002	−0.008	−0.016	−0.032	−0.064	−0.096	−0.127

Table 14.9(continued)

Values of $\left(\frac{h_{ideal} - h_{actual}}{RT_c}\right)^{(1)}$ for Equation (14.198)

P_r							
1.000	*1.200*	*1.500*	*2.000*	*3.000*	*5.000*	*7.000*	*10.000*
11.062	11.055	11.044	11.027	10.992	10.935	10.872	10.781
10.640	10.637	10.632	10.624	10.609	10.581	10.554	10.529
10.121	10.121	10.121	10.122	10.123	10.128	10.135	10.150
9.525	9.527	9.531	9.537	9.549	9.576	9.611	9.663
8.888	8.892	8.899	8.909	8.932	8.978	9.030	9.111
8.238	8.243	8.252	8.267	8.298	8.360	8.425	8.531
7.596	7.603	7.614	7.632	7.669	7.745	7.824	7.950
6.980	6.987	6.997	7.017	7.059	7.147	7.239	7.381
6.388	6.395	6.407	6.429	6.475	6.574	6.677	6.837
5.824	5.832	5.845	5.868	5.918	6.027	6.142	6.318
5.285	5.293	5.306	5.330	5.385	5.506	5.632	5.824
4.763	4.771	4.784	4.810	4.872	5.008	5.149	5.358
4.249	4.255	4.268	4.298	4.371	4.530	4.688	4.916
3.934	3.937	3.951	3.987	4.073	4.251	4.422	4.662
3.712	3.713	3.730	3.773	3.873	4.068	4.248	4.497
3.470	3.467	3.492	3.551	3.670	3.885	4.077	4.336
3.332	3.327	3.363	3.434	3.568	3.795	3.992	4.257
3.164	3.164	3.223	3.313	3.464	3.705	3.909	4.178
2.471	2.952	3.065	3.186	3.358	3.615	3.825	4.100
1.375	2.595	2.880	3.051	3.251	3.525	3.742	4.023
1.180	1.723	2.650	2.906	3.142	3.435	3.661	3.947
0.877	0.878	1.496	2.381	2.800	3.167	3.418	3.722
0.617	0.673	0.617	1.261	2.167	2.720	3.023	3.362
0.459	0.503	0.487	0.604	1.497	2.275	2.641	3.019
0.349	0.381	0.381	0.361	0.934	1.840	2.273	2.692
0.203	0.218	0.218	0.178	0.300	1.066	1.592	2.086
0.111	0.115	0.108	0.070	0.044	0.504	1.012	1.547
0.049	0.046	0.032	−0.008	−0.078	0.142	0.556	1.080
0.005	−0.004	−0.023	−0.065	−0.151	−0.082	0.217	0.689
−0.027	−0.040	−0.063	−0.109	−0.202	−0.223	−0.028	0.369
−0.051	−0.067	−0.094	−0.143	−0.241	−0.317	−0.203	0.112
−0.070	−0.088	−0.117	−0.169	−0.271	−0.381	−0.330	−0.092
−0.085	−0.105	−0.136	−0.190	−0.295	−0.428	−0.424	−0.255
−0.106	−0.128	−0.163	−0.221	−0.331	−0.493	−0.551	−0.489
−0.120	−0.144	−0.181	−0.242	−0.356	−0.535	−0.631	−0.645
−0.130	−0.156	−0.194	−0.257	−0.376	−0.567	−0.687	−0.754
−0.137	−0.164	−0.204	−0.269	−0.391	−0.591	−0.729	−0.836
−0.142	−0.170	−0.211	−0.278	−0.403	−0.611	−0.763	−0.899
−0.152	−0.181	−0.224	−0.294	−0.425	−0.650	−0.827	−1.015
−0.158	−0.188	−0.233	−0.306	−0.442	−0.680	−0.874	−1.097

An actual change in enthalpy between two states is expressed as the sum of an ideal gas term and two enthalpy departure terms, viz.

$$(h_2 - h_1)_{actual} = (h_2 - h_1)_{ideal} - \left[(h_2)_{ideal} - (h_2)_{actual}\right]_{T=T_2} + \left[(h_1)_{ideal} - (h_1)_{actual}\right]_{T=T_1} \quad (14.199)$$

where the ideal gas term is given by

$$(h_2 - h_1)_{ideal} = \int_{T_1}^{T_2} c_{P0}\, dT \quad (14.200)$$

We can execute a similar set of calculations for the generalized entropy departure. When the ideal gas terms of equation (14.160) are transposed to the left side of the equation, we can write the entropy departure, viz.

$$(s_{ideal} - s_{actual})_T = \left[\int_{P}^{P=0}\left[\frac{R}{P} - \left(\frac{\partial v}{\partial T}\right)_P\right] dP\right]_T \quad (14.201)$$

When equations (14.192) through (14.195) are used to express equation (14.201) in dimensionless form, we have

$$(s_{ideal} - s_{actual})_T = \frac{R}{M}\left[\int_{P_r=0}^{P_r}\left\{(z-1) + T_r\left(\frac{\partial z}{\partial T_r}\right)_{P_r} d(\ln P_r)\right\}\right]_T \quad (14.202)$$

In a manner similar to the enthalpy departure, the entropy departure can be written

$$(s_{ideal} - s_{actual})_T = \frac{R}{M}\left[\left(\frac{s_{ideal} - s_{actual}}{R}\right)^{(0)} + \omega\left(\frac{s_{ideal} - s_{actual}}{R}\right)^{(1)}\right] \quad (14.203)$$

where the terms $[(s_{ideal} - s_{actual})/R]^{(0)}$ and $[(s_{ideal} - s_{actual})/R]^{(1)}$ represent the spherical and non-spherical contribution to the entropy departure. Values of these terms are tabulated in Tables 14.10 and 14.11 taken from the data of Lee and Kesler (*op. cit.*). An actual change in entropy between two states is calculated in terms of the entropy departures in the same way that the change in enthalpy is computed in terms of the enthalpy departures, equation (14.191). The ideal gas contribution to the entropy change is

$$(s_2 - s_1)_{ideal} = \int_{T_1}^{T_2} \frac{c_{P0}}{T}\, dT - R \ln \frac{P_2}{P_1} \quad (14.204)$$

As an alternate approach, tabulated values of ideal gas entropies can be used in place of equation (14.204). In such cases, care must be exercised to account for differences in pressure between the ideal gas states of interest and the tabulated states since tabulated values are often for pressures of 1 atm or 1 bar.

Table 14.10

Values of $\left(\frac{s_{ideal} - s_{actual}}{R}\right)^{(0)}$ for Equation (14.203)

	P_r						
T_r	0.010	0.050	0.100	0.200	0.400	0.600	0.800
0.30	11.614	10.008	9.319	8.635	7.961	7.574	7.304
0.35	11.185	9.579	8.890	8.205	7.529	7.140	6.869
0.40	10.802	9.196	8.506	7.821	7.144	6.755	6.483
0.45	10.453	8.847	8.157	7.472	6.794	6.404	6.132
0.50	10.137	8.531	7.841	7.156	6.479	6.089	5.816
0.55	0.038	8.245	7.555	6.870	6.193	5.803	5.531
0.60	0.029	7.983	7.294	6.610	5.933	5.544	5.273
0.65	0.023	0.122	7.052	6.368	5.694	5.306	5.036
0.70	0.018	0.096	0.206	6.140	5.467	5.082	4.814
0.75	0.015	0.078	0.164	5.917	5.248	4.866	4.600
0.80	0.013	0.064	0.134	0.294	5.026	4.649	4.388
0.85	0.011	0.054	0.111	0.239	4.785	4.418	4.166
0.90	0.009	0.046	0.094	0.199	0.463	4.145	3.912
0.93	0.008	0.042	0.085	0.179	0.408	0.750	3.723
0.95	0.008	0.039	0.080	0.168	0.377	0.671	3.556
0.97	0.007	0.037	0.075	0.157	0.350	0.607	1.056
0.98	0.007	0.036	0.073	0.153	0.337	0.580	0.971
0.99	0.007	0.035	0.071	0.148	0.326	0.555	0.903
1.00	0.007	0.034	0.069	0.144	0.315	0.532	0.847
1.01	0.007	0.033	0.067	0.139	0.304	0.510	0.799
1.02	0.006	0.032	0.065	0.135	0.294	0.491	0.757
1.05	0.006	0.030	0.060	0.124	0.267	0.439	0.656
1.10	0.005	0.026	0.053	0.108	0.230	0.371	0.537
1.15	0.005	0.023	0.047	0.096	0.201	0.319	0.452
1.20	0.004	0.021	0.042	0.085	0.177	0.277	0.389
1.30	0.003	0.017	0.033	0.068	0.140	0.217	0.298
1.40	0.003	0.014	0.027	0.056	0.114	0.174	0.237
1.50	0.002	0.011	0.023	0.046	0.094	0.143	0.194
1.60	0.002	0.010	0.019	0.039	0.079	0.120	0.162
1.70	0.002	0.008	0.017	0.033	0.067	0.102	0.137
1.80	0.001	0.007	0.014	0.029	0.058	0.088	0.117
1.90	0.001	0.006	0.013	0.025	0.051	0.076	0.102
2.00	0.001	0.006	0.011	0.022	0.044	0.067	0.089
2.20	0.001	0.004	0.009	0.018	0.035	0.053	0.070
2.40	0.001	0.004	0.007	0.014	0.028	0.042	0.056
2.60	0.001	0.003	0.006	0.012	0.023	0.035	0.046
2.80	0.000	0.002	0.005	0.010	0.020	0.029	0.039
3.00	0.000	0.002	0.004	0.008	0.017	0.025	0.033
3.50	0.000	0.001	0.003	0.006	0.012	0.017	0.023
4.00	0.000	0.001	0.002	0.004	0.009	0.013	0.017

Table 14.10(continued)

Values of $\left(\frac{s_{ideal} - s_{actual}}{R}\right)^{(0)}$ for Equation (14.203)

P_r							
1.000	*1.200*	*1.500*	*2.000*	*3.000*	*5.000*	*7.000*	*10.000*
7.099	6.935	6.740	6.497	6.182	5.847	5.683	5.578
6.663	6.497	6.299	6.052	5.728	5.376	5.194	5.060
6.275	6.109	5.909	5.660	5.330	4.967	4.772	4.619
5.924	5.757	5.557	5.306	4.974	4.603	4.401	4.234
5.608	5.441	5.240	4.989	4.656	4.282	4.074	3.899
5.324	5.157	4.956	4.706	4.373	3.998	3.788	3.607
5.066	4.900	4.700	4.451	4.120	3.747	3.537	3.353
4.830	4.665	4.467	4.220	3.892	3.523	3.315	3.131
4.610	4.446	4.250	4.007	3.684	3.322	3.117	2.935
4.399	4.238	4.045	3.807	3.491	3.138	2.939	2.761
4.191	4.034	3.846	3.615	3.310	2.970	2.777	2.605
3.976	3.825	3.646	3.425	3.135	2.812	2.629	2.463
3.738	3.599	3.434	3.231	2.964	2.663	2.491	2.334
3.569	3.444	3.295	3.108	2.860	2.577	2.412	2.262
3.433	3.326	3.193	3.023	2.790	2.520	2.362	2.215
3.259	3.188	3.081	2.932	2.719	2.463	2.312	2.170
3.142	3.106	3.019	2.884	2.682	2.436	2.287	2.148
2.972	3.010	2.953	2.835	2.646	2.408	2.263	2.126
2.178	2.893	2.879	2.784	2.609	2.380	2.239	2.105
1.391	2.736	2.798	2.730	2.571	2.352	2.215	2.083
1.225	2.495	2.706	2.673	2.533	2.325	2.191	2.062
0.965	1.523	2.328	2.483	2.415	2.242	2.121	2.001
0.742	1.012	1.557	2.081	2.202	2.104	2.007	1.903
0.607	0.790	1.126	1.649	1.968	1.966	1.897	1.810
0.512	0.651	0.890	1.308	1.727	1.827	1.789	1.722
0.385	0.478	0.628	0.891	1.299	1.554	1.581	1.556
0.303	0.372	0.478	0.663	0.990	1.303	1.386	1.402
0.246	0.299	0.381	0.520	0.777	1.088	1.208	1.260
0.204	0.247	0.312	0.421	0.628	0.913	1.050	1.130
0.172	0.208	0.261	0.350	0.519	0.773	0.915	1.013
0.147	0.177	0.222	0.296	0.438	0.661	0.799	0.908
0.127	0.153	0.191	0.255	0.375	0.570	0.702	0.815
0.111	0.134	0.167	0.221	0.325	0.497	0.620	0.733
0.087	0.105	0.130	0.172	0.251	0.388	0.492	0.599
0.070	0.084	0.104	0.138	0.201	0.311	0.399	0.496
0.058	0.069	0.086	0.113	0.164	0.255	0.329	0.416
0.048	0.058	0.072	0.094	0.137	0.213	0.277	0.353
0.041	0.049	0.061	0.080	0.116	0.181	0.236	0.303
0.029	0.034	0.042	0.056	0.081	0.126	0.166	0.216
0.021	0.025	0.031	0.041	0.059	0.093	0.123	0.162

Table 14.11

Values of $\left(\frac{s_{ideal} - s_{actual}}{R}\right)^{(1)}$ for Equation (14.203)

	P_r						
T_r	0.010	0.050	0.100	0.200	0.400	0.600	0.800
0.30	16.782	16.774	16.764	16.744	16.705	16.665	16.626
0.35	15.413	15.408	15.401	15.387	15.359	15.333	15.305
0.40	13.990	13.986	13.981	13.972	13.953	13.934	13.915
0.45	12.564	12.561	12.558	12.551	12.537	12.523	12.509
0.50	11.202	11.200	11.197	11.192	11.182	11.172	11.162
0.55	0.115	9.948	9.946	9.942	9.935	9.928	9.921
0.60	0.078	8.828	8.826	8.823	8.817	8.811	8.806
0.65	0.055	0.309	7.832	7.829	7.824	7.819	7.815
0.70	0.040	0.216	0.491	6.951	6.945	6.941	6.937
0.75	0.029	0.156	0.340	6.173	6.167	6.162	6.158
0.80	0.022	0.116	0.246	0.578	5.475	5.468	5.462
0.85	0.017	0.088	0.183	0.408	4.853	4.841	4.832
0.90	0.013	0.068	0.140	0.301	0.744	4.269	4.249
0.93	0.011	0.058	0.120	0.254	0.593	1.219	3.914
0.95	0.010	0.053	0.109	0.228	0.517	0.961	3.697
0.97	0.010	0.048	0.099	0.206	0.456	0.797	1.570
0.98	0.009	0.046	0.094	0.196	0.429	0.734	1.270
0.99	0.009	0.044	0.090	0.186	0.405	0.680	1.098
1.00	0.008	0.042	0.086	0.177	0.382	0.632	0.977
1.01	0.008	0.040	0.082	0.169	0.361	0.590	0.883
1.02	0.008	0.039	0.078	0.161	0.342	0.552	0.807
1.05	0.007	0.034	0.069	0.140	0.292	0.460	0.642
1.10	0.005	0.028	0.055	0.112	0.229	0.350	0.470
1.15	0.005	0.023	0.045	0.091	0.183	0.275	0.361
1.20	0.004	0.019	0.037	0.075	0.149	0.220	0.286
1.30	0.003	0.013	0.026	0.052	0.102	0.148	0.190
1.40	0.002	0.010	0.019	0.037	0.072	0.104	0.133
1.50	0.001	0.007	0.014	0.027	0.053	0.076	0.097
1.60	0.001	0.005	0.011	0.021	0.040	0.057	0.073
1.70	0.001	0.004	0.008	0.016	0.031	0.044	0.056
1.80	0.001	0.003	0.006	0.013	0.024	0.035	0.044
1.90	0.001	0.003	0.005	0.010	0.019	0.028	0.036
2.00	0.000	0.002	0.004	0.008	0.016	0.023	0.029
2.20	0.000	0.001	0.003	0.006	0.011	0.016	0.021
2.40	0.000	0.001	0.002	0.004	0.008	0.012	0.015
2.60	0.000	0.001	0.002	0.003	0.006	0.009	0.012
2.80	0.000	0.001	0.001	0.003	0.005	0.008	0.010
3.00	0.000	0.001	0.001	0.002	0.004	0.006	0.008
3.50	0.000	0.000	0.001	0.001	0.003	0.004	0.006
4.00	0.000	0.000	0.001	0.001	0.002	0.003	0.005

Table 14.11(continued)

Values of $\left(\frac{s_{ideal} - s_{actual}}{R}\right)^{(1)}$ for Equation (14.203)

P_r							
1.000	*1.200*	*1.500*	*2.000*	*3.000*	*5.000*	*7.000*	*10.000*
16.586	16.547	16.488	16.390	16.195	15.837	15.468	14.925
15.278	15.251	15.211	15.144	15.011	14.751	14.496	14.153
13.896	13.877	13.849	13.803	13.714	13.541	13.376	13.144
12.496	12.482	12.462	12.430	12.367	12.248	12.145	11.999
11.153	11.143	11.129	11.107	11.063	10.985	10.920	10.836
9.914	9.907	9.897	9.882	9.853	9.806	9.769	9.732
8.799	8.794	8.787	8.777	8.760	8.736	8.723	8.720
7.810	7.807	7.801	7.794	7.784	7.779	7.785	7.811
6.933	6.930	6.926	6.922	6.919	6.929	6.952	7.002
6.155	6.152	6.149	6.147	6.149	6.174	6.213	6.285
5.458	5.455	5.453	5.452	5.461	5.501	5.555	5.648
4.826	4.822	4.820	4.822	4.839	4.898	4.969	5.082
4.238	4.232	4.230	4.236	4.267	4.351	4.442	4.578
3.894	3.885	3.884	3.896	3.941	4.046	4.151	4.300
3.658	3.647	3.648	3.669	3.728	3.851	3.966	4.125
3.406	3.391	3.401	3.437	3.517	3.661	3.788	3.957
3.264	3.247	3.268	3.318	3.412	3.569	3.701	3.875
3.093	3.082	3.126	3.195	3.306	3.477	3.616	3.796
2.399	2.868	2.967	3.067	3.200	3.387	3.532	3.717
1.306	2.513	2.784	2.933	3.094	3.297	3.450	3.640
1.113	1.655	2.557	2.790	2.986	3.209	3.369	3.565
0.820	0.831	1.443	2.283	2.655	2.949	3.134	3.348
0.577	0.640	0.618	1.241	2.067	2.534	2.767	3.013
0.437	0.489	0.502	0.654	1.471	2.138	2.428	2.708
0.343	0.385	0.412	0.447	0.991	1.767	2.115	2.430
0.226	0.254	0.282	0.300	0.481	1.147	1.569	1.944
0.158	0.178	0.200	0.220	0.290	0.730	1.138	1.544
0.115	0.130	0.147	0.166	0.206	0.479	0.823	1.222
0.086	0.098	0.112	0.129	0.159	0.334	0.604	0.969
0.067	0.076	0.087	0.102	0.127	0.248	0.456	0.775
0.053	0.060	0.070	0.083	0.105	0.195	0.355	0.628
0.043	0.049	0.057	0.069	0.089	0.160	0.286	0.518
0.035	0.040	0.048	0.058	0.077	0.136	0.238	0.434
0.025	0.029	0.035	0.043	0.060	0.105	0.178	0.322
0.019	0.022	0.027	0.034	0.048	0.086	0.143	0.254
0.015	0.018	0.021	0.028	0.041	0.074	0.120	0.210
0.012	0.014	0.018	0.023	0.035	0.065	0.104	0.188
0.010	0.012	0.015	0.020	0.031	0.058	0.093	0.158
0.007	0.009	0.011	0.015	0.024	0.046	0.073	0.122
0.006	0.007	0.009	0.012	0.020	0.038	0.060	0.100

14.9 Stability of Thermal-fluid Systems

The various models described above, including the pure substance model, assume that the state of the fluid is a stable equilibrium state, i.e., stable with respect to perturbations or fluctuations in its properties. In general, this may not necessarily be the case. We have already seen that the van der Waals model admits a whole host of states that are unstable as well as a domain of unstable states. Furthermore, it is common in engineering practice for the pure substance to be in a metastable state such that the smallest perturbation to that state will drive the fluid into a stable equilibrium state. It would be valuable, then, at this point in our development to examine in detail the conditions that determine the stability of the states of the pure substance model.

For this purpose, we consider an isolated system with fixed values of energy U and volume V. At equilibrium, the entropy of this system is maximum. Thus, any departure from equilibrium will decrease the entropy. In response to this departure, the system undergoes irreversible processes that generate entropy and drive the system back toward equilibrium. It follows, then, that the state of equilibrium is stable with respect to any departure that results in a decrease in entropy.

In a perturbed state, the entropy S can be expanded in a power series such that

$$S = S_{eq} + \delta S + \frac{1}{2}\delta^2 S + \ldots \tag{14.205}$$

where δS represents the first-order departure of the entropy from the equilibrium value, S_{eq}, and contains first-order perturbations δT, δV, δP, ... The term $\delta^2 S$ represents the second-order departures $(\delta T)^2$, $(\delta V)^2$, $(\delta P)^2$, ...

Since entropy is a maximum in the equilibrium state, the first-order term in equation (14.205) vanishes, i.e., $\delta S = 0$. Then it is the second-order term that we need to consider in establishing the conditions for stability. True stability requires that the system be stable with respect to both thermal and mechanical perturbations. Let us consider each of these in turn. first the conditions for thermal stability.

14.9.1 Thermal Stability

The approach is to consider the aforementioned isolated system with fixed values of energy and volume. We now divide the system into two subsystems as shown schematically in Figure 14.7: a large subsystem denoted by the symbol L and a small subsystem denoted by the symbol S with the departure from equilibrium occurring in the small subsystem.

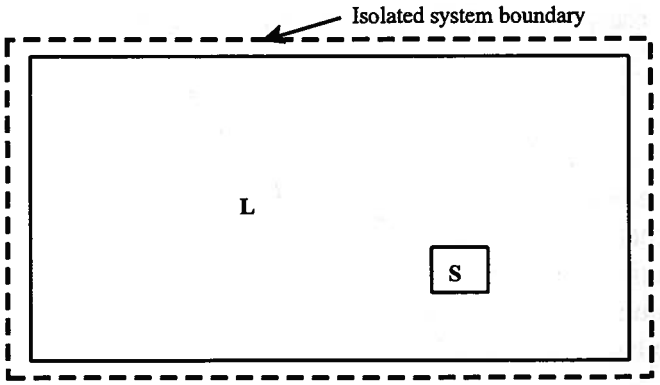

Figure 14.7 Subsystems of the Isolated System

The entropy of the composite system is given by

$$S = S_S + S_L \tag{14.206}$$

where

$$S_S = S_S(U_S, V_S) \quad \text{and} \quad S_L = S_L(U_L, V_L) \tag{14.207}$$

If we now expand the entropy in a Taylor series about its equilibrium value, we have

$$S - S_{eq} = \Delta S = \left(\frac{\partial S_S}{\partial U_S}\right)_{V_S} \delta U_S + \left(\frac{\partial S_L}{\partial U_L}\right)_{V_L} \delta U_L + \left(\frac{\partial^2 S_S}{\partial U_S{}^2}\right)_{V_S} \frac{(\delta U_s)^2}{2} + \left(\frac{\partial^2 S_L}{\partial U_L{}^2}\right)_{V_L} \frac{(\delta U_L)^2}{2} + \ldots \tag{14.208}$$

Physically, there is a perturbation in temperature of the small subsystem which causes a heat transfer interaction between subsystems S and L. This, in turn, produces a disturbance in energy. Since the total energy of the isolated system is constant

$$\delta U_S = -\delta U_L = \delta U \tag{14.209}$$

Since by definition

$$\left(\frac{\partial U}{\partial S}\right)_V \equiv \frac{1}{T} \tag{14.210}$$

we have upon combining equations (14.208), (14.209), and (14.210)

$$\Delta S = \left(\frac{1}{T_S} - \frac{1}{T_L}\right)\delta U + \left[\frac{\partial}{\partial U_S}\left(\frac{1}{T_S}\right) + \frac{\partial}{\partial U_L}\left(\frac{1}{T_L}\right)\right]\frac{(\delta U)^2}{2} + \ldots \tag{14.211}$$

Comparing like terms in equations (14.211) and (14.208), we observe

$$\delta S = \left(\frac{1}{T_S} - \frac{1}{T_L}\right)\delta U \tag{14.212}$$

and

$$\frac{1}{2}\delta^2 S = \left[\frac{\partial}{\partial U_S}\left(\frac{1}{T_S}\right) + \frac{\partial}{\partial U_L}\left(\frac{1}{T_L}\right)\right]\frac{(\delta U)^2}{2} \tag{14.213}$$

Since the entropy at equilibrium is a maximum, it follows that $\delta S = 0$. Then from equation (14.212), we have at equilibrium

$$T_S = T_L = T \tag{14.214}$$

If we neglect the higher order terms in the Taylor series expansion of equation (14.208), the departure from equilibrium is then described in terms of the second-order terms which must cause the entropy to decrease. That is, $\delta^2 S < 0$ which we apply to equation (14.213). In equation (14.213) we note that

$$\frac{\partial}{\partial U}\left(\frac{1}{T}\right)_V = -\frac{1}{T^2}\left(\frac{\partial T}{\partial U}\right)_V = -\frac{1}{T^2}\left(\frac{1}{mc_v}\right) \tag{14.215}$$

where we have made use of the definition of the specific heat at constant volume, c_v, equation (14.49). We also note that because of their relative sizes, the small subsystem changes in temperature by an amount δT as a result of the disturbance while the large subsystem remains at the equilibrium temperature T. In effect, the large subsystem appears to the small subsystem as though it has an infinite heat capacity. Then equation (14.209) becomes

$$\delta U = m_S c_v \delta T \tag{14.216}$$

and the second-order term given by equation (14.213) becomes with the aid of equation (14.215)

$$\frac{1}{2}\delta^2 S = \left[-\frac{1}{(T+\delta T)^2}\left(\frac{1}{m_S c_v}\right) + \frac{1}{T^2}\left(\frac{1}{m_L c_v}\right)\right]\frac{(m_S c_v \delta T)^2}{2} \tag{14.217}$$

which can be written in the form

$$\frac{1}{2}\delta^2 S = \left[-\frac{1}{(T+\delta T)^2} + \frac{1}{T^2}\left(\frac{m_S c_v}{m_L c_v}\right)\right]\frac{(m_S c_v)^2 (\delta T)^2}{2(m_S c_v)} \tag{14.218}$$

Since $m_S << m_L$, the second term in the square brackets of equation (14.218) can be neglected compared with the first term. Then equation (14.218) reduces to

$$\frac{1}{2}\delta^2 S = \left[-\frac{1}{(T+\delta T)^2}\right]\frac{(m_S c_v)(\delta T)^2}{2} \tag{14.219}$$

However, from our previous observations, we know that $\delta T << T$. Then equation (14.219) becomes

$$\frac{1}{2}\delta^2 S = -\frac{(m_S c_v)(\delta T)^2}{2T^2} \tag{14.220}$$

Since the second-order term must cause a decrease in entropy as a result of the disturbance, it must be the case that

$$-\frac{(m_S c_v)(\delta T)^2}{2T^2} < 0 \tag{14.221}$$

From equation (14.221) it follows that

$$c_v > 0 \tag{14.222}$$

This is the condition of *thermal stability*.

Thus, a stable equilibrium state is stable to perturbations in temperature if $c_v > 0$.

14.9.2 Mechanical Stability

We now turn our attention to the condition that determines the stability of a thermal-fluid system subjected to a disturbance in mechanical equilibrium. Following the example of the previous section, we once again consider an isolated system divided into two subsystems, a small subsystem denoted by the symbol *S* and a large subsystem denoted by the symbol *L*. In the present case, the two subsystems are separated by a frictionless diathermal piston. The conditions of isolation for the composite system result in a situation in which the total volume is constant while the diathermal piston ensures that the temperature will be constant throughout the composite system. The situation is depicted schematically in Figure 14.8.

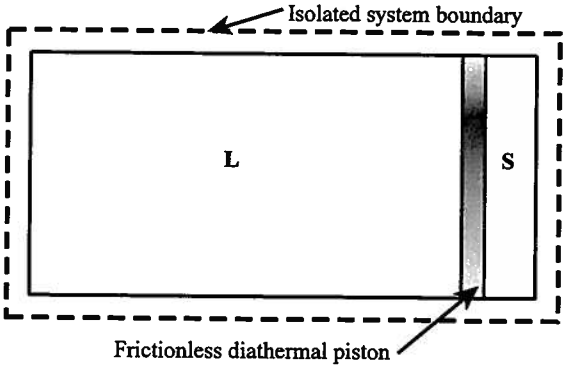

Figure 14.8 Isolated System with Two Subsystems Separated by a Frictionless Diathermal Piston

Since the volume and temperature of the isolated system are both constant, it is appropriate to describe the system in terms of the Helmholtz free energy, $F = F(T,V) = U - TS$. Then

$$dF = dU - TdS - SdT \tag{14.223}$$

From the canonical relation, we have

$$dU = TdS - PdV \tag{14.224}$$

From the second law, we have

$$dS = \delta S_{transfer} + \delta S_{gen} \tag{14.225}$$

Then combining equations (14.223) – (14.225), we get

$$dF = -SdT - PdV - T\delta S_{transfer} - T\delta S_{gen} \tag{14.226}$$

For the isolated system,

$$dT = 0 \quad \text{and} \quad dV = 0 \quad \text{and} \quad T\delta S_{transfer} = 0 \tag{14.227}$$

Then equation (14.226) becomes

$$-dF = T\delta S_{gen} > 0 \tag{14.228}$$

It follows, then, that the equilibrium condition is one for which the Helmholtz free energy is a minimum.

We now want to explore the departure from equilibrium that results from a small displacement of the piston between the two subsystems. Then expanding the Helmholtz free energy in a Taylor series about the equilibrium value, we obtain

$$F - F_{eq} = \Delta F = \left(\frac{\partial F_S}{\partial V_S}\right)_T \delta V_S + \left(\frac{\partial F_L}{\partial V_L}\right)_T \delta V_L + \left(\frac{\partial^2 F_S}{\partial V_S^{\,2}}\right)_T \frac{(\delta V_S)^2}{2} + \left(\frac{\partial^2 F_L}{\partial V_L^{\,2}}\right)_T \frac{(\delta V_L)^2}{2} + \ldots \tag{14.229}$$

where δV represents the disturbance in the Helmholtz free energy due to the aforementioned displacement of the common boundary between the subsystems S and L. Since the total volume is constant, we have

$$\delta V_S = -\delta V_L = \delta V \tag{14.230}$$

By definition,

$$\left(\frac{\partial F}{\partial V}\right)_T \equiv -P \tag{14.231}$$

Then with the aid of equations (14.230) and (14.231), equation (14.229) becomes

$$F - F_{eq} = \Delta F = (-P_S + P_L)\delta V + \left[-\frac{\partial P_S}{\partial V_S} + \frac{\partial P_L}{\partial V_L}\right]\frac{(\delta V)^2}{2} + \ldots \tag{14.232}$$

The power series expansion of the Helmholtz free energy is

$$F = F_{eq} + \delta F + \frac{1}{2}\delta^2 F + \ldots \tag{14.233}$$

Comparing equivalent terms in equations (14.232) and (14.233), we get

$$\delta F = (-P_S + P_L)\delta V \tag{14.234}$$

and

$$\frac{1}{2}\delta^2 F = \left[-\frac{\partial P_S}{\partial V_S} + \frac{\partial P_L}{\partial V_L}\right]\frac{(\delta V)^2}{2} \tag{14.235}$$

Since the Helmholtz free energy is a minimum at equilibrium, $\delta F = 0$ and equation (14.234) shows that the boundary between the two subsystems, the piston, is in mechanical equilibrium with $P_S = P_L = P$. If we neglect the higher order terms in the Taylor series expansion, the

departure from equilibrium is due to the second-order terms which cause the Helmholtz free energy to increase. Then $\delta^2 F > 0$.

From equation (14.62) we have

$$\left(\frac{\partial P}{\partial V}\right)_T = -\frac{1}{\kappa V} \tag{14.236}$$

where κ is the *isothermal compressibility*. Then the second-order term of equation (14.235) becomes

$$\frac{1}{2}\delta^2 F = \left[\frac{1}{\kappa V_S} - \frac{1}{\kappa V_L}\right]\frac{(\delta V)^2}{2} \tag{14.237}$$

Equation (14.237) can be written in the form

$$\frac{1}{2}\delta^2 F = \left[\frac{1}{\kappa} - \frac{1V_S}{\kappa V_L}\right]\frac{(\delta V)^2}{2V_S} \tag{14.238}$$

But from the geometry of the isolated system, $V_S << V_L$. Then the second term in square brackets in equation (14.238) is negligible compared to the first term. Then

$$\frac{1}{2}\delta^2 F = \frac{1}{\kappa}\frac{(\delta V)^2}{2V_S} > 0 \tag{14.239}$$

It follows, then, that the condition for *mechanical stability* is

$$\kappa > 0 \tag{14.240}$$

or equivalently

$$-\frac{1}{V}\left(\frac{\partial V}{\partial P}\right)_T > 0 \tag{14.241}$$

or

$$\left(\frac{\partial P}{\partial V}\right)_T < 0 \tag{14.242}$$

Thus in order for a state to be mechanically stable, the slope of the isotherm passing through the state must have negative slope in *P-V* coordinates. It is for this reason that the states along the path *m-o-n* in Figure 14.3 are not stable. This condition exposes one of the deficiencies of the van der Waals model.

14.9.3 Physical Significance of the Stability Criteria

Quite apart from simply establishing the conditions for stability in any model the might be used to describe the behavior of matter, the stability criteria also establish the relationship among many of the parameters used to characterize matter. For example, in equation (14.75), we presented a general relation between the specific heats of a model, viz.

$$c_P - c_v = \frac{Tv\beta^2}{\kappa} \tag{14.243}$$

where β is the coefficient of thermal expansion and κ is the coefficient of isothermal compressibility.

By the criterion of mechanical stability, equation (14.240), we have $\kappa > 0$. It followsfrom equation (14.243), then, that

$$c_P > c_v \tag{14.244}$$

and

$$\gamma = \frac{c_P}{c_v} > 1 \tag{14.245}$$

Thus, the specific heat at constant pressure is always greater than the specific heat at constant volume.

If we now define the coefficient of adiabatic compressibility, κ_S, by the relation

$$\kappa_S = -\frac{1}{v}\left(\frac{\partial v}{\partial P}\right)_s \tag{14.246}$$

we can show that

$$\kappa - \kappa_S = \frac{Tv\beta^2}{c_P} \tag{14.247}$$

Then by the criterion for thermal stability, equation (14.222), it follows that

$$\kappa > \kappa_S \tag{14.248}$$

Substituting the defining relations for κ and κ_S, we obtain

$$-\frac{1}{v}\left(\frac{\partial v}{\partial P}\right)_T > -\frac{1}{v}\left(\frac{\partial v}{\partial P}\right)_s \tag{14.249}$$

Then

$$\left(\frac{\partial P}{\partial v}\right)_s < \left(\frac{\partial P}{\partial v}\right)_T \tag{14.250}$$

Then for any stable equilibrium state located on the P-v plane, the slope of the isentrope through that state is steeper (more negative) than the slope of the isotherm through the same state. It is this fact that makes the Carnot cycle possible.

Problems

14.1 One kg of liquid is compressed in a reversible, adiabatic process from P_1 to P_2.

(a) If the liquid is modeled as a fluid with constant specific heats and a constant coefficient of thermal expansion, β, show that the final temperature after compression is approximately

$$T_2 = T_1 \exp\left[\frac{\beta v}{c_P}(P_2 - P_1)\right]$$

where

$$\beta = \frac{1}{v}\left(\frac{\partial v}{\partial T}\right)_P$$

(b) Experimental measurements of β and c_P show that for saturated liquid water at a pressure of 7 x 10^3 N/m^2,

$$\beta = 3.708 \text{ x } 10^{-4} \text{ (K)}^{-1} \quad \text{and} \quad c_P = 4.124 \text{ J/kg K}$$

What is the change in temperature for a reversible adiabatic, compression from this saturated state to a final pressure of 5 x 10^5 N/m^2?

(c) Suppose that saturated vapor at the same initial pressure of 7 x 10^3 N/m^2 is compressed in a reversible adiabatic manner to a final pressure of 5 x 10^5 N/m^2. What would the change in temperature be for this compression process? (Note from the temperature-entropy diagram that the initial state lies in a region where the vapor can be well represented by the ideal gas model.) How do you account for the difference between your answers to parts (a) and (b)?

14.2 Prove that the specific heat at constant pressure, c_P, for an ideal gas is a function of temperature only.

HINT: Use proof by contradiction. That is, assume $c_P = c_P(T,P)$ and show that $(\partial c_P/\partial P)_T = 0$.

14.3 Consider the classical example of a free expansion. A rigid, insulated container is divided into two compartments by a diaphragm. One compartment of volume V_1 contains a gas at a temperature T_1 and a pressure P_1. The other compartment of volume V_2 is evacuated. If the diaphragm separating the compartments is suddenly fractured, the gas will spontaneously expand to the volume of the whole container.

(a) Show that the temperature change for such a process is

$$T_2 - T_1 = \int_{V_1}^{V_1+V_2} \frac{1}{m}\left(\frac{P}{c_v} - \frac{T\beta}{c_v\kappa}\right)dV$$

where β is the coefficient of thermal expansion and κ is the coefficient of isothermal compressibility.

$$\beta = \frac{1}{V}\left(\frac{\partial V}{\partial T}\right)_P$$

$$\kappa = -\frac{1}{V}\left(\frac{\partial V}{\partial P}\right)_T$$

(b) Show that for an ideal gas there is no temperature change.

14.4 One method of liquefying gases is to compress the gas to a very high pressure and then expand the gas to a much lower pressure by means of a throttle. Since in a throttling process the enthalpy at inlet is identical to the enthalpy at outlet, the relevant performance parameter for this process is the Joule-Thomson coefficient defined as

$$\mu_{JT} = \left(\frac{\partial T}{\partial P}\right)_h$$

(a) Show that in general

$$\mu_{JT} = \frac{1}{c_P}\left[T\left(\frac{\partial v}{\partial T}\right)_P - v\right]$$

(b) Can an ideal gas be liquefied in this manner?

(c) Determine the Joule-Thomson coefficient for the incompressible fluid model.

14.5 The saturation pressure, P (N/m^2), for solid-vapor equilibrium in ammonia (molecular weight = 17.03 kg/kg-mole) is given by

$$\ln P = 11.552\left(\text{N/m}^2\right) - \frac{3255\ (\text{K})}{T}$$

where T is the temperature in K. The saturation pressure for liquid-vapor equilibrium in ammonia is given by

$$\ln P = 10.410\left(\text{N/m}^2\right) - \frac{3032\ (\text{K})}{T}$$

(a) What is the temperature of the triple point?

(b) What are the latent heats of sublimation and vaporization at the triple point?

(c) What is the latent heat of fusion at the triple point?

14.6 The expressions listed below have been proposed as characteristic thermodynamic functions for a system of mass m. Decide whether they are consistent with the requirements that must be fulfilled by functions of this type. For the ones that are physically acceptable, derive expressions for T and P.

The quantities v_0, θ, and R are positive constants.

(a) $u = \left(\frac{R\theta}{v_0}\right) mv \left(1 + \frac{s}{R}\right) \exp\left(-\frac{s}{R}\right)$

(b) $u = \left(\frac{v_0\theta}{R}\right) \frac{s^2}{v} \exp\left(\frac{s}{R}\right)$

(c) $u = \left(\frac{v_0\theta}{R^2}\right) \frac{m^2 s^3}{v}$

14.7 The speed of sound a in a homogeneous medium is defined as

$$a^2 = \left(\frac{\partial P}{\partial \rho}\right)_s$$

where ρ is the density and $\rho = 1/v$ where v is the specific volume.

(a) Show that the speed of sound can be written

$$a^2 = \frac{v\gamma}{\kappa}$$

where

$$\kappa \equiv -\frac{1}{v}\left(\frac{\partial v}{\partial P}\right)_T = \text{ isothermal compressibility}$$

$$\gamma = \frac{c_P}{c_v}$$

(b) Show that for an ideal gas

$$a^2 = \gamma RT$$

(c) Compute the speed of sound in R-22 saturated vapor at $T_{sat} = -120$ C where the saturation pressure is $P_{sat} = 230$ N/m^2 and $\rho_g = 0.01585$ kg/m^3, $(c_v)_g = 373.9$ J/kg K, and $(c_P)_g = 470.3$ J/kg K. Compare this with the reported value of $a = 136$ m/sec.

(d) Compute the speed of sound for both the saturated liquid and saturated vapor phases of R-22 at 20 C given the following data:

Liquid: $\rho_f = 1210$ kg/m^3, $(c_v)_f = 686.4$ J/kg K, $(c_P)_f = 1236$ J/kg K, $z_f = 0.02668$
Vapor: $\rho_g = 38.48$ kg/m^3, $(c_v)_g = 619.5$ J/kg K, $(c_P)_g = 840.4$ J/kg K, $z_g = 0.8390$

where z is the compressibility factor defined as

$$z = \frac{Pv}{RT}$$

14.8 As shown in the sketch below, a piston-cylinder apparatus contains 1 kg of H_2O in a metastable state, $P_1 = 5 \times 10^6$ N/m^2 and $T_1 = 260$ C. The area of the piston is $A_p = 0.25$ m^2. In effect, this is a supersaturated vapor since $T_1 < T_{sat}$. The H_2O undergoes a spontaneous transition to the stable equilibrium state, state 2.

(a) What is the temperature T_2?

(b) Using the van der Waals equation of state to describe the metastable state, estimate the change in volume $V_2 - V_1$.

The following data may be helpful: $R = 461.51$ J/kg K

$$c_{P0} = 0.046\tau + 1.47276 + \frac{0.83893}{\tau} - \frac{0.219989}{\tau^2} + \frac{0.244619}{\tau^3} - \frac{0.0970466}{\tau^4} \text{ in units of J/gram K}$$

where

$$\tau = \frac{1000\ (\text{K})}{T}$$

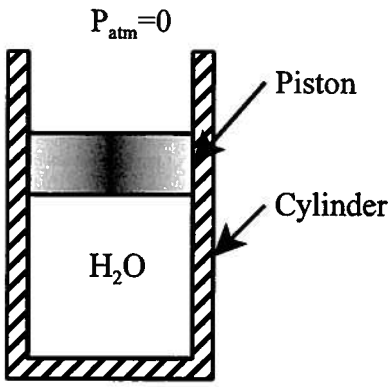

14.9 Using the van der Waals model, explain qualitatively how the value of the compressibility factor, z, can be greater than unity.

14.10 For the van der Waals model, we wish to formulate expressions for the various thermodynamic properties.

(a) Find expressions for $s = s(T,v)$, $u = u(T,v)$, $h = h(T,v)$.

(b) Find expressions for $s = s(T,P)$, $u = u(T,P)$, $h = h(T,P)$.

(c) Find $\mu_{JT} = \mu_{JT}(T,v)$.

(d) Find $c_P = c_P(T,v)$.

14.11 For an elastic material, the conjugate mechanical properties are the strain, ε, and the stress, σ. The thermodynamic coupling between the thermal and mechanical properties of an elastic material is weak. Nevertheless, when a load (stress) is applied to such a material, both the strain and the thermal properties, s and T, will change. One of the coefficients that provides a measure of this coupling is the thermal expansion coefficient β where

$$\beta = \left(\frac{\partial \varepsilon}{\partial T}\right)_{\sigma}$$

For the physical situation consisting of a bar under axial tensile load with uniform tensile stress, we wish to compare the extent of the coupling in bars made of steel, aluminum, and tugsten.

(a) For each of the materials, given the thermal expansion coefficient of the material, calculate the entropy change per unit mass for a change in stress from 0 to 50 x 10^6 N/m^2 if the bar is maintained at a temperature of 300 K.

(b) For each of the materials, calculate the heat transfer required to maintain the temperature at 300 K for the condition specified in part (a) above.

(c) Now suppose that the load is applied in a reversible, adiabatic manner. Formulate an expression for

$$\left(\frac{\partial T}{\partial \sigma}\right)_{s} = f(\beta, c_{\varepsilon}, Y)$$

where c_{ε} is the specific heat at constant strain and Y is Young's modulus, viz.

$$c_{\varepsilon} \equiv \left(\frac{\partial u}{\partial T}\right)_{\varepsilon} \quad \text{and} \quad Y = \left(\frac{\partial \sigma}{\partial \varepsilon}\right)_{T}$$

(d) For each of the materials, calculate the temperature change if the stress is changed from 0 to 50 x 10^6 N/m^2 in a reversible, adiabatic manner.

(e) What conclusions can you draw regarding the degree of coupling in these three materials? How does this coupling compare with that found in H_2O?

The following properties may be useful:
Steel: $\beta = 10.8 \times 10^{-6}$ K^{-1}, $c_{\varepsilon} = 419$ J/kg K, $\rho = 7850$ kg/m^3, $Y = 207 \times 10^9$ N/m^2
Aluminum: $\beta = 23.9 \times 10^{-6}$ K^{-1}, $c_{\varepsilon} = 962$ J/kg K, $\rho = 2700$ kg/m^3, $Y = 71 \times 10^9$ N/m^2
Tungsten: $\beta = 4.3 \times 10^{-6}$ K^{-1}, $c_{\varepsilon} = 138$ J/kg K, $\rho = 19{,}300$ kg/m^3, $Y = 355 \times 10^9$ N/m^2

14.12 Paramagnetic materials can have a change in internal energy due to a magnetic work transfer interaction. The magnetic work transfer per unit mass for these materials is given by

$$\delta W = -\mu_0 v H dM$$

where μ_0 is the permeability of free space, v is the specific volume of the material, H is the

magnetic field intensity, and M is the magnetization of the material.

(a) Formulate the canonical relation for a paramagnetic material.

(b) Formulate expressions for

$$dh_m = d\left(u - \mu_0 vHM\right)$$

$$df_m = d\left(u - Ts\right)$$

$$dg_m = d\left(u - \mu_0 vHM - Ts\right)$$

(c) Formulate the equivalent Maxwell relations for a paramagnetic material.

Suppose now that the property constitutive relation for a paramagnetic material is given by Curie's Law, viz.

$$M = C_C \frac{H}{T}$$

where C_C is a constant.

(d) Formulate an expression of the form $u = u(T,H)$ and the specific heat at constant $H = 0$, $c_{H=0}$.

(e) Formulate an expression of the form $s = s(T,H)$ and the specific heat at constant $H = 0$, $c_{H=0}$.

(f) One method of attaining very low temperatures is the adiabatic demagnetization of a paramagnetic material. Using the results of parts (d) and (e) above, explain how one would carry out such a cooling process.

14.13 Show that the difference in the specific heats $c_P - c_v$ may be expressed as

$$c_P - c_v = \frac{Tv\beta^2}{\kappa}$$

where β is the coefficient of thermal expansion and κ is the coefficient of isothermal compressibility.

$$\beta = \frac{1}{V}\left(\frac{\partial V}{\partial T}\right)_P$$

$$\kappa = -\frac{1}{V}\left(\frac{\partial V}{\partial P}\right)_T$$

14.14 The pressure of a 1 kg block of copper at a temperature of $T_1 = 0$ C is increased isothermally and reversibly from $P_1 = 10^5$ N/m^2 to $P_2 = 10^8$ N/m^2. Assume that the coefficient of thermal expansion β, the isothermal compressibility κ and the density ρ are constant.

(a) Calculate the work transfer and heat transfer for the copper during the compression.

(b) Does your answer violate the first law of thermodynamics?

(c) What would have been the rise in temperature if the process had been adiabatic instead of isothermal?

For copper:

$$\beta = 5.04 \text{ x } 10^{-5} \text{ K}^{-1}$$

$$\kappa = 8.56 \text{ x } 10^{-12} \text{ m}^2/\text{N}$$

$$\rho = 8009 \text{ kg/m}^2$$

14.15 An elastic rod has a length X and a temperature T when the tensile force on its ends is F. For this system, the energy U and the entropy S are given by the relations

$$U = C_X T$$

and

$$S = C_X \ln T - KX^2$$

where C_X and K are constants.

(a) Find the equation of state $f(F,X,T) = 0$ for this system.

(b) The elastic rod with $K = 17.2$ N/m^2 K and $C_x = 9.76$ J/K is taken through a Carnot cycle between heat reservoirs at 335 K and 315 K. The minimum length at the higher temperature is 3 m and the work transfer per cycle is 70 J. Show the Carnot cycle on the T-S and the F-X diagrams.

14.16 In a particular combustion test apparatus, it is necessary to provide a supply of ethane at a constant pressure of $P_1 = 7.3 \times 10^6$ N/m^2 and a constant temperature of $T_1 = 340$ C. To meet these requirements the research team built a piston-cylinder apparatus, shown in the sketch below, which uses a weighted piston to maintain constant pressure and a sensor and guard heater to maintain constant temperature. During one night while the supply valve is closed (no mass flow), the janitor unknowingly turns off the power supply to the guard heaters, and the temperature of the ethane falls due to heat losses to the environment. By the time the error is discovered the following morning, the temperature of the ethane has dropped to $T_2 = 63$ C. At this time, the research assistant turns on the guard heaters; however, unknown to her, the piston is now seized in the cylinder resulting in a gas volume V_2 corresponding to the temperature and pressure at the time the guard heaters were turned on. With the piston now locked in this position, the guard heaters return the temperature to $T_3 = 340$ C. The zero pressure specific heat of ethane is $c_{P0} = 1767$ J/kg K.

(a) Show the sequence of events on a P-v diagram assuming all processes are quasi-static.

(b) What is the pressure of the gas at the operating temperature of $T_3 = 340$ C if the piston remains seized?

(c) What is the heat transfer (per unit mass of ethane) for the surroundings during the cool down time 1 → 2 while the power is off?

(d) What is the heat transfer (per unit mass of ethane) for the guard heaters during the process 2 → 3 while the piston is seized?

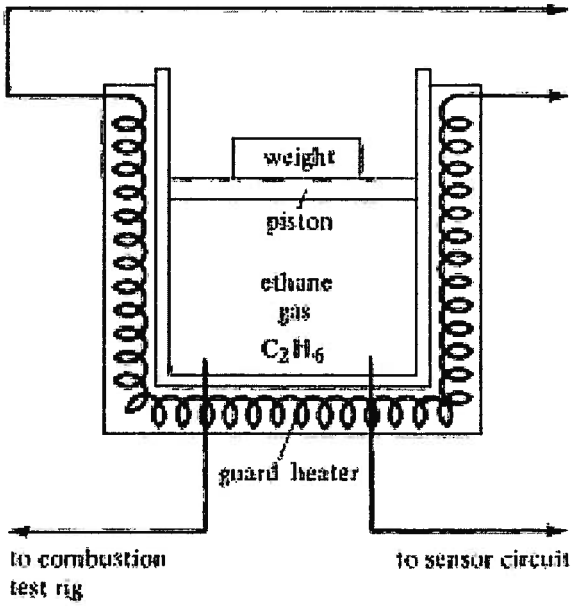

14.17 The equilibrium radiation within an evacuated uniform temperature enclosure is called blackbody radiation and Planck's law for blackbody radiation can be applied to this radiation. With the aid of Planck's law it can be shown that the energy density U/V of the radiation is

$$u = \frac{U}{V} = \frac{4}{c_0}\sigma T^4$$

where c_0 is the speed of light in the vacuum and σ is the Stefan-Boltzman radiation constant. The formulation of macroscopic thermodynamics can be applied to this equilibrium radiation field.

(a) For this constant volume system, derive an expression for the entropy of the enclosure in terms of T and V. Assume that $s = 0$ at $T = 0$.

(b) What are the Helmholtz free energy and the pressure of the equilibrium radiation field?

(c) What are the Gibbs free energy and the specific heats c_P and c_v for the equilibrium radiation field? Explain the physical significance of each result.

14.18 For a closed system, the specific heat is defined, in general, as the reversible heat transfer per unit mass per unit temperature change, viz.

$$c_y = \frac{1}{m}\left(\frac{\delta Q}{dT}\right)_y$$

where the subscript y denotes some property held constant or some constraint on the system during the heat transfer process.

(a) Show that for a single phase state, the specific heat at constant pressure is

$$c_P \equiv \frac{1}{m}\left(\frac{\delta Q}{dT}\right)_P = T\left(\frac{\partial s}{\partial T}\right)_P = \left(\frac{\partial h}{\partial T}\right)_P$$

(b) Show that for a closed system consisting of two phases in equilibrium, if we write

$$s_f = s_f\left[T, P(T)\right]_{sat} \quad \text{and} \quad s_g = s_g\left[T, P(T)\right]_{sat}$$

the specific heat of the saturated liquid along the locus of saturated states is

$$c_f \equiv \frac{1}{m}\left(\frac{\delta Q}{dT}\right)_f = T\left(\frac{ds_f}{dT}\right) \neq \left(\frac{dh_f}{dT}\right)$$

and the specific heat of the saturated vapor along the locus of saturated states is

$$c_g \equiv \frac{1}{m}\left(\frac{\delta Q}{dT}\right)_g = T\left(\frac{ds_g}{dT}\right) \neq \left(\frac{dh_g}{dT}\right)$$

(c) Show that if β represents the coefficient of thermal expansion

$$c_f = c_{P,f} - \beta_f v_f \frac{h_{fg}}{v_{fg}}$$

and

$$c_g = c_{P,g} - \beta_g v_g \frac{h_{fg}}{v_{fg}}$$

(d) Show that the variation of the latent heat h_{fg} along the locus of saturated states is given by *Planck's formula*, viz.

$$\frac{dh_{fg}}{dT} = c_{P,g} - c_{P,f} + \frac{h_{fg}}{T} - \frac{h_{fg}}{v_{fg}}\left(\frac{\partial v_{fg}}{\partial T}\right)_P$$

CHAPTER 15

Behavior of Steady-Flow Components of Thermal-Fluid Systems

15.1 Introduction

As we showed in Chapter 8, many complex thermal-fluid systems operate in a steady flow or periodic flow manner which greatly simplifies the analysis of their behavior. Typically, these systems employ a working fluid that can be modeled in terms of one of the fluid models already discussed in some detail in Chapters 4 and 13. The thermal-fluid systems themselves are constructed by interconnecting steady-flow components via pipes through which the working fluid is circulated. These steady-flow components are usually grouped into four classes according to function: (1) shaft work machines, (2) nozzles and diffusers, (3) throttles, and (4) heat exchangers. We have already addressed the analysis of heat exchangers in Chapter 12, and we now turn our attention to the other three classes of components. An understanding of the behavior of these components is essential to understanding the thermal-fluid plants to be presented in the Chapter 16.

Our objective in the present chapter is to determine the thermal-fluid behavior of the components of each class by modeling the component as a control volume and applying the equations that describe the thermal fluid behavior of the control volume in the manner of Chapter 8. This approach yields the "black box" characteristics of the component that must be known in order to evaluate the performance of the complete system of interconnected components. This does not mean that these equations do not apply or are not useful in determining the detailed internal processes of the component. On the contrary, in designing such a component, thorough consideration must be given to the complex internal processes. Whenever possible, we shall elaborate upon the details of these internal processes within the context of the present approach; however, in some cases, the analysis of these internal processes is outside the scope of our present objective and is better left to more advanced treatments of the subject.

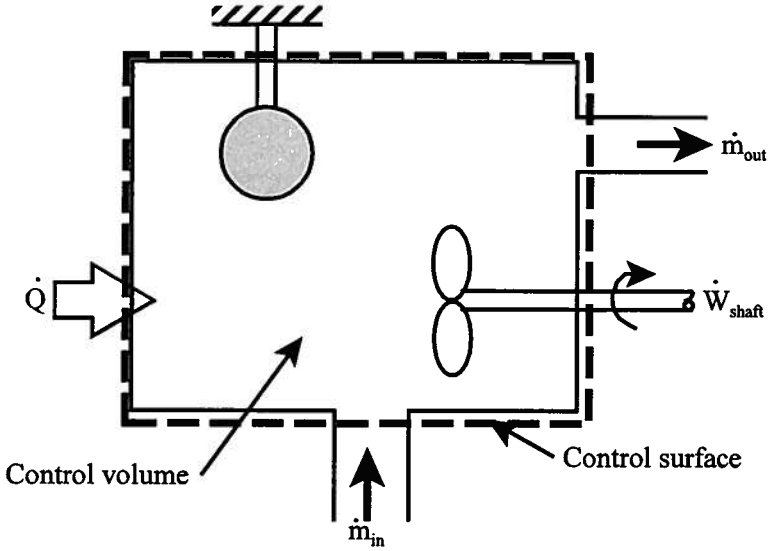

Figure 15.1 Steady-flow Control Volume with One Entry Port and One Exit Port

In the analyses of the present chapter, we shall apply the governing equations to a steady flow control volume with one inlet port and one exit port such as that shown schematically in Figure 15.1. In addition, it will also be useful to consider a control volume of infinitesimal extent

in the direction of flow. In such a control volume, the fluid experiences an infinitesimal change of state between inlet and outlet in response to infinitesimal rates of heat transfer and shear work transfer across the control surface. Under these circumstances, the governing equations then become differential relations.

The governing equations and their differential counterparts are:

Continuity Equation:

$$\frac{dM_{CV}}{dt} = \dot{m}_{in} - \dot{m}_{out} = 0 \tag{15.1}$$

$$d(\dot{m}) = 0 \tag{15.2}$$

First Law of Thermodynamics:

$$\frac{dE_{CV}}{dt} = \dot{Q} - \dot{W}_{shaft} + m_{in}\left(h + \frac{\vartheta^2}{2} + gz\right)_{in} - \dot{m}_{out}\left(h + \frac{\vartheta^2}{2} + gz\right)_{out} = 0 \tag{15.3}$$

$$\left(\frac{\delta\dot{Q}}{\dot{m}}\right) - \left(\frac{\delta\dot{W}}{\dot{m}}\right)_{shear} = dh + \vartheta d\vartheta + gdz \tag{15.4}$$

Second Law of Thermodynamics:

$$\frac{dS_{CV}}{dt} = \sum_i \left(\frac{\dot{Q}}{T}\right)_i + (\dot{m}s)_{in} - (\dot{m}s)_{out} + \dot{S}_{gen} = 0 \tag{15.5}$$

$$ds \geq \frac{1}{T}\left(\frac{\delta\dot{Q}}{\dot{m}}\right) \tag{15.6}$$

Equation of Linear Momentum:

$$\frac{d}{dt}\int_{CV}\rho\vec{\vartheta}dV = \int_{CS}(-P\vec{n})\,dA + \int_{CS}(\vec{\tau})\,dA + \int_{CV}\rho\vec{g}\,dV - \left(\dot{m}\vec{\vartheta}\right)_{out} + \left(\dot{m}\vec{\vartheta}\right)_{in} = 0 \tag{15.7}$$

$$d\vec{F} = P\vec{n}dA - \vec{\tau}dA_s - \vec{g}dz = d\left(\dot{m}\vec{\vartheta}\right) \tag{15.8}$$

Equation of Angular Momentum:

$$\frac{d}{dt}\left[\int_{CV}\left(\vec{r}\times\vec{\vartheta}\right)\rho dV\right] =$$

$$= \sum\left(\vec{r}\times\vec{F}_{surface}\right) + \int_{CV}(\vec{r}\times\vec{g})\rho dV + \vec{T}_{shaft} - \dot{m}_{out}\left(\vec{r}\times\vec{\vartheta}\right)_{out} + \dot{m}_{in}\left(\vec{r}\times\vec{\vartheta}\right)_{in} = 0 \tag{15.9}$$

$$\vec{r}\times d\vec{F} + (\vec{r}\times\vec{g})\,\rho dV + d\vec{T}_{shaft} = d\left[\dot{m}\left(\vec{r}\times\vec{\vartheta}\right)\right] \tag{15.10}$$

Notice that in each governing equation, the unsteady term will vanish in the present context since we are considering only steady-flow components.

For each category of components, the analysis will be illustrated by application to the flow of an incompressible fluid, the flow of an ideal gas, and the flow of a pure substance in two phase states through the component. These cases will serve to illustrate the basic behavior of each class of steady-flow components.

15.2 Shaft Work Machines

The first class of components is comprised of machines that change the state of a fluid

stream by positive or negative shaft work transfer. Machines with positive shaft work transfer are commonly called turbines, reciprocating engines, expanders, or fluid motors, depending upon the application and the method of developing the internal forces that produce the shaft work transfer. Machines with negative shaft work transfer are commonly called compressors, pumps, or fans depending upon the application.

The operation of a shaft work machine does not depend upon the attainment of thermal equilibrium between the flowing fluid and the walls of the apparatus; consequently, the rate of work transfer is not limited by the relatively slow processes of heat transfer. Rather, the work transfer depends upon the forces due to pressure acting on the moving surfaces internal to the apparatus. As we have shown previously in Chapter 4, pressure is distributed throughout a system by means of pressure waves that propagate at the speed of sound which is on the order of several hundred meters per second in gases and several thousand meters per second in liquids. Since these velocities are typically an order of magnitude or more faster than the velocities of moving boundaries, the time constants associated with work transfer processes are on the order of milliseconds or less.

There are two means by which these internal forces can be generated. In the first case, the machine is based upon the piston-cylinder configuration that we have examined in considerable detail heretofore. These machines are known as reciprocating or positive displacement machines since they operate by shuttling the piston back and forth in a reciprocal motion inside the cylinder. In this case, the internal forces are the result of equilibrium pressure (spatially uniform) acting on a moving piston face or the equivalent moving surface. The movement of the piston displaces the same amount of working fluid, usually a gas, over the course of its travel. Traditional internal combustion engines are examples of this type of shaft work machine as are reciprocating compressors.

In the second case, the internal structure of the machine consists of specially shaped blades that are mounted on a disk or rotor and extend outward in a radial fashion. The rotor, together with the attached blades, rotates about an axis perpendicular to the plane of the disk as the working fluid passes through it. In addition, depending upon the design, there may be other blade-like surfaces that are affixed to the housing of the machine and remain stationary. These surfaces form the stator of the machine and serve, in part, to control the direction of flow of the working fluid. In these machines, known as rotary machines or turbomachines, the operation of the machine is a consequence of the change in angular momentum of the working fluid as it passes through the machine.

Turbomachines can be grouped into two broad classes depending upon the direction of flow of the working fluid as it passes through the machine. If the flow path is essentially parallel to the axis of rotation of the rotor, the machine is said to be an axial flow machine. On the other hand, if the flow path is radially outward from the axis of rotation, the machine is said to be a radial flow turbomachine.

In a positive work transfer axial flow machine, the blades attached to the rotor are shaped so that the internal forces responsible for the torque output of the machine are generated by means of the change of momentum of the fluid stream as its direction is changed by the blades. There is a component of the resultant force that acts normal to the axis of rotation of the rotor thereby generating a torque. The blades of the stator form nozzle-shaped flow passages that accelerate the fluid, as well as change its direction of flow, before it passes over the rotor blades. Gas turbine engines found in commercial and military aircraft as well as stationary gas turbine power plants are examples of this type of shaft work machine. In fact, as we shall see in Chapter 16, gas turbine engines actual contain both positive and negative rotary shaft work machines in a single unit.

In a negative work transfer axial flow machine, the situation is somewhat more complicated since the objective of the operation is to increase the pressure of the working fluid in the direction of flow by decelerating the fluid. Since the flow is counter to the pressure gradient, this is an inherently unstable situation which requires the roles of the stator and rotor to be less specialized than is the case for a positive shaft work transfer axial flow machine. Both rotor and stator contribute to the deceleration process.

In radial flow turbomachines, the flow path can be either radially outward or radially inward. The choice is dictated by considerations of both size and the behavior of the working fluid. In most cases of radial flow machines, the flow is actually a combination of radial flow and axial flow. For example, radial inflow turbines with axial exhaust are the choice for the turbine component of automobile turbochargers. Water turbines used in hydroelectric dams are typically radial inflow with axial outflow. In radial inflow turbines, positive shaft power results from the decrease in kinetic energy of the working fluid as it passes from large radius to small radius on the rotor. The angular momentum of the fluid decreases as it passes through the rotor. In contrast, centrifugal pumps used, for example, to pump cooling water through automotive engine blocks are axial inflow and radial outflow. In radial outflow pumps, the pressure increase in the working fluid is the result of the deceleration of the fluid as it moves radially outward. The angular momentum of the fluid is increased as it passes through the rotor.

An alternative, but equally valuable classification of turbomachines is according to the manner in which fluid power is converted to shaft power and vice versa. In the *impulse* turbomachine, the pressure drop in the fluid (in the case of the impulse turbine) occurs in one or more nozzles outside the rotor. This accelerates the fluid stream which is then directed onto a series of blades on the rotor. As the fluid passes through the rotor, it experiences essentially no change in pressure, merely a change in direction which results in a change in angular momentum. Radial inflow turbines are frequently impulse turbines, for example. In the *reaction* turbomachine, the pressure drop (or pressure increase) in the fluid stream occurs as the fluid passes through the rotor. A centrifugal pump is an example of a reaction turbomachine. In practice, it is frequently the case that turbomachines are partly impulse machines and partly reaction machines. The axial flow air compressor is an example of this sort of operation.

In both reciprocating shaft work machines and turbomachines as outlined above, the limit on the rate of work transfer is related to the velocity of propagation of pressure waves (sound) in the fluid. This rate is often fast enough that the rate of work transfer for the machine is actually limited by the forces that result from the accelerations of the solid parts of the machine (inertia stress limit). Since the work transfer rate is rapid, the shaft work machine is small enough that the fluid remains within the machine for a time period that is small compared to the time period required to attain thermal equilibrium. Thus, the apparatus is essentially adiabatic. Note that some heat transfer does occur in virtually every case; however, the magnitude is negligible compared to the magnitude of the shaft work transfer, regardless of whether it is positive or negative.

A second result of the relatively rapid work transfer rate and the resulting small size of the machine is that the change in gravitational potential energy is usually negligible. This is usually true even for the large water turbines used in hydroelectric power stations provided the control volume does not include the penstock.

The preceding discussion indicates that shaft work machines can be reasonably modeled as adiabatic devices with negligible changes in gravitational potential energy. Further, in many practical cases the change in kinetic energy of the bulk flow is also negligible. Thus the first law

of thermodynamics, equation (15.3), applied to a control volume representing a machine of this type reduces to

$$-\dot{W}_{shaft} = \dot{m}\left(h_{out} - h_{in}\right) \tag{15.11}$$

For a machine with a unit mass flow rate of a fluid experiencing an infinitesimal change of state, equation (15.4) reduces to

$$-\left(\frac{\delta \dot{W}}{\dot{m}}\right)_{shaft} = dh \tag{15.12}$$

Equations (15.11) and (15.12) indicate that positive shaft work transfer occurs at the expense of the enthalpy of the flowing fluid and that negative shaft work transfer increases the enthalpy of the flowing fluid. In addition to equations (15.11) and (15.12), mechanical equilibrium requires that in a machine with a positive shaft work transfer, e.g., a turbine, the pressure of the flowing fluid must decrease as it passes through the device. On the other hand, in order to increase the pressure of a fluid stream in a shaft work machine (a pump or compressor), mechanical equilibrium requires a negative work transfer.

In applying equation (15.11) or (15.12) to a physical situation, one must always be careful to insure that the actual physical circumstances are consistent with the assumptions associated with these equations. For example, in gas turbines it is not uncommon for the kinetic energy of the flowing fluid to be significant. Also in a steam turbine exhausting steam at low pressure, the kinetic energy of the exhaust steam is often significant. In these more complex cases, equation (15.3) must be used to include changes in kinetic energy.

The evaluation of the performance of a shaft work machine is especially simple in the limiting case of the adiabatic machine that operates in a reversible manner with a negligible net change in the kinetic energy of the fluid as it passes through the machine. From equation (15.5) or (15.6) it is clear that the entropy of the fluid leaving the control volume is equal to the entropy of the fluid entering the control volume. Since according to the state principle (*cf.* Section 13.2) we need only specify two independent properties to establish the state of the fluid, the inlet entropy and the inlet pressure fix the inlet state of the working fluid. The outlet pressure and the outlet entropy (equal to the inlet entropy) then fix the outlet state of the reversible adiabatic shaft work machine.

To be more specific, consider the reversible adiabatic machine involving an infinitesimal change of state of the working fluid. From the definition of the enthalpy, the change in enthalpy can be related to the changes in entropy and pressure by means of the canonical relation, equation (13.1), viz.

$$dh = du + d\left(Pv\right) = Tds - Pdv + Pdv + vdP = Tds + vdP \tag{15.13}$$

For a reversible adiabatic machine, equation (15.6) gives $ds = 0$. Then since the entropy is constant in such a machine, equation (15.13) reduces to

$$\left(dh\right)_{\substack{constant\\entropy}} = vdP \tag{15.14}$$

Then equation (15.12) reduces to

$$-\left[\left(\frac{\delta \dot{W}}{\dot{m}}\right)_{shaft}\right]_{\substack{reversible\\adiabatic}} = dh = vdP \tag{15.15}$$

Thus, the shaft power of a reversible adiabatic machine is

$$-\left(\dot{W}_{shaft}\right)_{\substack{reversible\\adiabatic}} = \dot{m}\left[\int_{P_{in}}^{P_{out}} vdP\right]_{s=s_{in}} \tag{15.16}$$

Because the path of the process is specified as one of constant entropy, the volume is uniquely related to the pressure. Then the integral in equation (15.16) can be evaluated directly for a specific model for the fluid properties.

If the machine is adiabatic but irreversible, the second law of thermodynamics, equation (15.5), requires that the outlet entropy, s_{out}, be greater than the inlet entropy, s_{in}. As a result, the irreversible adiabatic machine has a smaller work transfer rate and a larger outlet enthalpy than the reversible machine with the same mass flow rate, inlet state, and outlet pressure. We can show this result of the irreversibility from the second law of thermodynamics and the relations for the properties of a pure substance. Let us compare an irreversible adiabatic machine with a reversible adiabatic machine, both with the same inlet state and the same outlet pressure. In this case, the outlet state of the irreversible machine will have the same pressure but a higher entropy than the outlet state of the reversible machine. Equation (15.13) implies that there exists a function $h = h(s,P)$ such that its differential is given by

$$dh = \left(\frac{\partial h}{\partial s}\right)_P ds + \left(\frac{\partial h}{\partial P}\right)_s dP \tag{15.17}$$

Comparing the coefficients of ds in equations (15.13) and (15.17), we conclude that

$$\left(\frac{\partial h}{\partial s}\right)_P = T \tag{15.18}$$

which is always positive. As a result, the locus of states with the same pressure (lines of constant pressure) on the h-s plane have a positive slope (*cf.* Figure 15.1). Thus the enthalpy of the outlet state for the irreversible machine will be greater than the enthalpy of the outlet state for the reversible machine at the same outlet pressure. From equation (15.11), the shaft work is proportional to $(h_{in} - h_{out})$ for both machines. Thus for a given inlet state and exit pressure

$$\left(\dot{W}_{shaft}\right)_{reversible} - \left(\dot{W}_{shaft}\right)_{irreversible} = \dot{m}\left[\left(h_{out}\right)_{irreversible} - \left(h_{out}\right)_{reversible}\right] \tag{15.19}$$

From equation (15.18), equation (15.19) becomes

$$\left(\dot{W}_{shaft}\right)_{reversible} - \left(\dot{W}_{shaft}\right)_{irreversible} = \dot{m}\left[\int_{s_{in}}^{s_{out}} \left(\frac{\partial h}{\partial s}\right)_P ds\right]_{P=P_{out}} = \dot{m}\left[\int_{s_{in}}^{s_{out}} T ds\right]_{P=P_{out}} \tag{15.20}$$

The irreversible work transfer rate is smaller in an algebraic sense. Consequently, the irreversible turbine will have a smaller positive work transfer than the reversible turbine; however, the irreversible compressor with its negative work transfer will require a work transfer of greater magnitude than the reversible compressor.

In practice, it has been found convenient to measure the work transfer rate of an actual adiabatic shaft work transfer machine in terms of the performance of a reversible adiabatic machine with the same inlet state and the same outlet pressure as the actual machine. It is conventional to express the ratio of these two work transfer rates as an efficiency; therefore, it is necessary to have one efficiency for machines with positive work transfer rates and a second efficiency for machines with negative work transfer rates. For the machine involving a positive work transfer, we use the conventional definition

$$\eta_+ = \frac{\dot{W}_{actual}}{\dot{W}_{reversible}} \tag{15.21}$$

Here η_+ is frequently known as the *adiabatic turbine efficiency* or the adiabatic expander efficiency. In equation (15.21), $\dot{W}_{actual}$ is the power output of the actual machine, and $\dot{W}_{reversible}$ is the power output of the reversible machine with the same inlet state and outlet pressure.

Substituting equation (15.11) into equation (15.21), we obtain

$$\eta_+ = \frac{\left[\dot{m}\left(h_{in} - h_{out}\right)\right]_{actual}}{\left[\dot{m}\left(h_{in} - h_{out}\right)\right]_{reversible}} = \frac{\left(h_{in} - h_{out}\right)_{actual}}{\left(h_{in} - h_{out}\right)_{reversible}} \tag{15.22}$$

For the machine involving a negative work transfer, we use the conventional definition

$$\eta_- = \frac{\dot{W}_{reversible}}{\dot{W}_{actual}} \tag{15.23}$$

where η_- is frequently known as the *adiabatic compressor efficiency* or *pump efficiency*. Again use of equation (15.11) yields

$$\eta_- = \frac{\left[\dot{m}\left(h_{in} - h_{out}\right)\right]_{reversible}}{\left[\dot{m}\left(h_{in} - h_{out}\right)\right]_{actual}} = \frac{\left(h_{in} - h_{out}\right)_{reversible}}{\left(h_{in} - h_{out}\right)_{actual}} \tag{15.24}$$

By formulating the definitions of efficiency as in equations (15.22) and (15.24), we always obtain a value of the efficiency which lies between zero and unity. Further, as the actual machine becomes more nearly reversible, its efficiency improves and approaches unity. Both of these features are consistent with our intuitive interpretations of efficiency.

Although most authors use the term efficiency to mean the adiabatic efficiencies as previously defined, other definitions for efficiency are sometimes used. It is prudent to verify the exact definition for the efficiency being employed when working with information from various sources. For example, in the study of compressors, it is common to employ the term isothermal efficiency which is used to compare the actual compressor to a reversible isothermal compressor.

15.2.1 Shaft Work Machines Processing an Ideal Gas

These conclusions can now be illustrated in detail for machines processing fluids with properties that can be adequately described by a simple model of the constitutive relations. If the fluid can be modeled as an ideal gas with constant specific heats, equation (15.11) becomes

$$-\left(\dot{W}_{shaft}\right)_{\substack{ideal\\gas}} = \dot{m} c_P \left(T_{out} - T_{in}\right) \tag{15.25}$$

which shows that in this case the rate of shaft work transfer (for a given mass flow rate) is determined solely by the temperature change of the gas. For the limiting case of the reversible adiabatic machine, the outlet temperature is related to the inlet temperature and the pressure ratio through the second law of thermodynamics. Thus, from the entropy constitutive relation for the ideal gas, equation (4.6), we have

$$s_{out} - s_{in} = c_P \ln\frac{T_{out}}{T_{in}} - R \ln\frac{P_{out}}{P_{in}} \tag{15.26}$$

Equation (15.26) then establishes the outlet temperature T_{out} from the pressure ratio P_{out}/P_{in} and the inlet temperature T_{in}. The rate of shaft work transfer is then given by equation (15.25) in terms of the inlet and outlet temperatures, T_{in} and T_{out}.

Alternatively, we could have used equation (15.16) and the fact that the pressure and volume of an ideal gas in a reversible adiabatic process are related by the expression

$$Pv^{\gamma} = \text{constant} \tag{15.27}$$

where $\gamma = c_P/c_v$. Then equation (15.16) can be integrated to give

$$-\left(\dot{W}_{shaft}\right)_{\substack{reversible\\adiabatic\\ideal\ gas}} = \frac{\dot{m}\gamma}{\gamma - 1}\left[P_{out} v_{out} - P_{in} v_{in}\right] \tag{15.28}$$

where v_{out} is uniquely related to v_{in} through the pressure ratio and equation (15.27). Note that equation (15.28) could have been obtained directly from equation (15.25) simply by substituting the ideal gas property constitutive relation and by making use of the definition of γ. Since

equation (15.25) holds for all adiabatic machines whether reversible or irreversible, it must be the case that for the ideal gas in general

$$-\left(\dot{W}_{shaft}\right)_{\substack{adiabatic\\ideal\ gas}} = \frac{\dot{m}\gamma}{\gamma-1}\left[P_{out}v_{out} - P_{in}v_{in}\right] \tag{15.29}$$

The significance of the reversibility is that only in the reversible case can we reduce equation (15.29) to the form

$$-\left(\dot{W}\right)_{\substack{reversible\\adiabatic\\ideal\ gas}} = \frac{\dot{m}\gamma}{\gamma-1}P_{in}v_{in}\left[\left(\frac{P_{out}}{P_{in}}\right)^{\gamma-1/\gamma} - 1\right] \tag{15.30}$$

That is, for a given mass flow rate the inlet state and pressure ratio uniquely determine the shaft work transfer rate for the reversible adiabatic machine. In an irreversible machine, both the inlet state and the outlet state must be known before equation (15.29) can be evaluated.

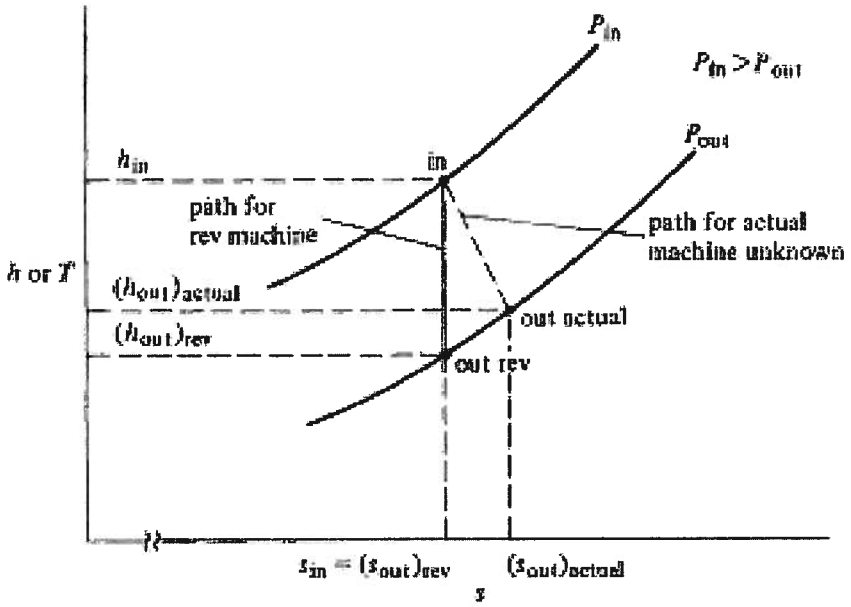

Figure 15.2 (a) States of the Ideal Gas Model in an Adiabatic, Positive Shaft Work Machine

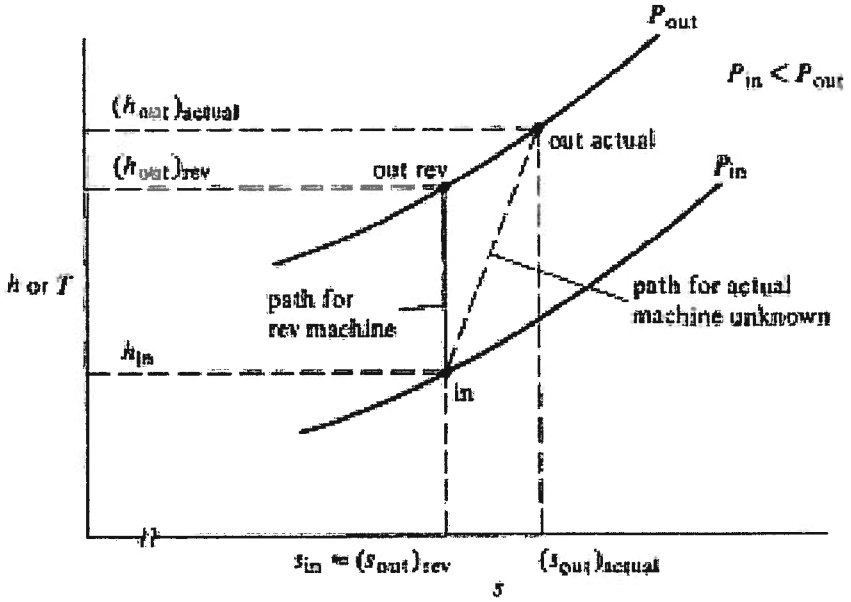

Figure 15.2 (b) States of the Ideal Gas Model in an Adiabatic, Negative Shaft Work Machine

This point is perhaps more clearly revealed in Figure 15.2 which shows the locus of states for the ideal gas as it passes through the shaft work machine. The information of Figure 15.2 is presented in terms of the coordinates h and s. The locus of states would have exactly the same appearance in terms of the coordinates T and s since the enthalpy and the temperature are directly related for the ideal gas. Note that in the case of the irreversible (actual) machine, the path of the process cannot be specified since some of the states involved may be non-equilibrium states. It is clear from Figure 15.2 that knowing the inlet state, the path, and the outlet pressure is the equivalent of knowing both the inlet state and the outlet state.

For the ideal gas, the adiabatic shaft work efficiencies reduce to

$$(\eta_+)_{\substack{ideal\\gas}} = \frac{(T_{in} - T_{out})_{actual}}{(T_{in} - T_{out})_{reversible}} \tag{15.31}$$

and

$$(\eta_-)_{\substack{ideal\\gas}} = \frac{(T_{in} - T_{out})_{reversible}}{(T_{in} - T_{out})_{actual}} \tag{15.32}$$

These efficiencies can be geometrically interpreted on Figure 15.2 as the ratios of the vertical distances between the inlet and outlet states for the reversible path and for the irreversible path.

Example 15E.1: Modern commercial aircraft are powered by turbo fan engines consisting of a gas turbine engine driving a single-stage axial flow fan. In a typical design, at take off power the gas turbine engine produces 25 MW. The conditions of the air at the fan inlet are $P_1 = 10^5$ N/m^2, $T_1 = 300$ K, and $\mathcal{V}_1 = 250$ m/sec. The exit conditions from the fan are $P_2 = 1.36 \times 10^5$ N/m^2, and $\mathcal{V}_2 = 250$ m/sec. The efficiency of the fan is $\eta_- = 0.85$ based on the same kinetic energy at the inlet and exit states. The ratio of the specific heats for air is $\gamma = 1.4$.

(a) What is the mass flow rate of air through the fan?

(b) What flow area is required at the fan inlet?

(c) What is the exit air temperature?

(d) What is the rate of entropy generation in the fan?

Solution: (a) The control volume selected for the analysis is shown in Figure 15E.1. For the reversible adiabatic fan the entropy of the fluid is constant. Thus from equation (5.47) and the ideal gas property constitutive relation

$$T_{2rev} = T_1 \left(\frac{P_2}{P_1}\right)^{\gamma-1/\gamma}$$

$$T_{2rev} = (300\text{ K})\left(\frac{1.36 \times 10^5\text{ N/m}^2}{1 \times 10^5\text{ N/m}^2}\right)^{0.4/1.4} = 327.55\text{ K}$$

The first law for the control volume, equation (15.3), around the reversible adiabatic fan gives

$$-\left(\frac{\dot{W}_{shaft}}{\dot{m}}\right) = \left(h_{2rev} + \frac{\mathcal{V}_{2rev}^2}{2}\right) - \left(h_1 + \frac{\mathcal{V}_1^2}{2}\right)$$

For the present case, $\mathcal{V}_{2rev} = \mathcal{V}_2 = \mathcal{V}_1$. Then

$$-\left(\frac{\dot{W}_{shaft}}{\dot{m}}\right)_{reversible} = c_P (T_{2rev} - T_1)$$

Substituting equation (15.32), we get

$$-\left(\frac{\dot{W}_{shaft}}{\dot{m}}\right)_{actual} = \frac{1}{\eta_-} c_P (T_{2rev} - T_1)$$

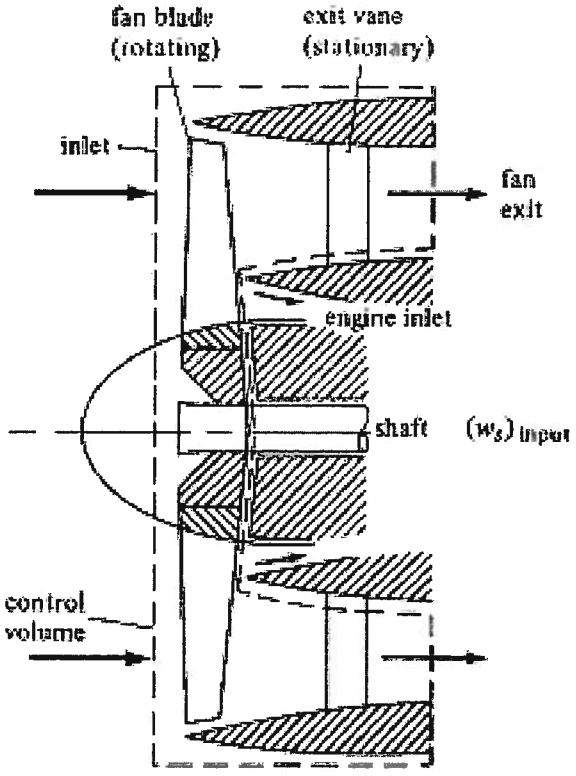

Figure 15E.1

Then

$$\dot{m} = \frac{-\left(\dot{W}_{shaft}\right)_{actual}\eta_{-}}{c_P\left(T_{2rev} - T_1\right)}$$

$$\dot{m} = \frac{\left(25 \text{ x } 10^6 \text{ W}\right)(0.85)}{(1003 \text{ J/kg K})(327.55 \text{ K} - 300 \text{ K})} = 769 \text{ kg/sec}$$

(b) The area of flow is given by

$$A = \frac{\dot{m}v}{\vartheta} = \frac{\dot{m}RT}{\vartheta P}$$

$$A = \frac{(769 \text{ kg/sec})(287 \text{ J/kg K})(300 \text{ K})}{(250 \text{ m/sec})\left(10^5 \text{ N/m}^2\right)} = 2.65 \text{ m}^2$$

(c) The exit temperature is given by the first law for the control volume around the actual fan. Thus, since the flow is adiabatic and $\vartheta_1 = \vartheta_2$, we have

$$-\left(\frac{\dot{W}_{shaft}}{\dot{m}}\right) = c_P\left(T_2 - T_1\right)$$

$$T_2 = T_1 - \frac{\dot{W}_{shaft}}{\dot{m}} = 300 \text{ K} - \left[\frac{-25 \text{ x } 10^6 \text{ W}}{(769 \text{ kg/sec})(1003 \text{ J/kg K})}\right] = 332.4 \text{ K}$$

(d) Since the flow is steady and adiabatic, the rate of entropy generation is the net rate at which entropy is convected out of the control volume, viz.

$$\cancel{\frac{dS_{cv}}{dt}} = \cancel{\sum_j \left(\frac{\dot{Q}}{T}\right)_j} + \dot{m}s_1 - \dot{m}s_2 + \dot{S}_{gen}$$

Substituting the entropy constitutive relation, we get

$$\dot{S}_{gen} = \dot{m}(s_2 - s_1) = \dot{m}\left(c_P \ln\frac{T_2}{T_1} - R\ln\frac{P_2}{P_1}\right)$$

$$\dot{S}_{gen} = (769 \text{ kg/sec})\left[(1003 \text{ Jkg K})\ln\frac{332.4 \text{ K}}{300 \text{ K}} - (287 \text{ J/kg K})\ln\frac{1.36 \text{ x } 10^5 \text{ N/m}^2}{1 \text{ x } 10^5 \text{ N/m}^2}\right]$$

$$\dot{S}_{gen} = 11,240 \text{ W/K}$$

15.2.1.1 Reciprocating Shaft Work Machines: Reciprocating shaft work machines are the oldest examples of shaft work machines in engineering practice, dating back at least as far as the machines of Thomas Newcomen (1664 – 1729). In their simplest form, reciprocating machines consist of one or more cylinders, each fitted with a piston that moves back and forth within the cylinder (hence the term reciprocating). The piston is connected to a crankshaft via a connecting rod that transmits force between the crankshaft and the piston and converts the reciprocating motion of the piston into rotary motion of the crankshaft. This force exerted on the crankshaft results in a torque that in the case of a positive shaft work machine can be used to turn some other mechanism such as an electric generator or the wheels of a vehicle, or, in the case of a negative shaft work machine, the torque input to the crankshaft can cause the piston to compress the gas contained between the piston face and the end of the cylinder.

For the purposes of illustrating the analysis of the foregoing section, we are going to focus our immediate attention on this latter example, namely that of the reciprocating compressor. In our analysis, we shall examine the internal details of the system and show how these details are consistent with the results obtained via the control volume approach.

The reciprocating compressor finds widespread use in industry to produce high pressure gas, most commonly high pressure air, that can be used in a variety of ways which include: (1) the operation of air motors in pneumatic tools for drilling, grinding, reaming, polishing, and sawing; (2) the operation of reciprocating pistons in tools like paving breakers, forge hammers, riveting hammers, and rock drills; (3) the atomization of liquids in paint sprayers; (4) the transport of materials like concrete or grain, or the transport of materials like sand for sand blasting operations in cleaning processes or shot for work hardening materials by shot peening; (5) the transmission of pressure in automatic control systems; and (6) the delivery of oxygen in combustion systems. Reciprocating compressors are also used to compress natural gas to the high pressures necessary to overcome the head loss in natural gas transmission lines and to compress various gases used in gas liquefaction systems such as air separation plants. Perhaps even more common is the use of reciprocating compressors in small scale refrigeration plants.

The performance of reciprocating machines can be determined by examining the details of the cyclic motion of the piston as it moves within the cylinder. Strictly speaking these machines are not steady flow since they operate in cyclic fashion with the apparatus, the cylinder, actually closed for a portion of the cycle. In steady flow machines, even though some time lapses between the time the gas is admitted to the machine and the time that it is discharged to its end use, to an observer stationed at the discharge from the machine the flow appears steady. However, in a single cylinder reciprocating machine, the discharge from the machine appears periodic to such an observer. Since the equations governing the behavior of steady flow devices apply to periodic flow devices as well, the performance of a cyclic device can be determined by applying these equations to the cyclic device. In practice, however, these devices usually consist of multiple cylinders whose pistons move in some phased manner at high speed so that the discharge state of the gas appears essentially constant with time to the observer stationed at the exit port.

Figure 15.3 is a schematic representation of a typical reciprocating compressor. The cylinder is fitted with an intake valve that facilitates the admission of a fresh charge of gas into the cylinder and an exhaust valve that enables the high pressure, high temperature gas to be discharged from the cylinder. The cycle of operation consists of the piston at "bottom dead center" (the extreme limit of its travel) and the cylinder filled with gas at the intake pressure (typically atmospheric pressure for air compressors). Both valves are closed. This is denoted as state 1 on Figure 15.4. The piston now begins to travel toward the cylinder head where the valves are located. During this inward motion of the piston, the pressure and temperature of the gas rise due to its thermodynamic coupling. This inward travel of the piston continues until the pressure of the gas reaches the design delivery pressure for the application. The position of the piston at this point is some distance from the cylinder head and is denoted as state 2 on Figure 15.4. When this state is reached, the exhaust valve opens and the piston continues its inward motion while delivering the high pressure, high temperature gas to a receiver, usually a large volume storage container. When the piston reaches the inward limit of its travel, a small volume, known as the *clearance volume*, remains in the cylinder. This clearance volume is filled with high pressure, high temperature gas. At this time, the exhaust valve closes and the piston reverses direction. This state is denoted as state 3 on Figure 15.4. The volume of gas within the cylinder expands as the piston moves outward. Due to the thermodynamic coupling of the gas, the pressure and temperature decrease during this motion. At some point in the outward motion of the piston, the pressure of the gas reaches the intake pressure. At this time, denoted as state 4 on Figure 15.4, the intake valve opens and fresh gas flows into the cylinder as the piston moves toward the extreme limit of its travel. When the extreme limit is reached in state 1, the intake valve closes and the cycle begins once again.

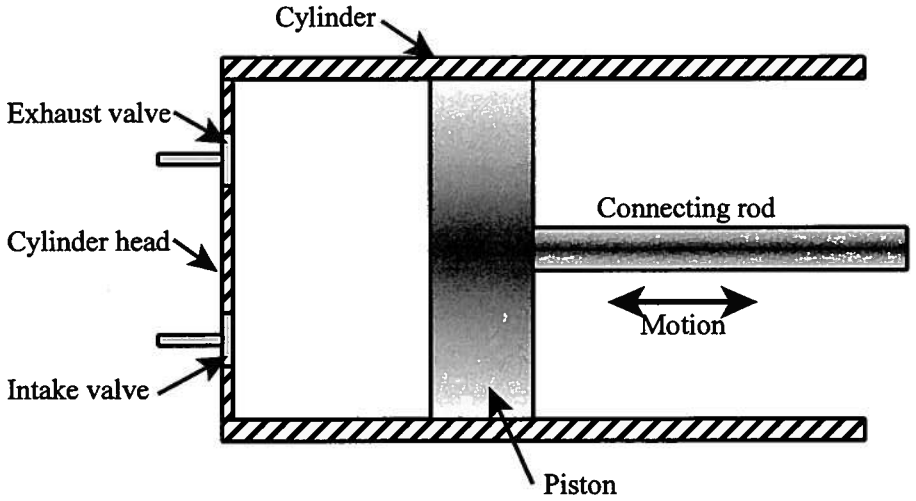

Figure 15.3 Schematic Representation of Reciprocating Compressor

Care must be exercised in the analysis of the gas compressor since part of the time the apparatus operates as an open system while the other part of the time the machine operates as a closed system. For the cycle shown in Figure 15.4, during processes 1 – 2 and 3 – 4 the compressor acts as a closed system with a fixed mass of gas experiencing reversible, adiabatic processes. During processes 2 – 3 and 4 – 1, the compressor operates as an open system and exchanges mass with the environment. For our purposes here, we are interested in the work transfer between the compressor and the environment. This information can be obtained by

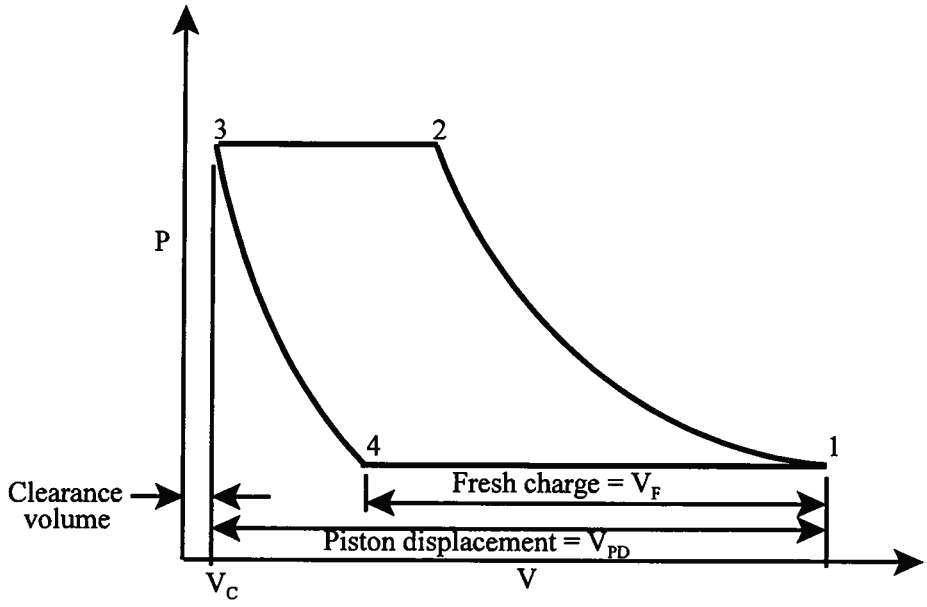

Figure 15.4 Gas Compressor Cycle

examining each process in turn and then summing the results to obtain the net work transfer for the cycle. The path of the process from state 1 to state 2 in the fixed mass of gas contained within the cylinder is reversible and adiabatic and is given by PV^{γ} = constant. Then the work transfer for the gas for this process is

$$(W_{1-2})_{\substack{rev \\ Q=0}} = \int_1^2 PdV = P_1V_1^{\gamma}\int_1^2 \frac{dV}{V^{\gamma}} = \frac{P_1V_1^{\gamma}}{1-\gamma}\left[V_2^{1-\gamma} - V_1^{1-\gamma}\right] = \frac{1}{1-\gamma}(P_2V_2 - P_1V_1) \qquad (15.33)$$

For the process from state 2 to state 3, the compressor is an open system as the mass of gas contained within the cylinder changes as the piston moves, but the force on the piston is constant at $P_2 = P_3$. Then the work transfer from the environment to the piston for the process 2 – 3 is

$$W_{2-3} = \int_2^3 Fdx = \int_2^3 PAdx = P_2(V_3 - V_2) = P_3V_3 - P_2V_2 \qquad (15.34)$$

For the process from state 3 to state 4, the compressor is a closed system and the path is again reversible and adiabatic with PV^{γ} = constant. Then in a manner similar to equation (15.33), the work transfer is

$$(W_{3-4})_{\substack{rev \\ Q=0}} = \frac{1}{1-\gamma}(P_4V_4 - P_3V_3) \qquad (15.35)$$

For the process from state 4 to state 1, the compressor is again an open system as mass is transferred to the environment, but the pressure on the piston face is constant $P_4 = P_1$. Then in a manner similar to equation (15.34)

$$W_{4-1} = P_1V_1 - P_4V_4 \qquad (15.36)$$

Then the net work transfer between the environment and the compressor is given by the sum of the work transfers for the individual processes that make up the compressor cycle, viz.

$$\oint \delta W = W_{net} = W_{1-2} + W_{2-3} + W_{3-4} + W_{4-1}$$

$$W_{net} = \frac{1}{1-\gamma}(P_2V_2 - P_1V_1) + (P_3V_3 - P_2V_2) + \frac{1}{1-\gamma}(P_4V_4 - P_3V_3) + (P_1V_1 - P_4V_4)$$

$$W_{net} = \frac{\gamma}{1-\gamma}(P_2V_2 - P_1V_1 + P_4V_4 - P_3V_3) \qquad (15.37)$$

Equation (15.37) can be rewritten in the form

$$\dot{W}_{net} = \frac{\gamma}{\gamma-1}\left[P_1V_1\left(1-\frac{P_2V_2}{P_1V_1}\right)-P_4V_4\left(1-\frac{P_3V_3}{P_4V_4}\right)\right] = \frac{\gamma}{\gamma-1}\left[P_1V_1\left(1-\frac{T_2}{T_1}\right)-P_4V_4\left(1-\frac{T_3}{T_4}\right)\right] \quad (15.38)$$

Since

$$\frac{T_2}{T_1} = \frac{T_3}{T_4} \quad \text{and} \quad \frac{T_2}{T_1} = \left(\frac{P_2}{P_1}\right)^{\gamma-1/\gamma} \quad (15.39)$$

Equation (15.38) can be rewritten in terms of the pressure ratio across the compressor, viz.

$$(W_{net})_{\substack{rev\\Q=0}} = \frac{\gamma}{\gamma-1}\left\{P_1V_1\left[1-\left(\frac{P_2}{P_1}\right)^{\gamma-1/\gamma}\right]-P_4V_4\left[1-\left(\frac{P_2}{P_1}\right)^{\gamma-1/\gamma}\right]\right\}$$

$$(W_{net})_{\substack{rev\\Q=0}} = \frac{\gamma}{\gamma-1}\left[1-\left(\frac{P_2}{P_1}\right)^{\gamma-1/\gamma}\right](m_1RT_1-m_4RT_4) = \frac{\gamma}{1-\gamma}RT_1\left[\left(\frac{P_2}{P_1}\right)^{\gamma-1/\gamma}-1\right](m_1-m_4) \quad (15.40)$$

Since $(m_1 - m_4)$ is the mass of compressed gas delivered each cycle and the compressor executes N cycles per second, the power required to drive the reversible adiabatic compressor is given by

$$(\dot{W}_{net})_{\substack{rev\\Q=0}} = \frac{\gamma}{1-\gamma}RT_1(Nm_{delivered})\left[\left(\frac{P_2}{P_1}\right)^{\gamma-1/\gamma}-1\right] = \frac{\gamma}{1-\gamma}\dot{m}RT_1\left[\left(\frac{P_2}{P_1}\right)^{\gamma-1/\gamma}-1\right] \quad (15.41)$$

With the aid of equation (15.39) and the fact that $\gamma/(1 - \gamma) = -c_P/R$, we can rewrite equation (15.41) in the form

$$(\dot{W}_{net})_{\substack{rev\\Q=0}} = -\frac{c_P}{R}\dot{m}RT_1\left(\frac{T_2}{T_1}-1\right) = -\dot{m}c_P\left[(T_2)_{rev}-T_1\right] \quad (15.42)$$

which is precisely the same result as equation (15.25) obtained by treating the compressor as a control volume. Thus, the analysis of the details of the internal operation of the apparatus inside the control volume and the control volume analysis itself are equivalent as they should be.

Departures from reversible operation of the gas compressor can be treated by means of the efficiency given in equation (15.32). The paths of the processes in the reversible and irreversible compressors are as shown in Figure 15.2(b). From Figure 15.2(b) it is apparent that the temperature of the gas following compression is increased substantially above the temperature at the inlet port. For example, an air compressor operating with a pressure ratio of 6 in one stage of compression would produce compressed air with an outlet temperature in excess of 500 K. These high temperatures can cause problems in devices downstream of the compressor, and for this reason, most compressors are fitted with heat exchangers at the exit port of the system. These heat exchangers use ambient air or water as the heat exchanger fluid to cool the compressed gas back down to the inlet temperature.

There are several noteworthy features of the compressor operating cycle. For example, in Figure 15.4, we note that if the extreme limit of travel of the piston is fixed, the clearance volume determines the amount air that can be delivered by the compressor. The greater the clearance volume, the less air that can be delivered. This influence of the clearance volume can be expressed in quantitative fashion in terms of a quantity known as the *volumetric efficiency* which is an important performance parameter for all reciprocating machines, be they positive or

negative shaft work machines. The volumetric efficiency is defined as the ratio of the mass of gas discharged per cycle to the mass of gas that would fill the volume displaced by the piston per cycle measured at inlet conditions. For air compressors (and internal combustion engines), inlet conditions are typically atmospheric temperature and pressure.

From Figure 15.4, it is apparent from the definition that the volumetric efficiency η_V is given by

$$\eta_V \equiv \frac{V_F v_0}{V_{PD} v_1} \tag{15.43}$$

where v_0 is the specific volume of the gas at inlet conditions and v_1 is the specific volume of the gas in the cylinder during the intake stroke. If the pressure drop across the intake valve is negligible (not necessarily the case for a real compressor), it follows that $v_0 = v_1$. Then

$$\eta_V = \frac{V_F}{V_{PD}} = \frac{V_1 - V_4}{V_1 - V_3} \tag{15.44}$$

The clearance C is usually expressed in terms of a fraction of the piston displacement, viz.

$$C = \frac{V_3}{V_1 - V_3} \tag{15.45}$$

Then for the reversible adiabatic machine

$$V_1 = \left(\frac{1+C}{C}\right) V_3 \quad \text{and} \quad V_4 = V_3 \left(\frac{P_2}{P_1}\right)^{1/\gamma} \tag{15.46}$$

Combining equations (15.46) and (15.44), we get

$$\eta_V = \frac{\left(\frac{1+C}{C}\right) V_3 - \left(\frac{P_2}{P_1}\right)^{1/\gamma} V_3}{\left(\frac{1+C}{C}\right) V_3 - V_3} = 1 - C\left[\left(\frac{P_2}{P_1}\right)^{1/\gamma} - 1\right] \tag{15.47}$$

Equation (15.47) shows that as the pressure ratio across the compressor increases, the compressor volume is used less and less effectively. In practice, clearance fractions are in the range of 5 to 15 percent; thus, for a clearance fraction of 5 percent and $\gamma = 1.4$, the volumetric efficiency decreases to zero for a pressure ratio of approximately 71. Since it is not uncommon for some applications to require pressure ratios as high as 200, it is clear that some other approach is required. The solution is to stage the compression, i.e., use several compressors in series, each with a modest pressure ratio, so that the volumetric efficiency is a reasonable value. In these cases, it is necessary to place a heat exchanger between any two stages so that the temperature of the gas at entry to the succeeding stage is as close to ambient as possible. Not only is the volumetric efficiency improved with this approach, but the power required to drive the compressor is substantially reduced over what might have been required for a single stage of compression. The optimum intermediate pressures for multi-stage compression will depend upon the overall pressure ratio and the number of stages. For example, for two stages of compression, it can be shown (See Example 15.2.) that with perfect intercooling, the intermediate pressure that results in the minimum power requirement is $P_i = (P_{inlet} P_{outlet})^{1/2}$. Note that as the number of stages approaches infinity in the limit, the compression process becomes isothermal and the required power approaches an absolute minimum (See Example 15.3).

In comparing the idealized models for reciprocating compressors with the actual hardware, several issues are worth noting. The valves typically used in these machines are spring

loaded so that the exhaust valve opens when the pressure of the gas in the cylinder exceeds the design delivery pressure just enough to overcome the inertia of the valve mass. There results some very small oscillations in pressure as the gas pressure adjusts to the motion of the valve and the gas, and the gas pressure gradually decreases to a value at which the valve closes. A similar set of events occurs during the intake stroke as the spring loaded intake valve opens when the pressure of the gas in the cylinder drops below atmospheric pressure and then oscillates slightly until it increases to a steady value of nearly atmospheric pressure at the end of the intake stroke. Clearly, if the spring loads on the intake and exhaust valves are too large, the volumetric efficiency will suffer. Other important issues for the real hardware are the leakage past the seals between the piston and the cylinder walls and the friction and lubrication of these seals as the piston moves relative to the cylinder walls.

Example 15.2: Consider a two-stage reciprocating air compressor ($\gamma = 1.4$) operating on a reversible, adiabatic cycle such as that shown in Figure 15.4. A heat exchanger with a heat exchanger effectiveness of $\varepsilon = 1$ is used as an intercooler between the two stages with a coolant at ambient temperature.

(a) Show that the power required to operate the machine will be a minimum when the intermediate pressure between the two stages is given by $P_i = (P_{inlet}P_{outlet})^{1/2}$.

(b) For the case in which the overall pressure ratio is 20, compare both the power required and the volumetric efficiency of the optimum two-stage machine with those of a single stage machine. The clearance fraction in both machines is 5 percent.

Solution: (a) For the reversible, adiabatic two stage machine, the power for each stage is given by equation (15.41). For a heat exchanger with $\varepsilon = 1$ and cooling provided by a fluid at ambient temperature, the temperature of the air entering the second stage is identical to the temperature of the air entering the first stage, i.e., $T_1 = T_5$. Then if the pressure of the gas entering the first stage is P_1 and the pressure of the gas leaving the first stage and entering the second stage is P_2 and the pressure of the gas leaving the second stage is P_6, it follows that

$$\left(\dot{W}_{net}\right)_{\substack{rev\\Q=0}} = \frac{\gamma}{1-\gamma}\dot{m}RT_1\left[\left(\frac{P_2}{P_1}\right)^{\gamma-1/\gamma} - 1\right] + \frac{\gamma}{1-\gamma}\dot{m}RT_5\left[\left(\frac{P_6}{P_5}\right)^{\gamma-1/\gamma} - 1\right]$$

$$\left(\dot{W}_{net}\right)_{\substack{rev\\Q=0}} = \frac{\gamma}{1-\gamma}\dot{m}RT_1\left\{\left[\left(\frac{P_2}{P_1}\right)^{\gamma-1/\gamma} - 1\right] + \left[\left(\frac{P_6}{P_2}\right)^{\gamma-1/\gamma} - 1\right]\right\}$$

Taking the derivative of this expression with respect to P_2 and setting the result equal to zero, we get

$$\frac{d}{dP_2}\left(\frac{-\left(\dot{W}_{net}\right)_{\substack{rev\\Q=0}}}{\dot{m}RT_1}\right) = \left[P_2^{-1/\gamma}P_1^{1-\gamma/\gamma} - P_2^{1-2\gamma/\gamma}P_6^{\gamma-1/\gamma}\right] = 0$$

$$P_2^{-1/\gamma}P_1^{1-\gamma/\gamma} = P_2^{1-2\gamma/\gamma}P_6^{\gamma-1/\gamma}$$

$$\left(P_1P_6\right)^{1-\gamma} = P_2^{2(1-\gamma)}$$

$$P_2 = \sqrt{P_1P_6}$$

(b) For an overall pressure ratio of 20, the intermediate pressure that gives the minimum power

requirement is $P_2 = \sqrt{20} = 4.472$. Then

$$\frac{(\dot{W}_{net})_{2stages}}{(\dot{W}_{net})_{1stage}} = \frac{\left[\left(\frac{4.472}{1}\right)^{1.4-1/1.4} - 1\right] + \left[\left(\frac{20}{4.472}\right)^{1.4-1/1.4} - 1\right]}{\left[\left(\frac{20}{1}\right)^{1.4-1/1.4} - 1\right]} = \frac{2(0.534)}{1.354} = 0.789$$

Thus the saving in power is 21 percent. The effect of staging on the volumetric efficiency is even more pronounced, viz.

$$\frac{(\eta_v)_{2stages}}{(\eta_v)_{1stage}} = \frac{1 - 0.05\left[\left(\frac{4.472}{1}\right)^{1/1.4} - 1\right]}{1 - 0.05\left[\left(\frac{20}{1}\right)^{1/1.4} - 1\right]} = \frac{0.904}{0.625} = 1.447$$

Thus there is a 45 percent increase in volumetric efficiency with the two-stage machine which results in a machine that is considerably smaller in size than the single-stage machine. The cost of this benefit is that there is an additional heat exchanger in the two-stage machine that is not required in the single-stage machine.

Example 15.E3: Consider a single stage reciprocating compressor with a pressure ratio of 20. Let the reversible, adiabatic paths during the compression stroke and the re-expansion stroke be replaced with polytropic paths described by PV^n = constant where $1 \le n \le 1.67$ such that the value $n = 1$ corresponds to a reversible, isothermal path and $n = 1.67$ corresponds to a reversible, adiabatic path in a monatomic gas (such as helium).

(a) Show that as the value of n decreases to unity, the power required to drive the compressor decreases to its minimum value.

(b) Derive an expression for the power required for reversible, isothermal compression in a reciprocating compressor that follows a cycle similar to that depicted in Figure 15.4 but with isothermal processes replacing the adiabatic ones. Evaluate this expression for a machine with a pressure ratio of 20.

Solution: (a) The expression for the power required in a single stage compressor with polytropic processes is given by equation (15.41) with γ replaced by n. Thus

$$(\dot{W}_{net})_{\substack{rev \\ Q=0}} = \frac{n}{1-n}\dot{m}RT_1\left[\left(\frac{P_2}{P_1}\right)^{n-1/n} - 1\right]$$

We can rewrite this expression in dimensionless form, viz.

$$\frac{-(\dot{W}_{net})_{\substack{rev \\ Q=0}}}{\dot{m}RT_1} = \frac{n}{n-1}\left[\left(\frac{P_2}{P_1}\right)^{n-1/n} - 1\right]$$

For a pressure ratio of 20, we can plot this equation as a function of the parameter n as shown in Figure 15E.3. Note that as $n \to 1$, the value of the dimensionless power approaches the minimum value.

(b) This minimum value can be determined by replacing the reversible, adiabatic paths from state 1 to state 2 and from state 3 to state 4 in Figure 15.4 with reversible, isothermal paths.

Then

$$W_{1-2} = \int_1^2 PdV = m_1 RT_1 \int_{V_1}^{V_2} \frac{dV}{V} = m_1 RT_1 \ln\left(\frac{V_2}{V_1}\right) = m_1 RT_1 \ln\left(\frac{m_2 RT_2}{m_1 RT_1}\frac{P_1}{P_2}\right) = -m_1 RT_1 \ln\left(\frac{P_2}{P_1}\right)$$

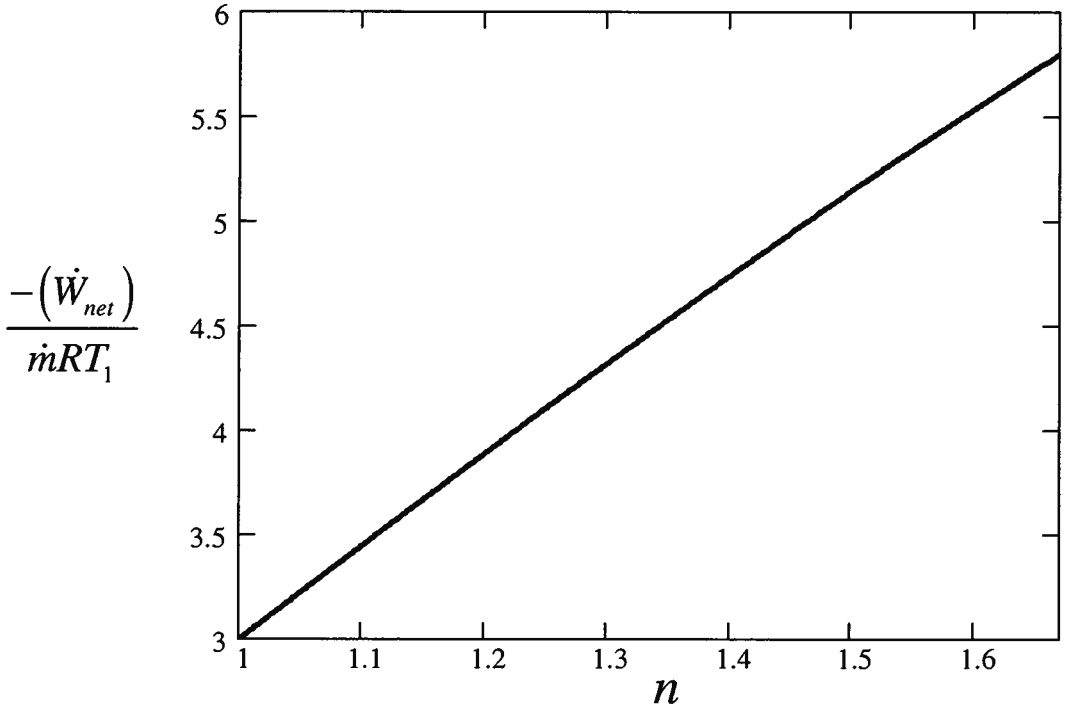

Figure 15E.3 Dimensionless Power for Reversible, Adiabatic Air Compressor with a Pressure Ratio of 20

Similarly for the process 3 – 4,

$$W_{3-4} = m_3 RT_1 \ln\left(\frac{P_2}{P_1}\right)$$

Then

$$W_{net} = (m_3 - m_1) RT_1 \ln\frac{P_2}{P_1} + P_3V_3 - P_2V_2 + P_1V_1 - P_4V_4$$

$$W_{net} = (m_3 - m_1) RT_1 \ln\frac{P_2}{P_1} + m_3RT_1 - m_2RT_1 + m_1RT_1 - m_4RT_1$$

$$W_{net} = (m_3 - m_1) RT_1 \ln\frac{P_2}{P_1} + RT_1(m_3 - m_2 + m_1 - m_4) = (m_3 - m_1) RT_1 \ln\frac{P_2}{P_1}$$

$$\frac{-(\dot{W}_{net})}{\dot{m}RT_1} = \ln\frac{P_2}{P_1}$$

For a pressure ratio of 20, $\frac{-(\dot{W}_{net})}{\dot{m}RT_1} = 2.996$ which is precisely the value obtained in part (a) above for the case of $n = 1$. Although the reversible, isothermal compressor achieves the minimum

power for a given pressure ratio and mass flow rate, it is not a practical solution since this design requires thermal equilibrium with the environment for each state. This requirement results in a machine that runs at an infinitesimally small rate. The practical compromise is to use an adiabatic design with as many stages as possible with intercooling after each stage.

15.2.1.2 Rotating Shaft Work Machines: Following the example of the preceding section, let us consider an axial flow compressor as an example of a rotating shaft work machine. The axial flow compressor represents an alternative design to the reciprocating compressor discussed above that uses rotary motion only and thereby eliminates the vibration associated with the reciprocating motion. Compared with reciprocating compressors, axial flow compressors are ideal for delivering large flow rates of gas at relatively low pressures. Also, the cylindrical shape and lighter mass of the axial flow compressor makes it well suited for its role as the compressor component of the gas turbine engine used to power aircraft.

A stage of an axial flow compressor consists of row of *rotor* blades, shaped like airfoils and mounted in a radial fashion on a disk that rotates about the axis of symmetry of the machine. The gas being compressed flows through the blades in a direction parallel to the axis of rotation. Located on the discharge side of the rotor is another row of blades that are held stationary and form a *stator*. In the space between the stator blades, the gas flow is decelerated with an attendant increase in pressure. The geometry of the stator blades is such that the gas flow is directed smoothly onto the blades of the next rotor located immediately downstream. The pressure ratio of compression in a single stage consisting of a rotor and a stator is rather small compared to a single stage of a typical reciprocating compressor, so many stages are required for even relatively moderate overall pressure ratios in axial flow compressors.

Figure 15.5 shows the cross-section of a rotor blade at some point along its span, e.g., at the midpoint, and the resulting velocity diagrams. The fluid enters the blade traveling in the axial

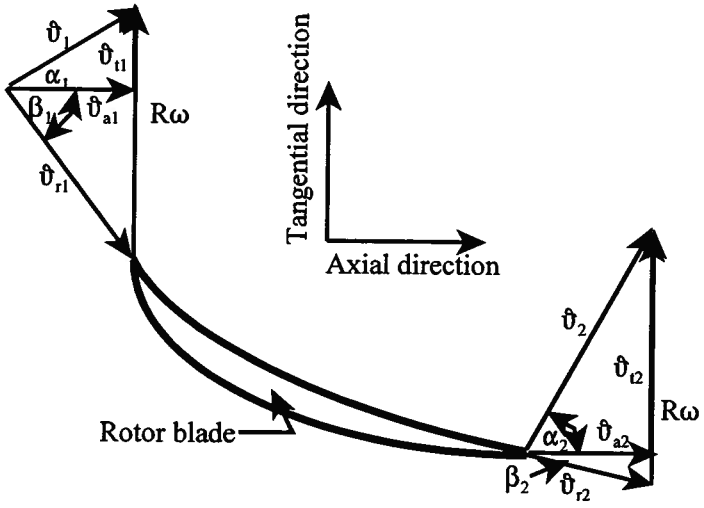

Figure 15.5 Velocity Diagrams for an Axial Flow Compressor at a Location R

direction with the absolute velocity ϑ_1. This velocity has a component relative to the blade of ϑ_{r1}. The absolute velocity can also be resolved into components in the axial direction, ϑ_{a1}, and the tangential direction, ϑ_{t1}. The tangential speed of the rotor blade at the location R is $R\omega$. The absolute velocity of the fluid at the exit from the blade is ϑ_2 with components ϑ_{r2}, ϑ_{a2}, and ϑ_{t2} as shown on Figure 15.5. The tangential component of fluid velocity increases in the direction of

flow through the compressor, thereby increasing the angular momentum of the fluid. According to the *Euler turbomachine equation*, equation (8.107), this increase in angular momentum is responsible for the torque required to drive the axial flow compressor, viz.

$$T_{shaft} = \dot{m}\left(R\vartheta_{t2} - R\vartheta_{t1}\right) \tag{15.48}$$

since the value of R is fixed in this case. Then the power required to drive the compressor is given by (thermodynamic sign convention)

$$-\left(\dot{W}_{shaft}\right)_{\substack{rev \\ Q=0}} = -T_{shaft}N = \dot{m}R\omega\left(\vartheta_{t2} - \vartheta_{t1}\right) \tag{15.49}$$

If we apply the first law to the control volume enclosing the blade, we obtain for steady, reversible, adiabatic flow

$$\cancel{\dot{Q}} - \left(\dot{W}_{shaft}\right)_{\substack{rev \\ Q=0}} = \dot{m}\left[\left(h_2 - h_1\right) + \left(\frac{\vartheta_2^2}{2} - \frac{\vartheta_1^2}{2}\right)\right] \tag{15.50}$$

Combining equations (15.49) and (15.50), we get

$$h_2 - h_1 = \frac{2R\omega\left(\vartheta_{t2} - \vartheta_{t1}\right) + \vartheta_1^2 - \vartheta_2^2}{2} \tag{15.51}$$

From the velocity diagrams of Figure 15.5, we have

$$\begin{aligned} \vartheta_1^2 &= \vartheta_{r1}^2 - R^2\omega^2 + 2R\omega\vartheta_{t1} \\ \vartheta_2^2 &= \vartheta_{r2}^2 - R^2\omega^2 + 2R\omega\vartheta_{t2} \end{aligned} \tag{15.52}$$

Then combining equations (15.51) and (15.52), we obtain

$$h_2 - h_1 = \frac{\vartheta_{r1}^2 - \vartheta_{r2}^2}{2} \tag{15.53}$$

Equation (15.53) shows that the enthalpy of the fluid changes as it passes over the blade by an amount that depends upon the flow geometry of the blade. We note that the quantity

$$h + \frac{\vartheta_r^2}{2} = \text{constant} \tag{15.54}$$

as the fluid passes through the various rotor stages of the machine. The quantity given in equation (15.54) is known as the *stagnation enthalpy*.

We can calculate the pressure ratio of the reversible rotor stage by combining equations (15.54) and (15.30), viz.

$$\frac{-\left(\dot{W}_{shaft}\right)_{\substack{rev \\ Q=0}}}{\dot{m}} = \frac{\gamma}{\gamma - 1}RT_1\left[\left(\frac{P_2}{P_1}\right)^{\gamma-1/\gamma} - 1\right] = h_2 - h_1 = \frac{\vartheta_{r1}^2 - \vartheta_{r2}^2}{2} \tag{15.55}$$

A complete stage consists of a rotor and a stator; thus the pressure increase given by equation (15.55) is only part of the total pressure increase for the stage. Typically, axial flow compressor stages are designed so that half the pressure rise occurs in the rotor and the other half occurs in the stator as the fluid is decelerated. This splitting of the pressure increase reduces the risk of flow separation due to the fact that the flow in the stage occurs in an adverse pressure gradient. We shall examine the flow in the stator later in this chapter when we take up the subject of *diffusers*.

It is important to note that the fluid velocity diagrams like those of Figure 15.5 depend upon the local tangential velocity of the blade, $R\omega$. Since R varies along the length of the blade, the local tangential velocity will also vary. The streamlines of the flow are essentially parallel to

the axis of rotation, so the velocity diagrams have unique shapes at each value of R. In order to maintain the axial component of the velocity constant from the root to the tip of the blade, it is necessary for the blade geometry to vary along this length. The net result is that the blades appear twisted about the blade axis as the airfoil shape of the blade changes from root to tip. This twist complicates the manufacture of the blades somewhat but is essential for proper performance of the compressor. Similar observations apply to axial flow turbines as well.

Example 15E.4: Consider a rotor stage of an axial flow air compressor with blade entry and exit angles $\beta_1 = 52.427°$ and $\beta_2 = 35°$, respectively (See Figure 15.5.). The gas enters at a temperature of $T_1 = 293$ K and a pressure of $P_1 = 2.5 \times 10^5$ N/m^2 with an axial velocity of $\vartheta_a = 137.5$ m/sec that is constant across the blade. For the ideal gas model, $\gamma = 1.4$ and $R = 287$ J/kg K. The compressor design is a reaction design with half the pressure rise occurring across the rotor and the other half across the stator. (Note that for a reaction design in which the pressure rise is split equally between the rotor and stator, the velocity diagrams are symmetric with $\beta_1 = \alpha_2$ and $\beta_2 = \alpha_1$.)

(a) Estimate the pressure ratio of the complete stage (rotor plus stator).

(b) Estimate the tangential velocity of the blade.

(c) Estimate the power required to drive this rotor.

Solution: (a) The change in kinetic energy of the gas as it flows across the blade is equal to the work done by the gas. Then according to equation (15.55), the pressure ratio across the blade is given by

$$\frac{\gamma}{\gamma-1}RT_1\left[\left(\frac{P_2}{P_1}\right)^{\gamma-1/\gamma}-1\right]=\frac{\vartheta_{r1}^2-\vartheta_{r2}^2}{2}$$

The velocities relative to the blade are given by the velocity diagrams of Figure 15.5, viz.

$$\vartheta_{r1}=\frac{\vartheta_a}{\cos\beta_1}=\frac{137.5\text{ m/sec}}{\cos 52.427^\circ}=225.494\text{ m/sec}$$

and

$$\vartheta_{r2}=\frac{\vartheta_a}{\cos\beta_2}=\frac{137.5\text{ m/sec}}{\cos 35^\circ}=167.857\text{ m/sec}$$

Then

$$\frac{P_2}{P_1}=\left\{1+\frac{\gamma-1}{\gamma RT_1}\left[\frac{\vartheta_{r1}{}^2-\vartheta_{r2}{}^2}{2}\right]\right\}^{\gamma/\gamma-1}$$

$$\frac{P_2}{P_1}=\left\{1+\frac{1.4-1}{1.4(287\text{ J/kg K})(293\text{ K})}\left[\frac{(225.494\text{ m/sec})^2-(167.857\text{ m/sec})^2}{2}\right]\right\}^{1.4/0.4}$$

$$\frac{P_2}{P_1}=1.1414$$

Then the pressure at exit from the blade is given by

$$P_2=1.1414P_1=1.1414(2.5\times10^5\text{N/m}^2)=2.8536\times10^5\text{ N/m}^2$$

and the pressure rise is

$$\Delta P=P_2-P_1=2.8536\times10^5\text{ N/m}^2-2.5\times10^5\text{ N/m}^2=3.536\times10^4\text{ N/m}^2$$

Since an equal pressure rise occurs in the stator, the pressure at exit from the stator is

$$P_3 = P_2 + \Delta P = 2.8536 \text{ x}10^5 \text{ N/m}^2 + 3.536 \text{ x } 10^4 \text{ N/m}^2 = 3.2071 \text{ x } 10^5 \text{ N/m}^2$$

Then the overall pressure ratio for the stage is

$$\frac{P_3}{P_1} = \frac{3.2071 \text{ x } 10^5 \text{ N/m}^2}{2.5 \text{ x } 10^5 \text{ N/m}^2} = 1.2828$$

This value for the pressure ratio is typical for stages of axial flow compressors designed for gas turbine engines.

(b) The blade speed can be determined from the velocity diagrams of Figure 15.5, viz.

$$\vartheta_b = \vartheta_a \left(\tan\alpha_1 + \tan\beta_1\right) = (137.5 \text{ m/sec})\left(\tan 35^\circ + \tan 52.427^\circ\right) = 275 \text{ m/sec}$$

(c) The power required to drive the rotor per unit mass flow rate can be determined from the Euler turbomachine equation, viz.

$$\frac{-\left(\dot{W}_{shaft}\right)}{\dot{m}} = R\omega\left(\vartheta_{t2} - \vartheta_{t1}\right)$$

The tangential components of the gas velocity at entrance and exit to the blade are given by

$$\vartheta_{t1} = \vartheta_a \tan\alpha_1 = 137.5 \tan 35^\circ = 96.279 \text{ m/sec}$$

and

$$\vartheta_{t2} = \vartheta_a \tan\alpha_2 = 137.5 \tan 52.427^\circ = 178.722 \text{ m/sec}$$

Then

$$\frac{-\left(\dot{W}_{shaft}\right)}{\dot{m}} = (275 \text{ m/sec})\left[(178.722 \text{ m/sec}) - (96.279 \text{ m/sec})\right] = 2.267 \text{ x } 10^4 \text{ W/kg/sec}$$

This example shows the importance of the blade design and the axial velocity on the performance of the axial flow compressor. The performance of axial flow compressors is limited by the competition between flow velocity and compressibility effects. In order to minimize the size of the machine, it is necessary to increase the flow velocity (axial velocity) as much as possible, but if the flow velocity is too large, shock waves can form locally and the machine becomes choked. For this reason the maximum Mach number in these shaft work machines is usually limited to about $M = 0.7$.

15.2.1.3 Polytropic Efficiency of Turbomachines: Although the adiabatic efficiencies defined in equations (15.22) and (15.24) are valid expressions of the performance of shaft work machines in general, they can be a bit misleading when comparing turbomachines of different pressure ratios. This is most easily illustrated for the case of a negative shaft work turbomachine processing an ideal gas, such as the multistage axial flow compressor described in the preceding section. From Figure 15.2(b), it would appear that the compression process occurs in a single step with the overall pressure ratio of P_{out}/P_{in}, but for reasons discussed above, for a pressure ratio of any practical value in a real axial flow compressor, it is impractical to execute the compression in a single stage. Rather, the compression process is carried out in a series of stages with identical, modest values of the pressure ratio. The overall pressure ratio of the compressor is then the product of the individual pressure ratios of the many stages. Since compressor designs vary with respect to the design of the individual stages, the efficiency of equation (15.24) is of limited value. We can, in fact, specify an adiabatic efficiency, η_{st}, for each individual stage in the manner of equation (15.24). This stage efficiency may be significantly different from the overall adiabatic efficiency of the compressor. Alternatively, we can define the polytropic efficiency, η_P, in light of the multi-stage nature of the compression process.

The *h-s* diagram for the compression process would then take on an appearance similar to that shown for a few stages in Figure 15.6. Consider the limiting case of an infinitesimal compression process in which the state

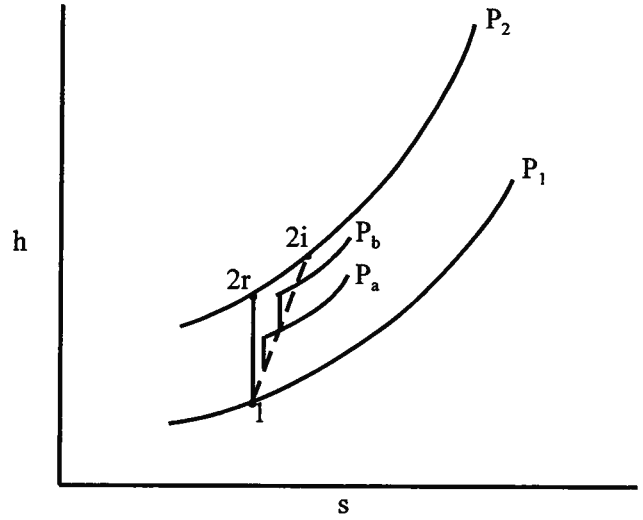

Figure 15.6 Multi-stage Compression of an Ideal Gas

of the gas is changed from P to $P + dP$. By virtue of the thermodynamic coupling in the gas, the temperature will change from T to $T + dT$. The work transfer required for this infinitesimal change of state is given by equation (15.12). For a reversible change of state, the necessary work transfer per unit mass flow rate is

$$-\left(\frac{\delta \dot{W}_{shaft}}{\dot{m}}\right)_{reversible} = (dh)_{reversible} \tag{15.56}$$

For the actual change of state, we have

$$-\left(\frac{\delta \dot{W}_{shaft}}{\dot{m}}\right)_{actual} = (dh)_{actual} \tag{15.57}$$

We now define a polytropic efficiency, η_P, for this small stage of compression such that

$$\eta_P = \frac{(dh)_{reversible}}{(dh)_{actual}} \tag{15.58}$$

From equation (15.13), we have for the reversible adiabatic compression

$$(dh)_{reversible} = \cancel{Tds} + vdP \tag{15.59}$$

and for the actual compression process, the enthalpy constitutive relation gives

$$(dh)_{actual} = c_P dT \tag{15.60}$$

Then

$$\eta_P = \frac{vdP}{c_P dT} = \frac{RT}{P}\frac{dP}{c_P dT} \tag{15.61}$$

where we have substituted the property constitutive relation for v. For the ideal gas model,

$$\frac{R}{c_P} = \frac{c_P - c_v}{c_P} = \frac{c_P/c_v - 1}{c_P/c_v} = \frac{\gamma - 1}{\gamma} \tag{15.62}$$

Then substituting equation (15.62) into equation (15.61) and separating variables, we get

$$\frac{dT}{T} = \frac{(\gamma - 1)}{\gamma \eta_P} \frac{dP}{P} \tag{15.63}$$

Integrating equation (15.63) for the overall compression process with the polytropic efficiency of each stage constant, we get

$$\frac{(T_2)_{actual}}{T_1} = \left(\frac{P_2}{P_1}\right)^{(\gamma-1)/\gamma\eta_P} \tag{15.64}$$

For the reversible compression process, we have from the entropy constitutive relation with $s_2 = s_1$,

$$\frac{(T_2)_{reversible}}{T_1} = \left(\frac{P_2}{P_1}\right)^{r/c_P} = \left(\frac{P_2}{P_1}\right)^{(\gamma-1)/\gamma} \tag{15.65}$$

Substituting equations (15.64) and (15.65) into equation (15.32), we get

$$\eta_- = \frac{\left[\left(\frac{P_2}{P_1}\right)^{\gamma-1/\gamma} - 1\right]}{\left[\left(\frac{P_2}{P_1}\right)^{\gamma-1/\gamma\eta_P} - 1\right]} \tag{15.66}$$

For the case $\gamma = 1.4$ (typical of diatomic gases like air), Figure 15.7 shows the effect of staging the compression process on the overall performance of the compressor. Except for the case of

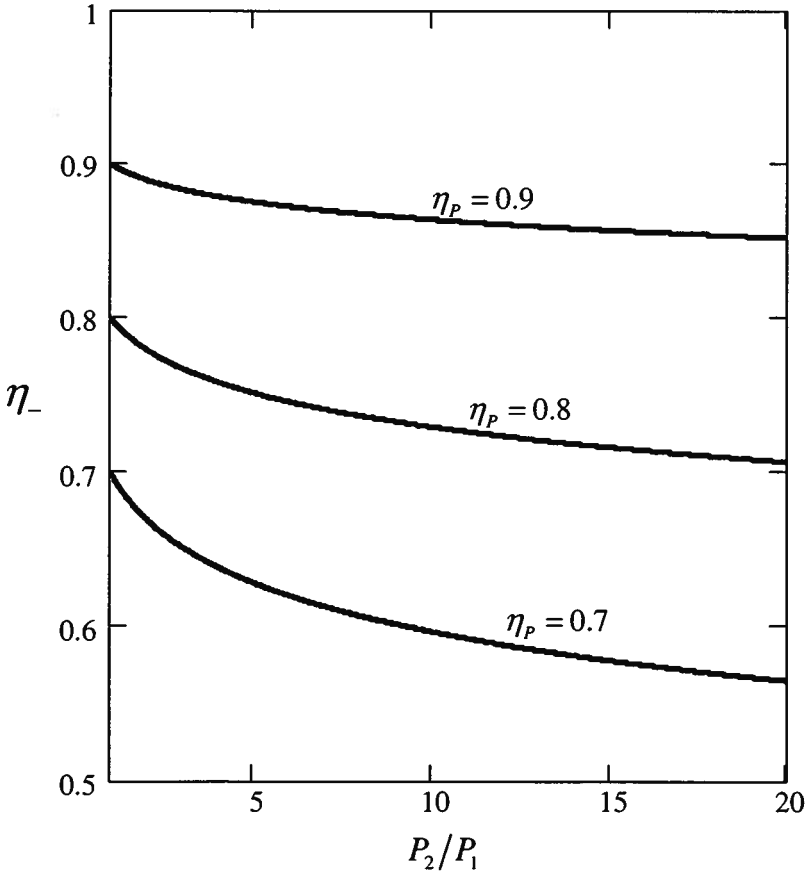

Figure 15.7 Adiabatic Efficiency of Multi-Stage Compression

single stage compression, the adiabatic efficiency of the compressor as a whole is always less than the efficiency of the individual stages. As the compression ratio increases, the staging effect becomes more pronounced. In effect, what we have done is to use a polytropic path defined by

$$Pv^n = \text{constant} \tag{15.67}$$

with $n > \gamma$, to get from the inlet state to the outlet state of the actual compressor. This path replaces the locus of states of the actual compression process. Unlike the actual sequence of states, this polytropic path is not an adiabatic path, but in fact, has a positive heat transfer. It should be noted that in a multi-stage axial compressor with many stages, the stage efficiency, η_{st}, may be approximately equal to the polytropic efficiency, η_P.

A similar result can be obtained for a positive shaft work turbomachine, such as a multi-stage, axial flow turbine. In this case, the polytropic efficiency is defined as

$$\eta_P = \frac{(dh)_{actual}}{(dh)_{reversible}} = \frac{c_P dT}{vdP} \tag{15.68}$$

After integrating equation (15.68) and substituting the result into equation (15.31), we obtain

$$\eta_+ = \frac{\left[1-\left(\frac{P_2}{P_1}\right)^{\eta_P(\gamma-1)/\gamma}\right]}{\left[1-\left(\frac{P_2}{P_1}\right)^{(\gamma-1)/\gamma}\right]} \tag{15.69}$$

Again for the case $\gamma = 1.4$, Figure 15.8 shows the effect of staging the expansion process on the overall performance of the turbine. In contrast to the compression process, the adiabatic

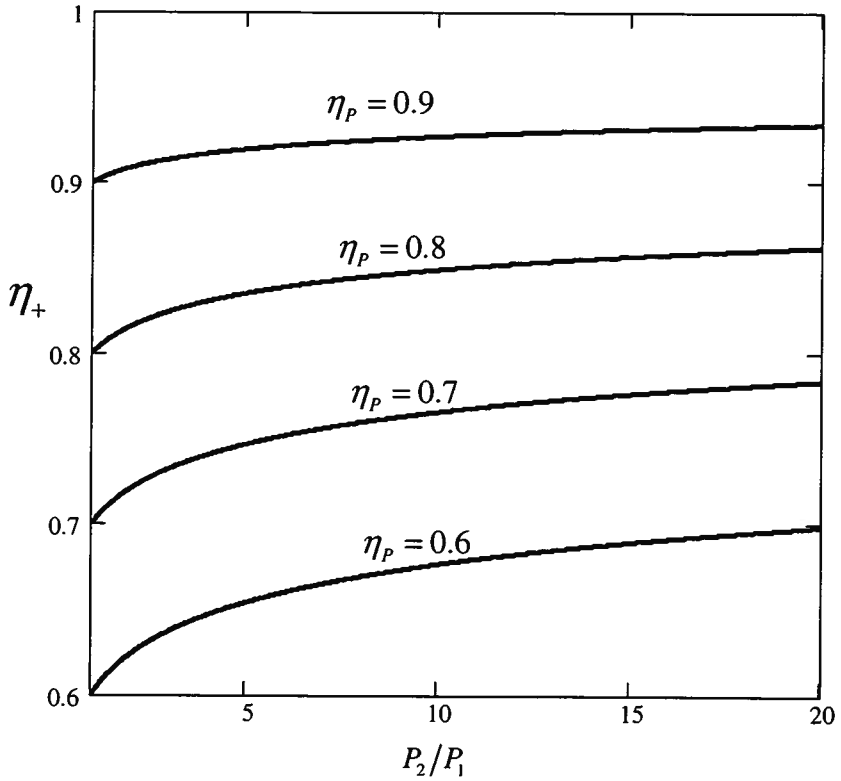

Figure 15.8 Adiabatic Efficiency of Multi-Stage Expansion

efficiency of the overall expansion process is greater than the small stage efficiency. This is one of the reasons that the adiabatic efficiency of turbines tends to be greater than the adiabatic efficiency of compressors even though the efficiency of the individual stages are the same in both cases. In practice, adiabatic efficiencies are usually reported on performance maps of shaft work turbomachines whereas polytropic efficiencies are usually used in the design process.

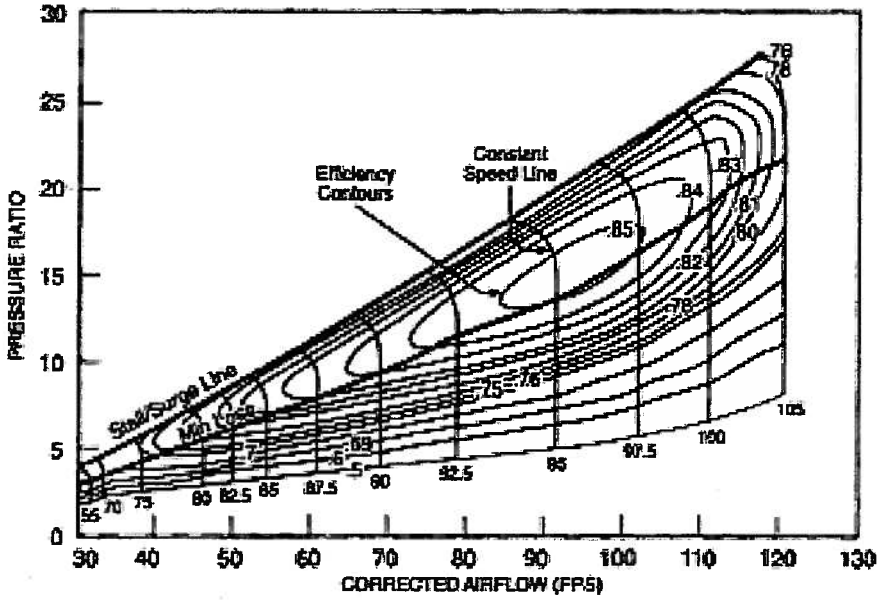

Figure 15.9 Performance Map of an Axial Flow Compressor

Figure 15.9 shows a typical performance map of a multi-stage axial flow compressor. Note the contours of constant (adiabatic) efficiency. A similar map can be developed for a turbine so that when a compressor and a turbine are to be used in tandem as in a gas turbine power plant, thermal-fluid engineers can make sure that the performance characteristics of the two shaft work machines properly match to insure continuity of flow and that the two units are optimized for the application.

Example 15E.4: A turbofan engine of the type shown in Example 15E.1 uses a compressor of $n = 17$ stages with an identical pressure ratio of $P_r = 1.2$ for each stage. The polytropic efficiency of each stage is $\eta_p = 0.9$. Estimate the adiabatic shaft efficiency of the compressor with air as the working fluid ($\gamma = 1.4$).

Solution: The overall pressure ratio of the compressor is given by

$$\frac{P_2}{P_1} = P_r^n = 1.2^{17} = 22.186$$

The adiabatic shaft machine efficiency is given by equation (15.44), viz.

$$\eta_- = \frac{\left[\left(\frac{P_2}{P_1}\right)^{\gamma-1/\gamma} - 1\right]}{\left[\left(\frac{P_2}{P_1}\right)^{\gamma-1/\gamma_p} - 1\right]} = \frac{22.186^{(1.4-1)/1.4} - 1}{22.186^{(1.4-1)/(1.4)(0.9)} - 1} = 0.8503$$

This is a typical value for an engine of this type.

15.2.1.4 Actuator Disks: Although this topic may seem somewhat misplaced in a section devoted to the analysis of the fundamental behavior of shaft work machines in general terms, we include shaft work machines that use the atmosphere as the working fluid in the present context for two reasons: (a) The internal details of this class of shaft work machines is analyzed in a slightly different manner than the broader classes of shaft work machines such as the turbines and compressors introduced above; and (b) these machines are finding more widespread deployment in the present energy marketplace than at any other time in history.

Actuator disks represent a class of machines that are a subset of the shaft work turbomachines described above. By definition, an actuator disk is an axial flow turbomachine consisting of a single rotor with an infinite number of frictionless blades that creates a pressure change without a change in velocity. That is, the fluid velocity through the actuator disk is continuous, but the fluid velocity far upstream is quite different from the fluid velocity far downstream. In this form, an actuator disk is a useful model for two common shaft work machines: (1) propellers used to propel aircraft or ships (negative shaft work turbomachines) and (2) wind turbines (positive shaft work turbomachines). Although the actuator disk uses air as the working fluid, the fluid velocity through the disk is relatively small ($M < 0.3$) so compressibility effects are negligible for both types of actuator disks. As a consequence, the air can be modeled as an incompressible fluid.

In the case of the *propeller*, the objective is to use the shaft power from a positive shaft work machine (such as a reciprocating piston engine or a gas turbine) driving the device to increase the linear momentum of a fluid stream. From the equation of linear momentum, it is apparent that this increase in linear momentum results in a thrust force applied to the air or water craft. In the general case, the shaft power delivered to the device appears in three forms: (1) propulsive power associated with the thrust applied to a moving mass, (2) an increase in the kinetic energy of the moving fluid stream, and (3) an increase in the stored thermal energy of the moving stream due to the irreversibility of the operation of the device. Thus, there is an efficiency associated with the device.

Consider the case of an aircraft propeller. The situation can be analyzed by using the control volume approach as shown in Figure 15.10. The boundaries of the control volume labeled CV_1 are coincident with a *streamtube* whose boundaries are streamlines passing through the propeller. Thus there is no fluid velocity component normal to the streamtube. The control volume CV_1 moves with constant velocity $\hat{v}_1$ through the quiescent atmosphere.

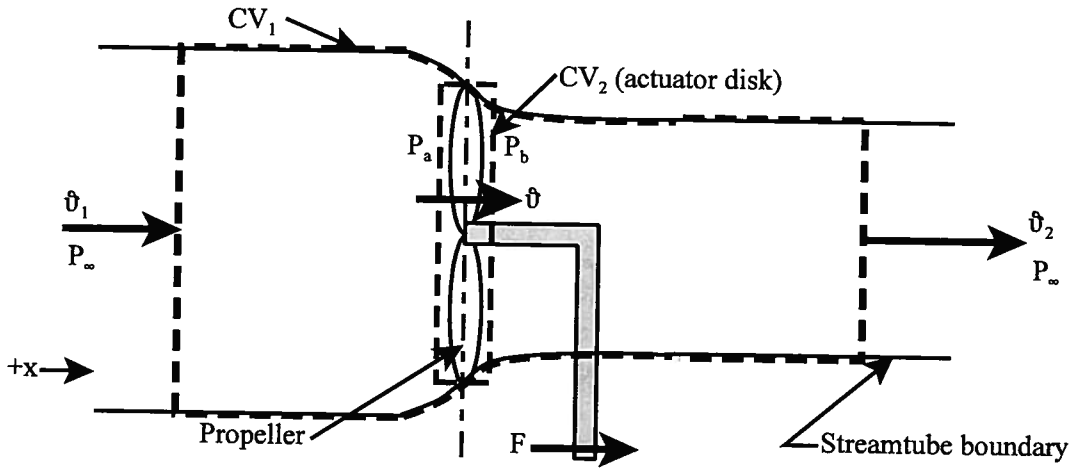

Figure 15.10 Control Volumes for Analysis of Propeller Performance

For control volume CV_1, the equation of linear momentum becomes

$$F + P_\infty A_1 - P_\infty A_2 - P_\infty A_p = \dot{m}\vartheta_2 - \dot{m}\vartheta_1 \tag{15.70}$$

where A_p is the surface area of the streamtube projected on to a plane normal to the axis of rotation of the propeller. Although $A_1 \neq A_2$, $A_2 + A_p = A_1$. Then equation (15.70) becomes

$$F = \dot{m}(\vartheta_2 - \vartheta_1) \tag{15.71}$$

For control volume CV_2, the actuator disk, the equation of linear momentum becomes

$$F + P_a A - P_b A = \dot{m}\vartheta_b - \dot{m}\vartheta_a \tag{15.72}$$

where A is the cross-sectional area of the actuator disk. Also, by definition, for the actuator disk $\vartheta_a = \vartheta_b = \vartheta$. Then combining equations (15.71) and (15.72), we obtain

$$F = (P_b - P_a)A = \dot{m}(\vartheta_2 - \vartheta_1) = \dot{m}\Delta\vartheta \tag{15.73}$$

where we have introduced the notation $\Delta\vartheta = (\vartheta_2 - \vartheta_1)$.

The pressure difference across the propeller appearing in equation (15.73) can be determined by applying the Bernoulli equation along a streamline leading into the propeller and also a different streamline leading away from the propeller. Note that these streamlines are straight when they cross the boundaries of CV_1. Thus

$$\frac{\vartheta_1^2}{2} + \frac{P_{atm}}{\rho} = \frac{\vartheta_a^2}{2} + \frac{P_a}{\rho} \tag{15.74}$$

$$\frac{\vartheta_2^2}{2} + \frac{P_{atm}}{\rho} = \frac{\vartheta_b^2}{2} + \frac{P_b}{\rho} \tag{15.75}$$

If we subtract equation (15.74) from equation (15.75), we obtain

$$P_b - P_a = \rho\left(\frac{\vartheta_2^2}{2} - \frac{\vartheta_1^2}{2}\right) \tag{15.76}$$

Since $\vartheta_2 = \vartheta_1 + \Delta\vartheta$, equation (15.76) can be rewritten as

$$P_b - P_a = \rho\left[\frac{(\vartheta_1 + \Delta\vartheta)^2}{2} - \frac{\vartheta_1^2}{2}\right] = \rho\left[\frac{\vartheta_1^2}{2} + \frac{2\vartheta_1\Delta\vartheta}{2} + \frac{(\Delta\vartheta)^2}{2} - \frac{\vartheta_1^2}{2}\right] = \rho\Delta\vartheta\left[\vartheta_1 + \frac{\Delta\vartheta}{2}\right] \tag{15.77}$$

Substituting equation (15.77) into equation (15.73), we get

$$(P_b - P_a)A = \rho A\Delta\vartheta\left(\vartheta_1 + \frac{\Delta\vartheta}{2}\right) = \dot{m}\Delta\vartheta \tag{15.78}$$

Comparing the left-hand side of equation (15.78) with the right-hand side, we conclude that for the mass flow through the actuator disk

$$\dot{m} = \rho A\left(\vartheta_1 + \frac{\Delta\vartheta}{2}\right) = \rho A\vartheta_a \tag{15.79}$$

Thus

$$\vartheta_a = \vartheta_1 + \frac{\Delta\vartheta}{2} \tag{15.80}$$

so that half of the total velocity increase through the actuator disk occurs leading up to the disk while the other half occurs leading away from the disk. Thus the velocity through the propeller (actuator disk) is the arithmetic average of the upstream and downstream velocities.

$$\vartheta_a = \vartheta_b = \vartheta = \vartheta_1 + \frac{\Delta\vartheta}{2} = \vartheta_1 + \frac{\vartheta_2 - \vartheta_1}{2} = \frac{\vartheta_1 + \vartheta_2}{2} \tag{15.81}$$

In designing a propeller using the actuator disk approach, the thermal-fluids engineer has to balance the diameter of the propeller, D, with the thrust, F, and aircraft velocity requirements. If we combine equation (15.79) with equation (15.73), we obtain an expression for the velocity change across CV_1, viz.

$$(\Delta v)^2 + 2v_1\Delta v - \frac{8F}{\rho\pi D^2} = 0 \tag{15.82}$$

where we have expressed the propeller area in terms of the propeller diameter, D. Solving for Δv, we obtain an expression for the velocity at exit from the streamtube, v_2. Thus,

$$\Delta v = v_2 - v_1 = v_1\left[\sqrt{1+K} - 1\right]$$

$$v_2 = v_1\sqrt{1+K} \tag{15.83}$$

where K is a dimensionless parameter that characterizes the design, viz.

$$K = \frac{8F}{\rho\pi D^2 v_1^2} \tag{15.84}$$

Note that v_1 is the aircraft velocity.

In order to gain some sense of performance of this negative shaft work machine, we examine the first law applied to the actuator disk.

$$\cancel{\dot{Q}} - \dot{W}_{shaft} = \dot{W}_{propulsive} + \dot{m}\left[(u_{out} - u_{in}) + \left(\frac{v_{out}^2}{2} - \frac{v_{in}^2}{2}\right) + \cancel{g(z_{out} - z_{in})}\right]$$

$$-\dot{W}_{shaft} = F v_{in} + \dot{m}\left[c(T_{out} - T_{in}) + \left(\frac{v_{out}^2}{2} - \frac{v_{in}^2}{2}\right)\right] \tag{15.85}$$

where we have used the property constitutive relation for the fluid model. Equation (15.85) shows that the shaft power from the engine into the propeller is consumed by the actual propulsion of the aircraft, irreversibilities of the operation of the device, and the kinetic energy of the air discharged into the atmosphere.

Some useful information can be obtained by considering the reversible case. In the reversible case, since the flow through the propeller is adiabatic, the second law applied to an incompressible fluid flowing through a control volume similar to CV_1 of Figure 15.10 gives

$$\dot{S}_{out} - \dot{S}_{in} = \cancel{\frac{\dot{Q}}{T}} + \cancel{\dot{S}_{gen}} = 0$$

$$\dot{m}(s_{out} - s_{in}) = \dot{m}\left(c\ln\frac{T_{out}}{T_{in}}\right) = 0 \tag{15.86}$$

Thus, the temperature of the fluid is constant as it passes through the reversible propeller. Then the first law applied to the reversible, adiabatic propeller becomes

$$-\left(\dot{W}_{shaft}\right)_{\substack{rev\\adiabatic}} = F v_{in} + \dot{m}\left[\cancel{c(T_{out} - T_{in})} + \left(\frac{v_{out}^2}{2} - \frac{v_{in}^2}{2}\right)\right] = \dot{m}v_{in}\Delta v + \dot{m}\left[\frac{(v_{in} + \Delta v)^2}{2} - \frac{v_{in}^2}{2}\right]$$

$$-\left(\dot{W}_{shaft}\right)_{\substack{rev\\adiabatic}} = \dot{m}v_{in}\Delta v + \dot{m}\left[\frac{v_{in}^2 + 2v_{in}\Delta v + (\Delta v)^2}{2} - \frac{v_{in}^2}{2}\right] = \dot{m}v_{in}\Delta v + \dot{m}v_{in}\Delta v\left(1 + \frac{\Delta v}{2v_{in}}\right) \tag{15.87}$$

The first term on the right-hand side of equation (15.87) represents the power required to propel the aircraft, but the second term on the right-hand side is power that is just dumped into the

atmosphere and serves no useful purpose. Thus we would like to maximize the former and minimize the latter. Unfortunately, the two terms are linked. The ratio of the two terms is a measure of the *propulsive efficiency* of the propeller. Thus,

$$\eta_{prop} = \frac{\dot{m}\vartheta_{plane}\Delta\vartheta}{\dot{m}\vartheta_{plane}\Delta\vartheta\left(1+\frac{\Delta\vartheta}{2\vartheta_{plane}}\right)} = \frac{1}{1+\frac{\Delta\vartheta}{2\vartheta_{plane}}} \tag{15.88}$$

From equation (15.88), it is clear that in order to make η_{prop} as large as possible, we need to make $\Delta\vartheta$ as small as possible. However, $\Delta\vartheta = 0$ is not an option because as equation (15.73) shows, there would then be no thrust. Then as we reduce $\Delta\vartheta$, we need to increase the diameter of the propeller and process more fluid in order to maintain thrust. Obviously, this trade-off has its limits in order to keep the propeller from hitting the fuselage in flight or the ground when landing. Note that this efficiency is not an efficiency in the sense of the adiabatic efficiency of a shaft work machine defined above.

Example15E.5: The Cessna Aircraft Company manufactures a particular aircraft design known as a Skylane (Model 182T). This plane uses a single engine (reciprocating piston shaft work machine) with a maximum power rating of 230 HP (171.5 kW). The aircraft is a monoplane with a three-bladed propeller with a diameter of D = 2 m. At an altitude of 6000 ft (1828.8 km), the aircraft cruises at 145 knots (nautical miles/hr) (74.594 m/sec) at a power level of 80 percent of maximum. Estimate the thrust of the propeller and the propulsive efficiency of the aircraft, η_{prop}, under these operating conditions.

Solution: In order to estimate the propulsive efficiency of the aircraft, we need to solve equation (15.88). This requires an estimate of the change in velocity of the air as it passes through the propeller of the aircraft. For the purposes of the estimate, we shall assume that the propeller operates in a reversible manner. Under cruise conditions, the shaft power input to the propeller is 80 percent of the maximum. Then

$$\wp_{cruise} = 0.8\wp_{max} = 0.8\left(1.715 \text{ x } 10^5 \text{ W}\right) = 1.372 \text{ x } 10^5 \text{ W}$$

In the absence of any irreversibilities in the propeller slipstream, this power goes into the power required to overcome the drag on the aircraft as it moves forward through the atmosphere and the kinetic energy of the propeller slipstream that eventually gets dissipated irreversibly in the atmosphere in the wake of the aircraft. Then from equation (15.65),

$$-\left(\dot{W}_{shaft}\right)_{\substack{rev\\adiabatic}} = \dot{m}\vartheta_{in}\Delta\vartheta + \dot{m}\vartheta_{in}\Delta\vartheta\left(1+\frac{\Delta\vartheta}{2\vartheta_{in}}\right) = 1.372 \text{ x } 10^5 \text{ W}$$

where $\vartheta_{in} = \vartheta_{plane}$ = 74.594 m/sec and $\dot{m}$ is given by the continuity equation applied to the propeller (actuator disk) itself. Thus, from equation (15.79)

$$\dot{m} = \rho A\left(\vartheta_{plane} + \frac{\Delta\vartheta}{2}\right)$$

From the U. S Standard Atmosphere model for the air, the altitude of z = 1828.8 m corresponds to the geopotential altitude of H = 1828.3 m. At this altitude, the pressure is P = 8.1205 x 10^4 N/m^2, the temperature is T = 276.27 K, and the density of the air is ρ = 1.024 kg/m^3. Then

$$\dot{m} = \left(1.024 \text{ kg/m}^3\right)\pi\left(\frac{2.0 \text{ m}}{2}\right)^2\left[\left(74.594 \text{ m/sec}\right)+\frac{\Delta\vartheta}{2}\right] = 239.97 \text{ kg/sec} + \left(3.217 \text{ kg/m}\right)\frac{\Delta\vartheta}{2}$$

Substituting this result into the first law, we get

$$\left\{239.97 \text{ kg/sec} + (3.217 \text{ kg/m})\frac{\Delta\vartheta}{2}\right\}(74.594 \text{ m/sec})\Delta\vartheta\left(2+\frac{\Delta\vartheta}{2\vartheta_{in}}\right) = 1.372 \text{ x } 10^5 \text{ W}$$

Solving for $\Delta\vartheta$, we obtain $\Delta\vartheta = 3.694$ m/sec. Then the thrust becomes

$$F = \dot{m}\Delta\vartheta = (1.024 \text{ kg/m}^3)\pi\left(\frac{2.0 \text{ m}}{2}\right)^2\left(74.549 \text{ m/sec} + \frac{3.694 \text{ m/sec}}{2}\right)(3.694 \text{ m/sec}) = 908.4 \text{ N}$$

and the propulsive efficiency becomes

$$\eta_{prop} = \frac{1}{1+\frac{\Delta\vartheta}{2\vartheta_{plane}}} = \frac{1}{1+\frac{3.694 \text{ m/sec}}{2(74.594 \text{ m/sec})}} = 0.976$$

This high value of propulsive efficiency can be attributed to several factors. The first, most obvious one, is the fact that this model assumes reversible operation. Clearly, there are irreversibilities associated with the operation of the device that will in fact degrade the performance. The second factor has to do with the fact that the operation of the propeller is much like that of a simple screw with a helical thread. As the screw (in this case, propeller) turns, the screw advances through the medium in which it is embedded. In fact, early designs of propellers were based upon this idea. The pitch of the propeller, i.e., the angle of the propeller blade with respect to the plane of rotation, provides the thrust that advances the aircraft forward, but the higher the pitch, the greater the possibility of flow separation and the losses that it incurs. Thus, modern propeller driven aircraft have automatic control systems that adjust this pitch under load so that the propeller operates in the most efficient manner possible while still maintaining the forward motion of the aircraft. This variable pitch design results in a high value of propulsive efficiency. Finally, the actuator disk theory is an overly simplified view of the operation of a propeller. The propeller blades are in fact shaped like aircraft wings in cross-section and attention must be paid to the aerodynamic character of the flow over the blades. This gives rise to a design approach known as *blade element theory.*

For the design of aircraft propellers, two basic ideas derive from blade element theory. First, the angle through which the axial flow is turned as it passes through the propeller should be kept as small as possible in order to avoid flow separation from the blades. Second, the velocity of the air as it approaches the propeller should be kept well below the speed of sound in order to avoid the formation of shock waves as the flow passes over the blades. These conditions are met easily in low speed, small aircraft. It should be kept in mind that blade element theory applies only so long as the *solidity* of the flow is small where the solidity is defined as the ratio of the actual blade area to the area of the actuator disk. Thus, blade element theory is appropriate for aircraft propellers for which solidity is indeed small, but not for marine propellers for which solidity is large.

This issue is further complicated by the fact that propeller performance is strongly dependent upon the number of blades that make up the device. Propellers with large numbers of blades tend to perform more efficiently than propellers with fewer blades. Modern aircraft propeller designs often employ as many as 12 blades. We shall return to this issue in Chapter 16 where we discuss aircraft propulsion systems in greater detail.

Propellers can also be run as positive shaft work machines that *extract* energy from the wind. Although such devices have been in existence for nearly two thousand years, it has only been in recent years that they have seen much attention from thermal-fluid engineers. In 16th century Europe, windmills or *wind turbines* provided the bulk of the power used to grind grains

and pump water, and the windmills of the Netherlands are classic examples of this technology. In rural areas of the United States, windmills provided not only the power required to pump water for irrigation of farm land, but also to operate sawmills in the late 19th and early 20th centuries. In the early to mid 20th century, windmills even provided electrical power for many farms in rural America that were not attached to the electrical power grid. In the 21st century as humankind has been forced to come to grips with the limited energy resources available, there has been a resurgence of interest in exploiting the wind as a renewable energy source. Germany, Denmark, and Ireland have been particularly active in developing wind turbines and wind farms for the production of electrical power. Although wind turbines have been installed in both on-shore and off-shore locations, the off-shore locations have been most promising because the wind speeds tend to be higher and more nearly constant. The Middelgrunden Off-shore Wind Farm off the coast of Denmark is presently the largest off-shore wind farm with a capacity of 40 MW, but the Cape Wind project planned for off-shore Cape Cod in Massachusetts will have a capacity of 420 MW.

The performance of wind turbines can be analyzed with the aid of the actuator disk model in much the same manner as propellers. The major difference, of course, is the fact that the wind turbine is a positive shaft work machine in which the fluid is decelerated instead of being accelerated. Figure 15.11 shows the streamtube and the corresponding control volumes for the wind turbine.

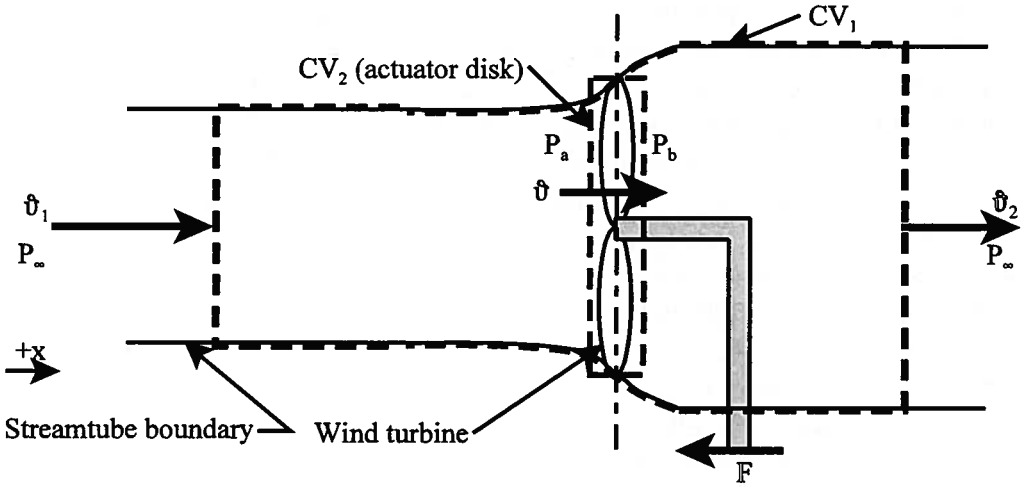

Figure 15.11 Control Volumes for Analysis of Wind Turbine Performance

From the momentum equation for CV_1, we have

$$-F = \dot{m}(v_2 - v_1) \tag{15.89}$$

Similarly for CV_2, the actuator disk,

$$-F + (P_a - P_b)A = \dot{m}(v_b - v_a) = 0 \tag{15.90}$$

Combining equations (15.89) and (15.90), we get

$$F = (P_a - P_b)A = \dot{m}(v_1 - v_2) \tag{15.91}$$

If we apply the Bernoulli equation from the inlet to CV_1 to the inlet to CV_2, we get

$$P_{atm+} + \frac{\rho v_1^2}{2} = P_a + \frac{\rho v^2}{2} \tag{15.92}$$

If we apply the Bernoulli equation from the outlet from CV_2 to the outlet of CV_1, we get

$$P_b + \frac{\rho \vartheta^2}{2} = P_{atm} + \frac{\rho \vartheta_2^2}{2} \tag{15.93}$$

Combining equations (15.91), (15.92), and (15.93), we get

$$P_a - P_b = \frac{1}{2}\rho\left(\vartheta_1^2 - \vartheta_2^2\right) = \frac{\dot{m}}{A}\left(\vartheta_1 - \vartheta_2\right) \tag{15.94}$$

From continuity,

$$\dot{m} = \rho \vartheta A \tag{15.95}$$

Combining equations (15.94) and (15.95), we get the expected result

$$\frac{1}{2}\rho\left(\vartheta_1^2 - \vartheta_2^2\right) = \rho \vartheta \left(\vartheta_1 - \vartheta_2\right)$$

$$\vartheta = \frac{\vartheta_1 + \vartheta_2}{2} \tag{15.96}$$

That is, like the propeller, the fluid velocity through the actuator disk is the arithmetic average of the inlet and outlet velocities and half the velocity change of the fluid in the streamtube occurs upstream of the actuator disk while the remainder occurs downstream.

If we now consider the reversible case, the first law applied to CV_2 becomes

$$\cancel{\dot{Q}} - \dot{W}_{shaft} = \dot{m}\left[\left(u_{out} - u_{in}\right) + \cancel{\left(\frac{\vartheta_{out}^2}{2} - \frac{\vartheta_{in}^2}{2}\right)} + \cancel{g\left(z_{out} - z_{in}\right)}\right]$$

$$\cancel{\dot{Q}} - \left(\dot{W}_{shaft}\right)_{\substack{rev \\ adiabatic}} = \dot{m}\left[\cancel{c\left(T_{out} - T_{in}\right)} + \left(\frac{P_{out}}{\rho} - \frac{P_{in}}{\rho}\right) + \cancel{\left(\frac{\vartheta_{out}^2}{2} - \frac{\vartheta_{in}^2}{2}\right)} + \cancel{g\left(z_{out} - z_{in}\right)}\right]$$

$$\left(\dot{W}_{shaft}\right)_{\substack{rev \\ adiabatic}} = \frac{\dot{m}}{\rho}\left(P_a - P_b\right) \tag{15.97}$$

Combining equations (15.94) – (15.97), we get

$$\left(\dot{W}_{shaft}\right)_{\substack{rev \\ adiabatic}} = \wp = \rho A \vartheta^2 \left(\vartheta_1 - \vartheta_2\right) = \frac{1}{4}\rho A\left(\vartheta_1^2 - \vartheta_2^2\right)\left(\vartheta_1 + \vartheta_2\right) \tag{15.98}$$

where the symbol $\wp$ denotes the power developed by the wind turbine under reversible, adiabatic conditions. There is a value of the discharge velocity ϑ_2 at which the power developed by the wind turbine becomes a maximum. This value can be determined by differentiating equation (15.98) with respect to ϑ_2 and setting the result equal to zero, viz.

$$\frac{d\wp}{d\vartheta_2} = \frac{1}{4}\rho A\left(\vartheta_1^2 - 2\vartheta_1\vartheta_2 - 3\vartheta_2^2\right) = 0 \tag{15.99}$$

Equation (15.99) is satisfied when the term in parentheses is equal to zero. This occurs for the roots of that expression, viz.

$$\vartheta_2 = -\vartheta_1 \quad \text{and} \quad \vartheta_2 = \frac{\vartheta_1}{3} \tag{15.100}$$

The first root gives the minimum power, namely zero when the turbine is not rotating. The second root gives the maximum power which can be determined by substituting this root into equation (15.99), viz.

$$\wp_{max} = \frac{1}{4}\rho A\left(\vartheta_1^2 - \frac{\vartheta_1^2}{9}\right)\left(\vartheta_1 + \frac{\vartheta_1}{3}\right) = \frac{8}{27}\rho A \vartheta_1^3 \tag{15.101}$$

The power in the wind flowing into the turbine is *nominally*

$$\wp_{wind} = \dot{m}\frac{\vartheta_1^2}{2} = \rho A\frac{\vartheta_1^3}{2} \tag{15.102}$$

(Note that for the sake of convenience in making estimates, this is a nominal value since we have used the wind velocity rather than the actual air velocity at the disk.) We can define a performance parameter, the power coefficient for the wind turbine, C_{power}, as the ratio of the power developed by the turbine to the power of the wind impinging on it, viz.

$$C_{power} = \frac{\wp}{\frac{\rho A\vartheta_1^3}{2}} \tag{15.103}$$

The maximum possible value for the power coefficient can be determined by substituting equation (15.101) into equation (15.103), viz.

$$\left(C_{power}\right)_{max} = \frac{\frac{8}{27}\rho A\vartheta_1^3}{\frac{1}{2}\rho A\vartheta_1^3} = \frac{16}{27} = 0.593 \tag{15.104}$$

This result is known as the Betz factor in honor of Albert Betz (1885 – 1968), a German physicist who was a colleague of Ludwig Prandtl at Aerodynamische Versuchsanstalt (AVA) in Gottingen. Betz, a pioneer in the development of wind turbines, first derived this factor in 1920. Through the efforts of Betz and his co-workers, Germany established a pre-eminent position in the use of the wind as a renewable energy source, a position it enjoys to this day.

From equation(15.98), it would appear that the power output of the wind turbine could be maximized by making the exit velocity zero, $\vartheta_2 = 0$. However, this would violate the continuity equation. Equation (15.100) is the result of maximizing the power output under the constraint of satisfying the continuity equation. The power coefficient of equation (15.104) then establishes an upper bound on our ability to extract power from the wind. However, in practice with current technology, power coefficients of well-designed wind turbines are somewhat less than the Betz limit and fall in the range $0.40 \le C_{power} \le 0.47$.

Figure 15.12 shows the performance of some modern wind turbines along with the performance of some classical windmills. Wind turbines can be designed with the axis of rotation either horizontal or vertical. The vertical axis wind turbine is insensitive the direction of the wind, but the horizontal axis wind turbine requires a rudder of some sort that turns the axis of rotation of the device parallel to the wind direction. Notice that the performance is optimum at a specific wind speed and falls off as wind speed either increases or decreases. In reality, the wind rarely blows at a steady speed so wind turbines are not really steady flow devices. The unsteady nature of the wind dictates a complex propeller design that greatly increases the cost of the device in order to achieve reasonable performance over a range of wind speeds.

Insert Figure 15.12 here.

Note that due to the viscous nature of air, the wind is a "boundary layer" phenomenon on the surface of the earth. That is, the local wind speed is a function of distance normal to the ground. As a consequence, the axes of rotation of wind turbines with horizontal axes of rotation (the most common in modern wind farms) are placed at some distance from the ground with heights of 100 m not uncommon. This requires a supporting structure that becomes a significant

fraction of the total cost of the device.

Example 15E.6: Throughout the 19th century and well into the first half of the 20th century, rural America relied heavily upon windmills of the type shown in Figure 15E.6 to provide the shaft power required to operate irrigation pumps and a wide variety of other farm machinery. A windmill was an essential piece of equipment on nearly every American farm. A typical 20th century design was a multi-blade design with a disk diameter of about 5 m. From the data of Figure 15.8, estimate the maximum shaft power that could be extracted from a wind of 11 m/sec on a day when the air temperature is 20 C and the air pressure is 1 atm. Also estimate the velocity of the wind downstream of the rotor disk.

Figure 15E.6 Windmill and Water Storage Tank on Farm on High Plains.
Gaines County, New Mexico (Russell Lee, photographer, 1940) Farm Security Administration - Office of War Information Photograph Collection, Library of Congress Prints & Photographs Division Washington, DC 20540

Solution: We first determine the air density ρ. The ideal gas model with R = 297 J/kg K provides an adequate description of the behavior of the air. Then since 1 atm = 1.01325 x 10^5 N/m^2,

$$\rho = \frac{P}{RT} = \frac{1.01325 \text{ x } 10^5 \text{ N/m}^2}{(287 \text{ J/kg K})(20 \text{ C} + 273.15 \text{ K})} = 1.204 \text{ kg/m}^3$$

For this design of windmill, the nominal maximum power of the wind is

$$\wp_{max} = \rho A \frac{v_1^3}{2} = (1.204 \text{ kg/m}^3)\left(\pi \frac{(5 \text{ m})^2}{4}\right)\left(\frac{(11 \text{ m/sec})^3}{2}\right) = 1.574 \text{ x } 10^4 \text{ W}$$

From Figure 15.8, the maximum power coefficient for the American multi-blade windmill design is $(C_{power})_{max}$ = 0.3. Then from the definition of the power coefficient

$$\wp = (C_{power})_{max}(\wp_{max}) = 0.3(1.574 \text{ x } 10^4 \text{ W}) = 4.721 \text{ kW}$$

It is interesting to note that this amount of power would be sufficient to power a modern home.

For purposes of an estimate of the downstream velocity, if we assume reversible, adiabatic operation of the windmill, equation (15.76) gives the power extracted from the wind.

Then

$$\wp = \rho A \vartheta^2 \left(\vartheta_1 - \vartheta_2\right) = \frac{1}{4}\rho A\left(\vartheta_1^2 - \vartheta_2^2\right)\left(\vartheta_1 + \vartheta_2\right)$$

$$4.721 \text{ x } 10^4 \text{ W} = \frac{1}{4}\left(1.204 \text{ kg/m}^3\right)\left(\pi\frac{(5 \text{ m})^2}{4}\right)\left[(11 \text{ m/sec})^2 - \vartheta_2^2\right](11 \text{ m/sec} + \vartheta_2)$$

$$\vartheta_2 = 3.606 \text{ m/sec}$$

It is interesting to note that as the electric power grid expanded in the mid 20th century to include rural America, windmills gradually disappeared from American farms. However, in the 21st century, as energy has become a more precious commodity with energy tax credits encouraging the deployment of renewable energy sources, windmills are once again returning to American farms.

15.2.2 Shaft Work Machines Processing an Incompressible Fluid

If the working fluid of the machine can be modeled as incompressible with a constant specific heat c, the enthalpy can be separated into a thermal energy cT and an uncoupled mechanical property Pv. Then the enthalpy can be written

$$h = cT + Pv \tag{15.105}$$

Then equation (15.11) becomes

$$-\left(\dot{W}_{shaft}\right)_{incompressible} = \dot{m}c\left(T_{out} - T_{in}\right) + \dot{m}v\left(P_{out} - P_{in}\right) \tag{15.106}$$

According to the entropy constitutive relation for the incompressible fluid as presented in Chapter 4, the entropy is related only to its thermal behavior. Then for the limiting case of the reversible adiabatic machine we have

$$s_{out} - s_{in} = c\ln\frac{T_{out}}{T_{in}} = 0 \tag{15.107}$$

Thus the outlet temperature is equal to the inlet temperature, and the shaft work transfer rate is directly related to the pressure difference and the volume flow rate $\dot{m}v$. Thus

$$-\left(\dot{W}_{shaft}\right)_{\substack{reversible\\adiabatic\\incompressible}} = \dot{m}v\left(P_{out} - P_{in}\right) = \frac{\dot{m}}{\rho}\left(P_{out} - P_{in}\right) \tag{15.108}$$

If the adiabatic machine is irreversible, the entropy of the fluid stream increases as it passes through the machine. From equation (15.107), it follows that the outlet temperature is greater than the inlet temperature. Thus, the first term in equation (15.106) is always positive for this class of adiabatic machines. This term represents the decrease in the shaft work transfer rate because of internal irreversibility which in this case is simply mechanical energy dissipation within the working fluid.

The locus of states for the incompressible fluid as it passes through the shaft work machine is shown in Figure 15.13. Again since some of the states in the actual machine are non-equilibrium states, the path cannot be specified for the irreversible (actual) machine. Also note that since the entropy and temperature of the incompressible fluid are directly related [equation (15.107)], the locus of states cannot be presented in terms of the coordinates T and s. For the incompressible fluid, the shaft work efficiencies reduce to a particularly simple form obtained by substituting equations (15.106) and (15.108) into equations (15.22) and (15.24).

$$\left(\eta_+\right)_{incompressible} = 1 - \frac{c\left(T_{out} - T_{in}\right)}{v\left(P_{out} - P_{in}\right)} \tag{15.109}$$

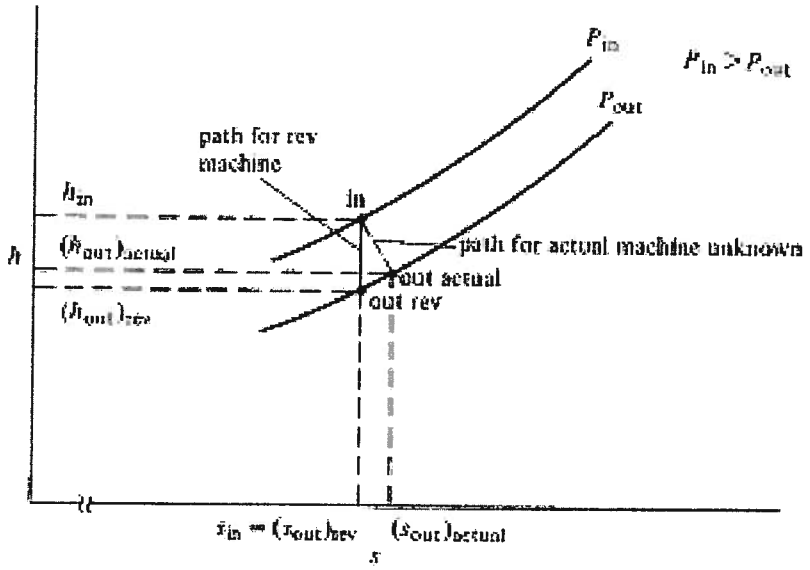

Figure 15.13(a) States of an Incompressible Fluid in a Positive Shaft Work Machine

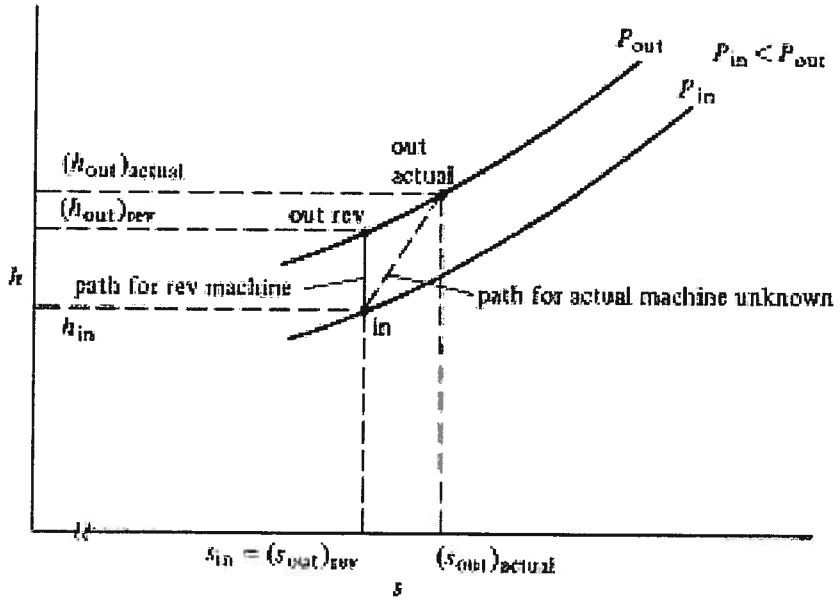

Figure 15.13 (b) States of an Incompressible Fluid in a Negative Shaft Work Machine

and

$$(\eta_{-})_{incompressible} = 1 - \frac{c(T_{out} - T_{in})}{c(T_{out} - T_{in}) + v(P_{out} - P_{in})} \tag{15.110}$$

In both cases, the outlet temperature is greater than the inlet temperature because of the irreversibility. For the positive shaft work machine the inlet pressure is greater than outlet pressure. However, for the negative shaft work machine the inlet pressure is less than the outlet pressure. Thus, in both equations (15.109) and (15.110) the second term on the right side is positive and less than unity and represents approximately the fraction of reversible shaft work transfer lost to irreversibility.

Negative shaft work machines processing an incompressible fluid are one of the most

common the steady flow components. These devices, known as pumps, are found in all sorts of thermal-fluid systems ranging from home heating systems and automobiles on the one hand to gigawatt power plants and petroleum refineries on the other. Because of the widespread application of pumps, thermal-fluid engineers have given special attention to quantifying their performance. Although the efficiency described above is certainly an important performance parameter, there is a collection of other parameters that is important in both designing and selecting these devices for service in larger systems. As shown in Appendix 15A, these parameters are most readily managed in non-dimensional form.

In Appendix 15A, we note that the dimensional analysis cannot give us the specific form of the function F identified by the Buckingham Pi Theorem. For this information we must examine the details of operation of the particular pump of interest. For this purpose, the most reasonable choice of pump is that of a centrifugal pump which, apart from the human heart, is probably the most common of all pump designs. A centrifugal pump consists of an impeller, mounted in bearings, that rotates in a housing shaped like a volute. The impeller is connected to some sort of positive shaft work machine such as an electric motor that drives it. Typically, the fluid to be pumped enters the rotor on the axis of rotation and then has its angular momentum increased by virtue of the rotation of the impeller that is fitted with vanes whose purpose is to guide the motion of the fluid. The fluid exits from the periphery of the circularly shaped rotor. The pressure increases in the direction of flow due to the increase in angular momentum of the fluid within the volute-shaped housing. Figure 15.10 shows an external view of a pump and drive motor assembly.

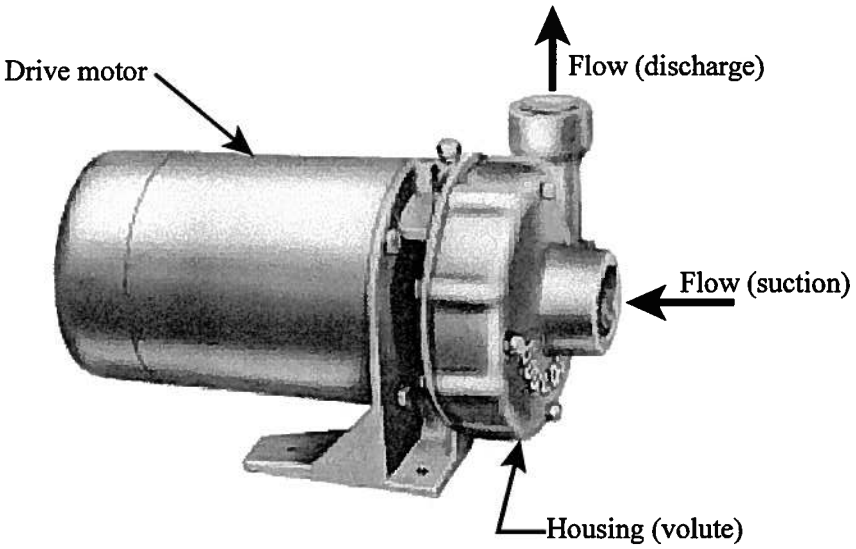

Figure 15.14 External View of Centrifugal Pump and Drive Motor Assembly
(Courtesy of Goulds Pumps)

Figure 15.15 shows a cross-sectional view of an impeller of the closed type that is used in the pump of Figure 15.14. The fluid enters the impeller axially and flows radially outward.

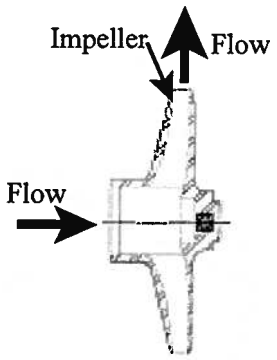

Figure 15.15 Cross-section of Closed Type of Impeller for a Centrifugal Pump

Figure 15.16 shows a view of an open impeller looking down the axis of rotation in the direction of travel of the fluid. The pump rotates in the clockwise direction in this view. This impeller is from a circulating pump used in a home heating system. Note the shape of the vanes.

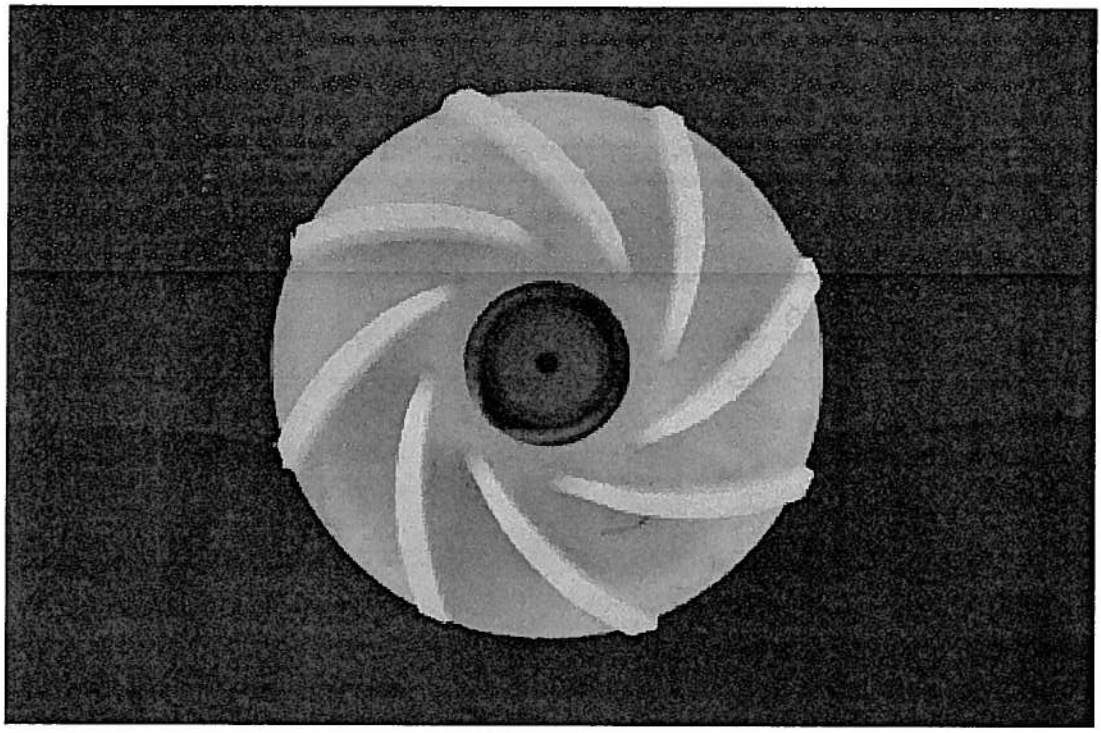

Figure 15.16 Open Impeller from Centrifugal Pump
(Photograph courtesy of Dr. Ruth Tuomala)

Figure 15.17 shows a schematic view of an impeller similar to that of Figure 15.16. Of particular interest is the velocity of the fluid as it exits the impeller. The velocity of the fluid relative to the surface of the blade is denoted by the symbol ϑ_{b2} while the velocity imparted to the fluid by the tangential velocity of the tip of the blade is $R_2\omega$ where ω is the rotational speed of the impeller. The vector sum of the velocity components ϑ_{b2} and R_2N gives the absolute velocity ϑ_A of the fluid particle relative to the stationary housing of the pump. The components of this velocity in the radial and tangential directions are ϑ_{r2} and ϑ_{t2}, respectively. There is a similar set of velocities at the entrance to the impeller.

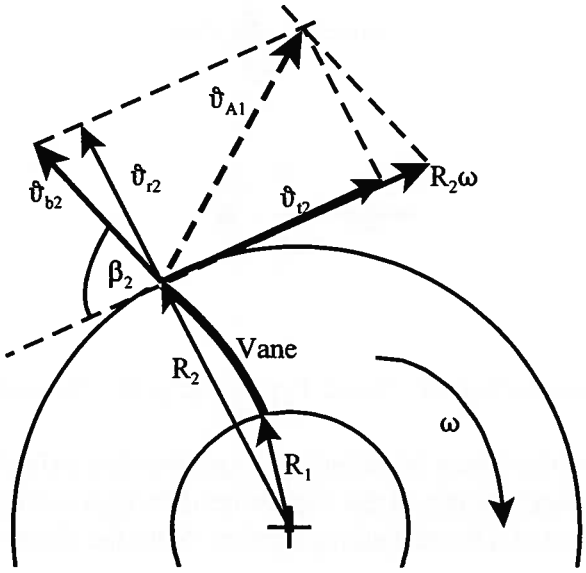

Figure 15.13 Velocity Components of a Fluid Particle at Exit from the Impeller of a Centrifugal Pump

The *Euler turbomachine equation*, equation (8.107), gives the torque that must be exerted on the impeller by the drive motor for the reversible operation of the pump.

$$T_{shaft} = \dot{m}\left(R_2\vartheta_{t2} - R_1\vartheta_{t1}\right) \tag{15.111}$$

Then the shaft power for reversible operation is given by

$$\left(\dot{W}_{shaft}\right)_{rev} = T_{shaft}N = \dot{m}\omega\left(R_2\vartheta_{t2} - R_1\vartheta_{t1}\right) \tag{15.112}$$

The pump head, h_{pump}, is by definition the reversible shaft power per unit mass flow rate. Then from equation (15.112)

$$h_{pump} = \frac{\left(\dot{W}_{shaft}\right)_{rev}}{\dot{m}} = \left(R_2\omega\vartheta_{t2} - R_1\omega\vartheta_{t1}\right) \tag{15.113}$$

In most centrifugal pump designs, there is no attempt to induce a tangential velocity component at the pump inlet. Then $\vartheta_{t1} = 0$ and equation (15.113) reduces to

$$h_{pump} = R_2\omega\vartheta_{t2} = R_2^2\omega^2 - R_2\omega\vartheta_{r2}\cot\beta_2 \tag{15.114}$$

which shows the significance of the vane exit angle in determining pump performance. Since

$$\dot{V} = \vartheta_{r2}\pi D_2 b_2 \tag{15.115}$$

where b_2 is the height of the vane at the outer periphery of the impeller, we can write equation (15.115) in the form

$$h_{pump} = \frac{\omega^2 D_2^2}{4} - \frac{\omega\dot{V}}{2\pi b_2}\cot\beta_2 \tag{15.116}$$

If we divide equation (15.116) through by $\omega^2 {D_2}^2$, we get

$$\frac{h_{pump}}{\omega^2 {D_2}^2} = \frac{1}{4} - \frac{\dot{V}D_2}{\omega D_2^3 2\pi b_2}\cot\beta_2$$

$$\Pi_{head} = \frac{1}{4} - \Pi_{flow}\frac{D_2}{2\pi b_2}\cot\beta_2 \tag{15.117}$$

In a similar manner, we could have started with equation (15.112). Then if $\vartheta_{t1} = 0$ and we make use of equation (15.115), equation (15.112) becomes

$$\left(\dot{W}_{shaft}\right)_{rev} = \dot{m}\omega\left(R_2\vartheta_{t2} - \cancel{R_1\vartheta_{t1}}\right) = \rho\dot{V}\omega\left(R_2\vartheta_{t2} - \cancel{R_1\vartheta_{t1}}\right)$$

$$\left(\dot{W}_{shaft}\right)_{rev} = \rho\dot{V}R_2^2\omega^2 - \rho\dot{V}R_2\omega\vartheta_{r2}\cot\beta_2 = \frac{\rho\dot{V}D_2^2\omega^2}{4} - \frac{\rho\dot{V}^2D_2\omega}{2\pi D_2 b_2}\cot\beta_2 \qquad (15.118)$$

If we divide equation (15.118) through by $\rho\omega^3 D_2^5$, we get

$$\frac{\left(\dot{W}_{shaft}\right)_{rev}}{\rho\omega^3 D_2^5} = \frac{\rho\dot{V}D_2^2\omega^2}{4\rho\omega^3 D_2^5} - \frac{\rho\dot{V}^2D_2\omega}{\rho\omega^3 D_2^5 2\pi D_2 b_2}\cot\beta_2 = \frac{\dot{V}}{4\omega D_2^3} - \frac{\dot{V}^2 D_2}{\omega^2 D_2^6 2\pi b_2}\cot\beta_2$$

$$\Pi_{power} = \frac{1}{4}\Pi_{flow} - \left(\Pi_{flow}\right)^2\left(\frac{D_2}{2\pi b_2}\right)\cot\beta_2 \qquad (15.119)$$

Equations (15.117) and (15.119) establish the functional relationships amongst the dimensionless parameters guaranteed by the Buckingham Pi Theorem. These relationships are shown schematically in graphical form in Figure 15.18 for a pump of a given diameter operating at fixed value of Reynolds number with a given fluid. It is worth noting that equations (15.117) and (15.119) apply to any negative shaft work machine processing an incompressible working fluid, be it a fan or a pump, provided the inlet is along the axis of rotation and the flow path is radially outward from the axis of rotation. Pumps that process a liquid always use vanes with $\beta_2 \leq \pi/2$ since the operating point becomes unstable otherwise. Vanes with $\beta_2 < \pi/2$ are said to be *backward curved* while vanes with $\beta_2 = \pi/2$ are said to be *radial.*

Fans, on the other hand, process gases that tend to have more stable operating points due to their lower values of viscosity. As a result, fan rotors (impellers) frequently have *forward curved* vanes with $\beta_2 > \pi/2$, especially in the smaller sizes.

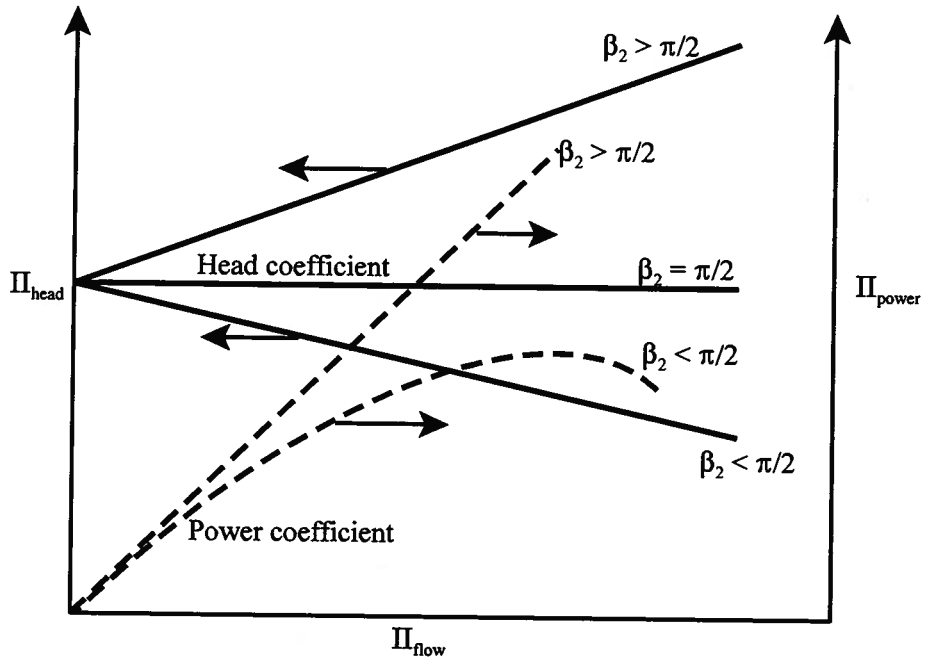

Figure 15.18 Dimensionless Performance Characteristics for a Negative Shaft Work Machine

While the head coefficient and the power coefficient of the pump are determined by the vane outlet angle β_2, the vane inlet angle β_1 determines the flow coefficient. The flow coefficient in turn determines the efficiency of the pump. For the case of a pump with pure axial flow at the inlet, there is no tangential component to the absolute velocity as shown in Figure 15.19. Then

$$\tan\beta_1 = \frac{\vartheta_{A1}}{R_1\omega} = \frac{\dot{V}}{\pi D_1 b_1}\frac{2}{D_1\omega} = \frac{\dot{V}}{\omega D_1^3}\left(\frac{2D_1}{\pi b_1}\right) \tag{15.120}$$

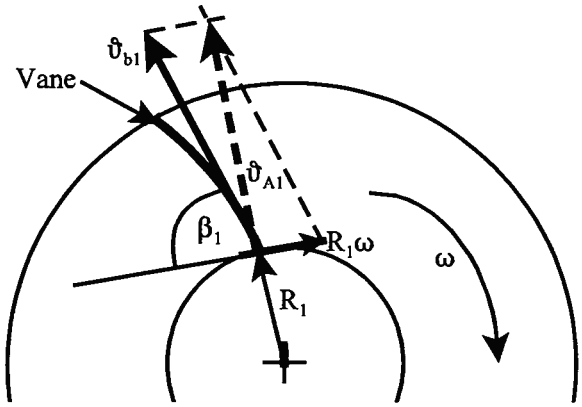

Figure 15.19 Velocity Components of a Fluid Particle at Entrance to the Impeller of a Centrifugal Pump

and it follows that the inlet vane angle is determined by $\dot{V}$, ω, D_1, and b_1. Then a pump of fixed dimensions D_1, b_1, and β_1 operating at a given rotational speed ω, will have a single volumetric flow rate $\dot{V}$ at which the operation will be optimal. This would be the point of maximum efficiency for the pump. At any other flow rate, the efficiency of this pump at this speed would be reduced. Figure 15.20 shows schematically this dependence of efficiency on flow rate for a given pump operating at a given rotational speed.

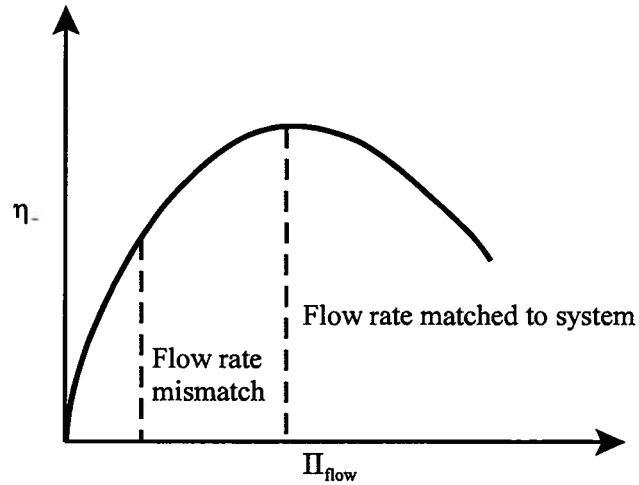

Figure 15.20 Optimal Operating Condition for Centrifugal Pump in Piping System

The optimal operating point for the pump can be characterized by another dimensionless parameter derived from the dimensionless parameters already formulated by eliminating the

pump geometry from the characterization. If we form the ratio of the square root of the flow coefficient to the one-fourth root of the head coefficient, we will have a new dimensionless parameter known as the *specific speed* of the pump, viz.

$$\omega_s = \frac{\left(\Pi_{flow}\right)^{1/2}}{\left(\Pi_{head}\right)^{3/4}} = \frac{\left(\dfrac{\dot{V}}{\omega D^3}\right)^{1/2}}{\left(\dfrac{h_{pump}}{\omega^2 D^2}\right)^{3/4}} = \frac{\omega \dot{V}^{1/2}}{\left(h_{pump}\right)^{3/4}} \tag{15.121}$$

When a particular pump is operated at the precise conditions for which its internal geometry is designed, the values of the parameters ω, h_{pump}, and $\dot{V}$ are uniquely defined and the efficiency is at its maximum value, η_{max}. The resulting value for the specific speed is the value usually reported by the manufacturer. The value of the specific speed characterizes the design of the device. Pumps with low values of specific speed are typically radial flow designs with high values for the pump head and low values for the volumetric flow rate. Pumps with high values of specific speed are typically axial flow designs with low values for the pump head and high values for the volumetric flow rate. A pump can be operated at a value of specific speed that is not the value specified by the manufacturer, but in that case, the efficiency will not be its maximum value. These results apply to fans as well as pumps.

There is another important issue that needs to be addressed in these pump/piping systems, namely the phenomena of cavitation. If the static pressure anywhere in the system falls below the vapor pressure of the flowing liquid at the prevailing temperature, the liquid will vaporize and form bubbles of vapor dispersed in the liquid. Over time, these vapor bubbles are capable of doing considerable damage to pumps, primarily in the form of erosion of pump surfaces exposed to two-phase flow. The process of erosion is caused by spalling of the pump surface due to alternating positive and negative Hertz contact stresses imposed by collapsing bubbles. Small particles of the pump material at the liquid interface literally jump off the surface as the surface experiences highly localized tensile forces. If the process is allowed to continue unchecked, pump performance degrades rapidly. The formation and collapse of vapor bubbles is usually accompanied by noise that becomes the "death rattle" of the pump.

Cavitation usually occurs within the pump, typically in the suction connection. Cavitation can be avoided by insuring that the there is available a *net positive suction head*, $NPSH_A$, at the pump inlet, viz.

$$NPSH_A = \frac{\left(P_0 - P_{sat}\right)}{\rho g} \tag{15.122}$$

where P_0 is the static pressure within the fluid at the pump inlet flange, P_{sat} is the saturation pressure of the fluid at the prevailing temperature, and ρ is the liquid density. Because of the nature of the internal flow geometry of the pump, there is usually a pressure drop within the pump so that at some internal location, the local static pressure is less than P_0. This minimum pressure establishes the *required net positive suction head*, $NPSH_R$. For a given pump design, the manufacturer measures the value of $NPSH_R$ and it then becomes incumbent upon the thermal-fluids engineer to ensure that for the piping system under consideration, the value of $NPSH_A$ exceeds the value of $NPSH_R$.

The value of $NPSH_A$ is just one of the parameters that the thermal-fluids engineer must determine in the application of a pump to a piping system design. The pump head and the volumetric flow rate are two parameters that are usually set by the piping system. The likelihood

that a pump will be found that exactly matches these requirements at maximum efficiency is small. However, the thermal-fluids engineer does have the option of introducing a throttle valve (to be discussed later in this chapter) into the system to match pump head and total head loss, as well as using a motor controller that allows the adjustment of the rotational speed of the pump. By means of these two control variables, the thermal-fluids engineer can find an appropriate pump to meet the requirements.

15.2.3 Shaft Work Machines Processing a Pure Substance

The locus of states of the pure substance as it passes through various shaft work machines is shown in Figures 15.21 and 15.22 on *h-s* and *T-s* coordinates. Note that one effect of the irreversibility present in the actual machine is to increase the amount of vapor resulting from the expansion process to a two-phase state in a positive shaft work machine. If the outlet state is a single-phase superheated vapor state, the irreversibilities increase the degree of superheat. Similarly, the vapor at the outlet of a negative shaft work machine is also superheated as a result of the irreversibilities present during the compression process. For both negative and positive shaft work machines operating in the subcooled liquid region, the irreversibility of the process reduces the degree of subcooling.

The example of a shaft work machine processing a pure substance that is of greatest interest in this context is an axial flow steam turbine. However, the internal construction of such a machine consists of two components: (1) a stator in the form of a nozzle and (2) a rotor with radially extending blades similar in form to those of the axial flow compressor discussed previously. The role of the nozzle is to accelerate a fluid stream to high velocity which is then deflected by the blades in such a manner as to produce a change in momentum of the fluid stream that results in a force on the blade. Since the blade is mounted on a disk that is free to rotate about a central axis, the force on the blade produces a torque about the axis of rotation. As a consequence, the internal details of the performance of the steam turbine are inextricably linked to the performance of the nozzle. Thus, our discussion of the internal details of the steam turbine must be delayed until we have developed the means to analyze the performance of the nozzle. (See Appendix 15B.) At this juncture, we content ourselves with an example of the control volume analysis of the steam turbine.

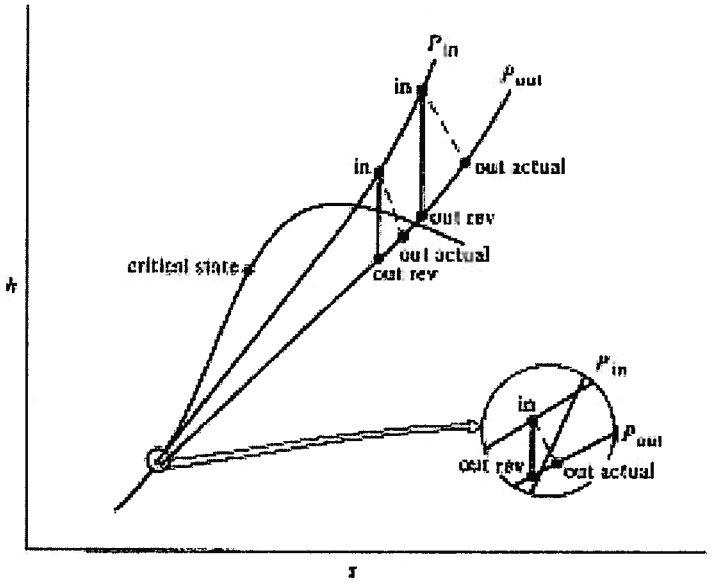

Figure 15.21(a) States of a Pure Substance in a Positive Shaft Work Machine

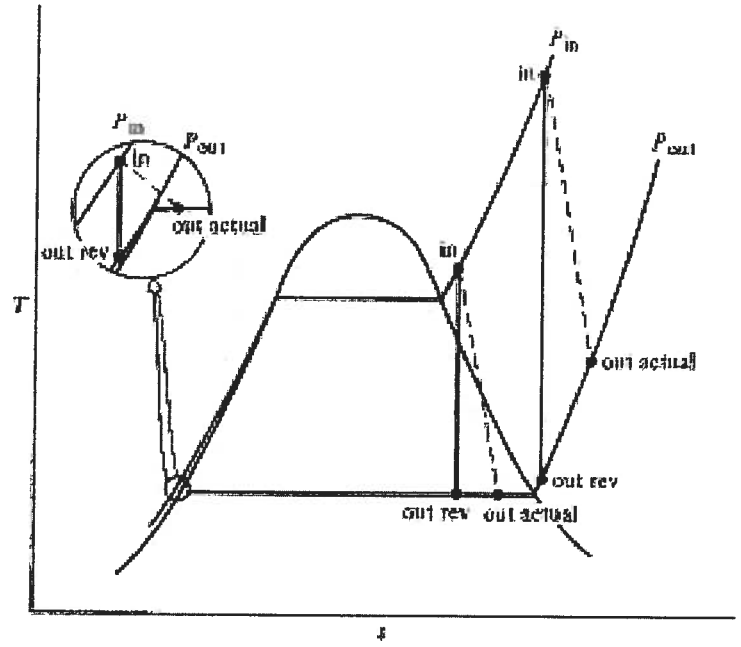

Figure 15.21(b) States of a Pure Substance in a Positive Shaft Work Machine

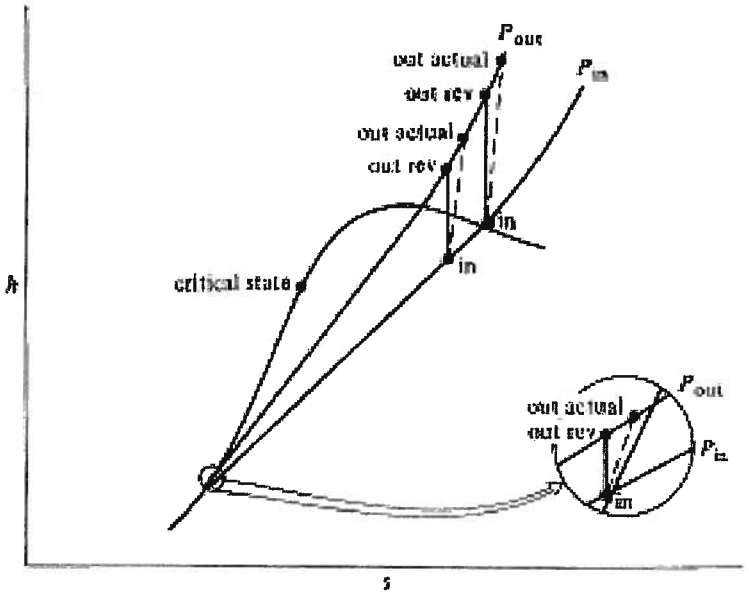

Figure 15.22(a) States of a Pure Substance in a Negative Shaft Work Machine

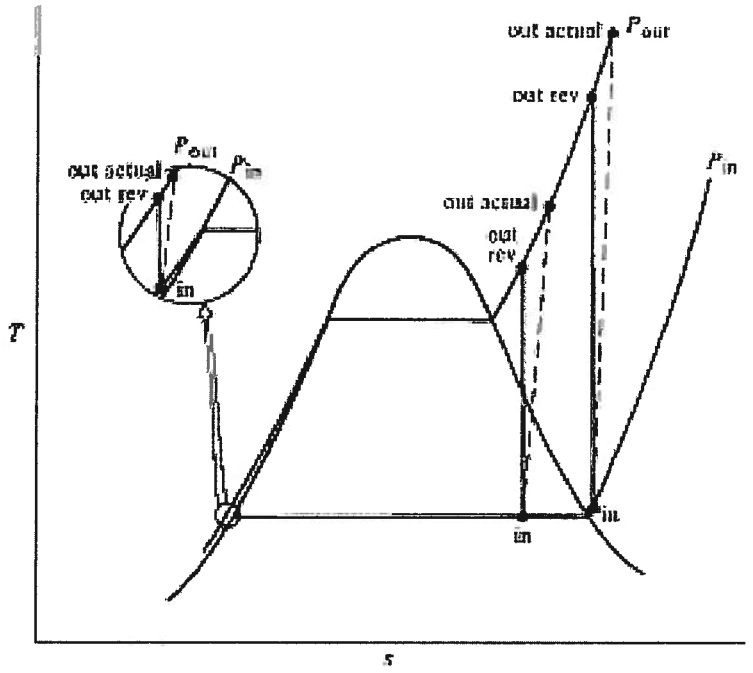

Figure 15.22(b) States of a Pure Substance in a Negative Shaft Work Machine

Example 15E.7: A four-stage steam turbine is to provide 1 MW to drive a boiler feed pump. The steam conditions at the turbine inlet are $P_1 = 3.0 \times 10^6$ N/m^2 and $T_1 = 260$ C. The turbine exhaust pressure is $P_2 = 2 \times 105$ N/m^2. The turbine efficiency is $\eta_+ = 0.85$.

(a) What mass flow rate of steam is required to achieve the necessary power?

(b) What is the quality of the exit steam?

(c) What is the rate of entropy generation in the turbine?

Solution: (a) The control volume selected for analysis of the turbine is shown in Figure 15E.7.

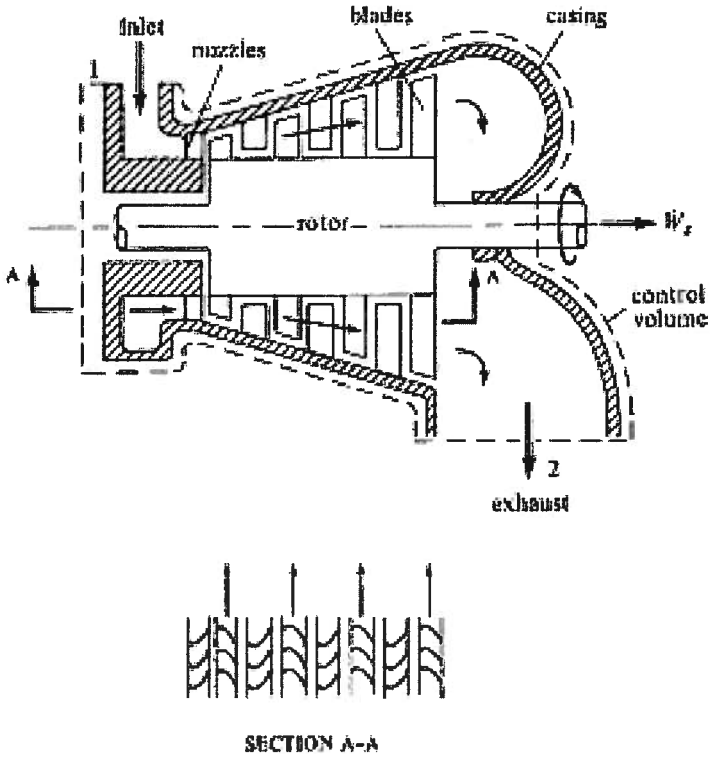

Figure 15E.7 Four-Stage Steam Turbine

The inlet state is a superheated vapor state with the following properties:

$$P_1 = 3 \text{ x } 10^6 \text{ N/m}^2,\ T_1 = 260 \text{ C},\ h_1 = 2886.4 \text{ kJ/kg},\ s_1 = 6.3459 \text{ kJ/kg K}$$

We first consider a reversible adiabatic turbine with the same state 1 and the same exhaust pressure . Two independent properties are required to specify the state at the exit of such a turbine. For this case the relevant properties are the exit pressure and the exit entropy, viz.

$$P_{2r} = P_2 = 2 \text{ x } 10^5 \text{ N/m}^2,\ s_{2r} = s_1 = 6.3459 \text{ kJ/kg K}$$

Since $s_f < s_{2r} < s_g$ at $P_2 = 2 \text{ x } 10^5$ N/m^2, state 2r is a two-phase state. Then the exit quality for the reversible adiabatic turbine is given by

$$x_{2r} = \frac{s_{2r} - s_f}{s_{fg}} = \frac{6.3459 \text{ kJ/kg K} - 1.5302 \text{ kJ/kg K}}{5.5967 \text{ kJ/kg K}} = 0.8604$$

Then the enthalpy at exit from the reversible adiabatic turbine is

$$h_{2r} = h_f + x_{2r} h_{fg} = 504.70 + (0.8605)(2201.5 \text{ kJ/kg}) = 2399.0 \text{ kJ/kg}$$

Then from equation (15.11) in which changes in kinetic and potential energies are neglected

$$\left(\frac{\dot{W}_{shaft}}{\dot{m}}\right)_{reversible} = h_1 - h_{2r}$$

$$\left(\frac{\dot{W}_{shaft}}{\dot{m}}\right)_{reversible} = 2886.4 \text{ kJ/kg} - 2399.0 \text{ kJ/kg} = 487.41 \text{ kJ/kg}$$

From the definition of turbine efficiency, equation (15.22), we have

$$\left(\frac{\dot{W}_{shaft}}{\dot{m}}\right)_{actual} = \eta_+ \left(\frac{\dot{W}_{shaft}}{\dot{m}}\right)_{reversible} = 0.85(487.41 \text{ kJ/kg}) = 414.30 \text{ kJ/kg}$$

The mass flow rate for a power output of 1 MW is

$$\dot{m} = \frac{\left(\dot{W}_{shaft}\right)_{actual}}{\left(\frac{\dot{W}_{shaft}}{\dot{m}}\right)_{actual}} = \frac{1000 \text{ kW}}{414.30 \text{ kJ/kg}} = 2.414 \text{ kg/sec}$$

(b) The quality of the steam at the turbine exit, state 2, is calculated from the enthalpy, h_2. From equation (15.11), we have

$$h_2 = h_1 - \left(\frac{\dot{W}_{shaft}}{\dot{m}}\right)_{actual}$$

$$h_2 = 2886.4 \text{ kJ/kg} - 414.30 \text{ kJ/kg} = 2472.1 \text{ kJ/kg}$$

$$x_2 = \frac{h_2 - h_f}{h_{fg}} = \frac{2472.1 \text{ kJ/kg} - 504.70 \text{ kJ/kg}}{2201.5 \text{ kJ/kg}} = 0.8936$$

(c) To calculate the entropy generated in the turbine we need the entropy at state 2.

$$s_2 = s_f + x_2 s_{fg} = 1.5302 \text{ kJ/kg} + (0.8937)(5.5967 \text{ kJ/kg}) = 6.5318 \text{ kJ/kg K}$$

Then the rate of entropy generation is

$$\dot{S}_{gen} = \dot{m}(s_2 - s_1) = (2.414 \text{ kJ/kg})(6.5318 \text{ kJ/kg K} - 6.3459 \text{ kJ/kg K}) = 0.4488 \text{ kW/K}$$

15.3 Nozzles

The operation of many engineering systems requires a fluid stream of high kinetic energy. For example, as we saw in Section 15.2, power output of a turbine is due to internal forces produced by the deflection of high velocity fluid streams. These high velocities can be achieved by accelerating the fluid stream in a device called a nozzle. A typical nozzle with a single inlet and a single outlet is shown in Figure 15.23. The fluid enters the nozzle with a low velocity at a specified temperature and pressure, and leaves the nozzle with a high velocity at a lower pressure. The pressure difference imposed across the nozzle accelerates the fluid. The mass flow rate is related to the nozzle cross sectional area by the continuity equation. The distribution of fluid velocity and state along the length of the nozzle is determined by its shape.

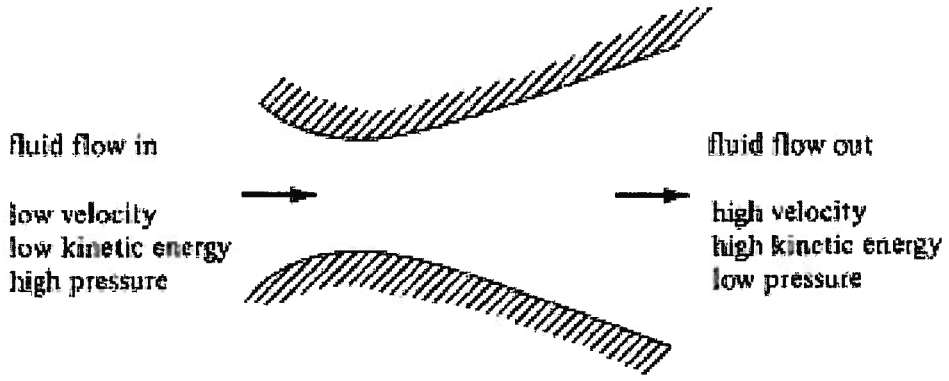

Figure 15.23 Nozzle with Converging-diverging Flow Area

The fluid velocity in the nozzle is high so the fluid does not attain thermal equilibrium with the nozzle walls. In addition, the surface area of contact between the fluid and the nozzle walls is relatively small. As a result, the heat transfer experienced by the fluid is negligibly small relative to the change in kinetic energy of the fluid stream, and the flow through the nozzle can be modeled as adiabatic. Also, the size of a typical nozzle is such that regardless of its orientation, the changes in the gravitational potential energy are negligible.

Since the flow through the nozzle is steady and adiabatic, and there is no shaft work transfer for a control surface coincident with the nozzle walls, the first law of thermodynamics, equation (15.3), applied to a control volume bounded by the inlet port and the outlet port becomes

$$\dot{m}\left(\frac{\vartheta_{out}^2}{2}-\frac{\vartheta_{in}^2}{2}\right)=\dot{m}\left(h_{in}-h_{out}\right) \tag{15.123}$$

For the nozzle in which unit mass flow rate experiences an infinitesimal change of state, the first law of thermodynamics, equation (15.4), becomes

$$\vartheta d\vartheta=-dh \tag{15.124}$$

Although equation (15.123) describes the performance of most nozzles in steady flow operation, one must always be certain that in a given situation all of the underlying assumptions of its derivation are satisfied.

Physically, equation (15.123) requires that the increase in the kinetic energy of the fluid stream is produced at the expense of the enthalpy of the fluid. From the definition of enthalpy, equation (15.123) can also be written

$$\frac{\vartheta_{out}^2}{2}-\frac{\vartheta_{in}^2}{2}=\left(u_{in}-u_{out}\right)+\left(P_{in}v_{in}-P_{out}v_{out}\right) \tag{15.125}$$

or for a control volume of infinitesimal extent in the direction of flow

$$\vartheta d\vartheta=-du-d\left(Pv\right) \tag{15.126}$$

From equations (15.125) and (15.126) it is apparent that any increase in the kinetic energy of the fluid may be the result of a decrease in the internal energy of the fluid and/or the net flow work.

As in the case of the shaft work machine, the evaluation of the performance of a nozzle is especially simple in the limiting case of reversible adiabatic operation. Since in this case the entropy of the fluid remains constant as it passes through the machine, it is necessary to specify only the inlet state and the outlet pressure in order to fix the states throughout the nozzle. The inlet state is normally specified by the pressure, temperature, and velocity. The pressure and the entropy (which is the same as the inlet entropy) then completely determine the exit state.

Consider, for example, the nozzle described by equation (15.126). For the reversible adiabatic case, the entropy is constant and the enthalpy is related to the pressure and volume by equation (15.13). Thus, equation (15.124) becomes

$$\left(\vartheta d\vartheta\right)_{\substack{reversible\\adiabatic}}=-vdP \tag{15.127}$$

Integrating equation (15.127), we obtain

$$\dot{m}\left(\frac{\vartheta_{out}^2}{2}-\frac{\vartheta_{in}^2}{2}\right)_{\substack{reversible\\adiabatic}}=-\dot{m}\left[\int_{P_{in}}^{P_{out}}vdP\right]_{s_{in}=s_{out}} \tag{15.128}$$

where the integral on the right side is evaluated along the path of constant entropy. For a nozzle, the value of the integral is clearly less than zero. The physical interpretation of equations (15.127) and (15.128) is that the change in the kinetic energy of each fluid particle at each point as it passes through the nozzle is produced only by the net normal forces due to pressure acting on the particle at that point. In addition, the local change in kinetic energy is proportional to the local specific volume of the fluid. This implies that for reversible fluid acceleration, the fluid shear stress must be zero everywhere throughout the fluid. The requirement of zero shear stress for reversible flow can be further verified by deriving equation (15.128) by integrating the momentum equation (with no shear stress) along the stream from inlet to outlet. As a result, the irreversible nozzle produces a smaller increase in kinetic energy of the fluid than the reversible nozzle with the same inlet state and outlet pressure.

This result may be shown from Figure 15.24 and equations (15.18) and (15.123). In Figure 15.24, $(s_{out})_{actual}$ is greater than $(s_{out})_{rev}$ and $(\partial h/\partial s)_P > 0$ by equation (15.18). Since the decrease in h is smaller in the actual nozzle, the increase in kinetic energy is smaller than in the reversible nozzle.

$$\left(h_{in}-h_{out}\right)_{actual}=\left(h_{in}-h_{out}\right)_{reversible}-\left[\int_{s_{in}}^{s_{out}}\left(\frac{\partial h}{\partial s}\right)_P ds\right]_{P=P_{out}} \tag{15.129}$$

$$\left(\frac{\vartheta_{out}^2}{2}-\frac{\vartheta_{in}^2}{2}\right)_{actual}=\left(\frac{\vartheta_{out}^2}{2}-\frac{\vartheta_{in}^2}{2}\right)_{reversible}-\left[\int_{s_{in}}^{s_{out}}Tds\right]_{P=P_{out}} \tag{15.130}$$

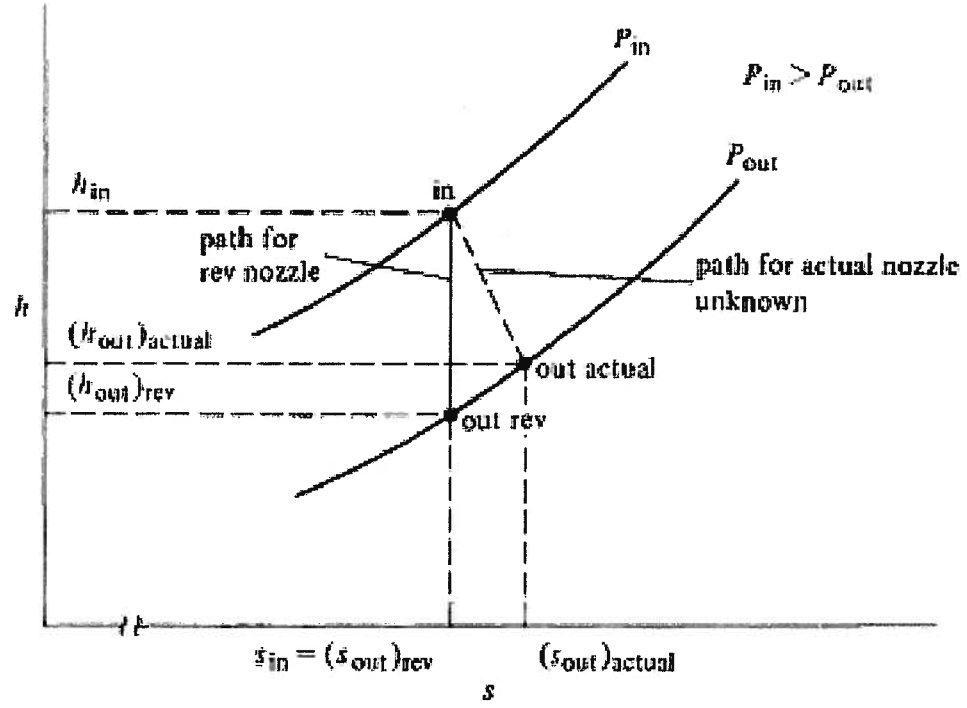

Figure 15.24 States of an Ideal Gas Flowing through a Nozzle

The origin of the irreversibility is the shear stress in the fluid due to the fluid viscosity and the relative velocity between the fluid and the wall. In a nozzle with smooth, gradual contours, the effects of the fluid shear stresses are usually confined to these thin boundary layers near the walls. (The flow of a veryviscous fluid is of course an exception. In that case, the boundary layer may extend across the entire flow area depending upon the magnitude of the viscosity.) As a consequence, the major part of the stream outside the thin boundary layer is accelerated reversibly and the flow can be treated as though it were inviscid.

We can define a nozzle efficiency that will provide us with an indication of the magnitude of the irreversibility of an irreversible (actual) nozzle. This efficiency is simply the ratio of the actual increase in kinetic energy of the fluid to the increase in kinetic energy that would have resulted from reversible, adiabatic operation between the same inlet state and the same outlet pressure. Thus,

$$\eta_N = \frac{\left(\frac{\vartheta_{out}^2}{2} - \frac{\vartheta_{in}^2}{2}\right)_{actual}}{\left(\frac{\vartheta_{out}^2}{2} - \frac{\vartheta_{in}^2}{2}\right)_{reversible}} \tag{15.131}$$

15.3.1 Nozzles Accelerating an Ideal Gas

If the fluid being accelerated can be modeled as an ideal gas with constant specific heats, equation (15.123) can be written

$$\dot{m}\left(\frac{\vartheta_{out}^2}{2} - \frac{\vartheta_{in}^2}{2}\right)_{\substack{ideal \\ gas}} = -\dot{m}c_P\left(T_{out} - T_{in}\right) \tag{15.132}$$

By making use of the relation between the specific heats and the gas constant, $c_P - c_v = R$, and the

ideal gas constitutive relation, we can write equation (15.132) in the form

$$\dot{m}\left(\frac{\vartheta_{out}^2}{2}-\frac{\vartheta_{in}^2}{2}\right)_{\substack{ideal\\gas}} = -\dot{m}\frac{\gamma}{\gamma-1}\left(P_{out}v_{out}-P_{in}v_{in}\right) \tag{15.133}$$

Equation (15.133) shows that for an ideal gas with constant specific heats, the increase in kinetic energy of the fluid stream depends upon the nature of the expansion process (the manner in which v_{out} depends upon P_{out}) and upon how strongly the fluid is coupled in the thermodynamic sense as determined by the value of γ.

For example, if the acceleration of the fluid through the nozzle is reversible as well as adiabatic, the path of the states for the ideal gas as it passes through the reversible nozzle is given by Pv^{γ} = constant. Then equation (15.133) becomes

$$\dot{m}\left(\frac{\vartheta_{out}^2}{2}-\frac{\vartheta_{in}^2}{2}\right)_{\substack{ideal\\gas}} = -\dot{m}\frac{\gamma}{\gamma-1}P_{in}v_{in}\left[\left(\frac{P_{out}}{P_{in}}\right)^{(\gamma-1)/\gamma}-1\right] \tag{15.134}$$

Thus for a particular ideal gas, the increase in kinetic energy in a reversible, adiabatic nozzle is uniquely determined by the inlet state and the outlet pressure. Note that by means of the ideal gas constitutive relation, we can write equation (15.134) in the form

$$\dot{m}\left(\frac{\vartheta_{out}^2}{2}-\frac{\vartheta_{in}^2}{2}\right)_{\substack{ideal\\gas}} = -\dot{m}\frac{\gamma}{\gamma-1}RT_{in}\left[\left(\frac{P_{out}}{P_{in}}\right)^{(\gamma-1)/\gamma}-1\right] \tag{15.135}$$

Thus for a fixed inlet temperature and pressure and a fixed outlet pressure, the ideal gas with the largest value of γ and R will provide the largest increase in kinetic energy. From Chapter 4 it is clear that a monatomic gas with a low molecular weight provides the desired combination. It is for this reason that helium is often used as the working fluid in a high velocity wind tunnel. (Actually hydrogen would be a better choice because of its extremely low molecular weight; however, helium is inert and therefore much safer to work with than the potentially explosive hydrogen.)

If the nozzle operates in a adiabatic but irreversible manner, the increase in kinetic energy of the ideal gas will be less than in the reversible case as shown in equation (15.130). For the ideal gas, the nozzle efficiency, equation (15.131) becomes

$$\left(\eta_N\right)_{\substack{ideal\\gas}} = \frac{\left(T_{out}-T_{in}\right)_{actual}}{\left(T_{out}-T_{in}\right)_{reversible}} \tag{15.136}$$

when combined with equation (15.132). Clearly the outlet temperature for reversible operation is lower than the outlet temperature for irreversible operation. Since $T_{out} < T_{in}$ regardless of whether the process is reversible or irreversible, $\eta_N < 1$. The locus of states of the ideal gas as it passes through the nozzle is shown in Figure 15.24 in terms of the enthalpy and entropy. Because of the relationship between temperature and enthalpy in the ideal gas, the locus of states shown in Figure 15.24 would have exactly the same appearance in terms of temperature and entropy. Geometrically the nozzle efficiency of equation (15.136) represents the ratio of the vertical distances between the inlet and outlet states for reversible and irreversible operation as shown in Figure 15.24.

The flow of an ideal gas through a nozzle is actually the basis of rocket propulsion. Modern rocket engines such as those used on the Space Shuttle are essentially a combustion

chamber used to produce a high temperature, high pressure gas that can be modeled to a first approximation as an ideal gas. This gas is discharged to space through a nozzle that provides the thrust necessary to propel the spacecraft through space. As we have already seen in Section 15.2, nozzles form an integral part of turbines used to provide shaft power. In gas turbine engines, the working fluid can be modeled as an ideal gas to a first approximation so that the flow of an ideal gas through a nozzle is an important aspect of the performance of gas turbine engines. For these reasons alone, it is worth investigating further the details of the performance of nozzles flowing an ideal gas. The following discussion is largely patterned after that presented by Ascher H. Shapiro (1916 – 2004) in his pioneering work *The Dynamics and Thermodynamics of Compressible Fluid Flow*, Vol. 1, John Wiley & Sons, 1953.

We now model the flow as one-dimensional such that the properties of the flow are uniform over any cross-section of the flow but change in the direction of the flow. Specifically, we are interested in analyzing the way an ideal gas behaves as it flows through a conduit, a nozzle, whose cross-sectional area changes in the direction of flow. The only conservation equation that explicitly contains the area is the continuity equation so this is the logical place to begin the analysis. For steady flow, the continuity equation can be written

$$\rho A \vartheta = \text{ constant} \tag{15.137}$$

Taking the logarithm of equation (15.137), we get

$$\ln \rho + \ln A + \ln \vartheta = \text{ constant} \tag{15.138}$$

Differentiating equation (15.138), we get

$$\frac{d\rho}{\rho} + \frac{dA}{A} + \frac{d\vartheta}{\vartheta} = 0 \tag{15.139}$$

As we saw in Section 15.3.1, the flow outside the boundary layer can be modeled as though it were inviscid. For one-dimensional, inviscid flow, the Euler equation (equation of linear momentum) reduces to

$$\vartheta \frac{d\vartheta}{dx} = -\frac{1}{\rho}\frac{dP}{dx} \tag{15.140}$$

which can be rewritten in the form

$$\vartheta d\vartheta = -\frac{dP}{\rho} = -\frac{dP}{d\rho}\frac{d\rho}{\rho} = -a^2\frac{d\rho}{\rho} \tag{15.141}$$

where for adiabatic flow without viscosity, the entropy is constant. Then by definition, the speed of sound, a, is

$$\frac{dP}{d\rho} = \left(\frac{dP}{d\rho}\right)_s = a^2 \tag{15.142}$$

Introducing the already familiar Mach number, M, which is defined as the ratio of the local fluid velocity to the velocity of sound

$$M \equiv \frac{\vartheta}{a} \tag{15.143}$$

equation (15.141) becomes

$$\frac{d\rho}{\rho} = -M^2\frac{d\vartheta}{\vartheta} \tag{15.144}$$

Substituting equation (15.144) into equation (15.139), we get

$$\frac{d\vartheta}{\vartheta} = -\frac{1}{1-M^2}\frac{dA}{A} \tag{15.145}$$

Equation (15.145) contains the essence of the influence of the compressibility of the fluid on the nature of the flow. In equation (15.145), we note that there are four possibilities:

1. $\boldsymbol{M = 0}$: For this case a decrease in area gives a proportional increase in velocity and the fluid behaves as though it were incompressible.

2. $\boldsymbol{0 < M < 1}$: For this case the flow is subsonic and the behavior of the velocity is relatively the same as the incompressible fluid case except that as M increases above $M = 0.3$, compressibility effects become important and velocity increases disproportionately as area decreases since $(1-M)$ is in the denominator of equation (15.145).

3. $\boldsymbol{M > 1}$: For this case the flow is supersonic and the continuity equation requires dA to be **positive** for $d\vartheta$ to be **positive** as it is in the case of the accelerating flow of the nozzle. This is a consequence of the fact that the density decreases faster than velocity increases and the flow is "driven" by continuity.

4. $\boldsymbol{M = 1}$: For this case the flow is sonic and $dA/A = 0$ if $d\vartheta/\vartheta$ is to be finite. Thus, this is the region of the conduit for which the area is a minimum in the direction of flow. This is called the "throat" of the conduit. Then if $M = 1$ anywhere in the flow, it occurs at the throat, but it is *not* necessarily the case that the flow in the throat is sonic, i.e., $M = 1$ at the throat.

We now identify a unique state in the flow, sometimes called the *critical state* (not to be confused with the thermodynamic critical state of Chapter 13 which is a universal definition in the science of thermodynamics), which we denote by the symbol *. In the present context, the critical state is simply a reference state in the flow where sonic conditions prevail, i.e., $M = 1$ with $\vartheta^* = a^*$. All the properties of the flow in that state are denoted by the symbol *. From continuity

$$\rho A\vartheta = \rho^* A^* \vartheta^* \tag{15.146}$$

where A^* denotes the area in the flow where the sonic conditions prevail. Then solving equation (15.146) for the area ratio, we get

$$\frac{A}{A^*} = \frac{\rho^* \vartheta^*}{\rho\vartheta} \tag{15.147}$$

but by definition

$$\frac{\vartheta^*}{\vartheta} = \frac{a^*}{\vartheta} \tag{15.148}$$

We now define a dimensionless velocity M^* such that

$$M^* \equiv \frac{\vartheta}{a^*} \tag{15.149}$$

At first glance, the definition of equation (15.149) can be somewhat confusing. It does *not* denote the state in the flow where $\vartheta^* = a^*$. Rather, in the case of flow in a nozzle, there may be at most

one, if any, location in the flow where the local velocity is the sonic velocity. At that location, a^* has a unique value, and this value can be used to non-dimensionalize the velocity at any other location in the flow field. The resulting non-dimensional parameter is denoted by the symbol M^* and has a different value at each location. M^* is a more convenient dimensionless velocity rather than the local Mach number M which depends upon the local sonic velocity which changes at each point in the flow as a consequence of the expansion process in the gas and the thermodynamic coupling of the gas. As we shall soon see, this non-dimensional parameter M^* is a convenient way of relating the local velocity to other parameters that describe the flow.

Consider the conditions in this one-dimensional flow field at two different points 1 and 2. From the first law for steady, one-dimensional bulk flow, we have

$$h_1 + \frac{\vartheta_1^2}{2} = h_2 + \frac{\vartheta_2^2}{2} \tag{15.150}$$

Suppose now that the flow originates from a reservoir where $\vartheta_1 = 0$ and $T_1 = T_0$, $P_1 = P_0$, and $\rho_1 = \rho_0$. These are known as the *stagnation* conditions. Also, suppose that the ideal gas model is a valid model for the fluid. Then we can substitute the ideal gas constitutive relation for the enthalpy and the first law becomes

$$c_P T_0 = c_P T + \frac{\vartheta^2}{2}$$

$$T_0 = T + \frac{\vartheta^2}{2c_P} \tag{15.151}$$

where the un-subscripted parameters can be the values of those parameters at any location in the flow. For the ideal gas model, we have

$$M = \frac{\vartheta}{a} \quad \text{and} \quad a = \sqrt{\gamma RT} \tag{15.152}$$

where $\gamma = c_P/c_v$. Then equation (15.151) can be written

$$T_0 = T + \frac{M^2 a^2}{2c_P} = T + \frac{\gamma RT}{2c_P} M^2 = T\left[1 + \frac{\gamma R}{2c_P} M^2\right]$$

$$\frac{T_0}{T} = 1 + \frac{\gamma - 1}{2} M^2 \tag{15.153}$$

If the flow is reversible and adiabatic, the entropy is constant throughout the flow and the locus of states with the same entropy is given by $Pv^\gamma = \text{constant}$. Then with the aid of the ideal gas model property constitutive relation

$$P_0 = P\left(\frac{T_0}{T}\right)^{\frac{\gamma}{\gamma-1}} \tag{15.154}$$

Then

$$\frac{P_0}{P} = \left[1 + \frac{\gamma - 1}{2} M^2\right]^{\frac{\gamma}{\gamma-1}} \quad \text{and} \quad \frac{\rho_0}{\rho} = \left[1 + \frac{\gamma - 1}{2} M^2\right]^{\frac{1}{\gamma-1}} \tag{15.155}$$

In Figure 15.25, we have plotted equations (15.153) and (15.155). It may be seen from Figure 15.25 that up to a Mach number of about $M = 0.3$, changes in density are essentially negligible. It is for this reason that we have been able to treat air as an incompressible fluid in so many flow situations that we have considered up to this point in our treatment of the subject.

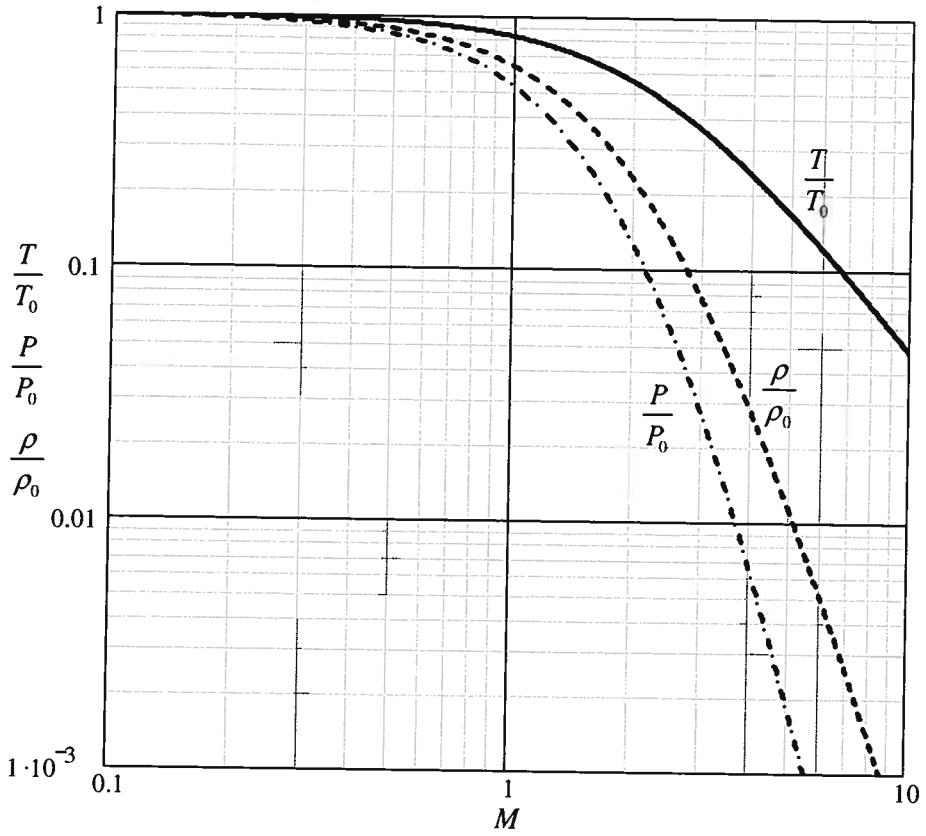

Figure 15.25 Isentropic Flow of a Gas with $\gamma = 1.4$

Let us now relate the reservoir and sonic conditions. Applying the first law to this situation, we have

$$T_0 = T^* \left[1 + \frac{\vartheta^{*2}}{2c_p T^*} \right] \tag{15.156}$$

But

$$\frac{\vartheta^{*2}}{2c_p T^*} = \frac{a^{*2}}{2c_p T^*} = \frac{\gamma R T^*}{2c_p T^*} = \frac{\gamma - 1}{2} \tag{15.157}$$

Then combining equations (15.156) and (15.157), we get

$$\frac{T^*}{T_0} = \frac{2}{\gamma + 1} \tag{15.158}$$

Similarly,

$$\frac{P^*}{P_0} = \left(\frac{2}{\gamma + 1} \right)^{\frac{\gamma}{\gamma - 1}} \quad \text{and} \quad \frac{\rho^*}{\rho_0} = \left(\frac{2}{\gamma + 1} \right)^{\frac{1}{\gamma - 1}} \tag{15.159}$$

For an ideal gas with $\gamma = 1.4$, equations (15.158) and (15.159) give

$$\frac{T^*}{T_0} = 0.8333 \quad \text{and} \quad \frac{P^*}{P_0} = 0.5283 \quad \text{and} \quad \frac{\rho^*}{\rho_0} = 0.6339 \tag{15.160}$$

The dimensionless velocity M^* is defined as

$$M^* \equiv \frac{\vartheta}{a^*} = \left(\frac{\vartheta}{a}\right)\left(\frac{a}{a^*}\right) = M\sqrt{\frac{T}{T^*}} \tag{15.161}$$

Then combining equations (15.153), (15.158), and (15.161), we get

$$M^* = M\left\{\frac{\gamma+1}{2}\left[1+\frac{\gamma-1}{2}M^2\right]^{-1}\right\}^{\frac{1}{2}} \tag{15.162}$$

Equation (15.162) is plotted in Figure 15.26.

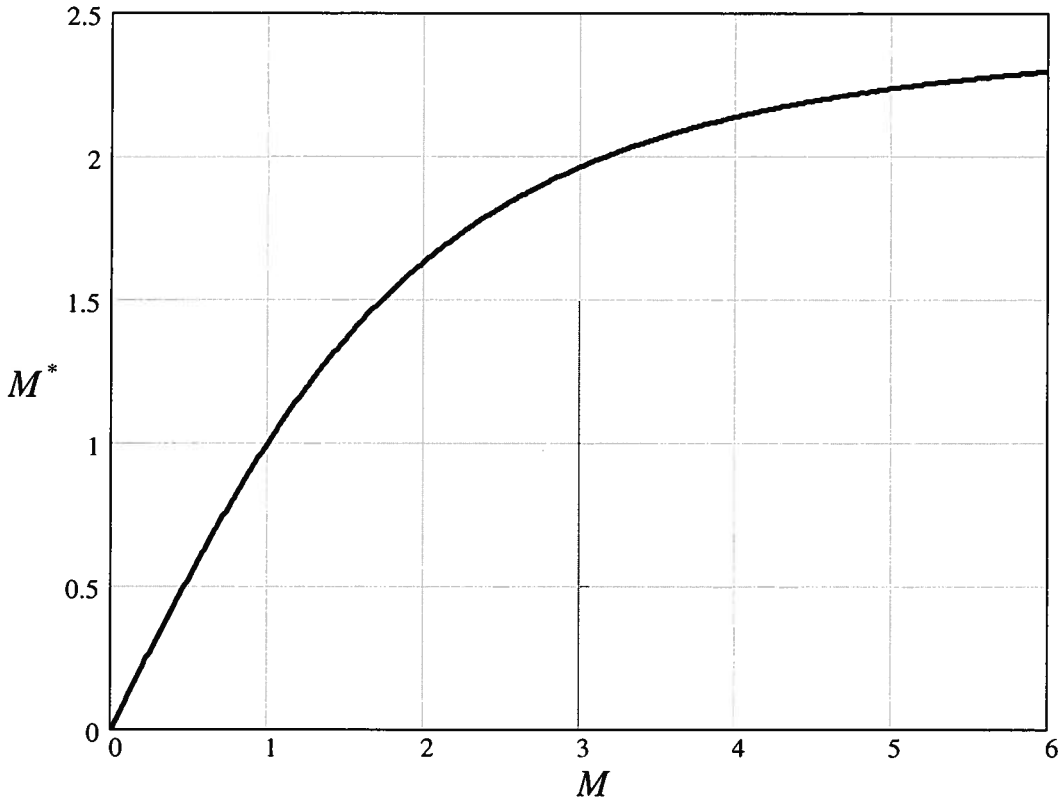

Figure 15.26 The Relation Between the Dimensionless Velocity M^* and the Local Mach Number M for the Flow of an Ideal Gas with $\gamma = 1.4$

Figure 15.26 has several interesting features. The Mach number M can be conveniently thought of as a measure of the square root of the ratio of the kinetic energy (velocity) of the flow to the internal energy of the fluid (since the denominator is the speed of sound which depends only upon the temperature as does the internal energy) whereas the dimensionless velocity M^* is a measure of the square root of the kinetic energy (velocity) only. In Figure 15.26, we see that for $M < 1$, the dimensionless velocity and the Mach number are essentially identical numerically. Thus, the acceleration of the fluid is a result of the flow work done on the fluid. The internal energy of the fluid contributes virtually nothing. However, as the fluid accelerates beyond the speed of sound, compressibility effects dominate the flow and the Mach number increases disproportionately relative to the dimensionless velocity (since the denominator is decreasing faster than the numerator is increasing). This means that the internal energy contributes a disproportionate amount to the acceleration of the fluid. In fact, as equation (15.162) shows, there is a limit to the acceleration of the fluid:

$$\text{as} \quad M \to \infty, \quad M^* \to \sqrt{\frac{\gamma+1}{\gamma-1}} \tag{15.163}$$

Equation (15.163) shows that for $\gamma = 1.4$, the limiting value of M^* is 2.449. This can be clearly seen in Figure 15.26. Thus, the maximum velocity of the flow is $\vartheta_{max} = 2.449a^*$. Thus,

$$\begin{aligned} &\text{when} \quad M < 1, \quad M^* < 1 \\ &\text{when} \quad M > 1, \quad M^* > 1 \\ &\text{when} \quad M = 1, \quad M^* = 1 \\ &\text{when} \quad M \to \infty, \quad M^* \to \sqrt{\frac{\gamma+1}{\gamma-1}} \end{aligned}$$

In practical applications of nozzle designs, it is worthwhile to know the mass flux through the nozzle. For example, the application of nozzles as thrusting mechanisms on spacecraft requires knowledge of the mass flow rate through the nozzle in order to determine the thrust available. The mass flux, i.e., the mass flow rate per unit area can be determined from the definition, viz.

$$\frac{\dot{m}}{A} = \rho\vartheta = \frac{P}{RT}\vartheta = \frac{P\vartheta}{\sqrt{\gamma RT}}\sqrt{\frac{\gamma}{R}}\sqrt{\frac{T_0}{T}}\frac{1}{\sqrt{T_0}} = \sqrt{\frac{\gamma}{R}}\frac{P}{\sqrt{T_0}}M\sqrt{1+\frac{\gamma-1}{2}M^2} \tag{15.164}$$

where we have made use of equation (15.153). If we solve equation (15.155) for M as a function of P/P_0 and substitute the result into equation (15.164), we can obtain an expression for the mass flux in terms of the pressure ratio. This can be expressed in dimensionless form, viz.

$$\frac{\dot{m}}{A}\frac{a_0}{P_0} = \gamma\sqrt{\frac{2}{\gamma-1}}\left(\frac{P}{P_0}\right)^{\frac{\gamma+1}{2\gamma}}\sqrt{\left(\frac{P}{P_0}\right)^{\frac{1-\gamma}{\gamma}}-1} \tag{15.165}$$

Equation (15.165) has been plotted in Figure 15.27 which clearly shows that the mass flux has a maximum value at the critical value of the pressure ratio. At values of the pressure ratio greater than the critical value, the flow is subsonic. At values of the pressure ratio less than the critical value, the flow is supersonic. In both cases, the dimensionless mass flux is less than the maximum value. The maximum value of the dimensionless mass flux can be obtained by recalling that the cross-sectional area for isentropic flow passes through a minimum when the Mach number is unity. Then the maximum value of the mass flux can be obtained by setting the Mach number equal to unity, $M = 1$, in equation (15.164), viz.

$$\left(\frac{\dot{m}}{A}\right)_{max}\frac{a_0}{P_0} = \gamma\sqrt{\left(\frac{2}{\gamma+1}\right)^{\frac{\gamma+1}{\gamma-1}}} \tag{15.166}$$

For $\gamma = 1.4$, equation (15.166) becomes

$$\left[\left(\frac{\dot{m}}{A}\right)_{max}\frac{a_0}{P_0}\right]_{\gamma=1.4} = 0.8102 \tag{15.167}$$

This value is clearly shown on Figure 15.27.

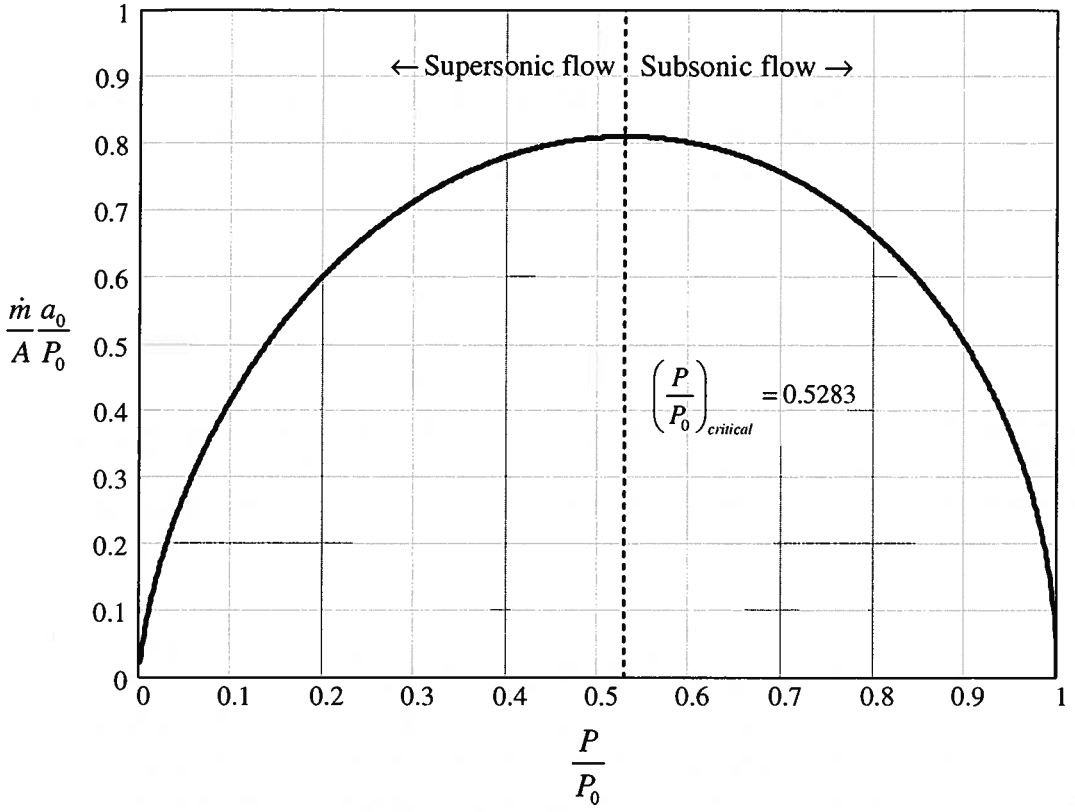

Figure 15.27 Dimensionless Mass Flux for Isentropic Flow with $\gamma = 1.4$

We now need to determine the shape of the flow passage that will insure that the flow is isentropic throughout. This will be a nozzle of converging-diverging configuration known as a *de Laval nozzle* in honor of Gustav de Laval (1845 – 1913), the Swedish engineer who first designed it. Combining equations (15.149), (15.156), and (15.161), we obtain

$$\frac{A}{A^*} = \frac{1}{M}\left\{\frac{2}{\gamma+1}\left[1+\frac{\gamma-1}{2}M^2\right]\right\}^{\frac{\gamma+1}{2(\gamma-1)}} \tag{15.168}$$

Equation (15.168) is plotted in Figure 15.28 which clearly shows the converging-diverging geometry of the nozzle, but there is another interesting feature. For each value of the local Mach number, there is a unique value of the ratio of the local area to the area where the flow is sonic (the throat if the flow is sonic at all); however, for any ratio of the two areas, there are two conditions of flow that satisfy the isentropic solution of the equations of motion. One of these solutions results in subsonic flow while the other results in supersonic flow. Which of these solutions prevails in a given situation depends upon the ambient pressure ("back" pressure) imposed on the discharge flow from the nozzle as we shall show below. This latter aspect of Figure 15.28 is important because once the nozzle is designed, the area is fixed for each location x along the flow axis, and the nozzle may operate at conditions other than the design conditions. The flow pattern that prevails is then dependent upon the conditions imposed.

Since de Laval nozzles find widespread use in thermal-fluids engineering, it is worthwhile to examine the manner in which these conditions influence their mode of operation.

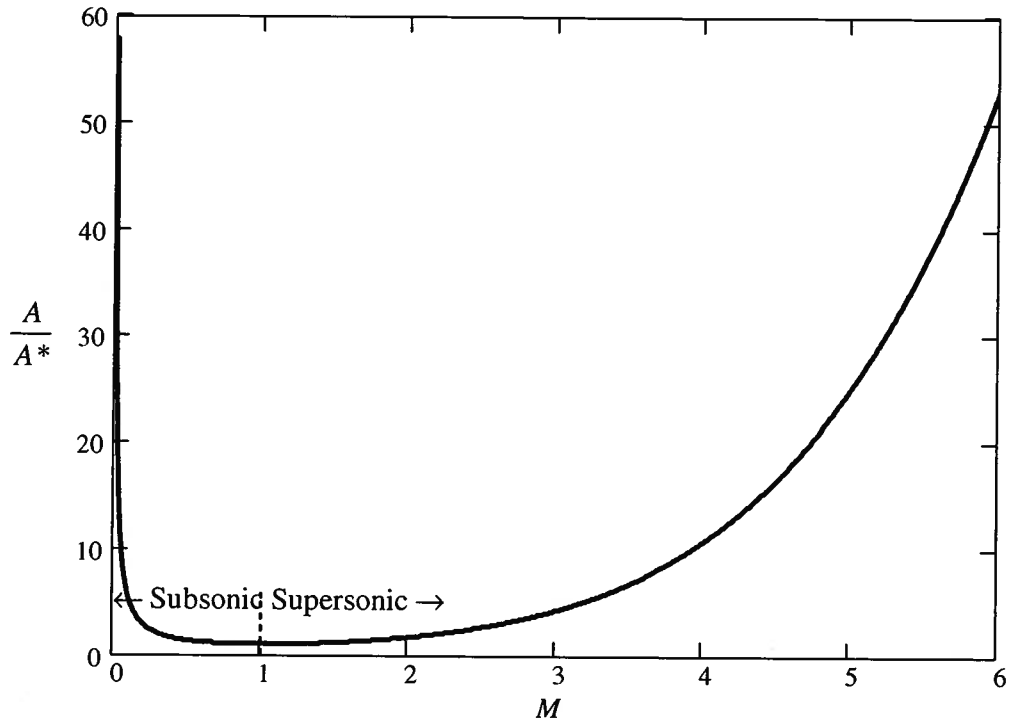

Figure 15.28 Area of Flow for Isentropic Flow of an Ideal Gas with $\gamma = 1.4$

Consider the case of an ideal gas flowing in a de Laval nozzle of fixed configuration determined by the specification of the cross-sectional area of flow at each point x along the direction of the flow axis as shown in Figure 15.28. The nozzle exhausts to a quiescent atmosphere where the pressure is maintained constant at P_{amb}. The flow originates from an upstream reservoir where the pressure is fixed at P_0 and the temperature is likewise fixed at T_0. There are four different regimes depending on the ratio P_{amb}/P_0, and these regimes are delineated by three unique flow patterns resulting from the following static pressure ratios:

1. $\frac{P_1}{P_0}$ where P_1 is the static pressure at exit that results in subsonic, isentropic expansion in the converging section, sonic flow at the throat, and subsonic, isentropic compression in the flow in the diverging section. The value of $P_1 = P_c$ in Figure 15.29 is determined from equation (15.168). The area of the exit plane A_e is known from the geometry of the nozzle and the ratio A_e/A^* is substituted into equation (15.168) to find the subsonic solution for M. This value of $M = M_1$ is then substituted into equation (15.155) to find the value of P_1/P_0, viz.

$$\frac{P_1}{P_0} = \left[1 + \frac{\gamma - 1}{2} M_1^2\right]^{\frac{\gamma}{1-\gamma}} \tag{15.169}$$

2. $\frac{P_2}{P_0}$ where P_2 is the static pressure at the exit plane that results in subsonic, isentropic expansion in the converging section, sonic flow at the throat, and supersonic isentropic expansion in the diverging section. $P_2 = P_j$ in Figure

15.29 where M_2 is the supersonic solution to the area–Mach number relation of equation (15.168) and

$$\frac{P_2}{P_0}=\left[1+\frac{\gamma-1}{2}M_2^{\,2}\right]^{\frac{\gamma}{1-\gamma}} \tag{15.170}$$

3. $\frac{P_3}{P_0}$ where P_3 is the static pressure achieved downstream of a normal shock wave at the exit where the conditions immediately upstream of the shock wave are supersonic with conditions specified by equations (15.154), (15.155) and (15.168). The pressure ratio across the shock wave is given by

$$\frac{P_3}{P_2}=1+\frac{2\gamma}{\gamma+1}\left(M_2^{\,2}-1\right) \tag{15.171}$$

where M_2 is the Mach number of the flow immediately upstream of the shock wave.

Regime I: If $P_{amb} < P_1$, (points *a*, *b*, and *c* on Figure 15.29) flow is isentropic and subsonic everywhere and the nozzle behaves like a Venturi meter. At the exit plane of the nozzle $P_e = P_{amb}$, and the mass flow rate is sensitive to changes in the ambient pressure P_{amb} and is given by

$$\dot{m}=\rho_0 a_0 A_{throat}\left(\frac{P_{amb}}{P_0}\right)^{\frac{1}{\gamma}}\sqrt{\frac{2}{\gamma-1}\left[1-\left(\frac{P_{amb}}{P_0}\right)^{\frac{\gamma-1}{\gamma}}\right]} \tag{15.172}$$

The Mach number at exit is given by

$$M_e=\sqrt{\frac{2}{\gamma-1}\left[\left(\frac{P_0}{P_{amb}}\right)^{\frac{\gamma-1}{\gamma}}-1\right]} \tag{15.173}$$

The boundary of Regime I is the isentropic flow condition determined by the pressure ratio of equation (15.169). With the exception of the case $P_1 = P_c$, throughout Regime I, there is an infinite number of pressure distributions in the direction of flow along the flow axis depending upon the ambient pressure. When $P_{amb} = P_c = P_1$, the flow accelerates with decreasing pressure in the converging section to the sonic velocity at the throat and then decelerates with increasing pressure in the diverging section to reach the ambient pressure $P_{amb} = P_c$. In this case, the flow is subsonic everywhere except at the throat where it is sonic. This is the limiting condition specified by equation (15.169) that marks the boundary between Regime I and Regime II.

Regime II: If $P_3 < P_{amb} < P_1$, (the region between points *c* and *f* on Figure 15.29) the flow is subsonic in the converging section, sonic at the throat, and supersonic over a portion of the diverging section and subsonic over the remainder. There is a shock wave normal to the flow within the diverging section and the pressure at the exit plane P_e is equal to the ambient pressure P_{amb}. The mass flow rate is given by equation (15.166), viz.

$$\dot{m}=\rho_0 a_0 A_{throat}\left(\frac{2}{\gamma+1}\right)^{\frac{\gamma+1}{2(\gamma-1)}} \tag{15.166}$$

This is "choked flow" at the throat. Note that $\dot{m}$ is independent of the ambient pressure. The exit Mach number is given by

$$M_e = \sqrt{-\frac{1}{\gamma-1} + \sqrt{\frac{1}{(\gamma-1)^2} + \frac{2\beta^2}{(\gamma-1)}}}$$

where (15.174)

$$\beta = \frac{P_0 A_{throat}}{P_{amb} A_e}\left(\frac{2}{\gamma+1}\right)^{\frac{\gamma+1}{2(\gamma-1)}}$$

Within Regime II there is a unique condition worthy of note. This is the condition that occurs when $P_{amb} = P_3 = P_f$ of Figure 15.29 and marks the boundary between Regime II and Regime III. In this case the flow accelerates with decreasing pressure in the converging section and reaches sonic velocity at the throat. In the diverging section, the flow continues to accelerate in the supersonic regime with decreasing pressure until the exit plane is reached. At this location, the pressure which has been attained through isentropic expansion does not match the ambient pressure and a normal shock wave forms to produce a discontinuity in pressure to reach the ambient pressure. That is, the normal shock wave that characterizes Regime II has moved downstream to the exit plane as the ambient pressure has decreased from P_c to P_f. A significant amount of entropy is generated in the shock wave. Immediately downstream of the shock wave the pressure at the exit plane is the ambient pressure $P_{amb} = P_f$, but immediately upstream of the shock wave, the pressure at the exit plane is determined by the area ratio as is typically the case in the supersonic regime. In the present case, knowing the area at the exit plane, we can solve equation (15.168) for the upstream Mach number at that location. With this value of the Mach number, we can solve equation (15.155) to determine the pressure upstream of the shock wave. There results

$$\frac{P_3}{P_2} = \frac{P_{amb}}{P_2} = 1 + \frac{2\gamma}{\gamma+1}\left(M_2^{\,2} - 1\right) \tag{15.175}$$

where M_2 is the Mach number in the exit plane immediately upstream of the shock wave.

Regime III: If $P_2 < P_{amb} < P_3$, (the region between points *f* and *j* on Figure 15.29) the flow is isentropic within the nozzle. It is subsonic in the converging section, sonic at the throat, and supersonic in the diverging section. Then the pressure in the exit plane is lower than the ambient pressure, $P_e = P_2$, and the gas is recompressed to the ambient pressure P_{amb} in an irreversible manner with a system of oblique shock waves external to the nozzle exit. This is referred to as an *over-expanded nozzle*. The flow is "choked" and the mass flow rate is given by equation (15.166) once again, viz.

$$\dot{m} = \rho_0 a_0 A_{throat}\left(\frac{2}{\gamma+1}\right)^{\frac{\gamma+1}{2(\gamma-1)}} \tag{15.166}$$

and the exit Mach number is determined by the supersonic solution to equation (15.168).

$$M_e = M_2$$

When $P_{amb} = P_2 = P_j$ of Figure 15.29, we have the "design condition" for the given geometry of the nozzle. The flow expands reversibly and adiabatically from the reservoir pressure P_0 to the ambient pressure P_{amb}. There is a perfect match between the pressure in the exit plane and the

ambient pressure. In this case, the exit Mach number is precisely that determined from the supersonic solution to equation (15.168) and the pressure is given by equation (15.170). This condition marks the boundary between Regime III and Regime IV.

Regime IV: If $P_{amb} < P_2$, (the region between point *j* and the horizontal axis in Figure 15.29) flow in the nozzle is supersonic throughout identical to that above except that now the pressure expands to the ambient pressure P_{amb} by a series of rarefaction waves that form external to the nozzle exit. This is an *under-expanded nozzle*. The flow is again "choked" and the mass flow rate is given by equation (15.166)

$$\dot{m} = \rho_0 a_0 A_{throat} \left(\frac{2}{\gamma+1} \right)^{\frac{\gamma+1}{2(\gamma-1)}} \tag{15.166}$$

and the exit Mach number is determined by the supersonic solution to equation (15.168), viz.

$$M_e = M_2$$

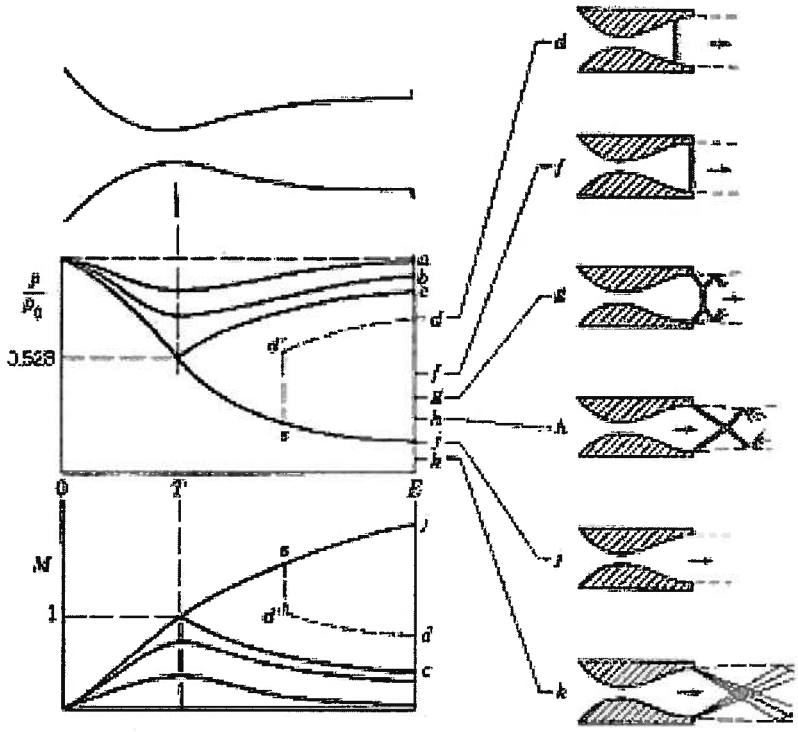

Figure 15.29 Effect of Pressure Ratio on Flow of an Ideal Gas with $\gamma = 1.4$ in a de Laval Nozzle
(From *Elements of Gasdynamics*, by H. W. Liepmann and A. Roshko, Dover Publications, Inc., New York, 1985, Fig. 5.3, p 127.)

Nozzles used for rocket propulsion, such as those used in the main engines of the Space Shuttle, usually have to operate in conditions that change during the ascent of the spacecraft. As a result, some of the flow conditions described above can be observed in photographs or television images of rocket propelled aircraft. In particular, during the launch of the Space Shuttle, the main shuttle engines operate in Regime III noted above. The atmospheric pressure during launch exceeds the design back pressure so that the engines operate in an *over-expanded* mode with the result that oblique shock waves form on the lips of the nozzles. As these shock waves interact with one another in a three-dimensional fashion due to the axisymmetric shape of the nozzle, they produce an observable phenomenon known as Mach diamonds where the flow turns parallel seen as light-colored cones in the exhaust plumes from the Space Shuttle main engines in Figure 15.30. These Mach diamonds are also shown schematically in Figure 15.31.

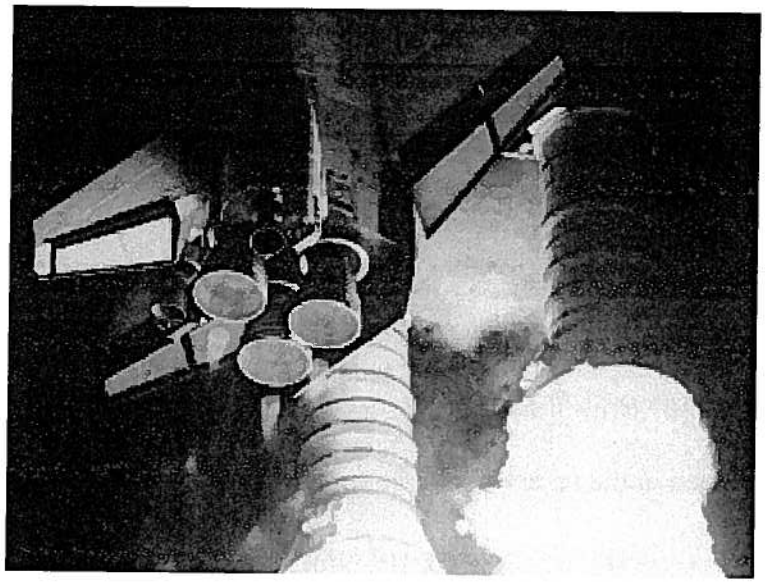

Figure 15.30 Mach Diamonds in the Exhaust from the Nozzles of Space Shuttle Main Engines
(From http://www.aerospaceweb.org/question/propulsion/q0224.shtml)

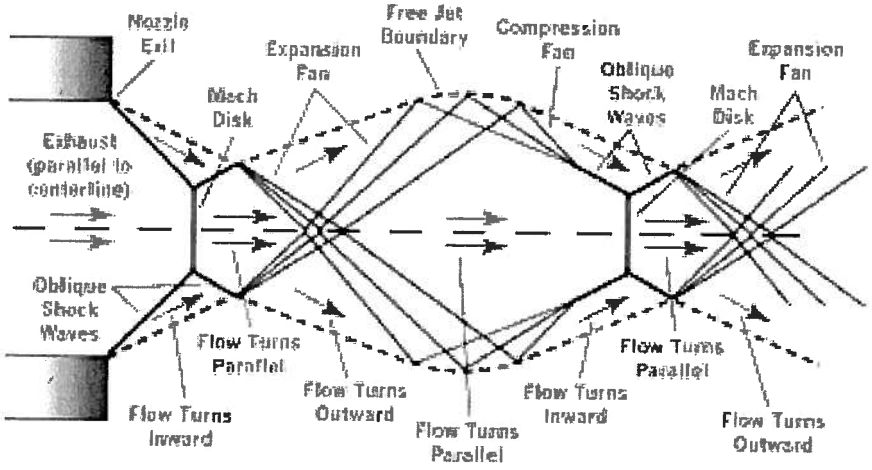

Figure 15.31 Schematic Representation of Mach Disks and Mach Diamonds
in the 3-dimensional Over-expanded Flow from a Rocket Nozzle
(From http://www.aerospaceweb.org/question/propulsion/q0224.shtml)

Example 15E.8: We wish to build a small nozzle for a classroom demonstration of nozzle design. The design is to be quasi-one-dimensional in the sense that the nozzle contour will be configured as a one dimensional nozzle sandwiched between two flat plates that are transparent for visualization. In order to have a design that can be seen easily, we arbitrarily set the throat dimensions to be 1 cm x 1 cm. The exit Mach number is to be $M_2 = 2.0$. The gas supply (nitrogen, $\gamma = 1.4$, $R = 297$ J/kg K) comes from a reservoir with fixed conditions of temperature,

T_0 = 300 K, pressure, and density. The ambient pressure is $P_{amb} = 10^5$ N/m^2 and the nozzle operates at the design condition with the pressure at the exit plane equal to the ambient pressure.

(a) Determine the supply conditions, P_0 and ρ_0, in the reservoir.

(b) Determine the exit area of the nozzle.

(c) Determine the mass flow rate of nitrogen through the nozzle.

(d) Determine the temperature of the nitrogen at exit from the nozzle.

Solution: (a) From equation (15.155),

$$\frac{P_0}{P_{amb}} = \left[1 + \frac{\gamma - 1}{2} M_2^{\,2}\right]^{\frac{\gamma}{\gamma-1}}$$

$$P_0 = \left(10^5 \text{ N/m}^2\right)\left[1 + \frac{1.4-1}{2}(2.0)^2\right]^{\frac{1.4}{1.4-1}} = 7.824 \text{ x } 10^5 \text{ N/m}^2$$

The density of the nitrogen in the reservoir can be calculated from the ideal gas property constitutive relation, viz.

$$\rho_0 = \frac{P_0}{RT_0} = \frac{7.824 \text{ x } 10^5 \text{ N/m}^2}{(297 \text{ J/kg K})(300 \text{ K})} = 8.781 \text{ kg/m}^3$$

The speed of sound at reservoir conditions is

$$a_0 = \sqrt{\gamma R T_0} = 353.19 \text{ m/sec}$$

(b) From equation (15.168), the area ratio is

$$\frac{A}{A^*} = \frac{1}{M}\left\{\frac{2}{\gamma+1}\left[1 + \frac{\gamma-1}{2}M^2\right]\right\}^{\frac{\gamma+1}{2(\gamma-1)}}$$

Since the flow is sonic at the throat by design,

$$A_e = A_{throat}\left[\frac{1}{M}\left\{\frac{2}{\gamma+1}\left[1 + \frac{\gamma-1}{2}M^2\right]\right\}^{\frac{\gamma+1}{2(\gamma-1)}}\right]$$

$$A_e = \left(10^{-2}\right)^2\left[\frac{1}{2.0}\left\{\frac{2}{1.4+1}\left[1 + \frac{1.4-1}{2}(2.0)^2\right]\right\}^{\frac{1.4+1}{2(1.4-1)}}\right]$$

$$A_e = 1.688 \text{ x } 10^{-4} \text{ m}^2$$

Since the side plates are separated by a dimension of 1 cm, the vertical dimension of the nozzle exit is L_e = 1.69 cm.

(c) The flow is determined by the sonic conditions at the throat, equation (15.166), viz.

$$\dot{m} = \rho_0 a_0 A_{throat}\left(\frac{2}{\gamma+1}\right)^{\frac{\gamma+1}{2(\gamma-1)}}$$

$$\dot{m} = \left(8.781 \text{ kg/m}^3\right)\left(353.19 \text{ m/sec}\right)\left(10^{-4} \text{ m}^2\right)\left(\frac{2}{1.4+1}\right)^{\frac{1.4+1}{2(1.4-1)}} = 0.1795 \text{ kg/sec}$$

(d) The exit temperature is that which results from a reversible adiabatic expansion, viz.

$$T_2 = T_0\left(\frac{P_0}{P_2}\right)^{\frac{1-\gamma}{\gamma}} = (300\text{ K})\left(\frac{7.824\text{ x }10^5\text{ N/m}^2}{10^5\text{ N/m}^2}\right)^{\frac{1-1.4}{1.4}} = 166.69\text{ K} = -106.48\text{ C}$$

15.3.2 Nozzles Accelerating an Incompressible Fluid

If the fluid flowing through the nozzle can be modeled as an incompressible fluid, the situation is somewhat different from that previously described. The difference arises because the thermal and mechanical aspects of an incompressible fluid are not coupled as they are in a gas. In fact, the temperature and pressure are completely uncoupled so the enthalpy can be separated into a thermal energy and an uncoupled mechanical property, Pv, in the manner of equation (15.105). Then for the incompressible fluid flowing in a horizontal nozzle, equation (15.123) can be written

$$\dot{m}\left(\frac{\vartheta_{out}^2}{2} - \frac{\vartheta_{in}^2}{2}\right) = \dot{m}\left[(u_{in} - u_{out}) + v(P_{in} - P_{out})\right] \tag{15.176}$$

where the specific volume v is constant. According to the energy constitutive relation for the incompressible fluid, the internal energy depends on temperature only. Then equation (15.176) becomes

$$\dot{m}\left(\frac{\vartheta_{out}^2}{2} - \frac{\vartheta_{in}^2}{2}\right) = \dot{m}\left[(T_{in} - T_{out}) + v(P_{in} - P_{out})\right] \tag{15.177}$$

The change in entropy experienced by the incompressible fluid as it flows through the nozzle is given by the entropy constitutive relation. Since in a reversible adiabatic expansion the entropy is constant, equation (15.107) requires that the temperature is also constant. For this situation, equation (15.177) reduces to

$$\dot{m}\left(\frac{\vartheta_{out}^2}{2} - \frac{\vartheta_{in}^2}{2}\right) = \dot{m}v(P_{in} - P_{out}) \tag{15.178}$$

Note that since the specific volume is constant, equation (15.178) could have been obtained directly from equation (15.127) by means of a simple integration. In any event, equation (15.178) again indicates that in the reversible adiabatic nozzle, the fluid is accelerated and increases in kinetic energy solely as a result of the net normal pressure forces on the fluid at the control surface (no shear stresses).

If in equation (15.178) we were to replace the specific volume with the density and were to consider unit flow rate, equation (15.178) becomes the familiar Bernoulli equation of incompressible fluid mechanics.

$$\frac{\vartheta_{out}^2}{2} - \frac{\vartheta_{in}^2}{2} = \frac{P_{in}}{\rho} - \frac{P_{out}}{\rho} \tag{15.179}$$

For a flow in which the acceleration process is irreversible and adiabatic, the second law of thermodynamics requires that the entropy should increase. Then from the entropy constitutive relation for the incompressible fluid, the temperature must also increase. Since the inlet state and outlet pressure are externally imposed, equation (15.178) shows that the increase in temperature and the associated increase in internal energy can occur only by dissipating uncoupled mechanical energy to uncoupled thermal energy. Thus, as shown in equation (15.130), the irreversible adiabatic acceleration of an incompressible fluid in a nozzle does not, for a given inlet state and outlet pressure, produce as large an increase in kinetic energy as a reversible

adiabatic expansion. This result becomes more obvious in the calculation of the nozzle efficiency. For the incompressible fluid, equation (15.131) reduces to

$$(\eta_N)_{incompressible} = 1 - \frac{c(T_{out} - T_{in})}{v(P_{in} - P_{out})} \tag{15.180}$$

Physically the second term on the right side of equation (15.180) represents the fraction of potentially available kinetic energy dissipated into internal energy through the action of irreversible processes.

The locus of states for the incompressible fluid flowing through the nozzle is shown in Figure 15.32. The nozzle efficiency has the usual geometric interpretation on this diagram.

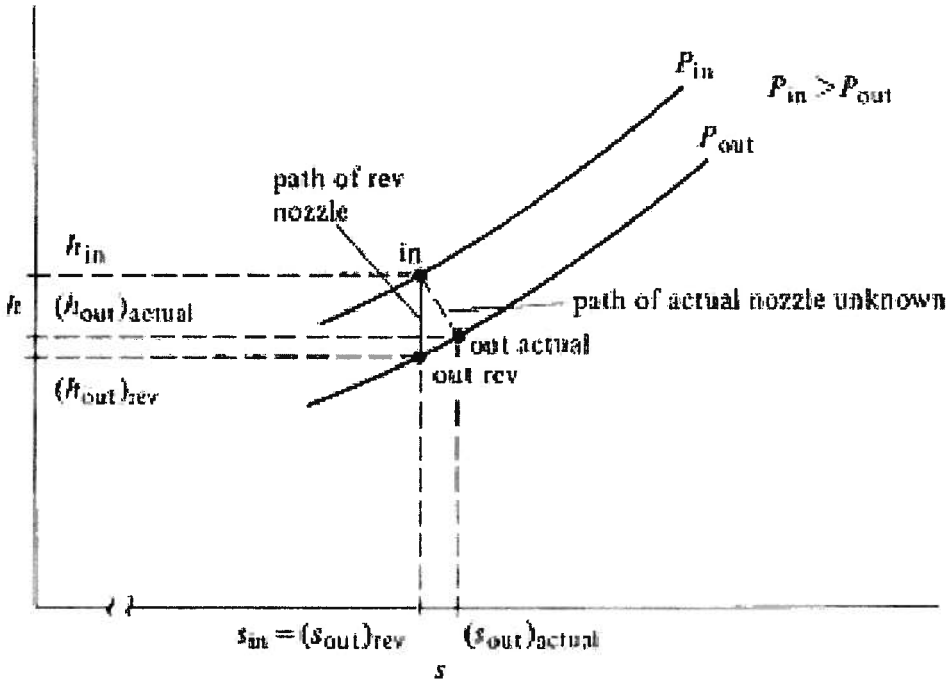

Figure 15.32 States of an Incompressible Fluid Flowing Through a Nozzle

Example 15E.9: The water in a fire hose flows steadily at $P = 10^6$ N/m^2 and $T = 25$ C, and approaches the nozzle with negligible kinetic energy. The stream leaving the nozzle is at atmospheric pressure, $P_2 = 10^5$ N/m^2. The nozzle efficiency is $(\eta_N)_{incompressible} = 0.95$.

(a) What is the velocity of the water leaving the nozzle?

(b) What is the temperature change of the water as it passes through the nozzle?

(c) What is the maximum height of fire that could be reached by the stream from the fire hose?

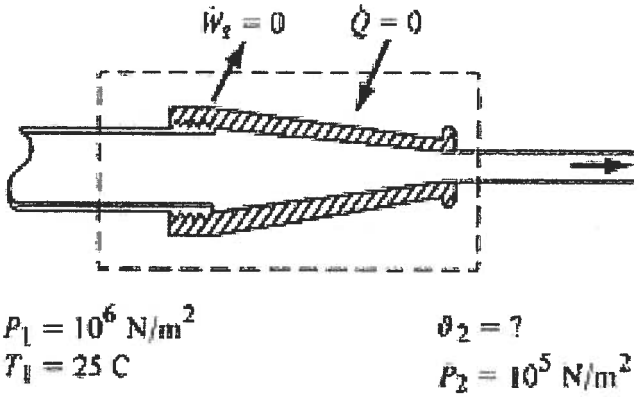

Figure 15E.9(a) Fire Nozzle Cross-section

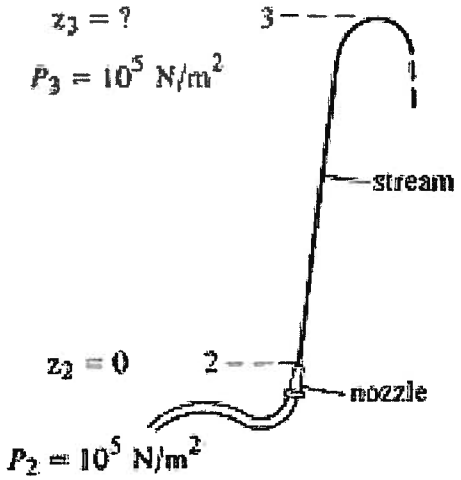

Figure 15E.9(b) Fire Nozzle

Solution: (a) The first law applied to the control volume shown in Figure 15E.9(a) gives the exit velocity from a steady-flow reversible nozzle with the same conditions as the actual nozzle.

$$\frac{dE_{cv}}{dt} = \dot{Q} - \dot{W}_{shaft} + \dot{m}\left(h_1 + \frac{\vartheta_1^2}{2} + gz_1\right) - \dot{m}\left(h_{2r} + \frac{\vartheta_{2r}^2}{2} + gz_2\right)$$

where $\vartheta_1^2/2$ has been assumed to be negligibly small compared to $\vartheta_{2r}^2/2$, the nozzle has been modeled as adiabatic, and the shear work transfer is zero. Changes in elevation are also assumed negligible.

$$\frac{\vartheta_{2r}^2}{2} = h_1 - h_{2r}$$

For the reversible nozzle, $s_{2r} = s_1$ since the nozzle is adiabatic. If we model the water as an incompressible fluid, then $T_{2r} = T_1$ since, according to the entropy constitutive relation, the entropy of an incompressible fluid depends only on temperature. Also, for an incompressible fluid $h = cT + Pv$. Thus for water with $v = 10^{-3}$ m^3/kg,

$$\frac{\mathcal{V}_{2r}^2}{2} = c(T_1 - T_{2r}) + v(P_1 - P_{2r})$$

$$\mathcal{V}_{2r}^2 = 2v(P_1 - P_{2r}) = 2\left(0.001 \text{ m}^3/\text{kg}\right)\left(10^6 \text{ N/m}^2 - 10^5 \text{ N/m}^2\right)$$

$$\mathcal{V}_{2r}^2 = 1800 \text{ Nm/kg} = 1800 \text{ m}^2/\text{sec}^2$$

The kinetic energy of the fluid leaving the actual nozzle is determined from the definition of nozzle efficiency, equation (15.131), with $\mathcal{V}_1^2 = 0$.

$$\mathcal{V}_2^2 = \eta_N \mathcal{V}_{2r}^2 0.95\left(1800 \text{ m}^2/\text{sec}^2\right) = 1710 \text{ m}^2/\text{sec}^2$$

$$\mathcal{V}_2 = 41.35 \text{ m/sec}$$

(b) The temperature change is determined by applying the first law to the actual nozzle.

$$h_1 - h_2 = \frac{\mathcal{V}_2^2}{2}$$

$$c(T_1 - T_2) + v(P_1 - P_2) = \frac{\mathcal{V}_2^2}{2}$$

$$T_2 - T_1 = \frac{v}{c}(P_1 - P_2) - \frac{\mathcal{V}_2^2}{2c}$$

$$T_2 - T_1 = \frac{0.001 \text{ m}^3/\text{kg}}{4180 \text{ J/kg K}}\left(10^6 \text{ N/m}^2 - 10^5 \text{ N/m}^2\right) - \frac{1710 \text{ m}^2/\text{sec}^2}{2(4180 \text{ J/kg K})} = 0.011 \text{ C}$$

(c) The maximum height is determined from the first law applied to the reversible constant pressure deceleration of the free stream from the nozzle exit (state 2) to the maximum height where the velocity is zero, state 3 in Figure 15E.9(b). For a reversible adiabatic deceleration at constant pressure, the first law becomes

$$\cancel{\frac{dE_{cv}}{dt}} = \cancel{\dot{Q}} - \cancel{\dot{W}_{shaft}} + \dot{m}\left(h_2 + \frac{\mathcal{V}_2^2}{2} + \cancel{gz_2}\right) - \dot{m}\left(h_3 + \cancel{\frac{\mathcal{V}_3^2}{2}} + gz_3\right)$$

Since $s_2 = s_3$, $T_2 = T_3$ for the incompressible fluid model. With $P_2 = P_3$, we have $h_3 = h_2$ since h is fixed by T and P. Then

$$\frac{\mathcal{V}_2^2}{2} - gz_3 = 0$$

$$z_3 = \frac{\mathcal{V}_2^2}{2g} = \frac{1710 \text{ m}^2/\text{sec}^2}{2\left(9.81 \text{ m/sec}^2\right)} = 87.16 \text{ m}$$

At this juncture, we would normally take up the matter of the detailed behavior of a nozzle accelerating an incompressible fluid; however, for the case in which the fluid viscosity can be ignored, we have already discussed the details of the fluid mechanics of the nozzle in Chapter 8. In particular, in Section 8.10.2 we discussed the details of the use of such a nozzle as a fluid metering device. Furthermore, when fluid viscosity is important, the details of the internal fluid mechanics of the nozzle accelerating an incompressible fluid can be reviewed in Chapter 9.

15.3.3 Nozzles Accelerating a Pure Substance

Nozzles accelerating a pure substance find widespread application in the stators of steam turbines as described in Appendix 15B. The behavior of a pure substance when accelerated in a

nozzle is between the two extremes represented by the incompressible fluid and the ideal gas models. The loci of states for a pure substance flowing through nozzles with various inlet states are shown in Figure 15.33. Of particular interest on these figures are the cases in which the fluid can undergo a change in phase from the vapor phase to the liquid phase. That is, the exhaust stream from the nozzle is in a two-phase state with both liquid and vapor phases present. When this phenomenon occurs in the nozzles of a steam turbine, the results can be quite damaging. The liquid forms as small droplets in the exhaust from the nozzle, and these droplets, which are traveling at high velocities on the order of the speed of sound, impinge upon the surface of the blades in the rotor. The liquid droplets are essentially incompressible and act as small projectiles when they strike the blade surface. The impact produces a compressive Hertz contact stress that actually causes a minute elastic deformation (depression) in the surface. When the contact stress is relaxed when the droplets bounce off, the local deformation also relaxes as the surface returns

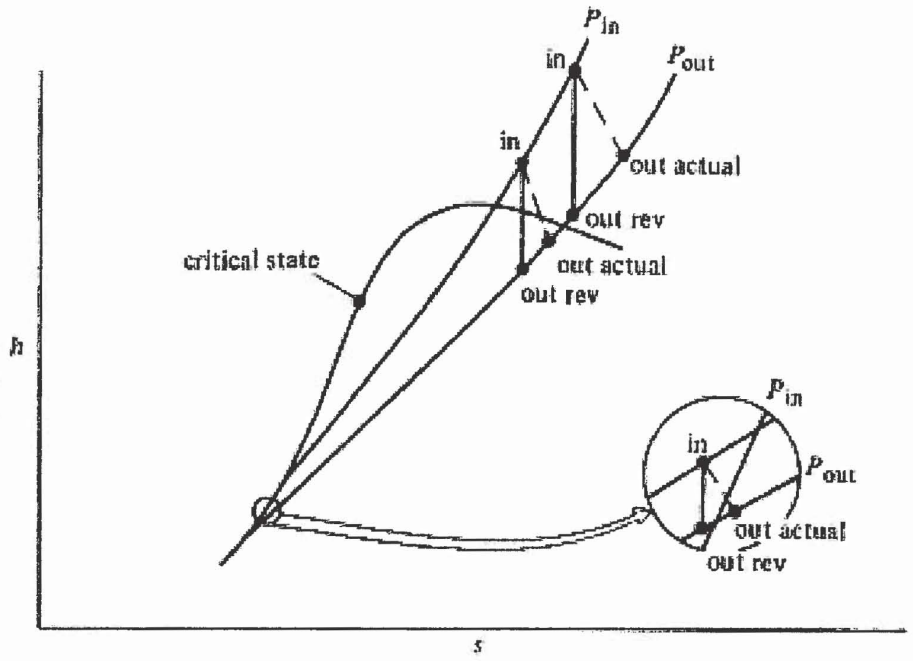

Figure 15.33(a) States of a Pure Substance Flowing Through a Nozzle

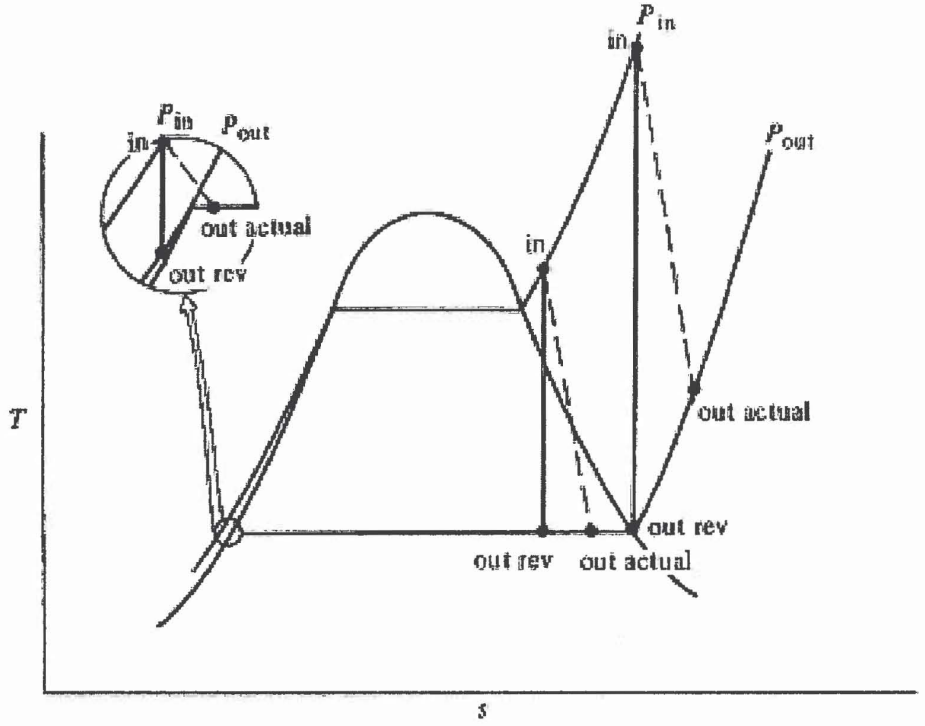

Figure 15.33(b) States of a Pure Substance Flowing Through a Nozzle

to its normal shape. However, if the stress that produced the deformation was high enough, the relaxation of the deformation through the elastic displacement of the surface produces local movement of the surface at velocities high enough that the resulting inertial forces are sufficient to exceed the tensile limit of the blade material and a small particle of the surface actually tears away from the surface. This phenomenon is called *spalling* and is the process by which the liquid droplets erode the surface. Over the course of time, this erosion produces a surface so rough that the friction between the fluid and the surface is high enough to increase the pressure drop in the rotor. As a result, the performance of the stage is degraded. Eventually, the loss in performance becomes so great that the turbine must be taken out of service and the blades repaired by welding new material on the surface and re-machining the blade in order to return the blade to its original design condition. This process of blade erosion determines the "mean time between failures" that sets the maintenance schedule for the turbine. Clearly, as can be seen from Figure 15.33, the erosion process is confined to the low pressure stages of the turbine where the liquid phase is most likely to be present.

Example 15E.10: Steam at a pressure $P_1 = 5 \times 10^5$ N/m^2 and a temperature of $T_1 = 300$ C enters a nozzle of a steam turbine. The initial velocity is essentially zero, $\vartheta_1 \approx 0$, and the steam is expanded adiabatically and irreversibly to a pressure of $P_2 = 10^5$ N/m^2. The nozzle efficiency is $\eta_N = 0.96$.

(a) Determine the state of the steam at the nozzle exit.

(b) Determine the velocity of the steam at the nozzle exit.

(c) If the mass flow rate of steam through the nozzle is $\dot{m} = 1$ kg/sec, determine the rate of entropy generation by the nozzle.

Solution: (a) The path followed by the steam in temperature-entropy coordinates would appear as shown in Figure 15.33(b). We first consider the reversible, adiabatic operation of the nozzle. Then the specific entropy of the steam remains unchanged as it passes through the reversible nozzle and $s_{2r} = s_1$. From the properties of the pure substance model of the H_2O, the initial state is a superheated state with $s_1 = 7.4614$ kJ/kg K and $h_1 = 3064.6$ kJ/kg. Then the exit state in reversible operation is established by the two independent properties, $P_2 = 10^5$ N/m^2 and $s_{2r} = 7.4614$ kJ/kg K. From the pure substance model, $h_{2r} = 2714.1$ kJ/kg. The exit specific enthalpy for irreversible operation can be determined from the definition of nozzle efficiency, viz.

$$\eta_N = \frac{(h_1 - h_2)_{rev}}{(h_1 - h_2)_{actual}}$$

$$(h_1 - h_2)_{actual} = \frac{(h_1 - h_2)_{rev}}{\eta_N} = \frac{(3064.6 \text{ kJ/kg} - 2714.1 \text{ kJ/kg})}{0.96} = 365.1 \text{ kJ/kg}$$

$$h_2 = h_1 - (h_1 - h_2)_{actual} = 3064.6 \text{ kJ/kg} - 365.1 \text{ kJ/kg} = 2699.5 \text{ kJ/kg}$$

Since the exit state of the steam is in the superheat region, the pressure and the specific enthalpy, P_2 and h_2, are sufficient to establish the exit state for irreversible operation.

(b) From the first law for the nozzle, the exit velocity is

$$\frac{\mathcal{V}_2^2}{2} - \frac{\mathcal{V}_1^2}{2} = h_1 - h_2$$

$$\mathcal{V}_2 = \sqrt{2(h_1 - h_2)} = \sqrt{2(3064.6 \text{ kJ/kg} - 2699.5 \text{ kJ/kg})}$$

$$\mathcal{V}_2 = 854.52 \text{ m/sec}$$

Although not specifically asked for in this case, we can calculate the Mach number at exit from the nozzle. Since the ideal gas model does not apply to the properties of H_2O in the vapor state, the speed of sound must be determined from the definition, viz.

$$a^2 = \left(\frac{\partial P}{\partial \rho}\right)_s$$

From the pure substance model, for the exit state, $a_2 = 480.27$ m/sec. Thus, $M_2 = 1.78$ which is clearly supersonic.

(c) The rate of entropy generation can be determined from the second law for the nozzle for adiabatic steady-flow, viz.

$$\cancel{\frac{dS_{cv}}{dt}} = \cancel{\sum_j \left(\frac{\dot{Q}}{T}\right)_j} + \dot{m}(s_1 - s_2) + \dot{S}_{gen}$$

$$\dot{S}_{gen} = \dot{m}(s_2 - s_1) = (1 \text{ kg/sec})(7.4614 \text{ kJ/kg K} - 7.4237 \text{ kJ/kg})$$

$$\dot{S}_{gen} = 37.70 \text{ W/K}$$

15.4 Diffusers

In some engineering systems, it is desirable to decelerate a fluid stream from a high velocity to a low velocity. One example is at the inlet to a jet aircraft engine. Here it is necessary to decelerate the air entering the engine so that it can be efficiently compressed in the engine

compressor. Another example is the inlet to the combustor on a jet engine. In this case it is necessary to decelerate the gas flow so that the heat transfer process inside the combustor can be more effective. In yet another example discussed in Section 15.1.3, the stators in an axial flow compressor act to decelerate the gas and increase the pressure.

The device in which this deceleration is effected is called a *diffuser* and the flow geometry by which it is accomplished involves a gradual increase in the cross-sectional area of the flow in the direction of flow. From continuity considerations, this increase in flow area results in a decrease in the average velocity, and the resulting change in momentum causes the static pressure to increase. In effect, the operation of the diffuser is essentially the inverse of the operation of the nozzle. As a result, some of the kinetic energy of bulk motion is converted into enthalpy of the flowing fluid. Thus equation (15.123) or (15.124) describes the operation of a diffuser as well as that of the nozzle. In fact, the reversible adiabatic diffuser is exactly the inverse process of the reversible adiabatic nozzle and the same relations apply to either. In practice, the difference between the nozzle and the diffuser results from the irreversibility of the processes, especially in the magnitude of the irreversibility. Ultimately, the difference can be traced to the dynamical behavior of the fluid itself.

The acceleration of a fluid produced by decreasing the pressure in the direction of motion as in a nozzle is inherently stable. The favorable pressure gradient is externally imposed and the fluid will accelerate smoothly through any reasonably smooth convergent flow passage in an almost reversible manner. However, as we saw in Section 15.3.2, the design of the supersonic (divergent) portion of a nozzle does require the proper passage contour to obtain reasonably reversible flow. We might then infer that by simply inverting the converging nozzle design, a diffuser should result in which it would be possible to increase the pressure and thereby decelerate the fluid almost reversibly. Although certainly true in principle, the realization of this situation is, in fact, another matter entirely.

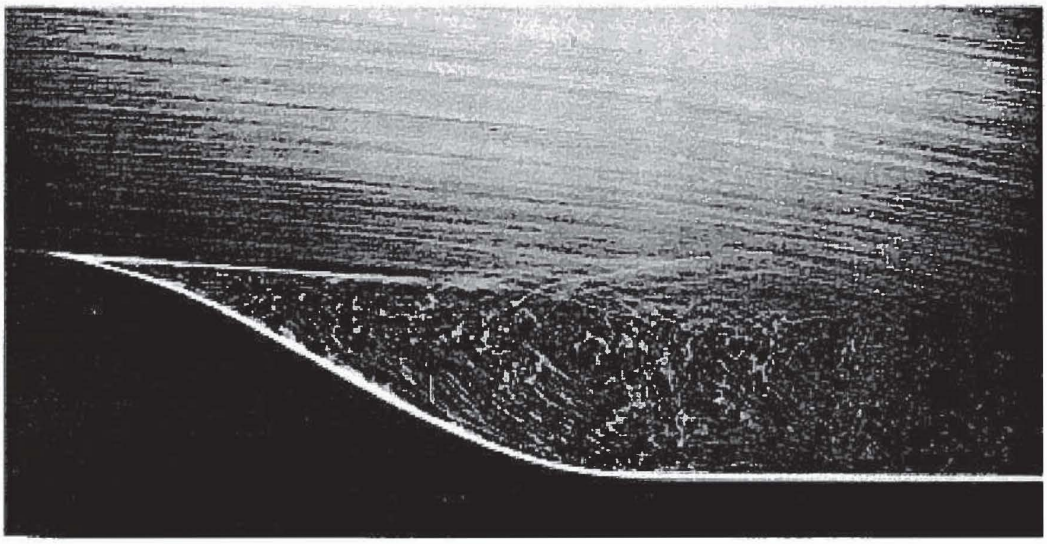

Figure 15.34 Flow in the Region of a Curved Wall Similar to the Wall of a Diffuser (From Figure 38, p. 27 of *An Album of Fluid Motion* by M. Van Dyke, Parabolic Press, Stanford, CA, 1982.)

The difficulty is that the deceleration of the fluid is inherently unstable. The fluid is decelerated by an increase in the pressure forces which oppose its motion. Furthermore, in the boundary layer near the wall of the diffuser, the fluid is being further decelerated by the action of viscous shear stresses. Unless careful consideration is given to the boundary layer of the flow, it is decelerated at a higher rate than the rest of the flow. The pressure forces and viscous shear stresses that oppose the fluid motion eventually overcome the forward motion in the boundary layer. The pressure gradient established by continued deceleration of the main flow then produces a region of backflow near the wall causing the main flow to separate from the wall as shown in Figure 15.34. In the backflow, eddies are formed in which kinetic energy of the fluid motion is dissipated irreversibly resulting in an increase in entropy. If the incoming flow velocity is increased above this threshold, the eddies form right at the start of the enlargement of the duct and the flow from duct becomes a jet as shown in Figure 9E.10(b). In the separated mode of diffuser operation, the flow is quite irreversible and pressure recovery is very poor.

Specifically, equation (15.123) shows that if the deceleration process is without work or heat transfer, the change in kinetic energy is the same for a given change in enthalpy regardless of the irreversibility of the process. However, note that equation (15.123) does not relate the change in kinetic energy directly to the pressure change. This relationship depends upon the irreversibility and the constitutive relations for the fluid. The effect of the irreversibility is shown in Figure 15.35. Since the slope of the constant pressure lines must be positive, an increase in entropy during the deceleration results in a lower final pressure for the same increase in enthalpy (or the same decrease in kinetic energy), Figure 15.35(a). Stated in another way, the increase in entropy due to irreversibility requires a larger increase in enthalpy (decrease in kinetic energy) to reach the same final pressure because the irreversible dissipation of some of the kinetic energy increased the entropy of the fluid as well as the enthalpy. If the objective were simply to eliminate the kinetic energy, the irreversible diffuser would be as satisfactory as the reversible diffuser.

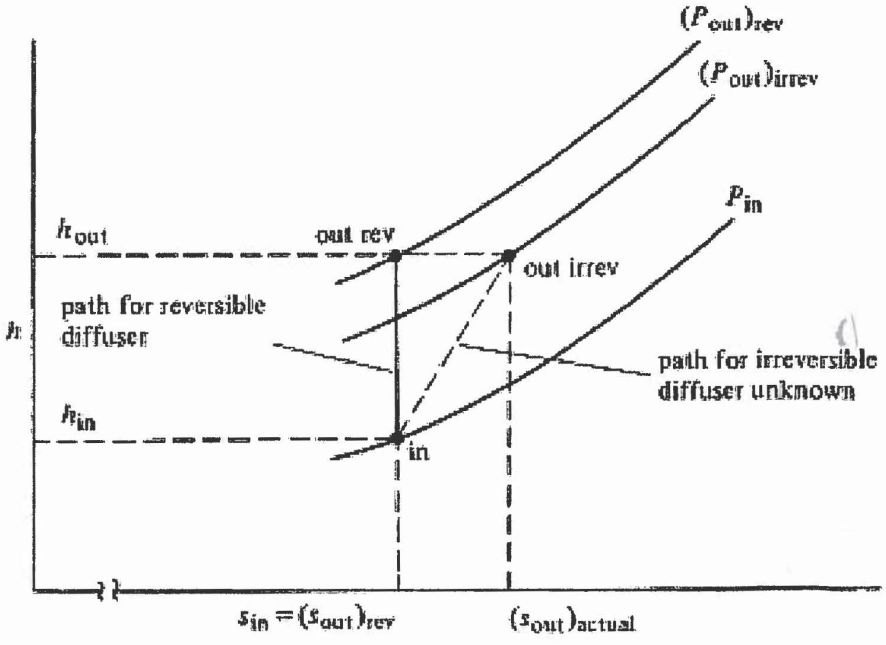

Figure 15.35(a) Pressure Increase for an Ideal Gas Flowing Through a Diffuser with Δh Fi

In engineering practice, the most convenient measure of the influence of irreversibility on the pressure recovery capability of a given diffuser design is the *pressure recovery factor*, C_P, defined as

$$C_P \equiv \frac{P_{out} - P_{in}}{\frac{1}{2}\rho_{in}\mathcal{V}_{in}^2} \tag{15.181}$$

Figure 15.35(a) illustrates the pressure increase that results from a given change in kinetic energy in a diffuser. Clearly $(P_{out})_{rev} > (P_{out})_{irrev}$. As we shall show shortly, the value of C_P, which is dimensionless, is usually determined by carefully controlled experiments and presented in terms of dimensionless characterizations of the geometry and flow of various diffuser designs. It is often compared with the value that would be obtained in the case of reversible, adiabatic operation of the diffuser, $(C_P)_{rev}$. The value of $(C_P)_{rev}$ for a given diffuser geometry will depend upon the nature of the fluid flowing through the diffuser. In the sections that follow, we shall provide more detailed information on the pressure recovery factor for the various fluid models.

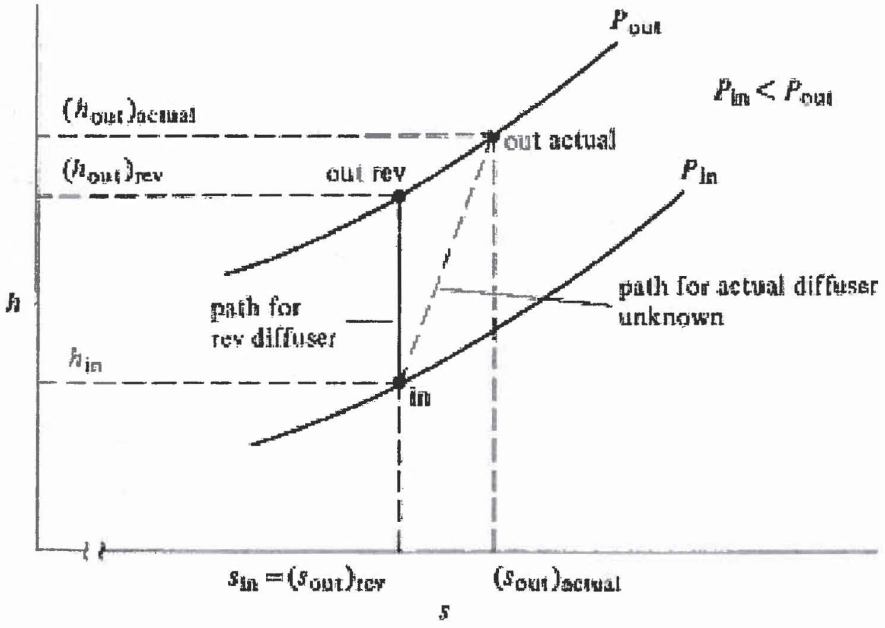

Figure 15.35(b) Kinetic Energy Decrease for an Ideal gas Flowing Through a Diffuser with P_{out} Fixed

In contrast to the situation depicted in Figure 15.35(a), we can adopt an alternative view of the diffuser and examine the way in which a given outlet pressure is achieved through a change in the kinetic energy of the flow. In this case the pressure of the outlet stream is fixed, and we compare the magnitudes of the kinetic energy changes necessary in the reversible and irreversible modes of operation to achieve this outlet pressure. As we would expect, the reversible diffuser utilizes the kinetic energy of the flow more effectively to create a given pressure rise than the irreversible diffuser, and the diffuser efficiency is the performance parameter that expresses the effectiveness of the conversion. The *diffuser efficiency* is defined as

the ratio of the kinetic energy decrease in an ideal reversible, adiabatic diffuser to the kinetic energy decrease in an actual irreversible, adiabatic diffuser where the two diffusers have the same inlet state and outlet pressure. Thus,

$$\eta_D = \frac{\left(\frac{\vartheta_{in}^2}{2} - \frac{\vartheta_{out}^2}{2}\right)_{rev}}{\left(\frac{\vartheta_{in}^2}{2} - \frac{\vartheta_{out}^2}{2}\right)_{actual}} \tag{15.182}$$

Substituting equation (15.123) into equation (15.182), we get

$$\eta_D = \frac{(h_{out} - h_{in})_{rev}}{(h_{out} - h_{in})_{actual}} \tag{15.183}$$

Note: Several definitions of diffuser efficiency other than equation (15.182) are currently in use. This must be kept in mind when reviewing the literature. One additional definition, in particular, is the total pressure recovery factor, $(P_0)_{out}/(P_0)_{in}$, defined as

$$\frac{(P_0)_{out}}{(P_0)_{in}} = \frac{\left(P + \frac{1}{2}\rho\vartheta^2\right)_{out}}{\left(P + \frac{1}{2}\rho\vartheta^2\right)_{in}} \tag{15.184}$$

where the total (stagnation) pressure is determined by bringing the fluid to rest adiabatically and reversibly. We now show how equations (15.183) and (15.184) are related to one another depending upon the model for the fluid flowing through the diffuser.

15.4.1 Diffusers Decelerating an Ideal Gas

The effect of the constitutive relations for the fluid on the performance of the diffuser can be illustrated by considering the two simple models – the ideal gas and the incompressible fluid. If the fluid can be modeled as an ideal gas, the change in kinetic energy can be determined from equation (15.133) in the general adiabatic case or from equation (15.134) in the reversible adiabatic case. For the irreversible case the diffuser efficiency, equation (15.183), reduces to

$$(\eta_D)_{\substack{ideal \\ gas}} = \frac{(T_{out} - T_{in})_{rev}}{(T_{out} - T_{in})_{actual}} \tag{15.185}$$

Figure 15.35(b) illustrates the change in kinetic energy that results for a given pressure increase in the fluid for both reversible and irreversible deceleration. The diffuser efficiency can be interpreted geometrically as the ratio of the vertical distances between the inlet and outlet states on Figure 15.35(b). The details of the ideal gas case are shown in Figure 15.36.

We can rewrite equation (15.185) in the form

$$(\eta_D)_{\substack{ideal \\ gas}} = \frac{T_{in}\left(\frac{T_{out}}{T_{in}} - 1\right)_{rev}}{T_{in}\left(\frac{T_{out}}{T_{in}} - 1\right)_{actual}} = \frac{\left(\frac{T_{out}}{T_{in}} - 1\right)_{rev}}{\left(\frac{T_{out}}{T_{in}} - 1\right)_{actual}} = \frac{\left(\frac{T_{out}}{T_{in}}\right)_{rev} - 1}{\frac{(T_{out})_{actual}}{(T_{out})_{rev}}\left(\frac{T_{out}}{T_{in}}\right)_{rev} - 1} \tag{15.186}$$

We now need to evaluate the ratio of the temperatures for the reversible case and the irreversible case. From the first law, the total enthalpy of the flow is constant, viz.

$$\frac{dE_{cv}}{dt} = \dot{Q} - \dot{W}_{shaft} + \dot{m}\left[h + \frac{\vartheta^2}{2} + gz\right]_{in} - \dot{m}\left[h + \frac{\vartheta^2}{2} + gz\right]_{out}$$
$$\left(h + \frac{\vartheta^2}{2}\right)_{in} = \left(h + \frac{\vartheta^2}{2}\right)_{out} \tag{15.187}$$

If the flow is brought to rest adiabatically and reversibly, equation (15.186) becomes

$$h_0 = \left(h + \frac{\vartheta^2}{2}\right)_i = \text{constant} \tag{15.188}$$

where i denotes any location in the flow field. As shown in Figure 15.36, the maximum value for the stagnation pressure in the flow must occur at the intersection of the locus of states given by $h = h_0$ and the locus of states with entropy $s = s_1$. All other possible values of the stagnation

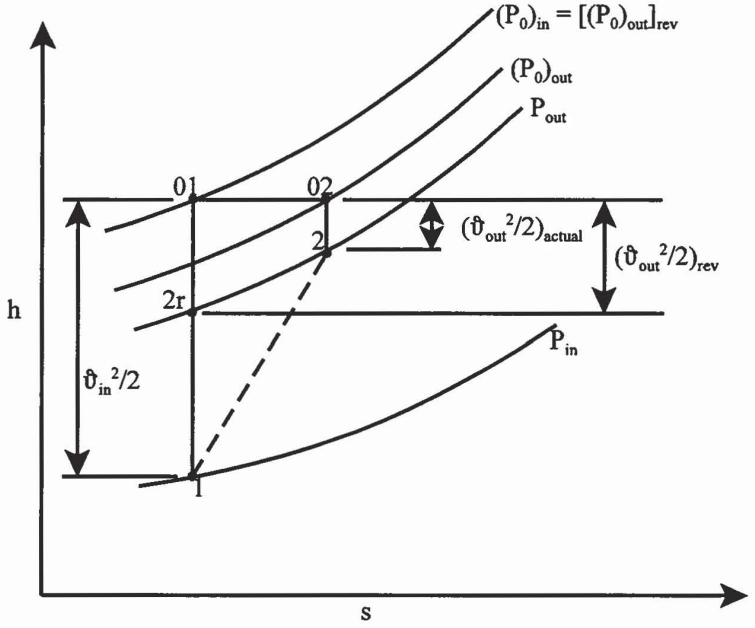

Figure 15.36 States of the Ideal Gas for Flow Through a Diffuser

pressure must lie along the locus of states $h = h_0$ and lesser values of pressure as entropy is generated by the irreversibility of the flow. In order to evaluate the temperatures at the discharge of the reversible and irreversible diffusers as they appear in equation (15.186), we need to establish the relationship between states 2r and 2 as shown in Figure 15.36 since $T_{2r} = (T_{out})_{rev}$ and $T_2 = (T_{out})_{actual}$. Along the isobar $P = P_{out}$, the temperature change is given by

$$dT = \left(\frac{\partial T}{\partial s}\right)_P ds \tag{15.189}$$

but by definition, the specific heat at constant pressure is given by

$$c_P \equiv T\left(\frac{\partial s}{\partial T}\right)_P \tag{15.190}$$

Then equation (15.189) becomes

$$dT = \frac{T}{c_P} ds \tag{15.191}$$

Then the entropy generated by the irreversible operation of the diffuser becomes

$$s_2 - s_1 = \int_{s_1}^{s_2} ds = \int_{T_{2r}}^{T_2} c_P \frac{dT}{T} = c_P \ln \frac{T_2}{T_{2r}} \tag{15.192}$$

It now remains to evaluate the entropy generated.

Along the locus of stagnation states $h = h_0 =$ constant shown in Figure 15.36, we have from equation (15.13)

$$dh = Tds + vdP \tag{15.13}$$

Then

$$dh_0 = 0 = T_0 ds_0 + v_0 dP_0$$

$$ds_0 = -\frac{v_0}{T_0} dP_0 = -\frac{RT_0}{T_0} \frac{dP_0}{P_0}$$

$$s_{02} - s_{01} = \int_{s_{01}}^{s_{02}} ds = -R \int_{P_{01}}^{P_{02}} \frac{dP_0}{P_0} = R \ln \frac{P_{01}}{P_{02}} \tag{15.193}$$

The entropy changes in equations (15.192) and (15.193) are identical. Then it follows that

$$c_P \ln \frac{T_2}{T_{2r}} = R \ln \frac{P_{01}}{P_{02}}$$

or

$$\frac{T_2}{T_{2r}} = \left(\frac{P_{01}}{P_{02}} \right)^{R/c_P} = \left(\frac{P_{01}}{P_{02}} \right)^{\gamma - 1/\gamma} \tag{15.194}$$

For the reversible operation of the diffuser,

$$\left(\frac{T_{out}}{T_{in}} \right)_{rev} = \left(\frac{P_{out}}{P_{in}} \right)^{\gamma - 1/\gamma} = \left(\frac{P_2}{P_1} \right)^{\gamma - 1/\gamma} \tag{15.195}$$

Then substituting equations (15.194) and (15.195) into (15.186), the diffuser efficiency for the ideal gas model becomes

$$(\eta_D)_{\substack{ideal \\ gas}} = \frac{\left(\frac{P_2}{P_1} \right)^{\gamma - 1/\gamma} - 1}{\left[\left(\frac{P_{01}}{P_{02}} \right) \left(\frac{P_2}{P_1} \right) \right]^{\gamma - 1/\gamma} - 1} \tag{15.196}$$

Equation (15.196) is plotted in Figure 15.37 for the case $\gamma = 1.4$. Since the stagnation pressure ratio serves as a measure of the irreversibility, Figure 15.37 clearly shows the effect of the irreversibility of the flow on the efficiency of the diffuser in utilizing the kinetic energy of the fluid to produce a given increase in pressure through deceleration of the flow. For a given static pressure ratio across the diffuser, the poorer the recovery of stagnation pressure, the greater the irreversibility of the flow and the smaller the value of efficiency.

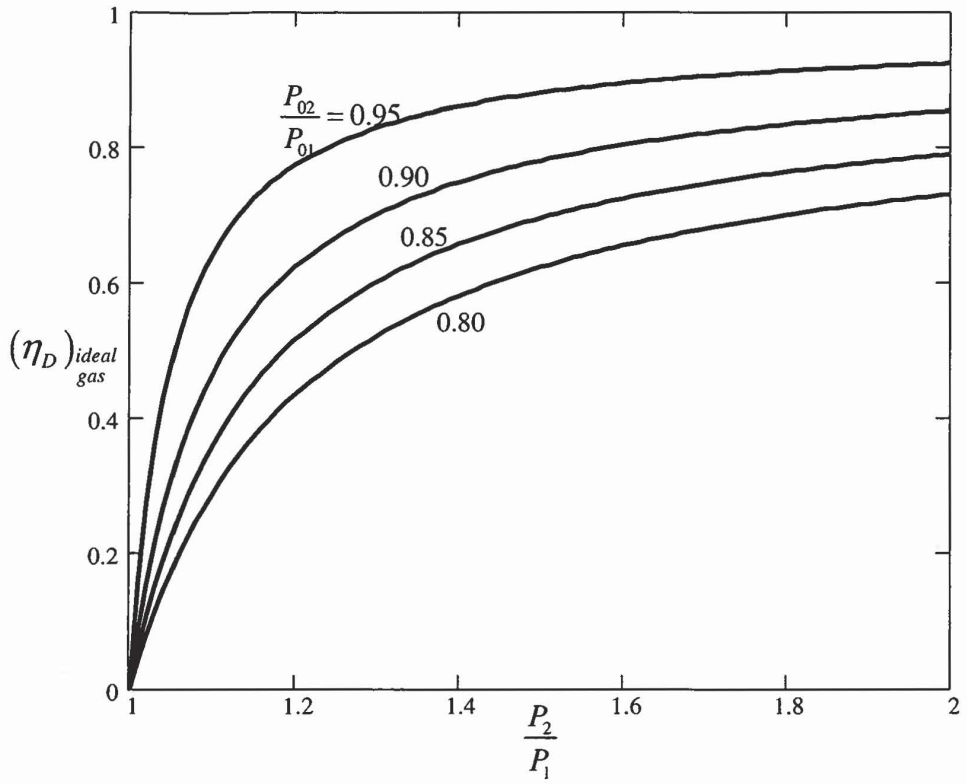

Figure 15.37 Effect of Pressure Recovery Ratio on Diffuser Efficiency for an Ideal Gas ($\gamma = 1.4$)

The details of the internal fluid dynamics of the flow of an ideal gas through a diffuser naturally divides into three regimes:

(1) If the flow is slow enough to be modeled as incompressible ($M \leq 0.3$), the compressibility effects can be neglected and the gas can be modeled as incompressible. This situation is treated in both Chapter 9 and the following section.

(2) If the flow Mach number is such that $0.3 < M < 1.0$, the case of reversible flow can be treated by the equations of reversible flow given in Section 15.3.1. For the irreversible case, flow should be divided into two regions: (1) the viscous boundary layer and (2) the inviscid core. For the latter region, the details of the flow field can be determined from a solution of Euler's equation or from potential flow theory, but for the former, the shape and thickness of the boundary layer must be determined from a solution of the Navier-Stokes equation. If the diffuser is long enough for the onset of turbulence, the turbulence is an additional factor that must be included in the analysis. The important point in this case is that the flow passage through the diffuser must be designed to minimize the possibility of flow separation.

(3) If the flow Mach number is such that the flow is supersonic ($M \geq 1.0$), the situation becomes very complicated by the presence of shock waves in the flow, both external to the diffuser as well as internal. In these cases the reader is referred to the many specialized treatments of this topic.

It should be noted that one of the most common applications of ideal gas flow in a diffuser is the case of diffusers at the inlet to gas turbine engines, specifically the inlet to axial

flow compressors. In such cases, one of the most important issues is the uniformity of the flow, so much so that the efficiency of the diffuser is often of secondary importance.

Example 15E.11: A subsonic diffuser suitable for use on the engine of a commercial aircraft has been tested at sea level conditions (T_∞ = 288.15 K, P_∞ = 1.01325 x 10^5 N/m^2) with an inlet area of A_1 = 0.140 m^2 and an inlet Mach number of M_1 = 0.9. At the outlet of the diffuser, M_2 = 0.2 but due to irreversibilities in the flow, the total pressure recovery is not complete and the total pressure at outlet is $P_{02} = 0.9P_{01}$. The fluid flowing is air which can be modeled as an ideal gas with γ = 1.4 and R = 287 J/kg K.

(a) Determine the change in kinetic energy per unit mass flow rate for the fluid as it flows through the diffuser.

(b) Determine the cross-sectional area A_2 of the diffuser at the outlet.

(c) Calculate the adiabatic efficiency η_D of the diffuser.

(d) Evaluate the static pressure recovery factor, C_P, for the device.

Solution: The Mach number of the flow is such that the analysis must include compressibility effects as presented in Section 15.3.1.

(a) Since we seek the change in kinetic energy of the fluid as it flows through the diffuser and we have information only for the Mach number, we need to evaluate the speed of sound at the entrance and exit. Using the ideal gas model we have

$$a_1 = \sqrt{\gamma R T_\infty} = \sqrt{1.4(287 \text{ J/kg K})(288.15 \text{ K})} = 340.26 \text{ m/sec}$$

Then the velocity at entrance is

$$\vartheta_1 = a_1 M_1 = (340.26 \text{ m/sec})(0.9) = 306.24 \text{ m/sec}$$

At the exit plane, we need to determine the local thermodynamic temperature first so that we can evaluate the local speed of sound. In equation (15.187) we showed that the stagnation enthalpy (total enthalpy) is constant throughout an adiabatic flow. If the specific heat at constant pressure is constant for the ideal gas model, then the stagnation temperature is also constant throughout the flow. Then at entrance, we have from equation (15.153)

$$T_{01} = T_\infty \left[1 + \frac{\gamma - 1}{2} M_1^2\right] = (288.15 \text{ K})\left[1 + \frac{1.4 - 1}{2}(0.9)^2\right] = 334.83 \text{ K}$$

Also from equation (15.153) we have

$$T_2 = T_{02}\left[1 + \frac{\gamma - 1}{2} M_2^2\right]^{-1} = (334.83 \text{ K})\left[1 + \frac{1.4 - 1}{2}(0.2)^2\right]^{-1} = 332.17 \text{ K}$$

Then the local speed of sound is

$$a_2 = \sqrt{\gamma R T_2} = \sqrt{1.4(287 \text{ J/kg K})(332.17 \text{ K})} = 365.33 \text{ m/sec}$$

and the local velocity at exit is

$$\vartheta_2 = a_2 M_2 = (365.33 \text{ m/sec})(0.2) = 73.066 \text{ m/sec}$$

Then the change in kinetic energy per unit mass flow rate becomes

$$\frac{(\Delta KE)_{actual}}{\dot{m}} = \frac{1}{2}\left(\vartheta_2^2 - \vartheta_1^2\right)_{actual} = \frac{1}{2}\left[(73.066 \text{ m/sec})^2 - (306.24 \text{ m/sec})^2\right] = 4.422 \text{ x } 10^4 \text{ J/kg}$$

(b) To determine the area at the exit plane of the diffuser, we make use of equation (15.164), viz.

$$\dot{m} = A_1\sqrt{\frac{\gamma}{R}}\frac{P_1}{\sqrt{T_0}}M_1\sqrt{1+\frac{\gamma-1}{2}M_1^2} = A_2\sqrt{\frac{\gamma}{R}}\frac{P_2}{\sqrt{T_0}}M_2\sqrt{1+\frac{\gamma-1}{2}M_2^2}$$

$$\frac{A_2}{A_1} = \frac{P_1M_1\sqrt{1+\frac{\gamma-1}{2}M_1^2}}{P_2M_2\sqrt{1+\frac{\gamma-1}{2}M_2^2}}$$

If we substitute equation (15.155) for the static pressure in terms of the total pressure, we can take into account the irreversibility of the flow, viz.

$$P_1 = P_{01}\left[1+\frac{\gamma-1}{2}M_1^2\right]^{\frac{\gamma}{1-\gamma}} \quad \text{and} \quad P_2 = P_{02}\left[1+\frac{\gamma-1}{2}M_2^2\right]^{\frac{\gamma}{1-\gamma}}$$

We get

$$\frac{A_2}{A_1} = \frac{P_{01}M_1\left[1+\frac{\gamma-1}{2}M_1^2\right]^{\frac{1+\gamma}{2(1-\gamma)}}}{P_{02}M_2\left[1+\frac{\gamma-1}{2}M_2^2\right]^{\frac{1+\gamma}{2(1-\gamma)}}} = \frac{P_{01}(0.9)\left[1+\frac{1.4-1}{2}(0.9)^2\right]^{\frac{1+1.4}{2(1-1.4)}}}{(0.9)P_{01}(0.2)\left[1+\frac{1.4-1}{2}(0.2)^2\right]^{\frac{1+1.4}{2(1-1.4)}}} = 3.2639$$

Then

$$A_2 = (3.2639)(0.140\ \text{m}^2) = 0.457\ \text{m}^2$$

(c) To determine the adiabatic efficiency of the diffuser, we can make use of equation (15.196), viz.

$$(\eta_D)_{\substack{ideal\\gas}} = \frac{\left(\frac{P_2}{P_1}\right)^{\gamma-1/\gamma}-1}{\left[\left(\frac{P_{01}}{P_{02}}\right)\left(\frac{P_2}{P_1}\right)\right]^{\gamma-1/\gamma}-1}$$

The ratio of the static pressures is given by

$$\frac{P_2}{P_1} = \frac{P_{02}\left[1+\frac{\gamma-1}{2}M_1^2\right]^{\frac{\gamma}{\gamma-1}}}{P_{01}\left[1+\frac{\gamma-1}{2}M_2^2\right]^{\frac{\gamma}{\gamma-1}}} = \frac{(0.9)P_{01}\left[1+\frac{1.4-1}{2}(0.9)^2\right]^{\frac{1.4}{1.4-1}}}{P_{01}\left[1+\frac{1.4-1}{2}(0.2)^2\right]^{\frac{1.4}{1.4-1}}} = 1.4803$$

Then

$$(\eta_D)_{\substack{ideal\\gas}} = \frac{\left(\frac{P_2}{P_1}\right)^{\gamma-1/\gamma}-1}{\left[\left(\frac{P_{01}}{P_{02}}\right)\left(\frac{P_2}{P_1}\right)\right]^{\gamma-1/\gamma}-1} = \frac{(1.4803)^{\frac{1.4-1}{1.4}}-1}{\left[\left(\frac{P_{01}}{(0.9)P_{01}}\right)(1.4803)\right]^{\frac{1.4-1}{1.4}}-1} = 0.776$$

(d) The static pressure recovery factor, C_P, is given by equation (15.181), viz.

$$C_P = \frac{P_2 - P_1}{\frac{1}{2}\rho_1 \vartheta_1^2} = \frac{\frac{P_2}{P_1}P_1 - P_1}{0.5\left(\frac{P_1}{RT_1}\right)\vartheta_1^2} = \frac{(1.01325 \times 10^5 \text{ N/m}^2)(1.4803-1)}{0.5\left[\frac{(1.01325 \times 10^5 \text{ N/m}^2)}{(287 \text{ J/kg K})(288.15 \text{ K})}\right](306.24 \text{ m/sec})^2} = 0.847$$

15.3.7 Diffusers Decelerating an Incompressible Fluid

For those cases in which the fluid can be modeled as an incompressible fluid and the outlet pressure is fixed, reversible diffuser operation can be described by equation (15.178). For the irreversible case, equation (15.177) must be used. From equation (15.177), it is apparent that in the irreversible case some of the mechanical kinetic energy is dissipated into uncoupled thermal energy. For this case the diffuser efficiency reduces to

$$(\eta_D)_{incompressible} = 1 - \frac{c(T_{out} - T_{in})}{c(T_{out} - T_{in}) + v(P_{out} - P_{in})} \tag{15.197}$$

Equation (15.197) has much the same interpretation as equation (15.180), i.e., the second term on the right-hand side represents the fraction of the kinetic energy converted into stored thermal energy as a result of the irreversibility in the flow. The locus of states for the incompressible fluid flowing through the diffuser with a fixed outlet pressure is shown in Figure 15.38(a).

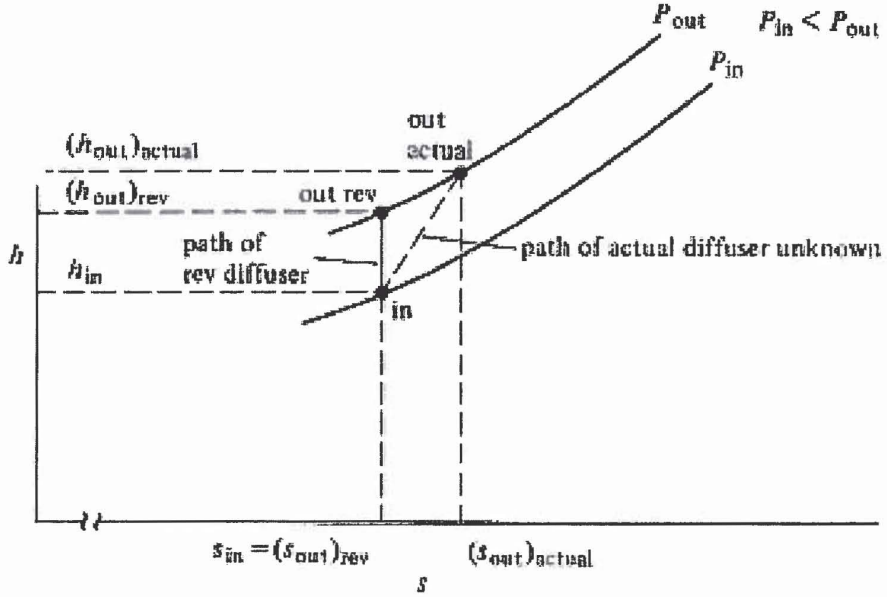

Figure 15.38(a) States of an Incompressible Fluid Flowing Through a Diffuser with P_{out} Fixed

For reversible operation with an incompressible fluid,

$$(h_{out} - h_{in})_{rev} = \frac{(P_{out} - P_{in})}{\rho} \tag{15.198}$$

and for irreversible operation

$$(h_{out} - h_{in})_{actual} = \left(\frac{\vartheta_{in}^2}{2} - \frac{\vartheta_{out}^2}{2}\right)_{actual} \tag{15.199}$$

Substituting equations (15.198) and (15.199) into equation (15.183), we get another expression

for the diffuser efficiency with an incompressible fluid flowing, viz.

$$(\eta_D)_{\rho=const} = \frac{2(P_{out} - P_{in})}{\rho\left(\vartheta_{in}^2 - \vartheta_{\substack{out \\ actual}}^2\right)} \tag{15.200}$$

Note that the outlet static pressure is the same in both the reversible and irreversible modes of operation but the velocities at outlet are different. Equation (15.200) can be expressed in terms of pressures only. Rewrite equation (15.183) in the form

$$\eta_D = \frac{\left(h_{\substack{out \\ rev}} - h_{in}\right)}{\left(h_{\substack{out \\ actual}} - h_{\substack{out \\ rev}}\right) + \left(h_{\substack{out \\ rev}} - h_{in}\right)} = \frac{1}{1 + \dfrac{\left(h_{\substack{out \\ actual}} - h_{\substack{out \\ rev}}\right)}{\left(h_{\substack{out \\ rev}} - h_{in}\right)}} \tag{15.201}$$

but

$$h_{\substack{out \\ actual}} - h_{\substack{out \\ rev}} = \left(h_{\substack{out \\ actual}} - h_{in}\right) - \left(h_{\substack{out \\ rev}} - h_{in}\right) \tag{15.202}$$

Substituting the first law and equation (15.200) into equation (15.202), we get

$$h_{\substack{out \\ actual}} - h_{\substack{out \\ rev}} = \left(\frac{\vartheta_{in}^2}{2} - \frac{\vartheta_{\substack{out \\ actual}}^2}{2}\right) - \left(\frac{P_{out} - P_{in}}{\rho}\right) = \frac{\left[(P_0)_{in} - (P_0)_{\substack{out \\ actual}}\right]}{\rho} \tag{15.203}$$

where we have made use of the total (stagnation) pressure, P_0. Substituting equation (15.203) into equation (15.201), we get

$$(\eta_D)_{\rho=const} = \frac{1}{1 + \dfrac{\left[(P_0)_{in} - (P_0)_{\substack{out \\ actual}}\right]}{(P_{out} - P_{in})}} \tag{15.204}$$

This is a particularly convenient form for the diffuser efficiency for the incompressible fluid model since stagnation pressures and static pressures are easy to measure with relatively simple instrumentation.

Alternatively, the thermal-fluids engineer might be interested in the pressure rise that could be achieved with a given decrease in kinetic energy. In this case the change in enthalpy of the fluid would be fixed and the path of the process would appear as shown in Figure 15.38(b). Then if the fluid (gas or liquid) can be modeled as an incompressible fluid, we can evaluate the pressure recovery coefficient for reversible, adiabatic operation rather simply. From the first law,

$$\frac{\vartheta_{in}^2}{2} + \frac{P_{in}}{\rho} = \frac{\vartheta_{out}^2}{2} + \frac{P_{out}}{\rho}$$

$$P_{out} - P_{in} = \rho\left(\frac{\vartheta_{in}^2}{2} - \frac{\vartheta_{out}^2}{2}\right) \tag{15.205}$$

From continuity,

$$\vartheta_{in} A_{in} = \vartheta_{out} A_{out}$$

$$\vartheta_{out} = \vartheta_{in} \frac{A_{in}}{A_{out}} \tag{15.206}$$

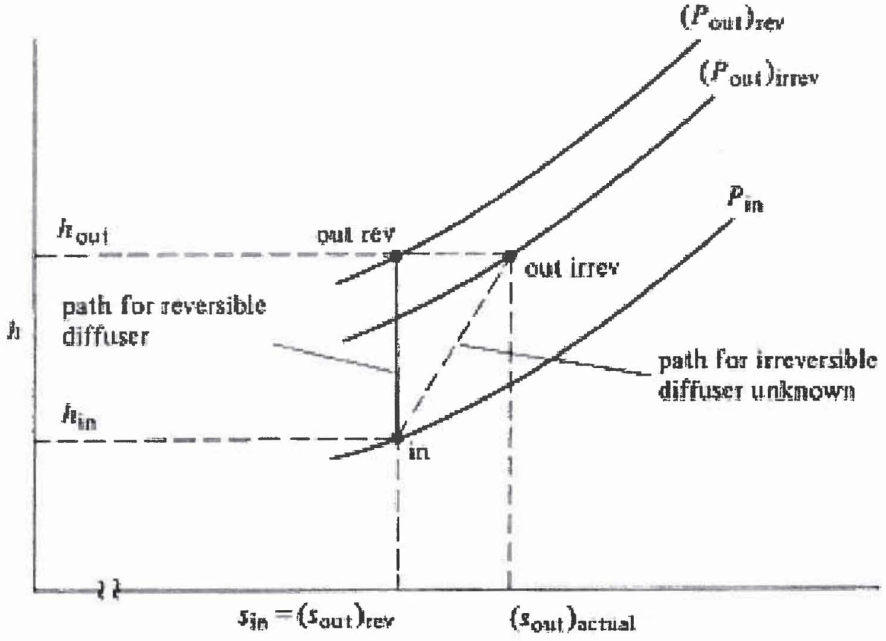

Figure 15.38(b) Pressure Increase for an Incompressible Fluid Flowing Through a Diffuser with Δh Fixed

Combining equations (15.205) and (15.206), we get for the reversible case

$$(P_{out} - P_{in})_{rev} = \frac{\rho \vartheta_{in}^2}{2}\left[1 - \left(\frac{A_{in}}{A_{out}}\right)^2\right] \tag{15.207}$$

Substituting equation (15.207) into equation (15.181), we get

$$(C_P)_{\substack{rev \\ \rho=const}} = \frac{\frac{\rho \vartheta_{in}^2}{2}\left[1 - \left(\frac{A_{in}}{A_{out}}\right)^2\right]}{\frac{\rho \vartheta_{in}^2}{2}} = 1 - \left(\frac{A_{in}}{A_{out}}\right)^2 \tag{15.208}$$

The area ratio $A_R = A_{out}/A_{in}$ is one of the dimensionless parameters used to characterize the geometry of a diffuser. Then equation (15.208) can be written

$$(C_P)_{\substack{rev \\ \rho=const}} = 1 - \left(\frac{1}{A_R^{\,2}}\right) = 1 - \left(\frac{\vartheta_{out}}{\vartheta_{in}}\right)^2 \tag{15.209}$$

The total (stagnation) pressures at inlet and outlet are given by

$$(P_0)_{in} = P_{in} + \frac{1}{2}\rho \vartheta_{in}^2 \quad \text{and} \quad (P_0)_{\substack{out \\ actual}} = (P_{out})_{irrev} + \frac{1}{2}\rho \vartheta_{out}^2 \tag{15.210}$$

Then

$$(\Delta P_0)_{actual} = (P_0)_{in} - (P_0)_{\substack{out \\ actual}} = \left[P_{in} - (P_{out})_{irrev}\right] + \frac{1}{2}\rho\left(\vartheta_{in}^2 - \vartheta_{out}^2\right)$$

$$(\Delta P_0)_{actual} = \left(P_{in} - P_{\substack{out \\ actual}}\right) + \frac{1}{2}\rho\vartheta_{in}^2\left(1 - \frac{\vartheta_{out}^2}{\vartheta_{in}^2}\right)$$

$$\frac{(\Delta P_0)_{actual}}{\frac{1}{2}\rho\vartheta_{in}^2} = \frac{\left(P_{in} - P_{\substack{out \\ actual}}\right)}{\frac{1}{2}\rho\vartheta_{in}^2} + \left(1 - \frac{\vartheta_{out}^2}{\vartheta_{in}^2}\right) = -(C_P)_{actual} + (C_P)_{rev}$$

$$(C_P)_{actual} = (C_P)_{rev} - \frac{(\Delta P_0)_{actual}}{\frac{1}{2}\rho\vartheta_{in}^2} \tag{15.211}$$

In thermal-fluids engineering practice, it is commonly the case that data obtained from carefully performed experiments are used to determine the values of the pressure recovery coefficient appropriate for a given situation. The geometry for a typical conical diffuser is shown in Figure 15.39 with experimental data in Figure 15.40.

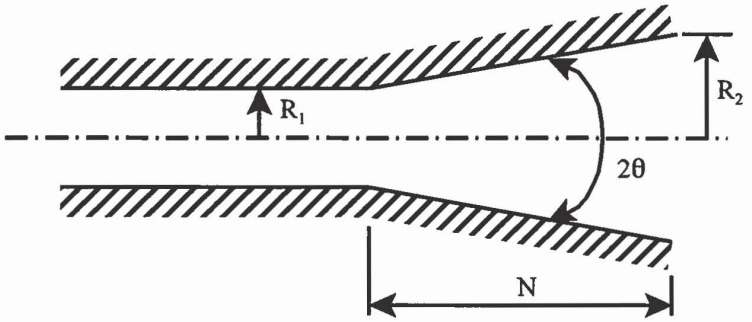

Figure 15.39 Geometry for a Conical Diffuser

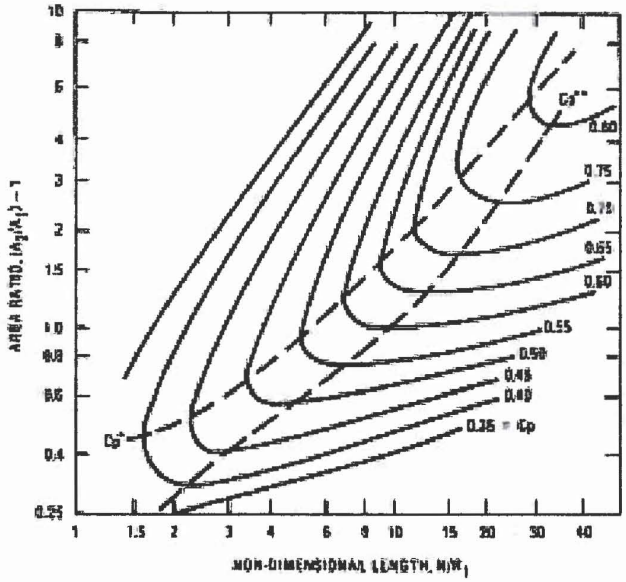

Figure 15.40 Static Pressure Recovery Coefficient for Conical Diffusers with $Re > 75 \times 10^3$

(From Fig. 7-12, p. 152, *Applied Fluid Dynamics Handbook*, by R. D. Blevins, Krieger Publishing Co., Malabar, FL, 1984.)

Note that for conical diffusers

$$A_R = \frac{A_2}{A_1} = \left(1 + \frac{N}{R_1}\tan\theta\right)^2 \tag{15.212}$$

Also note that on Figure 15.40, C_P^* is the locus of points that defines the diffuser area ratio A_R that produces the maximum static pressure recovery for a given dimensionless length, N/R_1, and $C_P^{**}$is the locus of points that defines the diffuser dimensionless length, N/R_1, that produces the maximum pressure recovery for a given area ratio, A_R.

It should also be noted that some investigators define a *diffuser effectiveness*, ε_D, such that

$$\varepsilon_D \equiv \frac{(C_P)_{actual}}{(C_P)_{rev}} \tag{15.213}$$

Data for the diffuser effectiveness can be found in the literature.

Example 15E.12: An air conditioning system in a large building has an air duct with a diameter of $D_1 = 0.5$ m. Air with a density of $\rho_1 = 1.2$ kg/m^3 and a temperature of $T_1 = 20$ C flows in the duct at a velocity of 2.5 m/sec. A diffuser must be installed to reduce the velocity and increase the air pressure to atmospheric pressure before the air can be discharged from the duct into a room. Space limitations suggest a dimensionless length ratio of $N/R_1 = 10$. The viscosity of the air is $\mu = 1.8249 \times 10^{-5}$ kg/m sec.

(a) Determine the area of the outlet of the diffuser.

(b) Determine the pressure at entrance to the diffuser that will result in an exit pressure of atmospheric pressure.

Solution: (a) The velocity of the air is clearly small enough that we can model the flow as incompressible. Then we can use Figure 15.40 to evaluate the pressure recovery factor so we need to make sure that the Reynolds number requirement is met. The Reynolds number for this flow is

$$Re = \frac{\vartheta_1 D_1 \rho_1}{\mu_1} = \frac{(2.5 \text{ m/sec})(0.5 \text{ m})(1.2 \text{ kg/m}^3)}{1.8249 \times 10^{-5} \text{ kg/m sec}} = 82.196 \times 10^3$$

The Reynolds number exceeds the lower limit of 75×10^3 for the data of Figure 15.40 so we can use these data. In Figure 15.40, we use the data for C_P^* since these values would give the maximum pressure recovery ratio for a given dimensionless length. From Figure 15.40 we have at the intersection of $N/R_1 = 10$ and the locus of C_P^*, an area ratio of 1.75 and $C_P^* = 0.66$. Then

$$\frac{A_2}{A_1} - 1 = 1.75$$

$$\frac{A_2}{A_1} = 2.75$$

Then the area of the diffuser outlet is

$$A_2 = 2.75\frac{\pi D_1^2}{4} = 2.75\frac{\pi(0.5 \text{ m})^2}{4} = 0.540 \text{ m}^2$$

This gives a diffuser outlet diameter of $D_2 = 0.829$ m. The velocity at the diffuser outlet would then be

$$\vartheta_2 = \frac{A_1}{A_2}\vartheta_1 = \frac{2.5 \text{ m/sec}}{2.75} = 0.909 \text{ m/sec}$$

This velocity is not so high that the occupants of the room would feel chilled by it, but it is a large enough velocity to move loose papers about. Therefore, the diffuser discharge should be directed into a region of the room where this is not likely to occur.

(b) The pressure of the air in the duct can be determined by the pressure recovery factor, viz.

$$P_1 = P_2 + \frac{C_P \rho_1 \vartheta_1^2}{2} = 1.01325 \text{ x } 10^5 \text{ N/m}^2 - \frac{0.66\left(1.20 \text{ kg/m}^3\right)\left(2.5 \text{ m/sec}\right)^2}{2}$$

Clearly, the second term on the right-hand side of the above expression is negligible, so the pressure in the duct just upstream of the diffuser is essentially atmospheric. To be sure, there is a measurable pressure difference, but it is so small that a differential manometer with water as the fluid is usually used to measure it. The duct-work of these air conditioning systems is usually sized on the basis of continuity considerations initially, and then the various head losses are determined using the analysis presented in Chapter 9 to determine the necessary blower capacity.

15.3.8 Diffusers Decelerating a Pure Substance

The behavior of a pure substance when decelerated in a diffuser is between the two extremes represented by the incompressible fluid and the ideal gas models. The loci of states for a pure substance flowing through diffusers with various inlet states are shown in Figure 15.41. In the compressed liquid region, the behavior of the fluid is essentially the same as that of the incompressible fluid model. In the superheat region, the behavior of the pure substance is essentially the same as that of the ideal gas model. However, the definition of the diffuser efficiency, equation (15.183), should be used rather than the expression derived explicitly for the ideal gas model, equation (15.196).

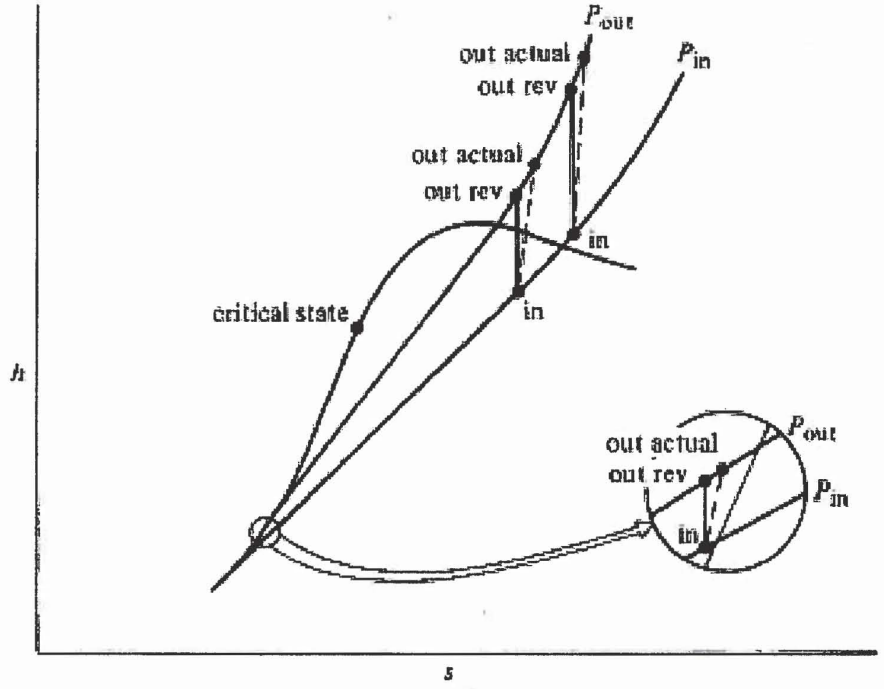

Figure 15.41(a) States of a Pure Substance Flowing Through a Diffuser

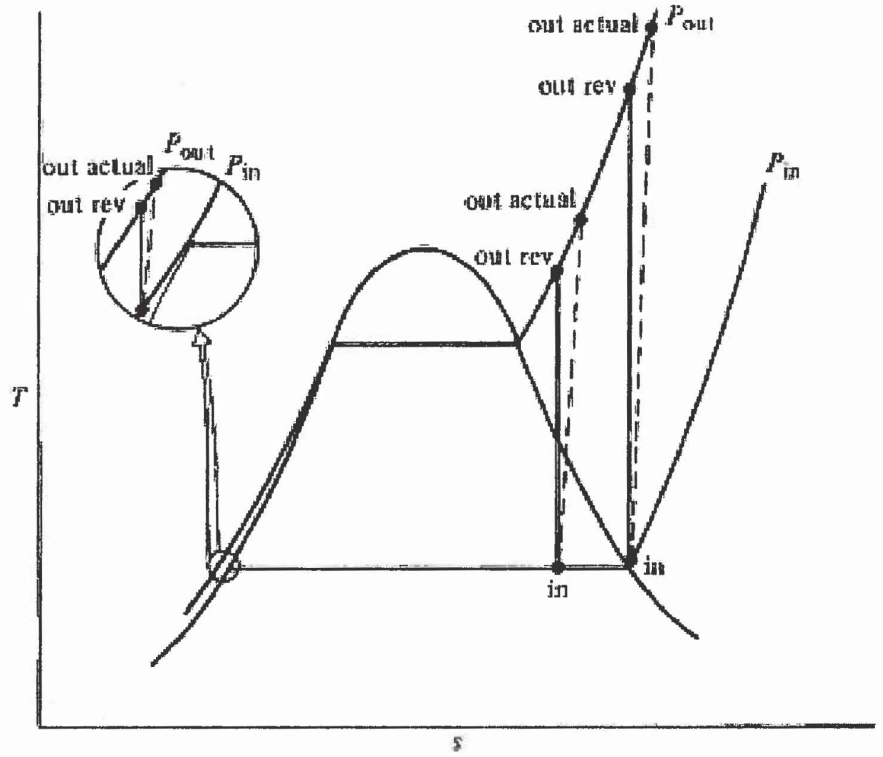

Figure 15.41(b) States of a Pure Substance Flowing Through a Diffuser

When the pure substance enters the diffuser with two phases present, it is usually the case that the exiting flow is superheated vapor. The evaporation of the liquid present at entry causes the density of the flow at exit to be substantially less than would have been the case with liquid present. The exit area of the diffuser must be designed with this in mind.

15.4 Throttle

In the two previous sections, it was stated that the pressure difference (or equivalently the pressure ratio) across the device was externally imposed. The throttle is the most common system component for controlling the pressures of a flowing stream. For specific applications the throttle is also known by various other names such as control valve, expansion valve, Joule-Thomson valve, porous plug, orifice, and flow resistance. Although the names are different, the principle of operation is the same.

In its simplest form, the throttle is nothing more than a port with an adjustable flow area which provides an adjustable resistance to the flow of fluid through the system. An increase in flow resistance requires a greater pressure difference across the throttle for a given flow rate. By adjusting the flow resistance of a throttle on the inlet of a device, we may adjust the inlet pressure while the supply pressure is fixed. Typically, the increase in flow resistance is produced by decreasing the cross sectional area of the flow at one section inside the throttle.

A typical throttle installation is shown schematically in Figure 15.42. The residence time of the fluid within the throttle is insufficient to permit significant heat transfer. The throttle can

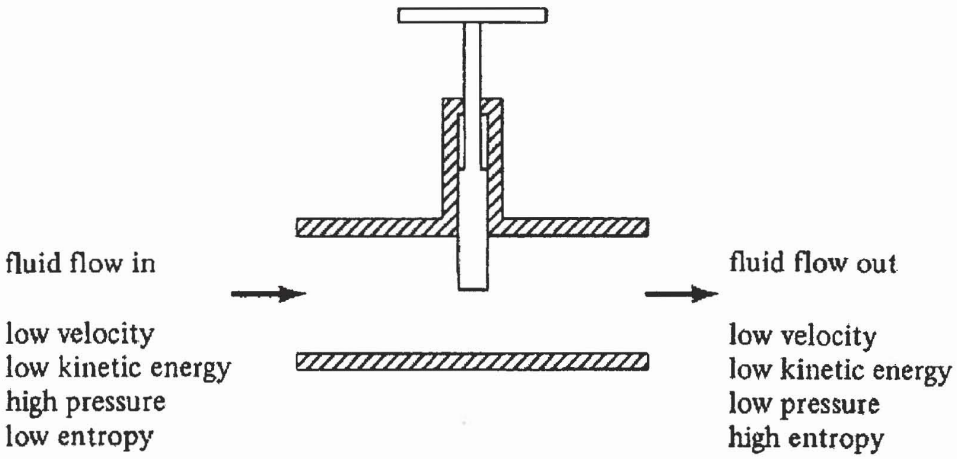

Figure 15.42 Throttle Valve

then be adequately modeled as an adiabatic device. In principle, the throttle is a nozzle in series with a very poor diffuser. In the nozzle section, the flow is accelerated to some velocity while the pressure is decreased to a value P. In the diffuser section, the flow is decelerated to the original velocity ϑ_{in}, but because the diffuser section operates in the separated mode, pressure recovery is poor and the stream returns to the inlet enthalpy with only a small pressure rise. The net result overall is a pressure drop with a significant generation of entropy. Essentially all of the flow irreversibility associated with the throttle is located in the diffuser section. By combining the governing equations for the nozzle and the diffuser, we obtain

$$\dot{m}\left[\left(h_{in}-h\right)+\left(h-h_{out}\right)\right]=\dot{m}\left[\left(\frac{\vartheta^2-\vartheta_{in}^2}{2}\right)+\left(\frac{\vartheta_{out}^2-\vartheta^2}{2}\right)\right] \tag{15.214}$$

or

$$h_{in}-h_{out}=\frac{\vartheta_{out}^2-\vartheta_{in}^2}{2} \tag{15.215}$$

In typical applications of the throttle, we locate the outlet port of the control volume far enough downstream so that the outlet velocity has essentially reached its final value. Typical values of the inlet and outlet velocities are such that the kinetic energies at the inlet and outlet ports are negligible (compared to the enthalpy). Thus,

$$\vartheta_{in}^2 \approx \vartheta_{out}^2 \approx 0 \tag{15.216}$$

Then equation (15.215) becomes

$$h_{in}=h_{out} \tag{15.217}$$

For the case of unit mass flow rate with an infinitesimal change of state, equation (15.1) reduces to

$$dh=0 \tag{15.218}$$

From equation (15.13)

$$dh=Tds+vdP \tag{15.219}$$

Combining equations (15.218) and (15.219), we see that for the throttle

$$Tds=-vdP \tag{15.220}$$

From equation (15.220), it is apparent that in order for there to be a pressure decrease in the

direction of flow through the throttle, the entropy must increase in the direction of flow. Since the throttle is adiabatic, it follows from the second law of thermodynamics that the operation of the throttle must be irreversible if the throttle is to operate in the desired manner. In fact, the throttle is the only thermal-fluid device that *must* be irreversible in order to operate properly.

Note that because the throttle operates in an irreversible manner, the locus of states of the fluid as it passes through the throttle is unknown. That is, even though the inlet and outlet enthalpies of the fluid are identical, the path is not necessarily one of constant enthalpy. The irreversibility internal to the throttle makes it impossible to identify the intermediate states.

15.4.1 Throttling an Ideal Gas

If the fluid can be modeled as an ideal gas, the enthalpy constitutive relation for the ideal gas model shows the enthalpy to be a function of temperature only. Then fore the ideal gas flowing through the throttle, equation (15.217) reduces to

$$T_{in} = T_{out} \tag{15.221}$$

The inlet and outlet states for the ideal gas flowing through the throttle are shown in Figure 15.43.

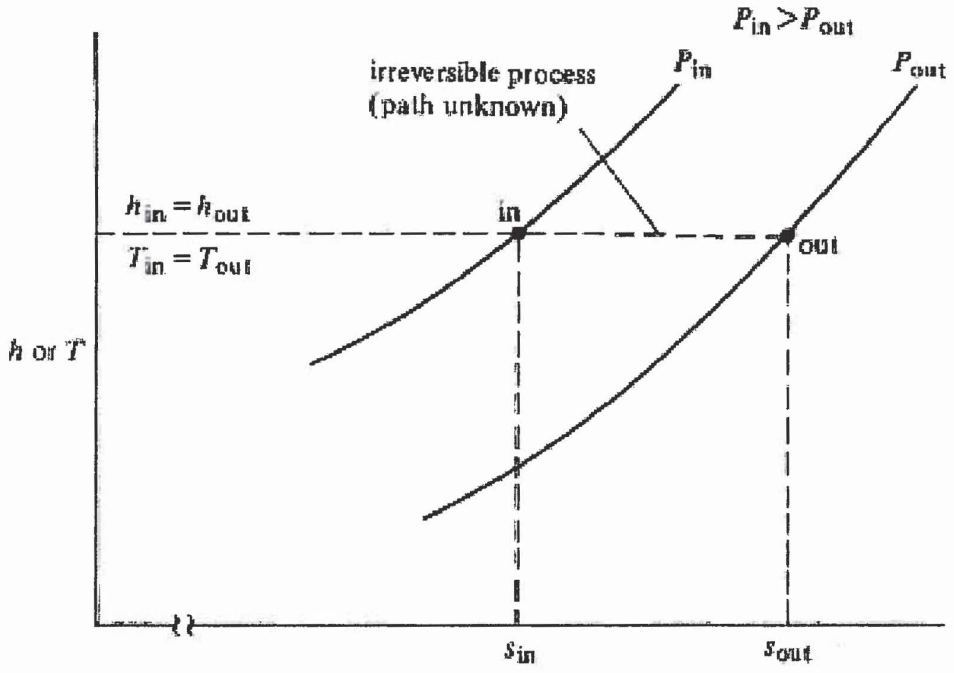

Figure 15.43 Inlet and Outlet States for an Ideal Gas Flowing Through a Throttle

The details of the dynamic behavior of the ideal gas flowing through the throttle cannot be readily elucidated because of the highly irreversible nature of the flow. The thermal-fluids engineer must be content with utilizing the expressions for head loss as presented in Chapter 9. For adjustable throttle valves, many manufacturers provide data for the flow coefficient of gases through their valves.

15.4.2 Throttling an Incompressible Fluid

If the fluid can be modeled as an incompressible fluid, equation (15.217) reduces to

$$u_{out} - u_{in} = v\left(P_{in} - P_{out}\right) \tag{15.222}$$

or

$$c(T_{in} - T_{out}) = v(P_{in} - P_{out}) \tag{15.223}$$

Since $P_{in} > P_{out}$, equation (15.223) shows that the temperature of the incompressible fluid increases as the fluid passes through the throttle. The source of this temperature increase is the irreversibility located in the diffuser section of the throttle. The inlet and outlet states for this case are shown in Figure 15.44.

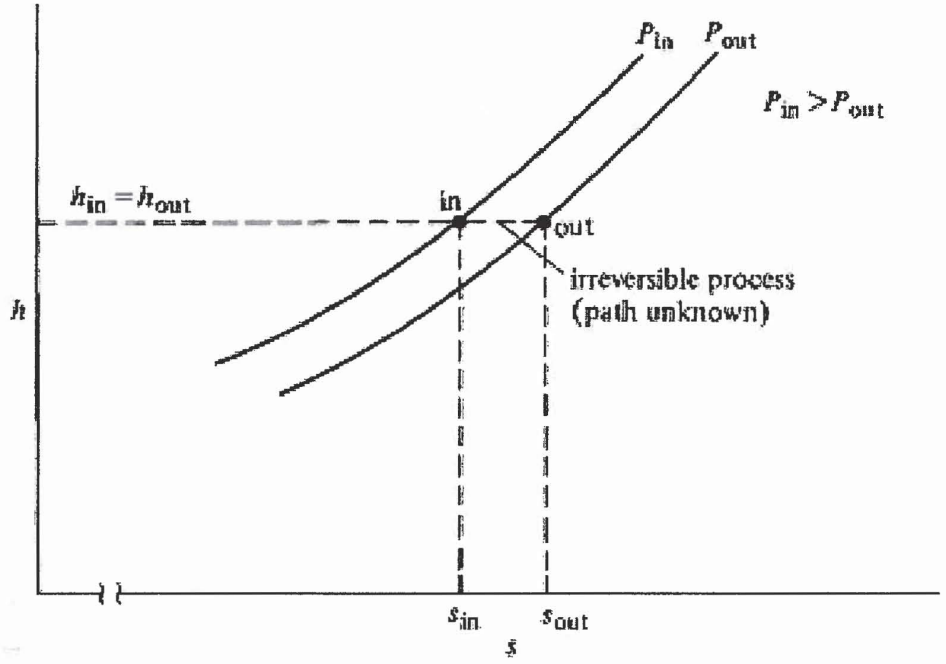

Figure 15.44 Inlet and Outlet States for an Incompressible Fluid Flowing Through a Throttle

15.4.3 Throttling a Pure Substance

In the case of a pure substance, the changes of state that may occur as the fluid passes through the throttle may be significantly different from either of the cases just discussed. The pure substance may either increase or decrease in temperature as a result of the internal dynamics of the throttle. If both the liquid and vapor phases are present, either at the inlet or at the outlet, the temperature of the pure substance will decrease. However, if only the vapor phase is present, at both inlet and outlet, the temperature may increase or decrease depending upon the inlet state. The performance parameter that indicates the outlet temperature of the pure substance as a result of a throttling process is known as the Joule-Thomson coefficient which is denoted by the symbol μ_{JT} and defined as

$$\mu_{JT} \equiv \left(\frac{\partial T}{\partial P}\right)_h \tag{15.224}$$

Although the sequence of states of the pure substance in the throttling process is not a sequence of states with the same values of enthalpy, the inlet and outlet states do have the same values for the enthalpy, and, hence, must lie on the locus of states of constant enthalpy. This is the reason that the partial derivative in equation of equation (15.224) must be formed while holding the enthalpy constant.

In Figure 15.45 we have plotted the locus of states of constant enthalpy as a function of temperature and pressure for the vapor phase of a pure substance. Also shown in Figure 15.45 is the locus of the maxima in the curves of constant enthalpy. This locus is called the inversion curve for the Joule-Thomson coefficient. For states to the left of the inversion curve, μ_{JT} is positive, while for states to the right of the inversion curve, μ_{JT} is negative. Thus, the inversion curve is the locus of states for which $\mu_{JT} = 0$. This is precisely the behavior of the ideal gas model.

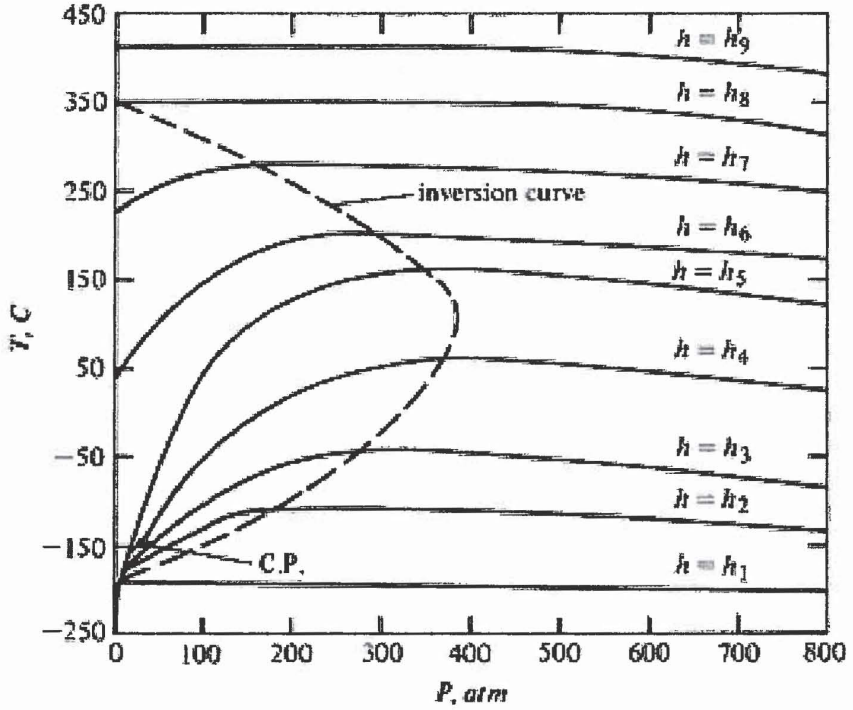

Figure 15.45 Inversion Curve for the Vapor Phase of a Pure Substance (Nitrogen)

If both of the end states are on the right of the inversion curve in Figure 15.45, the temperature must increase. This is behavior is typical of the incompressible fluid model as we saw above and could be termed liquid-like behavior. If both of the end states for a throttle are to the left of the inversion curve on Figure 15.45, the temperature must decrease as the fluid passes through the throttle. This type of behavior is true pure substance behavior. If the two end states are on opposite sides, the temperature may increase or decrease depending upon the exact states. Some typical throttling processes in the pure substance are shown in Figure 15.46.

In the region of positive μ_{JT}, the internal energy of the pure substance depends strongly on the volume as well as the temperature. In fact, the internal energy increases with volume at constant temperature which accounts for the pure substance behavior that differs from that of the ideal gas and the incompressible fluid which both have an internal energy which depends only upon T.

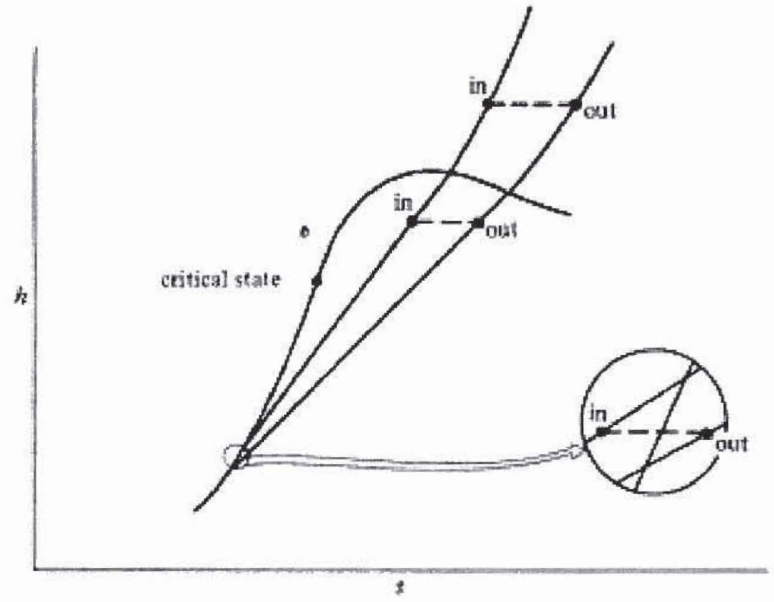

Figure 15.46(a) Throttling Processes for the Pure Substance

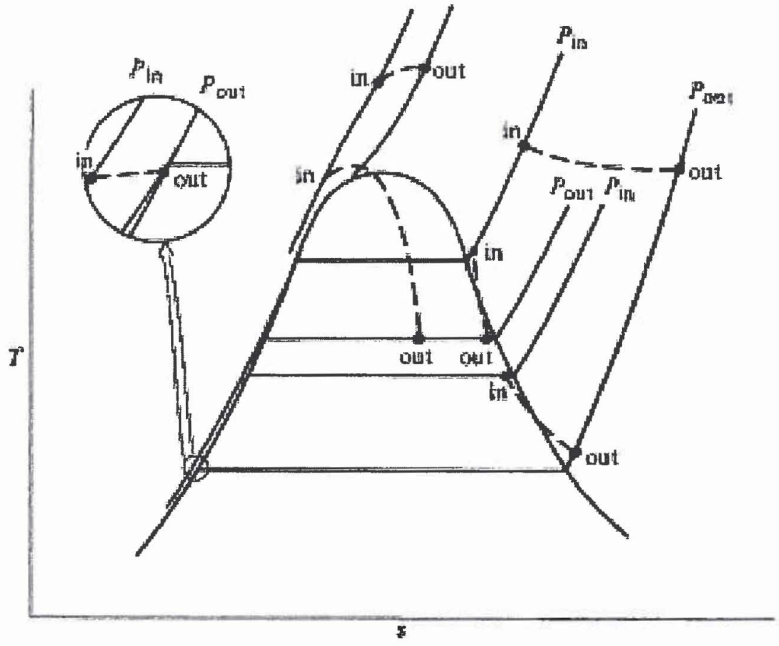

Figure 15.46(b) Throttling Processes for the Pure Substance

Example 15E.13: A supply of nitrogen is available at a pressure of $P_1 = 10^7$ N/m^2 as might be the case for high pressure nitrogen stored in a typical size A storage "bottle" similar to those used for the storage of welding gases or medical quality oxygen. We pose the following question: Can we take advantage of the pure substance behavior exhibited in Figure 14.45 and liquify the gas by throttling it from high pressure P_1 to low pressure $P_2 = 10^5$ N/m^2 through a

simple orifice?

Solution: The physical situation is shown schematically in Figure 15E.13(a).

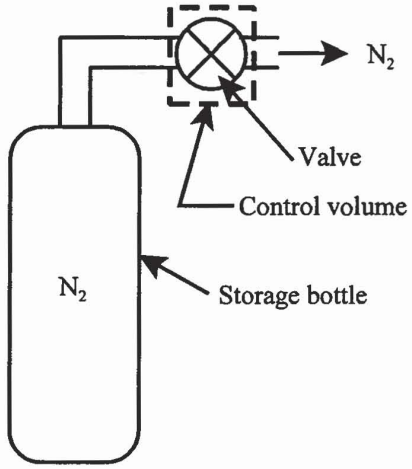

Figure 15E.13(a)

We need to find the state of the gas entering the throttle such that the state exiting from the throttle is just in the two-phase region. The limiting exit state would be that of a saturated vapor at the pressure P_2. If we apply the first law to the control volume shown in Figure 15E.13(a), we find from the tabulated properties of the pure substance model for nitrogen

$$h_1 = h_2 = h_{\substack{sat \\ vapor}} = 77.073 \text{ kJ/kg}$$

The state of the nitrogen entering the throttle is then $P_1 = 10^7$ N/m^2 and $h_1 = 77.073$ kJ/kg. From the tabulated properties of the pure substance model for nitrogen, these two independent properties correspond to $T_1 = 160.24$ K. If the temperature of the nitrogen entering the throttle is 160.24 K, there will be no liquid exiting the throttle, only vapor. For any inlet temperature less than 160.24 K, there will be a mixture of vapor and liquid leaving the throttle. The lower the inlet temperature, the greater the mass fraction in the liquid phase. For example, if the inlet temperature were 120 K, the enthalpy of the inlet fluid would be $h_1 = -27.821$ kJ/kg. At the outlet pressure of $P_2 = 10^5$ N/m^2, we have $h_f = -122.25$ kJ/kg and $h_{fg} = 199.323$ kJ/kg. Then the mass fraction in the liquid phase would be

$$y = 1 - x = 1 - \frac{h_1 - h_f}{h_{fg}} = 1 - \frac{-27.821 \text{ kJ/kg} - (-122.25 \text{ kJ/kg})}{199.323 \text{ kJ/kg}} = 1 - 0.474 = 0.526$$

Thus the fraction of mass flow in the liquid phase can be increased considerably by lowering the temperature at inlet to the throttle. The problem is, how can we accomplish this without introducing external refrigeration? The most direct method is to place a heat exchanger between the gas supply and the throttle valve. By also placing a phase separator downstream of the throttle, the mass flow that remains in the saturated vapor phase can be directed through the heat exchanger countercurrent to the supply stream to the throttle and the saturated liquid can be drawn off to a storage Dewar. By this means, the "waste" vapor can be used to pre-cool the nitrogen feed to the throttle. The configuration would be as shown in Figure 15E.13(b).

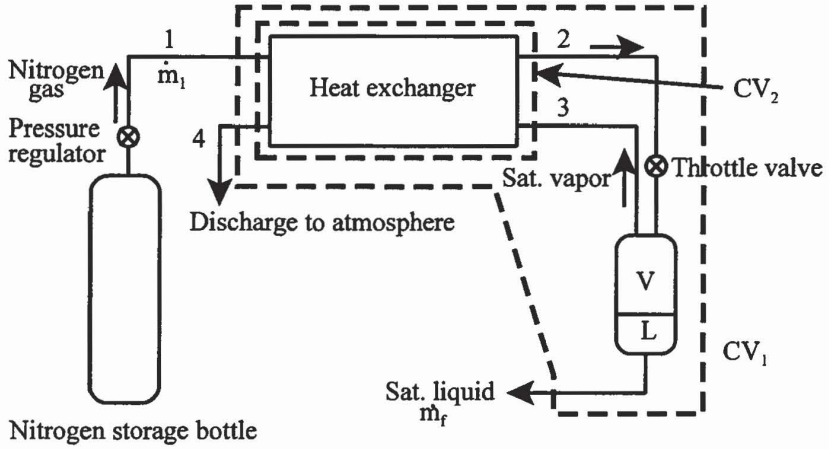

Figure 15E.13(b) Simple Joule-Thomson Liquefier

If we assume that the heat exchanger effectiveness is one, $\varepsilon = 1$, we can establish the limiting performance for this apparatus under conditions of steady flow. Then $T_3 = T_{sat} = 77.244$ K and $T_4 = 300$ K. The first law for control volume 1 in Figure 15E.13(b) becomes

$$\dot{m}_1 h_1 - \dot{m}_f h_f - (\dot{m}_1 - \dot{m}_f) h_4 = 0$$

If we set $\dot{m}_1$ equal to unity in this expression, we can determine the fraction of the nitrogen supply stream that can be liquified in this manner, viz.

$$\dot{m}_f = \frac{h_1 - h_4}{h_f - h_4}$$

From the pure substance model for nitrogen, we have

$$h_1 = 291.93 \text{ kJ/kg} \quad h_3 = 77.073 \text{ kJ/kg} \quad h_4 = 311.20 \text{ kJ/kg} \quad h_f = -122.25 \text{ kJ/kg}$$

The negative value for h_f is simply a consequence of the particular state selected as the datum state for the pure substance model for nitrogen. Then

$$\dot{m}_f = \frac{291.93 \text{ kJ/kg} - 311.20 \text{ kJ/kg}}{-122.25 \text{ kJ/kg} - 311.20 \text{ kJ/kg}} = 0.044 \text{ kg/sec}$$

Thus, 4.4 percent of the nitrogen supply stream can be liquified in this manner. The physical fact that makes this Joule-Thomson liquefier work is that the thermal-fluid properties of nitrogen are such a strong function of pressure for the pressure levels chosen. As a consequence, the heat exchanger can operate with an imbalance in mass flow rates between the high-pressure and low-pressure sides. If the properties were independent of pressure as is the case for the ideal gas model, the heat exchanger could not operate in this manner.

We can determine the state of the nitrogen entering the throttle by applying the first law to control volume 2 in Figure 15E.13(b). Then

$$h_1 + (1 - \dot{m}_f) h_g - h_2 - (1 - \dot{m}_f) h_4 = 0$$

$$h_2 = h_1 - (1 - \dot{m}_f)(h_4 - h_g)$$

$$h_2 = 291.93 \text{ kJ/kg} - (1 - 0.044 \text{ kg/sec})(311.20 \text{ kJ/kg} - 77.073 \text{ kJ/kg})$$

$$h_2 = 68.212 \text{ kJ/kg}$$

We now have two independent properties to establish state 2, namely $P_2 = 10^7$ N/m^2 and $h_2 =$ 68.212 kJ/kg. Then from the pure substance model for nitrogen, we have $T_2 = 156.97$ K.

For the throttle valve, $h_2 = h_3$. Then

$$h_3 = h_f + x_3 h_{fg}$$

$$x_3 = \frac{h_3 - h_f}{h_g - h_f} = \frac{68.212 \text{ kJ/kg} - (-122.25 \text{ kJ/kg})}{77.073 \text{ kJ/kg} - (-122.25 \text{ kJ/kg})} = 0.956$$

Then the fraction of nitrogen in the liquid phase is

$$y_3 = 1 - x_3 = 1 - 0.956 = 0.044$$

This is precisely the result we obtained from the first law for control volume 1.

The system shown in Figure 15E.13(b) is the essence of a system known as a Joule-Thomson liquefier that is the most basic of liquefiers. One notable feature of this design is that it is able to operate with a mass imbalance in the heat exchanger even though the fluid flowing in both the hot and cold streams is the same pure substance. This phenomenon is a consequence of the fact the properties of the pure substance are a function of both pressure and temperature, unlike those of the ideal gas model for which the properties are at most dependent upon temperature only. In designing liquefaction systems used for a wide variety of industrial processes, such as air separation plants to produce oxygen, nitrogen, and argon from atmospheric air, the challenge is to produce as much liquefied gas as possible from a given stream. As we shall see in Chapter 16, there are a number of innovative features that thermal-fluid engineers have introduced into the basic Joule-Thomson liquefier to increase the output significantly.

Appendix 15A

Dimensional Analysis of the Performance of a Negative Shaft Work Machine Processing an Incompressible Fluid – a Pump

In Section 9.10.3.5, we discussed briefly the characteristics of a pump and noted that pump characteristics that were useful for design of piping systems were volume flow rate, $\dot{V}$, and total dynamic head, H_{pump}. At that time we deferred further discussion of the other important pump characteristics until this point in our development of the subject. We now would like to develop a means of quantitating the performance of a pump in terms of all the parameters required to describe the characteristics of the pump. This can be most easily accomplished by means of the method of dimensional analysis.

Based upon our discussion of the Buckingham Pi Theorem of Section 10.6, we follow the list of steps presented there for dimensional analysis of pump characteristics:

Step 1: *List and count the n parameters required to describe the physical situation. If any important parameters are missing, dimensional analysis will fail.*

In addition to the volumetric flow rate, $\dot{V}$, and the total dynamic head, H_{pump}, or alternatively the pump head, h_{pump}, the evaluation of pump performance requires the rotational frequency of the pump, ω, that characterizes its speed, the diameter of the pump, D, that characterizes its size, and the power required to operate the pump, $\dot{W}_{shaft}$. The performance of the pump will also depend upon the character of the fluid that flows through it. The fluid can be characterized in terms of its density, ρ, and its viscosity, μ.

Step 2: *List the dimensions of each variable according to M, L, T, and Θ.*

For the volumetric flow rate,

$$\left[\dot{V}\right] = \frac{L^3}{T}$$

For the "head" developed by the pump, different investigators and different pump manufacturers use different terms to specify this quantity. The most common terminology used by pump manufacturers refers to the total dynamic head, H_{pump}, defined in equation (9.310) as the relevant pump characteristic. However, in the process of non-dimensionalization of the head of the pump, most treatments use the pump head, h_{pump}, defined in equation (9.307) as the relevant parameter. These two parameters differ by the factor g, viz.

$$h_{pump} = gH_{pump}$$

Clearly, the dimensions of the two parameters are different.

Following convention, we use the pump head as the parameter to be non-dimensionalized. Thus

$$\left[h_{pump}\right] = \frac{L^2}{T^2}$$

For the rotational speed of the pump

$$[\omega] = \frac{1}{T}$$

For the diameter of the pump

$$[D] = L$$

For the pump power

$$\left[\dot{W}_{shaft}\right] = \frac{ML^2}{T^3}$$

For the fluid density

$$[\rho] = \frac{M}{L^3}$$

For the fluid viscosity

$$[\mu] = \frac{M}{LT}$$

Thus there are 7 parameters required to characterize this situation.

Step 3: *Find the value of r. Initially guess r to be equal to the number of different dimensions present and then make sure the there are r parameters that do not form a Π-group. If this is unsuccessful, reduce r by one and look again.*

Let us guess the value of r to be the same as the number of dimensions required to characterize the situation. Then $r = 3$ and there would be $7 - 4$ dimensionless groups. The possible candidates for the parameters that do not form a dimensionless group are ρ, ω, and D. To test the hypothesis that these parameters do not form a dimensionless group, we need to find values of the exponents p, q, and r other than zero such that

$$\left[\rho^p \omega^q D^r\right] = 1$$

Then if these values exist, it must be the case that

$$\left(\frac{M}{L^3}\right)^p \left(\frac{1}{T}\right)^q (L)^r = 1$$

but

$$M: p = 0$$
$$L: 3p + r = 0 \Rightarrow r = 0$$
$$T: -q = 0 \Rightarrow q = 0$$

Since all of the dimensional exponents must be zero, it follows, then, that the parameters selected do not form a dimensionless group.

Step 4: *Select r parameters which do not form a Π-group among themselves. These parameters are the repeating parameters that will appear in all the Π-groups.*

According to the results of Step 3, we select ρ, ω, and D as the parameters to use in the non-dimensionalization process.

Step 5: *Select one of the remaining parameters that is not one of the r repeating parameters and non-dimensionalize that parameter using the r repeating parameters. Repeat the procedure until all the remaining parameters are non-dimensionalized. There should now be n − r Π-groups.*

For the volumetric flow rate, we seek the values of the exponents a, b, c such that

$$\left[\dot{V} \rho^a \omega^b D^c\right] = 1$$

Then

$$\left(\frac{L^3}{T}\right)\left(\frac{M}{L^3}\right)^a\left(\frac{1}{T}\right)^b(L)^c=1$$

$$M: a=0$$

$$L:\ 3-3a+c=0\Rightarrow 3+c=0\Rightarrow c=-3$$

$$T:\ -1-b=0\Rightarrow b=-1$$

and the first dimensionless group becomes

$$\Pi_1=\frac{\dot{V}}{\omega D^3}=\Pi_{flow} \tag{15A.1}$$

This dimensionless group is known as the *flow coefficient*, Π_{flow}.

To determine the second dimensionless group,

$$\left[h_{pump}\rho^d\omega^e D^f\right]=1$$

$$\left(\frac{L^2}{T^2}\right)\left(\frac{M}{L^3}\right)^d\left(\frac{1}{T}\right)^e(L)^f=1$$

$$M: d=0$$

$$L:\ 2-3d+f=0\Rightarrow f=-2$$

$$T:\ -2-e=0\Rightarrow e=-2$$

Then

$$\Pi_2=\frac{h_{pump}}{\omega^2 D^2}=\Pi_{head} \tag{15A.2}$$

and this dimensionless group is known as the *head coefficient*, Π_{head}.

To determine the third dimensionless group,

$$\left[\dot{W}_{shaft}\rho^g\omega^h D^i\right]=1$$

$$\left(\frac{ML^2}{T^3}\right)\left(\frac{M}{L^3}\right)^g\left(\frac{1}{T}\right)^h(L)^i=1$$

$$M: 1+g=0\Rightarrow g=-1$$

$$L:\ 2-3g+i=0\Rightarrow 2+3+i=0\Rightarrow i=-5$$

$$T:\ -3-h=0\Rightarrow h=-3$$

Then

$$\Pi_3=\frac{\dot{W}_{shaft}}{\rho\omega^3 D^5}=\Pi_{power} \tag{15A.3}$$

and this dimensionless group is known as the *power coefficient*, Π_{power}.

Finally, for the fourth dimensionless group,

$$\left[\mu\rho^j\omega^k D^l\right]=1$$

$$\left(\frac{M}{LT}\right)\left(\frac{M}{L^3}\right)^j\left(\frac{1}{T}\right)^k(L)^l=1$$

$$M: 1+j=0\Rightarrow j=-1$$

$$L:\ -1-3j+l=0\Rightarrow -1+3+l=0\Rightarrow l=-2$$

$$T:\ -1-k=0\Rightarrow k=-1$$

Then

$$\Pi_4 = \frac{\mu}{\rho\omega D^2}$$

It is actually the inverse of this dimensionless group that is of interest.

$$Re_{pump} = \frac{\rho\omega D^2}{\mu} \tag{15A.4}$$

This dimensionless group is the Reynolds number for a pump.

Step 6: *Check to see that all proposed Π-groups are dimensionless and write the functional relationship among them in dimensionless form.*

We have checked, and all the dimensionless groups are indeed dimensionless. According to the Buckingham Pi Theorem, there exists a function F such that

$$F(\Pi_1, \Pi_2, \Pi_3, \Pi_4) = 0$$

This is as far as dimensional analysis can take us. In order to determine the specific form of the function F, it is necessary to examine the details of the operation of the particular machine of interest.

At this point we should note that in some treatments of this subject and in much of the literature, especially that distributed by pump manufacturers, the dimensionless groups presented here are replaced by a set of groups that are not dimensionless, but rather are *dimensional*. These are derived from the set presented here by replacing the rotational speed, ω, in radians/sec by the rotational speed, N, in revolutions/sec or revs/min. Then

$$\Pi'_{flow} = \frac{\dot{V}}{ND^3}$$

$$\Pi'_{head} = \frac{h_{pump}}{N^2D^2}$$

$$\Pi'_{power} = \frac{\dot{W}_{shaft}}{\rho N^3 D^5}$$

$$\Pi'_{Reynolds} = \frac{\rho ND^2}{\mu}$$

Appendix 15B

Axial Flow Steam Turbines

15B.1 Introduction

In large-scale steam plants, it can be argued that the steam turbine plays the most pivotal role in the performance of the plant. However, in recent years, in modern, large-scale combined cycle energy conversion systems, the role of the steam turbine has been diminished somewhat in favor of that of the gas turbine plant. Nonetheless, the steam turbine finds such widespread use in both stationary and mobile energy conversion systems, it is worth examining the details of the performance of this steady-flow component.

The steam turbine has been in existence, in one form or another, for a long time. As early as the first century, Hero of Alexandria, an Egyptian engineer, demonstrated a crude form of steam turbine, the classic *Aeolipile*. Although it was little more than a toy, it did operate in a manner similar to modern turbines. (See Figure 15B.1.) It was basically a steam generator in which the steam exhausted into a sphere fitted with steam jets oriented perpendicular to the axis on which the sphere could rotate. The momentum of the steam leaving the jet produced a reaction force that caused the sphere to rotate.

Figure 15B.1 Aeolipile of Hero

In the millennia that followed Hero's early efforts, the first positive shaft work machines that used steam as the working fluid were of the reciprocating piston type. However, in the late nineteenth century, Charles Parsons (1854 – 1931), an Irish engineer who was a junior partner in the firm Clarke, Chapman, and Parsons, recognized the advantages of a rotating shaft work machine and built a multi-stage reaction turbine in 1884. In his first demonstration of the potential of the device, he utilized it to drive a dynamo, also of his own design, that generated about 7.5 kW of electrical power. He patented the device in April 1884 and shortly thereafter demonstrated of the potential of his invention as a marine power plant by using the machine to power his yacht *Turbinia*. Parsons's design was subsequently modified by Charles Curtis (1860 – 1953) who built a combined impulse-reaction turbine that incorporated the converging-diverging nozzle design of Gustav De Laval (1845 – 1913) for the stator. Curtis patented his design in 1896, and it was immediately adopted for use as the prime mover in stationary power plants. In the ensuing years, considerable development has gone into the steam turbine for both stationary and marine use, but the designs of Parsons and Curtis still form the basis for present configurations.

In modern applications, steam turbines are usually axial flow and range in size from one kW to 1.9 GW in output. Although the details of the internal construction vary somewhat with the application, the basic design consists of alternating rows of stators and rotors. Typically, the stators are configured as nozzles designed to accelerate the working fluid to high velocities while the rotors consist of blades shaped like airfoils and arranged radially on a disk centered on the axis of rotation. The deflection of the high velocity fluid stream by the rotor blades and the attendant change in momentum of the fluid stream result in a force applied to the blade. The rotation of the blade about the disk axis results in a torque that can be used to drive an electric generator or turn the propeller shaft of a vehicle.

Steam turbines are of two types: *impulse turbines* in which the stators are used simply to redirect the flow to the next rotor and *reaction turbines* in which the stator is configured as a nozzle and is used to accelerate the flow for the next rotor. In the ideal pure impulse turbine, the pressure drop in the flow occurs in the stators only and the fluid flows in a frictionless manner over the blades of the rotor. In the reaction turbine, a portion of the pressure drop occurs in the stator while the remainder occurs as the fluid passes over the blade. In typical designs, the pressure drop is divided equally between stator and rotor in the reaction turbine.

15B.2 Impulse Blade Design

The analysis of a single stage of an impulse turbine can be most easily accomplished with the aid of Figure 15B.2 and the velocity diagrams of Figure 15B.3. In performing such an analysis, one radial location on the blade is selected (typically the midpoint of the blade axis) and the velocity diagrams are constructed as in Figure 15B.3. Although the tangential velocity of the blade varies with radial position, one location is sufficient provided the fluid pressure is not too low. The lower the pressure, the longer the blade and the more approximate the analysis since the low-pressure blades can be quite long (on the order of a meter or more in large machines).

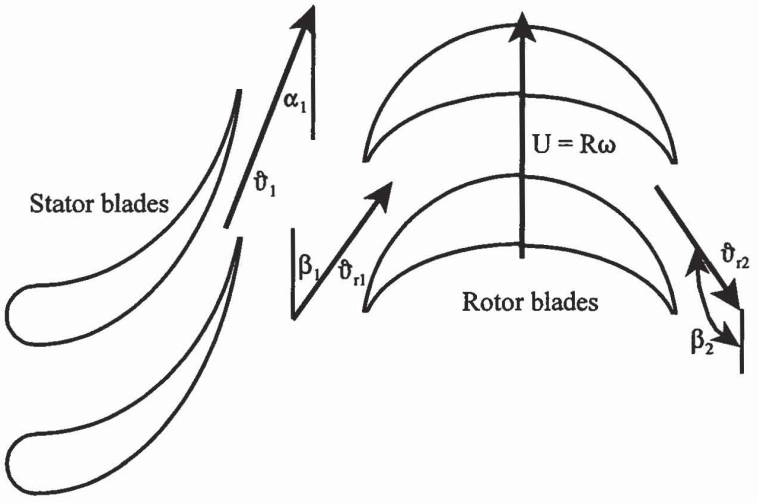

Figure 15B.2 Some Stator and Rotor Blades of a Single Stage Pure Impulse Turbine

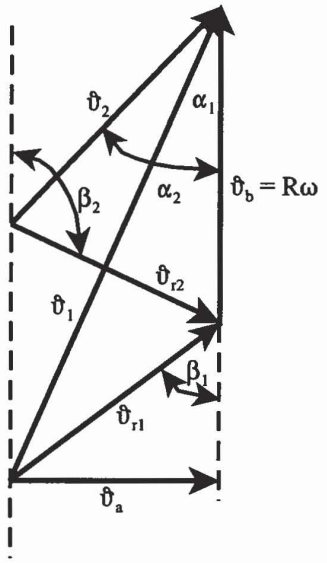

Figure 15B.3 Velocity Diagrams for a Pure Impulse Turbine with Constant Axial Velocity

In the present analysis, we consider an ideal machine in which the fluid flows across the blades with no pressure drop so that $\vartheta_{r1} = \vartheta_{r2}$. Thus, the orientation of the relative velocity component along the blade determines the performance of the blade. If we take the axial velocity as constant through the machine, the tangential component of force produced in this machine is given by the tangential component of the equation of linear momentum, viz.

$$F_t = \dot{m}\vartheta_{r1}\left(\cos\beta_1 - \cos\beta_2\right) \tag{15B.1}$$

According to the Euler turbomachine equation, equation (8.107), the power produced by the stage is then

$$\left(\dot{W}_{shaft}\right)_{\substack{rev \\ Q=0}} = \dot{m}R\omega\vartheta_{r1}\left(\cos\beta_1 - \cos\beta_2\right) = \dot{m}\vartheta_b\vartheta_{r1}\left(\cos\beta_1 - \cos\beta_2\right) \tag{15B.2}$$

where ϑ_b is the tangential component of blade velocity. If there are no net forces due to pressure acting on the rotor, which must be the case since the fluid flows along the blade with no pressure drop in this model, the axial component of the equation of linear momentum gives the axial force acting on the rotor, viz.

$$F_a = \dot{m}\vartheta_{r1}\left(\sin\beta_1 - \sin\beta_2\right) \tag{15B.3}$$

If the rotor blade is symmetric with respect to the entry and exit angles of the fluid stream, it follows that $\beta_2 = 180° - \beta_1$ and there is no net axial thrust on the rotor.

Consider the case of the first stage of such an impulse turbine in which the first stator is actually a nozzle. If the fluid enters the stator with negligible velocity and is accelerated to a velocity ϑ_1, the efficiency of the stage can be defined as the ratio of the power produced by the stage to the kinetic energy of the fluid stream entering the stage, viz.

$$\eta_{stage} = \frac{\left(\dot{W}_{shaft}\right)_{\substack{rev \\ Q=0}}}{\dot{m}\dfrac{\vartheta_1^2}{2}} = \frac{4\vartheta_b\vartheta_{r1}\cos\beta_1}{\vartheta_1^2} \tag{15B.4}$$

where we have made use of the fact that $\cos\beta_2 = \cos(\pi - \beta_1) = -\cos\beta_1$.

Then from the velocity diagrams of Figure 15B.3

$$\eta_{stage} = \frac{4\vartheta_b}{\vartheta_1^2}(\vartheta_1\cos\alpha_1 - \vartheta_b) = \frac{4\vartheta_b}{\vartheta_1}\left(\cos\alpha_1 - \frac{\vartheta_b}{\vartheta_1}\right) \tag{15B.5}$$

For maximum stage efficiency at a fixed exit angle from the stator, there is a particular relationship between the tangential component of blade velocity and the velocity at exit from the stator. This relationship can be determined by forming the derivative of equation (15B.5) with respect to the ratio ϑ_b/ϑ_1 and setting it equal to zero, viz.

$$\frac{d(\eta_{stage})}{d\left(\frac{\vartheta_b}{\vartheta_1}\right)} = 4\cos\alpha_1 - 8\frac{\vartheta_b}{\vartheta_1} = 0 \tag{15B.6}$$

Then at maximum stage efficiency

$$\frac{\vartheta_b}{\vartheta_1} = \frac{\cos\alpha_1}{2} \tag{15B.7}$$

Then the maximum stage efficiency becomes

$$(\eta_{stage})_{max} = \cos^2\alpha_1 \tag{15B.8}$$

Equation (15B.8) implies that $\alpha_1 = 0$ for maximum stage efficiency, but this is an absurd result from a practical point of view since the fluid exiting the stator at this angle would be unable to enter the rotor since it would be traveling parallel to it. At this angle, the optimum ratio of blade velocity to fluid velocity is 0.5.

From practical considerations, the stator exit angle in steam turbines is usually set between 15° and 20°. For $\alpha_1 = 15°$, $\vartheta_b/\vartheta_1 = 0.483$ and $(\eta_{stage})_{max} = 0.933$. For the case of maximum stage efficiency with $\alpha_1 = 15°$ and $\beta_2 = 180° - \beta_1$, it turns out that the absolute velocity of the fluid leaving the stage is purely axial as shown in Figure 15B.4 and that $\tan\beta_1 = 2\tan\alpha_1$ with $\beta_1 = 28.2°$.

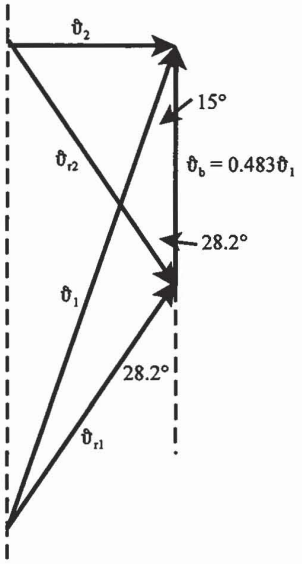

Figure 15B.4 Velocity Diagram for Maximum Stage Efficiency with $\alpha_1 = 15°$

If we were to assume that the flow in the stator is reversible and adiabatic, the first law applied to the stator gives

$$h_{in} - h_{out} = \frac{\vartheta_{out}^2}{2} - \frac{\vartheta_{in}^2}{2} \tag{15B.9}$$

If the inlet velocity is negligible, equation (15B.9) becomes

$$\vartheta_1 = \sqrt{2(h_{in} - h_{out})} \tag{15B.10}$$

If we combine equations (15B.10) and (15B.7) and solve for ϑ_b at maximum efficiency, we get

$$\vartheta_b = \frac{\cos\alpha_1}{2}\sqrt{2(h_{in} - h_{out})} = \frac{\cos\alpha_1}{2}\sqrt{2(\Delta h)} \tag{15B.11}$$

where Δh is the drop in enthalpy of the working fluid as it flows through the ideal impulse stage. Figure 15B.5 is a plot of equation (15B.11) for the case of $\alpha_1 = 15°$.

The utility of Figure 15B.5 lies in the fact that steam turbines are limited by the high stresses induced by high blade velocities rather than by fluid compressibility limits as in the case of axial flow air compressors. If, for example, stress considerations limit the tangential velocity of the blade depicted in Figure 15B.5 to a value of $\vartheta_b = 400$ m/sec, the maximum allowable enthalpy drop across the reversible stage would be $\Delta h = 343$ kJ/kg according to Figure 15B.5.

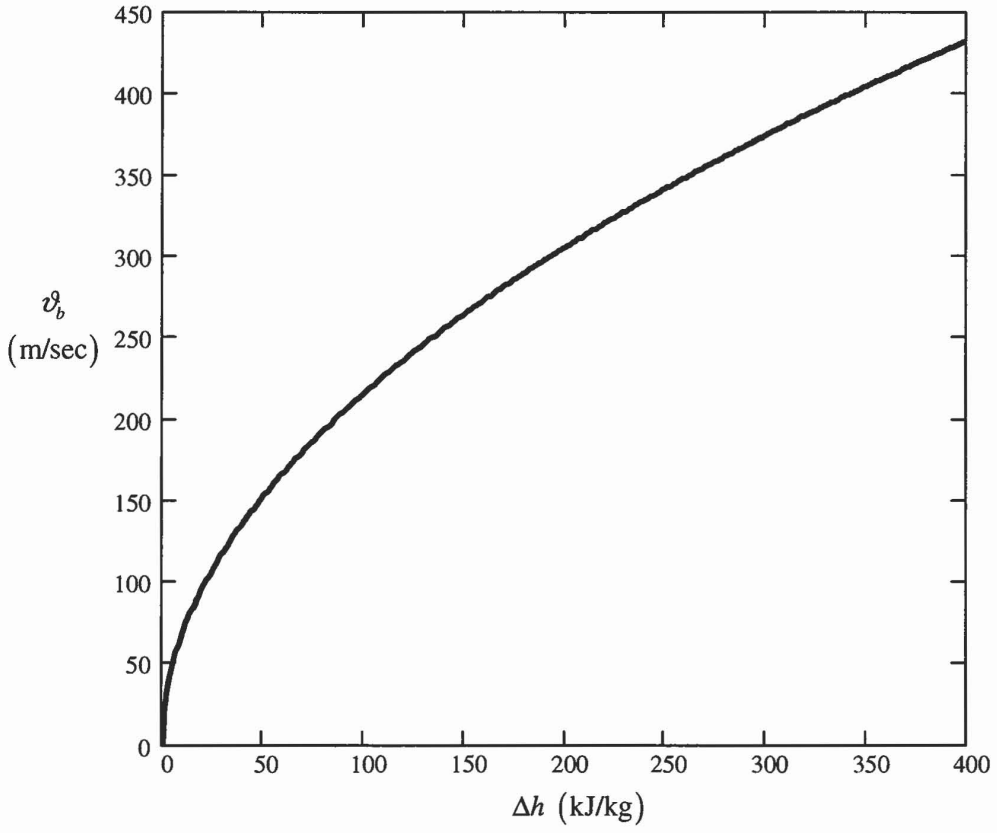

Figure 15B.5 Blade Tangential Velocity for an Ideal Impulse Stage at Maximum Blade Efficiency with $\alpha_1 = 15°$

A typical inlet state for the steam turbine would be T_{in} = 565 C and $P_{in} = 10^7$ N/m^2. Then from the properties of the pure substance model for H_2O, the outlet pressure for this isentropic stage would be $P_{out} = 3.5 \times 10^6$ N/m^2. This results in a pressure ratio of $P_{in}/P_{out} = 2.86$ across the stage. The speed of sound in the steam at outlet from the stage is $a_{out} = 610.7$ m/sec. This results in a blade Mach number of $M_{blade} = 0.65$ at the mean diameter which is a reasonable value. (In low pressure steam turbines, it is not uncommon for the lowest pressure stages with the longest blades for the blade *tip* Mach number to be as large as 1.2.) Note that in this example the absolute velocity of the fluid exiting the nozzle is 828.16 m/sec. Then the Mach number at exit of the supersonic nozzle is $M_{nozzle} = 1.36$. The velocity along the rotor blades is $\vartheta_{r1} = \vartheta_{r2} = 453.59$ m/sec and the Mach number is $M_r = 0.743$.

15B.3 Reaction Blade Design

We now take up the case of the *reaction stage* in which there is a pressure drop across the moving blade in addition to that across the stator. As a result, the passage between two blades is actually a moving nozzle. The stator forms a stationary nozzle with a portion of the total pressure drop of the stage while the rest of the stage pressure drop occurs across the blade. The turbine literature is somewhat divided on the point of view of what actually constitutes a *pure reaction* stage. Some investigators divide the total *pressure* drop of the stage equally between the stator and rotor while others divide the total *enthalpy* drop of the stage equally between the stator and rotor. In the present treatment, we shall develop the analysis in terms of the enthalpy drop.

Consider the case of a reaction blade designed with the velocity diagram shown in Figure 15B.6. The entering relative velocity has no tangential component and the blade is symmetrical with $\alpha_1 = \alpha_2$ and $\beta_2 = 180° - \alpha_1$. The stator directs the flow onto the rotor at an angle of α_1 with the tangential direction and with an absolute velocity of ϑ_1. The relative velocity at entrance to the blade is axial and the blade tangential velocity is $\vartheta_b = \vartheta_1 \cos \alpha_1$.

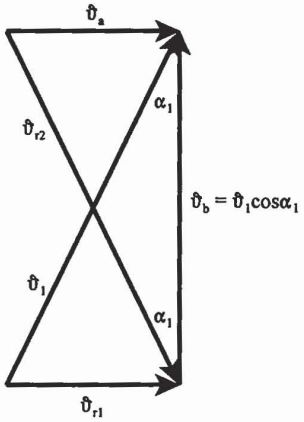

Figure 15B.6 Velocity Diagram for a Symmetrical Reaction Blade with Maximum Efficiency

For reversible adiabatic flow across the blade, the first law for a control volume attached to the blade gives

$$h_1 - h_2 = \frac{\vartheta_{r2}^2}{2} - \frac{\vartheta_{r1}^2}{2} \tag{15B.12}$$

With the aid of Figure 15B.6, equation (15B.12) becomes

$$h_1 - h_2 = \frac{\vartheta_1^2 \cos^2 \alpha_1}{2} = \frac{\vartheta_b^2}{2} \tag{15B.13}$$

The shaft power associated with this ideal reaction blade is

$$\left(\dot{W}_{shaft}\right)_{\substack{rev\\Q=0}} = \dot{m}\vartheta_b\vartheta_1\cos\alpha_1 = \dot{m}\vartheta_1^2\cos^2\alpha_1 = 2\dot{m}\left(h_1 - h_2\right) \tag{15B.14}$$

Then the efficiency of this blade is by definition

$$\eta_{blade} \equiv \frac{\left(\dot{W}_{shaft}\right)_{\substack{rev\\Q=0}}}{\dot{m}\left(\frac{\vartheta_1^2}{2} + \left(h_1 - h_2\right)\right)} = \frac{2\cos^2\alpha_1}{1+\cos^2\alpha_1} \tag{15B.15}$$

For a fluid entry angle of 15°, equation (15B.15) gives a blade efficiency of $\eta_{blade} = 0.965$.

If the blade tangential velocity is limited to $\vartheta_b = 400$ m/sec from stress considerations as in the case of the impulse blade, the maximum enthalpy drop across the blade that can be utilized is from equation (15B.13) $h_1 - h_2 = 80$ kJ/kg. If this is combined with the enthalpy drop in the nozzle,

$$h_0 - h_1 = \frac{\vartheta_1^2}{2} = \frac{1}{2}\left(\frac{\vartheta_b}{\cos\alpha_1}\right)^2 = \frac{1}{2}\left(\frac{400\text{ m/sec}}{\cos 15^\circ}\right)^2 = 85.74\text{ kJ/kg} \tag{15B.16}$$

we have $(\Delta h)_{stage} = 165.74$ kJ/kg which is about half that of the impulse stage at the same conditions of blade stress which reduces the pressure ratio of the reaction stage considerably compared with that of the impulse stage.

The performance of reaction blade designs compared with the impulse blade design depends heavily upon the relative balance between the enthalpy drop in the stator (nozzle) and that in the rotor. The enthalpy drop in the rotor is a function of the blade efficiency and the blade tangential velocity. For *maximum* stage efficiency with a given tangential blade velocity, there is a unique discharge velocity from the rotor, and, hence, enthalpy drop across the stage. To illustrate this point, let us consider a reaction blade design in which the flow of the fluid is reversible and adiabatic throughout with $\beta_2 = 180^\circ - \alpha_1$. The fluid enters the stator with negligible velocity in state 0 and expands to the pressure at entry to the rotor in state 1. Subsequently, the fluid expands in a reversible and adiabatic manner through the rotor to the discharge pressure in state 2. We define the degree of reaction of the design to be n where

$$n \equiv \frac{h_1 - h_2}{h_0 - h_2} \tag{15B.17}$$

that is, the ratio of the enthalpy drop in the rotor to the total enthalpy drop in the stage. Referring to the velocity diagram of Figure 15B.3, we find the shaft power produced in the stage is given by

$$\left(\dot{W}_{shaft}\right)_{\substack{rev\\Q=0}} = \dot{m}\vartheta_b\left(\vartheta_{t1} - \vartheta_{t2}\right) = \dot{m}\vartheta_b\left(\vartheta_1\cos\alpha_1 - \vartheta_2\cos\alpha_2\right)$$

$$\left(\dot{W}_{shaft}\right)_{\substack{rev\\Q=0}} = \dot{m}\vartheta_b\left(\vartheta_1\cos\alpha_1 - \vartheta_b + \vartheta_{r2}\cos\alpha_1\right) \tag{15B.18}$$

The velocity at discharge from the stator is determined from the first law applied to the control volume containing the stator, viz.

$$\vartheta_1 = \sqrt{2\left(h_0 - h_1\right)} = \sqrt{2(1-n)\left(h_0 - h_2\right)} = \vartheta_3\sqrt{1-n} \tag{15B.19}$$

where $n \le 1$ and ϑ_3 is the velocity at discharge from the reversible adiabatic expansion across the whole stage, viz.

$$\vartheta_3 = \sqrt{2\left(h_0 - h_2\right)} \tag{15B.20}$$

From the first law applied to the rotor blade, we have

$$\frac{\vartheta_{r2}^2}{2}=\frac{\vartheta_{r1}^2}{2}+(h_1-h_2)=\frac{\vartheta_{r1}^2}{2}+n(h_0-h_2)=\frac{\vartheta_{r1}^2}{2}+n\frac{\vartheta_3^2}{2} \tag{15B.21}$$

where we have made use of equation (15B.20). Using the velocity diagram of Figure 15B.3, equation (15B.21) can be written in the form

$$\vartheta_{r2}^2=\vartheta_1^2+\vartheta_b^2-2\vartheta_1\vartheta_b\cos\alpha_1+n\vartheta_3^2=\vartheta_3^2+\vartheta_b^2-2\vartheta_b\vartheta_3\sqrt{1-n} \tag{15B.22}$$

We can now use equations (15B.19) and (15B.22) to eliminate ϑ_1 and ϑ_{r2} from equation (15B.18). Then

$$\left(\dot{W}_{shaft}\right)_{\substack{rev\\Q=0}}=\dot{m}\vartheta_b\left[\vartheta_3\left(\sqrt{1-n}\right)\cos\alpha_1-\vartheta_b+(\cos\alpha_1)\sqrt{\vartheta_3^2+\vartheta_b^2-2\vartheta_b\vartheta_3(\cos\alpha_1)\sqrt{1-n}}\right] \tag{15B.23}$$

Then the stage efficiency becomes

$$\eta_{stage}=\frac{2\vartheta_b}{\vartheta_3}\left[\sqrt{1-n}\cos\alpha_1-\frac{\vartheta_b}{\vartheta_3}+(\cos\alpha_1)\sqrt{1+\left(\frac{\vartheta_b}{\vartheta_3}\right)^2-\frac{2\vartheta_b}{\vartheta_3}\sqrt{1-n}(\cos\alpha_1)}\right] \tag{15B.24}$$

Figure 15B.7 is a plot of equation (15B.24) and clearly shows that as the degree of reaction increases, i.e., as the enthalpy drop in the rotor increases relative to that in the stator, the maximum efficiency decreases and the ratio ϑ_b/ϑ_3 at which the maximum occurs increases.

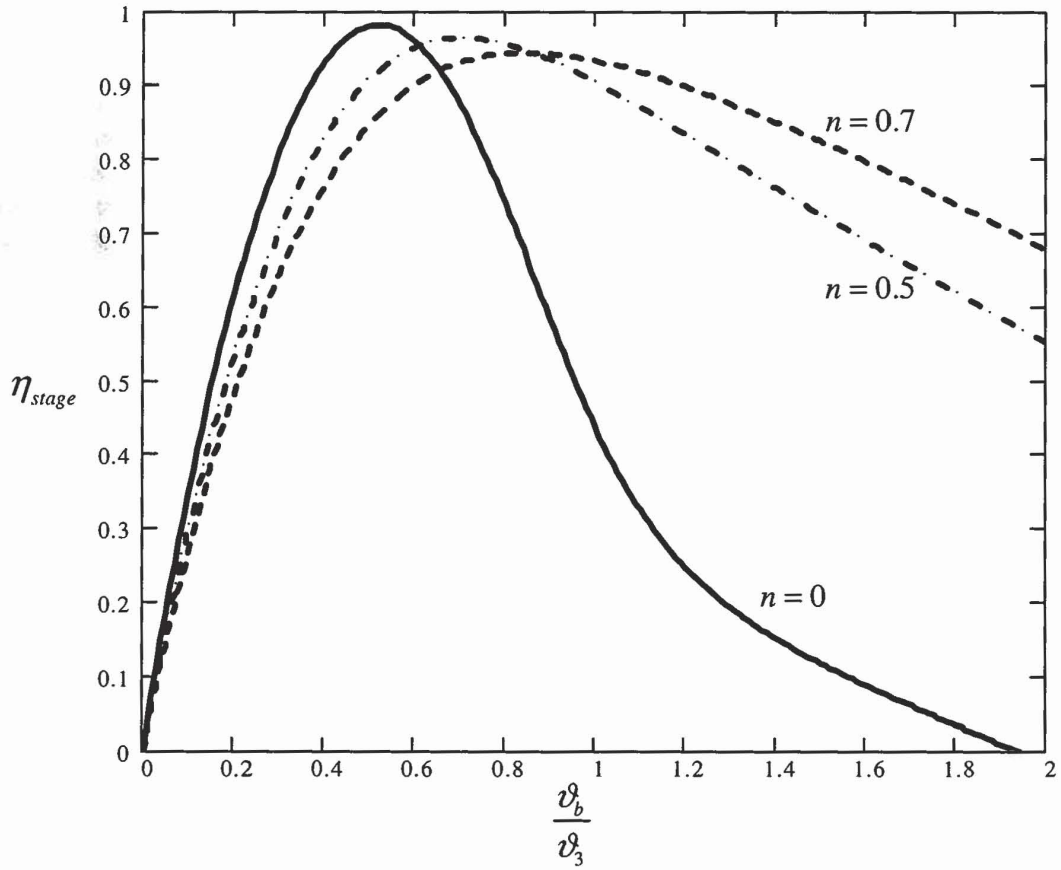

Figure 15B.7 Dependence of Stage Efficiency on Degree of Reaction for Reaction Blade Design

For maximum stage efficiency, the absolute velocity at exit from the blade must be axial.

It should be noted that the ideal impulse stage considered here ($n = 0$) is different from the one described in Section 15B.2. For the impulse stage of Section 15B.2, $\beta_2 = 180° - \beta_1$ and there was no axial thrust. In the case of this impulse stage, $\beta_2 = 180° - \alpha_1$ and there is an axial thrust. In the impulse stage design ($n = 0$), $\vartheta_{r2} = \vartheta_{r1}$. In the reaction stage design, ($n = 0.5$) $\vartheta_{r2} > \vartheta_{r1}$. From Figure 15B.7, it is apparent that in the reaction stage design ($n = 0.5$), the tangential blade velocity is about 40 percent greater than it is in the impulse stage design. In both designs, the discharge velocity from the stage is axial.

15B.4 Multi-staging

We have shown above, for the cases of reversible adiabatic flow, that the ratio of tangential blade velocity to the discharge velocity from the rotor has a particular value for maximum stage efficiency with a given blade design in a single stage. Due to stress considerations, the allowable tangential blade velocity is limited which, in turn, limits the allowable enthalpy drop across the stage for reversible adiabatic operation. The situation is further exacerbated by the irreversibilities in the flow. These irreversibilities reduce the stage efficiency as well as the enthalpy drop for a given pressure drop across the stage. One method of addressing these limits on performance is to stage the drop in enthalpy, or alternatively the drop in pressure, over a number of successive stages.

For example, for equal stage efficiencies, four stages with equal drops in enthalpy in each stage will reduce the required tangential blade velocity by a factor of two compared with a single stage. In addition, the in the presence of irreversibilities, the enthalpy at entrance to each succeeding stage will be higher than in the reversible case which in turn provides an opportunity for greater discharge velocities; however, the increase in entropy in each succeeding stage gradually reduces performance with each successive stage so that overall performance is reduced. However, as we saw for the case of the gas turbine, the loss in performance due to irreversibilities in the multi-stage machine is not so large as the loss in the single-stage machine. Furthermore, the reduction in velocity level in each stage reduces fluid friction which, in turn, reduces the loss of stage efficiency due to this factor. Finally, in the multi-stage machine, the pressure drop across each stage is smaller so that leakage losses between stages are reduced.

Typically in large multi-stage turbines, impulse blade designs are used in the high pressure stages because of their ability to utilize large drops in enthalpy with good efficiency at moderate tangential blade velocities. On the other hand, the larger leakage areas and lower enthalpy drops with good efficiency make the reaction blade design the choice for low pressure stages.

15B.5 Reheat Factor

The pressure ratios of typical large steam turbines used in central power plants can be quite large and may attain values of 10^3 or greater. In a manner similar to the case of the gas turbine, the expansion of the working fluid in the steam turbine does not occur in a single stage, but rather in multiple stages for the reasons given in the previous section. As a result, the pressure ratios across the various stages that make up the machine are only a fraction of that of the entire machine, and the expansion process in the steam turbine is not quite as shown in Figure 15.21. The process is more like that depicted in Figure 15B.8.

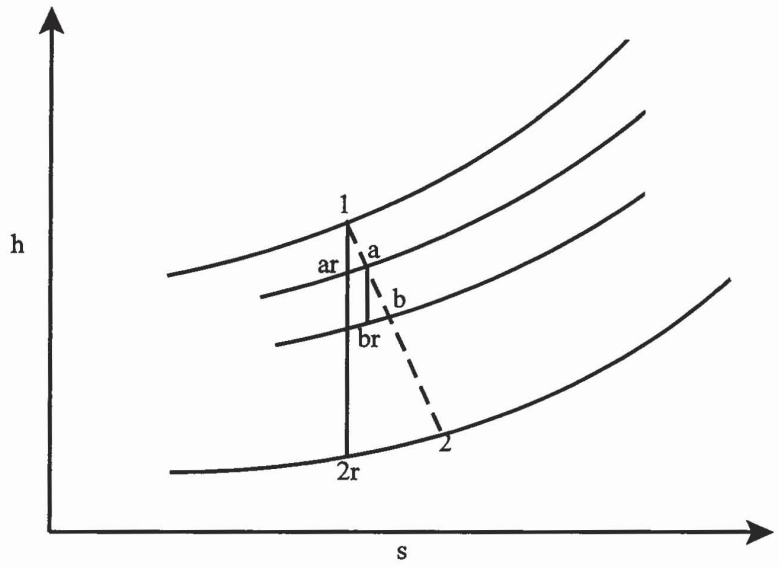

Figure 15B.8 Schematic Representation of Multi-Stage Expansion in a Steam Turbine

Figure 15B.8 shows just two stages in a multi-stage turbine. Due to irreversibilities in both the stator (nozzle) and the rotor, the entropy of the working fluid increases as it passes through each stage. Because the isobars diverge on the *h-s* plane as the entropy increases, the potential enthalpy drop across each succeeding stage is higher than it would have been at the original value of entropy. Thus the potential enthalpy drop for reversible operation of a multi-stage machine with N stages, is higher than the enthalpy drop for a single stage machine. Thus, in Figure 15B.8

$$\sum_{N}(h_1 - h_{ar}) + (h_a - h_{br}) + \ldots > (h_1 - h_{2r}) \tag{15B.25}$$

The irreversible, adiabatic multi-stage expansion has the *appearance* of a multi-stage expansion in which the working fluid experiences a positive heat transfer between each stage. In other words, the fluid *appears* to have been *reheated* between two successive stages. This leads to an expression of the inequality (15B.25) in terms of the parameter known as the *reheat factor*, *RF*, defined as

$$RF = \frac{\sum_{i}^{N}(\Delta h)_{i,rev}}{(h_{in} - h_{out})_{rev}} \tag{15B.26}$$

where $(\Delta h)_{i,rev}$ is the reversible, adiabatic enthalpy drop for stage i and $(h_{in} - h_{out})_{rev}$ is the reversible, adiabatic enthalpy drop for the given inlet state and the given outlet pressure for the turbine. Clearly, the reheat factor is greater than unity with typical values in the range of 1.03 to 1.08. There is a relationship between the reheat factor and the adiabatic efficiency.

Since the adiabatic efficiency η_+ for the turbine can be written

$$\eta_+ = \frac{(h_{in} - h_{out})_{actual}}{(h_{in} - h_{out})_{rev}} = \frac{(h_{in} - h_{out})_{actual}}{\sum_{i}^{N}(\Delta h)_{i,rev}} \frac{\sum_{i}^{N}(\Delta h)_{i,rev}}{(h_{in} - h_{out})_{rev}} \tag{15B.27}$$

the turbine adiabatic efficiency for the case of identical stages with identical enthalpy drops for each stage becomes

$$\eta_{+} = \eta_P (RF) \tag{15B.28}$$

where η_P is the polytropic efficiency, i.e., the stage efficiency, originally introduced in equation (15.68). Equation (15B.28) can be used to determine the power output for the turbine, viz.

$$\dot{W}_{shaft} = \dot{m}\left[\eta_{+}\left(h_{in} - h_{out}\right)_{rev}\right] = \dot{m}\left[\eta_P (RF)\left(h_{in} - h_{out}\right)_{rev}\right] \tag{15B.29}$$

From equation (15B.29) it would appear that we would want the value of RF to be as large as possible; however, the irreversible processes that increase the value of RF are precisely the processes that decrease the value of η_P. It turns out that for maximum turbine output for a given inlet state, the most desirable situation is to have the values of both η_P and RF be as close to unity as possible. This point can be illustrated as follows.

If we examine the behavior of the pure substance model for H_2O, we find that in the superheat region, along isotropes, i.e., paths of states with the same value for the specific entropy, the data can be fit with the expression Pv^n = constant where $n > 1$ but not equal to the ratio of the specific heats, c_P/c_v. For example, a typical state at entrance to a modern steam turbine might be P_{in} = 2 x 10^7 N/m^2 and T_{in} = 600 C. The value of the specific entropy is s_{in} = 6.5075 kJ/kg K. The locus of states with the same value of specific entropy would appear as in Figure 15B.9.

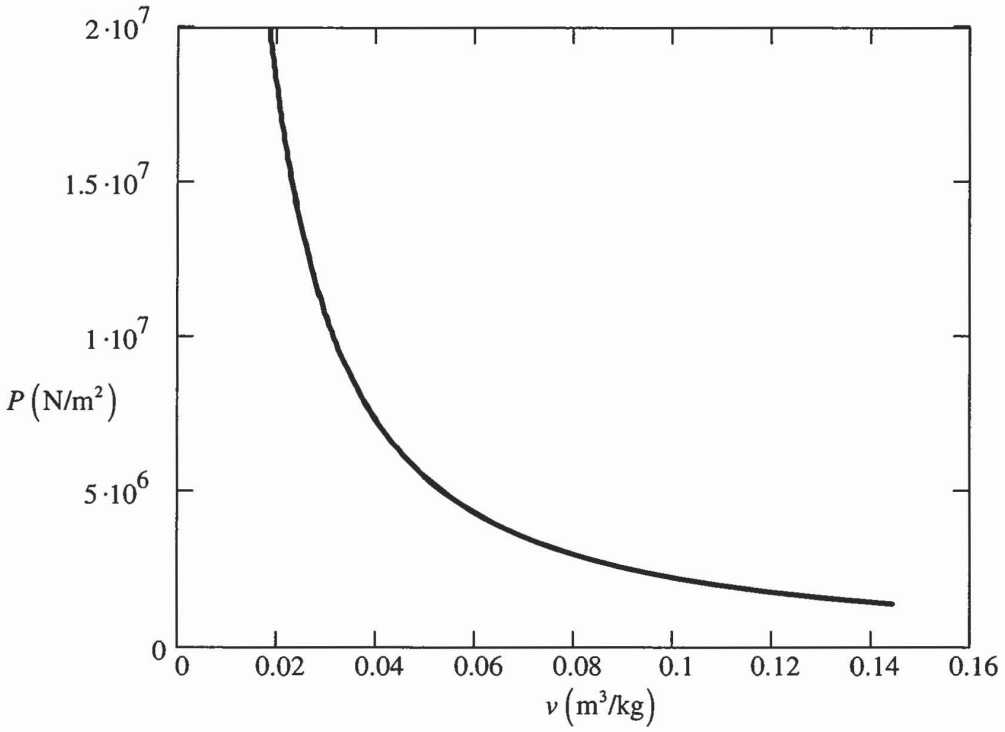

Figure 15B.9 Locus of States of H_2O with s = 6.5075 kJ/kg

Figure 15B.9 actually also shows a curve fit Pv^n = constant with n = 1.284 superimposed on the data, but the precision of the fit is so high, the two plots are indistinguishable. Then we can use equation (15.69) to quantify equation (15B.28) within the limits of the ideal gas model curve fit shown in Figure 15B.9. A plot of the result is shown in Figure 15B.10 with P_1/P_2 the pressure ratio across a typical stage.

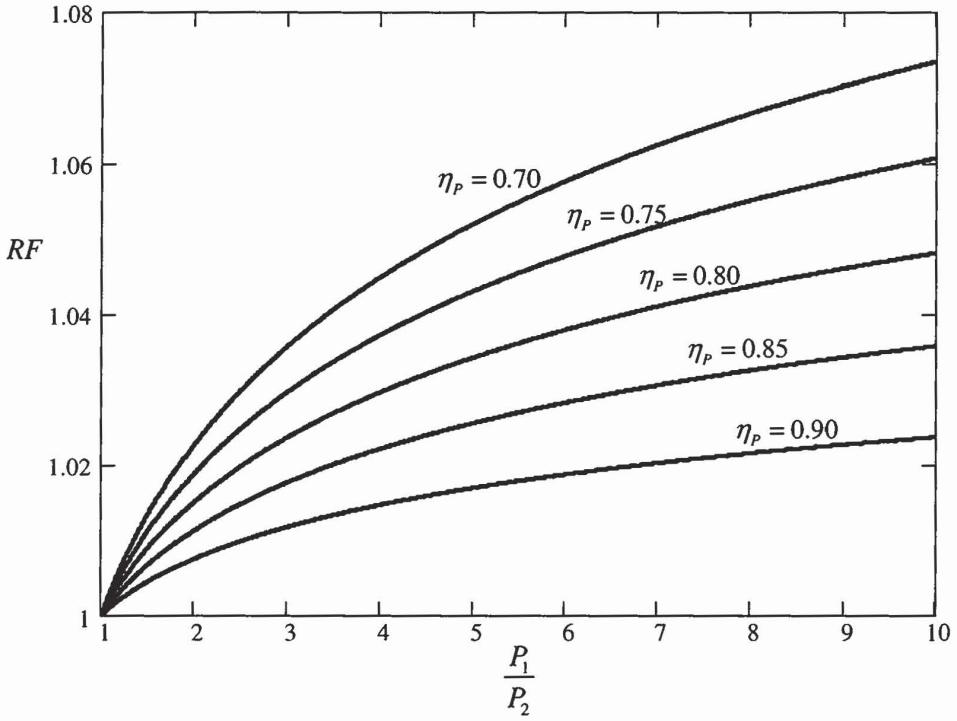

Figure 15B.10 Reheat Factor for Ideal Gas Model for Superheated Steam

Figure 15B.10 and equation (15B.29) together clearly show that although the reheat factor increases with increasing irreversibility, the polytropic efficiency decreases faster and the performance of the turbine declines.

PROBLEMS

15.1 The steady-state operating conditions of a water-cooled air compressor are shown in Figure 15P.1. The heat transfer between the compressor and the environment is negligible. If kinetic and potential energy effects are neglected, determine the power required to drive the compressor. The air can be modeled as an ideal gas with $c_v = 716$ J/kg K and $R = 287$ J/kg K. The cooling water can be modeled as an incompressible fluid with $c = 4187$ J/kg K and $\rho = 1000$ kg/m^3.

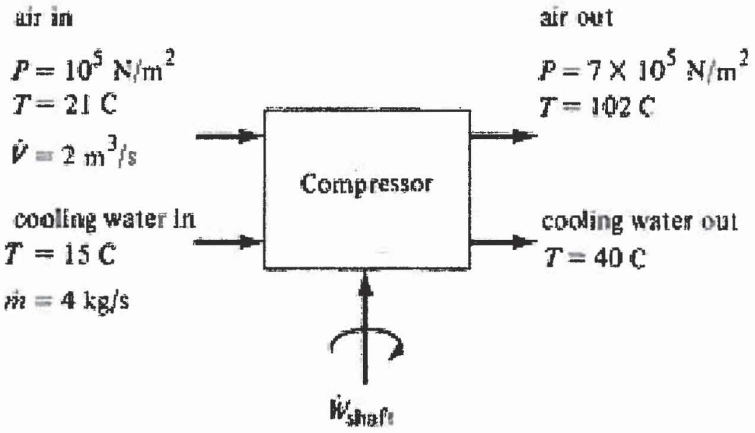

Figure 15P.1 Water-cooled Air Compressor

15.2 A steady flow pump receives saturated liquid H_2O at $T_1 = 25$ C. The pump delivers the liquid at a pressure of $P_2 = 7 \times 10^6$ N/m^2.

(a) Determine the shaft work transfer rate per unit mass flow rate if the pump is reversible and adiabatic.

(b) Estimate the outlet temperature from the pump if the efficiency is $\eta_{-} = 0.5$. (State clearly the model used for the constitutive relation for the fluid.)

(c) Repeat parts (a) and (b) for a pump discharge state with the exit 400 m above the pump inlet and a pressure at the elevated exit of $P_2 = 7 \times 10^6$ N/m^2.

15.3 The centrifugal air compressor is an alternate design for the compressor section of a gas turbine engine, particularly a small engine of low power output. This design operates in much the same manner as the centrifugal pump discussed in Chapter 15. In a particular application, the centrifugal air compressor of a gas turbine engine receives air from the ambient atmosphere where the pressure is $P_1 = 9 \times 10^4$ N/m^2 and the temperature is $T_1 = 27$ C. At the discharge of the compressor, the pressure is $P_2 = 3.7 \times 10^5$ N/m^2, the temperature is $T_2 = 205$ C, and the velocity is $\mathcal{V}_2 = 100$ m/sec. The mass flow rate into the compressor is a steady $\dot{m} = 20$ kg/sec.

(a) If the air can be modeled as an ideal gas with constant specific heats c_P and c_v, determine the power required to drive the compressor.

(b) Determine the adiabatic efficiency, η_C, of the compressor.

15.4 In the gas processing industry, nitrogen is separated from atmospheric air as a saturated liquid at a pressure of $P_1 = 10^5$ N/m^2. The nitrogen is then stored as a liquid until needed. The liquid is then vaporized and pumped into tanks for distribution at $P_3 = 2 \times 10^7$ N/m^2 and $T_3 = 27$

C for use in industrial facilities, welding operations, etc. Three schemes have been suggested for the vaporization and tank charging process as shown in Figure 15P.4. The first involves compressing the liquid from $P_1 = 10^5$ N/m^2 to $P_2 = 2 \times 10^7$ N/m^2 with a reversible, adiabatic pump and then vaporizing the high pressure liquid by heat transfer with the atmosphere. The second scheme involves first vaporizing the liquid and then compressing the gas in a reversible, adiabatic compressor so that the gas leaves the compressor at $P_3 = 2 \times 10^7$ N/m^2 and $T_3 = 27$ C. Finally, the third scheme involves vaporizing the liquid to produce a gas at $P_2 = 10^5$ N/m^2 and $T_2 = 27$ C and subsequently compressing the gas to $P_3 = 2 \times 10^7$ N/m^2 in a reversible isothermal compressor.

(a) Determine the heat transfer and work transfer per unit mass of nitrogen in each of the schemes suggested.

(b) Which scheme requires the minimum work transfer and why?

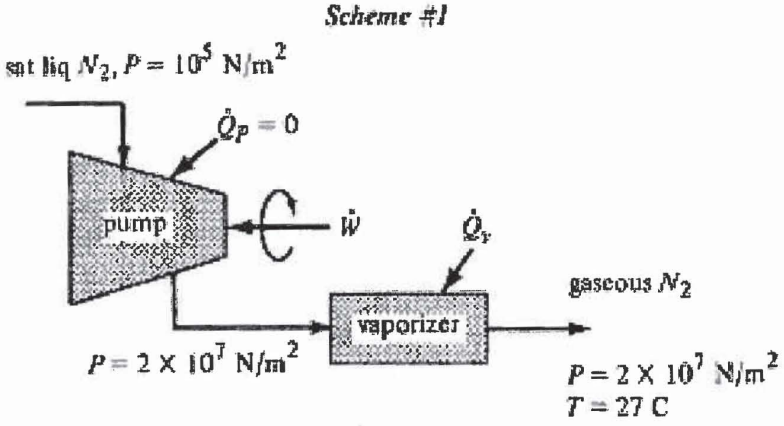

Figure 15P.4(a) Nitrogen Liquid Pump-Vaporizer System

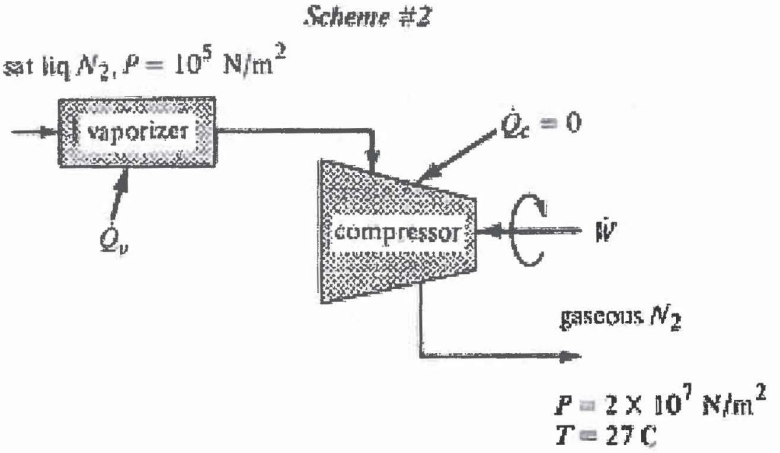

Figure 15P.4(b) Nitrogen Vaporizer-Adiabatic Compressor System

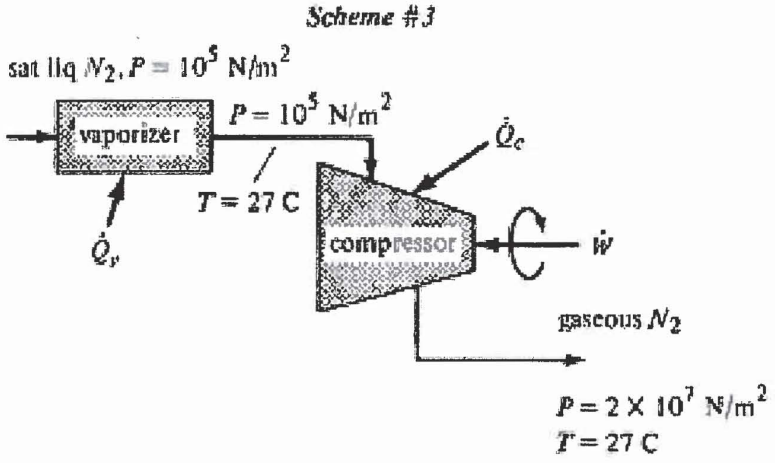

Figure 15P.4(c) Nitrogen Vaporizer-Isothermal Compressor System

15.5 Internal combustion engines such as those used to power automobiles and some trucks are basically a collection of piston-cylinder apparatuses much like those we have discussed previously. They can be modeled according to a cycle developed in the late 19th century by an engineer named Otto. During the cycle, the pressure inside the cylinder varies as the piston moves back and forth between the limits of its travel. Analysis of the Otto cycle shows that the power output of the engine is a function of the mean effective pressure inside the cylinder during the cycle.

In an effort to keep the size and mass of the vehicles as small as possible so that fuel efficiency can be as high as possible, thermal-fluids engineers are working to increase the power density (power per unit volume or power per unit mass) of the engine. One of the means of doing this is to increase the mean effective pressure inside the cylinder by increasing the inlet pressure to the engine through a device known as a supercharger. Superchargers are nothing more than air compressors mounted in the inlet air stream to the engine, and they can be powered by means of a shaft driven by the engine itself or by means of a small turbine that utilizes the "waste" energy in the exhaust stream from the engine. The later design is known as a "turbo-charger."

The compressor of a turbo-charger shown in Figure 15P.5 has an inlet flow rate of $\dot{m} =$ 7.5 m^3/min of air as measured at the inlet condition of $P_1 = 1.013 \times 10^5$ N/m^2 and $T_1 = 288$ K. The compressor has a pressure ratio of $P_2/P_1 = 1.5$ and an adiabatic shaft work efficiency of $\eta_C =$ 0.80. The compressor is driven directly by an exhaust turbine with an adiabatic shaft work efficiency of $\eta_T = 0.70$. The turbo-charger and engine are arranged so that they work on the "constant pressure system" which means both turbine and compressor operate under conditions of steady flow. The turbine pressure ratio is the same as that for the compressor and the mass of engine fuel may be neglected. Calculate the inlet temperature to the turbine and the power produced by the turbine. Assume air and exhaust gas can be modeled as an ideal gas with $\gamma = 1.4$ and $R = 287$ J/kg K.

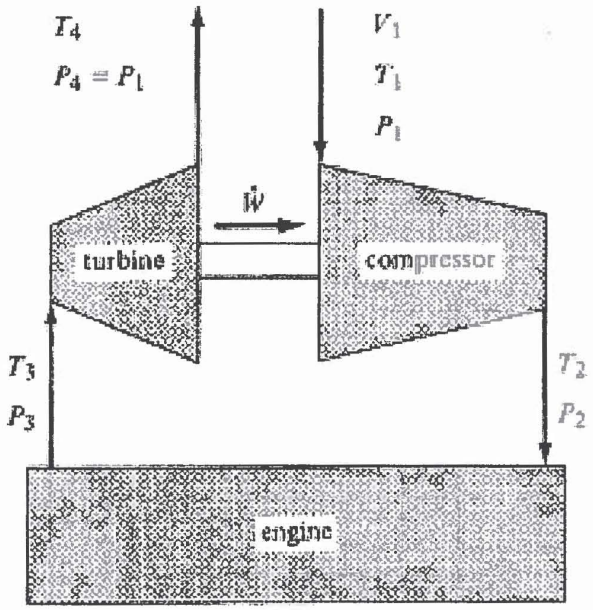

Figure 15P.5 Schematic of Automotive Turbo-charger

15.6 In the present energy market, it is common for power plants to adjust their output to meet the varying demand for energy. One simple way to do this is to install a throttle valve on the inlet side of the turbine and drop the pressure at the turbine inlet to reduce the power output as required. One problem with this method is that it generates a lot of entropy which degrades overall performance of the plant.

As shown in Figure 15P.6, H_2O is supplied to the throttle valve at a pressure of $P_1 = 3 \times 10^5$ N/m^2 and a temperature of $T_1 = 540$ C. The turbine has an adiabatic efficiency of 0.90. The condenser operates at a constant pressure of $P_3 = 3 \times 10^3$ N/m^2 and discharges saturated liquid H_2O at all operating conditions. The temperature of the cooling water at entrance to the condenser is $T_{cw,in} = 17$ C and at exit is $T_{cw,out} = 22$ C.

(a) Calculate the mass flow rate of H_2O through the turbine for a power output of 100 MW at full throttle (no pressure drop across the valve).

(b) What is the mass flow rate of cooling water for the full load condition?

(c) The throttle is adjusted so that the pressure at inlet to the turbine is $P_2 = 2 \times 10^5$ N/m^2 and the mass flow rate through the turbine is reduced to 75 % of the mass flow rate at full load. Calculate the turbine power output at this throttle setting.

(d) Calculate the cooling water flow rate for this new throttle setting.

(e) Calculate the rate of entropy generation due to the change in throttle setting.

(f) How does this entropy generation impact on plant performance?

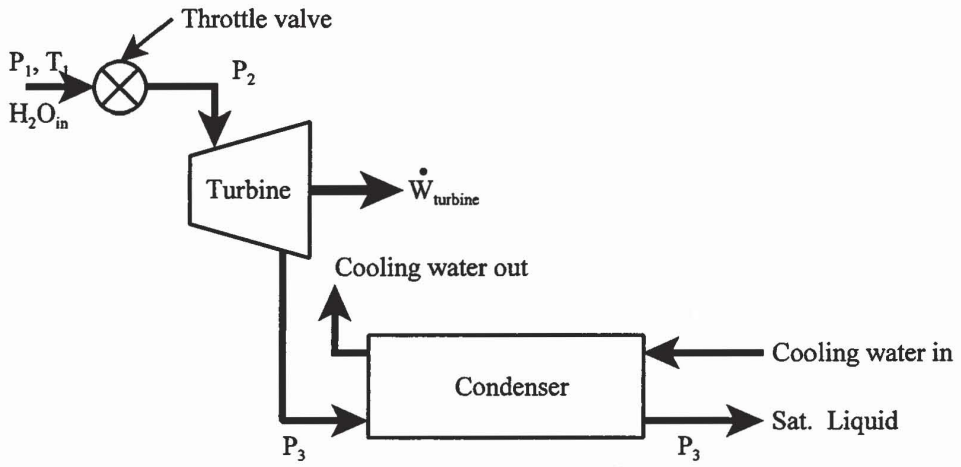

Figure 15P.6 Throttled Steam Turbine

15.7 As a consulting engineer, you are asked to specify the installation of a steam-powered turbo compressor unit for a large industrial plant. The purpose of the plant is to provide moderately high pressure air to operate air-actuated assembly line components and general service air for the plant. The two-stage centrifugal compressor is fitted with a combined intercooler and aftercooler as shown in the sketch below. The air leaving the first stage of the compressor at a pressure of P_1 = 3.873 x 10^5 N/m^2 enters the intercooler where it is cooled to a temperature of T_1 = 300 K. The air then returns to the compressor where it is further compressed to a pressure of $P_{air,out}$ = 1.5 x 10^6 N/m^2. The air then enters the aftercooler where it is cooled to a temperature of $T_{air,out}$ = 300 K. The volume flow rate from the aftercooler at the pressure of $P_{air,out}$ = 1.5 x 10^6 N/m^2 and the temperature of $T_{air,out}$ = 300 K is $\dot{V}$ = 10^4 m^3/hr. The steam used as the working fluid in the turbine component enters the turbine at a pressure of $P_{steam,in}$ = 2 x 10^6 N/m^2 and a temperature of $T_{steam,in}$ = 400 C and exits at a pressure of $P_{steam,out}$ = 10^5 N/m^2. The adiabatic efficiencies of the turbine and each stage of the compressor are η_T = 0.9 and η_C = 0.85, respectively. Cooling water enters the intercooler/aftercooler at a temperature of $T_{cw,in}$ = 20 C and exits at a temperature of $T_{cw,out}$ = 25 C.

The air entering the compressor can be modeled as an ideal gas with R = 287 J/kg K and c_P = 1003 J/kg K in state T_{atm} = 300 K and P_{atm} = 10^5 N/m^2. The cooling water in the intercooler can be modeled as an incompressible fluid with ρ_{cw} = 1000 kg/m^3 and c_{cw} = 4187 J/kg K.

(a) On a T-s diagram for air, show the states of the air as it passes through the compressor and intercooler/aftercooler.

(b) Determine the mass flow rate of steam required to power this unit.

(c) Determine the mass flow rate of cooling water through the intercooler/aftercooler necessary to achieve the operation described.

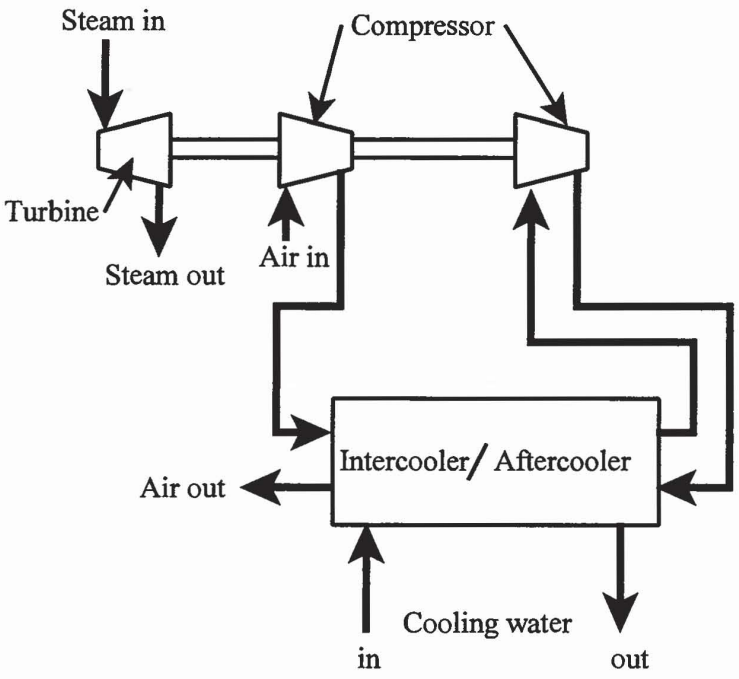

Figure 15P.7 Steam-powered Turbo Compressor

15.8 A steam power plant has a steam generator that operates at a supercritical pressure of 25 x 10^6 N/m^2. As shown in Figure 15P.8, the feed water pump supplies the steam generator with H_2O at this pressure by pumping saturated liquid H_2O from the condenser at a pressure of 10^4 N/m^2. The adiabatic shaft efficiency of the pump is $\eta_P = 0.70$. The feed water pump is powered by a small adiabatic steam turbine that utilizes steam that has been throttled to a pressure of $P_3 = 10^6$ N/m^2 from the steam supply at a pressure of $P_{supply} = 3 \times 10^6$ N/m^2 and a temperature of 540 C. The turbine exhausts the steam at a pressure of $P_4 = 10^4$ N/m^2. The adiabatic shaft efficiency of the turbine is $\eta_T = 0.90$.

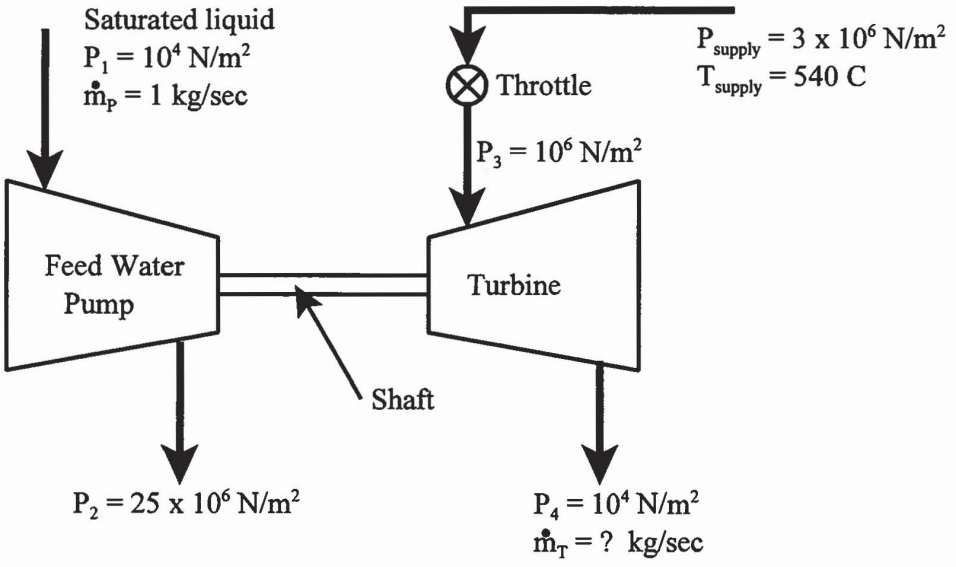

Figure 15P.8 Turbine Driven Feed Pump

(a) Show the processes in the turbine on a *T-s* diagram. Clearly identify the inlet and outlet states and their orientation to the locus of saturated states.

(b) Show the processes in the feed water pump on the same *T-s* diagram. Clearly identify the inlet and outlet states and their orientation to the locus of saturated states.

(c) For a turbine shaft power output of 1 W, calculate the mass flow rate of steam through the turbine.

(d) Use the result of part (c) above to estimate the mass flow rate (kg/sec) of steam through the turbine per unit mass flow rate (kg/sec) of H_2O through the feed water pump.

15.9 An ideal gas ($\gamma = 1.4$) flows through a three-stage axial flow air compressor that has the following stage pressure ratios and adiabatic efficiencies:

Stage	Pressure Ratio	Adiabatic Efficiency
1	1.6	0.87
2	1.4	0.89
3	1.3	0.90

(a) Calculate the overall pressure ratio and the overall adiabatic efficiency of the compressor.

(b) Assuming that the polytropic efficiency is constant for all three stages, calculate the polytropic efficiency.

(c) Consider the case in which the temperature ratios and the adiabatic efficiencies of the individual stages are identical and the overall temperature ratio is the same as that above. Compare the resulting stage efficiency with the polytropic efficiency.

15.10 The degree of reaction, n, of an axial compressor stage can be defined as the enthalpy increase across the rotor divided by the enthalpy increase across the stage, viz.

$$n = \frac{(h_2 - h_1)}{(h_3 - h_1)}$$

where the subscripts 1, 2, and 3 denote the state at entrance to the rotor, the state at exit from the rotor and at entrance to the stator, and the state at exit from the stator, respectively.

(a) Starting with equation (15.53) and Figure 15.5 and the fact that the absolute axial velocity is constant through the machine ($\vartheta_{a1} = \vartheta_{a2} = \vartheta_a$), show that

$$n = \frac{\vartheta_{r1}^{\,2} - \vartheta_{r2}^{\,2}}{2R\omega(\vartheta_{t2} - \vartheta_{t1})}$$

and

$$n = \frac{1}{2} + \frac{(\tan\beta_2 - \tan\alpha_1)\vartheta_a}{2R\omega}$$

(b) For an axial flow compressor with a ratio of hub radius to tip radius of 0.6 and the following conditions at the mean radius:

$$\frac{\vartheta_a}{R_{mean}\omega} = 0.4 \quad \text{and} \quad n = 0.5 \quad \text{and} \quad \alpha_1 = 30^\circ$$

calculate β_1 and n at the tip radius if $\vartheta_t \propto r^{-1}$.

15.11 Steam at a pressure of $P_1 = 6 \times 10^5$ and a temperature of $T_1 = 220$ C flows through a nozzle to a pressure of $P_2 = 10^5$ N/m^2. The mass flow rate through the nozzle is $\dot{m} = 5$ kg/sec and the nozzle efficiency is $\eta_N = 0.96$. The velocity of the H_2O at inlet is negligible compared to the velocity at exit.

(a) Calculate the exit velocity of the H_2O assuming that the H_2O is in a uniform state.

(b) Is there any liquid in the exit stream? If so, estimate the droplet size assuming homogeneous nucleation.

(c) Think about the motion of the droplets in the vapor medium. Under what conditions would the droplets travel at the same velocity as the vapor?

(d) We would like to estimate the Mach number of the exit stream. The software used to generate the thermal-fluid properties of H_2O calculates the speed of sound by forming the derivative

$$a^2 = \left(\frac{\partial P}{\partial \rho}\right)_s$$

but lacking this software we can estimate the speed of sound in the vapor phase by modeling the vapor as an ideal gas (not a very good model for the saturated vapor) and calculating the speed of sound accordingly. If we model the H_2O vapor as an ideal gas, it turns out that $\gamma = 1.3363$ and $R = 461.52$ J/kg K. Use this information to estimate the speed of sound and the Mach number in the vapor in the exit stream. Compare this estimated value of the speed of sound with the value from the pure substance model: $a = 472.0$ m/sec.

(e) Calculate the cross-sectional area of flow at the nozzle exit.

15.12 Consider a rocket engine shown schematically in Figure 15P.12. In a static test firing of the engine, a force $\mathfrak{I}$, known as the thrust force of the engine, must be applied to the housing of the engine to maintain it in static equilibrium. The engine generates gas steadily at stagnation conditions of P_0 and T_0, and these gases pass to the atmosphere, whose static pressure is P_{atm}, through a nozzle with throat area A_t. At the exit plane of the nozzle, the area is A_e and the pressure is P_e. Except under operating conditions far from the design point, sonic conditions occur at the throat and the flow throughout the nozzle is isentropic.

(a) Show that the thrust is given by

$$\mathfrak{I} = \dot{m}\vartheta_e + A_e\left(P_e - P_{atm}\right)$$

where $\dot{m}$ is the mass flow rate of gas through the nozzle and ϑ_e is the velocity of the exhaust gas at the exit plane.

(b) Show that the thrust can be cast in the dimensionless form

$$\frac{\mathfrak{I}}{P_0 A_t} = \gamma\sqrt{\frac{2}{\gamma-1}\left(\frac{2}{\gamma+1}\right)^{\frac{\gamma+1}{\gamma-1}}}\sqrt{1-\left(\frac{P_e}{P_0}\right)^{\frac{\gamma-1}{\gamma}}} + \frac{A_e}{A_t}\left(\frac{P_e}{P_0} - \frac{P_{atm}}{P_0}\right)$$

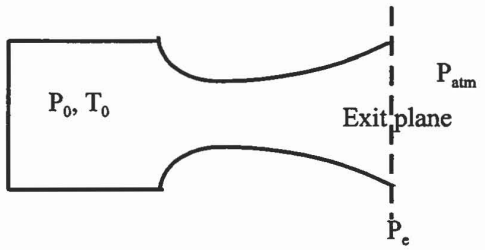

Figure 15P.12 Schematic of Rocket Engine

15.13 A child's toy is a small vehicle of mass $M = 0.5$ kg mounted on four wheels. The shape of the vehicle consists of a body of revolution with a cross-sectional diameter $D = 5$ cm and a drag coefficient of $C_D = 0.15$. The rolling resistance exclusive of aerodynamic drag is negligible. The vehicle is powered by the contents of a small cylinder initially containing a mass of $m_0 = 12$ gm of saturated CO_2 under pressure at a temperature of $T_0 = 20$ C. The cylinder volume is $V = 14$ ml (1 ml = 10^{-3} Liter; 1 L = 10^3 cm^3). The vehicle is set in motion by instantaneously piercing the end of the cylinder with a hole of diameter $d = 1.6$ mm. The CO_2 exits through this hole at sonic velocity.

(a) Describe an appropriate model for the state of the contents of the cylinder as a function of time after it is pierced.

(b) Estimate the speed of the vehicle after it has traveled 30 m.

(c) What mass of CO_2 remains in the cylinder after the vehicle has traveled 30 m?

The following table gives some properties of CO_2 under saturation conditions. Other properties can be found in the tabulation of thermal-fluid properties and at the NIST website http://webbook.nist.gov/chemistry/fluid/

Temperature (C)	Pressure (MPa)	Vapor Density (kg/m^3)	Vapor Speed of Sound (m/sec)
-20.000	1.9696	51.700	220.41
-15.000	2.2908	60.728	218.85
-10.000	2.6487	71.185	216.94
-5.0000	3.0459	83.359	214.68
0.00000	3.4851	97.647	212.04
5.0000	3.9695	114.621	208.97
10.000	4.5022	135.156	205.41
15.000	5.0871	160.730	201.21
20.000	5.7291	194.202	196.09
25.000	6.4342	242.732	189.12
30.000	7.2137	345.102	171.26

15.10 One method of producing liquid nitrogen is the Joule-Thomson liquefier shown in Figure 15P.10. Nitrogen gas at a pressure of $P_1 = 10^7$ N/m^2 and a temperature of $T_1 = 300$ K flows at a rate of $\dot{V}_1 = 10$ m^3/min (measured at 10^5 N/m^2) through the heat exchanger which can be modeled as a constant pressure device. The high-pressure discharge from the heat exchanger flows through the Joule-Thomson valve where its pressure is reduced to $P_3 = 10^5$ N/m^2. Some of the N_2 in state 3 is liquid and is collected in the storage Dewar. The vapor discharged from the J-T valve is directed back through the heat exchanger. The exhaust stream from the heat exchanger is at the temperature $T_5 = 297$ K. State 6 is saturated liquid nitrogen.

(a) Determine the rate $\dot{m}_6$ at which liquid nitrogen is delivered by this system in the steady state.

(b) Plot the temperature difference in the heat exchanger vs. the temperature of the low

pressure stream in the heat exchanger.

(c) Determine the rate of entropy generation in the heat exchanger and show how it could be reduced.

(d) Show how $\dot{m}_6$ is affected if the rate of entropy generation in the heat exchanger is reduced.

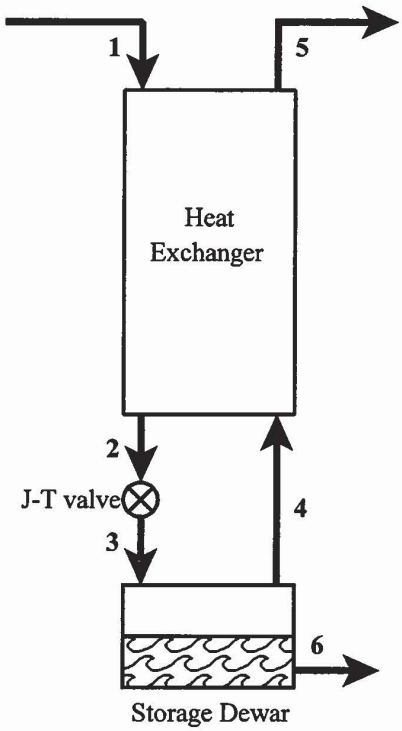

Figure 15P.10 Simple Joule-Thomson Liquefier

Chapter 17

Chemical Behavior of Thermal-Fluid Systems

17.1 Introduction

We now take up the situation in which a thermal-fluid system is comprised of several different components that can undergo chemical reactions that alter the composition of the system. Our objective in this case is to determine the manner in which the thermodynamic state of the system affects the composition as well as the manner in which the composition, in turn, affects the magnitudes of the interactions between the system and its environment. We shall use the second law to determine the composition and the first law to determine the magnitudes of the interactions. As an outgrowth of this study, we shall examine the behavior of ideal gas mixtures and mixtures of an ideal gas and a condensible vapor. Finally, we shall consider systems in the liquid phase that form solutions of varying composition.

17.2 Chemical Equilibrium

We first consider the case of a system consisting of a single phase in which a single reaction can occur. We represent this reaction by a chemical equation of the form

$$\nu_1 R_1 + \nu_2 R_2 + \ldots + \nu_j R_j \rightarrow \nu_{j+1} P_j + \ldots + \nu_c P_c \tag{17.1}$$

where $R_1 \ldots R_j$ are the reactants and $P_{j+1} \ldots P_c$ are the products of the reaction. The parameters $\nu_1 \ldots \nu_c$ are called the *stoichiometric coefficients* of the components 1,2, ...c and their values determine the conservation of atoms of the species involved in the reaction. It is important to note that in writing the chemical equation in this manner, the stoichiometric coefficients of the components that are formed as the reaction proceeds to the right have positive sign while those of the reactants, i.e., those components consumed in the reaction, are assumed to be negative.

We now introduce the Law of Definite Proportions which states that the increase in mass of a component i being formed in a reaction is proportional to its molecular mass M_i and its stoichiometric coefficient ν_i in the reaction. For each of the c components in the reaction, there is a mathematical expression of the law of the form

$$m_i - m_i^0 = \nu_i M_i \xi \tag{17.2}$$

where ξ is the *extent of reaction* or the *reaction coordinate*. At the time $t = 0$, $\xi = 0$, and the initial mass of component i is m_i^0. When $\xi = 1$, $\nu_1 \ldots \nu_j$ kmoles of $R_1 \ldots R_j$ reactants have been converted into $\nu_{j+1} \ldots \nu_c$ kmoles of $P_{j+1} \ldots P_c$. As the system passes from $\xi = 0$ to $\xi = 1$, one equivalent reaction has occurred.

If we sum all equations of the form (17.2) for the reaction, we obtain the conservation of mass, viz.

$$\sum_i \nu_i M_i = 0 \tag{17.3}$$

If we differentiate equations (17.2) with respect to time, we obtain

$$\frac{dm_i}{dt} = \nu_i M_i \frac{d\xi}{dt} \tag{17.4}$$

which can be also expressed as

$$\frac{d\xi}{dt} = \frac{dm_1}{\nu_1 M_1} = \frac{dm_2}{\nu_2 M_2} = \cdots = \frac{dm_c}{\nu_c M_c} \tag{17.5}$$

where $d\xi/dt$ is the rate of reaction, ϑ, at time t, viz.

$$\vartheta = \frac{d\xi(t)}{dt} \tag{17.6}$$

If we divide each of equations (17.2) through by the appropriate molecular mass, we obtain equations (17.2) in terms of mole numbers, viz.

$$n_i - n_i^0 = \nu_i \xi_i \tag{17.7}$$

where the mole number n_i is given by

$$n_i = \frac{m_i}{M_i} \tag{17.8}$$

Then

$$d\xi = \frac{dn_1}{\nu_1} = \frac{dn_2}{\nu_2} = \cdots = \frac{dn_c}{\nu_c} \tag{17.9}$$

It is often convenient to express the chemical composition of a system in terms of mole fractions, x_i, where the *mole fraction of component i*, is given by

$$x_i = \frac{n_i}{\sum_i n_i} = \frac{n_i^0 + \nu_i \xi}{\sum_i n_i^0 + \xi \sum_i \nu_i} = \frac{n_i^0 + \nu_i \xi}{n_0 + \nu \xi} \tag{17.10}$$

where we have introduced the short-hand notation

$$n_0 = \sum_i n_i^0 \quad \text{and} \quad \nu = \sum_i \nu_i \tag{17.11}$$

Note that $0 \le x_i \le 1$.

Given the fact that the composition of the single phase system can change as a result of the single chemical reaction, we are no longer dealing with a simple system. Then the specification of the state of the system requires the specification of more properties than were required heretofore. According to the state principle, one additional property is required for each departure from a simple system. Then for the system of interest, we could specify the state by specifying the temperature, pressure, and mole numbers, i.e., (T, P, n_1, ..., n_c), or we can make use of the extent of reaction and specify the state as (T, P, ξ). Note that since each of these parameters can be expressed in terms of time, we have

$$P = P(t) \quad \text{and} \quad T = T(t) \quad \text{and} \quad \xi = \xi(t) \tag{17.12}$$

and the reaction rate becomes

$$\frac{d\xi}{dt} = \vartheta(T, P, \xi) = \vartheta(t, \xi) \tag{17.13}$$

17.2.2 Entropy Generation due to Chemical Reactions under Various Conditions

We now introduce the notion of partial equilibrium. The systems of interest in the present case are in equilibrium with respect to certain properties, such as temperature and pressure, and there are no irreversibilities associated with changes in these properties. On the other hand, the system is not in equilibrium with respect to the redistribution of matter among the constituents susceptible to chemical reaction. The simplest example is a mixture of ideal gases capable of chemical reaction – an example we shall consider in detail shortly.

For the present, we wish to establish the extremum condition that applies under various conditions. Then from the first law, we have

$$dU = \delta Q - \delta W = \delta Q - PdV \tag{17.14}$$

From the second law, we have

$$dS = \frac{\delta Q}{T} - \delta S_{gen} \tag{17.15}$$

Substituting equation (17.15) into equation (17.14), we get

$$dU = TdS - T\delta S_{gen} - PdV \tag{17.16}$$

For irreversible reactions at constant S and V, we have

$$T\delta S_{gen} = -dU > 0 \tag{17.17}$$

If we apply the Legendre Transformation (*cf.* Chapter 14) to equation (17.17) and replace the property V with its canonically conjugate property $-P$, we get the extremum condition for a system experiencing irreversible chemical reaction at fixed values of S and P, viz.

$$T\delta S_{gen} = -\left[dU - d(-PV)\right] = -\left[d(U+PV)\right] = -dH > 0 \tag{17.18}$$

where H is the enthalpy.

Similarly, if we apply the Legendre Transformation (*cf.* Chapter 14) to equation (17.17) and replace the property S with its canonically conjugate property T, we get the extremum condition for a system experiencing irreversible chemical reaction at fixed values of T and V, viz.

$$T\delta S_{gen} = -\left[dU - d(TS)\right] = -\left[d(U-TS)\right] = -dF > 0 \tag{17.19}$$

where F is the Helmholtz free energy.

Finally, if we apply the Legendre Transformation (*cf.* Chapter 14) to equation (17.17) and replace both S and V with their canonically conjugate properties T and $-P$, we get the extremum condition for a system experiencing irreversible chemical reaction at fixed values of T and P, viz.

$$T\delta S_{gen} = -\left[dU - d(TS) - d(-PV)\right] = -\left[d(U-TS+PV)\right] = -dG > 0 \tag{17.20}$$

where G is the Gibbs free energy.

In practice it is most commonly the case that chemical reactions occur in systems with environments that can be modeled as combined heat and work reservoirs so that equation (17.20) is the extremum condition of greatest interest. Equation (17.20) states that for a system at constant T and P, the chemical reaction will proceed in the direction that results in a minimum value of the Gibbs free energy consistent with the fixed values of T and P.

17.2.3 Entropy Generation and the Affinity of Reaction

Consider a system in which a chemical reaction is the only irreversible change that takes place with ξ changing by an amount $d\xi$ during the time interval dt. Then the rate of entropy generation by the reaction is given by

$$\frac{\delta S_{gen}}{dt} = \frac{A}{T}\frac{d\xi}{dt} \geq 0 \tag{17.21}$$

where we have introduced A, the *affinity of reaction*. The concept of the affinity of reaction was first introduced in 1922 by Theophile De Donder of the University of Brussels as a means of using the entropy generated in a reaction as the determining factor for chemical equilibrium. In equation (17.21), inequality corresponds to spontaneous reaction in which entropy is generated as a means of minimizing the appropriate characteristic thermodynamic function, e.g., Gibbs free energy under conditions of fixed T and P. Equality in equation (17.21) sets the condition of chemical equilibrium.

We can combine equations (17.13) and (17.21) in the form

$$\frac{A}{T}\vartheta \geq 0 \tag{17.22}$$

such that when:

$$\begin{aligned} A>0, \vartheta>0 \\ A<0, \vartheta<0 \\ A=0, \vartheta=0 \end{aligned} \tag{17.22}$$

It follows then that the reaction rate always has the same sign as the affinity, and when chemical equilibrium prevails, the reaction rate is zero. The necessary and sufficient condition for chemical equilibrium is then

$$A(T,P,\xi)=0 \tag{17.23}$$

which defines an equilibrium surface on which all the states of thermodynamic and chemical equilibrium lie.

17.2.4 Affinity and the Characteristic Thermodynamic Functions

From the definition of the affinity and equations (17.17) through (17.20), the differentials of the characteristic thermodynamic functions for a chemically reacting system become

$$dU = TdS - PdV - Ad\xi \tag{17.24}$$

$$dH = TdS + VdP - Ad\xi \tag{17.25}$$

$$dF = -SdT - PdV - Ad\xi \tag{17.26}$$

$$dG = -SdT + VdP - Ad\xi \tag{17.27}$$

For the equilibrium energy surface we have

$$U = U(S,V,\xi) \tag{17.28}$$

Then the differential is

$$dU = \left(\frac{\partial U}{\partial S}\right)_{V,\xi} dS + \left(\frac{\partial U}{\partial V}\right)_{S,\xi} dV + \left(\frac{\partial U}{\partial \xi}\right)_{S,V} d\xi \tag{17.29}$$

Comparing equations (17.24) and (17.29), we find

$$T = \left(\frac{\partial U}{\partial S}\right)_{V,\xi} \quad \text{and} \quad -P = \left(\frac{\partial U}{\partial V}\right)_{S,\xi} \quad \text{and} \quad -A = \left(\frac{\partial U}{\partial \xi}\right)_{S,V} \tag{17.30}$$

In a similar fashion, we can write

$$H = H(S,P,\xi) \tag{17.31}$$

with

$$dH = \left(\frac{\partial H}{\partial S}\right)_{P,\xi} dS + \left(\frac{\partial H}{\partial P}\right)_{S,\xi} dP + \left(\frac{\partial H}{\partial \xi}\right)_{S,P} \tag{17.32}$$

Comparing equations (17.25) and (17.32), we find

$$T = \left(\frac{\partial H}{\partial S}\right)_{P,\xi} \quad \text{and} \quad V = \left(\frac{\partial H}{\partial P}\right)_{S,\xi} \quad \text{and} \quad -A = \left(\frac{\partial H}{\partial \xi}\right)_{S,P} \tag{17.33}$$

Also, we can write

$$F = F(T,V,\xi) \tag{17.34}$$

with

$$dF = \left(\frac{\partial F}{\partial T}\right)_{V,\xi} dT + \left(\frac{\partial F}{\partial V}\right)_{T,\xi} dV + \left(\frac{\partial F}{\partial \xi}\right)_{T,V} d\xi \tag{17.35}$$

Comparing equations (17.26) and (17.35), we find

$$-S = \left(\frac{\partial F}{\partial T}\right)_{V,\xi} \quad \text{and} \quad -P = \left(\frac{\partial F}{\partial V}\right)_{T,\xi} \quad \text{and} \quad -A = \left(\frac{\partial F}{\partial \xi}\right)_{T,V} \tag{17.36}$$

Finally, we can write

$$G = G(T, P, \xi) \tag{17.37}$$

with

$$dG = \left(\frac{\partial G}{\partial T}\right)_{P,\xi} dT + \left(\frac{\partial G}{\partial P}\right)_{T,\xi} dP + \left(\frac{\partial G}{\partial \xi}\right)_{T,P} d\xi \tag{17.38}$$

Comparing equations (17.27) and (17.38), we find

$$-S = \left(\frac{\partial G}{\partial T}\right)_{P,\xi} \quad \text{and} \quad V = \left(\frac{\partial G}{\partial P}\right)_{T,\xi} \quad \text{and} \quad -A = \left(\frac{\partial G}{\partial \xi}\right)_{T,P} \tag{17.39}$$

Thus, we have now established the affinity of reaction in terms of the slope along the reaction coordinate of the appropriate characteristic thermodynamic function, viz.

$$A = -\left(\frac{\partial U}{\partial \xi}\right)_{S,V} = -\left(\frac{\partial H}{\partial \xi}\right)_{S,P} = -\left(\frac{\partial F}{\partial \xi}\right)_{T,V} = -\left(\frac{\partial G}{\partial \xi}\right)_{T,P} \tag{17.40}$$

17.2.5 The Chemical Potential

Suppose that we now replace the reaction coordinate by the mole numbers in our specification of the state of the reacting system. Then the equilibrium energy surface is given by

$$U = U(S, V, n_1, n_2, \ldots n_c) \tag{17.41}$$

Then the differential becomes

$$dU = \left(\frac{\partial U}{\partial S}\right)_{V,n} dS + \left(\frac{\partial U}{\partial V}\right)_{S,n} dV + \sum_i \left(\frac{\partial U}{\partial n_i}\right)_{S,V,n_{j,j\neq i}} dn_i \tag{17.42}$$

where the subscript n indicates that the n_i are all constant which is equivalent to ξ = constant. Then from equations (17.30), we have

$$\left(\frac{\partial U}{\partial S}\right)_{V,n} = \left(\frac{\partial U}{\partial S}\right)_{V,\xi} = T \tag{17.43}$$

and

$$\left(\frac{\partial U}{\partial V}\right)_{S,n} = \left(\frac{\partial U}{\partial V}\right)_{S,\xi} = -P \tag{17.44}$$

Then equation (17.42) can be written

$$dU = TdS - PdV + \sum_i \left(\frac{\partial U}{\partial n_i}\right)_{S,V,n_{j,j\neq i}} dn_i \tag{17.45}$$

In a similar fashion, we can derive the exact differentials of the other characteristic thermodynamic functions

$$H = H(S, P, n_1, n_2, \ldots n_c) \tag{17.46}$$

$$F = F(T, V, n_1, n_2, \ldots n_c) \tag{17.47}$$

$$G = G(T, P, n_1, n_2, \ldots n_c) \tag{17.48}$$

with

$$dH = TdS + VdP + \sum_i \left(\frac{\partial H}{\partial n_i}\right)_{S,P,n_{j,j\neq i}} dn_i \tag{17.49}$$

$$dF = -SdT - PdV + \sum_i \left(\frac{\partial F}{\partial n_i}\right)_{T,V,n_{j,j\neq i}} dn_i \tag{17.50}$$

$$dG = -SdT + VdP + \sum_i \left(\frac{\partial G}{\partial n_i}\right)_{T,P,n_{j,j\neq i}} dn_i \tag{17.51}$$

If we now perform a series of Legendre transformations on equation (17.45), we get

$$dU - d(-PV) = d(U + PV) = dH = TdS + VdP + \sum_i \left(\frac{\partial U}{\partial n_i}\right)_{S,V,n_{j,j\neq i}} dn_i \tag{17.52}$$

$$dU - d(TS) = d(U - TS) = dF = -SdT - PdV + \sum_i \left(\frac{\partial U}{\partial n_i}\right)_{T,V,n_{j,j\neq i}} dn_i \tag{17.53}$$

$$dU - d(TS) - d(-PV) = d(U - TS + PV) = dG = -SdT + VdP + \sum_i \left(\frac{\partial U}{\partial n_i}\right)_{T,P,n_{j,j\neq i}} dn_i \tag{17.54}$$

Upon comparing equations (17.49) – (17.51) with equations (17.52) – (17.54), we conclude that

$$\left(\frac{\partial U}{\partial n_i}\right)_{S,V,n_{j,j\neq i}} = \left(\frac{\partial H}{\partial n_i}\right)_{S,P,n_{j,j\neq i}} = \left(\frac{\partial F}{\partial n_i}\right)_{T,V,n_{j,j\neq i}} = \left(\frac{\partial G}{\partial n_i}\right)_{T,P,n_{j,j\neq i}} \tag{17.55}$$

The result of equation (17.55), led J. Willard Gibbs to introduce the concept of the chemical potential. In his pioneering work "On the Equilibrium of Heterogeneous Substances," (*Transactions of the Connecticut Academy*, III. Oct. 1875 – May 1876, pp. 108 – 248 and May 1877 – July 1878, pp. 343 – 544) [*cf. The Scientific Papers of J. Willard Gibbs*, Vol. 1, *Thermodynamics*, Oxbow Press, Woodbridge, CT, 1993.], Gibbs defined the chemical potential as "the differential coefficient of the energy taken with respect to the variable expressing the quantity of that substance." Then equation (17.55) becomes

$$\mu_i = \left(\frac{\partial U}{\partial n_i}\right)_{S,V,n_{j,j\neq i}} = \left(\frac{\partial H}{\partial n_i}\right)_{S,P,n_{j,j\neq i}} = \left(\frac{\partial F}{\partial n_i}\right)_{T,V,n_{j,j\neq i}} = \left(\frac{\partial G}{\partial n_i}\right)_{T,P,n_{j,j\neq i}} \tag{17.56}$$

so that equations (17.45) and (17.49) – (17.51) become

$$dU = TdS - PdV + \sum_i \mu_i dn_i \tag{17.57}$$

$$dH = TdS + VdP + \sum_i \mu_i dn_i \tag{17.58}$$

$$dF = -SdT - PdV + \sum_i \mu_i dn_i \tag{17.59}$$

$$dG = -SdT + VdP + \sum_i \mu_i dn_i \tag{17.60}$$

The chemical potential is an intensive property and, as such, can have different values from point to point within the system boundary provided the system is not too far removed from equilibrium.

We now show the relationship of the affinity of reaction to the chemical potential. From equation (17.49) we have

$$A = -\left(\frac{\partial G}{\partial \xi}\right)_{T,P} \tag{17.61}$$

which, with the aid of equation (17.56), we can now write in the form

$$A = -\sum_i \left(\frac{\partial G}{\partial n_i}\right)_{T,P,n_{j,j\neq i}} \frac{dn_i}{d\xi} = -\sum_i \nu_i \left(\frac{\partial G}{\partial n_i}\right)_{T,P,n_{j,j\neq i}} = -\sum_i \nu_i \mu_i \tag{17.62}$$

At equilibrium, $A = 0$. Then from equation (17.62), the condition for chemical equilibrium is

$$\sum_i \nu_i \mu_i = 0 \tag{17.63}$$

Before we can make use of equation (17.63) to determine the relative amounts of the reacting species present in the equilibrium state, we need to establish the relationship between the chemical potential and the other thermodynamic properties that establish the equilibrium state. To this end, we exploit some of the mathematical properties of the thermodynamic functions. Specifically, we recall *Euler's Theorem.*

17.2.6 Euler's Theorem

The function $f = f(x,y,z...)$ is said to be homogeneous of degree m in the variables $x,y,z...$ if we have identically

$$f(\lambda x, \lambda y, \lambda z, \ldots) = \lambda^m f(x, y, z, \ldots) \tag{17.64}$$

where λ is an arbitrary constant. If we differentiate equation (17.64) with respect to λ, we get

$$\frac{\partial f(\lambda x, \lambda y, \lambda z, \ldots)}{\partial \lambda x} \cdot x + \frac{\partial f(\lambda x, \lambda y, \lambda z, \ldots)}{\partial \lambda y} \cdot y + \frac{\partial f(\lambda x, \lambda y, \lambda z, \ldots)}{\partial \lambda z} \cdot z \cdots \equiv m\lambda^{m-1} f(x, y, z, \ldots) \tag{17.65}$$

In particular, in equation (17.65) if $\lambda = 1$, we have

$$\frac{\partial f}{\partial x} x + \frac{\partial f}{\partial y} y + \frac{\partial f}{\partial z} z + \cdots = m f(x, y, z, \ldots) \tag{17.66}$$

Two cases are of particular interest in thermodynamics:

1. *Homogeneous functions of the first degree,* $m = 1$.

   Then

$$f(\lambda x, \lambda y, \lambda z, \ldots \lambda w, \ldots) = \lambda f(x, y, z, \ldots w, \ldots) \tag{17.67}$$

and

$$\sum_w \frac{\partial f}{\partial w} w = f(x, y, z, \ldots w, \ldots) \tag{17.68}$$

2. *Homogeneous functions of the zeroth degree,* $m = 0$.

   Then

$$f(\lambda x, \lambda y, \lambda z, \ldots \lambda w, \ldots) = f(x, y, z, \ldots w, \ldots) \tag{17.69}$$

and

$$\sum_w \frac{\partial f}{\partial w} w = 0 \tag{17.70}$$

17.2.7 Partial Molar Properties

As an example of the utility of Euler's Theorem applied to thermal-fluid systems, consider the volume of a multi-component system at fixed values of T and P. Then we can write

$$V = V(T, P, n_1, n_2, \ldots n_c) \tag{17.71}$$

If the system is increased in size λ times, we have

$$V(T, P, \lambda n_1, \lambda n_2, \ldots \lambda n_c) = \lambda V(T, P, n_1, n_2, \ldots n_c) \tag{17.72}$$

Then the volume is homogeneous of the first degree in $n_1, n_2, \ldots n_c$. Then by equation (17.68) we have

$$\sum_i \frac{\partial V(T, P, n_1, n_2, \ldots n_c)}{\partial n_i} n_i = V(T, P, n_1, n_2, \ldots n_c) \tag{17.73}$$

If we differentiate equation (17.74) with respect to n_j at constant T, P, we get for each value of j

$$\sum_i \frac{\partial^2 V}{\partial n_i \partial n_j} n_i + \frac{\partial V}{\partial n_j} = \frac{\partial V}{\partial n_j} \tag{17.74}$$

We now introduce the concept of *partial molar quantities* such that in the parlance of Gibbs the partial molar property is the differential coefficient of the property taken with respect to the variable expressing the quantity of that substance. Then the partial molar volume, υ_i, is defined as

$$\upsilon_i = \left(\frac{\partial V}{\partial n_i}\right)_{T,P,n_{j,j\neq i}} \tag{17.75}$$

Then equation (17.73) becomes

$$V = \sum_i n_i \upsilon_i \tag{17.76}$$

Equation (17.74) can now be written

$$\sum_i n_i \left(\frac{\partial \upsilon_i}{\partial n_j}\right)_{T,P} = 0 \tag{17.77}$$

or

$$\sum_i n_i \left(\frac{\partial \upsilon_j}{\partial n_i}\right)_{T,P} = 0 \tag{17.78}$$

Equation (17.78) satisfies equation (17.70). Then the partial molar volume is homogeneous of degree zero, and for all i we have

$$\upsilon_i(T, P, \lambda n_1, \lambda n_2, \ldots \lambda n_c) = \upsilon_i(T, P, n_1, n_2, \ldots n_c) \tag{17.79}$$

Thus the value of υ_i is independent of the size of the system so that the partial molar volume is an intensive property.

It is important to distinguish the difference between *partial molar properties* and *average molar properties*. If Φ is a property of a system and $\delta\Phi$ is the increase in that property when δn_i moles are added to the system at constant T and P, the partial molar value of that property, ϕ_i, is the limiting value of the ratio $\delta\Phi/\delta n_i$ as $\delta n_i \to 0$, viz.

$$\phi_i = \lim_{\delta n_i \to 0} \left(\frac{\delta\Phi}{\delta n_i}\right)_{T,P} = \left(\frac{\partial\Phi}{\partial n_i}\right)_{T,P} \tag{17.80}$$

The difference between the partial molar property and the corresponding average molar property can be made more apparent by computing the partial molar property from experimental data.

Consider, for example, a system comprised of two components 1 and 2 with n_1 moles of one component and n_2 moles of the other. The total volume of the mixture is V. Then the average molar volume $\bar{\upsilon}_i$ is

$$\bar{\upsilon}_i = \frac{V}{n_1 + n_2} \tag{17.81}$$

This is shown schematically in Figure 17.1 as a function of the mole fraction of component 2, x_2. Also shown in Figure 17.1 is the tangent to the curve of equation (17.81). The tangent intersects the line $x_2 = 0$ at the point A and the line $x_2 = 1$ at the point B.

From equation (17.77), we have for two components

$$n_1 \left(\frac{\partial \upsilon_1}{\partial n_2}\right)_{T,P} + n_2 \left(\frac{\partial \upsilon_2}{\partial n_2}\right)_{T,P} = 0 \tag{17.82}$$

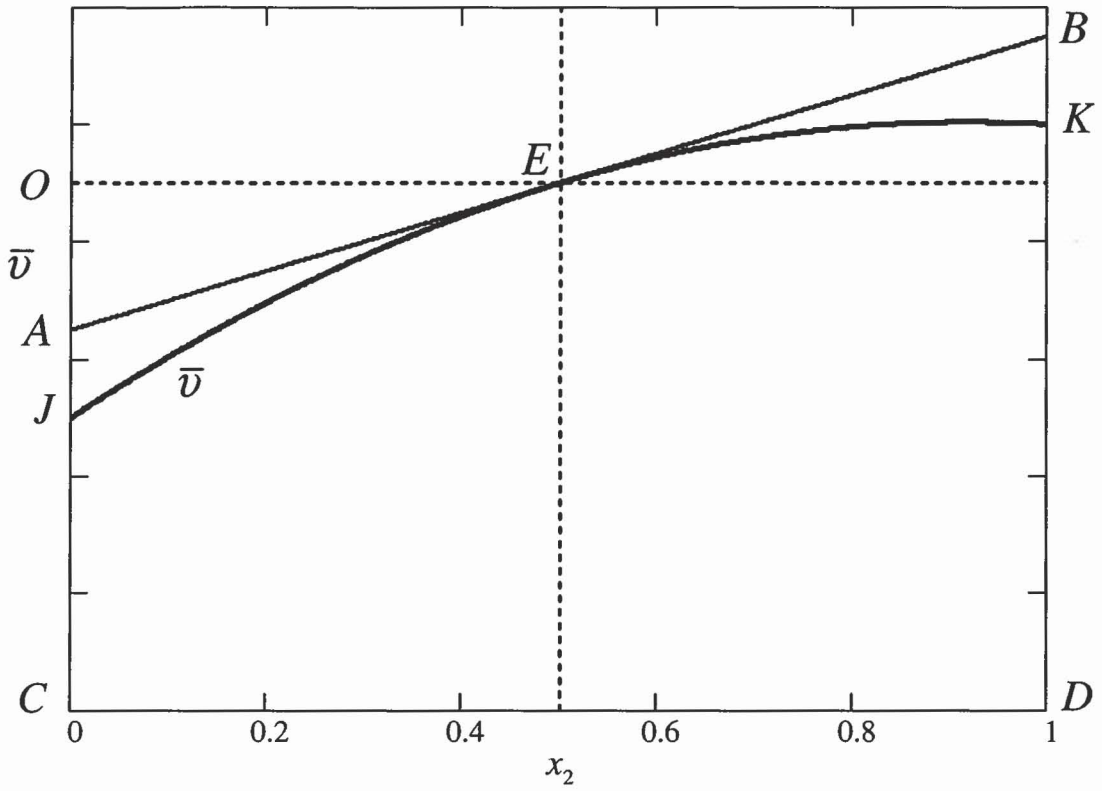

Figure 17.1 Schematic Representation of Experimental Data for Average Molar Volume of Two-component Mixture

where v_i is the partial molar volume. Dividing equation (17.82) by $n_1 + n_2$, we get

$$x_1\left(\frac{\partial v_1}{\partial n_2}\right)_{T,P} + x_2\left(\frac{\partial v_2}{\partial n_2}\right)_{T,P} = 0 \tag{17.83}$$

Applying the chain rule to equation (17.83), we get

$$x_1\left(\frac{\partial v_1}{\partial n_2}\right)_{T,P}\left(\frac{dn_2}{dx_2}\right) + x_2\left(\frac{\partial v_2}{\partial n_2}\right)_{T,P}\left(\frac{dn_2}{dx_2}\right) = x_1\left(\frac{\partial v_1}{\partial x_2}\right)_{T,P} + x_2\left(\frac{\partial v_1}{\partial x_2}\right)_{T,P} = 0 \tag{17.84}$$

The volume of the mixture is

$$V = n_1 v_1 + n_2 v_2 \tag{17.85}$$

Dividing equation (17.85) by $n_1 + n_2$, we get

$$\overline{v} = x_1 v_1 + x_2 v_2 = (1 - x_2) v_1 + x_2 v_2 \tag{17.86}$$

Taking the derivative of equation 917.86) with respect to x_2, we get

$$\left(\frac{\partial \overline{v}}{\partial x_2}\right)_{T,P} = -v_1 + v_2 + (1 - x_2)\left(\frac{\partial v_1}{\partial x_2}\right)_{T,P} + x_2\left(\frac{\partial v_2}{\partial x_2}\right)_{T,P} \tag{17.87}$$

Combining equations (17.84) and (17.87), we get

$$\left(\frac{\partial \overline{v}}{\partial x_2}\right)_{T,P} = v_2 - v_1 \tag{17.88}$$

Multiplying equation (17.88) through by x_2, we get

$$x_2\left(\frac{\partial \bar{v}}{\partial x_2}\right)_{T,P} = x_2 v_2 - x_2 v_1 \tag{17.89}$$

If we now add and subtract $x_1 v_1$ from equation (17.89), we get

$$x_2\left(\frac{\partial \bar{v}}{\partial x_2}\right)_{T,P} = \left(x_2 v_2 + x_1 v_1\right) - \left(x_1 v_1 + x_2 v_1\right) = \bar{v} - v_1 \tag{17.90}$$

Equation (17.90) can be rewritten in the form

$$v_1 = \bar{v} - x_2\left(\frac{\partial \bar{v}}{\partial x_2}\right) \tag{17.91}$$

From Figure 17.1, we can express equation (17.91) in terms of the lengths of the lines shown, viz.

$$v_1 = OC - OE\left(\frac{OA}{OE}\right) = AC \tag{17.92}$$

In a similar manner, we can show

$$v_2 = BD \tag{17.93}$$

When $x_2 = 0$, we have but a single component, 1, and $\bar{v} = v_1 = CJ$. Conversely, when $x_2 = 1$, we have but a single component, 2, and $\bar{v} = v_2 = DK$.

17.2.8 Characteristic Thermodynamic Functions and the Chemical Potential

We can write the Gibbs free energy surface in the form

$$G = G\left(T, P, n_1, n_2, \ldots n_c\right) \tag{17.94}$$

If we increase the size of the system by a factor λ, we have

$$G\left(T, P, \lambda n_1, \lambda n_2, \ldots \lambda n_c\right) = \lambda G\left(T, P, n_1, n_2, \ldots n_c\right) \tag{17.95}$$

Then the Gibbs free energy is homogeneous of the first degree in $n_1, n_2, \ldots n_c$. Then from Euler's Theorem [equation (17.68)], we have

$$\left(\frac{\partial G}{\partial n_1}\right)_{T,P,n_{j,j\neq 1}} n_1 + \left(\frac{\partial G}{\partial n_2}\right)_{T,P,n_{j,j\neq 2}} n_2 + \cdots + \left(\frac{\partial G}{\partial n_c}\right)_{T,P,n_{j,j\neq c}} n_c = G\left(T, P, n_1, n_2, \ldots n_c\right) \tag{17.96}$$

If we substitute equation (17.56) into equation (17.96), we obtain

$$G = \sum_i \mu_i n_i \tag{17.97}$$

Then since

$$G = U - TS + PV = H - TS = F + PV \tag{17.98}$$

we have

$$U = \sum_i \mu_i n_i + TS - PV \tag{17.99}$$

$$H = \sum_i \mu_i n_i + TS \tag{17.100}$$

$$F = \sum_i \mu_i n_i - PV \tag{17.101}$$

The function $G = G(T,P,n_1,\ldots,n_c)$ is a characteristic thermodynamic function and is equivalent to knowing all thermodynamic information about the system to which it applies. In particular, we can derive the various thermodynamic properties of the system by forming the appropriate partial derivatives, viz.

$$\left(\frac{\partial \mu_i}{\partial T}\right)_{P,n} = \frac{\partial}{\partial T}\left[\left(\frac{\partial G}{\partial n_i}\right)_{T,P}\right]_{P,n} = \frac{\partial}{\partial n_i}\left[\left(\frac{\partial G}{\partial T}\right)_{P,n}\right]_{T,P} = -\left(\frac{\partial S}{\partial n_i}\right)_{T,P} = -s_i \tag{17.102}$$

and

$$\left(\frac{\partial \mu_i}{\partial P}\right)_{T,n} = \frac{\partial}{\partial P}\left[\left(\frac{\partial G}{\partial n_i}\right)_{T,P}\right]_{T,n} = \frac{\partial}{\partial n_i}\left[\left(\frac{\partial G}{\partial P}\right)_{T,n}\right]_{T,P} = \left(\frac{\partial V}{\partial n_i}\right)_{T,P} = v_i \tag{17.103}$$

Now if we differentiate $G = U - TS + PV$ with respect to n_i with T and P constant, we have

$$\left(\frac{\partial G}{\partial n_i}\right)_{T,P} = \left(\frac{\partial U}{\partial n_i}\right)_{T,P} - T\left(\frac{\partial S}{\partial n_i}\right)_{T,P} + P\left(\frac{\partial V}{\partial n_i}\right)_{T,P} \tag{17.104}$$

Substituting equations (17.56), (17.102), and (17.103) into equation (17.104), we have a relation between the chemical potential and the partial molar properties, viz.

$$\mu_i = u_i - Ts_i + Pv_i \tag{17.105}$$

Similarly from $H = U + PV$, we have

$$\left(\frac{\partial H}{\partial n_i}\right)_{T,P} = \left(\frac{\partial U}{\partial n_i}\right)_{T,P} + P\left(\frac{\partial V}{\partial n_i}\right)_{T,P} \tag{17.106}$$

and

$$h_i = u_i + Pv_i \tag{17.107}$$

Then upon combining equations (17.105) and (17.107), we obtain

$$\mu_i = h_i - Ts_i \tag{17.108}$$

Now

$$\left[\frac{\partial}{\partial T}\left(\frac{\mu_i}{T}\right)\right]_{P,n} = \frac{1}{T}\left(\frac{\partial \mu_i}{\partial T}\right)_{P,n} - \frac{\mu_i}{T^2} \tag{17.109}$$

Substituting equation (17.102) and (17.108) into equation (17.109), we obtain

$$\left[\frac{\partial}{\partial T}\left(\frac{\mu_i}{T}\right)\right]_{P,n} = -\frac{1}{T}s_i - \frac{\mu_i}{T^2} = -\left(\frac{\mu_i + Ts_i}{T^2}\right) = -\frac{h_i}{T^2} \tag{17.110}$$

which is a result that will prove to be useful later.

17.2.9 Heat of Reaction

For a multi-component system undergoing a single reaction, we note that if we re-introduce the extent of reaction in the formulation for the enthalpy, we have an expression for the *heat of reaction* in terms of the partial molar enthalpy of the components of the reaction, viz.

$$\left(\frac{\partial H}{\partial \xi}\right)_{T,P} = \sum_i \left(\frac{\partial H}{\partial n_i}\right)_{T,P} \frac{dn_i}{d\xi} = \sum_i \nu_i h_i \tag{17.111}$$

where we have made use of equation (17.9) and the definition of the partial molar enthalpy. Recall that $\nu_i < 0$ for reactants and $\nu_i > 0$ for products of the reaction. Depending upon the individual values for the partial molar enthalpies of the various species involved in the reaction, the value of the heat of reaction can be positive or negative. From the first law, we see that for a reaction carried out at constant T and P, if

$$\left(\frac{\partial H}{\partial \xi}\right)_{T,P} > 0 \quad \text{reaction is endothermic} \tag{17.112}$$

but if

$$\left(\frac{\partial H}{\partial \xi}\right)_{T,P} < 0 \quad \text{reaction is exothermic} \tag{17.113}$$

17.2.10 Gibbs-Duhem Relation

If we form the differential of equation (17.97), we have

$$dG = \sum_i n_i d\mu_i + \sum_i \mu_i dn_i \tag{17.114}$$

Substituting equation (17.60) for dG into equation (17.114), we have the *Gibbs-Duhem relation*, viz.

$$SdT - VdP + \sum_i n_i d\mu_i = 0 \tag{17.115}$$

which is a relation amongst the changes in the intensive properties of a multi-component system.

For a system in partial equilibrium, that is a system in thermal and mechanical equilibrium but not chemical equilibrium, $dT = 0$ and $dP = 0$ and

$$\sum_i n_i d\mu_i = 0 \tag{17.116}$$

Thus, as the system seeks chemical equilibrium through chemical reaction the resulting changes in the chemical potential are not independent of one another.

In order to exploit fully the equilibrium concept embodied in the affinity of reaction, it is necessary for us to now develop a model of system behavior that will enable us to formulate the chemical potential in terms of the other thermodynamic properties. The model of the greatest practical utility is that of the *ideal chemical system.*

17.2.11 The Ideal Chemical System Model

The ideal chemical system model is defined in terms of the constitutive relation for the chemical potential, viz.

$$\mu_i^{ideal} = \mu_i^*(T,P) + \bar{R}T \ln x_i \tag{17.117}$$

where $\bar{R} = 8.3145 \text{ x } 10^3$ J/kmole-K and $\mu_i^*(T,P)$ is a function of T and P only and is the value of μ_i extrapolated to $x_i = 1$ at constant T and P. If a system satisfies equation (17.118) in a concentration range that extends to $x_i = 1$, we have

$$\mu_i^*(T,P) = \mu_i^0(T,P) \tag{17.118}$$

where μ_i^0 is the chemical potential of the pure component i at T and P.

Although the constitutive relation of equation (17.117) is a specialized form of the constitutive relation for the chemical potential in general, it is of considerable practical value. In particular, there are two examples of the ideal chemical system model that are of special interest:

1. *Perfect Mixture Model*: The *perfect mixture model* is a model of a mixture for which the ideal chemical system model holds for all values of x_i for all components i. Then

$$\mu_i^*(T,P) = \mu_i^0(T,P) \quad \text{for all } i \tag{17.119}$$

2. *Ideal Dilute Solution Model*: When all components of a mixture except for one are present in very small amounts, the mixture satisfies the constitutive relation (17.117) and is known as an *ideal dilute solution* in which the component present in a large amount is designated the *solvent* and is denoted by the subscript 1. Then

$$\mu_1^*(T,P) = \mu_1^0(T,P) \tag{17.120}$$

but for all other constituents of the mixture

$$\mu_i^*(T,P) \neq \mu_i^0(T,P) \tag{17.121}$$

We shall make use of these models in further developing the relations governing the state of chemical equilibrium.

17.2.12 Heat of Reaction of the Ideal Chemical System Model

We can rewrite the expression for the heat of reaction, equation (17.111), in the form

$$\left(\frac{\partial H}{\partial \xi}\right)_{T,P} = -T^2 \sum_i \nu_i \left(\frac{h_i^{ideal}}{T^2}\right) \tag{17.122}$$

From equations (17.110) and (17.117) we have

$$-\frac{h_i^{ideal}}{T^2} = \left[\frac{\partial}{\partial T}\left(\frac{\mu_i^{ideal}}{T}\right)\right]_{P,n} = \left[\frac{\partial}{\partial T}\left(\frac{\mu_i^*}{T}\right)\right]_{P,n} + \frac{\partial}{\partial T}\left(\bar{R}\ln x_i\right)_{P,n} = \left[\frac{\partial}{\partial T}\left(\frac{\mu_i^*}{T}\right)\right]_P \tag{17.123}$$

Then the heat of reaction for the ideal chemical system model becomes

$$\left(\frac{\partial H}{\partial \xi}\right)_{T,P} = -T^2 \sum_i \nu_i \left[\frac{\partial}{\partial T}\left(\frac{\mu_i^*}{T}\right)\right]_P \tag{17.124}$$

17.2.13 The Equilibrium Constant and the Law of Mass Action

From equation (17.62), we have for the affinity of the reaction of the ideal chemical system model

$$A^{ideal} = -\sum_i \nu_i \mu_i^{ideal} = -\sum_i \nu_i \mu_i^*(T,P) - \sum_i \nu_i \bar{R}T\ln x_i \tag{17.125}$$

Now we let

$$-\sum_i \nu_i \mu_i^*(T,P) = \bar{R}T\ln K(T,P) \tag{17.126}$$

where the quantity $K(T,P)$ is known as the equilibrium constant of the reaction. Then the affinity of the reaction becomes

$$A^{ideal} = \bar{R}T\ln K(T,P) - \bar{R}T\ln x_1^{\nu_1} x_2^{\nu_2}\ldots x_c^{\nu_c} \tag{17.127}$$

or alternatively

$$A^{ideal} = \bar{R}T\ln \frac{K(T,P)}{x_1^{\nu_1} x_2^{\nu_2}\ldots x_c^{\nu_c}} \tag{17.128}$$

In the equilibrium state of the ideal chemical model, $A^{ideal} = 0$. Then equation (17.128) gives us an expression for the equilibrium constant in the equilibrium state, viz.

$$K(T,P) = x_1^{\nu_1} x_2^{\nu_2}\ldots x_c^{\nu_c} \tag{17.129}$$

Equation (17.129) is known as the *Law of Mass Action*. It is possible to refine the expression for the equilibrium constant further, but in doing so, the results become model specific. We shall take just such an approach in the sections that follow.

17.2.14 The van't Hoff Relation

Without specializing the ideal chemical model any further, we can separate out the temperature dependence of the equilibrium constant. We can rewrite equation (17.126) in the form

$$-\sum_i \nu_i \left(\frac{\mu_i}{T}\right) = \bar{R}\ln K(T,P) \tag{17.130}$$

Then the variation in the equilibrium constant with temperature becomes

$$\bar{R}\frac{\partial}{\partial T}\left[\ln K(T,P)\right]_P = -\sum_i \nu_i \left[\frac{\partial}{\partial T}\left(\frac{\mu_i^*}{T}\right)\right]_P = \frac{1}{T^2}\left(\frac{\partial H^{ideal}}{\partial \xi}\right)_{T,P} \tag{17.131}$$

where we have substituted equation (17.124). Rearranging equation (17.131) and substituting

equation (17.122), we get the *van't Hoff relation*, viz.

$$\frac{\partial}{\partial T}\left[\ln K(T,P)\right]_P = \frac{1}{\bar{R}T^2}\left(\frac{\partial H^{ideal}}{\partial \xi}\right)_{T,P} = \frac{1}{\bar{R}T^2}\sum_i \nu_i h_1^{ideal} \tag{17.132}$$

From equation (17.132) it follows that for an endothermic reaction for which the heat of reaction is positive, i.e., $\sum_i \nu_i h_i^{ideal} > 0$, the equilibrium constant increases with temperature. On the other hand, for an exothermic reaction for which the heat of reaction is negative, i.e., $\sum_i \nu_i h_i^{ideal} < 0$, the equilibrium constant decreases as temperature increases.

17.3 Ideal Gas Mixtures

We now take up the first of the two special cases of the ideal chemical system models, namely a mixture of gases, each of which satisfies the ideal gas model. Such a mixture is a perfect mixture with the chemical potential of the constituent gases given by equation (17.117) together with equation (17.119). We shall examine two general classes of the behavior ideal gas mixtures; (1) reactive ideal gas mixtures and (2) a mixture of an ideal gas and a condensable vapor. The latter case is a subset of the science of thermodynamics known as *psychrometrics*.

17.3.1 Dalton's Law

In 1803, the English chemist and physicist John Dalton (1766 – 1844) published several papers in which he proposed a model for a mixture of ideal gases. This model is based upon the model of an ideal gas in which the molecules of the gas are considered to be point masses that do not interact with each other. Then in a mixture of such gases of different identities, none of the components are "aware" that the other components are present. Then in a volume V containing the mixture at a temperature T, each component in the mixture exists in the volume as though it alone occupied the entire volume. Each component gas i is said to exert a partial pressure P_i such that

$$P_i = n_i \frac{\bar{R}T}{V} \tag{17.133}$$

where n_i is the number of moles of component i in the mixture.

According to Dalton's hypothesis, now known as *Dalton's Law*, the total pressure of the mixture is simply the sum of the partial pressures of the constituent gases, viz.

$$P = \sum_i P_i \tag{17.134}$$

where

$$P = \sum_i n_i \frac{\bar{R}T}{V} \tag{17.135}$$

Combining equations (17.133) – (17.135), we obtain

$$P = \left(\sum_i n_i\right)\frac{P_i}{n_i} \tag{17.136}$$

and

$$P_i = \left(\frac{n_i}{\sum_i n_i}\right)P = x_i P \tag{17.137}$$

where x_i is the mole fraction of component i in the mixture.

Since a mixture of ideal gases in a volume V at a temperature T is a perfect mixture, the Helmholtz free energy F of the mixture is the sum of the of the free energies that the individual component gases would have if they alone occupied the volume at the temperature T. Then for the mixture

$$F = \sum_i F_i(T, V, n_i) = \sum n_i \bar{f}(T, \bar{v}_i) \tag{17.138}$$

where $\bar{f}_i(T, \bar{v}_i)$ is the molar free energy of the pure component and $\bar{v}_i$ is the molar volme, viz.

$$\bar{v}_i = \frac{V}{n_i} \tag{17.139}$$

Now by definition

$$\bar{f}_i(T, \bar{v}_i) = \bar{u}_i(T) - T\bar{s}_i(T, \bar{v}_i) \tag{17.140}$$

where we have made use of the fact that for the ideal gas model the internal energy is a function of temperature only, viz.

$$d\bar{u}_i(T) = \bar{c}_v(T)\,dT \tag{17.141}$$

The canonical relation can be written in molar form as

$$d\bar{u}_i = Td\bar{s}_i - Pd\bar{v}_i \tag{17.142}$$

The entropy constitutive relation also can be written in molar form as

$$d\bar{s}_i = \bar{c}_v \frac{dT}{T} + \bar{R}\frac{d\bar{v}_i}{\bar{v}_i} \tag{17.143}$$

which can be integrated to give

$$\bar{s}_i = \bar{s}_i(T_0, \bar{v}_{i0}) + \int_{T_0}^{T} \frac{\bar{c}_v(T)}{T} dT + \bar{R}\ln\frac{\bar{v}_i}{\bar{v}_{i0}} \tag{17.144}$$

or

$$\bar{s}_i = \bar{s}_i^{\dagger}(T) + \bar{R}\ln\bar{v}_i \tag{17.145}$$

where

$$\bar{s}_i^{\dagger}(T) = \bar{s}_i(T_0, \bar{v}_{i0}) + \int_{T_0}^{T} \frac{\bar{c}_v(T)}{T} dT - \bar{R}\ln\bar{v}_{i0} \tag{17.146}$$

Then the molar Helmholtz free energy becomes

$$\bar{f}_i(T, \bar{v}_i) = \bar{f}_i^{\dagger}(T) - T\bar{s}_i(T, \bar{v}_i) \tag{17.147}$$

where

$$\bar{f}_i^{\dagger}(T) = \bar{u}_i - T\bar{s}_i^{\dagger}(T) \tag{17.148}$$

Then

$$\bar{f}_i(T, \bar{v}_i) = \bar{f}_i^{\dagger}(T) - \bar{R}T\ln\bar{v}_i = \bar{f}_i^{\dagger}(T) - \bar{R}T\ln\frac{V}{n_i} \tag{17.149}$$

We now show that for a mixture of ideal gases, with the exception of the volume, the partial molar properties are identical to the corresponding molar properties. For the volume, we have

$$v_i = \left(\frac{\partial V}{\partial n_i}\right)_{T,P,n_{j,j\neq i}} = \frac{\partial}{\partial n_i}\left(\frac{\sum_i n_i \bar{R}T}{P}\right)_{T,P,n_{j,j\neq i}} = \frac{\bar{R}T}{P} \tag{17.150}$$

but

$$\overline{v}_i = \frac{\overline{R}T}{P_i} \tag{17.151}$$

Thus, comparing equations (17.150) and (17.151), we see the partial molar volume of a component of the ideal gas mixture is *not* equal to the molar volume of the component.

On the other hand, for the internal energy, since the component ideal gases of the mixture do not interact with one another, we have

$$U = \sum_i n_i \overline{u}_i \tag{17.152}$$

which gives for the partial molar internal energy

$$u_i = \left(\frac{\partial U}{\partial n_i}\right)_T = \overline{u}_i \tag{17.153}$$

For the chemical potential of component i, we have from equation (17.149)

$$\mu_i = \left(\frac{\partial F}{\partial n_i}\right)_{T,V} = \overline{f}_i^{\dagger}(T) + \overline{R}T + \overline{R}T \ln \frac{n_i}{V} \tag{17.154}$$

Then

$$\mu_i = \mu_i^{\dagger}(T) + \overline{R}T \ln P_i \tag{17.155}$$

where

$$\mu_i^{\dagger}(T) = \overline{f}_i^{\dagger}(T) + \overline{R}T + \overline{R}T \ln\left(\overline{R}T\right) \tag{17.156}$$

Equation (17.155) is identical to the formulation of μ_i for the pure component since it exerts the pressure P_i when it exists alone in the volume V. Thus

$$\mu_i = \overline{\mu}_i \tag{17.157}$$

For the enthalpy we have

$$h_i = u_i + Pv_i = u_i + \overline{R}T \tag{17.158}$$

and

$$\overline{h}_i = \overline{u}_i + P_i\overline{v}_i = \overline{u}_i + \overline{R}T \tag{17.159}$$

Thus in light of equation (17.153), comparison of equations (17.158) and (17.159) yields

$$h_i = \overline{h}_i \tag{17.160}$$

Similarly for the entropy, we have

$$\mu_i = h_i - Ts_i \tag{17.161}$$

and

$$\overline{\mu}_i = \overline{h}_i - T\overline{s}_i \tag{17.162}$$

Then in light of equations (17.157) and (17.160), it follows from equations (17.161) and (17.162) that

$$s_i = \overline{s}_i \tag{17.163}$$

Thus, for a mixture of ideal gases, the partial molar properties and the molar properties are indeed identical except for the volume.

17.3.2 Chemical Equilibrium in a Mixture of Ideal Gases

Consider now a mixture of ideal gases undergoing a single reaction. Since the partial pressure of component i in a mixture of ideal gases is $P_i = x_i P$, we can rewrite equation (17.155) in the form

$$\mu_i = \mu_i^0(T, P) + \overline{R}T \ln x_i \tag{17.164}$$

where $\mu_i^0(T,P)$ is the chemical potential of the pure component i at the temperature T and pressure P, viz.

$$\mu_i^{\,0}(T,P) = \mu_i^{\dagger}(T) + \bar{R}T \ln P \tag{17.165}$$

Recall from equation (17.62) that the affinity of the reaction is

$$A = -\sum_i \nu_i \mu_i \tag{17.166}$$

Substituting equation (17.155) into equation (17.166), we get

$$A = -\sum_i \nu_i \mu_i^{\dagger}(T) - \bar{R}T \sum_i \nu_i \ln P_i = -\sum_i \nu_i \mu_i^{\dagger}(T) - \bar{R}T \sum_i \ln P_i^{\nu_i} \tag{17.167}$$

If we now let

$$-\sum_i \nu_i \mu_i^{\dagger} = \bar{R}T \ln K_P(T) \tag{17.168}$$

we can rewrite equation (17.167) in the form

$$A = \bar{R}T \ln \frac{K_P(T)}{P_1^{\nu_1} P_2^{\nu_2} \ldots P_c^{\nu_c}} \tag{17.169}$$

At equilibrium, $A = 0$. Then the argument of the logarithm becomes unity and

$$K_P(T) = \prod_i P_i^{\nu_i} = P^{\sum_i \nu_i} \prod_i x_i \tag{17.170}$$

Comparing equations (17.129) and (17.170), we have

$$K(T,P) = P^{-\sum_i \nu_i} K_P(T) \tag{17.171}$$

Equation (17.171) shows that for the case of a mixture of ideal gases, we have separated the effects of temperature and pressure on the state of chemical equilibrium.

We can take the temperature dependence a step further. Since a mixture of ideal gases is an ideal chemical system, it satisfies the van't Hoff relation. Then from equation (17.132) we have

$$\frac{d}{dT}\left[\ln K_P(T)\right] = \frac{1}{\bar{R}T^2}\left(\frac{\partial H}{\partial \xi}\right)_{T,P} = \frac{1}{\bar{R}T^2}\sum_i \nu_i \bar{h}_i \tag{17.172}$$

If we integrate equation (17.172), we obtain

$$\ln K_P(T) - \ln K_P(T_0) = \int_{T_0}^{T} \frac{1}{\bar{R}T^2}\left(\frac{\partial H}{\partial \xi}\right)_{T,P} dT \tag{17.173}$$

For many ideal gas reactions, the temperature dependence of the heat of reaction is weak and the heat of reaction can be taken as a constant. Then the integral of equation (17.173) becomes

$$\ln K_P(T) = -\frac{1}{\bar{R}T}\left(\frac{\partial H}{\partial \xi}\right)_{T,P} + \text{constant} = -\frac{1}{\bar{R}T}\sum_i \nu_i \bar{h}_i + \text{constant} \tag{17.174}$$

Equation (17.174) can be used as an algebraic form to fit the experimental data for the equilibrium constant for gas phase reactions, viz.

$$\ln K_P(T) = \mathrm{A} + \frac{\mathrm{B}}{T(K)} \tag{17.175}$$

where A and B are constants. Table 17.1 lists the values of A and B for some gas phase reactions commonly found in engineering practice.